

TWENTY-SECOND ANNUAL REPORT
OF THE
NATIONAL ADVISORY COMMITTEE
FOR AERONAUTICS

1936

INCLUDING TECHNICAL REPORTS
Nos. 542 to 576



UNITED STATES
GOVERNMENT PRINTING OFFICE
WASHINGTON : 1937

TECHNICAL REPORTS

	Page		Page
No. 542. Potential Flow about Arbitrary Biplane Wing Sections. By I. E. Garrick.....	47	No. 559. The Forces and Moments Acting on Parts of the XN2Y-1 Airplane during Spins. By N. F. Seudder.....	305
No. 543. Tank Tests of N. A. C. A. Model 40 Series of Hulls for Small Flying Boats and Amphibians. By John B. Parkinson and John R. Dawson.....	77	No. 560. A Simplified Application of the Method of Operators to the Calculation of Disturbed Motions of an Airplane. By Robert T. Jones.....	313
No. 544. Combustion in a Bomb with a Fuel-Injection System. By Mildred Cohn and Robert C. Spencer.....	107	No. 561. Effect of Nozzle Design on Fuel Spray and Flame Formation in a High-Speed Compression-Ignition Engine. By A. M. Rothrock and C. D. Waldron.....	327
No. 545. Effects of Air-Fuel Ratio on Fuel Spray and Flame Formation in a Compression-Ignition Engine. By A. M. Rothrock and C. D. Waldron.....	119	No. 562. Air Flow in the Boundary Layer Near a Plate. By Hugh L. Dryden.....	339
No. 546. The Effect of Turbulence on the Drag of Flat Plates. By G. B. Schubauer and H. L. Dryden.....	129	No. 563. Calculated and Measured Pressure Distributions over the Midspan Section of the N. A. C. A. 4412 Airfoil. By Robert M. Pinkerton.....	365
No. 547. Wind-Tunnel Interference with Particular Reference to Off-Center Positions of the Wing and to the Downwash at the Tail. By Abe Silverstein and James A. White....	135	No. 564. Tests of a Wing-Nacelle-Propeller Combination at Several Pitch Settings up to 42°. By Ray Windler.....	381
No. 548. Effect of Tip Shape and Dihedral on Lateral-Stability Characteristics. By Joseph A. Shortall.....	149	No. 565. Measurements of Fuel Distribution within Sprays for Fuel-Injection Engines. By Dana W. Lee.....	389
No. 549. Wind-Tunnel Investigation of the Aerodynamic Balancing of Upper-Surface Ailerons and Split Flaps. By Carl J. Wenzinger.....	159	No. 566. Ground-Handling Forces on a 1/40-Scale Model of the U. S. Airship "Akron." By Abe Silverstein and B. G. Gulick.....	405
No. 550. Cooling Characteristics of a 2-Row Radial Engine. By Oscar W. Schey and Vern G. Rollin.....	177	No. 567. Propulsion of a Flapping and Oscillating Airfoil. By I. E. Garrick.....	419
No. 551. Aircraft Compass Characteristics. By John B. Peterson and Clyde W. Smith.....	187	No. 568. The Quiescent-Chamber Type Compression-Ignition Engine. By H. H. Foster.....	429
No. 552. Wind-Tunnel Tests of 10-Foot-Diameter Autogiro Rotors. By John B. Wheatley and Carlton Bioletti.....	199	No. 569. Wing-Nacelle-Propeller Interference for Wings of Various Spans Force and Pressure-Distribution Tests. By Russel G. Robinson and William H. Herrnstein, Jr.....	449
No. 553. Some Effects of Argon and Helium upon Explosions of Carbon Monoxide and Oxygen. By Ernest F. Fiock and Carl H. Roeder.....	213	No. 570. The Effect of Lateral Controls in Producing Motion of an Airplane as Computed from Wind-Tunnel Data. By Fred E. Weick and Robert T. Jones.....	465
No. 554. Wind-Tunnel Investigation of Ordinary and Split Flaps on Airfoils of Different Profile. By Carl J. Wenzinger.....	223	No. 571. Pressure Distribution over a Rectangular Airfoil with a Partial-Span Split Flap. By Carl J. Wenzinger and Thomas A. Harris.....	491
No. 555. Air Flow around Finned Cylinders. By M. J. Brevoort and Vern G. Rollin.....	237	No. 572. Determination of the Characteristics of Tapered Wings. By Raymond F. Anderson.....	503
No. 556. Further Studies of Flame Movement and Pressure Development in an Engine Cylinder. By Charles F. Marvin, Jr., Armistead Wharton, and Carl H. Roeder.....	251	No. 573. Aerodynamic Characteristics of N. A. C. A. 23012 and 23021 Airfoils with 20-Percent-Chord External-Airfoil Flaps of N. A. C. A. 23012 Section. By Robert C. Platt and Ira H. Abbott.....	523
No. 557. Preliminary Tests in the N. A. C. A. Free-Spinning Wind Tunnel. By C. H. Zimmerman.....	265	No. 574. Pressure Distribution over an Airfoil Section with a Flap and Tab. By Carl J. Wenzinger.....	543
No. 558. Turbulence Factors of N. A. C. A. Wind Tunnels as Determined by Sphere Tests. By Robert C. Platt.....	283	No. 575. Interference of Wing and Fuselage from Tests of 28 Combinations in the N. A. C. A. Variable-Density Tunnel. By Albert Sherman.....	555
		No. 576. Aircraft Accidents Method of Analysis. Report prepared by Committee on Aircraft Accidents.....	564

LETTER OF TRANSMITTAL

To the Congress of the United States:

In compliance with the provisions of the act of March 3, 1915, establishing the National Advisory Committee for Aeronautics, I transmit herewith the Twenty-second Annual Report of the Committee, covering the fiscal year ended June 30, 1936.

FRANKLIN D. ROOSEVELT.

THE WHITE HOUSE,
January 11, 1937.

LETTER OF SUBMITTAL

NATIONAL ADVISORY COMMITTEE FOR AERONAUTICS,
Washington, D. C., December 10, 1936.

MR. PRESIDENT:

In compliance with the provisions of the act of Congress approved March 3, 1915 (U. S. C., title 50, sec. 153), I have the honor to submit herewith the Twenty-second Annual Report of the National Advisory Committee for Aeronautics covering the fiscal year 1936.

During the past year there was continued improvement in the safety, efficiency, range, speed, comfort, and capacity of American aircraft. This gratifying progress in technical development was based largely upon the results of organized fundamental scientific research.

With the support of the President and of the Congress the research laboratories of this Committee at Langley Field, Va., have kept pace with the growing research needs of aviation, and they are as yet unsurpassed by the aeronautical research facilities of any other single nation. Increased recognition abroad of the value and of the vital necessity of aeronautical research has led to recent tremendous expansion in research programs and to multiplication of research facilities by other progressive nations. Thus has the foundation been laid for a serious challenge to America's present leadership in the technical development of aircraft.

This committee, alert to its responsibilities, has prepared plans for continued gradual expansion and improvement of its research facilities. In view of the increasing significance attaching to aircraft development in all parts of the world for both military and commercial purposes, this committee urges the wisdom and ultimate economy of its policy as the best insurance against falling behind in the development of an instrumentality so vital to national defense and so effective in the promotion of commerce and in the advancement of civilization.

Respectfully submitted.

J. S. AMES, *Chairman.*

THE PRESIDENT, *The White House, Washington, D. C.*

NATIONAL ADVISORY COMMITTEE FOR AERONAUTICS

HEADQUARTERS, NAVY BUILDING, WASHINGTON, D. C.

LABORATORIES, LANGLEY FIELD, VA.

Created by act of Congress approved March 3, 1915, for the supervision and direction of the scientific study of the problems of flight (U. S. Code, Title 50, Sec. 151). Its membership was increased to 15 by act approved March 2, 1929. The members are appointed by the President, and serve as such without compensation.

JOSEPH S. AMES, Ph. D., *Chairman*,
Baltimore, Md.

DAVID W. TAYLOR, D. Eng., *Vice Chairman*,
Washington, D. C.

CHARLES G. ABBOT, Sc. D.,
Secretary, Smithsonian Institution.

LYMAN J. BRIGGS, Ph. D.,
Director, National Bureau of Standards.

ARTHUR B. COOK, Rear Admiral, United States Navy,
Chief, Bureau of Aeronautics, Navy Department.

WILLIS RAY GREGG, B. A.,
Chief, United States Weather Bureau.

HARRY F. GUGGENHEIM, M. A.,
Port Washington, Long Island, N. Y.

SYDNEY M. KRAUS, Captain, United States Navy,
Bureau of Aeronautics, Navy Department.

CHARLES A. LINDBERGH, LL. D.,
New York City.

WILLIAM P. MACCRACKEN, Jr., LL. D.,
Washington, D. C.

AUGUSTINE W. ROBINS, Brigadier General, United States Army.
Chief, Matériel Division, Air Corps, Wright Field,
Dayton, Ohio.

EUGENE L. VIDAL, C. E.,
Director of Air Commerce, Department of Commerce.

EDWARD P. WARNER, M. S.,
New York City.

OSCAR WESTOVER, Major General United States Army,
Chief of Air Corps, War Department.

ORVILLE WRIGHT, Sc. D.,
Dayton, Ohio.

GEORGE W. LEWIS, *Director of Aeronautical Research*

JOHN F. VICTORY, *Secretary*

HENRY J. E. REID, *Engineer in Charge, Langley Memorial Aeronautical Laboratory, Langley Field, Va.*

JOHN J. IDE, *Technical Assistant in Europe, Paris, France*

TECHNICAL COMMITTEES

AERODYNAMICS

POWER PLANTS FOR AIRCRAFT

AIRCRAFT STRUCTURES AND MATERIALS

AIRCRAFT ACCIDENTS

INVENTIONS AND DESIGNS

Coordination of Research Needs of Military and Civil Aviation

Preparation of Research Programs

Allocation of Problems

Prevention of Duplication

Consideration of Inventions

LANGLEY MEMORIAL AERONAUTICAL LABORATORY

LANGLEY FIELD, VA.

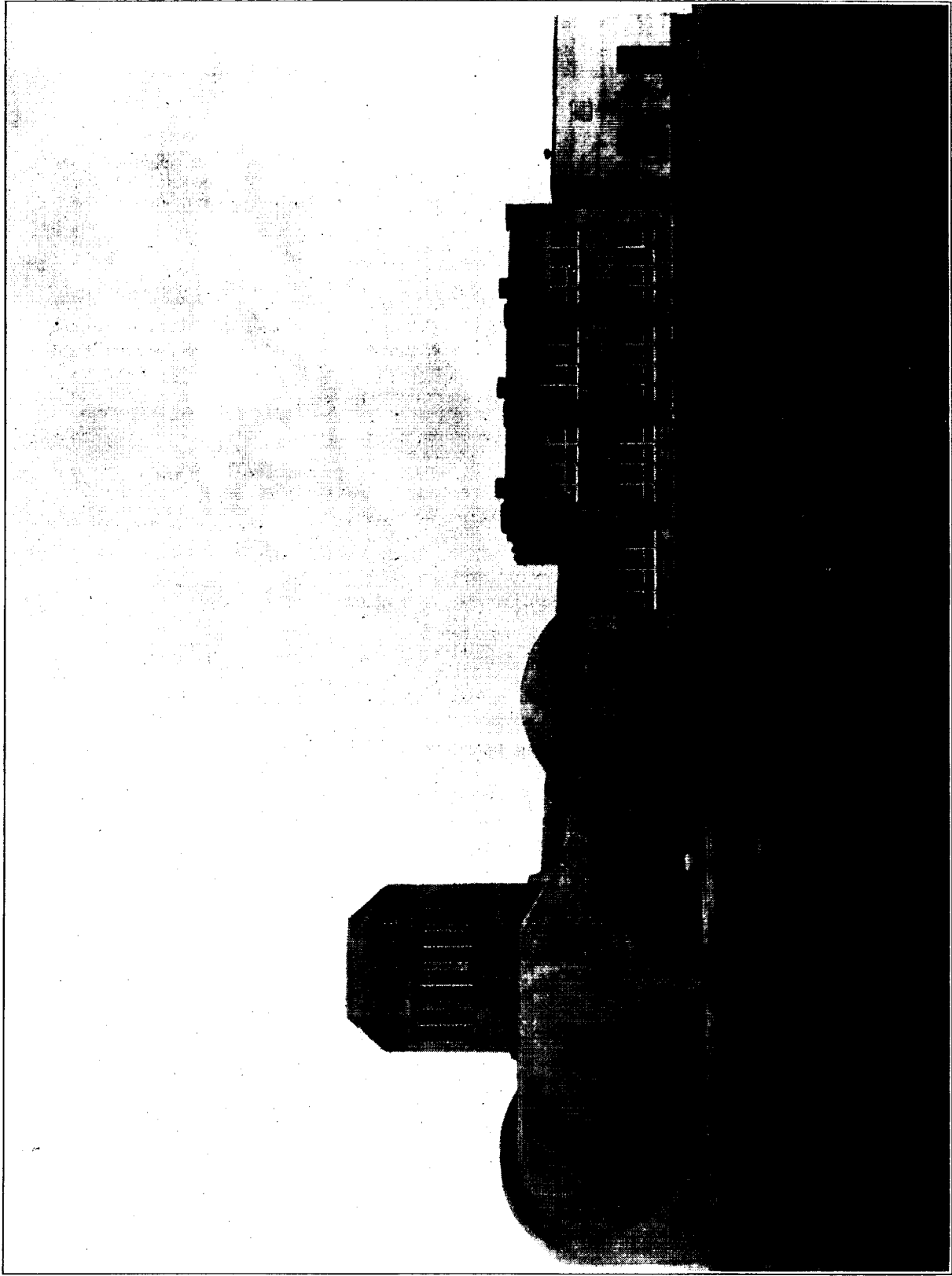
Unified conduct, for all agencies, of
scientific research on the fundamental
problems of flight.

OFFICE OF AERONAUTICAL INTELLIGENCE

WASHINGTON, D. C.

Collection, classification, compilation,
and dissemination of scientific and tech-
nical information on aeronautics.

IX



N. A. C. A. 8-FOOT HIGH-SPEED WIND TUNNEL, LANGLEY FIELD, VA.

TWENTY-SECOND ANNUAL REPORT

OF THE

NATIONAL ADVISORY COMMITTEE FOR AERONAUTICS

WASHINGTON, D. C., November 12, 1936.
To the Congress of the United States:

In accordance with the act of Congress approved March 3, 1915 (U. S. C., title 50, section 151), which established the National Advisory Committee for Aeronautics, this Committee submits herewith its twenty-second annual report, covering the fiscal year 1936.

Present status of research.—Improvement in aircraft performance, characteristic of the past few years, was continued in 1936. Important factors underlying the recent remarkable development of American aircraft have now been largely incorporated in the airplane designs of foreign nations. In the major European countries there has been intense effort in the development of improved aircraft and great expansion in aircraft programs and in production facilities. But what most directly interests this Committee is the increased appreciation abroad of the basic importance of scientific research in aeronautics. During the past two years there has been abundant evidence of the greatly increased appreciation by foreign powers of the essential role that research plays in the development of aviation. Intensive activity in the major European countries in building larger air fleets has been accompanied generally by extensive programs providing for research and development. This emphasizes the fact that when large sums of money are to be expended upon procurement of aircraft it is wise to predicate such expenditure upon adequate research and experimental development as being the only means of assuring the best possible return on the investment.

Increased responsibilities of this committee.—One result of the growing appreciation by European nations of the significance of the airplane in commerce and in modern warfare has been to increase the responsibilities of the National Advisory Committee for Aeronautics. It is one of the duties of this Committee to anticipate, and, with the support of the President and of the Congress, to provide for, the research needs of aviation, civil and military. The fundamental problems arising out of the rapid development of military, naval, and commercial airplanes have broadened in scope and variety and have become more and more urgent. The War, Navy, and Commerce Departments are each requesting priority in the conduct of special

investigations to meet their immediate requirements. In the rapidly advancing science of aeronautics the means and methods of conducting scientific research are changing and improving quite as rapidly as airplane design and performance change and improve. To meet adequately the increased requirements of the departments concerned, an enlarged research staff, modernization by this Committee of its research equipment, and provision of new research equipment are required.

Development of research facilities.—The Committee years ago recognized the importance and the value of conducting wind-tunnel investigations under approximately flight conditions; that is, at high values of Reynolds Number. In 1921 the Committee constructed the first variable-density wind tunnel. This was later duplicated abroad. In 1926 the Committee constructed what was then the largest wind tunnel in the world, having a throat diameter of 20 feet. With this wind tunnel it was possible for the first time to investigate full-scale propellers, engine nacelles, landing gears, and other parts of an airplane, but not a whole airplane. Wind tunnels of this size, improved in design and operating at higher wind velocities, have since been constructed in several countries. To study small full-size airplanes under flight conditions, the Committee constructed in 1930 the full-scale wind tunnel. This has since been duplicated abroad. The trend in the design and construction of wind tunnels abroad has followed in general the developments of large wind tunnels in this country.

In order to begin the study of air flow at very high speeds approximating the velocity of sound in air, the Committee constructed an 11-inch high-velocity jet-type wind tunnel and later a 24-inch tunnel of the same type.

During the past year this Committee placed in operation at Langley Field its new 500-mile-per-hour wind tunnel, which has a throat 8 feet in diameter. This new type of wind tunnel has more than met its designed performance. Early experience with its operation indicates that it will be a valuable addition to the Committee's research facilities and, by the use of larger models than can be used in the 24-inch tunnel, will make available to American airplane designers more accurate information and data regarding the

natural laws governing air flow and the flight of aircraft at high speed than thus far are available to designers in any other nation.

Additions and improvements.—The large seaplane is becoming an important factor in the development of transoceanic air transportation and of long-range naval aircraft. To meet the problems presented by this development, this Committee secured during the past year a supplemental appropriation to lengthen by approximately 900 feet the present seaplane towing basin, known as the "N. A. C. A. Tank." This extension, on which work has been started, will make the tank 2,900 feet long and will make it possible to study the hydrodynamic characteristics of seaplane floats and flying-boat hulls at water speeds up to at least 80 miles per hour.

The increasing size and speed of aircraft have made necessary the development of a new type of wind tunnel. During the past year a supplemental appropriation was granted by the Congress for the construction of a large pressure-type wind tunnel in which relatively large models can, by increasing the pressure in the tunnel to three or more atmospheres and thus increasing the Reynolds Number, be tested under conditions that will give results more nearly corresponding to the actual performance of large airplanes flying at high speed than it is possible to obtain in any wind tunnel in the United States at this time. Since starting work on this wind tunnel, the Committee has learned that a wind tunnel of similar type has recently been completed abroad.

To maintain leadership in the development and use of aircraft, it is essential that research laboratories in the United States have the latest and most efficient equipment for the study of problems arising as a result of the higher speeds and increased size of aircraft. Advantage was taken of advances that have been made in wind-tunnel technique, and during the past year the propeller-research tunnel and the 7- by 10-foot wind tunnel were modernized and brought to a more satisfactory and efficient operating condition.

At the present time the laboratories of this Committee comprise the following units: The 8-foot 500-mile-per-hour wind tunnel; the full-scale wind tunnel; the propeller-research tunnel; the variable-density wind tunnel; a 7- by 10-foot wind tunnel; a refrigerated wind tunnel; a vertical wind tunnel; a free-spinning wind tunnel; two high-velocity jet-type wind tunnels of 11- and 24-inch throat diameters, respectively; the N. A. C. A. Tank (now being lengthened); an engine research laboratory; a flight research laboratory; and an instrument laboratory. In addition there is under construction at the present time the new pressure-type wind tunnel previously referred to. The Committee's laboratories are known as the Langley Memorial Aeronautical Laboratory and are located at

Langley Field, Virginia, on land set aside by the War Department for the use of this organization. At the present time the laboratory staff comprises 370 employees.

Duplication avoided.—The Committee's laboratories as a whole are, we believe, as yet unexcelled by those of any other single nation. In this connection, it is worthy of note that during the preceding twelve months twenty-five delegations from twelve foreign nations have visited the laboratories of this Committee at Langley Field, Virginia. The Committee's laboratories, although located on an Army field, are under the direct control of this Committee. This Committee has been greatly assisted in its activities by the cordial and effective cooperation of the War, Navy, and Commerce Departments, and it has in turn endeavored in every way to meet their research requirements. In doing so, this Committee has coordinated the research needs of aviation, civil and military, and has effectively avoided duplication of effort in this field. The success of this Committee as a coordinating agency and as an agency to conduct in one central aeronautical laboratory the fundamental scientific research necessary to meet the needs of both military and civil aviation, has been made possible largely by the status of this Committee as an independent Government establishment, and also by the fact that all governmental agencies concerned with the development of aeronautics are represented on this Committee and on its subcommittees.

This Committee has also kept in close touch with the research needs of aviation as suggested by the aircraft industry. This Committee believes that the independent scientific direction of aeronautical research, together with the invaluable cooperation of the War, Navy, and Commerce Departments and of the aircraft industry, has promoted economy and efficiency and has been a vital factor in the successful development of American aircraft.

Functions of the Committee.—Any national aviation policy would be incomplete that did not provide adequately for the comprehensive planning and execution of long-range programs of fundamental scientific research. The law provides that this Committee shall "supervise and direct the scientific study of the problems of flight, with a view to their practical solution, and to determine the problems which should be experimentally attacked, and to discuss their solution and their application to practical questions." This Committee is also authorized by law to "direct and conduct research and experiment in aeronautics."

Thus the primary function of the National Advisory Committee for Aeronautics is to conduct scientific research. It does not have under the law broad advisory functions which its name may seem to imply. In 1926 a subordinate function was added by law giving to

this Committee the duty of advising and reporting upon the technical merits of aeronautical inventions and designs submitted to any branch of the Government for Government use. This Committee regards its primary function as the most fundamental activity of the Government in connection with the development of American aeronautics and as worthy of its sole and undivided attention. It does not seek any enlargement or change in its functions.

The formulation of research programs.—The technical subcommittees formulate comprehensive programs of fundamental research. All governmental agencies concerned are represented on these subcommittees, and in addition there are in some cases members selected from the industry and from educational institutions. The Army and Navy air organizations depend upon this Committee for the scientific study and investigation of fundamental problems connected with the design of improved military and naval aircraft. The Bureau of Air Commerce and the manufacturers of both military and civil aircraft also rely upon this Committee for fundamental data. This Committee institutes investigations and researches on the request of these governmental agencies, on the suggestion of the aircraft industry, and on its own initiative. Researches are usually so broadened in scope as to make the results applicable alike to military and to civil aircraft.

Supplementing this policy, and of equal importance, is the experimental engineering necessary to apply research results in the development of improved aircraft to meet varying needs. This experimental engineering is conducted for the Army Air Corps by the Matériel Division at Wright Field, Dayton, Ohio. For the Navy it is conducted by the Bureau of Aeronautics and the Naval Aircraft Factory. For civil and commercial aeronautics it is conducted by the manufacturers, acting in some cases in cooperation with the Bureau of Air Commerce and with educational institutions. The facilities of the National Bureau of Standards are also used by the War, Navy, and Commerce Departments, and by this Committee,

for the conduct of certain investigations for which that Bureau is particularly well equipped, principally in the fields of physics and of metallurgy. Such research activities are coordinated through the standing technical committees of the National Advisory Committee for Aeronautics. Thus one central governmental research organization, with the active cooperation of the War, Navy, and Commerce Departments, of the aircraft industry, and of educational institutions, supplies the research needs of aviation without overlapping or duplication of effort.

Summary.—The continued improvement in the safety, efficiency, range, speed, comfort, and capacity of American aircraft is especially gratifying to this Committee. The results, we believe, justify the long-continued and sound policy of coordination of effort and systematic prosecution of fundamental scientific research.

In the United States the airplane is an important factor in the development of our national defense and, with the extension of the air lines of Pan American Airways, will become a factor of tremendous importance in the development of commercial relations with South America and with the Far East. At the present time plans are nearing completion for the inauguration at an early date of regular air transportation across the North Atlantic.

We believe that fundamental scientific research in aeronautics is the foundation upon which the future of American aircraft development must be built. The maintenance of American leadership becomes more difficult in the face of tremendous expansion of research facilities in foreign nations. We recommend continued support by the Congress of a policy of gradual expansion of our research staff and equipment to meet the changing and increasing needs of American aviation development and also to insure that America shall not fall behind in an undertaking so vital to its national defense and at the same time so invaluable in promoting through commerce the progress of civilization.

PART I

REPORTS OF TECHNICAL COMMITTEES

In order to carry out effectively its principal function of the supervision, conduct, and coordination of the scientific study of the problems of aeronautics, the National Advisory Committee for Aeronautics has established a group of technical committees and subcommittees. These technical committees prepare and recommend to the main Committee programs of research to be conducted in their respective fields, and as a result of the nature of their organization, which includes representation of the various agencies concerned with aeronautics, they act as coordinating agencies, providing effectively for the interchange of information and ideas and the prevention of duplication.

In addition to its standing committees and subcommittees, it is the policy of the National Advisory Committee for Aeronautics to establish from time to time special technical subcommittees for the study of particular problems as they arise.

The Committee has three principal technical committees—the Committees on Aerodynamics, Power Plants for Aircraft, and Aircraft Structures and Materials—and under these committees eight standing and two special subcommittees. The membership of these committees and subcommittees is listed in part II.

The Committees on Aerodynamics and Power Plants for Aircraft have direct control of the aerodynamic and aircraft-engine research, respectively, conducted at the Committee's laboratory at Langley Field, and of special investigations conducted at the National Bureau of Standards. The greater part of the research under the supervision of the Committee on Aircraft Structures and Materials is conducted by the National Bureau of Standards. The experimental investigations in aerodynamics, aircraft power plants, and aircraft structures and materials undertaken by the Bureau of Aeronautics of the Navy, the Army Air Corps, the National Bureau of Standards, and other Government agencies are reported to these three committees.

REPORT OF COMMITTEE ON AERODYNAMICS

During the past year, two special subcommittees have been organized under the Committee on Aerodynamics. The first of these, the Special Subcom-

mittee on Aerodynamic Problems of Transport Construction and Operation, was established in March for the purpose of determining the research problems of particular interest and importance to air-transport operators which should be investigated by the Committee. In conjunction with the establishment of this subcommittee, a special conference of airplane pilots representing the air-transport operators and Government agencies concerned was held for the discussion of the handling characteristics and piloting technique of large transport airplanes. The activities of this special subcommittee and the work of the pilots' conference are described in part II of this report under the heading "Cooperation with the Aircraft Industry."

In April 1936, a Special Subcommittee on Vibration and Flutter was organized. This subcommittee was established at the suggestion of the Army Air Corps in view of the vital interest in and importance of the general problem of vibration, both to the military services and to commercial aeronautics. The work of this subcommittee is described at the close of the report of the Committee on Aerodynamics.

LANGLEY MEMORIAL AERONAUTICAL LABORATORY LANDING SPEED AND SPEED RANGE

Wing flaps are now used on nearly all high-performance airplanes and the Committee has continued its wind-tunnel and flight investigations of the promising forms. Some work has also been done on a new design of leading-edge slot.

Flaps.—The investigation of the external-airfoil flap, which consists of an airfoil pivoted at the rear of the main wing, has been extended in the 7- by 10-foot wind tunnel to include an N. A. C. A. 23012 flap having a chord 30 percent of that of the main airfoil, which was also of N. A. C. A. 23012 section. With this size of flap there is an increase of maximum lift coefficient over that obtained with the size 20 percent of the chord previously investigated (Technical Report No. 573) and similar low values of profile drag throughout the entire lift range. This investigation, moreover, has served to indicate a general method of combining airfoils of the well-known N. A. C. A. 230 series in external-airfoil flap arrangements, a method which not only will provide excellent speed-range characteristics but which should be definitely superior to devices now

commonly used in such items of performance as take-off, range, endurance, and ceiling.

At the request of the Navy Department, external-airfoil flaps have also been investigated on a Fairchild 22 airplane, both in the full-scale tunnel and in flight. The flap covered practically the entire span of the wing and the right and left halves were differentially deflected for lateral control. The flap was of Clark Y section and had a chord length equal to 20 percent of the chord of the main wing, which was of N. A. C. A. 23015 section. The investigation in the full-scale wind tunnel included tests in which the slot between the flap and the wing was covered, and the results showed that the slot effect appreciably increased the slope of the lift curve, the maximum lift coefficient, and the maximum value of lift-drag ratio. The maximum lift coefficient was found to be 1.51 with the flap set for minimum drag in cruising and 2.12 with the flap deflected downward 30°. The flight tests showed that the use of external-airfoil flaps reduced the low speed from 47 to 41 miles per hour and also reduced the take-off and landing distances. The position of the flap was found to be not critical as it is for split flaps, the reduction in take-off distance being about constant for the last third of the flap travel.

At the request of the Navy Department, tests were also made in the full-scale wind tunnel and in flight on a Fairchild 22 airplane equipped with a Cunningham-Hall wing. An internal air passage through the wing was provided by deflecting vanes in the under surface of the wing near the leading edge. Split trailing-edge flaps of Cunningham-Hall design were located on the under surface of the wing. In the deflected position a gap existed between the flap and the under surface of the wing. With the trailing-edge flap closed, opening the front vane to allow a passage of air through the wing increased the maximum lift coefficient obtained from 1.27 to 1.55. The trailing-edge flap increased the value further to 2.04. With the flap open, no increase in the maximum lift coefficient was obtained by opening the forward vane.

In the installation of the Cunningham-Hall wing tested on the Fairchild 22 airplane, the flap was intended to be automatic in operation by means of the action of a spring system sufficiently powerful to deflect fully the flap against the aerodynamic forces at low speeds. In the flight tests it was found that the automatic operation of the flap was unsatisfactory, however, because of internal friction in the mechanism. The internal air passage was found to have a negligible effect on the flight performance or on the flying qualities of the airplane. The flap was found to be effective in reducing the landing speed and the take-off distance.

A rather complete investigation has been made of ordinary trailing-edge flaps to provide extensive cor-

related data on their characteristics. Three airfoil sections, the Clark Y, the N. A. C. A. 23012, and the N. A. C. A. 23021, were tested in the 7- by 10-foot wind tunnel with ordinary flaps of three widths on the Clark Y airfoil and a flap of one width on each of the others. For purposes of comparison, one simple split flap was also investigated on the N. A. C. A. 23012 and on the 23021 airfoil. The aerodynamic characteristics of the airfoils with all the different flaps were measured and, in addition, hinge moments were obtained for the ordinary flaps on the Clark Y airfoil.

The results of the investigation are reported in Technical Report No. 554. It was found that the optimum width of ordinary flap for maximum lift attainable was the same as that of the split flap, 20 percent of the airfoil chord. The split flap produced somewhat greater increase in maximum lift coefficient on the airfoils tested than did the ordinary flap of the same width, but the lift-drag ratio at maximum lift was practically the same for the two types of flaps. Any gap between the airfoil and the leading edge of ordinary flaps had a very detrimental effect on the value of maximum lift coefficient attainable. On the basis principally of factors affecting airplane performance, the relative order of merit of the airfoils tested with either ordinary or split flaps is the N. A. C. A. 23012, the Clark Y, and the N. A. C. A. 23021. The hinge-moment coefficients of the ordinary flaps were practically the same as those of full-span split flaps of corresponding widths.

The report referred to last year on the effect of sudden operation of a flap on the motion of an airplane has been published as Technical Note No. 548. The results of the investigation of the Fowler flap reported previously have been published as Technical Note No. 578. The technical note presenting data on the Zap flap is now in preparation.

Maxwell slot.—Another investigation dealing with the improvement in speed range, carried out in the 7- by 10-foot wind tunnel at the request of the Bureau of Aeronautics, Navy Department, was concerned with the Maxwell leading-edge slot. This slot differs essentially from the Handley Page slot in that the moving parts operate solely by rotation. The Maxwell slot also provides a means for producing an unbroken leading-edge contour when it is in the closed condition. The test results, which are to be published in the form of a technical note, indicate that the aerodynamic characteristics of the Maxwell-type slot are substantially the same as those of the Handley Page type.

CONTROLLABILITY

In last year's report it was stated that in order to compute from the results of wind-tunnel tests the actual response to lateral-control devices in flight, it was

found necessary to make a rather complete mathematical analysis. This analysis included the secondary factors, such as the yawing moments given by the controls, their effect on the damping in roll, all the other lateral-stability derivatives of the airplane, and the moments of inertia of the airplane. The use of this method has been continued throughout the past year and some of the results have been published in Technical Report No. 570. The study of conditions above the stall indicated that satisfactory control could not be expected without some provision to maintain the damping in rolling and that a dangerous type of instability would arise if the damping was insufficient. From the information gained by the use of this method a critical analysis and comparison are being made of various lateral-control devices that have been tested in the 7- by 10-foot wind tunnel during the past several years.

The provision of an adequate degree of control with the expenditure of small operating effort is being given primary consideration in these comparisons. A matter of some interest in this connection is the possibility of reducing the operating force of aileron devices by means of an ordinary differential linkage. This method of balancing has shown so much promise that a separate study has been made of it. As a result of this study, charts that enable the designer to select an appropriate linkage arrangement for a given control device have been prepared for publication.

In the calculations of the actions of airplanes following control deflections or other disturbances, the operational calculus has proved a valuable device. Such calculations have been applied in a study of two-control operation of an airplane. Here the effects of a variety of possible procedures of control have been investigated and it is felt that the outcome of this study has shed some light on more general questions relating to lateral controllability and stability. An account of the simpler applications of the operational method has been prepared and published as Technical Report No. 560. A description of some more extensive applications is being incorporated in a report on two-control operation.

Slot-lip ailerons.—The investigation of slot-lip ailerons mentioned in last year's report has been continued both in the wind tunnels and in flight. Tests in flight and in the full-scale wind tunnel were made with the ailerons fitted to a Fairchild 22 airplane. The ailerons were tested at two chordwise positions on the wing, one with the hinge axis at 20 percent of the chord behind the leading edge and the other with the hinge axis at 45 percent. The wing was fitted with a split flap. The results from the full-scale wind tunnel showed that the forward aileron slot increased the minimum drag coefficient of the airplane by 7 percent and that the rear one increased it by 4 percent. These

drag increases are considered excessive for modern high-performance airplanes.

In the flight tests the ailerons in the forward position were found to be fairly effective in rolling the airplane for most flight conditions, but at moderately high speeds with the flap deflected the rolling action became very weak. It was apparent that unless otherwise limited, the maximum speed with flaps deflected would be limited by the value at which there was a total loss in lateral control. The control forces with the slot-lip ailerons were considerably greater than is desirable for an airplane of the size of the Fairchild 22. In the rear position, the ailerons were appreciably less effective than in the front position, but the effectiveness was maintained throughout the speed range. The control force was less than for the forward position. In both positions there was an apparent lag in the action of the ailerons. Instrument records showed that this was not exactly a lag between the operation of the aileron and the start of the response, but sluggishness in the attainment of maximum rolling velocity, or a low average acceleration in rolling.

The behavior of the slot-lip ailerons on this airplane did not seem to be in accord with the observed satisfactory behavior of the slot-lip ailerons on the W-1A airplane, as mentioned last year. To aid in the explanation of the apparent discrepancy between the results obtained with the two different installations of slot-lip ailerons, measurements of the rolling velocities were obtained with the W-1A airplane for comparison with similar measurements obtained with the Fairchild 22 airplane. These measurements showed that the W-1A ailerons were as effective as the ailerons in the forward location in the Fairchild 22 airplane and that they gave the same type of variation with speed as those located in the rearward position on the Fairchild 22 airplane. The results of measurements thus tend to verify the difference in observed behavior of the two airplanes but do not explain why this difference should exist. The slot-lip ailerons on the W-1A airplane were located at the point of 30 percent of the chord of the wing and were used in conjunction with a special type of slotted balanced flap instead of a split flap as installed on the Fairchild 22.

In this general connection a detailed analysis of flight records of the motion of the airplane following a movement of the control has been made and the relative sluggishness of ordinary and of slot-lip ailerons has been determined. A report is being prepared which will include results from both wind-tunnel and flight tests of slot-lip ailerons.

The investigation of the special form of slot-lip aileron, consisting of a plain aileron forming the trailing edge of an airfoil equipped with an external-air-

foil flap, has been continued in the 7- by 10-foot tunnel, and a report on this work is being prepared. This type of aileron, which provides a means of lateral control in combination with a full-span flap without adding appreciably to the drag of the wing, appears to offer unusual control possibilities in connection with flight at high lift coefficients. The results of the investigation of slot-lip ailerons in connection with wings equipped with external-airfoil flaps of various sizes are now being prepared for publication.

External-airfoil flaps deflected as ailerons.—As noted previously in the discussion in connection with high-lift devices, the external-airfoil flap on the Fairchild 22 airplane was used for lateral control as well as for high lift. The flap was divided at the center and the two parts were deflected relative to each other for lateral control. Because a differential linkage could not be used on account of overbalance difficulties in the flap-down position, an equal up-and-down deflection of 10° was used. This arrangement gave satisfactory response except for the large adverse yawing moments produced, and for the fact that the control forces were greater than are considered desirable. Recent analyses indicate, however, that by proper design both of these disadvantages can be substantially reduced.

Ailerons on tapered wings.—At the request of the Army Air Corps, an investigation of lateral control is being made both in the full-scale wind tunnel and in flight on a full-scale tapered wing fitted to a Fairchild 22 airplane for direct comparison with a straight wing having ailerons of the same size. These tests are now in progress.

In view of the present widespread use of partial-span split flaps on tapered wings, it was considered desirable to provide information on aileron design for this general arrangement. Tests of two wings having medium and high taper ratios have recently been completed in the 7- by 10-foot tunnel, and the results are being prepared for publication. The data include the aerodynamic information necessary for aileron design, together with aerodynamic characteristics of the wings themselves. The report should provide a more clear-cut basis than has heretofore been available to designers for optimum proportioning of ailerons and split flaps on wings of various taper ratios.

Floating tip ailerons.—The above-mentioned tapered wing on the Fairchild 22 airplane is fitted with removable tips that can be replaced by floating tip ailerons. The flight tests will include a comparison of the floating tip ailerons with the conventional ailerons on the same wing.

Failure of one engine on a two-engine airplane.—Two problems of special importance arise in connection with the failure of one engine on an airplane having two wing engines: (1) A sudden yawing moment due to the failure of thrust on one side which usually cannot

be overpowered by the rudder at low flight speeds; and (2) a large increase in drag and resulting loss of performance due to the yawed condition of the airplane and the deflected controls when flying on one engine.

These problems are of considerable importance to commercial operation and the Committee was asked to study the possibilities of improvement of the control and of reduction of drag. A large model of a low-wing airplane equipped with operating propellers was fitted with several new designs of tail surfaces and tested in the 20-foot tunnel. The model was tested with both single and double rudders, the latter inclined varying amounts in order to provide correcting yawing moments automatically. The nacelles were also inclined laterally to direct the slipstream on the vertical tail surfaces at an angle. Neither of these schemes provided more than about one-fourth the yawing moment needed to balance the thrust of the operating motor. One fact determined was that the tail surfaces of the low-wing monoplane were not completely in the slipstream on account of the fact that the downwash carried the slipstream down with it. The results of the yawing-moment tests, together with the results showing the loss of performance due to the increased drag in flight on one of two engines, are to be published in the near future.

Flying qualities of large airplanes.—An investigation has been initiated during the current year of the general stability, controllability, and maneuverability of large airplanes. This work has consisted of a review of the problem for the purpose of determining how much is known regarding the flying qualities of large airplanes in quantitative values, and also what the procedure should be in the investigation, on a quantitative basis, of the flying qualities of large airplanes. It is desired that all characteristics that influence the flying qualities of the airplane be actually measured and quantitative values obtained so as to remove guesswork concerning points of deficiency. This preliminary study has resulted in the preparation of a flight program of investigation in which all the quantities believed to be of importance will be measured. The procedure laid down is now being tried in flight on a five-place high-wing monoplane.

Magnitude of control forces available.—The paper mentioned in last year's report on the results of an investigation of the forces that a pilot is able to exert on the control column and rudder pedals of an airplane has been published as Technical Note No. 550. In accordance with a request of the Bureau of Air Commerce, the investigation has been extended to include measurements of the force that the pilot can exert on the wheel-type elevator and aileron control. The effect of wheel diameter and position and the difference between forces that can be applied with various hand grips have been investigated.

During the current year, considerable data pertaining to the control forces actually exerted by a pilot in flight have been obtained. In conjunction with investigations of lateral-control devices, the forces required to operate the ailerons have been recorded primarily for the purpose of determining the magnitude of the forces the pilots consider to be desirable and those that they consider to be excessive. For the Fairchild 22 airplane, with which most of the measurements were made, it appears that the stick forces required to operate the ailerons should be below, and possibly well below, about 8 pounds in order to be considered desirable. A lateral force of 15 pounds is considered to be excessive.

Measurements were also made of the control forces and movements on two naval airplanes in flight, primarily for the purpose of determining the requirements of an automatic pilot. On one of these airplanes, additional measurements were made in order to explain undesirable characteristics of the elevator control. Modifications of the airplane were recommended on the basis of these tests.

STABILITY

A review of all available previous and contemporary work on stability is now being undertaken. It is expected that a systematic correlation and analysis of available aerodynamic data will make possible the development of satisfactory semi-empirical formulas for the estimation of certain of the aerodynamic factors which govern stability characteristics.

A study is being made of the practicability of certain new types of apparatus that have been proposed for use in the determination of the stability characteristics of models. It is hoped that in the near future it will be possible to make systematic studies of the effects of changes in dimensional characteristics upon both the aerodynamic factors governing the free motion and the resulting free motion itself.

Lateral stability.—A report on lateral stability in power-off flight is being prepared for publication. This report will parallel Technical Report No. 521, which dealt with longitudinal stability. It will include a discussion of the problem and of the individual factors involved. A number of charts will be presented from which the lateral stability of a new design can be quickly and easily estimated.

Tests have been made in the 7- by 10-foot tunnel to determine the effect of dihedral angle and the effect of wing-tip shape on some of the aerodynamic characteristics affecting lateral stability, e. g., the rolling and yawing moments and the cross-wind force due to yaw and the damping in roll. The results of these tests are presented in Technical Report No. 548. It was found that the effect of dihedral angle could be predicted quite accurately but that the total "dihedral

effect" depends upon the particular shape of the wing in plan and elevation. The addition of a deflected flap to a wing changes the effective dihedral. Experience has shown that high-wing monoplanes have more effective dihedral than low-wing monoplanes, which indicates that wing-fuselage interference probably has an important influence on the effective dihedral. It is planned to obtain quantitative data on the dihedral effect with various wing and fuselage combinations.

Longitudinal stability.—The results of the investigation to determine the relation between the longitudinal stability and the flying qualities of several airplanes, as mentioned in the last annual report, have been prepared for publication.

Tail surfaces for airplanes equipped with wing flaps.—An analysis is being made of the horizontal tail surfaces required for airplanes equipped with wing flaps. This analysis, although not complete, indicates the need of larger tail surfaces to compensate for the larger couple about the aerodynamic center of the wing which is experienced with flaps. Consideration must be given to the setting of the tail surfaces to make certain that they do not stall when the airplane is flying at low angles of attack with the flap deflected. With wing flaps, such factors as the retardation of the flow by the wings and turbulence in the wake of the wings assume even more importance than they do with plain wings.

TAKE-OFF

The results of calculations of the effect of various flaps on take-off mentioned last year have been published as Technical Note No. 568. One interesting point brought out by those calculations was that, for an aspect ratio of 5 assumed for the wings, there appeared to be a fairly definite theoretical upper limit to the maximum lift coefficient that would result in reduction in take-off distance, even for an ideal high-lift device in which the only increase in drag with increased lift was the increase of induced drag. Subsequent calculations have been made to determine what this limiting maximum lift coefficient is as a function of aspect ratio. These latter calculations indicate that 3.5 is about the maximum lift coefficient desirable with a wing loading of 30 pounds per square foot and an aspect ratio of 12. With lower wing loadings and aspect ratios or with high-drag wings the desirable maximum lift coefficient is lower.

In calculations of the take-off distance of airplanes, three distinct phases of motion are ordinarily assumed: a horizontal ground run, a transition period of curvilinear flight, and a steady climb. A preliminary study of the take-off problem indicated that existing information regarding the rolling friction of airplane wheels was inadequate. The investigation of rolling friction of airplane wheels mentioned last year was

therefore undertaken. The results of this investigation are nearly ready for publication. As regards the second phase, or transition period, it was found that simplifying assumptions of unknown validity were required before the calculations could be made, and that an experimental study to determine the validity of these assumptions was advisable. Such a study is now being made. In this investigation the motion of an airplane during the transition period is being measured in flight and carefully studied.

As a result of experience obtained in making comparative take-off tests with various airplanes with high-lift wings on one type of airplane, as well as with different wing and power loadings, it has been found to be very difficult to obtain consistent data in consecutive runs. As a result of improvement in the apparatus used in measuring the take-off distance inconsistencies were traced in a large measure to air-speed variations. It was found that small differences between the speed at which the airplane in consecutive runs arrived at the point of take-off or a given altitude of, say, 50 feet, accounted for large discrepancies in the horizontal distance required for the ground run or the total run. It is very difficult for the pilot to reproduce speeds exactly enough for comparative performances without correction for these speed differences. This is particularly true with regard to an airplane having a rapid acceleration and a high initial rate of climb.

LANDING

Landing of airplanes equipped with wing flaps.—The technique of landing airplanes equipped with wing flaps has been discussed in Technical Note No. 553. Wing flaps cause the airplane to assume a steep nose-down attitude during the gliding approach to a landing. This fact must be accepted as inherent with conventional flapped airplanes. The use of power to hold the nose up during a glide may result in difficulty in placing the airplane in a three-point attitude for contact with the ground. Because of the steeper gliding angle and the more rapid deceleration resulting from the high drag of the airplane with wing flaps, it is essential that the airplane approach for the landing with a greater margin of speed above the stall than is normally the case with plain wings and that the elevator-control movements for leveling off prior to contact be made more abruptly.

Stable three-wheel landing gear.—The type of landing gear in which a swiveling wheel is located at the nose of the airplane and the fixed wheels are located slightly to the rear of the center of gravity has been utilized successfully by several designers of small light airplanes. The improvement in stability of the machine on the ground obtained with this type of landing gear, as well as certain other improvements in ground-handling characteristics, has given rise to considerable

interest in this type. The Committee has given consideration to the problems attendant on the use of such a landing-gear arrangement on a large airplane. It appears that instability of the castering wheel or wheel shimmy is likely to be a serious problem. Wheel shimmy is frequently encountered in tail wheels of conventional landing gears but would be even more objectionable if experienced with the large swiveling wheel that would be required at the forward end of the machine.

In order to determine what factors influence wheel shimmy, and to develop means for avoiding it by suitable design, an analytical and experimental study of the stability of castering wheels is being made. The experimental work is being carried out with small models of landing gears and landing-gear wheels fitted with pneumatic tires.

SPINNING

The 15-foot free-spinning wind tunnel has been in regular operation, most of the time being devoted to investigation of the spinning characteristics of scale models of service airplanes. During the past year the spinning characteristics of eight such models have been investigated and reported upon. A total of 17 models have been tested in the tunnel to date. Of these, eight have had definitely satisfactory spinning characteristics; i. e., it has been impossible to obtain unsatisfactory spins without major changes in design. The others have each shown unsatisfactory behavior with certain loadings or certain methods of handling the controls.

Tests are being made with a model of a low-wing monoplane for the purpose of making a direct quantitative comparison with the behavior of the airplane. Similar comparisons for two biplanes have been reported in Technical Report No. 557. The spinning characteristics of the biplane models were in reasonably good agreement with those of the respective airplanes. It is felt, however, that a comparison is desirable for a monoplane before conclusions are drawn as to the reliability of the model results as an indication of full-scale behavior.

It has been found desirable to include a determination of the effect of aileron setting when spinning tests of models were made. In certain cases the spinning characteristics have been found to vary widely with change in aileron setting. No general rule as to the aileron effect has become apparent. In certain cases setting the ailerons against the spin has improved recovery, in other cases such a setting has retarded recovery, and in still other cases it has had no appreciable effect.

A series of tests has been made with one model to determine the effects of certain systematic changes in tail arrangement. The results have been published in

Technical Note No. 570. They show that the spinning characteristics of the particular model are critically dependent upon the tail arrangement and confirm previous conclusions as to the desirability of keeping the vertical tail surfaces unshielded. This conclusion was supported by the results of tests of several models with small amounts of additional fin area placed in various locations around the periphery of the vertical surfaces and the after portion of the fuselage. Vertical fin area added underneath the fuselage has always resulted in improvement of the spinning characteristics. The improvement has been most marked when the added area was under the horizontal surfaces.

The spinning balance in the five-foot vertical wind tunnel has been altered to provide more accurate results and a direct-indicating force-measuring system has been installed. All six components of the aerodynamic forces and moments may now be measured simultaneously and the testing time has been materially reduced.

The experimental work in an extensive investigation on the spinning balance with a model of the Fleet biplane has been completed and a report is being prepared. The purpose of this investigation was to obtain a complete comparison of results from the spinning balance, free-spinning wind tunnel, and flight on the spinning characteristics of this airplane. A preliminary analysis shows that the differences in the moments between spinning-balance and flight results correspond to those found for two other biplane models reported in Technical Note No. 517. Predictions for a condition of equilibrium in a spin on the basis of spinning-balance data as compared with results from the free-spinning wind tunnel indicate that the aerodynamic pitching and rolling moments are of the same order of magnitude. Aerodynamic yawing moments deduced from the results from the free-spinning tunnel are between those obtained with the spinning balance and those obtained in flight.

The investigation with the spinning balance in the five-foot vertical wind tunnel on the spinning characteristics of wings to obtain fundamental information on the magnitudes of the aerodynamic forces and moments produced by the wings alone has been continued. In these investigations the six components of the aerodynamic forces and moments are measured for the entire ranges of angle of attack, rate of rotation, and angle of sideslip likely to be encountered in spins. The results of an investigation on a wing of rectangular plan form were reported in Technical Report No. 519. The tests have been completed on a Clark Y monoplane wing with elliptical tips. An investigation with a Clark Y monoplane wing having a taper of 5:2 and elliptical tips is planned to com-

plete a series on the effects of plan form with the Clark Y airfoil section.

The report on the forces and moments acting on various parts of the full-scale Fleet biplane in spins has been published as Technical Report No. 559.

Technical Note No. 575 has been prepared describing the procedure for calculating the moments of inertia of an airplane from design data pertaining to weight, position, dimensions, and component parts of the airplane. The paper was intended to be of assistance to designers required to submit models for spin tests.

In response to requests, the spinning experiences and studies of the Committee's test pilots have been summarized in a paper dealing with the piloting technique for recovery from spins, which has been published as Technical Note No. 555.

DRAG AND INTERFERENCE

In view of the demand for greater refinement in the design of airplanes of today, many practices that were regarded as entirely satisfactory a few years ago must be carefully scrutinized for possibilities of improvement. A question arises, for example, as to what shape of fuselage will give the least drag or whether the shape may be improved from the standpoint of cargo space without increasing the drag. An investigation of fuselage drag has been started in the variable-density wind tunnel with six streamline bodies of revolution with a systematic variation of shape and a fineness ratio of 5. The tests were made over a range of effective Reynolds Number from about 4,000,000 to 66,000,000. The streamline bodies of revolution are to be followed by bodies of more practical shape, and protuberances such as windshields and other necessary departures from ideal forms are to be added later. The results of the preliminary tests are being prepared for publication as a technical note.

Supplementing an investigation made last year of the air drag of seaplane hulls, a series of wing-tip floats has been investigated in the 20-foot wind tunnel. This series of floats had previously been investigated in the N. A. C. A. tank. The results are being prepared for publication in connection with the results from the tests in the tank.

Wing-fuselage interference.—The investigation of aerodynamic interference between the wing and the fuselage has been continued during the past year in the variable-density wind tunnel. The results for some 28 additional wing-fuselage combinations that were indicated by the program outlined in the basic report (Technical Report No. 540) are included in Technical Report No. 575. The investigation described in this paper practically concludes the study of combinations with a fuselage of rectangular sec-

tion and includes further information on the study of combinations of a round fuselage and a tapered wing.

An interesting conclusion of this phase of the study of wing-fuselage interference was the unexpectedly high speed-range index shown by the combination of the rectangular fuselage and the rectangular N. A. C. A. 4412 airfoil in a connected high-wing position. The study of the effect of fuselage cross-sectional shape was extended to cover tests of combinations with a fuselage of elliptical section and with a fuselage of modified triangular section. This phase of the investigation is almost completed and the results will appear as a technical note. Concurrently, further tests were made of combinations having split flaps, various wings, and various wing-root junctures. The most interesting development resulting from this part of the investigation is a type of wing-root juncture for certain low-drag combinations having efficient airfoils of moderate thickness and camber. This juncture eliminates the early flow breakdown at the wing roots and the loss in maximum lift that is usually associated with such low-drag combinations, even when the usual fillets are employed.

Wing - nacelle - propeller interference.—In connection with an investigation of wing-nacelle-propeller interference conducted in the 20-foot wind tunnel during the past two or three years, the question arose as to whether the span of the wing (15 feet) was sufficient to give the full effect of the wing-nacelle interference. To answer this question an investigation was made in the full-scale wind tunnel in which the same nacelle was tested on a wing of 30-foot span and the span later reduced to 25, 20, and 15 feet. Force and pressure-distribution measurements were made and the results showed that the influence of the propeller and nacelle extended laterally about five nacelle diameters or two propeller diameters from the thrust axis. The results thus established the validity of the method used in the 20-foot wind tunnel for a large number of wing-nacelle arrangements. The results of this investigation are published in Technical Report No. 569.

COWLING

As stated in previous reports, a systematic study of engine cowling has been under way in three main divisions: (1) the determination of the cooling requirements of an air-cooled engine; (2) the determination of the best cowling arrangement to obtain the necessary cooling with minimum drag; and (3) the verification of the results of divisions (1) and (2) by tests on complete full-size engines. Tests made on an actual engine were completed last year. The results did not completely verify those of divisions (1) and (2), and it was necessary to make an extensive series of supplementary tests in which the various elements of the cowling were separated and elaborate apparatus

installed to enable the numerous factors to be separated and their influence on the problem to be quantitatively determined. This research is more completely covered in the report of the Committee on Power Plants for Aircraft.

VIBRATION

The Committee has during the past year obtained numerous flight records of vibration in various airplanes. Such records are at the present time primarily useful in establishing a certain amount of practical information in regard to the magnitude and distribution of the vibrations to be normally expected. However, little has so far been achieved in regard to the explanation and classification of the vibrations. A systematic study of the engine proper as a source of vibration is planned as the next step in the program.

PROPELLER DESIGN

As mentioned last year, a program of propeller investigation has been prepared at the request of the Bureau of Aeronautics. The preliminary program has been reviewed by the Army Air Corps and by several propeller manufacturers and, as a result of many valuable suggestions, the final program will include tests of 2-, 3-, and 4-blade propellers of six different airfoil sections. The plan form of the propellers follows standard present-day practice and the airfoil sections include the familiar Clark Y and R. A. F. sections and four other sections which tests in the 12-inch high-speed tunnel and theoretical analysis indicate may show improved performance. The effect of various body shapes and pitch distributions will be determined. Apparatus is now being assembled and the tests are scheduled to be started soon.

The possibilities of propeller improvement and the indication of the direction that design changes should take have been studied by a comprehensive analysis of propeller application. The principal results have been given in a report, including several charts that enable the airplane designer to make a rapid yet fairly accurate estimate of the propeller requirements and performance of a design.

Complete tests were made of six full-scale propellers in conjunction with the investigation of propeller-cowling-nacelle combinations. These tests covered the complete range of flight conditions including ground, take-off, climbing, and normal high-speed flight. The range of the advance-diameter ratio has been extended far beyond that of earlier full-scale experiments, pitch settings up to 45° at 75 percent radius being included, which are equivalent to air speeds of more than 300 miles per hour for propellers of normal size and diameter. The propellers were all tested in conjunction with a standard nacelle unit equipped with six different N. A. C. A. cowlings.

The results showed that the conventional propeller reached its peak efficiency in the range between 200 to 350 miles per hour and at a pitch setting of approximately 35°. The inadequacy of the unconditional use of the propulsive efficiency as a figure of merit is shown. This efficiency was found consistently to exceed 100 percent on a certain cowling owing to the fact that that cowling has a very much decreased drag in the presence of the slipstream. The adoption of a standard nacelle unit that is free from this peculiarity is recommended as a basis for the comparative testing of propellers.

A report (Technical Note No. 557) has also been prepared describing the relation of the propeller to the take-off problem. It is shown that the static thrust is of practically no importance in reducing the take-off run. It is rather the thrust at the latter part of the run that is important. The superiority of the propeller of R. A. F. section over that of Clark Y section is again shown. Although this fact was brought out some years ago, the Clark Y propeller is still in quite general use.

PROPELLER NOISE

Further experimental work on the sound output from propellers was carried out at the request of the Air Corps upon certain special propellers. The rate of increase of radiated sound with rotational speed was determined for various frequency bands, and the distribution in space of the sound about the propellers was investigated.

A careful measurement of the sound output from two selected propellers is under way for the purpose of obtaining material for theoretical studies.

Attempts are under way to find a physical theory suitable for practical use that will account for the complex phenomena of the rotation noise to a first approximation. Such a theory, if available, would permit the prediction of the rotation noise in any specified direction and, since these components are the ones that usually determine the loudness, the effect on the ear at any distance along that direction could be estimated.

The paper dealing with the vortex noise from rotating cylindrical rods published as Technical Note No. 519 has been reprinted in the Journal of the Acoustical Society of America for January 1936. A paper on the dual nature of modulation has been published in the Philosophical Magazine for May 1936.

THEORETICAL AERODYNAMICS

Biplane interference.—Further work is planned in which the general biplane theory recently developed is to be employed in a more specific and detailed study of the interaction of two bodies in a uniform air stream.

Compressible flow.—The calculation of the compressible flow about symmetrical Joukowski profiles is

being carried out for the purpose of obtaining information as to the effect of compressibility on the lift and moment characteristics of airfoils of varying thickness and angle of attack. The ratio of the stream velocity to the velocity of sound in the stream, at which compressible potential flow ceases to exist, may also be calculated. This point of breakdown of potential flow is important because of the immediate appearance of shock waves and a subsequent sudden rise in the resistance of the airfoil.

Flow about bodies of revolution.—The investigation of rectilinear flow about bodies of revolution, the results of which were published in N. A. C. A. Report No. 516, has been extended to the case of an arbitrary body of revolution in steady motion in a circular path. The results are included in Technical Note No. 554. Applications of the results contained in these two papers are being made to the model of the airship *Akron*.

Nonuniform motion.—As an outgrowth of the flutter theory developed last year, further studies were made on the nonuniform motion of an airplane wing. In particular, the thrust or drag force experienced by a flapping and oscillating wing in a uniform air stream has been analyzed and formulas have been developed giving expressions for these forces in the case of three degrees of freedom, namely: vertical flapping, torsional oscillations about a fixed axis parallel to the span, and angular oscillations of the aileron about a hinge. It is shown that pure flapping always results in a propulsion (profile resistance being neglected) of which the theoretical efficiency is between 50 and 100 percent, depending on a single parameter $k = pb/v$, which is a simple combination of the oscillation frequency p , the velocity v , and the chord length $2b$. Pure torsional oscillations about an axis parallel to the span may result in either a thrust or a drag force, depending on k . This work which has bearing on the "Katzmayr" effect is also intimately related to certain problems which nature presents in bird and insect flight as well as in fish locomotion. The results are being published as Technical Report No. 567.

AIRFOILS

Systematic research directed toward higher flight speeds or more economical operation at a given speed is, of course, one of the Committee's most important activities. For several years the major research in the variable-density wind tunnel has been directed toward the reduction of wing drag or, more precisely, toward supplying the designing engineer with the aerodynamic data that will enable him to design the most efficient possible wing for a given application.

The first investigations were concerned with the shape of the wing section. Data were obtained for a large number of related airfoil-section shapes under the standard test conditions in the variable-density

wind tunnel. Although a few years ago these data were regarded as directly applicable to flight problems, as airplane design becomes more refined it is realized that they are not, in fact, directly applicable, owing partly to the fact that the tests were made at only one value of the Reynolds Number and partly to the fact that the characteristics derived were not the true section characteristics but were for complete airfoils, including tip effects. Nevertheless, the investigation resulted in the development of the now well-known N. A. C. A. airfoil section shapes, some of which have unusually desirable characteristics.

Applications of these airfoil data to wing design have emphasized the need for reliable airfoil section data for application to flight and for reliable methods of applying the section data to wing design. Such needs have been particularly emphasized by applications of the new efficient wing sections (such as those of the N. A. C. A. 230 series) to the wings that have been employed on many of the new airplanes that have been investigated in the Committee's large wind tunnels during the past year. The investigation of methods of obtaining reliable section data for this purpose and of applying them into flight at various values of the Reynolds Number has constituted a most important part of the airfoil research during the year.

A representative group of systematically related airfoils has now been investigated in the variable-density wind tunnel over a range of values of the Reynolds Number extending well into the flight range. The analysis of the results of the tests provides the information necessary for the application of the extensive airfoil data previously obtained from the variable-density wind tunnel. The result is that, for the first time, the designer will have reliable airfoil section data for direct application to the design of efficient wings.

This advance consists of three stages. The first stage, which is still in progress, is the correction of the test results for the turbulence present in the wind tunnel to the practically zero turbulence of flight conditions. Comparisons between results from the variable-density wind tunnel, full-scale wind tunnel, and flight permit the derivation of suitable corrections. Some comparisons of measurements on airfoils and spheres are presented in Technical Reports Nos. 530 and 558.

The second stage consists of the derivation, from the measurements on the models of rectangular plan form, of the true aerodynamic characteristics of the airfoil section itself. The problem is complicated by tip effects, by the variation of the lift along the span of the airfoil, and by certain shortcomings of the wing theory. A reasonably satisfactory empirical solution has, however, been reached so that airfoil section data are now derived from the test results.

The third and final stage consists of the determination of general scale-effect corrections; by the application of these corrections, the standard test data for one value of the Reynolds Number can be applied to flight at widely different values of the Reynolds Number. Satisfactory methods of correction were obtained as the result of the scale-effect tests of the related airfoils previously mentioned. The methods also supply a more satisfactory means than heretofore available of extrapolating the results to very large Reynolds Numbers above the range attainable in any existing wind tunnel. Thus reasonably satisfactory airfoil data are made available for the design of the new large and fast airplanes and flying boats. All this recent work on airfoil-section data for design is included in a report now being prepared for publication.

In addition to this more general work on airfoils, the tests of new airfoil sections have been continued to cover possible improvements of the N. A. C. A. 23012 section. These tests supply data for various related sections which, for some applications, will prove superior to that section.

Reference was made last year to an investigation of airfoil pressure distribution in the variable-density wind tunnel. It was pointed out that the differences between potential flow and measured pressures about the airfoil section were attributable to the neglect of the viscous boundary layer in the potential-flow theory. This investigation has been continued to study the variation of these differences with Reynolds Number and a report presenting the results is in preparation. It is shown that the scale effect on the aerodynamic characteristics can be traced to changes in the pressure distribution and that these changes are the result of changes in the character of the viscous boundary layer.

Aerodynamic effects at high speeds.—The more fundamental investigation of the compressibility burble, part of which was described in the last annual report, has been continued during the year to include the study of the flow conditions leading to the establishment of the compressibility burble (Technical Note No. 543). This work was conducted in the 24-inch high-speed wind tunnel and consisted chiefly of pressure-distribution measurements for the N. A. C. A. 4412 airfoil section. The experimental work has now been completed and these data are being analyzed. Measurements have also been made of the pressure loss in the compression shock that is associated with the compressibility burble. The measurements were made with a bank of total-head tubes placed 0.5 inch aft of the trailing edge of the model. These tests have also been completed and the data are being analyzed for inclusion in a report on the general investigation of the phenomenon.

An investigation of the drag of certain fundamental shapes, including circular and elliptical cylinders and

square and triangular prisms, through a large range of air speeds and Reynolds Numbers in the 11-inch high-speed wind tunnel, is nearing completion.

Tapered wings.—An investigation of methods for the application of the new section data to the calculation of the characteristics of tapered wings has been made and the results published as Technical Report No. 572. The characteristics of a number of tapered wings included in this report were found to agree well with calculated values. A number of other tapered wings have been tested and a comparison is being made of the calculated with the section characteristics as experimentally determined. The comparison includes the slope of the lift curve as well as the pitching moment, maximum lift, and drag coefficients.

The determination of the spanwise position at which stalling begins and of the value of the maximum lift coefficient has been made possible by the use of scale-effect data on airfoil sections. These calculations and data have been used to investigate the effect of taper ratio. Three wings of widely varying taper ratio were compared on an equal aerodynamic basis; that is, equal minimum drag, induced drag, and minimum speed. The comparison showed that the highly tapered wing had no advantage of structural weight but had the disadvantage of stalling at the tips. Methods of controlling the character of the stall to avoid objectionable tip stalling have also been investigated. The best results appear to be obtained by combining a moderate taper ratio with a little (about 2°) wash-out of incidence toward the tips and changing the section near the tips to one having a higher maximum lift coefficient.

Boundary-layer control.—The earlier work on boundary-layer control mentioned last year, which consisted mainly of tests in the 20-foot wind tunnel of several wings with a slot along the upper surface for boundary-layer control by suction, has been extended during the year to include study of the slot width and suction distribution along the span of a tapered wing. The course of the main investigation has, however, been somewhat changed. It is now planned to confine further testing to more fundamental investigations of control methods. In the meantime, possible applications of boundary-layer control to airplanes will be analyzed and the characteristics of the uncontrolled boundary layer will be more thoroughly investigated.

The fundamental investigations of boundary-layer behavior have been started in the variable-density, the 24-inch high-speed, and the smoke tunnels and will later be extended to other tunnels and to flight. Although most of this work has not progressed far enough to give results, one publication (Technical Note No. 544) dealing with the laminar boundary layer and its separation has been completed.

THE 8-FOOT HIGH-SPEED WIND TUNNEL

The 8-foot high-speed wind tunnel, sometimes referred to as the "full speed" wind tunnel, was placed in operation during the past year. A thorough investigation of the characteristics of the tunnel has been started and preliminary results indicate that the designed maximum speed of 500 miles per hour will be exceeded. The minimum speed of the tunnel is approximately 85 miles per hour, thus making it possible for the results to overlap in air speed and Reynolds Number the results from other wind tunnels. The air speed is continuously controllable between the minimum and maximum values. The air stream is steady and uniform, both in velocity and direction of flow.

Before completion of all the equipment in the tunnel a request of one of the military services was met by testing certain full-size airplane components at speeds greater than those obtainable heretofore in any tunnel over 2 feet in diameter. Future tests will include measurements of lift, drag, and pitching moment on large-scale wings at air speeds equaling and exceeding the present-day diving speeds, which produce serious compressibility effects.

WIND-TUNNEL CORRECTIONS

A theoretical study was made of the interference of the boundaries of a wind tunnel on the downwash behind an airfoil, and correction factors were determined for wind-tunnel test sections of several different shapes. The results are presented in Technical Report No. 547 in a practical form for application to wind-tunnel results.

In order to obtain a comparison between flow conditions in flight and in wind tunnels to supplement that afforded by previous sphere tests in flight and in the various wind tunnels of the Committee (Technical Report No. 558) an investigation is being made to determine the scale effect on the maximum lift of an airfoil. Tests of a wing mounted on a Fairchild 22 airplane are being made in flight. Tests of this wing in the full-scale wind tunnel have been completed. An appreciable variation of the Reynolds Number in flight is obtained, chiefly by varying the wing loading, but some additional variation is obtained by varying the flight altitude and utilizing the effect of seasonal temperature changes.

It is known from experience that the climbing performance of an airplane may be considerably affected by variations in wind velocity with altitude. If the climbing airplane encounters a head wind of increasing velocity but maintains a constant air speed, the continuous deceleration of the airplane increases the rate of climb over that which would normally be obtained. The reverse effect is experienced if the wind velocity decreases with altitude. Inasmuch as it ap-

pears that such effects can be experienced not only at very low altitudes but also at high altitudes, it is planned to make a systematic investigation to determine how serious the effect is likely to be and how error in the estimation of climbing performance can best be avoided.

In the past, considerable difficulty has been encountered when attempts have been made to predict climbing performance from tests made with power on in the full-scale wind tunnel. In order to determine the source of the discrepancies and how such discrepancies may be eliminated, a comprehensive investigation has been started in which flight tests will be made with an airplane that will later be tested in the full-scale wind tunnel. Velocities at various points along the span of the airplane and also at various fore-and-aft locations are to be measured for correlation with similar measurements in the wind tunnel. In the flight tests it is planned to deduce climbing performance from data obtained in tests in which the airplane will tow parachutes of various sizes to absorb the excess horsepower while in level flight, rather than to rely on actual measurements of rate of climb. The force required to tow the parachutes will be measured by means of suitable apparatus mounted in the airplane.

ICE PREVENTION

The Committee has investigated the effectiveness of the use of chemical solutions to prevent the formation of ice on airplanes. A study of various solutions showed that a 7:1 mixture of alcohol and glycerin was the most effective ice inhibitor. The remaining study was concerned with methods of proper distribution of the liquid to the exposed airplane surfaces.

The distribution to wings, struts, and similar surfaces is accomplished by means of a porous leather covering. The liquid is fed through tubes to the inner surface and the leather absorbs and distributes it evenly over the leading edge. The amount of liquid required varies with the type of ice formation encountered. On a modern transport airplane, approximately 1 gallon per hour would be sufficient to prevent accumulations in wet clouds at low temperature, which constitute about 95 percent of the icing conditions. The more severe condition in an ice-storm region may require as much as 5 gallons per hour. Aside from the liquid, the additional gross weight of the system is less than 0.5 pound per foot of span, or about 50 pounds for a transport.

ROTATING-WING AIRCRAFT

The detailed development and steady progress of rotating-wing aircraft during the past year are attested by the construction of several new models of autogiros far superior to any previous ones. The steadily widening field of application of this type of aircraft more

than justifies the vigorous prosecution of research directed toward increase in efficiency and the elimination of secondary difficulties arising in a design.

A report has been published (Technical Report No. 552) containing the results of wind-tunnel tests on a family of models of autogiro rotors of 10-foot diameter in the 20-foot wind tunnel. The investigation of systematic variations of blade airfoil section and blade plan form established the fact that the use of an airfoil 12 percent thick results in a higher lift-drag ratio than is obtained when an airfoil 18 percent thick is employed; and it was found that the reduction of blade chord near the rotor hub resulted in a reduction of rotor lift-drag ratio. The evaluation of the data obtained indicated the desirability of extending the tests to include other airfoil sections and established the necessity of making a study of blade twist in order to separate a composite influence on the test results into its constituent parts. The design of models to be used in this extension of the test program is well advanced.

During the past year two direct-control autogiros were purchased by the Army Air Corps for service test and experiment. The Committee conducted investigations in flight for the Air Corps of the control forces and general performance characteristics of these machines.

An experimental study of autogiro "jump take-off" on a rotor model of 10-foot diameter was recently completed. The maneuver involves the utilization of stored excess kinetic energy in the rotor blades for a take-off in which the flight path is initially vertical. The tests included a study of the three basic variables: blade pitch angle, initial rotor speed, and rotor disk loading. The experimental work was supplemented by an analysis of the problem through which it was found that the simple case of a jump take-off without forward speed could be accurately predicted from a solution of the differential equation of motion. The approximations required for the solution were justified by a comparison of analytical and experimental results. The results are to be published in a technical note.

Considerable study has been directed during the past year toward the extension of and improvement in the aerodynamic analysis of the autogiro rotor. One phase of this, which has been completed, is the analysis of the rotor-blade oscillation in the plane of the rotor disk. Study of this phenomenon disclosed that the flapping motion of the blade caused an oscillation in the plane of the rotor disk which was independent of the components of the air forces in the rotor disk and was the dominating factor determining the motion being studied. It was found that a satisfactory first approximation could be made if the air forces were neglected altogether. Experimental data

were found to agree satisfactorily with predicted values. The results of this work also will be published as a technical note.

Additional analytical work on the autogiro rotor completed and awaiting preparation in report form includes: a study of the rotor-torque equation, including correction factors graphically derived; a study of the effect of periodic blade twist on the rotor thrust and blade motion; a study of the instantaneous forces on a rotor blade, and their effect on rotor vibrations and rotor pitching and rolling moments; and a study of certain factors affecting the profile drag of an autogiro rotor.

AIRSHIPS

At the request of the Bureau of Aeronautics of the Navy, a series of investigations was made in the 20-foot wind tunnel on a 1/40-scale model of the airships ZRS-4 and ZRS-5 with the object of determining: (1) the effect of the aspect ratio of the fins on the aerodynamic forces and load distribution over them; (2) the effect of fins of various aspect ratios on the pressure distribution on the hull near the tail surfaces; (3) the effect on the pressure distribution on the fin of slots between the fin and the hull; and (4) the pressure distribution on the fin when the airship was in various angles of yaw and pitch as high as approximately 24°. A supplementary investigation on the same model has been made for the purpose of determining the effect of bow elevators on the resistance and controllability in pitch of an airship. Reports on these projects are in preparation.

Theoretical studies have indicated that considerable decrease in the drag of an airship should result by proper control of the boundary layer. An investigation to be conducted in the 20-foot tunnel on the application of boundary-layer control to airships has been initiated. The models and apparatus required are now being constructed.

FIELD-OF-VIEW MEASUREMENTS

The measurement of field of view from pilots' cockpits has been continued throughout the year. To date, charts of the field of view from 54 different military and commercial airplanes have been made.

MISCELLANEOUS TESTS OF MODELS OF COMPLETE AIRPLANES

The rapidly increasing size of modern military airplanes, as well as the general use of metal construction, makes alterations extremely difficult and emphasizes the importance of tests of complete models during the design stage. It is impossible at the present time to predict with certainty how the performance and handling characteristics of a new design may be affected by flow conditions arising from interference of the parts or by the presence of the slipstream. It is important that such tests be made at as high a Reynolds

Number as possible, and the Committee has received a number of requests during the past year from the Army and Navy for tests of large models in the 20-foot and the full-scale wind tunnels. Work of this nature interferes in a measure with systematic programs of research but, on the other hand, it has often been possible to take advantage of the presence of such models in the wind tunnels to make alterations and additional tests that fit in with established programs.

The Committee has also received a number of requests from manufacturers for tests of large models to be conducted at the expense of the manufacturers. If these tests are of such a nature that they cannot be conducted in existing commercial laboratories, it is the general policy of the Committee to make them. In these cases also it has often been possible to obtain data confirming results obtained in connection with established programs, and such projects have served the additional purpose of keeping the Committee in close touch with the current problems of designers. Several large commercial airplanes and seaplanes have been tested during the year in the larger wind tunnels, and there are indications that the Committee will be requested to do more work of this nature in the future.

NATIONAL BUREAU OF STANDARDS

WIND-TUNNEL INVESTIGATIONS

The aerodynamic activities of the National Bureau of Standards have been conducted in cooperation with the National Advisory Committee for Aeronautics.

Boundary layer near a plate.—A report has been completed on the air flow in the boundary layer near a plate. The paper reviews the published data of Burgers and van der Hegge Zijnen at Delft and of Hansen and Elias at Aachen, and presents the results of additional measurements carried out at the National Bureau of Standards on the distribution of speed and of the intensity of turbulence near a plate in the laminar, transition, and eddying regions. The report will be published as Technical Report No. 562.

Wind-tunnel turbulence.—Investigations of the nature of turbulence and its effects have been extended to cover the scale of the turbulence, or "average eddy size," as well as the intensity of the turbulence, which has hitherto been designated percentage turbulence. Work in this field was given additional impetus from the different response of the drag of a sphere to turbulence of given intensity produced by screens of different mesh sizes, which indicated that the aerodynamic effect of turbulence is dependent on its scale as well as on its intensity.

The scale of the turbulence was measured for screens varying in mesh from $\frac{1}{4}$ to 5 inches by the method outlined in the last annual report, in which two hot wires are utilized. With one wire fixed and the other movable, the correlation between the velocity fluctua-

tions at the two wires was determined as a function of the cross-stream separation of the two wires. The correlation coefficient was found to vary approximately exponentially with separation, and the scale of the turbulence was defined as the area under the curve of correlation coefficient versus separation. The scale defined in this manner was approximately equal to the diameter of the wires of which the screen was made for points near the screen, but increased linearly with distance downstream to several times the initial scale.

The intensity of the turbulence produced by these screens was measured at several distances downstream to study the decay of the turbulence. These measurements, together with the measurements of scale, gave new information on the mechanism of decay. G. I. Taylor's theoretical formula was found to be correct when allowance is made for the variation of the scale with distance from the screen.

The aerodynamic effect of the turbulence was studied by the use of the "pressure sphere" described in Technical Report No. 558. The critical Reynolds Number was found to depend on the product of the intensity of the turbulence by the fifth root of the ratio of the diameter of the sphere to the scale of the turbulence, in conformity with Taylor's theory.

A report of this work is in process of publication.

Corrections to hot-wire measurements of intensity of turbulence.—The studies of correlation between velocity fluctuations at different points showed that the wires used for turbulence measurements are often sufficiently long to introduce errors, because the fluctuations are not completely correlated over the length of the wire. The corrections for this effect to be applied to measurements of intensity and scale of turbulence by the hot-wire method have been computed.

Boundary layer near an elliptic cylinder.—The measurements in the boundary layer near an elliptic cylinder described in Technical Report No. 527 are being extended to higher speeds at which the layer becomes eddying before separation occurs.

The pressure distribution around the central section of the cylinder has been determined with the major axis parallel to the wind. The line of separation has been accurately located by means of a thin layer of kerosene and lampblack spread over the surface. Minute surface irregularities such as small particles of dirt were found to effect the position of the line of separation. The same technique was used to study the disturbance produced by the prongs supporting the exploring wire in the boundary layer and the disturbance produced by the wire itself. These disturbances could not be entirely eliminated but were made quite small by the use of prongs and wire of small diameter.

Boundary-layer investigation by diffusion of heat.—The method of thermal diffusion described in Technical

Report No. 524 is being applied to the study of a turbulent boundary layer. The boundary layer will be formed near a flat plate 10 feet wide and 24 feet long now being installed in the 10-foot wind tunnel. The traversing equipment has been constructed.

AERONAUTIC INSTRUMENT INVESTIGATIONS

The work on aeronautic instruments has been conducted in cooperation with the National Advisory Committee for Aeronautics and the Bureau of Aeronautics of the Navy Department.

Reports on aircraft instruments.—A report on the characteristics of aircraft compasses was published during the past year as Technical Report No. 551.

The development work on carbon-monoxide indicators for aircraft, which has been in progress for several years, is described in Technical Note No. 573.

The reports on electrical instruments in aircraft and on pressure drop in tubing used to connect aircraft instruments to vacuum pumps and pitot-static tubes are nearly completed.

Data are being collected for a report on the effect of vibration on service aircraft instruments.

Tests and test methods.—Work was completed during the year on an apparatus for testing aerographs. The apparatus consists essentially of a pressure-humidity chamber and a temperature chamber. The instruments under test are installed in the pressure-humidity chamber which in turn is placed within the temperature chamber, the temperature and pressure of the instruments being thus independently controlled. The relative humidity within the pressure-humidity chamber is controlled by means of a chemical drier and a device by means of which air bubbled through a water column is admitted to the chamber. A suction applied to the pressure-humidity chamber causes either dry or moist air to enter as desired.

Methods and equipment were devised for use in testing the suction-regulating valves used on aircraft to control the suction supplied to gyroscopic instruments.

New instruments.—Instruments designed and constructed for the Bureau of Aeronautics, Navy Department, include: A fuel-gas-volume indicator for the K airship; two improved models of a maximum-indicating accelerometer; and an improved design of a combination oxygen breathing mask and radio microphone.

SUBCOMMITTEE ON AIRSHIPS

The Subcommittee on Airships formulates and recommends programs of airship investigations for conduct at the Langley Memorial Aeronautical Laboratory, and maintains close contact with the work in progress.

During the past year an investigation has been completed in the full-scale wind tunnel on a large airship model at various heights above the ground board

and at various angles of yaw with reference to the wind, in order to obtain information on the forces acting on an airship during ground handling. The results of this study have been published in Technical Report No. 566. In conjunction with this study, tests were also made in the full-scale wind tunnel of the pressure distribution on a 1/40-scale model of the Lakehurst airship shed.

A study of the theory of potential flow as extended to the curvilinear motion of bodies of revolution has been conducted and the results, which are applicable to airships in flight, are presented in Technical Note No. 554.

During the past year a report outlining the procedure for the determination of the speed and climbing performance of airships has been published as Technical Note No. 564. This report represents the results of the experience of the Committee's laboratory over a period of several years in conducting investigations on full-scale airships in flight for the Army and Navy.

The Committee has recently completed a study of the effect of aspect ratio on the pressure distribution on airship fins, undertaken at the request of the Bureau of Aeronautics of the Navy for the information of the special airship subcommittee appointed by the Science Advisory Board.

The Committee's research program at the present time includes an investigation of boundary-layer control as applied to airship forms. This investigation is to be carried on in the 20-foot wind tunnel.

SUBCOMMITTEE ON METEOROLOGICAL PROBLEMS

During the past year the Subcommittee on Meteorological Problems has given consideration to a number of problems relating to atmospheric conditions which are of particular importance in connection with aircraft design and operation.

Gust conditions in relation to airplane acceleration.—The attention of the subcommittee was invited, as a result of discussion by the Special Subcommittee on Aerodynamic Problems of Transport Construction and Operation, to the desirability of obtaining all possible information on the structural effects of atmospheric disturbances. It was recognized that this problem was important from the viewpoint both of the correlation of structural effects with meteorological phenomena and of the determination of the most severe conditions for which design requirements must be formulated.

Arrangements are therefore being made for the installation of a number of special instruments to obtain records of accelerations, altitude, and air speed, to be installed on airplanes used in meteorological observations at Weather Bureau stations throughout the country.

The study of the effect of gust structure on airplane loads conducted at the Langley Memorial Aeronautical Laboratory has been extended to include measurements of the speed and accelerations on a Taylor Cub airplane and an Aeronca airplane in rough air. Data are being accumulated and analyzed for the purpose of establishing an effective gust gradient. The program as planned includes the obtaining of such records on towed gliders.

The accumulation and analysis of records of accelerations on transport airplanes in regular operation is being continued. A report presenting in a general way the information obtained in this study is now in preparation.

A program of triweekly flights to altitudes of about 19,000 feet is under way for the determination of a relation between effective gust velocities as measured by airplane accelerations and the degree of stability in the atmosphere at altitudes.

Investigation of wind gustiness.—The study of wind gustiness conducted for the past several years by the Daniel Guggenheim Airship Institute at Akron, Ohio, in cooperation with the Weather Bureau and the Bureau of Aeronautics of the Navy has been continued. This investigation includes two phases: first, a study of atmospheric turbulence under ordinary conditions; and second, a study of the fluctuations of wind velocity and direction during the passage of cold fronts. Records are being obtained from instruments installed in the radio tower at Akron and by means of balloons and theodolites. It is planned to extend the investigation by the addition of movable towers with instruments installed to obtain records at various positions.

Ice formation.—In accordance with recommendation of the Subcommittee on Meteorological Problems, the collection and analysis of data regarding the atmospheric conditions under which ice formation occurs on airplanes are being continued by the Weather Bureau. The problem of ice formation has been indicated by the transport operators as one of the most important in air-transport operation at the present time.

SUBCOMMITTEE ON SEAPLANES

The Subcommittee on Seaplanes was organized in 1935 to guide and direct the research on seaplanes and the work in the N. A. C. A. tank. With the continual improvement in the performance of seaplanes and the rapidly increasing demand for large, long-range flying boats, the work of the tank has become of greater and greater importance. The equipment at Langley Field permits the testing of larger models at higher speeds than can be done in other ship or seaplane tanks; hence there are many requests for quantitative information from agencies concerned with the problem of high speeds on the water. This year, as before, new

fundamental data from a number of tests of large models have been made available to seaplane designers while tests of a specific nature have been conducted for the military services and for private concerns.

THE N. A. C. A. TANK

Plant and equipment.—After five years of continuous operation, the tank was emptied, cleaned, and thoroughly inspected. Despite the extremely severe conditions of salt water and moist air to which they are subjected, the concrete and structure were found to be in excellent condition. During the past year, the rails and steelwork were cleaned and painted. Truck-type guide wheels were substituted for the original single guide wheels of the towing carriage to reduce the magnitude of lateral movements and, as a safety measure, the original pneumatic tires on the main wheels were replaced with new ones.

Historical series.—It is of great assistance to the designers of present-day seaplanes and to the Committee's staff in planning future research to know accurately the characteristics of hull forms that have been used and have proved successful in the past. As a part of a program to obtain such information, a 1/7-size model of the hull of the famous NC flying boat was tested over a wide range of operating conditions. This model was approximately twice the size of those originally tested in the experimental model basin of the Washington Navy Yard in 1917, when the form of the hull was developed. Its performance in the N. A. C. A. tank was found to compare favorably with that of many hulls of more modern design. The data obtained are published in Technical Note No. 566.

Effect of variations in dimensions and form of hull on take-off.—In spite of the increased facility in taking off the water given by more powerful engines and controllable propellers, the resistance to motion offered by the water remains a most important limitation of the performance of large seaplanes. The reduction of this resistance is, therefore, one of the primary objectives of the work at the tank and the development of forms having low water resistance has been continued. The N. A. C. A. pointed-step hull has shown definite promise in this direction but a valid criticism of the earlier forms was that the small angle of dead rise might result in heavy impact loads on the bottom in alighting on the water. Tank tests of a family of these hulls having three different angles of dead rise are described in Technical Note No. 551. It is shown that, while the high-speed resistance is somewhat greater for higher angles of dead rise than for low angles, the low-speed operation and spray characteristics are not impaired, and that, in spite of the increase in resistance at high speeds, the apparent advantages of the pointed-step form over conventional hulls are retained.

The single-float system for small seaplanes has certain aerodynamic and structural advantages. It is used extensively by the United States Navy but very little by private and commercial operators. Last year, 2/7-size models of two typical Navy floats were tested in the tank to obtain information to be used in attempts to design an improved form of float for this type of service. The results of these tests are published in Technical Note No. 563 and afford designers an opportunity to consider the single-float arrangement from the standpoint of water performance. A comparison of the test data of the conventional floats with those of a generally similar float having a pointed step is included in this note.

The form of the planing bottom of a hull forward of the step has in general a marked effect on water resistance. A previous investigation having established the superiority of a planing bottom longitudinally straight over the pronounced convex or "rocker" type, tests were made of a model of a flying-boat hull having a slightly concave bottom forward of the step. The results of these tests, reported in Technical Note No. 545, indicate that there is no great advantage in the concave type of planing bottom as tested, although the high-speed resistance was slightly less than that of the straight bottom.

Design data for hulls for small flying boats and amphibians.—The problems encountered in the design of hulls for small flying boats or amphibians are in some ways more difficult than those encountered in large craft. The combination of adequate strength, light weight, and good water performance with small size does not permit the elaborate structure that may be used where dimensions are not restricted. Under these conditions simplicity of form with good water performance becomes of the greatest importance. Technical Report No. 543 furnishes hydrodynamic data for five forms designed to be suitable for hulls of small flying boats and amphibians. The types used are simple in form and were tested in the tank for all values of speed, load, and trim which it was believed would apply. The data obtained are intended to aid the designer in selecting the most suitable size and type of hull as well as in verifying take-off performance in the early stages of a proposed design. Included in the series is a novel form of forebody the bottom surface of which can be expanded into a flat surface and hence can be fabricated without shaping the plating or planking near the bow. The tank tests indicated that this simplified form compared favorably with the conventionally shaped bottom, at least for the smooth-water conditions simulated in the tank.

Work for private concerns.—From time to time the tank has interrupted its regular work to perform tests for the manufacturers when such tests could not be satisfactorily done elsewhere.

SPECIAL SUBCOMMITTEE ON VIBRATION AND FLUTTER

The Special Subcommittee on Vibration and Flutter has held two meetings since its organization. At these meetings the special problems relating to the general subject which are being investigated by the Army Air Corps, the Bureau of Aeronautics of the Navy, the National Bureau of Standards, and the National Advisory Committee for Aeronautics were briefly outlined and the general program of future work was discussed.

At the second meeting, representatives of propeller manufacturers were present and described the progress made by their organizations in connection with the problem of propeller vibration and its relation to vibration in other parts of aircraft and to flutter.

One of the most important investigations in connection with this general problem is the study of engine vibration and the design of engine mounts, which has been carried on by the Matériel Division of the Army Air Corps. A special vibration-isolating mount for radial engines has been developed which effected considerable improvement in one of the airplanes in which it was installed. The Matériel Division is also investigating the vibration characteristics of engines, propellers, and various wings.

Under the sponsorship of the Bureau of Aeronautics of the Navy an investigation has been conducted at the Massachusetts Institute of Technology which resulted in the development of a vibration meter of the electrical pick-up type for measurement of the vibratory translational and rotational motion of airplane engines and structures in flight or on the ground.

The National Bureau of Standards has been engaged in a theoretical study of the effect of centrifugal force on the stress distribution and vibration frequency of propeller blades. Further study is being made of the theory and the literature on harmonic vibrations and on the vibration of mounting stands.

The National Advisory Committee at its laboratory at Langley Field has studied the effect of centrifugal force on propeller vibrations and the torsional vibration of engines. A comprehensive program is being initiated for the investigation of the vibration characteristics of airplane engines, particularly the periodic mass and gas forces and moments.

**REPORT OF COMMITTEE ON POWER PLANTS
FOR AIRCRAFT****LANGLEY MEMORIAL AERONAUTICAL LABORATORY
ENGINE POWER**

The designs of new aircraft are based upon aircraft engines developing twice the maximum power of the present engines. This large increase in engine power will be obtained by operating at higher engine speeds, by increasing the weight of the charge pumped into the cylinder, by using fuels having higher antiknock

ratings, and by improving the cooling of air-cooled engines. The investigations undertaken by the Committee indicate several promising methods by which this increased engine power may be efficiently obtained.

Increased engine speeds.—The power output of an engine is directly proportional to the rotative speed. The maximum rotative speed is limited, however, by the piston speed and by the loading of the engine bearings. In order to investigate the problems connected with higher rotative speeds a single-cylinder test engine is being designed to operate at a maximum speed of 4,000 r. p. m. The standard speed of the Committee's present laboratory test engines has been increased from 1,500 to 2,500 r. p. m. to simulate more closely the speed of multicylinder engines.

Improved fuels.—The maximum power that can be obtained from a given fuel is limited by its detonation characteristics. New processes of manufacture have made commercially available fuels having antidetonating characteristics superior to those of iso-octane. The use of these fuels results in a large increase in engine power because the aircraft engines can be operated at higher compression ratios and at increased manifold pressures. During the past year the necessary test equipment has been assembled for the determination of the maximum engine power available when fuels having a range of octane numbers from 87 to 100 are used. The engine tests will cover a range of inlet manifold pressures, air temperatures, and compression ratios. The fuels tested will be the same as those used by the Aviation Detonation Subcommittee of the Society of Automotive Engineers. Preliminary tests have been made of several types of detonation indicators for the purpose of obtaining a reliable indication of incipient detonation.

Detonation research.—Detonation in present aircraft engines is eliminated by the use of premium fuels. The development of aircraft engines capable of delivering high power outputs with cheaper fuels would result in an appreciable reduction in the operating cost of aircraft. A study of the detonation process occurring in internal-combustion engines is being made to obtain new knowledge concerning the phenomenon of detonation.

The N. A. C. A. combustion apparatus has been set up with a cylinder head having a pent-roof combustion chamber so that it can be operated as a spark-ignition engine. A rectangular glass window approximately 5 by 7 inches in size gives an unobstructed view of one-half the combustion chamber. The single fuel charge is injected through a fuel valve located in the cylinder head. The injection of the fuel, the occurrence of the spark, and the subsequent combustion are photographically recorded.

Three methods of photography are used. Motion pictures are taken of the fuel injection and the flame

propagation across the combustion chamber by means of a high-speed camera taking 2,500 frames per second. With the windows masked by a metal plate, schlieren photographs of the flame propagation are taken through a $\frac{1}{8}$ -inch slot. These data show phenomena that are not visible in the flame photographs because the temperature front is recorded instead of the flame. Schlieren photographs are also taken of the combustion visible through the unmasked window. In this case the light source consists of 10 electric sparks discharging at the rate of 2,000 per second. The variables investigated have been air-fuel ratio, engine speed, spark-plug arrangements, and fuels having a range of octane numbers from 65 to 100. Interesting records of the flame have been obtained with the charge fired by two diametrically opposite spark plugs, which indicate that the combustion front is from $\frac{1}{2}$ to 2 inches in depth. In all cases the flame occurring with detonation is decidedly more actinic than the flame preceding detonation.

Valve overlap.—At the request of the Bureau of Aeronautics, Navy Department, an investigation has been started to determine the increase in performance that may be obtained with a radial air-cooled engine equipped with a fuel-injection system and operating with a large valve overlap. The valve timing that will give maximum power will be determined from tests on a single-cylinder engine. The tests on a single-cylinder engine have been started with inlet and exhaust cams giving an overlap of 130 crank degrees.

Air intercoolers.—The inlet-air or the fuel-air mixture heated by the supercharger must be cooled before delivery to the engine cylinders to prevent the loss of engine power at high altitudes. Work has been continued on the study of air coolers for supercharged engines. Heat-transfer tests have been made on several samples of intercooler cores, and a few drag measurements have been made of an aluminum cooler, external fins being used to dissipate heat to the cooling air.

The 2-stroke-cycle engine.—The use of fuels having high antiknock ratings has permitted large increases to be made in the power output of aircraft engines. The favorable characteristics of the fuel should facilitate the obtaining of increased power and improved fuel economy for the spark-ignition 2-stroke-cycle engine operating with gasoline injection. A single-cylinder engine has been constructed and tests started to determine the performance characteristics of this type of engine for a range of speeds, scavenging pressures, injection methods, and inlet and exhaust timings.

FUEL CONSUMPTION

The demand for transport and military aircraft having a long range has intensified research on possible methods of reducing fuel consumption. At present,

the use of automatic mixture controls has given an appreciable reduction in fuel consumption. A reduction in fuel consumption of air-cooled engines has been obtained by the use of improved designs of cylinder finning. The design of aircraft engines to operate with fuels of high octane number should result in further reduction in fuel consumption because of the higher permissible compression ratios.

Fuel distribution.—The use of a fuel-injection system instead of a carburetor on aircraft engines has been found to result in reliable engine operation at all altitudes of the airplane, in increased engine power, and in more uniform distribution of fuel between individual cylinders. The distribution of the fuel within the cylinder is being studied by means of a spark-ignition fuel-injection engine fitted with a glass cylinder. The injection of the fuel and the movement of the air in the cylinder are being photographically recorded.

The distribution of fuel to the various cylinders of a multicylinder engine has been determined for a 500-horsepower radial air-cooled engine operated in the 20-foot wind tunnel. The method used was to collect and chemically analyze the exhaust gases from each cylinder for several conditions of engine speed, power output, and specific fuel consumption. The results showed that the variation in the quality of the mixture among individual cylinders was 4 percent and was independent of fuel consumption, air-fuel ratio, and engine power. It was found that the temperature of the spark-plug boss was not a good indicator of fuel distribution. The results of this investigation will be published as a technical note.

Mixture control.—For long-range aircraft it is necessary that the pilot maintain, especially under cruising conditions, an air-fuel mixture as lean as is compatible with safety. The use of the constant-speed propeller has made the usual "leaning-out" method obsolete. The normal mixture controls are being replaced by mechanisms that automatically maintain an economical mixture ratio at all altitudes. An investigation has been made to determine the operating characteristics of a commercial mixture indicator. The operation of this indicator is based on the change in thermal conductivity of the exhaust gases from the engine with change in air-fuel ratio. On the basis of a chemical analysis of the exhaust gases, the instrument gives accurate readings for a range of air-fuel ratios from 8 to 15. The instrument will not indicate satisfactorily, however, air-fuel ratios greater than 16.

Fuel injection.—An investigation has been started to determine the comparative performance obtained with an air-cooled cylinder of late design when operated with a carburetor, with fuel injection into the manifold, and with fuel injection into the cylinder. In this comparison of the three methods of carburetion

fuel consumption, power, and cylinder temperature are the important factors to be considered. Preliminary tests have shown that good performance can be obtained with any one of these methods; slightly greater power, however, is obtained by injecting into the cylinder and better fuel economy is obtained with the carburetor. The two injection-valve locations used in the cylinder head may not have given the maximum performance obtainable with injection into the cylinder. Locating the injection valve so as to take advantage of the air flow set up in the cylinder by the passage of the inlet air through the valve is expected to give an improvement in fuel consumption.

Long-range airplane.—A study is being made by the Committee of the factors affecting the design of long-range airplanes. One of the important phases of this study is to determine the fuel-consumption characteristics of the engine at various values of the engine speed and torque. The determination of these characteristics is being made on a single-cylinder air-cooled test engine having a compression ratio of 5.6. The results indicate that the improvement in the minimum specific fuel consumption becomes less as the engine torque is increased until, with a boost pressure of 5 pounds per square inch, no further improvement is secured. In addition, it has been found that the engine speed has no great effect on the minimum brake fuel consumption.

Exhaust-gas analysis.—Knowledge of the combustibles present in the exhaust gas of an internal-combustion engine makes possible the evaluation of the energy lost due to incomplete combustion. Analyses of exhaust gases by the use of several approved combustion methods have been found to give different results. A synthetic gas mixture of predetermined composition was prepared and analyzed by (1) slow combustion with air, (2) slow combustion with oxygen, (3) fractional combustion in a copper-oxide tube followed by slow combustion, and (4) fractional combustion in a copper oxide-cerium oxide tube followed by slow combustion. The fractional-combustion method depends on the oxidation of certain combustibles in the exhaust while others are unaffected. The tests indicated that the analysis by means of slow combustion with air gave the most reliable results.

COWLING AND COOLING

Cowling-propeller-nacelle investigation.—A comprehensive investigation has been carried on with full-scale models in the N. A. C. A. 20-foot wind tunnel, the general purpose of which is to supply information in regard to the physical functioning of the composite propeller-cowling-nacelle unit under all operating conditions of take-off, taxiing, and normal flight. The tests included numerous combinations of more than a dozen nose cowlings, about a dozen skirts, six pro-

pellers, two sizes of nacelles, various types of spinners, and other devices.

The optimum shape of a low-drag cowling has been determined. The shape of the leading edge and the contours of the exit passage are the causes of large losses when improperly designed. The importance of providing means for regulating the quantity of cooling air so as to keep it to a minimum to prevent excessive losses at high speeds was demonstrated. An N. A. C. A. cowling shows a remarkably high efficiency when considered as a pump for the cooling air. The superiority of a baffled over an unbaffled engine has been verified and it has furthermore been shown that tightly fitting baffles are superior to the deflector type.

The problem of cooling a radial air-cooled engine on the ground has been studied in detail. The influence of various forms of skirts, flaps, propellers, spinners, and special blowers has been investigated. Among the more interesting results are the demonstration of the comparative inefficiency of the adjustable skirt flaps, the detrimental effect of small-diameter front openings of the cowling, and the very beneficial effect of a carefully designed airfoil section near the hub of the propeller. A small axial fan of simple construction was found to give efficient cooling on the ground.

The cooling of a complete full-scale engine was studied in detail. A constant amount of heat was supplied to the cylinder by the use of an electrical heater. This arrangement gave the cooling directly by measurement of the outside temperatures. It was found that the baffled part of the cylinder was cooled directly by velocity flow and consequently the cooling was a direct function of the velocity or of the pressure drop across the baffles. The cooling of the front of the cylinder was of a different nature, as it was good in spite of the fact that there was no measureable velocity flow. This phenomenon was studied by the use of smoke flow and hot-wire anemometers, and it was found that a large-scale turbulence in front of the cowling materially aided the cooling. Spinners were found to affect this cooling materially.

The investigation of the cooling characteristics of a cowled Pratt & Whitney Wasp II engine installed in a nacelle and mounted in the 20-foot wind tunnel has been completed. Equally good cooling, for a particular pressure drop, resulted from each of the cowlings tested. Cooling of the front of the cylinder depended very little on pressure drop for those tests in which the pressure drop was varied by changing the skirt exit; the cooling of the front was accomplished by means of large-scale turbulence of the air. A controllable propeller used in the tests had no beneficial effect on cooling, and an adjustable propeller only improved the cooling slightly.

A new type of N. A. C. A. cowling has been developed as a result of the complete investigation of the

propeller-cowling-nacelle unit. This cowling is characterized by the feature that the exit opening discharging the cooling air is not, as usual, located behind the engine but at the nose of the cowling. This type of cowling is inherently capable of producing two to three times the pressure head obtainable with the normal type of cowling because the exit opening can be located in a field of considerable negative pressure. This arrangement makes possible more cooling at lower air speed or, if needed, more cooling at any speed. In general, the efficiency is found to be high, owing to the fact that higher velocities may be used in the exit opening. Flight tests made on a temporary installation have shown promising results.

The 2-row radial engine.—The results of an investigation conducted at the request of the Bureau of Aeronautics, Navy Department, on a 2-row radial engine installed in a service airplane and mounted in the full-scale wind tunnel have been given in Technical Report No. 550.

Fin dimensions.—The determination of the surface heat-transfer coefficients of closely spaced steel fins has been continued. Finned cylinders have been investigated having a range of fin width from 0.37 to 1.22 inches and of fin spacing from 0.022 to 0.131 inch. These cylinders were tested with and without baffles in a wind tunnel and with blower cooling, the cylinders being completely enclosed in a jacket. The results of an investigation in which the optimum fin spacing was determined for each of these three methods of cooling for cylinders having fins of 1.22-inch width are being prepared for publication. The results of an investigation made to determine the effect of fin width on the optimum fin spacing for each method of cooling are now being prepared for publication.

The effect of the conductivity of the metal of the fins on the heat transfer has been checked with aluminum, steel, and copper fins. The purpose of this investigation was to verify experimentally the use of the factor of thermal conductivity in the theoretical equation for the heat transfer from finned cylinders.

Flight tests have shown that for the same pressure drop across the cylinder fins the cooling in flight is considerably better than that obtained in laboratory tests with single-cylinder engines. This difference in cooling is attributed to the turbulent flow of air over the front of the cylinders that occurs in flight with the N. A. C. A. cowling. An investigation is being conducted to determine the effect of air turbulence on the cooling of finned cylinders.

Baffle study.—A study has been made to determine the effect of cylinder diameter, fin spacing, fin width, and baffle design on the energy loss of the air passing by the cylinder. The results show the relative cooling and the distribution of the energy loss for each baffle arrangement.

Blower power required.—For long-range airplanes, the air-cooled engines could be located within the wing and cooled by a blower. The results of the tests on two cylinders having widely differing fin pitches, enclosed in jackets and cooled with a blower, have been published in Technical Note No. 572. The minimum power required for satisfactory cooling with an overall blower efficiency of 100 percent varied from 2 to 6 percent of the engine power, depending on the operating conditions. The shape of the jacket had a large effect on the cylinder temperatures. The drop in total head across the cylinder varied approximately as the square of the weight of the cooling air. The temperature difference between the cylinder and the cooling air varied as the 0.51–0.56 power of the indicated horsepower.

An investigation has been made to determine the effect of changes in fin width and fin spacing on the pressure drop and power required to force air around finned cylinders at air speeds from 15 to 230 miles per hour. The effect of changes in the shape of the entrance and exit of the jacket on the pressure drop and power required to force the air around the finned cylinders has been investigated. The results of this investigation are being prepared for publication.

Cooling-air temperature.—For safe operation the temperatures of air-cooled cylinders must not exceed certain limiting values. Since air-cooled engines are required to operate over a wide range of conditions, it is important that the effect of the operating conditions on cylinder temperatures be known. In the acceptance testing of airplane engines the problem often arises of predicting engine temperatures for summer operation from tests made in the winter or of predicting altitude temperatures from tests at sea level.

An investigation has been made at the request of the Bureau of Aeronautics, Navy Department, to determine the effect of cooling-air temperature on cylinder temperature for the six cylinders representing service-type engines. For the range of conditions studied it was found that a single correction factor could be used for all cylinders for the variation in cylinder-head temperature with cooling-air temperature. Similar correction factors were also obtained for the cylinder barrel and flange. A report covering this investigation is being prepared.

A theoretical study has been made of the heat-transfer process in an air-cooled engine to provide a better insight into the relation between the various engine and cooling conditions. Equations have been derived for the relationship between cylinder temperatures and the important engine and cooling variables. The several empirical constants in the equations may readily be obtained from engine tests. An investigation has been made on a single-cylinder engine with two different designs of air-cooled cylinders to check the theo-

retical development and to provide values for the constants in the equations applicable to the respective cylinders for the particular conditions of the tests. The results of this investigation are being prepared for publication.

An investigation has been made to determine the effect of engine power, mass flow of the cooling air, and atmospheric temperature on the cylinder temperature of a Pratt & Whitney 1535 supercharged engine under actual flight conditions. A Grumman Scout (XSF-2) airplane was used in these tests. The results indicated that the difference in temperature between the cylinder wall and the cooling air varied as the 0.38 power of the brake horsepower for a constant mass flow of cooling air, cooling-air temperature, and engine speed. The difference in temperature was also found to vary inversely as the 0.39 power of the mass flow for points on the cylinder head, and the 0.35 power for points on the barrel, provided the engine power, engine speed, and cooling-air temperature were kept constant. A report of the results of this study has been prepared for publication.

Cooling at altitude.—An analysis has been made for the Bureau of Aeronautics, Navy Department, of the comparative cooling at altitude and at sea level of supercharged air-cooled engines in a high-speed transport and a pursuit airplane. The estimated cooling was based on data obtained from wind-tunnel tests of a multicylinder engine mounted in a nacelle and from single-cylinder engine tests.

Flame temperature.—A new technique for measuring combustion engine temperatures by the sodium line reversal method has been developed. The preliminary results obtained by this method are presented in Technical Note No. 559. Further measurements with a new cylinder head in which the temperature distribution will be studied are in progress.

COMPRESSION-IGNITION ENGINES

The rapid development of the compression-ignition, or Diesel type, engine for use in all forms of automotive equipment has not been followed in this country by the development of a successful Diesel aircraft engine. The low fuel consumption and reduction in fire hazard obtained by the use of the compression-ignition engine should be of particular interest to operators of long-range transport aircraft. The research work of the Committee on the compression-ignition engine has been continued with the object of obtaining fundamental knowledge concerning the fuel-injection and combustion process and of increasing the specific power output. A form of integral combustion chamber in which high-velocity air flow is utilized for distributing and mixing the fuel and the combustion air is being investigated. The specific power output obtained with a single-cylinder liquid-cooled

engine using this combustion chamber compares favorably with the maximum obtained from present supercharged spark-ignition aircraft engines.

Combustion research.—An investigation of the combustion characteristics of fuel sprays suitable for use in compression-ignition engines has been completed and the data are presented in Technical Report No. 545.

A constant-volume bomb has been used to investigate the effect of air temperature and density on the auto-ignition and subsequent combustion of Diesel fuel. The bomb is mounted in an electric furnace and can be heated to a maximum temperature of 1,100° F.; the density of the air in the bomb can be adjusted to any desired value. The minimum ignition lag obtained with this apparatus, the fuel being injected as in the compression-ignition engine, is 0.001 second. The amounts of ignition lag and combustion time obtained with the bomb are comparable with those obtained in the compression-ignition engine. An investigation is being conducted with the bomb to determine the effect of injection-nozzle design, air temperature, and pressure on the combustion.

The results of the investigation made of the combustion in a spherical bomb with a fuel-injection system at relatively low air temperatures have been published in Technical Report No. 544.

A research has been completed to determine the effect of increasing the degree of atomization of the fuel injected into a prechamber compression-ignition engine with forced air flow. The degree of atomization of the fuel was varied by increasing the fuel-injection pressure from 4,000 to 9,000 pounds per square inch. The results showed that the ignition lag decreased 35 percent and the brake mean effective pressure increased 19 percent with increase in the fuel-injection pressure. The results of an investigation covering the effects of several designs of fuel-valve nozzles on the fuel spray and flame formation in a high-speed compression-ignition engine have been published in Technical Report No. 561.

The effect on ignition lag and engine performance of heating the fuel oil before injection to a maximum temperature of 750° F. has been determined with a compression-ignition engine having a prechamber. The research is described in Technical Note No. 565.

Fuel-injection pumps.—Improved distribution of fuel within combustion chambers of certain forms for compression-ignition engines may be obtained by the use of more than one fuel-injection valve. An investigation has been completed on the rates of discharge from a single-cylinder fuel-injection pump connected to two injection valves. The variables investigated were pump speed, injection-tube length, injection valve-opening pressure, and discharge-orifice diameter. The results showed that by the proper choice of injection

valve-opening pressures and discharge-orifice diameters of the two injection valves, time rates of discharge can be obtained that cannot be obtained with a single injection valve. The use of unequal tube lengths connecting the two injection valves to the fuel pump resulted in erratic operation when the speed of the pump was varied. When the two injection tubes were of the same length, this erratic operation with change in pump speed did not occur.

A research has been started to determine the rates of discharge from a fuel-injection system in which the injection pump is connected directly to the fuel-injection valve. Preliminary tests indicate that with this system the rates of discharge are more nearly a function of pump speed than is the case with a long injection tube. The tests are being conducted for a range of pump speeds, injection valve-opening pressures, discharge-orifice diameters, and throttle settings.

A comparison of the distribution of fuel with several types of fuel sprays has been published in Technical Report No. 565.

Prechamber-type of combustion chamber.—This investigation has been completed and a report is being prepared summarizing the research work on the prechamber type of combustion chamber.

Integral type of combustion chamber.—Technical Report No. 568 has been prepared summarizing the work completed on the performance of an integral combustion chamber with no air flow, and concluding this investigation.

The investigation of engine performance has been continued on a single-cylinder engine having a displacer piston and a combustion chamber of vertical disk form. Results have been published in Technical Note No. 569 of the engine performance obtained at 2,000 r. p. m. for boost pressures up to 10 pounds per square inch. For these conditions brake mean effective pressures of over 200 pounds per square inch have been obtained with a specific fuel consumption of 0.46 pound per brake horsepower-hour. An investigation has been started at 2,500 r. p. m. on a single-cylinder engine having a 5-inch bore and a 7-inch stroke to determine the characteristics and performance possibilities of the displacer-piston combustion chamber at the higher engine speed.

Engine friction.—An investigation of the friction characteristics peculiar to compression-ignition engines has been completed and the results presented in Technical Note No. 577. The investigation included the determination of the effect of combustion-chamber shape, air-flow quantities, and compression ratio on the friction of single-cylinder compression-ignition engines.

Altitude performance.—Information is lacking concerning the performance of compression-ignition engines at altitude conditions. Equipment has been

assembled and an investigation started to determine the performance of a single-cylinder liquid-cooled compression-ignition engine in operation under conditions of inlet pressure and temperature and exhaust pressure equivalent to altitudes from sea level to a maximum of 30,000 feet.

Single-cylinder and multicylinder engines.—The problems of adopting the displacer-piston form of combustion chamber to a radial air-cooled engine and the requirements for adequate cooling have been given careful consideration. A preliminary design of air-cooled cylinder suitable for installation on a conventional radial engine has been completed. The necessary equipment is being assembled for an investigation of this design. In addition to giving information on power, economy, and cooling requirements, the results will permit direct comparisons to be drawn between the mechanical friction of spark-ignition and of compression-ignition radial air-cooled engines.

The 2-stroke-cycle engine.—Investigation of the 2-stroke-cycle compression-ignition engine has been continued with a determination of the optimum entry angle for the scavenging and combustion air with the inlet and exhaust systems arranged to eliminate ramming. An improvement of 15 percent in maximum performance was obtained by directing the air into the cylinder at a horizontal angle of 60° to the radial; all vertical entry angles with a flat-top piston adversely affected the engine performance. The single-cylinder engine developed 0.65 brake horsepower per cubic inch of displacement when operated at 1,800 r. p. m. with a scavenging air pressure of 8 pounds per square inch. The data indicate that a further improvement in performance may be expected by the use of higher scavenging pressures and engine speeds. A report presenting the results of this work is being prepared.

INSTRUMENTS

Fuel flowmeter.—The electrical type of indicating fuel flowmeter has been further developed to extend its range when either a potentiometer or a millivoltmeter is used for indication. The range of fuel flow that has been covered with a potentiometer is from 30 to 1,500 pounds per hour. The instrument is now being tested in flight.

High-speed camera.—The researches on combustion in a spark-ignition engine have indicated the need of taking high-speed motion pictures at rates greater than that of 2,500 frames per second now available with the present high-speed motion-picture camera. A new camera is being designed, to consist of a single rotating drum upon which will be mounted the photographic film and a system of prisms. The prisms are so arranged that the image focused on the film moves at the same linear speed as the film. The camera is being designed to take motion pictures of the combustion at rates up to 40,000 frames per second.

NATIONAL BUREAU OF STANDARDS

Phenomena of combustion.—The effects of the inert gases argon and helium upon flame speed and expansion ratio in mixtures of carbon monoxide, oxygen, and water vapor, measured by the bubble method, are described in Technical Report No. 553. The results of further studies of flame movement and pressure development in an engine cylinder are presented in Technical Report No. 556. A brief mimeographed note entitled "Practical Aims of Combustion Research" has been prepared for distribution to visitors and to others interested.

The construction of a spherical bomb of constant volume, equipped with (a) means for photographing the spread of flame from a central point of ignition, and (b) six indicators of the balanced-diaphragm type arranged to record the points at which predetermined pressures are reached, has been undertaken. Short cylinders of Pyrex glass, with ends ground parallel and with inside and outside surfaces given an optical polish, have been prepared to serve (singly) as windows through which the flame may be photographed.

The development of pressure indicators having sufficient accuracy has necessitated a special investigation of the characteristics of such instruments. These studies show that local regions of extremely high pressure may exist in passageways and crevices on the explosion side of the diaphragm. It is therefore desirable that the diaphragm be exposed directly to the explosive mixture. Studies of the effects of diaphragm diameter and thickness show that, for the present purpose, the inertia of the diaphragm is an important factor, particularly if measurements are to be made during the early stages of the explosion. An adequate compromise between sensitivity and inertia has been found experimentally, and the pressure indicators have been designed accordingly.

In the evolution of an accurate time-pressure record at least two other factors must be considered, namely (a) the time lag involved in the transfer of pressure from the flame front to the diaphragm, which is thought to be the time required for sound to travel from one to the other, and (b) the time between ignition and the attainment by the flame of its maximum, and temporarily constant, spatial speed. In the case of an explosive mixture for which flame speed and expansion ratio are already known, the observed and calculated time-pressure records are in good accord when the above corrections are determined and applied. Mathematical analyses of spherical burning at constant pressure (bubble) and at constant volume (bomb) have yielded fairly simple working equations whereby the desired characteristics may be derived from the observed quantities.

Ignition investigations.—The work on ignition problems for the Bureau of Aeronautics, Navy Department, has included laboratory tests of magnetos, ignition cable, spark plugs, and spark-plug elbows. In addition to the routine testing of magnetos, attention has been given to the improvement of test methods and a study was undertaken to ascertain the influence of various factors on the electrical characteristics of magnetos. The development of ignition cable capable of withstanding higher temperatures has been encouraged and experiments are in progress with a view to the possible replacement of rubber insulation. The mathematical analysis of heat flow in mica spark plugs has been extended and the accompanying calculations made. The theoretical results are being correlated with test results on spark plugs designed according to the theoretical principles. Routine temperature surveys have been made on about 20 airplanes and various cases of overheating have been found and corrected. Repeat tests on the same airplane at different ground temperatures have tended to show that the correction factors in current use are too small. Special temperature measurements have been made in connection with flight tests of spark plugs and spark-plug elbows.

Endurance tests of engines.—At the request of the Bureau of Air Commerce, a 25-hour torque-stand endurance test of an inverted 4-cylinder in-line air-cooled aircraft engine, in which battery ignition was used in place of the magnetos, was undertaken and successfully completed. The same engine had been run previously for about 25 hours during the cooling investigation and was subjected later to about 100 hours of additional running during a propeller test. A final report has been prepared covering the performance of the ignition system, and other parts, for the entire 150 hours.

A popular vee-type automobile engine, subjected to dynamometer test at full throttle and rated speed for the information of the Bureau of Air Commerce, suffered a crankshaft failure after running about 100 hours. A second test was terminated in a few hours by a connecting-rod bearing failure. Tests of a new engine, embodying the 1936 changes, developed two piston failures in the course of about 85 hours' running.

A well-known two-cylinder motorcycle engine is being given a 300-hour torque-stand endurance test to determine for the Bureau of Air Commerce the suitability of its parts for use in small and inexpensive aircraft engines. The propeller in this installation is driven by vee belts. Two 50-hour runs have been satisfactorily completed, about 15 horsepower per cylinder being developed at 3,000 r. p. m. The engine valves have given some trouble because of distortion of the cylinders by the cylinder-head studs. During the remainder of the test the engine is to be run at 4,000 r. p. m.

SUBCOMMITTEE ON AIRCRAFT FUELS AND LUBRICANTS

High octane number fuels.—The Subcommittee on Aircraft Fuels and Lubricants has prepared a program of tests of a single-cylinder engine to be conducted at the Langley Memorial Aeronautical Laboratory to determine the maximum performance that can be obtained with fuels having octane numbers from 87 to 100 without lead and for higher octane ratings with lead. The fuel to be used in these tests has been prepared for the Aviation Gasoline Detonation Subcommittee of the Society of Automotive Engineers. The maximum engine performance obtainable with a fuel having a specified octane number will be determined by two methods; first, by increasing the compression ratio and, second, by maintaining a constant compression ratio and increasing the boost pressure. The factor limiting each test will be the start of detonation. For check purposes, limited tests will be made by the laboratory on air-cooled single-cylinder engines and by the Matériel Division of the Air Corps on a liquid-cooled single-cylinder engine.

Detection and evaluation of knock.—A report on methods of measuring the intensity of knock in high-output aircraft engines was prepared at the request of the Bureau of Aeronautics of the Navy Department, and has been made available both to the Subcommittee on Aircraft Fuels and Lubricants and to the C. F. R. Aviation Gasoline Detonation Subcommittee. A satisfactory laboratory model of the photoelastic pressure gage has been completed and tested. This indicator will record directly either the pressure or the rates of pressure rise accompanying detonation. A portable instrument combining the pressure indicator and a thermal plug has been designed and is under construction.

Rating fuels in full-scale aircraft engines.—The results of the comparative tests of aviation fuels in representative aircraft engines, made by the National Bureau of Standards in cooperation with three engine companies, have been published. The final report includes a C. F. R. recommended procedure for rating fuels in full-scale aircraft engines and outlines the program of future work of the C. F. R. Aviation Gasoline Detonation Subcommittee with aviation fuels of high octane number. Arrangements have been made to set aside 70,000 gallons of technical iso-octane and 10,000 gallons of a straight-run gasoline of about 20 octane number for general use as reference fuels in full-scale engine tests of high octane fuels. The work of the C. F. R. subcommittee is being coordinated with the program of the Subcommittee on Aircraft Fuels and Lubricants so as to avoid possible duplication. The Army Air Corps, the Bureau of Aeronautics of the Navy, the National Bureau of Standards, and leading engine manufacturers are represented on both subcommittees.

Stability of aviation oil.—The investigation of the stability of aircraft engine lubricating oil, undertaken with the cooperation of the Bureau of Aeronautics of the Navy, was continued throughout the fiscal year. Engine tests with 22 representative aviation oils were completed after operation for approximately 30 hours each in a Pratt and Whitney Hornet engine at about 75 percent rated power. In cooperation with the Navy Department a large number of samples have been removed from engines in service and have been analyzed to provide a basis for further correlation with laboratory stability tests and a basis for recommendations regarding extension of the period between oil changes in service. A large volume of laboratory data was obtained on the 22 oils under various conditions of oxidation at various temperatures and a satisfactory correlation was found by the use of one set of laboratory test conditions and the results of the tests on the Hornet engine. Apparatus has been constructed for testing oil stability by an improved and somewhat simpler method which involves heating the oil in a cylinder under conditions analogous to those encountered in aircraft engines.

Oil acidity and bearing corrosion.—An investigation has been initiated for the Bureau of Aeronautics of the Navy involving a study of the effect of increase in oil acidity during service on the corrosion of master rod bearings. Apparatus for this purpose has been designed and the construction of a large part of it has been completed.

Wear and oiliness characteristics of aviation-engine lubricating oils.—An extensive investigation has been started with the cooperation of the Bureau of Aeronautics on the oiliness characteristics of lubricating oils and on the differences in cylinder-wall and piston-ring wear caused by different oils. Emphasis is being placed on the development of compounded oils which will have superior lubricating qualities and which will tend to reduce wear in high-output engines. Apparatus for this investigation has been designed and is practically completed. In conjunction with this investigation, data on oil stability and corrosion are being obtained on those compounded oils which show merit from the standpoint of wear reduction.

Aviation-engine wear.—In cooperation with the Subcommittee on Aircraft Fuels and Lubricants and a number of representative petroleum organizations, an investigation has been started on the relative wear with various oils in actual aircraft engines. In these tests it is planned to rely on accuracy of measurements rather than on long-time operation in order to obtain the desired information, and the engine will be largely rebuilt for each test, new pistons, cylinders, and rings being used each time. Considerable progress has been made in assembling the necessary equipment, both for measuring the various engine parts and for absorbing

the power. A special sound absorber has been designed and constructed in order to minimize engine noise and preliminary tests have indicated a fairly high degree of effectiveness.

REPORT OF COMMITTEE ON AIRCRAFT STRUCTURES AND MATERIALS

SUBCOMMITTEE ON METALS USED IN AIRCRAFT

Weathering of light-alloy structural sheet material.—The series of tests on aluminum-alloy sheet material which have been in progress at Washington, D. C.; Hampton Roads, Va.; and Coco Solo, C. Z., will be completed early in 1937 after four years' continuous exposure of the specimens to the weather. Although the initial test program was arranged to cover five years, it is felt that they will have essentially fulfilled the purpose in the somewhat shorter time. The results definitely establish the markedly superior properties, with respect to corrosion resistance, of the aluminum alloys containing magnesium as the alloying constituent over similar alloys containing copper as an essential alloying constituent. The tests have also given valuable information with respect to the coating processes which are dependable for use on aluminum-alloy structures which must withstand severe atmospheric conditions. The Alclad materials have proved very resistant under all conditions imposed upon them. These various classes of alloys can be depended upon to give eminent satisfaction over a stipulated minimum five-year service life of an aircraft.

In the summarizing report, detailed information is given on the microstructural aspect of the corrosion of aluminum-alloy sheet and its relation to the lowering of the mechanical properties of the material. The correlation of the results of laboratory tests by the salt-spray method on a large number of specimens with the results obtained with similar materials exposed continuously serves as a basis for a practical evaluation of this method of testing, which is extensively used in specifications in the aircraft industry.

A program to supplement these tests has been authorized and tests have been planned to give information on specific items of general importance in aircraft construction, such as spot welding, riveting, faying or contact surfaces, as well as newly developed protective coatings.

Protective surface treatment of magnesium alloys.—An electrolytic method has been developed for the surface treatment of magnesium alloys which is analogous to the anodic process used for aluminum alloys. The process is being applied on a commercial scale at the Naval Aircraft Factory. This method for treating the surface of magnesium has proved superior in a number of ways to other processes for the same purpose, although it is not so simple in application as the

corresponding anodic process for aluminum alloys, since the various types of magnesium alloys differ somewhat in their response to the treatment. Work is being continued for defining the proper conditions for each type of this class of alloy. The process has been described in a Research Paper of the National Bureau of Standards. Weather-exposure tests are in progress to supplement extensive laboratory tests by the salt-spray method to determine the relative merits of magnesium alloys treated by this and other methods, the treated specimens being coated with various kinds of priming and finishing coats recommended for magnesium.

Anodic oxidation for protective treatment of aluminum.—Work on this subject has been completed. The widely used chromic-acid method for this as initially described was essentially a batch process requiring an empirically determined voltage cycle. The work has demonstrated the feasibility of carrying out the process as a continuous one, and has, in addition, established the underlying principles for maintaining the bath in good working condition. The reasons for the deterioration of the bath with use have been set forth. The results are presented in a Research Paper of the National Bureau of Standards.

Elastic properties of high-strength aircraft metals.—In this investigation, which has recently been initiated, corrosion-resistant steel of the so-called 18-8 type is being used as the basis. This material already has been accepted for many important uses in aircraft, such as tie rods, cables, etc., and other important new uses are constantly being considered and tried. Austenitic steel of this kind owes its high strength to the cold working to which it is subjected in fabrication and definite information on the elastic properties and their limitations is very desirable, since, as is well known, the elastic properties of such a material are largely only nominal. None of the austenitic steels possess true elastic properties. In particular, information on the "over-load" characteristics of the material is desirable.

With the nominal elastic properties of the material as determined by the customary stress-strain measurements as a start, a study of the stress-permanent set relationship has been made, following which similar studies are being made of similar material which has undergone deformation prior to testing, such as might occur through accident in service. On the basis of the information secured by such studies it is expected that the maximum allowable stresses for materials of this kind which possess no true elastic properties can be fixed with more assurance than on a knowledge of only their nominal elastic properties or empirically determined yield strength.

Structural changes in aircraft metals occurring as a result of service stressing.—It is well established that

marked structural changes which are conducive to short service life occur in certain soft alloys as a result of the stress conditions which occur in service. An investigation has been started to show whether or not highly stressed aircraft metals, particularly propeller materials, may be subject to similar detrimental structural changes. The work has been confined to the propeller aluminum alloy, 25S, with special emphasis on its behavior under fatigue stress.

X-ray study by reflection methods at an angle of grazing incidence of the same spot on the surface of a fatigue-test specimen as it is fatigue-stressed at successively higher maximum fibre stresses from 12,000 to 18,000 pounds per square inch has shown no significant changes in the reflection pattern.

A testing program on the aluminum-alloy propeller material is now under way to show to what extent, if any, fatigue-stressing may affect the other mechanical properties of the material. Special attention is being given to the possible effect of fatigue-stressing on the impact resistance of the material. Information on this point is urgently needed.

Certain microstructural features, "slip-plane precipitation" and "veining", observed in 25S which have aroused some suspicion as to origin and significance have been found in individual grains throughout most of the length of practically all the blades studied. These features are evidently not characteristic of areas of maximum service stresses. Their appearance is associated with heat-treatment procedure. Results have been obtained which indicate that this condition can be more readily revealed in material which has been fatigue-stressed than in the same material initially. However, the practical significance of this fact, if it has any, is not apparent as yet.

Results of a systematic study of the rate of "growth" of the heat-treated 25S alloy indicate that growth in the material continues long after the maximum hardness of the alloy has been attained, which fact may have some significance with respect to internal stresses in the finished material as it goes into service.

Aircraft metals at subzero temperatures.—A program of tests has been carried on during the year for obtaining information requested by the Bureau of Aeronautics on the common mechanical properties of aircraft structural metals at subnormal temperatures, approximately those which occur in service. These properties were determined at a series of temperatures ranging from room temperature to -78.5°C . (-109°F). Information has been obtained on stainless steel, 18-8, and on the same material "stabilized" by means of titanium and by columbium; on representative aluminum alloys, cast and wrought; magnesium alloys, cast and wrought; chromium-nickel alloy, "inconel" (Cr 15 percent, Fe 6 percent, Ni 79

percent); chromium-nickel-molybdenum steel (C 0.47 percent, Cr 1.04 percent, Ni 1.80 percent, Mo .22 percent); high-chromium steel (C 0.11 percent, Cr 16.3 percent, Ni 1.72 percent).

Practically all of the materials have shown an increase in the yield strength and ultimate strength at the lowered temperature with no change in the modulus of elasticity and only slight or insignificant decrease in the ductility. A very reassuring result of the tests to date on many of the materials is the fact that the impact resistance of notched specimens determined at the low temperature, -78.5°C ., is not materially different from the value obtained on the same material at room temperature. For a few of the materials, however, some decrease in this property was noted. A report summarizing the work is in preparation as a Research Paper of the National Bureau of Standards.

Propeller materials.—The steel used in welded hollow steel propellers is a chromium-vanadium steel (S. A. E. No. 6130) having an ultimate tensile strength in a heat-treated condition of 120,000 to 155,000 pounds per square inch. The endurance limit determined on specimens cut from blades was 60,000 to 72,000 pounds per square inch; on specimens cut from the blade so as to contain a portion of the welded seam, it may be considerably lower, possibly as much as 30,000 pounds per square inch.

Miscellaneous aircraft metals.—In cooperation with the Bureau of Aeronautics, study has been made of the localized corrosion of a pitting type on rods of cold-rolled 18-8 stainless steel after a few months' marine service. Occasional rod failures were found which were of the fatigue type and which had originated at a pit. Improper surface finish is believed to be an important factor in this unsatisfactory behavior of the material.

Experiments are under way to determine the optimum annealing treatment for relief of internal stress in cold-rolled stainless tie rods without entailing marked lowering of the strength and corrosion-resistance. Heating to 1000°F . may be necessary for this purpose.

At the request of the Bureau of Aeronautics, Navy Department, studies are being made of a number of selected steels in an attempt to obtain information on the significance of elongation and reduction of area values in tensile tests, apart from their use as indications of quality of the materials. Information is desired bearing on the significance of the fact that for some metals the values for elongation and reduction of area in a tensile test are required to be two or three times as great as in others. Ordinary tensile tests, tensile-impact, notched-bar impact, torsion-impact, and hardness tests, as well as studies of the microstructure, are being made on the steels in several con-

ditions of heat treatment. Extensometer measurements are made of the elongations to the moment of fracture and reductions of area are measured simultaneously with the extensions.

SUBCOMMITTEE ON STRUCTURAL LOADS AND METHODS OF STRUCTURAL ANALYSIS

LANGLEY MEMORIAL AERONAUTICAL LABORATORY

Applied Loads on Airplane Structures—Gust loads.—Statistical measurements of acceleration and air speed on transport airplanes in regular service have been continued on the land types and extended to include the large flying boats in the Pacific and Caribbean services. Records covering a total of over 16,000 airplane hours have been accumulated under a wide variety of conditions. With the exception of one case, in which a land transport flew through a line squall, the maximum gust velocities deduced from the records on the basis of the sharp-edge-gust assumption have not exceeded ± 35 feet per second. In the exception noted the maximum gust velocities were $+ 33$ feet per second and $- 47$ feet per second. In the case of the large flying boats, the maximum gust velocities have extended to the same limits, namely, ± 35 feet per second, as those measured on the land transports, notwithstanding the much smaller total quantity of data on the flying boats.

Gust research.—Measurements of gust intensities and gradients have been made with light airplanes close to the ground under stable atmospheric conditions with large wind gradients. Analysis of a large number of gusts indicates that under these conditions the gust gradient decreases with increasing gust intensity so that the stronger gusts (30 feet per second) reach their maximum intensities in a horizontal distance of about 100 feet. This relation, however, cannot be considered well established without further verification by more extensive data.

A number of altitude surveys indicate that, aside from the gustiness associated with large wind gradients near the ground, strong gusts are usually found only within clouds of the cumulus type. An exception has been noted, however, at an altitude of 14,000 feet, in which case strong turbulence was found well under an alto-cumulus cloud layer associated with the over-running of a polar air mass by the outer reaches of a distant tropical hurricane. The strong wind gradient that presumably existed at the turbulent level caused accelerations of the airplane that were nearly as great as those measured within cumulo-congestus clouds.

Acceleration Measurements on Racing Airplanes.—Acceleration measurements have been made on several racing airplanes in actual races to supplement data previously obtained. The results, which do not include accelerations higher than those previously reported, have been presented in Technical Note No. 556.

Load Distribution.—A number of wind-tunnel experiments have been made to determine the pressure distribution on wings with flaps. Most of these tests have been made to establish the section characteristics, including the division of load between flap and wing, and the flap hinge moment. Flaps investigated in this section of the program include the split, plain (with and without tab), external-airfoil, and Fowler types. (See Technical Report No. 574).

Pressure-distribution measurements have also been made in the 7- by 10-foot wind tunnel and in the full-scale wind tunnel to determine the span-load distribution on wings with partial-span flaps (Technical Report No. 571). The results have been examined in the light of airfoil theory, and it has been found that the Lotz method of calculating the span-load distribution gives a sufficiently good approximation for structural purposes provided a sufficient number of harmonics are retained. A simple set of computing forms for determining the distribution by the Lotz method has been devised. These forms permit the use of a sufficient number of harmonics to obtain good precision, and at the same time keep the computations within reasonable limits.

NATIONAL BUREAU OF STANDARDS

Inelastic Behavior of Duralumin and Alloy Steels in Tension and Compression.—Tests by the pack method to study the behavior of thin sheet material in compression have been continued. The results suggest that the data from tensile tests on specimens cut transverse to the direction of rolling are more closely correlated with the compressive tests of specimens cut in the direction of rolling than the results from tensile specimens cut parallel to the direction of rolling.

Tubes Under Loads Other Than Torsion.—Some thirty odd 17ST tubes of varying length and of diameter-thickness ratios ranging from 15 to 70 have been tested for modulus of rupture under third point loading. The results are being analyzed, and the indications are that the test values of the modulus of rupture can be approximated within ± 5 percent by the equations of surfaces in which the ratio of diameter to thickness and the ratio of slenderness are the independent variables.

The modulus of rupture of chromium-molybdenum steel tubing has been determined for tubing with diameter-thickness ratios varying from about 15 to 60 and with loads applied in such a way as not to deform the tubing locally. Tests have also been made in which the load is applied in such a way as to deform the tubing locally; but the scattering of results is too great to determine the effect on the modulus of rupture of this method of loading, without further tests.

It should be noted that the variation of modulus of rupture with length or ratio of slenderness is due solely to the method of applying the load. When the load is applied in such a way as not to deform the tube

at the point of application of the load, the modulus of rupture is always found to be independent of the length of the tube. When, however, in the case of thin tubes, the load is applied as through a compression member, local deformation is produced by the load, which tends to dent the specimen, and failure occurs at lower values of the modulus of rupture for short specimens than for long. Thick tubes are little, if at all, affected. This effect of the method of applying the load has been studied and moduli of rupture have been determined under a conservative method of applying load, a method as severe as any likely to be met in practice. It has been found, of course, that the modulus of rupture increases with decreasing diameter-thickness ratio.

Work is in progress to correlate the results obtained from the tests for modulus of rupture and column strength of 17ST aluminum alloy tubing with the previous tests of this tubing under combined axial and transverse loads. In this connection it has been found that the so-called "add-area" method of designing is safe but probably uneconomical. It is hoped to improve the economy without endangering the safety.

Tubes with Torsional Loads.—The analysis of torsion tests of 61 chromium-molybdenum steel tubes and 102 tubes of 17ST had shown that the strength of the aluminum-alloy tubes could be expressed conveniently as a function of their wall thickness, outside diameter, length, and ultimate strength in tension. In the case of chromium-molybdenum steel tubes with their much more variable mechanical properties a knowledge of the yield point in tension is required in addition.

A report of this work has been prepared. It concludes with two design charts, one for chromium-molybdenum steel tubes and the other for 17ST tubes, from which the strength of such tubes within the range of sizes of those tested may be estimated with a minimum amount of labor.

Flat Plates Under Normal Pressure.—The tests so far made have given an answer to the problem of the amount of washboarding to be expected in a given plate, provided the plate is of the same material (17ST, 18-8) as those tested and provided it is supported in the same manner at the edges (clamped edges, supported edges) and falls into the range of sizes of those tested. To extend these results to cover other materials and other edge conditions requires either an extensive series of tests covering all the materials and all the edge conditions in question, or else the discovery of a satisfactory theoretical or semitheoretical relationship for these variables.

A comparison of the experimental results was made with the known theories for the deformation of rectangular plates of medium thickness in the hope of discovering such a theoretical or semitheoretical relationship. Unfortunately, the comparison did not lead to

the desired results because of the incompleteness of the theory, on the one hand, and the difficulties of securing the theoretical edge conditions in actual plates on the other. It was finally decided to search for an explanation by making additional tests of circular plates with clamped edges and comparing the results of these tests with the relatively complete theory of circular plates of medium thickness proposed by Way in 1933.

A fixture for testing circular plates with clamped edges has been constructed for conducting these tests. A proof test of the fixture showed that it held the plate clamped firmly to a pressure of about 600 pounds per square inch. The center deflection and the permanent set at the center of these plates showed the same type of variation with pressure as that found for the rectangular plates. This supports the expectation that the results of the tests of circular plates may throw light on the behavior of rectangular plates.

Strength of Welded Joints in Tubular Members for Aircraft.—A detailed report of this investigation has been prepared and is now in process of publication.

This report supplements the work described in Technical Report No. 348, which had shown that the use of inserted gusset plates was the most satisfactory way of strengthening a joint. The additional tests of the present series show that joints of this type could be improved by cutting out the portion of the plate between the intersecting tubes.

T and lattice joints in thin-wall tubing 1.5 by 0.020 inch have somewhat lower strength than joints in tubing of greater wall thickness because of failure by local buckling. In welding the thin-wall tubing only the recently developed carburizing-flux process was found to produce joints free from cracks. The magnetic-powder inspection was used to detect cracks in the joints and flaws in the tubing.

Heat-treating the chromium molybdenum T, lattice, and butt joints materially increased the strength. Butt joints in chromium-molybdenum sheet and tubing made by low-carbon welds, chromium-molybdenum welds, and carburizing-flux welds had about the same strength in the "as welded" condition. When heat-treated the chromium-molybdenum and carburizing flux welds were the strongest.

A number of welded joints that had been tested in this investigation were sectioned at the welds and etched to compare the quality of the welds with that found in the sections of welded joints taken from two airplanes that had failed. The comparison showed a much more intimate bond and a more gradual transition in section for the welds made for this investigation than for those taken from the airplanes. This indicates that there is room for improvement in the welding technique used in assembling aircraft.

Strength of Riveted Joints in Aluminum Alloy.—The work done to date in connection with this project has

been summarized in a report which has been mimeographed for distribution to Government agencies and manufacturers interested in the design of rivet connections.

The report contains a full account of the data obtained on the relation of head dimensions to driving stress, for various types of heads. The relation of shank upsetting to type of head used and to the ratio of rivet diameter to sheet thickness was also determined and the effects of this upsetting on the shearing strength of joints are discussed quantitatively. The tensile strength of joints for several types of driven rivet head was determined. Radial deformation of the sheet during driving of the rivets was investigated and found unsuitable as a criterion of excessive sheet buckling.

The report concludes with a tentative program for future work on this project. The exact nature of this program will be decided on the basis of the comments received relative to the report.

Investigation of Fatigue Resistance of Fabricated Structural Elements of Aircraft.—A machine for determining the endurance of wing beams under longitudinally reversed stress was constructed. The stress is provided by resonant motion of two weights relative to each other, one attached to each end of a section of the beam. The weights were chosen to resonate at a frequency of about 60 cycles per second; their motion is maintained by means of a push-pull or reciprocating motor. The weights required are so heavy (about 800 pounds) compared to the weight of the beam (25 pounds) that all sections of the beam are subjected to practically the same longitudinal force.

The test to destruction of one wing beam has been completed with the aid of this machine. In tests at constant over-all strain amplitude with zero mean stress, the nominal stress amplitude dropped continuously from 8,650 to 8,280 pounds per square inch during the test while the resonant frequency dropped steadily from 54.8 to 53.65 cycles per second. Failure occurred after 452,000 cycles. Cracks had formed at several points scattered over the length of the specimen, all but one being in the web. The crack distribution showed that substantially uniform load conditions had prevailed throughout the length of the specimen, and that cracks were generated more often at open holes than at rivets.

A comparison of the stress history of the beam with the diagrams of stress against cycles to failure of similar material indicated that failure should have occurred at the time it did if the stress concentration at the points of origin of the cracks was of the order of 3.

Beams and Stressed-Skin Research.—Compression tests have been completed on two sheet-stringer specimens submitted by the Bureau of Aeronautics of the Navy

Department to obtain a comparison with the strain distribution and the ultimate strength of similar sheet-stringer specimens tested at the Navy Model Basin.

The strain distribution was obtained from readings of twelve pairs of Tuckerman optical strain gages attached to various portions of the sheet and the stringers. The shape of the buckles was recorded by plaster casts. The progression of failure was followed by a large number of pointers attached to each stringer to indicate the amount of buckling and of twisting.

An analysis of the measured strains for one of the specimens showed that the median fiber strain in the center between stringers became a tensile strain under high compressive loads. This agrees with the paradoxical result predicted by Timoshenko for the stress distribution in square plates after buckling. Timoshenko's theory has been extended to include rectangular plates in order to apply it to the present case.

The comparison of the observed stringer loads with those calculated from Timoshenko's theory, extended to rectangular plates, leads to a fair agreement up to loads within about 20 percent of the ultimate load. The theory also predicts the strain distribution accurately and may, therefore, be taken as a good first approximation in the design of sheet-stringer combinations of the type tested and under conditions approaching those of the test.

Propeller Vibration.—A theoretical analysis of the effect of centrifugal force on the stress distribution and frequency of propeller blades vibrating with the fundamental mode in bending and second harmonic mode in bending (with one node near the tip) has been completed. The analysis shows that the stress per unit tip deflection changes only 10 to 20 percent at speeds of rotation around 1,700 r. p. m. It seems, therefore, that the ordinary engineering procedure of taking the extreme fiber stress at any point in a vibrating blade as the sum of the centrifugal stress and the bending stress for no rotation is adequate. The effect of rotation on frequency can be predicted conveniently from Lord Rayleigh's energy method provided the deflection curve for no rotation is known. The values so obtained agree satisfactorily with the more exact theoretical values and also with the values observed by Theodorsen at Langley Field on a particular type of propeller.

The above analysis rests on the assumption that the propeller blade bends like a simple beam when it vibrates with one of its modes in bending. This assumption was checked for the extreme case of a solid steel propeller blade whose section was so curved in shape that its neutral axis lay outside the blade near the center. The ratio of measured strain amplitudes for pairs of points on opposite sides of this blade were found to be nearly equal to the ratio of extreme fiber distances as given by the simple-beam theory.

Airplane Vibrations.—In the investigation of a case of undesirable vibrations in an airplane, it was found that air impulses from a two-blade propeller with a frequency of about 3,200 per minute excited resonant vibrations in the wings with a frequency of about 1,600 cycles per minute and these in turn excited resonant vibrations in the tail assembly with a frequency of about 800 cycles per minute. The natural frequencies of the wing and tail differed enough from the ratio 2:1 to produce strong beats by the interchange of energy between wing and tail. It was concluded that the vibration was a case of double submultiple resonance.

No direct reference was found to this phenomenon in the engineering literature, but it seems probable that submultiple resonance has been the unrecognized cause of a number of baffling cases of undue vibration in engineering structures.

A review of the literature on submultiple resonance has disclosed several interesting characteristics distinguishing it from ordinary resonance. Submultiple resonance requires either a modulation of the exciting force by the excited motion, or a marked deviation from the proportionality between load and deflection assumed in ordinary vibration problems; the amplitude of the resonant motion is not proportional to that of the exciting force; a finite initial impulse is required to start the vibration. A mechanical model has been constructed which demonstrates the characteristics of this type of resonance.

SUBCOMMITTEE ON RESEARCH PROGRAM ON MONOCOQUE DESIGN

Research on stressed-skin or monocoque structures for aircraft is in reality research in elasticity, structures, and strength of materials. The results of the research conducted under the supervision of this subcommittee, therefore, have broad applications in other fields besides aeronautics. Conversely, the results of much of the research conducted on these subjects in fields other than aeronautics have aeronautical applications. The objective of each research undertaken by the Committee is to obtain results that can be used directly in analysis or design.

Elastic axis of shell wings.—A report on the elastic axis of shell wings has been prepared and published as Technical Note No. 562. In the report the definitions of flexural center, torsional center, elastic center, and elastic axis are discussed. The calculation of elastic centers is also dealt with in principle and a suggestion is made for the design of shear webs.

Strain measurements on box beams in bending.—Strain-gage measurements were made on a number of small-size rectangular box beams subjected to bending. The main conclusion is that there is an inevitable scattering of test results in such structures and that this scat-

tering is sufficient to overshadow the effect of varying sheet thickness or bulkhead spacing within wide limits.

Although measurements were made chiefly on the tension side, some measurements were made on the compression side. One conclusion drawn from the latter tests is that the von Kármán formula for effective width gives very conservative values unless the yield point is approached.

Strength of stiffeners.—For several years a general study of the compressive strength of stiffeners used in stressed-skin structures has been in progress. This study is, in effect, a study of the strength of columns formed of thin metal. This year the study has resulted in the preparation of a report dealing with a theory for primary failure in straight centrally loaded columns, which is in the process of publication.

When a skin-stiffener combination fails by deflection normal to the skin, the accepted column curve for the material is applicable. When failure occurs by deflection of the outstanding portion of the stiffener in a direction parallel to the skin, however, there is a combined action of bending and twisting in the stiffener that requires for its solution a more general theory for primary failure in columns than has been available heretofore. "Primary failure", as here used, is any type of column failure in which the cross sections are displaced, rotated, or both displaced and rotated but not distorted. In keeping with this definition of primary failure, any failure in which the cross sections are distorted but not displaced or rotated is designated "local failure."

Wagner and Pretschner (see Technical Memorandum No. 784) present a theory for torsion-bending failure of open-section columns formed of thin metal when the cross sections rotate about an axis which is parallel to the column and passes through the center of twist for the section. When the column is attached to the skin of a stressed-skin structure, the stiffness of the skin in its own plane and the anchorage of the skin at the sides of the panel force the axis of rotation to lie in the plane of the skin. Consequently, for the solution of the skin-stiffener problem the Wagner-Pretschner theory was extended to include rotation of the cross sections about axes other than the one passing through the center of twist. The extended theory includes both Euler bending and the Wagner-Pretschner theory for twisting failure as special cases.

In the report mentioned above consideration is given only to primary failure and the application of the theory to a column of I section is given in detail. Its application to a number of other sections more commonly used as stiffeners in stressed-skin structures is now in progress. In addition to the study of primary failure, progress is also being made in the study of local failure in columns, but no reports have as yet been prepared.

Cross method of moment distribution.—A report on convergence of the Cross method of moment distribution is nearing completion. In this report it is shown how simple criterions can be derived by the methods of moment distribution to check the stability of compression members in rigid joint structures. These same criterions can also be used to determine the fixity coefficient for stiffeners in stressed-skin structures.

Compressive strength of corrugated sheet.—A report on the strength of corrugated sheet is being prepared in cooperation with Professor A. S. Niles of Stanford University.

SUBCOMMITTEE ON MISCELLANEOUS MATERIALS AND ACCESSORIES

The problems under the cognizance of the Subcommittee on Miscellaneous Materials and Accessories during the past year, which are being investigated by the National Bureau of Standards, concern the development of a flexible substitute for glass and the development of substitutes for linen webbing and silk shroud lines for parachutes. Consideration has also been given to the possibilities of plastics as a material for aircraft structures.

Development of flexible substitute for glass.—Commercial and experimental transparent plastics which have been investigated to determine their suitability for aircraft windshields and windows include acetate, nitrate, ethylcellulose and cellulose-acetobutyrate materials, and the acrylate and vinyl resins. Tests were made to determine their resistance to water and organic solvents; their dimensional stability on aging; and the effect of outside exposure on light transmission, haze, and general appearance.

During the latter part of the year, however, the importance of the impact resistance of a windshield which would withstand collision with relatively large hailstones and wild birds became apparent. Attention was accordingly directed to this phase of the problem, and the possibility of using laminated glass and plastic, as well as plastic alone, was given consideration. Im-

pact tests have been made both with the Charpy apparatus and by using falling weights. The results to date indicate that cellulose nitrate, cellulose acetate, ethylcellulose, and vinyl acetal materials are the strongest, while the polyvinyl-chloride, acetate, and acrylate resins are relatively weak.

Substitute for linen webbing.—At the suggestion of the military services, cotton manufacturers have been contacted to ascertain the possibility of making an all-cotton webbing to have the same properties as that now made from imported flax. The opinions are encouraging. It seems that certain mill experiments must be carried out to find out just how such a webbing should be made, but there is little doubt of the ability to do so. One mill has indicated its willingness to make the experiments provided that there is a sufficient potential market for the material. Data on this point are now being collected.

Substitute for silk shroud line.—The question of finding a domestic substitute for the imported silk now used in shroud lines has been under consideration. Inquiries have revealed that two manufacturers are willing to undertake the necessary experimental work. One plans to use Cordura rayon, the other American cotton. These experiments are now under way.

Development of plastic material for aircraft structures.—Consideration has been given to the compilation of information regarding the strength properties of plastics and reinforced plastics, with a view to their use as structural members. It is apparent that the collection of this information is in itself a large task, but it is necessary as a basis for planning any investigation of the subject. After a thorough review of the literature on the subject and contact with the manufacturers of plastics, a tabulation of the physical properties and weathering characteristics of laminated plastics will be made. Other points that will be determined are the uniformity of the material, the adhesion and corrosion between the plastic and the reinforcing metal, fabrication facilities, and relative cost as compared to other aircraft structural materials.

PART II

ORGANIZATION AND GENERAL ACTIVITIES

ORGANIZATION

The National Advisory Committee for Aeronautics was established by act of Congress approved March 3, 1915 (U. S. Code, title 50, sec. 151). The Committee is composed of fifteen members appointed by the President and serving as such without compensation. The law provides that the members shall include two representatives each from the War and Navy Departments and one each from the Smithsonian Institution, the Weather Bureau, and the National Bureau of Standards, together with not more than eight additional persons "who shall be acquainted with the needs of aeronautical science, either civil or military, or skilled in aeronautical engineering or its allied sciences." One of these eight is a representative of the Bureau of Air Commerce of the Department of Commerce. Under the rules and regulations governing the work of the Committee as approved by the President the Chairman and Vice Chairman of the Committee are elected annually. At the meeting held on October 22, 1936, Dr. Joseph S. Ames was reelected Chairman for the ensuing year and Dr. David W. Taylor was reelected Vice Chairman.

During the past year there were three changes in the membership of the main Committee, as follows:

Major General Oscar Westover, Chief of the Air Corps, United States Army, who had succeeded Major General Benjamin D. Foulois, Air Corps, United States Army, in that post on the latter's retirement from active duty, was appointed by the President a member of the National Advisory Committee for Aeronautics on January 25, 1936, to succeed General Foulois on this Committee.

Rear Admiral Arthur B. Cook, United States Navy, who had succeeded Rear Admiral Ernest J. King, United States Navy, as Chief of the Bureau of Aeronautics, Navy Department, was appointed by the President a member of the National Advisory Committee for Aeronautics on June 16, 1936, to succeed Admiral King on this Committee.

Captain Sydney M. Kraus, United States Navy, who had succeeded Commander Ralph D. Weyerbacher, United States Navy, as head of the material branch of the Bureau of Aeronautics, Navy Department, was appointed by the President a member of the National

Advisory Committee for Aeronautics on June 17, 1936, to succeed Commander Weyerbacher on this Committee.

The executive offices of the Committee, including its offices of aeronautical intelligence and aeronautical inventions, are located in the Navy Building, Washington, D. C., in close proximity to the air organizations of the Army and Navy.

The office of aeronautical intelligence was established in the early part of 1918 as an integral branch of the Committee's activities. Scientific and technical data on aeronautics secured from all parts of the world are classified, catalogued, and disseminated by this office.

To assist in the collection of current scientific and technical information and data, the Committee maintains a technical assistant in Europe with headquarters at the American Embassy in Paris.

CONSIDERATION OF AERONAUTICAL INVENTIONS

By act of Congress approved July 2, 1926, an Aeronautical Patents and Design Board was established consisting of Assistant Secretaries of the Departments of War, Navy, and Commerce. In accordance with that act as amended by the act approved March 3, 1927, the National Advisory Committee for Aeronautics passes upon the merits of aeronautical inventions and designs submitted to any aeronautical division of the Government, and submits reports thereon to the Aeronautical Patents and Design Board. That board is authorized, upon the favorable recommendation of the Committee, to "determine whether the use of the design by the Government is desirable or necessary and evaluate the design and fix its worth to the United States in an amount not to exceed \$75,000."

During the past year the inventions section received for consideration 2,049 new submissions. It conducted the necessary correspondence and granted interviews as requested by the inventors. Approximately twelve percent of the new submissions were received through the Aeronautical Patents and Design Board. In those cases reports on the merits of the submissions were made to that board, and in all other cases replies were submitted directly to the inventors.

ANALYSIS OF AIRCRAFT ACCIDENTS

During the past year the Committee on Aircraft Accidents has completed a revision of the report on the standard method for the analysis of aircraft accidents, and the revised report has been published as Technical Report No. 576, superseding the previous report, No. 357.

The Committee on Aircraft Accidents includes in its membership representatives of the air organizations of the War, Navy, and Commerce Departments, and the method of analysis and classification of aircraft accidents prepared by this Committee and revised from time to time has been followed for the past several years by these three departments in their study of accidents under their jurisdiction. The standard method includes provision for the classification of accidents according to their nature and according to their results, and a chart, together with explanatory definitions, for their analysis according to both immediate and underlying causes. The practical value of the method and the importance of the information which may be obtained by its use have been clearly demonstrated in its application in service in the three departments.

The revised report includes modifications in definitions and nomenclature introduced to answer questions of interpretation and provide against certain inadequacies of classification which had been encountered as a result of the recent rapid advances in aeronautics. These modifications, however, are in general conformity with the classifications previously established.

AERONAUTICAL RESEARCH IN EDUCATIONAL INSTITUTIONS

The recommendations of the Federal Aviation Commission on the subject of aeronautical research in educational institutions were put into effect by this Committee with the appropriation by Congress of \$25,000 for this purpose carried in the Second Deficiency Act approved August 12, 1935. Contracts for special reports requiring original research in aeronautics have been made by this Committee with eight educational institutions at a total cost of \$23,942.50.

COOPERATION WITH THE AIRCRAFT INDUSTRY

In formulating its program of research the Committee makes provision for the study of those problems that are of particular interest and importance to commercial aeronautics, both in design and operation. The problems of aircraft manufacturers and operators are frequently being presented to the Committee in correspondence and by personal contacts and informal conferences, and by these means the Committee is kept in continuous touch with the research needs of the aircraft industry. The Committee takes advantage of

every opportunity which is afforded to obtain the comments and suggestions of the industry in connection with its research programs.

Every effort is made to place in the hands of the industry as promptly as possible the results of researches which are of particular value to commercial aeronautics. When in the course of an investigation it appears that the results so far obtained will be of special interest and importance to the industry prior to the preparation of a formal report for publication, the Committee issues the data in advance form to American manufacturers and to the Government services for their confidential information. Some of the important subjects on which information has been made available to American manufacturers in this form during the past year are the new N. A. C. A. nose-type cowling, the cooling of airplane engines on the ground, the relative efficiencies and design characteristics of various engine-propeller combinations, corrections for scale effect for the application of airfoil section data from the variable-density wind tunnel, airfoil-section characteristics in relation to air forces and their distribution on airplane wings, and the wing-fuselage interference of twenty-eight combinations as determined in the variable-density wind tunnel.

Conferences With Aircraft Operators.—As previously stated, a Special Subcommittee on Aerodynamic Problems of Transport Construction and Operation was organized during the past year under the Committee on Aerodynamics. This subcommittee was established on recommendation of the Aerodynamics Committee with a view to determining the problems of particular importance in connection with transport operation which should be investigated by the National Advisory Committee. In conjunction with the establishment of this subcommittee a special conference of airplane pilots was held to discuss the handling characteristics and piloting technique of large transport airplanes.

The membership of both the special subcommittee and the pilots' conference included representatives of the principal commercial aircraft operating agencies in this country, namely the Air Transport Association of America, American Airlines, Eastern Air Lines, Northwest Air Lines, Pan American Airways, Transcontinental and Western Air, and United Air Lines; and representatives of the Army Air Corps, the Bureau of Aeronautics of the Navy, the Bureau of Air Commerce, and the National Advisory Committee for Aeronautics. In addition, the special subcommittee included representation of the United States Weather Bureau, and the pilots' conference was attended by representatives of the two principal manufacturers of large commercial flying boats, as well as by well-known individual pilots. Honorable Edward P. Warner, a member of the National Advisory Committee for Aero-

nautics and Chairman of the Committee on Aerodynamics, served as chairman both of the special subcommittee and of the pilots' conference.

The Special Subcommittee on Aerodynamic Problems of Transport Construction and Operation met on March 17, 1936, at the Committee's headquarters in Washington. The following problems, many of which are not within the scope of the functions of the National Advisory Committee, were presented by the transport operators at this meeting as of particular interest and importance:

1. Ice formation including the aerodynamic effect on wings and control surfaces, the aerodynamic effect of de-icers, and the elimination of ice in carburetors.
2. Instrument landing—development and installation of equipment.
3. Problems of high altitude flying.
4. Snow static in connection with radio.
5. Improved cowling providing better engine cooling.
6. Means of avoiding collisions in the air over crowded airports.
7. Development of alternate current source of electrical energy for various uses.
8. Increased propeller efficiency and proper location of propellers.

Each of these problems was discussed and the present status of development outlined by the representatives of the various agencies engaged in such development. In connection with problems 5 and 8, the work conducted by the National Advisory Committee and the program planned for the future were described briefly.

The conference of airplane pilots was held on March 16, 1936. Among the problems discussed at this conference were the effect of flaps on airplane performance; the effect of rough air on transport operation; the desirability of the establishment of a criterion for the proper control and stability characteristics of airplanes; handling problems such as crosswind landings, ground-looping tendencies, and lateral control in taxiing; the effect of ice formation, particularly on windshields; hull-bottom pressures on flying boats; and piloting technique in the landing of large flying boats in rough waves.

Annual Research Conference.—An important means of keeping the Committee in close contact with the needs of the aircraft industry is the annual aircraft engineering research conference held at the Committee's laboratories each May. This conference, which was initiated in 1926, has two principal purposes: first, to enable representatives of the industry to obtain first-hand information on the Committee's research facilities and the results obtained in its investigations; and second, to afford them an opportunity to present to the Committee their suggestions for investigations to be included in the Committee's research program.

Owing to the large number of those who desired to attend, the conference this year was for the first time

held in two sections. Section A, which was held on May 20, 1936, included in general the representatives of aircraft manufacturers and operators and Government officials. Section B, held on May 22, included the personnel of governmental agencies using aircraft, representatives of engineering societies, and members of the faculties of professional schools, as well as representatives of manufacturers and operators who were unable to attend Section A.

In the absence of the Chairman of the conference, Dr. Joseph S. Ames, who was prevented by illness from attending, Honorable William P. MacCracken, a member of the National Advisory Committee and Chairman of its Committee on Power Plants for Aircraft, presided over Section A, and Dr. Lyman J. Briggs, also a member of the Advisory Committee and Chairman of the Committee on Aircraft Structures and Materials, presided over Section B. At Section A the Committee was represented by its officers, members of the main Committee, and members of the Committees on Aerodynamics and Power Plants for Aircraft. Section B was attended by the officers of the Committee and by members of the Committee on Aircraft Structures and Materials and of the Subcommittee on Structural Loads and Methods of Structural Analysis.

At the morning session of both sections, the principal investigations under way at the laboratory, both in aerodynamics and power plants, were explained by the engineers in charge of the work, and charts were exhibited showing some of the results obtained. The guests were then conducted on a tour of inspection of the laboratory, and the research equipment was shown in operation.

In the afternoon, seven simultaneous conferences were held for the discussion of seven different subjects, namely, flying and handling characteristics, aerodynamic efficiency and interference, aerodynamic consideration of cowling and cooling, power plant consideration of cowling and cooling, aircraft-engine research, seaplanes, and autogiros. At these conferences the results of the Committee's researches were presented in further detail, and suggestions were submitted by the representatives of the industry for problems to be added to the Committee's program. These suggestions were referred to the Committee on Aerodynamics and the Committee on Power Plants for Aircraft and were considered by them in their preparation of the Committee's research program.

SUBCOMMITTEES

The Advisory Committee has organized three main standing technical committees, with subcommittees, for the purpose of supervising its work in their respective fields. The three main technical Committees

on Aerodynamics, Power Plants for Aircraft, and Aircraft Structures and Materials and their subcommittees supervise and direct the aeronautical research conducted by the Advisory Committee and coordinate the investigations conducted by other agencies.

During the past year the Subcommittee on Methods and Devices for Testing Aircraft Materials and Structures, which was a subcommittee of the Committee on Aircraft Structures and Materials, was discharged, as it was considered that the purpose for which the subcommittee had been organized had been served for all practical needs by special reports which had been prepared by the subcommittee for the Government agencies interested, and that any future work on the subject of methods and devices for the testing of aircraft materials and structures could be conducted under the direction of the Subcommittee on Structural Loads and Methods of Structural Analysis.

As previously stated, in accordance with the Committee's policy of establishing special subcommittees for the study of particular problems as they arise, two special technical subcommittees were organized during the past year under the Committee on Aerodynamics, namely, a Special Subcommittee on Aerodynamic Problems of Transport Construction and Operation, and a Special Subcommittee on Vibration and Flutter.

The work of the standing technical committees and subcommittees and of the Special Subcommittee on Vibration and Flutter have been described in part I. The activities of the Special Subcommittee on Aerodynamic Problems of Transport Construction and Operation have been outlined in part II under the heading "Cooperation with the Aircraft Industry."

The organization of the committees and of the standing and special subcommittees is as follows:

COMMITTEE ON AERODYNAMICS

Hon. Edward P. Warner, Chairman.

Dr. George W. Lewis, National Advisory Committee for Aeronautics, Vice Chairman.

Maj. H. Z. Bogert, Air Corps, United States Army, Matériel Division, Wright Field.

Dr. L. J. Briggs, National Bureau of Standards.

Theophile dePort, Matériel Division, Army Air Corps, Wright Field.

Lt. Comdr. W. S. Diehl (C. C.), United States Navy.

Dr. H. L. Dryden, National Bureau of Standards.

Lt. Col. O. P. Echols, Air Corps, United States Army, Matériel Division, Wright Field.

Richard C. Gazley, Bureau of Air Commerce, Department of Commerce.

Hon. Willis Ray Gregg, United States Weather Bureau.

Lawrence V. Kerber, Bureau of Air Commerce, Department of Commerce.

Lt. Comdr. R. D. MacCart (C. C.), United States Navy, Naval Aircraft Factory.

Commander A. C. Miles (C. C.), United States Navy.

Elton W. Miller, National Advisory Committee for Aeronautics.

Dr. David W. Taylor.

Dr. A. F. Zahm, Division of Aeronautics, Library of Congress.

SUBCOMMITTEE ON AIRSHIPS

Hon. Edward P. Warner, Chairman.

Starr Truscott, National Advisory Committee for Aeronautics, Vice Chairman.

Dr. Karl Arnstein, Goodyear-Zeppelin Corporation.

Maj. H. Z. Bogert, Air Corps, United States Army, Matériel Division, Wright Field.

Commander Garland Fulton (C. C.), United States Navy.

Dr. George W. Lewis, National Advisory Committee for Aeronautics (ex officio member).

Ralph H. Upson, Ann Arbor, Mich.

SUBCOMMITTEE ON METEOROLOGICAL PROBLEMS

Hon. Willis Ray Gregg, United States Weather Bureau, Chairman.

Dr. W. J. Humphreys, United States Weather Bureau.

Dr. J. C. Hunsaker, Massachusetts Institute of Technology.

Dr. George W. Lewis, National Advisory Committee for Aeronautics (ex officio member).

Delbert M. Little, United States Weather Bureau.

Dr. Charles F. Marvin.

Lt. Comdr. F. W. Reichelderfer, United States Navy, Naval Air Station, Lakehurst.

Dr. C. G. Rossby, Massachusetts Institute of Technology.

Capt. B. J. Sherry, United States Army, Signal Corps, War Department.

Eugene Sibley, Bureau of Air Commerce, Department of Commerce.

SUBCOMMITTEE ON SEAPLANES

Capt. H. C. Richardson (C. C.), United States Navy, Chairman.

Maj. H. Z. Bogert, Air Corps, United States Army, Matériel Division, Wright Field.

Theophile dePort, Matériel Division, Army Air Corps, Wright Field.

Lt. Comdr. W. S. Diehl (C. C.), United States Navy.

Richard C. Gazley, Bureau of Air Commerce, Department of Commerce.

J. T. Gray, Bureau of Air Commerce, Department of Commerce.

Dr. George W. Lewis, National Advisory Committee for Aeronautics (ex officio member).

Lt. Comdr. A. O. Rule, United States Navy.

Starr Truscott, National Advisory Committee for Aeronautics.

SPECIAL SUBCOMMITTEE ON AERODYNAMIC PROBLEMS OF TRANSPORT CONSTRUCTION AND OPERATION

Hon. Edward P. Warner, Chairman.

E. T. Allen, New York City.

Paul Collins, Boston and Maine Airways.

D. B. Colyer, United Air Lines.

Smith J. DeFrance, National Advisory Committee for Aeronautics.

Lt. Col. O. P. Echols, Air Corps, United States Army, Matériel Division, Wright Field.

Col. E. S. Gorrell, Air Transport Association of America.

Croll Hunter, Northwest Airlines.

L. V. Kerber, Bureau of Air Commerce, Department of Commerce.

Dr. George W. Lewis, National Advisory Committee for Aeronautics (ex officio member).

D. M. Little, United States Weather Bureau.

William Littlewood, American Airlines.

Commander A. C. Miles (C. C.), United States Navy.

A. A. Priester, Pan American Airways.

Richard V. Rhode, National Advisory Committee for Aeronautics.

Paul Richter, Transcontinental and Western Air.

Capt. E. V. Rickenbacker, Eastern Air Lines.

Maj. R. W. Schroeder, Bureau of Air Commerce, Department of Commerce.

Wesley L. Smith, Cranford, New Jersey.

Fred E. Weick, National Advisory Committee for Aeronautics.

SPECIAL SUBCOMMITTEE ON VIBRATION AND FLUTTER

Henry J. E. Reid, National Advisory Committee for Aeronautics, Chairman.

Lt. Comdr. W. S. Diehl (C. C.), United States Navy.

C. H. Helms, National Advisory Committee for Aeronautics.

Capt. P. H. Kemmer, Air Corps, United States Army, Matériel Division, Wright Field.

Dr. George W. Lewis, National Advisory Committee for Aeronautics (ex officio member).

Lt. Comdr. R. D. MacCart (C. C.), United States Navy, Naval Aircraft Factory.

Dr. Walter Ramberg, National Bureau of Standards.

F. R. Shanley, Bureau of Air Commerce, Department of Commerce.

Capt. T. A. Sims, Jr., Air Corps, United States Army, Matériel Division, Wright Field.

Dr. Theodore Theodorsen, National Advisory Committee for Aeronautics.

COMMITTEE ON POWER PLANTS FOR AIRCRAFT

Hon. William P. MacCracken, Jr., Chairman.

Dr. George W. Lewis, National Advisory Committee for Aeronautics, Vice Chairman.

Dr. H. C. Dickinson, National Bureau of Standards.

John H. Geisse, Bureau of Air Commerce, Department of Commerce.

Carlton Kemper, National Advisory Committee for Aeronautics.

Lt. Comdr. T. C. Lonnquest, United States Navy.

Gaylord W. Newton, Bureau of Air Commerce, Department of Commerce.

Maj. E. R. Page, Air Corps, United States Army, Matériel Division, Wright Field.

Prof. C. Fayette Taylor, Massachusetts Institute of Technology.

SUBCOMMITTEE ON AIRCRAFT FUELS AND LUBRICANTS

Dr. H. C. Dickinson, National Bureau of Standards, Chairman.

Dr. O. C. Bridgeman, National Bureau of Standards.

H. K. Cummings, National Bureau of Standards.

Lt. C. E. Ekstrom, United States Navy.

L. S. Hobbs, The Pratt & Whitney Aircraft Company.

Capt. F. D. Klein, Air Corps, United States Army, Matériel Division, Wright Field.

Dr. George W. Lewis, National Advisory Committee for Aeronautics (ex officio member).

Lt. Comdr. T. C. Lonnquest, United States Navy.

Gaylord W. Newton, Bureau of Air Commerce, Department of Commerce.

Arthur Nutt, Wright Aeronautical Corporation.

Maj. E. R. Page, Air Corps, United States Army, Matériel Division, Wright Field.

Addison M. Rothrock, National Advisory Committee for Aeronautics.

COMMITTEE ON AIRCRAFT STRUCTURES AND MATERIALS

Dr. L. J. Briggs, National Bureau of Standards, Chairman.
Prof. H. L. Whittemore, National Bureau of Standards, Vice Chairman.

Maj. H. Z. Bogert, Air Corps, United States Army, Matériel Division, Wright Field.

S. K. Colby, Aluminum Co. of America.

Lt. C. F. Cotton (C. C.), United States Navy.

Warren E. Emley, National Bureau of Standards.

Commander Garland Fulton (C. C.), United States Navy.

Richard C. Gazley, Bureau of Air Commerce, Department of Commerce.

J. T. Gray, Bureau of Air Commerce, Department of Commerce.

C. H. Helms, National Advisory Committee for Aeronautics.

Dr. Zay Jeffries, American Magnesium Corporation.

J. B. Johnson, Matériel Division, Army Air Corps, Wright Field.

Dr. George W. Lewis, National Advisory Committee for Aeronautics (ex officio member).

H. S. Rawdon, National Bureau of Standards.

E. C. Smith, Republic Steel Corporation.

Starr Truscott, National Advisory Committee for Aeronautics.

Hon. Edward P. Warner.

SUBCOMMITTEE ON METALS USED IN AIRCRAFT

H. S. Rawdon, National Bureau of Standards, Chairman.

Commander Garland Fulton (C. C.), United States Navy.

Dr. Zay Jeffries, American Magnesium Corporation.

J. B. Johnson, Matériel Division, Army Air Corps, Wright Field.

Dr. George W. Lewis, National Advisory Committee for Aeronautics (ex officio member).

E. C. Smith, Republic Steel Corporation.

John Vitol, Bureau of Air Commerce, Department of Commerce.

Prof. H. L. Whittemore, National Bureau of Standards.

SUBCOMMITTEE ON STRUCTURAL LOADS AND METHODS OF STRUCTURAL ANALYSIS

Starr Truscott, National Advisory Committee for Aeronautics, Chairman.

M. P. Crews, Bureau of Air Commerce, Department of Commerce.

Richard C. Gazley, Bureau of Air Commerce, Department of Commerce.

Lt. Comdr. L. M. Grant (C. C.), United States Navy.

Maj. C. F. Greene, Air Corps, United States Army, Matériel Division, Wright Field.

Capt. P. H. Kemmer, Air Corps, United States Army, Matériel Division, Wright Field.

Dr. George W. Lewis, National Advisory Committee for Aeronautics (ex officio member).

Lt. Comdr. R. D. MacCart (C. C.), United States Navy, Naval Aircraft Factory.

Prof. J. S. Newell, Massachusetts Institute of Technology.

Lt. Comdr. H. R. Oster (C. C.), United States Navy, Naval Aircraft Factory.

Henry J. E. Reid, National Advisory Committee for Aeronautics.

Richard V. Rhode, National Advisory Committee for Aeronautics.

Dr. L. B. Tuckerman, National Bureau of Standards.

SUBCOMMITTEE ON RESEARCH PROGRAM ON MONOCOQUE DESIGN

Dr. George W. Lewis, National Advisory Committee for Aeronautics, Chairman.

Richard C. Gazley, Bureau of Air Commerce, Department of Commerce.

Lt. Comdr. L. M. Grant (C. C.), United States Navy.

Maj. C. F. Greene, Air Corps, United States Army, Matériel Division, Wright Field.

Capt. P. H. Kemmer, Air Corps, United States Army, Matériel Division, Wright Field.

Eugene E. Lundquist, National Advisory Committee for Aeronautics.

Lt. Comdr. R. D. MacCart (C. C.), United States Navy, Naval Aircraft Factory.

F. R. Shanley, Bureau of Air Commerce, Department of Commerce.

Dr. L. B. Tuckerman, National Bureau of Standards.

SUBCOMMITTEE ON MISCELLANEOUS MATERIALS AND ACCESSORIES

Warren E. Emley, National Bureau of Standards, Chairman.
C. J. Cleary, Matériel Division, Army Air Corps, Wright Field.

John Easton, Bureau of Air Commerce, Department of Commerce.

C. H. Helms, National Advisory Committee for Aeronautics.

Dr. George W. Lewis, National Advisory Committee for Aeronautics (ex officio member).

J. E. Sullivan, Bureau of Aeronautics, Navy Department.

G. W. Trayer, Forest Service, Department of Agriculture.

P. H. Walker, National Bureau of Standards.

COMMITTEE ON AIRCRAFT ACCIDENTS

Hon. Edward P. Warner, Chairman.

Lieut. J. F. Greenslade, United States Navy.

Maj. E. V. Harbeck, Jr., Air Corps, United States Army.

J. W. Laukford, Bureau of Air Commerce, Department of Commerce.

Dr. George W. Lewis, National Advisory Committee for Aeronautics.

Lt. Comdr. A. O. Rule, United States Navy.

J. T. Shumate, Bureau of Air Commerce, Department of Commerce.

Maj. Lowell H. Smith, Air Corps, United States Army.

COMMITTEE ON AERONAUTICAL INVENTIONS AND DESIGNS

Dr. L. J. Briggs, National Bureau of Standards, Chairman.

Hon. Willis Ray Gregg, United States Weather Bureau.

Capt. S. M. Kraus, United States Navy.

Brig. Gen. A. W. Robins, Air Corps, United States Army, Matériel Division, Wright Field.

Dr. David W. Taylor.

John F. Victory, Secretary.

COMMITTEE ON PUBLICATIONS AND INTELLIGENCE

Dr. Joseph S. Ames, Chairman.

Hon. Willis Ray Gregg, United States Weather Bureau, Vice Chairman.

Miss M. M. Muller, Secretary.

COMMITTEE ON PERSONNEL, BUILDINGS, AND EQUIPMENT

Dr. Joseph S. Ames, Chairman.

Dr. David W. Taylor, Vice Chairman.

John F. Victory, Secretary.

TECHNICAL PUBLICATIONS OF THE COMMITTEE

The Committee has four series of publications, namely technical reports, technical notes, technical memorandums, and aircraft circulars.

The technical reports present the results of fundamental research in aeronautics. The technical notes are mimeographed and present the results of short research investigations and the results of studies of specific detail problems which form parts of long investigations. The technical memorandums are mimeographed and contain translations and reproductions of important foreign aeronautical articles. The aircraft circulars are mimeographed and contain descriptions of new types of foreign aircraft.

The Committee issued during the past year a bibliography of aeronautics for the year 1932. It had previously issued bibliographies for the years since 1909. All issues of the Bibliography of Aeronautics to date were prepared by Paul Brockett.

The following are lists of the publications issued:

LIST OF TECHNICAL REPORTS ISSUED DURING THE PAST YEAR

- | | |
|------|--|
| No. | |
| 542. | Potential Flow About Arbitrary Biplane Wing Sections. By I. E. Garrick, N. A. C. A. |
| 543. | Tank Tests of N. A. C. A. Model 40 Series of Hulls for Small Flying Boats and Amphibians. By John B. Parkinson and John R. Dawson, N. A. C. A. |
| 544. | Combustion in a Bomb with a Fuel-Injection System. By Mildred Cohn and Robert C. Spencer, N. A. C. A. |
| 545. | Effects of Air-Fuel Ratio on Fuel Spray and Flame Formation in a Compression-Ignition Engine. By A. M. Rothrock and C. D. Waldron, N. A. C. A. |
| 546. | The Effect of Turbulence on the Drag of Flat Plates. By G. B. Schubauer and H. L. Dryden, National Bureau of Standards. |
| 547. | Wind-Tunnel Interference with Particular Reference to Off-Center Positions of the Wing and to the Downwash at the Tail. By Abe Silverstein and James A. White, N. A. C. A. |
| 548. | Effect of Tip Shape and Dihedral on Lateral-Stability Characteristics. By Joseph A. Shortal, N. A. C. A. |
| 549. | Wind-Tunnel Investigation of the Aerodynamic Balancing of Upper-Surface Ailerons and Split Flaps. By Carl J. Wenzinger, N. A. C. A. |
| 550. | Cooling Characteristics of a 2-Row Radial Engine. By Oscar W. Schey and Vern G. Rollin, N. A. C. A. |

551. Aircraft Compass Characteristics. By John B. Peterson and Clyde W. Smith, Bureau of Aeronautics, Navy Department.
552. Wind-Tunnel Tests of 10-Foot-Diameter Autogiro Rotors. By John B. Wheatley and Carlton Bioletti, N. A. C. A.
553. Some Effects of Argon and Helium upon Explosions of Carbon Monoxide and Oxygen. By Ernest F. Flock and Carl H. Roeder.
554. Wind-Tunnel Investigation of Ordinary and Split Flaps on Airfoils of Different Profile. By Carl J. Wenzinger, N. A. C. A.
555. Air Flow Around Finned Cylinders. By M. J. Brevoort and Vern G. Rollin, N. A. C. A.
556. Further Studies of Flame Movement and Pressure Development in an Engine Cylinder. By Charles F. Marvin, Jr., Armistead Wharton, and Carl H. Roeder, National Bureau of Standards.
557. Preliminary Tests in the N. A. C. A. Free-Spinning Wind Tunnel. By C. H. Zimmerman, N. A. C. A.
558. Turbulence Factors of N. A. C. A. Wind Tunnels as Determined by Sphere Tests. By Robert C. Platt, N. A. C. A.
559. The Forces and Moments Acting on Parts of the XN2Y-1 Airplane During Spins. By N. F. Seudder, N. A. C. A.
560. A Simplified Application of the Method of Operators to the Calculation of Disturbed Motions of an Airplane. By Robert T. Jones, N. A. C. A.
561. Effect of Nozzle Design on Fuel Spray and Flame Formation in a High-Speed Compression-Ignition Engine. By A. M. Rothrock and C. D. Waldron, N. A. C. A.
562. Air Flow in the Boundary Layer Near a Plate. By Hugh L. Dryden, National Bureau of Standards.
563. Calculated and Measured Pressure Distributions Over the Midspan Section of the N. A. C. A. 4412 Airfoil. By Robert M. Pinkerton, N. A. C. A.
564. Tests of a Wing-Nacelle-Propeller Combination at Several Pitch Settings up to 42°. By Ray Windler, N. A. C. A.
565. Measurements of Fuel Distribution within Sprays for Fuel-Injection Engines. By Dana W. Lee, N. A. C. A.
566. Ground-Handling Forces on a $\frac{1}{10}$ Scale Model of the U. S. Airship "Akron." By Abe Silverstein and B. G. Gulick, N. A. C. A.
567. Propulsion of a Flapping and Oscillating Airfoil. By I. E. Garrick, N. A. C. A.
568. The Quiescent-Chamber Type Compression-Ignition Engine. By H. H. Foster, N. A. C. A.
569. Wing-Nacelle-Propeller Interference for Wings of Various Spans. Force and Pressure-Distribution Tests. By Russell G. Robinson and William H. Herrstein, Jr., N. A. C. A.
570. The Effect of Lateral Controls in Producing Motion of an Airplane as Computed from Wind-Tunnel Data. By Fred E. Weick and Robert T. Jones, N. A. C. A.
571. Pressure Distribution Over a Rectangular Airfoil with a Partial-Span Split Flap. By Carl J. Wenzinger and Thomas A. Harris, N. A. C. A.
572. Determination of the Characteristics of Tapered Wings. By Raymond F. Anderson, N. A. C. A.
573. Aerodynamic Characteristics of N. A. C. A. 23012 and 23021 Airfoils with 20-Percent-Chord External-Airfoil Flaps of N. A. C. A. 23012 Section. By Robert C. Platt and Ira H. Abbott, N. A. C. A.
574. Pressure Distribution Over an Airfoil Section with a Flap and Tab. By Carl J. Wenzinger, N. A. C. A.
575. Interference of Wing and Fuselage from Tests of 28 Combinations in the N. A. C. A. Variable-Density Tunnel. By Albert Sherman, N. A. C. A.
576. Aircraft Accidents. Method of Analysis. Prepared by Committee on Aircraft Accidents, N. A. C. A.

LIST OF TECHNICAL NOTES ISSUED DURING THE PAST YEAR

- | No. | |
|------|---|
| 543. | The Compressibility Burble. By John Stack, N. A. C. A. |
| 544. | An Application of the Von Kármán-Millikan Laminar Boundary-Layer Theory and Comparison with Experiment. By Albert E. von Doenhoff, N. A. C. A. |
| 545. | Tank Tests of a Model of a Flying-Boat Hull Having a Longitudinally Concave Planing Bottom. By J. B. Parkinson, N. A. C. A. |
| 546. | Comparative Tests of Pitot-Static Tubes. By Kenneth G. Merriam and Ellis R. Spaulding, Worcester Polytechnic Institute. |
| 547. | Development of the N. A. C. A. Slot-Lip Aileron. By Fred E. Weick and Joseph A. Shortal, N. A. C. A. |
| 548. | Flight Tests of a Balanced Split Flap with Particular Reference to Rapid Operation. By H. A. Soulé, N. A. C. A. |
| 549. | Drag of Prestone and Oil Radiators on the YO-31A Airplane. By S. J. DeFrance, N. A. C. A. |
| 550. | Limitations of the Pilot in Applying Forces to Airplane Controls. By M. N. Gough and A. P. Beard, N. A. C. A. |
| 551. | Tank Tests of Three Models of Flying-Boat Hulls of the Pointed-Step Type with Different Angles of Dead Rise—N. A. C. A. Model 35 Series. By John R. Dawson, N. A. C. A. |
| 552. | Wind-Tunnel Tests of Wing Flaps Suitable for Direct Control of Glide-Path Angle. By Fred E. Weick, N. A. C. A. |
| 553. | Notes on the Technique of Landing Airplanes Equipped with Wing Flaps. By Melvin N. Gough, N. A. C. A. |
| 554. | Circular Motion of Bodies of Revolution. By Carl Kaplan, N. A. C. A. |
| 555. | Piloting Technique for Recovery from Spins. By W. H. McAvoy, N. A. C. A. |
| 556. | Further Measurements of Normal Accelerations on Racing Airplanes. By N. F. Seudder and H. W. Kirschbaum, N. A. C. A. |
| 557. | Considerations of the Take-Off Problem. By Edwin P. Hartman, N. A. C. A. |
| 558. | The Performance of a DePalma Roots-Type Supercharger. By Oscar W. Schey and Herman H. Ellerbrock, Jr., N. A. C. A. |
| 559. | Combustion-Engine Temperatures by the Sodium Line-Reversal Method. By Maurice J. Brevoort, N. A. C. A. |
| 560. | A Comparison of Corrosion-Resistant Steel (18 Percent Chromium—8 Percent Nickel) and Aluminum Alloy (24ST). By J. E. Sullivan, Bureau of Aeronautics, Navy Department. |
| 561. | Full-Scale Wind-Tunnel Tests to Determine a Satisfactory Location for a Service Pitot-Static Tube on a Low-Wing Monoplane. By John F. Parsons, N. A. C. A. |
| 562. | Remarks on the Elastic Axis of Shell Wings. By Paul Kuhn, N. A. C. A. |
| 563. | Tank Tests of Models of Floats for Single-Float Seaplanes—First Series. By J. B. Parkinson, N. A. C. A. |
| 564. | Procedure for Determining Speed and Climbing Performance of Airships. By F. L. Thompson, N. A. C. A. |

565. Influence of Fuel-Oil Temperature on the Combustion in a Prechamber Compression-Ignition Engine. By Harold C. Gerrish and Bruce E. Ayer, N. A. C. A.
566. Tank Tests of a Model of the NC Flying-Boat Hull—N. A. C. A. Model 44. By Joe W. Bell, N. A. C. A.
567. Tests of N. A. C. A. Airfoils in the Variable-Density Wind Tunnel. Series 230. By Eastman N. Jacobs and Robert M. Pinkerton, N. A. C. A.
568. Calculated Effect of Various Types of Flap on Take-Off Over Obstacles. By J. W. Wetmore, N. A. C. A.
569. Boosted Performance of a Compression-Ignition Engine with a Displacer Piston. By Charles S. Moore and Hampton H. Foster, N. A. C. A.
570. Effect of Changes in Tail Arrangement upon the Spinning of a Low-Wing Monoplane Model. By C. H. Zimmerman, N. A. C. A.
571. A Method of Estimating the Aerodynamic Effects of Ordinary and Split Flaps of Airfoils Similar to the Clark Y. By H. A. Pearson, N. A. C. A.
572. Performance of Air-Cooled Engine Cylinders Using Blower Cooling. By Oscar W. Schey and Herman H. Ellersbrock, Jr., N. A. C. A.
573. Carbon-Monoxide Indicators for Aircraft. By S. H. J. Womack and J. B. Peterson, National Bureau of Standards.
574. Tank Tests of Models of Flying-Boat Hulls Having Longitudinal Steps. By John M. Allison and Kenneth E. Ward, N. A. C. A.
575. Estimation of Moments of Inertia of Airplanes from Design Data. By H. W. Kirschbaum, N. A. C. A.
576. Tank Tests of a Model of the Hull of the Navy PB-1 Flying Boat—N. A. C. A. Model 52. By John M. Allison, N. A. C. A.
577. Friction of Compression-Ignition Engines. By Charles S. Moore and John H. Collins, Jr., N. A. C. A.
578. Full-Scale Wind-Tunnel and Flight Tests of a Fairchild 22 Airplane Equipped with a Fowler Flap. By C. H. Dearborn and H. A. Soule, N. A. C. A.
579. Charts for Calculating the Performance of Airplanes Having Constant-Speed Propellers. By Roland J. White and Victor J. Martin, California Institute of Technology.
580. A General Tank Test of a Model of the Hull of the British Singapore IIC Flying Boat. By John R. Dawson and Starr Truscott, N. A. C. A.
581. A Study of Autogiro Rotor-Blade Oscillations in the Plane of the Rotor Disk. By John B. Wheatley, N. A. C. A.
782. Status of Wing Flutter. By H. G. Küssner. From *Luftfahrtforschung*, October 3, 1935.
783. Analysis of the Three Lowest Bending Frequencies of a Rotating Propeller. By F. Liebers. From *Luftfahrtforschung*, August 31, 1935.
784. Torsion and Buckling of Open Sections. By H. Wagner and W. Pretschner. From *Luftfahrtforschung*, December 5, 1934.
785. Methods and Formulas for Calculating the Strength of Plate and Shell Constructions as Used in Airplane Design. By O. S. Heck and H. Ebner. From *Luftfahrtforschung*, February 6, 1935.
786. The Formation of Ice on Airplanes. By H. Noth and W. Polte. From *Luftwissen*, vol. II, no. 11, 1935.
787. Investigations on the Amount of Downwash Behind Rectangular and Elliptical Wings. By H. Muttray. From *Luftfahrtforschung*, March 28, 1935.
788. The 5- by 7-Meter Wind Tunnel of the DVL. By M. Kramer. From *Luftfahrtforschung*, October 3, 1935.
789. Turbulent Jet Expansion. By E. Förthmann. From *Ingenieur-Archiv*, vol. V, no. 1, 1934.
790. Ignition and Flame Development in the Case of Diesel Fuel Injection. By Otto Holfelder. From supplement to *Forschung auf dem Gebiete des Ingenieurwesens*, September–October 1935.
791. Behavior of Turbulent Boundary Layers on Curved Convex Walls. By Hans Schmidbauer. (Thesis)
792. General Instability Criterion of Laminar Velocity Distributions. By W. Tollmien. From *Nachrichten von der Gesellschaft der Wissenschaften zu Göttingen (Mathematik)*, vol. I, no. 5, 1935.
793. Bending of Beams of Thin Sections. By Maximilian T. Huber. From *Instytut Badań Technicznych Lotnictwa Sprawozdanie Kwartalne No. 3*, Warsaw, 1930.
794. Chief Characteristics and Advantages of Tailless Airplanes. By A. Dufaure De Lajarte. From *Association Technique Maritime et Aéronautique*, June 1935.
795. Similitude in Hydrodynamic Tests Involving Planing. By M. F. Gruson. Paper presented on the occasion of the inauguration of the Institute of Mechanics of Fluids of the University of Lille, April 5–8, 1934.
796. Contribution to the Problem of Airfoils Spanning a Free Jet. By J. Stüper. From *Luftfahrtforschung*, December 25, 1935.
797. Ignition Process in Diesel Engines. By W. Wentzel. From *Forschung auf dem Gebiete des Ingenieurwesens*, May–June 1935.
798. Flow Phenomena on Plates and Airfoils of Short Span. By H. Winter. From *Verein deutscher Ingenieure, Special Issue (Aviation)*, 1936.
799. The Transport of Vorticity through Fluids in Turbulent Motion. (In the light of the Prandtl and Taylor theories.) By C. Ferrari. From *L'Aerotechnica*, November–December 1935.
800. Charts for Checking the Stability of Compression Members in Trusses. By K. Borkmann. From *Luftfahrtforschung*, January 20, 1936.
801. Correction of Downwash in Wind Tunnels of Circular and Elliptic Sections. By Irmgard Lotz. From *Luftfahrtforschung*, December 25, 1935.
802. Automatic Stabilization. By Fr. Haus. From *L'Aéronautique*, October 1935; January and February 1936.
803. Details of the Construction and Production of Fuel Pumps and Fuel Nozzles for the Airplane Diesel Engine. By W. S. Lubenetsky. From *Dieselelectroenergie*, No. 6, Moskva, 1935.

LIST OF TECHNICAL MEMORANDUMS ISSUED DURING THE PAST YEAR

- | |
|---|
| <p>No.</p> <p>777. Tests of Spheres with Reference to Reynolds Number, Turbulence, and Surface Roughness. By S. Hoerner. From <i>Luftfahrtforschung</i>, March 28, 1935.</p> <p>778. Method for the Determination of the Spanwise Lift Distribution. By A. Lippisch. From <i>Luftfahrtforschung</i>, June 17, 1935.</p> <p>779. Weldability of High-Tensile Steels from Experience in Airplane Construction, with Special Reference to Welding Crack Susceptibility. By J. Müller. From <i>Luftfahrtforschung</i>, October 1, 1934.</p> <p>780. Glider Development in Germany. A Technical Survey of Progress in Design in Germany Since 1922. By B. S. Shenstone and S. Scott-Hall. From <i>Aircraft Engineering</i>, October 1935.</p> <p>781. Reduction of Lift of a Wing Due to Its Drag. By J. Stüper. From <i>Zeitschrift für Flugtechnik und Motorluftschiffahrt</i>, August 28, 1933.</p> |
|---|

804. The Stress Criterion of a Tension Member with Graded Flexural Stiffness. (Contribution to the Problem of "Clamping Effect" Outside of the Elastic Range.) By Hans W. Kaul. From *Luftfahrtforschung*, June 20, 1936.

LIST OF AIRCRAFT CIRCULARS ISSUED DURING THE PAST YEAR

- No.
200. The Short "Scion Senior" Commercial Airplane (British). A Four-Engine High-Wing Cantilever Monoplane. From *Flight*, October 31, 1935; and *The Aeroplane*, October 30, 1935.
201. The Avro "Anson" General-Purpose Airplane (British). A Two-Engine Low-Wing Cantilever Monoplane. From *Flight*, January 30, and *The Aeroplane*, January 29, 1936.
202. The Latécoere 521 "Lieutenant de Baisseau Paris" Commercial Flying Boat (French). A Two-Deck Six-Engine Semicantilever Sesquiplane. From *L'Aéronautique*, November 1935.
203. The Vickers-Supermarine "Scapa" (British). A Military Flying Boat. From *Flight*, April 26, 1934; *Flight*, February 27, 1936; and *The Aeroplane*, February 26, 1936.

FINANCIAL REPORT

The general appropriation for the National Advisory Committee for Aeronautics for the fiscal year 1936, as contained in the Independent Offices Appropriation Act approved February 2, 1935, was \$820,800. The Second Deficiency Act of 1935, approved August 12, 1935, provided an additional amount of \$338,050 for the same purposes, making the total amount available for expenditure during the fiscal year 1936 \$1,158,850. The amount expended and obligated was \$1,157,746, itemized as follows:

Personal services.....	\$775,114
Supplies and materials.....	63,364
Communication service.....	3,192
Travel expenses.....	16,085
Transportation of things.....	3,329
Furnishing of electricity.....	29,418
Repairs and alterations.....	18,746
Special investigations and reports.....	89,493
Equipment.....	159,005
Expended and obligated.....	1,157,746
Unobligated balance.....	1,104

Total, general appropriation..... 1,158,850

The appropriation for printing and binding for 1936 was \$18,700, of which \$18,663 was expended.

The amount of the regular appropriation for the fiscal year 1937, as provided in the Independent Offices Appropriation Act approved March 19, 1936, is \$1,158,850. A supplemental appropriation of \$1,367,000 was made available in the First Deficiency Appropriation Act, fiscal year 1936, approved June 22, 1936, for the same purposes specified in the Committee's regular appropriation act for 1936, to continue available until June 30, 1937. It provided not to exceed \$1,100,000 for the construction and equipment of an additional wind tunnel, and not to

exceed \$267,000 for increasing the length of the present seaplane model testing tank and for additional equipment therefor. The total amount available for general expenses during the fiscal year 1937 therefore is \$2,525,850. An additional amount of \$18,700 was appropriated for printing and binding, fiscal year 1937.

The amount expended and obligated during the fiscal year 1936 for the completion of the 500-mile-per-hour wind tunnel at Langley Field was \$8,741.20, under the total allotment of \$478,300 made for this purpose by the Public Works Administration during the fiscal year 1934.

The sum of \$5,945 was received by this Committee during the fiscal year 1936 as special deposits to cover the estimated cost of scientific services to be furnished private parties. The total cost of investigations completed for private parties during the fiscal year 1936, amounting to \$2,795.80, was deposited in the Treasury of the United States to the credit of Miscellaneous Receipts.

Of the allotment of \$3,000 for participation by this Committee in the California Pacific International Exposition which opened at San Diego, California, on May 27, 1935, there was on June 30, 1935, an unexpended balance of \$2,045.74. The exposition closed in November 1935, and in March 1936 the unexpended balance of \$610.13 was deposited in the Treasury. The amount of \$1,410.13 was on April 4, 1936, allotted to this Committee for continued participation in the exposition, which reopened in February 1936. Of this allotment the amount of \$545.79 was expended and obligated as at June 30, 1936, leaving a balance of \$864.34.

An allotment of \$15,500 was received by this Committee for participation in the Texas Centennial Exposition at Dallas, Texas, which opened June 6, 1936. Of this allotment the amount of \$12,652.82 was expended and obligated as at June 30, 1936, leaving a balance of \$2,847.18.

From allotments from the Department of Commerce to a working fund during the fiscal years 1934 and 1935 for work performed by this Committee in connection with the furtherance of the improvement of safety and efficiency in civil aviation, there was an unexpended balance of \$403 as at June 30, 1935. An additional allotment of \$8,000 was received in July 1935, making the total amount available for this purpose \$8,403. Of this amount \$6,314.16 was expended and obligated during the fiscal year 1936, leaving a balance of \$2,088.84 as at June 30, 1936.

An allotment of \$7,600 was received from the State Department for payments during the fiscal year 1936 to employees stationed abroad, on account of exchange losses due to appreciation of foreign currencies, and of this amount \$5,409.79 was paid to employees of the

Committee stationed in the Paris Office during the fiscal year, leaving a balance of \$2,190.21 to be turned back into the Treasury.

CONCLUDING STATEMENT

The continued progress in aviation is shrinking distances and bringing the nations of the world closer together. Air trade routes are being extended by progressive nations in order to develop their commercial and national influence. Scheduled air passenger transportation across the North Atlantic by airship and across the Pacific by seaplane was inaugurated in 1936. It is expected that regular seaplane service across the North Atlantic will soon be inaugurated.

Air travel in the United States is increasing. Comfortable sleeping berths are being provided for overnight transportation. Mail and express are being carried in greater quantities. The economic status of air transportation is improving to such an extent that cargo airplanes are being developed for freight only. The safety of the airplane and the safety precautions surrounding air travel are being steadily improved. Commercial aeronautics is more highly developed in the United States than in any other country.

Military aircraft developed in the United States are highly efficient and dependable. In the major European nations tremendous emphasis is being placed upon the military significance of aircraft. Their construction programs and factories are being enlarged and research laboratories and facilities multiplied.

The development of superior aircraft is dependent upon fundamental scientific research. The encouragement and freedom of those engaged in scientific research is essential to this development. The status of the National Advisory Committee for Aeronautics as an independent Government establishment gives it the necessary freedom of action, and its researches are largely responsible for the present superiority of American aircraft. The United States may justly take pride in the remarkable development of American aviation to date. But in order to insure that this country shall not fall behind, this Committee urges the wisdom and ultimate economy of increased appropriations for research personnel and for new research equipment.

Respectfully submitted.

NATIONAL ADVISORY COMMITTEE
FOR AERONAUTICS,
JOSEPH S. AMES, *Chairman*.

REPORT No. 542

POTENTIAL FLOW ABOUT ARBITRARY BIPLANE WING SECTIONS

By I. E. GARRICK

SUMMARY

A rigorous treatment is given of the problem of determining the two-dimensional potential flow around arbitrary biplane cellules. The analysis involves the use of elliptic functions and is sufficiently general to include the effects of such elements as the section shapes, the chord ratio, gap, stagger, and decalage, which elements may be specified arbitrarily. The flow problem is resolved by making use of the methods of conformal representation. Thus the solution of the problem of transforming conformally two arbitrary contours into two circles is expressed by a pair of simultaneous integral equations, for which a method of numerical solution is outlined. It is pointed out that an inverse method of transforming conformally two circles into the wing profiles of a biplane arrangement leads readily to the development of related families of biplane combinations. Flow formulas are developed giving the velocity and pressure at any point of the surface of either profile of the arbitrary biplane arrangement, for any angle of attack. The theory of the monoplane wing section in potential flow is shown to be a degenerate case in which the elliptic functions reduce to trigonometric functions. The general method presented may be employed to determine the potential flow in any doubly connected region and hence may be applied to the single slotted wing or to the auxiliary-airfoil wing.

As an example of the numerical process, the pressure distribution over certain arrangements of the N. A. C. A. 4412 airfoil in biplane combinations is presented and compared with the monoplane pressure distribution.

INTRODUCTION

It is the purpose of this paper to develop a general theory of arbitrary biplane cellules of infinite span in potential flow. No attempt is made here to treat the case of finite span or to consider viscosity; rather it is the object of this work to bring the two-dimensional theory of biplane cellules in uniform, steady potential flow to the same degree of exactness and generality to which the two-dimensional monoplane airfoil theory has been brought. The analysis will be sufficiently general to include such elements as profile shapes, chord ratio, gap/chord, stagger, and decalage, and

will contain as special cases the monoplane theory, as well as the theories of the slotted monoplane wing, of the auxiliary-airfoil wing, and of the influence of the ground or plane barriers on a monoplane airfoil in two-dimensional potential flow.

In order to arrive in a natural manner at a perspective of the biplane analysis it is advantageous to consider first the simpler case of the monoplane wing section and to keep in view the essential concepts that carry over to the biplane analysis. It is well known that by virtue of the methods of conformal representation the two-dimensional potential flow around a single obstacle can be obtained by the following process. In the first place, a standard contour is selected, the region about which is simply connected and the flow function of which in uniform potential flow is known or obtainable. The transformation must then be found that transforms conformally the region of the given obstacle into this standard region. This transformation, in combination with the known flow function, gives the desired flow function for the obstacle. In the case of monoplane wing profiles, the standard flow region may be chosen to be that about a circle and the theorem which states that it is possible to transform conformally the contour of the given obstacle into a circle is known as Riemann's theorem. (Cf., for example, reference 1.) In the case of two obstacles, the region is termed "doubly connected" and the process is again applicable except that the standard doubly connected region is chosen to be the region about two circles. The theorem that states the existence of a transformation function bringing the doubly connected region (region of the biplane contours) into the region of two circles is Koebe's theorem (reference 2).

The flow function giving the uniform potential flow for a circular cylinder is well known and, in determining the flow about a monoplane airfoil section, the main problem is the transforming of the airfoil contour into a circle. In order to attain this result in a simple manner it is necessary to perform a few intermediate transformations. The airfoil profile itself may be regarded as a contour described about a conveniently chosen line segment or chord. An

initial transformation of a simple type exists (the so-called "Joukowski transformation") that transforms the chord into a unit circle and automatically maps the airfoil contour into a nearly circular contour described about the unit circle. There remains then the final task of transforming the nearly circular contour into a true circle, and this may be performed by a method given by Theodorsen (reference 3). This method leads directly to a simple integral equation which can be solved by a process of iteration or successive approximations and which converges with extreme rapidity. (Cf. reference 1.) It is important in regard to practical considerations to observe that the method is so powerful that one step in the process is quite sufficient in all ordinary cases.

The standard *doubly* connected region has been chosen as the region about two circles; and it is worthy of mention that only as recently as 1929 was the complex flow potential for two circles rigorously developed (by Lagally, reference 4). Dupont, Bonder, and Müller (references 5, 6, and 7) have also contributed to this problem but Lagally's solution is the more elegant. The flow function for two circles being known, the main problem in finding the flow about a biplane arrangement is the obtaining of the transformation mapping the two contours into two circles.

In a manner analogous to the case of the single airfoil section, the contours of a biplane arrangement may be considered to be described about a skeleton of two conveniently placed mean lines or chords. Hence, to maintain the analogy it is seen that initially it is desired to find a transformation function which transforms the two line segments into two circles. This problem has been touched upon by Kutta who has given the uniform potential flow for the special case of two parallel equal line segments (reference 8). The transformation function bringing two circles into any two *parallel* line segments has been developed by C. Ferrari (reference 9). In the first part of the present paper the more general problem of decalage of the line segments has been studied and a function developed that transforms two circles into any two nonintersecting line segments in any relative positions. This function that transforms the skeleton or chords of the biplane arrangement into two circles also transforms the contours themselves into two nearly circular contours described about the skeleton circles. There remains then the problem of transforming the two nearly circular contours into two true circles. In order to accomplish this task, the method of Theodorsen is generalized in the present paper to apply to doubly connected regions by employing the concentric circular ring region as a standard region and by utilizing a Laurent series development instead of a one-way power series. There is obtained finally a pair of simultaneous integral equa-

tions expressing the conformal representation of the two nearly circular contours into two circles. Just as in the case of the single integral equation in the monoplane case, there exists an analogous process of successive approximations or iteration that converges with the same remarkable degree of rapidity.

The general transformation from the biplane contours to two circles together with the Lagally formula for the flow about two circles yields an expression for the velocity and pressure at each point of the surface of either profile of the biplane arrangement. There are two arbitrary circulations in the flow formula, viz, the separate circulations around each contour, and these are determined uniquely by applying the well-known Kutta-Joukowski condition to the trailing edges of both contours, specifying thereby that the flow leaves these edges smoothly.

In the case of monoplane wing theory it has been shown (reference 1) that theoretical shapes can be conveniently developed by an inverse method of transforming conformally a circle into a wing profile. The Joukowski airfoils and the other so-called "theoretical" airfoils are special examples of this process. In an analogous manner it is possible to develop theoretical biplane combinations by an inverse process of transforming two circles into two contours resembling wing profiles. A general and flexible method of obtaining these shapes is presented; the results are especially instructive in that, in this process, the integral equations referred to in a preceding paragraph reduce to definite integrals.

Elliptic functions arise in a natural manner in the analysis and the problem treated provides a good illustration of the power and beauty of these remarkable functions. The general theory of the single, arbitrary wing section is shown to be a degenerate case in which the imaginary period of the doubly periodic elliptic functions becomes infinite, and hence the elliptic functions reduce to ordinary trigonometric functions. A few pages are devoted to the monoplane theory in view of the light that it throws on the more general biplane analysis.

Numerical results are presented only to furnish an illustration of the theory. In particular, the pressure distribution is determined for certain arrangements of the N. A. C. A. 4412 airfoil in biplane combinations. The elliptic functions that arise in the analysis and that are to be evaluated in a numerical case may fortunately, when necessary, be developed in rapidly convergent expansions.

Statement of the problem.—The problem treated in this paper may be restated as follows. Given, an arbitrary biplane arrangement oriented in a specified manner in a nonviscous, incompressible fluid medium and translated with uniform velocity V . To determine the velocity and pressure distribution in two-dimen-

sional potential flow in the field of motion for all angles of attack, particularly, at each point of the surface of the biplane profiles.

As has been pointed out, it is well recognized that the aforementioned problem may be treated in two stages. In the first place, the complex function expressing the conformal transformation of the region of the biplane into a standard doubly connected region must be obtained and, finally, the complex flow function for this standard region, which is chosen as the region about two circles, must be known. The region external to the two contours of a biplane arrangement will be brought into the region about two circles by the intermediate use of two nearly circular contours. Before this result can be accomplished, however, it is desirable to discuss several preliminary transformations.

1. PRELIMINARY TRANSFORMATIONS

First, the transformation bringing the region external to two nonintersecting circles (t plane) into the annular region between two concentric circles (w plane) will be obtained. This annular region will then be mapped into a rectangular region (s plane) and the rectangular region into the region about two line segments (u plane). (See fig. 1.)

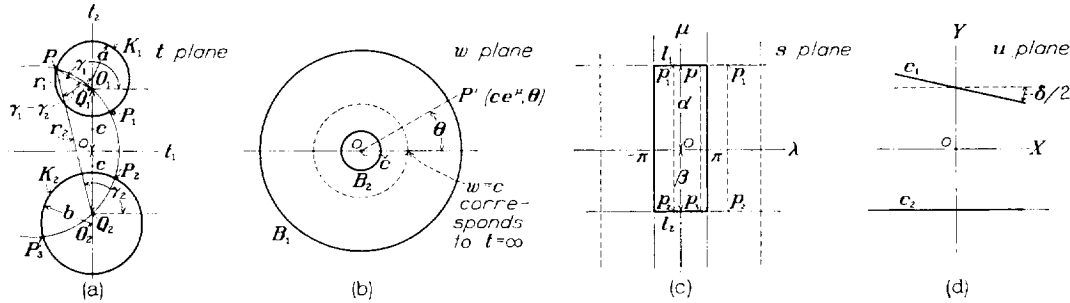


FIGURE 1.—Mapping of: (a) two coaxial circles in the t plane into (b) two concentric circles in the w plane, (c) rectangular region in the s plane, (d) two line segments in the u plane.

Transformation of a coaxial system of circles into a concentric system.—A coaxial system of circles may be described most simply by the use of bipolar coordinates. Consider a complex t plane where $t=t_1+it_2$. Let $Q_1(0, ic)$ and $Q_2(0, -ic)$ located on the t_2 axis be the origins of two polar coordinate systems r_1, γ_1 and r_2, γ_2 . The variable t may be written in the two forms:

$$t = ic + r_1 e^{i\gamma_1} = -ic + r_2 e^{i\gamma_2}$$

Then in the relation

$$\frac{t+ic}{t-ic} = \frac{r_2}{r_1} e^{i(\gamma_2-\gamma_1)} \quad (1)$$

there are expressed in a convenient form, the bipolar coordinates $\frac{r_2}{r_1}$ and $\gamma_2 - \gamma_1$. (See fig. 1 (a).)

The curves $r_2/r_1 = \text{constant}$ are circles with centers lying along the t_2 axis (theorem of Apollonius). This family of circles contains the points Q_1 and Q_2 as limiting circles of zero radius. For points in the upper half plane ($t_2 > 0$) we have $r_2/r_1 > 1$, for points in the lower half plane $r_2/r_1 < 1$, while on the t_1 axis, $r_2/r_1 = 1$. The curves given by $\gamma_2 - \gamma_1 = \text{constant}$ also form a family of circles (theorem of the constant angle subtended by the chord of a circle) which is orthogonal to the first system and each circle of which contains the limit points Q_1 and Q_2 on its circumference.

A new complex variable $w = ce^{\mu+i\theta}$ is now introduced by the following relation

$$\frac{w}{c} = e^{\mu+i\theta} = \frac{t+ic}{t-ic} = \frac{r_2}{r_1} e^{i(\gamma_2-\gamma_1)} \quad (2)$$

Hence

$$\left. \begin{aligned} \mu &= \log \frac{r_2}{r_1} \\ \theta &= \gamma_2 - \gamma_1 \end{aligned} \right\} \quad (3)$$

Also

$$t = ic \frac{w+c}{w-c} \quad (4)$$

These equations transform conformally the coaxial system of circles of the t plane into a concentric system of circles in the w plane. In particular, two circles K_1 and K_2 in the t plane, K_1 located in the upper half

plane and K_2 in the lower half plane and defined by $\log r_2/r_1 = \alpha$ and $\log r_2/r_1 = -\beta$, respectively ($\alpha > 0, \beta > 0$), transform into two concentric circles B_1 and B_2 about the origin in the w plane, of radii ce^α and $ce^{-\beta}$, respectively (fig. 1 (b)). It is noted also that the t_1 axis transforms into the circle of radius c in the w plane, and that the region at infinity in the t plane maps into the neighborhood of the point $w=c$. It may also be remarked that the circles orthogonal to K_1 and K_2 transform into radial lines through the origin.

Transformation of the circular systems into rectangular systems.—There is now introduced another variable $s = \lambda + i\nu$ defined by the relation

$$s = i \log \frac{w}{c} = i \log \frac{t+ic}{t-ic} \quad (5)$$

Separating into real and imaginary parts

$$\left. \begin{aligned} \lambda &= -(\gamma_2 - \gamma_1) = -\theta \\ \nu &= \log \frac{r_2}{r_1} = \mu \end{aligned} \right\} \quad (6)$$

Hence the variable s may hereafter be denoted by

$$s = -\theta + i\mu \text{ or also by } s = \lambda + i\mu$$

Also from (5) we have

$$w = ce^{-is} \quad (7)$$

and

$$t = ic \left(\frac{1 + e^{is}}{1 - e^{is}} \right) = -c \cot \frac{s}{2} \quad (8)$$

The circles in the t plane, $r_2/r_1 = \text{constant}$ (or the circles in the w plane $ce^\mu = \text{constant}$), correspond uniquely to the straight lines $\mu = \text{constant}$ in the s plane. In particular, the limiting points Q_1 and Q_2 correspond to $\mu = \infty$ and $\mu = -\infty$, respectively. Also the t_1 axis corresponds to the axis $\mu = 0$, the point at infinity in the t plane going into the origin $s = 0$. The circular arcs $\gamma_1 - \gamma_2 = \text{constant}$ between Q_1 and Q_2 correspond to the lines $\lambda = \text{constant}$. It is noted, however, that this latter correspondence is infinitely many-valued since the addition of integral multiples of 2π to γ_1 or γ_2 does not alter the circular arc considered; hence, $\gamma_1 - \gamma_2 = \text{constant}$ corresponds to the infinite number of parallel lines $\lambda = \text{constant} + 2k\pi$, where k is any integer (fig. 1 (c)).

The whole t plane has thus infinitely many values on the s plane, but there is a one-to-one correspondence between the whole t plane and a strip of width 2π bounded by two parallels to the μ axis. In the following investigation, the strip in the s plane bounded by the lines $\lambda = -\pi$ and $\lambda = \pi$ will be considered as the representation of the t plane cut along the length $Q_1 Q_2$.

Equation (5) thus defines a conformal transformation of the coaxial system of circles in the t plane, or of the concentric system of circles in the w plane, to a rectangular system in the s plane. In particular, consider again the two definite circles K_1 and K_2 of the coaxial pencil. The circle K_1 is defined by $\log r_2/r_1 = \mu = \alpha$ and the circle K_2 by $\log r_2/r_1 = \mu = -\beta$ where α and β are positive constants. It is then noted that the region of the t plane external to the circles K_1 and K_2 (or the ring region within B_1 and B_2) corresponds uniquely to the rectangular region bounded by the lines $\mu = \alpha$, $\mu = -\beta$, $\lambda = -\pi$, and $\lambda = \pi$. (The two sides $\lambda = -\pi$ and $\lambda = \pi$ correspond to the right and left edges respectively of a cut along the t_2 axis drawn between the two circles.) The rectangle contains, necessarily, the point $s = 0$ as an internal point.

Geometrical relations.—Attention may be momentarily diverted to some geometrical relations existing in the various planes. Let the radii of K_1 and K_2 be a and b , respectively, and let the centers of K_1 and K_2 be situated at O_1 and O_2 , respectively (fig. 1 (a)).

The quantities a and b may be expressed in terms of α and β . The equation of K_1 in bipolar coordinates is, by equation (2)

$$\frac{r_2}{r_1} = \frac{|t + ic|}{|t - ic|} = e^\alpha$$

Writing $t = t_1 + it_2$ there results upon expansion

$$t_1^2 + t_2^2 - 2ct_2 \coth \alpha + c^2 = 0$$

which is the equation of a circle whose center O_1 is situated at

$$t_2 = c \coth \alpha$$

and whose radius is

$$a = c \operatorname{csch} \alpha$$

Similarly, for the second circle K_2 , the center O_2 is at

$$t_2 = -c \coth \beta$$

and the radius is

$$b = c \operatorname{csch} \beta$$

Denoting by d the center-to-center distance $O_1 O_2$ (fig. 1), there may be written the equations:

$$\left. \begin{aligned} a &= c \operatorname{csch} \alpha \\ b &= c \operatorname{csch} \beta \\ d &= c (\coth \alpha + \coth \beta) \end{aligned} \right\} \quad (9)$$

which suffice to fix a , b , and d in terms of α , β , and c . Forming the auxiliary quantity $d^2 - a^2 - b^2$, it is found that $d^2 - a^2 - b^2 = 2abc \cosh(\alpha + \beta)$. It immediately follows that

$$\left. \begin{aligned} c &= \frac{ab}{d} \sinh(\alpha + \beta) \\ \sinh \alpha &= \frac{b}{d} \sinh(\alpha + \beta) \\ \sinh \beta &= \frac{a}{d} \sinh(\alpha + \beta) \end{aligned} \right\} \quad (10)$$

We observe that the quantity $\alpha + \beta$ on the right-hand side is expressed in terms of a , b , and d by the relation

$$\cosh(\alpha + \beta) = \frac{d^2 - a^2 - b^2}{2ab}$$

2. TRANSFORMATION OF TWO CIRCLES INTO TWO ARBITRARY LINE SEGMENTS

The transformation that maps the rectangular region in the s plane into the region external to two nonintersecting line segments in a u plane will now be derived. In combination with the preliminary transformations of the preceding section this result will then transform the region of the two circles K_1 and K_2 of the t plane, or the ring region of the w plane, into the region of the line segments. Let the u plane (fig. 1 (d)) contain the two line segments c_1 and c_2 and let $u(t) = X + iY$ be the analytic function that transforms the circles K_1 and K_2 into the desired line segments. With no loss in generality, the system of coordinates in the u plane may be so chosen that the X axis is parallel to c_2 . Let the line segment c_1 be inclined at an angle $-\delta/2$ with respect to the X axis. (The negative sign before δ is a matter of later convenience; fig. 1(d)) may be

regarded as illustrating the definition of *positive* decalage.) Let l_1 and l_2 denote the two lines $\mu=\alpha$ and $\mu=-\beta$ of the rectangular s plane that correspond to K_1 and K_2 , then, it is evident that $\frac{dY}{dX}=0$

for points of K_2 or l_2 and $\frac{dY}{dX}=-\tan \frac{\delta}{2}$ for points along

K_1 or l_1 . Let $f(s)=\frac{du}{ds}$ be the derivative of the function $u(s)$ that gives the desired correspondence between the u and s planes. From the well-known property of conformal mapping, viz, that tangents at corresponding points in the two planes differ in direction by the argument of the derivative function, it follows that the argument of $f(s)$ equals 0 (or π) along l_2 and equals $-\delta/2$ (or $-\delta/2+\pi$) along l_1 , or

$f(s)$ is a real quantity along l_2

$f(s)e^{i\delta/2}$ is a real quantity along l_1

By a principle of Schwarz the as yet undetermined function $f(s)$ has the property of being extended by analytic continuation to the whole strip region in the s plane (fig. 1(c)) for, since $f(s)$ is real along l_2 , its values for a pair of reflected points mirrored in the line l_2 are conjugate complex. Similarly the function $f(s)e^{i\delta/2}$ may be reflected about the line l_1 . With successive alternate reflections in l_1 and l_2 $f(s)$ takes on values as shown in figure 2. For every two successive reflections the original values of $f(s)$ are repeated except for a multiplying factor $e^{-i\delta}$. Hence it is clear that $f(s)$ must satisfy the relation

$$f[s+2i(\alpha+\beta)]=f(s)e^{-i\delta} \quad (1)$$

Also, since $f(s)$ is a single-valued function of t , it satisfies the condition

$$f(s+2\pi)=f(s) \quad (2)$$

If $\delta=0$, then $e^{-i\delta}=1$ and it is seen at once that $f(s)$ is then a *doubly periodic* function, hence an elliptic function (of the first kind), of real period $2\omega=2\pi$ and of imaginary period $2\omega'=2i(\alpha+\beta)$. In the general case where $\delta \neq 0$, the function $f(s)$ is not a purely doubly periodic function but, since one of its periods gives rise to a multiplying factor, is an elliptic function of the second kind. It is completely determined, except for a constant, by its behavior at its poles, in the neighborhood of which the function becomes infinite (Hermite's theorem). In the present analysis, we shall consider the fundamental periodic rectangle as formed by the original transformed rectangle and its reflection in the line l_2 (fig. 2).

We now investigate the poles of the function $f(s)=\frac{du}{ds}$. We assume that at infinity $|u|=|t|$, in order that the regions at infinity in the u and t planes be

equally magnified and map into each other (except for a possible change in direction), and we have

$$\left|\frac{du}{dt}\right|_{t=\infty}=1$$

or noting equation (1.8)¹

$$\left|\frac{du}{dt}\right|_{t=\infty}=\left|\frac{du}{ds}\right|_{s=0}\cdot\left|\frac{ds}{dt}\right|_{t=\infty}=\left|\frac{du}{ds}\right|_{s=0}\cdot\left|\frac{2c}{t^2+c^2}\right|_{t=\infty}=1 \quad (3)$$

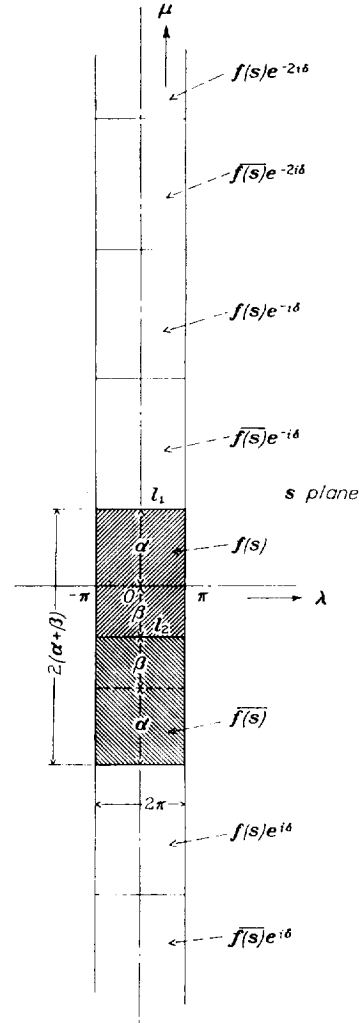


Figure 2.—Illustrating the properties of $\frac{du}{ds}=f(s)$ in the strip region: $\overline{f(s)}$ is the conjugate complex quantity of $f(s)$.

This relation shows at once that $f(s)$ possesses a singular point at $s=0$, and hence has one also at the point obtained by reflection of $s=0$ in l_2 , viz, $s=-2i\beta$. In the neighborhood of these points $f(s)$ becomes infinite in the order of t^2 as $t \rightarrow \infty$ or as $\frac{1}{s^2}$ as $s \rightarrow 0$, i. e., has poles of *order two* at the origin $s=0$ and at $s=-2i\beta$.

¹This notation denotes equation (8) of sec. 1.

The fundamental function having a single pole of *first order* (with residue unity) at the origin and satisfying the foregoing period requirements is (reference 10, p. 416, and reference 11, p. 369)

$$A(s) = \frac{e^{-\frac{\pi}{\omega} \delta s} \sigma(s + \delta)}{\sigma(\delta) \sigma(s)} \quad (4)$$

where σ denotes the sigma function of Weierstrass and possesses the following period properties

$$\begin{aligned} \sigma(u + 2\omega) &= -e^{-2\eta(u+\omega)} \sigma(u) \\ \sigma(u + 2\omega') &= -e^{-2\eta'(u+\omega')} \sigma(u) \end{aligned} \quad (5)$$

The expression (4) for $A(s)$ may also be written as follows

$$A(s) = \frac{H'(0)H(s+\delta)}{H(\delta)H(s)} \quad (4')$$

where the Jacobi $H(\eta)$ function is defined by the equation (cf. references 11 and 12)

$$H(u) = 2q^{1/4} \sin \frac{\pi u}{2\omega} - 2q^{9/4} \sin \frac{3\pi u}{2\omega} + 2q^{25/4} \sin \frac{5\pi u}{2\omega} - \dots \quad (6)$$

and possesses the period properties

$$\begin{aligned} H(u + 2\omega) &= -H(u) \\ H(u + 2\omega') &= -q^{-1} e^{-i\frac{\pi}{\omega} u} H(u) \end{aligned}$$

where

$$q = e^{\frac{i\pi\omega'}{\omega}}$$

The relation existing between the σ and H functions is (reference 11, p. 488)

$$\sigma(u) = e^{\frac{\eta u}{2\omega}} \frac{H(u)}{H'(0)} \quad (7)$$

A function such as we are seeking, having a single pole of the *second order* at the origin and the required period properties, may be obtained by taking the *negative* derivative of $A(s)$ with regard to s . From equation (4') we have

$$A'(s) = -\frac{dA(s)}{ds} = -\frac{H'(0)}{H(\delta)} \frac{d}{ds} \frac{H(s+\delta)}{H(s)} \quad (8)$$

The function $f(s)$ is now determined except for constants a_1 and a_2 is given by

$$f(s) = \frac{du}{ds} = a_1 A'(s) + a_2 A'(s + 2i\beta) + a_3 \quad (9)$$

To determine the constants, observe that by means of equation (3), and by the fact that the expansion of $A'(s)$ about the origin begins with the term $\frac{1}{s^2}$, we have in the neighborhood of $s=0$

$$\left| \frac{du}{dt} \right|_{t=\infty} = \left| \frac{a_1}{s^2} \right|_{s=0} \cdot \left| \frac{2c}{t^2} \right|_{t=\infty} = 1$$

and since from equation (1.8) $|t|_{t=\infty} = \left| \frac{2c}{s} \right|_{s=0}$ there results $|a_1| = 2c$. Thus the magnitude of a_1 is determined

and, in general, we may put $a_1 = 2ce^{i\gamma}$ where γ is an arbitrary real parameter that determines the stagger of the segments, and the significance of which will be seen shortly. It may be observed at this point that with $a_1 = 2ce^{i\gamma}$ the following relation holds

$$\left. \frac{du}{dt} \right|_{t=\infty} = e^{i\gamma} \left. \frac{du}{dt} \right|_{t=\infty} = e^{i\gamma} \quad (10)$$

i. e., the regions at infinity in the u and t planes agree in magnitude but differ by angle γ in direction. In order to determine a_2 it is sufficient to recall that $f(s)$ must remain real on l_2 hence it may be seen that a_2 must equal $2ce^{-i\gamma}$. Then finally equation (9) may be expressed as

$$\frac{du}{ds} = 2c[A'(s)e^{i\gamma} + A'(s + 2i\beta)e^{-i\gamma}] \quad (11)$$

The general function relating the u and s planes is then by integration with regard to s

$$u(s) = -2c[A(s)e^{i\gamma} + A(s + 2i\beta)e^{-i\gamma}] + k \quad (12)$$

where the function $A(s)$ is given by (4) or (4') and where k is an arbitrary constant that is independent of s but may contain the parameter δ .²

The singular points of transformation (12) are given by the roots of the equation $\frac{du}{ds} = 0$. It is possible to draw at once certain conclusions with regard to the singular points. There exists a theorem on elliptic functions (reference 11, p. 366) which states that the number of zeros of an elliptic function (of the first or second kind) in a periodic rectangle is equal to the number of poles. Since $f(s) = \frac{du}{ds}$ has 2 poles of second order in the periodic rectangle it follows that the equation $\frac{du}{ds} = 0$ possesses 4 roots in this rectangle. It is demonstrable without difficulty that 2 of the zeros are located on the boundary $\mu = \alpha$ and the remaining 2 on the boundary $\mu = -\beta$. These zeros correspond to the end points of the line segments c_1 and c_2 of the u plane. It may be stated for reference that on l_2 the singular values of λ are obtained from the equation

$$\frac{du}{ds} = 0 = A'(\lambda - i\beta)e^{i\gamma} + A'(\lambda + i\beta)e^{-i\gamma}$$

or since $A'(\lambda - i\beta)$ and $A'(\lambda + i\beta)$ are conjugate complex quantities, the singular points are given by the solutions of

$$\text{Re. } A'(\lambda - i\beta)e^{i\gamma} = 0$$

where Re. denotes "real part of." On l_1 , we employ the period property (1) of $A(s)$ and obtain for the equation satisfied by the singular values of λ

$$\text{Re. } A'(\lambda + i\alpha)e^{i(\gamma + \delta/2)} = 0$$

² The remainder of this section is commentary to this equation. The reader may, without loss of continuity, proceed to sec. 3, p. 56.

Developments of $A(s)$ convenient for numerical purposes will be discussed shortly. It may be of value to consider first several useful special examples of equation (12).

(a) **Parallel segments of zero stagger**³ ($\delta=0$, $\gamma=0$).—It is necessary to observe first the limiting form of $A(s)$ as $\delta \rightarrow 0$. From equations (4) or (4') (or cf. reference 10, p. 425) we have that

$$\begin{aligned} \lim_{\delta=0} \left(A(s) - \frac{1}{\delta} \right) &= \frac{\sigma'(s)}{\sigma(s)} - \frac{\eta s}{\omega} = \zeta(s) - \frac{\eta s}{\omega} \\ &= \frac{H'(s)}{H(s)} = Z_1(s) \end{aligned} \quad (13)$$

where the various forms are equivalent. The functions σ and ζ are Weierstrass elliptic functions, and H and Z_1 (eta and zeta functions) are the elliptic functions of Jacobi and Hermite. Then putting for convenience the arbitrary constant $k = \frac{4c}{\delta} - ic$ in equation (12) we obtain

or we may put down the complete equation for reference as follows. Noting that

$$Z_1'(s) = -\frac{d}{ds} \left[\zeta(s) - \frac{\eta s}{\omega} \right] = p(s) + \frac{\eta}{\omega}$$

where the Weierstrass p function is defined by

$$p(s) = -\frac{d}{ds} \zeta(s), \text{ and writing } s = \lambda + i\alpha \text{ the equation}$$

determining the singular points of c_1 is

$$p(\lambda + i\alpha) + p(\lambda - i\alpha) + \frac{2\eta}{\pi} = 0 \quad (15)$$

The addition theorem (reference 10, p. 140) of the p function may be written

$$p(\lambda + i\alpha) = \frac{[p'(\lambda) - i\bar{p}'(\alpha)]^2}{4[p(\lambda) + \bar{p}(\alpha)]^2} - p(\lambda) + \bar{p}(\alpha) \quad (16)$$

Here, $\bar{p}(\alpha) = -p(i\alpha)$ and the bar designates that the elliptic function \bar{p} is based on periods $2\bar{\omega}$ and $2\bar{\omega}'$ con-

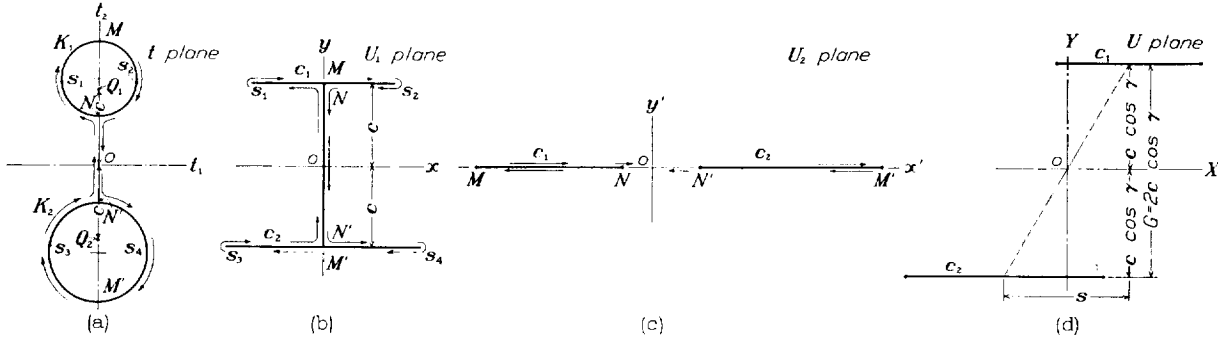


FIGURE 3.—Illustrating the case of parallel line segments: (a) t plane, (b) U_1 plane ($\delta=0$, $\gamma=0$), (c) U_2 plane ($\delta=0$, $\gamma=\pi/2$), (d) U plane ($\delta=0$, γ arbitrary).

$$\begin{aligned} \lim_{\delta=0, \gamma=0} u(s) &= U_1(s) = x + iy \\ &= -2c[Z_1(s) + Z_1(s + 2i\beta)] - ic \end{aligned} \quad (14)$$

or (as given by Ferrari),

$$= -2c \left[\zeta(s) + \zeta(s + 2i\beta) - \frac{2\eta s}{\omega} \right] + \text{const.}$$

Observing that the Z_1 function has the following period properties

$$\begin{aligned} Z_1(s + 2\omega) - Z_1(s) &= 0 \\ Z_1(s + 2\omega') - Z_1(s) &= -i \end{aligned}$$

it follows that for $\mu = \alpha$, $y = c$ and for $\mu = -\beta$, $y = -c$. Hence the gap G between the line segments is $2c$. The case is illustrated in figure 3 (b).

The singular values of λ are in this case given by

$$\begin{aligned} \text{Re. } Z_1'(s + i\alpha) &= 0 \\ \text{Re. } Z_1'(s - i\beta) &= 0 \end{aligned}$$

³The case of parallel line segments has been studied by Ferrari (reference 9).

jugate to the periods of p , i. e., $2\bar{\omega} = \frac{2\omega'}{i}$ and $2\bar{\omega}' = 2i\omega$ (reference 10, p. 32). Making use of (16) and of the differential equations for the p and \bar{p} functions:

$$\begin{aligned} p'(\lambda)^2 &= 4p^3(\lambda) - g_2p(\lambda) - g_3 \\ \bar{p}'(\alpha)^2 &= 4\bar{p}^3(\alpha) - g_2\bar{p}(\alpha) + g_3 \end{aligned}$$

equation (15) becomes

$$Ap(\lambda)^2 + Bp(\lambda) + C = 0 \quad (17)$$

where

$$\begin{aligned} A &= 4[\eta/\pi - \bar{p}(\alpha)] \\ B &= 4\bar{p}(\alpha)^2 + 8(\eta/\pi)\bar{p}(\alpha) - g_2 \\ C &= 4(\eta/\pi)p(\alpha)^2 + g_2\bar{p}(\alpha) - 2g_3 \end{aligned}$$

This equation determines the two singular points for the upper segment c_1 . In general, there is only one positive value of the root $p(\lambda)$, hence the singular points, $\lambda = \pm \lambda_s$, are symmetrical with respect to the origin. The negative root does not give real values for λ . For the lower line segment c_2 it is only necessary to replace α by β . (Cf. reference 10, p. 272: Given $p(\lambda)$, to find λ .)

The line segments c_1 and c_2 given by transformation 14) are without "stagger" since the midpoint of each segment is located on the y axis (fig. 3 (b)). In order to obtain further insight into the general transformation let us consider the case $\delta=0$, $\gamma=90^\circ$.

(b) **Tandem parallel segments** ($\delta=0$, $\gamma=\frac{\pi}{2}$).—In this case let the arbitrary constant $k=-c$ in transformation (12), and noting equation (13), we obtain

$$\begin{aligned} \lim_{\delta=0, \gamma=\frac{\pi}{2}} u(s) &= U_2(s) \\ &= -2ic[Z_1(s) - Z_1(s+2i\beta)] - c \quad (18) \\ &= -2ic[\zeta(s) - \zeta(s+2i\beta)] - c \end{aligned}$$

It can be shown directly that the singular values of λ are 0 and π , for we have

$$\frac{dU_2}{ds} = 0 = p(s) - p(s+2i\beta) \quad (19)$$

and if

$$\begin{aligned} p(u) &= p(v) \text{ we must have} \\ u &= \pm v + 2m\omega + 2m'\omega' \quad \text{where } m \text{ and } m' \end{aligned}$$

are any integers. Hence, writing $s = \lambda + i\mu$ we have for the solutions of (19) in the fundamental periodic rectangle $\lambda_s = 0$ and $\lambda_s = \pi$. Figure 3(c) shows a typical correspondence for this case.

(c) **Parallel segments of arbitrary stagger.**—Let the arbitrary constant $k = \left(\frac{4c}{\delta} - ic\right) \cos \gamma - c \sin \gamma$ in equation (12), and noting relation (13),

$$\begin{aligned} \lim_{\delta=0} u(s) &= U(s) = U_1(s) \cos \gamma + U_2(s) \sin \gamma \\ &= -2c[Z_1(s)e^{i\gamma} + Z_1(s)e^{-i\gamma}] - ice^{-i\gamma} \quad (20) \end{aligned}$$

The function $U(s)$ is the general relation bringing the region about any two parallel line segments into a rectangular region in the s plane. In this transformation the values of the parameters α , β , and γ suffice to fix uniquely the chord ratio c_1/c_2 , the gap/chord G/c_2 , and the stagger/chord S/c_2 of the parallel segments. The gap between the line segments is $2c \cos \gamma$. Figure 3(d) illustrates the definitions of the various quantities. In the general case of parallel segments of arbitrary stagger, there are given the three ratios $c_1:c_2:G:S$ and the parameters α , β , and γ are to be determined. This problem involves the solution of transcendental relations; in this connection it is convenient to draw up charts, e. g., figure 4. This figure shows a cross plot that presents G/c_2 , S/c_2 in terms of ω' and γ in the case of equal chords $c_1/c_2=1$, i. e., $\alpha=\beta$.

The singular points of equation (20) are defined by the relation

$$\frac{dU}{ds} = 0 = p(s)e^{i\gamma} + p(s+2i\beta)e^{-i\gamma} + \frac{2\eta}{\pi} \cos \gamma \quad (21)$$

Writing $s = \lambda + i\alpha$ in (21) we have

$$\begin{aligned} &\cos \gamma [p(\lambda + i\alpha) + p(\lambda - i\alpha) + 2\eta/\pi] \\ &+ i \sin \gamma [p(\lambda + i\alpha) - p(\lambda - i\alpha)] = 0 \end{aligned}$$

Employing the notation of equation (17) and the relations preceding equation (17), there results

$$a_4 p^4(\lambda) + a_3 p^3(\lambda) + a_2 p^2(\lambda) + a_1 p(\lambda) + a_0 = 0 \quad (22)$$

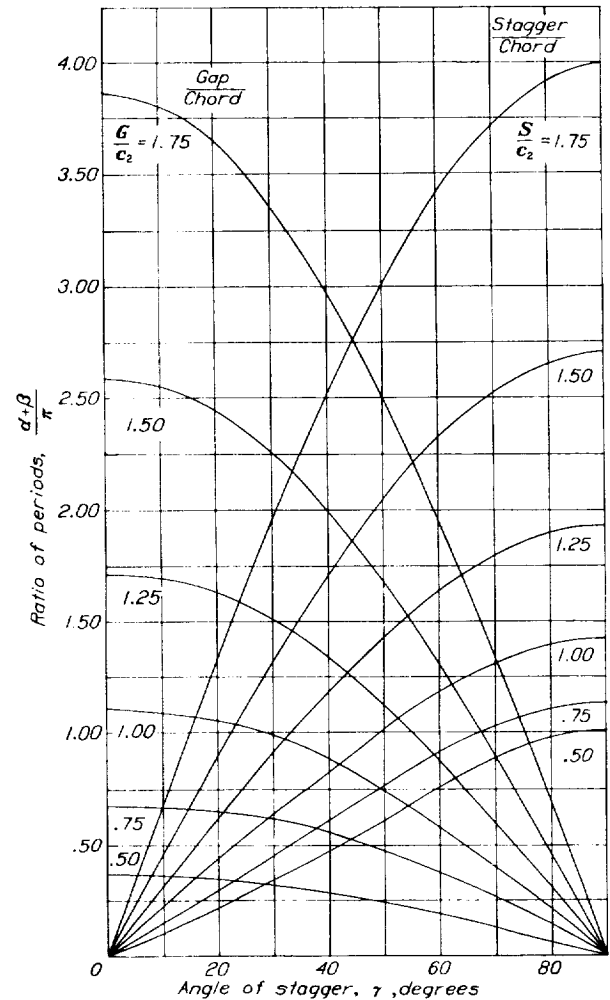


FIGURE 4.—Chart presenting the angle of stagger γ and the ratio of the periods $\frac{\alpha+\beta}{\pi}$ against gap/chord G/c_2 , and stagger/chord S/c_2 in the special case of equal parallel line segments, ($\delta=0$, $\alpha=\beta$)

where

$$\begin{aligned} a_4 &= A^2 d^2 \\ a_3 &= 2ABd^2 - 4 \\ a_2 &= (B^2 + 2AC)d^2 \\ a_1 &= 2BCd^2 + g_2 \\ a_0 &= C^2 d^2 + g_3 \text{ and } d = \frac{1}{2} \frac{\cot \gamma}{p'(\alpha)} \end{aligned}$$

This equation suffices to determine the values of λ corresponding to the end points of the upper line seg-

ments c_1 . In the case of the lower segment α is to be replaced by β . In general, there are only two positive solutions for $p(\lambda)$; and it may be observed that the solutions for both angles of stagger $\pm\gamma$ are contained in equation (22). (In sec. 4 approximations for the singular values of λ are given by simple formulas.)

Jacobi series—In order to obtain further insight into the general relation (12) and to separate $u(s) = X + iY$ into its real and imaginary parts it is necessary to revert to Jacobi expansions. These developments are especially useful where numerical evaluations are required.

By reference 10, page 416, we have the following expansion for the function $A(s)$:

$$A(s) = \frac{e^{-\frac{\gamma}{2}s} \sigma(s+\delta)}{\sigma(\delta)\sigma(s)} = \frac{1}{2} \left(\cot \frac{s}{2} + \cot \frac{\delta}{2} \right) + 2 \sum_{m=1}^{\infty} \sum_{n=1}^{\infty} q^{2mn} \sin(ms+n\delta) \quad (23)$$

where

$$q = e^{\frac{i\pi\omega'}{\omega}} = e^{i\omega'} = e^{-(\alpha+\beta)}$$

The expression for $Z_1(s)$ occurring in the case of parallel segments is

$$\lim_{\delta \rightarrow 0} \left(A(s) - \frac{1}{2} \cot \frac{\delta}{2} \right) = Z_1(s) = \frac{1}{2} \cot \frac{s}{2} + 2 \sum_{m=1}^{\infty} \sum_{n=1}^{\infty} q^{2mn} \sin ms \quad (23')$$

To separate $A(s)$ into real and imaginary parts, replace s by $\lambda + i\mu$ and note that

$$\cot \frac{\lambda + i\mu}{2} = \frac{\sin \lambda - i \sinh \mu}{\cosh \mu - \cos \lambda} \quad (24)$$

Then

$$A(s) = M(\lambda, \mu) + iN(\lambda, \mu) + \frac{1}{2} \cot \frac{\delta}{2} \quad (25)$$

where ⁴

$$M(\lambda, \mu) = -\frac{\sin \lambda}{2(\cosh \mu - \cos \lambda)} + \sum_{m=1}^{\infty} \sum_{n=1}^{\infty} q^{2mn} \sin(m\lambda + n\delta) \cosh m\mu$$

$$N(\lambda, \mu) = -\frac{\sinh \mu}{2(\cosh \mu - \cos \lambda)} + \sum_{m=1}^{\infty} \sum_{n=1}^{\infty} q^{2mn} \cos(m\lambda + n\delta) \sinh m\mu$$

⁴ The value of $q = e^{-(\alpha+\beta)}$ may always be kept less than $e^{-\pi} = 0.0432$ by resorting when necessary, e. g., $\alpha + \beta$ small, to transformations that interchange the real and imaginary periods of the elliptic functions (reference 10, p. 260). Thus the expressions can always be made to converge very rapidly. Indeed, there exist several other expansions for $A(s)$ which though less simple in form are more rapidly convergent than the formula given here (reference 10, p. 422).

Let us put the arbitrary constant k equal to $(2c \cot \frac{\delta}{2} - ic) \cos \gamma - c \sin \gamma$ in equation (12) and separate $u(s)$ as follows

$$u(s) = X + iY = u_1(s) \cos \gamma + u_2(s) \sin \gamma \quad (26)$$

where

$$u_1(s) = x + iy = -2c[A(s) + A(s+2i\beta)] + 2c \cot \frac{\delta}{2} - ic \quad (27)$$

and

$$u_2(s) = x' + iy' = -2ic[A(s) - A(s+2i\beta)] - c \quad (28)$$

It is evident that $u_1(s)$ and $u_2(s)$ are generalizations of $U_1(s)$ and $U_2(s)$, given by equations (14) and (18) for the cases $(\delta=0, \gamma=0)$ and $(\delta=0, \gamma=\pi/2)$, respectively.

Employing relation (25), equation (27) giving $u_1(s)$ may be separated into

$$\left. \begin{aligned} x &= -2c[M(\lambda, \mu) + M(\lambda, \mu+2\beta)] \\ y &= -2c[N(\lambda, \mu) + N(\lambda, \mu+2\beta)] - c \end{aligned} \right\} \quad (27a)$$

It is observed that for $\mu = -\beta$, the coordinates become

$$\left. \begin{aligned} x_\beta &= -4cM(\lambda, \beta) \\ y_\beta &= -c \end{aligned} \right\} \quad (27b)$$

Equation (27a) is most useful in the neighborhood of $\mu = -\beta$. For values of μ near α , relation (27) is first rewritten by making use of the period property $A(s+2\omega') = A(s)e^{-i\delta}$, and we have

$$\left. \begin{aligned} x &= -2c[M(\lambda, \mu) + M(\lambda, \mu-2\alpha) \cos \delta] \\ &\quad + N(\lambda, \mu-2\alpha) \sin \delta] + c \sin \delta \\ y &= -2c[N(\lambda, \mu) + N(\lambda, \mu-2\alpha) \cos \delta] \\ &\quad - M(\lambda, \mu-2\alpha) \sin \delta] + c \cos \delta \end{aligned} \right\} \quad (27c)$$

For $\mu = \alpha$, equation (27c) becomes

$$\left. \begin{aligned} x_\alpha &= -2c[M(\lambda, \alpha)(1 + \cos \delta) - N(\lambda, \alpha) \sin \delta] \\ &\quad + c \sin \delta \\ y_\alpha &= -2c[N(\lambda, \alpha)(1 - \cos \delta) - M(\lambda, \alpha) \sin \delta] \\ &\quad + c \cos \delta \end{aligned} \right\} \quad (27d)$$

It may be remarked that equations (27), which hold also for the special case $\delta=0$, show immediately that in this case $y_\beta = -c$ and $y_\alpha = c$, or that the gap of the parallel segments is $2c$. In the general case ($\delta \neq 0, \gamma=0$) it is clear from (27d) that the point $(x_\alpha, y_\alpha) = (0, c)$ lies on c_1 . The "gap" as measured along the y axis (i. e., from $x_\beta=0$ to $x_\alpha=0$) is therefore again $2c$. The effect of decalage may be considered to a first order to be a rotation of the segment c_1 for the case ($\delta=0, \gamma=0$) by the angle $\delta/2$ about the point $(0, c)$.

Employing relation (25), equation (28) giving $u_2(s)$ may be separated into

$$\left. \begin{aligned} x' &= -2c[-N(\lambda, \mu) + N(\lambda, \mu+2\beta)] - c \\ y' &= -2c[M(\lambda, \mu) - M(\lambda, \mu+2\beta)] \end{aligned} \right\} \quad (28a)$$

It is observed that for $\mu = -\beta$ the coordinates become

$$\left. \begin{aligned} x'_\beta &= -4cN(\lambda, \beta) - c \\ y'_\beta &= 0 \end{aligned} \right\} \quad (28b)$$

In the neighborhood of $\mu=\alpha$, it may be preferable to express equation (28a) as follows

$$\left. \begin{aligned} x' &= -2c[-N(\lambda, \mu) + N(\lambda, \mu - 2\alpha) \cos \delta] \\ &\quad - M(\lambda, \mu - 2\alpha) \sin \delta] + c \cos \delta \\ y' &= -2c[M(\lambda, \mu) - M(\lambda, \mu - 2\alpha) \cos \delta \\ &\quad - N(\lambda, \mu - 2\alpha) \sin \delta] - c \sin \delta \end{aligned} \right\} \quad (28c)$$

For $\mu=\alpha$ the coordinates are seen to be

$$\left. \begin{aligned} x_\alpha' &= 2c[N(\lambda, \alpha)(1 + \cos \delta) \\ &\quad + M(\lambda, \alpha) \sin \delta] + c \cos \delta \\ y_\alpha' &= -2c[M(\lambda, \alpha)(1 - \cos \delta) \\ &\quad + N(\lambda, \alpha) \sin \delta] - c \sin \delta \end{aligned} \right\} \quad (28d)$$

For $\delta=0$ it is clear from (28b) and (28d) that $y_\alpha' = y_\beta' = 0$. In general, for $\delta \neq 0$ it can be seen that the coordinates $(x_\alpha', y_\alpha') = (-c, 0)$ satisfy equation (28d), hence this point lies on c_1 .

The general equation (12) or (26) may now be separated into

$$u(s) = X + iY \quad (29)$$

where

$$\begin{aligned} X &= x \cos \gamma + x' \sin \gamma \\ Y &= y \cos \gamma + y' \sin \gamma \end{aligned}$$

In particular, it is clear from the foregoing that the lower segment c_2 is situated at $Y_\beta = -2c \cos \gamma$ and that the point $(X_\alpha, Y_\alpha) = (-c \sin \gamma, c \cos \gamma)$ lies on the segment c_1 .

If there are given any two line segments in position, the three ratios $c_1:c_2:G:S$ are known (in addition δ is known), and the quantities α , β , and γ are to be determined. Equation (29) is transcendental and a direct solution for a given case is not available; however, an indirect procedure of building up charts similar to figure 4 (for which $\delta=0$) for different values of δ may be resorted to. The case of parallel segments, as well as the degenerate monoplane case (cf. sec. 4), will prove helpful in this procedure.

For later reference, the derivative expression $\frac{du}{ds}$ may be put down. We have

$$\frac{du}{ds} = \frac{du_1}{ds} \cos \gamma + \frac{du_2}{ds} \sin \gamma \quad (30)$$

where

$$\begin{aligned} \frac{1}{2c} \frac{du_1}{ds} &= A'(s) + A'(s + 2i\beta) \\ &= P(\lambda, \mu) + iQ(\lambda, \mu) \\ \frac{1}{2c} \frac{du_2}{ds} &= i[A'(s) - A'(s + 2i\beta)] \\ &= P'(\lambda, \mu) + iQ'(\lambda, \mu) \end{aligned}$$

In order to determine P , Q , P' , and Q' , the following development is noted

$$\begin{aligned} A'(s) &= \frac{1}{4 \sin^2 s/2} \sum_{m=1}^{\infty} \sum_{n=1}^{\infty} m q^{2mn} \cos (ms + n\delta) \\ &= M'(\lambda, \mu) + iN'(\lambda, \mu) \end{aligned} \quad (31)$$

where

$$\begin{aligned} M'(\lambda, \mu) &= \frac{1 - \cos \lambda \cosh \mu}{2(\cosh \mu - \cos \lambda)} \\ &\quad - \sum_{m=1}^{\infty} \sum_{n=1}^{\infty} m q^{2mn} \cos (m\lambda + n\delta) \cosh m\mu \end{aligned}$$

$$\begin{aligned} N'(\lambda, \mu) &= \frac{-\sin \lambda \sinh \mu}{2(\cosh \mu - \cos \lambda)} \\ &\quad - \sum_{m=1}^{\infty} \sum_{n=1}^{\infty} m q^{2mn} \sin (m\lambda + n\delta) \sinh m\mu \end{aligned}$$

Hence,

$$\begin{aligned} P &= M'(\lambda, \mu) + M'(\lambda, \mu + 2\beta) \\ Q &= N'(\lambda, \mu) + N'(\lambda, \mu + 2\beta) \\ P' &= -N'(\lambda, \mu) + N'(\lambda, \mu + 2\beta) \\ Q' &= M'(\lambda, \mu) - M'(\lambda, \mu + 2\beta) \end{aligned}$$

And finally

$$\frac{du}{ds} = 2c[P' \cos \gamma + P' \sin \gamma + i(Q \cos \gamma + Q' \sin \gamma)] \quad (32)$$

The equations of this section may be simplified in the noteworthy special case in which $\alpha=\beta$. The constant $2i\beta$ is in this case equal to half the imaginary period, i. e., $2i\beta = \omega'$ and, in particular, the line segments c_1 and c_2 are equal. By reference 10, page 422, we have

$$\begin{aligned} A(s + \omega') &= \frac{\sigma_3(s + \delta)}{\sigma_3(s) \sigma(\delta)} e^{-\frac{\pi \delta}{\omega}} e^{-\frac{\delta}{2}} \\ &= e^{-\frac{\delta}{2}} \left(\frac{1}{2} \csc \frac{\delta}{2} + \sum_{m=1}^{\infty} \sum_{n=1}^{\infty} q^{(2n-1)m} \sin [ms + (n-1/2)\delta] \right) \end{aligned}$$

This expression may therefore replace $A(s + 2i\beta)$ in equations (26), (27), and (28). Similarly in equation (30) $A'(s + 2i\beta)$ may be replaced by $A'(s + \omega')$ where

$$A'(s + \omega') = -e^{-\frac{\delta}{2}} \sum_{m=1}^{\infty} \sum_{n=1}^{\infty} m q^{(2n-1)m} \cos [ms + (n-1/2)\delta]$$

3. TRANSFORMATION OF A NEARLY CIRCULAR RING REGION IN THE w PLANE INTO A TRULY CIRCULAR RING REGION IN THE z PLANE

In the foregoing sections, there have been obtained the equations transforming the region external to two circles (in the t plane); or the annular region between two concentric circles (in the w plane); or also a rectangular region (in the s plane); into the region external to any two nonintersecting line segments (in the u plane). It may now be imagined, for definiteness, that two airfoil profiles are generated about the two line segments as chords in the u plane (fig. 5 (a)). In the plane of the rectangle, the two profiles will correspond to curves of small amplitude extending

from $\lambda = -\pi$ to $\lambda = \pi$ near the boundary lines $\mu = \alpha$ and $\mu = -\beta$, respectively. In the ring region, the profiles will correspond to two nearly circular contours forming an annular region (fig. 5 (c)). It is intended to show how this annular region may be transformed into a concentric circular ring region (fig. 5 (e)).

At present it is assumed that the nearly circular ring region in the w plane corresponding to a given biplane cellule in the u plane is known. It is observed that this knowledge implies that equation (2.12) may be inverted and the variables λ, μ solved for in terms of x and y . How this task may be done is taken up in section 4. It is recalled here that the variable λ corresponds to $-\theta$ (equation (1.6)) and that the

where the radii are respectively,

$$R_1 = ce^{\sigma_1}, R_2 = ce^{\sigma_2}, \sigma_1 > 0, \sigma_2 < 0$$

(At times it will be found convenient to denote σ_1 by α' and σ_2 by $-\beta'$).

Let the function that transforms the w plane conformally into the z plane be written as

$$w = ze^{h(z)} \quad (5)$$

where $z = ce^{\sigma + i\varphi} = Re^{i\varphi}$ and where $h(z)$ represents a Laurent series with complex coefficients:

$$h(z) = a_0 + \sum_{n=1}^{\infty} (a_n z^n + a_{-n} z^{-n}) \quad (6)$$

where $R_2 \leq |z| \leq R_1$, or with $z = Re^{i\varphi}$

$$h(z) = f(R, \varphi) + ig(R, \varphi) \quad (6')$$

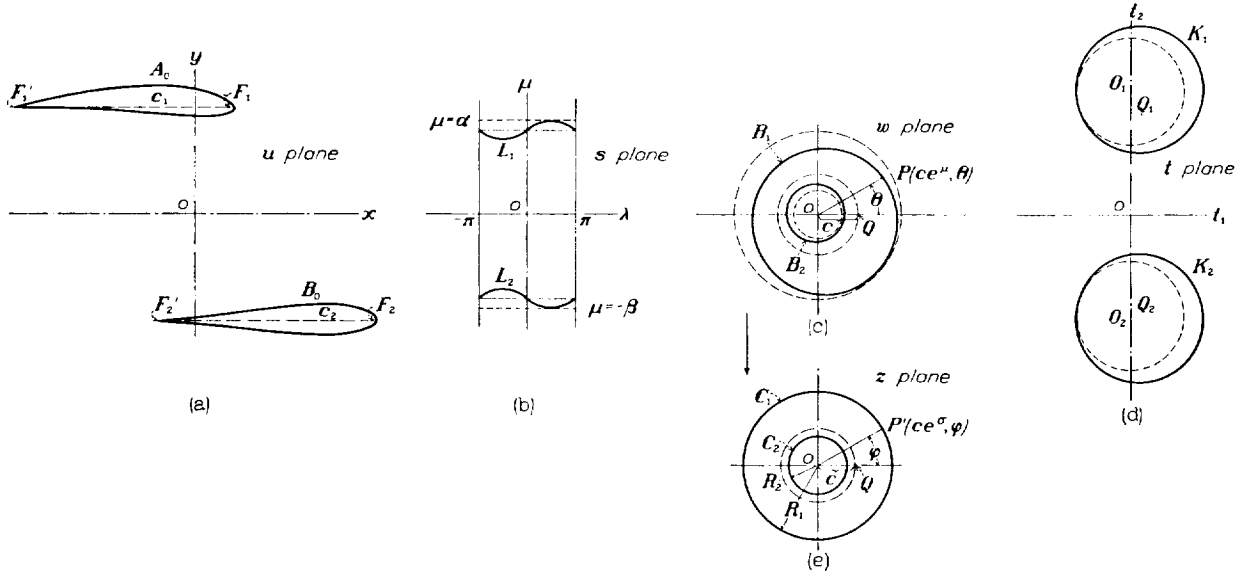


FIGURE 5.—Mapping of: (a) two contours A_0 and B_0 of a biplane arrangement into (b) two curved lines L_1 and L_2 in the s plane, (c) two nearly circular contours B_1 and B_2 of an annular region in the w plane, (d) two nearly circular contours K_1 and K_2 in the t plane, (e) two true circles C_1 and C_2 of the concentric ring region in the z plane.

neighborhood of the point $w = c$, which corresponds to the region at infinity in the t or u planes, must be an internal point of the annular region.

The annular region in the w plane then contains two boundary contours, an outer contour B_1 and an inner contour B_2 . Let the contour B_1 be defined by

$$w = ce^{\mu_1(\theta) + i\theta} \quad (1)$$

and the contour B_2 by

$$w = ce^{\mu_2(\theta) + i\theta} \quad (2)$$

where the range of θ may be chosen as $0 \leq \theta \leq 2\pi$.

Consider now a z plane (fig. 5 (e)) containing two concentric circles about the origin, an outer circle C_1 that corresponds to B_1 and an inner circle C_2 that corresponds to B_2 . The circle C_1 may be defined by

$$z = ce^{\sigma_1 + i\varphi} \quad (3)$$

and the circle C_2 by

$$z = ce^{\sigma_2 + i\varphi} \quad (4)$$

It is seen that on C_1 ,

$$\log \frac{w}{z} = h(z) = h(R_1, \varphi) = f(R_1, \varphi) + ig(R_1, \varphi) = \mu_1 - \sigma_1 + i(\theta - \varphi)_1$$

or, in short,

$$h_1(\varphi) = f_1(\varphi) + ig_1(\varphi) = \mu_1 - \sigma_1 + i(\theta - \varphi)_1 \quad (7)$$

where $(\theta - \varphi)_1$ means that the quantity $\theta - \varphi$ is evaluated around C_1 . On C_2 similarly

$$h_2(\varphi) = f_2(\varphi) + ig_2(\varphi) = \mu_2 - \sigma_2 + i(\theta - \varphi)_2 \quad (8)$$

Let the complex coefficients in equation (6) be expressed as

$$\left. \begin{aligned} a_n &= A_n + iB_n \\ a_{-n} &= A_{-n} + iB_{-n} \end{aligned} \right\} \quad (9)$$

Then, from equations (6) and (7), it is found that

$$f_1(\varphi) = A_0 + \sum_{n=1}^{\infty} [(A_n R_1^n + A_{-n} R_1^{-n}) \cos n\varphi - (B_n R_1^n - B_{-n} R_1^{-n}) \sin n\varphi] \quad (10)$$

$$g_1(\varphi) = B_0 + \sum_{n=1}^{\infty} [(B_n R_1^n + B_{-n} R_1^{-n}) \cos n\varphi + (A_n R_1^n - A_{-n} R_1^{-n}) \sin n\varphi] \quad (11)$$

Similarly

$$f_2(\varphi) = A_0 + \sum_1^{\infty} [(A_n R_2^n + A_{-n} R_2^{-n}) \cos n\varphi - (B_n R_2^n - B_{-n} R_2^{-n}) \sin n\varphi] \quad (12)$$

$$g_2(\varphi) = B_0 + \sum_1^{\infty} [(B_n R_2^n + B_{-n} R_2^{-n}) \cos n\varphi + (A_n R_2^n - A_{-n} R_2^{-n}) \sin n\varphi] \quad (13)$$

From equation (10),

$$\left. \begin{aligned} A_n R_1^n + A_{-n} R_1^{-n} &= a_{1,n} = \frac{1}{\pi} \int_0^{2\pi} f_1(\varphi) \cos n\varphi d\varphi \\ -B_n R_1^n + B_{-n} R_1^{-n} &= b_{1,n} = \frac{1}{\pi} \int_0^{2\pi} f_1(\varphi) \sin n\varphi d\varphi \end{aligned} \right\} \quad (14)$$

and

$$A_0 = a_{1,0} = \frac{1}{2\pi} \int_0^{2\pi} f_1(\varphi) d\varphi = \frac{1}{2\pi} \int_0^{2\pi} \mu_1 d\varphi - \sigma_1$$

Similarly from equation (12),

$$\left. \begin{aligned} A_n R_2^n + A_{-n} R_2^{-n} &= a_{2,n} = \frac{1}{\pi} \int_0^{2\pi} f_2(\varphi) \cos n\varphi d\varphi \\ -B_n R_2^n + B_{-n} R_2^{-n} &= b_{2,n} = \frac{1}{\pi} \int_0^{2\pi} f_2(\varphi) \sin n\varphi d\varphi \end{aligned} \right\} \quad (15)$$

and

$$A_0 = a_{2,0} = \frac{1}{2\pi} \int_0^{2\pi} f_2(\varphi) d\varphi = \frac{1}{2\pi} \int_0^{2\pi} \mu_2 d\varphi - \sigma_2$$

The equality $a_{1,0} = a_{2,0} = A_0$ is a condition of uniformity that is necessary since $h(z)$ is a regular analytic function in the ring region. There is, in addition, an arbitrary element in equations (10) to (13) (which may be chosen in a number of ways) viz, there is at our disposal the choice of the point in the z plane that shall correspond to, say $w=c$. This choice, which will be introduced at a later point (p. 14), is $z=c$ when $w=c$, and will fix the constants A_0 and B_0 in terms of R_1 and R_2 and the remaining coefficients.

From the first parts of equations (14) and (15),

Denoting the variable in equation (17) by φ' instead of φ and substituting by means of equations (14) and (15), it appears that

$$\begin{aligned} g_1(\varphi') &= B_0 + \frac{1}{\pi} \sum_1^{\infty} \int_0^{2\pi} f_1(\varphi) (-\sin n\varphi \cos n\varphi' + \cos n\varphi \sin n\varphi') \coth n\tau d\varphi \\ &\quad + \frac{1}{\pi} \sum_1^{\infty} \int_0^{2\pi} f_2(\varphi) (\sin n\varphi \cos n\varphi' - \cos n\varphi \sin n\varphi') \operatorname{csch} n\tau d\varphi \end{aligned}$$

or

$$g_1(\varphi') = B_0 + \frac{1}{\pi} \sum_1^{\infty} \left[\int_0^{2\pi} f_2(\varphi) \sin n(\varphi - \varphi') \operatorname{csch} n\tau d\varphi - \int_0^{2\pi} f_1(\varphi) \sin n(\varphi - \varphi') \coth n\tau d\varphi \right] \quad (19)$$

In a similar manner,

$$g_2(\varphi') = B_0 + \frac{1}{\pi} \sum_1^{\infty} \left[\int_0^{2\pi} f_2(\varphi) \sin n(\varphi - \varphi') \coth n\tau d\varphi - \int_0^{2\pi} f_1(\varphi) \sin n(\varphi - \varphi') \operatorname{csch} n\tau d\varphi \right] \quad (20)$$

there is obtained on solving for A_n , A_{-n} , B_n , and B_{-n}

$$\left. \begin{aligned} A_n &= \frac{a_{1,n} R_2^{-n} - a_{2,n} R_1^{-n}}{\left(\frac{R_1}{R_2}\right)^n - \left(\frac{R_2}{R_1}\right)^n}, \quad B_n = \frac{-b_{1,n} R_2^{-n} + b_{2,n} R_1^{-n}}{\left(\frac{R_1}{R_2}\right)^n - \left(\frac{R_2}{R_1}\right)^n} \\ A_{-n} &= \frac{-a_{1,n} R_2^n + a_{2,n} R_1^n}{\left(\frac{R_1}{R_2}\right)^n - \left(\frac{R_2}{R_1}\right)^n}, \quad \text{and } B_{-n} = \frac{-b_{1,n} R_2^n + b_{2,n} R_1^n}{\left(\frac{R_1}{R_2}\right)^n - \left(\frac{R_2}{R_1}\right)^n} \end{aligned} \right\} \quad (16)$$

Let

$$\frac{R_2}{R_1} = e^{-\tau} = q$$

where

$$\tau = \sigma_1 - \sigma_2 (= \alpha' + \beta')$$

Substituting by means of equation (16) in equation (11), it is seen that

$$\begin{aligned} g_1(\varphi) &= B_0 + \sum_1^{\infty} \left(\frac{b_{1,n} e^{n\tau} + b_{2,n}}{e^{n\tau} - e^{-n\tau}} + \frac{-b_{1,n} e^{-n\tau} + b_{2,n}}{e^{n\tau} - e^{-n\tau}} \right) \cos n\pi \\ &\quad + \sum_1^{\infty} \left(\frac{a_{1,n} e^{n\tau} - a_{2,n}}{e^{n\tau} - e^{-n\tau}} + \frac{a_{1,n} e^{-n\tau} - a_{2,n}}{e^{n\tau} - e^{-n\tau}} \right) \sin n\pi \\ g_1(\varphi) &= B_0 + \sum_1^{\infty} \left[-b_{1,n} \left(\frac{e^{n\tau} + e^{-n\tau}}{e^{n\tau} - e^{-n\tau}} \right) \right. \\ &\quad \left. + b_{2,n} \left(\frac{2}{e^{n\tau} + e^{-n\tau}} \right) \right] \cos n\varphi \\ &\quad + \sum_1^{\infty} \left[a_{1,n} \left(\frac{e^{n\tau} + e^{-n\tau}}{e^{n\tau} - e^{-n\tau}} \right) - a_{2,n} \left(\frac{2}{e^{n\tau} - e^{-n\tau}} \right) \right] \sin n\varphi \end{aligned}$$

or also

$$\begin{aligned} g_1(\varphi) &= B_0 + \sum_1^{\infty} (-b_{1,n} \coth n\tau + b_{2,n} \operatorname{csch} n\tau) \cos n\varphi \\ &\quad + \sum_1^{\infty} (a_{1,n} \coth n\tau - a_{2,n} \operatorname{csch} n\tau) \sin n\varphi \quad (17) \end{aligned}$$

Similarly, by substitution of equation (16) in equation (13),

$$\begin{aligned} g_2(\varphi) &= B_0 + \sum_1^{\infty} (-b_{1,n} \operatorname{csch} n\tau + b_{2,n} \coth n\tau) \cos n\varphi \\ &\quad + \sum_1^{\infty} (a_{1,n} \operatorname{csch} n\tau - a_{2,n} \coth n\tau) \sin n\varphi \quad (18) \end{aligned}$$

The two series expressions

$$\begin{aligned} a) & \sum_1^{\infty} \sin n(\varphi - \varphi') \coth n\tau \\ b) & \sum_1^{\infty} \sin n(\varphi - \varphi') \operatorname{csch} n\tau \end{aligned}$$

that occur in equations (19) and (20) may be evaluated in terms of elliptic functions. Consider the expansion for $\zeta(u)$ (reference 10, p. 403)

$$\begin{aligned} \zeta(u) - \frac{\eta u}{\omega_1} &= Z_1(u) = \frac{H'(u)}{H(u)} \\ &= \frac{\pi}{2\omega_1} \cot \frac{\pi u}{2\omega_1} + \frac{2\pi}{\omega_1} \sum_1^{\infty} \frac{q^{2n}}{1-q^{2n}} \sin \frac{n\pi u}{\omega_1} \end{aligned}$$

In order not to confuse the periods occurring here with those of the preceding section, the real period is denoted by $2\omega_1 = 2\pi$, and the imaginary period by $2\omega_2 = 2i\tau$,

$$q = e^{i\pi \frac{\omega_2}{\omega_1}} = e^{-\tau} = \frac{R_2}{R_1}$$

Then

$$\begin{aligned} Z_1(u) &= \frac{1}{2} \cot \frac{u}{2} + 2 \sum_1^{\infty} \frac{e^{-2n\tau}}{1-e^{-2n\tau}} \sin nu \\ &= \sum_1^{\infty} \sin nu + \sum_1^{\infty} \left(\frac{1+e^{-2n\tau}}{1-e^{-2n\tau}} - 1 \right) \sin nu \\ &= \sum_1^{\infty} \coth n\tau \sin nu \end{aligned} \quad (21)$$

Consider the expansion for $\zeta(u + \omega_2)$ (reference 10, p. 426)⁵

$$\begin{aligned} \zeta(u + \omega_2) - \frac{\eta(u)}{\pi} - \eta' &= Z(u) = \frac{\Theta'(u)}{\Theta(u)} \\ &= \frac{2\pi}{\omega_1} \sum_1^{\infty} \frac{q^n}{1-q^{2n}} \sin \frac{n\pi u}{\omega_1} \end{aligned}$$

For $\omega_1 = \pi$ this expression becomes

$$\begin{aligned} Z(u) &= \sum_1^{\infty} \frac{2e^{-n\tau}}{1-e^{-2n\tau}} \sin nu \\ &= \sum_1^{\infty} \operatorname{csch} n\tau \sin nu \end{aligned} \quad (22)$$

Then replacing u by $\varphi - \varphi'$, equations (19) and (20) become

$$\begin{aligned} g_1(\varphi') &= B_0 + \frac{1}{\pi} \int_0^{2\pi} f_2(\varphi) Z(\varphi - \varphi') d\varphi \\ &\quad - \frac{1}{\pi} \int_0^{2\pi} f_1(\varphi) Z_1(\varphi - \varphi') d\varphi \end{aligned} \quad (23)$$

$$\begin{aligned} g_2(\varphi') &= B_0 + \frac{1}{\pi} \int_0^{2\pi} f_2(\varphi) Z_1(\varphi - \varphi') d\varphi \\ &\quad - \frac{1}{\pi} \int_0^{2\pi} f_1(\varphi) Z(\varphi - \varphi') d\varphi \end{aligned} \quad (24)$$

Since $Z(u) = \frac{\Theta'(u)}{\Theta(u)}$ and $Z_1(u) = \frac{H'(u)}{H(u)}$, there is obtained also by integration by parts:

$$\begin{aligned} g_1(\varphi') &= B_0 - \frac{1}{\pi} \int_0^{2\pi} f_2'(\varphi) \log \Theta(\varphi - \varphi') d\varphi \\ &\quad + \frac{1}{\pi} \int_0^{2\pi} f_1'(\varphi) \log H(\varphi - \varphi') d\varphi \end{aligned} \quad (23')$$

$$\begin{aligned} g_2(\varphi') &= B_0 - \frac{1}{\pi} \int_0^{2\pi} f_2'(\varphi) \log H(\varphi - \varphi') d\varphi \\ &\quad + \frac{1}{\pi} \int_0^{2\pi} f_1'(\varphi) \log \Theta(\varphi - \varphi') d\varphi \end{aligned} \quad (24')$$

where the logarithm operates only on the absolute value of the quantities $\Theta(\varphi - \varphi')$ and $H(\varphi - \varphi')$.

In a manner similar to the foregoing procedure it is possible to solve for the coefficients in equations (11) and (13), substitute in equations (10) and (12), and obtain as the reciprocal relations to (23) and (24) the following:

$$\begin{aligned} f_1(\varphi') &= A_0 - \frac{1}{\pi} \int_0^{2\pi} g_2(\varphi) Z(\varphi - \varphi') d\varphi \\ &\quad + \frac{1}{\pi} \int_0^{2\pi} g_1(\varphi) Z_1(\varphi - \varphi') d\varphi \end{aligned} \quad (25)$$

$$\begin{aligned} f_2(\varphi') &= A_0 - \frac{1}{\pi} \int_0^{2\pi} g_2(\varphi) Z_1(\varphi - \varphi') d\varphi \\ &\quad + \frac{1}{\pi} \int_0^{2\pi} g_1(\varphi) Z(\varphi - \varphi') d\varphi \end{aligned} \quad (26)$$

Equations (23) and (24), which essentially express a pair of boundary-value relations for a concentric ring region, permit the obtaining of the imaginary parts of a complex function $h(z)$ along the boundary circles of a ring region from a knowledge of the real parts along the boundaries. These equations are fundamental in a potential-theory study of ring regions; they have been developed in a different manner and for another purpose by Henri Villat in 1912 (reference 13, p. 147). It will be shown shortly that equations (23) and (24), when generalized and regarded as integral equations instead of being considered as definite integrals, make it possible to obtain the complete correspondence which we are seeking for doubly connected regions.

⁵ For reference, note the definition of the Θ function (cf. references 11 and 12)

$$\Theta(u) = 1 - 2q \cos \frac{\pi u}{\omega} + 2q^4 \cos \frac{2\pi u}{\omega} - 2q^9 \cos \frac{3\pi u}{\omega} + \dots$$

The H function is defined in equation (2.6) of the preceding section. Some writers on elliptic functions use Θ_0 and Θ_1 to denote the Θ and H functions.

The function giving the value of $h(z)$ at any point *interior* to the ring region may also be expressed in terms of the real parts of $h(z)$ along the boundaries C_1 and C_2 . From equation (16),

$$a_n = A_n + iB_n - \frac{1}{2\pi \sinh n\tau} \left[R_2^{-n} \int_0^{2\pi} f_1(\varphi) e^{-in\varphi} d\varphi - R_1^{-n} \int_0^{2\pi} f_2(\varphi) e^{-in\varphi} d\varphi \right]$$

$$a_{-n} = A_{-n} + iB_{-n} - \frac{1}{2\pi \sinh n\tau} \left[-R_2^n \int_0^{2\pi} f_1(\varphi) e^{in\varphi} d\varphi + R_1^n \int_0^{2\pi} f_2(\varphi) e^{in\varphi} d\varphi \right]$$

Then equation (6)

$$h(z) = a_0 + \sum_1^{\infty} (a_n z^n + a_{-n} z^{-n})$$

becomes

$$h(z) = a_0 - \frac{1}{\pi} \int_0^{2\pi} f_1(\varphi) M d\varphi + \frac{1}{\pi} \int_0^{2\pi} f_2(\varphi) N d\varphi \quad (27)$$

where

$$M = \sum_1^{\infty} \frac{R_2^n z^{-n} e^{in\varphi} - R_2^{-n} z^n e^{-in\varphi}}{2 \sinh n\tau}$$

$$N = \sum_1^{\infty} \frac{R_1^n z^{-n} e^{in\varphi} - R_1^{-n} z^n e^{-in\varphi}}{2 \sinh n\tau}$$

The quantities M and N may be readily expressed in terms of elliptic functions. Let

$$e^{in\varphi_2} = R_2^n z^{-n} e^{in\varphi}$$

Then by equation (22),

$$M = \sum_1^{\infty} \frac{i \sin nv_2}{\sinh n\tau} = \frac{O'(v_2)}{i\Theta(v_2)} = iZ(v_2)$$

Similarly let

$$e^{in\varphi_1} = R_1^n z^{-n} e^{in\varphi}$$

Then

$$N = i \frac{\Theta'(v_1)}{\Theta(v_1)} = iZ(v_1)$$

Then finally

$$h(z) = a_0 - \frac{i}{\pi} \int_0^{2\pi} f_1(\varphi) Z(v_2) d\varphi + \frac{i}{\pi} \int_0^{2\pi} f_2(\varphi) Z(v_1) d\varphi \quad (28)$$

where

$$v_2 = i \log \frac{z}{R_2} + \varphi$$

$$v_1 = i \log \frac{z}{R_1} + \varphi$$

or writing

$$z = ce^{\sigma + i\varphi'}$$

$$v_2 = \varphi - \varphi' + i(\sigma - \sigma_2)$$

$$v_1 = \varphi - \varphi' + i(\sigma - \sigma_1)$$

Determination of the constants A_0 and B_0 .—It will be recalled that the neighborhood of the point $w=c$ corresponds to the region at infinity in the t and u planes. In order to make the correspondence of the w and z planes unique the following condition is put down. Let $z=c$ when $w=c$, hence causing the region about $z=c$ to correspond also to the region at infinity in the t and u planes. There is, however, an essential fact to be noted, viz, $\frac{dw}{dz}$ evaluated for $z=c$ is, in general, different from unity, hence generally a magnification and rotation of the regions near $w=c$ and $z=c$ exists in the two planes.

The conditions to be studied are

$$w=c \quad (29)$$

$$\frac{dw}{dz} = re^{i\xi}, \text{ evaluated for } z=c \quad (29')$$

From equation (5)

$$w = ze^{h(z)}$$

there is obtained

$$\frac{dw}{dz} = e^{h(z)} \left(1 + z \frac{dh(z)}{dz} \right) \quad (30)$$

The condition (29) then corresponds to

$$[h(z)]_{z=c} = 0 \quad (31)$$

And, in view of the preceding relations, equation (29') corresponds to

$$\left[z \frac{dh(z)}{dz} \right]_{z=c} = re^{i\xi} - 1 = p + iq \quad (31')$$

where it is noted that r and ξ are given in terms of p and q as follows:

$$r^2 = (1+p)^2 + q^2$$

$$\xi = \tan^{-1} \frac{q}{1+p}$$

By equations (6) and (9), it is found that equation (31) separates into

$$A_0 + \sum_1^{\infty} (A_n c^n + A_{-n} c^{-n}) = 0 \quad (32)$$

$$B_0 + \sum_1^{\infty} (B_n c^n + B_{-n} c^{-n}) = 0 \quad (33)$$

Also equation (31') becomes

$$\sum_1^{\infty} n (A_n c^n - A_{-n} c^{-n}) = p \quad (34)$$

$$\sum_1^{\infty} n (B_n c^n - B_{-n} c^{-n}) = q \quad (35)$$

These equations may also be expressed in other forms. For example, from equation (28), since $z=c$ corresponds to $\sigma=0$, $\varphi'=0$, we have that

$$h(c) = 0 = A_0 + iB_0 - \frac{i}{\pi} \int_0^{2\pi} f_1(\varphi) Z(v_2) d\varphi$$

$$+ \frac{i}{\pi} \int_0^{2\pi} f_2(\varphi) Z(v_1) d\varphi$$

where

$$v_2 = \varphi - i\sigma_2,$$

and

$$v_1 = \varphi - i\sigma_1$$

Employing equation (22), this separates into

$$A_0 - \frac{1}{\pi} \sum_{n=1}^{\infty} \frac{\sinh \frac{n\sigma_2}{n\tau}}{\sinh \frac{n\sigma_1}{n\tau}} \int_0^{2\pi} f_1(\varphi) \cos n\varphi d\varphi \\ + \frac{1}{\pi} \sum_{n=1}^{\infty} \frac{\sinh \frac{n\sigma_1}{n\tau}}{\sinh \frac{n\sigma_2}{n\tau}} \int_0^{2\pi} f_2(\varphi) \cos n\varphi d\varphi = 0 \quad (32')$$

$$B_0 - \frac{1}{\pi} \sum_{n=1}^{\infty} \frac{\cosh \frac{n\sigma_2}{n\tau}}{\sinh \frac{n\sigma_1}{n\tau}} \int_0^{2\pi} f_1(\varphi) \sin n\varphi d\varphi \\ + \frac{1}{\pi} \sum_{n=1}^{\infty} \frac{\cosh \frac{n\sigma_1}{n\tau}}{\sinh \frac{n\sigma_2}{n\tau}} \int_0^{2\pi} f_2(\varphi) \sin n\varphi d\varphi = 0 \quad (33')$$

In these equations f_1 and f_2 may each be altered by the addition of a constant without altering the values of the integrals. Hence, if $f_1(\varphi) - A_0$, $f_2(\varphi) - A_0$ are known (i. e., only the variational parts of f_1 and f_2 are known) and if there are also given or known the quantities $R_1 = ce^{\sigma_1}$, $R_2 = ce^{\sigma_2}$, equations (32') and (33') determine directly the constants A_0 and B_0 so that condition (31) is satisfied.

Since μ_1 and μ_2 differ from f_1 and f_2 by constants (cf. equations (7) and (8)) they may replace f_1 and f_2 in equations (32') and (33'). Also, by equations (14) and (15) it is recalled that

$$A_0 = \frac{1}{2\pi} \int_0^{2\pi} \mu_1 d\varphi - \sigma_1 = \frac{1}{2\pi} \int_0^{2\pi} \mu_2 d\varphi - \sigma_2$$

or that $\tau = \sigma_1 - \sigma_2 = \frac{1}{2\pi} \int_0^{2\pi} (\mu_1 - \mu_2) d\varphi$. Hence, if there are given the functions μ_1 and μ_2 (therefore τ is known), equation (32') determines the individual quantities σ_1 and σ_2 (i. e., the radii R_1 and R_2). Equation (33') then again defines the value of the constant B_0 .

By the use of equations (15) and (16), the conditions (34) and (35) may also be written in other forms. Thus

$$p = \frac{1}{\pi} \sum_{n=1}^{\infty} \frac{n \cosh \frac{n\sigma_2}{n\tau}}{\sinh \frac{n\sigma_1}{n\tau}} \int_0^{2\pi} f_1(\varphi) \cos n\varphi d\varphi \\ - \frac{1}{\pi} \sum_{n=1}^{\infty} \frac{n \cosh \frac{n\sigma_1}{n\tau}}{\sinh \frac{n\sigma_2}{n\tau}} \int_0^{2\pi} f_2(\varphi) \cos n\varphi d\varphi \quad (34')$$

$$q = \frac{1}{\pi} \sum_{n=1}^{\infty} \frac{n \sinh \frac{n\sigma_2}{n\tau}}{\sinh \frac{n\sigma_1}{n\tau}} \int_0^{2\pi} f_1(\varphi) \sin n\varphi d\varphi \\ - \frac{1}{\pi} \sum_{n=1}^{\infty} \frac{n \sinh \frac{n\sigma_1}{n\tau}}{\sinh \frac{n\sigma_2}{n\tau}} \int_0^{2\pi} f_2(\varphi) \sin n\varphi d\varphi \quad (35')$$

Further study of equations (23) and (24).—It has already been mentioned that there are two points of view from which the simultaneous equations (23) and (24) may be studied. In one, the equations are re-

garded as definite integral evaluations and the functions $f_1(\varphi)$ and $f_2(\varphi)$ are known as functions of the variable φ . In the other, the equations are regarded as integral equations and the functions are known in terms of θ , not φ . In the next few paragraphs the definite-integral viewpoint will first be employed and it will be shown how it may be used to develop biplane arrangements in an artificial or indirect manner. The results obtained by this method will also be of some interest and value when the more direct integral-equation point of view is investigated in the subsequent section.

Families of biplane arrangements.—When $f_1(\varphi)$ and $f_2(\varphi)$ are known functions, the evaluation of equations (23) and (24) determine the "conjugate" functions $g_1(\varphi)$ and $g_2(\varphi)$. It may be observed that the Fourier series expansions of $f_1(\varphi)$ and $g_1(\varphi)$ and of $f_2(\varphi)$ and $g_2(\varphi)$ are related by the peculiar interchange of coefficients as seen in equations (10) to (13). The existence of the integrals in equations (23) and (24) requires only that $f_1(\varphi)$ and $f_2(\varphi)$ be piecewise continuous and differentiable, and have no poles of order equal to or greater than one. In this paper, however, the only interest is in continuous, single-valued functions f_1 and f_2 , of period 2π , and satisfying the conditions of uniformity (cf. paragraph following equation (15)), such functions as may always be associated with the conformal transformation of doubly connected regions bounded by continuous closed contours for a proper choice of coordinates.⁶

When the functions $g_1(\varphi)$ and $g_2(\varphi)$ are known, the correspondence of θ and φ is immediately known along the boundary contours since $g(\varphi) = \theta - \varphi$. Also, the functions $f_1(\varphi)$ and $f_2(\varphi)$ together with the constants σ_1 and σ_2 determine⁷ the functions $\mu_1(\varphi)$ and $\mu_2(\varphi)$. The quantities μ_1 and μ_2 expressed as functions of $\theta (= -\lambda)$ then permit the defining of two contours in the u plane, the external region of which is in one-to-one correspondence with the ring region. Some specific examples will shortly be given. With an insight gained by experience, the functions $\mu_1(\varphi)$ and $\mu_2(\varphi)$ may be so chosen that certain desired classes of practical biplane arrangements may be obtained. It may be remarked here that once there is obtained a definite biplane arrangement by means of this process, the problem may immediately be considered reversed and thus insight is obtained into the solution of the associated integral equation. This notion will be later examined; in this section, some illustrations of the afore-mentioned process are briefly presented.

⁶ There is an additional condition on $g_1(\varphi)$ or $g_2(\varphi)$ necessary in order that the contours shall be free of double points (cf. reference 1, p. 10), viz,

$$-1 \leq \frac{dg_1}{d\varphi} \leq \infty, \quad -1 \leq \frac{dg_2}{d\varphi} \leq \infty$$

⁷ It is understood that the minor equation (31) is to be satisfied.

By reference to the Fourier series developments for $f_1(\varphi)$ and $f_2(\varphi)$, equations (10) and (12), it may be observed that a particularly simple example is the following:

$$\begin{aligned} f_1(\varphi) &= \mu_1(\varphi) - \sigma_1 = A_0 - 0.1 \sin \varphi \\ &= A_0 - (B_1 R_1 - B_{-1} R_1^{-1}) \sin \varphi \end{aligned} \quad (36a)$$

$$\begin{aligned} f_2(\varphi) &= \mu_2(\varphi) - \sigma_2 = A_0 + 0.1 \sin \varphi \\ &= A_0 - (B_1 R_2 - B_{-1} R_2^{-1}) \sin \varphi \end{aligned} \quad (36b)$$

Also let $\sigma_1 = \frac{\pi}{2} - 0.1 = 1.4708$, and let $\sigma_2 = -1.4708$. (Hence $\tau = \sigma_1 - \sigma_2 = 2(1.4708)$ and $2\omega_2 = 2i\tau = 5.8832i$.)

or finally,

$$\mu_1(\varphi) = 1.4708 - 0.1 \sin \varphi = -\mu_2(\varphi)$$

$$g_1(\varphi) = -0.04851 + 0.11114 \cos \varphi = g_2(\varphi)$$

It is now possible to define the variable $\theta = \varphi + g(\varphi)$ along each contour:

$$\theta_1 = -\lambda_1 = \varphi + g_1(\varphi)$$

$$\theta_2 = -\lambda_2 = \varphi + g_2(\varphi)$$

In addition to the choice of f_1 and f_2 , the line segments, or chords, and their relative positions (deter-

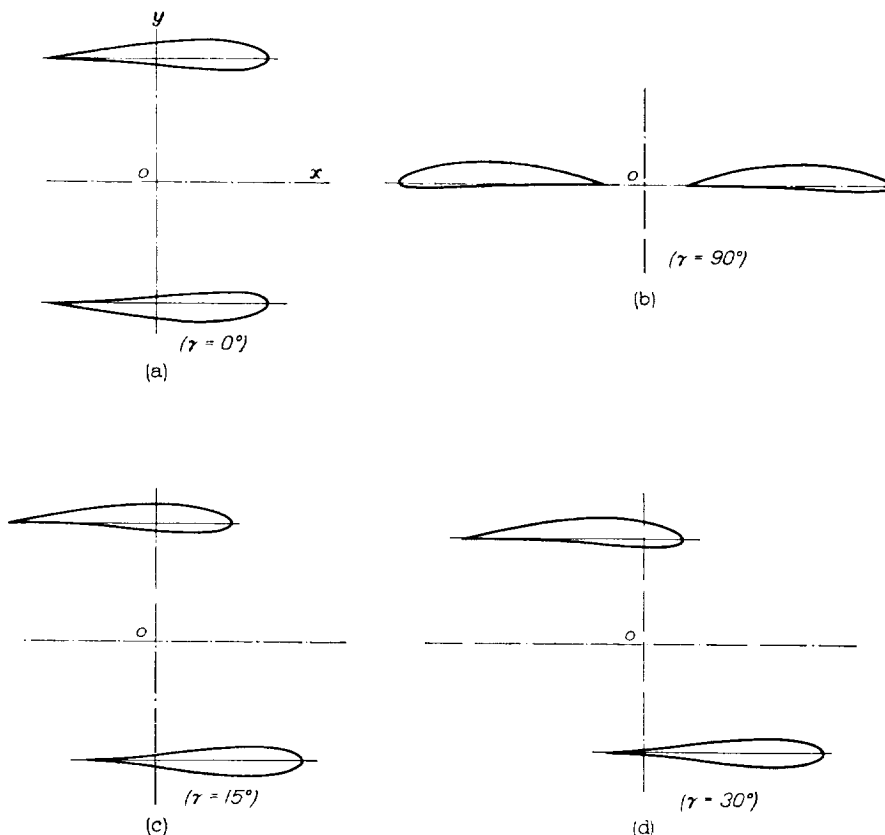


FIGURE 6.—Biplane arrangements defined by special choice of f_1 and f_2 and other parameters. (See equations (36a) and (36b).)

By equations (11) and (13), there may be written for $g_1(\varphi)$ and $g_2(\varphi)$

$$g_1(\varphi) = (\theta - \varphi)_1 = B_0 + (B_1 R_1 + B_{-1} R_1^{-1}) \cos \varphi$$

$$g_2(\varphi) = (\theta - \varphi)_2 = B_0 + (B_1 R_2 + B_{-1} R_2^{-1}) \cos \varphi$$

The conditions on A_0 and B_0 , equations (32) and (33), give $A_0 = 0$; $B_1 = B_{-1} = \frac{0.1}{2} \operatorname{csch} \frac{\tau}{2}$ (cf. equation (16)), hence $B_0 = -2B_1$. (Also, note that for this example, equations (34) and (35) give $p = q = 0$, i. e., $\left[\frac{dw}{dz}\right]_{z=c} = re^{i\epsilon} = 1$). Then,

$$g_1(\varphi) = -0.1 \operatorname{csch} \frac{\tau}{2} + 0.1 \coth \frac{\tau}{2} \cos \varphi = g_2(\varphi)$$

mined by α , β , γ , and δ) about which the biplane contours will be generated may be chosen. (See fig. 5.)

Choose $\delta = 0$ and $\alpha = \beta = \frac{\pi}{2}$ (hence $2\omega' = 2\pi i$). The rectangular Cartesian coordinates of the biplane contours are now given by equation (2.29). Figure 6 shows the arrangements obtained in this numerical case for a number of values of the angle of stagger γ .

In the elementary example just described the profiles for zero stagger are mirror images (fig. 6 (a)). A simple numerical case for which this is not true is given by

$$f_1(\varphi) = \mu_1(\varphi) - \sigma_1 = A_0 - 0.1 \sin (\varphi + 30^\circ) \quad (37a)$$

$$f_2(\varphi) = \mu_2(\varphi) - \sigma_2 = A_0 + 0.1 \sin (\varphi - 30^\circ) \quad (37b)$$

Here, also, choose $\alpha = \beta = \frac{\pi}{2}$, $\sigma_1 = -\sigma_2 = 1.4708$. Then

$$g_1(\varphi) = (\theta - \varphi)_1 = B_0 + 0.09625 \cos \varphi - 0.0450 \sin \varphi$$

$$g_2(\varphi) = (\theta - \varphi)_2 = B_0 + 0.09625 \cos \varphi + 0.0450 \sin \varphi$$

The constants A_0 and B_0 determined by equations (32) and (33) are

$$A_0 = 0.0216, B_0 = -0.0420$$

$$\left(\text{Again, in this example } \left[\frac{dw}{dz} \right]_{z=c} = re^{\theta} = 1. \right)$$

Forming θ_1 and θ_2 , the rectangular coordinates of the contours are obtained as was shown in the preceding

Indeed, if the process is considered in the light of a boundary-value problem of the concentric ring region, it is seen that it is sufficiently general to yield any biplane arrangement (more generally, any doubly connected region).

Equations (23) and (24) as integral equations.—It is desirable at this point to introduce the following notation. Frequent use will be made of subscripts. The first subscript will usually be 1 or 2 and will indicate that the designated quantity is to be evaluated at the boundary C_1 or C_2 , respectively (or also B_1 and B_2 , respectively). A second subscript will sometimes be employed to denote the variable in terms of which the quantity is expressed. Thus $\mu_{1,\theta}$ represents the quan-

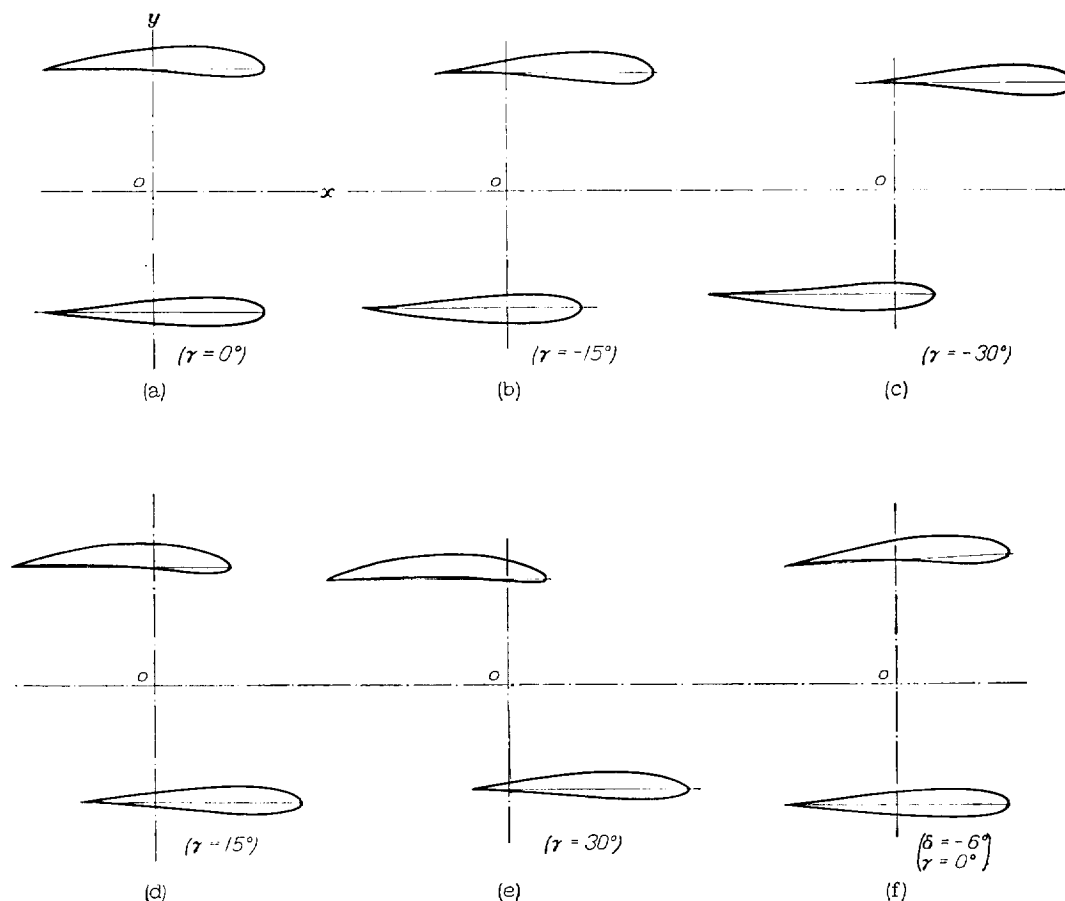


FIGURE 7.—Biplane arrangements defined by special choice of f_1 and f_2 and other parameters. (See equations (37a) and (37b).)

example. Figure 7 shows some arrangements for various values of the angle of stagger γ . Figure 7 (f) shows the arrangement obtained (for $\gamma = 0$, cf. fig. 7 (a)) when an angle of decalage $\delta/2 = -3^\circ$ is further introduced in this numerical example.

In this manner, by employing appropriate values for $f_1(\varphi)$ and $f_2(\varphi)$ (or $g_1(\varphi)$ and $g_2(\varphi)$) and for the other parameters involved, it is possible readily to develop arrangements of a great variety of contour shapes, gap/chord values, chord ratios, stagger, and decalage.

tity μ evaluated around C_1 (or B_1) expressed as a function of θ ; also, $\mu_{2,\varphi}$ denotes the quantity μ evaluated on C_2 expressed as a function of φ .

It is recalled that by equations (7) and (8)

$$\begin{aligned} f_{1,\varphi} &= \mu_{1,\varphi} - \sigma_1 \\ f_{2,\varphi} &= \mu_{2,\varphi} - \sigma_2 \end{aligned}$$

or f_1 and μ_1 , and f_2 and μ_2 differ by constants. Then in the integrands of equations (23) and (24) the functions f_1 and f_2 may be replaced by μ_1 and μ_2 , since the

additive constants do not contribute to the integrals. If a definite biplane arrangement is preassigned or, what is essentially the same, if there is given a definite nearly circular annular region (in a w plane; $w = ce^{u+i\theta}$), it is the functions $\mu_{1,\theta}$ and $\mu_{2,\theta}$ that may be considered directly defined or known.⁸ Thus, from an initial knowledge of $\mu_{1,\theta}$ and $\mu_{2,\theta}$ and with the aid of equations (23) and (24), it is desired to obtain a knowledge of the functions $\mu_{1,\varphi}$ and $\mu_{2,\varphi}$. From this point of view the expressions (23) and (24) then represent a pair of simultaneous integral equations, whose process of solution is more intricate than that involved in the process of evaluating the definite integrals. The problem may be restated more precisely:

Given two functions $\mu_{1,\theta}$ and $\mu_{2,\theta}$ that define two continuous contours of an annular region with respect to an origin contained by both contours. Then two pairs of functions $\mu_{1,\varphi}$ and $g_{1,\varphi}$, and $\mu_{2,\varphi}$ and $g_{2,\varphi}$ are to be obtained such that they are interrelated in the manner shown by the interchange of coefficients in the Fourier expansions, equations (10) to (13), which also satisfy certain local specified conditions at $z=c$ (equation (31)), and for which the relations $g_1 = (\theta - \varphi)_1$, $g_2 = (\theta - \varphi)_2$, which permit an interchange of the arguments θ and φ on each boundary, are consistent with the given functions $\mu_{1,\theta}$ and $\mu_{2,\theta}$; that is to say, when $\mu_{1,\varphi}$ is expressed as a function of θ by means of the function $g_{1,\varphi}$ there results the original function $\mu_{1,\theta}$; in symbols

$$\mu_{1,\varphi} \equiv \mu_{1,\theta} \\ \text{when } \theta = \varphi + g_{1,\varphi} \text{ or } \varphi = \theta - g_{1,\varphi}$$

and similarly

$$\mu_{2,\varphi} \equiv \mu_{2,\theta} \\ \text{when } \theta = \varphi + g_{2,\varphi} \text{ or } \varphi = \theta - g_{2,\varphi}$$

The process employed in this paper to obtain the desired solution of the simultaneous integral equations is one of successive approximations or iteration. The degree of convergence of most methods of successive approximations usually depends on how good the initial approximation is. In this regard it is rather fortunate that the contours of practically any biplane arrangement transform, under the transformations already developed (with proper choice of coordinates), into nearly circular contours in the w plane. The nearness of these boundary contours to circular contours is very significant and enables the initial approximations to be so chosen that the process converges ordinarily with great rapidity, one step in the process being sufficient for most practical purposes.

Outline of the method of successive approximations.—The various steps in the process of successive approximations will be written down schematically. (Allowing for a difference of notation the process is essentially similar to that employed in reference 1.)

⁸ The process of forming $\mu_{1,\theta}$ and $\mu_{2,\theta}$, assuming as known only the rectangular coordinates of the biplane contours, is outlined in section 4, p. 66.

An extension in the use of subsequent notation must first be noted. The symbol $f_{1,\theta}$ represents, as mentioned previously, the function f evaluated on C_1 and expressed as a function of θ . The symbol $f_{1,k,\theta}$ shall now be employed to denote the value of f_1 as given in the k th step in the process of successive approximations, expressed as a function of θ . Thus the symbol $g_{2,4,\varphi_{2,3}}$ denotes the value of g_2 given by the fourth step in the process, expressed as a function of φ_2 as given by the third step in the process.

We start with the two functions $\mu_{1,\theta}$ and $\mu_{2,\theta}$ that define the contours B_1 and B_2 completely. Employing θ instead of φ in the integrals,⁹ equations (32') define the constants $\sigma_{1,1}$ and $\sigma_{2,1}$ and equation (33') determines the constant $B_{0,1}$. The simultaneous equations (23) and (24) then determine completely the functions $g_{1,1,\theta}$ and $g_{2,1,\theta}$ as follows:

$$\left. \begin{aligned} \varphi_{1,1} &= \theta - g_{1,1,\theta} \\ \varphi_{2,1} &= \theta - g_{2,1,\theta} \end{aligned} \right\} \quad (38a)$$

The values $\mu_{1,\varphi_{1,1}}$ and $\mu_{2,\varphi_{2,1}}$ may now be defined and these functions may be considered as known. Employing $\varphi_{1,1}$ and $\varphi_{2,1}$ as variables instead of φ , equations (32') and (33') determine $\sigma_{1,2}$, $\sigma_{2,2}$, and $B_{0,2}$. Equations (23) and (24) determine then the functions $g_{1,2,\varphi_{1,1}}$ and $g_{2,2,\varphi_{2,1}}$, which may be expressed as functions of θ in view of equation (38a). The variables $\varphi_{1,2}$ and $\varphi_{2,2}$ are now given by

$$\left. \begin{aligned} \varphi_{1,2} &= \theta - g_{1,2,\theta} \\ \varphi_{2,2} &= \theta - g_{2,2,\theta} \end{aligned} \right\} \quad (38b)$$

The functions $\mu_{1,\varphi_{1,2}}$ and $\mu_{2,\varphi_{2,2}}$ are now determined and the process may be continued as outlined for $\mu_{1,\varphi_{1,1}}$ and $\mu_{2,\varphi_{2,1}}$. It is noteworthy that this process converges, in practice, with extreme rapidity, that is to say, the functions $\mu_{1,\varphi_{1,k}}$ and $\mu_{2,\varphi_{2,k}}$ approach identity with $\mu_{1,\varphi_{1,k+1}}$ and $\mu_{2,\varphi_{2,k+1}}$ for small values of k . Experience has shown (cf. also reference 1) that in ordinary cases one, or at most two, steps in the process are sufficient for great accuracy. It must be noted, however, that a completely rigorous discussion of the convergence process is lacking.

In order to illustrate the method, consider the biplane arrangements of figure 7 defined by the functions in equations (37a) and (37b). Forgetting for the moment that the various functions are known, assume only $\mu_{1,\theta}$ and $\mu_{2,\theta}$ to be given and attempt to obtain $\mu_{1,\varphi}$ and $\mu_{2,\varphi}$. Figure 8 shows the various functions described. It is seen that the set of curves $g_{1,\varphi_{1,1}}$, $g_{2,\varphi_{2,1}}$, $\mu_{1,\varphi_{1,1}}$, and $\mu_{2,\varphi_{2,1}}$ (obtained by a 20-point numerical process similar to that sketched in

⁹ Denoting the initial approximation by a zero subscript, observe that the initial approximation employed here is $\varphi_{1,0} = \theta - g_{1,0}$ and $\varphi_{2,0} = \theta - g_{2,0}$ where $g_{1,0} = g_{2,0} = 0$. More generally, the initial transformation may be better defined where $g_{1,0}$ and $g_{2,0}$ are arbitrary functions, so chosen that they are better approximations to the final solutions g_1 and g_2 . Then employing $\varphi_{1,0}$ and $\varphi_{2,0}$ as variables instead of θ the functions $\mu_{1,\varphi_{1,0}}$ and $\mu_{2,\varphi_{2,0}}$ may be defined from which $g_{1,1}$ and $g_{2,1}$ are determined and the process continued as outlined. (Cf. reference 1, p. 13.)

the appendix of reference 1) are completely coincident with the known solutions $g_{1,\varphi}$, $g_{2,\varphi}$, $\mu_{1,\varphi}$, and $\mu_{2,\varphi}$. A further application of the process can cause no further noticeable change.

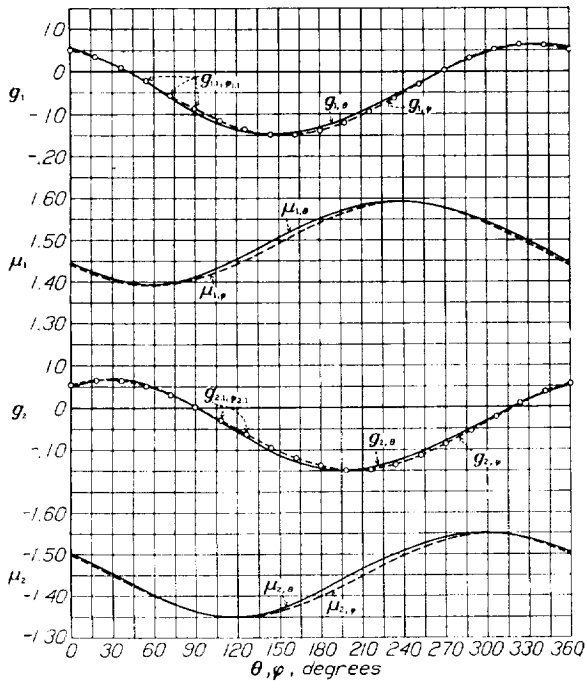


FIGURE 8.—Illustrating the process of successive approximations.

For future reference, the derivative expression $\frac{dw}{dz}$ evaluated at the boundary circles will be required. From equation (30)

$$\frac{dw}{dz} = w \left(1 + z \frac{dh(z)}{dz} \right)$$

On C_1

$$h(z) = f_{1,\varphi} + i g_{1,\varphi}$$

Then

$$\left[\frac{dw}{dz} \right]_{C_1} = \left| \frac{w}{z} \right|_{C_1} \cdot \left[\left(1 + \frac{dg_{1,\varphi}}{d\varphi} \right) - i \frac{df_{1,\varphi}}{d\varphi} \right] \quad (39)$$

Observing that $d\varphi = d(\theta - g)$ this may also be expressed

$$\left[\frac{dw}{dz} \right]_{C_1} = \left| \frac{w}{z} \right|_{C_1} \left(\frac{1 - i \frac{df_{1,\theta}}{d\theta}}{1 - \frac{dg_{1,\theta}}{d\theta}} \right) \quad (39')$$

For the boundary C_2 , the subscript 1 is replaced by 2.

4. GENERAL MONOPLANE WING SECTION THEORY—A DEGENERATE CASE OF THE BIPLANE ANALYSIS

It may be of some interest to discuss in this section briefly the case of the single airfoil section considered as a special case of the biplane analysis. A biplane arrangement in a two-dimensional field of flow corresponds mathematically to a doubly connected region. The degenerate case in which one of the biplane con-

tours reduces to a (regular) point leads to the monoplane-wing profile the external region of which is simply connected.¹⁰ It should therefore be possible to obtain the complete theory of monoplane wing sections in potential flow as limiting values of the formulas already developed for biplane wing sections, as will be outlined in the present section. Conversely, the monoplane case is of further significance in that it permits a more complete understanding of the biplane analysis and, too, considerably simplifies the practical evaluations. The numerical process employed in the monoplane case, it will appear, needs to be modified in a relatively minor way to yield the results for ordinary biplane combinations. Indeed, according to a method outlined by Koebe (reference 2), it is known that even the more general problem of transforming a multiply connected region (multiplane problem) into a region bounded by circles may be resolved by a process of successive approximations employing only the separate cases for the simply connected regions. The details of this problem remain for a future investigation; it is mentioned here merely as a further possible application of the degenerate case.

It may first be observed that as one of the circles in the t plane reduces to a point the value of α or β (according as the upper or lower circle degenerates) becomes infinite. Hence in the degenerate case, the elliptic functions introduced in the analysis become circular functions having a real period $2\omega = 2\pi$ and an imaginary period $2\omega'$, which is infinite. From equation (2.23) it is clear that $\omega' = i\infty$ corresponds to $q = 0$ and that

$$\lim_{q=0} A(s) = \frac{1}{2} \cot \frac{\delta}{2} + \frac{1}{2} \cot \frac{s}{2} \quad (1)$$

Let $\beta = \infty$, then employing this equation and relation (1.8) it is found that equation (2.12) becomes

$$\lim_{q=0} u(s) e^{t\delta/2} = U_1 = T_1 + \frac{a^2}{T_1} \quad (2)$$

where the origin in the U_1 plane is referred to the midpoint of the line segment and where

$$T_1 = e^{t(\gamma + \delta/2)} (t - ic \coth \alpha)$$

$$a = c \operatorname{csch} \alpha$$

It is seen that the T_1 plane corresponds simply to the t plane translated to a new origin (O_1 in fig. 1) and rotated by an angle $\gamma' = \gamma + \frac{\delta}{2}$. Equation (2) is nothing more than the well-known transformation leading to Joukowski airfoils. The line segment in this case ($\beta = \infty$) is equal to twice the diameter of the circle in the T_1 plane, i. e., $c_1 = 4a$.

¹⁰ Strictly speaking, the point at infinity represents another boundary and the flow regions are respectively, triply connected and doubly connected. This fact corresponds to the circumstance that in the flow formula for the biplane case there may be two arbitrary circulations specified, and in the monoplane flow formula, one. The flow formula for a simply connected region without singular points cannot be multiply valued, i. e., cannot possess an arbitrary circulation.

If α instead of β , is allowed to approach infinity there is obtained

$$\lim_{\alpha \rightarrow \infty} u(s) = U_2 = T_2 + \frac{b^2}{T_2}$$

where the origin in the U_2 plane is referred to the midpoint of the line segment, and where

$$T_2 = e^{i\gamma} (t + ic \coth \beta)$$

$$b = c \operatorname{csch} \beta$$

The chord length $c_2 = 4b$.

In what immediately follows we show how to express λ , μ in the degenerate case in terms of the coordinates x , y of the airfoil section. These results will be of value in the later determination of λ , μ from x , y for the biplane case.

It has been seen that in the degenerate case ($\beta = \infty$) the origin of coordinates may be referred to the midpoint of the chord and

$$U_1 = T_1 + \frac{a^2}{T_1} \quad (2)$$

where the rectangular coordinates in the U_1 plane are (x_1, y_1) i. e.,

$$U_1 = x_1 + iy_1$$

$$T_1 = e^{i\gamma'} (t - ic \coth \alpha)$$

$$a = c \operatorname{csch} \alpha \text{ and } \gamma' = \gamma + \delta/2$$

Let T_1 be written in the form

$$T_1 = ae^{i\psi_1 + i\theta_1} \quad (3)$$

Then

$$U_1 = x_1 + iy_1 = 2a \cosh (\psi_1 + i\theta_1) \quad (4)$$

where

$$x_1 = 2a \cosh \psi_1 \cos \theta_1$$

$$y_1 = 2a \sinh \psi_1 \sin \theta_1$$

And upon inversion (cf. reference 1)

$$\left. \begin{aligned} 2 \sin^2 \theta_1 &= p + \sqrt{p^2 + \frac{y^2}{a^2}} \\ 2 \sinh^2 \psi_1 &= -p + \sqrt{p^2 + \frac{y^2}{a^2}} \end{aligned} \right\} \quad (5)$$

where

$$p = 1 - \left(\frac{x}{2a}\right)^2 - \left(\frac{y}{2a}\right)^2$$

By equation (1.8)

$$t = -c \cot \frac{s}{2} \text{ where } s = \lambda + i\mu$$

Hence,

$$\lambda + i\mu = -2 \cot^{-1} \frac{t}{c} = -2 \cot^{-1} (T_1 e^{-i\gamma'} + ic \coth \alpha) \frac{1}{c}$$

or also

$$\lambda + i\mu = -2 \cot^{-1} (l + im) \quad (6)$$

where

$$l = \frac{a}{c} e^{i\psi_1} \cos (\theta_1 - \gamma')$$

$$m = \frac{a}{c} (e^{i\psi_1} \sin (\theta_1 - \gamma') + \cosh \alpha)$$

It is known that

$$\begin{aligned} \cot^{-1} (l + im) &= -\frac{i}{2} \log \frac{l + im + i}{l + im - i} \\ &= -\frac{i}{4} \log \frac{(l^2 + m^2 - 1)^2 + 4l^2}{[l^2 + (m-1)^2]^2} + \frac{1}{2} \tan^{-1} \frac{2l}{l^2 + m^2 - 1} \end{aligned}$$

So that finally equation (6) separates into

$$\left. \begin{aligned} \lambda &= -\tan^{-1} \frac{2l}{l^2 + m^2 - 1} \\ \mu &= \frac{1}{2} \log \frac{(l^2 + m^2 - 1)^2 + 4l^2}{[l^2 + (m-1)^2]^2} \end{aligned} \right\} \quad (7)$$

These relations express λ and μ in the monoplane case in terms of θ_1 and ψ_1 and hence by (5) also in terms of x_1 and y_1 .

Similarly, in order to obtain λ and μ for the degenerate case in which $\alpha = \infty$, replace a by b ($=c \operatorname{csch} \beta$) and let

$$\begin{aligned} T_2 &= e^{i\gamma} (t + ic \coth \beta) \\ &= be^{i\psi_2 + i\theta_2} \end{aligned} \quad (3')$$

Then finally λ and μ are given by equation (7) in which

$$\left. \begin{aligned} l &= l_2 = \frac{b}{c} e^{i\psi_2} \cos (\theta_2 - \gamma) \\ m &= m_2 = \frac{b}{c} (e^{i\psi_2} \sin (\theta_2 - \gamma) - \cosh \beta) \end{aligned} \right\} \quad (6')$$

Inversion of equation (2.12).—It is quite evident that the direct inversion of the elliptic transcendental equation (2.12) (p. 52), if at all possible, would be very laborious. However, an indirect method which employs the results of the degenerate cases and which performs this inversion readily, to any degree of approximation, will now be outlined.

Thus, let a definite biplane arrangement be given (fig. 5(a)). The chords or line segments c_1 and c_2 may first be chosen in the following *convenient* manner. Let the chord c_1 be defined by the line $F_1 F_1'$, where F_1 is the midpoint of the distance between the leading edge and the center of curvature of the leading edge and F_1' is the midpoint of the distance between the trailing edge and the center of curvature of the trailing edge. It is observed at this point that the only *theoretical* restriction upon the choice of the chords is that the singular points (the end points of the line segments) be within the contours, or, at most, on the boundaries themselves. The above-mentioned choice is one merely of convenience, the object in view being the defining of a smooth (λ, μ) relationship. (In reference 1, a similar situation is described in detail.) The above-outlined procedure may be also applied to determine the chord c_2 of the lower contour of the biplane cellule.¹¹

¹¹ In the event that the chords so determined are almost, but not quite, parallel it is of some advantage numerically to vary from the foregoing procedure sufficiently to cause the chords to become exactly parallel and to maintain approximately the foci F and F' . Small variations from the choice of chords outlined are of minor importance and will not affect the smoothness of the (λ, μ) relationship. The desirability of maintaining the chords exactly parallel, if they are reasonably parallel to start with, is due to the circumstance that elliptic functions of the second kind are then avoided.

The chords c_1 and c_2 having been conveniently chosen, it is possible to determine uniquely by means of the charts outlined previously (fig. 4), or indirectly from the equations themselves, the values of the constants α , β , γ , and δ . The quantity c may be regarded throughout as a convenient unit reference length.

Equation (7), it will be recalled, for these values of α , β , γ , and δ , determines the values of λ and μ (in terms of the rectangular coordinates of the profile sections), which in the degenerate cases correspond to profiles geometrically similar to the upper or lower profiles of the given biplane cellule, the only differences being that the chords are $4a=4c \operatorname{csch} \alpha$ and $4b=4c \operatorname{csch} \beta$, respectively. When, however, the values of λ and μ thus determined are inserted in equation (2.29) (employing the proper periods $2\omega=2\pi$, $2\omega'=2i(\alpha+\beta)$) there is obtained a biplane arrangement which has, necessarily, the required chords and position (i. e., the proper skeleton) and around this skeleton has generated contour shapes A_1 and B_1 which, in ordinary cases, are almost identical with the given original contours A_0 and B_0 . Thus, the use of the values (λ, μ) of the degenerate cases in the *biplane* analysis is equivalent to a replacement of the original biplane arrangement by a new arrangement defined by the contours A_1 and B_1 . The differences between A_0 and A_1 , and B_0 and B_1 are remarkably small in practice. Mathematically the foregoing procedure represents, however, only a first, although important, step in a process of successive approximations which we outline as follows.

Consider only A_0 and A_1 . The contour A_1 defines, by means of equation (7), a new degenerate (λ, μ) relation. The differences between this new (λ, μ) relation of A_1 and the original degenerate (λ, μ) relation of A_0 is a proper criterion of the differences between the contours A_0 and A_1 themselves since, if these (λ, μ) functions coincide, the contours must coincide. Hence, by a shifting process similar to that commonly employed in methods of successive approximations, the first approximation to the desired (λ, μ) relation of A_0 (this first approximation has been here considered to be the degenerate (λ, μ) relation itself of A_0) may be corrected by these differences to give a second and better approximation. The process may be repeated k times, if necessary, until the degenerate (λ, μ) relation of A_k coincides with the degenerate (λ, μ) relation of A_0 , hence A_k coincides with A_0 , and therefore the actual (λ, μ) relation that defines the contour A_k itself in the biplane case (i. e., by equation (2.29)) is the desired (λ, μ) relation of A_0 .

Singular points in the monoplane case.—The monoplane case may also be useful in obtaining the singular points of the biplane transformation to a good first approximation. From equation (2):

$$U_1 = T_1 + \frac{a^2}{T_1}$$

the singular points are given by

$$\frac{dU_1}{dT_1} = 0 = 1 - \frac{a^2}{T_1^2}$$

or by

$$T_1 \pm a$$

Since by equation (3)

$$T_1 = ae^{\psi_1 + i\theta_1}$$

it is evident that the singular points correspond to $(\psi_1, \theta_1) = (0, 0)$ and $(0, \pi)$, respectively. On replacing ψ_1 and θ_1 in equations (6) and (7) by these values it is seen that the singular points $(\lambda = \lambda_s)$ of the upper chord ($\mu = \alpha$) are given by

$$-\tan \lambda_s = \frac{\sinh \alpha \cos \gamma'}{1 \pm \cosh \alpha \sin \gamma'} \quad (8)$$

Similarly for the chord of the lower profile ($\mu = -\beta$) we get

$$\tan \lambda_s = \frac{\sinh \beta \cos \gamma}{1 \pm \cosh \beta \sin \gamma} \quad (8')$$

It may also be useful to note that to a first approximation (the approximation being better the greater $\alpha + \beta$) the chords of a biplane cellule are given by $c_1 = 4c \operatorname{csch} \alpha$, $c_2 = 4c \operatorname{csch} \beta$. Hence the chord ratio is approximately

$$\frac{c_1}{c_2} = \frac{\sinh \beta}{\sinh \alpha}$$

It has been shown thus far that the degenerate monoplane case may be of value in the determination of μ and λ for a biplane cellule. The limiting forms of the simultaneous integral equations will now be briefly discussed.

Forms of the integral equations (3.23) and (3.24) for the monoplane case.—Consider the simultaneous equations (23) and (24) of section 3, which define the distortion of two contours from two circles. Let $\beta' = -\sigma_2 = \infty$, i. e., $R_2 = 0$, the interior circle of figure 5 (e) degenerates to a point. It is seen then that the Laurent series, equation (3.6), becomes a one-way ascending power series and $a_{-n} = A_{-n} + iB_{-n} = 0$. We have also since $\tau = \alpha' + \beta' = \infty$ that equations (3.21) and (3.22) give

$$Z(\varphi - \varphi') = 0, \quad Z_1(\varphi - \varphi') = \frac{1}{2} \cot \frac{\varphi - \varphi'}{2}$$

Equations (3.23) and (3.24) then reduce to a single equation

$$g_1(\varphi') = B_0 - \frac{1}{2\pi} \int_0^{2\pi} f_1(\varphi) \cot \frac{\varphi - \varphi'}{2} d\varphi \quad (9)$$

or also

$$g_1(\varphi') = B_0 + \frac{1}{\pi} \int_0^{2\pi} f_1(\varphi) \log \sin \left| \frac{\varphi - \varphi'}{2} \right| d\varphi \quad (9')$$

Equation (9), considered as an integral equation, enables the transforming of the contour of a simply connected region into a circle. The process of iteration outlined in the preceding section is directly applicable in this simpler case. (Cf. reference 1.) The constants A_0 , B_0 , and $\sigma_1 = \alpha'$ may be determined, as before, from equations (3.32) and (3.33).

In the event that $\alpha' = \infty$, the outer circle of figure 5(e) becomes infinitely large, i. e., $R_1 = \infty$. Then the Laurent series (3.6) becomes a descending power series and $a_n = A_n + iB_n = 0$. With $f_1 = g_1 = 0$ and $\tau = \infty$ we find that equations (3.23) and (3.24) reduce to

$$g_2(\varphi') = B_0 + \frac{1}{2\pi} \int_0^{2\pi} f_2(\varphi) \cot \frac{\varphi - \varphi'}{2} d\varphi \quad (10)$$

or also

$$g_2(\varphi') = B_0 - \frac{1}{\pi} \int_0^{2\pi} f_2(\varphi) \log \sin \left| \frac{\varphi - \varphi'}{2} \right| d\varphi \quad (10')$$

The functions $g_1(\varphi)$ and $g_2(\varphi)$, determined by equations (9) and (10) by separate treatment of the two monoplane cases, may when known be employed as a convenient initial approximation (cf. footnote 9) in the more general case.

The well-known flow function for a single circular cylinder may be brought into combination with the results of this section to yield the flow about an arbitrary

single airfoil as has been already obtained in reference 3. We proceed at once to the more general case to introduce the flow function for two circular cylinders into the biplane analysis.

respond to the contours of the biplane arrangement and are not to be confused with the contours K_1 and K_2 of the t plane (fig. 5 (d)) which, in general, are not circles. The primes will be retained to denote this difference. The relation between the z and t' planes is (cf. equation (1.4))

$$t' = ic \frac{z+c}{z-c} \quad (1)$$

Also by the relation

$$t' = -c \cot \frac{s'}{2} \quad (2)$$

the region external to the circles K_1' and K_2' is mapped into a rectangular region in the s' plane bounded by the lines l_1' and l_2' (cf. equation (1.8) and fig. 9). For later reference the relation between s' and z is also noted here:

$$z = ce^{-is'} \quad (3)$$

and since $z = ce^{i\sigma + i\varphi}$ and $s' = \lambda' + i\mu'$ it is clear that

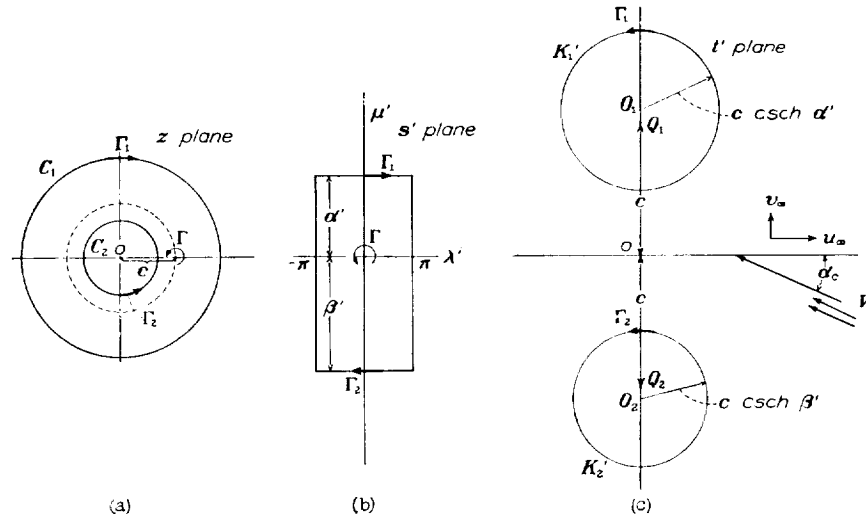


FIGURE 9.—Illustrating the flow regions in the z , s' , and t' planes.

trary single airfoil as has been already obtained in reference 3. We proceed at once to the more general case to introduce the flow function for two circular cylinders into the biplane analysis.

5. POTENTIAL FLOW ABOUT THE BIPLANE CONTOURS

Potential flow around two circles.—It has thus far been shown how the two contours of a biplane arrangement, in a u plane, may be transformed into two concentric circles in the z plane. It is desirable in what follows to transform the concentric circles C_1 and C_2 of the z plane into the coaxial ones K_1' and K_2' in a t' plane (fig. 9). The circles K_1' and K_2' will thus also corre-

$$\left. \begin{aligned} \lambda' &= -\varphi \\ \mu' &= \sigma \end{aligned} \right\} \quad (4)$$

Hence the boundary lines l_1' and l_2' are given respectively by

$$\mu' = \alpha' = \sigma_1, \quad \mu' = -\beta' = \sigma_2$$

where

$$\alpha' > 0, \quad \beta' > 0$$

(It will also be recalled from section 3 (cf. line following equation (3.16)) that $\sigma_1 - \sigma_2 = \alpha' + \beta' = \tau$.)

In a noteworthy paper (reference 4) Lagally has given the complex flow potential for uniform flow past two circles. His formula makes use of the interme-

diate s' plane and the complex flow potential in the s' plane, is given by¹²

$$\Omega(s') = \frac{\Gamma'}{4\pi}s' - \frac{\Gamma}{4\pi} \left[2i \log \frac{\sigma(s')}{\sigma(s'+2i\beta')} + \left(1 - \frac{4\beta'\eta_1}{\pi} \right) s' \right] - 2cu_\infty \left[\zeta(s') + \zeta(s'+2i\beta') - \frac{2}{\pi}\eta_1 s' \right] + 2icv_\infty [\zeta(s') - \zeta(s'+2i\beta')] \quad (5)$$

In this equation $\Gamma = -(\Gamma_1 + \Gamma_2)$ where Γ_1 and Γ_2 are the individual arbitrary circulations about K_1' and K_2' , respectively (see fig. 9; the *positive* direction of Γ_1 or Γ_2 , which is opposite to that of Γ , is chosen such that as one traverses the contour in this direction the flow region is on the right). The symbol Γ' denotes the "countercirculation" $\Gamma' = \Gamma_1 - \Gamma_2$. The velocity at infinity is $u_\infty + iv_\infty$. The periods of the elliptic functions are, as in section 3, $2\omega_1 = 2\pi$, $2\omega_2 = 2i(\alpha' + \beta') = 2i\tau$.

Equation (5) shows directly that the whole flow is built up by linear superposition of four separate flows, for each of which one of the quantities Γ , Γ' , u_∞ , and v_∞ is different from zero.

In the first partial flow with the factor Γ' , both circulations are equal and opposite about the two circles, $\Gamma_1 = -\Gamma_2 = \frac{\Gamma'}{2}$. The streamlines are the circles of the coaxial pencil. The velocity at infinity is zero. In the second partial flow with the factor Γ , the two circulations are equal. $\Gamma_1 = \Gamma_2 = -\frac{\Gamma}{2}$. The velocity at infinity is again zero. The third partial flow with the factor u_∞ is a translatory flow without circulation, normal to the line of centers of the two circles. The fourth partial flow with the factor v_∞ is a translatory flow without circulation in the direction of the line of centers of the two circles.

The flow at the surface of the two circles, and the determination of Γ and Γ' .—It is convenient to define the velocity at infinity, whose rectangular components are u_∞ and v_∞ , in another manner, by introducing a magnitude V_c and an angle of attack α_c (fig. 9 (c)). Let

$$\begin{aligned} u_\infty &= -V_c \cos \alpha_c \\ v_\infty &= V_c \sin \alpha_c \end{aligned} \quad (6)$$

¹² Lagally's formula as presented in reference 4 employs elliptic functions of periods $\bar{\omega}_1$ and $\bar{\omega}_2$ which are conjugate to the periods ω_1 and ω_2 employed here, i. e., $\bar{\omega}_1 = \omega_2/\tau$, $\bar{\omega}_2 = i\omega_1$. The formula of reference 4 is brought into equation (5) by putting Lagally's symbols iZ , u_∞ , v_∞ equal to s' , u_∞ , $-u_\infty$, respectively.

or, in a single expression,

$$u_\infty + iv_\infty = -V_c e^{-i\alpha_c}.$$

By derivation of equation (5) with regard to s' , we obtain the complex velocity function in the s' plane as

$$\begin{aligned} W(s') &= \frac{\Gamma'}{4\pi} - \frac{\Gamma}{4\pi} \left\{ 2i [\zeta(s') - \zeta(s'+2i\beta')] + 1 - \frac{4\beta'\eta_1}{\pi} \right\} \\ &\quad - 2cV_c \cos \alpha_c [p(s') + p(s'+2i\beta') + 2\eta_1/\pi] \\ &\quad - 2icV_c \sin \alpha_c [p(s') - p(s'+2i\beta')] \end{aligned} \quad (7)$$

This expression gives the velocity components $U_1 - iV_1$ at any point of the rectangular region in the s' plane. It is a real quantity on each of the boundaries, $\mu' = \alpha'$, $\mu' = -\beta'$ of the rectangle since these boundaries are streamlines and the normal flow V_1 vanishes.

Let us evaluate W for each of the two cases: (1) $s' = \lambda' + i\alpha'$ corresponding to the boundary l_1' (2) $s' = \lambda' - i\beta'$ corresponding to the boundary l_2' . In case (1) we obtain

$$\begin{aligned} W_1 &= \frac{\Gamma'}{4\pi} - \frac{\Gamma}{2\pi} \left\{ i [\zeta(\lambda' + i\alpha') - \zeta(\lambda' - i\alpha')] + \frac{2\eta_1\alpha'}{\pi} - \frac{1}{2} \right\} \\ &\quad - 2cV_c \cos \alpha_c [p(\lambda' + i\alpha') + p(\lambda' - i\alpha') + 2\eta_1/\pi] \\ &\quad - 2icV_c \sin \alpha_c [p(\lambda' + i\alpha') - p(\lambda' - i\alpha')] \end{aligned} \quad (8)$$

or

$$\begin{aligned} W_1 &= \frac{\Gamma'}{4\pi} - \frac{\Gamma}{2\pi} R_1(\lambda', \alpha') - 2cV_c \cos \alpha_c R_2(\lambda', \alpha') \\ &\quad - 2cV_c \sin \alpha_c R_3(\lambda', \alpha') \end{aligned} \quad (9)$$

where R_1 , R_2 , and R_3 are real quantities introduced for brevity in notation and defined by the following equations (the primes are dropped for convenience):¹³

$$\begin{aligned} R_1(\lambda, \alpha) &= i [\zeta(\lambda + i\alpha) - \zeta(\lambda - i\alpha)] + \frac{2\eta_1\alpha}{\pi} - \frac{1}{2} \\ &= -\frac{1}{2} + \frac{\sinh \alpha}{\cosh \alpha - \cos \lambda} - 4 \sum_{m=1}^{\infty} \frac{q^{2m}}{1 - q^{2m}} \sinh m\alpha \cos m\lambda \end{aligned} \quad (10)$$

¹³ The developments given here for R_1 , R_2 , and R_3 are rapidly convergent when $\tau = \alpha' + \beta'$ is large, say greater than $\frac{\pi}{2}$. Other expansions are possible (cf. reference 10, p. 422) and, in certain cases, more desirable. For example, when τ is small, say less than $\frac{\pi}{2}$, it is possible by a simple transformation to interchange the real and imaginary periods of the elliptic functions (cf. footnote 4) and obtain more rapidly convergent developments.

$$R_2(\lambda, \alpha) = p(\lambda + i\alpha) + p(\lambda - i\alpha) + \frac{2\eta_1}{\pi} \quad (11)$$

$$= \frac{1 - \cos \lambda \cosh \alpha}{(\cosh \alpha - \cos \lambda)^2} - 4 \sum_1^{\infty} \frac{mq^{2m}}{1 - q^{2m}} \cosh m\alpha \cos m\lambda$$

$$R_3(\lambda, \alpha) = i[p(\lambda + i\alpha) - p(\lambda - i\alpha)] \quad (12)$$

$$= \frac{\sin \lambda \sinh \alpha}{(\cosh \alpha - \cos \lambda)^2} - 4 \sum_1^{\infty} \frac{mq^{2m}}{1 - q^{2m}} \sinh m\alpha \sin m\lambda$$

where

$$q = e^{-\tau}$$

In case (2) there is obtained similarly

$$W_2 = \frac{\Gamma'}{4\pi} + \frac{\Gamma}{4\pi} R_1(\lambda', \beta') - 2cV_c \cos \alpha_c R_2(\lambda', \beta') + 2cV_c \sin \alpha_c R_3(\lambda', \beta') \quad (13)$$

In order to specify the circulation Γ and the counter-circulation Γ' , we make use of the Kutta-Joukowski

Solving for $\frac{\Gamma}{2\pi}$ and $\frac{\Gamma'}{4\pi}$ in (14)

$$\left. \begin{aligned} \frac{\Gamma}{2\pi} &= -2cV_c \left[\frac{\cos \alpha_c (R_{21} - R_{22}) + \sin \alpha_c (R_{31} + R_{32})}{R_{11} + R_{12}} \right] \\ \frac{\Gamma'}{4\pi} &= 2cV_c \left[\frac{\cos \alpha_c (R_{11}R_{22} + R_{21}R_{12}) - \sin \alpha_c (R_{11}R_{32} - R_{31}R_{12})}{R_{11} + R_{12}} \right] \end{aligned} \right\} \quad (15)$$

In order to obtain the angle of zero lift β_c , in the plane of the circles, we equate $\Gamma = 0$ and solve for the particular value of the angle of attack α_c , which is denoted as $-\beta_c$ (i. e., for $\alpha_c = -\beta_c$, $\Gamma = 0$). Then we have at once from (15)

$$\tan \beta_c = \frac{R_{21} - R_{22}}{R_{31} + R_{32}} \quad (16)$$

with this definition of β_c , the total circulation may be expressed as

$$\Gamma = -4\pi cKV_c \sin (\alpha_c + \beta_c) \quad (17)$$

where the constant K is

$$K = \frac{1}{\cos \beta_c} \frac{R_{31} + R_{32}}{R_{11} + R_{12}}$$

(In the limiting cases $\beta' = \infty$, $\alpha' = \infty$, cK is equal to $c \operatorname{csch} \alpha'$ or $c \operatorname{csch} \beta'$, respectively, which are the radii of K_1' or K_2' , respectively.)

Similarly, the angle γ_c may be defined as the angle of attack for which counter-circulation Γ' vanishes (i. e., for $\alpha_c = -\gamma_c$, $\Gamma' = 0$). Then from (15)

$$\tan \gamma_c = -\frac{R_{11}R_{22} + R_{21}R_{12}}{R_{11}R_{32} - R_{31}R_{12}} \quad (18)$$

and Γ' may be expressed as

¹⁴ The values of λ_1' and λ_2' may be determined as follows: Let λ_1 and λ_2 denote the values of λ ($= -\theta$) that correspond to the end points of the chords, i. e., λ_1 and λ_2 , or $-\theta_1$ and $-\theta_2$, are the singular points of equation (2.12). Then the values of λ_1' ($= -\varphi$) corresponding to λ_1 and λ_2 are given by λ_1' and λ_2' , or $-\varphi_1$ and $-\varphi_2$, where (cf. sec. 3) $\varphi_1 = \theta_1 - \theta_1$, $\varphi_2 = \theta_2 - \theta_2$, $\varphi_3 = \theta_3 - \theta_3$.

¹⁵ The total lift is, as in the monoplane case, $L = \rho V \Gamma$ (cf. p. 25) per unit spanlength.

condition for finite velocities at the sharp trailing edges. Equations (9) and (13) must vanish for the particular values of λ' that correspond to the trailing edges of the upper and lower contours of the biplane combination. Let λ_1' and λ_2' be the values of λ corresponding to the trailing edges of the two contours.¹⁴ Then we have

$$\left. \begin{aligned} W(\lambda_1', \alpha') &= \frac{\Gamma'}{4\pi} - \frac{\Gamma}{2\pi} R_{11} - 2cV_c \cos \alpha_c R_{21} \\ &\quad - 2cV_c \sin \alpha_c R_{31} = 0 \\ W(\lambda_2', \beta') &= \frac{\Gamma'}{4\pi} + \frac{\Gamma}{2\pi} R_{12} - 2cV_c \cos \alpha_c R_{22} \\ &\quad + 2cV_c \sin \alpha_c R_{32} = 0 \end{aligned} \right\} \quad (14)$$

where the R 's with double subscripts are constants defined as follows. (See equations (10)–(12).)

$$R_{11} = R_1(\lambda_1', \alpha'), R_{21} = R_2(\lambda_1', \alpha'), R_{31} = R_3(\lambda_1', \alpha')$$

$$R_{12} = R_1(\lambda_2', \beta'), R_{22} = R_2(\lambda_2', \beta'), R_{32} = R_3(\lambda_2', \beta')$$

$$\Gamma' = -8\pi cJV_c \sin (\alpha_c + \gamma_c) \quad (19)$$

where the constant J is

$$J = \frac{1}{\cos \gamma_c} \frac{R_{11}R_{32} - R_{31}R_{12}}{R_{11} + R_{12}}$$

Velocity at the boundary contours of the biplane combination.—Let the complex potential function in the plane containing the biplane contours (u plane) be Ω , then the complex velocity function is

$$\frac{d\Omega}{du} = v_x - iv_y \quad (20)$$

or

$$v = \sqrt{v_x^2 + v_y^2} = \left| \frac{d\Omega}{du} \right|$$

where v_x and v_y are the velocity components in the direction of the coordinate axes in the u plane. Introducing the intermediate planes, we have

$$\frac{d\Omega}{du} = \frac{d\Omega}{ds'} \cdot \frac{ds'}{dz} \cdot \frac{dz}{dw} \cdot \frac{dw}{ds} \cdot \frac{ds}{du} \quad (21)$$

It is first of importance to consider the changes that a velocity at infinity in the u plane undergoes when transformed to the t' (or s') planes. (It will be recalled that $u = \infty$ corresponds to $t = \infty$, $s = 0$, $w = c$, $z = c$, $s' = 0$, $t' = \infty$.) Let $-Ve^{-i\alpha_0}$ denote the velocity at infinity in the u plane and, as before, $-Ve^{-i\alpha_c}$ denotes the velocity at infinity in the t' plane. (See figs. 9 and 10; the velocity magnitudes are V and V_c and the angles of attack are α_0 and α_c , respectively.)

Then noting equations (2.10) and (3.29) it is found from (21) that

$$\left. \begin{aligned} V_c &= rV \\ \alpha_c &= \alpha_0 + \gamma + \xi \end{aligned} \right\} \quad (22)$$

where r and ξ are determined by equation (3.31') (r is generally near unity, ξ near zero), and γ is the angle of stagger of the biplane chords.

The angle of zero lift for the biplane combination is given by

$$\beta_0 = \beta_c + \gamma + \xi$$

i. e., for $\alpha_0 = -\beta_0$ the lift vanishes.

In order to determine the velocities at each boundary contour of the biplane combination, it is sufficient to obtain the magnitudes of the individual terms in equation (21) at each boundary. For the upper profile we have by equation (9)

$$\left| \frac{d\Omega}{ds'} \right| = W_1$$

From equation (3)

$$\left| \frac{ds'}{dz} \right| = \left| \frac{1}{z} \right|$$

$$v_1 = \frac{W_1}{2c} \left[\left(1 + \frac{dg_1}{d\varphi} \right)^2 + \left(\frac{df_1}{d\varphi} \right)^2 \right]^{-\frac{1}{2}} [(P_1 \cos \gamma + P_1' \sin \gamma)^2 + (Q_1 \cos \gamma + Q_1' \sin \gamma)^2]^{-\frac{1}{2}} \quad (23)$$

Similarly for the velocity at each point of the surface of the lower profile

$$v_2 = \frac{W_2}{2c} \left[\left(1 + \frac{dg_2}{d\varphi} \right)^2 + \left(\frac{df_2}{d\varphi} \right)^2 \right]^{-\frac{1}{2}} [(P_2 \cos \gamma + P_2' \sin \gamma)^2 + (Q_2 \cos \gamma + Q_2' \sin \gamma)^2]^{-\frac{1}{2}} \quad (24)$$

It may be worth while to point out in résumé of equations (23) and (24) that these relations do contain the necessary parameters for the study of the potential flow in any doubly connected region. It is observed that the uniform stream velocity V and the angle of attack α_0 for the biplane cellule occur only in W_1 or W_2 (equations (9) and (13)) and are related to the velocity V_c and angle of attack α_c for the two circles in the t' plane by equation (22). The circulation Γ and the countercirculation Γ' , also occur in W_1 and W_2 . These circulations are, in general, arbitrary but may be considered specified or fixed in the case of biplane contours by equations (17) and (19). The parameters α , β , γ , and δ determine the position and attitude of the profile chords, i. e., the gap/chord, chord ratio, stagger, and decalage. The variables λ , μ define the shapes of the contours, having the chosen line segments as chords. The functions f and g furnish the means of transition from the two arbitrary contours to two circular boundaries (i. e., from θ , μ to φ , σ). The parameters α' and β' determine the radii of the circles and are fixed by the local conditions at $z=c$ corresponding to the region at infinity (equation (3.29)).

From equation (3.40) or (3.40')

$$\left| \frac{dw}{dz} \right| = \left| \frac{w}{z} \right| \left[\left(1 + \frac{dg_{1,\varphi}}{d\varphi} \right)^2 + \left(\frac{df_{1,\varphi}}{d\varphi} \right)^2 \right]^{\frac{1}{2}}$$

or also

$$\left| \frac{dw}{dz} \right| = \left| \frac{w}{z} \right| \frac{\left[\left(1 + \frac{df_{1,\theta}}{d\theta} \right)^2 \right]^{\frac{1}{2}}}{1 - \frac{dg_{1,\theta}}{d\theta}}$$

From equation (1.7)

$$\left| \frac{dw}{ds} \right| = |w|$$

And from equation (2.32)

$$\frac{1}{2c} \left| \frac{dw}{ds} \right| = [(P_1 \cos \gamma + P_1' \sin \gamma)^2 + (Q_1 \cos \gamma + Q_1' \sin \gamma)^2]^{\frac{1}{2}}$$

(The subscript 1 in P_1 , P_1' , Q_1 , and Q_1' denotes that the values of (λ, μ) which define the upper contour are to be used.) Hence, finally for the velocity v_1 at any point (x, y) or (λ, μ) of the surface of the upper profile there is obtained

The local superstream pressure at points of the boundary surfaces, in terms of the dynamic pressure of the uniform stream, is given by

$$\frac{p_1}{q} = 1 - \left(\frac{v_1}{V} \right)^2, \quad \frac{p_2}{q} = 1 - \left(\frac{v_2}{V} \right)^2 \quad (25)$$

where

$$q = \frac{1}{2} \rho V^2$$

The general formulas can be somewhat simplified in certain special cases. For example, in the case of biplane contours described about parallel segments as chords the parameter $\delta=0$ and, in addition, if the chords are equal, $\alpha=\beta$.

Application may be made of the Blasius formulas for obtaining the total lift of the biplane combination. It is readily found that the total lift is, as in the monoplane case given by $L=\rho V\Gamma$ per unit span length, where Γ is the total circulation, and the lift vector L is perpendicular to the direction of the uniform stream V . The total integrated moment as well as the forces on the separate contours may also be developed without regard to the local pressure formula (25) though the expressions are not of particularly simple forms. In

the special case of biplane combinations composed of the framework of the line segments themselves, the formulas for the forces and moments will reduce somewhat. These and further special applications are reserved for the future.

As an example of the application of the formulas presented in this paper the pressure distribution for the biplane cellule shown in figure 10 (N. A. C. A. 4412 air-

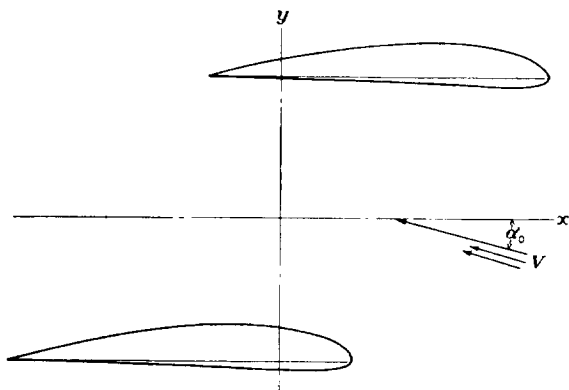


FIGURE 10.—Biplane arrangement (N. A. C. A. 4412 section).

foil section) is developed. The curves representing the g_1 , g_2 , μ_1 , and μ_2 functions are shown in figure 11. The pressure distribution is given in figure 12 for values of the biplane combination lift coefficient: $C_L=0, 0.5, 1.0$, and 1.5 . The pressure distribution for the monoplane case (cf. reference 14) is also presented for comparison. The numerical procedure is outlined under table I.

LANGLEY MEMORIAL AERONAUTICAL LABORATORY,
NATIONAL ADVISORY COMMITTEE FOR AERONAUTICS,
LANGLEY FIELD, VA., June 8, 1935.

REFERENCES

1. Theodorsen, T., and Garrick, I. E.: General Potential Theory of Arbitrary Wing Sections. T. R. No. 452, N. A. C. A., 1933.
2. Koebe, P.: Abhandlungen zur Theorie der konformen Abbildung. Journal für die Reine u. Angewandte Mathematik, vol. 145, 1914, p. 223. (Also scattered papers in Mathematischen Annalen, 1909-1912.)
3. Theodorsen, Theodore: Theory of Wing Sections of Arbitrary Shape. T. R. No. 411, N. A. C. A., 1931.
4. Lagally, M.: Die reibungslose Strömung im Aussengebiet zweier Kreise. Zeitschrift für Angewandte Math. u. Mech., vol. 9, no. 4, Aug. 1929, pp. 299-305. (Translated in N. A. C. A., T. M. No. 626.)

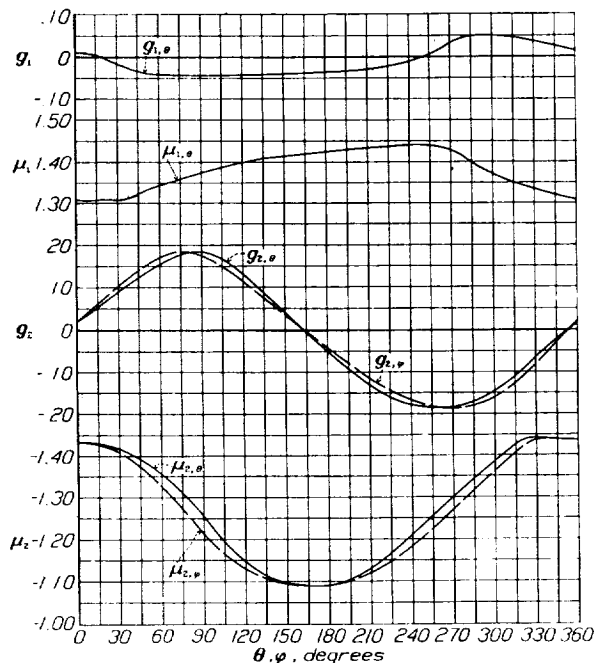
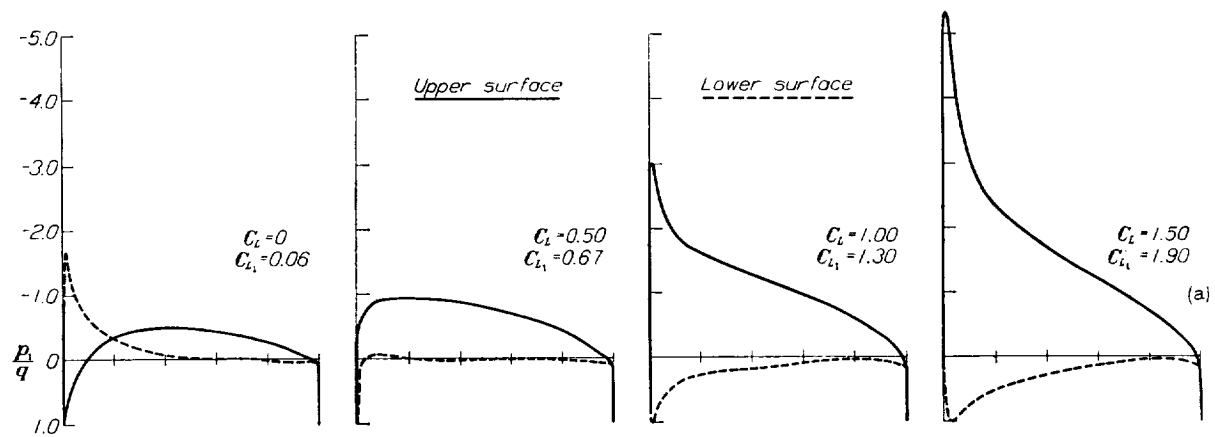
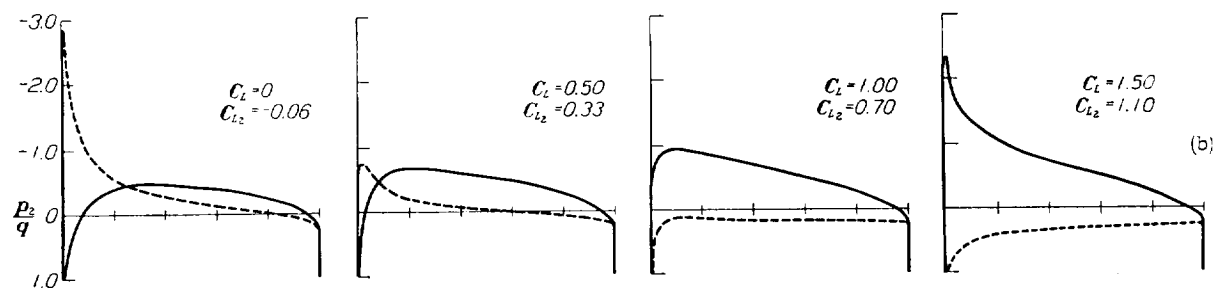


FIGURE 11.—The μ_1 , μ_2 , g_1 , and g_2 functions for the arrangement in figure 10.

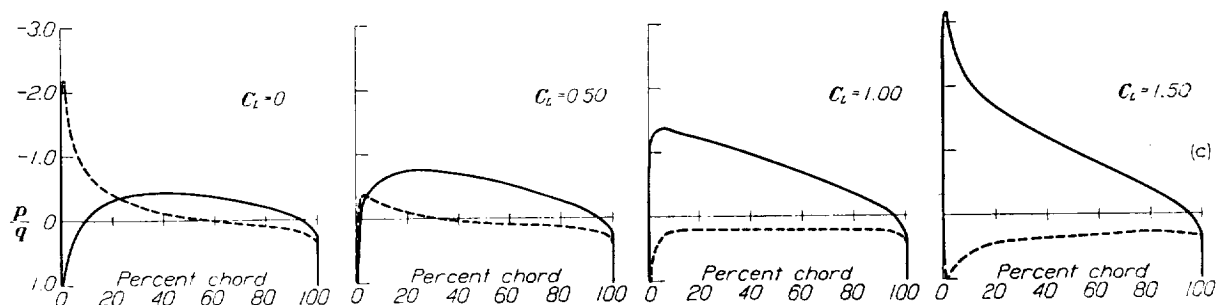
5. Dupont, P.: Introduction à l'étude du biplan: interaction de deux corps non contigus. IV Congresso Int. di Navig. Aerea, Rome, 1927.
6. Bonder: Sul moto di due cilindri in un fluido perfetto. Bollettino della Soc. Politecnica di Varsavia, 1929.
7. Müller, W.: Systeme von Doppelquellen in der ebenen Strömung, insbesondere die Strömung um zwei Kreiszylinder. Z. A. M. M. vol. 9, June 1929, pp. 200-213.
8. Kutta, W. M.: Über ebene Zirkulationsströmungen nebst flugtechnischen Anwendungen. Sitzungsber. der Bayr. Akad. d. Wissensch., München, 1911, p. 65.
9. Ferrari, Carlo: Sulla trasformazione conforme di due cerchi in due profili alari. Memorie della Reale Accad. della Scienze di Torino. June 1930. Serie II, vol. 67, 1930.
10. Halphen, G. H.: Traité des Fonctions Elliptiques et de leurs Applications. Vol. I, Gauthier-Villars, Paris, 1886.
11. Appell, P., and Lacour, E.: Principes de la Théorie des Fonctions Elliptiques et Applications. Gauthier-Villars, Paris, 1922.
12. Wilson, Edwin Bidwell: Advanced Calculus. Ginn and Co., Boston, 1912, p. 468.
13. Villat, Henri: Le problème de Dirichlet dans une aire annulaire. Rendiconti del Circolo Matematico di Palermo, vol. 33, 1912, pp. 134-175.
14. Garrick, I. E.: Determination of the Theoretical Pressure Distribution for Twenty Airfoils. T. R. No. 465, N. A. C. A., 1933.



(a) Pressure distribution for the upper wing section of the biplane combination in figure 10.



(b) Pressure distribution for the lower wing section of the biplane combination in figure 10.



(c) Pressure distribution for the monoplane airfoil section (N. A. C. A. 4412).

FIGURE 12.

EXPLANATION OF TABLE I

Table I presents in outline the numerical procedure in obtaining the velocities and pressures at the boundaries of the biplane combination shown in figure 10. The gap/chord=0.825, stagger/chord=0.530, chord/chord=1, and the decalage=0. The parameters α , β , γ , and δ are: $\alpha=\beta=1.4436$, $\gamma=-30^\circ$, and $\delta=0$. The rectangular coordinates x , y of the profiles are given in columns 1 and 2. (c =unity.) The values of λ , μ which correspond (i. e., satisfy equation (2.29)) are given in columns 3 and 4 and have been calculated by the method outlined in section 4. The constants $A_0=0.0467$, $B_0=-0.0106$, $r=1.025$, $\xi=-0^\circ3'$, $\alpha'=1.333$, $\beta'=1.303$, $\tau=2.636$ and the angular distortion functions g_1 and g_2 (column 5) are determined by the method outlined in section 3. Column 6 presents the angle $\varphi=\theta-g$ where $\theta=-\lambda$. The functions R_1 , R_2 , and R_3 given in columns 7, 8, and 9 are determined by equations (5.10)–(5.12). Column 10 gives the quantity $h=\left[\left(1+\frac{dg}{d\varphi}\right)^2+\left(\frac{df}{d\varphi}\right)^2\right]^{-1/2}$ for each profile obtained graphically. (See fig. 11.) Column 11 gives the quantity $k=[(P \cos \gamma + P' \sin \gamma)^2 + (Q \cos \gamma + Q' \sin \gamma)^2]^{-1/2}$ for each profile. In determining the next column, we require the singular points of the chords as determined by equation (2.22), $\lambda_1=91^\circ49'$, $\lambda_2=40^\circ58'$. Hence $\varphi_1=-93^\circ22'$, $\varphi_2=-35^\circ14'$ (cf. footnote 14). The constants occurring in equation (5.14) are then $R_{11}=0.3444$, $R_{21}=0.2617$, $R_{31}=0.3659$, $R_{12}=0.9431$, $R_{22}=-0.4890$, $R_{32}=0.7117$. Equation (5.16) gives then $\beta_c=34^\circ51'$ and equation

(5.17) determines $K=1.020$. The circulation is now $\Gamma=-4\pi c V_c(1.020) \sin(\alpha_c+34^\circ51')$. Equation (5.18) determines $\gamma_c=38^\circ5'$ and (5.19) gives $J=-0.0987$. The countercirculation $\Gamma'=8\pi c V_c(0.0987) \sin(\alpha_c+38^\circ5')$. The lift coefficient may be expressed as $C_L=\frac{\rho V \Gamma}{q(\text{chord})}$ where $q=\frac{1}{2}\rho V^2$. The chord for each profile in the example considered is equal to $(2.106)c$, hence $C_L=-2\pi(0.985) \sin(\alpha_c+34^\circ51')$. (In the monoplane case the lift coefficient for the N. A. C. A. 4412 airfoil in two-dimensional potential flow is obtained as (cf. reference 14) $2\pi(1.114) \sin(\alpha+\text{constant})$ or the slope of the lift curve in the monoplane case is about 13 percent greater than that in the biplane example treated). Putting $C_L=0, 0.5, 1.0$, and 1.5 , respectively, the angles α_c are determined as $\alpha_c=-34^\circ51'$, $-30^\circ8'$, $-25^\circ24'$, and $-20^\circ35'$, respectively (i. e., by equation (5.22) $\alpha_0=-4^\circ48', 0^\circ5', 4^\circ33', 9^\circ22'$, respectively). Columns 12–15 of the table give the values of $\frac{W_1}{2cV}$ and $\frac{W_2}{2cV}$ for the foregoing four values of α_c , and are determined by equations (5.9) and (5.13). The velocities at each profile surface v_1 and v_2 are given in terms of the stream velocity V by the formulas (5.23) and (5.24), $\frac{v_1}{V}=\frac{W_1 h_1 k_1}{2cV}$ and $\frac{v_2}{V}=\frac{W_2 h_2 k_2}{2cV}$. The pressure ratios $\frac{p_1}{q}$ and $\frac{p_2}{q}$ shown in figure 12 are given by equation (5.25).

The Smithsonian Tables of Hyperbolic Functions were found useful in the numerical work.

TABLE I. BIPLANE ARRANGEMENT N. A. C. A. 4412

(SEE FIG. 10)

A. UPPER PROFILE

x	y	λ	μ	ϕ_1	$\phi (= -\lambda')$	$R_1(\lambda')$	$R_2(\lambda')$	$R_3(\lambda')$	h_1	k_1	$\frac{C_L=0}{W_1}$ $2cV$	$\frac{C_L=0.5}{W_1}$ $2cV$	$\frac{C_L=1.0}{W_1}$ $2cV$	$\frac{C_L=1.5}{W_1}$ $2cV$
UPPER SURFACE														
1.6458	0.8731	-39 4	1.3132	-1 34	40 38	0.8627	-0.3665	-0.6883	1.063	7.940	-0.0670	0.0574	0.2021	0.3434
1.6121	.9195	-29 36	1.3096	-0 51	30 27	.6995	-.5870	-.6380	1.076	4.160	.1227	.2849	.4459	.6013
1.5839	.9379	-26 6	1.3099	-0 34	26 40	1.0225	-.6687	-.5972	1.076	3.250	.2131	.3778	.5410	.6918
1.5282	.9641	-21 7	1.3111	-0 16	21 23	1.0893	-.7922	-.5305	1.070	2.422	.3424	.5341	.6904	.8533
1.4742	.9836	-17 22	1.3118	0 12	17 10	1.1097	-.8541	-.4931	1.064	2.112	.4247	.5978	.7678	.9291
1.4198	1.0066	-14 2	1.3061	0 18	13 44	1.1251	-.9108	-.3652	1.052	1.858	.5443	.7123	.8764	1.0302
1.3140	1.0323	-8 43	1.3068	0 34	8 9	1.1630	-.9777	-.2265	1.037	1.585	.6784	.8429	1.0027	1.1519
1.2094	1.0504	-4 8	1.3080	0 47	3 21	1.1766	-1.0093	-.0950	1.038	1.424	.7796	.9375	1.0900	1.2307
1.0000	1.0694	3 53	1.3117	1 10	-4 3	1.1753	-1.0064	.1146	1.047	1.267	.8869	1.0400	1.1770	1.3017
.7921	1.0690	11 14	1.3181	1 26	-12 40	1.1405	-.9257	.3407	1.054	1.198	.9599	1.0808	1.1952	1.2971
.6731	1.0460	18 42	1.3251	1 47	-20 29	1.0824	-.7958	.5051	1.030	1.244	.9472	1.0382	1.1386	1.2190
.5799	1.0333	25 55	1.3327	2 1	-27 56	1.0092	-.6421	.6127	1.039	1.311	.8826	.9611	1.0336	1.0949
-.1745	1.0036	34 8	1.3408	2 13	-36 21	.9138	-.4577	.6787	1.036	1.477	.7679	.8258	.8786	.9213
-.0314	.9660	43 54	1.3514	2 35	-46 29	.7924	-.2496	.6852	1.024	1.829	.6019	.6398	.6738	.6995
-.2180	.9340	57 2	1.3675	2 52	-59 54	.6380	-.0274	.6224	1.013	2.746	.3834	.4033	.4204	.4314
-.3364	.8952	66 56	1.3818	2 58	-69 54	.5357	-.0936	.5491	.988	4.184	.2426	.2530	.2625	.2672
LOWER SURFACE														
-.4280	0.8657	93 54	1.4333	1 26	-95 20	0.3342	0.2707	0.3507	0.904	65	-0.0162	-0.0164	-0.0165	-0.0168
-.3046	.8935	127 10	1.4364	-1 3	-126 7	.1933	.3560	.1787	.957	5.248	-.1855	-.1893	-.1917	-.1938
-.1891	.8618	143 31	1.4345	-1 32	-141 59	.1570	.3590	.1197	.976	4.463	-.2207	-.2236	-.2248	-.2257
-.0359	.8567	169 13	1.4274	-1 69	-167 14	.1218	.3691	.0343	.990	3.655	-.2776	-.2782	-.2786	-.2788
.2550	.8520	-169 13	1.4208	-2 10	171 23	.1199	.3696	-.0234	.994	3.253	-.3111	-.3080	-.3014	-.2850
.4680	.8455	-160 5	1.4126	-2 11	152 16	.1335	.3672	-.0796	.994	3.021	-.3412	-.3327	-.3159	-.2892
.6696	.8408	-133 7	1.4078	-2 22	135 39	.1699	.3547	-.1412	.994	2.799	-.3662	-.3498	-.3309	-.3092
.8906	.8294	-116 15	1.3938	-2 29	118 44	.2229	.3334	-.2176	.993	2.739	-.3924	-.3653	-.3355	-.3040
1.0912	.8212	-100 40	1.3830	-2 30	103 10	.2676	.2909	-.2987	.994	2.703	-.4112	-.3718	-.3290	-.2843
1.2812	.8148	-84 57	1.3710	-2 30	87 27	.3887	.2309	-.4117	.998	2.824	-.4191	-.3601	-.2984	-.2354
1.3763	.8083	-77 17	1.3606	-2 30	79 47	.4477	.1810	-.4708	.999	2.993	-.4120	-.3417	-.2687	-.1950
1.4602	.8125	-68 40	1.3520	-2 30	71 10	.5236	.1066	-.5391	1.001	3.367	-.3899	-.3053	-.2181	-.1306
1.5158	.8149	-63 58	1.3463	-2 28	66 6	.5730	.0520	-.5783	1.005	3.714	-.3675	-.2736	-.1773	-.0810
1.5621	.8209	-58 39	1.3413	-2 22	61 0	.6261	-.0123	-.6150	1.014	4.330	-.3358	-.2320	-.1261	-.0207
1.6068	.8320	-52 11	1.3340	-2 18	54 29	.6913	-.1087	-.6548	1.031	5.250	-.2800	-.1631	-.0452	.0716
1.6287	.8430	-47 41	1.3290	-2 4	49 46	.7535	-.1891	-.6759	1.040	6.000	-.2256	-.0990	-.0289	.1548
1.6458	.8731	-39 4	1.3132	-1 34	40 38	.8627	-.3665	-.6883	1.063	7.940	-.0870	.0574	.2021	.3434

B. LOWER PROFILE

x	y	λ	$-\mu$	ϕ_2	$\phi (= -\lambda')$	$R_1(\lambda')$	$R_2(\lambda')$	$R_3(\lambda')$	h_2	k_2	$\frac{C_L=0}{W_2}$ $2cV$	$\frac{C_L=0.5}{W_2}$ $2cV$	$\frac{C_L=1.0}{W_2}$ $2cV$	$\frac{C_L=1.5}{W_2}$ $2cV$
UPPER SURFACE														
0.4440	-0.8606	-93 23	1.2379	10 32	82 51	0.4168	0.2164	-0.4584	1.022	11.756	0.0899	0.0217	-0.0467	-0.1145
.4096	-.8025	-110 37	1.1703	8 51	101 46	.2924	.3021	-.3209	1.112	6.918	-.0189	-.1108	-.1626	-.2370
.3791	-.7807	-117 23	1.1516	7 48	109 35	.2600	.3251	-.2695	1.138	5.964	-.1073	-.1490	-.2000	-.2440
.3191	-.7498	-127 47	1.1275	6 15	121 32	.2008	.3470	-.2044	1.158	5.010	-.1624	-.2007	-.2378	-.2638
.2612	-.7269	-136 12	1.1102	4 37	131 35	.1693	.3583	-.1589	1.170	4.485	-.1977	-.2307	-.2623	-.2917
.2050	-.7153	-143 24	1.1050	3 23	140 11	.1464	.3653	-.1215	1.173	4.238	-.2248	-.2536	-.2806	-.3056
.0911	-.6881	-156 50	1.0944	1 8	155 42	.1221	.3716	-.0720	1.175	3.819	-.2582	-.2818	-.3036	-.3229
-.0215	-.6700	-168 55	1.0880	-0 14	169 9	.1118	.3766	-.0313	1.175	3.575	-.2856	-.3057	-.3238	-.3394
-.2419	-.6540	-169 35	1.0976	-4 35	165 0	.1127	.3739	.0377	1.160	3.241	-.3228	-.3380	-.3511	-.3614
-.4555	-.6388	-150 30	1.1306	-7 27	143 7	.1402	.3669	.1103	1.121	3.012	-.3586	-.3708	-.3806	-.3872
-.6711	-.6768	-132 36	1.1741	-9 30	123 6	.1923	.3502	.1926	1.070	2.835	-.3919	-.4020	-.4091	-.4133
-.8667	-.7019	-117 11	1.2191	-10 20	106 51	.2663	.3080	.2903	1.018	2.718	-.4125	-.4203	-.4253	-.4260
-.1.0690	-.7333	-101 51	1.2648	-10 34	91 17	.3513	.2656	.3386	.986	2.678	-.4344	-.4405	-.4438	-.4421
-.1.2628	-.7713	-86 32	1.3110	-10 26	78 6	.4740	.1660	.5146	.957	2.735	-.4347	-.4280	-.4285	-.4234
-.1.4622	-.8149	70 2	1.3594	-9 26	60 36	.6309	-.0056	.6419	.898	3.243	-.3566	-.3566	-.3543	-.3463
-.1.5589	-.8391	69 57	1.3855	-8 23	51 34	.7368	-.1492	.6992	.861	4.312	-.2715	-.2700	-.2669	-.2680
LOWER SURFACE														
-1.6490	-0.8664	39 16	1.4371	-5 25	-33 51	0.9582	-0.5229	0.7030	0.832	33	0.0330	0.0327	0.0320	0.0357
-1.5126	-.8650	21 30	1.4404	-2 8	-19 22	1.1317	-.8647	.5270	.829	2.766	.4140	.4020	.3872	.3749
-1.4050	-.8706	14 20	1.4399	-1 0	-13 20	1.1648	-.9544	.3822	.848	1.992	.5736	.5536	.5284	.5058
-1.2189	-.8742	4 8	1.4375	0 18	-4 26	1.2056	-1.0546	.1341	.854	1.488	.7944	.7574	.7149	.6727
-.9847	-.8815	-4 8	1.4335	1 45	2 23	1.2092	-1.0634	-.0728	.862	1.307	.9198	.8686	.8020	.7528
-.7785	-.8861	-11 39	1.4311	2 33	9 8	1.1880	-1.0151	-.2705	.862	1.247	.9931	.9277	.8466	.7620
-.5784	-.8910	-18 48	1.4279	3 31	15 17	1.1500	-.9254	-.4288	.861	1.238	1.0100	.9329	.8399	.7534
-.3649	-.9033	-26 43	1.4186	4 45	21 59	1.0926	-.7967	-.6660	.860	1.342	.9827	.8953	.7921	.7052
-.1651	-.9125	-35 7	1.4082	5 46	29 21	1.0125	-.6285	-.6668	.859	1.524	.9024	.8064	.6969	.6030
-.0513	-.9201	-45 13	1.3919	7 6	38 7	.9056	-.4248	-.7214	.862	1.905	.7654	.6674	.5632	.4577
-.1492	-.9246	-50 57	1.3775	7 50	43 7	.8425	-.3151	-.7254	.869	2.241	.6787	.5797	.4763	.3719
-.2510	-.9236	-58 13	1.3600	8 41	49 32	.7618	-.1864	-.7085	.882	2.896	.5634	.4667	.3656	.2656
-.3014	-.9213	-62 39	1.3474	9 10	53 29	.7136	-.1157	-.6891	.889	3.403	.4943	.3998	.3022	.2044
-.3514	-.9152	-68 6	1.3325	9 41	58 25	.6555	-.0370	-.6575	.900	4.351	.4117	.3579	.2273	.1339
-.3996	-.9037	-75 27	1.3094	10 10	65 17	.5798	.0557	-.6052	.921	6.340	.3057	.2207	.1337	.0474
-.4248	-.8922	-81 7	1.2907	10 33	70 34	.5260	.1146	-.5614	.965	8.770	.2323	.1523	.0710	-.0099
-.4440	-.8606	-93 23	1.2379	10 32	82 51	.4168	.2164	-.4584	1.022	11.756	.0899	.0217	-.0467	-.1145

REPORT No. 543

TANK TESTS OF N. A. C. A. MODEL 40 SERIES OF HULLS FOR SMALL FLYING BOATS AND AMPHIBIANS

By JOHN B. PARKINSON and JOHN R. DAWSON

SUMMARY

The N. A. C. A. model 40 series of flying-boat hull models consists of 2 forebodies and 3 afterbodies combined to provide several forms suitable for use in small marine aircraft. One forebody is of the usual form with hollow bow sections and the other has a bottom surface that is completely developable from bow to step. The afterbodies include a short pointed afterbody with an extension for the tail surfaces, a long afterbody similar to that of a seaplane float but long enough to carry the tail surfaces, and a third obtained by fitting a second step in the latter afterbody.

The various combinations were tested in the N. A. C. A. tank by the general method over a suitable range of loadings. Fixed-trim tests were made for all speeds likely to be used and free-to-trim tests were made at low speeds to slightly beyond the hump speed. The characteristics of the hulls at best trim angles have been deduced from the data of the tests at fixed trim angles and are given in the form of nondimensional coefficients applicable to any size of hull.

Comparisons among the forms are shown by suitable cross plots of the nondimensional data and by photographs of the spray patterns. The difference between the results obtained with the two forebodies was small for the smooth-water conditions simulated in the tank. With the same forebody in each case, the resistance of the no-step afterbody was least at the hump speed and that of the pointed afterbody was least at high speeds.

Take-off examples of an 8,000-pound flying boat or amphibian having a power loading of 13.3 pounds per horsepower and a 2,000-pound flying boat having a power loading of 18.2 pounds per horsepower are included to illustrate the application of the data.

INTRODUCTION

A "general" test of a given form of hull as made in the N. A. C. A. tank provides data for all speeds, loads, and trim angles for which the form is suitable. These data may be used to compare the water characteristics with those of other forms and to estimate the

water performance of possible applications of the lines over a considerable range of full-size dimensions. The results of such tests on 11 forms have been published to date by the Committee.

The models tested have, in general, the forms found in a limited number of large flying boats. A need has been expressed for general test data regarding forms similar to those used on the smaller flying boats and amphibians of 2,000 to 10,000 pounds gross weight. The hulls of flying boats in this class appear to have higher length-beam ratios and higher beam loadings (C_{Δ} values) than are usual for the hulls of the larger craft thus far investigated. The amphibians also have higher angles of afterbody keel. Because the hulls are relatively narrow, a moderate angle of dead rise gives satisfactory shock-absorbing qualities and, because they are heavily loaded for their size, some means of suppressing spray such as hollow sections or spray strips is particularly desirable.

Simplicity of form seems to be a conspicuous feature of the designs in this class. Excessive flaring of the forebody sections requiring extensive forming of the plating is avoided; likewise, a simple form of afterbody is usually adopted. Because of the low power loadings generally employed, the compromises made among water and flight characteristics favor those of flight. These smaller craft are less seaworthy than the large flying boats but usually operate in inland waters, which do not demand the degree of seaworthiness necessary in the open sea.

The N. A. C. A. model 40 series of flying-boat hulls was designed with the foregoing considerations in mind. It includes 2 forebodies and 3 afterbodies in various combinations that are of interest to the designers of small marine aircraft. General tests of 5 of the 6 possible combinations were made in the N. A. C. A. tank during 1934. From the results of the tests, the water performance of full-size hulls having their lines may be estimated and the effect of changes in form within the limits covered by the series may be determined.

DESCRIPTION OF MODELS

LINES

General.—The lines developed for the series are shown in figures 1 and 2. The faired offsets for the models are given in tables I to IV. The following particulars apply to all the variations:

	Inches	Percentage of maximum beam
Forebody length.....	42.00	311.80
Over-all length.....	100.00	742.39
Beam over chine.....	13.00	96.51
Beam over spray strips.....	13.47	100.00
Depth.....	11.00	103.93
Width of spray strip.....	.25	1.86
Width of keel flat.....	.20	1.48
Depth of step.....	.50	3.71

Angle of dead rise, stations 6 and aft, 20°.

The V bottom cross section with the spray strip added at the chine was considered to be the most economical arrangement for this class of hull. In the tank, the water breaks cleanly from the edge of the strip before the hump speed is reached; hence this edge, rather than the chine, is considered to be the boundary of the bottom. It is suggested that in full-size applications the strip be extended to the bow.

Forebodies.—The length of the forebody was made as short as was thought to be practicable for the loadings intended in order to keep the structure forward of the portion of the hull that is used for passengers or cargo as light as possible. Forward of the step the planing bottom is longitudinally straight for good planing characteristics while farther forward the bottom

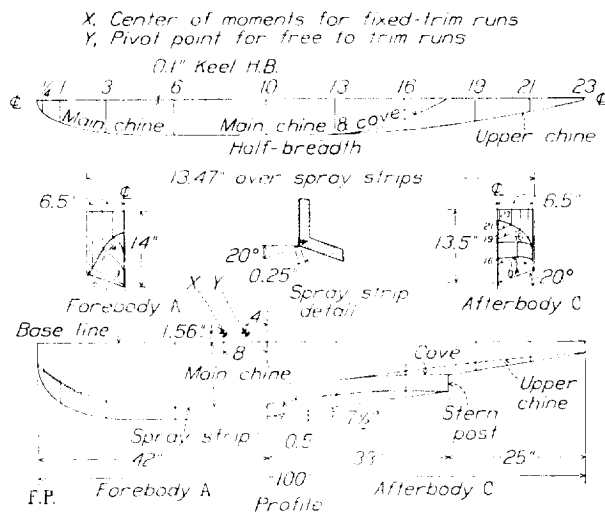


FIGURE 1.—Lines of forebody A and afterbody C.

risers sharply toward the bow. The bow sections of forebody A are slightly flared in the usual manner as an aid in meeting oncoming waves. The plan form of its chine is rounded at the bow to facilitate rounding the deck above it when desirable from aerodynamic considerations.

Forebody B was developed to be used where extreme simplicity of form is desirable. The bottom surface forward of the flat planing bottom is generated by a straight line moving parallel to itself with the chine as a directrix. The bottom surface is therefore that of a cylinder which may be unrolled into a flat sheet and

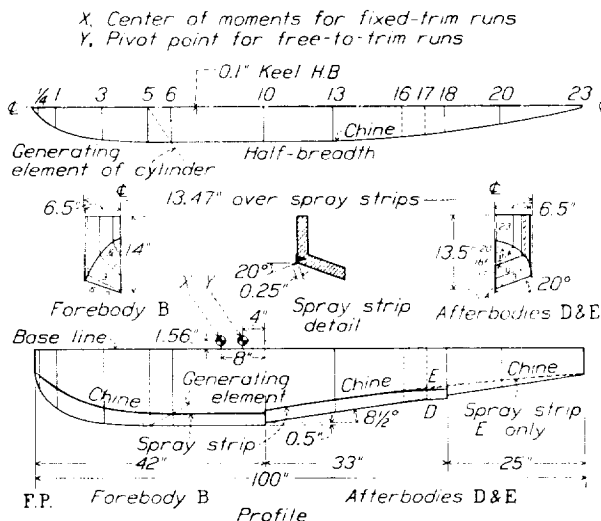


FIGURE 2.—Lines of forebody B, afterbody D, and afterbody E.

the entire surface of the hull is developable, no forming of the plating or planking being necessary in its construction. The slanting of the generating element in space as shown in figure 2 causes the angle of dead rise to increase toward the bow like that of the usual forms. As a result of this method of determining the surface, the conventional stations and water lines become slightly convex; hence, for practical applications, the use of a spray strip would be particularly desirable.

For the completely developable surface of forebody B, the plan form at the bow cannot be rounded but must be pointed so that the generating element will remain within the surface from keel to chine. Aft of station 6, forebodies A and B are identical.

Afterbodies.—Afterbody C is pointed in plan form and terminates in a narrow stern post. The extension of the hull, which carries the tail surfaces of the flying boat, is above the portion that is active during the take-off or immersed while at rest. The resulting form is an adaptation of the original NC type of afterbody, which has been favored by American designers. It is believed that the "cove" may be filleted with small effect on the water performance.

The angle of afterbody keel is made higher than that used on most large flying boats having this form of afterbody in order to provide a greater ground clearance for amphibians and to reduce high-speed resistance.

Afterbodies D and E provide second-step and no-step arrangements that are probably more economical

to construct than is a pointed type like afterbody C. The no-step afterbody is like that of a seaplane float and is much used in Europe for small craft. In some cases a second step is added to aid in controlling the trim angle at the hump speed or to provide additional lift while the afterbody is immersed. In afterbody D the portion ahead of the second step is curved down to give a higher effective trim angle for this portion of the bottom.

Combinations.—The forebodies and afterbodies were grouped for the tests as follows:

Model 40-AC: Normal forebody, pointed afterbody.

Model 40-AD: Normal forebody, second-step afterbody.

Model 40-AE: Normal forebody, no-step afterbody.

Model 40-BC: Developable forebody, pointed afterbody.

Model 40-BE: Developable forebody, no-step afterbody.

Tests of these combinations make it possible to compare the performances obtained when using the normal forebody with the three types of afterbody and when using the developable forebody with the pointed and no-step afterbodies. It was not considered necessary to test the developable forebody with the second-step afterbody as the characteristics of this combination may be inferred from the foregoing comparisons.

CONSTRUCTION

The various forebodies and afterbodies were constructed separately of mahogany to a tolerance of ± 0.02 inch and were bolted together at the step to form the combinations desired. In accordance with the usual practice at the N. A. C. A. tank, the surfaces were smoothly finished and given several coats of gray-pigmented varnish.

The spray strips were made of brass sheet 0.035 inch thick and 0.25 inch wide and were attached at the chines with wood screws through tabs formed on the strips at intervals. Unavoidable spaces between the inner edge of the strips and the model were filled with plasticine.

APPARATUS AND PROCEDURE

The N. A. C. A. tank and its testing apparatus are described in reference 1. The method of towing the model described therein introduced systematic errors because of the use of a "towing gate." The towing gate has been replaced by a counterbalanced girder as described in reference 2, and these errors are now eliminated. In the present towing gear the trimming moments are measured by a very stiff spring rigidly attached to the model. Water moments applied to the model cause the spring to deflect and the model to rotate slightly, but the deflections of the spring are so small that the change of trim angle due to the rotation of the model is within the limits of the accuracy to

which the trim angle is set. The deflections of this spring are measured by a dial gage. The center of moments was arbitrarily placed at the point shown in figures 1 and 2.

The tests were made by the general method which consists of measuring resistance, trimming moment, and draft at a fixed trim angle for a number of loads throughout the speed range considered practicable. The trim angle is then changed and the procedure repeated until a sufficient number of trim angles are obtained to determine the trim angle that gives least resistance at each load and speed. The loads taken are expected to cover the useful range for the models tested.

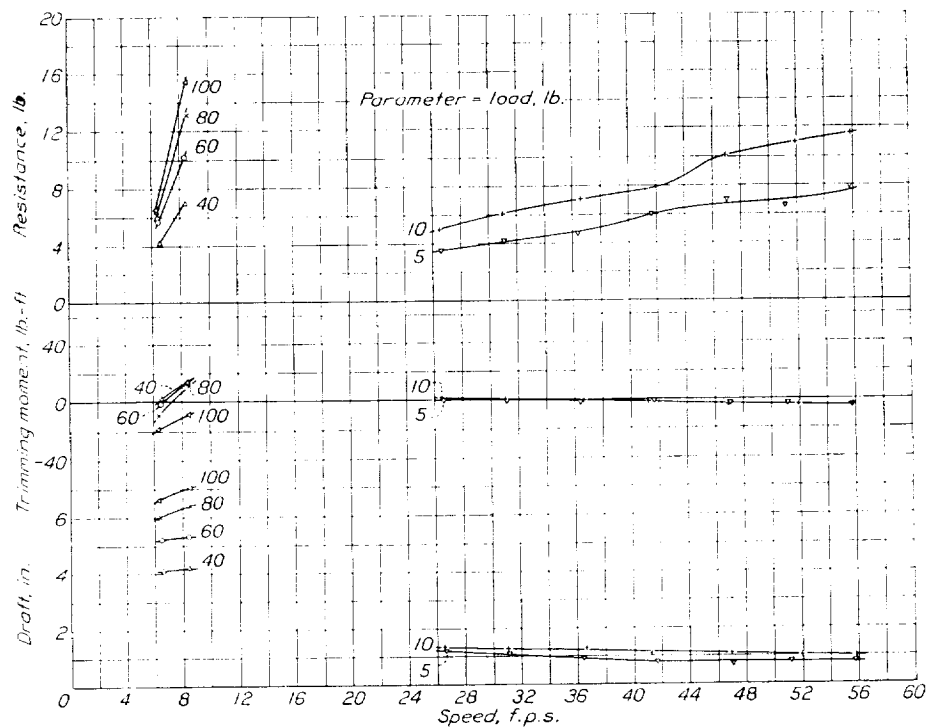
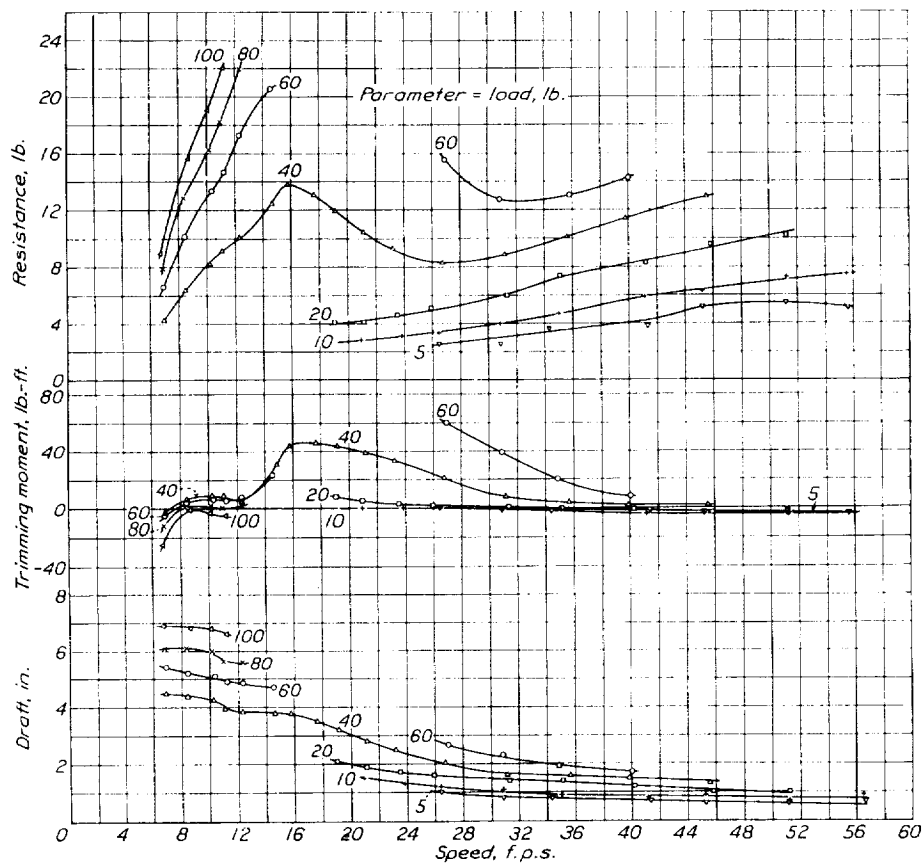
At the lowest speeds the curves of resistance plotted against trim angle failed to show a minimum resistance within the range of trim angles at which it was possible to test these models. Instead, the resistance continued to decrease as the trim angle was increased. At speeds below the hump speed the resistance is generally of only minor interest in the take-off problem and it makes little difference whether minimum resistance is obtained or not. Since it is generally considered that in the average flying boat only a small amount of longitudinal control is available at low speeds, there is some justification for using free-to-trim (zero trimming-moment) resistance up to the hump when the values of the aerodynamic moments are unknown. Results from the general tests of these models showed, however, that, with the center of moments used in the tests, the free-to-trim resistance at very low speeds would be a great deal higher than the resistance encountered at the speed corresponding to the usual free-to-trim hump and would be even greater than the minimum hump resistance corresponding to best angle. Moving the center of gravity back toward the step would, of course, allow the model to trim at greater angles and thus reduce the free-to-trim resistance at low speeds.

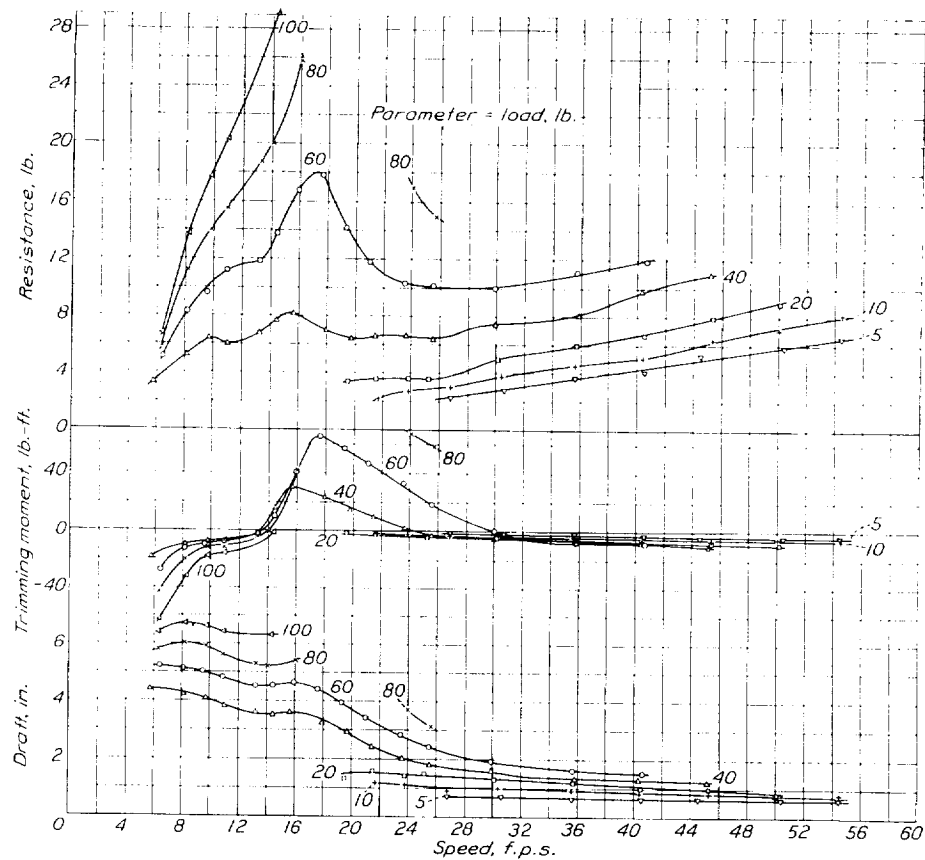
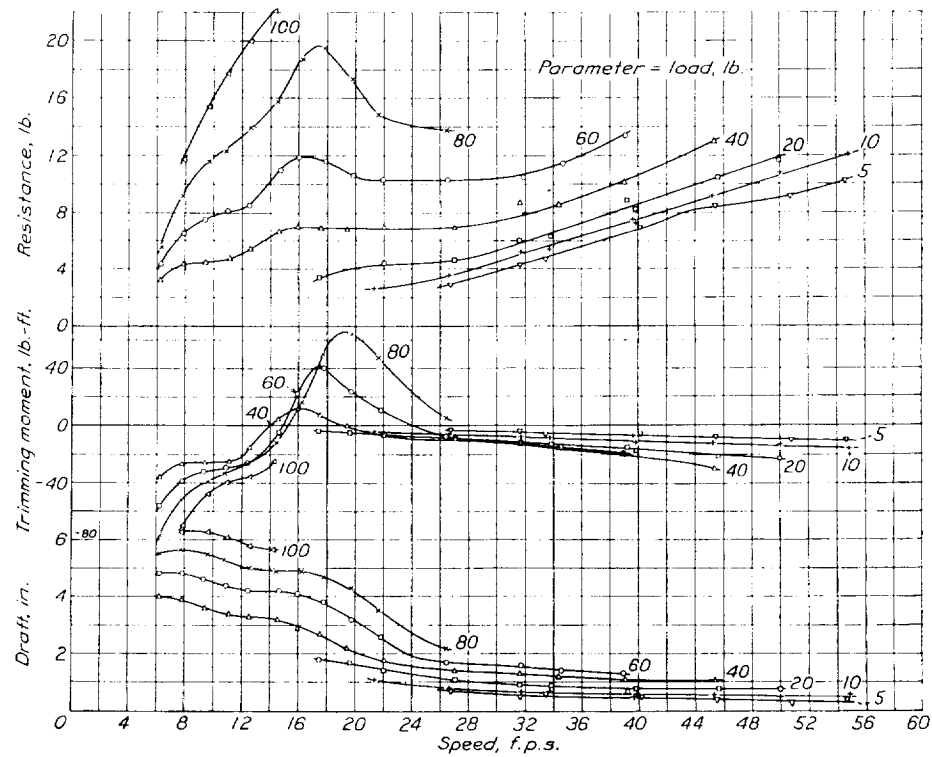
Although the free-to-trim curves for any position of the center of gravity that does not produce trim angles outside the range of those tested may be determined from the general test data, it was decided to test all five models free to trim, up to and including the hump, with the center of gravity 4 inches forward of the step. These tests presented an opportunity to observe the free-to-trim performance of the models as well as to check the accuracy of zero trimming-moment curves obtained from the general test results.

RESULTS

GENERAL TEST DATA

The data obtained from the tests of the five combinations are plotted against speed in figures 3 to 32. The plotted resistance is the water resistance plus the air drag of the model and was obtained by deducting

FIGURE 3.—Model 40-AC. Resistance, trimming moment, and draft. $\tau = 2^\circ$.FIGURE 4.—Model 40-AC. Resistance, trimming moment, and draft. $\tau = 3^\circ$.

FIGURE 5.—Model 40-AC. Resistance, trimming moment, and draft. $\tau = 5^\circ$.FIGURE 6.—Model 40-AC. Resistance, trimming moment, and draft. $\tau = 7^\circ$.

the air drag of the towing gear from the values weighed by the dynamometer. The trimming moments are referred to the center of moments shown in figures 1 and 2, which is 8 inches forward of the step. Positive moments tend to raise the bow. The drafts are the distances from the free-water surface to the keel at the main step. The main step is a convenient point of reference although the afterbody is deeper in the water at high angles of trim.

The exact conversion of trimming moments to the actual center of gravity used in a given design is laborious. The correction for a shift of the center of

STATIC PROPERTIES

The trimming moments and drafts obtained with the models at rest in the tank are given in figures 33 to 37. The moments are referred to the same center of moments as that used in the fixed-trim tests, which is located 8 inches forward of the step. The drafts are measured from the free-water surface to the keel at the main step. The position of the load water line and the longitudinal stability at rest for a given application may be deduced from these curves without performing the extensive calculations necessary to obtain this information from the lines.

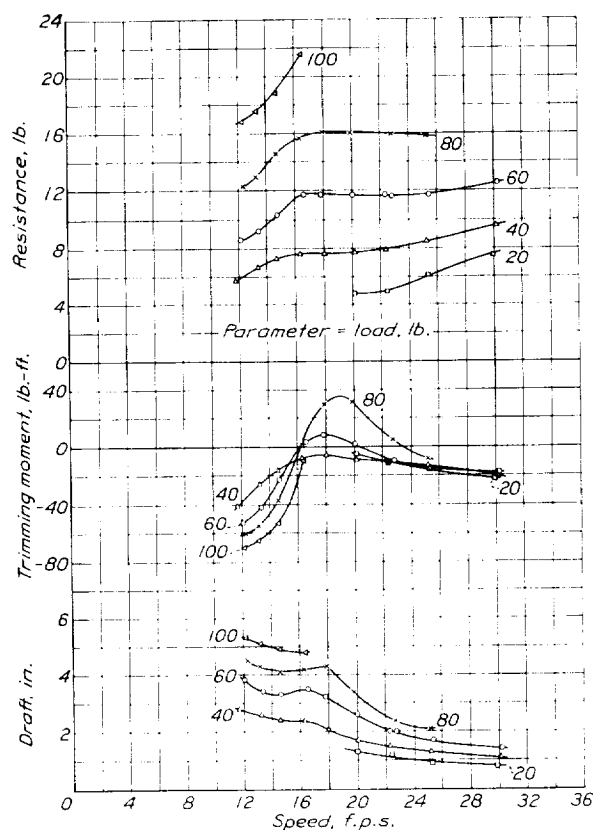


FIGURE 7.—Model 40-AC. Resistance, trimming moment, and draft. $\tau=9^\circ$.

moments parallel to the base line for these hulls is given with sufficient accuracy, however, by the expression ΔX where Δ is the load on the water in pounds and X is the distance of the center of gravity aft of the center of moments in feet. At low speeds this simplification depends on the fact that the resultant-force vector is nearly equal in magnitude to its load component and the direction of the resultant force is nearly perpendicular to the base line at usual trim angles; at high speeds, although the resultant-force vector no longer has these properties, the absolute error introduced is small and may be neglected. The corrections for shift in the center of moments perpendicular to the base line will be small in the range of center-of-gravity positions usually encountered.

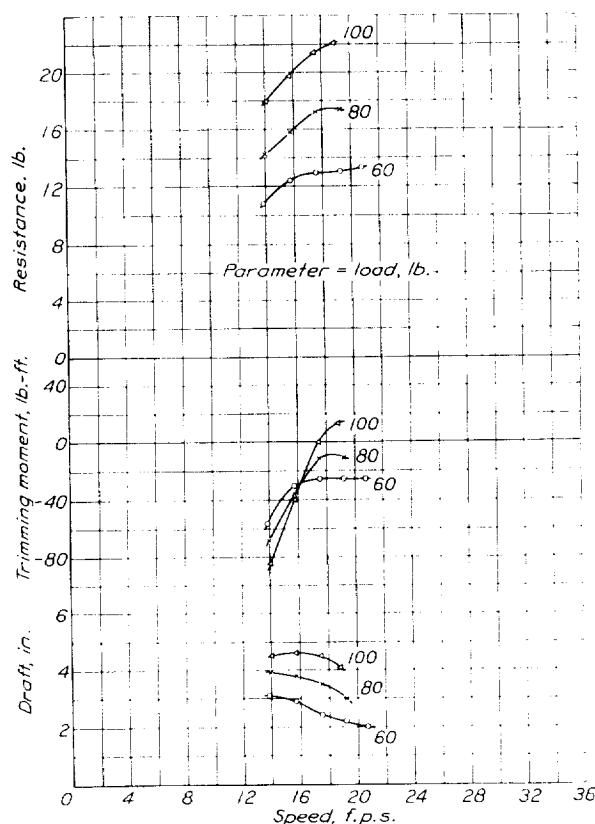
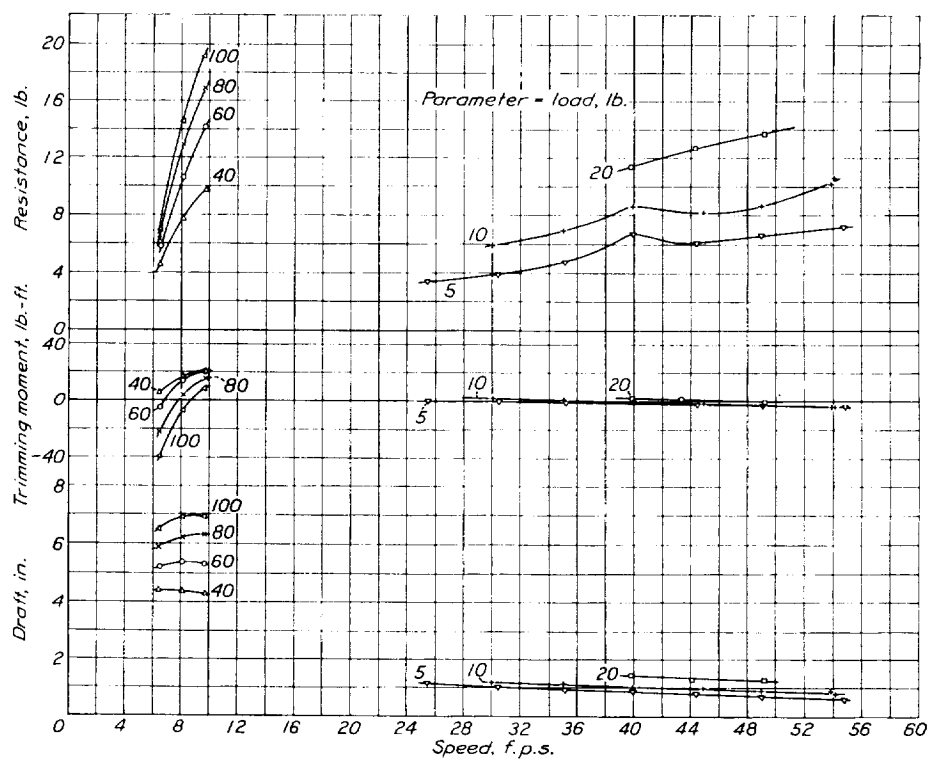
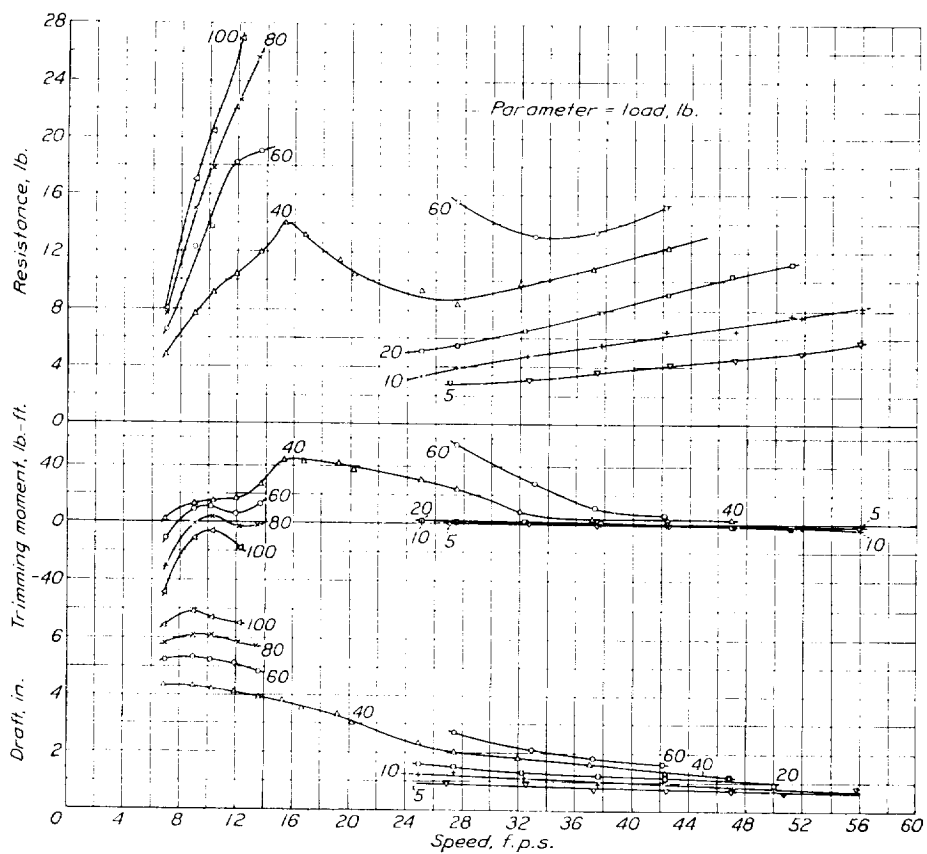
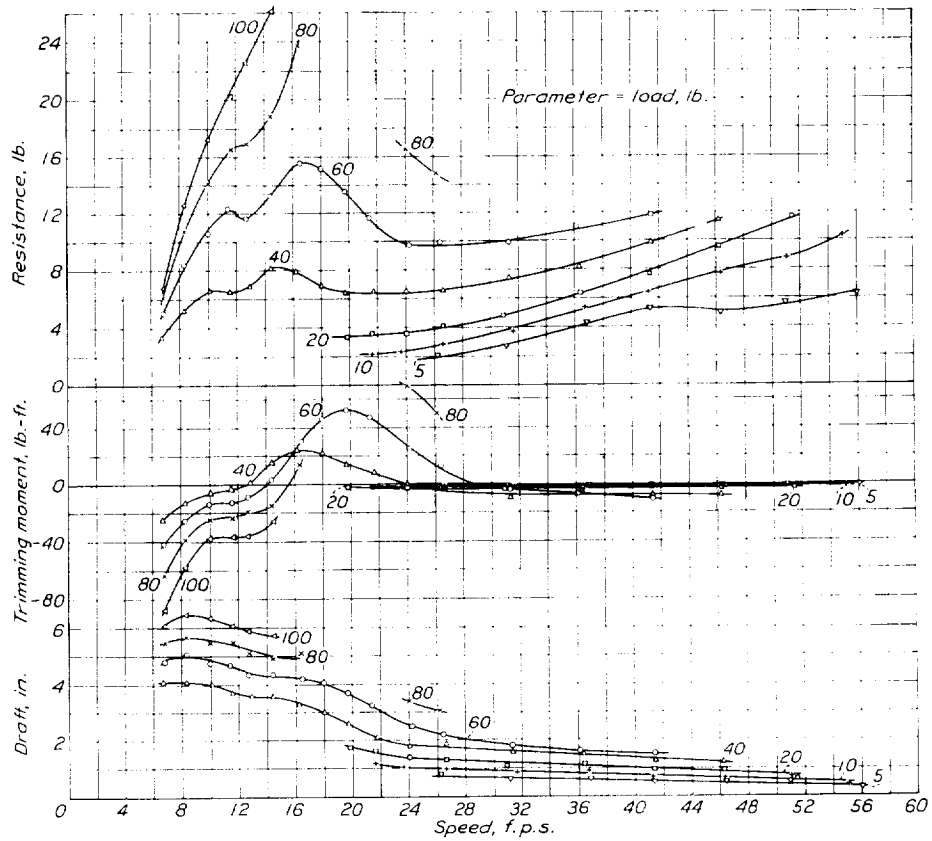
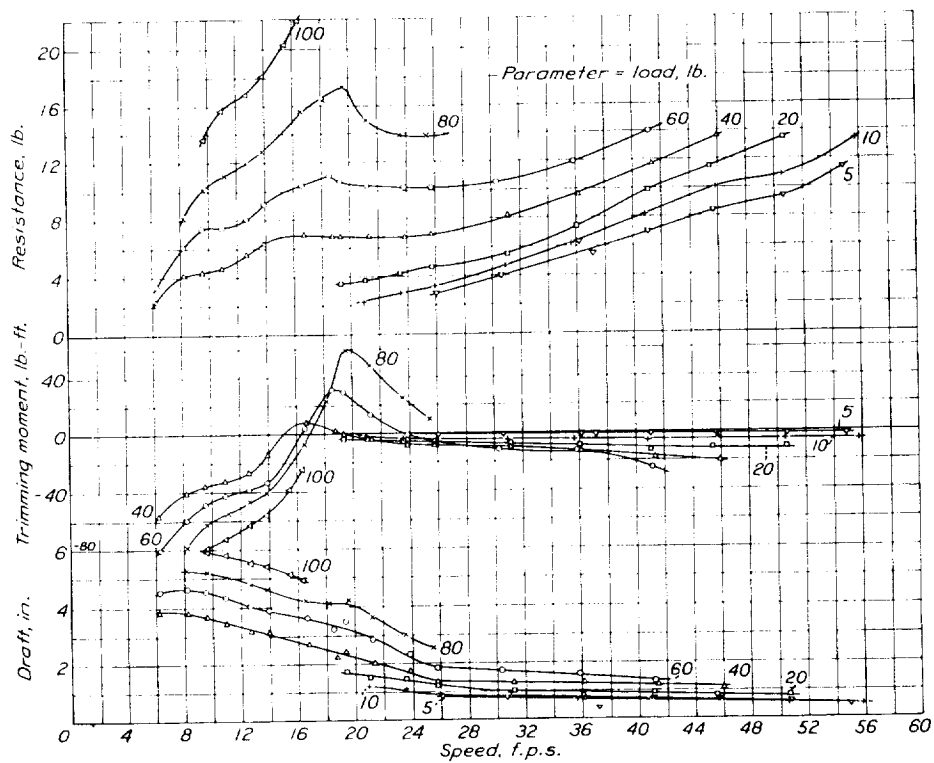


FIGURE 8.—Model 40-AC. Resistance, trimming moment, and draft. $\tau=11^\circ$.

The center of gravity of most seaplanes will be aft of the center of moments to which the trimming moments at rest are referred. Where the difference in height is small, the trimming-moment correction is approximately $\Delta_0 X$, where Δ_0 is the displacement and X is the distance of the center of gravity aft of the center of moments parallel to the model base line. Using this correction for an abscissa shift on the trimming-moment curves, the trim angle at rest for each load parameter may be read directly. A cross plot of these trim angles against load will enable the trim at the designed load to be determined. The draft at this trim being read from the draft curves, the water line for the assumed conditions may be drawn on the hull profile

FIGURE 9.—Model 40-AD. Resistance, trimming moment, and draft. $\tau=2^\circ$.FIGURE 10.—Model 40-AD. Resistance, trimming moment, and draft. $\tau=3^\circ$.

FIGURE 11.—Model 40-AD. Resistance, trimming moment, and draft. $\tau = 5^\circ$.FIGURE 12.—Model 40-AD. Resistance, trimming moment, and draft. $\tau = 7^\circ$.

BEST-ANGLE DATA

The characteristics of the hulls as given in the curves of figures 3 to 32 are for three independent variables—speed, load, and trim angle. As it is desirable for a hull to remain near its best angle of trim and there is, in general, one angle for minimum resistance at each speed and load, it has been found desirable to derive the hull characteristics at best trim angle throughout the speed range. The trim-angle variable is thus eliminated and the optimum performance of the hull is determined.

The procedure consists of plotting the resistance and trimming moment for each load parameter against

where

V is speed, f. p. s.

Δ , load on the water, lb.

R , water resistance plus air drag of hull, lb.

M , trimming moment, lb.-ft.

b , beam over spray strips, ft.

g , acceleration of gravity, 32.2 ft. per sec.²

w , specific weight of water, lb. per cu. ft.

NOTE: w was 63.5 lb. per cu. ft. during the tests and is usually taken as 64 lb. per cu. ft. for sea water.

The results of the best-angle analysis are given as curves of C_R against C_V in figures 38 to 42, C_R against C_Δ in figures 43 to 47, best trim angle τ_0 against C_V

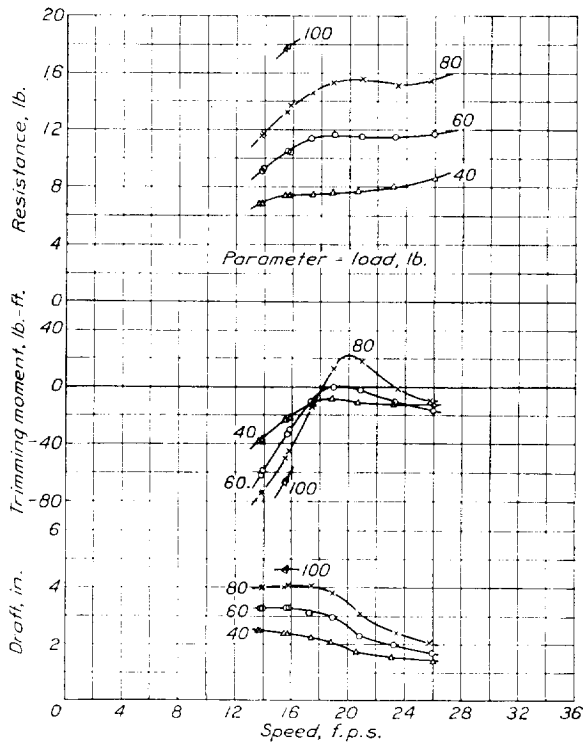


FIGURE 13.—Model 40-AD. Resistance, trimming moment, and draft. $\tau = 9^\circ$.

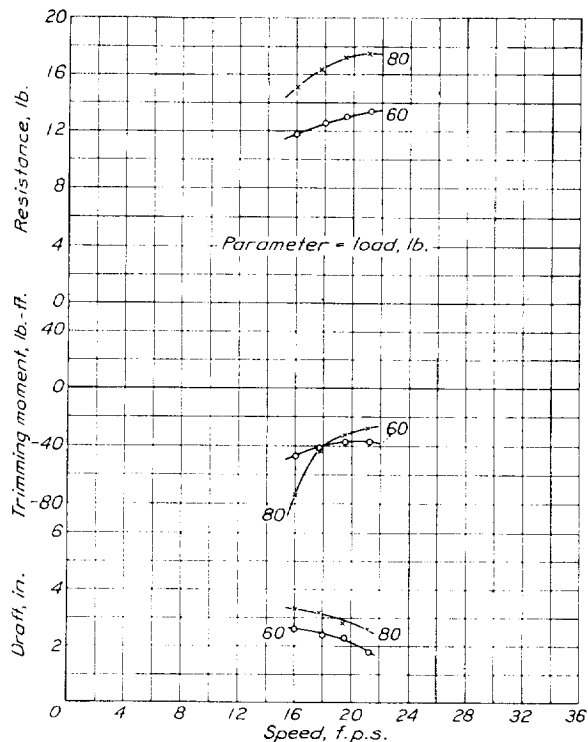


FIGURE 14.—Model 40-AD. Resistance, trimming moment, and draft. $\tau = 11^\circ$.

trim angle at a series of speeds. From these cross plots the minimum resistance, the best trim angle, and the trimming moment existing at that angle are determined for each load and speed. The data found are then converted to nondimensional coefficients, based on Froude's law of comparison and using the maximum beam over the spray strips as the characteristic dimension. The coefficients are defined as follows:

$$\text{Speed coefficient, } C_V = \frac{V}{\sqrt{gb}}$$

$$\text{Load coefficient, } C_\Delta = \frac{\Delta}{wb^3}$$

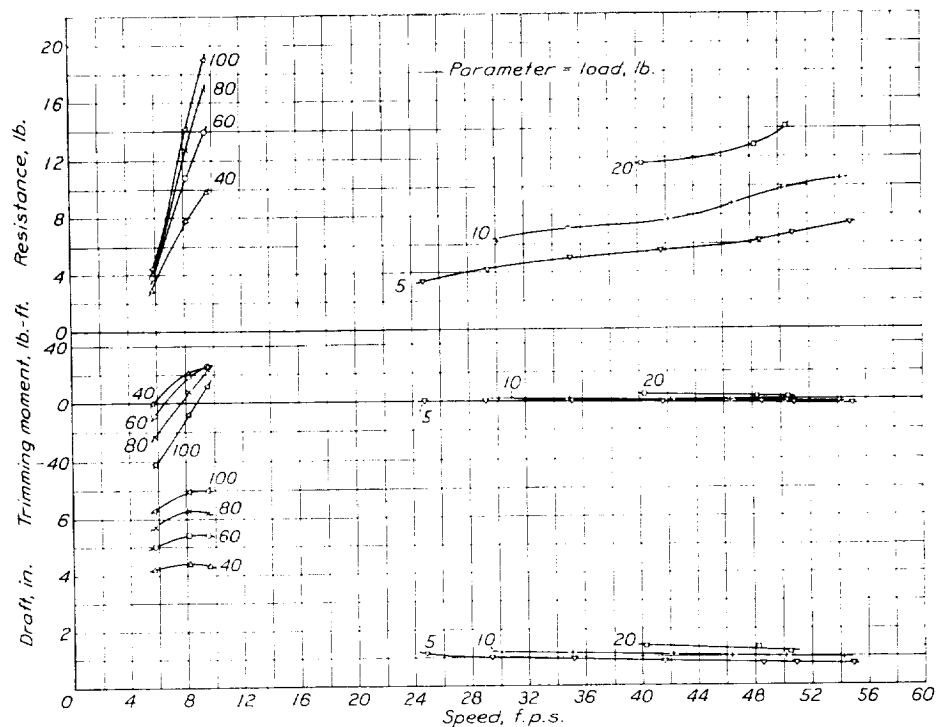
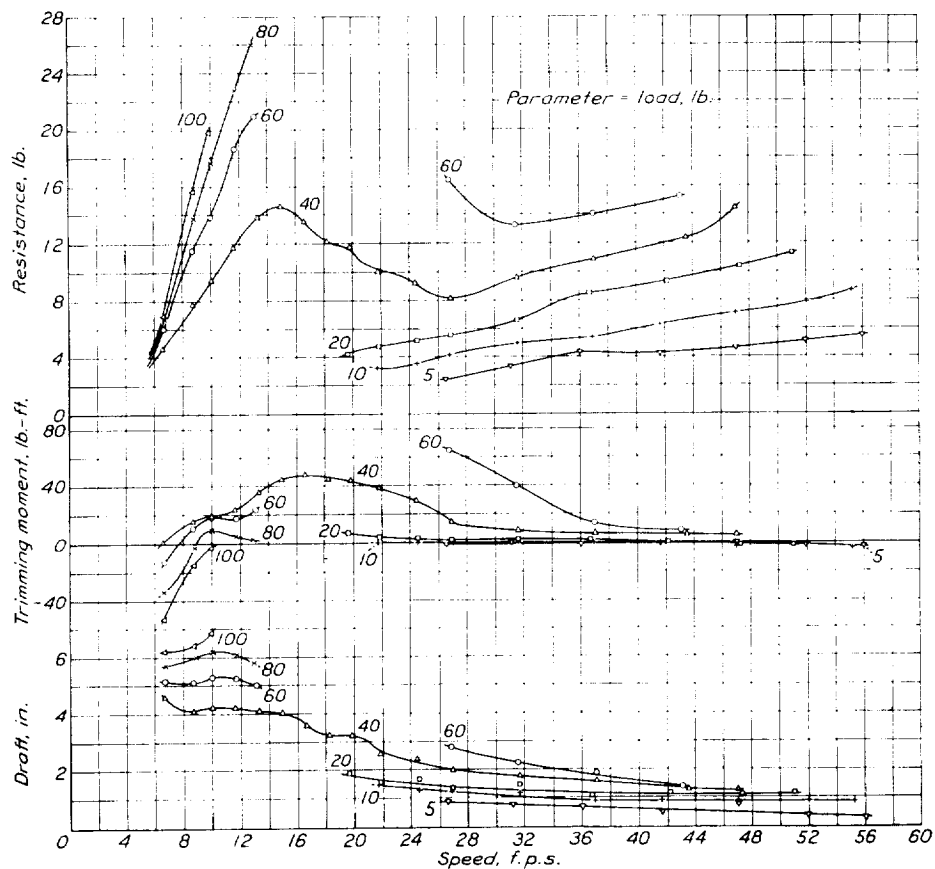
$$\text{Resistance coefficient, } C_R = \frac{R}{wb^3}$$

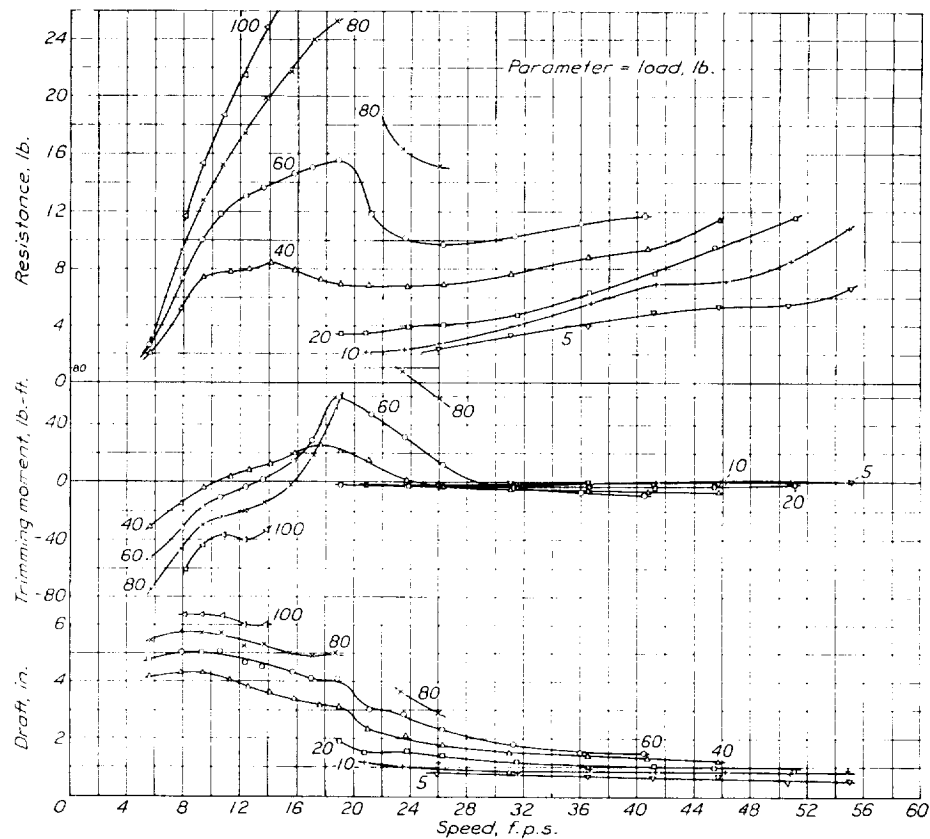
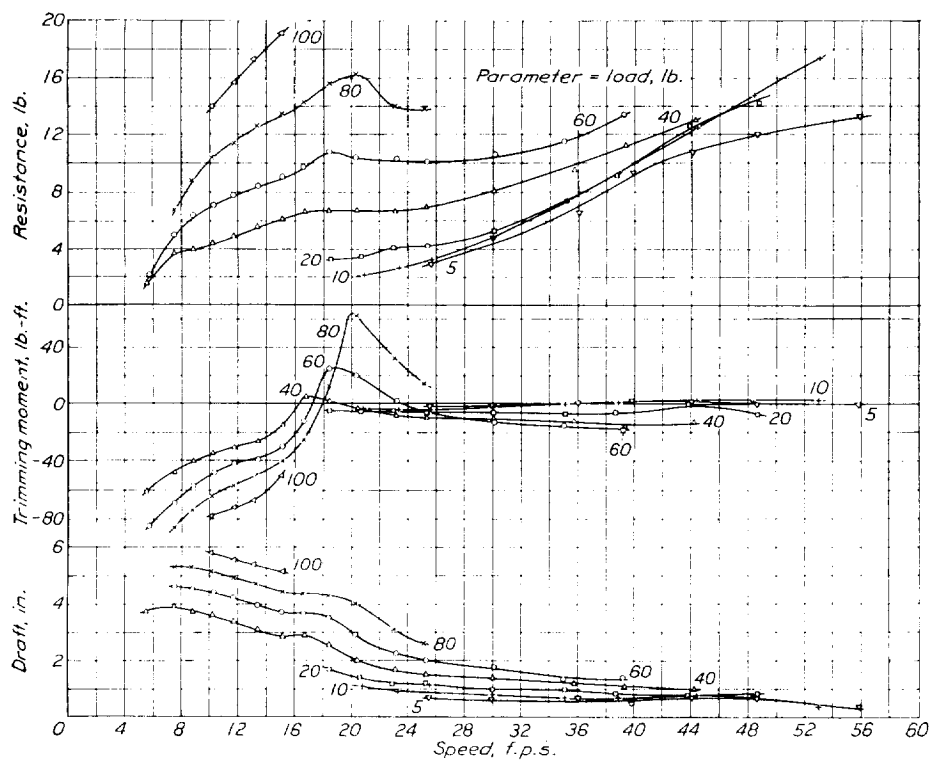
$$\text{Trimming-moment coefficient, } C_M = \frac{M}{wb^4}$$

in figures 48 to 52, and C_M against C_V in figures 53 to 57. The application of these curves in the determination of the take-off characteristics of a seaplane using the hull to which they refer is described in detail in reference 3.

FREE-TO-TRIM DATA

For speed coefficients below 2.0, the resistance continues to decrease with increase in trim angle, the best angles being above any practical range. As soon as the best angle is determinate, the trimming moments existing are found to have a high negative value but to decrease rapidly with speed until they become positive at the hump speed. The performance at low speeds is then best investigated by assuming the hull to be free to trim, as previously explained, or to be under the influence of the nearly constant thrust moment.

FIGURE 15.—Model 40-AE. Resistance, trimming moment, and draft. $\tau = 2^\circ$.FIGURE 16.—Model 40-AE. Resistance, trimming moment, and draft. $\tau = 3^\circ$.

FIGURE 17.—Model 40-AE. Resistance, trimming moment, and draft. $\tau=5^\circ$.FIGURE 18.—Model 40-AE. Resistance, trimming moment, and draft. $\tau=7^\circ$.

The resistance coefficient at zero moment and the angle for zero moment referred to a center of moments 4 inches ahead of the step on the model are plotted against speed in figures 58 to 67. Although these values were obtained from the free-to-trim tests in the tank, the values deduced from the data for the fixed-trim runs were found to check them closely. The characteristics at zero trimming moment or at an assumed thrust moment may be deduced for other

high planing speeds. When the developable forebody is used with the pointed afterbody, the maximum positive trimming-moment coefficient is slightly lower and the values at $C_V=7.0$ are larger in the negative direction. With the no-step afterbody, the maximum positive C_M is slightly lower at heavy loads and greater at light loads, whereas the high speed C_M values closely correspond. The differences in the best angle of trim are within the accuracy of determination.

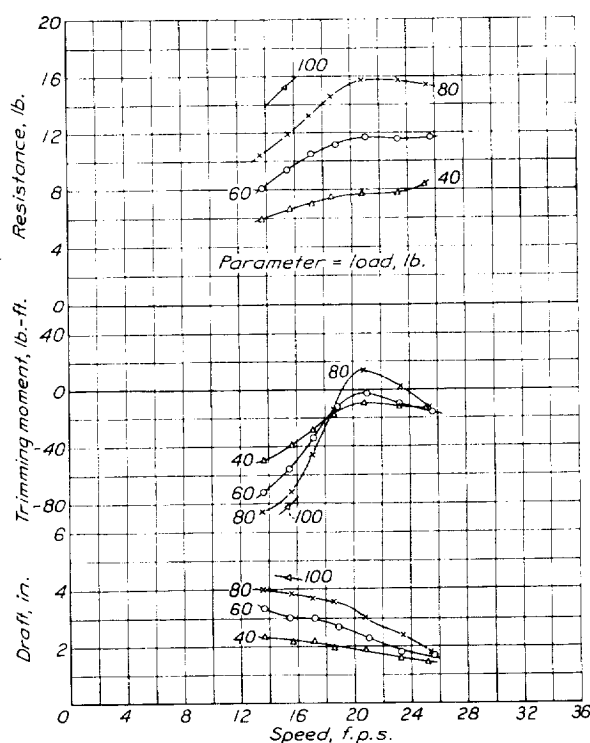


FIGURE 19.—Model 40-AE. Resistance, trimming moment, and draft. $\tau=9^\circ$.

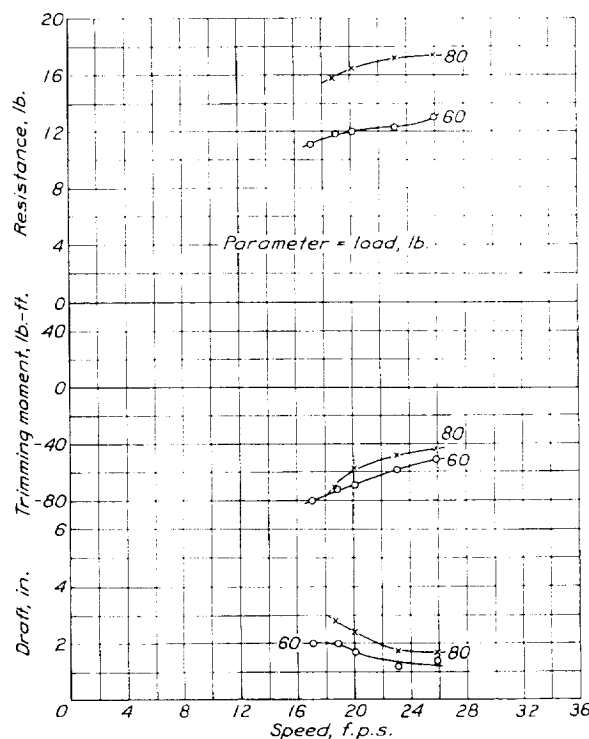


FIGURE 20.—Model 40-AE. Resistance, trimming moment, and draft. $\tau=11^\circ$.

positions of the center of gravity from suitable cross plots of figures 3 to 32.

DISCUSSION OF RESULTS

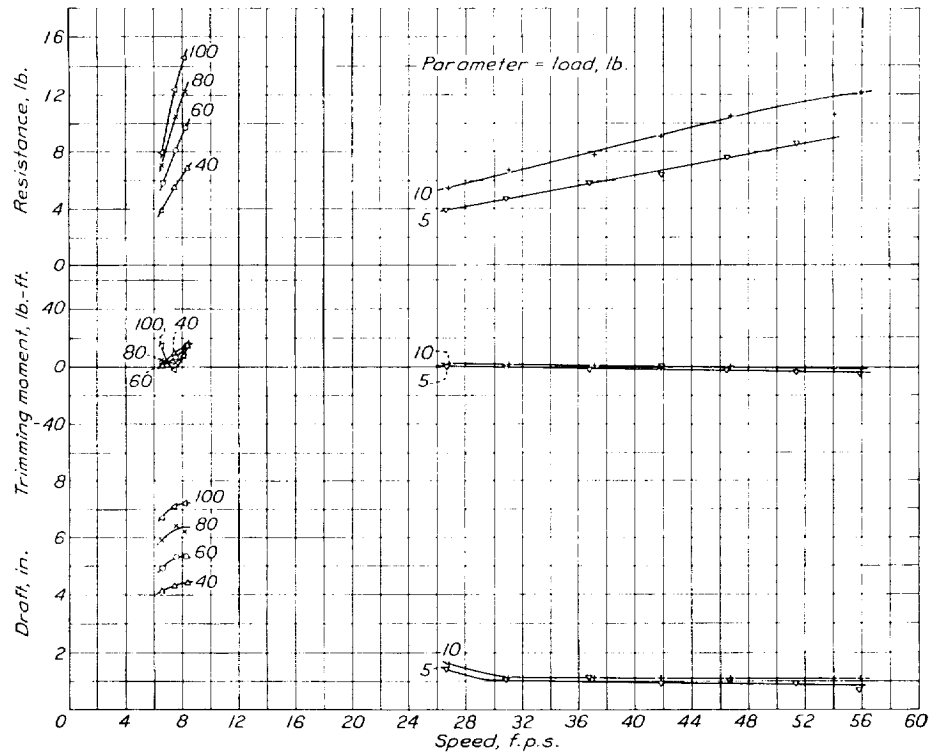
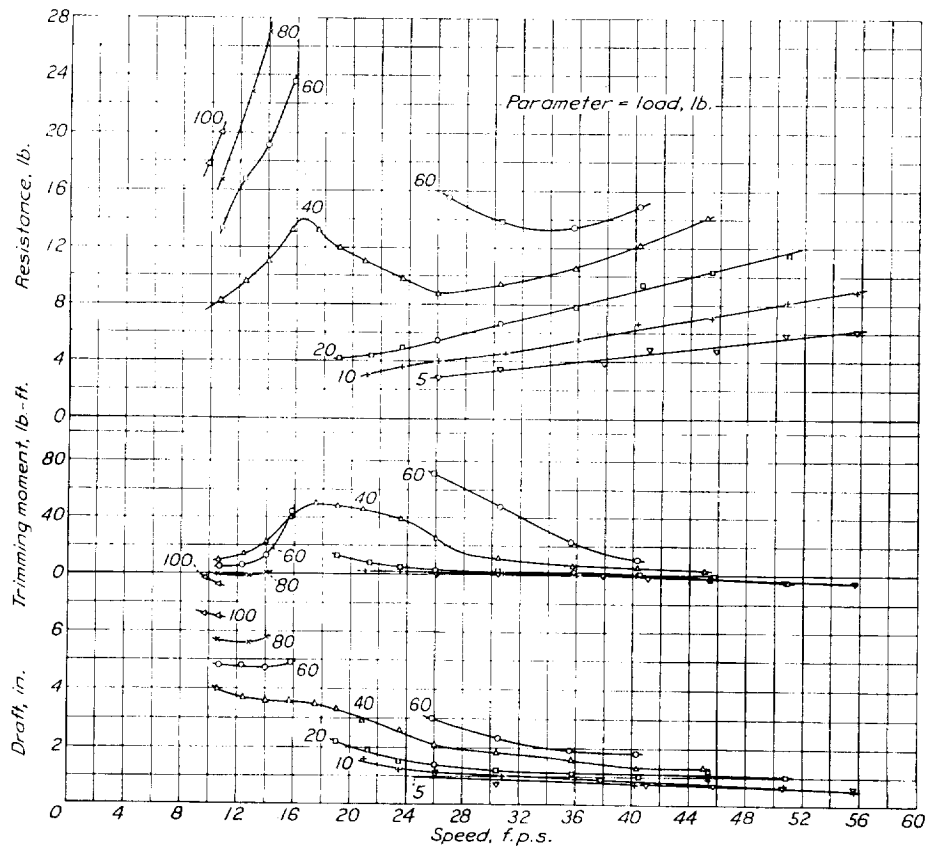
BEST-ANGLE DATA

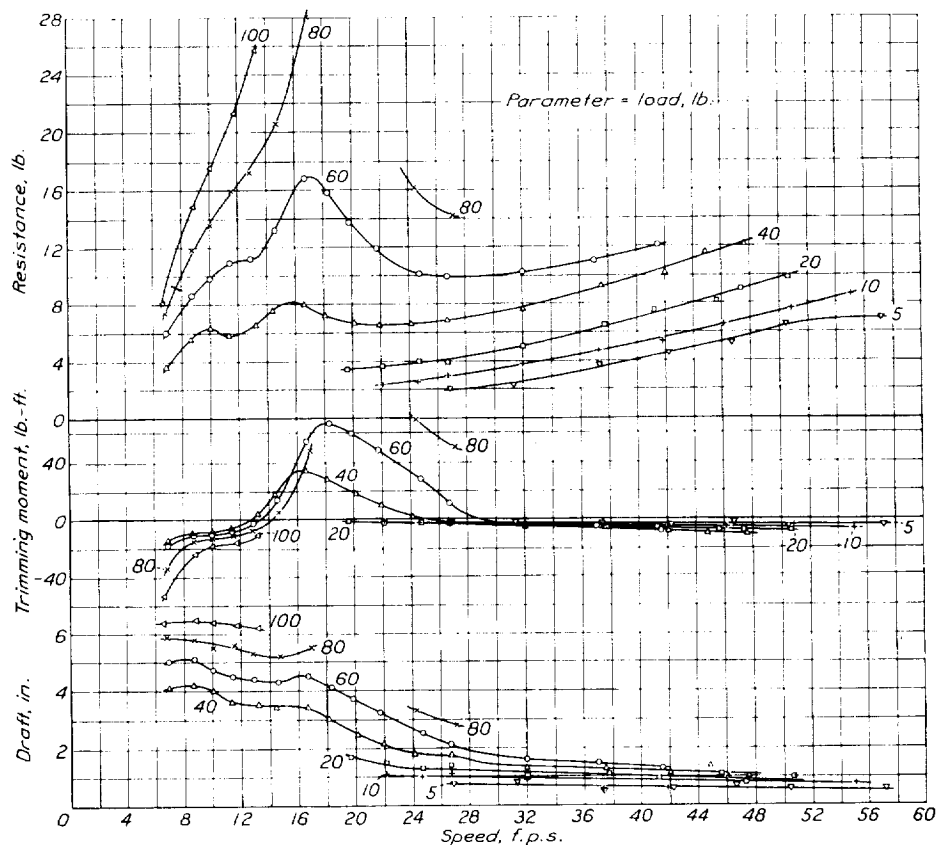
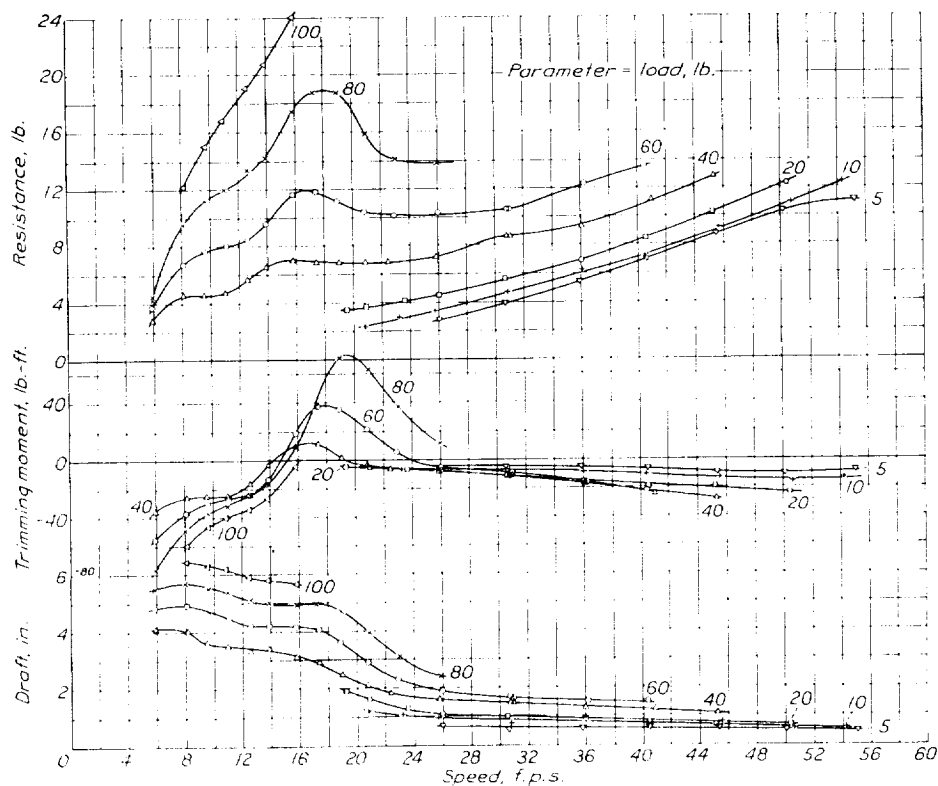
Comparisons of the characteristics of the hull forms may be made by cross-plotting the values of figures 38 to 57 against load coefficient at representative speed coefficients. Suitable cross curves for comparisons among the hulls are shown in figures 68, 69, and 71. The spray patterns may be compared by means of the photographs of figures 70 and 72.

Effect of form of forebody.—From figures 68 and 69 it is seen that the differences between the characteristics of the normal and developable forebodies are small for the smooth-water and fixed-trim conditions reproduced in the tank tests. The load-resistance ratios Δ/R for the developable form are slightly higher at the hump of the C_R curves and slightly lower at

Figure 70 shows the height and volume of spray thrown from the two types of forebodies to be practically identical for smooth-water operation. The water line does not extend far enough forward, however, to judge the action of the bow in rough water in the conditions shown. Apparently, the desirability of using the form of developable surface found on forebody B depends on its cleanness of running and the effect of the convex bow sections on resistance when driving through waves. An experimental determination of such qualities in the tank is difficult to carry out at the present time and is at best only an approximation of actual sea conditions.

Effect of form of afterbody.—The characteristics of the models consisting of the normal forebody and the various afterbodies are compared in figures 71 and 72. The Δ/R values with the pointed afterbody are lowest at the hump in the C_R curves and generally slightly higher at high planing speeds. With the no-step

FIGURE 21.—Model 40-BC. Resistance, trimming moment, and draft. $\tau = 2^\circ$.FIGURE 22.—Model 40-BC. Resistance, trimming moment, and draft. $\tau = 3^\circ$.

FIGURE 23. Model 40-BC. Resistance, trimming moment, and draft. $\tau=5^\circ$.FIGURE 24.—Model 40-BC. Resistance, trimming moment, and draft. $\tau=7^\circ$.

afterbody the Δ/R values at the hump are slightly superior to those with the second-step afterbody; at medium planing speeds, inferior; and at high planing speeds, practically equal. The second-step afterbody gives the highest positive C_M and the no-step afterbody gives the lowest. There is little choice in trimming-moment characteristics at high speeds. The most favorable trim with the second-step afterbody is slightly lower near the hump speed. At high speeds, the best trim angle with all the afterbodies is practically the same.

The superiority of the performance with the second-step and no-step afterbodies at the best trim hump is attributed to the larger planing area provided by them when immersed at low speeds. The slight improve-

of the model to those from the forebody indicates that at these speeds the afterbodies produce lift with the exception of the pointed afterbody, which seems to be clear at 19.7 feet per second. In general, the various models are fairly clean considering the heavy loads carried in proportion to their size.

FREE-TO-TRIM DATA

Figures 58 to 67 show the performance of the hulls at zero trimming moment around a center-of-gravity position 4 inches ahead of the step on the model. At low speeds and heavy loads some of the forms, particularly 40-BE, tend to remain below the best trim to such an extent that the resulting resistance peak is higher than what may be called the "real hump" cor-

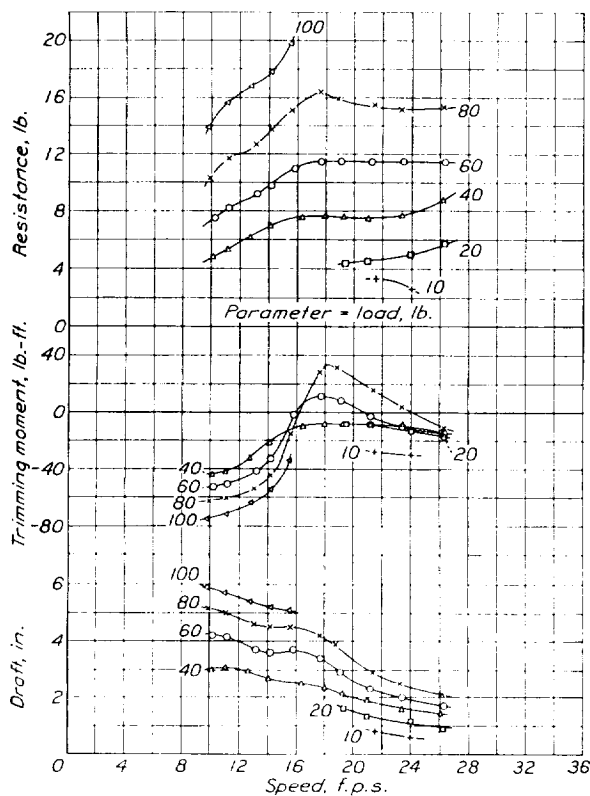


FIGURE 25.—Model 40-BC. Resistance, trimming moment, and draft. $\tau=9^\circ$.

ment given by the pointed afterbody at high speeds is probably because of the smaller area offered to the water coming from the forebody because the lift is produced chiefly by the main planing bottom forward of the step. From considerations of high-speed resistance, it appears desirable to carry the load on the forebody of a hull because the afterbody is operating in its wake and contributes a greater share of frictional resistance in proportion to the load it carries.

The photographs of figure 72 show the blisters coming from the forebody and also make it possible to get an idea of the action of the afterbody. The similarity of the secondary blisters coming from the after part

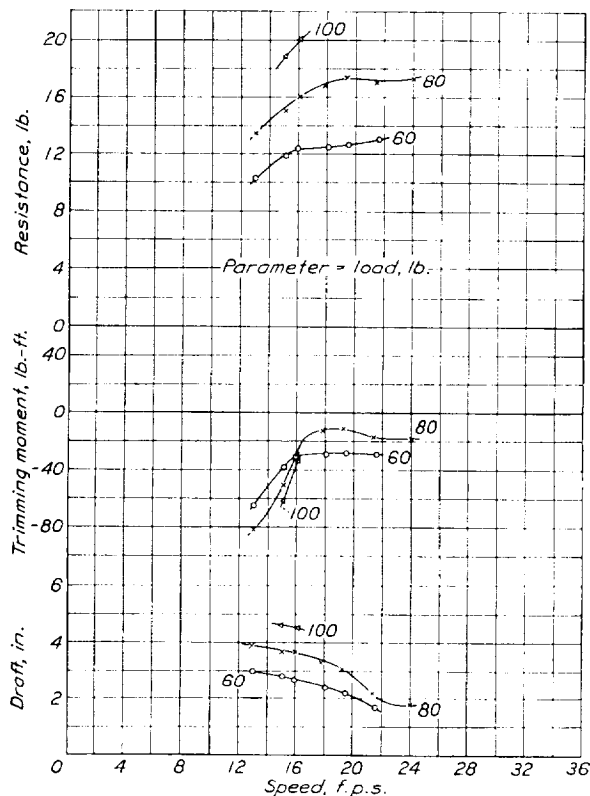
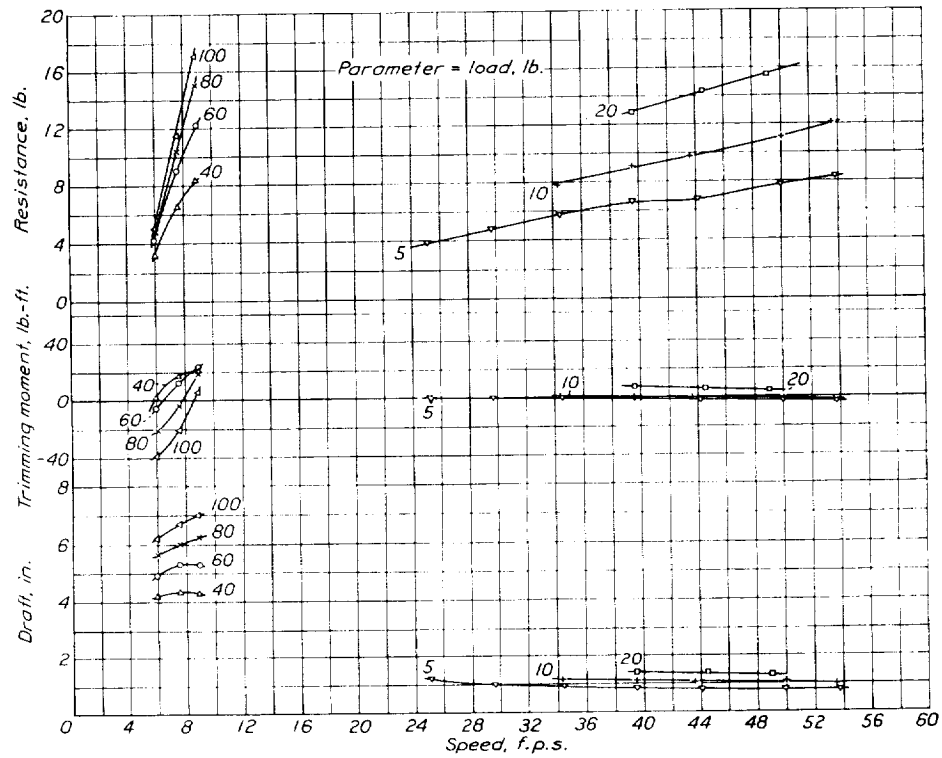
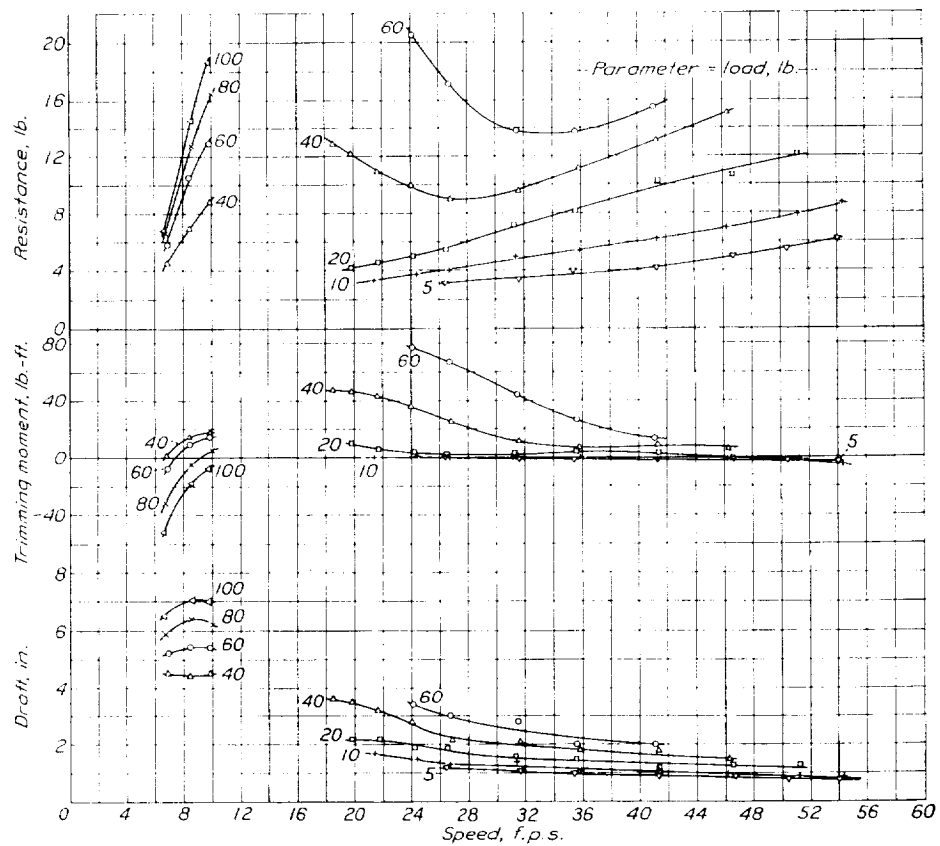
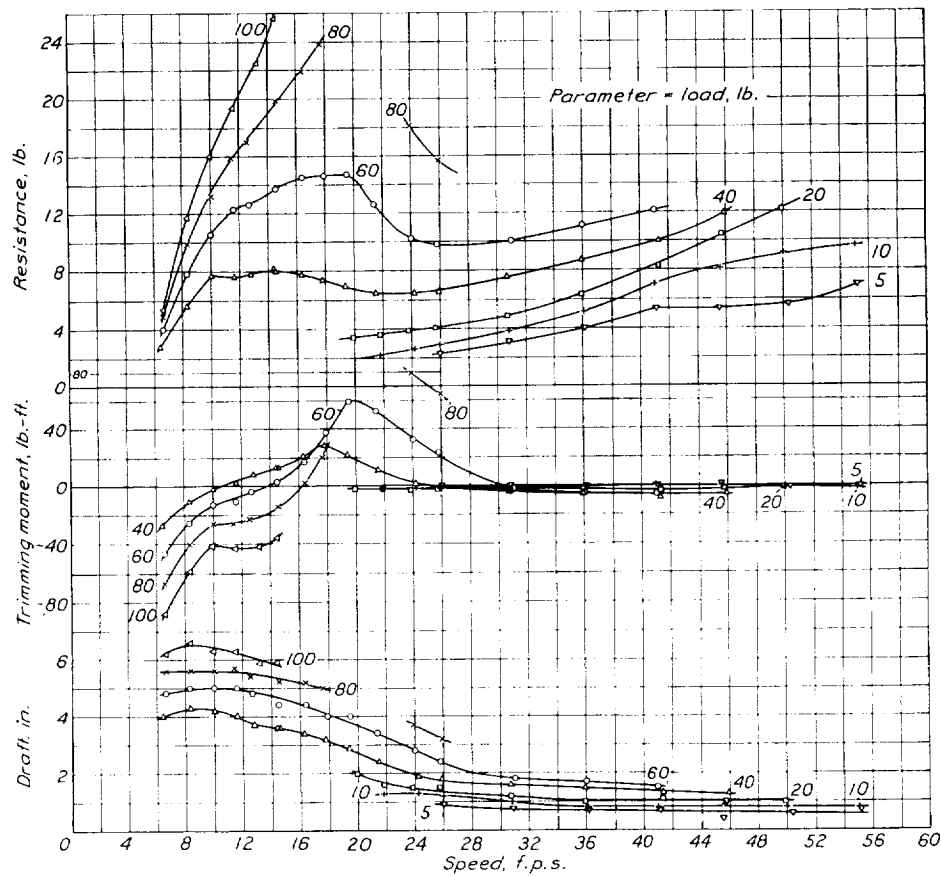
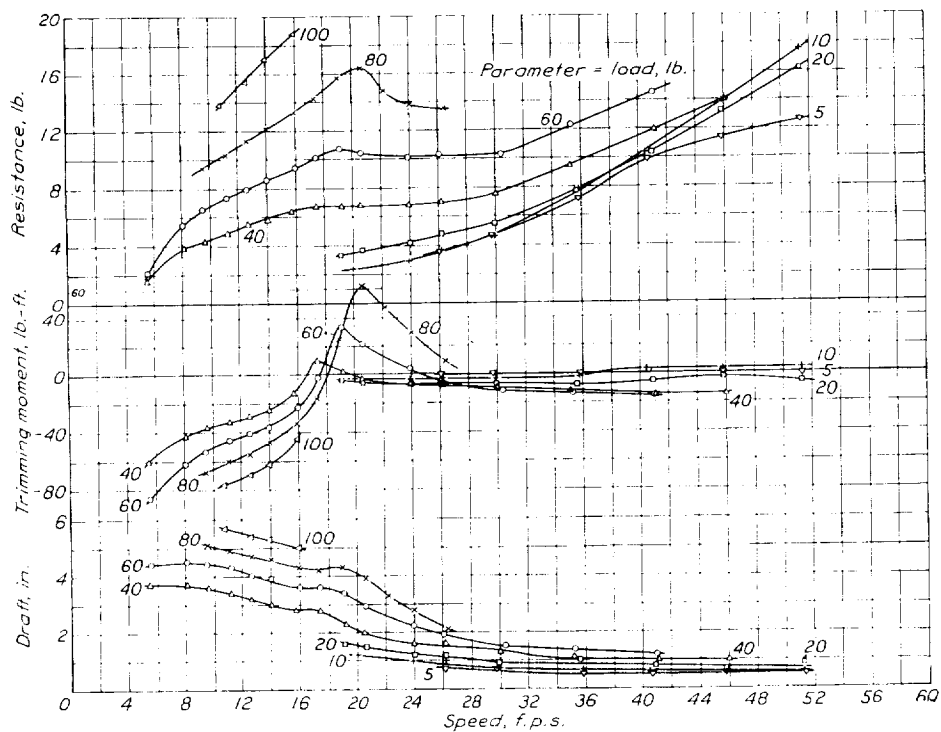


FIGURE 26.—Model 40-BC. Resistance, trimming moment, and draft. $\tau=11^\circ$.

responding to the maximum resistance at best trim angle. The negative thrust moment that usually exists would aggravate this condition. At speed coefficients corresponding to the real hump, however, the trim at zero moment is higher than the best trim so that the thrust moment would tend to lower the resistance. Any control moment available from the elevators in the slipstream at these low speeds can, of course, be used to favor the take-off. The performance before the hulls attain planing speeds is therefore dependent on the position of the center of gravity, the magnitude of the thrust moment, and the amount of control that the pilot can bring into play to maintain the best trim angle.

FIGURE 27.—Model 40-BE. Resistance, trimming moment, and draft. $\tau = 2^\circ$.FIGURE 28.—Model 40-BE. Resistance, trimming moment, and draft. $\tau = 3^\circ$.

FIGURE 29.—Model 40-BE. Resistance, trimming moment, and draft. $\tau = 5^\circ$.FIGURE 30.—Model 40-BE. Resistance, trimming moment, and draft. $\tau = 7^\circ$.

TAKE-OFF EXAMPLES

The application of the data obtained from these models is illustrated by the following examples:

Example 1.—A hypothetical flying boat or amphibian suitable for cargo or passenger service is represented by the following assumed data:

Gross load, lb.	8,000
Wing area, sq. ft.	550
Horsepower	600
Effective aspect ratio including ground effect	10
Parasite-drag coefficient excluding hull	0.03
Airfoil section	Clark Y

Model 40-BC is selected as the hull and a maximum beam of 5.2 feet is used. This beam will give a moderately high beam loading at the hump (C_A = about 0.75) where about 85 percent of the gross weight will be on the water. The best angle of wing setting is found by

ably more excess thrust at the hump than at the second critical point near get-away. A somewhat smaller hull should then give a little better take-off performance. The take-off time and distance are determined from the $1/a$ and V/a curves, respectively, both of which are plotted in figure 73 (b). The time is found to be 24.2 seconds and the length of run 1,480 feet.

The trim-angle curve for this take-off is plotted in figure 74 (a) and the trimming moments to obtain these trim angles are plotted in figure 74 (b). This trimming-moment-curve was obtained from figure 56 and was corrected for the difference between the center of gravity chosen and the center of moments used in the fixed-trim tests. If the center of gravity chosen had been other than that used for the free-to-trim tests it would have been necessary to compute the free-to-trim resistance from the test results given in figures 21 to 26.

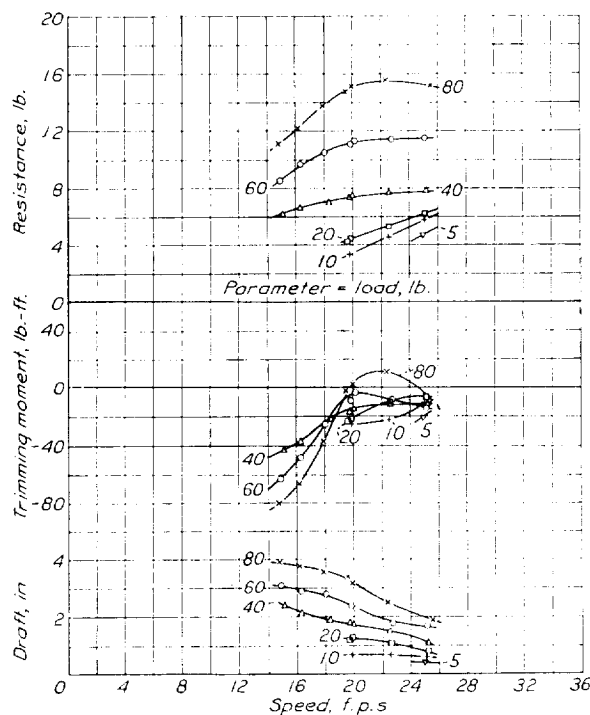


FIGURE 31.—Model 40-BE. Resistance, trimming moment, and draft. $\tau=9^\circ$.

the method of reference 3 to be about 5° . The center of gravity of the complete boat is taken to be the same as that used in the free-to-trim tests on these models and it is arbitrarily assumed that the craft will run free to trim to a speed coefficient of 2.4 and at best trim angle at higher speeds. The water resistance plus air drag ($R+D$) is computed by the method of reference 3 using the free-to-trim curves up to $C_V=2.4$. The resultant curve is plotted in figure 73 together with the thrust obtained from the curves of reference 4. From this figure it may be seen that there is consider-

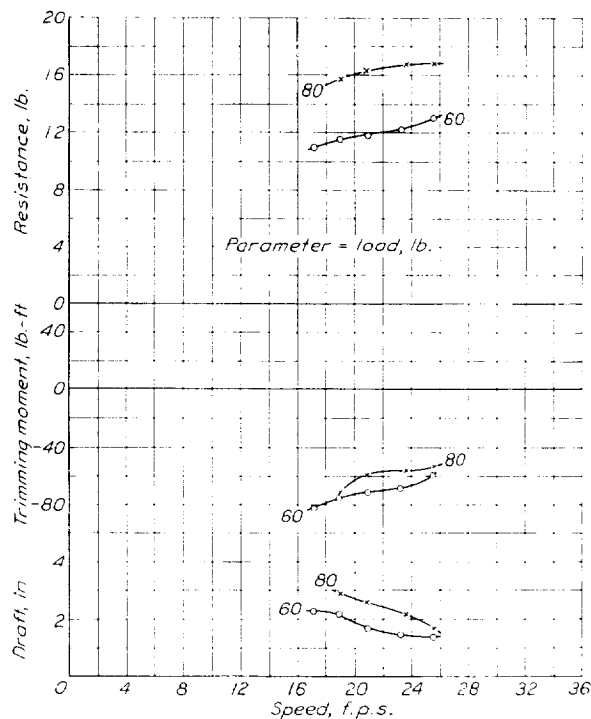


FIGURE 32.—Model 40-BE. Resistance, trimming moment, and draft. $\tau=11^\circ$.

In practice, if the free-to-trim calculations indicate that there is a reasonable amount of excess thrust at low speeds, the free-to-trim resistance may be used in the calculations for take-off time and distance without appreciable error. If, however, it appears desirable and the design is sufficiently advanced to determine the aerodynamic moments, the minimum resistance obtainable may be calculated from the test data.

Example 2.—A hypothetical small low-powered flying boat will be considered. This craft is presumably to be built at a reasonable cost without a great number

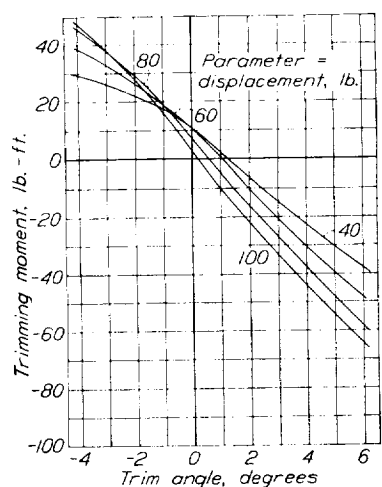


FIGURE 33.—Model 40-AC. Trimming moments and drafts at rest.

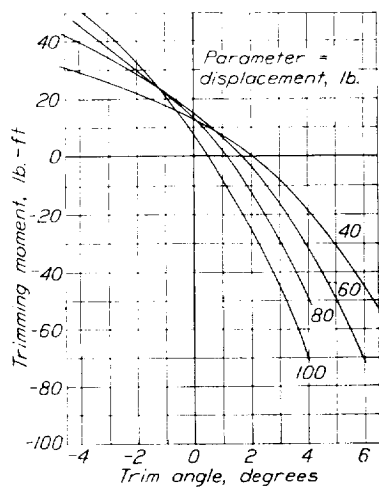


FIGURE 34.—Model 40-AD. Trimming moments and drafts at rest.

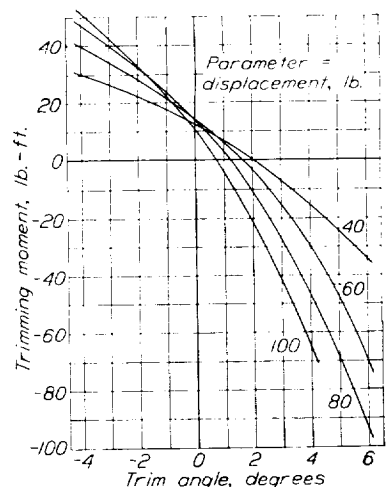


FIGURE 35.—Model 40-AE. Trimming moments and drafts at rest.

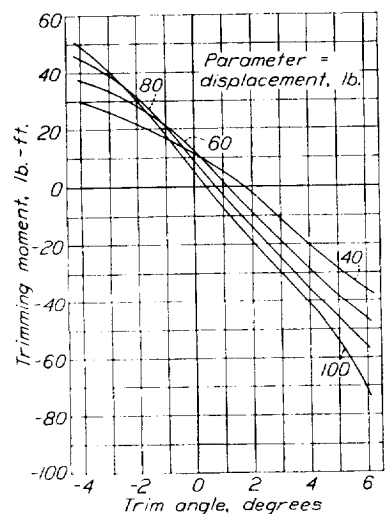


FIGURE 36.—Model 40-BC. Trimming moments and drafts at rest.

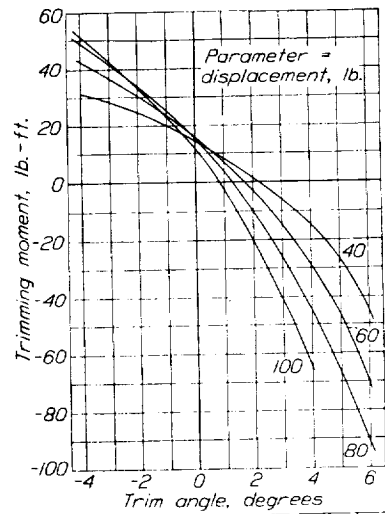


FIGURE 37.—Model 40-BE. Trimming moments and drafts at rest.

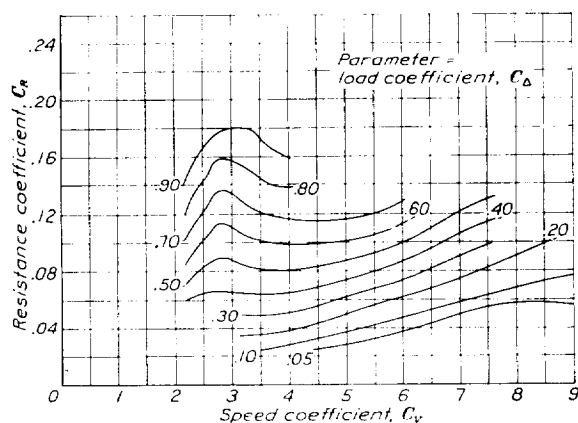


FIGURE 38.—Model 40-AC. Variation of resistance coefficient at best trim angle with speed coefficient.

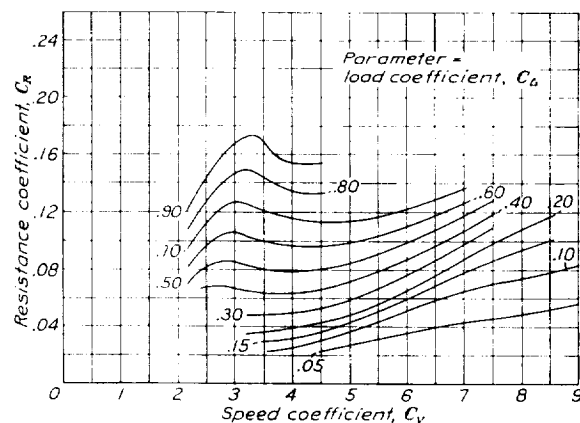


FIGURE 39.—Model 40-AD. Variation of resistance coefficient at best trim angle with speed coefficient.

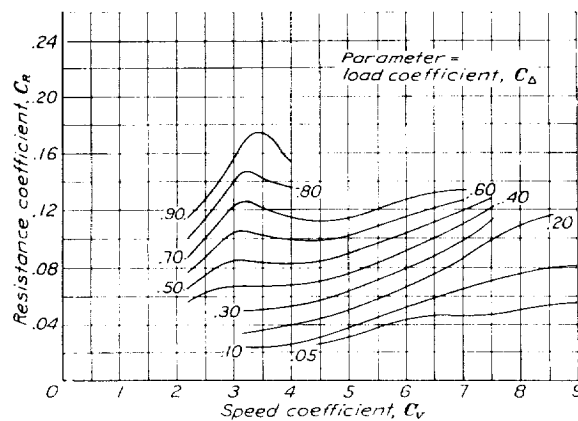


FIGURE 40.—Model 40-AE. Variation of resistance coefficient at best trim angle with speed coefficient.

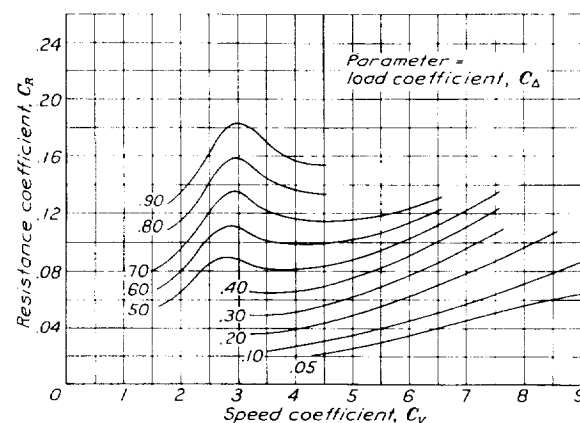


FIGURE 41.—Model 40-BC. Variation of resistance coefficient at best trim angle with speed coefficient.

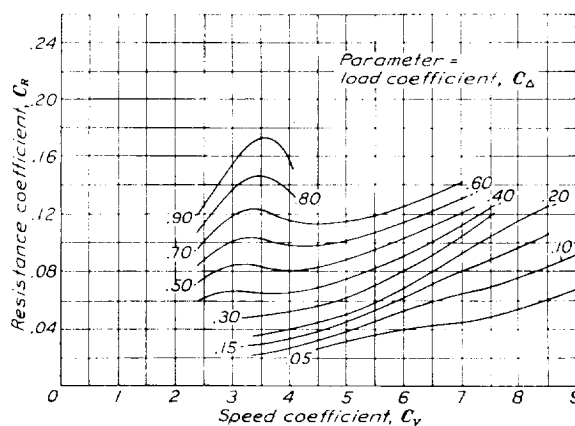


FIGURE 42.—Model 40-BE. Variation of resistance coefficient at best trim angle with speed coefficient.

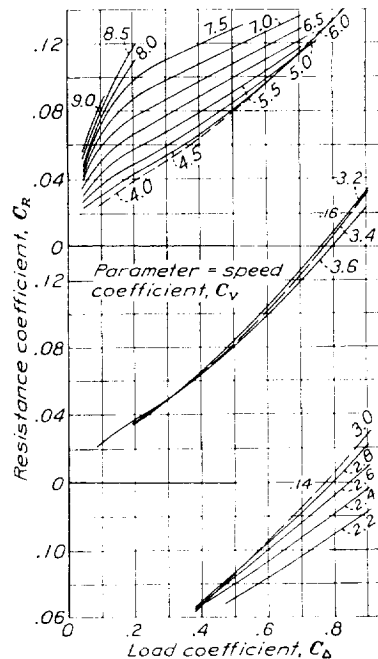


FIGURE 44.—Model 40-A-D. Variation of resistance coefficient at best trim angle with load coefficient.

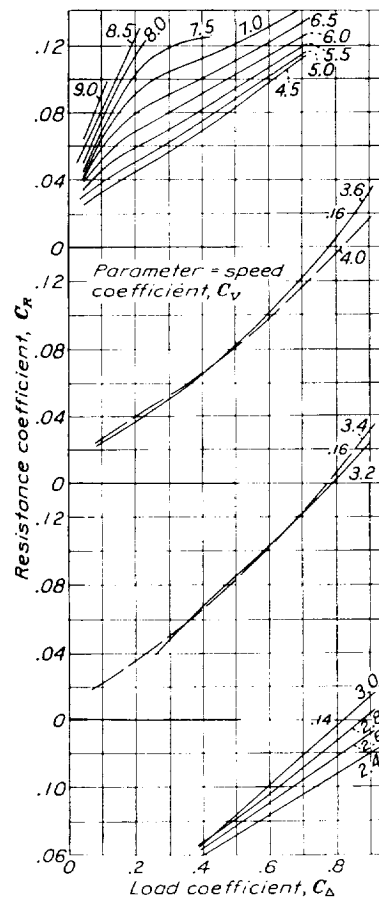


FIGURE 47.-- Model 40-BE. Variation of resistance coefficient at best trim angle with load coefficient.

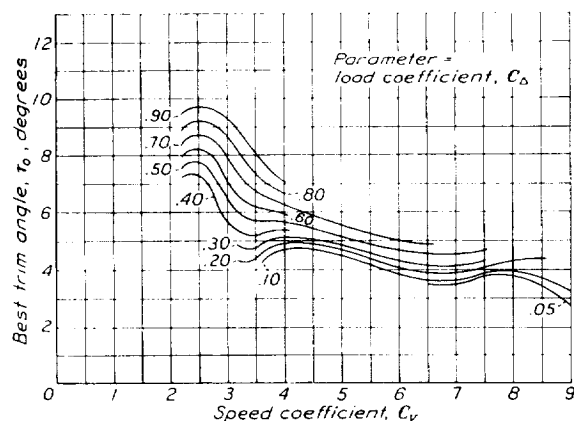


FIGURE 48.—Model 40-AC. Variation of best trim angle with speed coefficient.

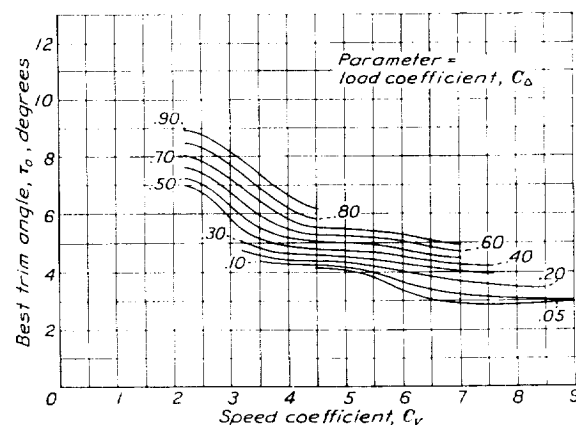


FIGURE 49.—Model 40-AD. Variation of best trim angle with speed coefficient.

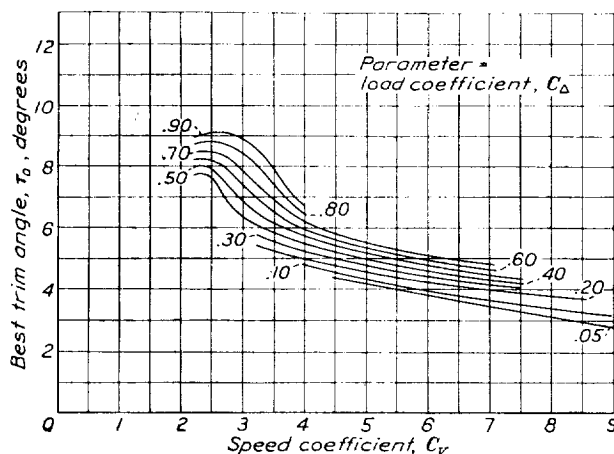


FIGURE 50.—Model 40-AE. Variation of best trim angle with speed coefficient.

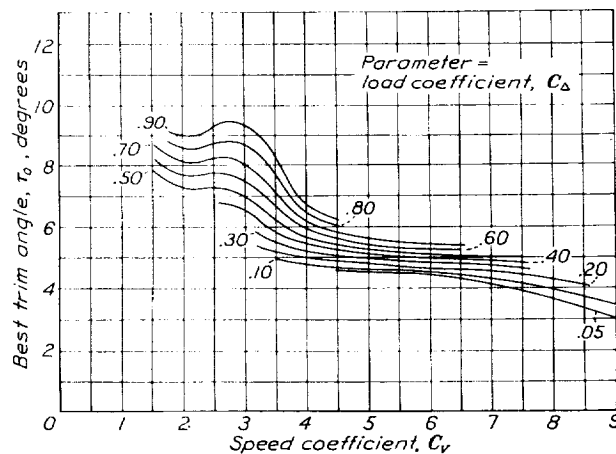


FIGURE 51.—Model 40-BG. Variation of best trim angle with speed coefficient.

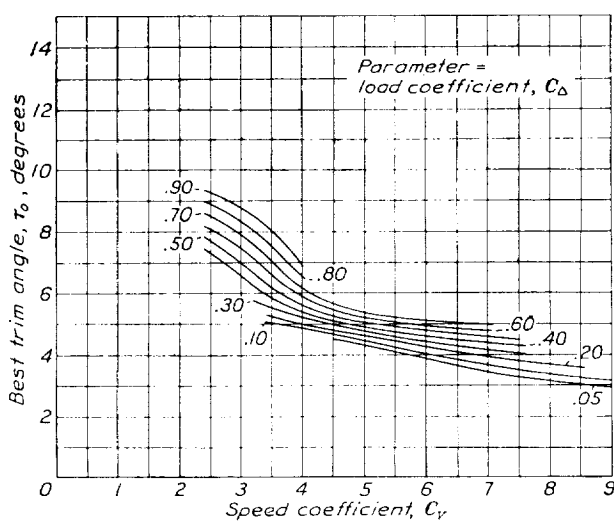


FIGURE 52.—Model 40-BE. Variation of best trim angle with speed coefficient.

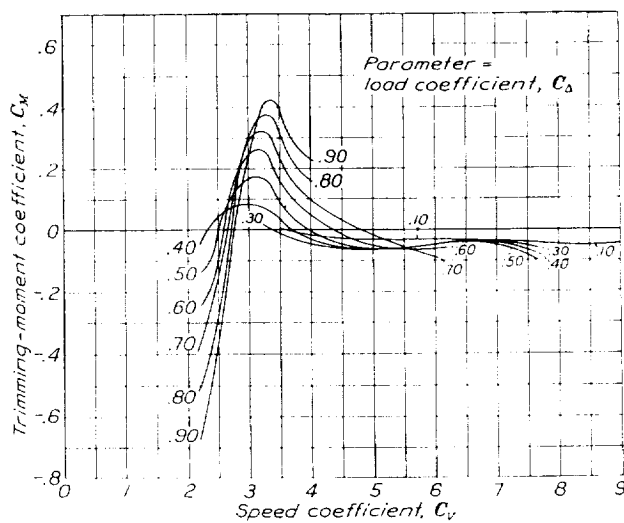


FIGURE 53.—Model 40-AC. Variation of trimming-moment coefficient at best trim angle with speed coefficient.

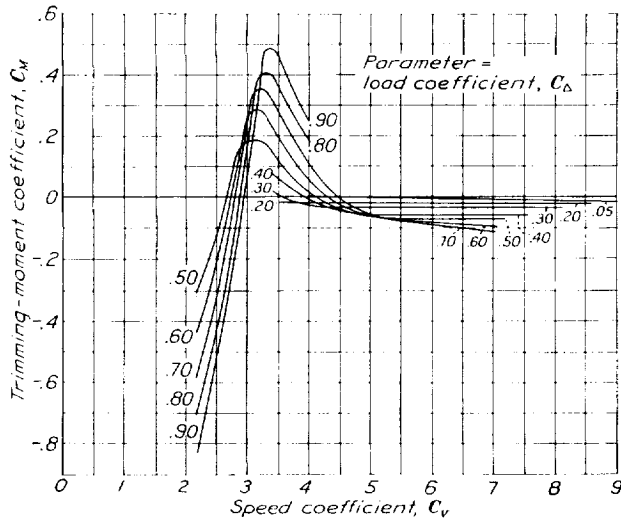


FIGURE 54.—Model 40-AD. Variation of trimming-moment coefficient at best trim angle with speed coefficient.

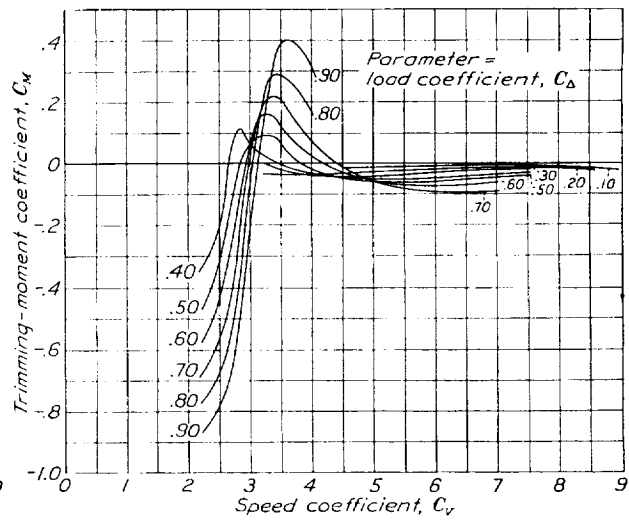


FIGURE 55.—Model 40-AE. Variation of trimming-moment coefficient at best trim angle with speed coefficient.

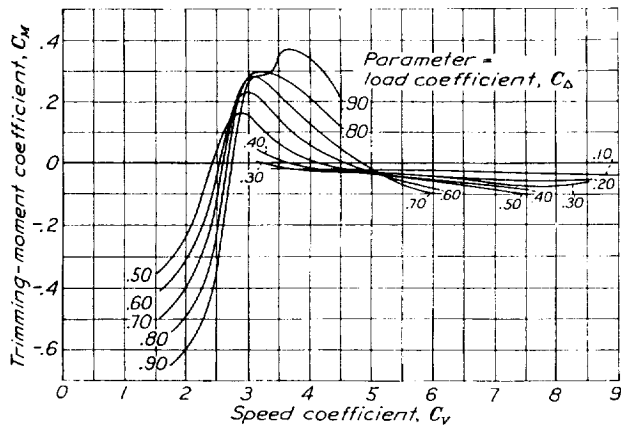


FIGURE 56.—Model 40-BC. Variation of trimming-moment coefficient at best trim angle with speed coefficient.

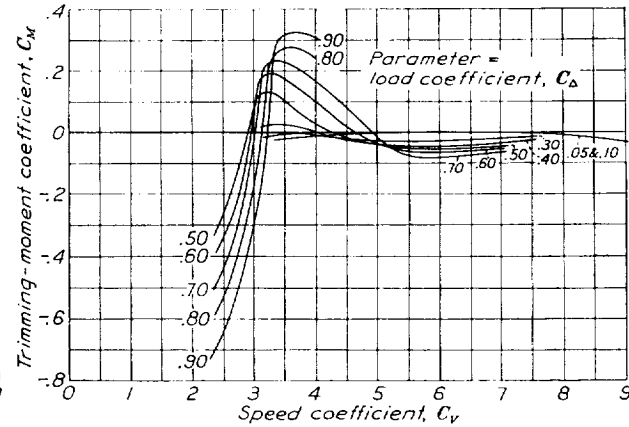


FIGURE 57.—Model 40-BE. Variation of trimming-moment coefficient at best trim angle with speed coefficient.

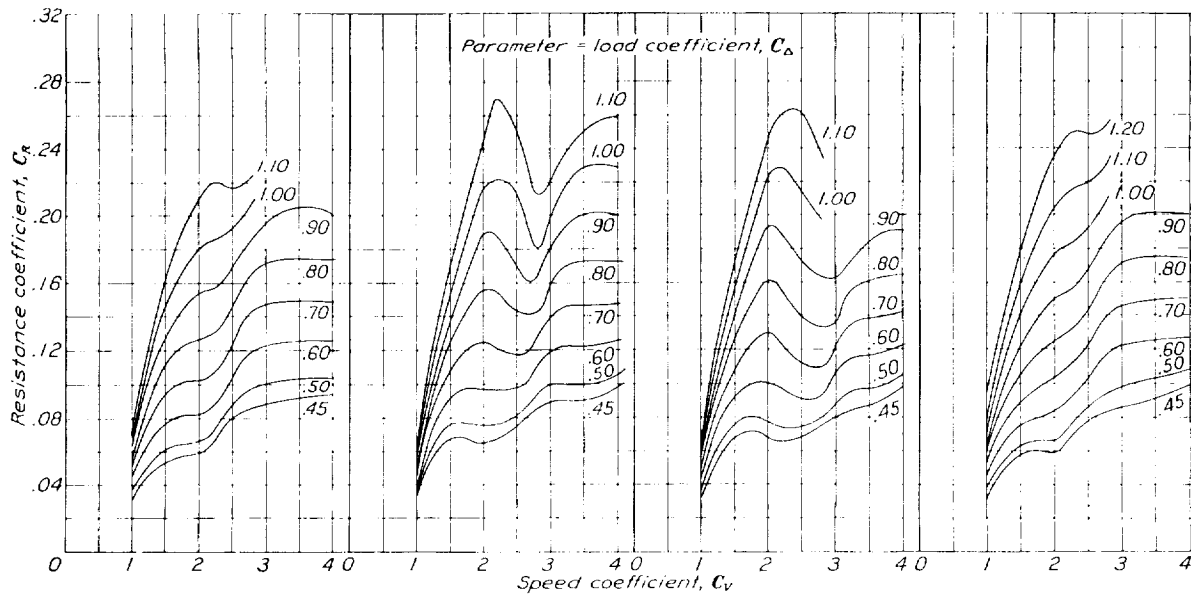


FIGURE 58.—Model 40-AC.

FIGURE 59.—Model 40-AD.

FIGURE 60.—Model 40-AE.

FIGURE 61.—Model 40-BC.

Variation of resistance coefficient at zero trimming moment with speed coefficient. Free-to-trim tests.

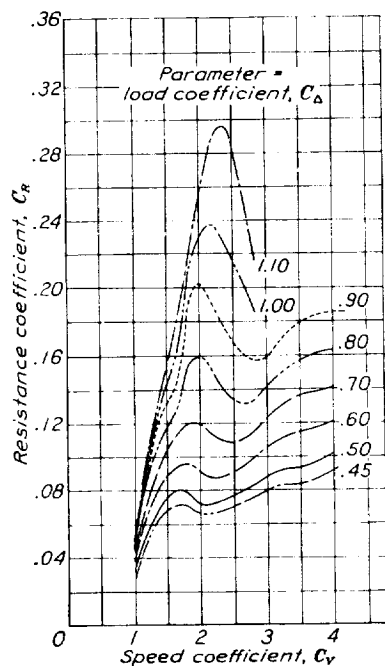


FIGURE 62.—Model 40-BE. Variation of resistance coefficient at zero trimming moment with speed coefficient. Free-to-trim tests.

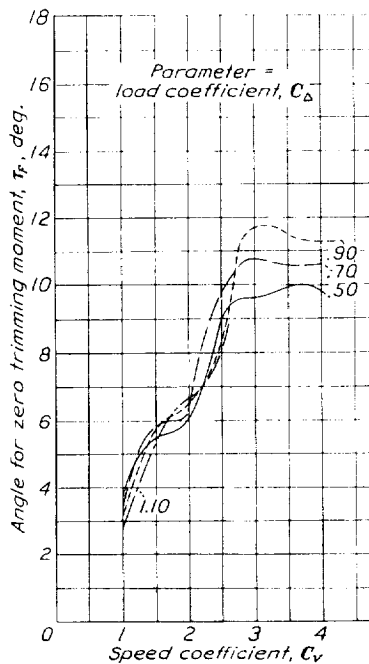


FIGURE 63.—Model 40-AC. Variation of trim angle for zero trimming moment with speed coefficient. Free-to-trim tests.

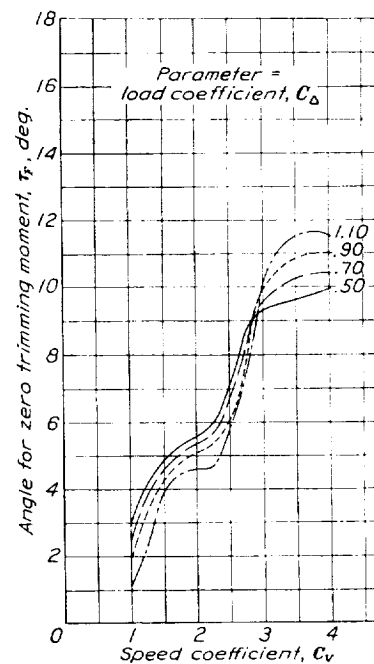


FIGURE 64.—Model 40-AD. Variation of trim angle for zero trimming moment with speed coefficient. Free-to-trim tests.

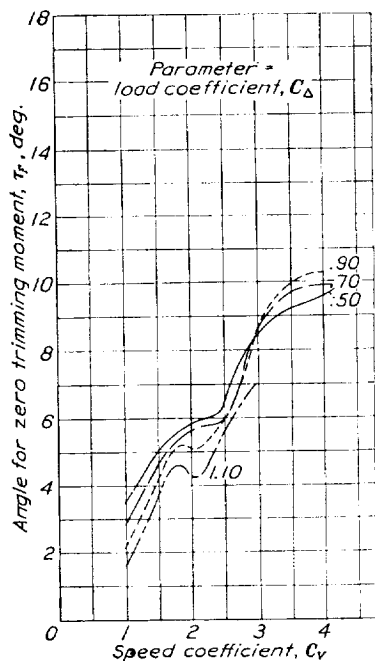


FIGURE 65.—Model 40-AE. Variation of trim angle for zero trimming moment with speed coefficient. Free-to-trim tests.

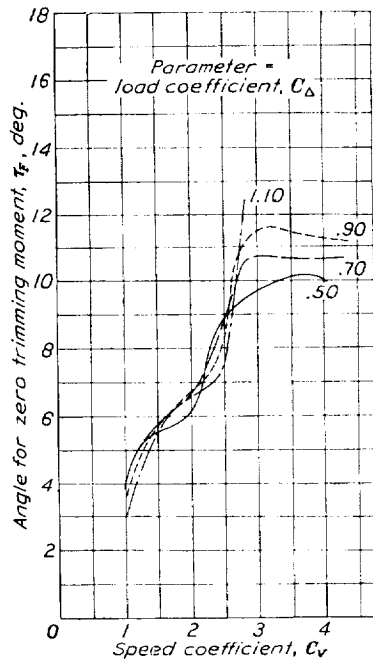


FIGURE 66.—Model 40-BC. Variation of trim angle for zero trimming moment with speed coefficient. Free-to-trim tests.

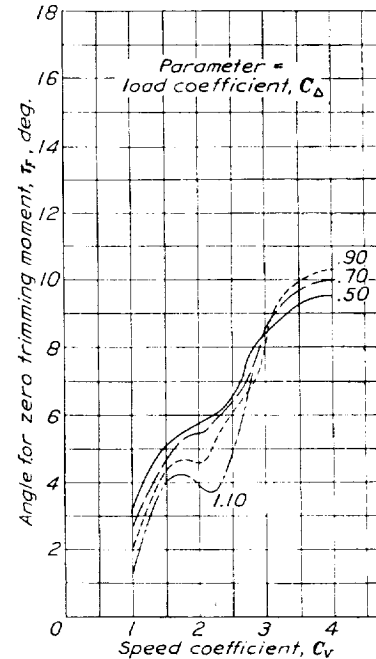


FIGURE 67.—Model 40-BE. Variation of trim angle for zero trimming moment with speed coefficient. Free-to-trim tests.

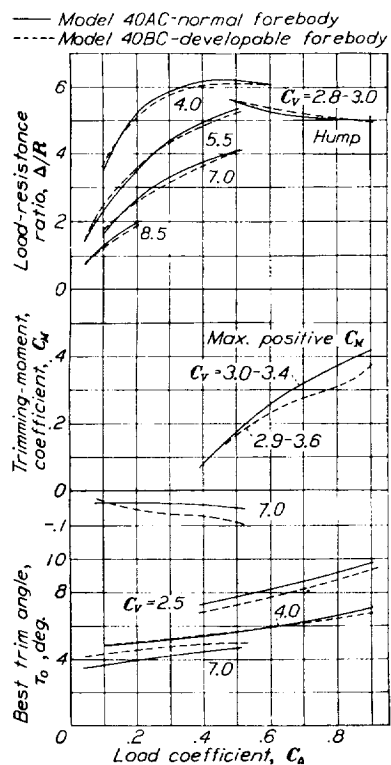


FIGURE 69.—Effect of developable forebody surface on characteristics at best trim angle. Pointed afterbody.

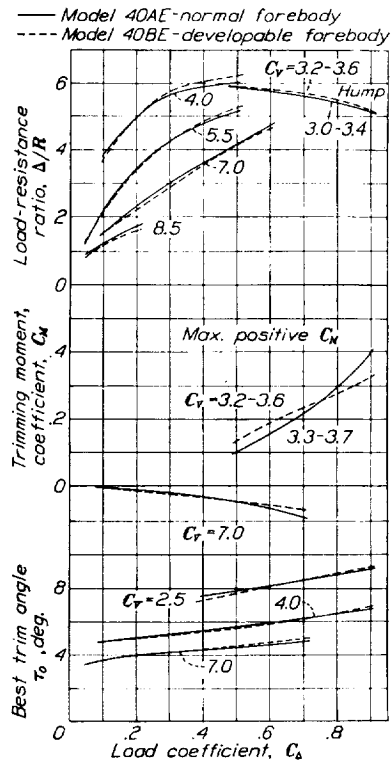


FIGURE 69.—Effect of developable forebody surface on characteristics at best trim angle. No-step afterbody.

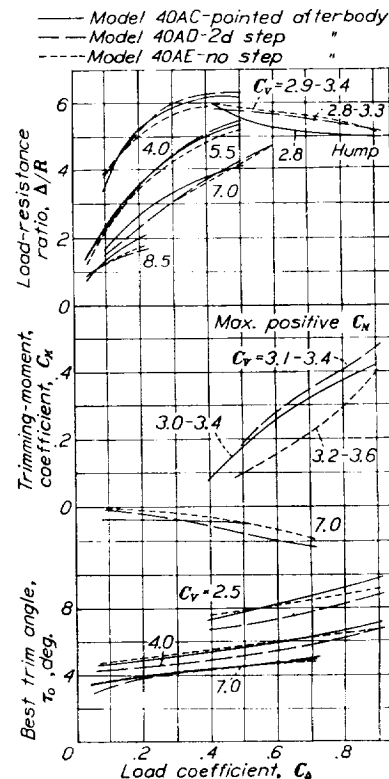


FIGURE 71.—Effect of afterbody form on characteristics at best trim angles. Normal forebody.

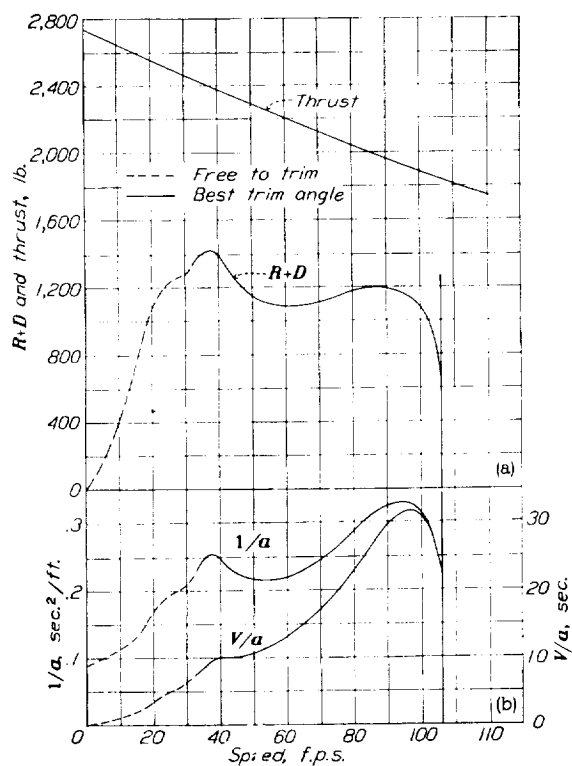


FIGURE 73.—Curves for determining take-off time and run for the 8,000-pound example.

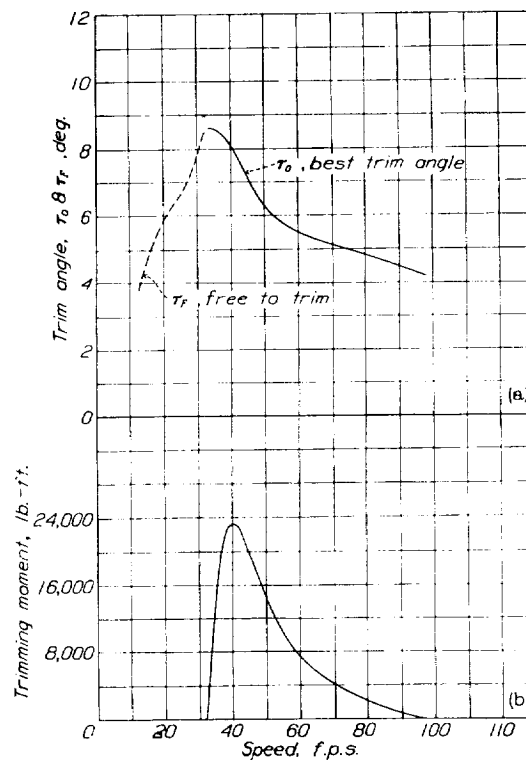


FIGURE 74.—Trim angle and trimming moment for the 8,000-pound example.

of refinements. The parasite drag is purposely assumed to be quite high. The following data are assumed:

Gross load, lb.....	2,000
Wing area, sq. ft.....	200
Horsepower.....	110
Effective aspect ratio including ground effect.....	10
Parasite-drag coefficient excluding hull.....	0.05
Airfoil section.....	Clark Y

best-angle total resistance at the hump. If sufficient controlling moment to increase the trim angles is available at low speeds, the low-speed resistance can be reduced. Examination of the $1/a$ and V/a curves shows, however, that this early resistance peak increases the take-off time less than 1 second and that the effect on the take-off distance is almost negligible. In fact, the excess thrust is found to be smallest at the

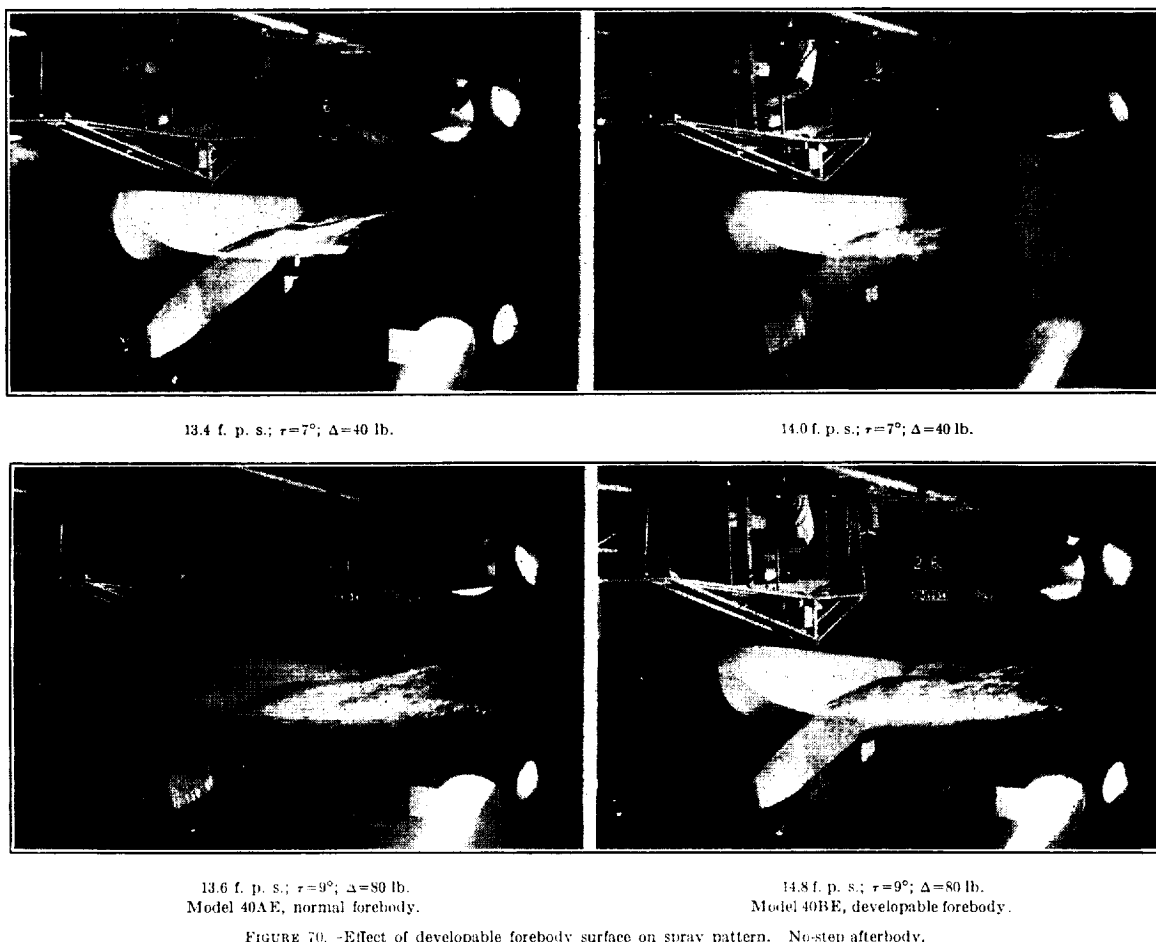


FIGURE 70. -Effect of developable forebody surface on spray pattern. No-step afterbody.

Model 40-BE is chosen for the hull and a maximum beam of 3.15 feet is used to give the maximum hull loading that can be used without extrapolating some of the curves. The angle of wing setting used is 4° . Again, the center of gravity is conveniently taken to be the same as that used in the free-to-trim tests of the hull.

Thrust, $R+D$, $1/a$, and V/a are plotted in figure 75. Trim angle and trimming moment are plotted in figure 76. The take-off time and distance are computed using the free-to-trim resistance curve to the point where it meets the best-angle resistance curve. The take-off time is 23.7 seconds and the length of run 1,300 feet.

It is seen that the free-to-trim total resistance ($R+D$) at low speeds is considerably greater than the

critical point near get-away. It would seem from this fact that a smaller hull would give a substantial improvement in water performance but the loading used here appears to be very close to the practical limit. Any further increase of the load coefficient would probably result in too much spray at low speeds. Some improvement could be obtained by a higher wing setting as the high-speed hump occurs very near the stalling speed, but the improvement in take-off performance would probably be gained at the cost of a poorer flying attitude. Furthermore, if the angle of wing setting is increased too much, the problem may be complicated by the stalling of the wing at the high trim angles required near the hump.

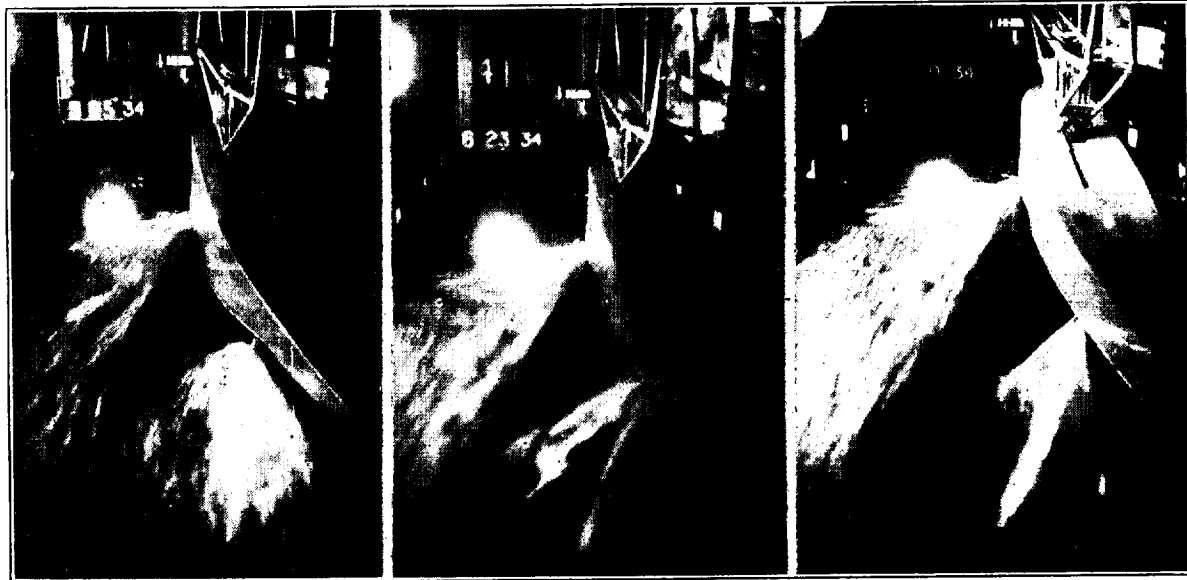
If the trimming moment required to obtain best trim angle at the hump (fig. 76(b)) is found to be

excessive, an angle somewhere between the best angle and the zero trimming-moment angle can probably be obtained that will increase the hump only slightly, as indicated by the comparatively small difference between the minimum $R+D$ and the free-to-trim $R+D$ at a speed of 38 feet per second (fig. 75(a)). In fact,

angle at the hump if the new center-of-gravity position does not produce undesirable stability characteristics.

CONCLUDING REMARKS

The selection of the best of these hulls for a given design will probably be governed by considerations



14.5 f. p. s.; $\tau=7^\circ$; $\Delta=40$ lb.

13.9 f. p. s.; $\tau=7^\circ$; $\Delta=40$ lb.

13.4 f. p. s.; $\tau=7^\circ$; $\Delta=40$ lb.



19.7 f. p. s.; $\tau=7^\circ$; $\Delta=80$ lb.
Model 40AC, pointed afterbody.

19.5 f. p. s.; $\tau=7^\circ$; $\Delta=80$ lb.
Model 40AD, second-step afterbody.

18.4 f. p. s.; $\tau=7^\circ$; $\Delta=80$ lb.
Model 40AE, no-step afterbody.

FIGURE 72.—Effect of afterbody form on spray pattern. Normal forebody.

the critical peak of the free-to-trim resistance curve can be eliminated by moving the center of gravity sufficiently far aft and accepting the accompanying higher trimming moment required to obtain best trim

other than the water-resistance characteristics because of the comparatively small differences in the resistance curves of the five models. Model 40-BE offers least resistance at the hump and model 40-AC the least at

high speeds but, in general, the differences are not sufficiently great to be a determining factor.

The developable forebody apparently offers a satisfactory solution for the problem of simplified construction without an accompanying sacrifice in performance. In the smooth water of the tank there was little choice between the two forebodies in regard to the spray. In rough water the developable forebody would probably have slightly poorer spray characteristics than the other forebody.

It is suggested that the spray strips be continued forward until they meet at the bow.

It appears from the take-off examples that the margin of excess thrust is likely to be less near get-away speed than it is at the hump. Exceptions to this statement may be found when controllable propellers

It should be possible to use even greater angles of afterbody keel than were used in the present case without greatly increasing take-off time or run. In fact, there may be an appreciable improvement if the high-speed resistance is critical. (See reference 5.)

LANGLEY MEMORIAL AERONAUTICAL LABORATORY,
NATIONAL ADVISORY COMMITTEE FOR AERONAUTICS,
LANGLEY FIELD, VA., June 19, 1935.

REFERENCES

1. Truscott, Starr: The N. A. C. A. Tank. A High-Speed Towing Basin for Testing Models of Seaplane Floats. T. R. No. 470, N. A. C. A., 1933.

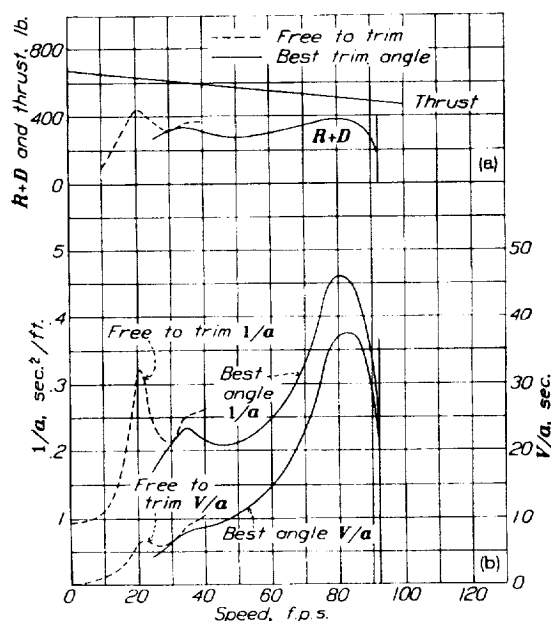


FIGURE 75.—Curves for determining take-off time and run for the 2,000-pound example.

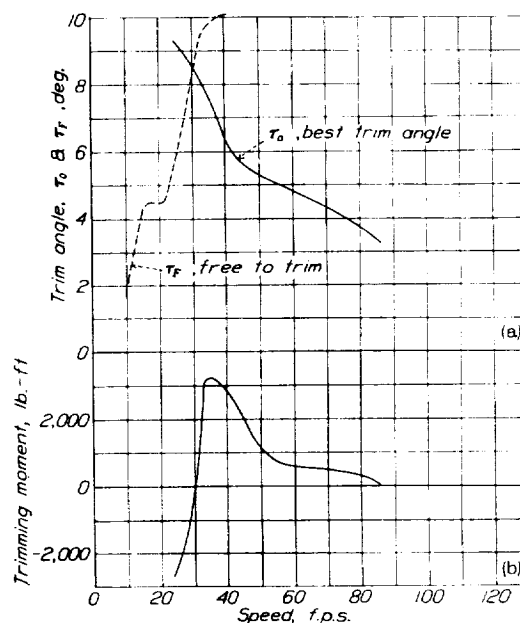


FIGURE 76.—Trim angle and trimming moment curves for the 2,000-pound example. $\Delta=80$ lb.

and/or very low wing loadings are used. An increase in the load coefficient will usually raise the hump $R+D$ and lower the high speed $R+D$ but, in the case of these models, it is not recommended that the initial load be increased beyond the maximum load tested because the spray may become excessive, particularly at the bow. In fact, if very rough water is to be encountered in service it would appear advisable to use only a moderately high load coefficient.

2. Shoemaker, James M.: Tank Tests of Flat and V-Bottom Planing Surfaces. T. N. No. 509, N. A. C. A., 1934.
3. Shoemaker, James M., and Parkinson, John B.: A Complete Tank Test of a Model of a Flying-Boat Hull—N. A. C. A. Model No. 11. T. N. No. 464, N. A. C. A., 1933.
4. Hartman, Edwin P.: Working Charts for the Determination of Propeller Thrust at Various Air Speeds. T. R. No. 481, N. A. C. A., 1934.
5. Allison, John M.: The Effect of the Angle of Afterbody Keel on the Water Performance of a Flying-Boat Hull Model. T. N. No. 541, N. A. C. A., 1935.

TABLE I.—OFFSETS FOR FOREBODY A, INCHES

Station	Distance from F. P.	Distance below base line						Half-breadths					
		Keel	B 1, 1.30	B 2, 2.60	B 3, 3.90	B 4, 5.20	Chine	Chine	WL 1, 12.40	WL 2, 10.80	WL 3, 9.20	WL 4, 7.60	WL 5, 6.00
F. P.	0	Tangent at 4.00					4.00	Tan- gent					
1/4	1.05	7.79	5.40				4.84	2.07				0.16	0.85
1/2	2.10	9.24	6.96	5.81			5.66	2.92			0.12	.87	2.27
1	4.20	11.01	9.22	7.89	7.16		7.13	3.99		0.23	1.32	3.00	
1 1/2	6.30	12.13	10.71	9.48	8.67		8.38	4.74		1.23	2.99		
2	8.40	12.86	11.74	10.67	9.88	9.40	9.63	5.29	0.57	2.44			
3	12.60	13.66	12.90	12.12	11.44	10.92	10.64	5.98	2.11	5.46			
4	16.80	13.95	13.39	12.81	12.25	11.75	11.31	6.33	3.54				
5	21.00	14.00					11.59	6.46					
6-10	25.20-42.00	14.00					11.67	6.50					

¹ Distance from center line (plane of symmetry) to buttock (section of hull surface made by a plane parallel to plane of symmetry).² Distance from base line to water line (section of hull surface made by a horizontal plane parallel to base line.)

TABLE II.—OFFSETS FOR FOREBODY B, INCHES

Sta- tion	Distance from F. P.	Distance below base line						Half-breadths					
		Keel	B 1, 1.30	B 2, 2.60	B 3, 3.90	B 4, 5.20	Chine	Chine	WL 1, 12.40	WL 2, 10.80	WL 3, 9.20	WL 4, 7.60	WL 5, 6.00
F. P.	0	Tangent at 4.00					4.00	0.10					
$\frac{1}{4}$	1.05	7.36	5.19				4.75	1.45					0.90
$\frac{1}{2}$	2.10	8.83	7.37				5.54	2.46				1.13	2.21
1	4.20	10.72	9.70	8.46			7.06	3.84			1.85	3.39	
$1\frac{1}{2}$	6.30	11.91	11.09	10.12	9.08		8.37	4.72		1.70	3.75		
2	8.40	12.69	11.99	11.19	10.35	9.43	9.36	5.29	0.59	3.22			
3	12.60	13.55	12.99	12.37	11.75	11.05	10.64	5.98	2.53	5.68			
4	16.80	13.88	13.42	12.88	12.34	11.79	11.31	6.33	3.74				
5	21.00	14.00	13.54	13.06	12.57	12.07	11.59	6.46	4.32				
6-10	25.20-42.00	14.00					11.67	6.50					

TABLE III.—OFFSETS FOR AFTERBODY C, INCHES

[Elements of stations are straight lines]

Sta- tion	Dis- tance from station 10A	Distance below base line				Half-breadths	
		Keel	Main chine	Cove	Upper chine	Main chine and cove	Upper chine
10A	0	13.50	11.17			6.50	
11	4.2		10.62			6.50	
12	8.4		10.08			6.47	
13	12.6		9.55	7.09	7.09	6.39	6.39
14	16.8		9.13	6.56	6.49	6.04	6.23
15	21.0		8.89	6.20	5.91	5.18	5.98
16	25.2		8.84	6.05	5.36	3.77	5.68
17	29.4		8.95	6.04	4.83	1.97	5.30
18F	33.0	9.15	9.11	6.11	4.41	.20	4.89
18A	33.0	6.15			4.41		4.89
19	38.0				3.86		4.22
20	43.0				3.35		3.44
21	48.0				2.88		2.54
22	53.0				2.46		1.52
23	58.0	2.19			2.08		.40

TABLE IV.—OFFSETS FOR AFTERBODIES D AND E, INCHES

[Elements of stations are straight lines]

Sta- tion	Dis- tance from station 10A	Chine half- breadth	Distance below base line			
			Afterbody D		Afterbody E	
			Keel	Chine	Keel	Chine
10A	0	6.50	13.50	11.17	13.50	11.17
11	4.2	6.50		10.54		10.54
12	8.4	6.47		9.93		9.93
13	12.6	6.39		9.33		9.33
14	16.8	6.23		8.76		8.76
15	21.0	5.98	10.36	8.22		8.22
16	25.2	5.68	9.80	7.77		7.71
17	29.4	5.30	9.37	7.48		7.22
18F	33.0	4.89	9.15	7.41		6.84
18A	33.0	4.89	8.57	6.83		6.83
19	38.0	4.22		6.32		6.32
20	43.0	3.44		5.85		5.85
21	48.0	2.54		5.44		5.44
22	53.0	1.52		5.06		5.06
23	58.0	.40	4.83	4.72	4.83	4.72

REPORT No. 544

COMBUSTION IN A BOMB WITH A FUEL-INJECTION SYSTEM

By MILDRED COHN and ROBERT C. SPENCER

SUMMARY

Fuel injected into a spherical bomb filled with air at a desired density and temperature could be ignited with a spark a few thousandths of a second after injection, an interval comparable with the ignition lag in fuel-injection engines. The effect of several variables on the extent and rate of combustion was investigated: Time intervals between injection and ignition of fuel of 0.003 to 0.06 second and one of 5 minutes; initial air temperatures of 100° C. to 250° C.; initial air densities equivalent to 5, 10, and 15 absolute atmospheres pressure at 100° C.; and air-fuel ratios of 5 to 25.

The 5-minute interval between injection and spark permitted the fuel to vaporize completely; for the shorter periods the explosion took place with liquid-vapor mixtures. For the short periods, the time of reaction increased as the period was increased and the response of combustion to changes in the initial conditions was more marked than it was for the long period, indicating the significance of distribution and vaporization. An increase in initial temperature decreased the time of reaction for both types but increased the extent of combustion for only the short-period mixtures. For the uniform vapor-air explosions, an increase in air density lengthened the reaction time. For the nonuniform liquid-vapor-air explosions, an increase in air density from 0.00473 to 0.0095 gram per cubic centimeter (equivalent to 5 and 10 atmospheres pressure at 100° C.) shortened the time of reaction but (with the exception of the tests at 100° C.), as the density was increased to 0.0142 gram per cubic centimeter (equivalent to 15 atmospheres pressure at 100° C.), the reaction time tended to lengthen. The leanest mixture that would explode with a delay period of 5 minutes corresponded to an air-fuel ratio of 20.7. For a delay period of 0.004 second it corresponded to one of 25. The reaction time was a minimum and the maximum pressure a maximum at an air-fuel ratio of 10 for the delayed explosions. At the higher densities and temperatures, the two types of explosions acted more alike.

INTRODUCTION

The National Advisory Committee for Aeronautics has carried out investigations of the formation, penetration, and combustion of fuel sprays. The N. A. C. A. combustion apparatus (reference 1) has been used to

photograph the combustion of fuel under conditions analogous to those existing in the combustion chamber of a high-speed compression-ignition engine. This apparatus has also been used for an investigation in which the injected fuel was ignited by a spark (reference 2). The individual effects of such variables as the time interval between the injection and the spark, the air temperature, the air density, and the turbulence cannot, however, be determined with the combustion apparatus.

An analysis of the effects of such variables on the combustion of fuel sprays would be very helpful in explaining the phenomena observed in engines. A spherical bomb was therefore constructed into which the fuel could be injected under varying conditions and be ignited by a spark at any desired time after injection. Homogeneous mixtures of vaporized fuel and air can be obtained by allowing sufficient time to elapse between injection and ignition and the combustion of such uniform mixtures can be compared with the combustion of nonuniform mixtures of liquid fuel, fuel vapor, and air.

The combustion apparatus has recently been utilized for tests in which ignition was effected by compression (reference 3). When compared with the data of reference 2, the results indicated that the data obtained with spark ignition would be useful in studying combustion obtained by compression ignition. The results obtained with the bomb, particularly those at high temperatures and pressures, should be an aid in interpreting phenomena in compression-ignition engines. The present paper covers the results obtained when a hydrogenated safety fuel was used in the spherical bomb and the conditions varied. The tests were conducted at the Langley Field laboratories during the winter of 1933-34.

APPARATUS AND METHOD

THE BOMB AND AUXILIARY EQUIPMENT

The spherical bomb designed for this investigation is constructed of stainless steel and has a volume of 600 cubic centimeters. The bomb is equipped with an optical-type pressure indicator, a spark plug, an injection valve, and an air inlet and exhaust fitting. The bomb is immersed in a liquid bath thermostatically controlled to within 1° C. Tests showed that

after the bath temperature had been held constant for 10 minutes, no appreciable difference could be detected between the temperature of the air within the bomb and that of the bath. The assembled test apparatus is shown in figure 1. Fuel is sprayed into the bomb (fig. 2) through a 13-orifice nozzle (fig. 3) designed according to the recommendations of Spanogle and Foster (reference 4).

The experimental arrangement is shown by the sketch of figure 4. The system consists of a high-

the reservoir. The fuel weight can be controlled within ± 2 percent. The fuel is circulated under pressure through the injection valve by a pump in order to control the temperature of the fuel at the valve. The temperature of the fuel was maintained at 45°C . in all the tests.

The electrodes of the spark plug were extended by nichrome wires ending in nichrome balls 2.5 millimeters in diameter. The spark gap was kept adjusted to about 0.46 millimeter, as less clearance apparently

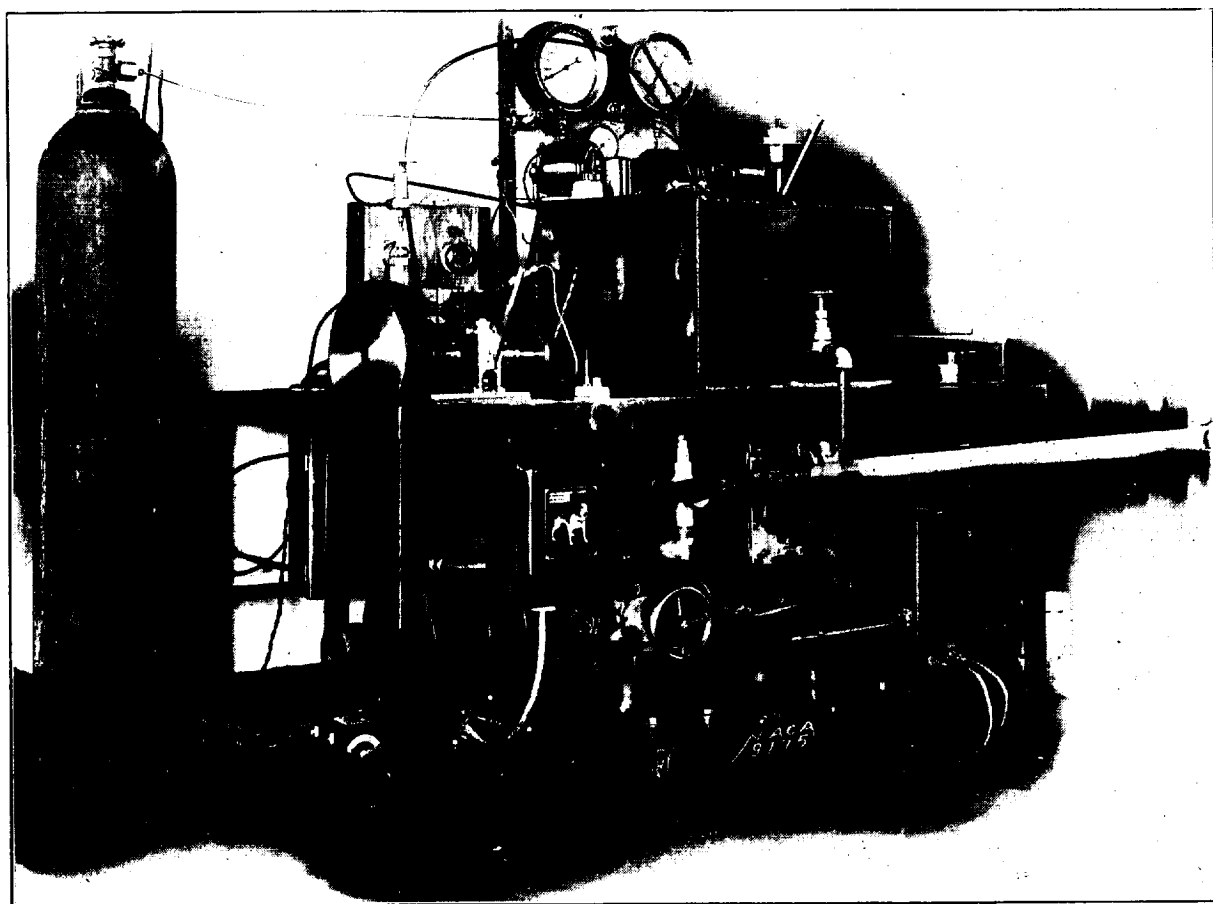


FIGURE 1.—The assembled apparatus.

pressure hand pump, a reservoir, a poppet valve, an injection valve, and a clutch mechanism for operating the poppet valve. The clutch is engaged by pulling a trip lever; the camshaft then makes a single revolution. The pressure of the fuel above the poppet valve is sufficient to hold it closed as the spring is compressed by the cam follower. When the cam follower strikes the valve and opens it slightly, the pressure is no longer effective and the compressed spring completes the opening of the valve very rapidly. A pressure wave then traverses the injection tube to the injection valve, causing the injection of the fuel.

The fuel quantity may be changed by varying the pressure in the reservoir or by changing the size of

caused considerable difficulty in igniting the mixture. The spark gap was located at the center of the bomb, and the injection valve was so mounted that the spray from the center orifice of the nozzle impinged directly upon the gap. This arrangement insured the presence of fuel at the spark gap but, because of the wetting of the plug, it necessitated the use of a heavy spark discharge. The timing of the spark with respect to the spray could be varied by the phase-changing device indicated in figure 4. This device permitted a variation in spark timing from 0 to 0.063 second after injection start. Longer intervals had to be manually timed, and the range between 0.063 second and about 10 seconds could not be investigated.

In order to set the timing of the spark with respect to the spray, the spark-timing switch was connected as the switch for a neon-tube stroboscope and the start of injection was then visually determined. These settings were checked by wrapping heavy paper around a pulley, mounting the injection valve and the end of the ignition cable just above the pulley, and making an injection against the paper while the pulley was

11,000 vibrations per second, respectively. The indicator was calibrated by means of a dead-weight gage tester at temperatures up to 250°C . The film speed used during most of the tests was 100 inches per second, but a few tests were made with a film speed of 33 inches per second. The indicator is provided with a spark gap for recording the time of passage of the igniting spark.

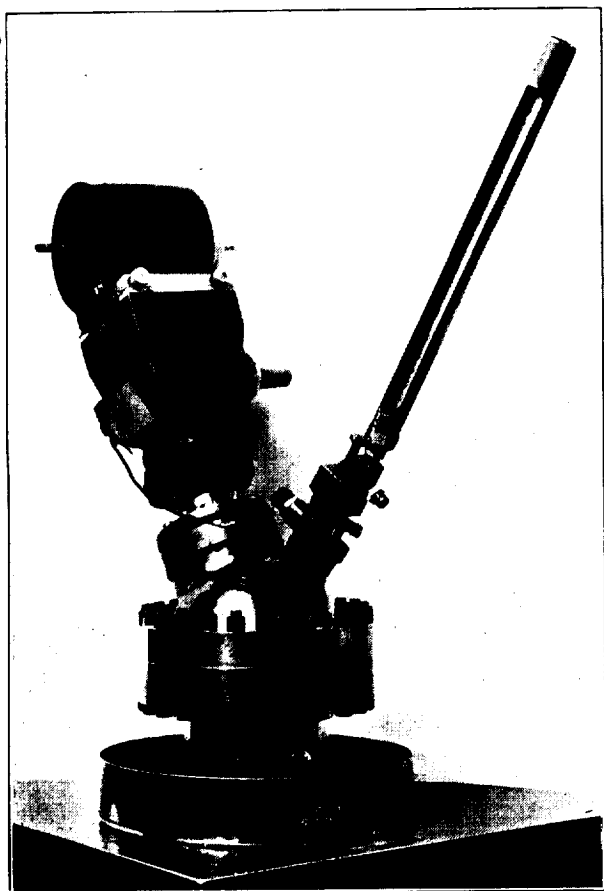


FIGURE 2.—The bomb assembled with the optical indicator.

turning at a known speed. The timing of the spark with respect to the spray was determined by measuring the distance between the mark of the spark and the mark of the injection. As a result of these tests it is estimated that the spark timing did not vary more than 0.0001 second for any one setting of the switch.

The pressure indicator is of the optical type and has been described in reference 3. The two diaphragms used in the test were designed for pressures of the order of 70 and 120 atmospheres. The natural frequencies of the diaphragm and the optical gear were 9,600 and

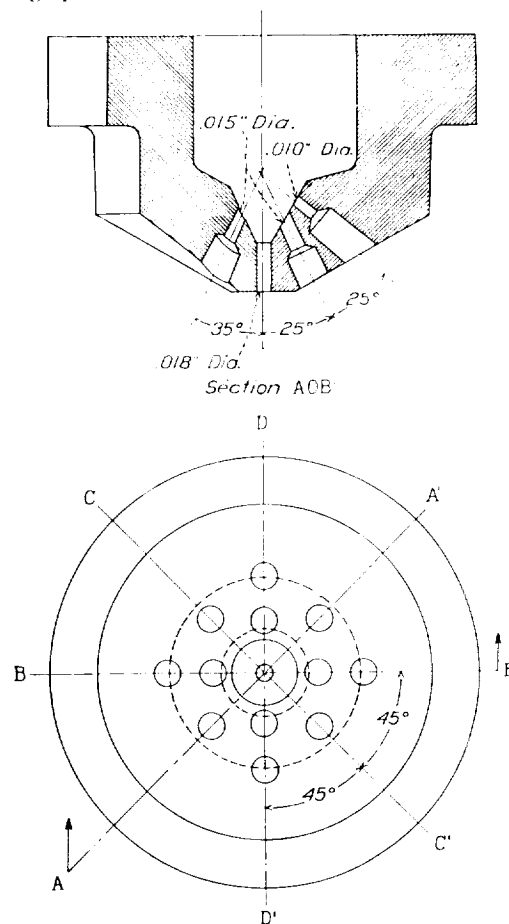


FIGURE 3.—The 13-orifice nozzle. Plane DD' is identical with BB' and plane CC' is identical with AA' .

THE FUEL

Hydrogenated safety fuel (reference 5) was used throughout these tests. The properties peculiar to this fuel are its high octane number and its high flash point (41°C . as compared with -32°C . to -43°C . for gasolines). The percentage of aromatic and naphthenic compounds is much higher in hydrogenated fuel than it is in ordinary straight-run or cracked distillates. The results of actual engine tests conducted at this laboratory with the safety fuel are

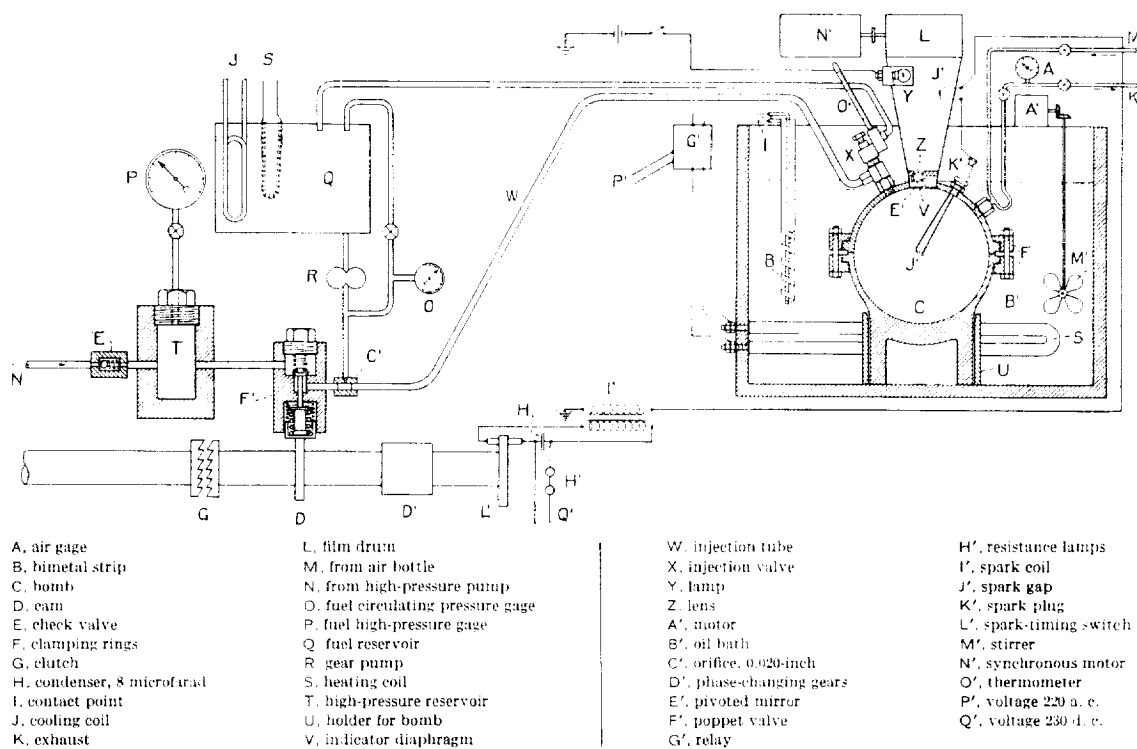
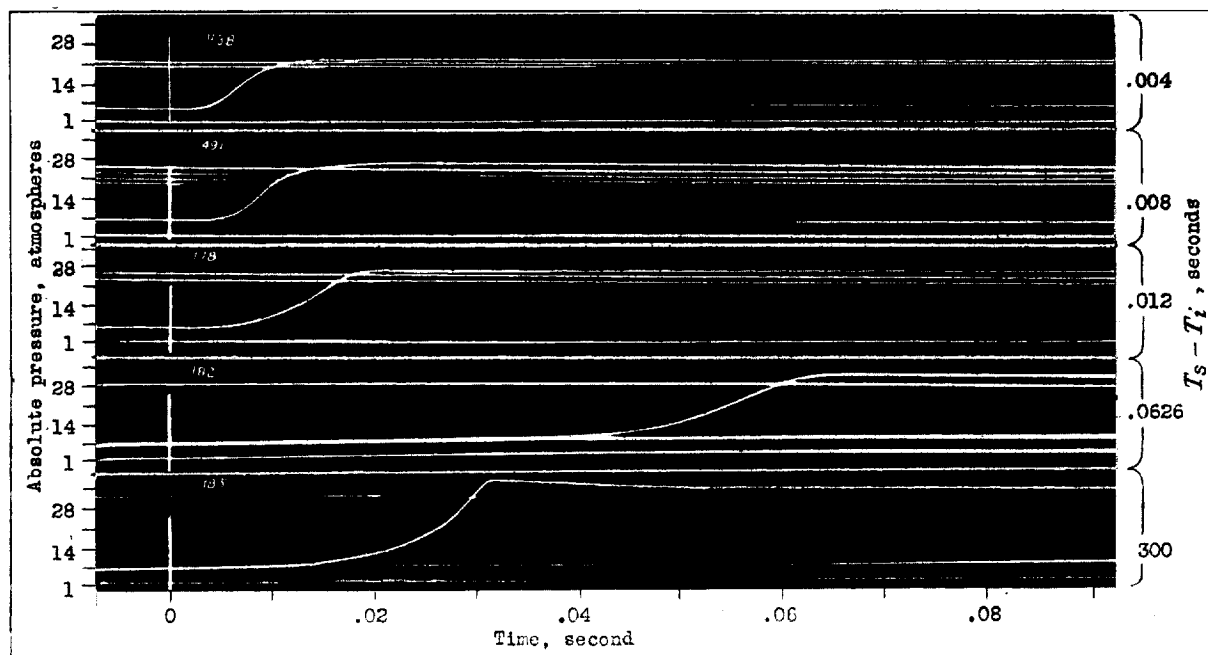


FIGURE 4.—Diagram of the apparatus.

FIGURE 5. Effect of time interval ($T_s - T_i$) between injection and spark. Initial air temperature, 200° C.; initial air pressure, 6.3 atmospheres, absolute; air-fuel ratio, 15.

presented in reference 6. The properties of the fuel are listed below:

Properties of hydrogenated safety fuel

Specific gravity.....	0.882
Initial boiling point.....	156° C.
50 percent point.....	180° C.
80 percent point.....	190° C.
90 percent point.....	193° C.
Final boiling point.....	206° C.
Recovery, percent.....	99
Octane number ¹	95
Flash point (Abel closed-cup method).....	41° C.
Percentage carbon.....	88.5
Percentage hydrogen.....	11.5
Heat of combustion ² (constant volume at 30° C.), calories/gram.....	10,400

ANALYSIS OF RECORDS

The data obtained from the pressure-indicator records included the time from the injection to the spark ($T_s - T_i$), the time from the spark to the start of pressure rise, the time for completion of the total reaction when possible, and the time for the completion of a definite percentage of the reaction, as well as the time of attaining the maximum pressure. (See table I.) In the determination of the time for the attainment of maximum pressure, the line recorded by the passage of the spark was considered zero.

Difficulty was encountered in the determination of the time of attainment of maximum pressure owing to the long duration of a more or less constant pressure (fig. 5) at the end of the explosion when the rate of heat input is apparently balanced by the rate of heat loss. Owing to the uncertainty of the location of the point of maximum pressure, for comparative purposes, another point in the pressure-time curve was arbitrarily chosen at $P = 2.5 P_i$, where P_i is the initial pressure. In figure 6 both the time interval from the spark to $2.5 P_i$ and the interval from the spark to maximum pressure are plotted for the delayed explosions. As figure 7 shows, no difficulty was experienced in determining the location of maximum pressure for these explosions. Figure 8 shows that, for comparative purposes, the chosen time interval ($T_{2.5P_i} - T_s$) may be used as an equivalent of the total time between the passage of the spark and the attainment of maximum pressure ($T_{P_{max}} - T_s$).

¹ Determined against iso-octane and heptane blends on series 30 Ethyl Gasoline Corporation test engine; jacket temperature, 300° F.; engine speed, 600 r. p. m.; compression pressure, 190 to 200 pounds per square inch.

² Determined by the National Bureau of Standards.

Owing to the change in the specific heats with temperature, the percentage of reaction does not remain constant for the same P/P_i ratio at different initial temperatures. Assuming that the products of the reaction are CO_2 and H_2O and using Lewis and Randall's values for the specific heats of gases (reference 7) and Cragoe's values for the specific heat of the fuel (reference 8), the following results are obtained:

Temperature °C.	Percentage reaction $P = 2.5 P_i$
100.....	17.3
150.....	20.0
200.....	22.4
250.....	25.8

If the time necessary to achieve a definite percentage of reaction had been chosen instead of the time necessary to reach $2.5 P_i$, the same trends would have been observed qualitatively.

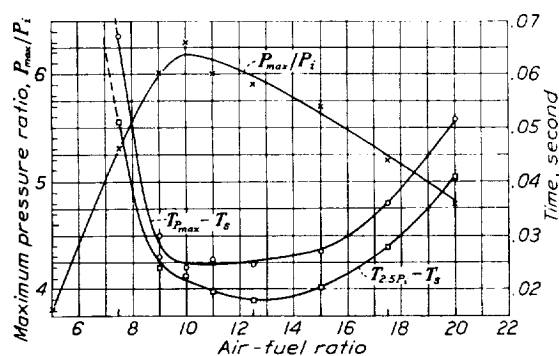


FIGURE 6.—Effect of air-fuel ratio on maximum pressure ratio and time of reaction. Time interval between injection and spark ($T_s - T_i$), 5 minutes; initial air temperature, 200° C.; initial air pressure, 6.3 atmospheres, absolute.

TEST RESULTS

The test results are summarized in table I. The data are not complete at 100° C. because ignition would not take place over a complete range of time intervals between the injection of the fuel and the passage of the spark. The three densities used at each temperature (100°, 150°, 200°, and 250° C.) were equivalent to 5, 10, and 15 atmospheres absolute pressure at 100° C. and shall hereinafter be referred to as 5, 10, and 15 atmospheres. At a density of 5 atmospheres the range extended from 0.003 to 0.020 second; at 10 atmospheres the limits were from 0.003 to 0.052 second; and at a density of 15 atmospheres the range was from 0.004 to 0.056 second. At all other temperatures the mixture would explode throughout the entire range investigated, after the limiting value in spark timing, at 0.003 or 0.004 second after injection.

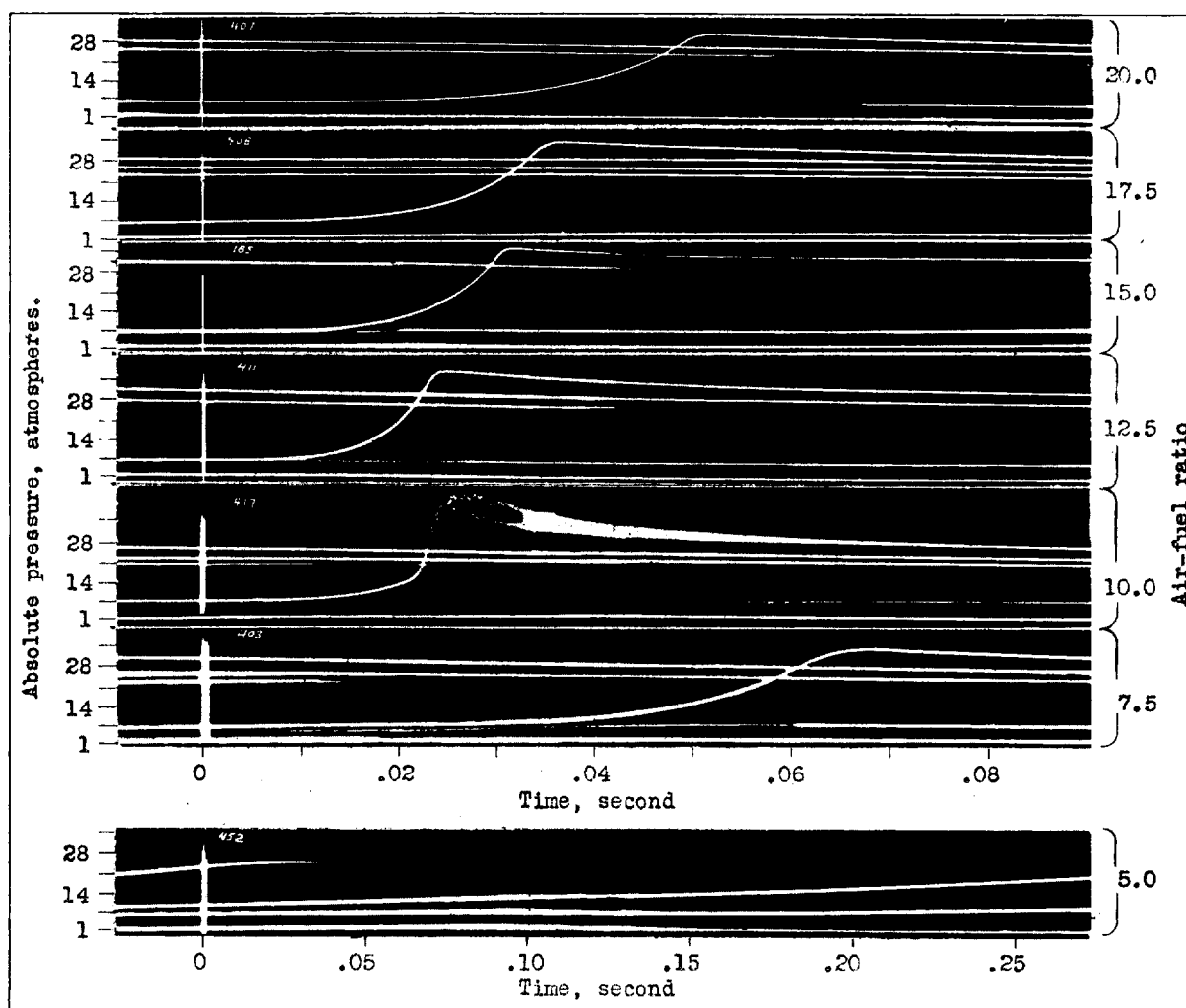


FIGURE 7.—Effect of air-fuel ratio. Initial air temperature, 200° C.; initial air pressure, 6.3 atmospheres, absolute; interval between injection and spark, 5 minutes.

TABLE I.—THE RATE AND EXTENT OF COMBUSTION FOR HYDROGENATED SAFETY FUEL INJECTED INTO AIR AT DIFFERENT DENSITIES

(Air-fuel ratio, 15)

Initial temperature	Initial pressure P_i (abs.)	Time intervals between—			Maximum pressure Initial pressure P_{max}/P_i
		Injection and spark ($T_s - T_i$)	Spark and start of pressure rise	Spark and 2.5 initial pressure ($T_{2.5P_i} - T_i$)	

DENSITY OF 5 ATMOSPHERES (REFERRED TO 100° C.)

° C.	Atmospheres	Seconds	Second	Second	
100	5.0	0.0040	0.0055		1.5
		.0080	.0075		2.4
		.0120		(1)	
150	5.7	.0040	.0055	0.0155	3.3
		.0080	.0070	.0200	3.3
		.0120	.0105	.0375	3.3
		.0630	(1)	.27	3.75
200	6.3	300	.0140	.0240	6.2
		.0040	.0030	.0085	3.4
		.0080	.0045	.0095	4.0
		.0120	.0045	.0140	3.9
		.0630	.0385	.0540	4.3
250	7.0	300	.0100	.0205	5.7
		.0040	.0030	.0060	3.6
		.0080	.0030	.0085	3.8
		.0120	.0035	.0095	3.9
		.0630	.0120	.0150	4.2
	300		.0100	.0205	5.3

DENSITY OF 10 ATMOSPHERES (REFERRED TO 100° C.)

° C.	Atmospheres	Seconds	Second	Second	
100	10.0	0.0040	0.0040	0.0125	4.2
		.0080	.0095	.0275	4.0
		.0120	.0085	.0305	3.8
150	11.4	.0040	.0035	.0100	4.2
		.0080	.0040	.0120	4.5
		.0120	.0070	.0175	4.2
		.0630	.0785	.1355	4.1
200	12.7	300	.0115	.0205	6.0
		.0040	.0025	.0050	4.4
		.0080	.0040	.0095	4.4
		.0120	.0050	.0105	4.5
		.0630	.0130	.0325	4.6
250	14.0	300	.0090	.0260	5.6
		.0040	.0020	.0045	4.3
		.0080	.0025	.0055	4.3
		.0120	.0025	.0075	4.4
		.0630	.0090	.0175	4.9
	300		.0110	.0260	5.1

DENSITY OF 15 ATMOSPHERES (REFERRED TO 100° C.)

° C.	Atmospheres	Seconds	Second	Second	
100	15.0	0.0040	0.0040	0.0095	5.0
		.0080	.0075	.0250	4.5
		.0120	.0075	.0275	4.5
150	17.0	.0040	.0030	.0070	4.9
		.0080	.0060	.0150	4.6
		.0120	.0070	.0195	4.3
		.0630	.0575	.1015	4.1
200	19.1	300	.0175	.0425	5.8
		.0040	.0020	.0055	4.7
		.0080	.0035	.0080	4.5
		.0120	.0055	.0125	4.5
		.0630	.0480	.0695	4.5
250	21.1	300	.0100	.0320	5.5
		.0040	.0020	.0045	4.6
		.0080	.0025	.0055	4.6
		.0120	.0040	.0075	4.7
		.0630	.0150	.0240	5.2
	300		.0080	.0245	5.5

¹ Value not measurable.

MAXIMUM PRESSURES

The ratio of maximum pressure to initial pressure (P_{max}/P_i) is tabulated for the various temperatures and pressures because this ratio is indicative of the extent of effective combustion. No attempt has been made to correct the values of the maximum pressure for heat losses, although the time required to attain maximum pressure varies.

It will be noted from the table that the ratios of maximum to initial pressure for the so-called "delayed"

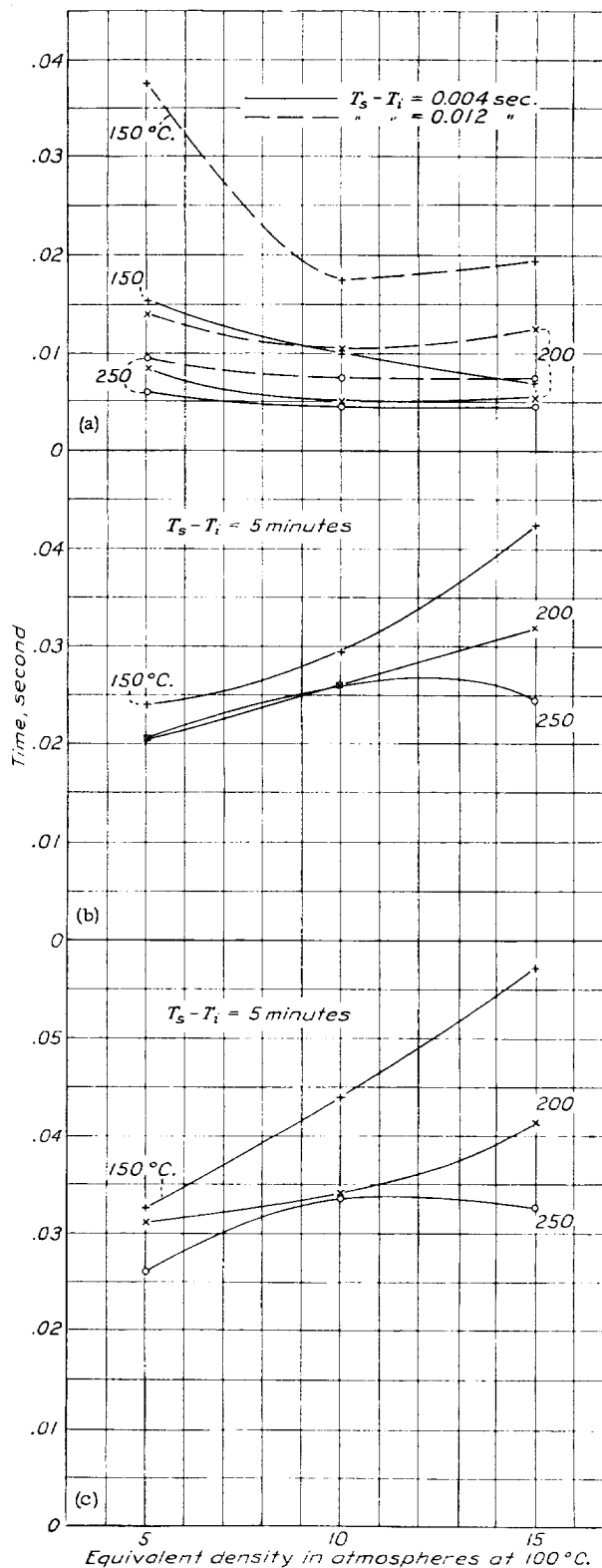


FIGURE 8.—Effect of air density on time of reaction. Air-fuel ratio, 15.
(a) Time required for pressure to reach 2.5 P_i . $T_s - T_i$, 0.004 and 0.012 second.
(b) Time required for pressure to reach 2.5 P_i . $T_s - T_i$, 5 minutes. (c) Time required for pressure to reach maximum. $T_s - T_i$, 5 minutes.

explosions (spark occurring several minutes after injection of the fuel) greatly exceed those for the explosions with short time intervals between injection and ignition, this effect being more marked at low temperatures and air densities. For those mixtures exploding at a very short time after injection, the pressure ratio (P_{max}/P_i) increases with increased air density and, in general, increases with increased temperature. On the other hand, for the delayed explosions the pressure ratio decreases with increased temperature. The delayed explosions exhibited no definite trend of P_{max}/P_i with change of density although, in general, the ratio decreased slightly with an increase of density.

For the delay period of 0.004 second the variation of maximum pressure with air-fuel ratio was direct; whereas for the delayed explosions the maximum pressure ratio reached a maximum value at an air-fuel ratio of 10. The leanest mixture that would explode

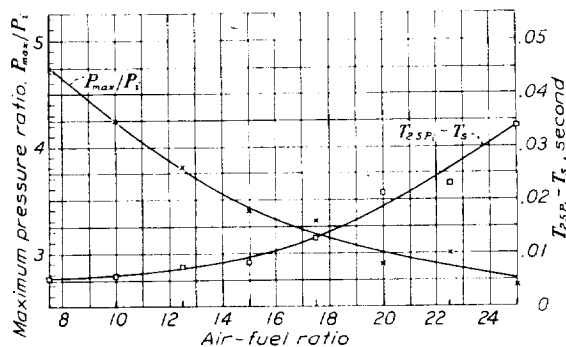


FIGURE 9.—Effect of air-fuel ratio on maximum pressure ratio and on time of reaction. $T_s - T_i$, 0.004 second; initial air temperature, 200°C.; initial air pressure, 6.3 atmospheres, absolute.

with a delay period of 5 minutes (figs. 6 and 7) corresponded to an air-fuel ratio of 20.7. With a delay period of 0.004 second (fig. 9) an air-fuel ratio of 25 would explode.

With air-fuel ratios in the neighborhood of 10 in the case of delayed explosions, the reaction was, in fact, so intense in this range that severe vibrations were set up which continued for some time after the maximum pressure was attained (see fig. 7). The explosions were accompanied by a high-pitched whistle or "squeak." The frequency of the vibrations was approximately 6,000 per second. The appearance of the highest frequency at the point of greatest pressure (that is, highest temperature) indicated that the vibrations were actually in the gas.

TIME OF REACTION

The values for the time interval $T_{2.5P_i} - T_s$ are tabulated for all conditions except that of a pressure of 5 atmospheres and a temperature of 100°C., where the pressure never reached 2.5 times its initial value. Under the same temperature and pressure conditions the shortest reaction time corresponds to the shortest

$T_s - T_i$ interval; as the time between the injection of the fuel and the passage of the spark increased, the rate of pressure rise decreased and the time between the occurrence of the spark and the beginning of a perceptible rise increased. The typical series of records shown in figure 5 illustrates this trend. As the temperature increases, the time $T_{2.5P_i} - T_s$ decreases. An increase in air density at first decreases the time of reaction for the liquid-vapor-air explosions but, at the higher densities and the temperatures above 100°C., there is a tendency for the interval to lengthen with further increase in density. For the vapor-air explosions, an increase in air density increases the time of reaction. It will be seen that, notably at the lower temperatures, the time between the spark and the attainment of a pressure equal to $2.5P_i$ was sometimes shorter for the delayed explosions than it was for some of the others. If the maximum rates of pressure rise are compared, however, the delayed explosions always yield the higher values because the reaction autoaccelerates and the delayed explosions attain the higher pressures. The effect of fuel concentration on reaction time is shown in figures 6 and 9. For the delayed explosions, the reaction time was a minimum at an air-fuel ratio of 10.

SUMMARY OF TEST RESULTS

The test results may be summarized as follows:

For the explosions having $T_s - T_i$ periods between 0.003 and 0.06 second, the extent of effective combustion, as measured by P_{max}/P_i —

- varied directly with temperature;
- varied directly with density; and
- varied directly with fuel concentration.

The time of reaction—

- varied directly with the $T_s - T_i$ interval;
- varied inversely with temperature;
- varied inversely with density at low densities and directly with density at the higher densities; and
- varied inversely with fuel concentration.

For the explosions having a $T_s - T_i$ period of 5 minutes, the extent of effective combustion—

- varied inversely with temperature owing to changing specific heats;
- exhibited no definite trend with increase of density but tended to decrease slightly; and
- reached a maximum at an air-fuel ratio of 10.

The time of reaction—

- varied inversely with temperature;
- varied directly with density; and
- reached a minimum at an air-fuel ratio of 10.

PRECISION OF RESULTS

Excellent agreement was generally obtained between records taken under the same conditions. With a $T_s - T_i$ period of 0.063 second, however, the variation in the time of reaction sometimes reached

50 percent. The usual variation of the maximum pressure was between 2 and 3 percent with a maximum variation of 10 percent. The maximum pressure could be measured within one-half atmosphere. Time intervals could be measured on the film drum to within 0.0005 second as the film drum was driven by a synchronous motor.

When a number of records were taken without cleaning the bomb, the time of reaction increased. The inside of the bomb was therefore never allowed to accumulate a coating of carbon but was cleaned very thoroughly after every few tests. At least one test for each condition was made with the clean bomb. The usual procedure was to make a test with the clean bomb and then to make several check tests with the bomb uncleaned but flushed thoroughly with air. The tabular data represent the average of at least three records for each recorded value; the conclusions result from the trends exhibited by approximately 650 individual records.

DISCUSSION

The validity of drawing analogies between the combustion in a fuel-injection engine and the combustion of a homogeneous mixture of fuel and air can be judged from these results. With respect to each variable considered—air temperature, air density, and air-fuel ratio—the behavior of the vapor-air mixture differs from that of the liquid-vapor-air mixture. It must not be forgotten, however, that the temperatures encountered in an engine at the moment of ignition are considerably higher than the corresponding temperatures used in these tests. When the initial density is comparable with densities in an engine (the two higher densities correspond to compression ratios of 7.9 and 11.8, respectively), the two types of explosion become more similar in behavior, particularly at the higher temperatures.

VARIATION IN TIMING

As the time between injection of the fuel and passage of the spark was increased, the rate of pressure rise decreased considerably, accompanied by an increase in the time between the spark and the start of pressure rise. The phenomena are similar to those found with the N. A. C. A. combustion apparatus (reference 2), and at the time of the reported tests an explanation was suggested on the basis of a change in the composition of the mixture with increased time due to vaporization and decomposition of the fuel. In the present tests, however, it is believed that the temperatures were too low for the occurrence of appreciable decomposition (references 9 and 10).

An analysis of the significance of the time variable presents the following potential effects: (1) change in distribution of fuel with a consequent change in the air-fuel ratio at the point of ignition; (2) increase in quan-

tity of fuel vaporized, which may involve a change in the ratio of air to fuel vapor, a greater predominance of the rate of homogeneous reaction over the heterogeneous liquid-air surface reaction if the latter exists, and perhaps a change in composition of the vapor because of preferential vaporization of certain components; (3) chemical reactions occurring before ignition, which include preflame oxidation, decomposition of the fuel, formation of highly activated molecules of very short life; and (4) change in the degree of turbulence, gradual decrease after the primary disturbance due to injection. Although no satisfactory explanation of the phenomena has been found, a brief discussion of the foregoing possibilities will be given here.

The first possibility was eliminated by the tests varying the air-fuel ratio. Although the rate of pressure rise varied with the air-fuel ratio, the initial rate for the delayed explosions, regardless of the air-fuel ratio, was never as great as it was for the short $T_s - T_i$ periods. Even the maximum rate of pressure rise of the delayed explosions did not exceed that of some of the short-interval ones, as shown by the records for an air density of 15 atmospheres and a $T_s - T_i$ period between 0.003 and 0.004 second in which the maximum rate of pressure rise was as great as the highest maximum rate obtainable with the delayed explosions, namely, that at an air-fuel ratio of 10. (See fig. 7.) The time lag preceding the start of pressure rise was longer for the delayed explosions. (See figs. 5 and 7.) These comparisons conclusively prove that the air-fuel ratio is not the sole cause of the variation in pressure rise observed with different timing.

The second possible explanation, a predominance of the homogeneous over the heterogeneous reaction, implies the existence of a greater percentage of the fuel in the vapor phase and also assumes that the rate of the homogeneous reaction is slower than that of the heterogeneous reaction (an assumption that is, a priori, very doubtful). At least qualitatively, an increase in temperature with the same $T_s - T_i$ period should be equivalent to increasing the $T_s - T_i$ period and holding the temperature constant. Quantitatively, the effect would depend somewhat upon the relative temperature coefficients of the reactions. It is obvious, however, from the data that an elevation of the initial temperature decreases the time and increases the rate of reaction; whereas an increase in the time interval between injection and spark has the reverse effect. It may therefore be concluded that an increase in the proportion of fuel in the vapor phase does not account for the decrease in the rate of reaction unless an increase in initial temperature in some way has an effect unrelated to vaporization that more than compensates the effect of increased vaporization.

The possibility of chemical reactions occurring before ignition was not investigated. Such reactions would normally be expected to increase the rate of

pressure rise with increased time before ignition as well as to shorten the lag between the spark and the start of pressure rise. In order to explain the observed phenomena, it is necessary to postulate a preflame reaction that is detrimental to the flame reaction. If the presence of highly activated, unstable, intermediate compounds were ascertained, whose concentration decreased with time due to their short life, the reaction might be expected to proceed more slowly as the $T_s - T_i$ period was lengthened. Various investigators have suggested the primary formation of such intermediate compounds (reference 10) but their existence as well as their behavior remains a controversial point.

Injection of the fuel undoubtedly introduces some turbulence in the medium; this turbulence decreases with increase of time after injection. Turbulence has been found to increase the rate of reaction (reference 11 and reference 12, p. 243). In an engine the amount of turbulence set up by the injection of the fuel is negligible in comparison with the turbulence induced by the air intake and the piston movement. Were the effects of the variation in timing in the bomb to be attributed solely to turbulence, it would be necessary to view them as phenomena entirely unrelated to the effects of variation of the injection advance angle on the rate of combustion in the N. A. C. A. combustion apparatus (reference 2).

EFFECT OF TEMPERATURE

When discussing the effect of temperature on an explosive reaction, the initial temperature of the mixture must be clearly distinguished from the temperature of the explosive reaction, that is, the flame temperature. The initial temperature is primarily significant in the initial stages of the reaction, particularly when a liquid fuel is used and when heat transfer and vaporization are of importance. As a result, the temperature has a much greater influence on the heterogeneous reactions, that is, the reactions in which the spark occurs very shortly after injection, than on the homogeneous reactions with a completely vaporized fuel. The term "homogeneous" as used here is meant to eliminate the possibility of a heterogeneous liquid-gas reaction, not a reaction at the wall of the bomb.

Temperature does, nevertheless, affect the rates of the fuel-vapor-air explosions (delayed explosions) somewhat and also affects the maximum pressure attainable, owing to changes in the specific heats of gases with temperature. The calculations of maximum pressure attainable, based on the specific heats given by Lewis and Randall (reference 7) and on the heat of combustion (10,400 calories per gram at 30° C.) determined by the National Bureau of Standards,

yield the following results for an air density of 5 atmospheres.

Temperature	P_{max}/P_i	
	Calculated	Experimental
°C.		
100	7.9	
150	7.0	6.2
200	6.3	5.7
250	5.8	5.3

Corrections have been made for the increase in the number of molecules on the assumption of complete combustion and for dissociation of carbon dioxide and water at the maximum temperature and pressure using Bjerrum's dissociation values (reference 12, p. 264) that check with the free-energy equations of Lewis and Randall (reference 7). After these computations were made, new values for thermodynamic quantities calculated from spectroscopic data were published (reference 13); the maximum pressures attainable were then recalculated using these values but the same results were obtained. Since the specific heats introduce an error of at least 10 percent in the calculations in addition to the error introduced by neglecting the heat loss, the experimental values obtained show good agreement with the calculated ones. The calculated values point out the variation to be expected with temperature.

It will be noted that for the explosions with short time intervals between injection and spark, the ratios of maximum to initial pressure fall far short of the theoretically attainable ones. For these explosions the ratio also increases slightly with temperature. These results are not surprising and merely indicate that distribution and vaporization play a significant part. The fact that density is much more effective than temperature in raising the P_{max}/P_i ratio may be correlated with the fact that density is much more effective than temperature in improving distribution. In the whole series the greatest effect of temperature occurs with a change from 100° to 150° C. at the lowest air density (5 atmospheres at 100° C.) where distribution is very poor. (See table I.)

It has already been observed that, regardless of the air density, no explosion would occur at 100° C. when the usual procedure of allowing 5 minutes to elapse between injection and spark was followed. It was thought that the vapor pressure of the fuel at this temperature might be too low, which would result in the formation of a mixture that was too lean to ignite. Calculations were made that yielded a value of 100 mm of Hg for the vapor pressure of hydrogenated safety fuel at 100° C. The calculations were based on empirical equations presented by Miss Elizabeth

Aldrich (paper presented at the S. A. E. summer meeting, 1932, entitled "The Vapor Pressures of Automotive Diesel Fuels"). If a molecular weight of 136 is assumed (this value corresponds to a formula $C_{10}H_{18}$ and agrees well with the percentage composition and lies in the correct boiling range for the pure hydrocarbons $C_{10}H_{22}$ and $C_{10}H_{14}$), the quantity of fuel that can be vaporized is 0.365 gram. This value corresponds to an air-fuel ratio of 23.3 at the highest density, which is beyond the value of 20.7 that marks the limit of ignition even at 200° C. Furthermore, the limit of ignition has been found to change with temperature, decreasing to 18.4 at 150° C., so that the possibility exists that at 100° C. a richer mixture than one with an air-fuel ratio of 15 would be required for ignition. From the vapor-pressure calculations it is seen that only at an absolute pressure of 5 atmospheres could a mixture richer than one with air/fuel = 15 be obtained; it was found that with an air-fuel ratio of 12.5 an explosion would occur with a delay period of 5 minutes at an initial temperature of 100° C.

Further calculations were made, using the equations given by Miss Aldrich, and it was found that at 150° C. approximately 1.5 grams of fuel could be vaporized in the bomb. A combustible mixture could therefore always be obtained at this temperature.

At temperatures of 150° C. or greater, ignition would take place with any time interval between injection and spark greater than 0.003 or 0.004 second. The effect of temperature on the maximum pressures and on the time of reaction was greater at the lower temperatures. Because of the contradictory data and the differences in experimental method of investigators in the field, it is difficult to interpret the significance of the effect of temperature. Mardles (reference 14) found an interesting correlation between the temperature coefficient of the nonflame oxidation and the knocking tendency of the fuel. A brief review of the effect of initial temperature found by other investigators will be found in reference 15.

EFFECT OF DENSITY

From physical considerations the most significant effect of air density is probably its influence on the distribution of the fuel. Lee (reference 16) has shown that the distribution of the fuel within the spray becomes more uniform as the density of the medium increases. The continued appearance of spots of deposited carbon on the walls of the bomb showed definitely that the sprays always impinged upon the walls; any increase in the density causing a corresponding decrease in the penetration would therefore improve the distribution throughout the bomb (reference 17).

Since the injection pressure is increased as the fuel quantity is increased, the atomization as well as the distribution is improved at the higher densities that correspond to the higher fuel quantities. The results are consistent with the expected improvement of distribution and atomization because a greater percentage of the total fuel is burned (higher P_{max}/P_i ratio) with increasing air density. The increased oxygen concentration at the higher densities would have no effect on the percentage of fuel burned, since the fuel concentration is increased to the same extent. The implication, however, is that the effect of the density on the distribution in the liquid phase caused the continual increase in the pressure ratios (P_{max}/P_i) for the explosions with short T_s-T_i periods. The ratio P_{max}/P_i for the delayed explosions decreased slightly as the density increased, which may be due to increased heat losses at the higher temperatures accompanying the higher pressures.

As the air density was increased, the time of reaction increased under certain conditions and decreased under others. For the delayed explosions the reaction time always increased with density. For the explosions with short T_s-T_i periods an increase in air density from 5 to 10 atmospheres caused a decided decrease in reaction time, again probably due to the influence of density on distribution in this range. At an initial temperature of 100° C. a further increase in density to 15 atmospheres caused a further decrease in reaction time but, at the higher temperatures, consistent with the general tendency to approach the behavior of the delayed explosions, the reaction time increased with further increase in density. In figure 8, the reaction time is plotted against the density for both types of explosion.

Fenning found both for methane-air explosions (reference 18) and for air-fuel-vapor (petrol, hexane, and benzene) explosions (reference 19) that the explosion time increased with density, just as it did in the present experimental work for the delayed explosions. In exploding CO-air mixtures at high initial pressures, Bone and Townend (reference 12, p. 282) noted a similar effect on the time of reaction as the initial pressure is increased. They offer an explanation of this phenomenon in the form of an energy-absorbing effect of nitrogen, which they claim is vitiated by the presence of hydrogen. This explanation, however, is not completely satisfying even for CO-air explosions and excludes hydrocarbon-air explosions in contradiction to Fenning's as well as to the present work.

AIR-FUEL RATIO

The difference between the vapor-air explosions and the liquid-vapor-air explosions is most clearly exhibited by the variation with air-fuel ratio of each type. For both types the air concentration was held constant.

In the homogeneous reactions (delayed explosions) the maximum pressure developed reached a maximum at an air-fuel ratio of 10. This maximum is beyond the theoretically correct mixture ratio of 15.6 and corresponds to an air-fuel ratio that is just sufficient to burn all the fuel to H_2O and CO . Dr. R. F. Selden, of this laboratory, has calculated the over-all energy of activation of the oxidation of safety fuel using the data at different air-fuel ratios. The calculations yielded a value of 31.1 kilogram-calories, which is of the correct order of magnitude.

The leanest mixture that will ignite varies with the temperature. As the limits of ignition are determined by the initial stage of the reaction, the initial temperature is a significant variable. The limits corresponded to air-fuel ratios of approximately 23, 21, 18.5, and 12.5 at temperatures of 250° , 200° , 150° , and $100^\circ C.$, respectively.

When the fuel was ignited 0.004 second after injection, the air-fuel ratio varied from point to point in the bomb and only qualitatively may it be said that the air-fuel ratio increased as the fuel quantity increased. In the immediate neighborhood of the spark the mixture must have been richer than that indicated by ratio of the air and fuel quantities because ignition would occur with an apparent air-fuel ratio of 25. The true air-fuel ratio at the ignition limit for the vapor-air explosions was 21 under the same conditions ($200^\circ C.$, 6.3 atmospheres absolute pressure). On the other hand, ignition could not be effected at an apparent air-fuel ratio of 5, although the vapor-air mixtures would explode at this ratio.

As the fuel quantity was increased in the heterogeneous mixtures at $200^\circ C.$, the maximum pressures developed upon explosion continuously increased and the time of reaction continuously decreased. The pressure rise per gram of fuel, however, decreased as the fuel concentration increased, probably because of poor distribution. The highest P_{max}/P_i ratio attained was 4.75 at an apparent air-fuel ratio of 7.5, but it is obvious that even in this case all the available oxygen was not consumed.

CONCLUSIONS

From the results obtained it must be concluded that the extent and rate of combustion of a fuel injected in the liquid state, particularly at low air temperatures and densities, are dependent upon the distribution and the condition of the fuel at the moment of ignition. At high air temperatures and densities, a marked similarity exists in the course of combustion of liquid fuel injected into the bomb and ignited immediately and that of a fuel allowed to vaporize completely before ignition.

LANGLEY MEMORIAL AERONAUTICAL LABORATORY,
NATIONAL ADVISORY COMMITTEE FOR AERONAUTICS,
LANGLEY FIELD, VA., August 9, 1935.

REFERENCES

1. Rothrock, A. M.: The N. A. C. A. Apparatus for Studying the Formation and Combustion of Fuel Sprays and the Results from Preliminary Tests. T. R. No. 429, N. A. C. A., 1932.
2. Rothrock, A. M., and Cohn, Mildred: Some Factors Affecting Combustion in an Internal-Combustion Engine. T. R. No. 512, N. A. C. A., 1934.
3. Rothrock, A. M., and Waldron, C. D.: Some Effects of Injection Advance Angle, Engine-Jacket Temperature, and Speed on Combustion in a Compression-Ignition Engine. T. R. No. 525, N. A. C. A., 1935.
4. Spanogle, J. A., and Foster, H. H.: Basic Requirements of Fuel-Injection Nozzles for Quiescent Combustion Chambers. T. N. No. 382, N. A. C. A., 1931.
5. Haslam, R. T., and Bauer, W. C.: Production of Gasoline and Lubricants by Hydrogenation. S. A. E. Jour., March 1931, pp. 307-314.
6. Schey, Oscar W., and Young, Alfred W.: Performance of a Fuel-Injection Spark-Ignition Engine Using a Hydrogenated Safety Fuel. T. R. No. 471, N. A. C. A., 1933.
7. Lewis, Gilbert Newton, and Randall, Merle: Thermodynamics. McGraw-Hill Book Co., Inc., 1923, p. 80.
8. Cragoe, C. S.: Thermal Properties of Petroleum Products. Misc. Publication No. 97, Bur. Standards, 1929.
9. Boerlage, G. D., and Van Dyck, W. J. D.: Causes of Detonation in Petrol and Diesel Engines. R. A. S. Jour., Dec. 1934, pp. 953-986.
10. Frey, F. E.: Pyrolysis of Saturated Hydrocarbons. Ind. & Eng. Chem., vol. 26, no. 2, Feb. 1934, p. 201.
11. Marek, L. F., and Hahn, Dorothy A.: The Catalytic Oxidation of Organic Compounds in the Vapor Phase. The Chemical Catalog Co., Inc., 1932, chap. XI.
12. Bone, William A., and Townend, Donald T. A.: Flame and Combustion in Gases. Longmans, Green & Co., Ltd., (London) 1927.
13. Lewis, Bernard, and von Elbe, Guenther: Heat Capacities and Dissociation Equilibria of Gases. Amer. Chem. Soc. Jour., vol. 57, 1935, pp. 612-614.
14. Mardles, E. W. J.: The Oxidation of Fuel Vapours in Air. Faraday Soc. Trans., vol. XXVII, Part II, Nov. 1931, pp. 681-721.
15. Brown, George Granger: The Relation of Motor Fuel Characteristics to Engine Performance. Dept. Eng. Research Bull. No. 7, Univ. Mich., May 1927.
16. Lee, Dana W.: Experiments on the Distribution of Fuel in Fuel Sprays. T. R. No. 438, N. A. C. A., 1932.
17. Joachim, W. F., and Beardsley, Edward G.: The Effects of Fuel and Cylinder Gas Densities on the Characteristics of Fuel Sprays for Oil Engines. T. R. No. 281, N. A. C. A., 1927.
18. Fenning, R. W.: Gaseous Combustion at Medium Pressures. Part I.—Carbon Monoxide-Air Explosions in a Closed Vessel. Part II.—Methane-Air Explosions in a Closed Vessel. R. & M. No. 998, British A. R. C., 1925.
19. Fenning, R. W.: Closed Vessel Explosions of Mixtures of Air and Liquid Fuel (Petrol, Hexane, and Benzene) over a Wide Range of Mixture Strength, Initial Temperature and Initial Pressure. R. & M. No. 979, British A. R. C., 1925.

REPORT No. 545

EFFECTS OF AIR-FUEL RATIO ON FUEL SPRAY AND FLAME FORMATION IN A COMPRESSION-IGNITION ENGINE

By A. M. ROTHROCK and C. D. WALDRON

SUMMARY

High-speed motion pictures were taken at the rate of 2,500 frames per second of the fuel spray and flame formation in the combustion chamber of the N. A. C. A. combustion apparatus. The compression ratio was 13.2 and the speed 1,500 revolutions per minute. An optical indicator was used to record the time-pressure relationship in the combustion chamber. The air-fuel ratio was varied from 10.4 to 365. The results showed that as the air-fuel ratio was increased definite stratification of the charge occurred in the combustion chamber even though moderate air flow existed. The results also showed the rate of vapor diffusion to be relatively slow.

INTRODUCTION

One of the advantages of the compression-ignition engine is that as the fuel quantity injected into the combustion chamber is decreased the air quantity inducted can remain constant so that the fuel is burned with a large excess of air. As a result, the combustion efficiency of the engine increases as the air-fuel ratio is increased. As the combustion efficiency increases the mechanical efficiency decreases; therefore the overall efficiency tends to remain constant. It is this fact that causes the fuel-consumption curve of the compression-ignition engine to show so little change for a wide range of load conditions.

Tests on compression-ignition engines have shown the fuel to auto-ignite with an estimated air-fuel ratio of about 1,000 (reference 1). In practice, an engine will use ratios as high as 70 to 80. Although the fuel is undoubtedly stratified at the high ratios so that the actual ratio in the combustible mixture is considerably lower, no information has been obtained on the extent of the stratification. Data on the stratification of the fuel may be obtained by exploring the combustion chamber with a gas-sampling valve such as that developed by Spanogle and Buckley (reference 2). High-speed motion pictures, such as those presented in reference 3, may be taken of the fuel spray and flame formation under conditions of varying air-fuel ratio. The present report discusses the results of tests made during the latter part of 1934 in which the motion-

picture method was used. These tests are part of a general program of research on combustion in a compression-ignition engine being conducted with the N. A. C. A. combustion apparatus. Reports describing other parts of this program are given in references 3, 4, 5, and 6.

APPARATUS AND METHOD

The data were obtained with the N. A. C. A. combustion apparatus (references 3 and 4) in conjunction with a special high-speed motion-picture camera described in reference 7. The combustion apparatus consists essentially of a single-cylinder test engine in which the sides of the combustion chamber are two 2.5-inch diameter glass windows. The engine has a bore of 5 inches, a stroke of 7 inches, and an intake-port height of one-half inch. After the apparatus has been brought to the desired speed by an electric motor, a single charge of fuel is injected into the combustion chamber. The engine is consequently operated under power for a single cycle. Figure 1 of reference 3 shows the apparatus with the indicator installed in one side of the combustion chamber. Figure 1 of the present report shows the apparatus with the windows in both sides of the chamber so that high-speed motion pictures may be taken of both the fuel sprays and the flame.

Since the tests presented in reference 3, the injection system has been altered by replacing the engine-operated pump with a reservoir in which the pressure is regulated with a hand pump. This change was made to increase the accuracy of the amount of fuel injected. The fuel quantity is varied by changing the pressure in the reservoir. The timing spark has been placed between the prismatic shutter on the camera and the film. With this arrangement the timing sparks at top center and 90° after top center are recorded on the film for each engine cycle.

A calibration curve of injection pressure against fuel quantity injected (fig. 2) was first obtained. Five separate discharges of fuel were weighed at each injection pressure. From this curve the injection pressure for the desired fuel quantity was chosen. The indicator was installed and two indicator cards were taken at the

given fuel quantity. The fuel-quantity weight was then checked and two series of high-speed motion pictures of the sprays and combustion were taken. The indicator was again installed and two more indicator cards taken.

The injection nozzle (fig. 3) has a smaller total area than that used in the tests described in reference 3 and, as a result, fuel was discharged from all six orifices.

The diesel fuel used in the tests was designated fuel 2 in reference 3. The fuel temperature was measured as the fuel left the injection valve through the hollow injection-valve stem.

indicator cards taken before and after the photographing of the fuel and the spray agreed very well, generally within the width of the recorded line. Originals of similar cards have been reproduced in reference 3. The flame pictures showed variation in both the positions of flame start and in the flame spread. Nevertheless, all the general characteristics were reproduced in both runs for any one condition. In each case the photographs reproduced in this report appeared to be representative.

The air quantity was estimated from the air temperature and pressure in the cylinder at the start of the

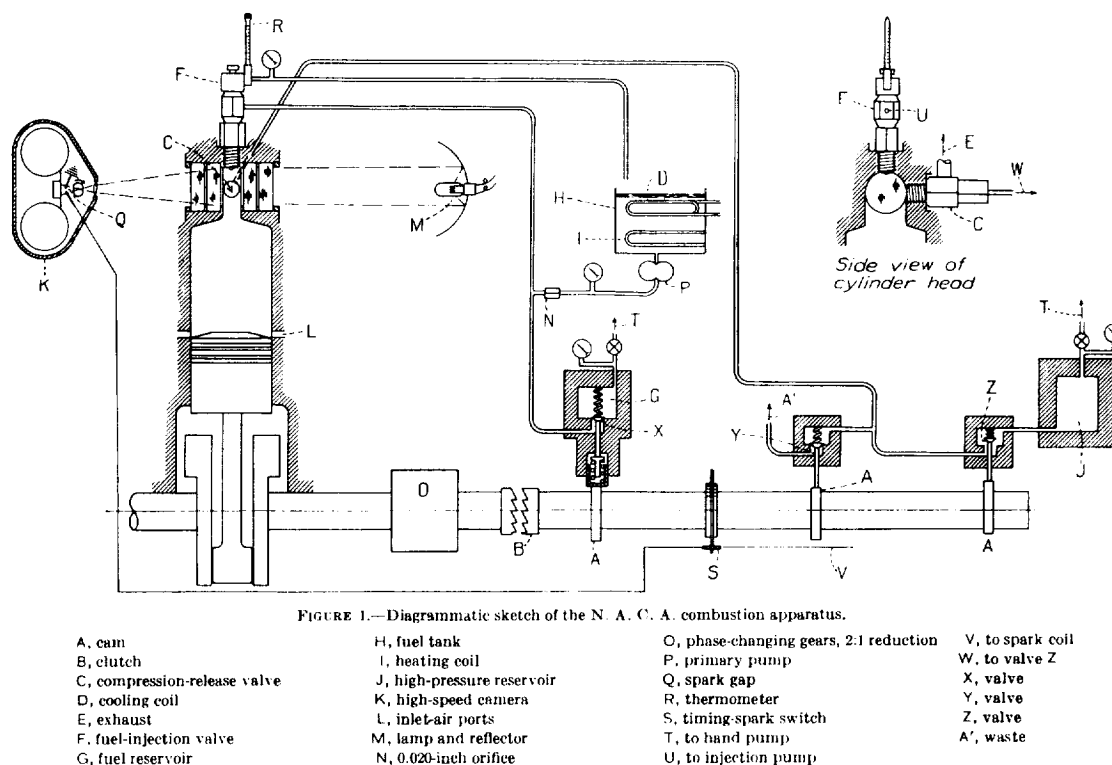


FIGURE 1.—Diagrammatic sketch of the N. A. C. A. combustion apparatus.

The following test conditions were maintained constant:

Engine speed.....	1,500 r. p. m.
Engine-jacket temperature.....	150° F. \pm 5°.
Fuel temperature at injection valve.....	110° F. \pm 2°.
Compression ratio (based on 6.5-inch stroke):	
With indicator installed.....	13.9.
With glass windows in each side.....	13.2.

The value of 150° F. for the engine-jacket temperature was that of the outgoing temperature of the glycerin used to heat the jacket; this temperature was measured both at the cylinder and at the combustion chamber. The incoming temperature of the glycerin was about 10° higher than the outgoing.

The curve of figure 2 shows that the fuel quantities did not vary more than ± 3 percent. The weighing of the fuel just before each run served as a check. The

compression stroke and from the displacement of the engine. The temperature of the air was assumed to be between that of the room, approximately 85° F., and that of the engine jacket. The air pressure at the time the intake ports were closed was assumed to be 750 millimeters of mercury.

The start of the injection was determined by injecting against a paper mounted on the flywheel of the engine. When the injection valve was mounted in the engine, however, the injection-valve opening pressure was decreased somewhat because of the force exerted by the air pressure on the end of the injection-valve stem. As a result the timing at the small fuel quantities was advanced. The injection start therefore increased from about 9° before top center at the lowest air-fuel ratio to about 15° before top center at the highest air-fuel ratio. This decrease in the injection-valve opening pressure also increased by an unknown

amount the fuel quantity injected. Comparison of the indicator cards with cards from an engine indicates that the increase was insufficient to affect the precision of the results.

RESULTS AND DISCUSSION

The reproductions of the indicator cards are shown in figure 4. When the air-fuel ratio was increased from 10.4 to 13.0, the maximum cylinder pressure showed a slight increase, possibly because less heat was given to the unburned fuel. As the ratio was

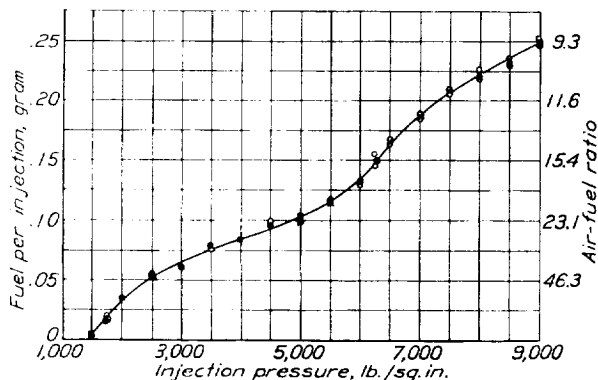


FIGURE 2.—Calibration of the fuel-injection system of the combustion apparatus.

further increased, the maximum cylinder pressure and the power output decreased. When considering the effect of air-fuel ratio on the thermal efficiency of the engine, two factors must be considered: the combustion efficiency and the cycle efficiency. It must also be remembered that there are two fluids entering into the chemical reaction, the fuel and the air. In order to obtain the maximum and most efficient heat input both fluids must be completely utilized. With the

tion of the fuel in the air. Figure 5 is a composite from prints of the original 16-millimeter film¹ taken with the high-speed motion-picture camera. Figures 6 to 9 are enlargements of the photographs of the fuel sprays and the initial flame formation. In the assembly of figure 5 the top center may vary by half a frame width because the strips of film were alined so that the photographs are directly under each other. In the enlargements the true top centers are used.

When an excess of fuel was injected into the combustion chamber (figs. 5 and 6), the sprays penetrated across the visible portion of the chamber. The two outside sprays from the smallest orifices are difficult to

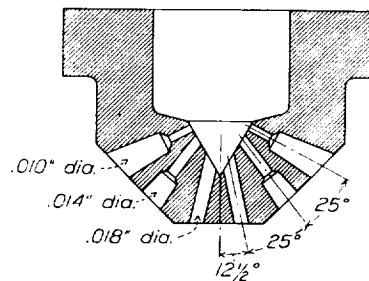


FIGURE 3.—The 6-orifice injection nozzle.

distinguish because they are very close to the edge of the chamber. The flame fills most of the chamber for 6 or 7 photographs, 22 to 25 crankshaft degrees. The chamber then starts to become fogged and the flame is either slowly obscured by the smoke or dies out; the flame finally disappears at 90° after top center or later. From a fuel-air ratio of 17.2 to one of 25.7, the duration of the maximum flame spread seems to increase, reaching a value of about 30 crankshaft degrees. These data compare favorably with the data shown in figure 14 of reference 9 in which the rate of

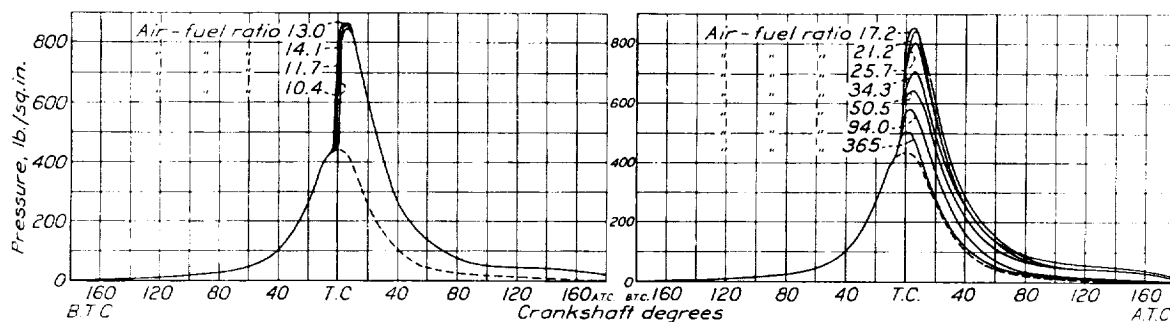


FIGURE 4.—Effect of air-fuel ratio on instantaneous pressures in the combustion chamber.

present knowledge of methods of distributing the fuel in the combustion chamber, either fluid can be completely utilized only at the expense of an excess of the other. Of course, in practice the air is present in excess because a low specific fuel consumption is more important than a low specific air consumption.

The photographs of the fuel sprays and of the combustion (figs. 5 to 9) indicate the extent to which both fuel and air are utilized and also indicate the distribu-

tion of the fuel in the air. Figure 5 is a composite from prints of the original 16-millimeter film¹ taken with the high-speed motion-picture camera. Figures 6 to 9 are enlargements of the photographs of the fuel sprays and the initial flame formation. In the assembly of figure 5 the top center may vary by half a frame width because the strips of film were alined so that the photographs are directly under each other. In the enlargements the true top centers are used.

¹ The motion-picture film is available on loan. (See reference 8.)

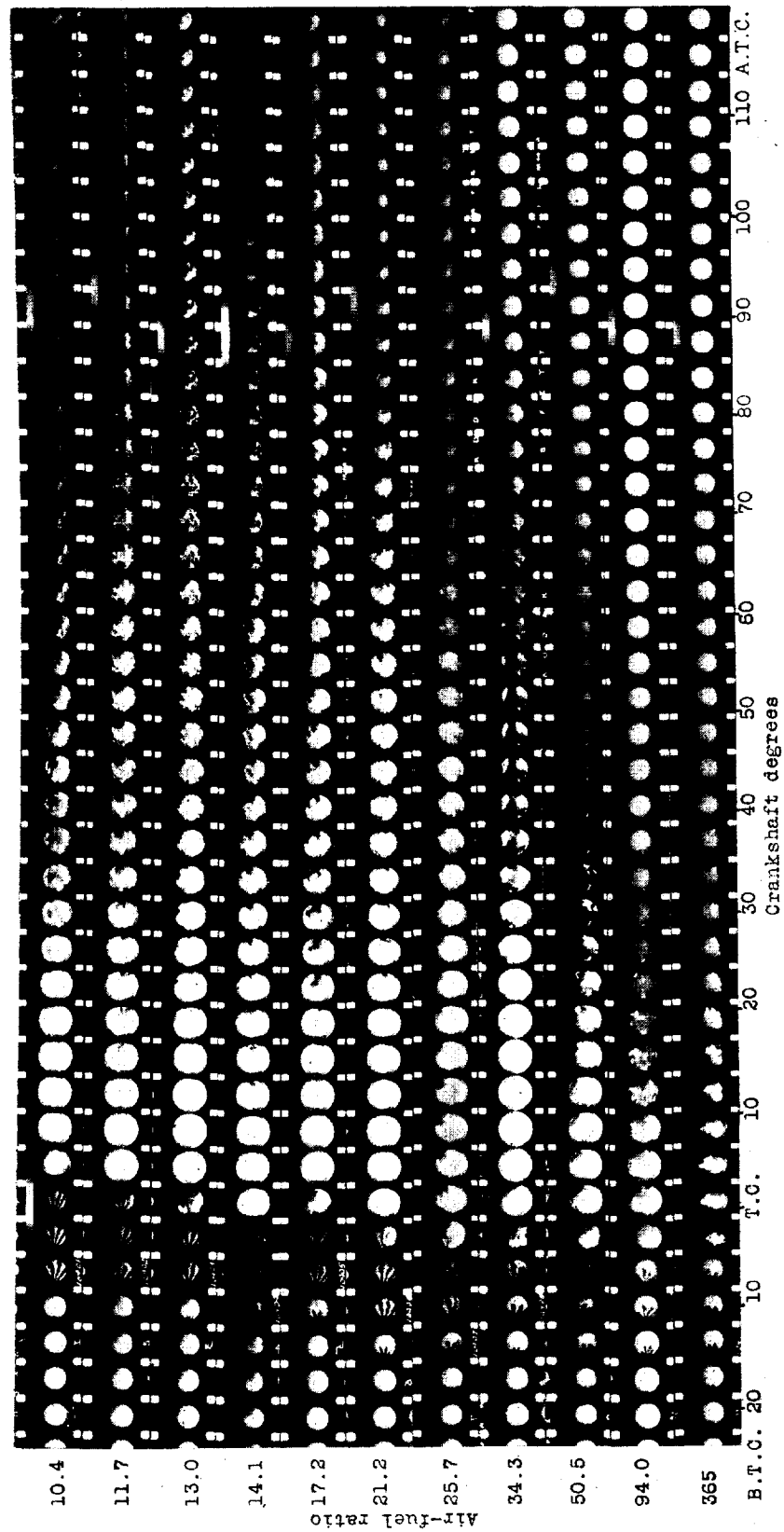


FIGURE 5.—Effect of air-fuel ratio on fuel spray and flame formation.

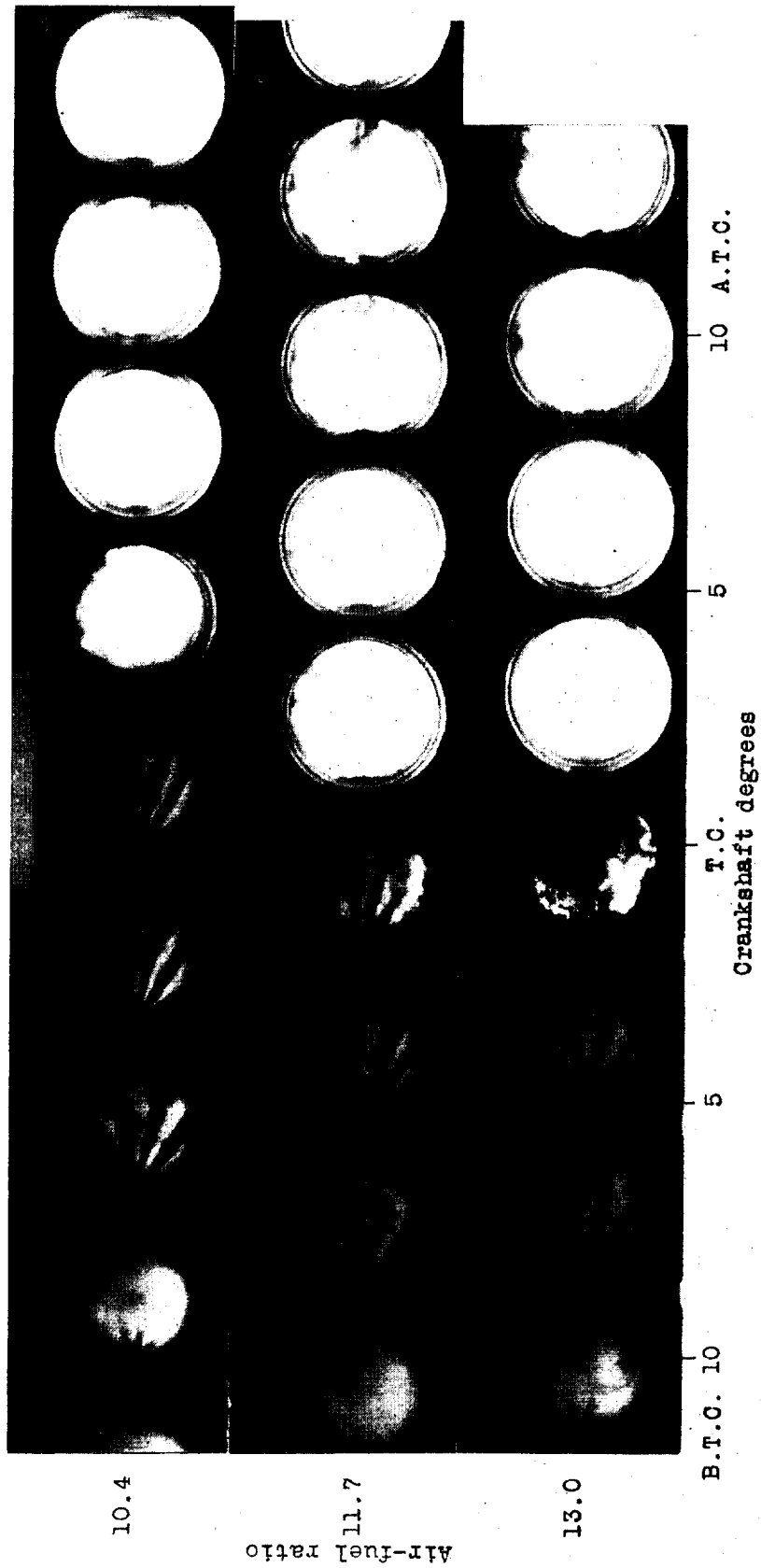


FIGURE 6. Enlargements of photographs of fuel sprays and first part of flame for air-fuel ratios from 10.4 to 13.0.

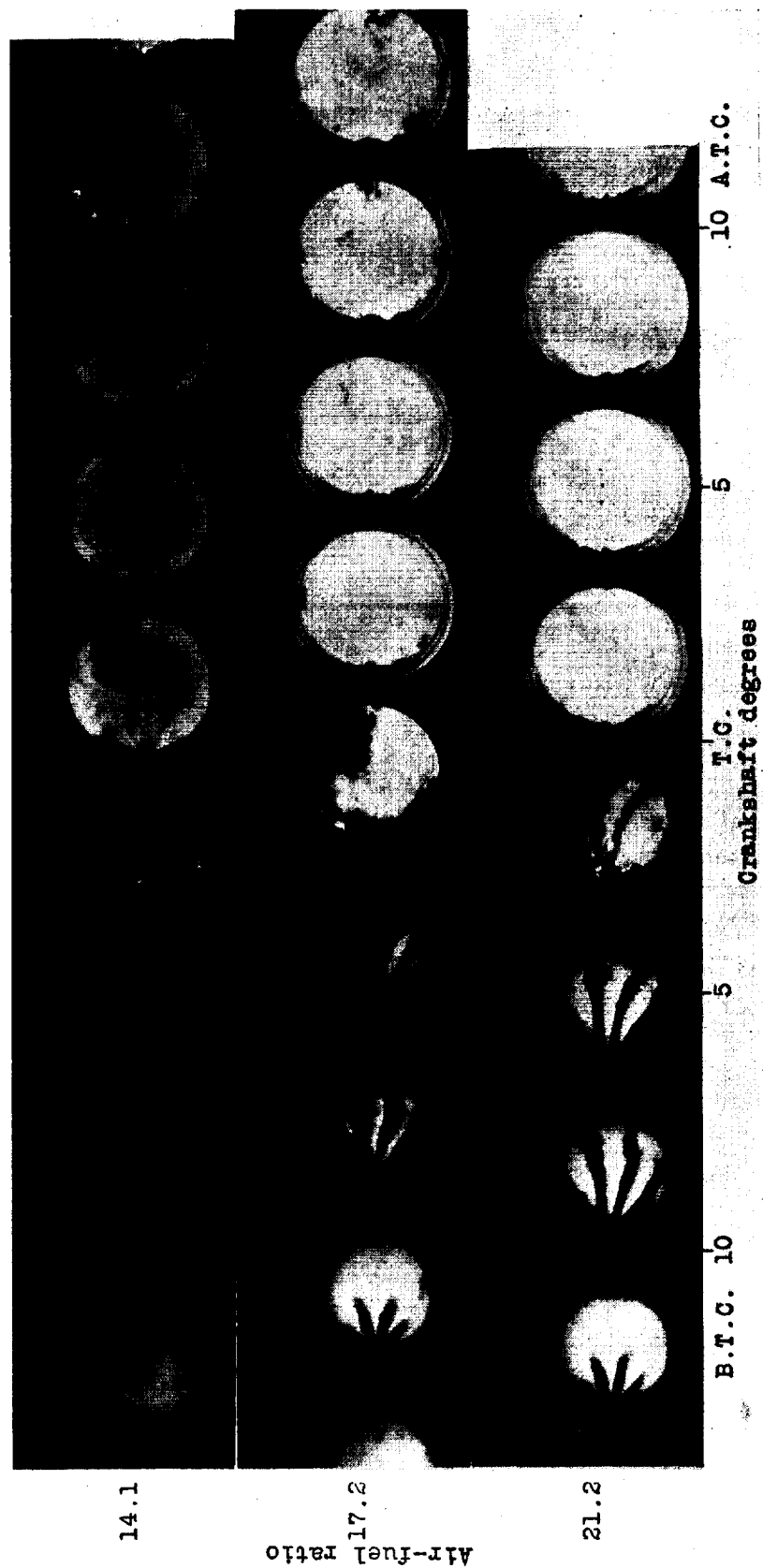


FIGURE 7.—Enlargements of photographs of fuel sprays and first part of flame for air-fuel ratios from 14.1 to 21.2.

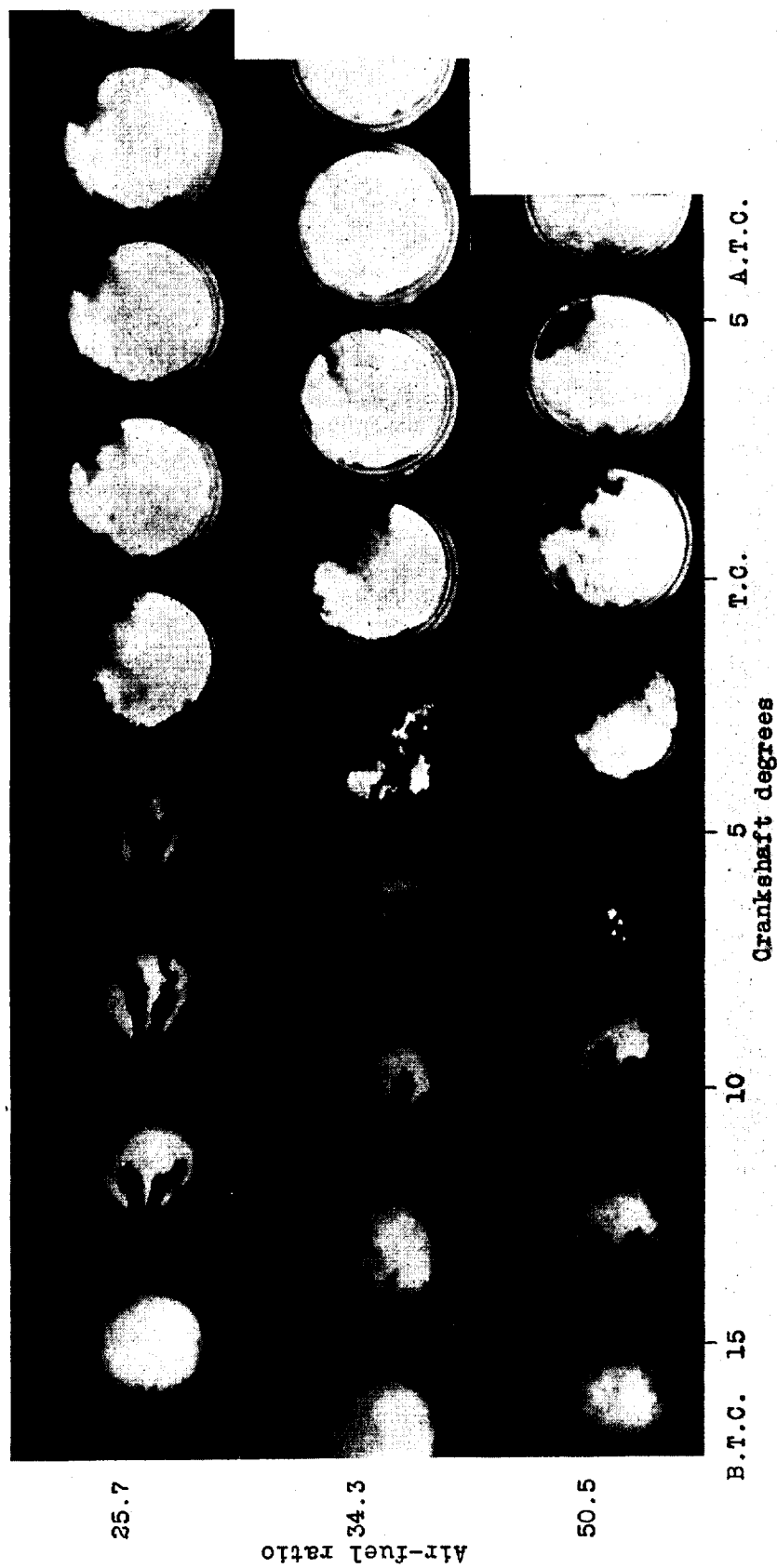


FIGURE 8.—Enlargements of photographs of fuel sprays and first part of flame for air-fuel ratios from 25.7 to 50.5.

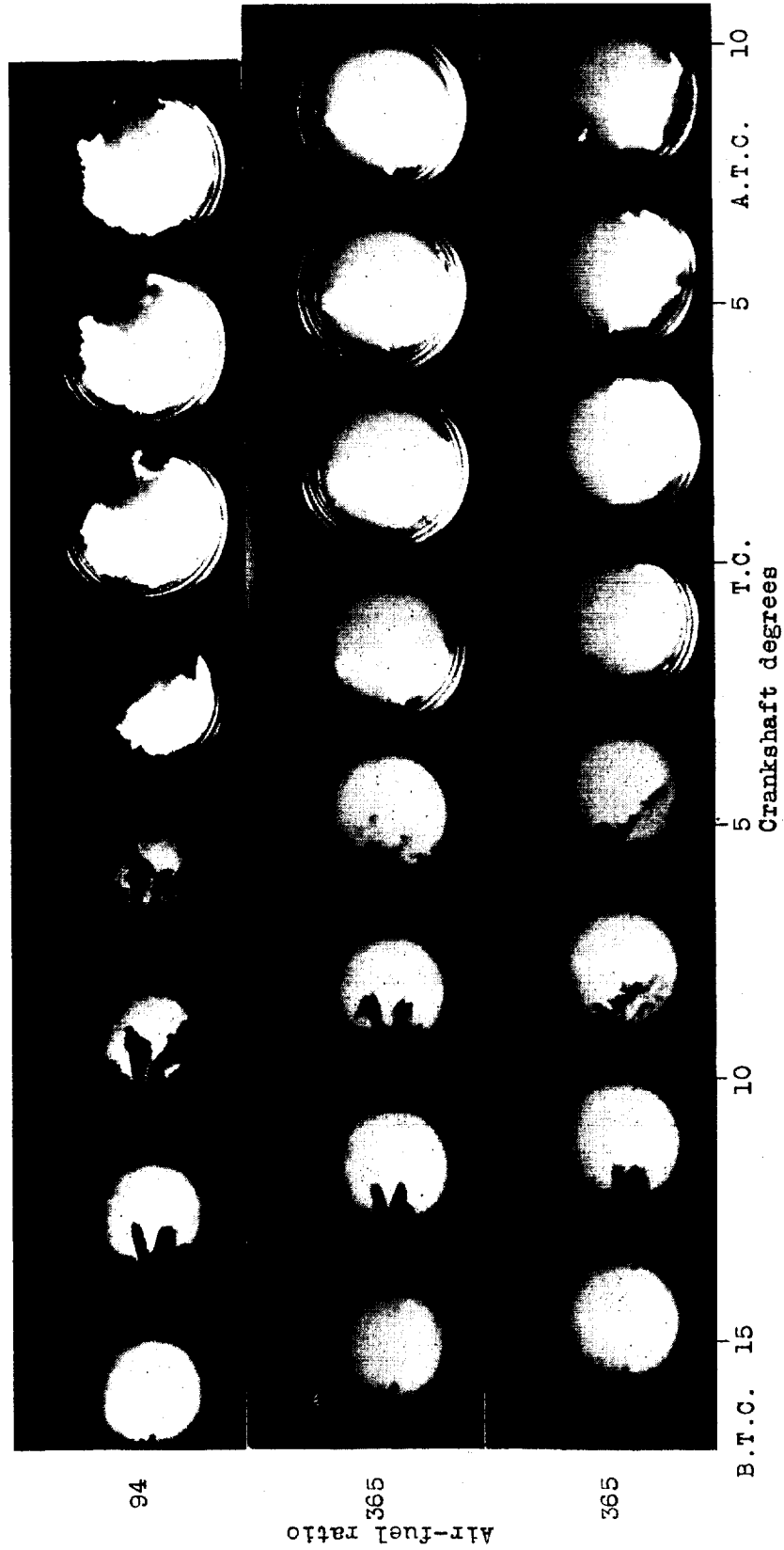


FIGURE 9 - Enlargements of photographs of fuel sprays and first part of flame for air-fuel ratios from 94 to 365.

smoke. The end of the appearance of the flame also occurred earlier in the cycle. These results indicate that both the combustion efficiency and the cycle efficiency are increased as the fuel quantity is decreased. Computations made of data obtained on a test engine at the same time that the data presented in reference 9 were obtained showed that as the air-fuel ratio was increased from 15.4 to 31.8 the combustion and cycle efficiencies were increased, respectively, from 70 and 44 percent to 84 and 49 percent, causing an increase in the indicated thermal efficiency of from 31 to 41 percent.

The enlargements (figs. 6 and 7) show that there was little change in either the spray or the initial-flame formation as the air-fuel ratio was increased from 10.4 to 21.2. It is interesting to note that the burning is always recorded as starting in more than one place. Also, in those series of photographs in which the start of burning is not recorded, the fuel sprays at the injection nozzle are still visible after the flame has filled most of the portion of the chamber between the glass windows. There is a tendency for a small portion of the chamber to remain free of flame, but otherwise the chamber is surprisingly well filled. The sprays show no appreciable effect of any air flow persisting in the chamber although there is some air movement, probably caused by the air entering through the intake ports.

At an air-fuel ratio of 21.2, a slight decrease in spray penetration is noticed. This decrease becomes more marked until at a ratio of 365 the sprays penetrate to a distance of only about 1 inch. The stratification of the charge becomes noticeable at a ratio of 25.7 and is very marked at the ratios of 94 and 365 (figs. 8 and 9). The sprays at the three highest ratios show marked effects of air movement, being blown to the left side of the chamber (the bottom in the figures). Comparing the two series of photographs for a ratio of 365 shows that this effect is not constant. The second series at this ratio shows clearly how the flame appears in that part of the chamber in which the spray last appeared and that the flame spreads to a slightly larger area than that covered by the spray just before it disappeared because of its vaporization.

CONCLUSIONS

The results presented show that definite stratification of the fuel charge does occur in the combustion

chamber of the compression-ignition engine even though moderate air flow exists. The start of burning relative to the fuel sprays is not affected by the air-fuel ratio, nor is the rate of flame spread greatly affected by the ratio.

The results at the higher ratios showed that the rate of diffusion of the gases in the combustion chamber, as indicated by the flame spread after the maximum pressure has been reached, was relatively slow. This result in itself indicates why it is difficult to obtain a good mixture of the air and fuel in the combustion chamber of a compression-ignition engine.

LANGLEY MEMORIAL AERONAUTICAL LABORATORY,
NATIONAL ADVISORY COMMITTEE FOR AERONAUTICS,
LANGLEY FIELD, VA., August 26, 1935.

REFERENCES

1. Spanogle, J. A.: A Comparison of Several Methods of Measuring Ignition Lag in a Compression-Ignition Engine. T. N. No. 485, N. A. C. A., 1934.
2. Spanogle, J. A., and Buckley, E. C.: The N. A. C. A. Combustion Chamber Gas-Sampling Valve and Some Preliminary Test Results. T. N. No. 454, N. A. C. A., 1933.
3. Rothrock, A. M., and Waldron, C. D.: Some Effects of Injection Advance Angle, Engine-Jacket Temperature, and Speed on Combustion in a Compression-Ignition Engine. T. R. No. 525, N. A. C. A., 1935.
4. Rothrock, A. M.: The N. A. C. A. Apparatus for Studying the Formation and Combustion of Fuel Sprays and the Results from Preliminary Tests. T. R. No. 429, N. A. C. A., 1932.
5. Rothrock, A. M., and Waldron, C. D.: Fuel Vaporization and Its Effect on Combustion in a High-Speed Compression-Ignition Engine. T. R. No. 435, N. A. C. A., 1932.
6. Rothrock, A. M., and Cohn, Mildred: Some Factors Affecting Combustion in an Internal-Combustion Engine. T. R. No. 512, N. A. C. A., 1934.
7. Tuttle, F. E.: A Non-Intermittent High-Speed 16 mm Camera. Soc. Motion Picture Eng. Jour., vol. XXI, no. 6, December 1933, pp. 474-477.
8. Rothrock, A. M., Buckley, E. C., and Waldron, C. D.: Effect of Air-Fuel Ratio on Combustion in a High-Speed Compression-Ignition Engine. Technical Film No. 3, N. A. C. A., 1935.
9. Rothrock, A. M.: Combustion in a High-Speed Compression-Ignition Engine. T. R. No. 401, N. A. C. A., 1931.

REPORT No. 546

THE EFFECT OF TURBULENCE ON THE DRAG OF FLAT PLATES

By G. B. SCHUBAUER and H. L. DRYDEN

SUMMARY

In determining the effect of turbulence on the forces exerted on bodies in the air stream of a wind tunnel, it is commonly assumed that the indications of the standard pitot-static tube used to determine the air speed are not dependent on the turbulence. To investigate the truth of this assumption, the drag of a normally exposed flat plate, the difference in pressure between the front and rear of a thin circular disk, the rate of rotation of a vane anemometer, and the pressure developed by a standard pitot-static tube were measured in an air stream for several conditions of turbulence. The results may be interpreted as indicating that there is no appreciable effect of turbulence on the vane anemometer and the standard pitot-static tube, but that there is a small effect on the drag of a flat plate and the pressure difference between front and rear of a disk. This drag was found to be independent of the speed or Reynolds Number and hence the observed turbulence effect is of a different nature from the effects observed on skin-friction plates and air-ship hulls or on spheres.

This work was conducted by the National Bureau of Standards with the cooperation and financial assistance of the National Advisory Committee for Aeronautics.

INTRODUCTION

It is now well known that all aerodynamic measurements are to some extent dependent on the magnitude of the small fluctuations of speed, collectively called "turbulence", which are present in the air stream. The effects of turbulence are supposed to be related to the effects of Reynolds Number in that both are the expression of the same basic phenomenon. A brief summary of the status of knowledge in April 1934 is given in reference 1.

In determining the effect of turbulence and Reynolds Number on aerodynamic force coefficients for various body forms, it is assumed that the force on the body is affected by turbulence and Reynolds Number, but that the pressure developed by the standard pitot-static tube, from which the dynamic pressure q ($= \frac{1}{2} \rho V^2$ where ρ is the density and V the speed of the air stream) is computed, is not. In support of this assumption it is often possible to point to changes in

pressure and velocity distribution about the body, indicating with little doubt that the force on the body also changes. While it has been possible to show, by means of whirling arm tests, that the pressure difference obtained from the standard pitot-static tube is equal to the dynamic pressure q over the usual range of Reynolds Number (reference 2), no such fundamental test has been devised to show that this pressure difference is the same as q when the air is turbulent. It is generally assumed that turbulence can have little or no effect on the readings as long as the direction changes introduced by the turbulent motions are not over 3° (turbulence about 5 percent). The effect on the boundary layer about the static orifices in the wall of the tube is certainly negligible.

The drag coefficient ¹ for a flat disk normal to the wind is constant over part of the range of Reynolds Numbers.² The explanation of this fact is simply that the separation lines must lie at the edges of the plate and consequently cannot shift as the Reynolds Number changes. The same kind of reasoning would deny the possibility of a turbulence effect, and indeed the argument appears to be as strong as that advanced in the case of the pitot-static tube.

In the course of some investigations at the National Bureau of Standards in 1932, an attempt was made to test the correctness of a calibration for the wall orifice of the $4\frac{1}{2}$ -foot wind tunnel, used to indicate the speed of the air stream, by measuring the drag coefficient for a 2- by 12-inch rectangular flat plate placed normal to the wind. The stream had been previously made very turbulent by placing a screen with loosely attached aluminum tags across the upstream section of the tunnel. The drag coefficient was found to be higher than that obtained in some earlier work. A check calibration of the wall orifice against the standard

¹ The drag coefficient is equal to the drag divided by q and by the area of the plate.

² In the early experiments of Eiffel and others, various sources of error, such as tunnel wall effects, spindle interference, and lack of geometrical similarity, were not recognized and an apparent variation with Reynolds Number was found. The careful experiments of C. Wieselsberger described in *Ergebnisse Aerodyn. Versuchsanstalt, Göttingen, II*, p. 25, show that there is no variation as great as 1 percent between a Reynolds Number of 10,000 and 1,000,000 for the circular disks tested. In other experiments, some variation is found. It is the opinion of the authors that all of the published data considered together supports the conclusion that the drag of a given thin flat plate with sharp square edges is independent of Reynolds Number in the range 10^4 to 10^6 .

pitot-static tube showed that the calibration was not at fault. Later when the screen was removed and the turbulence was much lower, the drag determination was repeated. In this case the drag coefficient was lower and agreed well with earlier values. The difference in the two results appeared to be an effect of turbulence, but whether on the plate or the pitot-static tube was not known. Since the speed was not equally uniform over the area occupied by the plate in the two cases, and accordingly the difference in results might have been due to the failure to get a correct average calibration for the region occupied by the plate, the data were not considered to be conclusive.

For this reason it was decided to investigate the turbulence effect more fully before reporting it. The object of the present investigation was to repeat the earlier work under a greater variety of conditions, paying close attention to speed distribution in every case, and to obtain data which would show whether the effect was on the flat plate or the standard pitot-static tube.

METHOD OF PRODUCING TURBULENCE

Before the present investigation was begun, considerable attention had been given to methods of varying the turbulence of the 4½-foot wind tunnel of the National Bureau of Standards. The placing of square-mesh screens, made from cylindrical wires or rods, over the entire cross section of the tunnel at some upstream position, was found to be satisfactory both from the standpoint of turbulence production and uniformity of speed (reference 3). In order to avoid a regular pattern in the speed distribution from the individual wires, it was necessary to work at distances greater than 65 wire diameters from the screens. These screens were installed one at a time and the turbulence measured at several distances back of each of them by the "hot-wire" method (reference 4).

Turbulence measured by this method is expressed as the ratio of the root-mean-square of the speed fluctuation at a point to the average speed. This quotient times 100 is termed the percentage turbulence. Values of the turbulence back of the two screens used in the present investigation are shown in figure 1.

TEST EQUIPMENT AND PROCEDURE

Since the aerodynamic balance used in the 4½-foot tunnel was fixed in position, and it was not practicable to change the position of the screens, measurements of the drag coefficient for the 2-by 12-inch flat plate could be made only at 2.7 and 1.1 percent turbulence with the screens and 0.7 percent for the free tunnel condition.

In order to get a device to indicate the presence or absence of the effect over a wider range of turbulence, the so-called "pressure disk" shown in figure 2 was devised. This is simply a 3-inch disk with one orifice

at the center of the front face and four others at the back where the supporting spindle is connected to the plate. By means of these orifices, the pressure difference across the plate can be determined. This difference, denoted by Δp , when divided by q yields a pressure coefficient, which should vary with turbulence somewhat like the drag coefficient. It was not intended that the drag coefficient be determined from the pressure coefficient. This would be a very doubtful procedure. The work on the disk was intended to bring out independent evidence of the effect on drag coefficients by another method. Both the 2-by 12-inch plate and the 3-inch disk had sharp square edges. The thickness of the plate was 0.046 inch and that of the disk 0.043 inch.

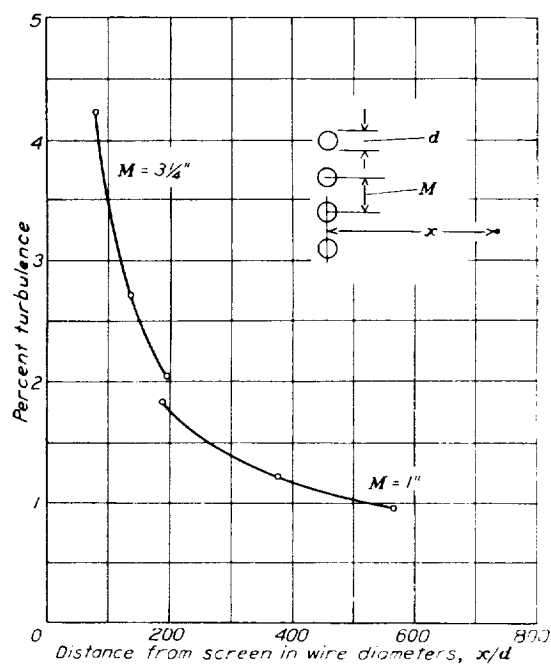


FIGURE 1. Variation of percentage turbulence with distance from screens. Distance expressed in wire diameters.
 $d = 0.625$ inch for 3/4-inch mesh
 $d = 0.192$ inch for 1-inch mesh

Being faced with the problem of deciding whether to place the effect of turbulence on the flat plate or the pitot-static tube, it was desirable to obtain an entirely independent indication of the speed at the position where the pitot-static tube and the flat plates were run. A vane anemometer³ (shown in fig. 2) having about the same diameter as the pressure disk was used for this purpose. The anemometer was not to be used to measure the air speed, but rather the speed indicated by it was to be compared with that indicated by the pitot-static tube, as in a calibration of the instrument.

³ Vane anemometer built by Davis Instrument Co. Eight-blade, low-speed type, rated at 3,000 feet per minute maximum speed.

Working positions back of the two screens were selected according to the amount of turbulence desired. At any given position the procedure consisted of making three separate sets of runs covering a given speed range, one on the pressure disk, another on the vane anemometer, and still another on the standard pitot-static tube. Taking the pitot-static tube as an example, a run consisted of reading the manometer to which the pitot-static tube was connected simultaneously with another manometer connected to the tunnel wall orifice. The factor obtained from the ratio of the two readings amounted to a calibration factor for the wall orifice, to be used to obtain the value of q and hence of the air speed when the pitot-static tube was removed. Having calibrated the wall

In connection with the force measurements a similar procedure was followed at the position determined by the balance. The pitot-static tube runs in this case were distributed over the area occupied by the 2- by 12-inch plate, and the vane anemometer was calibrated at the position later occupied by the center of the plate. Both were run with the shielded balance arm protruding into the stream.

The force measurements were made on a balance of the N. P. L. type. The plate was attached to the shielded balance arm by a spindle 9 inches long fastened rigidly to one end of the plate. The drag of this spindle was determined by making a separate run with a dummy spindle attached to the balance and with the plate mounted separately above it. By deducting

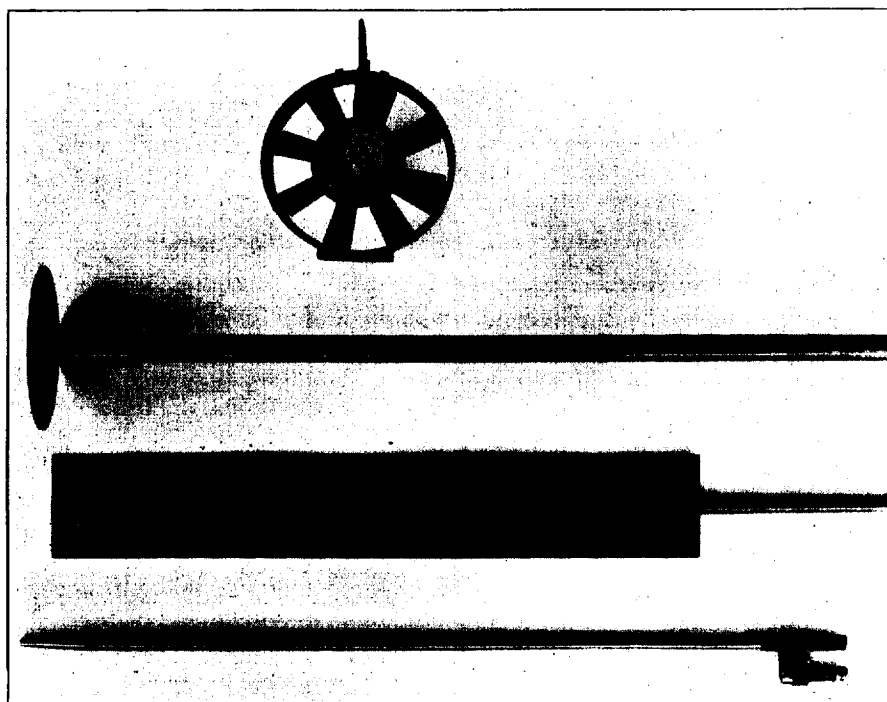


FIGURE 2. - Vane anemometer, 3-inch pressure disk and spindle, 2- by 12-inch flat plate and spindle, and standard pitot-static tube.

orifice, readings from it, taken simultaneously with those from the pressure disk, allowed $\Delta p/q$ to be calculated. Similarly, in calibrating the vane anemometer, readings from the wall orifice were used to indicate the air speed. Hence the results are expressed in terms of the speed indicated by the pitot-static tube, assuming no effect of turbulence.

The disk and vane anemometer responded to the average conditions over an area, presumably over their frontal area. The indications of the pitot-static tube were obtained therefore at a number of points over the areas swept out by the disk and the anemometer in order to obtain a similar integrated effect. Measurements were made at the center of this area and at several points on a 1- and 2-inch radius.

the spindle drag from the drag of the plate and spindle combined, the drag of the plate alone was obtained. The interference of the spindle on the plate drag was not corrected for by this procedure, but a preliminary investigation showed that this interference was too small to be detected.

RESULTS

Great care was taken to secure accurate values of the mean velocity pressure over the area to be occupied by the plate or anemometer at a given reading of the manometer connected to the wall orifice. Thus, for the 2- by 12-inch plate, readings were taken at 7 points for 6 speeds. Considering the results obtained with the $3\frac{1}{4}$ -inch screen, the average deviation of a single

observation from the mean at any one point was about 0.5 percent, the maximum deviation 1 percent. For all points considered together, the average deviation was 1 percent, the maximum 2 percent. It seems

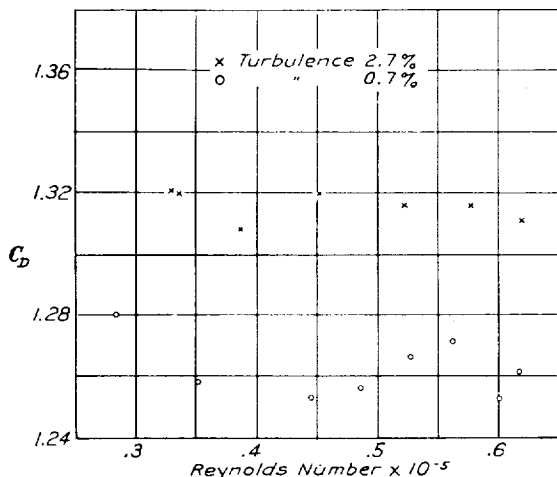


FIGURE 3.—Drag coefficients for 2-by-12-inch flat plate for various Reynolds Numbers. The length term in the expression for Reynolds Number is the width of the plate, i. e., 2 inches.

conservative, taking account of "sampling" errors, to assume that the mean value for the 42 points is equal to the correct average over the area of the plate within 0.5 percent. The probable error computed by con-

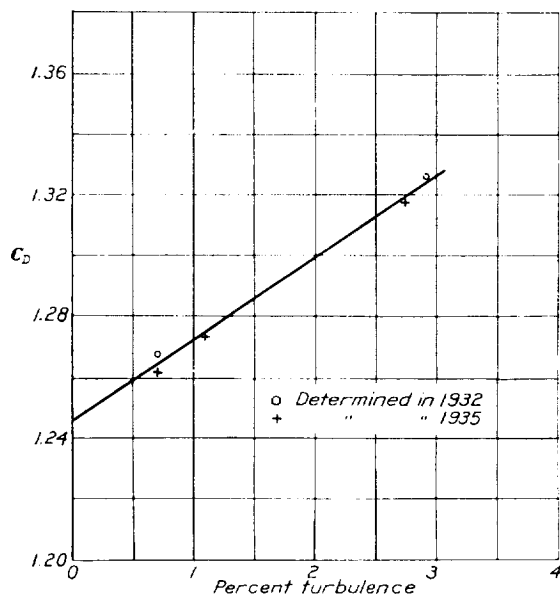


FIGURE 4.—Relation between percentage turbulence and drag coefficient for 2-by-12-inch flat plate. $C_D = \frac{D}{qS}$, where S =area of plate, q =dynamic pressure, and D =drag.

sidering the 42 observations as being made on the same quantity is only 0.1 percent.

The deviations which have been given for the $3\frac{1}{4}$ -inch screen represent the worst condition. Over smaller

areas and with the 1-inch screen or with no screen, the deviations were much smaller, and a fair average value of the mean deviation for those conditions would be about 0.3 percent.

Two series of determinations of the drag coefficient of the rectangular plate are shown in figure 3. Whereas there is no definite variation of the drag coefficient with Reynolds Number over the range from 30,000 to 60,000, there is a marked change in the coefficient with turbulence. This variation with turbulence is shown more clearly in figure 4 where the coefficients have been averaged over the Reynolds Number range and plotted against turbulence. Determinations made in 1932, shown on the same figure, agree well with those

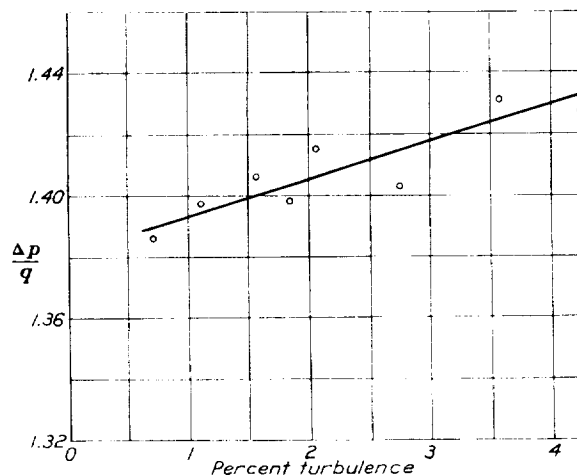
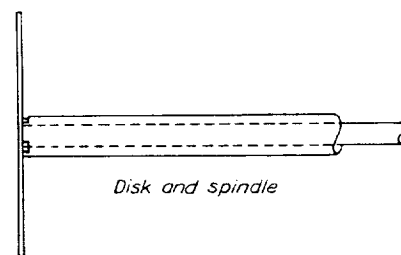


FIGURE 5.—Relation between percentage turbulence and pressure coefficient for 3-inch diameter disk.

of 1935. Extrapolating to zero turbulence, we find a drag coefficient of 1.246. Since wind tunnels may vary in turbulence from near zero to 2 percent or possibly more, a dispersion among results in various tunnels of perhaps 4 percent may be expected. This is nothing like the disagreement found in sphere drag results; nevertheless it is enough to be of importance in precise work.

Figure 5 shows the variation of the pressure coefficient of the pressure disk with turbulence. While the scatter in this diagram is considerable, there is a definite upward trend to the coefficient with increasing turbulence. Here again the coefficient was independent of the speed.

We may contrast the results for the plates with those shown in figure 6 for the vane anemometer. Here there is no evidence of any dependence of the

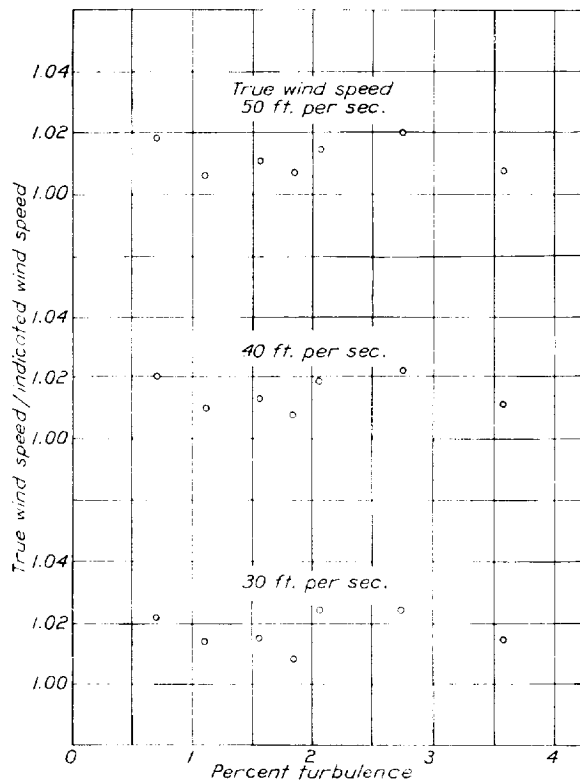


FIGURE 6.—Calibration of vane anemometer for various amounts of turbulence.

calibration factor on turbulence. This means either that the indications of the anemometer and the pitot-static tube both vary with the turbulence in such a way as to mask any effect, or that there is no turbulence effect on either instrument. Since the two

are radically different both in construction and principle of operation, it seems very unlikely that turbulence should affect the two alike. Hence the conclusion: Both the pitot-static tube and the vane anemometer are free from any effect of turbulence. The dynamic pressure q is therefore determined correctly by the pitot-static tube, and the variation of the flat plate coefficient is due to the effect of turbulence on the plate itself.

It is usual to attribute the effect of wind-tunnel turbulence on aerodynamic forces to a shift in the point of transition from laminar to turbulent boundary-layer flow. The result is a different skin friction and a different separation point. It is difficult to see how this explanation can be applied in the case of the flat plate. We have here a case where the turbulence apparently affects the wake of the plate; or, if we wish to imagine a separated boundary layer enveloping the wake, perhaps the exterior turbulence affects the stability of this layer. Whatever the explanation, the work with the pressure disk indicates that turbulence does lower the pressure in the wake.

NATIONAL BUREAU OF STANDARDS,
WASHINGTON, D. C., June 22, 1935.

REFERENCES

1. Dryden, Hugh L.: Turbulence, Companion of Reynolds Number. *Jour. Aero. Sci.*, vol. I, no. 2, April 1934, p. 67.
2. Ower, E., and Johansen, F. C.: On a Determination of the Pitot-Static Tube Factor at Low Reynolds Numbers, with Special Reference to the Measurement of Low Air Speeds. R. & M. No. 1437, British A. R. C., 1931.
3. Schubauer, G. B.: A Turbulence Indicator Utilizing the Diffusion of Heat. T. R. No. 524, N. A. C. A., 1935.
4. Mock, W. C., Jr., and Dryden, H. L.: Improved Apparatus for the Measurement of Fluctuations of Air Speed in Turbulent Flow. T. R. No. 448, N. A. C. A., 1932.

REPORT No. 547

WIND-TUNNEL INTERFERENCE WITH PARTICULAR REFERENCE TO OFF-CENTER POSITIONS OF THE WING AND TO THE DOWNWASH AT THE TAIL

By ABE SILVERSTEIN and JAMES A. WHITE

SUMMARY

The theory of wind-tunnel boundary influence on the downwash from a wing has been extended to provide more complete corrections for application to airplane test data. The first section of the report gives the corrections at the lifting line for wing positions above or below the tunnel center line; the second section shows the manner in which the induced boundary influence changes with distance aft of the lifting line.

Values of the boundary corrections are given for off-center positions of the wing in circular, square, 2:1 rectangular, and 2:1 elliptical tunnels. Aft of the wing the corrections are presented for only the square and the 2:1 rectangular tunnels, but it is believed that these may be applied to jets of circular and 2:1 elliptical cross sections. In all cases results are included for both open and closed tunnels.

INTRODUCTION

The influence of wind-tunnel boundaries on the downwash at the lifting line of an airfoil has been the subject of considerable theoretical and experimental study. The investigations have been primarily confined to the problem of determining the average downwash over the span of an airfoil located in the center of a wind-tunnel test section. Prandtl (reference 1) first demonstrated the general method of analysis and gave numerical values for the magnitude of boundary influence on airfoils of finite span tested at the center of either an open or a closed circular tunnel. Glauert, Terazawa, Theodorsen, Rosenhead, and Tani and Sanuki (references 2 to 8) extended this theory to include all the more conventional tunnel sections; that is, square, rectangular, and elliptical. The theoretical results for the central wing position are presented in figure 1 (from reference 9), the circular and square sections being represented by $\lambda=1.0$ for the ellipse and rectangle, respectively.

When testing airplanes and airplane models in wind tunnels, it is often necessary to locate the wing above the horizontal center line of the jet; otherwise at large angles of attack the tail is too near the edge of the air stream. Numerical values of the downwash resulting from the boundary influence have hitherto not been available for off-center positions of the wing. Further-

more, the influence of the boundaries on the downwash behind the wing in the region of the tail has been only briefly and approximately treated (reference 10). This information is necessary for correcting wind-tunnel downwash measurements and elevator angles for flight trim. The theory has therefore been extended to show the magnitude of the boundary influence on airfoils tested above or below the horizontal center line of the tunnel and the dependence of the magnitude of the boundary influence on the distance aft of the wing.

The general problem for any wind tunnel in either the two- or three-dimensional case is that of determining a stream function which, added to that of the flow produced by the airfoil, satisfies the conditions that must exist at the boundaries of the air stream. The effect of the boundaries may then be replaced by this stream function and the boundary-induced velocity computed for any point in the wind tunnel. The conditions at the boundary of the closed tunnel may be exactly expressed as a zero flow normal to the walls; whereas, the open-tunnel boundary condition closely approximates one of constant pressure from the quiescent air around the jet.

In many of the cases of practical importance the solution may be simplified by the use of an external arrangement of vortices that mirror the wing horseshoe vortex in a manner which satisfies the specified boundary conditions. The external image arrangements in these cases are equivalent to the desired stream function.

The value of the interference at any point in a wind tunnel is a function of many factors. Foremost among these factors are: the relative size of the model and the tunnel, the span loading of the airfoil, the test-section shape and constraint, the position of the model in the jet, and the relative location of the point investigated to the airfoil position. Each of these variables has been considered in the present study. The results are presented over a practical range of the ratio of the wing vortex span to the tunnel width for both open and closed tunnels. The span employed is not the geometric one but is an effective span based on the assumption that the wing vortex sheet rolls up into two trailing vortices with a spacing of about 0.8 to 0.9 of the wing length.

The correct ratio of effective to geometric span for various types of loading and aspect ratios is given in reference 2; however, sufficient accuracy for practical purposes is obtained by assuming a uniform loading over the effective span have shown a close agreement with the calculations based on the actual loading over the geometric span. This

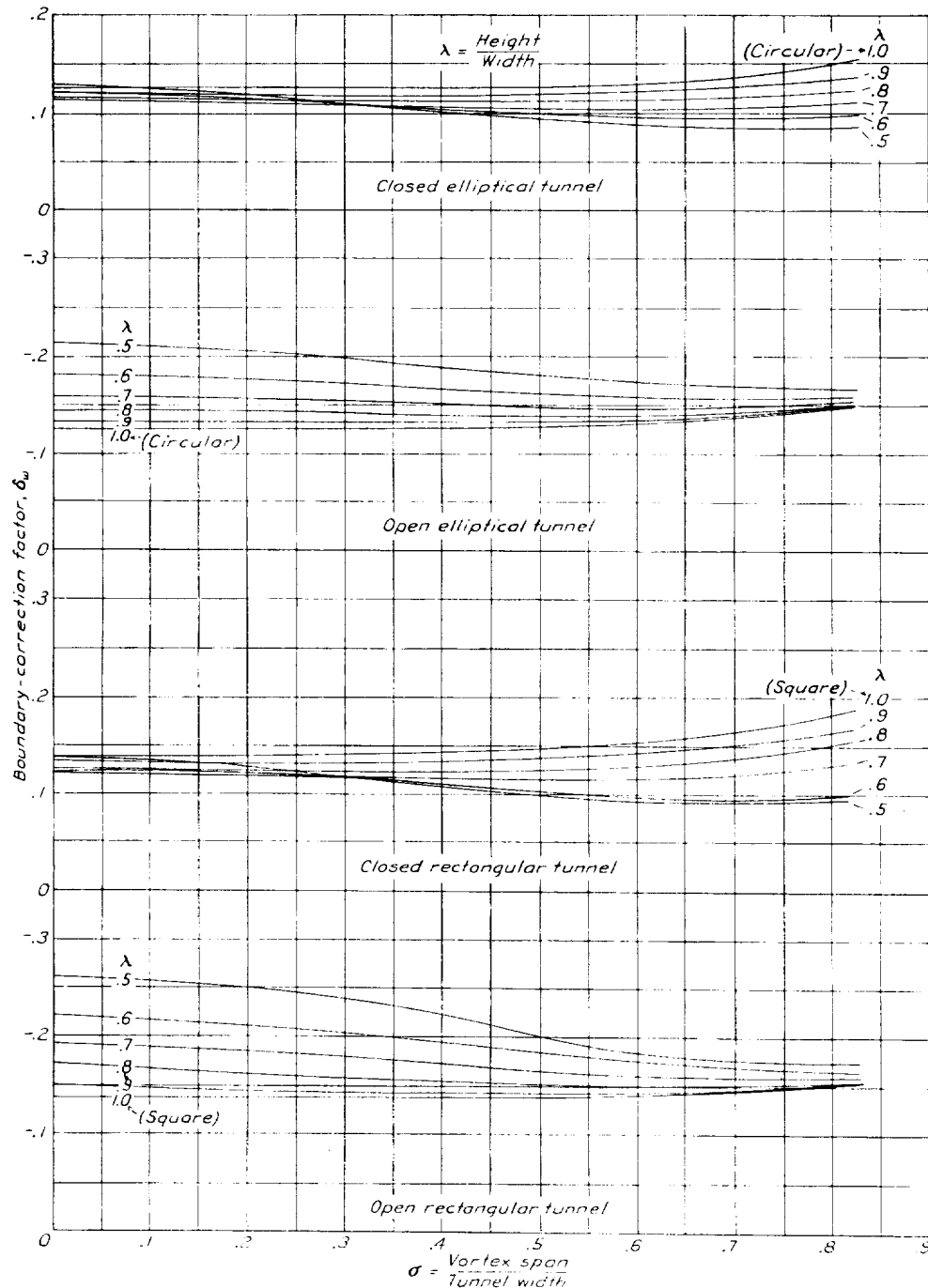


FIGURE 1.—Boundary-correction factors for airfoils of finite span in the center of conventional tunnel sections.

purposes is obtained by using a value of 0.8 for a tapered and 0.85 for a rectangular wing. Computations of theoretical boundary influence based on the assumption is therefore followed throughout the report and it provides a simplification of the problem without a sacrifice of accuracy.

This analysis covers boundary influence on downwash for circular, square, 2:1 elliptical, and 2:1 rectangular tunnels at the wing, and for square and 2:1 rectangular tunnels in the region aft of the wing. The wing positions analyzed are those on the center line and 0.1 and 0.2 of the tunnel height above the center of the jet.

BOUNDARY INFLUENCE AT THE AIRFOIL

Elliptical tunnel.—A general solution for the boundary influence at the lifting line of an airfoil at any position in an elliptical tunnel has been made by Tani and Sanuki (reference 8). The numerical values of the boundary-correction factor δ_w were not given, however, except for the case of the wing on the tunnel center line.

Following the method of Tani and Sanuki, we may write in the elliptical coordinates (ξ, η) , for the closed elliptical tunnel,

$$\delta_w = -\frac{c}{4a\sigma^2} \left[\sum_{n=1}^{\infty} \frac{e^{-n\xi_0}}{n \cosh n\xi_0} \cosh^2 n\xi_1 \cos^2 n\eta_1 + \sum_{n=2}^{\infty} \frac{e^{-n\xi_0}}{n \sinh n\xi_0} \sinh^2 n\xi_1 \sin^2 n\eta_1 \right] \quad (1)$$

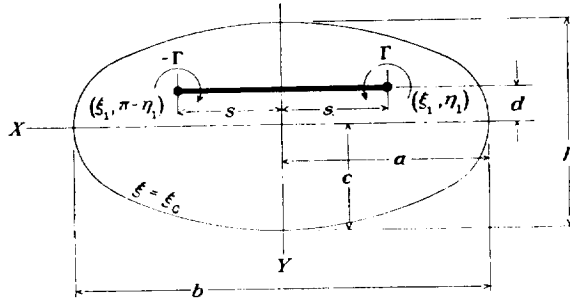


FIGURE 2.—Off-center location of airfoil in an elliptical wind tunnel.

and, for the open elliptical tunnel,

$$\delta_w = -\frac{c}{4a\sigma^2} \left[\sum_{n=1}^{\infty} \frac{e^{-n\xi_0}}{n \sinh n\xi_0} \cosh^2 n\xi_1 \cos^2 n\eta_1 + \sum_{n=2}^{\infty} \frac{e^{-n\xi_0}}{n \cosh n\xi_0} \sinh^2 n\xi_1 \sin^2 n\eta_1 \right] \quad (2)$$

in which a and c are, respectively, the major and minor semi-axes of the ellipse (fig. 2), and σ is the ratio of the span of the trailing vortices to the tunnel width ($b = 2a$). The symbol Σ' implies that only odd values of n are to be summed and Σ'' indicates the use of only even values of n . The usual boundary-correction factor δ_w is defined by

$$\Delta\alpha_w = \delta_w \frac{S}{C} C_L$$

in which S and C are the areas of the wing and test section, respectively, and $\Delta\alpha_w$ is the induced downwash angle at the lifting line of the wing due to the influence of the boundaries. The subscript w refers to the location at the lifting line.

The elliptical coordinates ξ and η are related to the rectangular coordinates x and y as follows:

$$\begin{cases} x = k \cosh \xi \cos \eta \\ y = k \sinh \xi \sin \eta \end{cases}$$

in which k is a constant required to preserve the scale of dimensions. The boundary ellipse is defined by $\xi = \xi_0$, so that

$$\begin{aligned} a &= k \cosh \xi_0 \\ c &= k \sinh \xi_0 \end{aligned}$$

or

$$\begin{aligned} \xi_0 &= \coth^{-1} \frac{a}{c} \\ k &= \sqrt{a^2 - c^2} \end{aligned}$$

The elliptical coordinates (ξ_1, η_1) of the vortex position (x_1, y_1) are given by

$$\begin{aligned} 2 \sin^2 \eta_1 &= p \pm \sqrt{p^2 + \left(\frac{2y_1}{k}\right)^2} \\ \sinh \xi_1 &= \frac{y_1}{k \sin \eta_1} \end{aligned}$$

in which

$$p = 1 - \left(\frac{x_1}{k}\right)^2 - \left(\frac{y_1}{k}\right)^2$$

Substitution of the foregoing values of ξ_0 , ξ_1 , and η_1 in equations (1) and (2) permits the obtaining of the values of δ_w for the closed and open tunnels. The series converges rapidly and the use of only the first two terms is sufficient.

For an infinitely small airfoil, σ approaches 0 and equations (1) and (2) reduce, for the closed tunnel, to

$$\delta_w = -\frac{ac}{4(a^2 - c^2)} \left[\sum_{n=1}^{\infty} \frac{ne^{-n\xi_0} \cosh^2 n\xi_1}{\cosh n\xi_0 \cosh^2 \xi_1} + \sum_{n=2}^{\infty} \frac{ne^{-n\xi_0} \sinh^2 n\xi_1}{\sinh n\xi_0 \cosh^2 \xi_1} \right]$$

and for the open tunnel, to

$$\begin{aligned} \delta_w &= -\frac{ac}{4(a^2 - c^2)} \left[\sum_{n=1}^{\infty} \frac{ne^{-n\xi_0} \cosh^2 n\xi_1}{\sinh n\xi_0 \cosh^2 \xi_1} \right. \\ &\quad \left. + \sum_{n=2}^{\infty} \frac{ne^{-n\xi_0} \sinh^2 n\xi_1}{\cosh n\xi_0 \cosh^2 \xi_1} \right] \end{aligned}$$

The values of δ_w are given in figures 3 and 4 plotted against the distance of the airfoil from the center line for the open and closed 2:1 elliptical tunnels. The factors are the same for wing positions above and below the center of the tunnel.

Circular tunnel.—The circular tunnel is a special case of the elliptical tunnel in which the boundary-ellipse parameter ξ_0 approaches ∞ , and the values of δ_w for the circular tunnel may thus be computed from equations (1) and (2). A simpler and more direct method of solution is revealed, however, by employing the inverse-image method (fig. 5).

Let the effect of the vortex A at a point x of the wing be considered. Since the radius r equals $\sqrt{(x' - x)^2 + y'^2}$

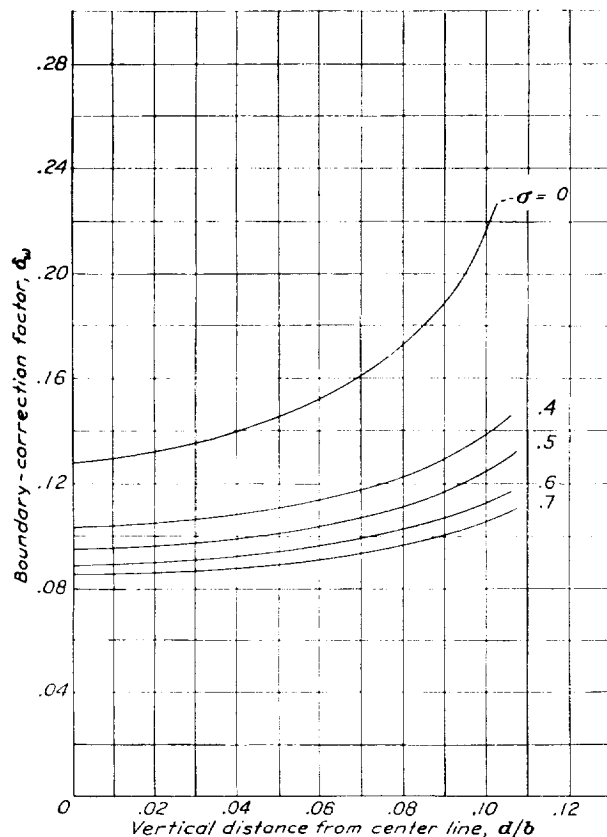


FIGURE 3.—Boundary-correction factors at the airfoil lifting line for the closed 2:1 elliptical tunnel. Airfoil locations are above or below the tunnel center line.

and $\cos \alpha$ equals $\frac{x' - x}{\sqrt{(x' - x)^2 + y'^2}}$, the downward velocity is

$$v = \frac{\Gamma}{4\pi} \frac{(x' - x)}{(x' - x)^2 + y'^2}$$

in which x' and y' are constants depending on the wing position and tunnel radius, and are given by

$$x' = \frac{R^2 s}{s^2 + d^2}$$

$$y' = d \left(\frac{R^2 - s^2 - d^2}{s^2 + d^2} \right)$$

The total induced flow D over the span from both A and B is

$$D = 2 \int_{-s}^s v dx = \frac{\Gamma}{2\pi} \int_{-s}^s \frac{(x' - x) dx}{(x' - x)^2 + y'^2}$$

$$D = \frac{\Gamma}{4\pi} \left[\log \frac{(x' + s)^2 + y'^2}{(x' - s)^2 + y'^2} \right]$$

Letting \bar{v} be the average induced velocity over the span, $\bar{v} = \frac{D}{2s}$ and $\Delta \alpha_w = \frac{\bar{v}}{V}$. To simplify, we may write

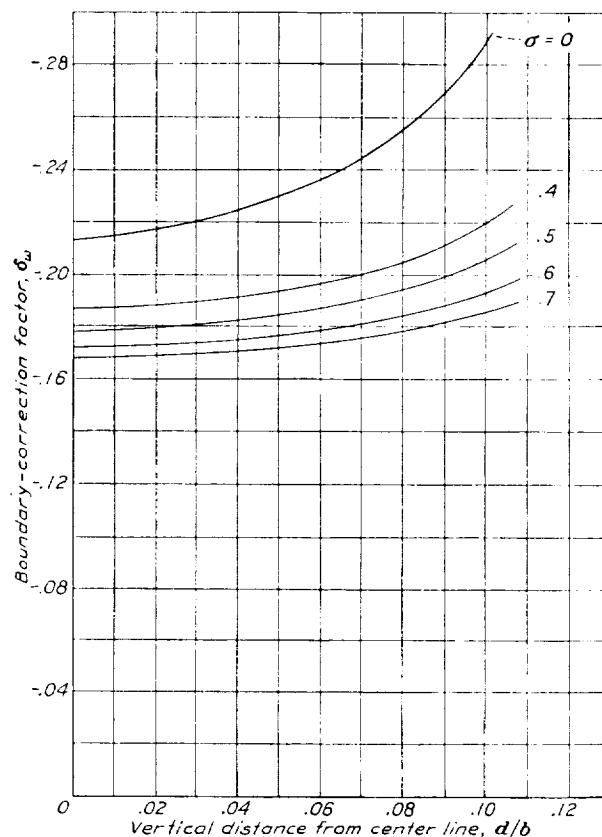


FIGURE 4.—Boundary-correction factors at the airfoil lifting line for the open 2:1 elliptical tunnel. Airfoil locations are above or below the tunnel center line.

$\Gamma = \frac{C_L V S}{4s}$, then

$$\Delta \alpha_w = \frac{C_L S}{32\pi s^2} \left[\log \frac{(x' + s)^2 + y'^2}{(x' - s)^2 + y'^2} \right] = \delta_w \frac{S}{C} C_L$$

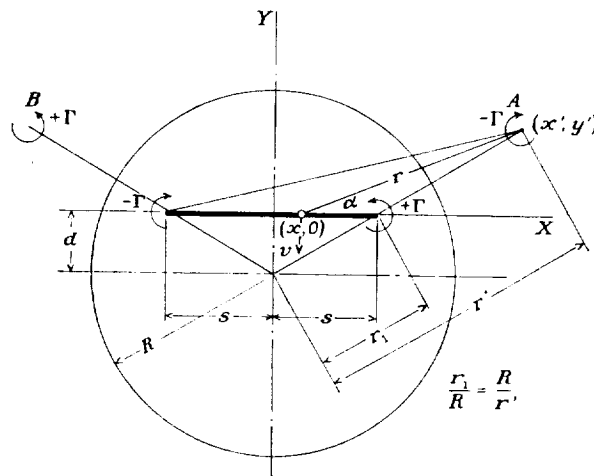


FIGURE 5.—Location of image vortices for off-center wing locations in the circular tunnel.

Since $\sigma = \frac{s}{R}$ and $C = \pi R^2$, then

$$\delta_w = \frac{1}{32\sigma^2} \left\{ \log \frac{1 + 2 \left[\sigma^2 - \left(\frac{d}{R} \right)^2 \right] + \left[\sigma^2 + \left(\frac{d}{R} \right)^2 \right]^2}{1 - 2 \left[\sigma^2 + \left(\frac{d}{R} \right)^2 \right] + \left[\sigma^2 + \left(\frac{d}{R} \right)^2 \right]^2} \right\}$$

For an infinitely small airfoil the equation reduces to

$$\delta_w = \frac{1}{8 \left[1 - \left(\frac{d}{R} \right)^2 \right]^2}$$

The boundary-correction factors δ_w for off-center positions in the circular tunnel are given in figure 6.

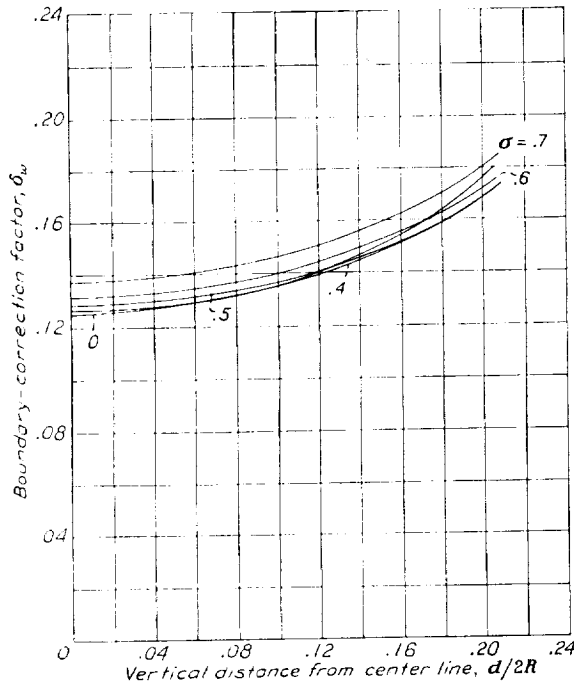


FIGURE 6.—Boundary-correction factors at the airfoil lifting line for the open and closed circular tunnels. The factor δ_w is positive for the closed tunnel and negative for the open. Airfoil locations are above or below the tunnel center line.

As a check, the values were computed by both the methods described. Numerically, they are the same for open and closed circular tunnels but are of positive sign (upwash) for the closed and negative (downwash) for the open.

Rectangular tunnel.—The images that satisfy the boundary conditions of the rectangular tunnel are arranged in a checkerboard pattern of vortices extending to infinity. The circulation strength of the images corresponds to that of the airfoil. For the closed tunnel the condition of zero velocity normal to the wall is satisfied by alternate horizontal rows of positive and negative vortices (fig. 7); in the free jet the uniform-pressure criterion is met by alternate vertical rows of

positive and negative images (fig. 8). When the airfoil is not on the tunnel center line, the pattern becomes asymmetrical with regard to the origin, but the boundary conditions are fulfilled if the wing vortex is repeatedly reflected in the boundaries. Figure 9 shows the pattern for the closed rectangular tunnel with the wing above the tunnel center line. If the images are divided into two superimposed groups, one with origin at the airfoil on line A-A in figure 9 and the other with origin at the first image B-B, two symmetrical groups of images emerge with a vertical spacing of twice the tunnel height. The problem of determining the downwash at the wing is simplified and expedited since Theodorsen (reference 6) gives the equation for the group with the origin at the airfoil (line A-A) directly as

$$\delta_{w1} = -\frac{1}{4\pi r_1 \sigma^2} \left[\log \frac{\sinh \pi r_1 \sigma}{\pi r_1 \sigma} + \sum_{n=1}^{\infty} (-1)^n \log \left(1 - \frac{\sinh^2 \pi r_1 \sigma}{\sinh^2 \pi n r_1} \right) \right] \quad (3)$$

for the open tunnel, in which r_1 is the ratio of tunnel width to the doubled height, and σ is the ratio of the span of the tip vortices to the tunnel width. If we write

$$\Delta \alpha_{w1} = \delta_{w1} \frac{S}{C} C_L$$

the effective value of the jet area C , owing to the doubled effective tunnel height, becomes twice the true area and the values of δ_{w1} from equation (3) must be halved for application to the true tunnel. Equation (3) as written applies to the open tunnel; the closed-tunnel values are obtained by deleting from the summation the factor $(-1)^n$, which takes into account the signs of the vertical rows of images, the minus sign in front being retained. It may be remarked that, whereas δ_{w1} for the open tunnel is the same as δ_w for an open tunnel of doubled height with the wing on the center line, the same is not true of the closed tunnel, as may be seen from a study of the corresponding image patterns.

There remains, then, the problem of computing the flow over a span $2s$ at a distance y below the origin (origin on line B-B) contributed by an infinite pattern of vortices symmetrical about B-B and with vertical spacing of twice the tunnel height. By the method of Theodorsen (reference 6), the velocity function for an infinite vertical row of equidistant semi-infinite vortices at $x=0$ may be written as

$$v = \frac{\Gamma}{8h} \frac{\sinh \frac{\pi x}{h}}{\cosh \frac{\pi x}{h} - \cos \frac{\pi y}{h}}$$

in which v is the vertical velocity and $2h$ is the vertical spacing of the images.

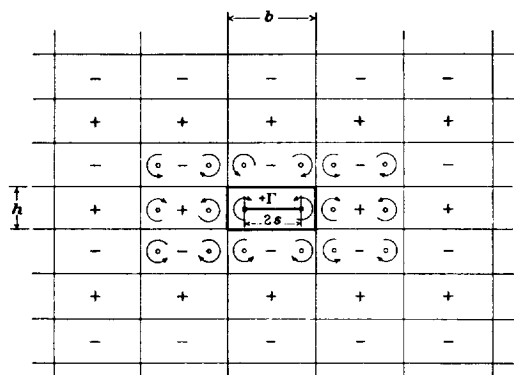


FIGURE 7.—Arrangement of the infinite image pattern to satisfy the boundary conditions of the closed rectangular tunnel.

At any value of the parameter y the stream function from this row of semi-infinite vortex filaments is evaluated by integrating with respect to x . Thus

$$\psi = \int v dx = \int \frac{\Gamma}{8h} \frac{\sinh \frac{\pi x}{h}}{\cosh \frac{\pi x}{h} - \cos \frac{\pi y}{h}} dx$$

integrated

$$\psi = \frac{\Gamma}{8\pi} \log \left(\cosh \frac{\pi x}{h} - \cos \frac{\pi y}{h} \right)$$

The result may now be extended to include two vertical rows of vortices of opposite sign at a distance s and

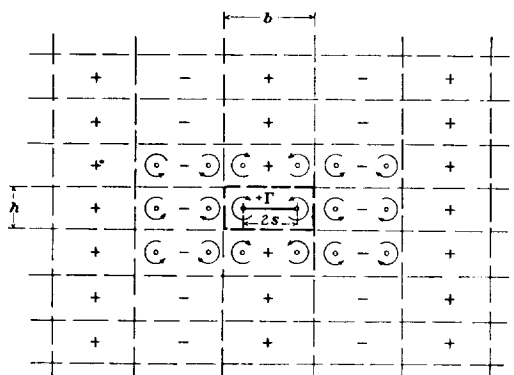


FIGURE 8.—Arrangement of the infinite image pattern to satisfy the boundary conditions of the open rectangular tunnel.

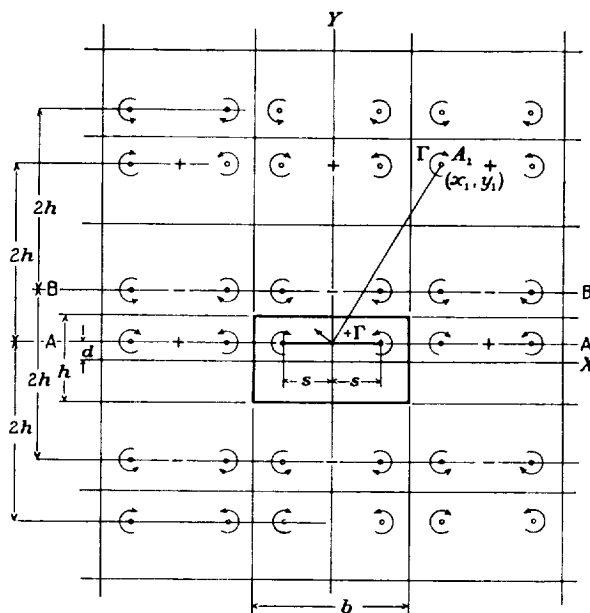


FIGURE 9.—Arrangement of the infinite image pattern to satisfy the boundary conditions for off-center locations of the wing in a closed rectangular tunnel.

— s from the y axis. The stream function then becomes

$$\begin{aligned} \psi &= \frac{\Gamma}{8\pi} \left\{ \log \left[\cosh \frac{\pi(x-s)}{h} - \cos \frac{\pi y}{h} \right] \right. \\ &\quad \left. - \log \left[\cosh \frac{\pi(x+s)}{h} - \cos \frac{\pi y}{h} \right] \right\} \\ \psi &= -\frac{\Gamma}{8\pi} \log \frac{\cosh \frac{\pi(x+s)}{h} - \cos \frac{\pi y}{h}}{\cosh \frac{\pi(x-s)}{h} - \cos \frac{\pi y}{h}} \end{aligned} \quad (4)$$

The total vertical flow may be determined by adding the effect of all the double rows of vortices to infinity. The contribution to the vertical flow of any double row of vortices, say the n th, is numerically the same as the vertical flow at the location of the n th row induced by the double row at the origin. It is therefore only necessary to calculate the flow induced by this double row at the origin, between the limits

$$x = nb - s \text{ and } x = nb + s$$

For the actual vertical flow at the first exterior row of vortices with center at $x = b$, the limits $x = b - s$ and $x = b + s$ are substituted in equation (4). The vertical flow from this row is, disregarding signs,

$$D = \frac{\Gamma}{8\pi} \log \frac{\left[\cosh \frac{\pi(b+2s)}{h} - \cos \frac{\pi y}{h} \right] \left[\cosh \frac{\pi(b-2s)}{h} - \cos \frac{\pi y}{h} \right]}{\left(\cosh \frac{\pi b}{h} - \cos \frac{\pi y}{h} \right)^2}$$

For the n th double row, consequently

$$D = \frac{\Gamma}{8\pi} \log \frac{\left[\cosh \frac{\pi(nb+2s)}{h} - \cos \frac{\pi y}{h} \right] \left[\cosh \frac{\pi(nb-2s)}{h} - \cos \frac{\pi y}{h} \right]}{\left(\cosh \frac{\pi nb}{h} - \cos \frac{\pi y}{h} \right)^2}$$

The entire vertical flow for all the rows from $x = -\infty$ to $+\infty$ becomes

$$D = -\frac{\Gamma}{8\pi} \sum_{-\infty}^{\infty} \log \frac{\left[\cosh \frac{\pi(nb+2s)}{h} - \cos \frac{\pi y}{h} \right] \left[\cosh \frac{\pi(nb-2s)}{h} - \cos \frac{\pi y}{h} \right]}{\left(\cosh \frac{\pi nb}{h} - \cos \frac{\pi y}{h} \right)^2}$$

or $\frac{\Gamma}{8\pi} \psi$ in which ψ represents the negative of the infinite sum. We may write

$$2s\Gamma\rho V = \frac{1}{2} C_L \rho V^2 S$$

in which V is the velocity, ρ the density of the medium, and S is the airfoil area. Simplifying,

$$\Gamma = \frac{C_L V S}{4s}$$

The angular deflection caused by the induced flow is

designated

$$\Delta\alpha = \frac{\bar{v}}{V} = \frac{D}{2sV} = \frac{C_L S}{64s^2\pi} \psi = \delta \frac{S}{C} C_L$$

or with $bh = C$, the cross-sectional area of the jet; $\frac{b}{h} = r$, the ratio of the tunnel width to height; and σ equals the ratio of vortex span $2s$ to the tunnel width b ; the final result for the group with origin at B-B may be written for the open tunnel

$$\delta_{w_2} = -\frac{1}{16\sigma^2\pi r} \sum_{-\infty}^{\infty} (-1)^n \log \frac{\left[\cosh \pi r(n+\sigma) + \cos 2\pi r \frac{d}{b} \right] \left[\cosh \pi r(n-\sigma) + \cos 2\pi r \frac{d}{b} \right]}{\left(\cosh \pi nr + \cos 2\pi r \frac{d}{b} \right)^2} \quad (5)$$

The summation converges rapidly and the terms for values of n greater than 2 are negligible. The same equation applies for the closed tunnel except that the factor $(-1)^n$ is omitted and the sign before the expression becomes positive.

For an infinitely small wing, equations (3) and (5) reduce to

$$\delta_1 = -\frac{\pi r}{4} \left(\frac{1}{6} - \sum_{n=1}^{\infty} \frac{(-1)^n}{\sinh^2 \pi nr} \right)$$

$$\delta_2 = -\frac{\pi r}{16} \sum_{n=-\infty}^{\infty} (-1)^n \left[\frac{1 + \cosh \pi nr \cos 2\pi r \frac{d}{b}}{\left(\cosh \pi nr + \cos 2\pi r \frac{d}{b} \right)^2} \right]$$

The total boundary-correction factor at the airfoil is

$$\delta_w = \frac{1}{2} \delta_{w_1} + \delta_{w_2} \quad (6)$$

By means of the foregoing equations the correction factors δ_w have been computed over a practical range of span ratios and wing positions for the square and 2:1 rectangular tunnels with open and closed test sections. These results are presented in figures 10 to 13, inclusive.

Wing locations and effective spans are expressed as fractions of the tunnel width b .

BOUNDARY INFLUENCE AFT OF THE AIRFOIL IN RECTANGULAR TUNNELS

Thus far consideration has been given only to the conditions at a plane through the lifting line of the wing, where the transverse portion of the horseshoe vortex representing the effect of the wing does not affect the boundary condition and the problem reduces to that of finding the effect of vortices extending from zero to infinity in only one direction. If the induced vertical velocity due to the boundary interference were constant along the tunnel axis, the only effect of the interference would be to change the general direction of the air stream with respect to the airplane and balance system without in any way changing the local flow over the airplane for any given attitude with respect to the relative wind. The tunnel-wall interference, however, is not constant along the tunnel axis. The variation of boundary influence with distance downstream causes the tail of the airplane to be operating at a different angle of attack than it would in free air for the same angle of the wing to the relative wind, the discrepancy being equal to the difference in

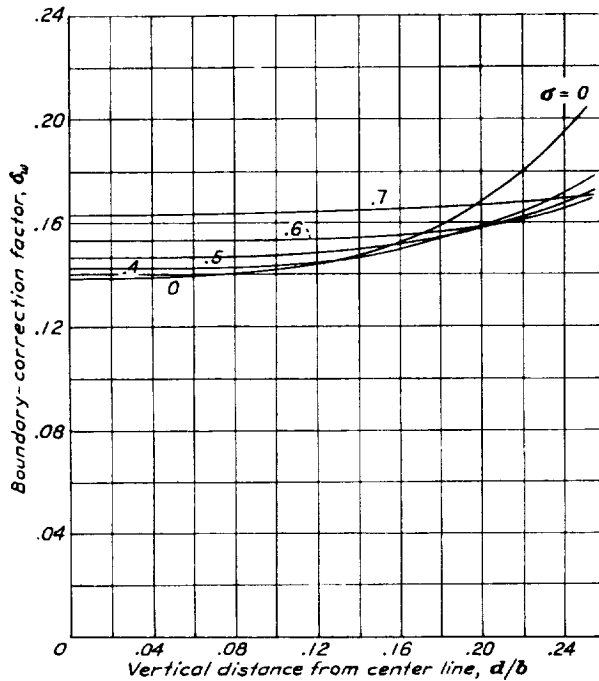


FIGURE 10.—Boundary-correction factors at the airfoil lifting line for the closed square tunnel. Airfoil locations are above or below the tunnel center line.

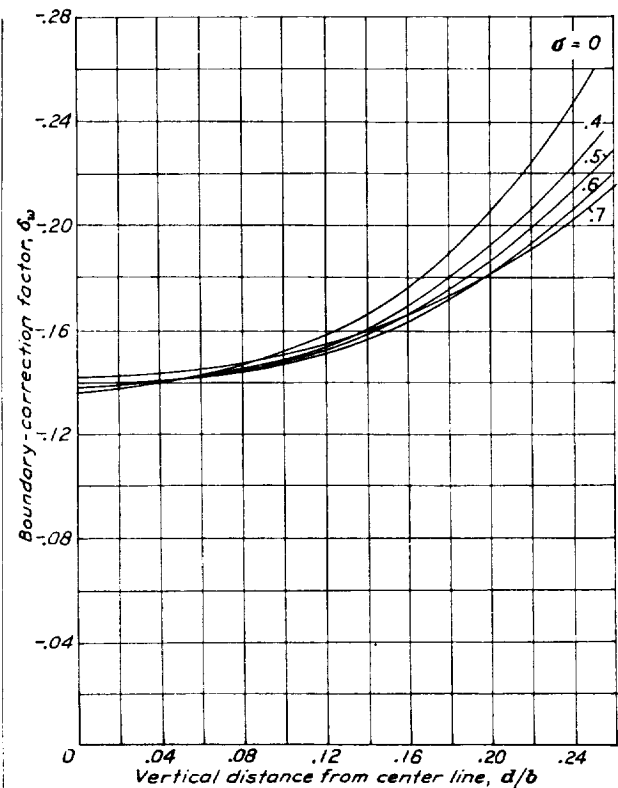


FIGURE 11.—Boundary-correction factors at the airfoil lifting line for the open square tunnel. Airfoil locations are above or below the tunnel center line.

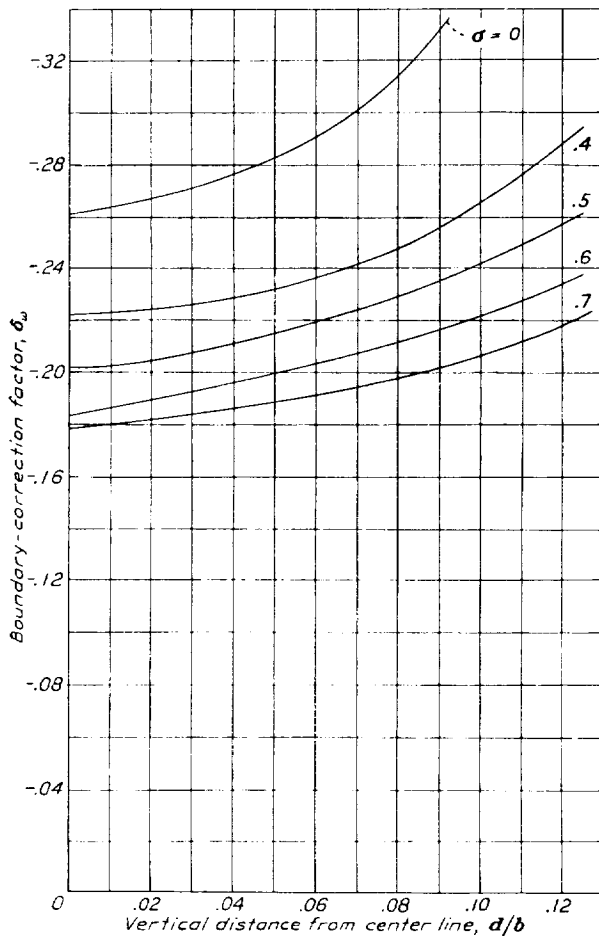


FIGURE 13.—Boundary-correction factors at the airfoil lifting line for the open 2:1 rectangular tunnel. Airfoil locations are above or below the tunnel center line.

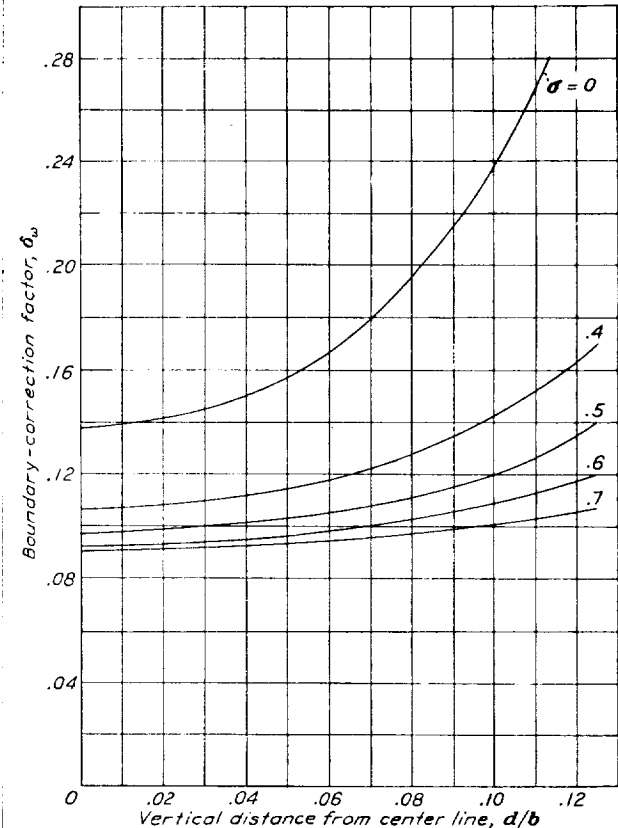


FIGURE 12.—Boundary-correction factors at the airfoil lifting line for the closed 2:1 rectangular tunnel. Airfoil locations are above or below the tunnel center line.

the induced angle of flow at the wing and tail. The tail surface also acts as an airfoil affecting the boundary conditions but the tail area is so small that this effect may be neglected.

At any cross-sectional plane behind the lifting line, the influence of the horseshoe vortex system at the tunnel boundary differs from that at the wing owing to the transverse and longitudinal segments of the wing horseshoe vortex system that extend between the wing and this plane. The longitudinal vortices downstream from the plane may still be considered to be of infinite length. A corresponding variation in the influence of the images is required in order that the boundary conditions may be satisfied.

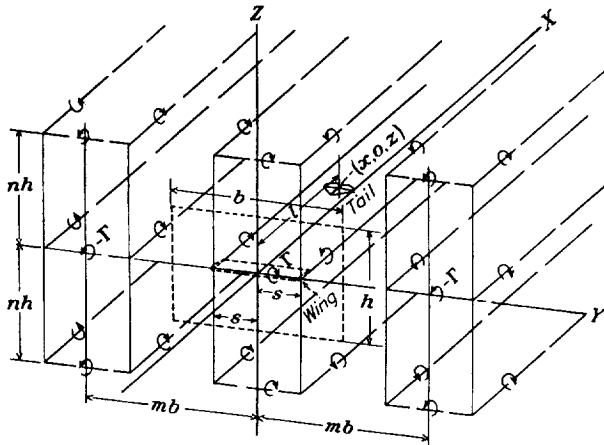


FIGURE 14.—Three-dimensional arrangement of wing and image vortices to satisfy the boundary conditions aft of the airfoil for the open rectangular tunnel.

No simple extension of the image system has been found for the circular or elliptical tunnels that satisfies the boundary conditions at all points. For the rectangular tunnel, it can easily be seen that the boundary condition is satisfied at all points by the same system of images as in the two-dimensional problem, each pair of vortices including a transverse segment to make it a complete image of the horseshoe vortex representing the wing (fig. 14). At an infinite distance behind the airfoil, the induced velocities from the transverse images become zero and the total induced velocity from the longitudinal branches, which may then be considered as extending to infinity in both fore and aft directions, reaches twice the value at the wing.

If the increment of induced angle at points behind the wing be designated $\Delta\alpha_A$, the total influence at any location from the boundaries is

$$\Delta\alpha_T = \Delta\alpha_w + \Delta\alpha_A$$

in which $\Delta\alpha_w$ is the value at the wing, from the foregoing discussion of downflow at the lifting line.

If the origin of coordinates is chosen at the center of the airfoil lifting line with the x axis coincident with the horizontal axis of the jet, the y axis along the span,

and the z axis vertical, a doubly infinite series of images is located at points $y=mb$ and $z=nh$ for a rectangular tunnel of breadth b and height h (fig. 14). The variables m and n assume all positive and negative integral values except (0, 0).

Although the pattern is infinite, the images adjacent to the tunnel boundaries are the most effective and the first two rows of images exterior to the tunnel boundaries ordinarily contribute more than 90 percent of the induced flow. The validity of this statement is demonstrated by the rapidity with which the series representing the effects of consecutive rows converge and by computations showing the negligible contributions from the exterior rows.

The method followed in this paper has therefore been to determine exactly and individually the induced vertical velocity from each vortex in the first two exterior double rows of images and to sum the effects of the remaining rows to infinity by an approximate method demonstrated in reference 10.

For the additional vertical velocity w_{A_1} at a point $(x, 0, 0)$ contributed by an image with circulation Γ located at (y, z) , we may readily write

$$w_{A_1} = \frac{\Gamma}{4\pi\sqrt{x^2+y^2+z^2}} \left(\frac{1}{x^2+z^2} + \frac{1}{y^2+z^2} \right) \quad (7)$$

Since

$$\Gamma = \frac{C_L V S}{4s} \quad \text{and} \quad \frac{w_{A_1}}{V} = \Delta\alpha_{A_1}$$

$$\frac{4\pi w_{A_1}}{\Gamma} = \frac{16\pi s \Delta\alpha_{A_1}}{C_L S}$$

and

$$\Delta\alpha_{A_1} = \left(\frac{4\pi w_{A_1}}{\Gamma} \right) \frac{C_L S}{16\pi s}$$

If

$$h = \lambda b \quad \text{and} \quad C = \lambda b^2$$

$$\Delta\alpha_{A_1} = \frac{\left(\frac{4\pi w_{A_1}}{\Gamma} \right) \lambda b^2}{16\pi s} \frac{S}{C} C_L$$

which may be written

$$\Delta\alpha_{A_1} = \delta_{A_1} \frac{S}{C} C_L$$

therefore

$$\delta_{A_1} = \frac{\left(\frac{4\pi w_{A_1}}{\Gamma} \right) \lambda b^2}{16\pi s}$$

If the term $\left(\frac{4\pi w_{A_1}}{\Gamma} \right)$ be evaluated by equation (7) for

each of the vortices in the first two exterior double rows, with positive sign for images that create upflow in the tunnel and negative for those inducing downflow, we may express the correction factor that accurately repre-

sents more than 90 percent of the interference flow as

$$\delta_{A_1} = \frac{\lambda b^2}{16\pi s} \sum_{A_1} \frac{4\pi w_{A_1}}{\Gamma} \quad (8)$$

For the remaining rows to infinity the equation for the closed tunnel may be written by the approximate method of reference 10 as

$$\begin{aligned} \Delta\alpha_{A_2} = \frac{xS}{2hC} C_L \left[\left(\frac{\lambda^2}{\pi} \right) \sum_{m=3}^{\infty} \sum_{n=1}^{\infty} (-1)^n \frac{m^2 - 2\lambda^2 n^2}{(m^2 + \lambda^2 n^2)^{5/2}} \right. \\ \left. + \left(\frac{\lambda^2}{\pi} \right) \sum_{m=1}^2 \sum_{n=3}^{\infty} (-1)^n \frac{m^2 - 2\lambda^2 n^2}{(m^2 + \lambda^2 n^2)^{5/2}} \right. \\ \left. + \frac{\lambda^2}{2\pi} \sum_{m=3}^{\infty} \frac{1}{m^3} + \frac{1}{\lambda\pi} \sum_{n=3}^{\infty} \frac{(-1)^{n+1}}{n^3} \right] \quad (9) \end{aligned}$$

and for the open tunnel

$$\begin{aligned} \Delta\alpha_{A_2} = \frac{xS}{2hC} C_L \left[\left(\frac{\lambda^2}{\pi} \right) \sum_{m=3}^{\infty} \sum_{n=1}^{\infty} (-1)^m \frac{m^2 - 2\lambda^2 n^2}{(m^2 + \lambda^2 n^2)^{5/2}} \right. \\ \left. + \left(\frac{\lambda^2}{\pi} \right) \sum_{m=1}^2 \sum_{n=3}^{\infty} (-1)^m \frac{m^2 - 2\lambda^2 n^2}{(m^2 + \lambda^2 n^2)^{5/2}} \right. \\ \left. + \frac{\lambda^2}{2\pi} \sum_{m=3}^{\infty} \frac{(-1)^m}{m^3} - \frac{1}{\lambda\pi} \sum_{n=3}^{\infty} \frac{1}{n^3} \right] \quad (10) \end{aligned}$$

The assumptions are made that the wing may be represented by a doublet at the center of the jet and that the distances to the exterior vortices are large compared with the span $2s$ and the distance along the axis x . Positive values of $\Delta\alpha_{A_2}$ indicate upflow in the tunnel.

If the terms in the brackets of equations (9) and (10) are denoted by ψ , then

$$\Delta\alpha_{A_2} = \frac{xS}{2hC} C_L \psi$$

or

$$\Delta\alpha_{A_2} = \delta_{A_2} \frac{S}{C} C_L$$

and

$$\delta_{A_2} = \frac{x\psi}{2b\lambda}$$

The total increment of induced angle behind the airfoil is

$$\Delta\alpha_A = \Delta\alpha_{A_1} + \Delta\alpha_{A_2}$$

therefore

$$\delta_A = \delta_{A_1} + \delta_{A_2}$$

The values of δ_A in terms of the wing correction δ_w are presented in figures 15 to 26 for the open and closed square tunnels and for the 2:1 rectangular tunnels. They cover a practical range of wing and tail positions in the test section. The wing positions and distances to the rear are given as fractions of the tunnel breadth b . The tail heights for a particular wing height correspond to the positions that the tail occupies over a range of angles of attack of the airplane thrust axis.

Although no theoretical solution has been made, it is believed that the values of δ_A/δ_w for the square and the

2:1 rectangular tunnels apply to the circular and 2:1 elliptical tunnels, respectively, with an accuracy sufficient for practical use.

A special case of some interest is that of a wing at the center and extending through the walls of a closed rectangular tunnel. For this case there are no trailing vortices and therefore there is no induced vertical velocity at the plane of the wing due to boundary interference. There is, however, an interference at downstream points from the images of the transverse vortex and, since this interference varies with distance along the tunnel, there is an effective curvature of the air stream.

Since a wing spanning a closed rectangular tunnel may be considered the same as an infinitely long wing between an upper and lower boundary, the image system consists simply of a single vertical row of infinite transverse vortices of alternating signs with a vertical spacing equal to the height of the tunnel. The vertical velocity due to the n th image vortex above the wing at any point x downstream from the airfoil lifting line and z above the center of the tunnel is

$$w = -\frac{\Gamma}{2\pi} \frac{(-1)^n x}{(nh - z)^2 + x^2}$$

The total induced velocity is that from all the vortices from $n = -\infty$ to $n = +\infty$ except the one at $n=0$, which is that of the wing itself. Or,

$$w = -\frac{\Gamma}{2\pi} \left[\sum_{n=-\infty}^{\infty} \frac{(-1)^n x}{(nh - z)^2 + x^2} - \frac{x}{z^2 + x^2} \right] \quad (11)$$

If only points along the center of the tunnel are of interest, $z=0$ and (11) reduces to

$$w = -\frac{\Gamma}{2\pi} \left[\sum_{n=-\infty}^{\infty} (-1)^n \frac{x}{x^2 + n^2 h^2} - \frac{1}{x} \right]$$

which can be expressed very simply as

$$w = -\frac{\Gamma}{2\pi} \left(\frac{\frac{\pi}{h}}{\sinh \frac{\pi x}{h}} - \frac{1}{x} \right)$$

(See reference 5.)

Putting $\Gamma = \frac{C_L V S}{4s}$ and $\Delta\alpha = \frac{w}{V}$

$$\Delta\alpha_A = -\frac{C_L S}{8sh} \left(\frac{1}{\sinh \pi \frac{x}{h}} - \frac{1}{\pi \frac{x}{h}} \right)$$

$$\delta_A = -\frac{1}{4} \left(\frac{1}{\sinh \pi \frac{x}{h}} - \frac{1}{\pi \frac{x}{h}} \right)$$

If c is the chord of the airfoil

$$\Delta\alpha_A = \delta_A \frac{S}{C} C_L = \delta_A \frac{c}{h} C_L$$

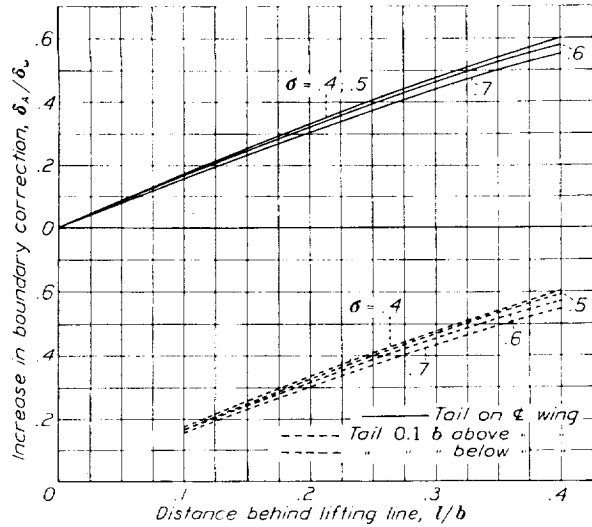


FIGURE 15.—Boundary-correction factors aft of the airfoil lifting line for the closed square tunnel with wing on tunnel center line. Value of δ_w from figure 10.

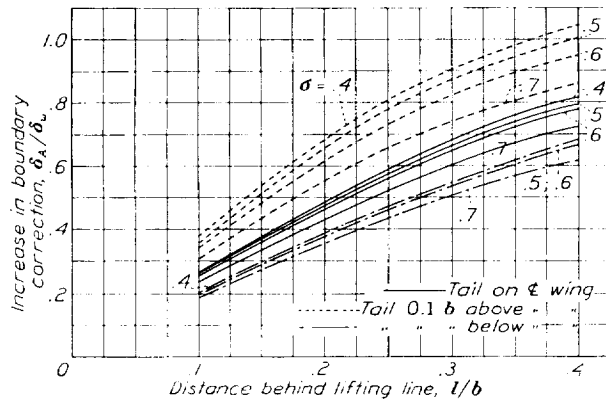


FIGURE 17.—Boundary-correction factors aft of the airfoil lifting line for the closed square tunnel with wing 0.2 b above tunnel center line. Value of δ_w from figure 10.

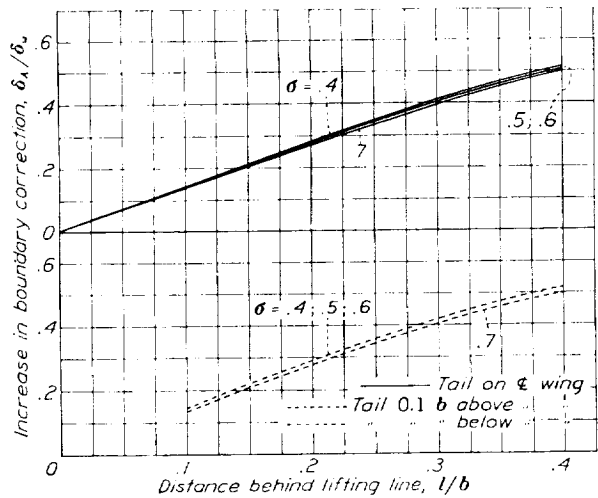


FIGURE 18.—Boundary-correction factors aft of the airfoil lifting line for the open square tunnel with wing on tunnel center line. Value of δ_w from figure 11.

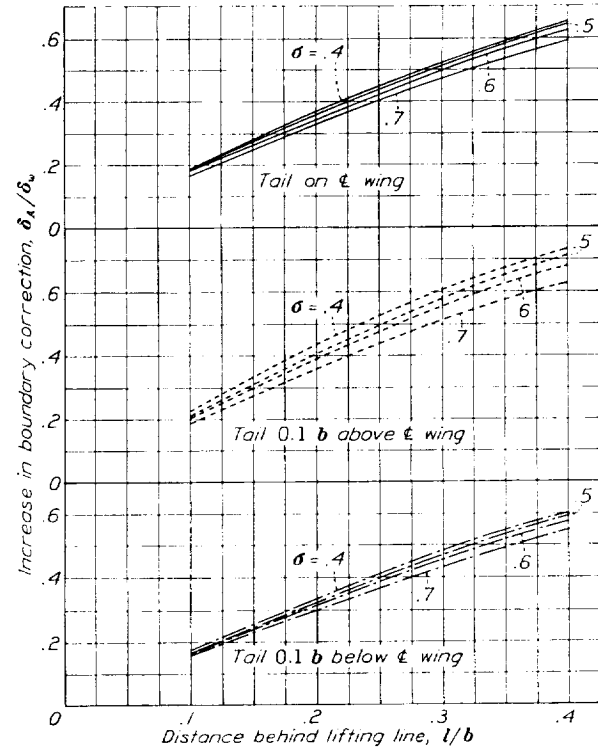


FIGURE 16.—Boundary-correction factors aft of the airfoil lifting line for the closed square tunnel with wing 0.1 b above tunnel center line. Value of δ_w from figure 10.

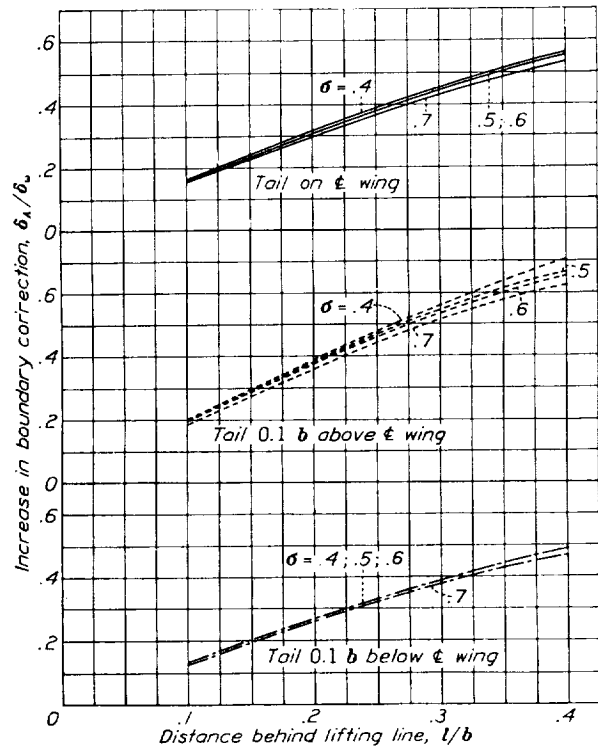


FIGURE 18.—Boundary-correction factors aft of the airfoil lifting line for the open square tunnel with wing 0.1 b above tunnel center line. Value of δ_w from figure 11.

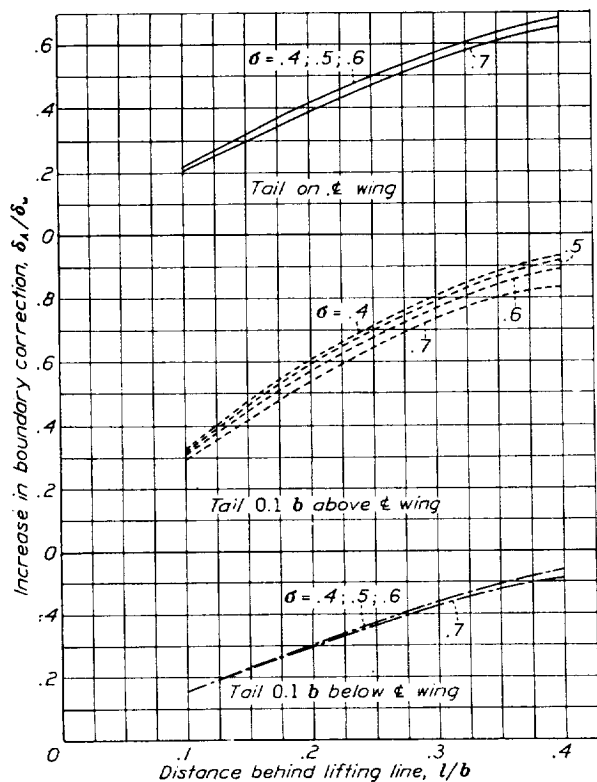


FIGURE 20.—Boundary-correction factors aft of the airfoil lifting line for the open square tunnel with wing 0.2b above tunnel center line. Value of δ_w from figure 11.

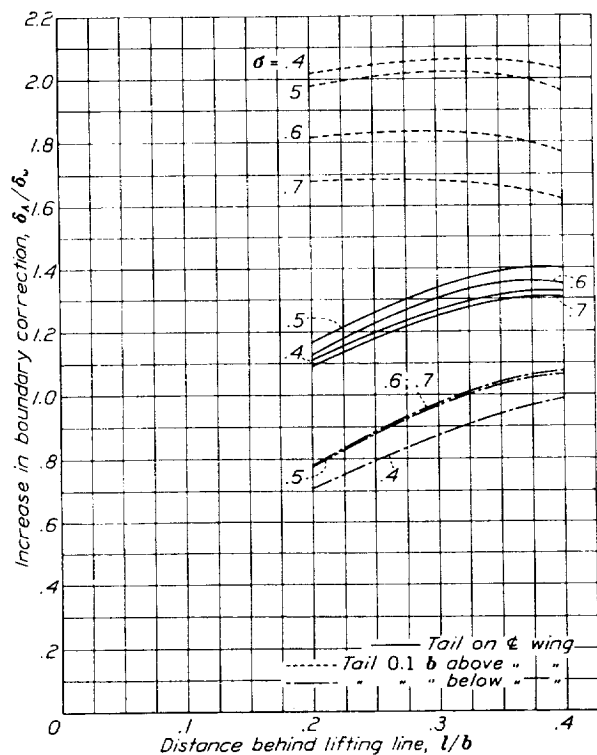


FIGURE 23.—Boundary-correction factors aft of the airfoil lifting line for the closed 2:1 rectangular tunnel with wing 0.1b above tunnel center line. Value of δ_w from figure 12.

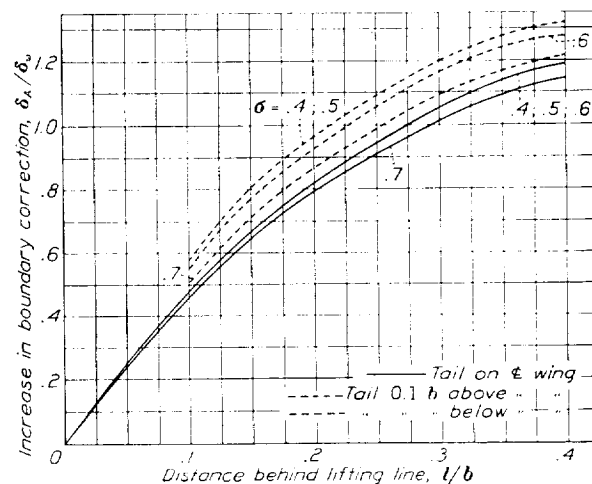


FIGURE 21.—Boundary-correction factors aft of the airfoil lifting line for the closed 2:1 rectangular tunnel with wing on tunnel center line. Value of δ_w from figure 12.

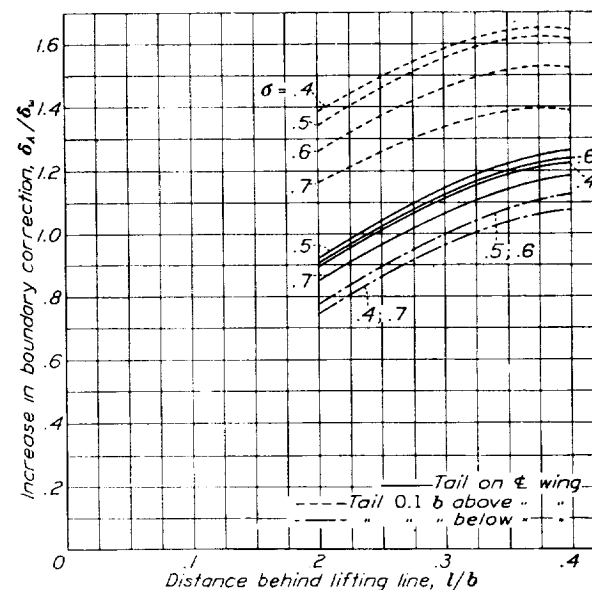


FIGURE 22.—Boundary-correction factors aft of the airfoil lifting line for the closed 2:1 rectangular tunnel with wing 0.05b above tunnel center line. Value of δ_w from figure 12.

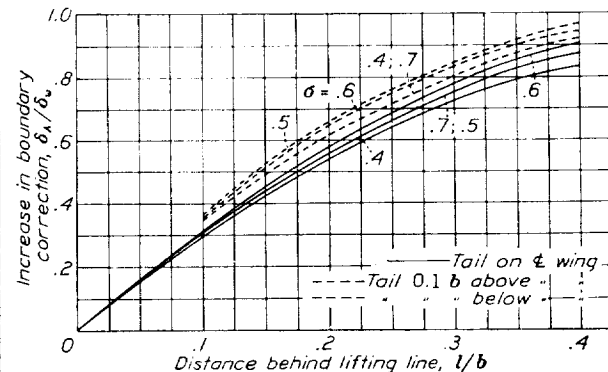


FIGURE 24.—Boundary-correction factors aft of the airfoil lifting line for the open 2:1 rectangular tunnel with wing on tunnel center line. Value of δ_w from figure 13.

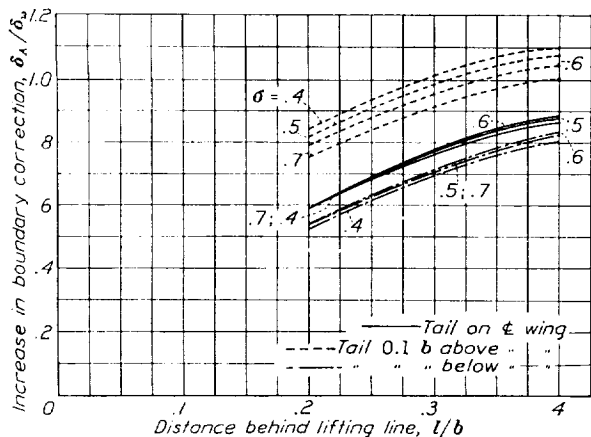


FIGURE 25.—Boundary-correction factors aft of the airfoil lifting line for the open 2:1 rectangular tunnel with wing 0.05 b above tunnel center line. Value of δ_∞ from figure 13.

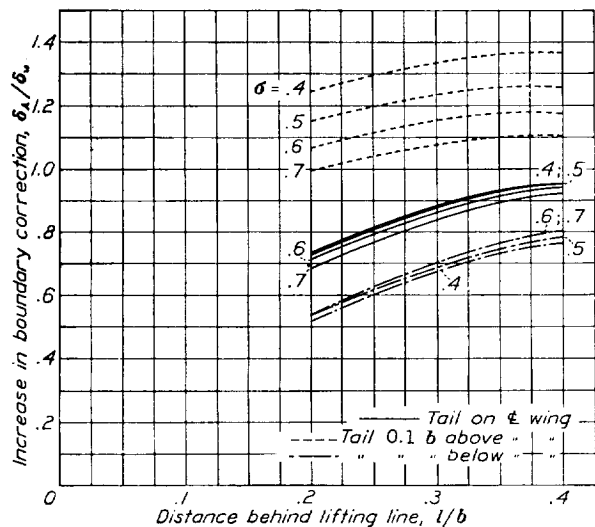


FIGURE 26.—Boundary-correction factors aft of the airfoil lifting line for the open 2:1 rectangular tunnel with wing 0.1 b above tunnel center line. Value of δ_∞ from figure 13.

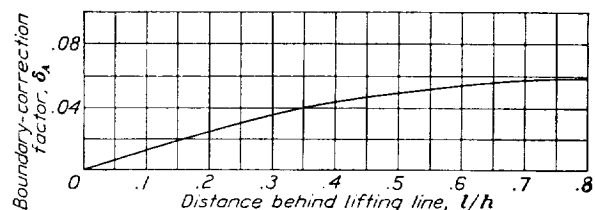


FIGURE 27.—Boundary-correction factors aft of the infinite span airfoils in closed rectangular tunnels. δ_∞ is zero.

The values of δ_A are plotted against distance downstream in figure 27. They are small as compared with the corrections obtained for finite wings. It may be noted that these corrections are independent of the height-breadth ratio of the tunnel and may be used for closed rectangular tunnels of any dimensions.

It is expected that these results for the boundary influence behind the wing will check experimental results for closed rectangular tunnels. In the case of open tunnels, however, the problem is not so definite because other factors, such as the proximity to and shape of the exit cone, may seriously alter the flow behind the wing. Thus it is desirable to verify the validity of the results for any given open tunnel.

LANGLEY MEMORIAL AERONAUTICAL LABORATORY,
NATIONAL ADVISORY COMMITTEE FOR AERONAUTICS,
LANGLEY FIELD, VA., June 28, 1935.

REFERENCES

1. Prandtl, L.: Tragflügeltheorie. II C, Göttingen Nachrichten, 1919.
2. Glauert, H.: The Elements of Aerofoil and Airscrew Theory. Chaps. XII and XIV, Cambridge University Press, 1926.
3. Glauert, H.: The Interference on the Characteristics of an Aerofoil in a Wind Tunnel of Rectangular Section. R. & M. No. 1459, British A. R. C., 1932.
4. Terazawa, Kwan-ichi: On the Interference of Wind Tunnel Walls of Rectangular Cross-Section on the Aerodynamical Characteristics of a Wing. Report No. 44, Aero. Res. Inst., Tokyo Imperial University, 1928.
5. Theodorsen, Theodore: The Theory of Wind-Tunnel Wall Interference. T. R. No. 410, N. A. C. A., 1931.
6. Theodorsen, Theodore: Interference on an Airfoil of Finite Span in an Open Rectangular Wind Tunnel. T. R. No. 461, N. A. C. A., 1933.
7. Rosenhead, L.: The Effect of Wind Tunnel Interference on the Characteristics of an Aerofoil. Roy. Soc. Proc., Math. and Phys., 129A, (London), 1930, pp. 115-135.
8. Tani, Itiro, and Sanuki, Matao: The Wall Interference of a Wind Tunnel of Elliptic Cross Section. Proceedings of the Physics-Math. Soc. of Japan, 3d Series, vol. 14, no. 10, 1932.
9. Theodorsen, Theodore, and Silverstein, Abe: Experimental Verification of the Theory of Wind-Tunnel Boundary Interference. T. R. No. 478, N. A. C. A., 1934.
10. Glauert, H., and Hartshorn, A. S.: The Interference of Wind Channel Walls on the Downwash Angle and the Tailsetting to Trim. R. & M. No. 947, British A. R. C., 1924.

REPORT No. 548

EFFECT OF TIP SHAPE AND DIHEDRAL ON LATERAL-STABILITY CHARACTERISTICS

By JOSEPH A. SHORTAL

SUMMARY

Tests were conducted in the N. A. C. A. 7- by 10-foot wind tunnel to determine the effect of wing-tip shape and dihedral on some of the aerodynamic characteristics of Clark Y wings that affect the performance and lateral stability of airplanes. Force tests at several angles of yaw and rotation tests at zero yaw were made. From these tests the rates of change of rolling-moment, yawing-moment, and cross-wind force coefficients with angle of yaw and the rate of change of rolling-moment coefficient with rolling were determined.

The tests showed that the plan form of a wing tip as well as the elevation shape had considerable effect on the rate of change of rolling- and yawing-moment coefficients with angle of yaw. The tests also showed that with dihedral of only the outer one-fourth of each semispan, the dihedral effect was maintained to a much higher angle of attack than when the complete semispan had dihedral. At normal angles of attack, the increments of rate of change of rolling moment with angle of yaw due to dihedral may be calculated with satisfactory accuracy.

INTRODUCTION

As part of a general program on the improvement of safety in flight the N. A. C. A. has instituted a research of various means for improving the lateral stability of airplanes. That part of the investigation reported herein was made to provide fundamental data on the effect of wing-tip shape and dihedral on some of the lateral-stability factors. The part of the program dealing with tip shape was requested by the Army Air Corps.

The particular wing-tip shapes tested were chosen after a study of existing pertinent data. The pressure-distribution tests of reference 1 revealed that the high local loading near the extreme tips of rectangular wings could be reduced by rounding the tips and also that the centers of pressure could be located nearly on spanwise straight lines by having the extreme tip at least as far forward as 35 percent of the basic chord from the leading edge. Force tests of references 2 to 5 showed that the maximum L/D ratio of a wing with a square tip could be improved by substituting prac-

tically any other shape of tip, the greatest improvement being found with tips having a ratio of the tip length to the basic chord of between 0.75 and 1.50. (See fig. 6.) The maximum lift coefficient was increased with tip-length/basic-chord ratios greater than 0.75 but was decreased with shorter tips. For the present tests, two tips were designed having tip-length/basic-chord ratios of 0.75 and 1.00 and similar plan forms with the extreme tip 35 percent of the basic chord aft of the leading edge. In addition, several modifications so small as to be classed as "tip fairings" rather than as new shapes were tested to determine the effect of such fairings on the aerodynamic characteristics of a rectangular wing since in actual practice small fairings are used to improve the otherwise blunt-end appearance of rectangular wings.

The effect of elevation shape of a particular tip on lift and drag was tested by the Navy (unpublished data). It was found that, although the effect was not great, there was a definite improvement in general performance characteristics in having the lower surface of the tip curve upward. In order to measure this improvement and to determine the effective dihedral angle of such shapes, three elevation shapes of a particular tip were included in the present tests.

The effect of dihedral on the aerodynamic characteristics of airplanes has been experimentally determined in several instances but with small wing models at low air speeds (references 6 to 8). The tests reported herein included the determination of the effect of dihedral angle of the outer 25, 50, and 93 percent of the semispan of a rectangular wing equipped with the rounded tip determined to be the optimum in the first part of the tests. Tests of a rectangular wing with dihedral were included for comparison.

The effect of the various wing shapes on the rates of change of rolling-moment, yawing-moment, and cross-wind force coefficients with angle of yaw and the rate of change of rolling-moment coefficient with rolling was determined in addition to the general aerodynamic characteristics. The results are presented in such a form that they may be directly applied in lateral-stability calculations.

APPARATUS

The N. A. C. A. 7- by 10-foot wind tunnel, which was used in this investigation, has a closed return passage and an open test section (reference 9). The

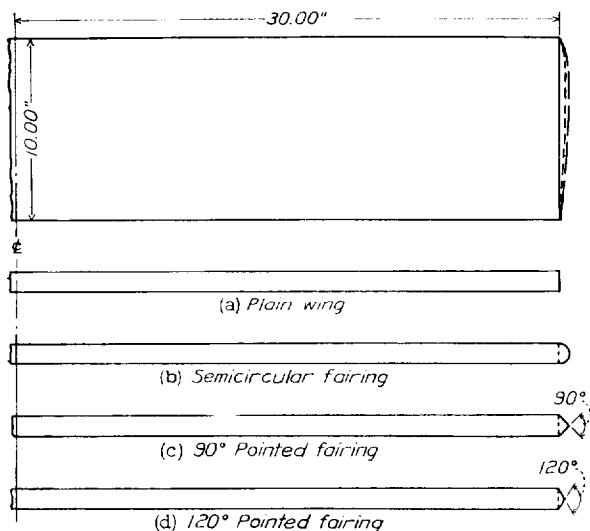


FIGURE 1.—A rectangular wing with small tip fairings.

model under test is attached to a small mounting plate resting on the balance tripod so that the center of moments on the model is at the midspan quarter-chord point. The six-component balance indicates the forces and moments with respect to the wind, or tunnel, axes. The mounting plate is fastened to a

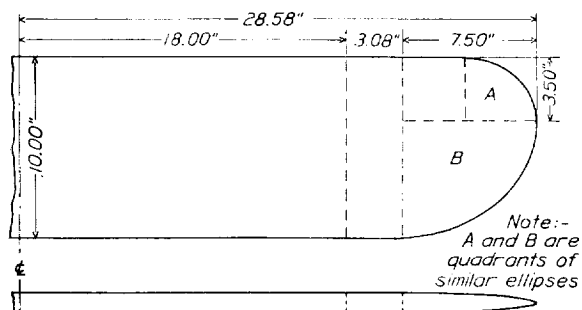


FIGURE 2.—A wing with three-quarters-chord length modified elliptical tip.

spindle that may be rotated in yaw about a vertical axis through a system of gears actuated from without the tunnel. The angle of attack may be changed while the tunnel is in operation. In order to apply a rolling velocity to the model so that the rolling moment accompanying the rolling about the wind axis may be measured, a special rotation mounting replaces the force-test tripod.

Eleven wing models were used in the present investigation. All but the ones with small tip fairings shown in figure 1 are listed in the first column of table I. Laminated mahogany was used in the construction of

the models, which were accurate to within ± 0.005 inch of the specified Clark Y ordinates. The small tip fairings were screwed directly to the ends of the rectangular wing of aspect ratio 6. For the other models, a common center segment of 10-inch chord and 36-inch span was used, the tips under test being sufficiently long to make the aspect ratio of the wing equal to 6 when they were attached to the ends of the common center segment.

For the wings with rounded tips Clark Y sections were maintained without washout to the tips. Two of the tips had the same elevation shape (maximum ordinate points on mean lines in one plane) but different plan forms. One of these had a length equal to three-quarters of the basic wing chord (fig. 2) and the other a length equal to the basic wing chord (fig. 3 (b)). The tips were similar in that they were composed of two quadrants of similar ellipses and a rectangle with the extreme tip 35 percent of the basic chord back of the leading edge of the center section. The other two tips had the same plan form as the above-described larger tip but had different elevation

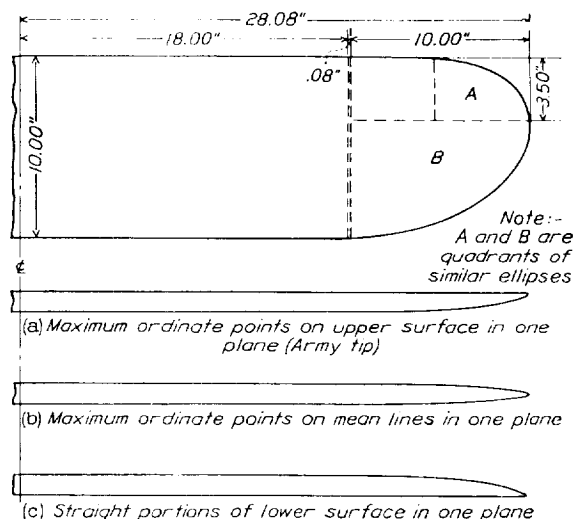


FIGURE 3.—A wing with one-chord length modified elliptical tip having three elevation shapes.

shapes. For one the maximum ordinate points on the upper surface were in one plane (fig. 3 (a)), adopted as the standard Army tip, and for the other the straight portions of the lower surface were in one plane (fig. 3 (c)). In order to find the effect of aspect ratio, the Army tip was attached to the 60-inch span rectangular wing, making the aspect ratio 8.39 instead of 6.

For the dihedral tests, the wing was cut at the proper sections and held at the desired dihedral angles by metal straps set in the surface. With the Army tip in use, these cuts were made 25, 50, and 93 percent of the wing semispan from the tip. (See fig. 4.) With the square tips, dihedral straps were used only at the 93-percent semispan cut. (See fig. 5.)

TESTS

The tests were made at a dynamic pressure of 16.37 pounds per square foot, which corresponds to 80 miles per hour under standard conditions, making the aver-

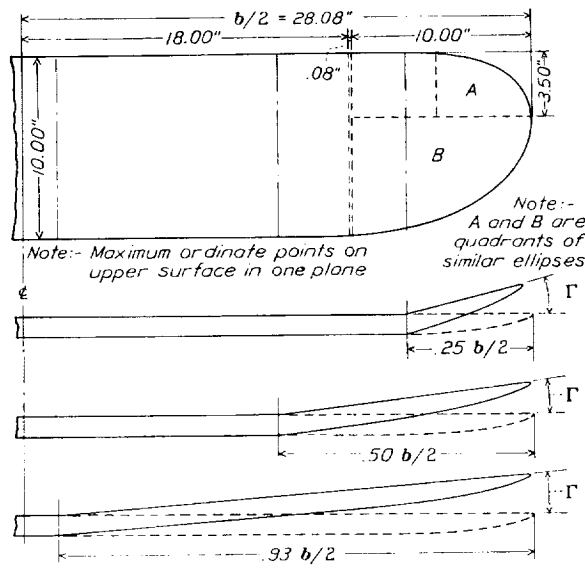


FIGURE 4.—A wing with Army tip showing various dihedral arrangements

age Reynolds Number 609,000 computed on the basic chord of the wing.

With the rectangular wing, force tests were made at a large number of angles of yaw (ψ') to determine the

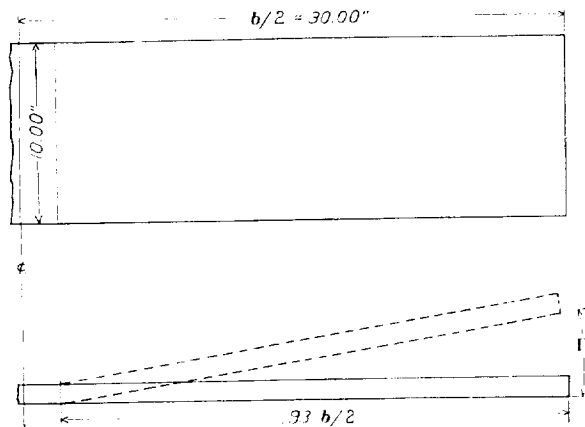


FIGURE 5.—A rectangular wing with dihedral.

minimum number of angles necessary to define the slope of the curves of rolling- and yawing-moment and cross-wind force coefficients against angle of yaw. Values of $\psi' = -5^\circ, 0^\circ$, and 5° having been found sufficient, the tests of the other models were made at these settings and also at $\psi' = 10^\circ$ and $\psi' = 20^\circ$ to cover the range likely to be encountered in flight.

Rolling tests were made with the rectangular wing driven in rotation at values of $\frac{p'b}{2V}$ of 0.02 and 0.05 in

both directions, where p' is the angular velocity in roll about the wind axis. These tests showed that the slope of the curves of rolling-moment coefficient against rate of rotation at zero rotation could be determined from the tests at $\frac{p'b}{2V} = 0.05$ in both directions for angles of attack encountered in normal flying below the stall. Consequently, the remainder of the rotation tests were made only at this rate.

RESULTS

The results, uncorrected for tunnel effects, are presented in the form of standard absolute coefficients with respect to wind axes that intersect on the wing model at the midspan quarter-chord point of the basic chord. The wing area, span, and average chord used in computing the coefficients were those of the wing with no dihedral.

A copy of the extensive tabulated results of the tests herein analyzed is available upon request from the National Advisory Committee for Aeronautics.

The force-test data were plotted against angle of yaw; the rates of change of rolling-moment coefficient $\left(\frac{dC_l'}{d\psi'}\right)_0$, yawing-moment coefficient $\left(\frac{dC_n'}{d\psi'}\right)_0$, and cross-wind force coefficient $\left(\frac{dC_x}{d\psi'}\right)_0$ with angle of yaw

were determined at 0° yaw. In addition, increments of rates of change due to dihedral (designated by Δ) were determined for angles of attack of $0^\circ, 10^\circ$, and 15° and are plotted against angle of dihedral. From the rotation tests the rates of change of rolling-moment coefficient with rate of rotation were determined by summing the values for positive and negative rotation at a rate of $\frac{p'b}{2V} = 0.05$ and dividing by 0.10. These rates of change are designated $\left(\frac{dC_l'}{d\frac{p'b}{2V}}\right)_0$.

The above-mentioned slopes at zero yaw are sufficient for the normal range of angles of attack and yaw encountered in flight and for computations based on the theory of small oscillations. At the angles of attack above the stall and for displacements in yaw greater than 10° , however, the factors cannot be computed directly from the slopes at zero yaw. Unsymmetrical stalling of the wing and the generally unsteady conditions encountered at high angles of attack cause the results to vary widely.

The addition of small tip fairings had such a minor effect on the characteristics of the rectangular wing that the results have not been included. The interesting result of the tests is that small tip fairings may be added to a rectangular wing of aspect ratio 6 without appreciably altering the aerodynamic characteristics.

ACCURACY OF RESULTS

The dynamic pressure was maintained constant within ± 0.25 percent. The angles of attack, yaw, and dihedral were accurate within $\pm 0.10^\circ$. The coefficients for a particular model are believed to be accurate within the following limits:

$$C_{L_{max}} \pm 0.005$$

$$C_{D_{min}} \pm 0.0005$$

$C_l' \pm 0.001$ except at angles of attack above 25° where angles of yaw of opposite sign may give values differing by 0.020.

$C_n' \pm 0.001$ except at high angles of attack where it may be ± 0.010 .

$$C_c \pm 0.002$$

Because of slight inaccuracies in the models resulting from alterations made during the tests, it is believed that for purposes of comparison between models the accuracy should be considered to be ± 0.001 for $C_{D_{min}}$ and ± 0.010 for $C_{L_{max}}$.

PERFORMANCE CRITERIONS

The criterions used to measure the effect of the wing shapes on airplane performance are: The maximum lift coefficient $C_{L_{max}}$, which gives an indication of the landing speed; the minimum drag coefficient $C_{D_{min}}$, which is a high-speed criterion; the ratio of maximum lift coefficient to minimum drag coefficient $C_{L_{max}}/C_{D_{min}}$, a speed-range criterion; and the lift-drag ratio L/D at a lift coefficient of 0.70, which is a criterion of the rate of climb. The values of these criterions for the wings tested have been tabulated in table I for a direct comparison.

TABLE I.—PERFORMANCE CRITERIONS OF RECTANGULAR WINGS HAVING VARIOUS TIP SHAPES AND DIHEDRAL ANGLES

[All wings not otherwise designated have an aspect ratio of 6]

Wing shape	Dihedral angle 1°	Criterion			
		$C_{L_{max}}$	$C_{D_{min}}$	$\frac{C_{L_{max}}}{C_{D_{min}}}$	$\frac{L}{D}$ at $C_L = 0.70$
Rectangular tip, 0.93 b/2 dihedral	0	1.268	0.0158	80.3	15.2
Do	5	1.242	.0162	76.6	14.0
Do	10	1.222	.0168	72.7	14.7
0.75c rounded tip ¹	0	1.265	.0160	79.5	15.9
1.00c rounded tip ¹	0	1.278	.0154	82.9	16.6
Do ²	0	1.277	.0155	82.3	16.3
1.00c rounded tip, ³ 0.25 b/2 dihedral	0	1.281	.0156	82.1	16.2
Do	7	1.293	.0159	81.3	16.4
Do	15	1.289	.0163	79.0	15.9
Do	30	1.262	.0167	75.5	15.5
Do	45	1.225	.0168	73.0	15.3
1.00c rounded tip, ³ 0.50 b/2 dihedral	0	1.298	.0162	80.1	15.4
Do	5	1.295	.0162	80.0	15.4
Do	10	1.288	.0162	79.9	15.4
Do	15	1.262	.0169	74.7	15.3
1.00c rounded tip, ³ 0.93 b/2 dihedral	0	1.288	.0162	79.5	15.2
Do	2	1.295	.0168	77.0	15.2
Do	5	1.275	.0164	77.7	15.2
Do	10	1.248	.0162	77.0	15.2
Do	15	1.205	.0156	77.2	14.8
1.00c rounded tip ³ (A. R. 8.39)	0	1.321	.0148	89.3	18.5

¹ Maximum ordinate points on mean lines in one plane.

² Straight portions of lower surface in one plane.

³ Maximum ordinate points on upper surface in one plane (Army tip).

Effect of plan form.—The rectangular wing with rounded tips of a length equal to three-quarters the basic chord had practically the same performance characteristics as the plain rectangular wing of the same aspect ratio except for the rate-of-climb criterion, which was increased in the order of 4 percent. The rounded tip equal to the basic chord in length had, however, improved performance characteristics; the speed-range ratio was increased about 3 percent and the climb criterion about 9 percent. Although these percentages are within the experimental error, it is believed that they indicate a definite trend. The effect of these two similarly shaped tips of different lengths is in fair agreement with previous systematic tests of the effect of plan form as shown in figure 6. The improvement in rate-of-climb criterion is explained by the fact that the span load distribution for the wings with rounded tips approaches the ideal, which results in a lower induced drag.

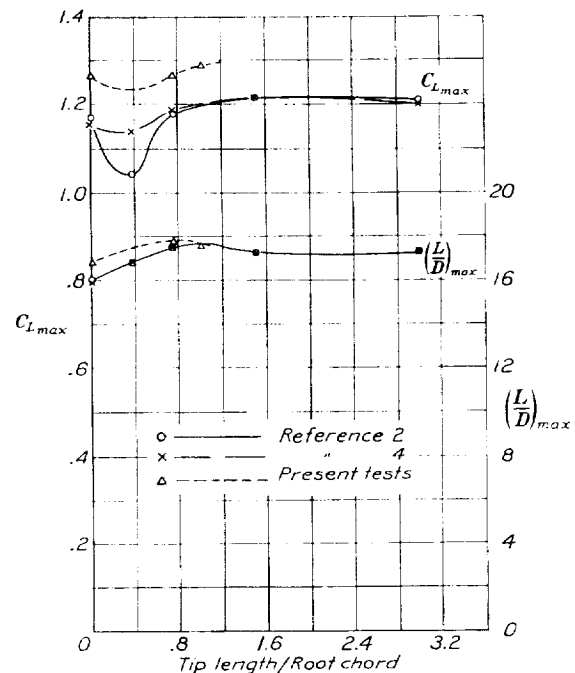


FIGURE 6.—Effect of tip length on $C_{L_{max}}$ and $(L/D)_{max}$.

Effect of elevation shape.—The effect of elevation shape of the one-chord length tip on the performance criterions is shown in table I. The results of these tests are in agreement with previous unpublished Navy tests in that, although the effect of elevation shape on the performance criterions is not great, there is a certain advantage in raising the extreme tip at least as high as the midpoint. The tip adopted by the Army as their standard rounded tip is the longer rounded tip with the maximum ordinate points on the upper surface in one plane.

Effect of aspect ratio.—The wing with aspect ratio 8.39 was made by adding the Army tip to the rectangular wing of aspect ratio 6, which makes the tip portion a smaller percentage of the span than the wing of aspect ratio 6 with Army tip. An appreciable im-

provement was obtained in all the performance criterions with the wing of aspect ratio 8.39 over those of the same wing of aspect ratio 6.

Effect of dihedral.—The effects of the various dihedral arrangements on the performance criterions are

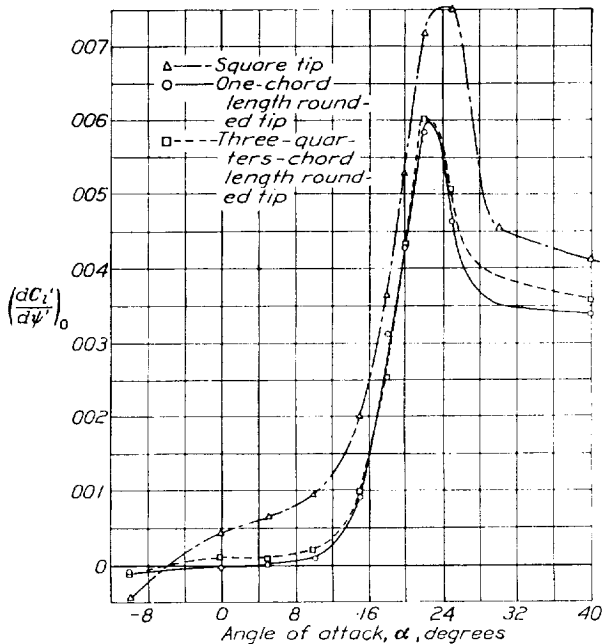


FIGURE 7.—Effect of wing tip plan form on rate of change of rolling-moment coefficient with angle of yaw. Maximum ordinate points on mean lines in one plane.

compared in table I. As the coefficients are based on the area of the wings with no dihedral, the maximum lift would be expected to be lower with dihedral because of the reduction of the projected area of the wing on a lateral plane. Such was the case in the actual tests; the reduction in maximum lift coefficients was proportional to the reduction in the projected area. The minimum drag coefficients, however, increased slightly in every case except with the Army tip with 93 percent semispan dihedral. The coefficients used would be expected to remain constant except for interference effects at the juncture of the portions of the wing forming the dihedral angle. In all cases the effect was no larger than about 5 percent. Since the maximum lift coefficient was decreased and the minimum drag coefficient was increased, the speed-range ratio was reduced about 10 percent for extreme dihedral angles except for the wing with Army tip and 93 percent semispan dihedral, for which the ratio remained practically constant. For dihedral angles normally used (5° or less), however, the effect is negligible. All the dihedrals reduced the rate-of-climb criterion by a slight amount.

AERODYNAMIC CHARACTERISTICS AFFECTING LATERAL STABILITY

In order to make a complete determination of the asymmetric motions and the lateral stability of an air-

plane, there are required nine resistance derivatives determined from the rate of change of rolling moment, of yawing moment, and of cross-wind force with cross-wind velocity, with rolling velocity, and with yawing velocity. The results are presented in such a manner that a direct determination is possible of four of the derivatives, namely, the three computed from the rate of change of rolling moment, of yawing moment, and of cross-wind force with cross-wind velocity, and the one computed from the rate of change of rolling moment with rolling velocity. Although these four factors are the important ones affected by the wing shapes tested, it is considered outside the scope of this report to make detailed lateral-stability calculations in which assumptions for the remaining factors would be required. Consequently, only the quantitative effects of the wing shapes on the four above-mentioned factors will be discussed.

Effect of plan form.—When a wing is yawed, the span load distribution is considerably changed and a rolling moment results that may become very large at high angles of attack. The particular changes that occur are clearly shown by means of pressure-distribution tests in reference 10. The particular plan form of the wing has an appreciable effect on the results as shown in figure 7 where the rates of change of rolling-moment coefficient with angle of yaw $\left(\frac{dC_l'}{d\psi'}\right)_0$ is given for three wings of the same elevation shape but having different plan forms. The effect is pronounced at an angle of attack of 10° , which corresponds to a lift coefficient of about 1.0, where the rate of change given by

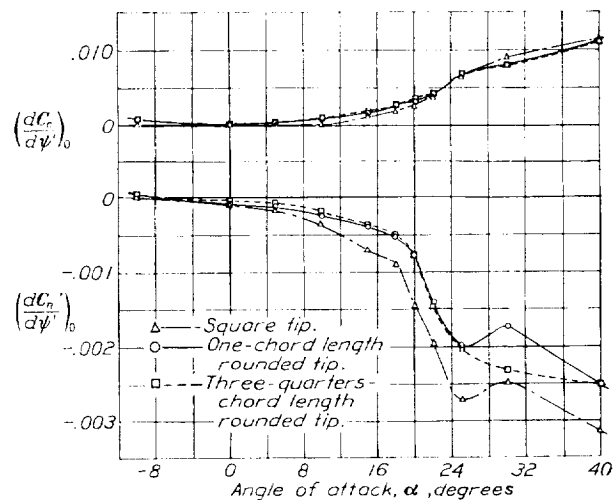


FIGURE 8.—Effect of wing tip plan form on rate of change of cross-wind force and yawing-moment coefficients with angle of yaw. Maximum ordinate points on mean lines in one plane.

the square tip was about four times that of the rounded tip. The effect of plan form on $\left(\frac{dC_l'}{d\psi'}\right)_0$ and $\left(\frac{dC_n'}{d\psi'}\right)_0$ as shown in figure 8 is small compared with the values due to the fuselage and tail. At angles of attack near that

for minimum speed, the values of $\left(\frac{dC_n'}{d\psi'}\right)_0$, which is a measure of the directional stability, were about twice as high for the rectangular wing as for the wings with rounded tips. The values of rates of change of rolling-moment coefficient with rolling $\left(\frac{dC_l'}{d\psi'}\right)_0$ as shown in figure 9 were reduced by rounding the tips in the order

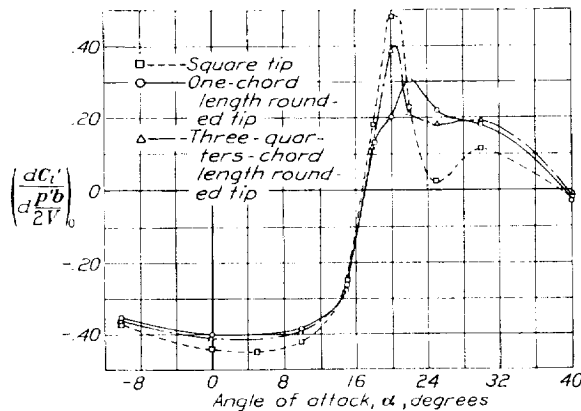


FIGURE 9.—Effect of wing tip plan form on rate of change of rolling-moment coefficient with rate of roll. Maximum ordinate points on mean lines in one plane.

that would be expected, the greatest values being for the rectangular wing.

Effect of elevation shape.—In figure 10 is shown the effect of elevation shape of a one-chord length rounded tip on $\left(\frac{dC_l'}{d\psi'}\right)_0$. Up to 15° angle of attack, changing

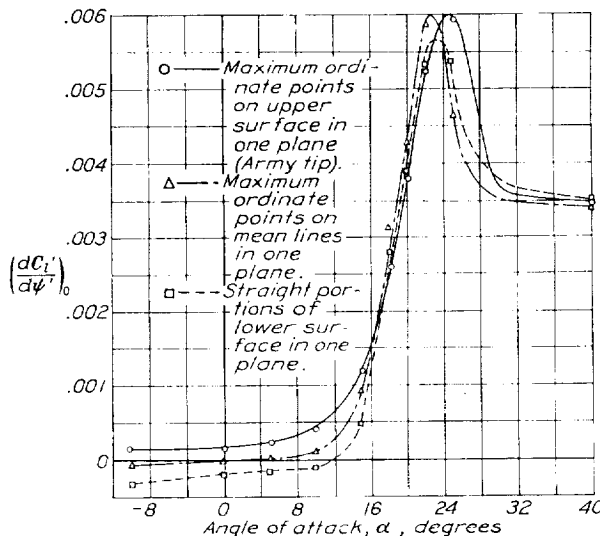


FIGURE 10.—Effect of elevation shape of a one-chord length rounded tip on rate of change of rolling-moment coefficient with angle of yaw.

the elevation shape resulted in a parallel shifting of the curves. Later tests showed that this shift could be expressed in terms of effective full-span dihedral; placing the maximum ordinate points on mean lines in one plane was equivalent to giving a wing with the Army

tip (maximum ordinate points on upper surface in one plane) a negative dihedral angle of 1½°; whereas placing the straight portions of the lower surface in one plane

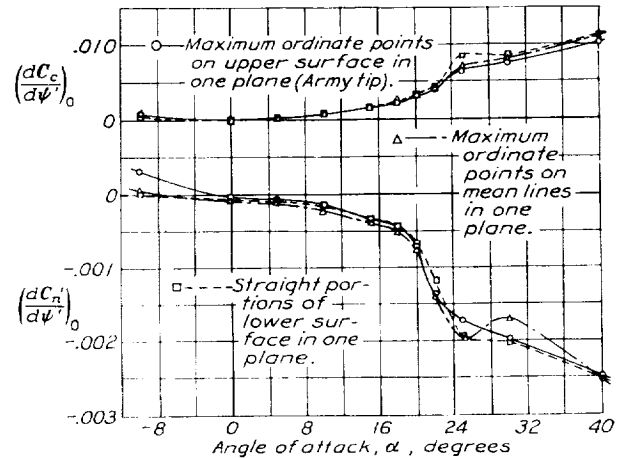


FIGURE 11.—Effect of elevation shape of a one-chord length rounded tip on rate of change of cross-wing force and yawing-moment coefficients with angle of yaw.

was equivalent to a negative dihedral angle of 2½°. Above 15° angle of attack, the elevation shape had practically no effect. Neither the values of $\left(\frac{dC_n'}{d\psi'}\right)_0$

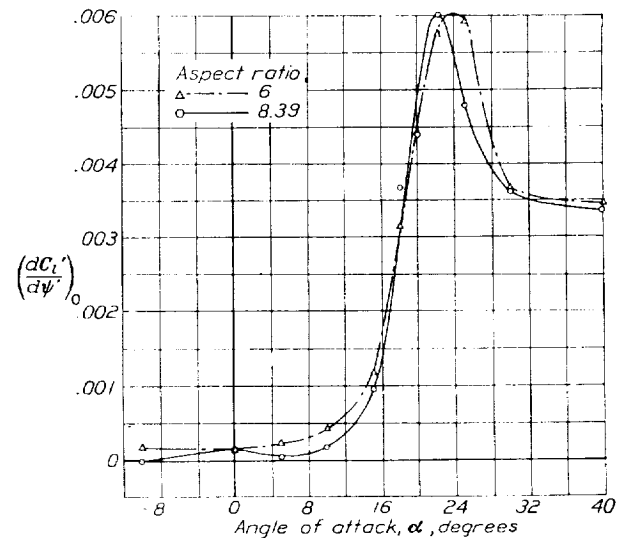


FIGURE 12.—Effect of aspect ratio of a wing with Army tip on rate of change of rolling-moment coefficient with angle of yaw. Maximum ordinate points on upper surface in one plane.

and $\left(\frac{dC_ε'}{d\psi'}\right)_0$, given in figure 11, nor the values of $\left(\frac{dC_l'}{d\psi'}\right)_0$ were affected by elevation shape.

Effect of aspect ratio.—It had been previously found that increasing the aspect ratio of a wing decreased $\left(\frac{dC_l'}{d\psi'}\right)_0$. (See reference 11.) The results of the present tests (see fig. 12) show that the reduction in $\left(\frac{dC_l'}{d\psi'}\right)_0$ for the wing of aspect ratio 8.39 was equivalent

to a negative dihedral angle of $1\frac{1}{2}^\circ$ for the wing of aspect ratio 6. On the other hand, the values of $\left(\frac{dC_n}{d\psi'}\right)_0$ and $\left(\frac{dC_c}{d\psi'}\right)_0$ were unaffected by aspect ratio.

Effect of dihedral.—As previously mentioned, most of the dihedral tests were made with the Army tip

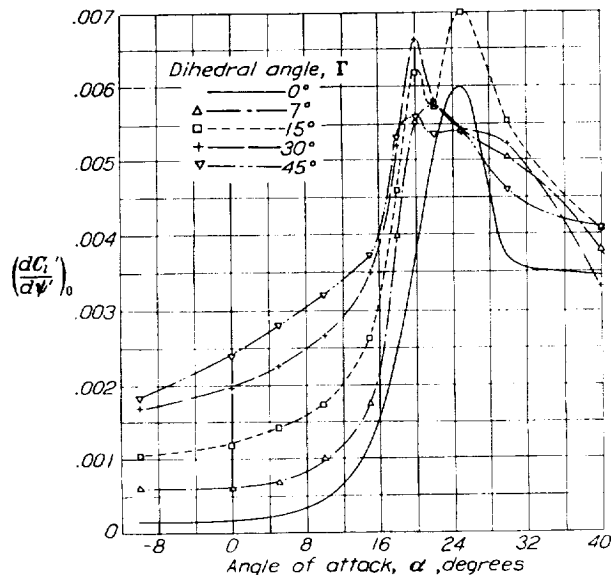


FIGURE 13.—Effect of dihedral of 25 percent semispan of wing with Army tip on rate of change of rolling-moment coefficient with angle of yaw.

although a few tests were made with the rectangular tip. The dihedral axis for the wing with the Army tip was located successively 25, 50, and 93 percent of the semispan from the tip of the wing. With the dihedral

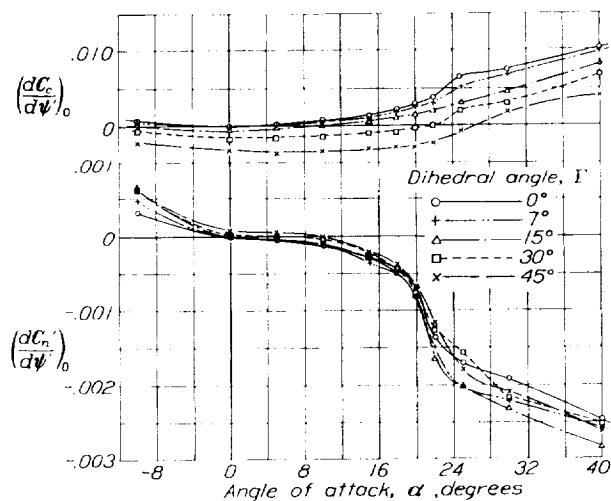


FIGURE 14.—Effect of dihedral of 25 percent semispan of wing with Army tip on rate of change of cross-wind force and yawing-moment coefficients with angle of yaw.

axis at the 25-percent point, the values of $\left(\frac{dC_l'}{d\psi'}\right)_0$ (fig. 13) are increased by dihedral up to angles of attack as high as 22° ; with the dihedral axis at the 50-percent point (fig. 16), the values are increased up through

20° angle of attack; and with 93 percent of the semispan in use (fig. 18), the increase in $\left(\frac{dC_l'}{d\psi'}\right)_0$ due to dihedral is reduced to zero at 19° angle of attack. This action is explained by the manner in which a rectangular

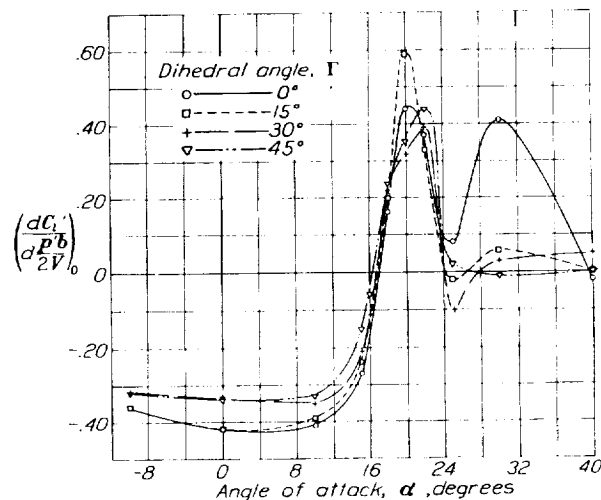


FIGURE 15.—Effect of dihedral of 25 percent semispan of wing with Army tip on rate of change of rolling-moment coefficient with rate of roll.

wing stalls. The burble starts at the center section and spreads toward the tips, the tips remaining unaffected for several degrees after the center-section flow breaks down. The effect of dihedral on $\left(\frac{dC_c}{d\psi'}\right)_0$

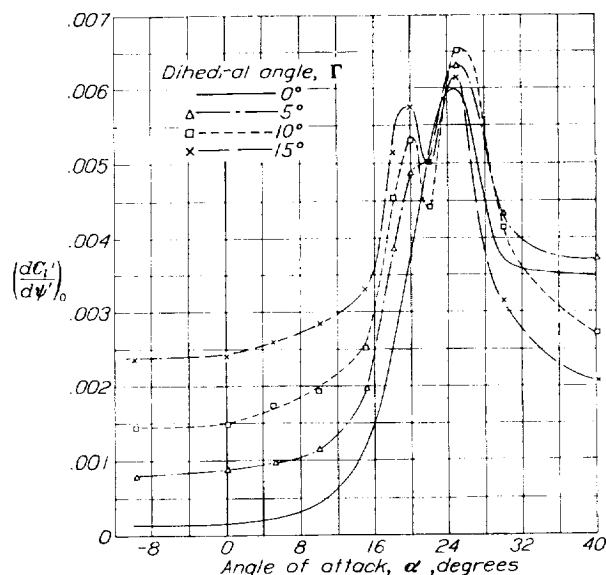


FIGURE 16.—Effect of dihedral of 50 percent semispan of wing with Army tip on rate of change of rolling-moment coefficient with angle of yaw.

and $\left(\frac{dC_l'}{d\psi'}\right)_0$ shown in figures 14, 17, and 19, although not large, is fairly consistent for the three dihedral axes used. The values of $\left(\frac{dC_c}{d\psi'}\right)_0$ were reduced for the wing alone as would be expected but the values of

$\left(\frac{dC_n'}{d\psi'}\right)_0$, the directional-stability criterion, became more positive. The values of $\left(\frac{dC_l'}{d\psi'}\right)_0$ were decreased somewhat when the dihedral axis was at 25-percent semispan (fig. 15) and the dihedral angle was greater

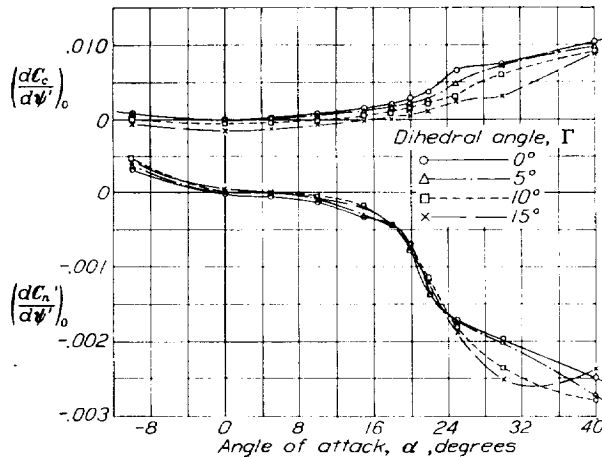


FIGURE 17.—Effect of dihedral of 50 percent semispan of wing with Army tip on rate of change of cross-wind force and yawing-moment coefficients with angle of yaw.

than 15° . For the other dihedral-axis locations, the values were hardly affected for the angles up to 15° . When the wing with square tips was given dihedral the values of $\left(\frac{dC_l'}{d\psi'}\right)_0$, $\left(\frac{dC_n'}{d\psi'}\right)_0$, $\left(\frac{dC_c}{d\psi'}\right)_0$, and $\left(\frac{dC_l'}{d\psi'}\right)_0$ were

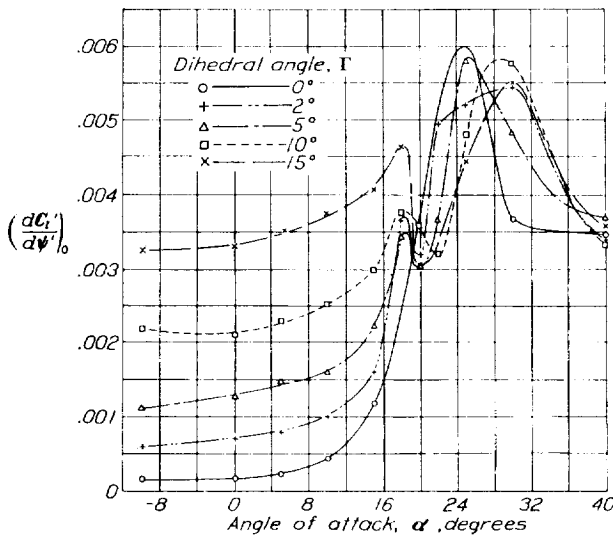


FIGURE 18.—Effect of dihedral of 93 percent semispan of wing with Army tip on rate of change of rolling-moment coefficient with angle of yaw.

affected in about the same manner as were the values for the wing with the Army tip, except that the values of $\left(\frac{dC_l'}{d\psi'}\right)_0$ due to dihedral reversed in effect at 18°

angle of attack and considerably reduced the total $\left(\frac{dC_l'}{d\psi'}\right)_0$ for the wing. (See figs. 20 and 21.)

A more direct comparison of the effects of the dihedrals tested was made by computing the increments of

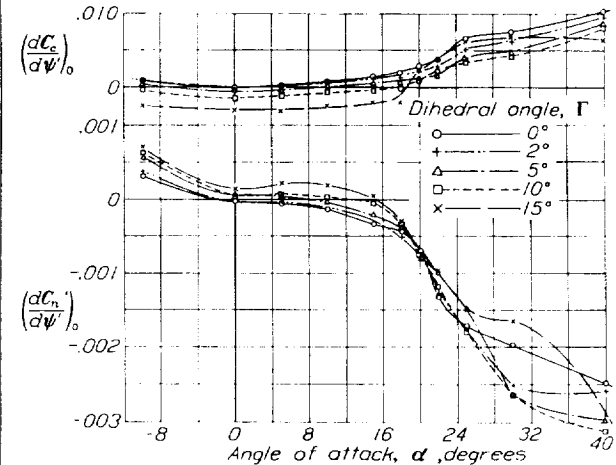


FIGURE 19.—Effect of dihedral of 93 percent semispan of wing with Army tip on rate of change of cross-wind force and yawing-moment coefficients with angle of yaw.

rates of change due to dihedral angle, $\Delta\left(\frac{dC_l'}{d\psi'}\right)_0$, $\Delta\left(\frac{dC_n'}{d\psi'}\right)_0$, and $\Delta\left(\frac{dC_c}{d\psi'}\right)_0$ for 0° , 10° , and 15° angles of attack and plotting them against dihedral angle in figure 22. It

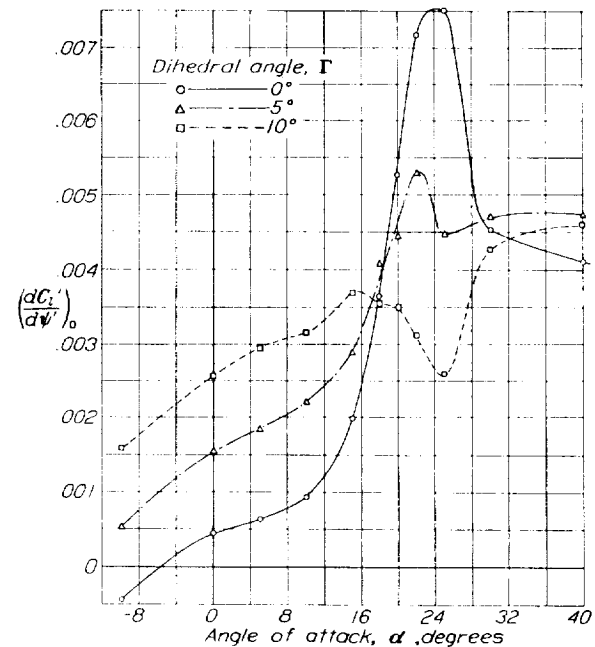


FIGURE 20.—Effect of dihedral of 93 percent semispan of a rectangular wing on rate of change of rolling-moment coefficient with angle of yaw.

may be seen that the increments with the rectangular wing are practically the same as for the wing with the Army tip when the same percentage of the semispan is

used in both cases. This agreement is an indication that the effects due to a dihedral angle with practically the full semispan in use may be added directly to the basic 0° dihedral curves regardless of tip shape.

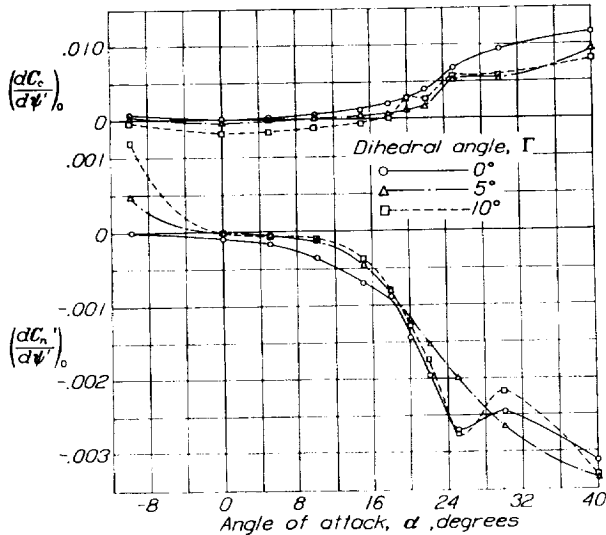


FIGURE 21.—Effect of dihedral of 93 percent semispan of rectangular wing on rate of change of cross-wind force and yawing-moment coefficients with angle of yaw.

The increments $\Delta\left(\frac{dC_l'}{d\psi'}\right)_0$ and $\Delta\left(\frac{dC_n'}{d\psi'}\right)_0$ lend themselves to further evaluation since they vary as a straight line with the angle of dihedral Γ up to an angle of 15° .

An average curve has been drawn through the sets of points and the equations of the curves have been determined to be

$$\frac{d}{d\Gamma} \Delta\left(\frac{dC_l'}{d\psi'}\right)_0 = 0.000333K - 0.000118K^{2.35}$$

$$\frac{d}{d\Gamma} \Delta\left(\frac{dC_n'}{d\psi'}\right)_0 = 0.000024K^{1.5}$$

where K is the fraction of the semispan in use.

These equations may be used with sufficient accuracy in determining the effect of dihedral of any fraction of the semispan of a rectangular wing of Clark Y or similar section having an aspect ratio of 6 with the Army tip. These values, of course, must be added to the basic values for the wing with 0° dihedral. If the entire semispan has dihedral, K becomes 1.0, $\frac{d}{d\Gamma} \Delta\left(\frac{dC_l'}{d\psi'}\right)_0 = 0.000215$, and $\frac{d}{d\Gamma} \Delta\left(\frac{dC_n'}{d\psi'}\right)_0 = 0.000024$. Blenk (reference 6) found corresponding values of 0.000204 and 0.000030 for a rectangular wing with square tips.

Comparison of calculated and experimental results.—When a wing with a dihedral angle Γ is yawed through an angle ψ' , the new wing chord along the wind direction is

$$c' = \frac{c}{\cos \psi'}$$

and the spanwise displacement of the trailing edge relative to the leading edge of the chord line is

$$l = c' \sin \psi'$$

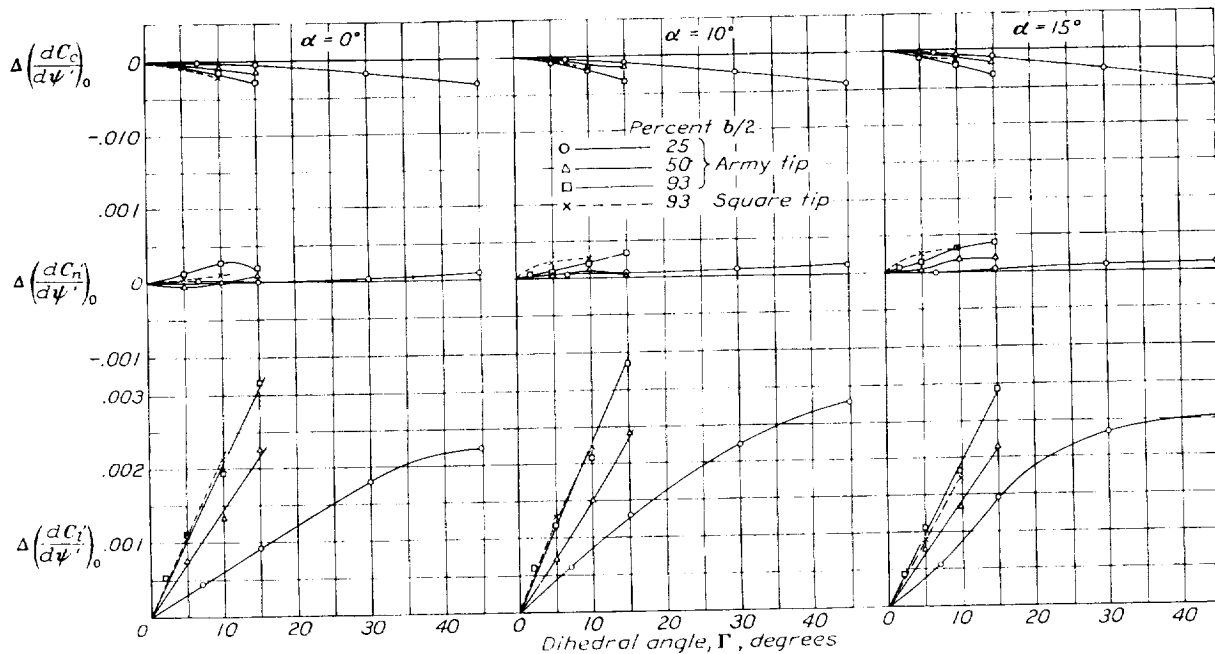


FIGURE 22.—Effect of dihedral on rates of change of rolling-moment, yawing-moment, and cross-wind force coefficients with angle of yaw.

Consequently, the values of $\frac{d}{d\Gamma} \Delta\left(\frac{dC_l'}{d\psi'}\right)_0$ and $\frac{d}{d\Gamma} \Delta\left(\frac{dC_n'}{d\psi'}\right)_0$ were determined from figure 22 for the wing with the Army tip and have been plotted against fraction of wing semispan in figure 23 for the three angles of attack.

Then, owing to the dihedral angle, the trailing edge of the new chord of the rearward wing is higher than its leading edge by an amount

$$h = l \sin \Gamma$$

which may be written

$$h = c' \sin \psi' \sin \Gamma$$

This value makes the angle of attack of c' less than the angle of attack of c so that

$$\sin \Delta\alpha' = \frac{h}{c'} = \sin \psi' \sin \Gamma$$

Now for small angles the sine equals the angle in radians, so that

$$\Delta\alpha' = \psi' \Gamma \text{ (all in radians)}$$

Likewise, on the forward wing the angle of attack is increased by

$$\Delta\alpha' = \psi' \Gamma$$

Wieselsberger has shown (reference 12) that the rolling moment due to an unsymmetrical span load distri-

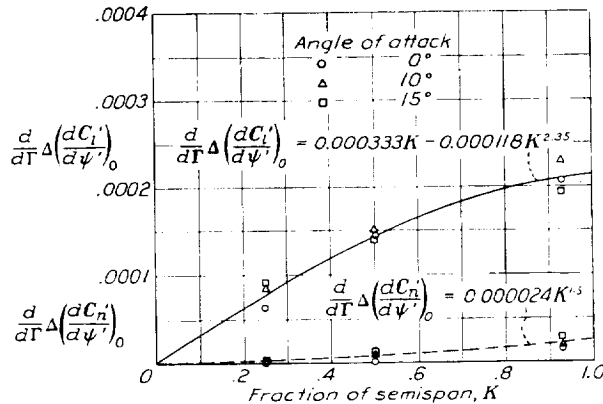


FIGURE 21.—Effect of dihedral span on rate of change with dihedral angle of the rate of change of rolling moment with angle of yaw.

bution resulting from equal changes in angle of attack of opposite sign on the two halves of a rectangular wing may be expressed by

$$M_y' = \frac{\rho V^2}{2} b^3 \zeta \alpha_q$$

where ζ is a factor dependent on the aspect ratio and the slope of the lift curve for a wing of infinite aspect ratio and α_q is the change in angle of attack.

Expressing this equation in coefficient form results in

$$C_l' = \zeta \alpha_q \left(\frac{b^2}{S} \right)$$

Substituting for α_q its equal $\frac{\psi' \Gamma}{57.3^\circ}$ for $\left(\frac{b^2}{S} \right)$ the value of 6, and for ζ the value 0.127 from Wieselsberger and Asano (reference 13) for a change in angle of attack over 93 percent of the span,

$$C_l' = 0.127 \frac{\psi' \Gamma}{57.3^\circ} \times 6$$

Then differentiating with respect to ψ' and Γ ,

$$\frac{d}{d\Gamma} \left(\frac{dC_l'}{d\psi'} \right)_0 = 0.000232$$

which is, within the limits of accuracy, equal to the value found from the experiments reported herein.

CONCLUSIONS

1. The rate of change of rolling moment with angle of yaw was greatly affected by wing-tip shape.
2. Agreement was obtained between computed and experimental values of the rate of change of rolling moment with angle of yaw due to dihedral of a rectangular wing.
3. The dihedral effect was maintained to a higher angle of attack with dihedral of only the outer one-fourth of each semispan than when the entire semispan had dihedral.

LANGLEY MEMORIAL AERONAUTICAL LABORATORY,
NATIONAL ADVISORY COMMITTEE FOR AERONAUTICS,
LANGLEY FIELD, VA., August 27, 1935.

REFERENCES

1. Rhode, Richard V.: The Influence of Tip Shape on the Wing Load Distribution as Determined by Flight Tests. T. R. No. 500, N. A. C. A., 1934.
2. Beisel, R. B.: Wing Tip Forms. Aircraft Tech. Note No. 106, Navy Dept., Bur. Constr. and Repair, 1921.
3. Irving, H. B., and Powell, C. H.: The Effect of Rounding the Wing Tips of an Aerofoil Having a High Value of Maximum Lift Coefficient. R. & M. No. 330, British A. C. A., 1917.
4. Relf, E. F.: Effect of Shape of Wing Tips on the Lift, Drag, and Centre of Pressure of an Aerofoil. R. & M. No. 152, Section I.—(iv), British A. C. A., 1914.
5. Parkin, J. H., Crane, H. C., and Galbraith, S. L.: Wing Tip Research. Part I.—Effect of Outline and Washout of Camber on the Aerodynamic Efficiency. Univ. Toronto Eng. Res. Bull. No. 2, pp. 78–110. Aero. Res. Paper No. 4, Dec. 1920.
6. Blenk, Herman: Göttingen Six-Component Measurements on Wings with Dihedral, Sweepback, and Warp. A. C. T. R., Translation No. 250, Matériel Div., Army Air Corps, 1929.
7. Relf, E. F., and Landells, A.: Forces and Moments on an Aerofoil Having a Dihedral Angle. R. & M. No. 152, Section I (iii), British A. C. A., 1914.
8. Hunsaker, J. C., and Douglas, D. W.: Experiments on a Dihedral Angle Wing. Smithsonian Misc. Collections, vol. 62, no. 4, 1916.
9. Harris, Thomas A.: The 7- by 10-Foot Wind Tunnel of the National Advisory Committee for Aeronautics. T. R. No. 412, N. A. C. A., 1931.
10. Williams, D. H.: Pressure Distribution Over a Yawed Aerofoil. R. & M. No. 1203, British A. R. C., 1928.
11. Zimmerman, C. H.: Characteristics of Clark Y Airfoils of Small Aspect Ratios. T. R. No. 431, N. A. C. A., 1932.
12. Wieselsberger, C.: Theoretical Investigation of the Effect of the Ailerons on the Wing of an Airplane. T. M. No. 510, N. A. C. A., 1929.
13. Wieselsberger, C., and Asano, T.: Determination of the Air Forces and Moments Produced by the Ailerons of an Airplane. T. M. No. 488, N. A. C. A., 1928.

REPORT No. 549

WIND-TUNNEL INVESTIGATION OF THE AERODYNAMIC BALANCING OF UPPER-SURFACE AILERONS AND SPLIT FLAPS

By CARL J. WENZINGER

SUMMARY

An investigation was made in the N. A. C. A. 7- by 10-foot wind tunnel to determine the effectiveness of various methods of reducing the high control forces of unbalanced upper-surface ailerons and of unbalanced split flaps. An unusual test installation was used in which a large-chord wing model was mounted on the regular balance between two large end planes. The tests included many different aileron-axis and flap-axis locations and several arrangements of aileron and flap slots, all on a Clark Y wing. In addition to the hinge moments, the rolling and the yawing moments as well as the lift and drag characteristics of the various arrangements were determined.

As a result of the investigation, a balanced split flap was developed that required control forces about half those of the unbalanced split flap when the balanced split flap was deflected to give approximately the same maximum lift. No entirely satisfactory arrangement of balanced upper-surface ailerons was found but one arrangement was developed that appeared satisfactory except for the stick-force characteristics with small aileron deflections at high angles of attack with the flaps neutral. Another arrangement also appeared satisfactory for all flight conditions except the lowest speeds obtainable with flaps neutral, in which case the indicated rolling moments were low.

INTRODUCTION

For a wing with full-span split flaps, the lateral control may be obtained by "upper-surface ailerons" formed by hinging the upper portion of the split trailing edge and deflecting it upward. Wind-tunnel tests (reference 1) of a wing equipped with such a device indicated that reasonably satisfactory control would be available below the stall with the flaps neutral and somewhat less satisfactory control with the flaps down for high lift.

The main disadvantage of upper-surface ailerons appears to be the high control force required for their operation in comparison with the forces required for similar ordinary ailerons having conventional movement (reference 2). The aileron characteristics are affected to a considerable extent by the deflected split flaps. The control forces required to operate the

flaps are also very high (reference 3); their full deflection usually requires many turns of a crank.

The present tests were undertaken to determine the effectiveness of various methods of reducing the control forces required for both upper-surface ailerons and split flaps. The locations of the axes of the ailerons and the flaps were varied, and several arrangements of aileron and flap slots were investigated. The effects of the ailerons and flaps on the lift and drag of the wing were measured and the rolling and yawing moments were calculated.

MODELS AND APPARATUS

For the present tests it was desirable to use a wing model with a chord considerably longer than the 10-inch-chord models customarily used for tests in the 7- by 10-foot wind tunnel in order to enable easier modifications of the ailerons and flaps. A large-chord model of short span was therefore mounted between two end planes. With such an installation it was hoped to obtain approximately two-dimensional flow and so measure the section characteristics of the model under test.

The basic wing model of laminated mahogany was built to the Clark Y profile and was 20 inches in both span and chord. The full-span ailerons and flaps were also of laminated mahogany. Circular metal end plates 24 inches in diameter were fastened rigidly to the tips of the wing model with the centers of the plates located at the midchord point of the wing chord line. The ailerons and flaps were supported at each end by rods passing through holes in the end plates and were supported at their midspan by thin metal fixtures attached to the wing. The hinge-axis locations could be easily and quickly changed. The ailerons and flaps could either be locked at a desired deflection or be arranged to swing freely about any hinge axis.

The model was mounted at its 50-percent-chord point on the regular force-test tripod of the N. A. C. A. 7- by 10-foot open-throat wind tunnel. (See reference 4.) Two large wooden end planes were mounted so as to include the model and its end plates between them. (See fig. 1.) A circular cut-out in each end plane allowed the model to rotate freely; any contact between the end plates and the end planes was indicated by the flashing of a neon bulb.

Lift and drag forces were read directly on the regular wind-tunnel balances. Hinge moments were measured by the twist of a long calibrated slender steel rod connected at one end to the aileron or flap (free to

general, from 0° to 25° ; the aileron and flap deflections ranged in most cases from neutral to 90° up and 90° down.

PRELIMINARY TESTS

Air-flow surveys.—Dynamic-pressure surveys were made between the end planes at the model location to obtain a calibration for use with the static reference pressure plates of the wind tunnel. The wing model was removed for these tests, and the metal end plates were attached rigidly to the wooden end planes. The dynamic-pressure distribution between the planes was found to be satisfactory, and a static-pressure survey was then made along the jet center line. The static pressure showed a considerable gradient along that portion of the jet occupied by the model and this condition was taken into account by making a suitable correction to the measured drag.

Tare forces.—It was necessary to determine the tare forces due to the metal end plates in order to obtain the net forces. One series of tests was therefore made with the end plates attached to the wing equipped with an unbalanced split flap, the tests being made with flap

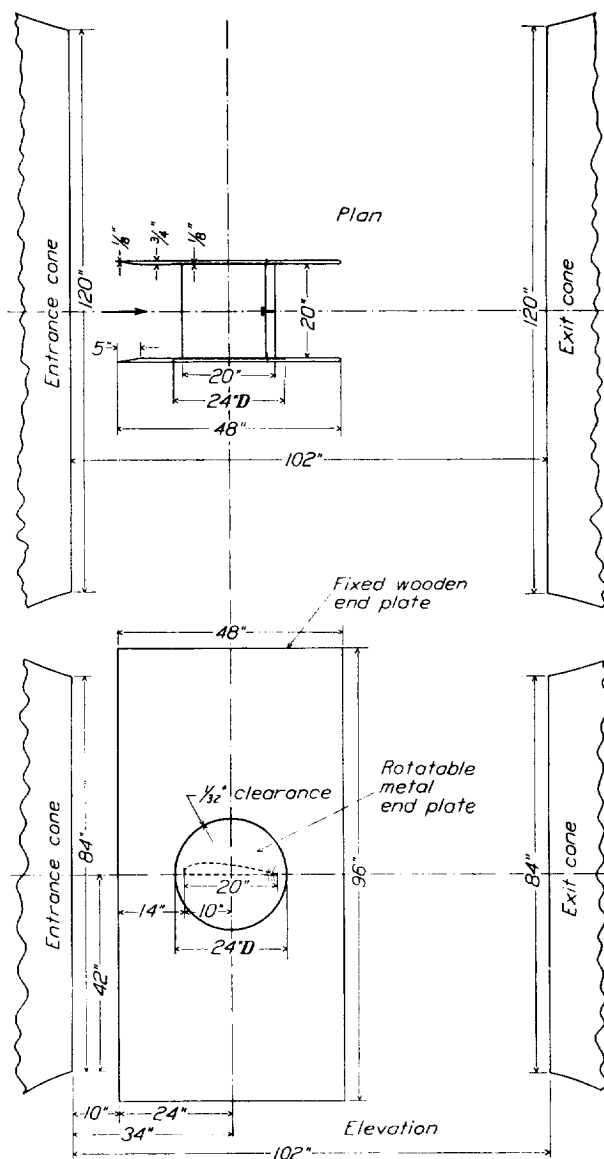


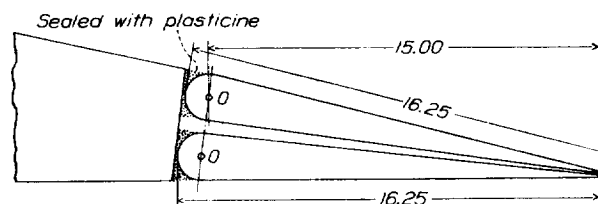
FIGURE 1.—Wind-tunnel installation of wing model between end planes.

swing) and at the other end to a clamp with pointer and dial outside the air stream.

METHODS

GENERAL TEST CONDITIONS

The tests all were made at a dynamic pressure of 16.37 pounds per square foot corresponding to an air speed of 80 miles per hour under standard sea-level conditions. The average Reynolds Number, based on the test air speed and on the wing chord, was 1,218,000 (twice that of the tests usually made in the 7- by 10-foot wind tunnel). The angles of attack ranged, in



Note: All dimensions in percent wing chord

FIGURE 2.—Unbalanced upper-surface aileron and unbalanced split flap.

both neutral and down 60° . Another series of tests was made with the end plates supported on the balance, the wing being in place but supported separately, flap both neutral and down 60° and a small gap being maintained between the wing and the end plates. The difference between the measured forces for the two series of tests gave the tare forces due to the plates. The greatest effect was on the drag, in which case the tare forces amounted to about 75 percent of the minimum drag of the plain airfoil.

A few tests were made with and without the thin metal fittings used to support the aileron and flap at midspan. As the results showed no consistent differences, the effect of the fittings was considered to be negligible.

Comparison of two-plane installation and standard wind-tunnel tests.—Tests were made to obtain a comparison between the results from the two-plane installation and the usual wind-tunnel results from rectangular wings in the free jet. The Clark Y wing with 0.15c unbalanced upper-surface ailerons and 0.15c unbalanced split flap was used as the basis for comparison. (See fig. 2.) The gaps between the wing and the aileron and between the wing and the flap were kept sealed for all tests with this arrangement because other tests had

shown that any gap produced an adverse effect on the aerodynamic characteristics.

The hinge moments of the aileron are compared in figure 3 with those for a full-semispan unbalanced upper-

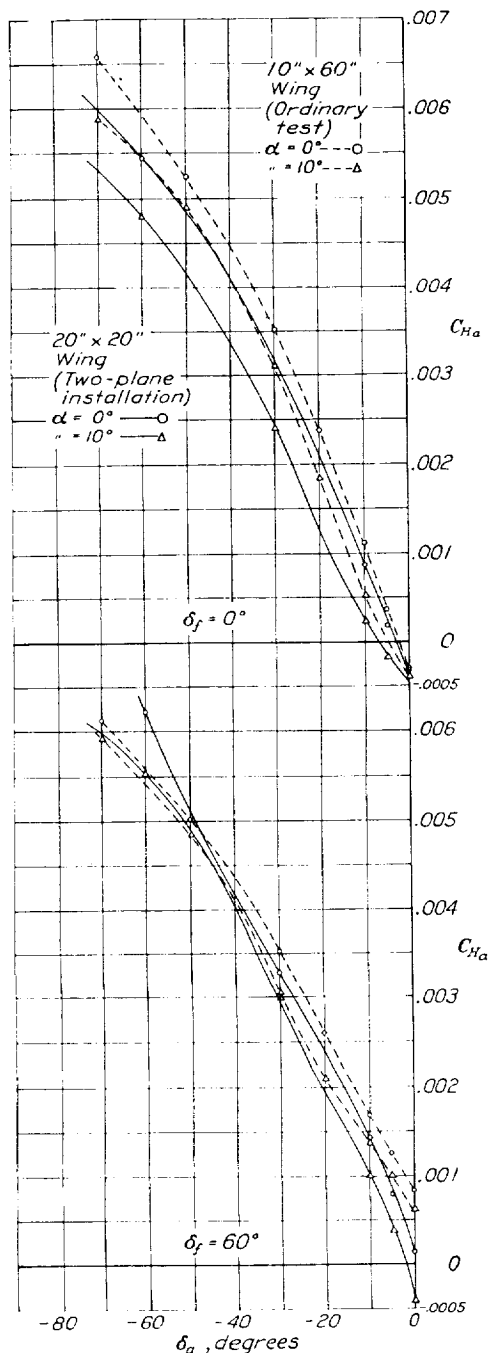


FIGURE 3.—Aileron hinge-moment coefficients obtained with two-plane installation and with ordinary wind-tunnel test. 0.15c by 1.00 b/2 unbalanced upper-surface aileron on wing with flap neutral and down 60°.

surface aileron on a wing of aspect ratio 6. The data for the tests of aspect ratio 6 were converted from data in reference 1 for a partial-semispan aileron. In gen-

eral, the agreement is fair and is better for the conditions with a split flap deflected for maximum lift than for the flap neutral.

Lift and drag coefficients of wings with unbalanced split flaps as obtained in the two types of wind-tunnel test installation are shown in figure 4. (Data for tests of the wing of aspect ratio 6 are from reference 1.) None of these data were corrected for effects of the jet boundaries, but corrections were applied for tares and for the effect of the static-pressure gradient. The static-pressure gradient produces an additional downstream force on the models, corresponding to values of ΔC_D of 0.0015 and of 0.009 on the small- and large-chord wings, respectively. The values of this correction were obtained in accordance with the methods given in reference 5.

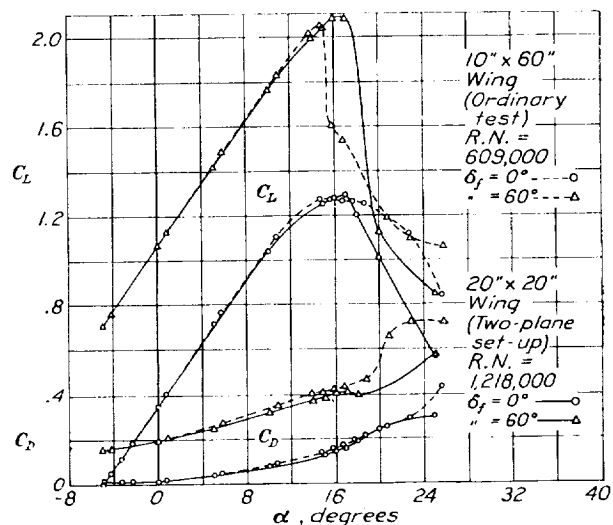


FIGURE 4.—Comparison of lift and drag coefficients of wings with 0.15c full-span unbalanced split flaps for two types of wind-tunnel test. (Uncorrected for effects of jet boundaries.)

The maximum lift coefficients are about the same with either test arrangement for the two conditions of flaps neutral or deflected. In addition, the lift curves are almost identical up to the stall. The drag curves diverge slightly in the region from zero to maximum lift, the values for the wing in the two-plane installation being the lower ones.

Agreement of the lift and drag curves for the two types of test without corrections for tunnel effects or reduction to a common aspect ratio was unexpected, and the fact that the lift curves did agree closely could only be regarded as a coincidence. In order to determine whether the data from the two types of test could be corrected to a common aspect ratio, the data given in figure 4 for the flap-neutral conditions were corrected for tunnel effects and reduced to infinite aspect ratio

for comparison. The standard jet-boundary corrections,

$$\Delta\alpha = \delta \frac{S}{C} C_L \times 57.3, \text{ degrees}$$

$$\Delta C_D = \delta \frac{S}{C} C_L^2$$

where S is the total wing area, and C the jet cross-sectional area, were applied to the results for the 10- by 60-inch wing. A theoretical value of $\delta = -0.165$ (reference 6) was taken as most nearly representative of the boundary effect in the 7- by 10-foot wind tunnel.

The induced angle of attack and induced drag coefficient

$$\alpha_i = -\frac{C_L}{\pi R}(1 + \tau) \times 57.3, \text{ degrees}$$

$$C_{Di} = -\frac{C_L^2}{\pi R}(1 + \sigma)$$

were calculated for the rectangular wing of aspect ratio 6 using values of $\tau = 0.179$ and $\sigma = 0.054$.

The results of the 20- by 20-inch wing in the two-plane installation were corrected for the downward deflection of the jet behind the wing and for the induced curvature of the flow in the neighborhood of the wing. (See reference 5.) In this case

$$\Delta\alpha = -\left[\left(0.25\frac{c}{h}C_L\right) + \frac{\pi}{12}\left(\frac{c}{h}\right)^2\left(\frac{C_L}{2} + C_{m0}\right)\right] \times 57.3, \text{ degrees}$$

$$\Delta C_D = -0.25\frac{c}{h}C_L^2$$

where c is the wing chord.

h is the height of the jet.

C_{m0} is the pitching-moment coefficient at zero lift.

Lift coefficients against angle of attack for infinite aspect ratio and profile-drag coefficients against lift coefficients are plotted in figure 5. The slope of the lift curve for the wing tested between end planes is not quite so great as that of the rectangular wing tested in the free jet. Over the straight portion of the lift curve (up to a lift coefficient of about 1.0) the slopes are respectively 0.096 and 0.101 per degree. The profile-drag coefficients show a good agreement over the same range of lift coefficients, the values for the wing between end planes being slightly lower.

The comparisons made indicate that two-dimensional flow conditions are closely approximated for the wing between end planes. Consequently, the test data may be corrected to any aspect ratio desired and comparisons made with other wind-tunnel tests with a reasonable degree of accuracy.

CALCULATION OF COEFFICIENTS

Because of the close agreement between the results from the two types of wind-tunnel test, it was possible to calculate the coefficients from the two-plane tests without applying jet-boundary corrections and to have

the results comparable with those from wings of aspect ratio 6 ordinarily tested in the 7- by 10-foot tunnel. The measured lift and drag data were therefore not corrected for boundary effects but the corrections were applied for the effect of the longitudinal static-pressure gradient in the tunnel jet and for the tares due to the metal end plates.

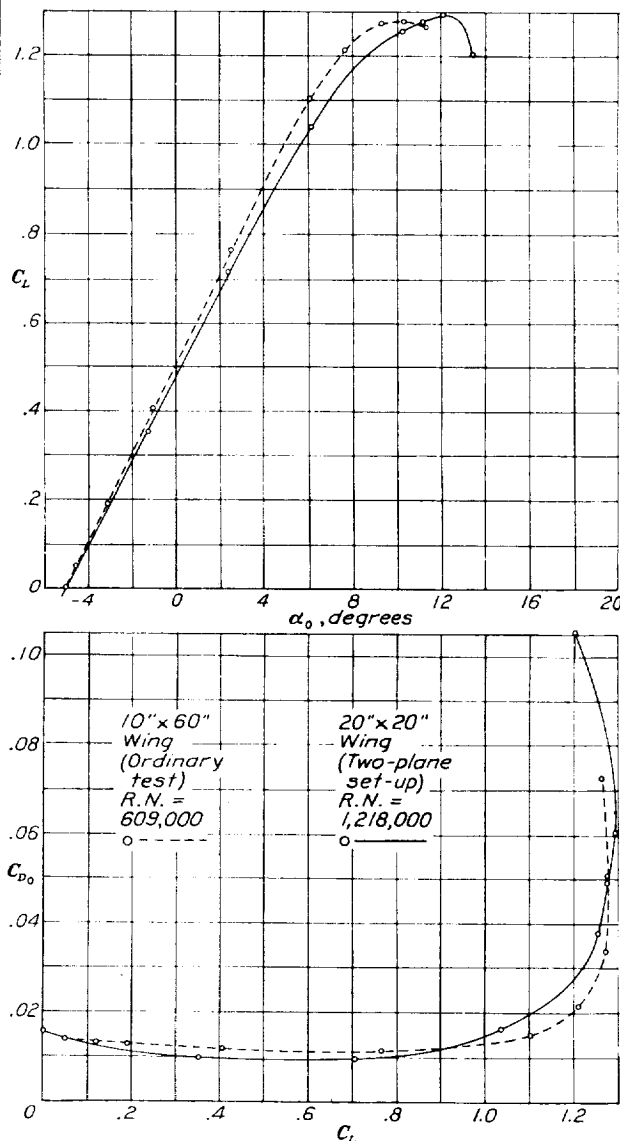


FIGURE 5.—Comparison of lift and profile-drag coefficients of wings with unbalanced split flaps neutral for two types of wind-tunnel test. (Corrected to infinite aspect ratio.)

The results are given in the form of absolute coefficients:

Hinge-moment coefficient,

$$C_H = \frac{H}{qcS}$$

where H is the moment of a semispan aileron, or of a full-span flap, about the hinge axes, and q is the

dynamic pressure. Lift and drag coefficients are, as usual, C_L and C_D .

Rolling-moment and yawing-moment coefficients about the wind axes C_l' and C_n' were calculated for a semispan aileron on a wing of aspect ratio 6, utilizing methods described in references 7 and 8. The rolling-moment coefficient

$$C_l' = \frac{1}{2} \left(R \zeta \frac{1}{d\alpha} \Delta C_L \right)$$

where ζ depends upon the proportion of the semispan covered by the aileron.

$\frac{dC_L}{d\alpha}$ is the actual slope of the lift curve.

ΔC_L is the change in lift due to deflecting the aileron at a given angle of attack.

The yawing-moment coefficient is the sum of two coefficients, an induced yawing-moment coefficient and a profile yawing-moment coefficient, $C_n' = C_{n_i}' + C_{n_p}'$. The induced yawing-moment coefficient

$$C_{n_i}' = -\mu C_l' C_L$$

where μ depends upon the proportion of the semispan covered by the aileron.

C_l' is the rolling-moment coefficient computed as previously explained.

C_L is the given lift coefficient.

The profile yawing moment

$$N_p = \zeta \Delta C_{D_0} q b S$$

and the coefficient

$$C_{n_p}' = \zeta \Delta C_{D_0}$$

where ζ depends upon the proportion of the semispan covered by the aileron.

ΔC_{D_0} is the change in profile drag produced by deflecting the aileron at a given lift.

DEVELOPMENT OF BALANCED UPPER-SURFACE AILERONS AND BALANCED SPLIT FLAPS

UNBALANCED UPPER-SURFACE AILERON AND UNBALANCED SPLIT FLAP

The combination of unbalanced upper-surface aileron and unbalanced split flap (fig. 2) is used as the basic arrangement for comparison with all the ailerons and flaps tested. Rolling-, yawing-, and hinge-moment coefficients of the unbalanced upper-surface aileron are given in figure 6 with the split flap neutral and in figure 7 with the flap down 60°. Lift and drag coefficients for the wing with unbalanced split flap are given in figure 8. Maximum lift coefficients, drag coefficients and ratios of L/D at maximum lift, and hinge-moment coefficients for different deflections of the unbalanced split flap are given in figure 9.

BALANCED UPPER-SURFACE AILERON AND BALANCED SPLIT FLAP

Slot arrangement 1 (fig. 10).—An airfoil section was used for both ailerons and flaps throughout the tests of the balancing arrangements. (See table I.) The ailerons and flaps using this section were of the same size in plan form as the unbalanced upper-surface ailerons and the unbalanced split flaps.

The first slot arrangement tested of balanced upper-surface aileron and balanced split flap with a slot for each is shown dotted in figure 10. The flap was kept neutral for the series of tests with this arrangement. Only hinge moments were measured for the aileron with the different axis locations shown in figure 10. These locations were so chosen that, when the axis was moved back for balancing, the nose of the aileron would just clear the flap during deflection of the aileron.

The results of these tests indicated that the aileron axis should be about 30 percent of the aileron chord back from the leading edge of the aileron for any considerable reduction of the aileron hinge moment. This location requires that the aileron axis be about 60 percent of the aileron chord out from the upper surface because of the geometrical arrangement of aileron, flap, and slot (axis A12).

Slot arrangement 2 (figs. 10 and 11).—Slot arrangement 2, shown by the solid outline in figure 10, differs from arrangement 1 in that the aileron and flap have smaller slots. Aileron characteristics were determined for axis locations A8, A12, and A14 (flap neutral). As no appreciable differences were found between the hinge moments for the two slot arrangements, arrangement 2 was used for further tests because of the smaller slots.

The lift and the drag of the wing, and the hinge moments of the flap, were next measured with the flap deflected about axis locations F1, F12, and F14. The most promising characteristics were obtained with the flap deflected 60° about axis F12.

The aileron characteristics were then determined for axis location A12 with the flap deflected 60° about axis location F12. The results were not satisfactory because the hinge moments of the aileron were considerably overbalanced at the low deflections and the indicated rolling moments were in the wrong direction at moderately high angles of attack. Both of these conditions required improvement.

In order to improve the low lifts produced by the flap with slot arrangement 2, the open aileron slot was completely sealed with plasticine. Measurements of maximum lift were made with the flap deflected different amounts at axis locations F8, F12, and F14. The results with aileron slot open and sealed are plotted in figure 11. It will be noted that a large improvement was obtained with the aileron slot sealed and only the flap slot open. This balanced split flap produced a somewhat higher maximum lift than the unbalanced split flap. For the further arrangements of balanced

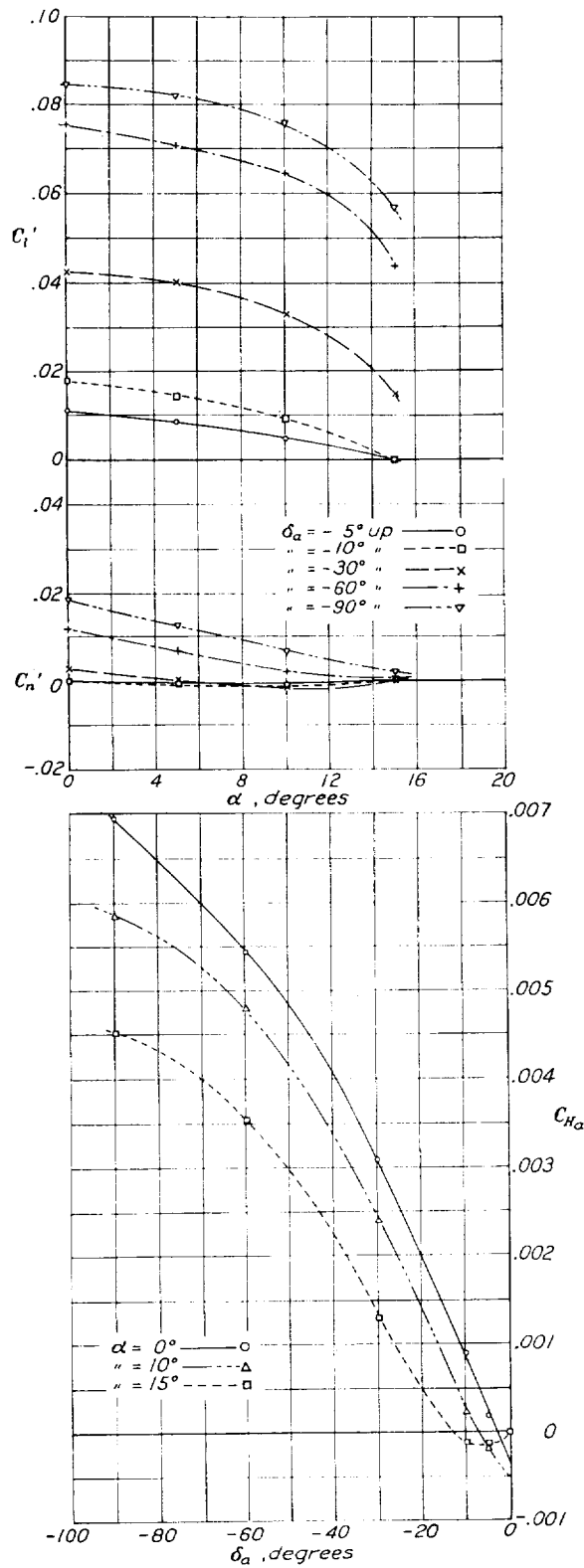


FIGURE 6.—Rolling, yawing, and hinge-moment characteristics of unbalanced upper-surface aileron. Flap neutral.

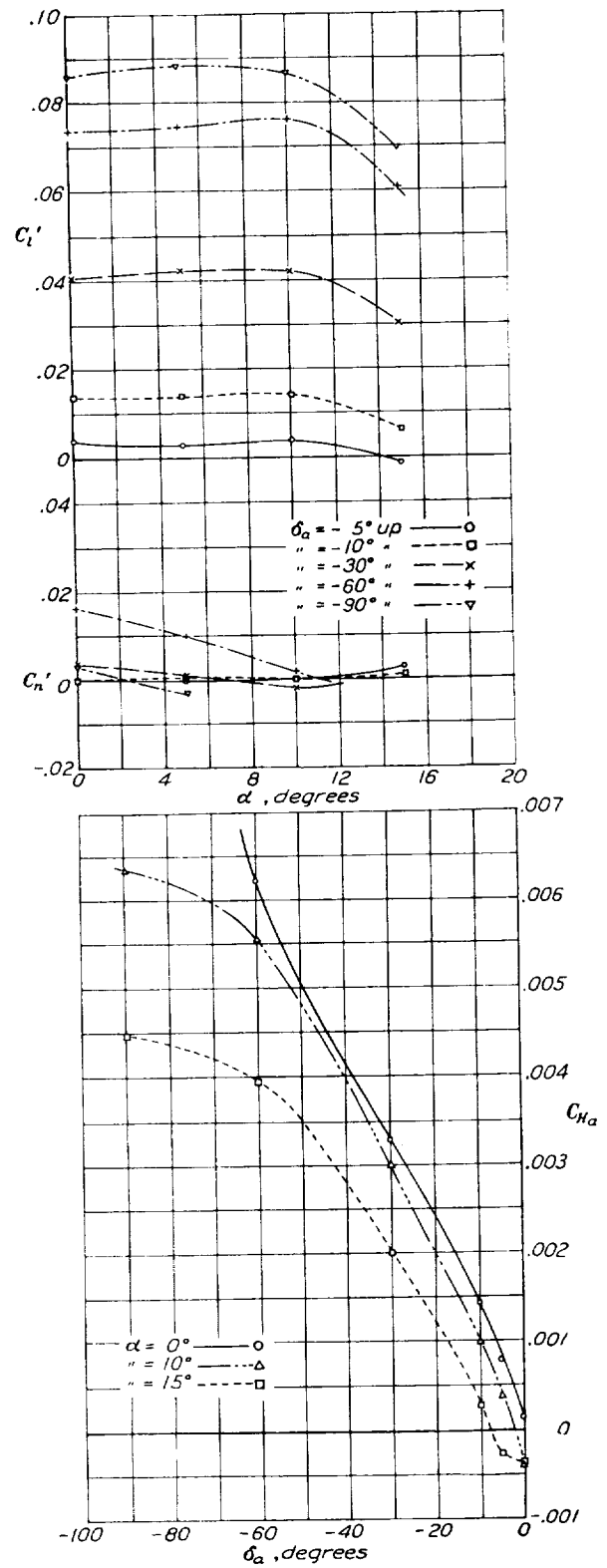


FIGURE 7.—Rolling, yawing, and hinge-moment characteristics of unbalanced upper-surface aileron. Flap down 60° .

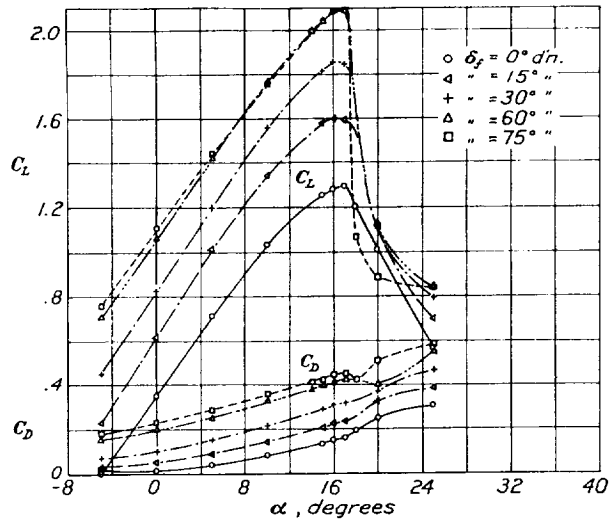


FIGURE 8.—Lift and drag coefficients for wing with unbalanced split flap.

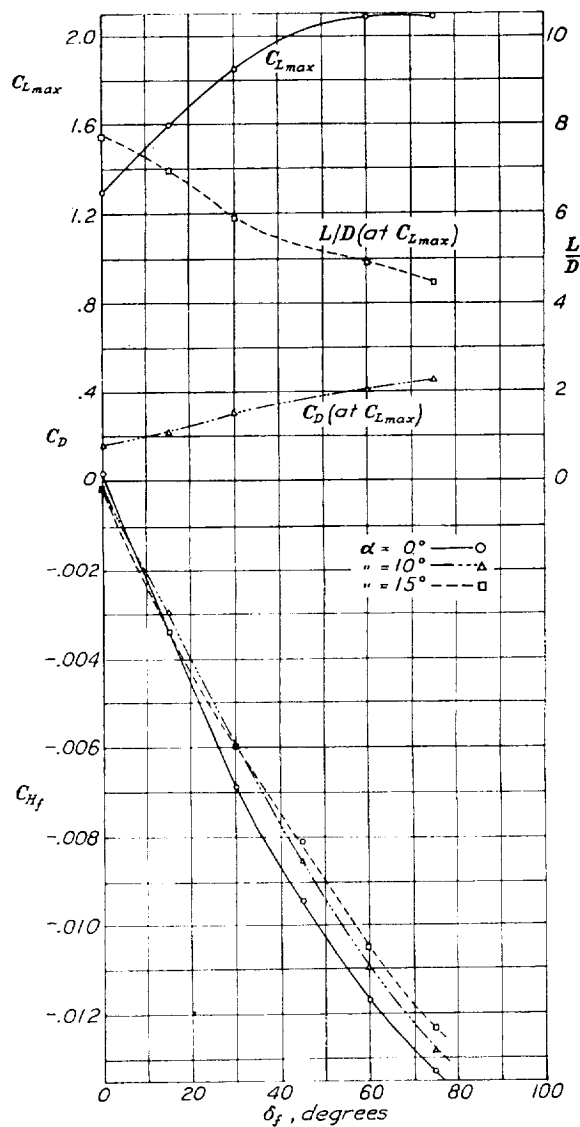
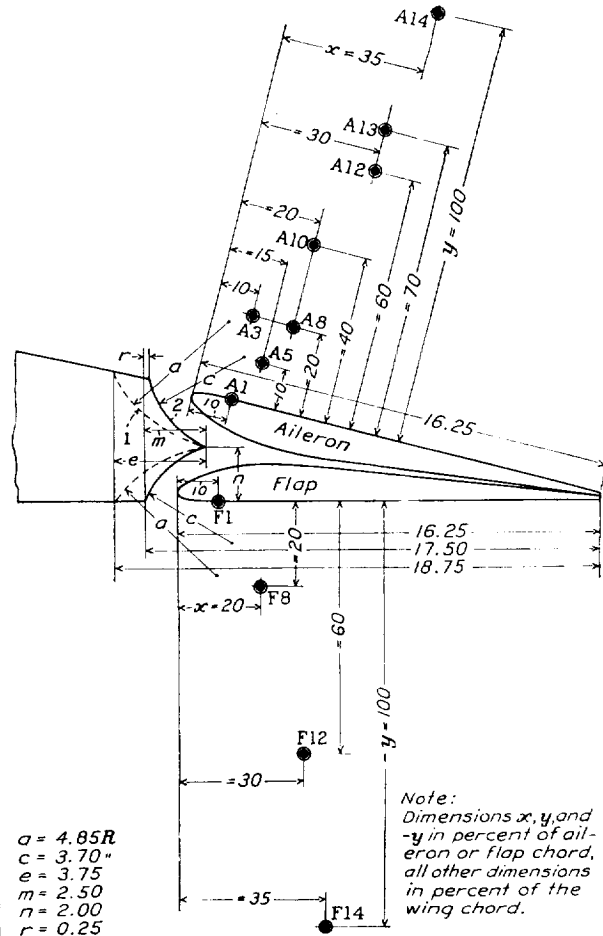
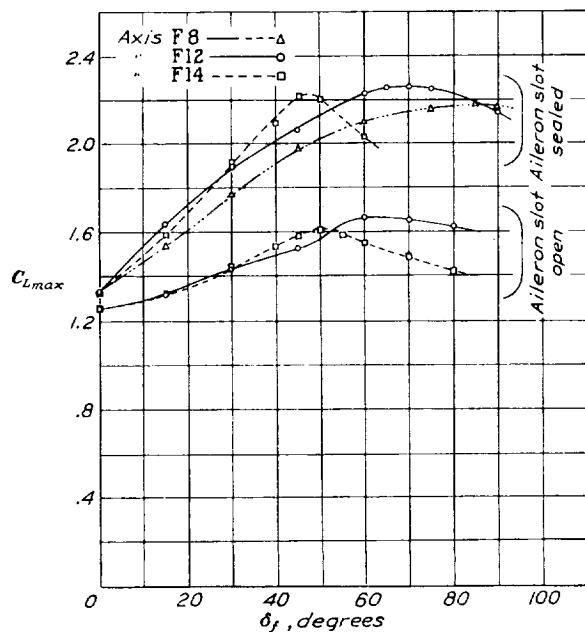
FIGURE 9.— C_{Lmax} , C_D and L/D at C_{Lmax} , and C_H for different deflections of unbalanced split flap.

FIGURE 10.—Balanced upper-surface aileron and balanced split flap. Slot arrangement 1 and 2 with aileron and flap axes tested.

FIGURE 11.—Effect on C_{Lmax} with aileron slot open and sealed. Balanced split flap at different axis locations.

upper-surface ailerons and split flaps with slots the aileron slot was therefore kept sealed to as great an extent as was practicable when the aileron was neutral.

Slot arrangement 3 (figs. 12 to 20).—Slot arrangement 2 was changed to arrangement 3 (fig. 12) because it was desired to retain the high maximum lifts obtained with a closed aileron slot, and it was thought that the overbalance of the aileron could be improved at the same time. The flap characteristics were obtained at axis locations F1, F8, and F12. The most promising locations on the basis of high lift and low hinge moments were F8 and F12, although the flap-hinge moments were somewhat erratic beyond 35° deflection at axis location F12.

The aileron characteristics were then determined for axis locations A12 and A8 with the flap deflected 60°

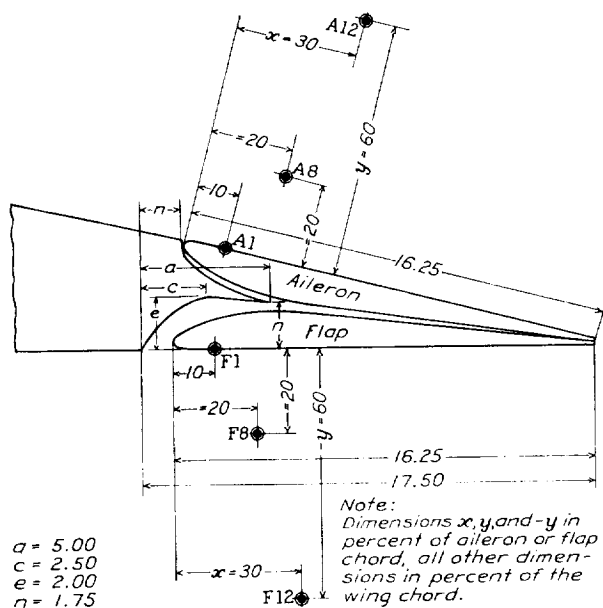


FIGURE 12.—Balanced upper-surface aileron and balanced split flap. Slot arrangement 3 with aileron and flap axes tested.

about axis location F12. The results of these tests (figs. 13, 14, 15, and 16) showed only a slight improvement in the aileron hinge-moment overbalance. The rolling- and yawing-moment characteristics, however, appeared to be very good for the aileron-axis locations tested with the flap deflected, the indicated rolling moments being much greater than for the flap-neutral condition.

The aileron characteristics were also determined for several axis locations with the flap both neutral and deflected about axis location F8. The results for axis location A8 are given in figure 17 and for axis location A12, in figure 18. It will be seen that with aileron axis location A12, flap deflected about axis location F8, the aileron hinge moments are satisfactory up to the stall. The indicated rolling moments, however, are somewhat lower with this arrangement than with the flap deflected about axis location F12.

The similarity of the hinge-moment curves of the balanced upper-surface aileron at axis location A12 (fig. 14) with flap deflected about axis location F12 to those of ordinary ailerons indicated that the overbalanced hinge moments could probably be overcome by rigging the ailerons up 10° for neutral and using a differential deflection. In this manner the favorable rolling- and yawing-moment characteristics for axis location A12 would be retained without overbalance of the aileron hinge moments.

The aileron was then rigged up 10° at several axis locations, and the effect on the flap characteristics was measured. The results for the flap at axis location F8 with the aileron rigged up 10° at axis location A8 are given in figure 19 and for similar conditions but with the respective axes F12 and A12, in figure 20. The effect of rigging the aileron up 10° was mainly a reduction in the maximum lift and in the drag at maximum lift. Hinge moments of the flap were practically unaffected.

Slot arrangement 3A (figs. 21 to 25).—Because rigging the aileron up 10° for neutral with slot arrangement 3 left a break in the wing upper surface, that arrangement was modified as 3A having no sharp break in the upper surface. (See fig. 21.) This modification was accomplished by raising the aileron bodily for its neutral position and by changing the slot shape somewhat. A new axis location was then used for the aileron because of the geometrical arrangement. The object was to keep the aileron and flap axes as close to the surface as possible and still obtain low hinge moments, together with other favorable characteristics.

With the aileron rigged up 10° for neutral at axis location A9, the flap characteristics were obtained for the flap at axis locations F1, F8, and F12. The flap at axis location F8 appeared to be the most promising of these three, and it was noted that, because of the geometrical arrangement, a similar reduction in flap-hinge moments would be possible with an axis the same distance back from the flap nose but closer to the surface. The flap characteristics were then measured at this new axis location, F6.

Aileron characteristics of the balanced upper-surface aileron at axis location A9 are given in figure 22 with the split flap neutral and in figure 23 with the flap deflected 60° about axis location F6. The indicated rolling and yawing moments appear to be satisfactory, and no overbalance of aileron hinge moments occurs up to the stall. Lift and drag coefficients for the wing with balanced split flap at axis location F6 are given in figure 24. Maximum lift coefficients, drag coefficients and ratios of L/D at maximum lift, and hinge-moment coefficients for different deflections of the balanced split flap are given in figure 25.

Slot arrangement 4 (fig. 26).—A short series of tests was made with slot arrangement 4 to determine the effect of closing the flap slot in a manner similar to that

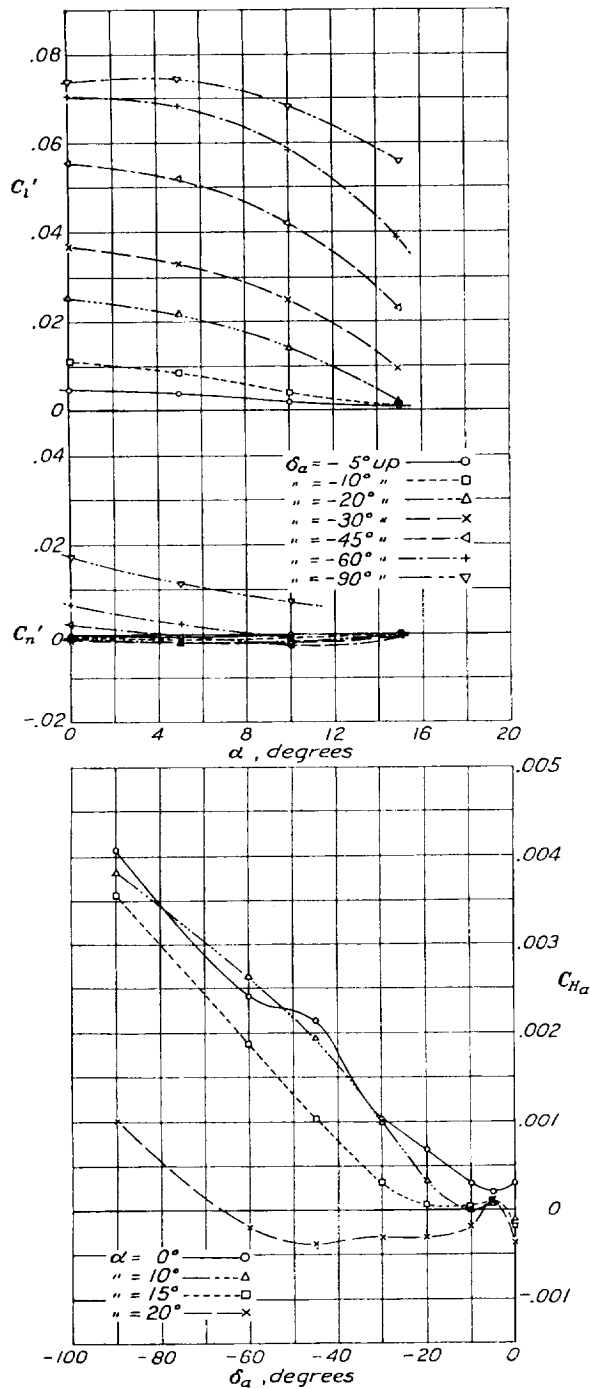


FIGURE 13. Rolling-, yawing-, and hinge-moment characteristics of balanced upper-surface aileron at axis A12. Flap neutral. Slot arrangement 3.

in which the aileron slot had been closed but leaving the aileron slot open. With the aileron slot open a low maximum lift was again produced by the flap. The aileron characteristics were practically the same as those obtained with slot arrangement 3. Since slot arrangement 4 possessed no particular advantages for

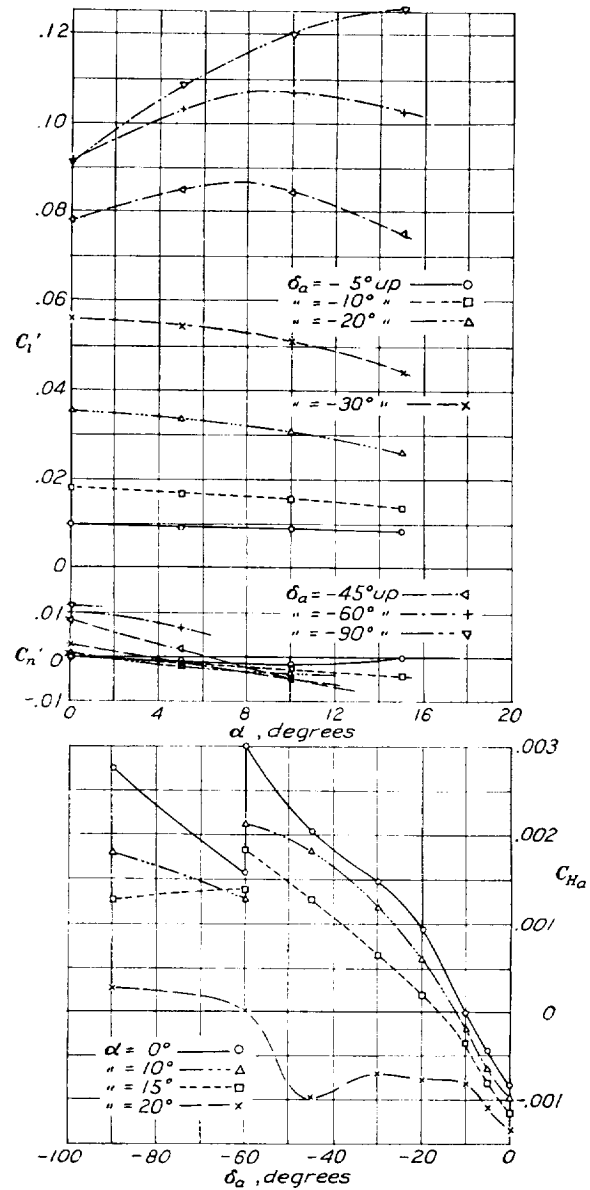


FIGURE 14. Rolling-, yawing-, and hinge-moment characteristics of balanced upper-surface aileron at axis A12. Flap down 60° at flap axis F12. Slot arrangement 3.

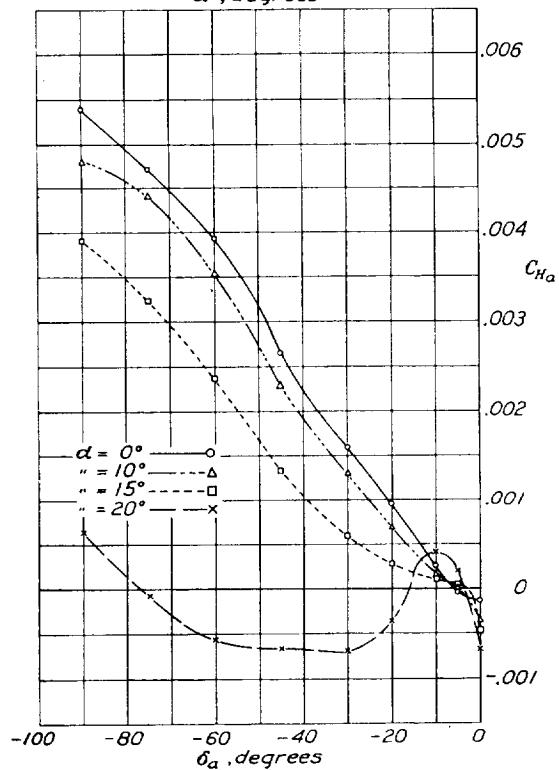
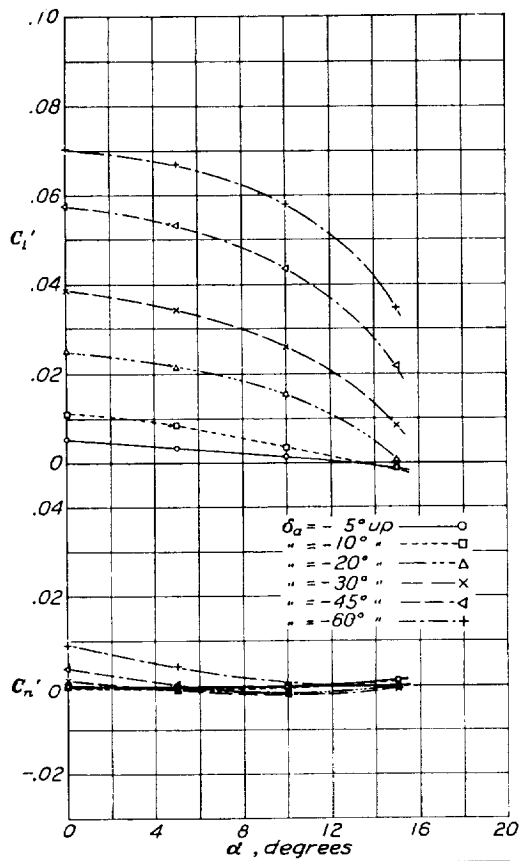


FIGURE 15.—Rolling, yawing, and hinge-moment characteristics of balanced upper-surface aileron at axis A8. Flap neutral. Slot arrangement 3.

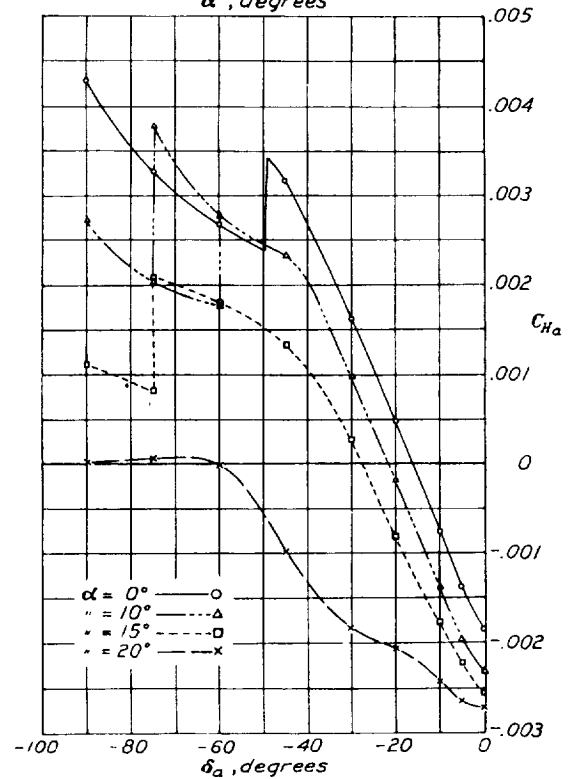
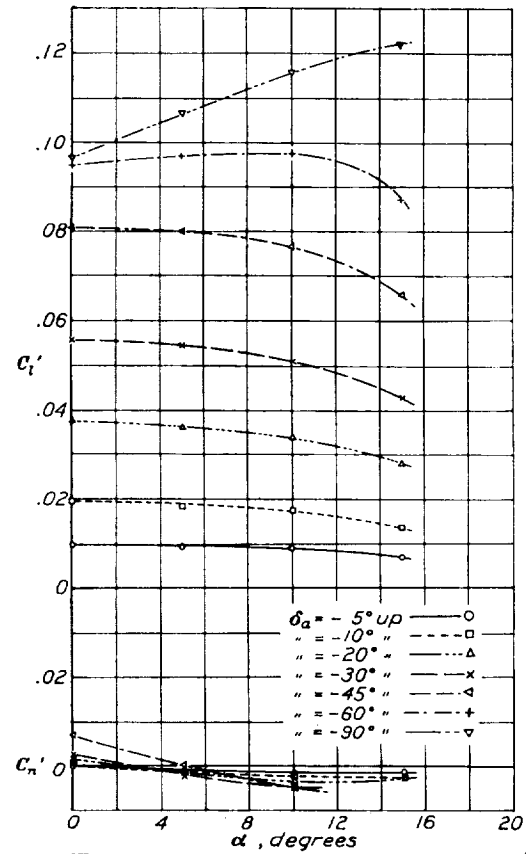


FIGURE 16.—Rolling, yawing, and hinge-moment characteristics of balanced upper-surface aileron at axis A8. Flap down 60° at flap axis F12. Slot arrangement 3.

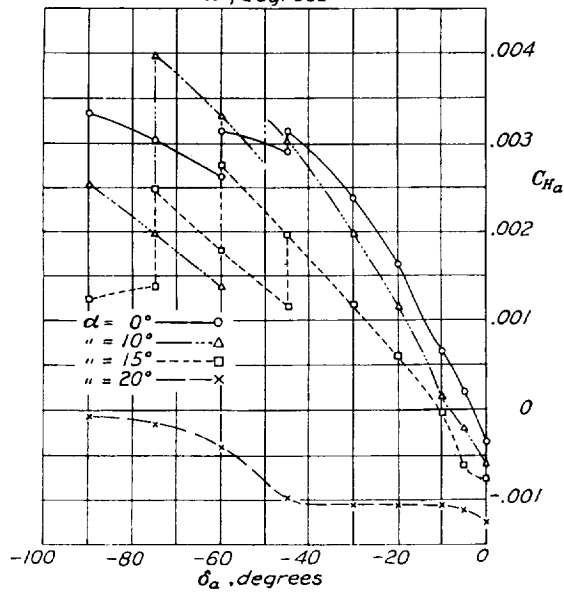
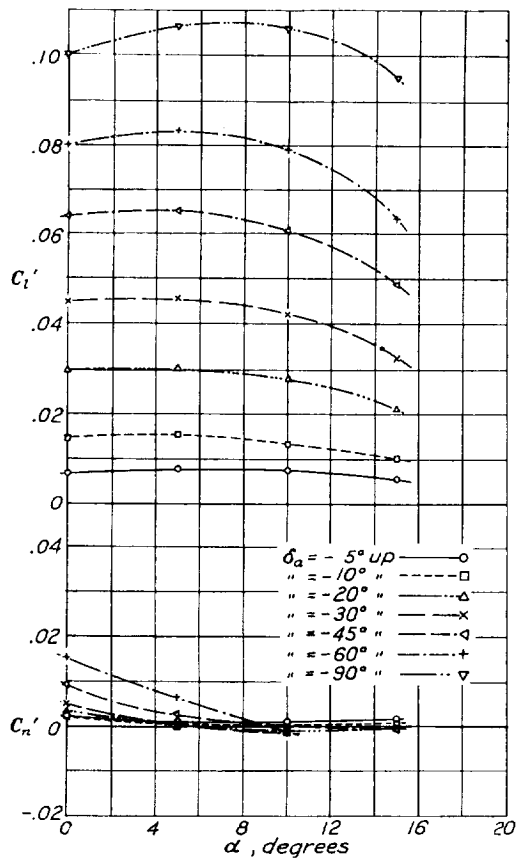


FIGURE 17. -Rolling, yawing, and hinge-moment characteristics of balanced upper-surface aileron at axis A8. Flap down 75° at flap axis F8. Slot arrangement 3.

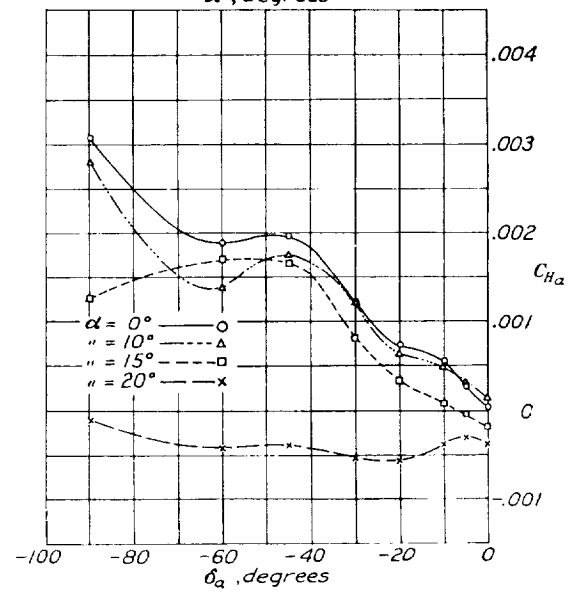
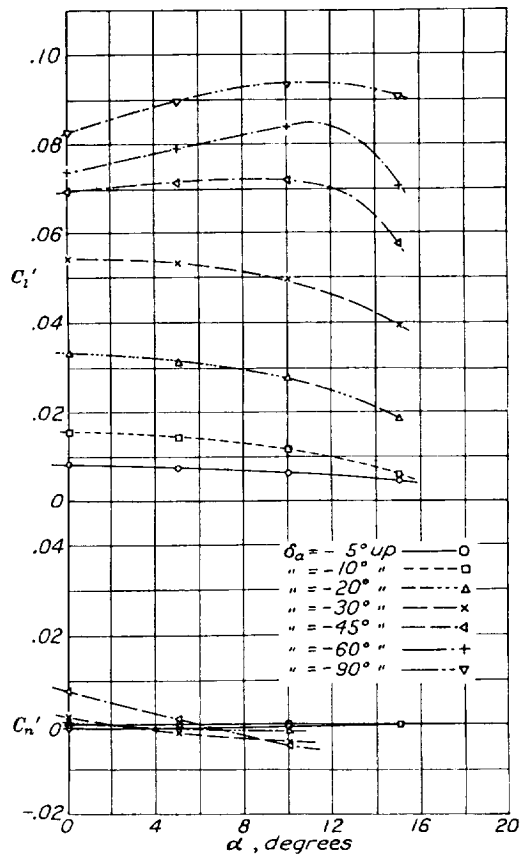


FIGURE 18. -Rolling, yawing, and hinge-moment characteristics of balanced upper-surface aileron at axis A12. Flap down 75° at flap axis F8. Slot arrangement 3.

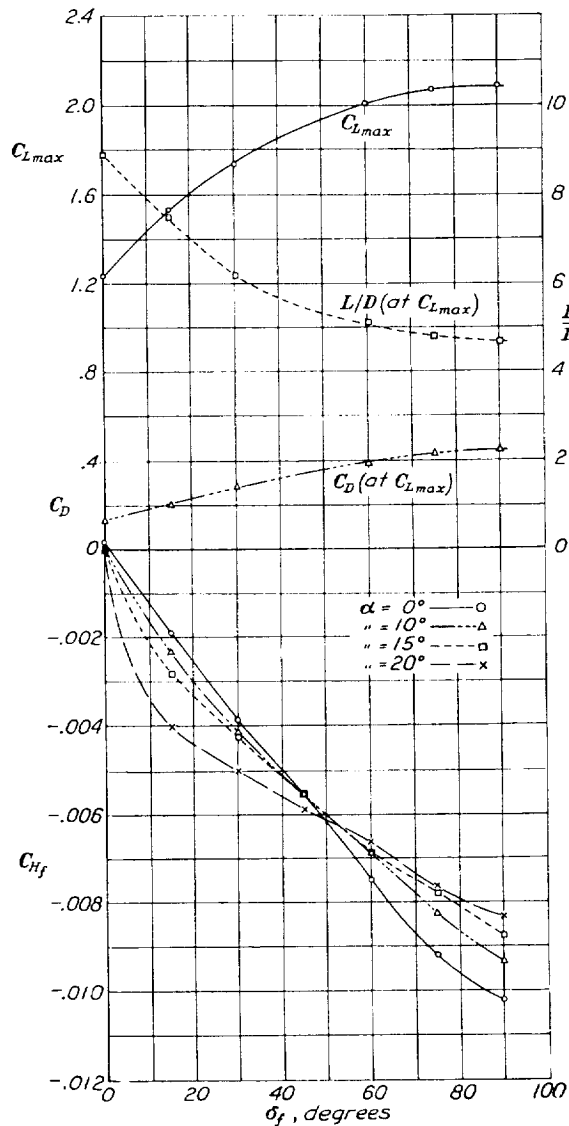


FIGURE 19.— C_{Lmax} , C_D and L/D at C_{Lmax} , and C_{Hf} for different deflections of balanced split flap at axis F8. Aileron rigged up 10° at aileron axis A8. Slot arrangement 3.

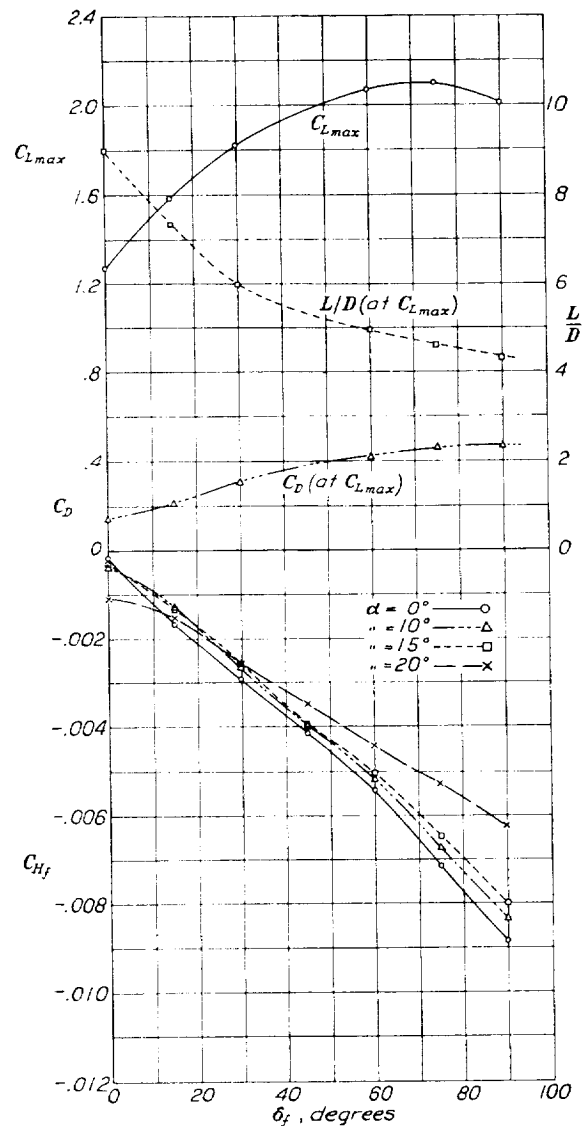


FIGURE 20.— C_{Lmax} , C_D and L/D at C_{Lmax} , and C_{Hf} for different deflections of balanced split flap at axis F12. Aileron rigged up 10° at aileron axis A12. Slot arrangement 3.

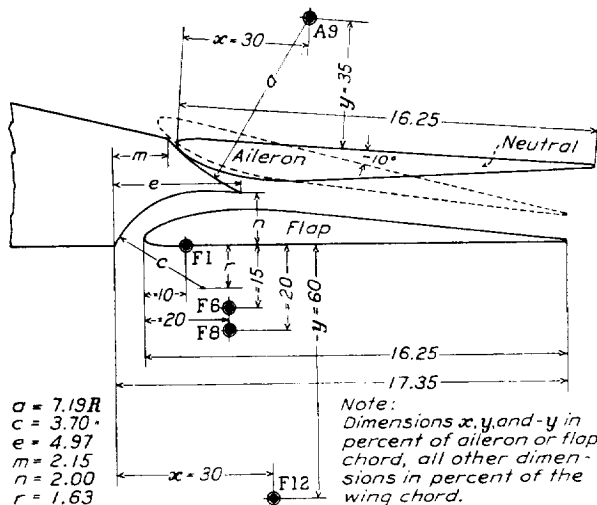


FIGURE 21.—Balanced upper-surface aileron rigged up 10° and balanced split flap. Slot arrangement 3A with aileron and flap axes tested.

the aileron and was detrimental to the maximum lift, tests were discontinued.

The range of balancing upper-surface ailerons now appeared to have been sufficiently well covered but it seemed desirable to make a few additional tests further to decrease the flap hinge moments and possibly to increase the flap effectiveness.

BALANCED SPLIT FLAP

Slot arrangement 5 (figs. 27 to 29).—The slot and balanced split-flap arrangement shown in figure 27 was obtained by disregarding the upper-surface aileron and making the wing upper surface solid and continuous. Axis location F6 again gave the greatest reduction in flap hinge moments without locating the axis a considerable distance out from the surface.

Lift and drag coefficients for the wing with the balanced split flap at axis location F6 are given in

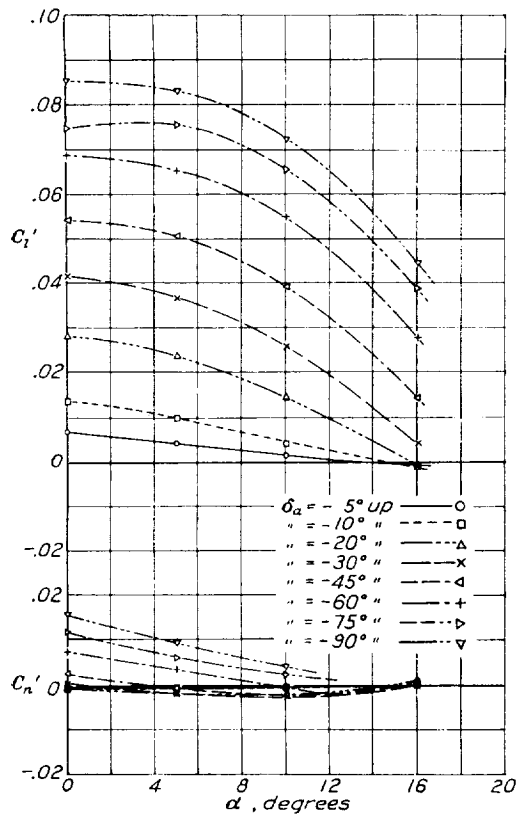


FIGURE 22.—Rolling-, yawing-, and hinge-moment characteristics of balanced upper-surface aileron at axis A9. Flap neutral. Slot arrangement 3A.

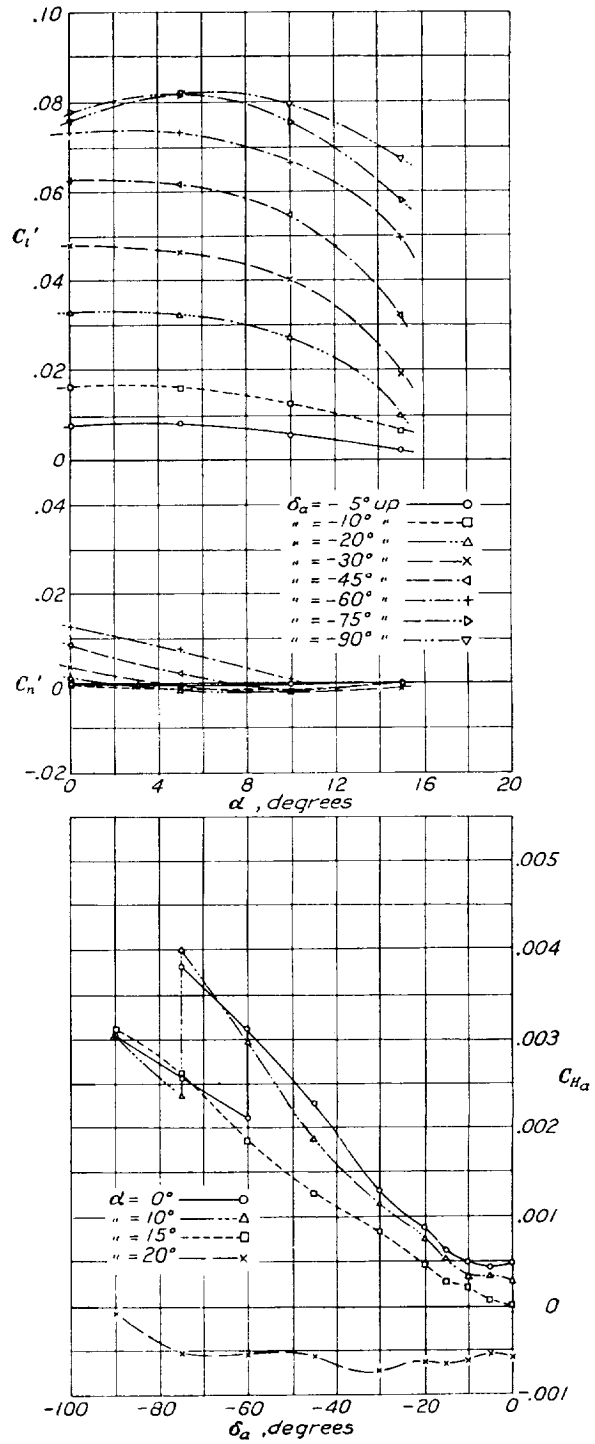


FIGURE 23.—Rolling-, yawing-, and hinge-moment characteristics of balanced upper-surface aileron at axis A9. Flap down 60° at flap axis F6. Slot arrangement 3A.

figure 28. Maximum lift coefficients, drag coefficients and ratios of L/D at maximum lift, and hinge-moment coefficients for different deflections of the balanced split flap are given in figure 29.

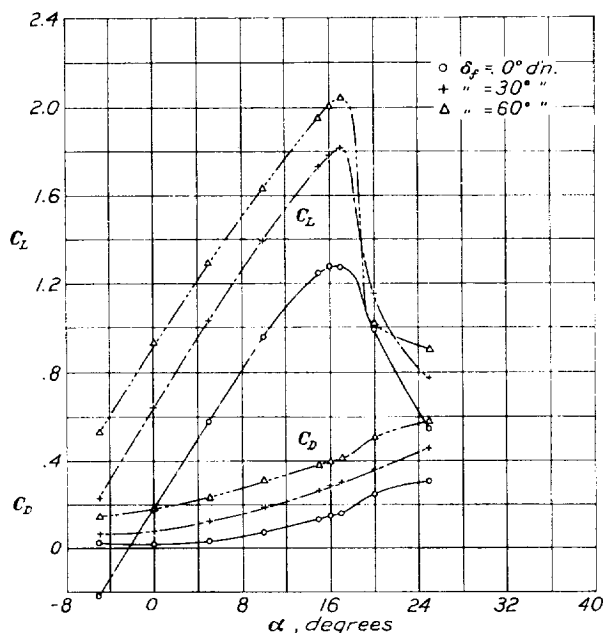


FIGURE 24.—Lift and drag coefficients for wing with balanced split flap at axis F6. Aileron rigged up 10° at aileron axis A9. Slot arrangement 3A.

Slot arrangement 5A (figs. 30, 31, and 32).—A new axis location F7, giving still further balancing, was obtained by making the wing upper surface thinner

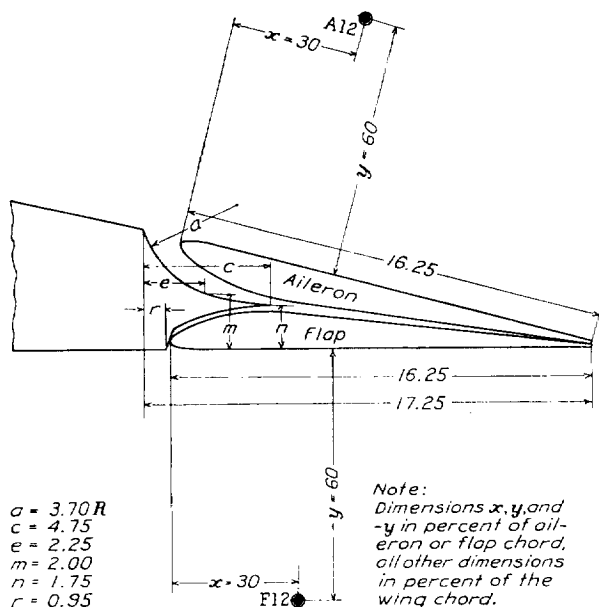


FIGURE 26.—Balanced upper-surface aileron and balanced split flap. Slot arrangement 4 with aileron and flap axes tested.

and moving the flap axis back, keeping it as close to the surface as axis 6 (fig. 30).

Lift and drag coefficients for the wing with arrangement 5A are given in figure 31. Maximum lift coefficients, drag coefficients and ratios of L/D at maximum lift, and hinge-moment coefficients for different

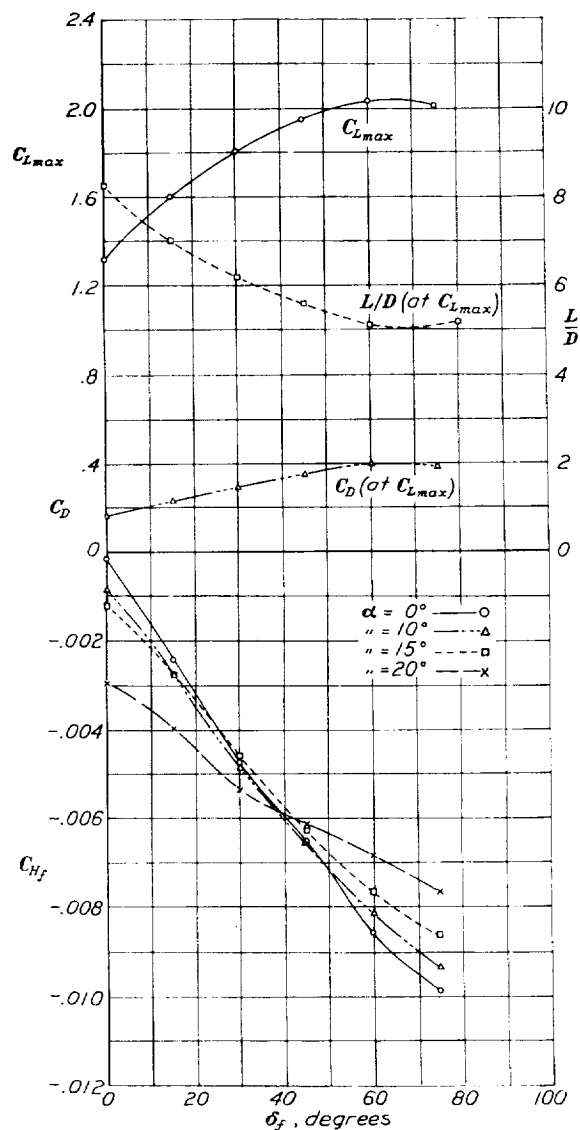


FIGURE 25.— $C_{L_{max}}$, C_D and L/D at $C_{L_{max}}$, and C_H for different deflections of balanced split flap at axis F6. Aileron rigged up 10° at aileron axis A9. Slot arrangement 3A.

deflections of the balanced split flap are given in figure 32.

DISCUSSION

In order to facilitate a discussion of some of the arrangements of balanced upper-surface ailerons and balanced split flaps, the factors that appear suitable for a comparison of the different arrangements in this investigation are listed in table II. A differential deflection of the ailerons was used for most cases, assuming two semispan ailerons, one up 30° and the

other down 10° from a neutral position rigged up 10° . The ailerons are compared on the basis of hinge-, rolling-, and yawing-moment characteristics, at two angles of attack 0° and 10° , with flaps both neutral and deflected. In the case of the flaps, the characteristics of the unbalanced split flap neutral and deflected for maximum lift were used as the basis of

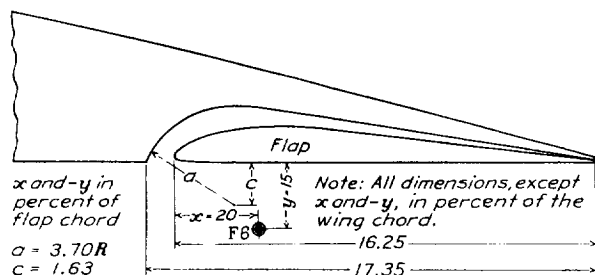


FIGURE 27.—Balanced split flap with slot arrangement 5.

comparison. The balanced flaps were then deflected to give approximately the same maximum lift and comparisons were made of flap hinge moments and ratios of L/D at this maximum lift.

For the same aileron deflections the rolling moments and the hinge moments of unbalanced upper-surface ailerons (flap neutral) are higher than those obtained

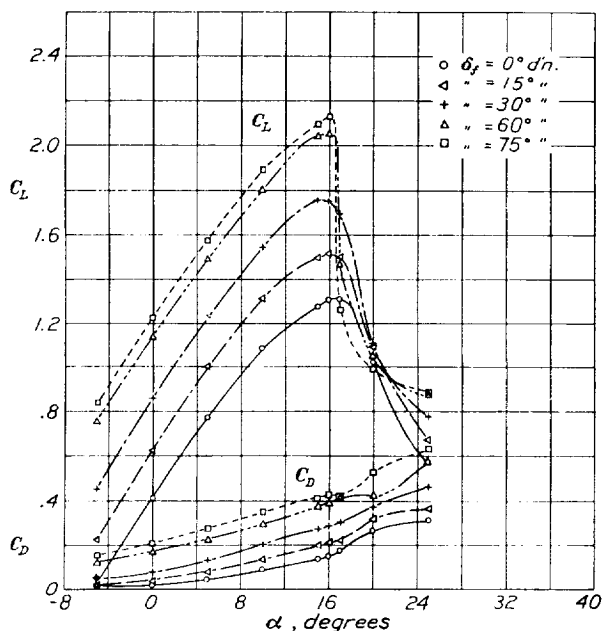


FIGURE 28.—Lift and drag coefficients for wing with balanced split flap at axis F6. Slot arrangement 5.

with balanced ailerons. The indicated yawing moments appear to be small for the unbalanced upper-surface ailerons near the stall of the wing; they are slightly adverse for the condition with flap deflected. Rigging the unbalanced upper-surface ailerons up 10° for neutral had very little effect on the aileron characteristics.

Of all the balanced upper-surface ailerons tested, slot arrangement 3, with the aileron at axis location A12 (rigged up 10° for neutral) and the balanced split flap at axis location F12, shows probably the best rolling-moment characteristics with the flap either neutral or deflected for maximum lift. With the flap neutral, the indicated rolling moments are about 15 percent lower than those of the unbalanced upper-

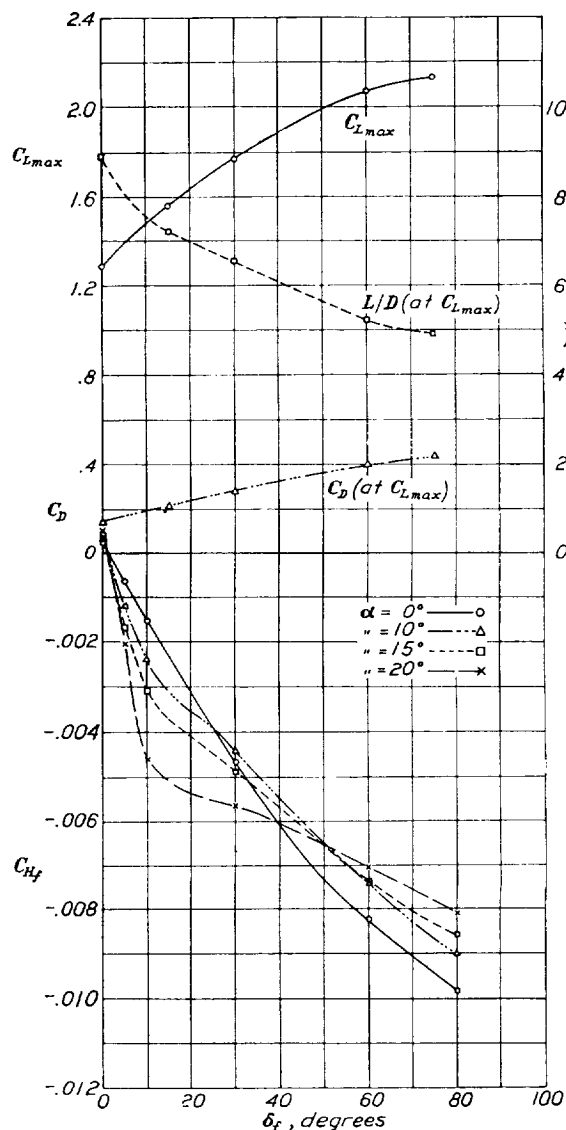


FIGURE 29.— $C_{L_{max}}$, C_D and L/D at $C_{L_{max}}$, and C_H for different deflections of balanced split flap at axis F6. Slot arrangement 5.

surface ailerons. With flap deflected, however, the rolling moments are 30 to 60 percent higher. The indicated yawing moments appear to be satisfactory at low angles of attack but are somewhat adverse near the stall with flap deflected.

The hinge moments are about half those of the unbalanced upper-surface ailerons, flaps neutral, and are increased to roughly 70 percent those of the unbal-

anced ailerons with flap deflected. On the basis of rolling moments equal to those obtained with the unbalanced ailerons, the hinge moments of the balanced ailerons would become about 60 percent those of the unbalanced ailerons, flap neutral, but only 45 percent with flap deflected. A point that should be noted, however, is that at high angles of attack, with the flap

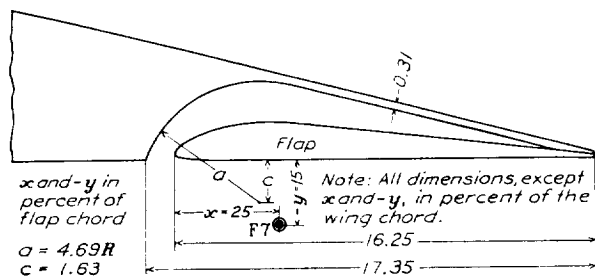


FIGURE 30.—Balanced split flap with slot arrangement 5A.

neutral, the stick forces may not be satisfactory for small aileron deflections because the hinge-moment curves (fig. 13) indicate no moment over a small range of deflections for the differential motion used. With this arrangement of aileron and flap, the axes are located 60 percent of the aileron or flap chord out from

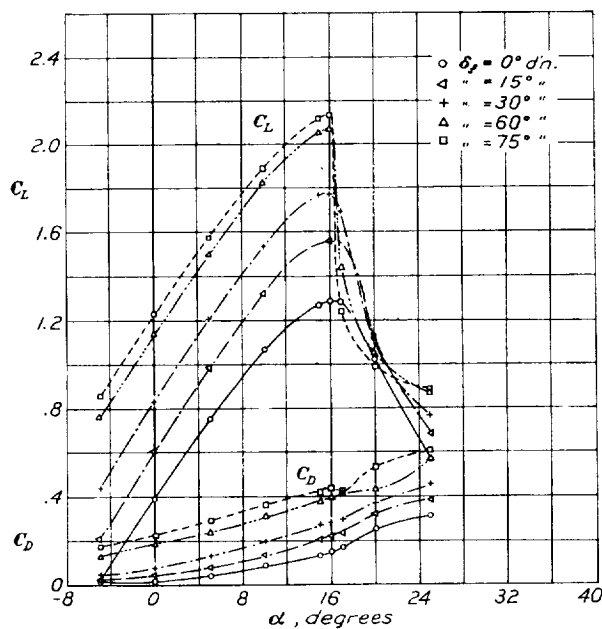


FIGURE 31.—Lift and drag coefficients for wing with balanced split flap at axis F7. Slot arrangement 5A.

the surface. On a wing having a chord of 6 feet this distance would amount to about 6 inches, which should be considered in comparisons with other arrangements.

Another arrangement of balanced upper-surface ailerons and balanced split flap which might be used is that of slot arrangement 3A with the aileron at axis location A9 and the flap at axis location F6. The

aileron in this case have the lowest hinge moments of any of the balanced arrangements tested, the moments being about 50 percent those of the unbalanced upper-surface ailerons when the flaps are neutral and about 40 percent when the flaps are deflected. On the basis of rolling moments equal to those of the unbalanced ailerons, the hinge moments would become about 65

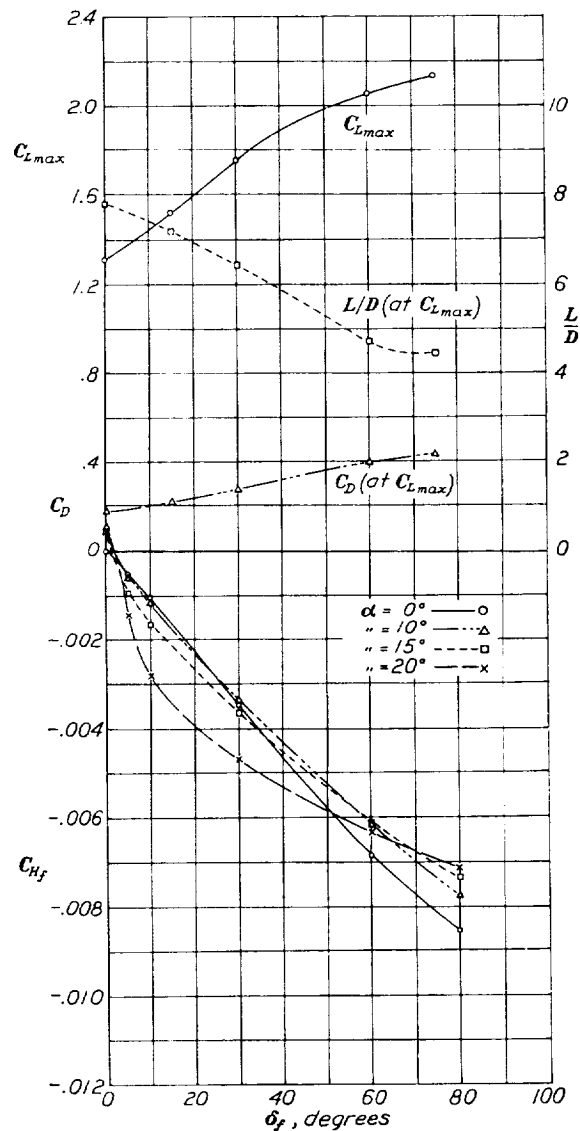


FIGURE 32.— $C_{L_{max}}$, C_D and L/D at $C_{L_{max}}$, and C_H for balanced split flap at axis F7. Slot arrangement 5A.

percent those of the unbalanced ailerons, flap neutral, and 50 percent with flap deflected. As regards lateral control, the rolling- and yawing-moment characteristics indicate that reasonably satisfactory control would be expected at all flight conditions excepting at the lowest speeds obtainable with the flaps neutral. This point, however, may be of sufficient importance to make the arrangement unsatisfactory.

The balanced split flap at axis location F12 with slot arrangement 3 gives a high maximum lift with exceptionally low hinge moments. The hinge moments are only about 50 percent those of the unbalanced split flap and are the lowest of any of those tested. The axis location is 60 percent of the flap chord out from the surface, an item that should be considered in comparisons with other balanced split flaps.

The balanced split flap at axis location F6 with slot arrangement 3A also gives a high maximum lift with reasonably low hinge moments. These moments are roughly 75 percent those of the unbalanced split flap for a flap deflection required to give the same maximum lift. With this arrangement the flap axis is only 15 percent of the flap chord out from the lower surface.

CONCLUSIONS

1. A balanced split flap has been developed that requires control forces about half those of the unbalanced split flap for approximately the same maximum lift.

2. A gap allowing flow of air from the lower to the upper surface of the wing in the vicinity of a split flap has an adverse effect on the maximum lifts attainable.

3. No entirely satisfactory arrangement of balanced upper-surface ailerons was found but one arrangement was developed that appeared to be satisfactory except for the stick-force characteristics with small aileron deflections at high angles of attack, flap neutral. Another arrangement also appeared to be satisfactory for all flight conditions except the lowest speeds obtainable with flaps neutral in which case the indicated rolling moments were low.

LANGLEY MEMORIAL AERONAUTICAL LABORATORY,
NATIONAL ADVISORY COMMITTEE FOR AERONAUTICS,
LANGLEY FIELD, VA., August 20, 1935.

REFERENCES

1. Weick, Fred E., and Wenzinger, Carl J.: Wind-Tunnel Research Comparing Lateral Control Devices, Particularly at High Angles of Attack. XII. Upper-Surface Ailerons on Wings with Split Flaps. T. R. No. 499, N. A. C. A., 1934.
2. Soulé, H. A., and McAvoy, W. H.: Flight Investigation of Lateral Control Devices for Use with Full-Span Flaps. T. R. No. 517, N. A. C. A., 1935.
3. Wenzinger, Carl J.: Wind-Tunnel Measurements of Air Loads on Split Flaps. T. N. No. 498, N. A. C. A., 1934.
4. Harris, Thomas A.: The 7- by 10-Foot Wind Tunnel of the National Advisory Committee for Aeronautics. T. R. No. 412, N. A. C. A., 1931.
5. Glauert, H.: Wind-Tunnel Interference on Wings, Bodies, and Airscrews. R. & M. No. 1566, British A. R. C., 1933.
6. Theodorsen, Theodore: Interference on an Airfoil of Finite Span in an Open Rectangular Wind Tunnel. T. R. No. 461, N. A. C. A., 1933.
7. Wieselsberger, C.: Theoretical Investigation of the Effect of the Ailerons on the Wing of an Airplane. T. M. No. 510, N. A. C. A., 1929.
8. Munk, Max M.: A New Relation Between the Induced Yawing Moment and the Rolling Moment of an Airfoil in Straight Motion. T. R. No. 197, N. A. C. A., 1924.

TABLE I.—ORDINATES OF BALANCED UPPER-SURFACE AILERON AND BALANCED SPLIT FLAP IN PERCENT AILERON OR FLAP CHORD

[Radius: L. E., 0.62; T. E., 0.37]

Distance from L. E.	Upper	Lower	Distance from L. E.	Upper	Lower
0.....	1.38	1.38	40.....	7.00	0
1.25.....	2.94	.42	50.....	6.00	0
2.5.....	3.72	.23	60.....	4.92	0
5.....	4.85	.03	70.....	3.84	0
7.5.....	5.81	0	80.....	2.81	0
10.....	6.65	0	90.....	1.73	0
15.....	7.81	0	95.....	1.07	0
20.....	8.43	0	100.....	.74	0
30.....	8.08	0			

REPORT No. 550

COOLING CHARACTERISTICS OF A 2-ROW RADIAL ENGINE

By OSCAR W. SCHEY and VERN G. ROLLIN

SUMMARY

Cooling tests were conducted on a calibrated GR-1535 Pratt & Whitney Wasp, Jr. engine installed in a Vought XO4U-2 airplane. The tests were made in the N. A. C. A. full-scale tunnel at air speeds from 60 to 120 miles per hour, at engine speeds from 1,500 to 2,600 r. p. m., and at manifold pressures from 19 to 33 inches of mercury absolute. A Smith controllable propeller was used to facilitate obtaining the different combinations of engine speed, power, and manifold pressure.

The results of the tests showed that an air speed of 120 miles per hour was necessary for the satisfactory cooling of this engine, as installed in a Vought XO4U-2 airplane with air of standard sea-level density when operating at full throttle at an engine speed of 2,500 r. p. m. Increasing the brake horsepower 50 percent resulted in an increase of 13 to 20 percent in the temperature difference between the air and the cooling surface. When the air speed was increased from 60 to 120 miles per hour, there was a decrease in the temperature difference between the cooling air and the cooling surface of only 17 percent. The same percentage change in temperature difference between the cooling air and the cooling surface was obtained for a given change in power when the manifold pressure was varied as when the engine speed was varied. The effect of the attitude of the airplane on the cylinder temperatures was small; the temperatures increased or decreased slightly, depending on the location of the cylinder. The difference in cylinder temperatures obtained with 3-blade and 2-blade propellers was negligible. The heat loss through the oil radiator was equal to from 3 to 6 percent of the heat going into indicated power, depending on engine speed and mixture strength.

INTRODUCTION

Many investigations have been conducted on air-cooled engines, particularly engines of the single-row radial type, for the purpose of studying the cooling obtained with different types of cowlings. Although most of these investigations have yielded a large amount of valuable information, there still remain important factors to be investigated.

Remarkable progress has been made in the cooling of air-cooled engines but cooling difficulties frequently occur because aircraft engines are required to operate, at least part of the time, under very severe conditions. Furthermore, reduction gears, controllable propellers, increased specific outputs, superchargers, and, in some

cases, low-drag cowlings have all intensified cooling difficulties.

The present investigation was undertaken at the request of the Bureau of Aeronautics, Navy Department, to determine the cooling of a 2-row radial engine under conditions closely simulating those in flight, especially those of the full-throttle climb. In these tests the many factors influencing the cooling were varied over a range sufficiently large that their effects could be established. In general, the cylinder temperatures were measured at various engine speeds, manifold pressures, speeds of cooling air, and fuel consumptions. Tests were also made with a 2-blade and 3-blade propeller and with the airplane at different angles of attack.

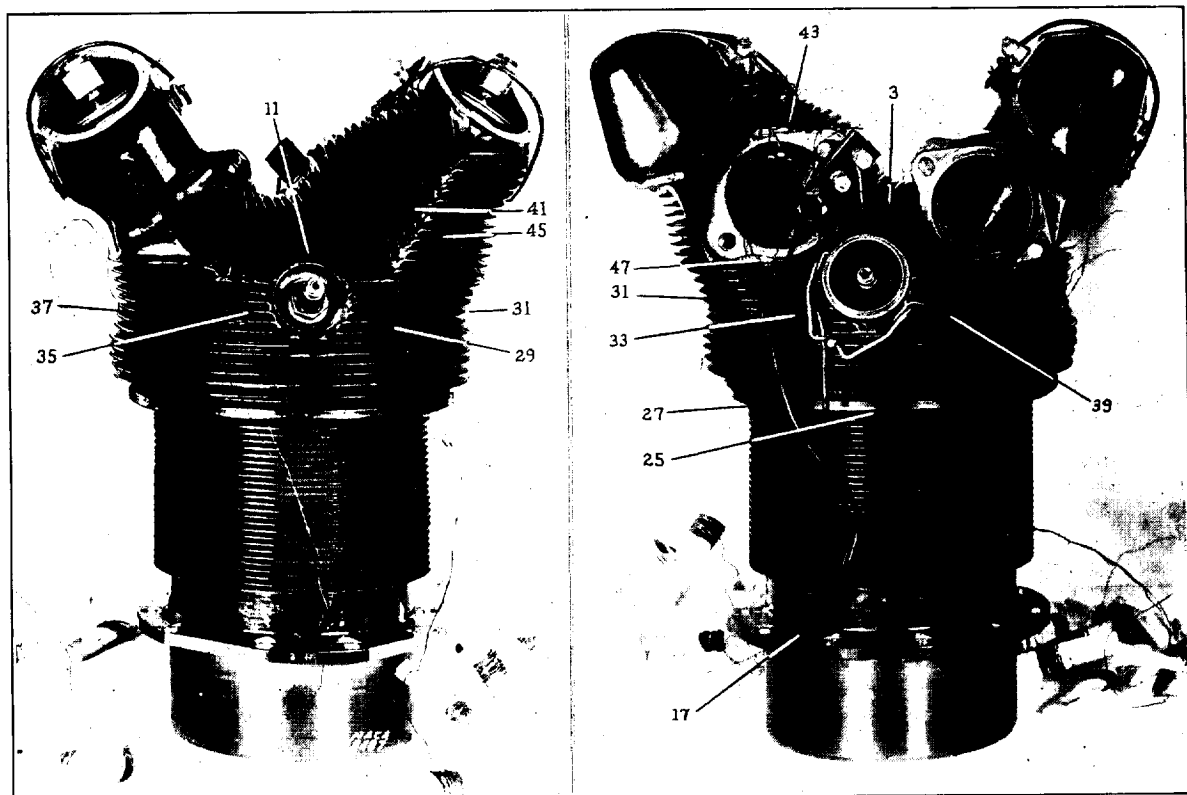
The tests were conducted by the National Advisory Committee for Aeronautics during April and May 1933.

DESCRIPTION OF EQUIPMENT

Engine.—The engine used for these tests is a 14-cylinder 2-row radial, designated a GR-1535 Pratt & Whitney Wasp, Jr. The engine has an over-all diameter of 43 $\frac{3}{4}$ inches. It is rated at 700 horsepower at 2,500 r. p. m., has a compression ratio of 6.5, and is equipped with a geared centrifugal supercharger that operates at eight times engine speed. This supercharger will maintain a manifold pressure of approximately 33 inches of mercury absolute at sea level when the engine is operating at 2,600 r. p. m. The propeller is driven through a 3:2 reduction gear. For the greater part of the investigation the engine was equipped with a 2-blade Smith controllable propeller having a diameter of 10 feet; the remaining tests were made with a 3-blade adjustable propeller having a diameter of 10 feet 6 inches.

The rear-row cylinders on this engine have more finning around the exhaust ports than the cylinders in the front row (fig. 1). Intercylinder baffles limit the amount of cooling air flowing past the cylinders. These baffles, as shown in figure 2, fit closely to the cylinders and are supplemented by pieces that fit closely to the fins at the top of the cylinder and extend outward to an N. A. C. A. cowling ring, forming a wall blocking off the area between the cowling and the engine. These baffles keep the air close to the cylinder and guide it to the rear of the cylinder (reference 1).

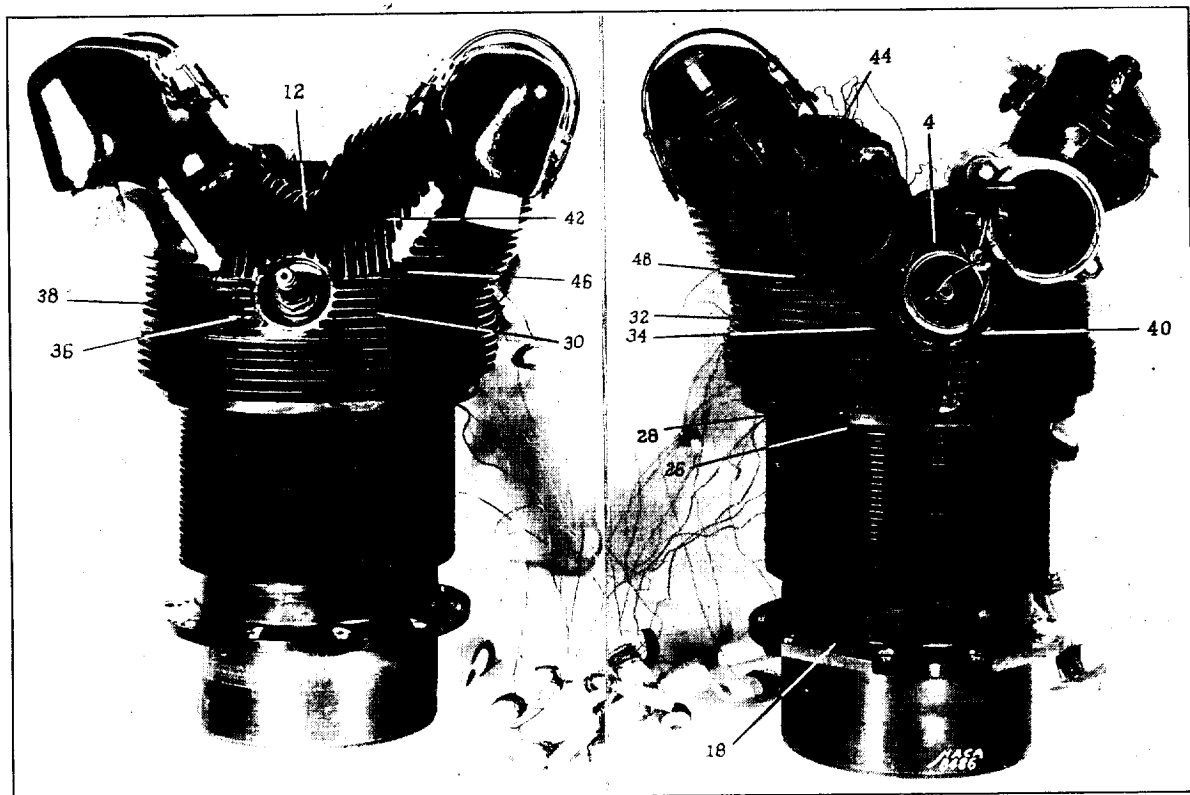
In these tests the oil radiator was modified so that water instead of air was used for carrying the heat



Front view.

Cylinder 3.

Rear view.



Front view.

Cylinder 4.

Rear view.

FIGURE 1.—Comparative finning on the rear-row (cylinder 3) and the front-row (cylinder 4) cylinders and also the location of thermocouples.

away from the oil. This change was necessary in order to obtain sufficient cooling when operating at high power output with low air speeds.

Airplane.—The engine was mounted in a Vought XO4U-2 airplane, a 2-place observation airplane of conventional design with a maximum speed of 185 miles per hour.

Full-scale tunnel.—All the tests except a few high-speed flight tests were made in the Committee's full-scale tunnel (reference 2). This tunnel has a 30- by 60-foot jet and a maximum air speed of approximately 120 miles per hour. Figure 3 shows the airplane mounted on the balance in the full-scale tunnel.

Instruments.—Iron-constantan thermocouples connected to two Brown recording pyrometers were used for measuring the cylinder temperatures. The thermocouples were made from 0.016-inch diameter enameled and silk-covered wire. The thermocouples were peened to the cylinder heads and electrically spot-welded to the steel barrels. The location of the 47 thermocouples used is given in table I and figure 1. These thermocouples were located as shown in order to obtain the difference in temperature between front- and rear-row cylinders, the maximum temperature on a front- and a rear-row cylinder, and an indication of temperature difference between several cylinders in each row.

TABLE I.—LOCATION OF THERMOCOUPLES

Thermocouple	On cylinder ¹	Corresponding thermocouple on cylinder 3 ²
1	1	3
2	2	3
5	5	3
6	6	3
7	7	3
8	8	3
9	9	3
10	10	3
13	5	11
14	6	11
15	7	11
16	8	11
19	5	17
20	6	17
21	7	17
22	8	17
23	Front section of crankcase.	
24	Blank, for synchronizing records.	

¹ Cylinders are numbered in accordance with the customary practice. (See fig. 2 (b).)

² For location of thermocouples on cylinders 3 and 4 see fig. 1.

In addition to the cylinder-temperature measurements the following temperature measurements were obtained:

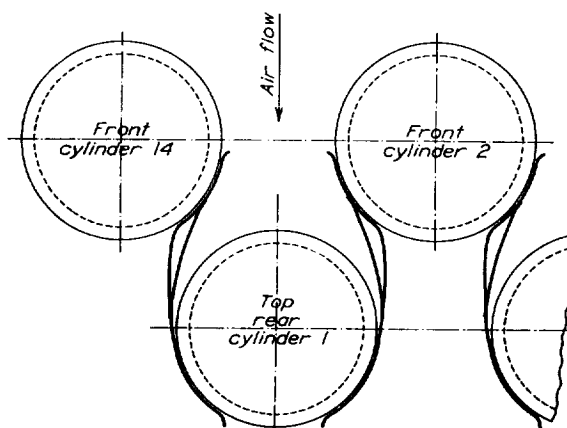
- Oil in.
- Oil out.
- Carburetor air.
- Air stream.
- Cold junction of thermocouples.
- Accessory compartment.
- Oil radiator, water in.
- Oil radiator, water out.

Electrical-resistance thermometers were used for measuring the first six temperatures and vapor-pressure thermometers for those of the oil radiator.

The engine speed was measured with an electrical tachometer and the manifold pressure with a mercury



(a) Baffles assembled on a rear-row cylinder.



(b) Plan view of inter-cylinder baffles.

FIGURE 2.—Arrangement of inter-cylinder baffles on Pratt & Whitney GR-1535 2-row radial engine.

manometer. The wind-tunnel air speed was obtained from a static-plate calibration of the tunnel for each test condition. Fuel-consumption measurements were obtained with a calibrated displacement-type fuel flowmeter. The water passing through the air passages of the oil radiator was measured with a calibrated water meter.

With the exception of the static-plate manometer and the water-in and water-out thermometers in the oil radiator all instruments were located in the scale room directly below the airplane.

METHOD OF TESTING

The effect on the cylinder temperatures of operating at several engine speeds from 1,700 to 2,500 r. p. m. was investigated for full-throttle conditions at air speeds of 85, 102, and 119 miles per hour. Tests were also made at several engine speeds from 1,500 to 2,500 r. p. m. with manifold pressures of approximately 29, 24, and 20 inches of mercury absolute and at an air speed of 116 miles per hour. For each of these runs the desired engine speed was obtained at each air-speed and manifold-pressure condition by varying the pitch of the propeller.

Four full-throttle runs were made at an engine speed of 2,500 r. p. m. and at an air speed of 120 miles per hour to determine the variation in cylinder temperature with mixture ratio by varying the rate of fuel flow. The lowest rate was determined by the maximum cylinder-head temperature, which was limited to 600° F., and by the general operation and power output of the engine. The maximum rate was with the mixture control set full rich.

The difference in cylinder temperatures obtained with 2-blade and 3-blade propellers was determined for full-throttle operation at engine speeds of 2,000 and

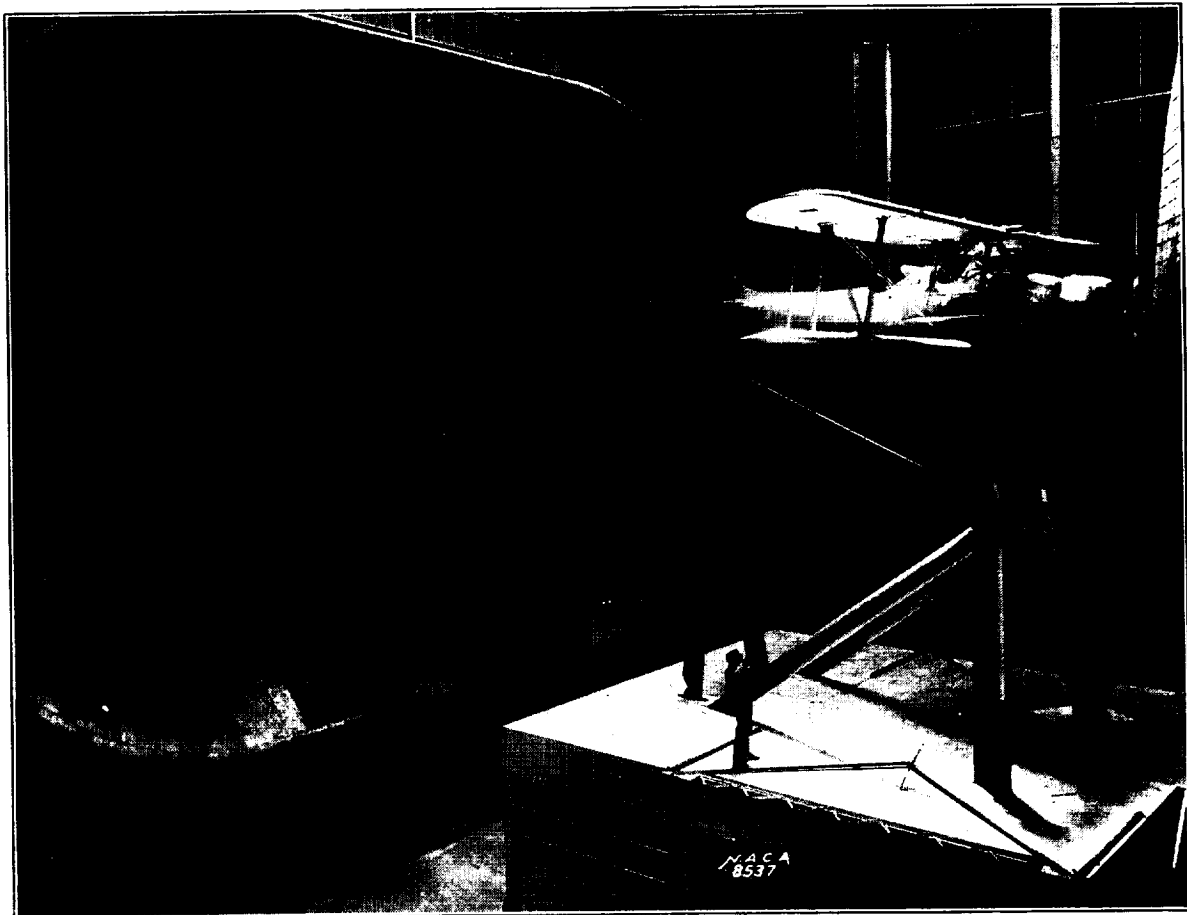


FIGURE 3. The NACA 8537 2-airplane mounted in the full-scale tunnel ready for test.

The effect of engine speed on the cylinder temperatures for a constant brake horsepower and a constant air speed of 119 miles per hour was determined. The power was maintained constant by changing the propeller pitch and the manifold pressure. The manifold pressure required to give constant power when the engine speed was varied was obtained from the calibration curves for the engine. Although engine manufacturers have limited the temperature of the rear spark plug boss to 500° F. for satisfactory cooling, long engine life, and reliability, higher temperatures were tolerated in some runs in order to extend the range of the tests.

2,100 r. p. m. and at air speeds of 85 and 120 miles per hour, respectively.

The effect of the attitude of the airplane on the cylinder temperatures was determined for four different angles of attack (based on the thrust axis): -4°, 0°, 4°, and 8°. These tests were made at an air speed of 100 miles per hour, at an engine speed of 2,100 r. p. m., and at full-open throttle.

The lubricating oil used in these tests conformed to the Navy specifications for a 3120 oil. Gasoline conforming to Army specifications Y-3557-G and having an octane number of 87 was used in most of the investigation. For the most severe conditions sufficient

ethyl fluid was added to the gasoline to increase the octane number to 92.

Air speed.—The observed air speed was corrected to an air speed at 29.92 inches of mercury and 70° F. from

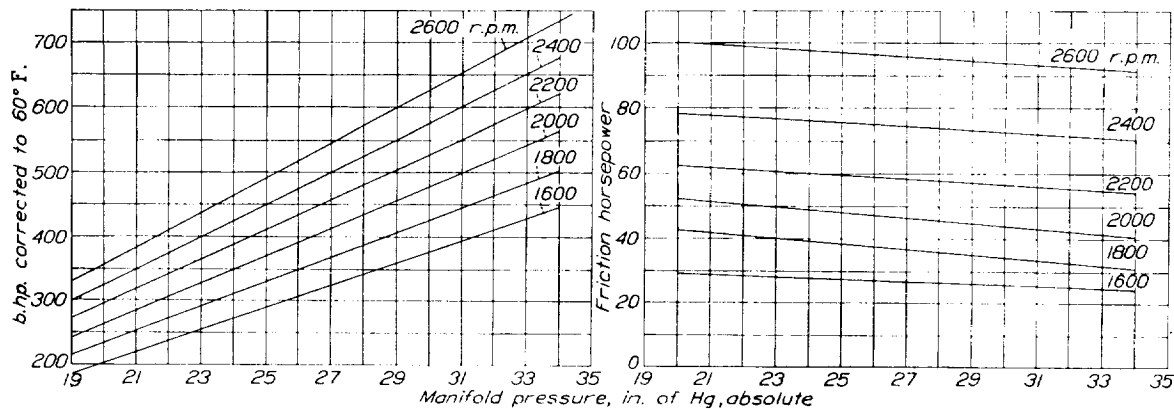


FIGURE 4.—Calibration curves showing brake and friction horsepower at various engine speeds and manifold pressures.

A few runs were also made at what might be called "normal" operation with a fixed-pitch propeller. The propeller pitch was set so that 2,500 r. p. m. could be obtained at an air speed of approximately 120 miles per hour when operating at full-open throttle. With this pitch setting, performance measurements were obtained at full-open throttle for air speeds of 80, 100, and 120 miles per hour. A similar series of runs was made with the propeller pitch set to give a full-throttle engine speed of 2,150 r. p. m. at an air speed of 120 miles per hour. Test runs were then made with this fixed-pitch setting when operating at full-open throttle at air speeds of 60, 80, 100, and 120 miles per hour.

COMPUTATIONS

Engine power.—The engine was calibrated before and after these cooling tests by the Research Division of the United Aircraft and Transportation Corporation (reference 3). The calibration curves of friction and brake horsepower for various speeds and manifold pressures are shown in figures 4 and 5. In the preparation of these curves the power developed was corrected to a standard atmosphere (29.92 inches of mercury pressure and 60° F. temperature).

The power developed was obtained from the calibration curves for the observed manifold pressure and engine speed. A correction was then applied to the power obtained from the calibration curves for the difference in carburetor-air temperature during the calibration and during the test according to the relation

$$\text{Observed b. hp.} = \text{b. hp. (at 60° F.)} \sqrt{\frac{T_s + 460}{T_0 + 460}}$$

where

T_0 , observed air temperature at the carburetor.

T_s , standard air temperature at the carburetor (60° F.).

Cylinder temperatures.—The pyrometer readings of cylinder temperatures were corrected for instrument calibration and cold-junction variation and were converted to a standard cooling-air temperature of 70° F.

pressure and temperature measurements according to the relation

$$V_s = \frac{V_0 \rho_0}{\rho_s}$$

where

V_0 , observed air speed.

V_s , air speed at 29.92 inches of mercury pressure and 70° F.

ρ_0 , observed density.

ρ_s , standard density.

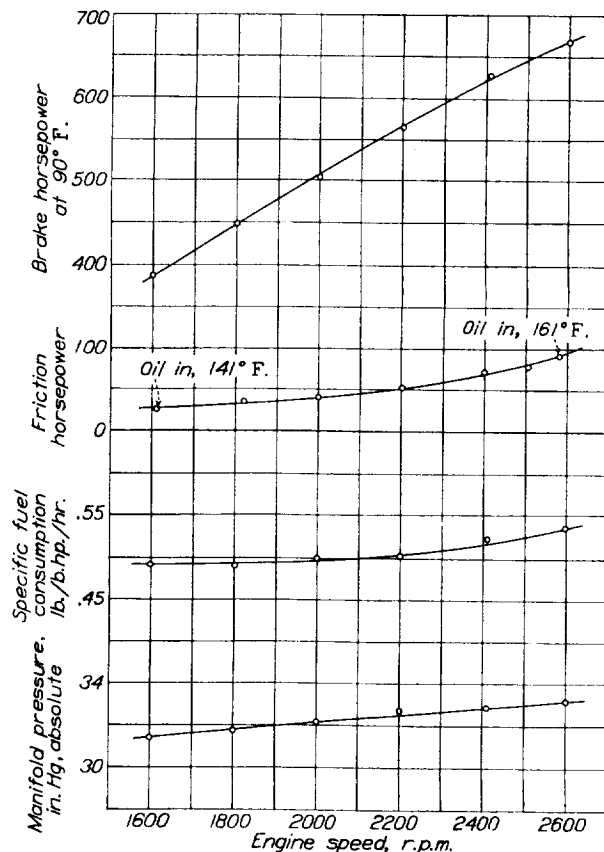


FIGURE 5.—Full-throttle calibration of GR-1535 engine.

Heat loss to the oil.—The heat loss to the oil was calculated from the quantity and increase in temperature of the water flowing through the oil cooler.

Fuel consumption.—The specific fuel consumption was calculated from the fuel flow, observed horsepower, and density of the fuel.

RESULTS AND DISCUSSION

Effect of specific fuel consumption.—The curves in figure 6 (a) for full throttle show that the leaning of a very rich mixture so as to obtain a reduction in specific fuel consumption of 0.10 pound per brake horsepower per hour resulted in only a small increase in cylinder

mixture ratio of the charge delivered to each cylinder. Temperature differences between cylinders are often attributed to poor distribution or to nonuniform cooling of the cylinders because of their location with respect to other engine parts. These curves show that temperature differences between cylinders can be definitely attributed to poor distribution only after a sufficient number of runs have been made to establish the curve of cylinder temperature against specific fuel consumption. The cylinders that are operating on a lean mixture will show the greatest variation in temperature with change in mixture strength. On the basis of these curves the variation in mixture strength for

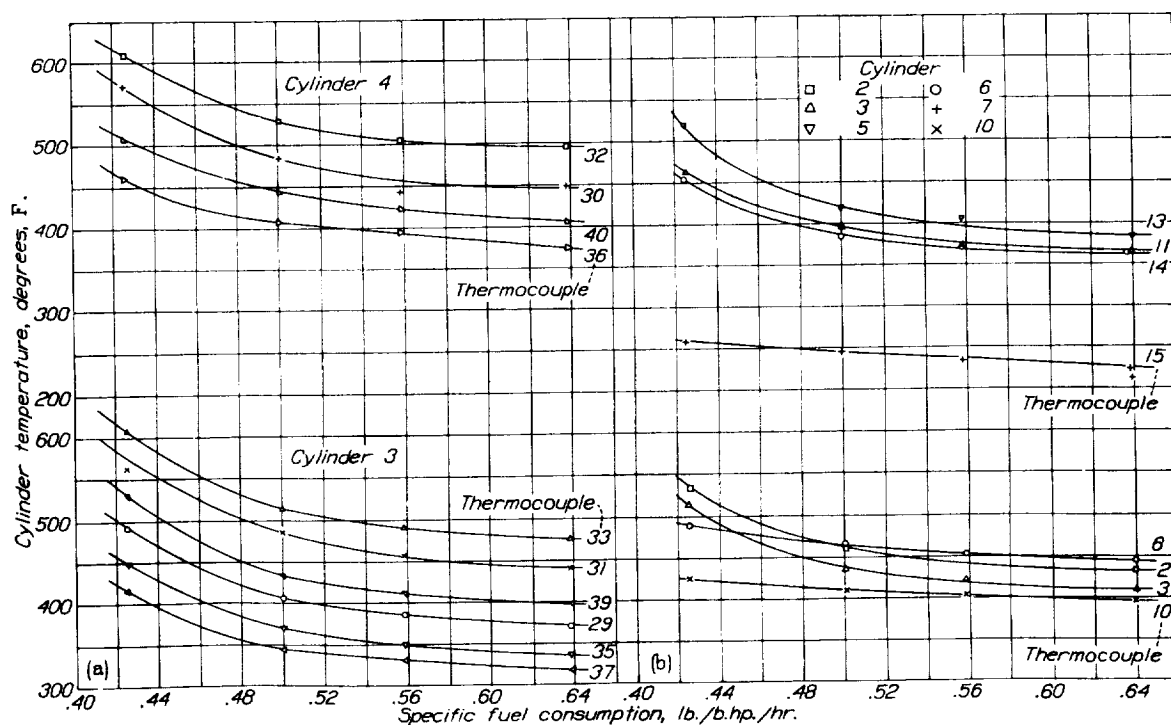


FIGURE 6.—Effect of specific fuel consumption at full throttle on the cylinder temperatures. In these tests the horsepower varied from 675 to 695; the engine speed from 2,427 to 2,498 r. p. m.; the manifold pressure from 33.33 to 33.61 in. Hg. absolute, and the air speed from 116.2 to 119.2 m. p. h.

temperatures; whereas the leaning of a lean mixture so as to obtain the same reduction in specific fuel consumption resulted in a large increase in cylinder temperatures. The temperatures at different points on the same cylinder varied consistently with the mixture strength; those that are high showed the greatest variation. As a lean mixture burns slowly the cylinder walls are exposed to burning gases during a large part of the expansion stroke; with a rich mixture some of the heat is carried out through the exhaust by the excess fuel.

A comparison of the curves of temperature variation with specific fuel consumption for several cylinders (fig. 6(b)) shows that the temperature of each cylinder did not vary the same amount when the mixture strength was changed. The amount of this variation depends upon how much difference there is in the

different cylinders is estimated to be at least 10 percent.

Effect of engine speed and air speed when operating at full throttle.—The cylinder temperatures obtained when operating full throttle at engine speeds between 1,800 and 2,600 r. p. m. and at average air speeds of 85, 102, and 119 miles per hour are shown in figure 7. These temperature measurements from the 6 thermocouples on cylinder 4 and from the 6 on cylinder 3 are only a part of the temperature data obtained; they have been selected after comparison with other temperatures observed as a fair representation of all engine temperatures. When the engine speed was increased from 1,800 to 2,600 r. p. m., the brake horsepower was increased 50 percent (fig. 5) and the indicated horsepower 59 percent; whereas the difference

in temperature between the cylinder and the air increased 15 to 24 percent (fig. 7).

It may be well to state that these results have been substantiated in laboratory tests of a single-cylinder air-cooled engine. The much more rapid increase of the engine power than of the cylinder temperatures indicates that considerably more power can be obtained from an air-cooled cylinder with small improvements in the finning. The specific fuel consumption and the manifold pressures increased slightly in these tests. The increase in specific fuel consumption

installed in the XO4U-2 airplane can be operated at a full-throttle speed of 2,500 r. p. m. without exceeding the safe cylinder-head operating temperature (500° F.), provided that the speed of the airplane is 120 miles per hour and that the mass flow is equal to that of cooling air at 70° F. and at standard sea-level density. Without a controllable propeller these high engine speeds could not be obtained in climb unless the propeller pitch were set so low that level flight at full-open throttle would be impossible without excessive engine speeds. Flight tests conducted elsewhere on

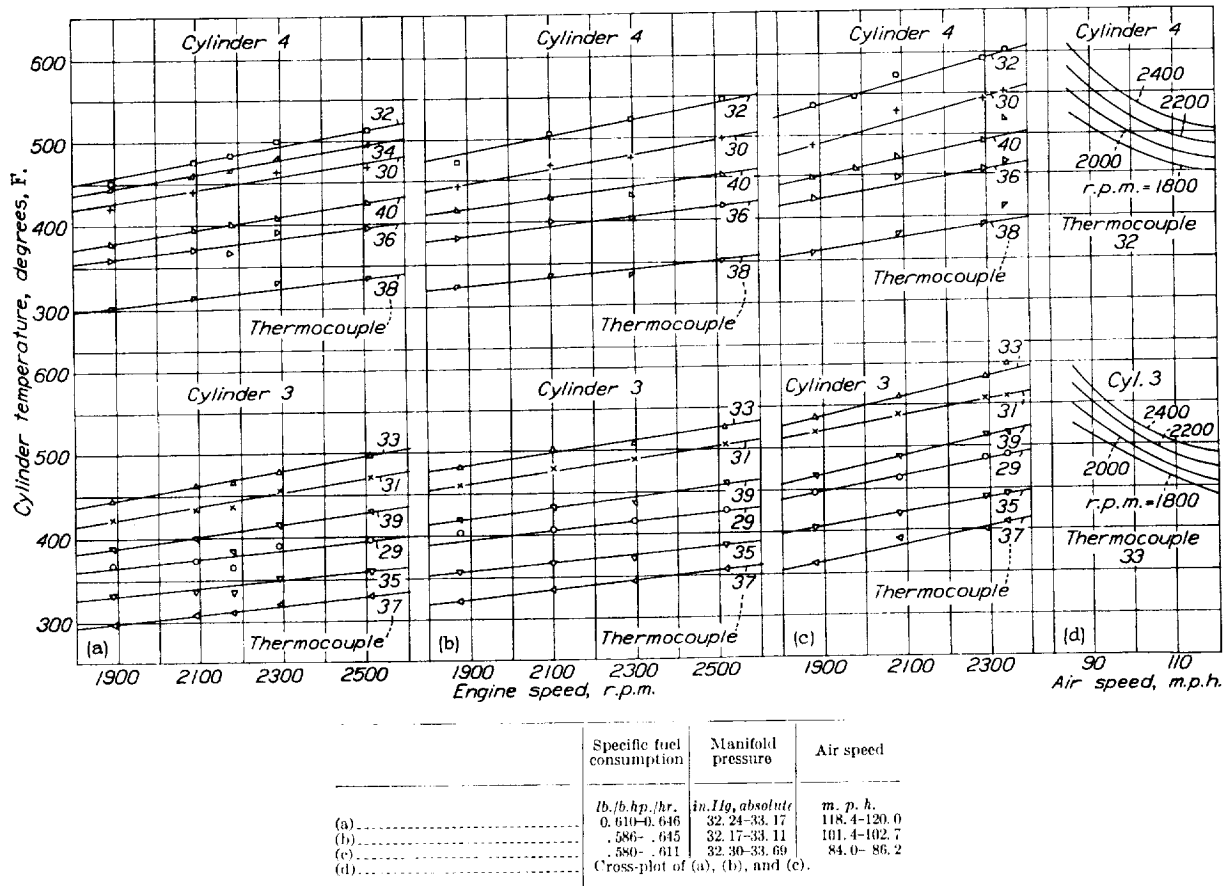


FIGURE 7.—Effect of engine speed and air speed on cylinder temperatures when operating at full throttle.

caused by increasing the engine speed from 1,800 to 2,600 r. p. m. resulted in a reduction in cylinder temperature of approximately 10° F.; whereas the increase in manifold pressure would result in an increase in cylinder temperature of less than 5° F.

The results shown in figure 7 closely simulate those obtainable in full-throttle climbs at higher engine speeds. At air speeds of 85 to 90 miles per hour, the best climbing range for this airplane, the highest cylinder-head temperatures at 2,500 r. p. m. were more than 600° F., which is appreciably higher than what would be considered permissible for long life and reliability. The results indicate that this engine as

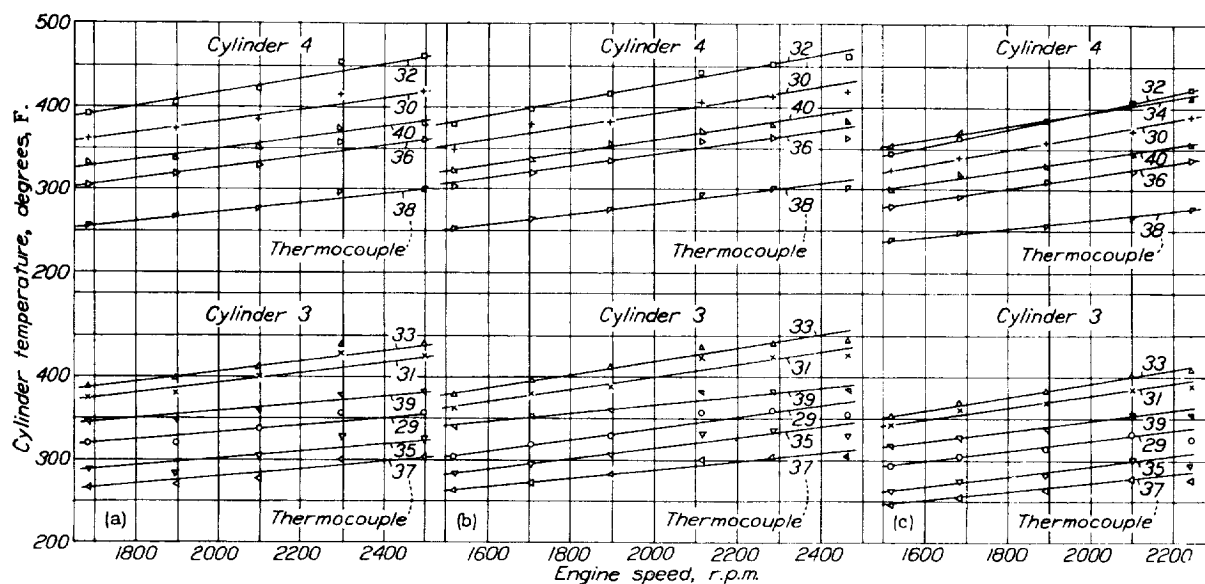
this airplane indicate that, when an adjustable propeller having the best setting for high speeds is used, the engine speed in climb will be so low that the safe operating temperature is not exceeded at air speeds of 80 to 90 miles per hour.

Flight tests conducted at air speeds higher than those obtainable in the tunnel showed that the cooling was satisfactory for these conditions. In full-throttle climbs at high engine speeds, however, the cylinder temperatures, like those in the tunnel, were high. No attempt was made to reduce the temperatures obtained in flight to the same standard because the magnitude

of the various corrections is not sufficiently well established to justify comparison.

Effect of engine speed when operating at various throttle settings.—The cylinder temperatures obtained when operating at different throttle settings at various engine speeds and at approximately constant air speed are shown in figure 8. These curves show that, regardless of the amount of throttling or of the manifold pressure at which the engine operates, a certain percentage increase in power due to increase in engine speed will, for each condition, result in approximately the same percentage increase in temperature. For example, when operating at a manifold pressure of

constant speed and varying manifold pressure and the other with varying speed and constant manifold pressure. The average temperature for thermocouples 29, 31, 33, 35, 37, and 39 on cylinder 3 were used in the preparation of these curves. It is interesting to note that increasing the brake horsepower by increasing the speed results in a slightly greater rate of change in temperature than is obtained by increasing the manifold pressure. On an indicated-power basis the temperatures for each of the two conditions of varying the power fall on the same straight line. Within the range of these tests it is apparent that nothing is to be gained in reduced cylinder temperatures by in-



	Specific fuel consumption	Manifold pressure	Air speed
	<i>lb./b.h.p./hr.</i>	<i>in. Hg. absolute</i>	<i>m. p. h.</i>
(a)	0.614-0.654	28.36-28.53	116.0-117.4
(b)563-.647	23.67-23.91	114.5-115.5
(c)607-.652	19.15-19.27	115.8-117.0

FIGURE 8. —Cylinder temperatures obtained with varying manifold pressures and engine speeds when the air speed is practically constant.

19.2 inches of mercury an increase in engine speed sufficient to cause a 50 percent increase in brake horsepower will result in an average increase in the temperature difference between the cooling air and the cylinder of 21 percent on the front-row cylinder and of 17 percent on the rear row. At a manifold pressure of 28.44 inches of mercury absolute a 50 percent increase in power will result in an average increase in cylinder temperature difference of 22 percent for cylinder 4 and an increase of 15 percent for cylinder 3. The largest percentage increase in temperature difference in each case is for the front-row cylinders, which have the least amount of finning around the head.

The curves in figure 9 show the relation between the average cylinder temperatures and the brake and indicated horsepower for two conditions, one with

creasing either function of the power in preference to the other.

Effect of engine speed when operating at approximately constant power.—The results in figure 10 show that the cylinder temperatures are not influenced by the engine speed or pitch setting provided that the power and other conditions remain constant. In these tests the brake horsepower decreased from 530 to 503 and the indicated horsepower increased from 570 to 600 when the engine speed was increased from 2,000 to 2,600 r. p. m. It has been shown earlier that a 5 to 6 percent variation in engine power would cause a change of approximately 2 percent in the cylinder temperatures. The slightly higher temperatures obtained at a speed of 2,000 r. p. m. were mostly due to a low specific fuel consumption, the specific fuel consumption being

0.606 pound per brake horsepower per hour for this run and more than 0.638 pound per brake horsepower per hour for the other runs. The difference in specific

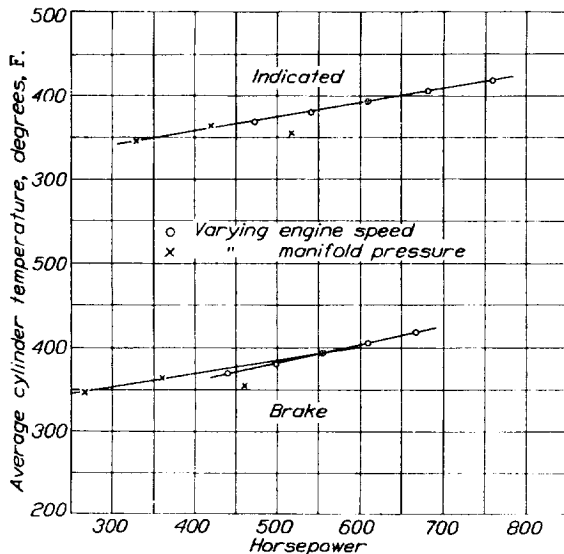


FIGURE 9.—Effect on cylinder temperatures of increasing power by increasing either engine speed or manifold pressure.

fuel consumption would cause a variation in temperature of from 10° to 15° F.

Effect of changing air speed when propeller pitch is constant.—The two sets of runs (fig. 11) in which the

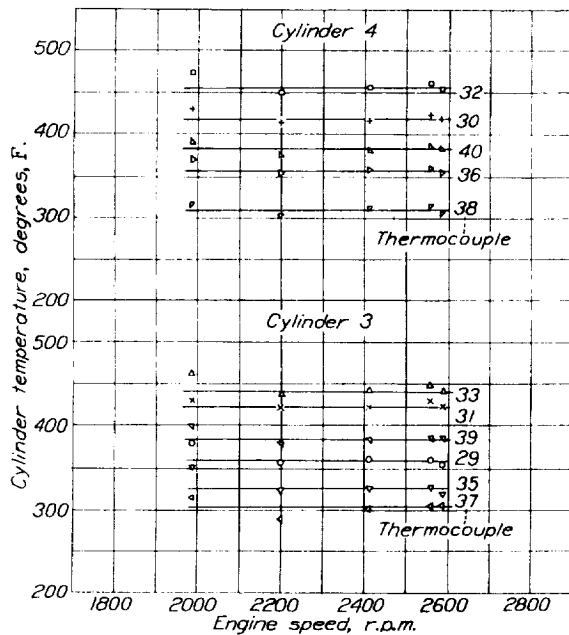


FIGURE 10.—Effect on cylinder temperatures of operating at various engine speeds when the power and the air speed are constant. In these tests the brake horsepower varied from 503 to 532; the specific fuel consumption from 0.606 to 0.651 lb. per b.h.p. per hr.; the air speed from 118.0 to 119.3 m. p. h.; and the manifold pressure from 25.46 to 33.44 in. Hg. absolute.

propeller pitch was set to give full-throttle engine speeds of 2,500 and 2,150 r. p. m. showed that when the air speed was reduced the cylinder temperatures

increased to exceed the safe operating temperature at the lower air speed.

Heat loss to lubricating oil.—The curves in figure 12 show the ratio between the heat loss to the oil and the heat going into indicated power at different engine

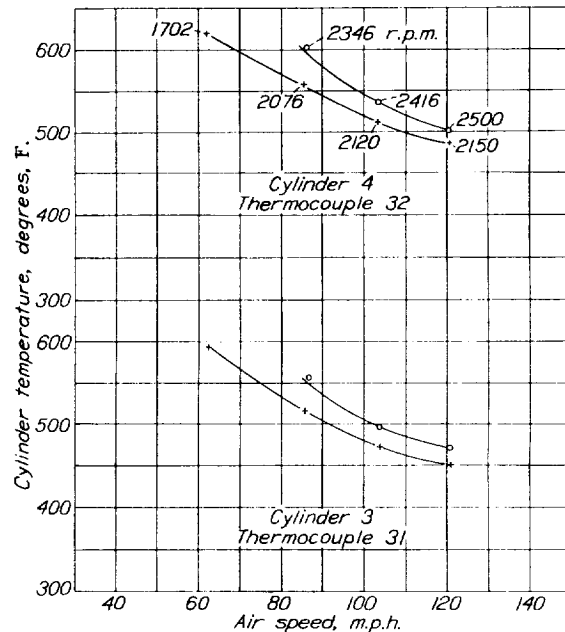


FIGURE 11.—Effect on cylinder temperature of changing air speed when propeller pitch is constant.

speeds when operating at a constant engine power of 530 brake horsepower and when operating with the engine power varying from 498 to 692 brake horsepower. Increasing the speed when the power was held constant resulted in an increasing amount of heat being carried away from the oil. The total quantity of heat carried

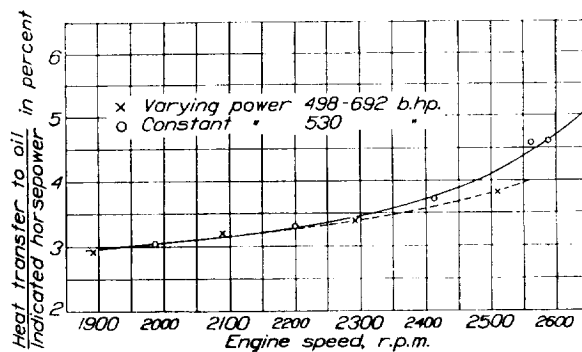


FIGURE 12.—Heat loss to the oil.

away with varying power may appear to be less than with constant power but such is not the case, however, for the lower curve is based on a higher brake horsepower.

When the mixture is leaned, the heat loss to the oil increased from approximately 4 to 6 percent of the heat going into indicated power because of the increase in temperature of the cylinder walls.

The heat loss to the oil in these tests was higher than would be obtained in regular service because the cylinder temperature in many runs exceeded the specified service temperatures. Recent tests on this engine by the Bureau of Aeronautics, Navy Department, gave a heat loss to the oil equal to 1.72 percent of the heat going into useful work.

In the most severe of these tests excessive oil-out and accessory-compartment temperatures were obtained. When the mixture was leaned, the accessory-compartment temperatures reached a maximum of 220° F. and the oil-out, 200° F. In all other tests the oil-out and accessory-compartment temperatures varied between 150° and 190° F. depending on power output and air speed.

Effect of angle of attack.—Increasing the angle of attack of the airplane (based on thrust axis) from -4° to 8°, which includes the high-speed and climbing attitude at full throttle, caused the temperature of the top cylinders in the front row to increase 15° to 20° F. and the temperature of the bottom cylinders in the front row to decrease the same amount. The other cylinders did not show any consistent change with angle of attack. The change in temperature on the rear-row cylinders was slightly less than on the front row. The results indicate that a reduction in temperature can be obtained by setting the fins at a slight angle with respect to the air stream.

Cylinder temperatures obtained with 2-blade and 3-blade propellers.—These tests showed that at low air speeds the use of 3-blade propellers resulted in lower cylinder temperatures than that of 2-blade propellers. At an air speed of approximately 120 miles per hour the average temperature for all thermocouples on the cylinders was practically the same with each propeller; whereas at an air speed of 80 miles per hour the average temperature for all thermocouples was 17° F. lower when using a 3-blade propeller.

CONCLUSIONS

The results of this investigation show that with a GR-1535 engine installed in a Vought XO4U-2 airplane:

1. When operating at full-open throttle at an engine speed of 2,500 r. p. m., an air speed of 120 miles per hour must be maintained for satisfactory cooling (500°

F. cylinder-head temperature) with air at a pressure of 29.92 inches of mercury and a temperature of 70° F.

2. Increasing the brake horsepower 50 percent resulted in a 15 to 24 percent increase in the temperature difference between the cooling surface and the cooling air.

3. The same percentage change in temperature difference between the cooling air and the cooling surface was obtained for a given change in power when the manifold pressure was varied as when the engine speed was varied.

4. Increasing the air speed from 60 to 120 miles per hour resulted in a decrease of 17 percent in the average difference in temperature between the cylinder and the cooling air.

5. The heat loss to the oil under these particular test conditions was equal to from 3 to 6 percent of the heat going into indicated power depending on the engine speed and fuel-air ratio.

6. The amount the temperature of different cylinders changes when the mixture strength is varied was found to be a good indication of mixture distribution in the engine.

7. The effect of the attitude of the airplane on the cylinder temperatures was small and slightly dependent on location of the cylinder.

8. There was practically no difference in the cylinder temperatures obtained with either 2-blade or 3-blade propellers at an air speed of 120 miles per hour; at an air speed of 80 miles per hour the average cylinder temperature for all the thermocouples was 17° F. lower with the 3-blade propeller.

LANGLEY MEMORIAL AERONAUTICAL LABORATORY,
NATIONAL ADVISORY COMMITTEE FOR AERONAUTICS,
LANGLEY FIELD, VA., *December 4, 1934.*

REFERENCES

1. Beisel, Rex B., MacClain, A. Lewis, and Thomas, F. M.: The Cowling and Cooling of Radial Air-Cooled Aircraft Engines. S. A. E. Jour., May 1934, pp. 147-166.
2. DeFrance, Smith J.: The N. A. C. A. Full-Scale Wind Tunnel. T. R. No. 459, N. A. C. A., 1933.
3. Chance Vought Corporation: Power Plant Tests on Pratt & Whitney 3:2 Geared R-1535 No. 2 Installed in Vought Model XO4U-2. Report No. 1944, Issue No. 1, Feb. 1933.

REPORT No. 551

AIRCRAFT COMPASS CHARACTERISTICS

By JOHN B. PETERSON and CLYDE W. SMITH

SUMMARY

A description of the test methods used at the National Bureau of Standards for determining the characteristics of aircraft compasses is given. The methods described are particularly applicable to compasses in which mineral oil is used as the damping liquid. Data on the viscosity and density of certain mineral oils used in United States Navy aircraft compasses are presented. Characteristics of Navy aircraft compasses IV to IX and some other compasses are shown for the range of temperatures experienced in flight.

Results of flight tests are presented. These results indicate that the characteristic most desired in a steering compass is a short period and, in a checking compass, a low overswing.

INTRODUCTION

Liquid-damped compasses have been extensively used in the navigation of surface ships, but it was not until their use in faster maneuvering aircraft that the dynamic characteristics of the card became of foremost importance. Numerous attempts have been made to analyze the motion of the liquid-damped compass card (references 1, 2, 3, 4, and 5), on the assumption that such an analysis would aid in the evaluation of the characteristics that a compass to be used in a specified manner should have. These attempts have yielded only approximate solutions, which have not aided the authors materially in clarifying the problem of the selection of suitable compass characteristics.

The data presented herein were obtained at the request, and with the financial support, of the Bureau of Aeronautics, Navy Department. The National Advisory Committee for Aeronautics furnished the financial support essential for the preparation of the report. The authors wish to acknowledge the close cooperation of W. G. Brombacher, National Bureau of Standards, C. L. Seward, Bureau of Aeronautics, Navy Department, and Ira E. Hobbs, lieutenant, United States Navy.

MOTION OF LIQUID-DAMPED COMPASS CARDS

The effect of the liquid that is carried around by the card is as if there were another disk of varying moment of inertia connected to the magnetic card by viscous

friction of varying magnitude. The complicated nature of the motion is indicated by the data presented in figure 1, which shows the motion of a Navy IX aircraft compass card after release from rest at a deflection of 30° (solid line) and after release from rest at a deflection of 10.5° (dotted line). The decrement in successive amplitudes of the first motion is far from constant, an observation not in agreement with the usual simplified theories. Although the card comes to rest at the end of the first overswing of 10.5° , the liquid continues in motion and reduces the second overswing, so that the ratio $10.5:2=5.25$ of second to third amplitude is much greater than the ratio $30:10.5=2.86$ of first to second amplitude. If the card is held steady at a deflection of 10.5° until the liquid has had time to come to rest and then released, the overswing is 3.7° and the ratio is $10.5:3.7=2.84$.

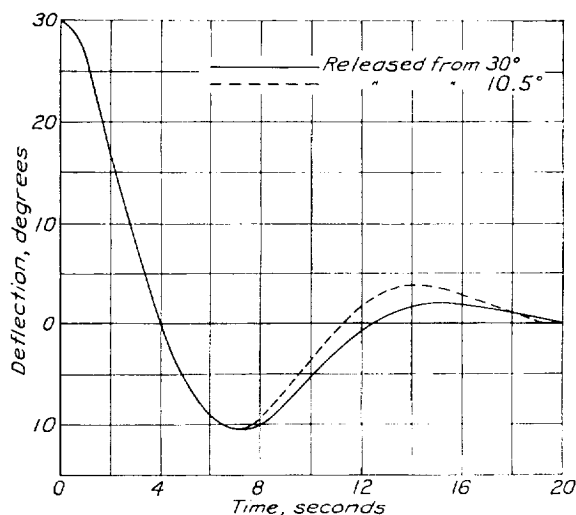


FIGURE 1.—Time-deflection curves for United States Navy IX liquid-damped aircraft compass at a temperature of 20°C .

In order to produce the motion indicated in figure 1, only the compass card was deflected, the case remaining stationary. In actual use both the compass card and the case are moving and there will be an additional effect on the motion of the card owing to the motion of the case from which it is separated by a relatively narrow layer of liquid. The authors have reached the

conclusion that a satisfactory analysis of the motion of the card including all of the factors involved would be extremely complicated.

OPERATING CHARACTERISTICS

In the absence of a satisfactory theory, the relation between operating characteristics that can be measured in the laboratory and behavior in flight must be determined empirically. For practical convenience, the operating characteristics of a compass are defined by three constants, which can easily be measured in the laboratory as described below. These constants are:

(1) The time of swing 30° to 5° , which is closely related to the period of the compass.

(2) The overswing from 30° , which depends principally upon the relative values of the moment of inertia and magnetic moment of the card and the viscosity of the damping liquid.

(3) The swirl, which serves as a measure of the effect of motion of the case on the motion of the card.

Following is a detailed description of the methods used at the National Bureau of Standards for determining these characteristics.

Time 30° to 5° .—The card is magnetically deflected 30° from its equilibrium position, held at this position long enough for the liquid to come to rest, released, and the time observed for it to pass through an angle of 25° toward its equilibrium position. The same test is repeated, deflecting the card 30° in the opposite direction. The position of the compass should not be changed between the two tests. The average of the observed times is defined as the "time 30° to 5° ." The purpose of making observations for deflections in both directions is to average out any error due to incorrect setting of the lubber line with reference to the equilibrium position of the card.

Overswing.—The card is magnetically deflected 30° from its equilibrium position, held at this position long enough for the liquid to come to rest, released, and the overswing past the equilibrium position noted. The test is repeated, deflecting the card in the opposite direction. The position of the compass should not be changed between the two tests. The average of the two observations is defined as the "overswing." In practice it is convenient to combine the test for the time 30° to 5° and for the overswing.

Swirl.—The compass is mounted on a motor-driven turntable, and turned through an angle of 90° at a rate of 30° per second. During the turn, a swirling motion is transmitted to the damping liquid, and some of this motion is transmitted to the card. The maximum deflection of the card from its true position, which occurs after the turn has been completed, is noted and defined as the "swirl."

These three operating characteristics are affected in the first order of magnitude by two variable factors, (1) the temperature and (2) the horizontal magnetic

field strength. It has been determined by experiment that temperature affects only the viscosity and density of the damping liquid. Temperature has a negligible effect on the magnetic moment of the permanent magnets. The International Critical Tables give 0.0002 per degree centigrade as the temperature coefficient of magnetic moment of cobalt magnet steel. This amounts to a change of 1 percent for a 50° C. change in temperature. The magnetic moment increases as the temperature is decreased. Variation of the operating characteristics with viscosity of the damping liquid is both more conveniently and more accurately determined by filling the compass with mineral oil having the required viscosity at room temperature than by changing the temperature of the compass. It is not necessary to make a separate determination of the effect of density, since the density of the liquids used can be expressed as a function of the viscosity alone.

DAMPING LIQUIDS

The method developed by Cragoe (reference 6) for representing changes in viscosity of liquids with changes in temperature and composition has been used. The reader is referred to Cragoe's article for full details of the method, but a short description will be given here. Cragoe has found that, to a very good approximation, a certain function of absolute viscosity (or of kinematic viscosity) for which the name "liquidity" has been suggested, is linearly related to temperature, that its reciprocal is linearly related to pressure, and that a linear mixture rule is applicable to such a function.

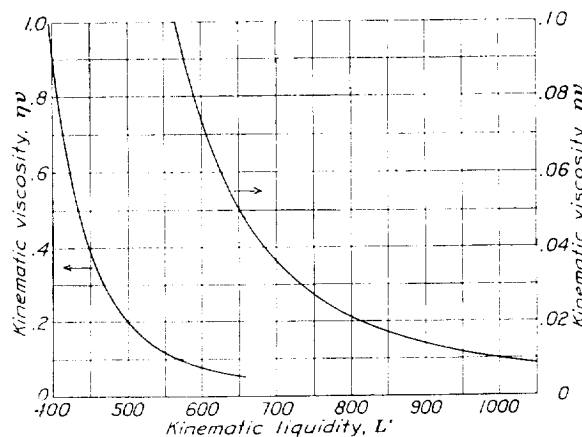


FIGURE 2.—Cragoe's kinematic liquidity as a function of kinematic viscosity.

Designating the liquidity by L when it refers to absolute viscosity and by L' when it refers to kinematic viscosity, it is defined by the equations

$$\eta = Ae^{B/L}$$

$$\eta\nu = Ae^{B/L'}$$

where η is the absolute viscosity, and v is the specific volume, both in cgs units; A and B are the same constants in the two equations. The numerical value of A is 5×10^{-4} and that of B is $1000 \log_e 20$.

Figure 2 shows the relation between the kinematic liquidity L' , and the kinematic viscosity ηv . The relation between kinematic liquidity and temperature for some representative compass liquids is shown in figure 3.

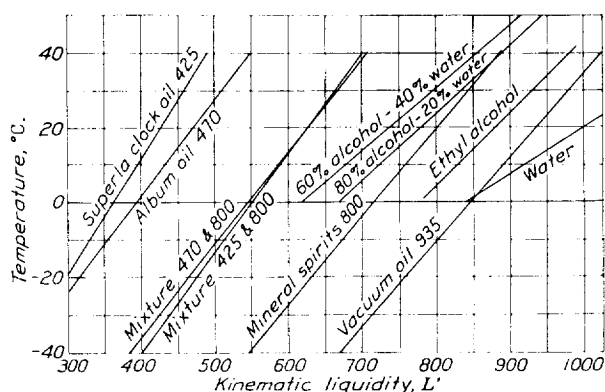


FIGURE 3.—Temperature-liquidity curves for compass damping liquids.

It has been found that Cragoe's equation for mixtures is directly applicable to mixtures of mineral oils used as compass damping liquids.

$$L'm = xL'_1 + (1-x)L'_2$$

$L'm$ = the kinematic liquidity of the mixture.

L'_1 and L'_2 = the kinematic liquidities of the component liquids.

x = the fraction by weight of component No. 1.

The rule does not, however, apply to mixtures of alcohol and water as will be seen by reference to the curves for these liquids in figure 3. The viscosity data on alcohol and water have been taken from Bingham and Jackson (reference 7).

Figure 4 shows that except for the alcohol-water mixtures, which also showed an anomalous behavior in figure 3, the density is a single-valued function of the liquidity for all the liquids considered. In other words, the density of the damping liquid varies with the liquidity, independent of the particular mineral oil used. For example, if the liquidity of vacuum oil at -15°C ., is equal to the liquidity of mineral spirits at 15°C ., the densities are also approximately equal.

The data at 16°C . shown in figure 4 were obtained by actual measurement of the density and liquidity of damping liquids. The densities at -15°C . and 40°C . were extrapolated on the basis of the value at 16°C .

from the National Standard Petroleum Oil Tables (reference 8). The liquidities for these temperatures were obtained from figure 3.

EFFECT OF TEMPERATURE AND LIQUIDITY

The variation in the characteristics of some representative compasses with temperature and liquidity of the damping fluid are shown in figures 5 to 21. The characteristics of time, overswing, and swirl are plotted against liquidity. The temperature-liquidity

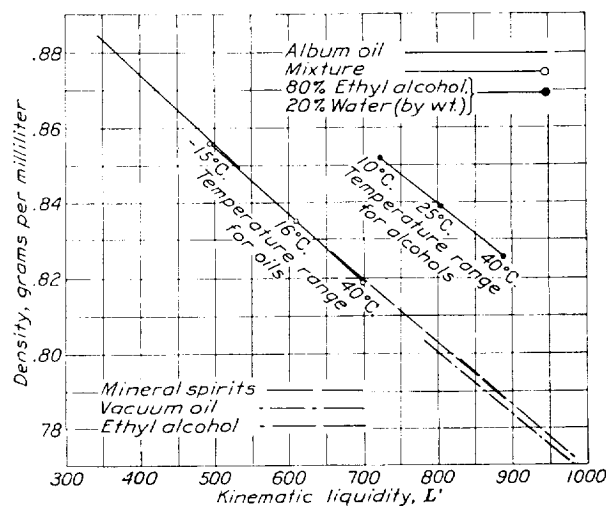


FIGURE 4.—Density liquidity curves for compass damping liquids.

relations for several liquids are shown by the several straight lines. To determine the characteristics of a compass at a given temperature, enter the chart at the temperature value on the right-hand scale, determine the liquidity for the liquid being used, and read the characteristics corresponding to this liquidity. The liquidity lines for the liquids commonly used in the compass are shown as solid lines.

The characteristics were usually determined for one compass, picked as representative of the type. When possible, five compasses were tested at room temperature with the original liquid and, on the basis of the data thus obtained, the average compass of the five was selected for complete tests. Another compass of the same type might have slightly different characteristics. The observed points are indicated on the curve sheets and the best smooth curves are drawn through the points.

Some specifications regarding the details of the compasses tested are given in table I. The values omitted were not available to the authors.

The Navy Department now uses or in the past has used as damping liquids, mineral oils of four different

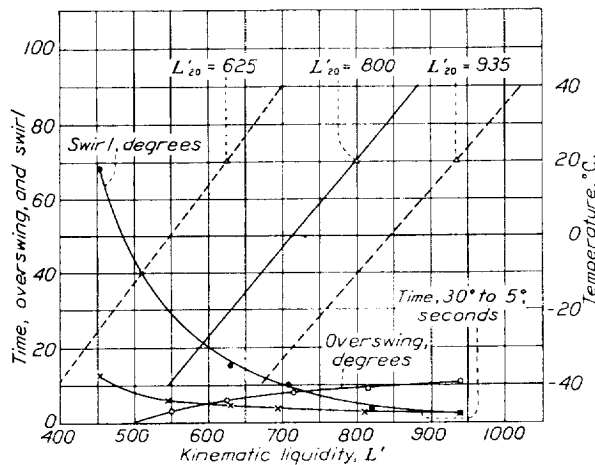


FIGURE 5.—Characteristics of United States Navy NSII aircraft compass.

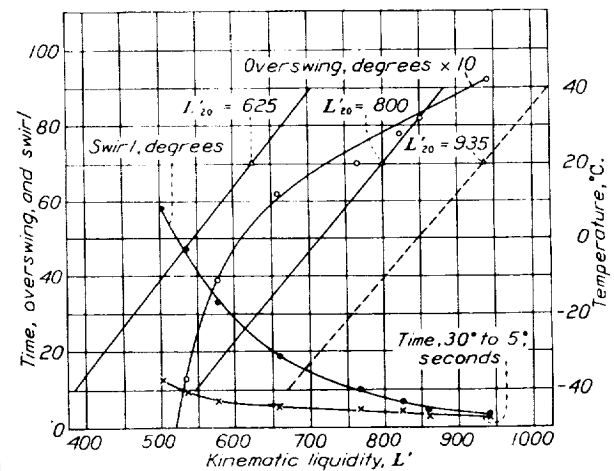


FIGURE 8.—Characteristics of United States Navy VB and VC aircraft compasses

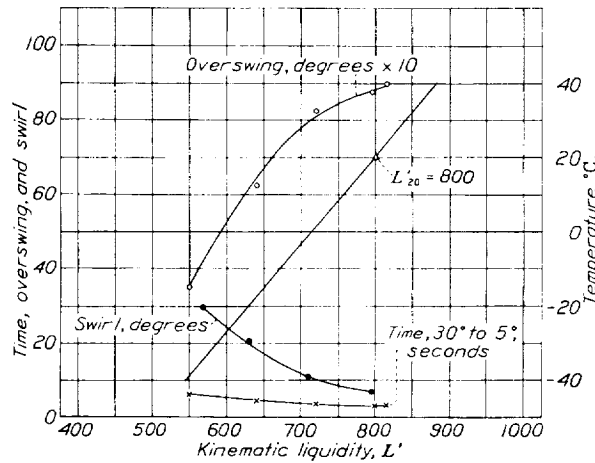


FIGURE 6.—Characteristics of United States Navy IV aircraft compass.

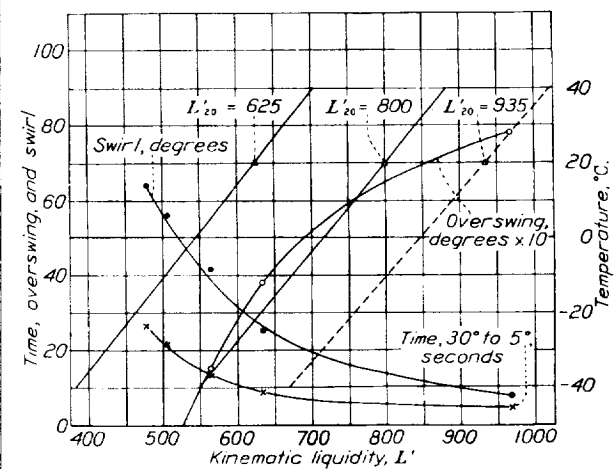


FIGURE 9.—Characteristics of United States Navy VI and VIA aircraft compasses

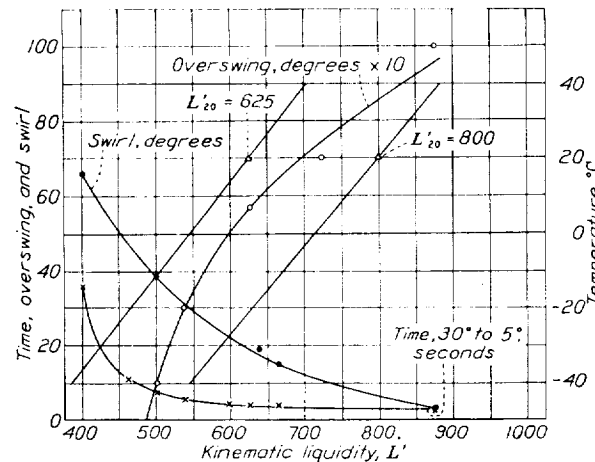


FIGURE 7.—Characteristics of United States Navy V and VA aircraft compasses.

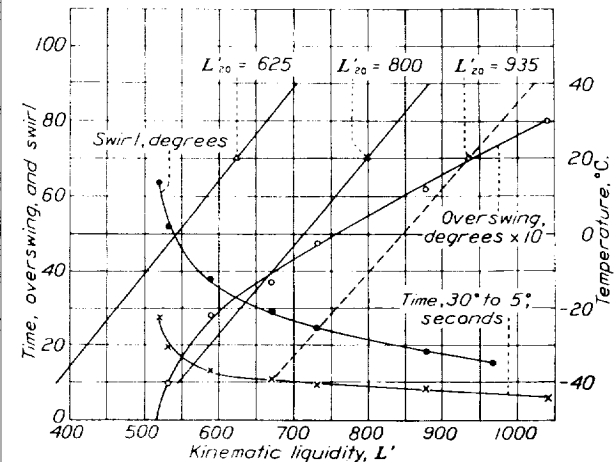


FIGURE 10.—Characteristics of United States Navy VIB aircraft compass.

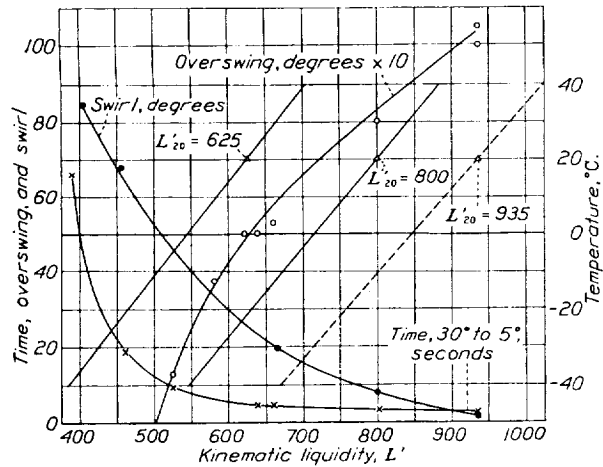


FIGURE 11.—Characteristics of United States Navy VII and VIIA aircraft compasses.

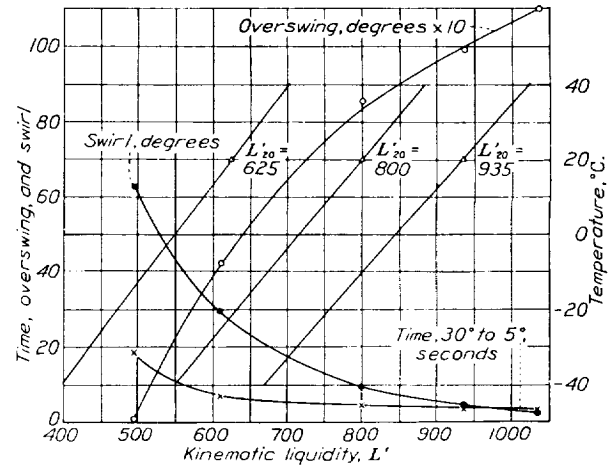


FIGURE 14.—Characteristics of United States Navy IX aircraft compass.

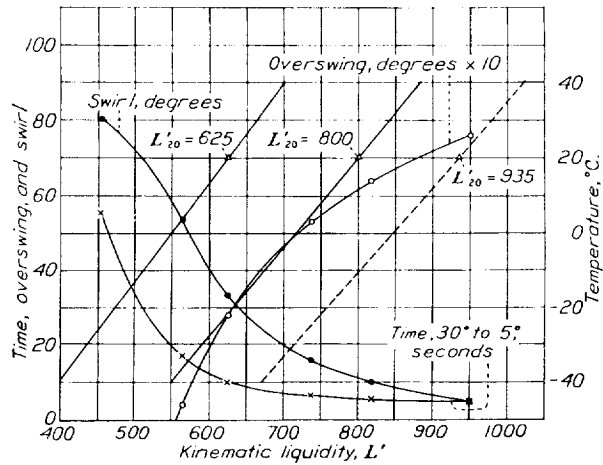


FIGURE 12.—Characteristics of United States Navy VIIIB aircraft compass.

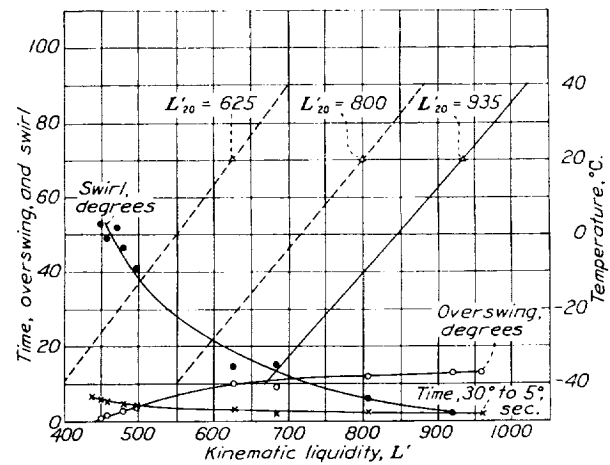


FIGURE 15.—Characteristics of United States Army B8 aircraft compass.

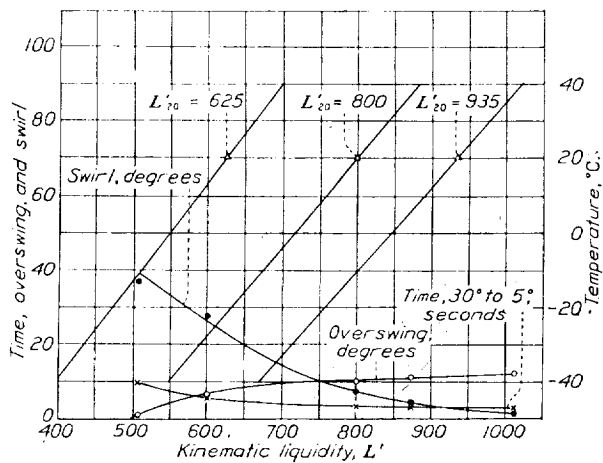


FIGURE 13.—Characteristics of United States Navy VIII aircraft compass.

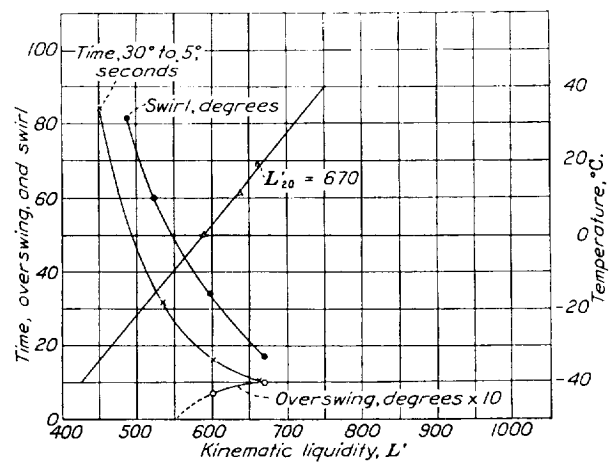


FIGURE 16.—Characteristics of United States Army D4 aircraft compass.

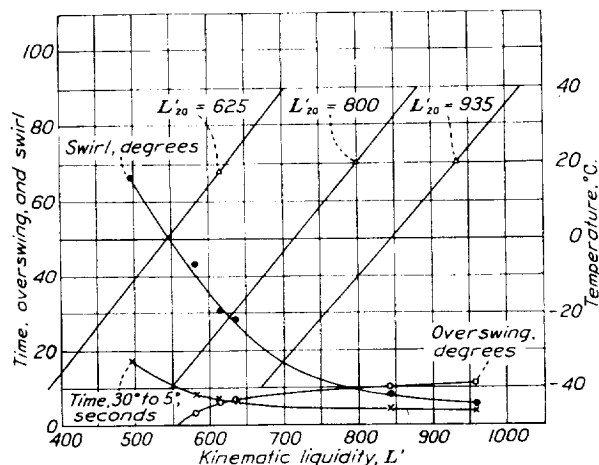


FIGURE 17.—Characteristics of KT58 aircraft compass.

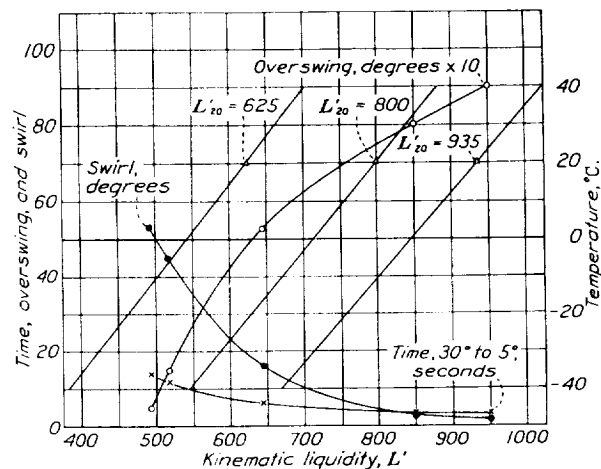


FIGURE 18.—Characteristics of KT65 aircraft compass.

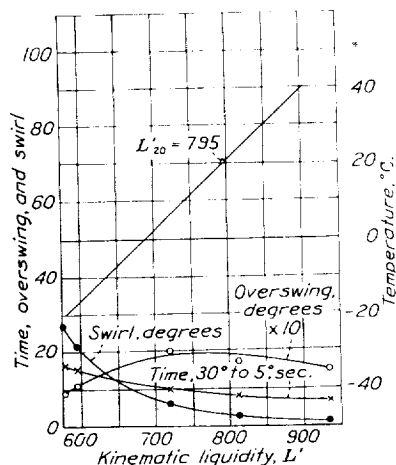


FIGURE 19.—Characteristics of British S. O. 2 aircraft compass.

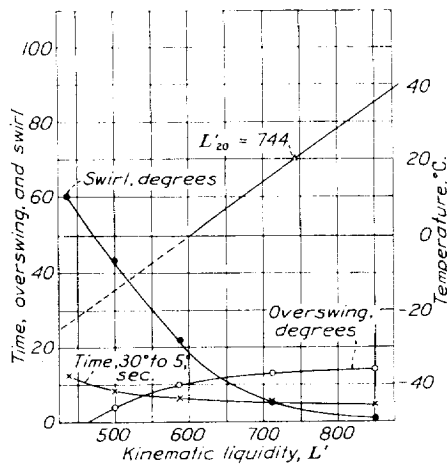


FIGURE 20.—Characteristics of Morel Petit model 28 aircraft compass.

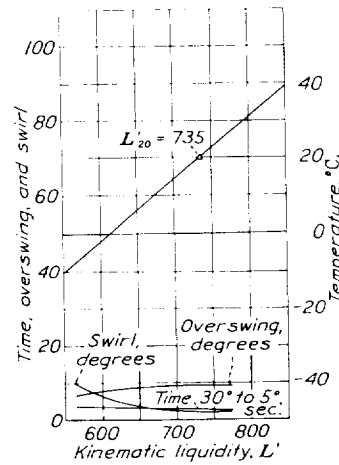


FIGURE 21.—Characteristics of Dobrie type 860 aircraft compass.

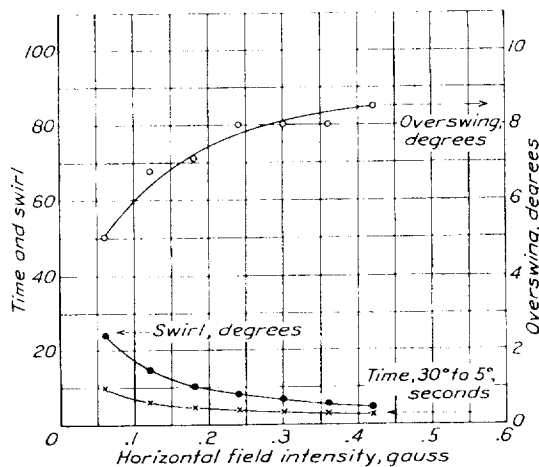


FIGURE 22.—Effect of magnetic field intensity on the characteristics of Navy VB aircraft compass at 20° C.

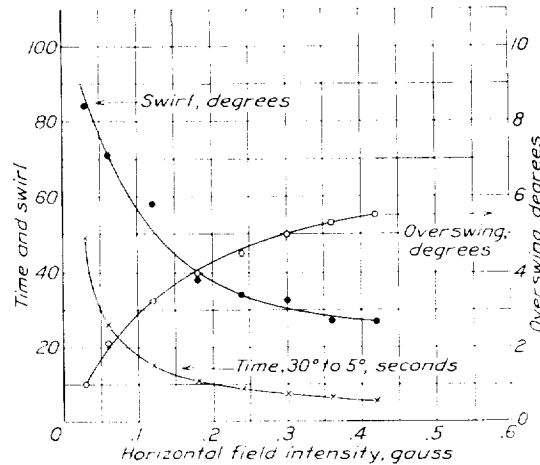


FIGURE 23.—Effect of magnetic field intensity on the characteristics of Navy V1B aircraft compass at 20° C.

liquidities, the trade names and liquidities of which are:

	Kinematic liquidity L' at 20° C.
Superla clock oil.....	430
Album oil.....	470
Mineral spirits.....	800
Vacuum oil.....	935

A liquid of any intermediate liquidity may be obtained by mixing two of these mineral oils in the proportions given by Cragoe's equation for mixtures. Although the foregoing figures are representative, the liquidities of individual samples have been found to vary as much as ± 5 percent.

compass without arresting the card was employed. In the method a magnetometer is used to measure the change in the strength of the magnetic field caused by the presence of the compass.

The magnetometer is a short piece of magnetized cobalt steel suspended from a phosphor bronze strip at the center of a coil of known dimensions. The magnetometer is set up so that the axis of the coil is horizontal and parallel to the magnetic meridian. A torsion is applied to the suspension to cause the magnet to take a position perpendicular to the magnetic meridian and perpendicular to the axis of the coil, which will be called the "zero" position. When

TABLE I
AIRCRAFT COMPASS SPECIFICATIONS

	U. S. Navy compasses										U. S. Army		KT (U. S.)		Foreign		
	NSII	IV	V	VB	VI	VIB	VII	VIIIB	VIII	IX	B8	D4	58	65	A	B	C
Number of magnets.....	2	2	2	2	2	2	2	2	2	2	2	2	2	2	4		
Diameter of magnets, inches.....	$\frac{3}{32}$	$\frac{3}{32}$	$\frac{1}{8}$	$\frac{3}{32}$	$\frac{3}{32}$	$\frac{3}{32}$	$\frac{1}{4}$	$\frac{3}{32}$	$\frac{1}{4}$	$\frac{1}{4}$	$\frac{3}{32}$	$\frac{1}{4}$	$\frac{3}{32}$	$\frac{1}{4}$			
Length of magnets, inches.....	2	$1\frac{1}{8}$	$1\frac{1}{2}$	$1\frac{1}{4}$	$1\frac{1}{4}$	$1\frac{1}{4}$	$1\frac{1}{4}$	$1\frac{1}{4}$	$1\frac{1}{4}$	$1\frac{1}{4}$	$1\frac{1}{4}$	$1\frac{1}{4}$	$1\frac{1}{4}$	$1\frac{1}{4}$			
Magnetic moment, cgs units.....	240	216	308	80	240	116	308	91	160	320	176	43	80	256	60	400	352
Card diameter, inches.....			$2\frac{1}{4}$	$2\frac{1}{4}$	4	4	3	3	$2\frac{1}{2}$	$3\frac{1}{4}$	$1\frac{3}{4}$			$3\frac{1}{4}$		$3\frac{1}{4}$	
Card weight in air, grams.....	7.4	7.2	8.4	5.4	7.8	6.4	8.4	5.8	12.5	17.2	8.2	2.9					
Period in air, seconds.....				8.2		11.4		8.4									
Card weight in liquid, grams.....				4.3		5.1		4.7	1.0	1.5							3
Float.....	No	No	No	No	No	No	No	No	Yes	Yes	No	No	Yes	Yes	No	Yes	Yes
Damping liquid.....	M	M	M	M	M	M	M	M	M	M	M	M	M	M	N	O	P
Liquidity at 20° C.....	800	800	625	(625) (800)	625	(625) (800)	625	(625) (800)	800	935	935	670	625	800	795	740	735

A. Type S. O. 2 (large) compass (British).
B. Morel Petit model 28 compass (French).
C. Debie type 860 compass (French).
M. Mineral oil.
N. 86 percent ethyl alcohol (by weight).
O. 31 percent ethyl alcohol (by weight).
P. 60 percent ethyl alcohol (by weight).

The Navy IV compass is filled with the liquid for which L' is 800. The Navy V, VI, and VII compasses were originally filled with a mixture of 47 percent mineral spirits and 53 percent album oil, the kinematic liquidity L' of the mixture being 625 at 20° C. (See fig. 3.) Navy V, VI, and VII compasses now in stock are being refilled with mineral spirits for which L' is 800 at 20° C. The VIII and IX compasses have damping liquids the kinematic liquidities of which are 800 and 935, respectively.

MAGNETIC FIELD STRENGTH

The standard horizontal magnetic field strength at which the time of swing, overswing, and swirl were measured, was 0.18 gauss, which is an average value for the United States. In order to give an idea of the variation in characteristics to be expected from variation in horizontal field strength, two representative compasses were tested at field strengths between 0.06 and 0.42 gauss. The characteristics of the two compasses for this range of field strength are shown in figures 22 and 23.

MAGNETIC MOMENT

A modification of the method described by Sanford (reference 9) for measuring the magnetic moment of a

making a measurement, the compass is brought to a definite position on the axis of the coil, causing a deflection of the magnetometer. The electric current in the coil necessary to restore the deflection to zero is determined. From this current, the dimensions of the coil, and the distance of the compass from the magnetometer, the moment of the magnetic system of the compass is calculated. Since the change in field strength due to the compass magnets is a very small percentage of the total field strength, it is essential that this measurement be made at a location where the field will be undisturbed.

The magnetic moment for each type of compass, as derived by this procedure, is given in table I.

FLIGHT TESTS

In Navy practice there are two distinct uses of a compass. It may be used as a steering indicator, the pilot steering the airplane according to its indications. It may be used as a checking compass to check occasionally the course of an airplane that is being steered on a straight course according to the indications of a directional gyro.

In an attempt to compare compasses of different characteristics in flight, a series of tests were made on compasses in pairs. As representative of the results

obtained in this series of tests a part of the comparative tests on Navy IV and VIB compasses are shown in figures 24 and 25. In the steering tests the pilot steered by the compass and an observer took about 30 readings per minute on a directional gyro. In the checking tests, the pilot steered by the directional gyro and an observer took readings on the compass.

Each compass was tested on north and on south courses, both as a steering compass and as a checking compass. As a steering compass, the performance is worse on a north course because of the northerly turning error. When an airplane turns from a north course, the centrifugal acceleration of the turn causes the compass card to tilt out of the horizontal position into such a position that the earth's vertical magnetic field will cause the card to deflect in the direction in which the airplane has turned. It is easily possible for the card of any unstabilized compass to turn faster than the airplane, indicating to the pilot a turn in the

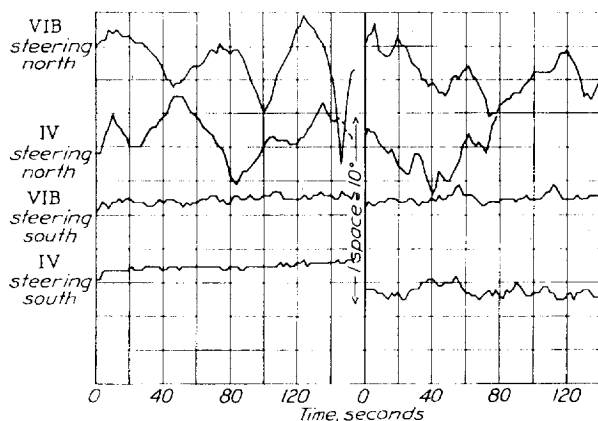


FIGURE 24.—Flight tests of steering compasses.

opposite direction. At the magnetic equator there is no northerly turning error and south of the magnetic equator the southerly turning error becomes troublesome.

The results of these tests are shown in table II. The values given are the average deviations of the readings from a straight line faired between the plotted points. Comparisons should be made only between two compasses of the same pair, because another pair may have been tested at another time when the air may have been rougher or smoother. It is assumed that the air conditions remained constant during the time required to test one pair.

Although definite conclusions should not be drawn from the results of the few tests presented here, there is a strong indication that the short-period compass is better for steering and the long-period compass with a low overswing is better for checking. It is the belief of the authors that the yawing oscillations of an airplane being steered according to the indications of a

compass may vary greatly with different pilots. Practically all of the flight data of this report were obtained by the junior author and by Ira E. Hobbs, lieutenant, United States Navy. It is very desirable that flight tests be continued with other compasses, other pilots, and automatic pilots. Probably also, photographic methods of recording the instrument readings should be utilized.

The results of these flight tests can be explained on the basis of the difference in the periods of the compass and the yawing of the airplane. An airplane steering on a north course, according to the indications of a compass, oscillates with a period longer than the period of the compass, while an airplane steered according to the indications of the relatively stable directional gyro oscillates with a period shorter than the periods of the compasses in this group. The curves of figure 24 show clearly that the period of the yawing oscillation of the airplane steered according to the indication of a compass on a north course is much longer than the period of the compass by which it is being steered (approx-

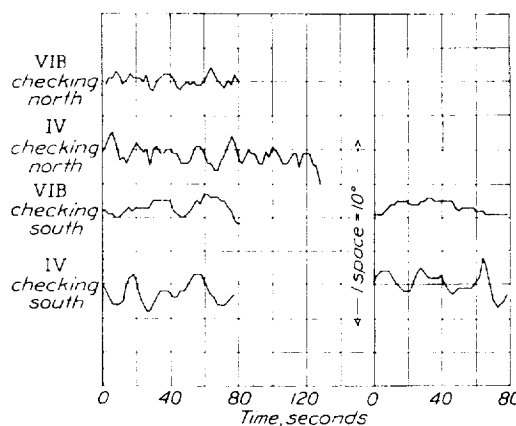


FIGURE 25.—Flight tests of checking compasses.

mate periods, airplane, 60 seconds; compass IV, 19 seconds; compass VIB, 30 seconds).

TABLE II
RESULTS OF FLIGHT TESTS ON COMPASSES

Compass	Time, 30° to 5°	Over-swing	Swirl	Steering error		Checking error	
				North	South	North	South
VIB.....	Seconds	Degrees	Degrees	Degrees	Degrees	Degrees	Degrees
V.....	11.6	3.5	29	4.1	-----	1.5	-----
	14.0	1.5	45	7.0	-----	1.3	-----
IV.....	4.8	6.2	10	3.0	1.1	3.7	-----
V.....	14.0	1.5	45	6.8	1.1	1.7	-----
IV.....	5.0	6.0	11	4.6	1.1	2.0	2.5
VIB.....	8.0	6.5	14	5.3	1.2	1.4	1.7
VIB.....	8.0	6.5	14	5.3	.9	1.1	3.1
VIB.....	12.0	3.5	31	6.8	1.3	1.2	1.2
IV.....	3.2	8.5	8.2	2.8	2.1	1.8	3.3
S. O. 2.....	9.2	2.0	5.0	3.1	2.4	2.1	5.8

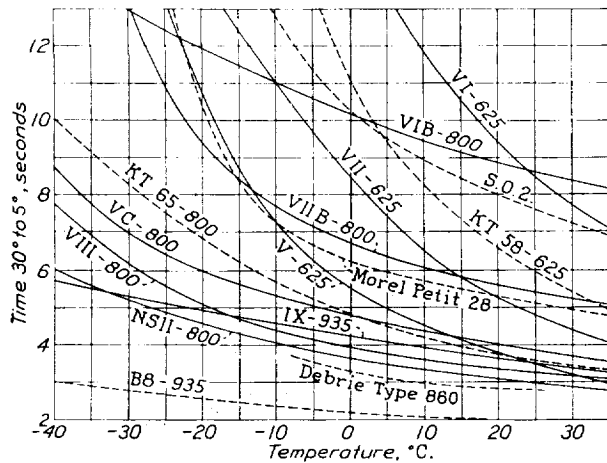


FIGURE 26.—Summary chart, time of swing against temperature.

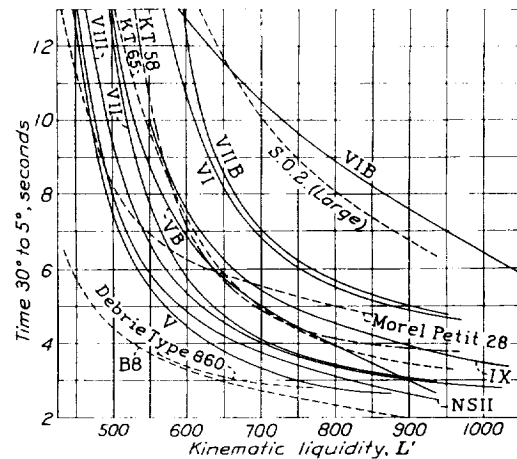


FIGURE 29.—Summary chart, time of swing against liquidity.

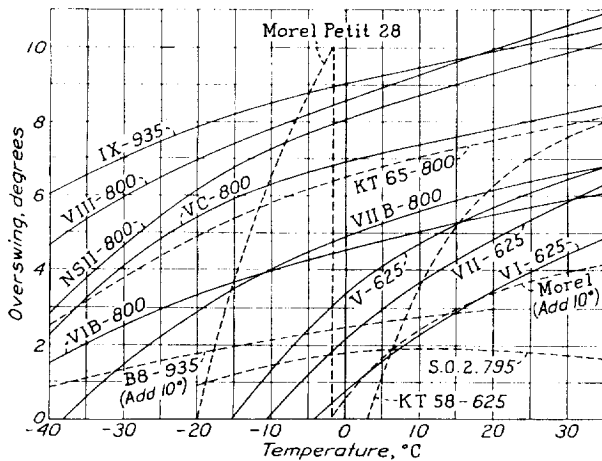


FIGURE 27.—Summary chart, overswing against temperature

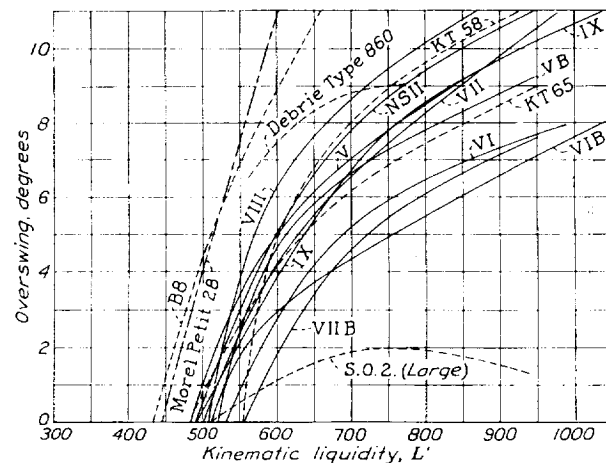


FIGURE 30.—Summary chart, overswing against liquidity.

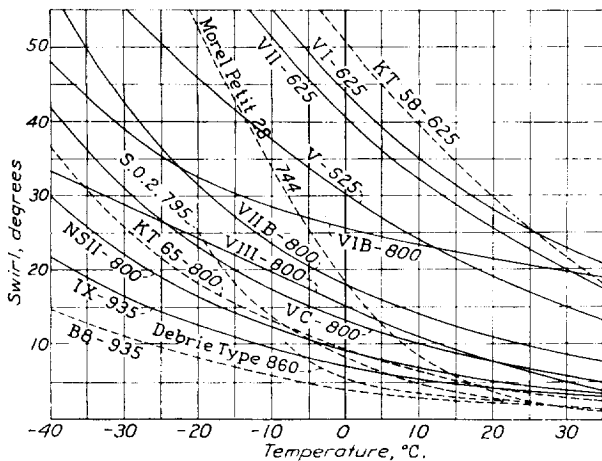


FIGURE 28.—Summary chart, swirl against temperature.

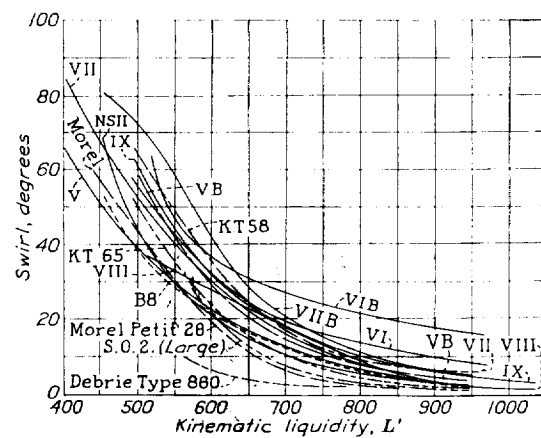


FIGURE 31.—Summary chart, swirl against liquidity.

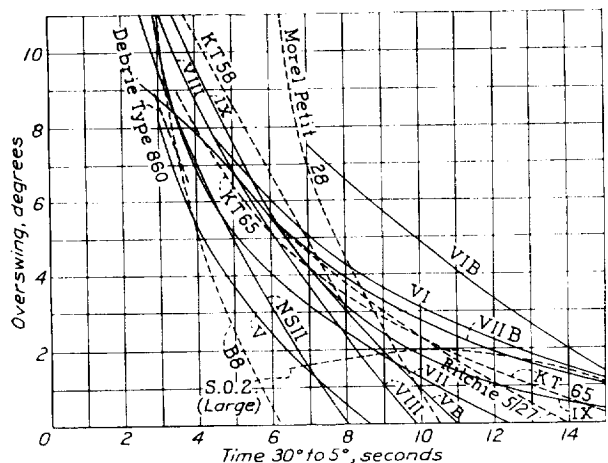


FIGURE 32.—Summary chart, overswing against time of swing.

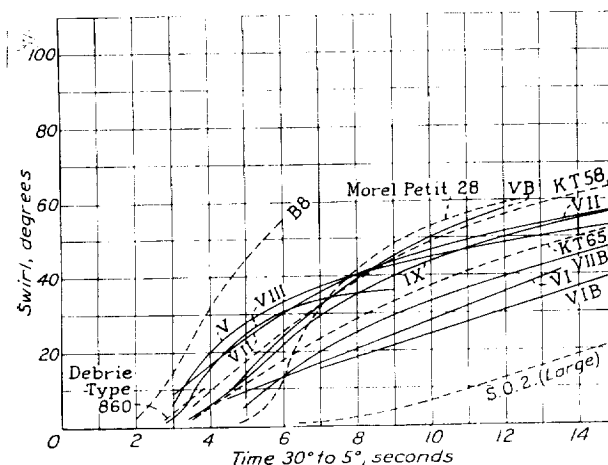


FIGURE 33.—Summary chart, swirl against time of swing

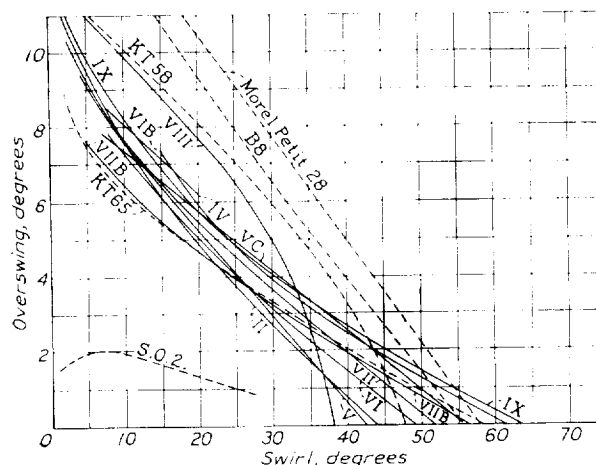


FIGURE 34.—Summary chart, overswing against swirl.

DISCUSSION

The curves for time of swing, overswing, and swirl shown in figures 5 to 21, for the individual compasses are summarized from various points of view in figures 26 to 34. Figures 26, 27, and 28 show the variations of time of swing, overswing, and swirl with temperature. Figures 29, 30, and 31 show the variations of the same quantities with liquidity. Figures 32, 33, and 34 show the variations of time of swing, overswing, and swirl, one relative to the other. The variations in the characteristics were obtained by varying the liquidity of the damping liquid.

It is very probable that low time of swing, low overswing, and low swirl are desirable characteristics for good performance in flight. These requirements are not simple to meet because low overswing and low swirl are conflicting requirements as may be seen in figure 34. Low overswing may be obtained by the use of weak magnets and a viscous damping liquid but their use causes a long time of swing and a high swirl. A low swirl and a short time of swing may be obtained by the use of strong magnets and a thin damping liquid of low viscosity but a high overswing is thereby produced.

Opposite extremes of performance are shown in figures 32, 33, and 34 by the British S. O. 2. compass and the French Morel Petit model 28 compass. The low overswing and low swirl of the S. O. 2. compass are obtained by the use of an extremely light and relatively fragile magnetic card. It has been the experience of the authors that this instrument is too fragile for service use. The magnetic moment is so low that the pivot must be in perfect condition if excessive friction is to be avoided. On the other extreme, the Morel compass has a very heavy floated card and a high magnetic moment. Practically all American compasses have characteristics between the British and French extremes. Of the American compasses in this report, only the Navy VIII and IX and the two KT compasses have cards with floats.

The curves of figures 32, 33, and 34 are an aid in the selection of compasses for flight tests. As an example of the use of these curves it will be seen that by a suitable choice of damping liquids the Army B8 and Navy VIB compasses may be given any of the following characteristics at any selected temperature of the compass.

The chief reason for the difference in characteristics of the B8 and the VIB is the difference in size of the card. The B8 card has a diameter of $1\frac{1}{8}$ inches and the VIB card has a diameter of 4 inches. The clearance

between the bowl and the card is approximately the same for both compasses.

TABLE III

Compass	Time 30° to 5°	Over- swing	Swirl
	<i>Seconds</i>	<i>Degrees</i>	<i>Degrees</i>
B8.....	6.0	0.4	55
VIB.....	6.0	8.5	12
B8.....	4.0	5.0	36
VIB.....	9.8	5.0	24
B8.....	3.9	6.0	30
VIB.....	11.8	3.9	30

NATIONAL BUREAU OF STANDARDS,
WASHINGTON, D. C., December 14, 1935.

REFERENCES

1. Stewart, C. J.: Aircraft Instruments. Chapman & Hall, Ltd. (London), 1930.
2. Field, M. B.: The Navigational Magnetic Compass Considered as an Instrument of Precision. Inst. Elec. Eng. Jour., May 1919, pp. 349-386.
3. Capon, R. S., and Lee, A.: Preliminary Report on the Forced Oscillations of Aircraft Compasses. R. & M. No. 874, British A. R. C., 1920.
4. Wimperis, H. E., and Rowe, A. P.: Some Characteristics of Aircraft Compasses. R. & M. No. 735, British A. R. C., 1921.
5. Rowe, A. P.: The Northerly Turning Error of Compasses in Aircraft. R. & M. No. 875, British A. R. C., 1921.
6. Cragoe, C. S.: Changes in the Viscosity of Liquids with Temperature, Pressure and Composition. World Petroleum Congress Proc., vol. II (London), 1933, p. 529.
7. Bingham, E. C., and Jackson, R. F.: Standard Substances for the Calibration of Viscometers. Scientific Paper 298, vol. 14, no. 1, Bur. Standards, 1917, p. 76.
8. National Bureau of Standards: National Standard Petroleum Oil Tables. Circular No. 154, Bur. Standards, 1924.
9. Sanford, R. L.: Testing of Magnetic Compasses. Scientific Paper No. 382, Bur. Standards, 1920.

REPORT No. 552

WIND-TUNNEL TESTS OF 10-FOOT-DIAMETER AUTOGIRO ROTORS

By JOHN B. WHEATLEY and CARLTON BIOLETTI

SUMMARY

A series of 10-foot-diameter autogiro rotor models were tested in the N. A. C. A. 20-foot wind tunnel. Four of the models differed only in the airfoil sections of the blades, the sections used being the N. A. C. A. 0012, 0018, 4412, and 4418. Three additional models employing the N. A. C. A. 0012 section were tested, in which a varying portion of the blade near the hub was replaced by a streamline tube with a chord of about one-fourth the blade chord.

With maximum L/D used as a criterion, the order of merit of the airfoil sections tested is: N. A. C. A. 4412, 0012, 4418, and 0018. The elimination of blade area near the hub was found to have a detrimental effect on the rotor L/D . The results indicate the possibility of obtaining further improvements in the L/D by using thinner airfoil sections and by employing tapered blades with a tip chord smaller than the root chord. The results also demonstrate the necessity for a study of the effect of blade twist on the rotor characteristics and show the advisability of improving testing technique to reduce the errors occurring in the determination of the tare drag.

INTRODUCTION

The high-speed performance of the autogiro is at present inferior to that of the airplane, although no inherent reason for the existing large difference has appeared. The N. A. C. A. has accordingly decided to investigate different types of autogiro rotors with the purpose of establishing a means of improving the efficiency (the lift-drag ratio) of the rotor.

The results given in this paper were obtained by a wind-tunnel investigation of 10-foot-diameter model rotors in which the influence on rotor characteristics of the blade airfoil section and a variation in the blade plan form were determined. Four airfoil sections differing in camber and thickness and four plan forms were tested; the aerodynamic characteristics of each rotor were determined at several pitch settings over the entire range of tip-speed ratios in which the rotors would autorotate.

APPARATUS

The model rotors were tested in the N. A. C. A. 20-foot wind tunnel described in reference 1. The test set-up is shown in figure 1, which shows that the rotor was supported by a small mast projecting from a large fairing. The entire supporting structure, with the exception of the mast and part of the sting and tailpost also shown in figure 1, was shielded from the air stream to reduce the tare drag. The mast was attached to an electric motor enclosed in the shielding; the motor employed to start the model rotating was mounted in trunnion bearings to permit a change in the rotor angle of attack by means of the sting and tailpost. The rotors were mounted inverted so that at 90° angle of attack the rotor was upstream from the bulky supporting structure. A magneto tachometer geared to the rotor shaft measured the rotor speed.

The model rotor hub used for all rotor tests had journal bearings at the horizontal and vertical pin articulations; the use of these bearings made it necessary that the hub be considerably larger in proportion than a full-scale hub. The horizontal pin was placed at a radius of 1.125 inches (1.88 percent R) and the radius of the vertical pin was 2.50 inches (4.17 percent R). Damping was supplied at the vertical pins by means of adjustable washers, which provided a friction torque of about 6 inch-pounds. The rotor blades were attached to the hub by steel forks bolted to the blades and screwed into sockets connected to the vertical pins. Pitch adjustments were made at these screw connections, which were locked by clamping bolts. The blade butts were at $7\frac{1}{2}$ -inch radii (12.5 percent R) and the outer ends of the forks at 12-inch radii (20 percent R).

All seven rotors had diameters of 10 feet and consisted of three blades, which were constructed of laminated mahogany, hollowed to reduce their weight, balanced about the quarter-chord point by brass nosepieces forming part of the airfoil section. Four sets of blades differed only in the airfoil section used; the sections tested were the N. A. C. A. 0012, 0018,

4412, and 4418. These rotors are designated A (N. A. C. A. 0012), A (N. A. C. A. 4418), etc., where A indicates the plan form. Three additional sets of blades employing the N. A. C. A. 0012 profile were constructed in which a systematic variation of plan form was effected; these rotors are designated B

axes of $0.25c$ and $0.75c$. The physical characteristics of the blades are shown in table 1; the ordinates of the airfoil sections are given in reference 2.

The motion of the rotor blade about the horizontal pin was recorded throughout several revolutions by a stylus scratching on waxed paper. The stylus was



FIGURE 1.—A 10-foot autogiro rotor mounted for test.

(N. A. C. A. 0012), C (N. A. C. A. 0012), and D (N. A. C. A. 0012). Rotors B, C, and D differed in that the inner 30 percent, 45 percent, and 60 percent, respectively, of the blade was replaced by a $1\frac{1}{4}$ -inch-diameter streamline tube having a chord of about one-fourth the blade chord, as shown in figure 2. The tip shape of all blades was semielliptical; the trailing edge was a circular quadrant with a radius of $0.75c$, and the leading edge was an elliptical quadrant with

linked to the blade so that the deflections of the stylus and blade were proportional, and the waxed paper was wound on a drum concentric with the rotor axis immediately beneath the rotor disk. The record was oriented in azimuth by a prick punch fixed with reference to the air stream. Successive records were obtained by winding the paper on spools within the drum; the spools were manually operated from the balance house.

TESTS AND PROCEDURE

Each rotor was tested at several pitch settings from 0° to the highest angle at which autorotation could be obtained over a reasonably wide range of tip-speed ratios. Pitch settings were measured from the angle of zero lift of the blade section using the data given in reference 2. The test data are incomplete in some cases at low tip-speed ratios and low pitch settings because at the lowest tunnel speed available (40 feet per second) the rotor speed became dangerously high. In general, the range of tip-speed ratios tested became smaller as the pitch setting was increased because autorotation broke down at successively lower values of the tip-speed ratio. No tests were made of the B (N. A. C. A. 0012) rotor at tip-speed ratios below 0.1 because the model vibrated violently in that range.

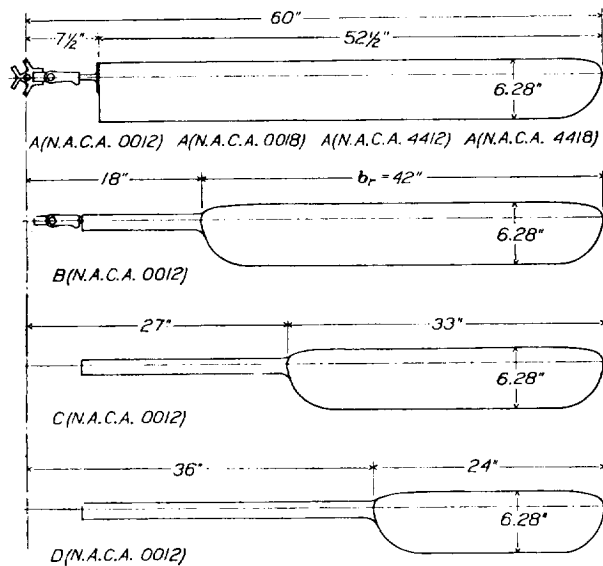


FIGURE 2.—Plan forms of model autogiro blades.

At the beginning of a test the rotor was driven at about 400 revolutions per minute with the electric motor. The tunnel fan was then started and the model was allowed to autorotate. In general, all tests were made at a rotor speed of 550 revolutions per minute, giving a tip speed of 288 feet per second. Data were obtained at each tunnel speed between 40 feet per second and 140 feet per second by adjusting the angle of attack. When the tunnel speed reached 140 feet per second, which corresponds to a tip-speed ratio of about 0.5 for a rotor speed of 550 revolutions per minute, it was kept constant and tip-speed ratios greater than 0.5 were obtained by successive reductions in the rotor speed. In this manner, except for the limitations previously mentioned, all tip-speed ratios from 0 to 0.7, corresponding to angles of attack from 90° to the minimum obtainable, were investigated.

At any tunnel speed, when steady conditions had been obtained, simultaneous visual observations of

lift, drag, dynamic pressure, rotor speed, and angle of attack were made. Records of blade motion were obtained during the tests at intervals of the tip-speed ratio of about 0.03.

The tare forces on the set-up were determined with the rotor and hub removed over the same range of air speeds as that in which the rotor tests were made. There was an appreciable scale effect on the tare forces so that the coefficients of tare lift and drag used for correcting the observed data corresponded to the particular air speed at which the observed data were obtained. The method used for obtaining the tare forces results in the inclusion of the hub forces in the net lift and drag forces.

RESULTS

The terminology and symbols used in this paper are the same as those given in reference 3. For convenience, a list of the symbols and definitions follows:

- V , true air speed, ft. per second.
 Ω , angular velocity, radians per second.
 R , rotor radius, ft.
 α , rotor angle of attack, deg. (acute angle between relative wind and a plane perpendicular to the rotor axis).
 L , rotor lift, lb.
 D , rotor drag, lb.
 T , rotor thrust, lb. (component of rotor force parallel to rotor axis).
 θ , pitch setting, deg. (blade angle measured from zero lift position when blade is at rest).

$$C_L, \text{ lift coefficient, } \frac{L}{\frac{1}{2}\rho V^2 \pi R^2}$$

$$C_D, \text{ drag coefficient, } \frac{D}{\frac{1}{2}\rho V^2 \pi R^2}$$

$$C_R, \text{ resultant-force coefficient, } (C_L^2 + C_D^2)^{1/2}$$

$$C_T, \text{ thrust coefficient, } \frac{T}{\rho \Omega^2 \pi R^4}$$

$$\mu, \text{ tip-speed ratio, } \frac{V \cos \alpha}{\Omega R}$$

$$\psi, \text{ blade azimuth angle from down wind in direction of rotation, deg.}$$

$$\beta, \text{ angle between blade axis and a plane perpendicular to rotor axis, deg. (positive in the direction of thrust), expressed by: } \beta = a_0 - a_1 \cos \psi - b_1 \sin \psi - a_2 \cos 2\psi - b_2 \sin 2\psi - \dots$$

$$a_0, \text{ constant term in Fourier series that expresses } \beta.$$

$$a_n, \text{ coefficient of } \cos n\psi \text{ in Fourier series that expresses } \beta.$$

$$b_n, \text{ coefficient of } \sin n\psi \text{ in Fourier series that expresses } \beta.$$

$$\sigma, \text{ solidity, ratio of blade area to swept disk area.}$$

$$I_1, \text{ moment of inertia of one blade about the horizontal pin, slug-ft.}^2$$

$$c, \text{ chord of blade, ft.}$$

$$a, \text{ lift-curve slope with angle of attack, in radian measure.}$$

$$\gamma, \text{ mass constant of blade, } \frac{c \rho a R^4}{I_1}$$

The results of the force measurements corrected for tare and jet-boundary interference are presented in figures 3 to 40, inclusive. For each rotor, values of C_L , L/D , C_R , C_T , α , and the blade-motion coefficients a_0 , a_1 , and b_1 are presented in curve form for each pitch setting tested, as functions of the tip-speed ratio μ . The coefficients C_L , L/D , and C_R for the A (N. A. C. A. 4412) and A (N. A. C. A. 4418) rotors were cross-faired against the pitch setting and then replotted against tip-speed ratio, a procedure made possible in these cases by the large number of pitch settings tested. It will be noted that L/D has been given in preference to the drag coefficient C_D ; this usage was found advisable because the minimum and maximum values of C_D were in the ratio of approximately 1:150 and an abnormal scale would have been required to present the results accurately.

The measured blade motion was transformed into the coefficients of a Fourier series by the 12-point harmonic analysis described in reference 4, resulting in a series of 12 terms. The blade motion of a full-scale rotor is such that the coefficients a_2 and b_2 are not negligible in comparison with a_0 , a_1 , and b_1 . The mass constant γ of the model blades was so small, however, that all coefficients of order greater than the first were found to be equal to or smaller than the probable error in the results and, for this reason, no coefficients of higher order than the first have been included in the blade-motion data.

Figure 23 shows the effect of a variation in blade plan form on the maximum L/D for optimum pitch setting and on C_T at $\mu=0.35$. Figure 40 illustrates the effect of airfoil section on the maximum L/D and on C_T at $\mu=0.35$ as functions of the pitch setting. Figure 41 shows the significant effect of a change in the rotor speed on C_L and L/D ; figure 42 shows the effect of rotor speed on a_1 .

No test data on moments or centers of pressure were obtained; the geometry of the balance system rendered such results too inaccurate to be of value.

ACCURACY

The accidental errors occurring in these tests arise from nonsimultaneous observations, the human error in reading instruments, the failure to obtain steady conditions when taking data, and similar factors. The influence of these types of error on the final results has been minimized by obtaining a large number of test points during all tests.

There are three principal sources of consistent errors in the final results: The jet-boundary effect, the blocking effect in the tunnel, and the errors due to the method of obtaining the tare drag. A correction for the effect of the jet boundary on the rotor was applied by assuming the rotor to be equivalent to an airfoil of the same span and same total lift. This correction is justified principally by expediency, since no information exists that can be used for the

accurate correction of the jet-boundary effect on a rotor. The use of this correction assumes a vortex field behind the rotor similar to the one behind the equivalent wing, an assumption obviously not exactly true. This error can, however, be considered small and especially so near maximum L/D , where the jet-boundary correction in all cases had almost vanished. The blocking effect, which is essentially a disturbance in the uniform velocity distribution across the jet by the presence of a body in the jet, has been estimated from disk tests to be as high as 20 percent for a disk normal to the air stream. Since this effect depends mostly upon the projected area of the body on a plane normal to the air stream, and upon the drag of the body, it can be neglected at angles of attack of less than 30° ($\mu > 0.125$). Thus the blocking effect does not influence the maximum L/D , which occurs at $\mu=0.35$. The tare lift was small and the error arising from it can be neglected, but the tare drag is the source of an error of unknown magnitude. The tare forces were determined by testing the set-up with the rotor and hub removed, which leaves the interference effects in the net results; in addition, the hub drag, which was, because of the size of the hub, considerably greater than that of a full-scale rotor, was included in the net drag. These considerations indicate that the net drags obtained are appreciably larger than the correct values.

The nature of the consistent errors precludes an attempt at their evaluation; the following table summarizes the magnitude of the errors in the faired curves caused by the accidental factors:

μ	± 3 percent.
α	$\pm 0.1^\circ$.
C_L	± 3 percent.
L/D	± 5 percent.
C_T	± 3 percent.
a_0, a_1, b_1	$\pm 0.2^\circ$.

DISCUSSION

Before the detailed discussion, it is advisable to consider the effect of an erroneous tare drag on the results. As previously explained, the tare drag used was probably smaller than the correct value because the model rotor hub was disproportionately large. The net drag coefficients used in obtaining rotor lift-drag ratios are consequently considered too large. A constant decrement to the experimental net drag coefficients would increase the L/D at low-pitch settings more than at high-pitch settings because the rotor forces and coefficients increase with pitch setting. By reference to the curves of C_L and L/D it can be determined that C_L for maximum L/D at optimum pitch setting lies between 0.085 and 0.120 and occurs at $\mu=0.35$ for all rotors, showing that there is no great difference in the rotor forces at optimum pitch setting and, consequently, that the relative merit of

the different rotors will not be changed by a small error in the tare drag. The only important change will be a decrease in the optimum pitch setting and an increase in the values of the lift-drag ratios obtained.

Most of the results require little discussion. On all rotors an increase in angle of pitch setting increases the lift coefficient at any tip-speed ratio greater than that corresponding to maximum lift, which occurs at about $\mu=0.13$, and increases the thrust coefficient and the blade-motion coefficients at all tip-speed ratios. The lift-drag curves show that for each rotor there is an optimum angle of pitch setting considerably lower than the highest pitch setting at which autorotation occurs.

The variation of angle of attack with pitch setting is reasonably consistent. At tip-speed ratios in the approximate range 0 to 0.15 the angle of attack increases with pitch setting for pitch settings greater than 2° ; at higher tip-speed ratios the angle of attack decreases with pitch setting until within 1° or 2° of the maximum pitch setting tested, at which point the angle of attack begins to increase.

A much greater range of operating pitch settings was obtained with the two cambered airfoils (N. A. C. A. 4412 and N. A. C. A. 4418) than with the two symmetrical ones (N. A. C. A. 0012 and N. A. C. A. 0018). The principal reason for this result is thought to be the twist of the blade during its operation. A twisting couple is applied to each blade if the normal component of the blade centrifugal force is not applied at the center of pressure of the air force. The centrifugal force is applied at the center of gravity of the blade, which is at $0.25c$ on all blades. The center of pressure of the symmetrical blades occurs also at $0.25c$; consequently, the twisting moment on the symmetrical blades is negligible. The cambered blades, however, have a center of pressure that changes with angle of attack and has a mean position at about $0.35c$. An upward force at $0.35c$ and an equal downward force at $0.25c$ obviously tend to decrease the blade pitch angle, which results in an operating pitch appreciably less than the pitch setting. This condition is illustrated in figure 40 by the difference in the thrust coefficients at equal pitch settings for the four airfoil sections used. The illustrated differences between the mean curve for the two symmetrical sections and the curves for the two cambered sections are then consistent with the explanation given when it is remembered that the N. A. C. A. 4418 is torsionally stiffer than the N. A. C. A. 4412 and that the N. A. C. A. 4418 and N. A. C. A. 4412 have almost identical center-of-pressure characteristics.

The preceding argument leads also to the conclusion that the twist, and consequently the rotor characteristics determined by the twist, will depend upon rotor speed because the centrifugal force and thrust vary with the square of the rotor speed, while the rigidity remains constant. This deduction is verified in figures 41 and 42, showing the A (N. A. C. A. 4412) rotor characteristics at 400 and 550 revolutions per minute. The lift coefficient L/D and the flapping coefficient a_1 at 7° pitch setting and 400 revolutions per minute correspond more closely to the characteristics for 8° than for 7° pitch setting when the test was made at 550 revolutions per minute. These curves show that at 400 revolutions per minute the operating pitch was greater than at 550 revolutions per minute although the pitch setting was the same.

The general information on maximum L/D is summarized in figures 23 and 40. Figure 40 shows that the order of merit of the airfoil sections based on maximum L/D is: N. A. C. A. 4412, 0012, 4418, and 0018, indicating that camber is advantageous and that a thickness of 18 percent is less efficient than one of 12 percent. Figure 23 shows that the maximum lift-drag ratio is affected adversely by reducing blade area near the hub. When quantitative conclusions are drawn from the results in this report, it is important to remember that the blade twist of the different airfoils was not constant; this factor may have influenced the relative L/D ratios of the rotors. It is therefore not known whether the increased efficiency of the cambered blades should be ascribed to the camber or the twist. The plan-form results also contain another variable, a change in solidity, which would affect the L/D ; in this case, however, calculations indicate that the decrease in solidity should increase the L/D , whereas the sum of the two effects was a decrease in L/D . It then seems safe to conclude that the effect of reducing the blade area near the hub is, if anything, more disadvantageous than the results indicate.

The test results indicate that rotor efficiency can possibly be increased by extending the tests of blade thickness and by a further investigation of the effect of twist. The employment of tapered blades with the maximum chord at the hub also appears promising. The L/D results in this paper are, however, of only relative value because of the error inherent in the tare-drag results, and these values of L/D are at present exceeded on full-scale rotors with less efficient airfoil sections.

CONCLUSIONS

1. Cambered rotor blades with a center of gravity at $0.25c$ are appreciably reduced in pitch while operating because of the dynamic twist.

2. Owing to the different airfoil characteristics and possibly because of the blade twist, cambered blades develop a greater L/D than symmetrical ones.

3. An increase in blade thickness ratio from 12 percent to 18 percent results in an appreciably lower L/D .

4. The order of merit based on maximum L/D of the airfoil sections tested is: N. A. C. A. 4412, 0012, 4418, 0018.

5. Test results are quantitatively reliable for $\mu > 0.15$ except for the L/D , which is probably lower than the correct value.

6. Rotor lift-drag ratios are adversely affected by removing blade area near the hub.

7. A possibility exists of improving the rotor lift-drag ratio by tapering the blade to a smaller chord at the tip than at the hub.

8. The tests should be extended to include other airfoil sections and tapered blades, and the effect of blade twist should be carefully studied.

LANGLEY MEMORIAL AERONAUTICAL LABORATORY,
NATIONAL ADVISORY COMMITTEE FOR AERONAUTICS,
LANGLEY FIELD, VA., October 10, 1935.

TABLE I.—BLADE CHARACTERISTICS

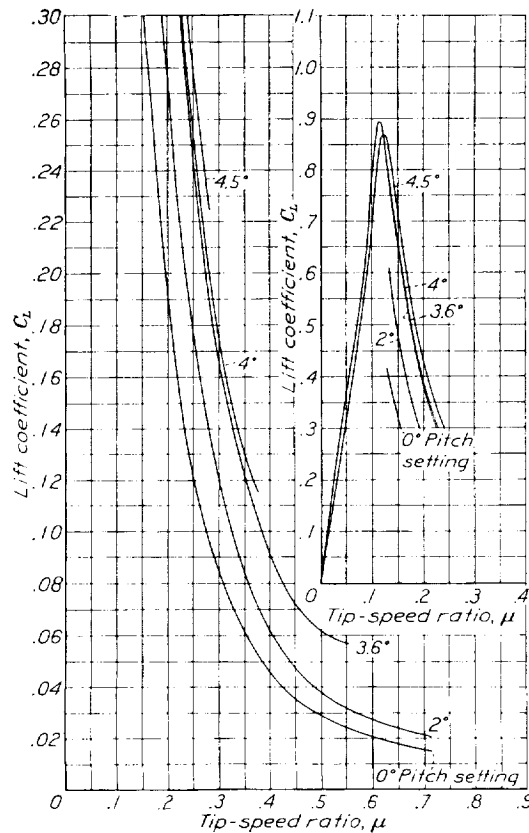
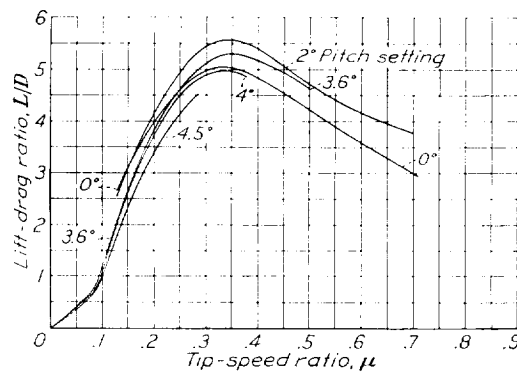
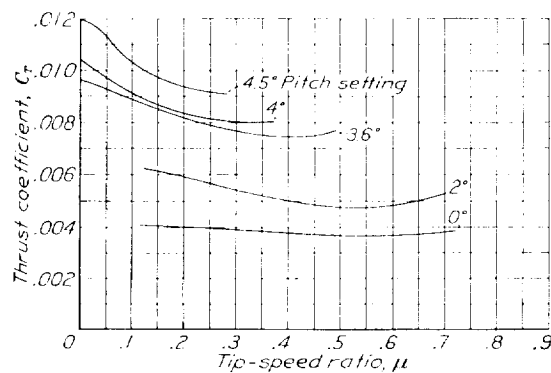
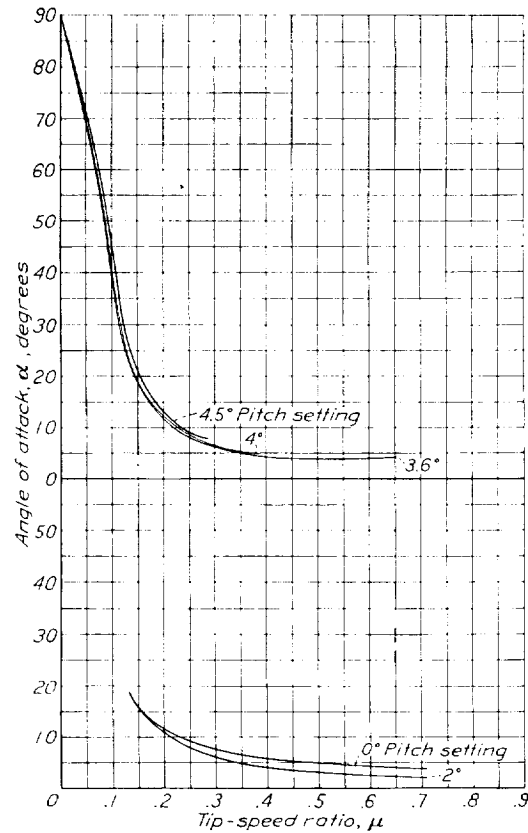
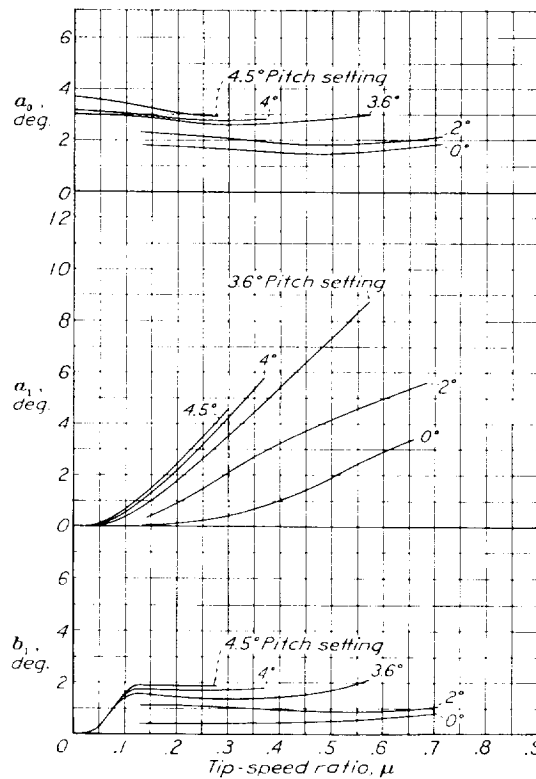
Blade designation	Radius R	Span t_r	Chord c	Angle of zero lift α_{L_0}	Mass con- stant: $\gamma = \frac{c \rho \alpha R^4}{I_1}$	Torsional rigidity ² (deg. twist per in. length per in.- lb.)
	<i>Feet</i>	<i>Feet</i>	<i>Foot</i>	<i>°</i>		
A (N. A. C. A. 0012)....	5.00	4.375	0.523	0	5.31	0.00119
B (N. A. C. A. 0012)....	5.00	3.50	.523	0	5.28	.00088
C (N. A. C. A. 0012)....	5.00	2.75	.523	0	4.93	.00074
D (N. A. C. A. 0012)....	5.00	2.00	.523	0	4.62	.00057
A (N. A. C. A. 0018)....	5.00	4.375	.523	0	4.32	.00047
A (N. A. C. A. 4412)....	5.00	4.375	.523	-3.9	5.00	.00121
A (N. A. C. A. 4418)....	5.00	4.375	.523	-3.7	3.65	.00041

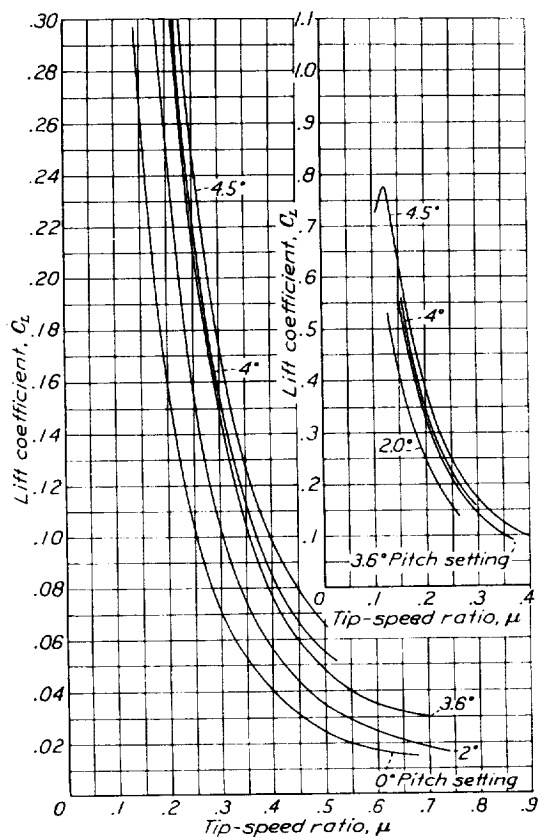
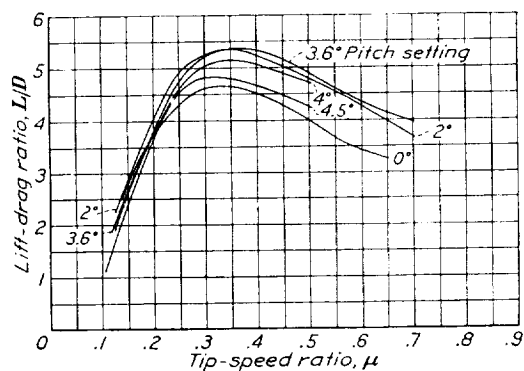
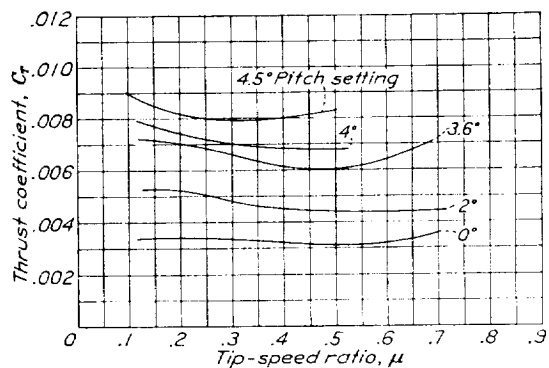
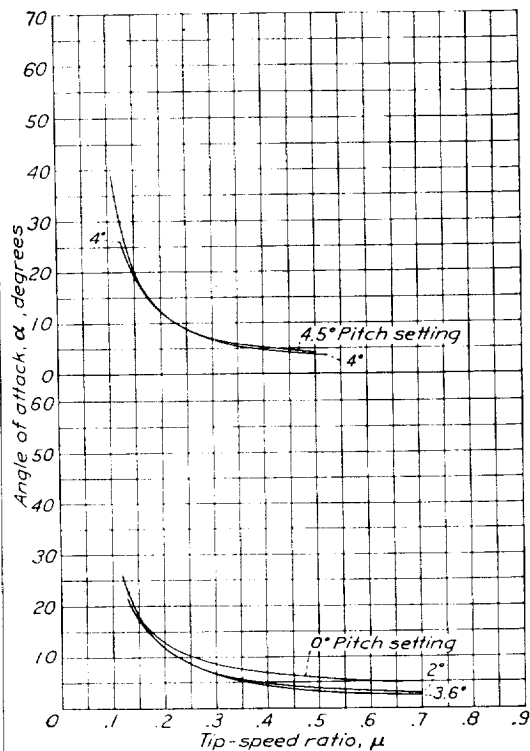
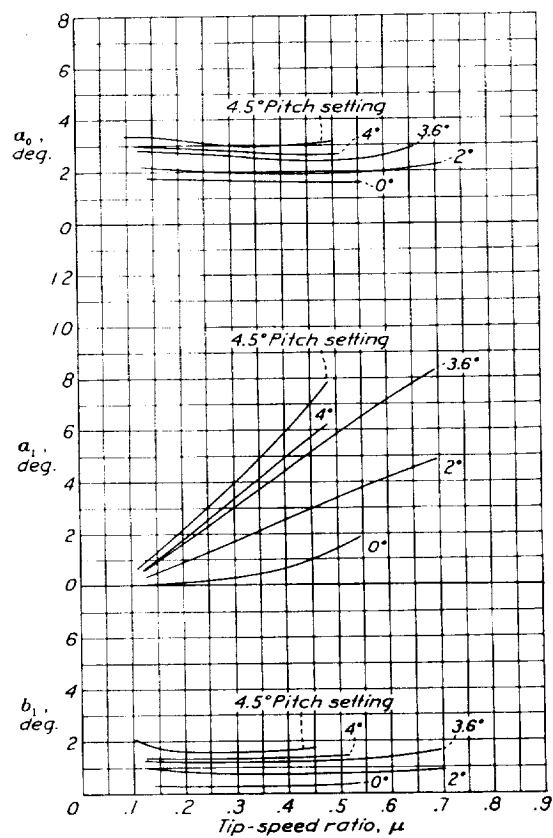
¹ Calculated for $\rho = 0.002378$ slug/cu. ft.

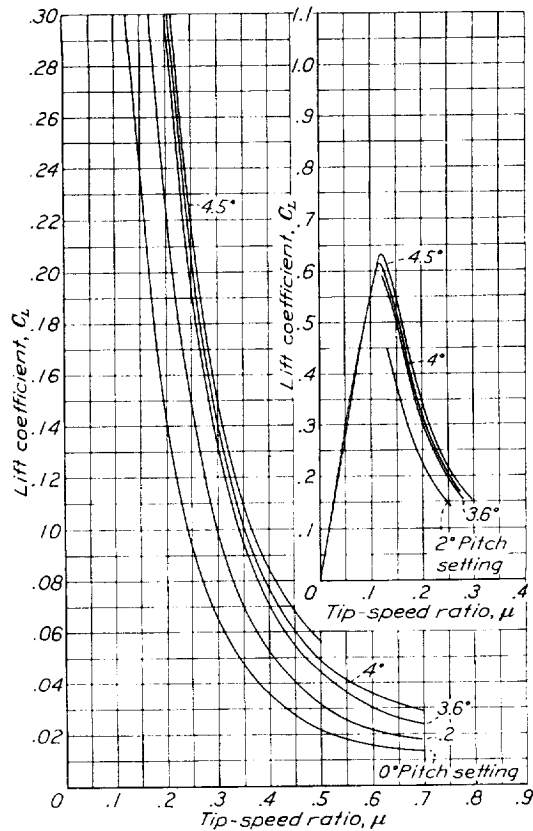
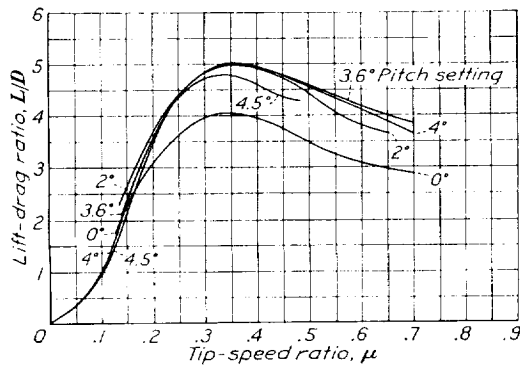
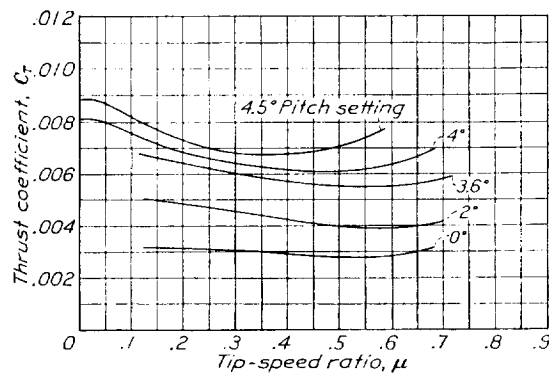
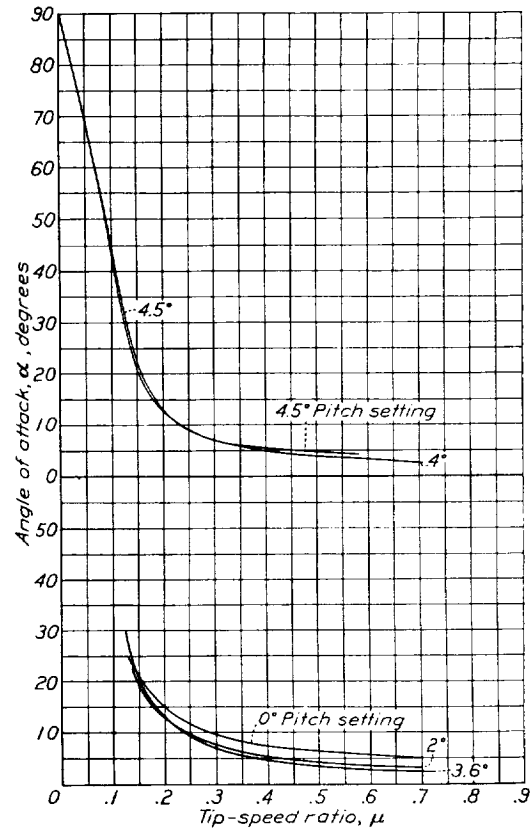
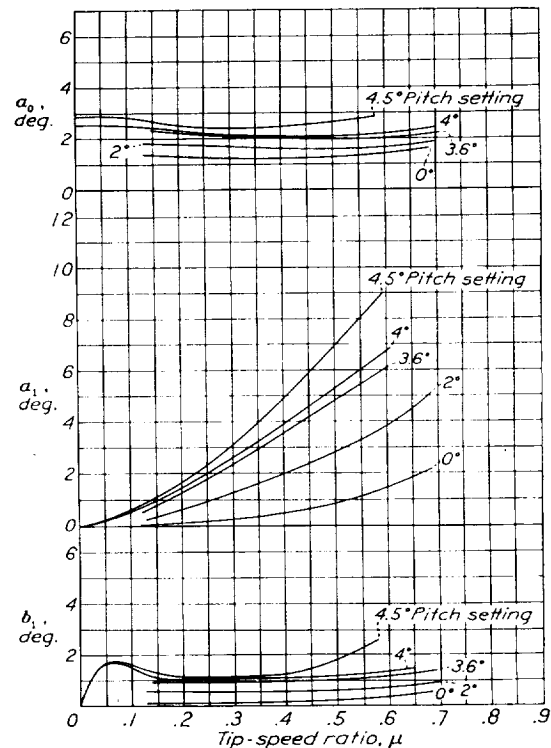
² For torsional moment constant along blade.

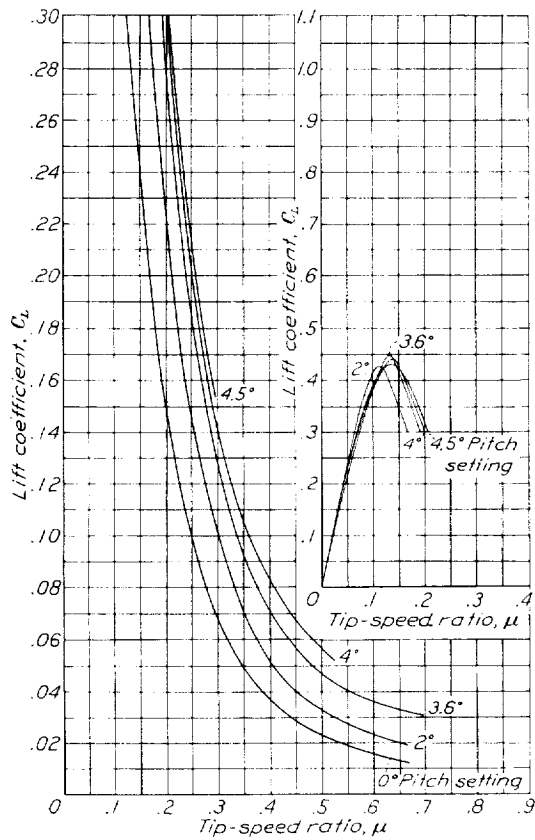
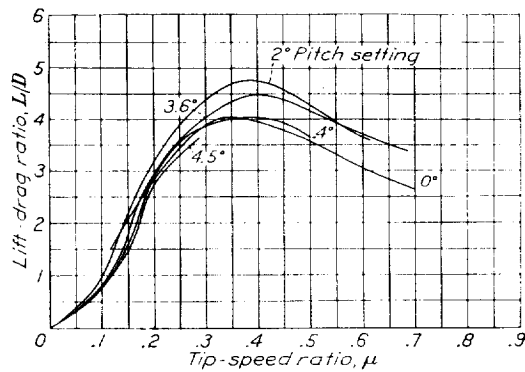
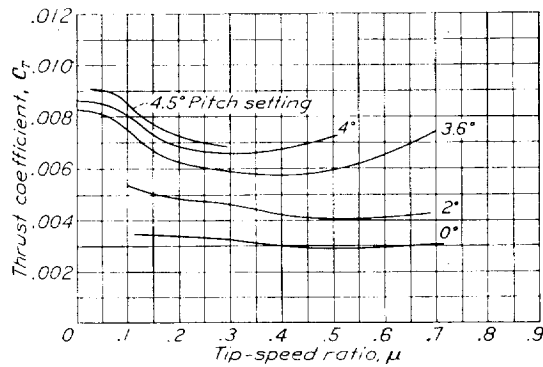
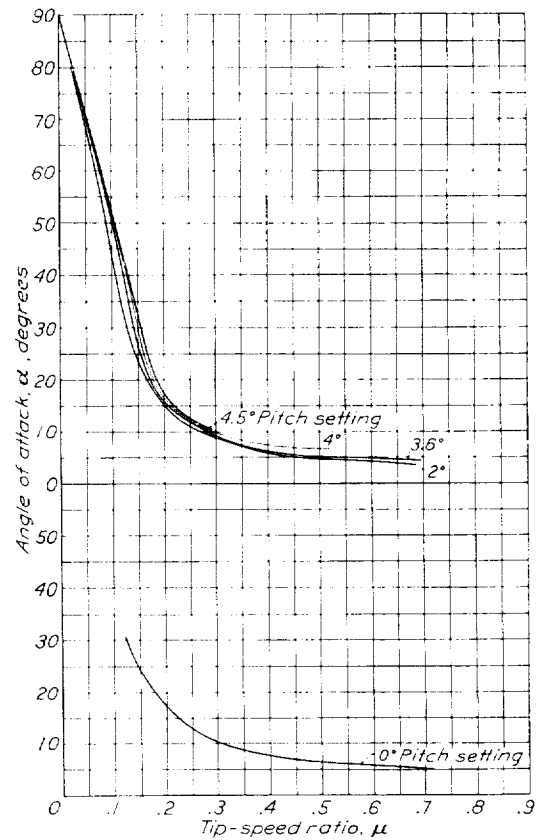
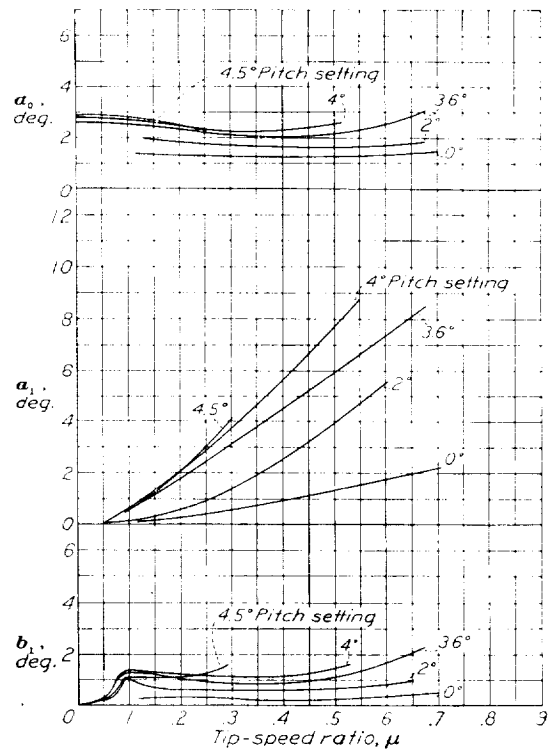
REFERENCES

1. Weick, Fred E., and Wood, Donald H.: The Twenty-Foot Propeller Research Tunnel of the National Advisory Committee for Aeronautics. T. R. No. 300, N. A. C. A., 1928.
2. Jacobs, Eastman, N., Ward, Kenneth E., and Pinkerton, Robert M.: The Characteristics of 78 Related Airfoil Sections from Tests in the Variable-Density Wind Tunnel. T. R. No. 460, N. A. C. A., 1933.
3. Wheatley, John B.: An Aerodynamic Analysis of the Autogiro Rotor with a Comparison between Calculated and Experimental Results. T. R. No. 487, N. A. C. A., 1934.
4. Whittaker, E. T., and Robinson, G.: The Calculus of Observations. Blackie and Son, Ltd. (London), 1924.

FIGURE 3.—Lift coefficient C_L of 10-foot autogiro rotor. A (N. A. C. A. 0012).FIGURE 4.—Lift-drag ratio L/D of 10-foot autogiro rotor. A (N. A. C. A. 0012).FIGURE 5.—Thrust coefficient C_T of 10-foot autogiro rotor. A (N. A. C. A. 0012).FIGURE 6.—Angle of attack α of 10-foot autogiro rotor. A (N. A. C. A. 0012).FIGURE 7.—Blade-motion coefficients a_0 , a_1 , and b_1 of 10-foot autogiro rotor. A (N. A. C. A. 0012).

FIGURE 8.—Lift coefficient C_L of 10-foot autogiro rotor. B (N. A. C. A. 0012).FIGURE 9.—Lift-drag ratio L/D of 10-foot autogiro rotor. B (N. A. C. A. 0012).FIGURE 10.—Thrust coefficient C_T of 10-foot autogiro rotor. B (N. A. C. A. 0012).FIGURE 11.—Angle of attack α of 10-foot autogiro rotor. B (N. A. C. A. 0012).FIGURE 12.—Blade-motion coefficients a_0 , a_1 , and b_1 of 10-foot autogiro rotor. B (N. A. C. A. 0012).

FIGURE 13.—Lift coefficient C_L of 10-foot autogiro rotor. C (N. A. C. A. 0012).FIGURE 14.—Lift-drag ratio L/D of 10-foot autogiro rotor. C (N. A. C. A. 0012).FIGURE 15.—Thrust coefficient C_T of 10-foot autogiro rotor. C (N. A. C. A. 0012).FIGURE 16.—Angle of attack α of 10-foot autogiro rotor. C (N. A. C. A. 0012).FIGURE 17.—Blade-motion coefficients a_0 , a_1 , and b_1 of 10-foot autogiro rotor. C (N. A. C. A. 0012).

FIGURE 18.—Lift coefficient C_L of 10-foot autogiro rotor. D (N. A. C. A. 0012).FIGURE 19.—Lift-drag ratio L/D of 10-foot autogiro rotor. D (N. A. C. A. 0012).FIGURE 20.—Thrust coefficient C_T of 10-foot autogiro rotor. D (N. A. C. A. 0012).FIGURE 21.—Angle of attack α of 10-foot autogiro rotor. D (N. A. C. A. 0012).FIGURE 22.—Blade-motion coefficients a_0 , a_1 , and b_1 of 10-foot autogiro rotor. D (N. A. C. A. 0012).

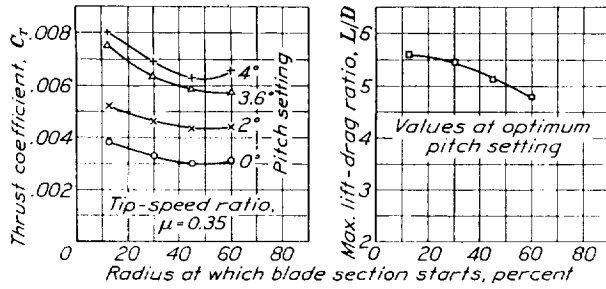


FIGURE 23.—Influence of blade span on maximum lift-drag ratio and thrust coefficient (at $\mu=0.35$) of 10-foot autogiro rotor.

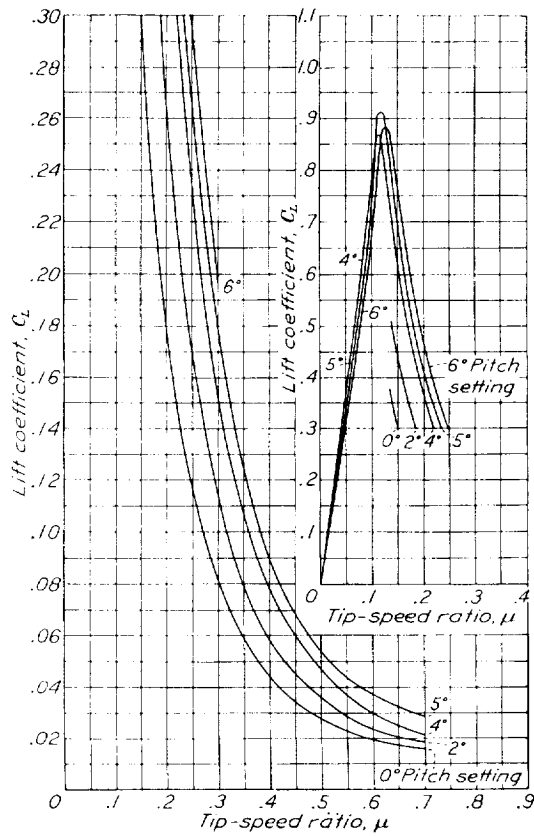


FIGURE 24.—Lift coefficient C_L of 10-foot autogiro rotor. A (N. A. C. A. 0018).

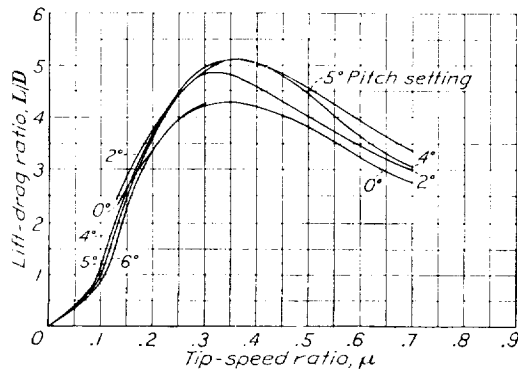


FIGURE 25.—Lift-drag ratio L/D of 10-foot autogiro rotor. A (N. A. C. A. 0018).

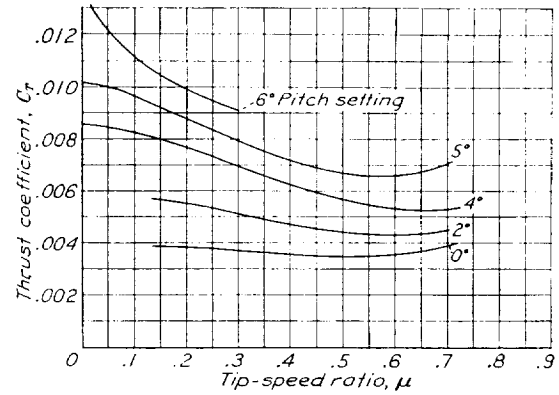


FIGURE 26.—Thrust coefficient C_T of 10-foot autogiro rotor. A (N. A. C. A. 0018).

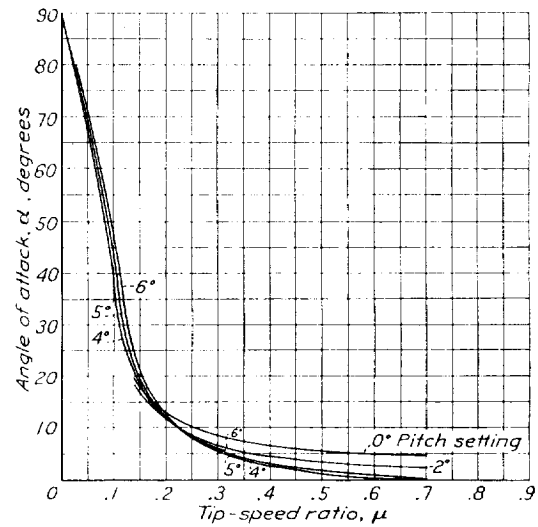


FIGURE 27.—Angle of attack α of 10-foot autogiro rotor. A (N. A. C. A. 0018).

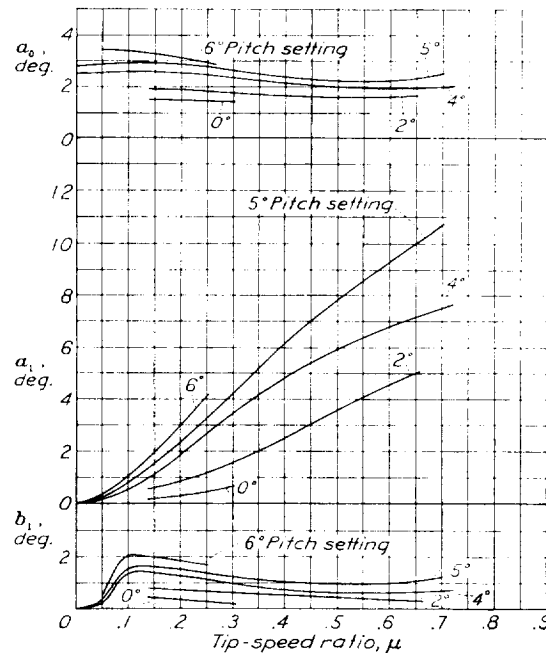
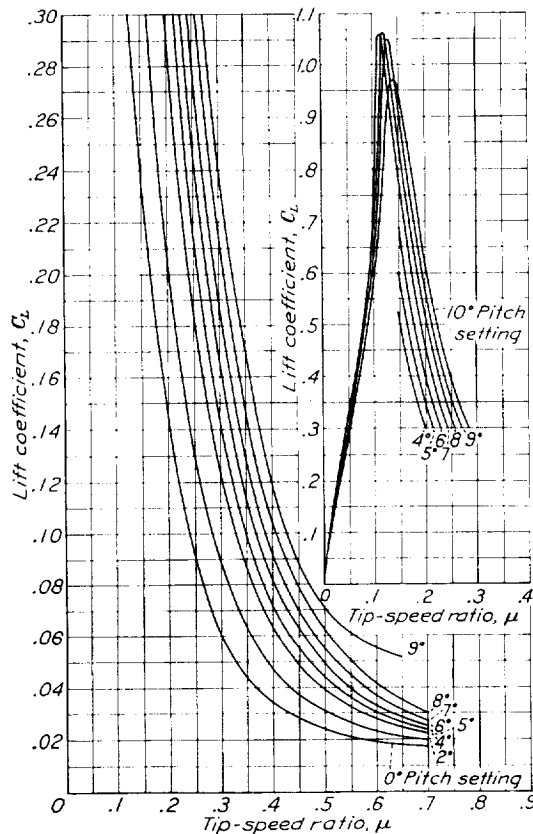
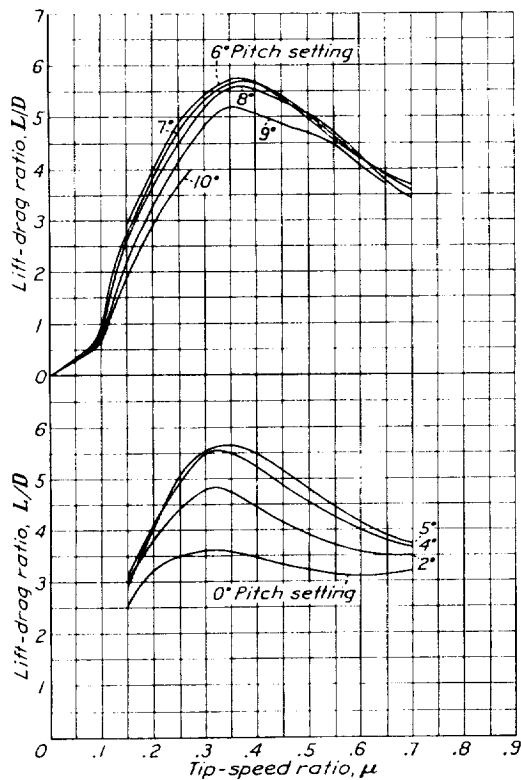
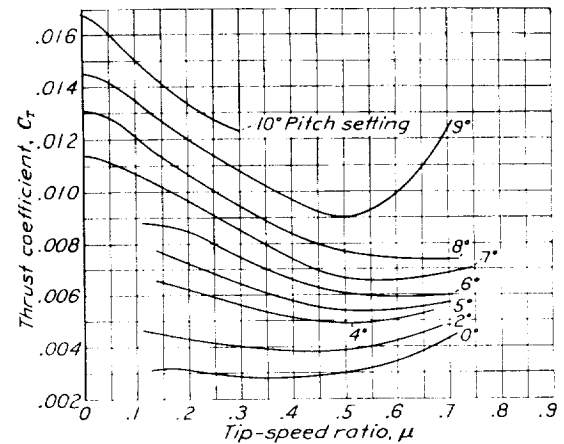
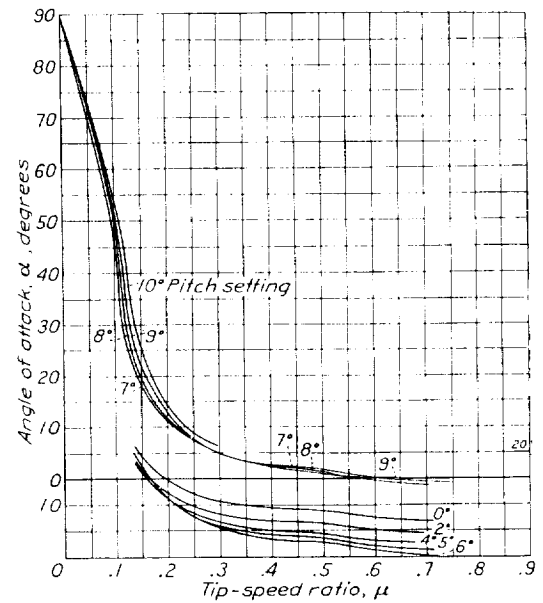
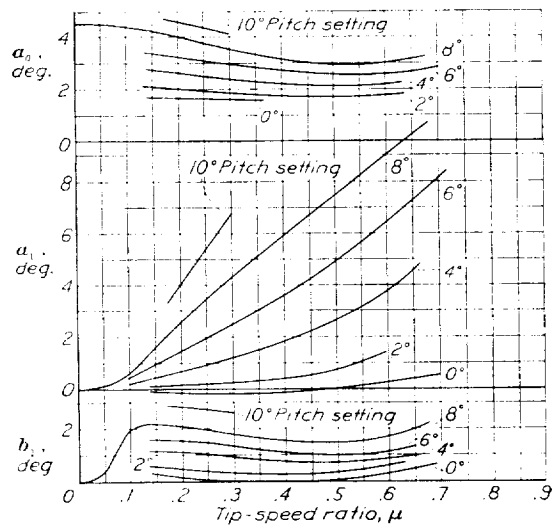
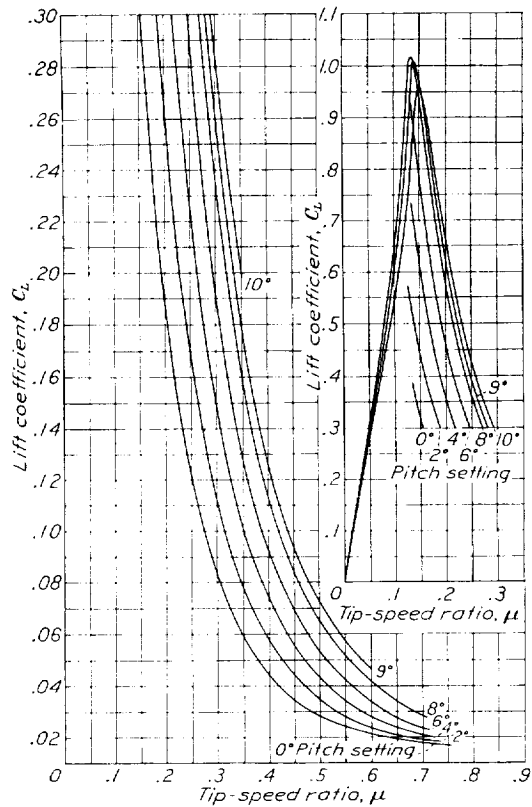
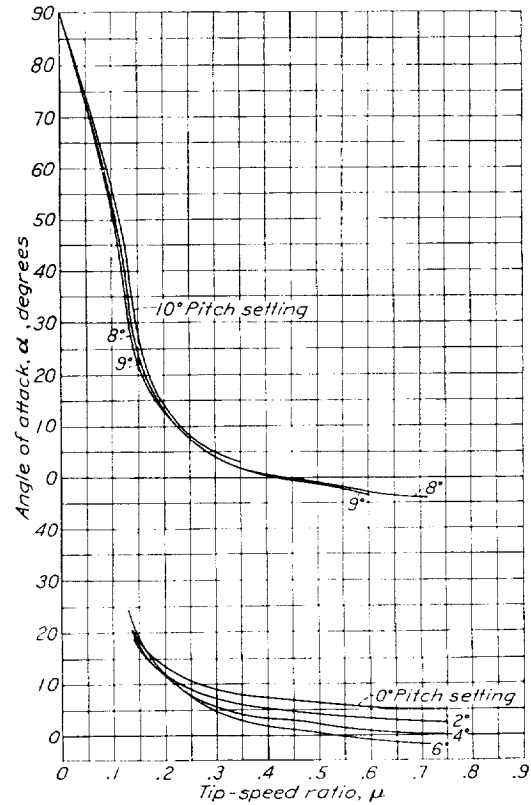
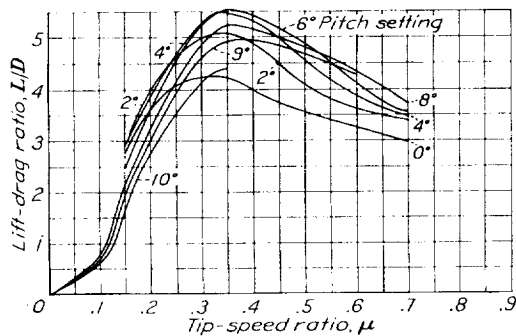
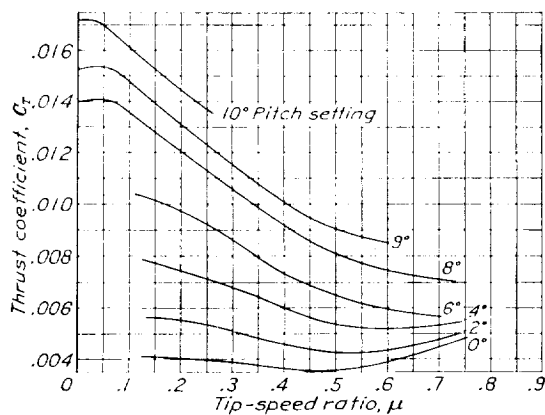
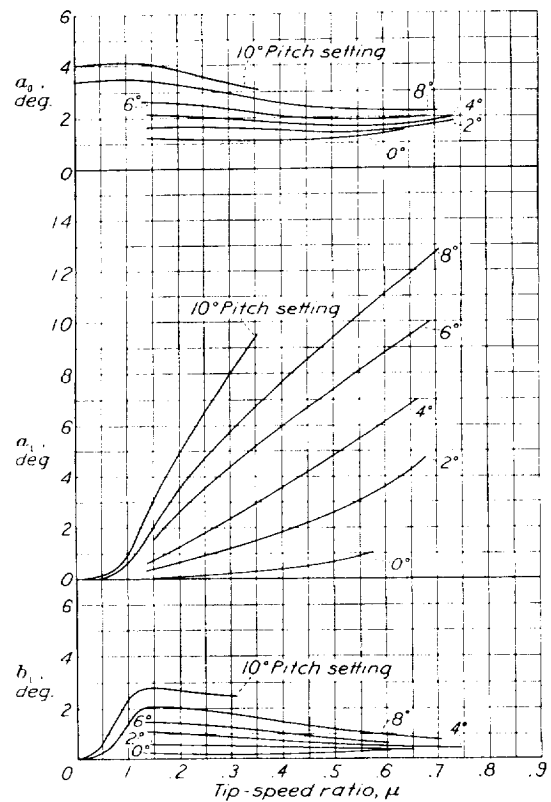


FIGURE 28.—Blade-motion coefficients a_0 , a_1 , and b_1 of 10-foot autogiro rotor. A (N. A. C. A. 0018).

FIGURE 29.—Lift coefficient C_L of 10-foot autogiro rotor. A (N. A. C. A. 4412).FIGURE 30.—Lift-drag ratio L/D of 10-foot autogiro rotor. A (N. A. C. A. 4412).FIGURE 31.—Thrust coefficient C_T of 10-foot autogiro rotor. A (N. A. C. A. 4412).FIGURE 32.—Angle of attack α of 10-foot autogiro rotor. A (N. A. C. A. 4412).FIGURE 33.—Blade-motion coefficients a_0 , a_1 , and b_1 of 10-foot autogiro rotor A (N. A. C. A. 4412).

FIGURE 34.—Lift coefficient C_L for 10-foot autogiro rotor. A (N. A. C. A. 4418).FIGURE 37.—Angle of attack α of 10-foot autogiro rotor. A (N. A. C. A. 4418)FIGURE 35.—Lift-drag ratio L/D of 10-foot autogiro rotor. A (N. A. C. A. 4418).FIGURE 36.—Thrust coefficient C_T of 10-foot autogiro rotor. A (N. A. C. A. 4418).FIGURE 38.—Blade-motion coefficients a_0 , a_1 , and b_1 of 10-foot autogiro rotor. A (N. A. C. A. 4418).

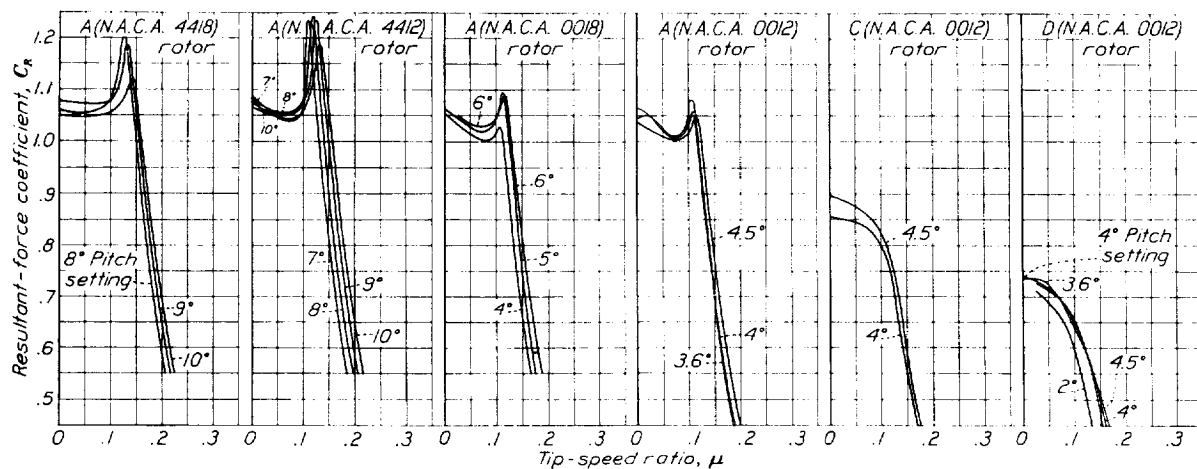
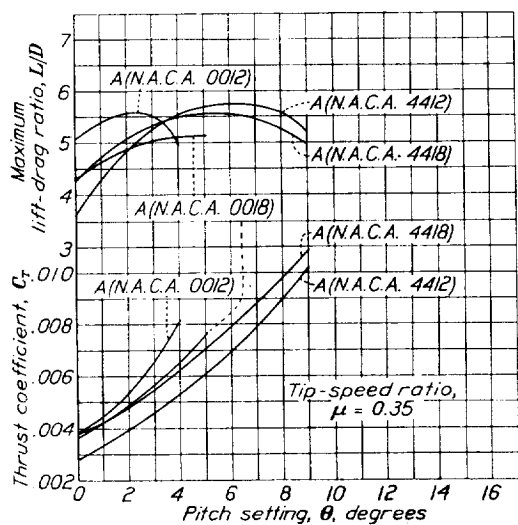
FIGURE 39.—Resultant force coefficient C_R of 10-foot autogiro rotors.

FIGURE 40.—Influence of pitch setting on maximum lift-drag ratio and thrust coefficient of 10-foot autogiro rotors.

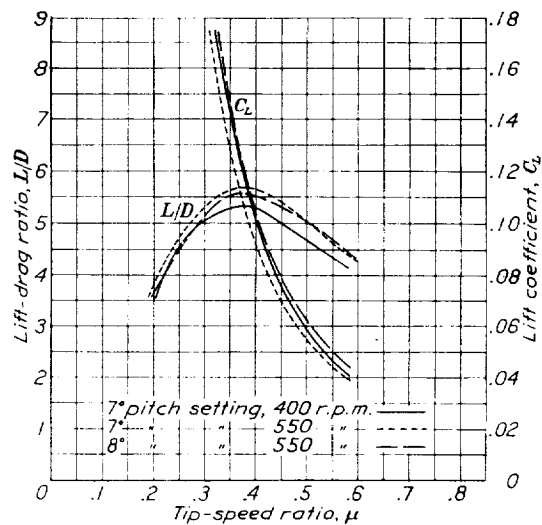
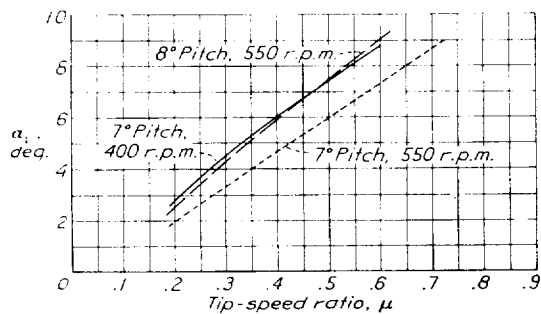


FIGURE 41. Influence of rotor speed on lift coefficient and lift-drag ratio of 10 foot autogiro rotor. A(N.A.C.A. 4412).

FIGURE 42.—Influence of rotor speed on flapping coefficient a_1 of 10-foot autogiro rotor. A(N.A.C.A. 4412).

REPORT No. 553

SOME EFFECTS OF ARGON AND HELIUM UPON EXPLOSIONS OF CARBON MONOXIDE AND OXYGEN

By ERNEST F. FLOCK and CARL H. ROEDER

SUMMARY

This investigation, performed at the National Bureau of Standards at the request and with the financial assistance of the National Advisory Committee for Aeronautics, is a study of the effects of the inert gases argon and helium upon flame speed and expansion ratio in exploding mixtures of CO, O₂, and H₂O. For the particular gas mixtures investigated the results show that (1) with the possible exception of He in small amounts the addition of inert gas always produces decreased flame speed and expansion ratio, (2) like volumes of A and He have very different effects upon flame speed but practically the same effect upon expansion ratio, and (3) the difference in the effect of these two gases upon flame speed is independent of the ratio of CO to O₂. A discussion of some possible modes by which inert gases may produce the observed effects is included.

INTRODUCTION

The majority of practical advances that have been made in the application of gaseous explosions to the production of useful work are of an empirical nature. So rapid have been these advances that at present our knowledge of the fundamental processes of the explosion itself lags far behind. It seems unlikely, however, that all of the possible means for improving the efficiency and performance of an internal-combustion engine will be discovered without the aid of an exact knowledge of the mechanism of the ignition and subsequent combustion of the explosive mixture within the cylinder.

It is believed that the practical value of results obtained by isolating and evaluating the effects of the individual operating variables under carefully controlled conditions will be amply demonstrated when a complete and comprehensive picture of the explosive process has been evolved. A portion of the necessary information can be obtained by the study of the effect of operating variables upon the speed with which flame transforms an explosive mixture. Experiments of this nature, using the comparatively simple fuel CO, have been in progress for some time at the National Bureau of Standards.

In reference 1 the effect of water vapor upon the speed of flame in equivalent CO-O₂ mixtures at various pressures was reported. In reference 2, means were described for improving the precision of results obtained by the soap-bubble, or constant-pressure method, developed and used by Stevens (reference 3) and data were reported showing the variation with composition of the spatial and transformation velocity of flame and of expansion ratio.

Further information upon the mechanism of the CO-O₂ reaction is presented in this report, in which the effects upon flame speed and expansion ratio of replacing a portion of the explosive mixture with the inert gases A and He are studied. These results may eventually prove of value in explaining the effects of the nitrogen that is always present in the engine cylinder.

In order to isolate the effects of the diluent gases upon flame speed and expansion ratio the present study was made at constant pressure in quiescent gas mixtures of carefully controlled composition and initial temperature. The truly inert gases A and He are better suited to the present study of the mechanism of the oxidation of CO than N₂, because it is probable that the latter is not totally inert. Carbon monoxide was selected as the fuel because it can be readily prepared in a very pure state, because it produces a highly actinic flame, and because numerous data on explosions of this fuel in the absence of diluents are already available.

A previous investigation, similar in nature to the present one, was reported by Stevens (reference 3). The subsequent study of the characteristics of the soap-bubble method (reference 2) revealed that the precision of the results could be much improved, and indicated the desirability of repeating and extending the earlier observations.

EXPERIMENTAL PROCEDURE

The method employed consists essentially in taking a photographic record on a film moving at constant speed of the travel of flame initiated by a spark at the

center of a soap bubble filled with explosive mixture. From such a record, which also contains time signals recorded simultaneously with the explosion, the spatial velocity (S_s) of flame and the final radius of the sphere of hot products (R_2) can be readily obtained. If the initial radius of the bubble (R_1) is known, the speed (S_t) with which the flame transforms the unburned gases can be calculated through the relation

$$S_t = S_s \left(\frac{R_1}{R_2} \right)^3$$

The details of the method, apparatus, and technic have been described in reference 2. The necessary connections for admitting the inert gases constituted the only significant change in the apparatus.

The A was an especially purified sample furnished by the Westinghouse Lamp Co. of Bloomfield, N. J., and specified by them to be 99 percent pure. It was used without further treatment, save drying over P_2O_5 .

The He, obtained from the Navy Department, was freed of combustibles by passage over hot CuO and of O_2 and other impurities by passage through charcoal immersed in liquid air. It also was dried with P_2O_5 before being admitted to the mixing vessel.

The bubbles were blown in a sealed chamber in which a temperature of 25° C. was maintained. The partial pressure of water vapor in this chamber was kept at 20.44 mm Hg and, by varying the composition of the soap solution, its vapor pressure at 25° C. was adjusted to as nearly this same value as was practicable. The temperature of the distilled water that was used for humidifying the gas mixtures was kept at 22.5° C., so that the partial pressure of H_2O in each of the gas mixtures was likewise 20.44 mm. Under these conditions the calculated concentration of H_2O vapor in each mixture, before the bubbles were blown, was 0.0269 ± 0.0001 mole percent and no change in the partial pressure of H_2O in the mixture should have occurred during the formation and life of the bubbles. Practically, however, it was impossible entirely to eliminate all temperature and humidity gradients in the chamber, and the resulting variations in the H_2O content of the mixtures at the time of firing are believed to account for a considerable portion of the spread in the observed results.

The first series of observations in the present study shows the effect of varying the ratio of CO to O_2 at a constant partial pressure of H_2O of 20.44 mm in the absence of inert gas. The results of this series were desired for comparison with the corresponding values of S_s previously obtained by the constant-volume method (fig. 5 of reference 2) and for reference values of S_s , R_2 , and S_t to serve as termini for the curves obtained in the presence of the inert gases. Each of the other eight series of experiments was made with the addition of measured quantities of A and He (separately) to a previously prepared mixture of CO, O_2 , and H_2O .

The method of making the mixtures was modified slightly from that given in reference 2. In order that a complete series of observations with A and with He could be made at the same ratio of CO to O_2 it was desirable to make the latter mixture in a comparatively large quantity (ca. 20 liters).

Since no provision was made for the precise determination of the temperature of the storage flasks, the direct measurement of the composition of the CO- O_2 mixtures was only approximate. More precise values of composition were obtained by measuring S_s in the absence of inert gas and reading the concentration of CO from the previously determined S_s curve, which will be presented later in figure 1. It will be shown that exact knowledge of this composition is not important so far as the comparative effect of the two inert gases is concerned. The approximate composition of each CO- O_2 mixture indicated whether it was on the rich or lean side of chemical equivalence.

Each mixture was prepared as follows. Water vapor at a pressure of 20.44 mm was admitted to the evacuated mixing vessel, and the dry mixture of CO and O_2 was then admitted to a previously chosen total pressure. Finally the inert gas was added in amount sufficient to bring the total pressure to 760 mm Hg. When a steady state was reached after each addition of gas to the mixing vessel, the pressure and temperature were observed. In order to insure complete uniformity the final mixtures (1 liter total volume) were always allowed to stand 1 hour before blowing a bubble. Each mixture consisted of enough gas for three bubble experiments, though the usual practice was to make but two observations if both appeared satisfactory.

The eight different ratios of CO to O_2 used with inert gases were distributed throughout the range of mixture ratios for which it is believed that the bubble method can be most advantageously employed. The number of observations with A was restricted by the limited available supply of this gas.

RESULTS OF THE EXPERIMENTS

The type of photographic records obtained and the method of calculating the results therefrom have already been described in reference 2. The data obtained in this way during the present investigation are most conveniently presented in graphical form.

Figure 1 shows the variation of final radius (R_2), speed of flame in space (S_s), and speed of transformation of the unburned charge (S_t) for a range of CO- O_2 mixtures containing a constant mole fraction of H_2O of 0.0269 ± 0.0001 . The square of the mole fraction of CO is plotted along the axis of abscissas to render the curves more nearly symmetrical. Each circle on the curves for R_2 and S_s represents the mean of two or more determinations. The S_t curve is derived from the other two through the relation $S_t = S_s \left(\frac{R_1}{R_2} \right)^3$, in

which the initial radius R_1 was constant throughout and equal to 4.5 cm.

The reasons for including this series of measurements have already been presented. The values of S_s given in figure 1 are directly comparable with those determined by the constant-volume method, as presented in figure 5 of reference 2. In the deviation chart (fig. 2) the mean values of S_s obtained by averaging the two sets of measurements are represented by the straight base line, while the curves show the deviations from this mean of the values of S_s obtained by the

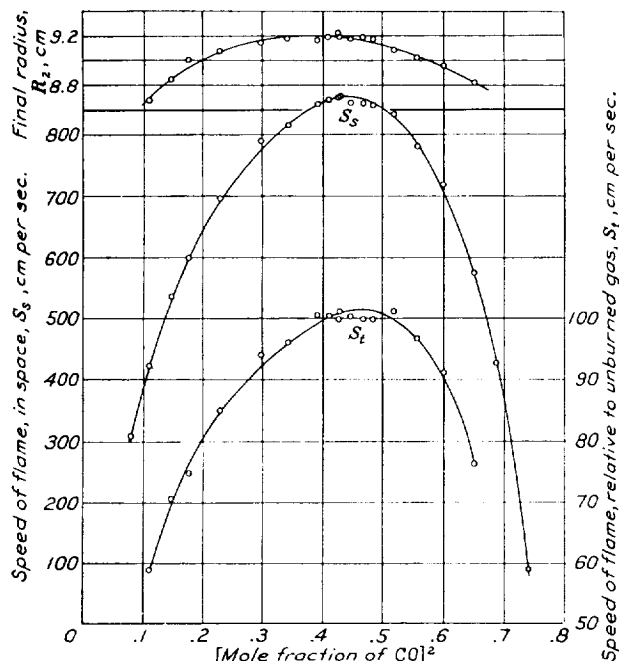


FIGURE 1.—Variation of R_2 , S_s , and S_t with the mole fraction of CO in the absence of inert gas (mole fraction of $H_2O = 0.0269$).

two methods. At both the rich and lean extremes the values of S_s are changing rapidly and the personal factor involved in drawing the curves through the experimental points may be responsible for a considerable part of the deviation. The deviations in the region embracing equivalence are probably due in a large measure to failure to adjust the vapor pressure of the soap solution at 25° C. to exactly 20.44 mm. The deviation is in the direction indicating that this vapor pressure was slightly below the chosen value.

Despite this indication the differences between the values of S_s determined by the two methods seem about as small as could be expected when it is considered that an error of from 5 to 10 cm per sec. may reasonably be present in each series. It seems safe to conclude that no large systematic error occurs in one method and not in the other. Accidental errors in the reduction of the data from the photographic records are common to both methods, but their effects are greatly reduced by the fairing applied to both series of observations. It is believed that values of S_s can be determined by

either method with substantially the same precision and that at no point on either of the curves is the value of S_s in error by more than 10 cm per sec.

Some further comparisons of the data of figure 1 with those of figures 6 and 7 of reference 2 are of value in showing the effect of water vapor upon the explosive oxidation of CO. The water-vapor content in the present series of measurements was 0.0269 mole percent and in the earlier series 0.0331, while all other factors were the same for both. A change in water content from the higher to the lower of these values, no matter what the mixture ratio, always produced a decrease in S_s , an increase in R_2 , and a correspondingly large decrease in S_t . The decrease in R_2 is greatest for lean mixtures and approaches zero for very rich mixtures. The decrease in S_t is least for lean mixtures and increases gradually as the mixtures become richer. The decrease in S_s , which is of course a function of the changes in R_2 and S_s , has a minimum value near equivalence and larger values for both lean and rich mixtures. From these facts it follows that, if a mixture in a bubble at the time of firing should for some unrecognized cause contain an excess of water vapor, the observed value of S_s will be too high, of R_2 will be too low, and of S_t will be too high. These relations among the errors in the observed quantities are illustrated by several of the observations plotted in figure 1 and in the figures to be presented later in this report. The inference is that, for mixtures of CO, O_2 , and H_2O , in spite of all the precautions that have been taken to control the concentration of the latter, uncertainty in the H_2O content still remains as one of the outstanding sources of error in the results obtained by the bubble method.

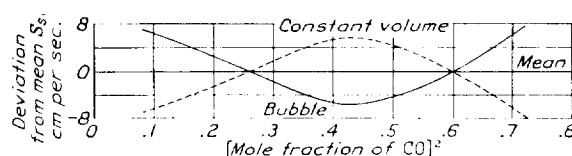


FIGURE 2.—Differences in the values of S_s observed by the constant-volume and bubble methods.

The gases A and He were selected for the present study of the effect of inert diluents for these reasons: First, it was considered that the rare gases were most likely to be inert under the conditions prevailing in an explosion; second, these two gases are the most readily obtainable of the rare gases in the desired state of purity; and, third, the heat capacities are practically identical while there is a large difference in thermal conductivity.

The data obtained in the presence of A and He for different CO/ O_2 ratios are presented in figures 3 to 10, inclusive. The same quantities (R_2 , S_s , and S_t) are plotted along the axis of ordinates as in figure 1. The mole fraction of inert gas is in each case plotted along the axis of abscissas. The crosses represent the

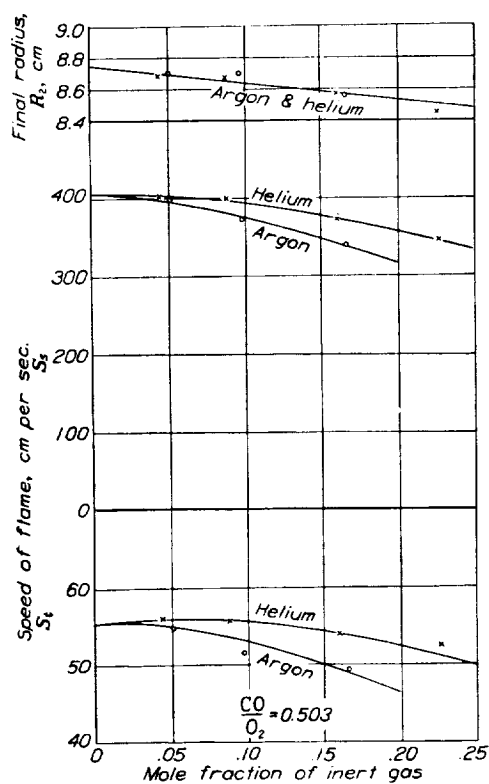


FIGURE 3.

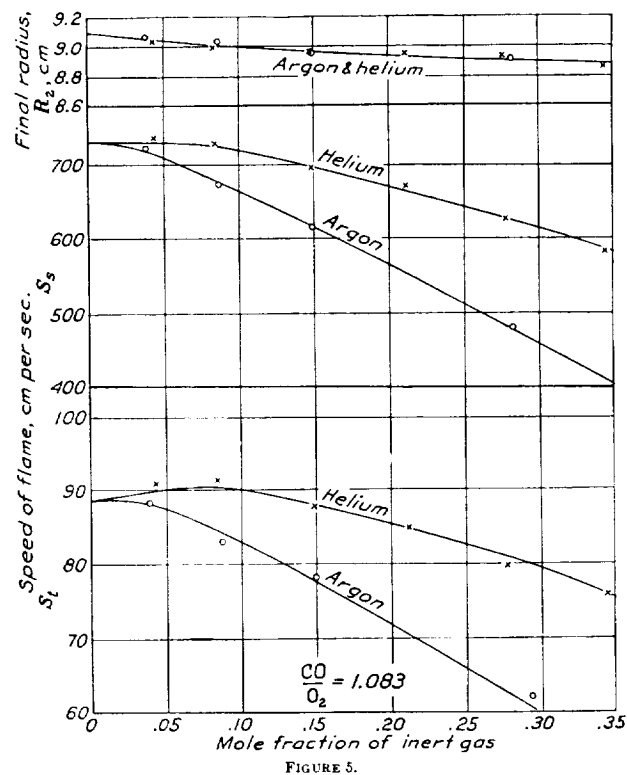


FIGURE 5.

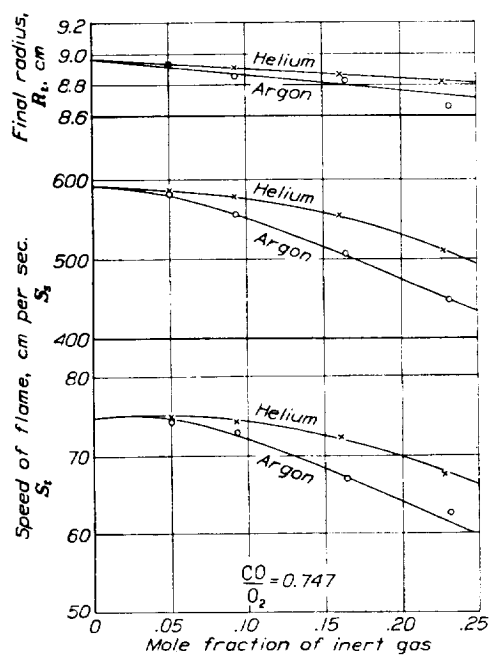


FIGURE 4.

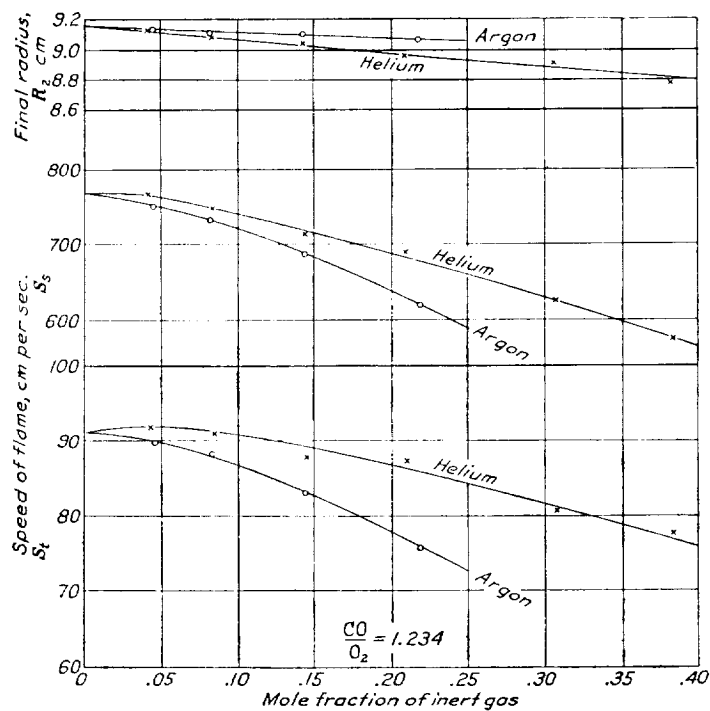


FIGURE 6.

FIGURES 3 to 6 inclusive.—Effects of argon and helium on R_2 , S_s , and S_t in CO-O₂ explosions (mole fraction of H₂O = 0.029).

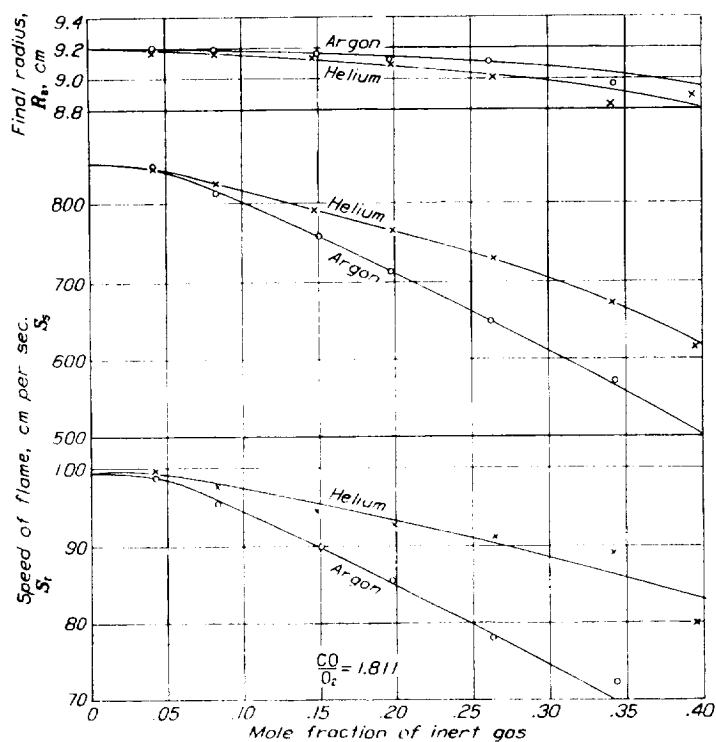


FIGURE 7.

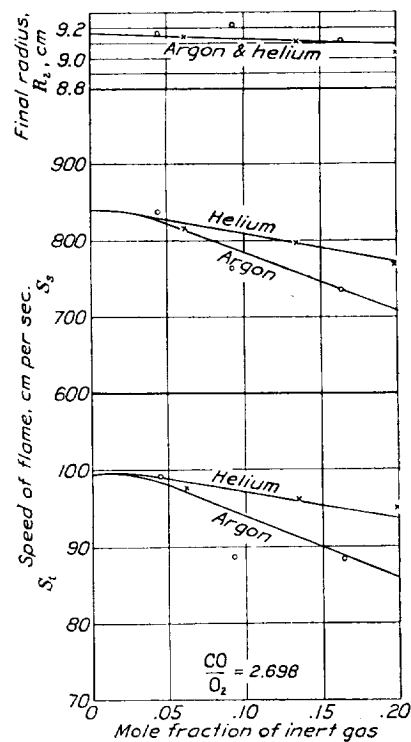


FIGURE 8.

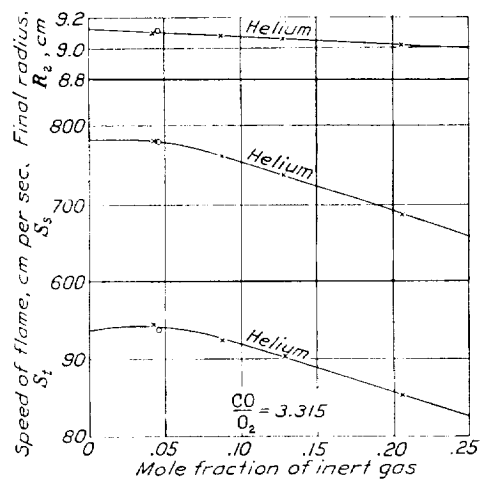


FIGURE 9.

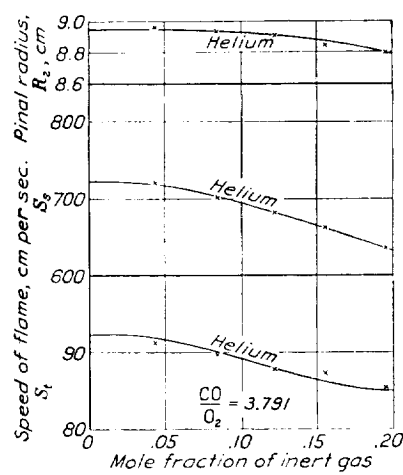


FIGURE 10.

FIGURES 7 to 10 inclusive.—Effects of argon and helium on R_2 , S_s , and S_t in CO-O₂ explosions (mole fraction of H₂O = 0.0269).

experimental points for He and the open ones, those for A. Exhaustion of the A supply prevented determinations for this gas in the mixtures represented by figures 9 and 10.

ANALYSIS OF THE RESULTS

It is convenient, when analyzing the present results, to discuss separately the effects of varying the concentration of a particular inert gas and of changing from one inert gas to another.

Changes in the concentration of A or He.—In any analysis of results obtained by the present method it should be kept in mind that the total pressure and the partial pressure of H_2O were essentially constant in all the experiments and that, when inert gas was introduced, it replaced a portion of the active mixture of CO and O_2 . Therefore, an increase in the mole fraction of inert gas, as represented along the axes of abscissas in figures 3 to 10, actually involves three simultaneous and significant changes in composition: (1) A reduction in the partial pressure of CO- O_2 mixture, (2) an increase in the ratio of H_2O to active mixture, and (3) an increase in the concentration of inert gas.

The effect of each of these changes may be evaluated for the specific case of S_s in equivalent CO- O_2 mixtures, since data on the effect of pressure and concentration of H_2O vapor in such mixtures are available in reference 1. For this purpose let us consider the experiment in which 20 percent by volume of A was used. It is convenient to refer to four different mixtures, each of which represents an isolated stage in the whole process of replacing 20 volume percent of the reference mixture, in the form of CO and O_2 , with A. The characteristics of these mixtures may be tabulated as follows:

	Mixture number			
	I	II	III	IV
Total pressure (mm Hg).....	760.0	608.0	765.3	760.0
Partial pressure of H_2O (mm Hg).....	20.44	20.44	25.71	20.44
Mole fraction of CO.....	0.6487	0.6443	0.6443	0.5154
Mole fraction of O_2	0.3244	0.3221	0.3221	0.2577
Mole fraction of H_2O	0.0269	0.0336	0.0336	0.0269
Mole fraction of A.....	0.0000	0.0000	0.0000	0.2000
Speed of flame in space S_s (cm per sec.).....	860	894	910	730

Mixture I is a reference mixture fired under the actual conditions of the present measurements. The value of S_s is taken from the appropriate curve in figure 1. If the total pressure of mixture I is reduced 20 percent by removal of CO and O_2 in equivalent proportions, mixture II results. The value of S_s for this mixture was obtained by interpolation of the data of figure 2 of reference 1. Mixture III is obtained by adding H_2O to mixture I until its mole fraction becomes the same as in mixture II. The value of S_s for mixture III was likewise taken from figure 2 of reference 1. Mixture IV results if A is added to mixture II in suffi-

cient quantity to restore the total pressure to the same value as that of mixture I. Mixture IV can be fired in a bubble and the value of S_s was obtained by interpolation of the present data.

The difference in S_s for mixtures III and I is $910-860=50$ cm per sec., and shows the effect of changing the ratio of H_2O to explosive mixture by an amount equivalent to that which automatically occurs when 20 percent of inert gas is added at constant total pressure and partial pressure of H_2O . The partial pressure of CO+ O_2 is the same in mixtures I and III.

The difference in S_s for mixtures II and I, $894-860=34$ cm per sec., shows the effect of simultaneous changes in partial pressure of CO+ O_2 and of the ratio of H_2O to combustible. This increase of 34 cm per sec. is thus the resultant of an increase of 50 cm per sec. due to the latter and a decrease of $50-34=16$ cm per sec., which is the effect of the pressure decrease alone.

The difference in S_s for mixtures II and IV, $894-730=164$ cm per sec., represents the true effect of the A alone, since no other differences exist in the composition of these two mixtures.

The difference in S_s for mixtures I and IV, $860-730=130$ cm per sec., is the combined effect of the three significant changes in composition that occur when 20 percent of inert gas is introduced. This decrease of 130 cm per sec. is the observed resultant of an increase of 50 cm per sec. due to the increase in the ratio of H_2O to explosive mixture, a decrease of 16 cm per sec. due to the reduction in the partial pressure of the CO+ O_2 and a decrease of 164 cm per sec. due to the A.

As already shown, the true effect of introducing 20 percent of A is a decrease in S_s of 164 cm per sec., while the observed effect of the three simultaneous changes in composition is only 130 cm per sec. Similar calculations for other concentrations of both A and He show that this same order is always maintained in equivalent mixtures of CO and O_2 . Quantitative data for mixtures of CO and O_2 in other proportions are not available, but it has been shown that, qualitatively, the effect of water vapor is in the same direction for all ratios of CO to O_2 as at equivalence. It is therefore concluded that, if curves showing the effect upon S_s of the inert gases alone could be obtained, they would lie below the S_s curves of figures 3 to 10 at all points except those for zero concentration of inert gas, and that the separation would increase with the concentration of inert gas.

Unfortunately sufficient reliable data to permit a similar isolation of the effects of inert gases upon R_2 and S_s do not exist. A qualitative estimate is possible, however, for it has been shown that in the range of concentration of water vapor here involved, an increase in the mole fraction of H_2O always produces a decrease in R_2 . This is probably a direct result of the increase in the amount of heat retained by the H_2O

as kinetic energy. Nothing very definite can be said about the effect of pressure upon R_2 for want of reliable experimental results. Some decrease in the volume of hot products is to be expected when the initial pressure is reduced at a constant mole fraction of H_2O because of the greater dissociation of CO_2 at lower pressures. The changes in R_2 resulting from the addition of inert gas as displayed in figures 3 to 10 are therefore the resultant of the three decreases due to the increase in the ratio of H_2O to unburned gas, to the decrease in partial pressure of the active mixture and consequent less complete oxidation of the CO, and to the presence of the inert gas. The effect of the latter alone would therefore be expected to be less than is shown in the figures.

If the curves given for R_2 are too low and those for S_s too high, it follows that those for S_t are also too high.

It is concluded that when the effects of inert gases upon flame speed and expansion ratio are investigated by a method in which it is practicable to eliminate the effect of varying the initial partial pressure of the unburned gas and the ratio of H_2O to unburned mixture, it will be found that A and He actually produce less decrease in R_2 and greater decreases in S_s and S_t than are shown in the figures.

Differences in the effects of A and He.—In contrast with the rather obscure effect of the change in concentration of inert gas, the differences in the effects produced by like volumes of A and He can be obtained directly from the figures, since the substitution of one inert gas for the other involves no further change in the initial composition of the mixture.

It will be noted that in figures 6 and 7 the values of final radius (R_2) seem slightly higher for A; in figure 4 the He gave the higher values, and in figures 3, 5, and 8 the effect of these two gases on R_2 seems to be identical. In those cases where differences are shown they are of an order of magnitude comparable with the error that may reasonably be expected in the observed values of R_2 . Therefore the present measurements should not be considered sufficiently precise to show definitely that like volumes of A and He may produce different changes in final radius. If real differences actually exist, the present results show that they are very small and, for the purpose of the following discussion, it is necessary to consider only one of the flame speeds (either S_t or S_s) since these are exactly proportional for identical values of R_2 .

Slight increases in S_t at low concentrations of He are shown in some of the figures. These increases are of a magnitude comparable with the experimental error and may or may not be significant.

It is evident in each of figures 3 to 8 that a given volume of He offers less hindrance to the progress of the reaction zone than a like volume of A. From each of these figures a series of differences in S_s , when like volumes of He and A are present, may be

read off at arbitrarily chosen values of the mole fraction of inert gas. An assembly of such data is presented in figure 11. The horizontal dashes represent the individual differences and the dots the means of these differences. Each horizontal dash in any vertical line thus represents the difference in S_s for mixtures containing corresponding amounts of He and A at a chosen ratio of CO to O_2 . The order of the departure of the dashes from the mean does not show

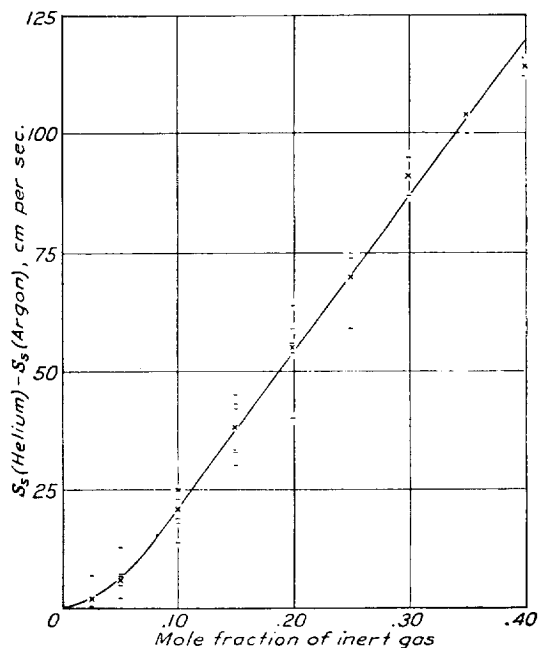


FIGURE 11.—Differences in the effect upon S_s of argon and helium for all ratios of CO to O_2 .

any systematic relation to mixture ratio. In addition, the ordinates of the dashes are differences between two quantities to each of which a tentative tolerance of ± 10 cm per sec. has been assigned. For these reasons the spread of the dashes is believed to be no greater than the experimental error and the curve that has been fitted to the dots is considered a satisfactory representation of the present results.

From this curve it is concluded that, within the limits of error of these experiments, the difference in the effect of A and He upon flame speed is independent of the ratio of CO to O_2 and that this difference increases linearly with the concentration of the inert above 7 percent. No logical explanation for the curvature at low concentrations of inert gas has been found. The curve must pass through the origin, but no straight line through this point represents the data satisfactorily.

The problem of explaining the observed differences in the effects of A and He is difficult because we do not know the mechanism of the action of either. We do know that with the possible exception of He in small amounts, both reduce flame speed, that identical vol-

umes retain virtually the same fraction of the total chemical energy liberated by the oxidation of the fuel, and that at room temperature the specific thermal conductivity of He is over 8 times that of A. This last fact, together with the rather natural supposition that the ability of gases to conduct heat is important in fixing the speed at which flame travels through an explosive mixture, seems to offer at once a qualitative explanation of the present results. Before such an explanation is accepted, however, it may be well to see how it agrees with other known facts.

It was predicted by the kinetic theory of gases, and has since been experimentally verified, that the thermal conductivity, viscosity, and diffusivity of a gas are related properties, since each is intimately connected with the mean free path of the molecules. The question at once arises as to why the thermal conductivity has been selected as the one of these four properties most significant in the propagation of flame. One reason may be that, by its use, an easily visualized physical picture has been evolved by numerous authors, on the assumption that heat is conducted from the flame to the active gas where inflammation occurs when the so-called ignition temperature is reached. Lewis and von Elbe (reference 4) give numerous citations to such theoretical treatments. Although the simplicity of such a picture is very appealing, it does not seem to be in complete accord with other related ideas or with various experimental results in the field.

In the first place it would seem that if this picture were correct, greater theoretical advances would have been made since its initial appearance more than 40 years ago. In spite of the fact that the velocity of an average molecule is high compared with normal flame velocities, the actual rate of resultant displacement of such a molecule is much less than the rate of propagation of flame. Stated in other words, the interdiffusion of gases is a comparatively slow process. These facts suggest that the commonly pictured process of conduction of heat in a gas is too slow to have much influence upon flame speed.

As pointed out by Lewis and von Elbe (reference 4) there is considerable evidence that inflammation of an active mixture can be produced at temperatures much below the ignition temperature by the introduction of a comparatively small number of active particles. If such particles are produced in the flame it seems logical to suppose that some of them will advance into the unburned charge at a faster rate than the flame itself. Physically, then, the chief difference between the mechanism proposed by Lewis and von Elbe and that involving the idea of thermal conduction is one of degree, the former requiring the advance of a much smaller number of particles ahead of the reaction zone than the latter. In spite of the fact that the conduction of heat and the interdiffusion of gases are comparatively slow processes, it is not difficult to conceive that a

relatively small number of particles from the flame are at all times advancing through the flame front and into the unburned gas ahead of it. Such action may result from the fact that some of the particles are moving at velocities far in excess of the average, or that, even though all the particles capable of producing activation were possessed of the same velocity, through sheer chance some of them would move farther than others before suffering collision or loss of the power of activation.

From the material that has been presented there seems to be some reason to suppose that the rate of flame propagation should depend to a considerable extent upon the free paths of some of the particles borne in the flame and that the free paths of particular interest are far in excess of the average or mean free path of all members of the species.

Regardless of the mechanism by which flame propagates, the replacement of active mixture with inert gas, as was done in the present measurements, may be thought of as the introduction of a resistance, in the form of intermediate collisions, to the transfer of energy in some form from the flame to the unburned gas. The magnitude of the resistance depends upon characteristics of the inert gas that have not yet been definitely identified. Some reasons for and against the selection of thermal conductivity have already been stated. On the basis of the activation theory of Lewis and von Elbe (reference 4) the explanation of the observed differences in the effects of A and He is possibly not quite so obvious.

In the first place, it is impossible to calculate the rate of diffusion of any species from the flame into the mixture of gases ahead of the flame front. We do know, however, that the mean free path of He is approximately three times that of A and that gases therefore diffuse more rapidly through He. In other words, it would be expected that with identical conditions both as to concentration and average translational energy prevailing in the flame, a greater number of particles from the flame would advance per unit time into an unburned charge containing He than into one containing the same volume concentration of A. This being the case it seems logical that flame should progress more rapidly in the mixtures containing the He. Furthermore, once a molecule of unburned gas has received the necessary energy from the flame to cause it to react upon the next collision with its complement molecule, it must first diffuse through the comparatively cold gases until the complement molecule is found. The presence of He would offer less resistance to this process than the presence of a like volume of A.

It may be well to point out also that if activation is electrical in nature, that is, if it is accomplished by reason of charges borne by the activators, the mass absorption coefficient of A for electrons and for positive

ions is greater than that of He, so that the charged particles would have a greater probability of reaching the unburned charge before losing their activity in the presence of He.

If it be true that the two rates of diffusion, namely, (1) that of active particles from the flame into the unburned charge and (2) that of the activated molecules through the charge to their complement molecules, are primarily responsible for fixing the speed of flame relative to the unburned gases, then it is to be expected that the heat capacity of the diluent gas will have little or no effect upon this speed. Such an expectation would not be fulfilled if it were found that the probability of an activator losing its potency upon collision with a molecule of inert gas varied with the nature of the inert gas. The heat capacity of the inert gas will, however, be important in fixing the final temperature attained by the products of combustion, and by this means it will influence expansion ratio and the speed of flame in space.

COMPARISON WITH THE RESULTS OF STEVENS

The present measurements are essentially a repetition and extension of those which Stevens (reference 1) made by the same method. The results of the two series, however, disagree even qualitatively. It has already been pointed out in reference 2 that in the earlier measurements the control of the water-vapor content of the bubbles at the time of firing was inadequate for explosions of CO. This fact alone will hardly account for the difference in results shown by the two series of measurements, because Stevens concluded that "argon has practically the same effect on the rate of propagation of the reaction zone in the CO-O₂ explosive reaction as the inert gas helium." In addition, his values for the transformation velocity S_t in mixtures containing 40 percent of CO or less are higher than those which he obtained in the absence of inert gas. This latter result is not only at wide variance with the present data, which show that a decrease in S_t results upon addition of both A and He regardless of the ratio of CO to O₂, but is also quite difficult to explain.

It is likewise very difficult to find a logical reason for the fact that his observed results vary as they do from the present results. The deviation is particularly noticeable for his results in the presence of A. Both the A and the He used in the present measurements were taken from cylinders procured by Stevens and it is probable that the gases which he used came from these same cylinders. In a few experiments with lean mixtures the He was used directly from the cylinder without purification, and an increase in flame speed was observed up to a certain concentration of impure He. This result indicates the presence of combustible material that burns more rapidly than CO. The presence of such materials in the He during Stevens'

measurements might account for a portion of the increase in flame speed in his lean mixtures containing this inert gas. As has been stated, these impurities were removed in the present experiments by passage over hot copper oxide and then charcoal immersed in liquid air.

The A, however, was used in both series without purification, except the passage over P₂O₅ in the present experiments. It is highly improbable that the A contains any impurities besides other members of the rare gas group and atmospheric air. None of these could conceivably produce the high values of flame speed observed by Stevens, this contention being amply verified by the present measurements. No satisfactory explanation has been found for the high values he obtained with A or for the identity of his values for A and He.

Since it is certain that large errors exist in the earlier measurements with A and He and since it is known, both from the results reported in reference 2 and those here presented, that an equation of the type $S_t = K[\text{CO}]^2[\text{O}_2]$ is inadequate to represent the more precise results in the absence of inert gas, it is futile to modify an equation of this type by an additive term to take into account the effect of inert gases. Stevens' equation

$$S_t = K_1[\text{CO}]^2[1 - \text{CO}]^a + \beta G_i$$

in which K_1 , a , and β are empirical constants, and G_i is the concentration of the inert gas, is therefore untrustworthy and the values of the constants K_1 and β found by Stevens are very different from those indicated by the more precise results. In fact, no constant values of K_1 and β , when substituted in the above equation, give an adequate representation of the present results.

CONCLUSIONS

The following conclusions are drawn from the results that have been presented.

1. The earlier belief (reference 2) that satisfactory agreement existed between values of S_t determined by the constant-volume and bubble methods has been confirmed over the entire range of mixture ratios.

2. Previous results (reference 1) indicated that an increase in the concentration of water vapor up to saturation at room temperature always produced an increase in the spatial velocity of flame in equivalent mixtures of CO and O₂. A comparison of the present results with those of reference 2 shows that this statement may be extended to include all values of mixture ratio, and that increasing the H₂O content of any mixture (up to saturation at least 25° C.) likewise results in decreased values of R_2 and increased values of S_t . The magnitude of these changes varies somewhat with mixture ratio.

3. The substitution of A or He for active mixture always produces a decrease in R_2 . Like quantities of

these inert gases have almost, if not exactly, the same effect upon R_2 .

4. Argon always produces a greater decrease in flame speed, both in space (S_s) and relative to the active gas (S_r), than does a like volume of helium.

5. Simultaneous changes in the concentration of H_2O and inert gas are inherent in the bubble method. It is shown that when the effects of the former are eliminated the values of R_2 become higher and those of S_s and S_r become lower than those shown in figures 3 to 10. In other words, the effects of A and He alone upon flame speed are actually somewhat greater than is shown in the graphs, while the effect upon expansion ratio is less.

6. The difference in the effect of A and He, which is shown directly in the present results, is independent of the ratio of fuel to oxygen.

7. This difference is a linear function of the concentration of inert gas above 7 percent. No explanation has been found for the different shape of this function at low concentrations of inert gas.

8. It is believed that the heat capacity of the inert gas influences the expansion ratio, and through it the spatial velocity of flame, but is of little or no importance in fixing the velocity of transformation of the active gases.

9. It is also believed that the free path of the molecules of an inert gas, which governs the rate at which other particles diffuse through it, is of primary impor-

tance in determining the effect of the inert gas upon the transformation velocity.

10. The present results disagree with previous measurements made by Stevens (reference 3) using the same method. The differences may be assigned in part to the inadequacy of the control of the concentration of water vapor in his experiments. Impurities in the He used by Stevens may have been responsible for a portion of the increase in flame speed which he observed upon addition of this gas to lean mixtures. For A, however, the cause of the difference still remains obscure.

NATIONAL BUREAU OF STANDARDS,
WASHINGTON, D. C., *September 25, 1935.*

REFERENCES

1. Flock, Ernest F., and King, H. Kendall: The Effect of Water Vapor on Flame Velocity in Equivalent CO-O₂ Mixtures. T. R. No. 531, N. A. C. A., 1935.
2. Flock, Ernest F., and Roeder, Carl H.: The Soap-Bubble Method of Studying the Combustion of Mixtures of CO and O₂. T. R. No. 532, N. A. C. A., 1935.
3. Stevens, F. W.: The Gaseous Explosive Reaction at Constant Pressure. The Effect of Inert Gases. Jour. Amer. Chem. Soc., vol. 50, no. 12, 1928, pp. 3244-3258.
4. Lewis, Bernard, and von Elbe, Guenther: On the Theory of Flame Propagation. Jour. Chem. Phys., vol. 2, August 1934, pp. 537-546.

REPORT No. 554

WIND-TUNNEL INVESTIGATION OF ORDINARY AND SPLIT FLAPS ON AIRFOILS OF DIFFERENT PROFILE

By CARL J. WENZINGER

SUMMARY

The Clark Y, the N. A. C. A. 23012, and the N. A. C. A. 23021 airfoils equipped with full-span ordinary flaps and with full-span simple split flaps were tested in the N. A. C. A. 7- by 10-foot wind tunnel. The principal object of the tests was to determine the characteristics of the airfoils with ordinary flaps and, in addition, to determine the relative merits of the various airfoils when equipped with either ordinary flaps or with simple split flaps. The Clark Y airfoil was tested with 3 widths of ordinary flap, 10, 20, and 30 percent of the airfoil chord. The optimum width of the ordinary and the simple split flap based on the maximum lift attained with the Clark Y airfoil was then tested on each of the other two airfoils.

The optimum width of ordinary flap for maximum lift attainable was found to be the same as that of the split flap, 20 percent of the airfoil chord. The split flap produced somewhat greater increases in $C_{L_{max}}$ on the airfoils tested than did the ordinary flap of the same width, but the L/D at maximum lift was practically the same for the two types of flap. Any gap between the airfoil and the leading edge of ordinary flaps had a very detrimental effect on the $C_{L_{max}}$ attainable. Based principally on factors affecting airplane performance, the relative order of merit of the airfoils tested with either ordinary or split flaps is N. A. C. A. 23012, Clark Y, and N. A. C. A. 23021. The hinge-moment coefficients (based on flap chord and area) of the full-span ordinary flaps were practically independent of flap chord; the actual hinge moments varied approximately as the square of the chord. In addition, the hinge-moment coefficients of the split flaps were practically the same as those of full-span ordinary flaps of corresponding widths.

INTRODUCTION

Many experimental investigations have been made of various types of flap for increasing, in particular, the maximum lift of airplanes as an aid to improved performance. Among the devices already investigated in considerable detail by the N. A. C. A. are simple split flaps, split flaps of the Zap type, Fowler flaps, and external-airfoil flaps. Some uncorrelated data are also available from various sources on slotted flaps and on

ordinary flaps. Because of the simplicity of ordinary flaps and the lack of correlated data on them as a lift-increasing device, it appeared desirable to make a more complete investigation of this type of flap.

Three basic airfoil sections were used in the present tests to obtain an estimate of the effect of airfoil section and thickness. In addition to the Clark Y, the N. A. C. A. 23012 airfoil was selected as being representative of the best airfoils at present available for use on conventional airplanes, and the N. A. C. A. 23021 airfoil was selected as a representative thick section. Three widths of ordinary flap were tested on the Clark Y airfoil, and one width on each of the other two airfoils. For purposes of comparison one simple split flap was also tested on the N. A. C. A. 23012 and 23021 airfoils, and data are included from previous tests of the Clark Y airfoil with a split flap. The aerodynamic characteristics of the airfoils with all the different flaps were measured and, in addition, hinge moments were obtained for the ordinary flaps on the Clark Y airfoil.

MODELS AND TESTS

Models.—Mahogany models of the Clark Y, the N. A. C. A. 23012, and the N. A. C. A. 23021 airfoil sections were tested. The span of each model was 60 inches and the chord 10 inches. The Clark Y airfoil with the 3 widths of ordinary flap tested (10, 20, and 30 percent of the wing chord) is shown in figure 1. These flaps are arranged to lock rigidly to the airfoil or to rotate freely about their respective hinge axes. The other two airfoils are shown with ordinary flaps in figure 2 and with split flaps in figure 3.

The ordinates of the airfoil sections are included with the charts of their aerodynamic characteristics in figures 4, 5, and 6. The size of flap that gave the highest value of the maximum lift coefficient for the Clark Y airfoil together with reasonable hinge moments (20-percent-chord flap) was used with the N. A. C. A. 23012 and the N. A. C. A. 23021 airfoils.

Tests.—The tests were made in the N. A. C. A. 7- by 10-foot wind tunnel which, together with associ-

ated apparatus and standard test procedure, is described in reference 1. The dynamic pressure was maintained constant at 16.37 pounds per square foot, which corresponds to an air speed of 80 miles per hour under standard sea-level conditions. The average Reynolds Number for the tests was 609,000, based on the air speed and on the 10-inch airfoil chord. Lift,

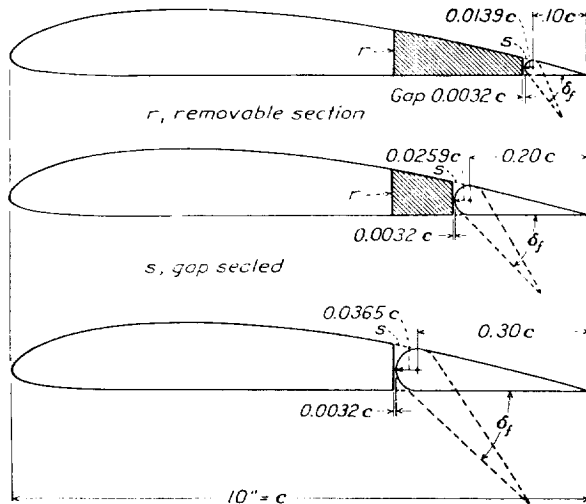


FIGURE 1.—Full-span ordinary flaps tested on the Clark Y airfoil.

drag, and pitching moments were measured for all flap arrangements with flap deflections from 0° to beyond those for maximum lift. The angle-of-attack range covered was from below zero lift to beyond the stall of the airfoil. Hinge moments were also measured for the three widths of ordinary flap on the Clark Y airfoil.

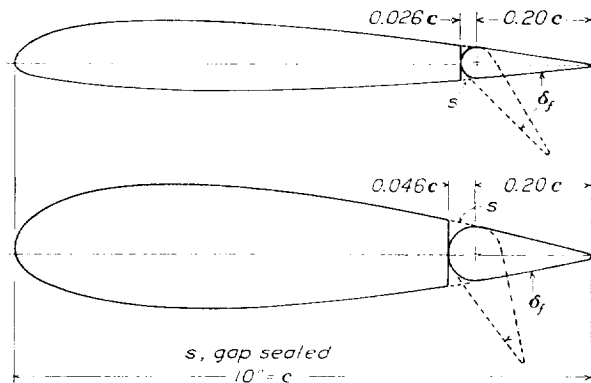


FIGURE 2.—Full-span ordinary flaps tested on the N. A. C. A. 23012 and N. A. C. A. 23021 airfoils.

These moments were obtained by the methods given in reference 2, which presents results of hinge-moment tests on split flaps of various chords.

RESULTS

Results of the investigation are given in standard nondimensional coefficient form for the following four coefficients:

$$C_L = \frac{\text{lift}}{qS}$$

$$C_D = \frac{\text{drag}}{qS}$$

$$C_{m_{c/4}} = \frac{\text{pitching moment about quarter chord}}{qSc}$$

$$C_{h_f} = \frac{\text{flap hinge moment}}{qS_f c_f}$$

in which

S , airfoil area.

S_f , flap area.

c , airfoil chord.

c_f , flap chord.

q , dynamic pressure.

The data were corrected for the effects of the jet boundaries and for the tunnel static-pressure

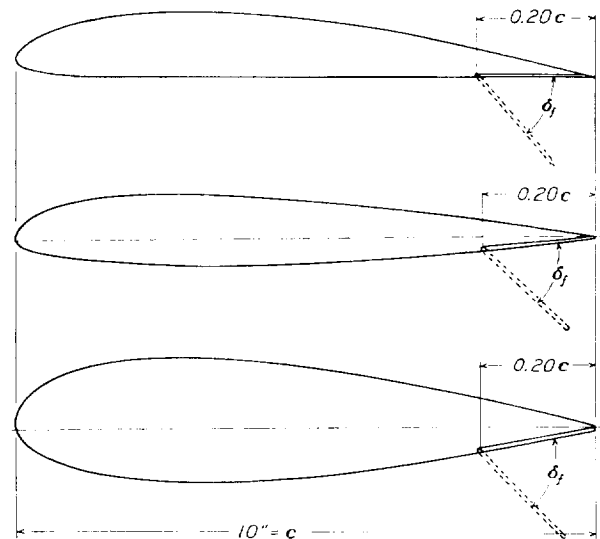


FIGURE 3.—Full-span split flaps tested on the Clark Y, the N. A. C. A. 23012, and the N. A. C. A. 23021 airfoils.

gradient. The standard jet-boundary corrections, $\Delta\alpha = \delta \frac{S}{C} C_L \times 57.3$, in degrees, and $\Delta C_D = \delta \frac{S}{C} C_L^2$, where C is the jet cross-sectional area, were used. The value of factor $\delta = -0.165$ was taken as being most nearly representative of the boundary effect in the 7- by 10-foot wind tunnel. (See reference 3.) The longitudinal static-pressure gradient in the 7- by 10-foot wind tunnel produces an additional downstream force on the model. This force corresponds to a value of $\Delta C_D = 0.0015$ for rectangular airfoils of thickness equal to 12 percent of the chord and $\Delta C_D = 0.0029$ for an airfoil having a thickness of 21 percent of the chord. These values were obtained in accordance with methods given in reference 4.

DISCUSSION

PLAIN AIRFOILS

Complete aerodynamic characteristics of the three plain airfoils are given in figures 4, 5, and 6. These characteristics include those for the three airfoils of

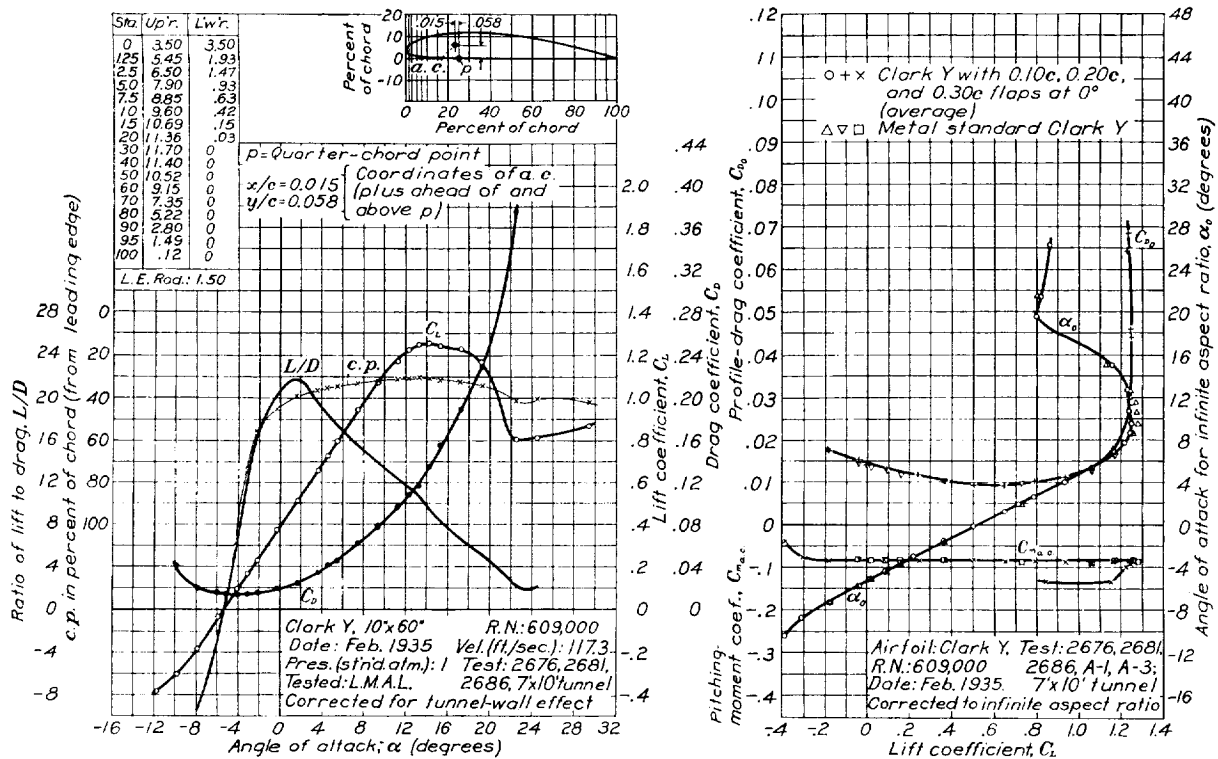


FIGURE 4.—The Clark Y airfoil.

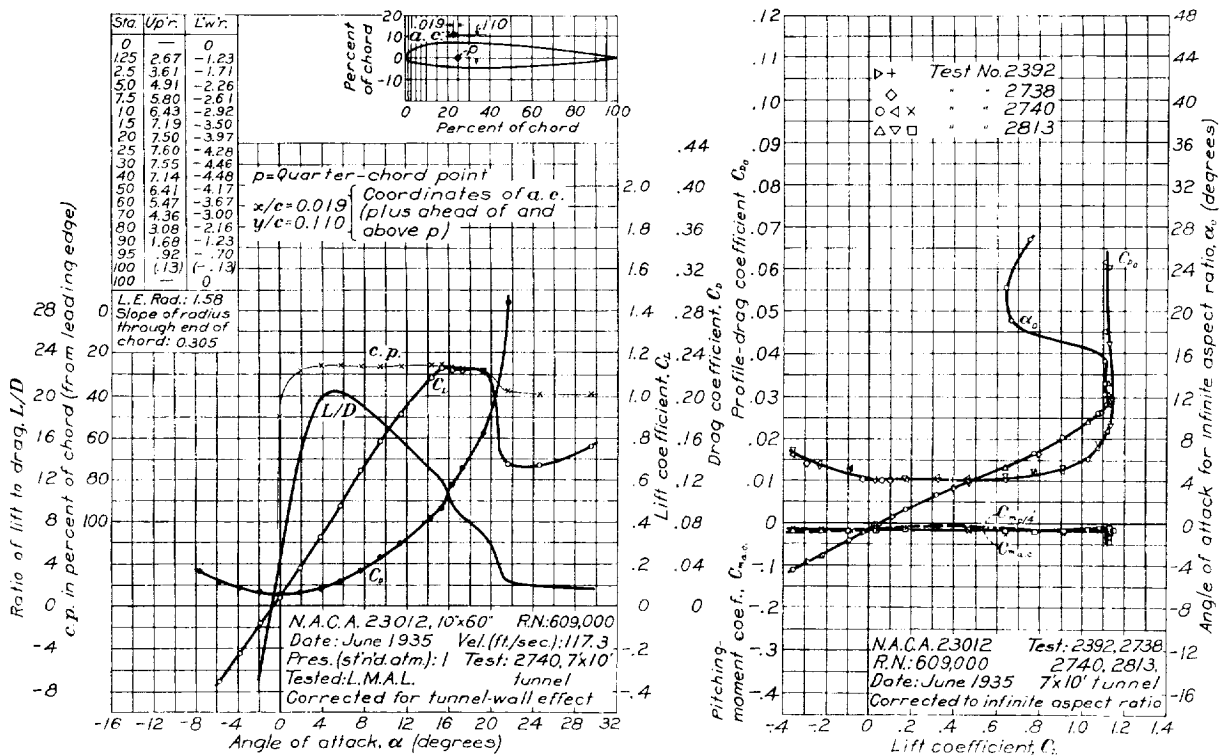


FIGURE 5.—The N. A. C. A. 23012 airfoil

aspect ratio 6 corrected to free-air conditions, profile-drag coefficients, and angle of attack for infinite aspect ratio.

AIRFOILS WITH FLAPS

Clark Y airfoil with ordinary flap.—Lift, drag, and center-of-pressure characteristics for the airfoil with the 10-percent-chord flap are given in figure 7. These results are for the airfoil with the gap between the flap and main portion of the airfoil completely sealed with plasticine. Values of L/D and $C_{m_{c/4}}$ for the 10-percent-chord flap are given in figure 8. Values of $C_{L_{max}}$ and values of L/D and C_D at $C_{L_{max}}$ are given in figure 9 for different deflections of the 10-percent-chord flap. The latter characteristics are given for the conditions in which the gap between the flaps and the main portion

from references 5 and 6.) The effects on $C_{L_{max}}$ are shown and the effects on L/D and C_D at $C_{L_{max}}$. From these results it may be concluded that split flaps of the same width give somewhat higher maximum lifts than do ordinary flaps. Values of L/D and C_D at $C_{L_{max}}$ are nearly the same for both types of flap. Practically no further gain in maximum lift is obtained by increasing the flap chord beyond 20 percent of the airfoil chord, the data indicating that with wider split flaps the maximum lift remains about the same but that it drops off with wider ordinary flaps. The optimum width of either ordinary or split flaps for maximum lift appears to be 20 percent of the airfoil chord.

Clark Y airfoil with a 20-percent-chord split flap.—For comparison with tests of the N. A. C. A. 23012 and N. A. C. A. 23021 airfoils having split flaps, the

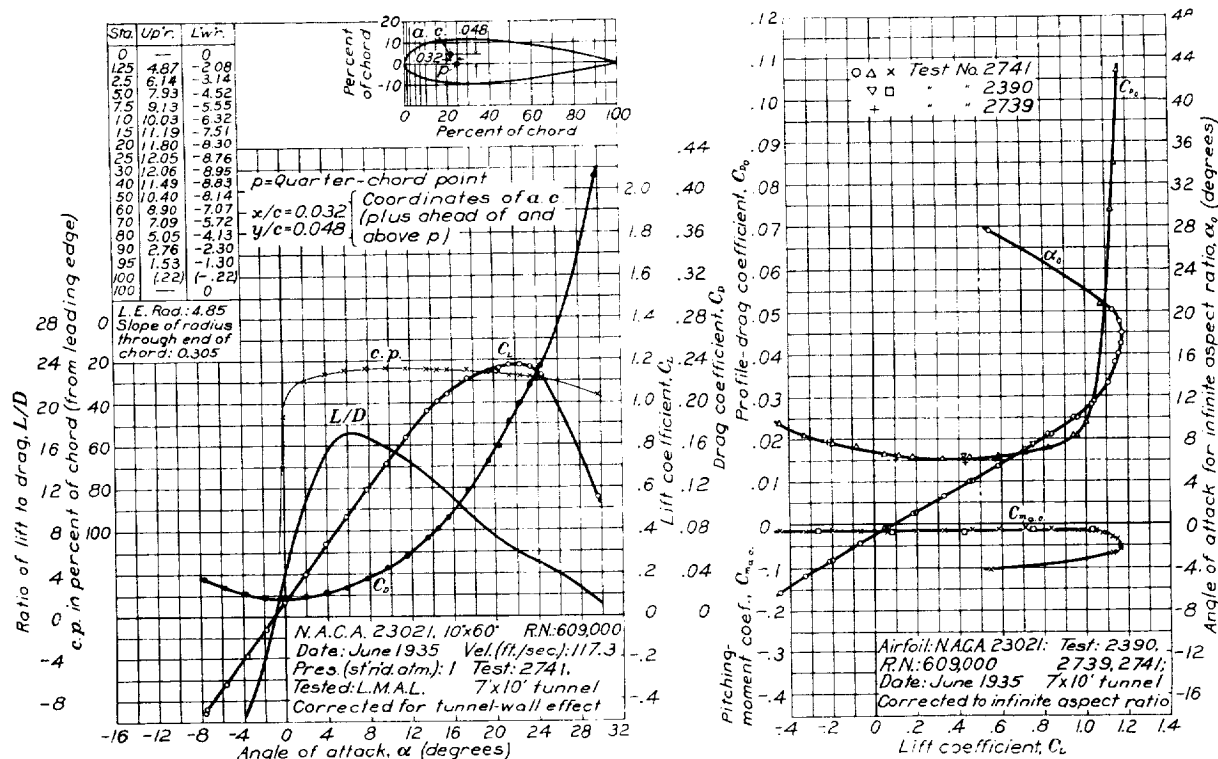


FIGURE 6.—The N. A. C. A. 23021 airfoil.

of the airfoil is both open and sealed. It will be noted from figure 9 that even a small open gap had a very detrimental effect on the maximum lift of the airfoil. It is therefore essential to keep the flap gaps completely sealed to obtain the best characteristics with ordinary flaps. Similar charts for the airfoil with a 20-percent-chord flap are shown in figures 10, 11, and 12. Charts for the airfoil with a 30-percent-chord flap are given in figures 13, 14, and 15.

Optimum sizes of ordinary and split flaps on the Clark Y airfoils.—Figure 18 gives a comparison of different widths of ordinary and of split flaps on Clark Y airfoils. (The data for the split flaps are taken

lift, the drag, and the center-of-pressure characteristics for a Clark Y airfoil with a 20-percent-chord split flap are given in figure 16. These data were taken from reference 6 and have been corrected for a wing of aspect ratio 6 in free air. The L/D and $C_{m_{c/4}}$ for the Clark Y airfoil with split flap are given in figure 17. A comparison of 20-percent-chord ordinary and split flaps on a Clark Y airfoil is given in figure 19. This figure shows the variation of $C_{L_{max}}$ and of L/D and C_D at $C_{L_{max}}$ for different flap deflections. As previously noted, the split flap gives a somewhat higher maximum lift than does the ordinary flap but has slight effect on the other factors.

N. A. C. A. 23012 airfoil with 20-percent-chord ordinary and split flaps.—Lift, drag, and center-of-pressure characteristics are given in figure 20 for a

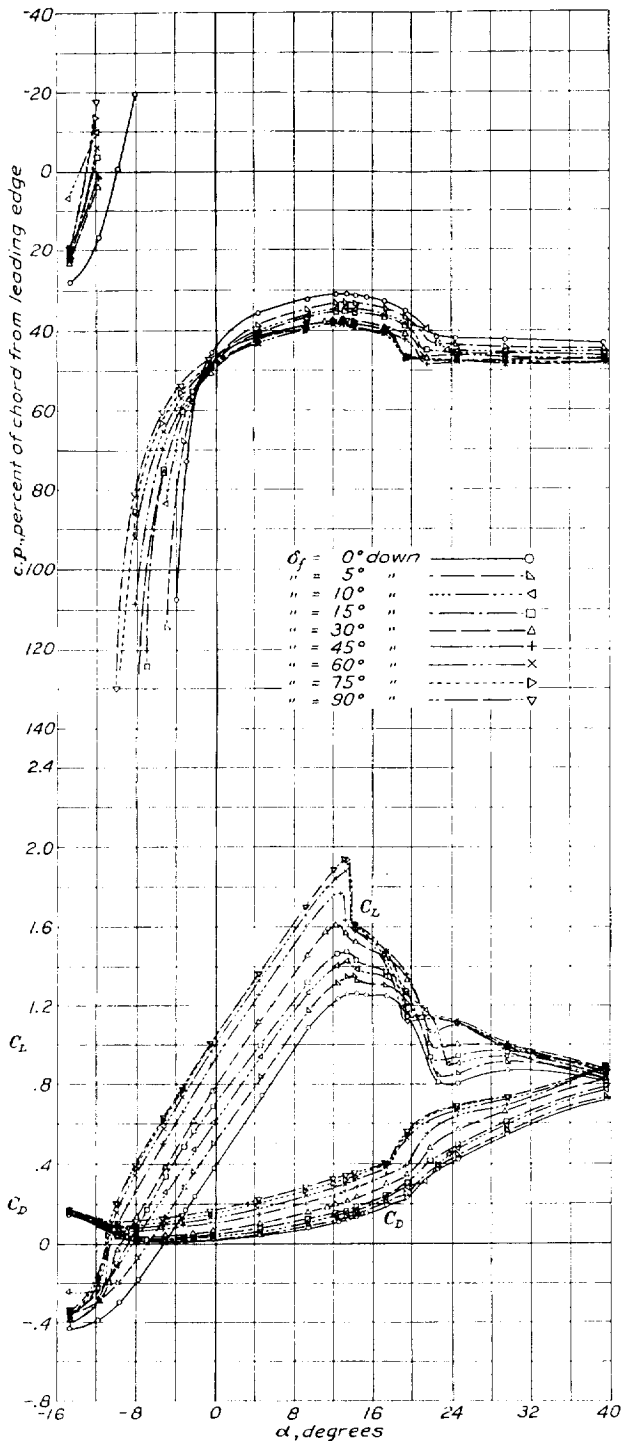


FIGURE 7.—Lift, drag, and center of pressure for the Clark Y airfoil with 0.10c full-span ordinary flap. Flap gap sealed.

20-percent-chord ordinary flap on the N. A. C. A. 23012 airfoil. The L/D and $C_{m_{c/4}}$ for the 20-percent-chord ordinary flap are given in figure 21. Similar

curves for 20-percent-chord split flaps are given in figures 22 and 23. A comparison of ordinary and

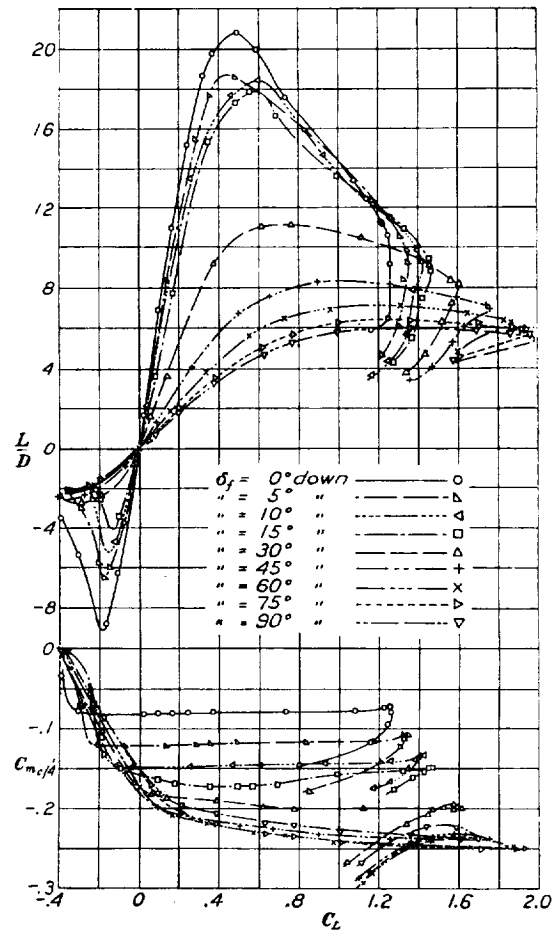


FIGURE 8.—Lift-drag ratio and pitching-moment coefficient for the Clark Y airfoil with 0.10c full-span ordinary flap. Flap gap sealed.

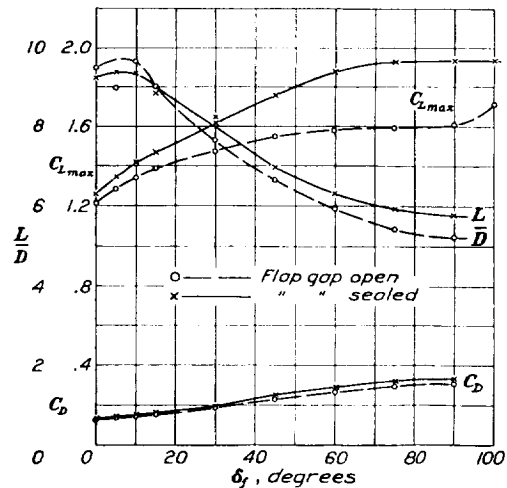


FIGURE 9.—Effect of flap deflection on maximum lift, and on lift-drag ratio and drag at maximum lift. The 0.10c full-span ordinary flap on the Clark Y airfoil.

split flaps on the N. A. C. A. 23012 airfoil is given in figure 24. This figure shows the effects of $C_{L_{max}}$ as well as of L/D and C_D at $C_{L_{max}}$ for different flap deflec-

tions. As in the case of the Clark Y airfoil, the split flap gave a higher maximum lift on the N. A. C. A.

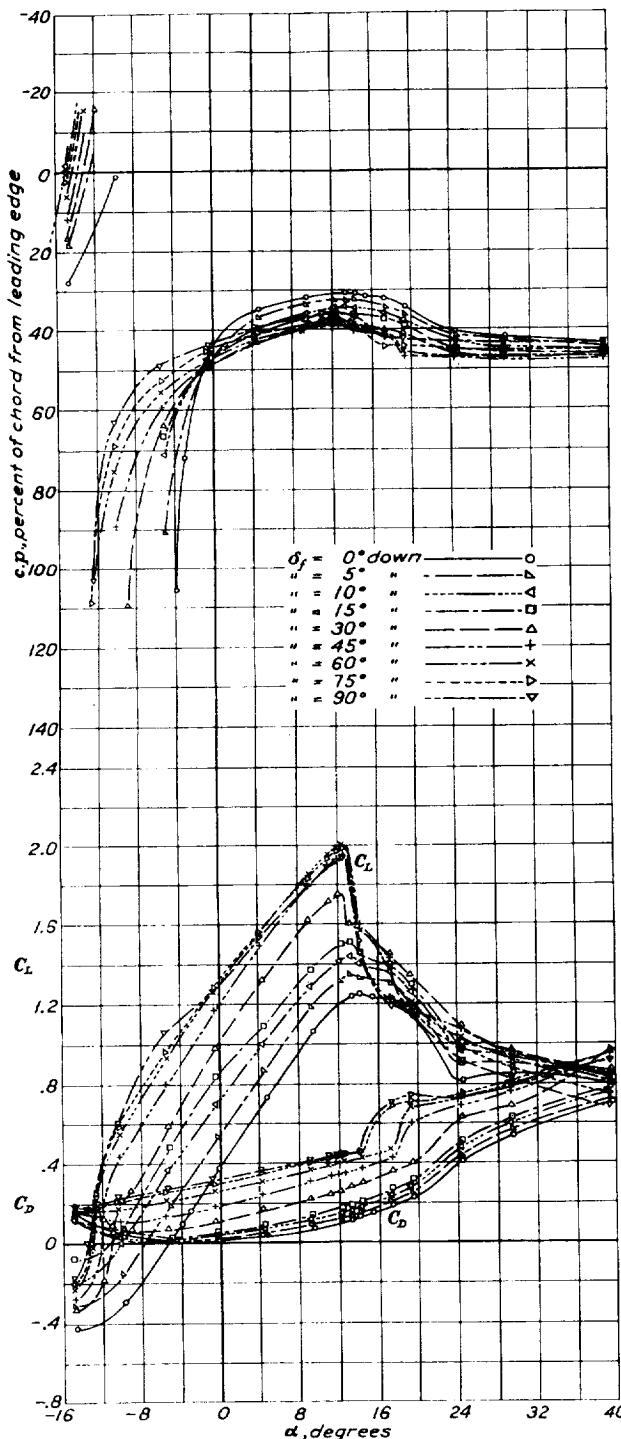


FIGURE 10.—Lift, drag, and center of pressure for the Clark Y airfoil with 0.20c full-span ordinary flap. Flap gap sealed.

23012 airfoil than did the ordinary flap. In addition, the two types of flap had almost the same effect on the other factors considered.

N. A. C. A. 23021 airfoil with 20-percent-chord ordinary and split flaps.—Charts similar to those for

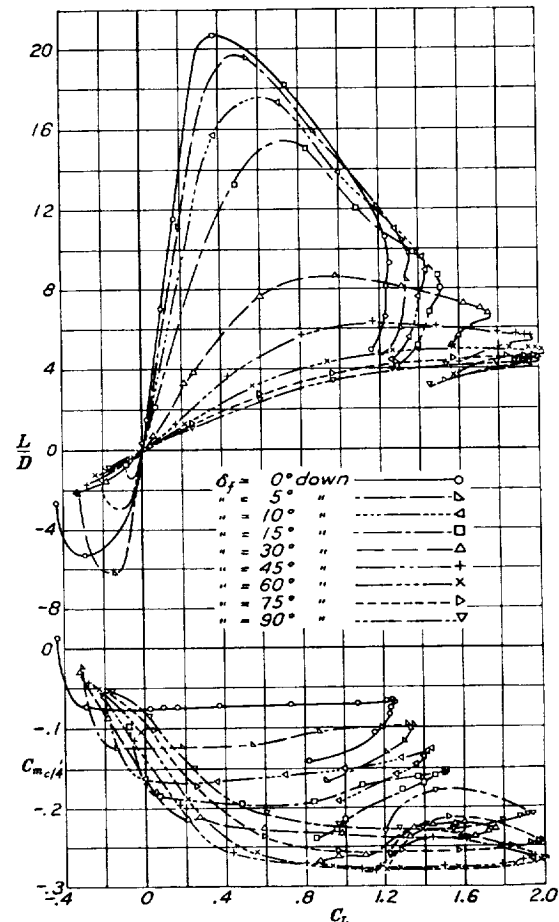


FIGURE 11.—Lift-drag ratio and pitching-moment coefficient for the Clark Y airfoil with 0.20c full-span ordinary flap. Flap gap sealed.

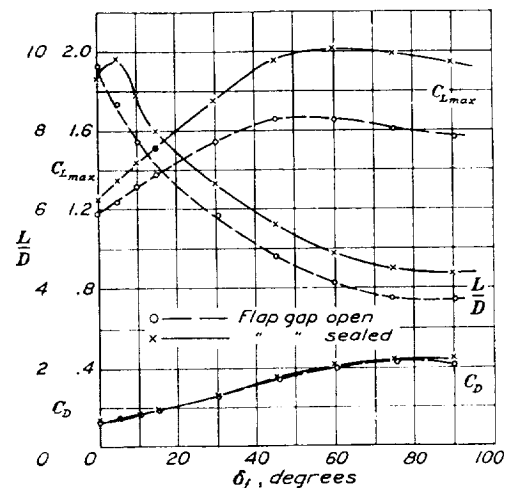


FIGURE 12.—Effect of flap deflection on maximum lift, and on lift-drag ratio and drag at maximum lift. The 0.20c full-span ordinary flap on the Clark Y airfoil.

the N. A. C. A. 23012 airfoil are given for the N. A. C. A. 23021 airfoil with flaps in figures 25, 26, 27, 28,

and 29. The ordinary and split flaps on the N. A. C. A. 23021 airfoil also showed the same relative

Comparison of lift effects of 20-percent-chord ordinary and split flaps on Clark Y, N. A. C. A. 23012,

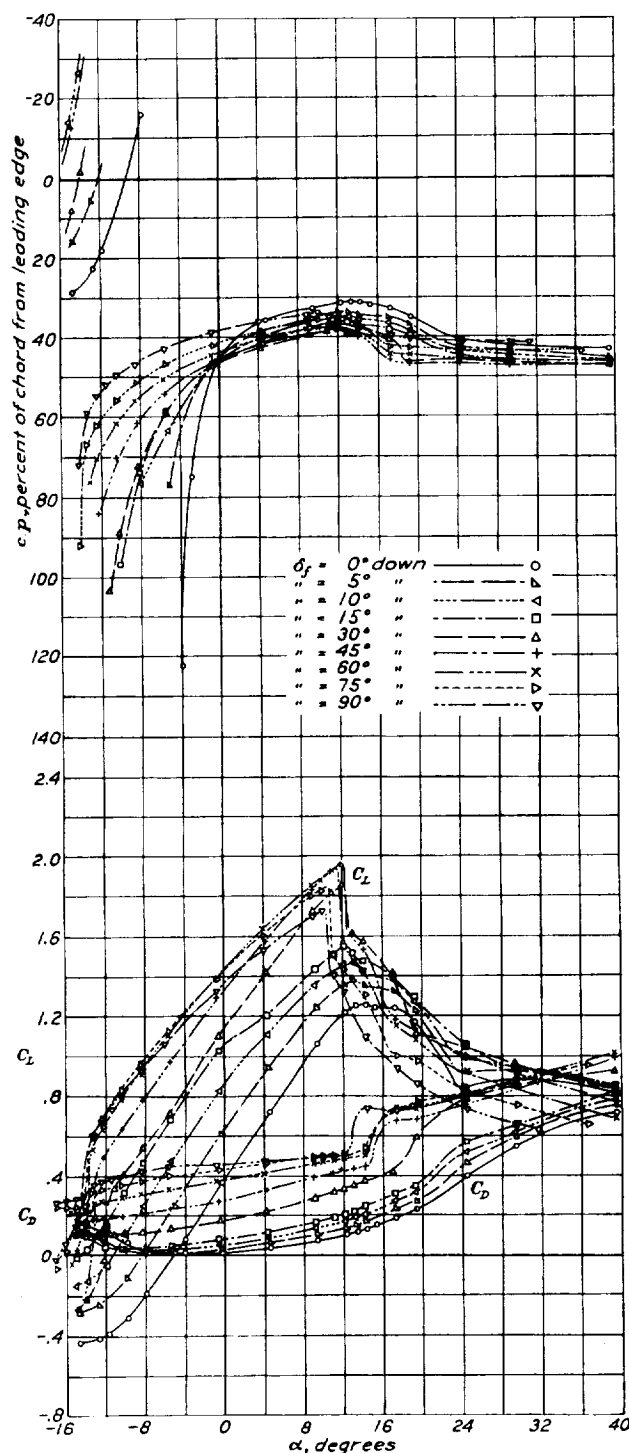


FIGURE 13.—Lift, drag, and center of pressure for the Clark Y airfoil with 0.30c full-span ordinary flap. Flap gap sealed.

effects as they did on the Clark Y and on the N. A. C. A. 23012 airfoils.

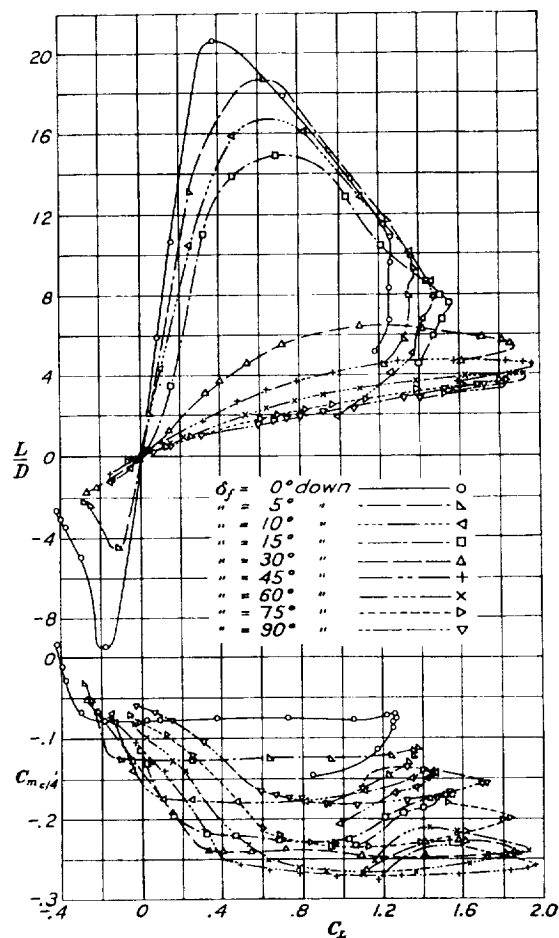


FIGURE 14.—Lift-drag ratio and pitching-moment coefficient for the Clark Y airfoil with 0.30c full-span ordinary flap. Flap gap sealed.

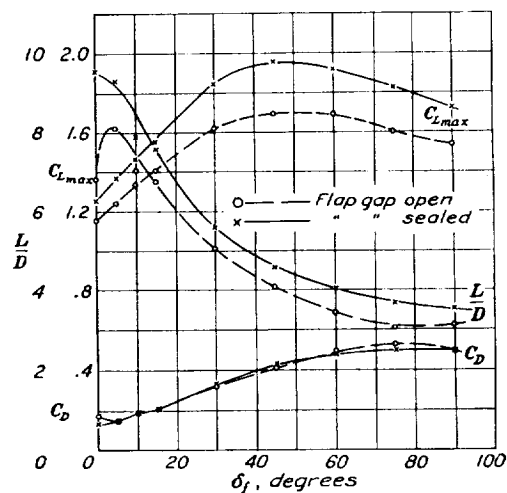


FIGURE 15.—Effect of flap deflection on maximum lift, and on lift-drag ratio and drag at maximum lift. The 0.30c full-span ordinary flap on the Clark Y airfoil.

and N. A. C. A. 23021 airfoils.—Table I shows the effects at a test Reynolds Number of 609,000 on the

maximum lift coefficient with flaps neutral; on the maximum lift coefficient with flaps deflected; on the increment in maximum lift coefficient due to the two

Somewhat higher maximum lift coefficients and greater increments in maximum lift were given by the

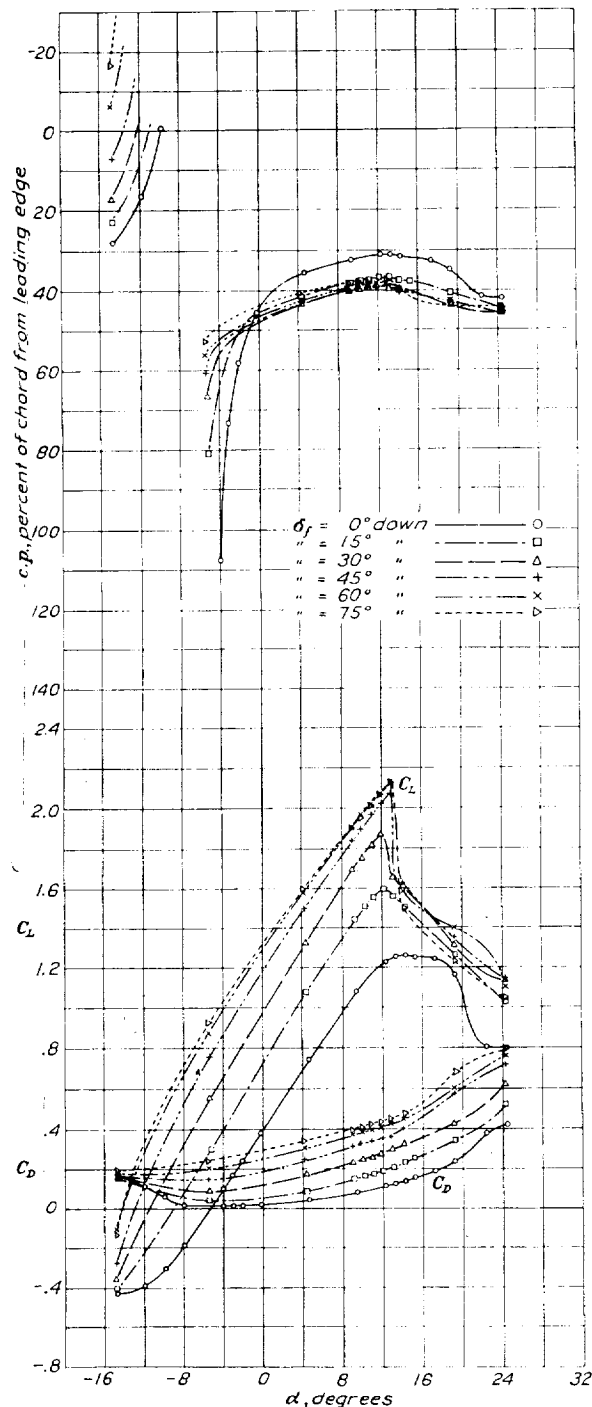


FIGURE 16.—Lift, drag, and center of pressure for Clark Y airfoil with 0.20c full-span split flap. (Data from reference 6.)

types of flaps on various airfoils; on the ratio of maximum lift to minimum drag; and on the ratio of lift to drag at maximum lift.

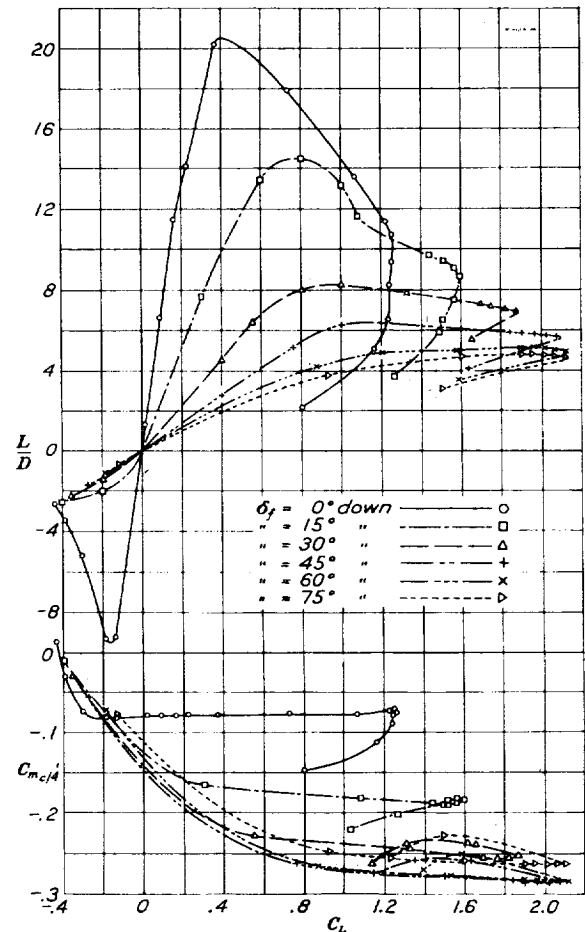


FIGURE 17.—Lift-drag ratio and pitching-moment coefficient for the Clark Y airfoil with 0.20c full-span split flap.

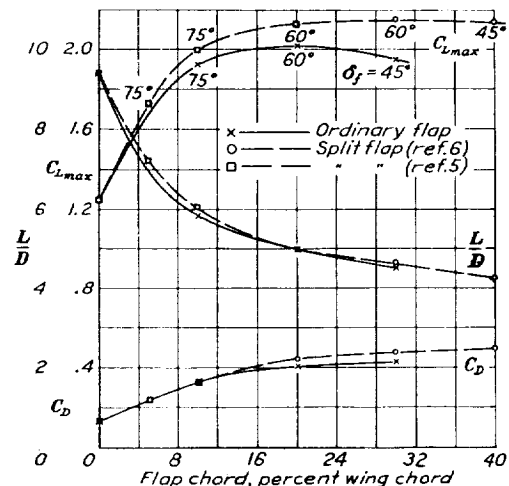


FIGURE 18.—Effect of flap chord on maximum lift, and on lift-drag ratio and drag at maximum lift for both ordinary and split flaps on the Clark Y airfoil.

split flap than by ordinary flaps on the three airfoils tested. The highest maximum lift coefficient and the

greatest increment in maximum lift were both given by flaps on the N. A. C. A. 23021 airfoil. In this case an lift above that of the plain airfoil of more than 100 percent. The highest speed-range ratio $C_{L_{max}}/C_{D_{min}}$ was given, however, by flaps on the N. A. C. A. 23012 air-

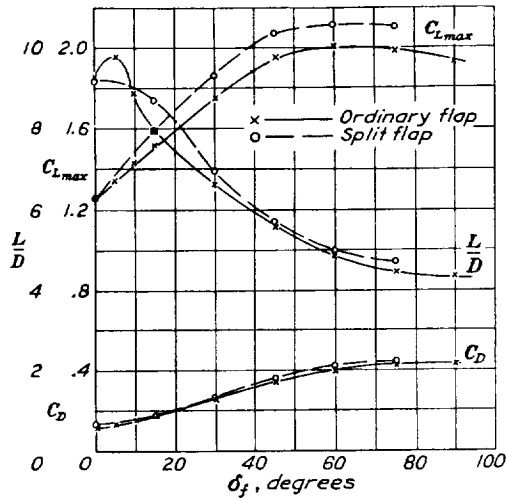


FIGURE 19.—Effect of flap deflection on maximum lift, and on lift-drag ratio and drag at maximum lift. The 0.20c full-span ordinary and split flaps on the Clark Y airfoil.

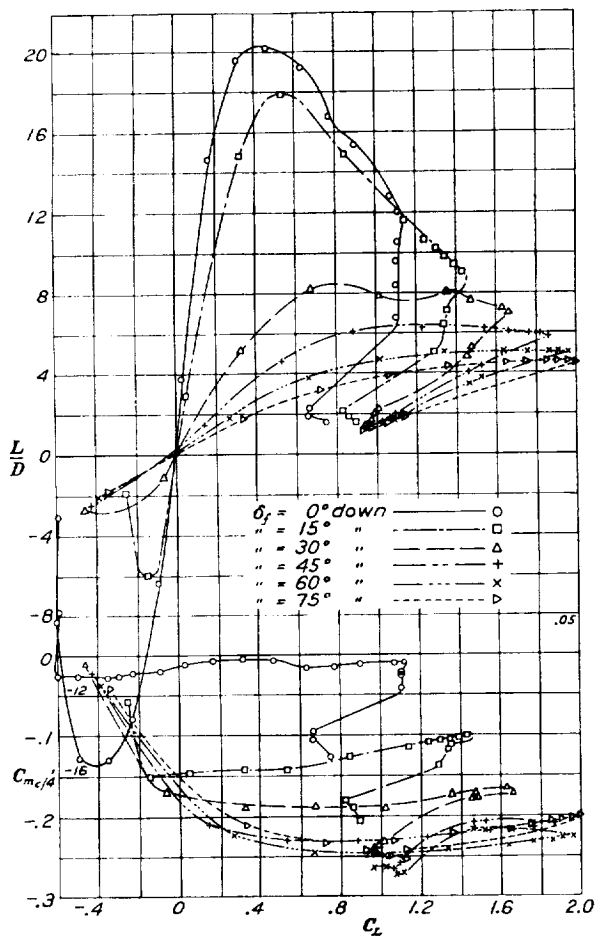


FIGURE 21.—Lift-drag ratio and pitching-moment coefficient for the N. A. C. A. 23012 airfoil with 0.20c full-span ordinary flap. Flap gap sealed.

increment in maximum lift coefficient of 1.193 was obtained, which represents an increase in the maximum

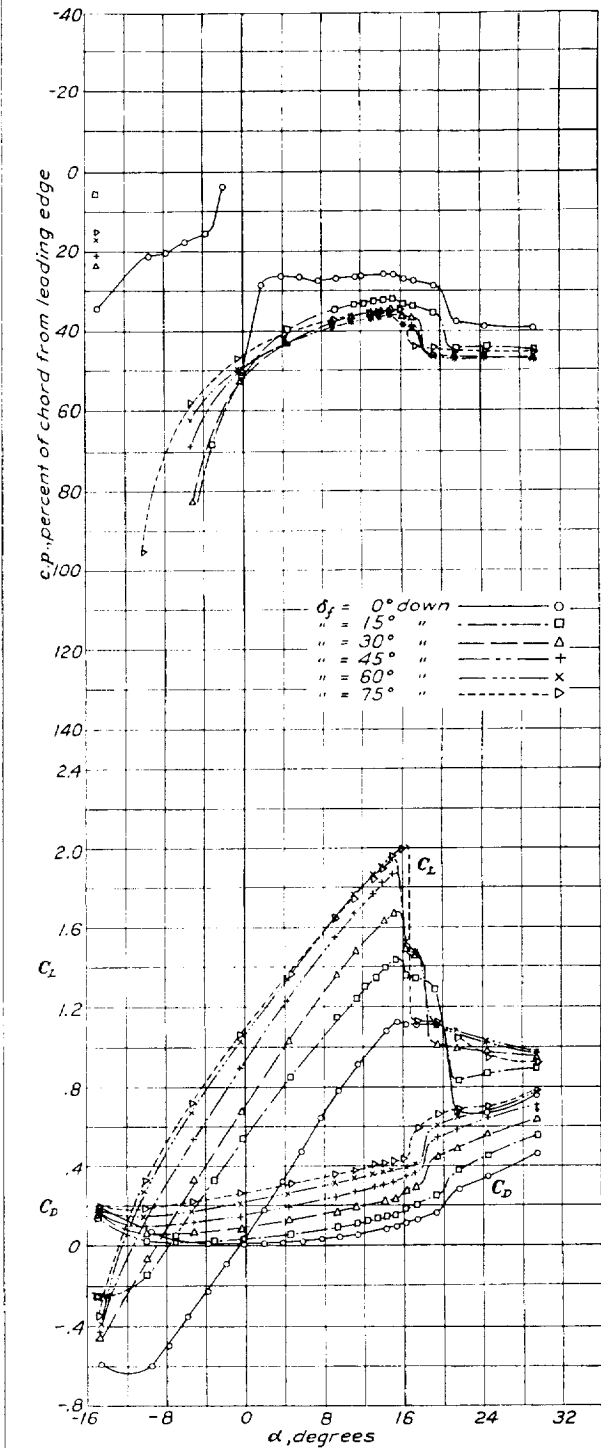


FIGURE 20.—Lift, drag, and center of pressure for the N. A. C. A. 23012 airfoil with 0.20c full-span ordinary flap. Flap gap sealed.

foil, which has a lower maximum lift but which also has a considerably lower minimum drag. The steepest

gliding angle attainable (indicated by L/D at $C_{L_{max}}$) is the same with either type of flap on the particular airfoil considered.

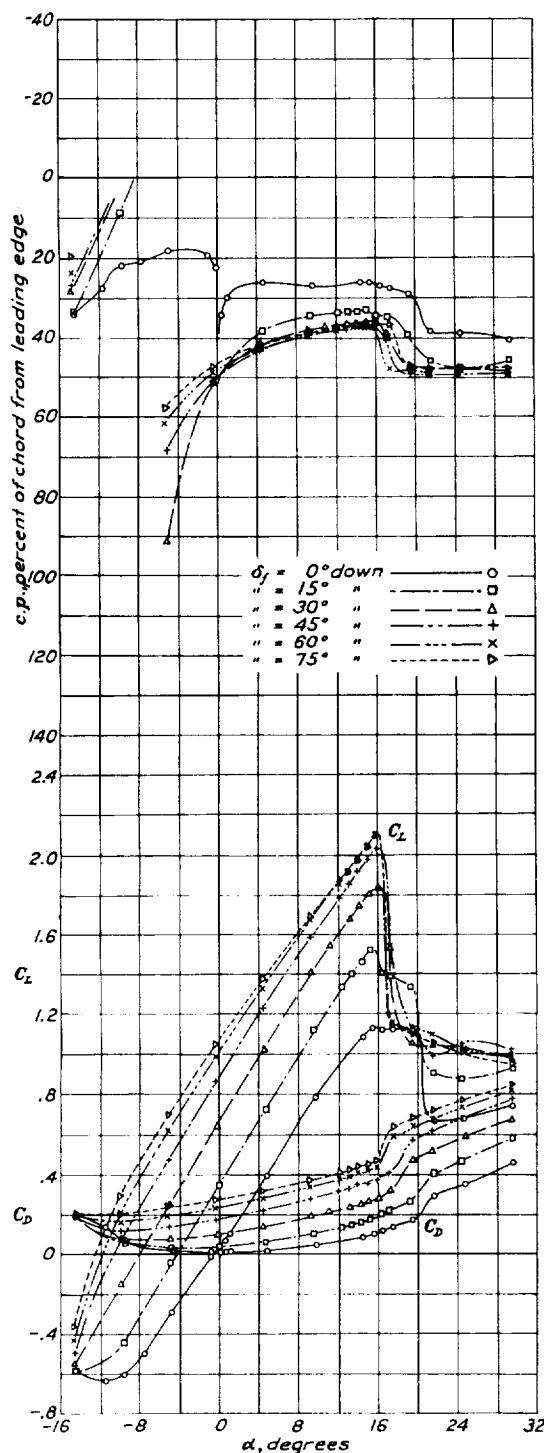


FIGURE 22.—Lift, drag, and center of pressure for the N. A. C. A. 23012 airfoil with 0.20c full-span split flap.

Some tests in the full-scale tunnel and in the variable-density tunnel (reference 7) indicate that the maximum

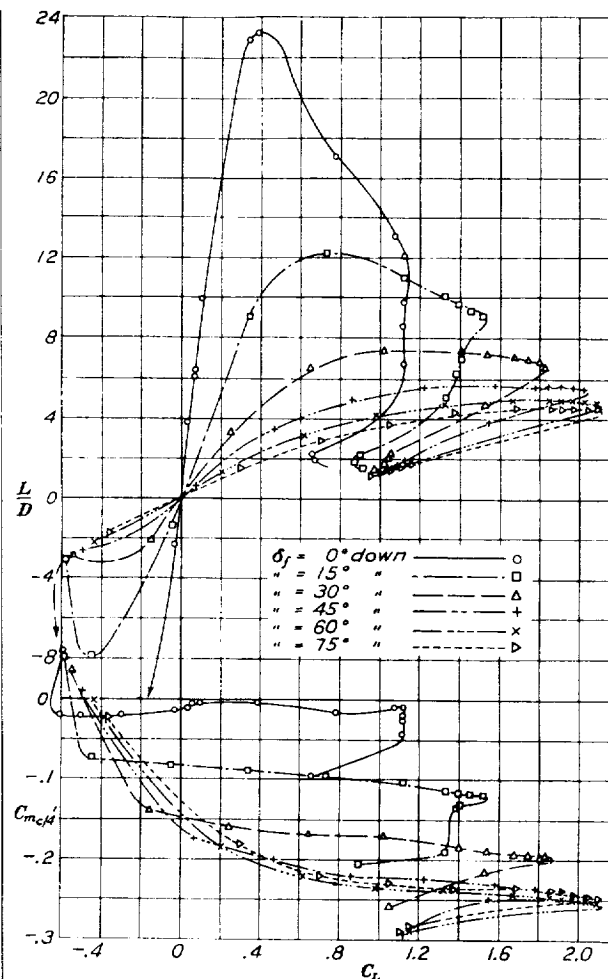


FIGURE 23.—Lift-drag ratio and pitching-moment coefficient for the N. A. C. A. 23012 airfoil with 0.20c full-span split flap.

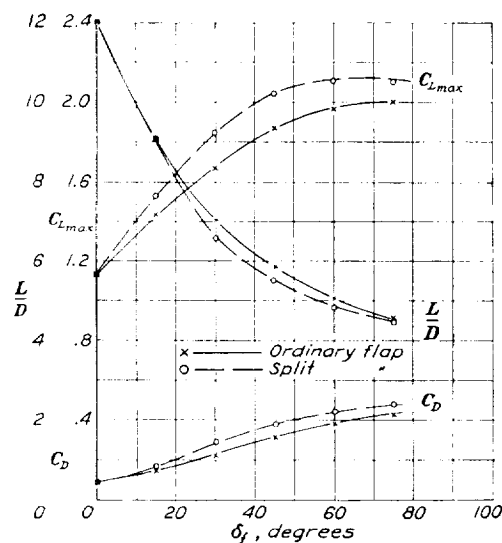


FIGURE 24.—Effect of flap deflection on maximum lift, and on lift-drag ratio and drag at maximum lift. The 0.20c full-span ordinary and split flaps on the N. A. C. A. 23012 airfoil.

lift of the N. A. C. A. 23012 airfoil is equal to or slightly greater than that of the Clark Y airfoil in the normal full-scale range of the Reynolds Number. Further-

maximum lift than the Clark Y. Thus, it appears that the N. A. C. A. 23012 plain wing will have some ad-

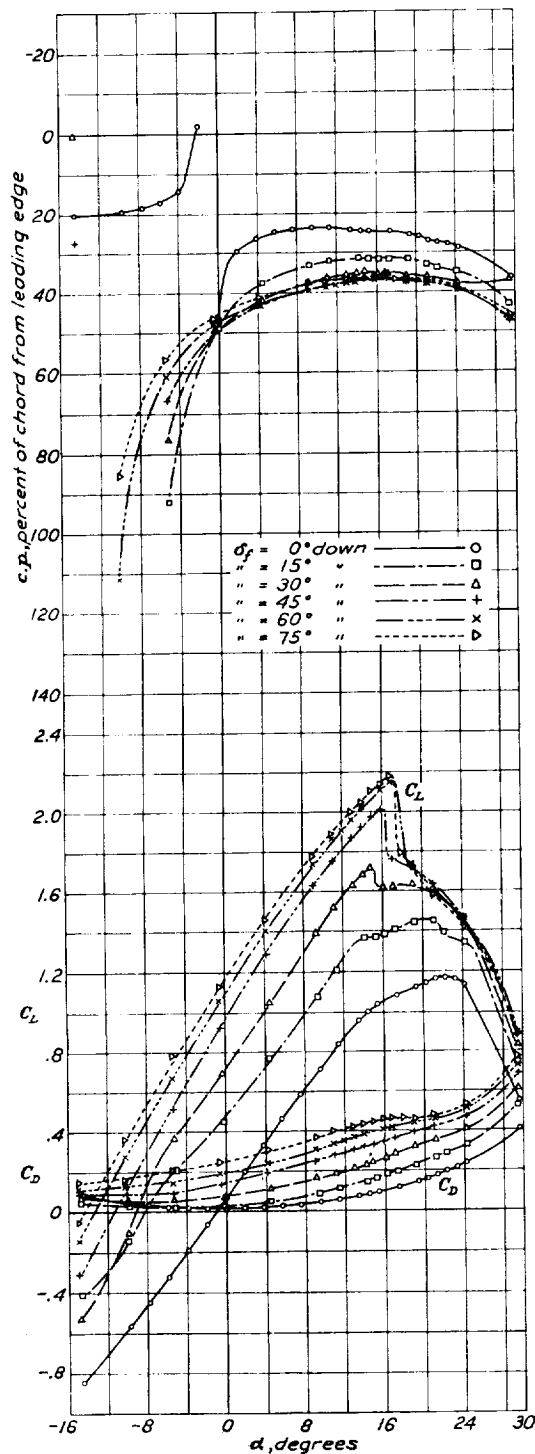


FIGURE 25.—Lift, drag, and center of pressure for the N. A. C. A. 23021 airfoil with 0.20c full-span ordinary flap. Flap gap sealed.

more, recent tests in the variable-density tunnel show that at large as well as at small Reynolds Numbers the N. A. C. A. 23021 airfoil has considerably lower

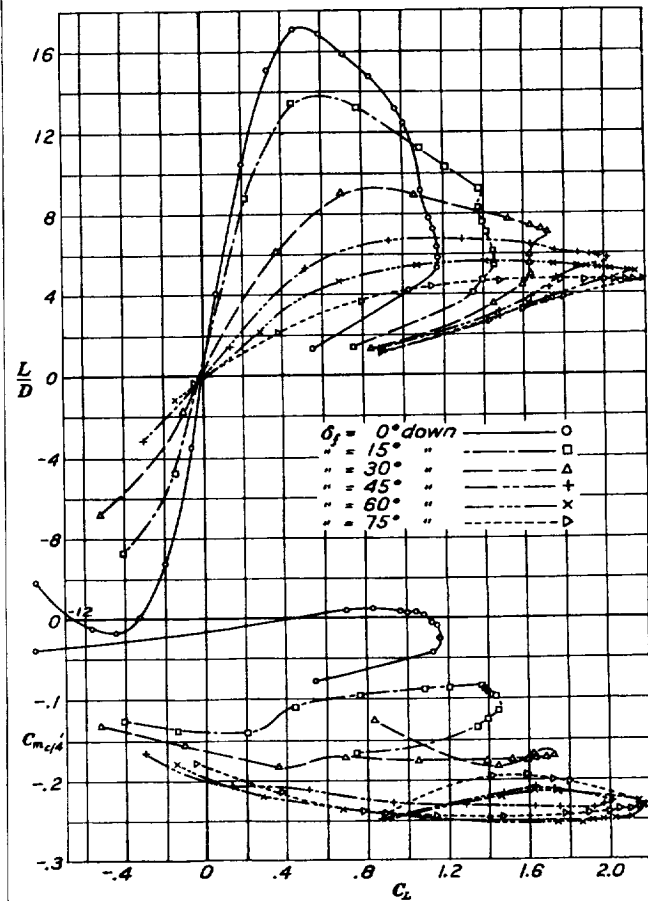


FIGURE 26.—Lift-drag ratio and pitching-moment coefficient for the N. A. C. A. 23021 airfoil with 0.20c full-span ordinary flap. Flap gap sealed.

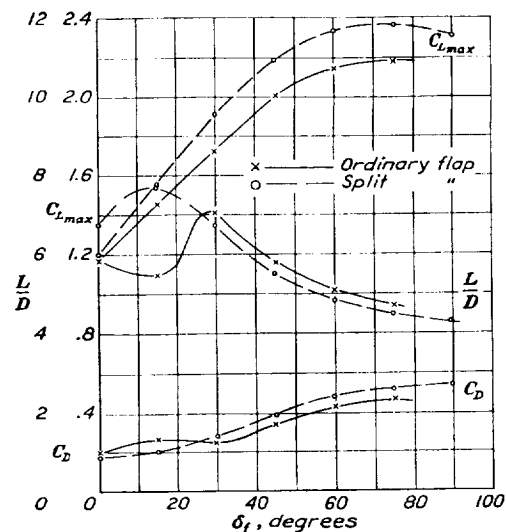


FIGURE 27.—Effect of flap deflection on maximum lift, and on lift-drag ratio and drag at maximum lift. The 0.20c full-span ordinary and split flaps on the N. A. C. A. 23021 airfoil.

vantages over the Clark Y or N. A. C. A. 23021 wings in the full-scale range of the Reynolds Number that

are not shown by low-scale tests if the lift increments due to the flaps are not adversely affected. Experimental data (unpublished) have shown that actually the increments in maximum lift due to split flaps on medium-thick airfoils vary but little with Reynolds Number. In connection with the present investigation, a few tests were made in the variable-density tunnel to determine the scale effect on $C_{L_{max}}$ at high

(Effective Reynolds Number = test $R \times \frac{\text{critical } R \text{ free air}}{\text{critical } R \text{ tunnel}}$. See reference 7.) The value of the factor is 1.4 for the 7- by 10-foot wind tunnel and 2.6 for the variable-density wind tunnel. The data show that the scale effect is about the same for the N. A. C. A. 23021 airfoil with the flap deflected downward 75° as it is for

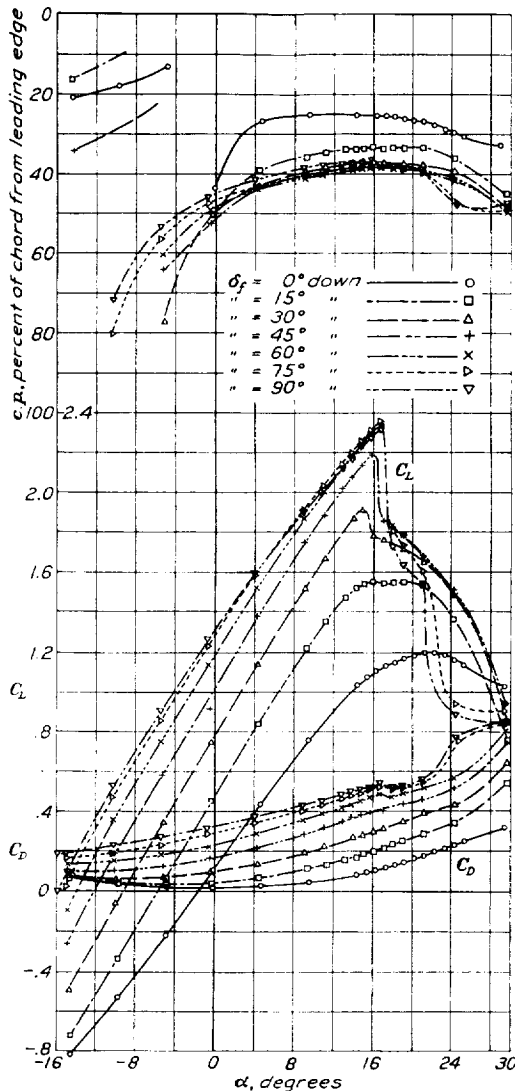


FIGURE 28.—Lift, drag, and center of pressure for the N. A. C. A. 23021 airfoil with 0.20c full-span split flap.

Reynolds Numbers of the N. A. C. A. 23021 airfoil (a thick section) with a 20-percent-chord split flap. The results of the scale-effect tests are given in figure 30 in which $C_{L_{max}}$ for the N. A. C. A. 23021 airfoil with the flap neutral and with the flap deflected downward 75° is plotted against "effective" Reynolds Number both for the 7- by 10-foot and the variable-density wind tunnels.

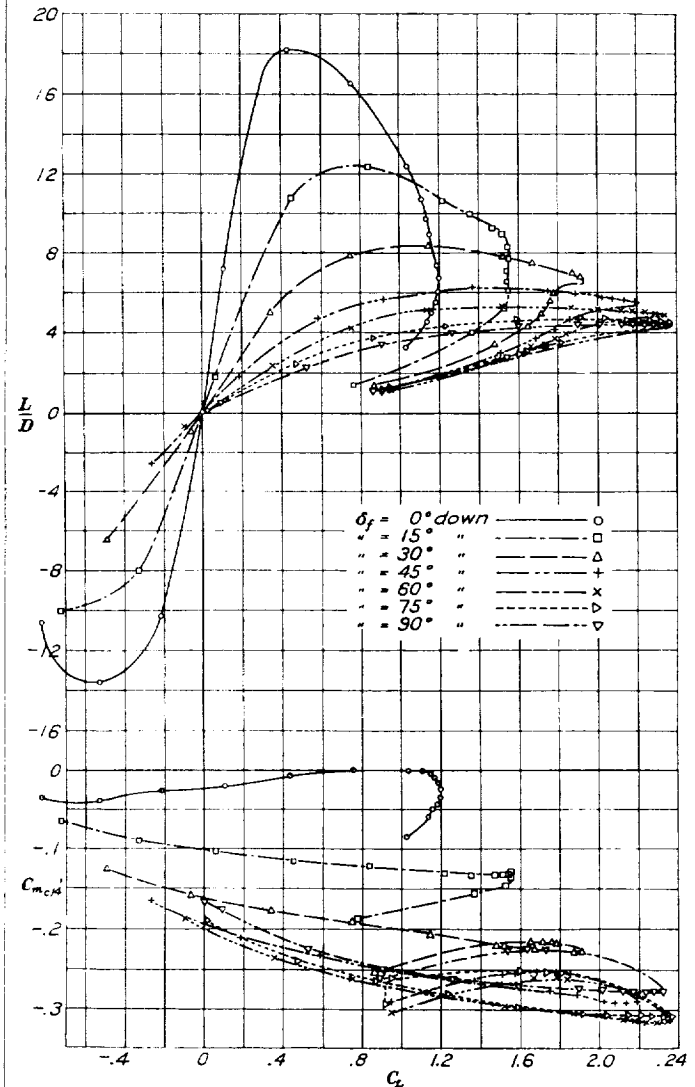


FIGURE 29.—Lift-drag ratio and pitching-moment coefficient for the N. A. C. A. 23021 airfoil with 0.20c full-span split flap.

the plain airfoil and that the increment in $C_{L_{max}}$ due to the deflected split flap is, therefore, practically independent of scale effect. It seems fairly well established that increments of $C_{L_{max}}$ due to split flaps on medium-thick and thick airfoils are independent of scale effect, so that values of the increments obtained at the relatively low scale of the present tests may be directly applied to full-scale wings.

TABLE I
COMPARISON OF CLARK Y, N. A. C. A. 23012, AND
N. A. C. A. 23021 AIRFOILS WITH BOTH ORDINARY
AND SPLIT 0.20c FLAPS

[The 7- by 10-foot wind tunnel. R. 609, 000]

Type of flap	Flap neutral		Flap deflected			
	$C_{L_{m0.2}}$	$C_{L_{m0.2}}/C_{D_{min}}$	$C_{L_{m0.2}}$	$\Delta C_{L_{m0.2}}$	$^a C_{L_{m0.2}}/C_{D_{min}}$	F/D at $C_{L_{m0.2}}$
Clark Y						
Ordinary.....	1.250	89.4	2.105	0.765	144	4.8
Split.....	1.250	89.4	2.118	.868	151	4.8
N. A. C. A. 23012						
Ordinary.....	1.126	107	2.000	0.874	191	4.5
Split.....	1.126	107	2.100	.974	200	4.5
N. A. C. A. 23021						
Ordinary.....	1.170	73.2	2.187	1.017	137	4.6
Split.....	1.170	73.2	2.363	1.193	148	4.6

^a $C_{D_{min}}$ values for flap neutral.

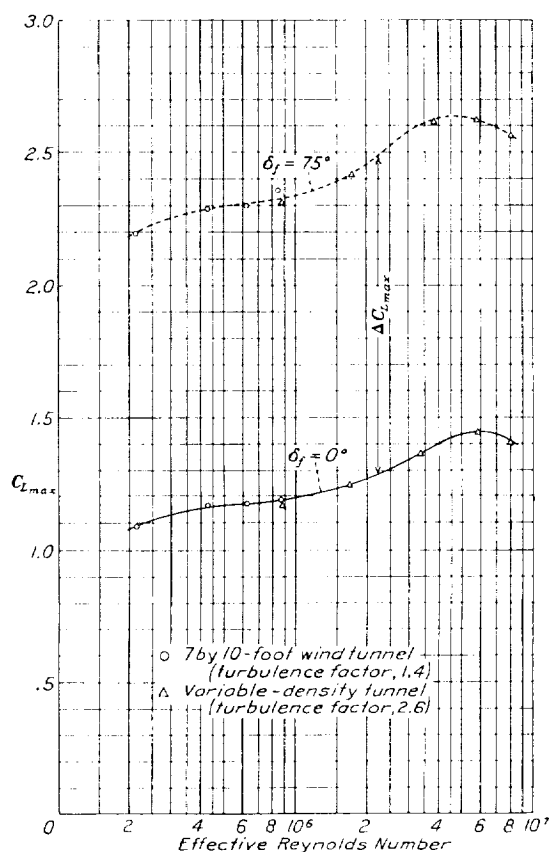


FIGURE 30.—Scale effect on maximum lift coefficient of the N. A. C. A. 23021 airfoil with 0.20c split flap neutral and deflected 75°.

Hinge moments of ordinary flaps.—The hinge moments were obtained for the three widths of ordinary flap on the Clark Y airfoil. These results are given in figures 31, 32, and 33 as coefficients of flap hinge

moment against flap deflection for various angles of attack. Comparison of hinge-moment coefficients for the three widths of ordinary flap indicates that they are practically independent of the flap chord. Comparison of the hinge-moment coefficients of ordinary flaps with those of the split flaps given in reference

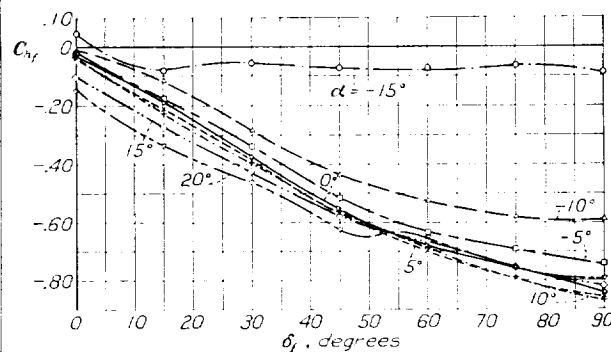


FIGURE 31.—Hinge-moment coefficients of 0.10c ordinary flap on the Clark Y airfoil. Flap gap sealed.

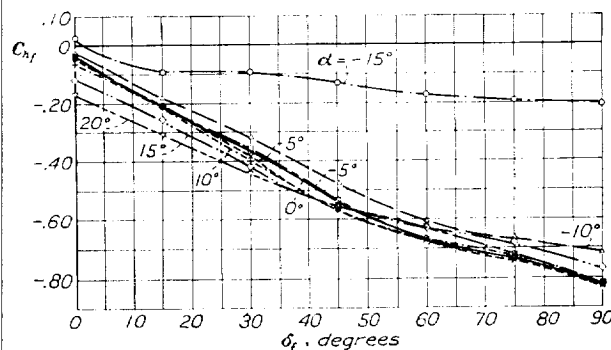


FIGURE 32.—Hinge-moment coefficients of 0.20c full-span ordinary flap on the Clark Y airfoil. Flap gap sealed.

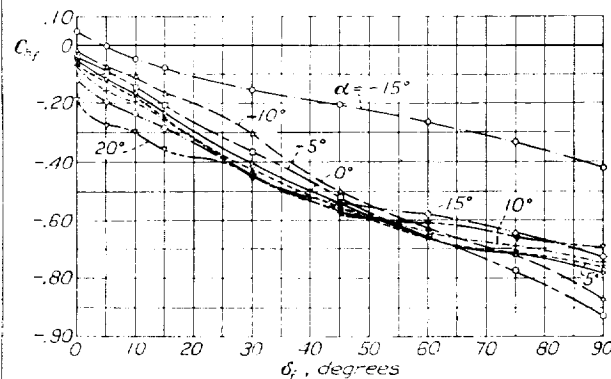


FIGURE 33.—Hinge-moment coefficients of 0.30c full-span ordinary flap on the Clark Y airfoil. Flap gap sealed.

2 indicates also that the hinge-moment coefficients are practically the same for the two types of flap. The actual hinge moments in inch-pounds are plotted against flap chord to a logarithmic scale in figure 34 for different deflections of the ordinary flaps and for several angles of attack. The slope of these curves is approximately 2, indicating that the actual hinge

moment varies as the square of the flap chord for a given flap deflection.

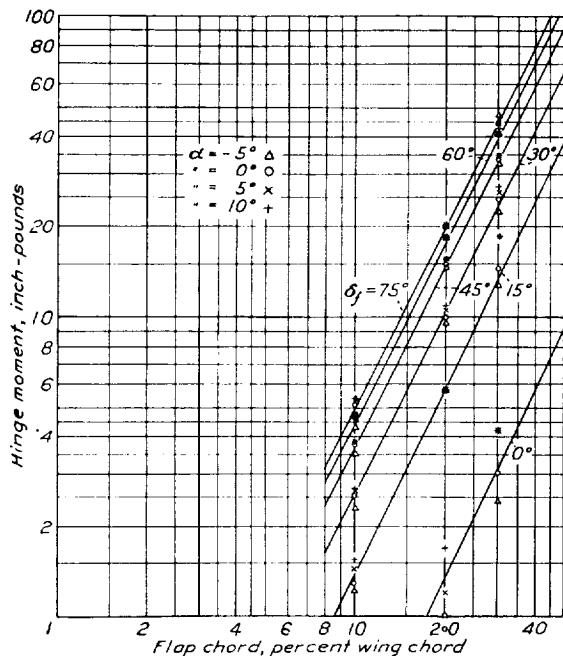


FIGURE 34.—Variation of hinge moment with flap chord for full-span ordinary flaps on the Clark Y airfoil. $q = 16.37$ lb./sq. ft.

CONCLUSIONS

1. Full-span split flaps produced somewhat greater increases in $C_{L_{max}}$ of the three airfoils tested than did full-span ordinary flaps of the same width, but the L/D at $C_{L_{max}}$ was practically the same for the two types of flap.
2. Based principally on the speed-range ratio $C_{L_{max}}/C_{D_{min}}$, the relative order of merit of the airfoils tested with either ordinary or split flaps is N. A. C. A. 23012, Clark Y, and N. A. C. A. 23021.

3. Any gap between the wing and the leading edge of ordinary flaps had a very detrimental effect on the $C_{L_{max}}$ attainable.

4. The hinge-moment coefficients of the full-span ordinary flaps were practically independent of flap chord; the actual hinge moments varied approximately as the square of the flap chord. Both of these findings accord with theory.

5. The hinge-moment coefficients of the full-span ordinary flaps were practically the same as those of split flaps of similar size.

LANGLEY MEMORIAL AERONAUTICAL LABORATORY,
NATIONAL ADVISORY COMMITTEE FOR AERONAUTICS,
LANGLEY FIELD, VA., October 25, 1935.

REFERENCES

1. Harris, Thomas A.: The 7 by 10 Foot Wind Tunnel of the National Advisory Committee for Aeronautics. T. R. No. 412, N. A. C. A., 1931.
2. Wenzinger, Carl J.: Wind-Tunnel Measurements of Air Loads on Split Flaps. T. N. No. 498, N. A. C. A., 1934.
3. Theodorsen, Theodore: Interference on an Airfoil of Finite Span in an Open Rectangular Wind Tunnel. T. R. No. 461, N. A. C. A., 1933.
4. Glauert, H.: Wind Tunnel Interference on Wings, Bodies, and Airscrews. R. & M. No. 1566, British A. R. C., 1933.
5. Gruschwitz, Eugen, and Schrenk, Oskar: A Simple Method for Increasing the Lift of Airplane Wings by Means of Flaps. T. M. No. 714, N. A. C. A., 1933.
6. Weick, Fred E., and Harris, Thomas A.: The Aerodynamic Characteristics of a Model Wing Having a Split Flap Deflected Downward and Moved to the Rear. T. N. No. 422, N. A. C. A., 1932.
7. Jacobs, Eastman N., and Clay, William C.: Characteristics of the N. A. C. A. 23012 Airfoil from Tests in the Full-Scale and Variable-Density Tunnels. T. R. No. 530, N. A. C. A., 1935.

REPORT No. 555

AIR FLOW AROUND FINNED CYLINDERS

By M. J. BREVOORT AND VERN G. ROLLIN

SUMMARY

A study was made to determine the air-flow characteristics around finned cylinders. Air-flow distribution is given for a smooth cylinder, for a finned cylinder having several fin spacings and fin widths, and for a cylinder with several types of baffle with various entrance and exit shapes.

The results of these tests show: That flow characteristics around a cylinder are not so critical to changes in fin width as they are to fin spacing; that the entrance of the baffle has a marked influence on its efficiency; that properly designed baffles increase the air flow over the rear of the cylinder; and that these tests check those of heat-transfer tests in the choice of the best baffle.

INTRODUCTION

Several investigations of the flow of air over flat plates and around smooth cylinders have yielded valuable information on boundary-layer phenomena. No published results are available, however, of the interfin velocities of the air flow around a finned cylinder. The velocity distribution in the fin space determines the boundary-layer characteristics at a given position around the cylinder. The fact that the entire mechanism of cooling is not given by these measurements does not influence the conclusions to be drawn relative to fin spacing, fin width, and pressure drop around the cylinder.

The present investigation was made to determine the effect of changes in fin width, fin pitch, and cylinder diameter on the interfin velocity of a cylinder model. Baffles found to be the best in tests of electrically heated cylinders (reference 1) were also tested. Interfin velocities with and without baffles for each of several positions around the cylinder were measured for five tunnel air speeds from approximately 38 to 145 miles per hour. The velocities in the exit passage of the baffles were in most cases measured for the same tunnel air speeds. The method of measurement made it impossible to measure the air flow in the boundary layer; it was possible, however, to measure the velocity distribution throughout the space between adjacent fins.

In a study of the entire problem of engine cooling it is imperative that the complete picture of air flow about the individual cylinders and baffles be known, for ob-

viously the study of air flow is a very effective means of learning the conditions that give the best cooling with the least drag. Separate studies of flows over flat plates and over cylinders might supposedly be sufficient to give a working picture of the desired phenomena. It is believed, however, that the fins on the cylinder create a mutual interference, so that conclusions drawn from tests other than those of the combination itself might be misleading. The acceleration of the air around the front part of the cylinder, the deceleration around the rear, and the effect of the cylinder fins in stimulating the formation of the boundary layer on the cylinder are known to exist but are difficult to visualize in their proper perspective except by measurement.

Temperature measurements must be supplemented by air-flow measurements to show why one condition is good and another poor. Temperature measurements alone show only the condition; air-flow measurements, correlated with temperature measurements, show the cause.

APPARATUS

Wind tunnel.—The air-flow measurements around the cylinders were made in a 30-inch closed-throat wind tunnel designed to give air speeds up to 200 miles per hour. (See reference 2.) The tunnel air speeds were measured with a pitot-static tube located to one side and ahead of the test specimen to reduce the interference effect. A honeycomb grill in the tunnel entrance reduced air disturbances.

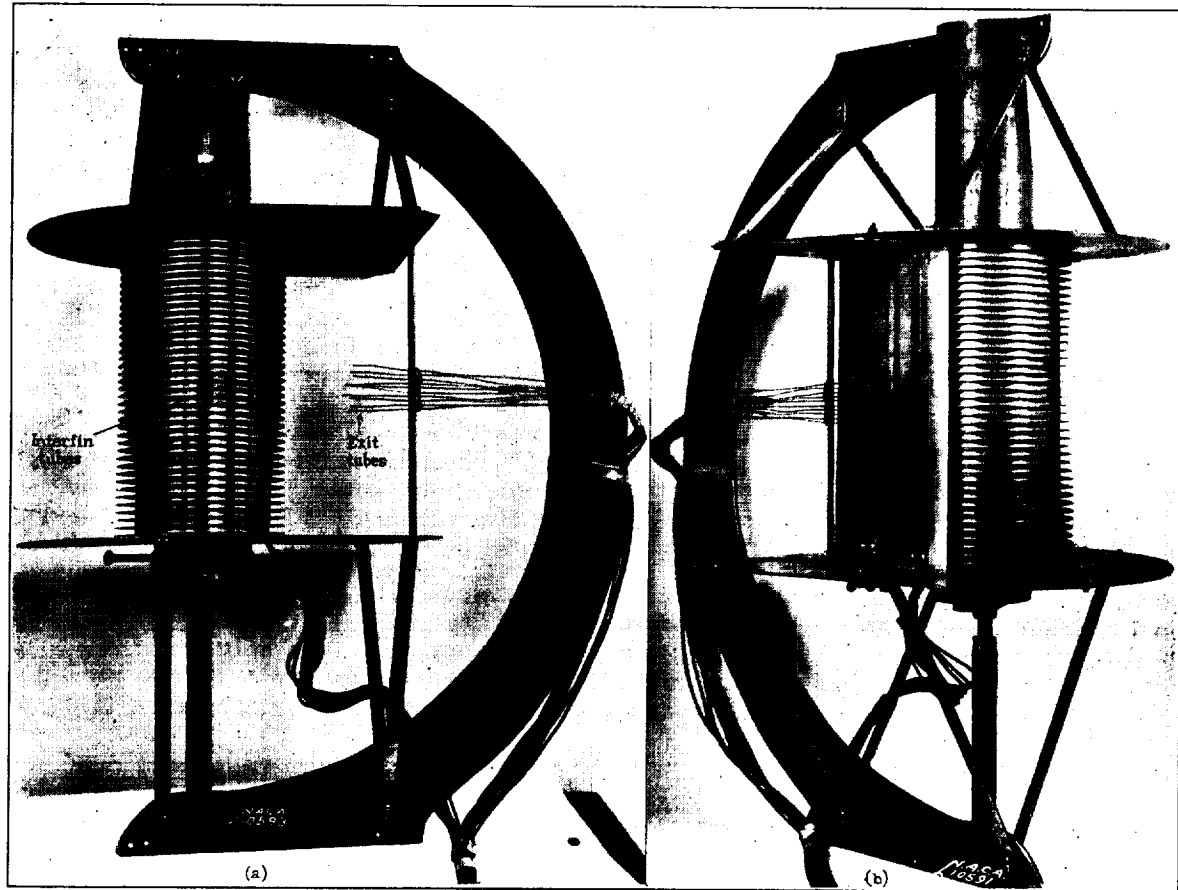
Apparatus for measuring the air flow around a cylinder.—The air flow between the fins and in the front and rear of the cylinder was in all cases measured with impact and static tubes. The tubes between the fins were placed tangential to the cylinder wall; the holes in the static tubes and open ends of the impact tubes were in a given plane passing through the axis of the cylinder. Never more than two tubes were located in a given space between two fins. An impact tube was located in one space and a static tube in the same position in an adjacent space, a procedure based upon the assumption that the flow through all the spaces used is identical. No justification can be given for such an assumption except that both static and impact pressures vary in a regular and reasonable manner from

cylinder wall to fin tip. Of the various means by which such a survey might have been made this method was the most practicable for such an extended survey.

The pitot-static tubes were made of stainless steel seamless tubing with a 0.002-inch thick wall. Two tube sizes were used; the 0.040-inch outside diameter tubes were used for the velocity survey ahead of the cylinder and in the baffle exit passages, and the 0.015-inch outside diameter tubes were installed between the fins to obtain the interfin velocities. The impact

inch to the cylinder wall. Measurements across the fin spacing showed no measurable variation in velocity, indicating that the boundary layer along the fin was less than 0.010 inch. In the determination of the average velocity between the fins at a given position on the cylinder, the velocity was assumed to be constant across the fin spacing.

Cylinders and baffles.—The finned cylinders used in these tests were made of flat circular disks of different diameters clamped together with a $\frac{1}{2}$ -inch rod



(a) Interfin and exit tubes.

(b) Baffles mounted in place.

FIGURE 1.—Assembly of finned test cylinder. The cylinder can be rotated about its central axis to obtain measurements at various angles with respect to the air stream.

tubes were made by cutting the tubes off square and removing the burs from the ends. The static tubes were made by closing and rounding off the ends and then drilling four 0.004-inch holes symmetrically around each tube about $\frac{1}{4}$ inch from the closed end. Although, as previously stated, never more than two tubes were located in a given space, all subsequent references to the tubes will be made as though they were all located in one space. Usually eight pairs of tubes were used to determine the air flow between the fins. Tubes were located both along the center line between the fins, and as close as 0.010 inch to the fins and 0.020

through their central axis. (See fig. 1 (a).) The fin disks were made of $\frac{1}{2}$ -inch flat steel stock and the spacers of sheet aluminum. Two sets of disks were required to make up a cylinder, one set of large diameter serving as fins and another group of smaller diameter and the proper thickness forming the cylinder proper and giving the desired spacing between the fins. Both sets were always made from selected materials to secure perfectly flat surfaces and uniform thicknesses. The variation in fin spacing was never greater than 0.002 inch. Enough disks were assembled to give a cylinder 5 to 11 inches in length, depending on the

spacing. Cylinders of two base diameters, 4.66 and 7 inches, were used. The 4.66-inch cylinders had fin widths of $\frac{3}{8}$, $\frac{3}{4}$, $1\frac{1}{2}$, and 3 inches and fin spaces of $\frac{1}{32}$, $\frac{1}{16}$, $\frac{1}{8}$, $\frac{1}{4}$, and $\frac{1}{2}$ inch. The cylinder could be rotated about its central axis to obtain readings at several points with one set of pitot-static tubes.

Baffles (figs. 1 (b) and 2) were made of $\frac{1}{8}$ -inch sheet aluminum annealed and rolled into shape. They were mounted around the cylinder symmetrically with respect to its central axis. One set of inner baffles (fig. 2, II-M) was made and tested to see if it were possible to guide the air farther around the rear of the cylinders. These baffles were partly slotted so that they could be installed between the fins.

TESTS

Air-flow measurements of the unbaflled cylinder com-

2 percent and the velocities are believed to be accurate to within ± 5 percent.

Most of the baffle tests were conducted on the 4.66-inch cylinder having $\frac{3}{4}$ -inch fins with $\frac{1}{4}$ -inch spacers. The baffle used, found to be the best from previous tests (reference 1), fitted tightly against the fins and had an entrance angle of 140° and 3-inch extensions. The width of the exit passage was so proportioned that the ratio of exit area to area between fins at right angles to the direction of the air stream was 1.6, giving the optimum exit opening for the aforementioned cylinder a width of 2.1 inches.

Baffle I was a standard shell baffle with an entrance angle of 140° and an optimum exit 2.1 inches wide with 3-inch plates. (See fig. 2.) A complete velocity survey was made with the baffles in contact with and separated $\frac{1}{2}$ inch from the fin tips. (See I_X and I_L , fig. 2.)

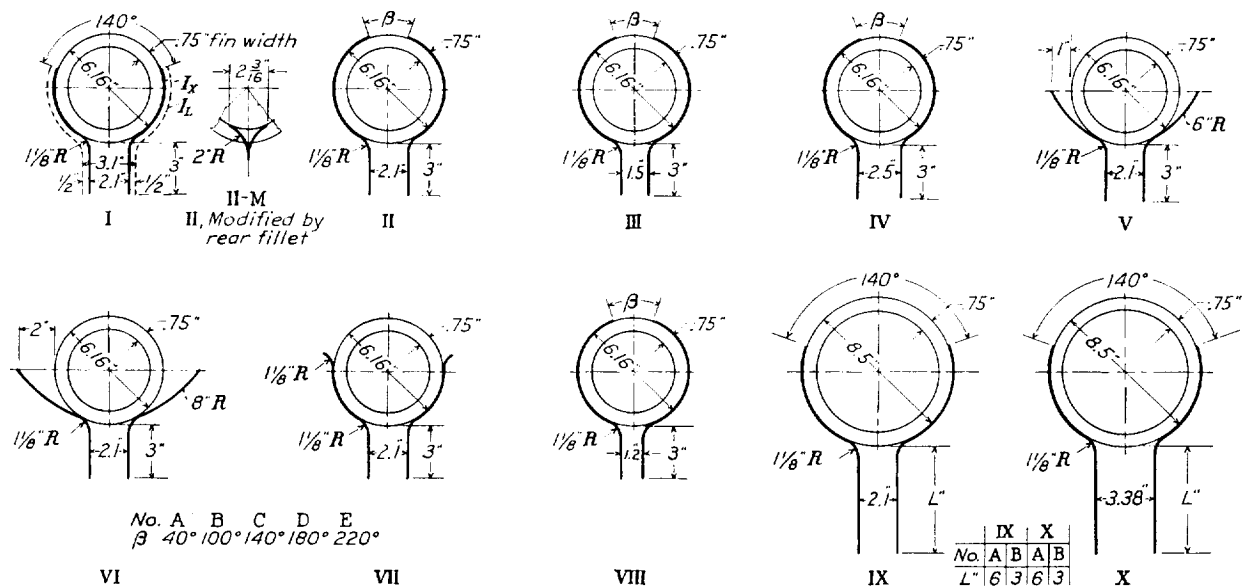


FIGURE 2.—Plan view of cylinder and baffle arrangements tested.

binations were made with air speeds of approximately 38, 56, 80, 110, and 145 miles per hour, at positions of $\theta = 15^\circ, 45^\circ, 90^\circ, 120^\circ$, and 135° from the front of the cylinder with fin spacings of $\frac{1}{16}$, $\frac{1}{8}$, $\frac{1}{4}$, and $\frac{1}{2}$ inch and fin widths of $\frac{3}{8}$, $\frac{3}{4}$, $1\frac{1}{2}$, and 3 inches. Tests of the 3-inch fins were limited to spacings of $\frac{1}{8}$, $\frac{1}{4}$, and $\frac{1}{2}$ inch. The vibration of these fins made it necessary to use four sets of small interfin spacers located to offer a minimum of interference to the air flow in the vicinity of the pitot-static tubes. One set of tests was also made of the $\frac{3}{4}$ -inch fins using $\frac{1}{32}$ -inch spacing.

Both the velocity and the static pressure, read on a U-tube water manometer, were measured for all tests. The static pressure was used as a guide to detect errors or to determine any anomalous behavior. The manometer fluid showed no fluctuation because the small tubes damped the fluctuations in the air stream. The tubes checked a standard pitot-static tube to within

Complete velocity surveys with baffles II, III, and IV were made to determine the effect of changes in entrance angle and exit width on the flow characteristics around the cylinder and through the exit of the baffle. Five entrance angles ($40^\circ, 100^\circ, 140^\circ, 180^\circ$, and 220°) were tested with each of the three exit widths (1.5, 2.1, and 2.5 inches). The velocity survey for the baffle tests was made at angles of $15^\circ, 45^\circ, 90^\circ$, and 135° and, in addition, at points 5° ahead of and behind the forward edge of the baffle (e. g., 85° and 95° for the 180° entrance).

Baffles V and VI were tested to determine the effect of a pressure-type baffle on the flow characteristics around the cylinder. They had standard exit passages and flared entrances of 6- and 8-inch radii, respectively.

Baffle VII resembles II-D very closely and shows the effect of a small flare on the flow characteristics when used with a closely fitting baffle.

Baffle VIII was tested on the 4.66-inch diameter cylinder with $\frac{3}{8}$ -inch fins and $\frac{1}{32}$ -inch spacers. Velocity surveys were taken around the fins and through the exit passage for entrance angles of 40° , 100° , 140° , 180° , and 220° . The optimum exit passage was used on this baffle so that the width of the exit opening for this fin spacing was 1.2 inches.

Baffles IX and X were tested on the 7-inch diameter cylinder with $\frac{3}{8}$ -inch fins and $\frac{1}{32}$ -inch spacers. Velocity surveys were made with each baffle having 6-inch and 3-inch exit-passage lengths to determine the effect of the cylinder diameter on the optimum exit passage. Baffle X had the same entrance opening as baffle IX

pendicular to the tunnel axis. The results of these surveys are shown in figure 3; the calculated curves are based upon a nonviscous potential flow in free space.

Although an integration of the experimental curves for air-speed distribution across the tunnel indicates that the pitot-static tube is so located that the readings are about 5 percent high, no correction has been applied because the uncorrected results will be more directly comparable with other studies made in the tunnel. Furthermore, the results presented here are more valuable for the comparison of flow characteristics under different conditions than for absolute values.

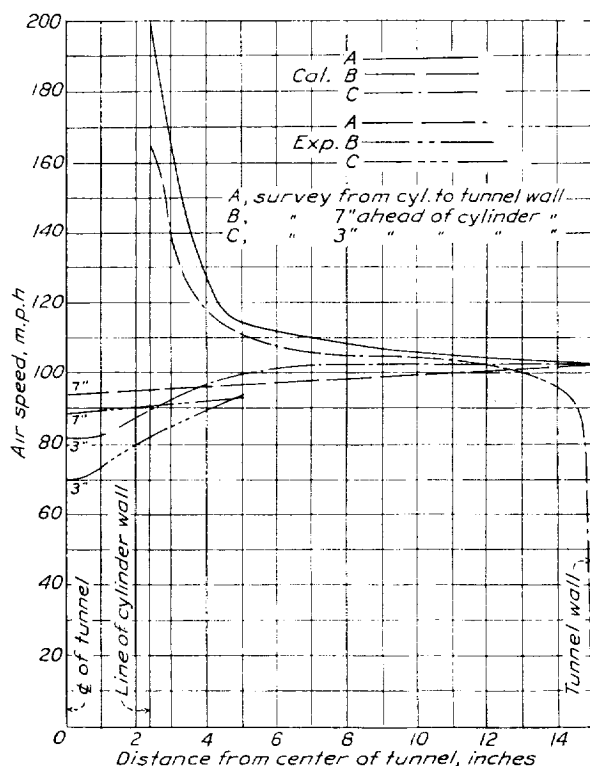


FIGURE 3.—Velocity survey of tunnel test section. V_a 100 m. p. h.

but the exit opening, instead of being 1.6 times the cross-sectional area between the fins, had the same angular opening in the rear as baffle II, so that the exit width was 3.38 inches.

In addition to the tests of finned cylinders, a similar velocity survey was made on a smooth cylinder 4.66 inches in diameter to compare the results with theoretical calculations.

RESULTS

Two velocity surveys were made in the throat of the tunnel at a tunnel air speed of 100 miles per hour; one along the diameter of the cylinder (extended) perpendicular to the axis of the tunnel, and the other at two stations ahead of the cylinder along horizontal lines per-

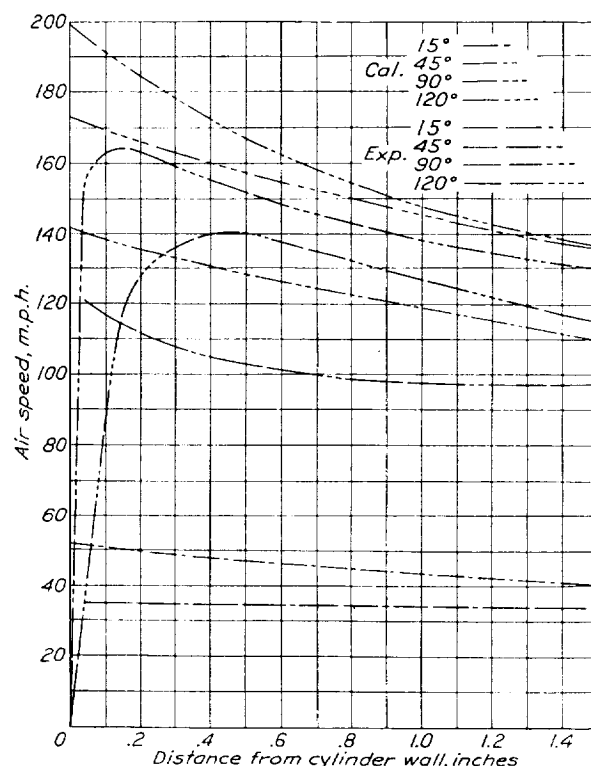
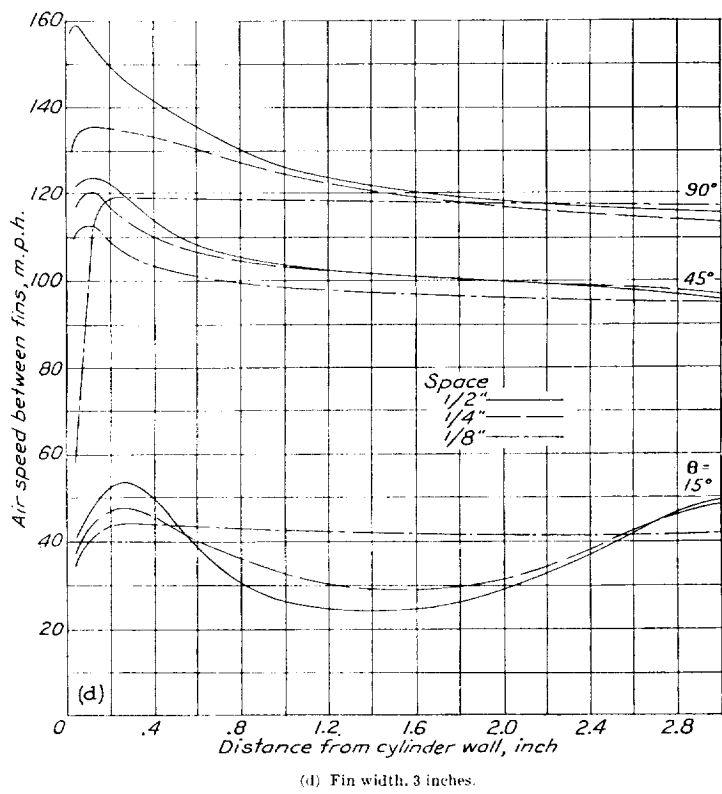
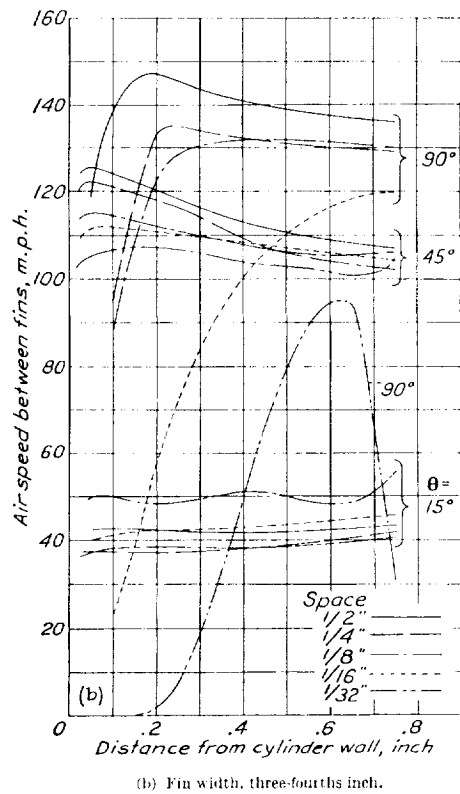
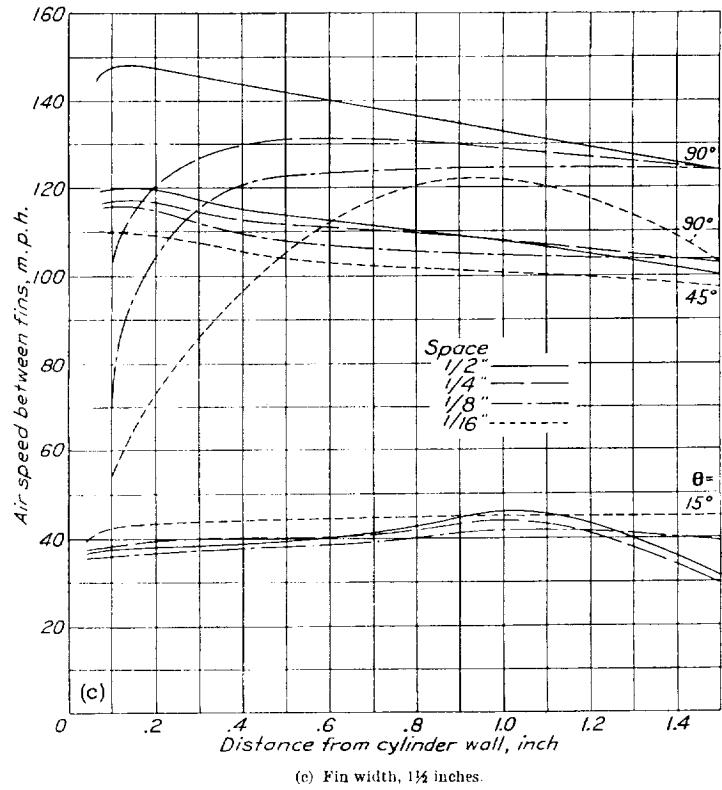
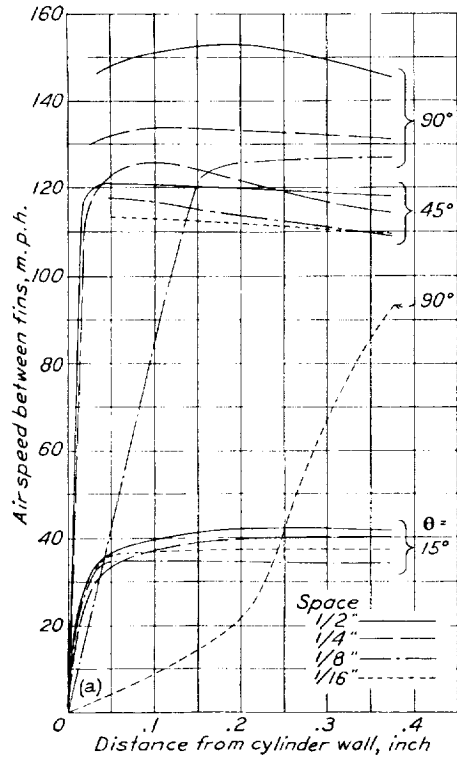


FIGURE 4.—Calculated and experimental air flow around a smooth cylinder of 1.66 inch diameter. V_a 100 m. p. h.

Preliminary measurements were made of the air flow around a smooth cylinder. Figure 4 shows both the measured and the calculated air speeds. It is interesting to note that the experimental curves gradually approach the theoretical curves as the distance from the cylinder wall is increased and that the boundary-layer thickness for some of the settings is less than 0.040 inch, the closest point measured.

The data were reduced to values of V_a , average interfin velocity, and V_t , tunnel air speed, and the results were tabulated at $100 V_a/V_t$. The data on the unbaffled cylinder are tabulated in table I; tables II to IV give the data for the complete series of baffle tests on three different cylinders, including the variations of baffle shape and of entrance and exit openings.

FIGURE 5.—Effect of fin space on interfin velocity distribution of a finned cylinder. V_∞ , 100 m. p. h.

The results are given in two forms: As figures showing the air flow for typical cases, and as tables giving the ratio of average velocity (V_a) to the tunnel air speed (V_t) for the interfin and exit measurements. The plotted values are for a tunnel air speed of 100 miles per hour and the tabular data are for tunnel air speeds of 50, 100, and 150 miles per hour.

The results of tests of the unbauffed 4.66-inch diameter cylinder for all fin widths and spacings are shown in table I and figure 5. The fin spacing and the angular station (θ) at which the measurements were made are designated on the figure. Each group of curves is for a particular fin width. Similar results for the 7-inch diameter cylinder are shown in table V and in figure 6.

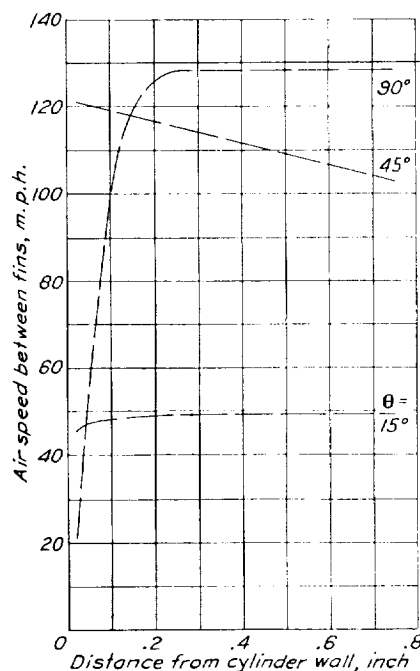


FIGURE 6.—Velocity distribution between fins of a 7-inch diameter cylinder. V_t , 100 m. p. h.; fin width, three-fourths inch; fin space, one-fourth inch.

Figure 7 helps to explain part of the phenomena encountered in the tests of cylinders with baffles. The curves are plots of θ against the average air speed multiplied by a factor K , which is the ratio of the cooling area of the particular fin spacing to the cooling area of the $\frac{1}{4}$ -inch spacing. The results presented are those for the 4.66-inch diameter cylinder with a $\frac{3}{4}$ -inch fin width. The factor K multiplied by the air speed, although it is not an exact measure, should give a good indication of relative cooling for a given fin width at a particular point on the cylinder. The curves show definitely that better cooling should result from closely spaced fins. The best entrance angle (β) for a cylinder baffle for maximum cooling of the cylinder is given by

the angle corresponding to the maximum value of KV_a .

All the test data for the 4.66-inch cylinder with $\frac{1}{4}$ -inch fin spaces for various baffles are shown in figures 8 (a), 8 (b), 8 (c), and 9 and in tables II to IV. In figure 10 and in table VI similar results are given for the $\frac{1}{32}$ -inch spacing on the same cylinder diameter. Results of tests of the 7-inch cylinder are shown in figure 11 and table V. The results plotted in figures 8, 9, 10, and 11 agree with those shown in figure 7 in that the maximum air flow occurs with the baffle opening predicted by measurements on the unbauffed cylinder.

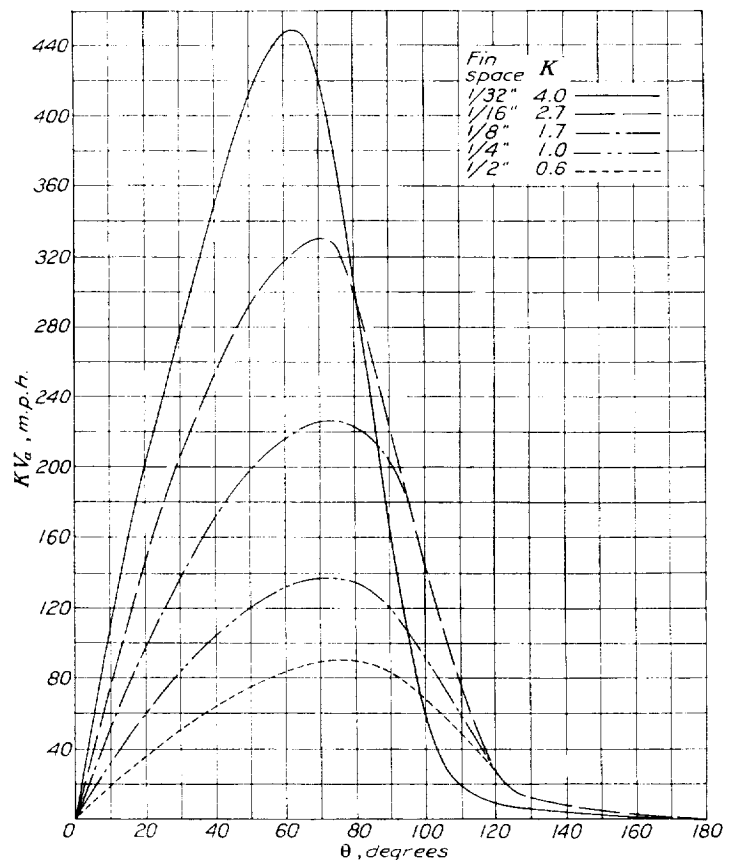


FIGURE 7.—Effect of fin space on cooling of a 4.66-inch diameter cylinder without baffles. V_t , 100 m. p. h. The best entrance angle for each fin space for a cylinder baffle for maximum cooling of a cylinder is given by the angle corresponding to a maximum value of KV_a .

The most desirable entrance angle, as shown by the figures, is 140° .

The results from tests of baffles II, III, and IV are shown in figure 12. The baffle with the 140° opening and 2.1-inch exit gave the maximum air flow between the fins.

Figure 13 gives a direct comparison of the relative cooling of several of the arrangements tried in addition to the calculated and experimental velocity distribution around the 4.66-inch cylinder without baffles. Baffle II-C and VII are the best of the five plotted.

There are many published studies on boundary layer for various types of bodies. Doetsch, Éliás, Thom, Fage, and Pye are among those who have made experiments and calculations that are most directly applicable to this problem. (See references 3 to 10.) Doetsch studied the problem of velocity and temperature gradient near the surface of a heated flat plate in an air stream. His results check theory in that both gradient curves have the same form. The tests were run at low velocities so that the boundary layer was laminar. Thom has made boundary-layer experiments and calculations for the flow around a cylinder which are in close agreement but which, like those of Doetsch,

thickness at 45° for a tunnel air speed of 100 miles per hour is calculated to be 0.035 inch. Pye has analyzed the entire mechanism of cooling around a finned cylinder. His article is a complete summary of the whole problem rather than a detailed study of any one part.

In figure 14 a comparison is made between a cooling and a velocity curve. The curves indicate how much cooler a given location is than the rear position on the cylinder wall at which the cooling is considered zero. This comparison, although not physically correct, is presented to correlate temperature and velocity measurements. The discrepancy is caused by the fact that the cooling is not shown to be due directly to boundary-

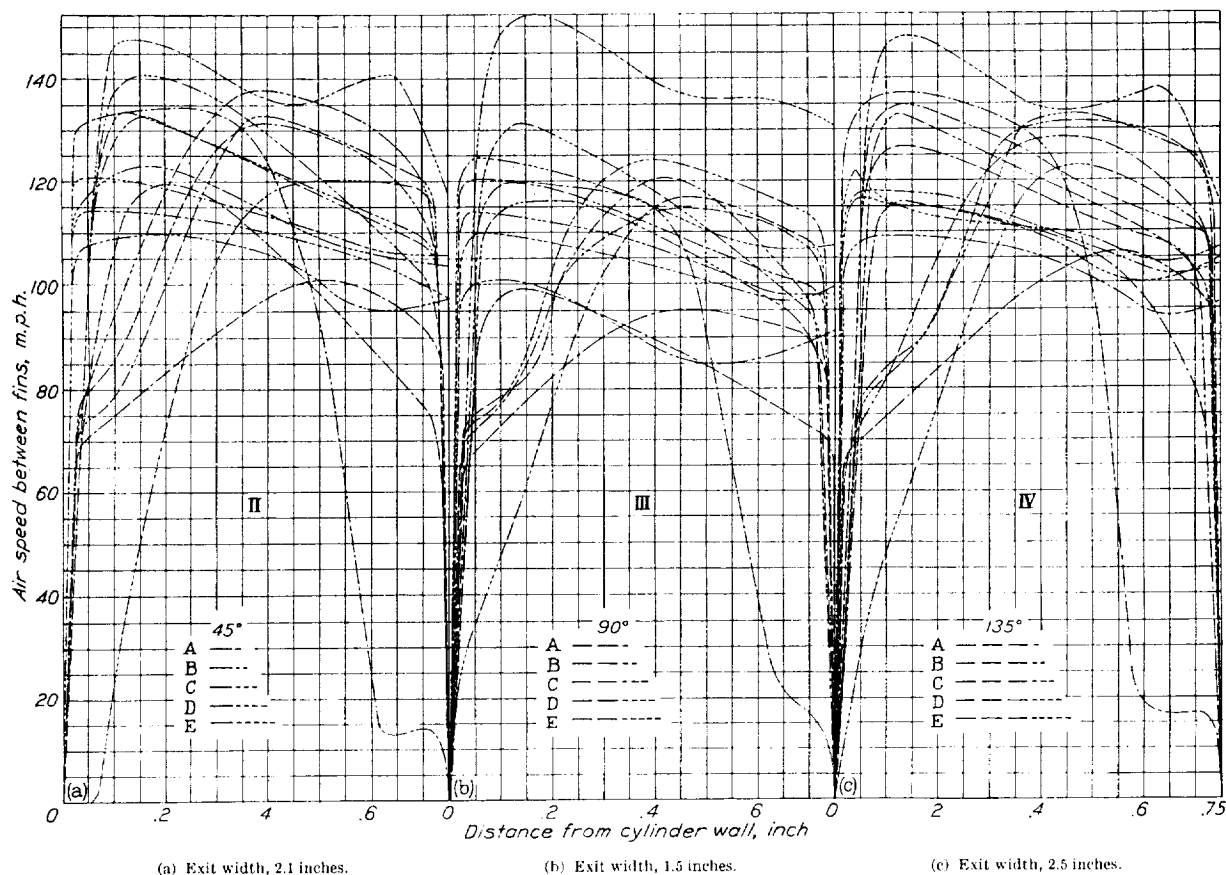


FIGURE 8.—Effect of exit width on interfin velocity of baffled cylinders having several entrance angles. V_∞ 100 m. p. h.; fin width, three-fourths inch; fin space, one-fourth inch.

are for laminar flow. Fage presents results, both experimental and calculated, for turbulent flow about a cylinder. Although the results given in the subject paper for a smooth cylinder at 45° (fig. 4) do not present satisfactory boundary-layer measurements, they do, however, agree with Fage's experiments at 49° in that the boundary-layer thickness is less than the closest point taken in these experiments. It is evident from the shape of the curves that the boundary layer is less than 0.040 inch thick. The boundary-layer

layer conditions. The boundary layer and the velocities outside the boundary layer, however, are dependent upon each other, and therefore the comparison presented here has real physical significance even though it is slightly out of proportion.

The velocity corresponds to a tunnel air speed of 50 miles per hour. Two cases are presented: (a) No baffle, and (b) with the II-C baffle.

In both cases the cooling and velocity curves near the front of the cylinder are dissimilar, owing to the

fact that an unmeasured radial component of velocity and a relatively thin boundary layer over the front of the cylinder exist and that relatively cool air comes directly in contact with the cooling surfaces. In view of these considerations, the lack of similarity is to be expected.

Farther around the cylinder the two cases must be treated separately. The expected similarity of the two curves of the un baffled cylinder is evident. It would be incorrect, however, to ascribe the cooling over the rear two-thirds of the cylinder directly to velocity because the cooling-air temperature is rising, the boundary layer is getting thicker, and there is

The velocity distributions shown in figure 8 indicate that the decrease in cooling is caused by the thick boundary layer next to the cylinder, emphasizing the importance of using closely fitting baffles.

Another factor of considerable importance in actual cooling is the type of cylinder baffle used, as shown in previous tests. The loss in total head as the air flows around a baffle-enclosed cylinder (fig. 15) is typical of all the combinations studied.

The curve for the 40° opening is obviously incorrect as energy once lost cannot be regained. It is believed that this erratic behavior is caused by the extreme turbulence at the entrance.

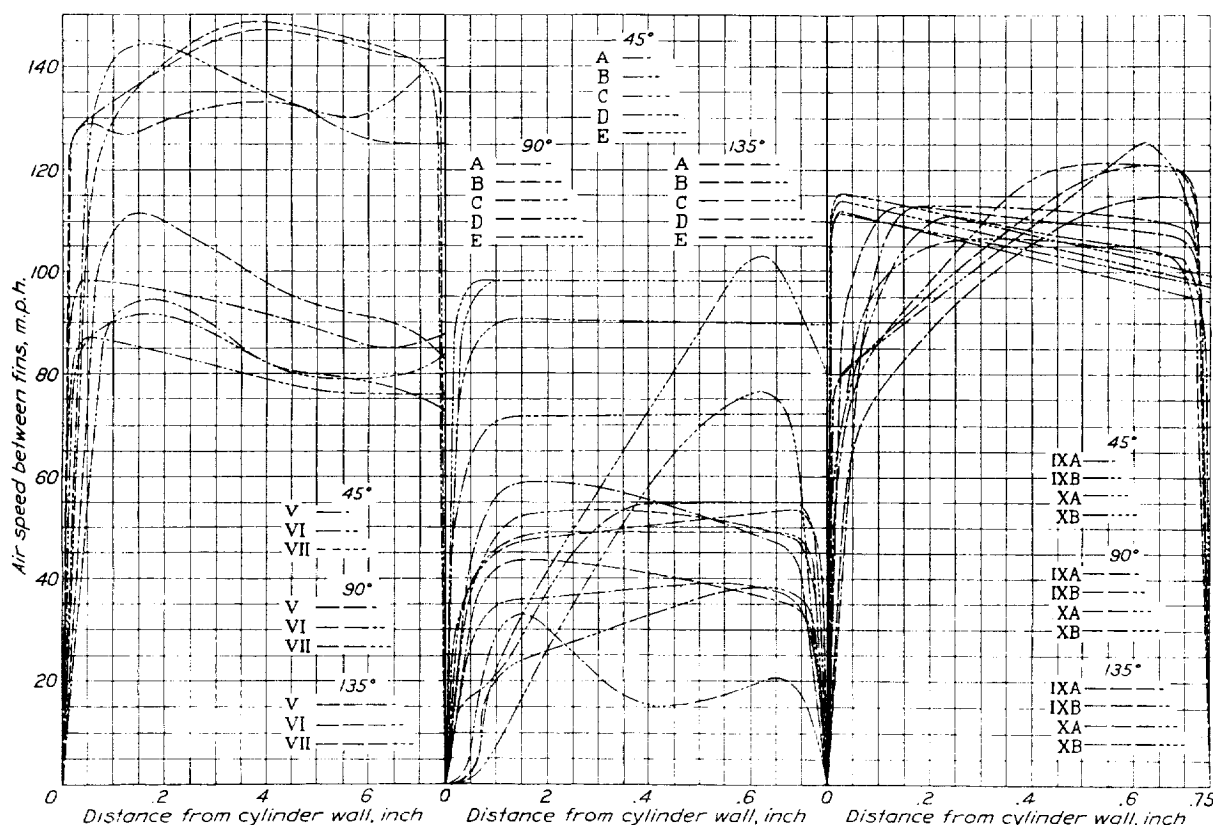


FIGURE 9.—Effect of baffle shape on interfin velocity. V_0 , 100 m. p. h.; fin width, three-fourths inch; fin space, one-fourth inch.

FIGURE 10.—Effect of entrance angle on interfin velocity. V_0 , 100 m. p. h.; fin width, three-fourths inch; fin space, one thirty-second inch.

FIGURE 11.—Effect of exit width and length on interfin velocity. V_0 , 100 m. p. h.; fin width, three-fourths inch; fin space, one-fourth inch.

breakaway of the air flow from the rear that gives cooling phenomena rather easy to visualize but extremely difficult to predict. The vortices released at the breakaway certainly give excellent cooling in particular regions and undoubtedly keep the cylinder temperature in the rear much cooler than would be expected.

The baffled cylinder is even more illustrative than the un baffled one because of the simpler phenomena. The velocity must remain the same; therefore, any change in the cooling must be due to changes of the boundary layer and the temperature of the cooling air.

The effect of the entrance angle β on the loss in total head is clearly shown in figure 15 for various positions θ around the cylinder. An entrance angle of 140° gives the most uniform loss in head and, as previously shown, provides the best cooling. It is apparent from these curves why one baffle is better than another.

Figure 16 shows the loss in total head through the baffles per inch of mean fin circumference for the 4.66-inch cylinder with $\frac{1}{4}$ - and $\frac{1}{32}$ -inch spacings. Curve A is plotted for four sets of data, two exit widths and two entrance angles; and curve B is plotted for only one condition. The results show that the rate of pres-

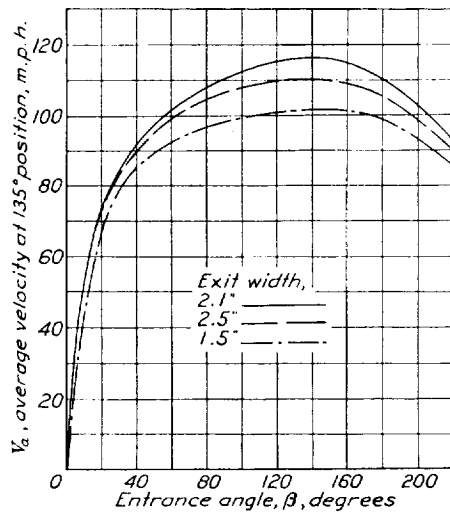


FIGURE 12.—Effect of entrance angle on V_a for a 4.66-inch diameter cylinder. V_a , 100 m. p. h.; fin width, three-fourths inch; fin space, one-fourth inch.

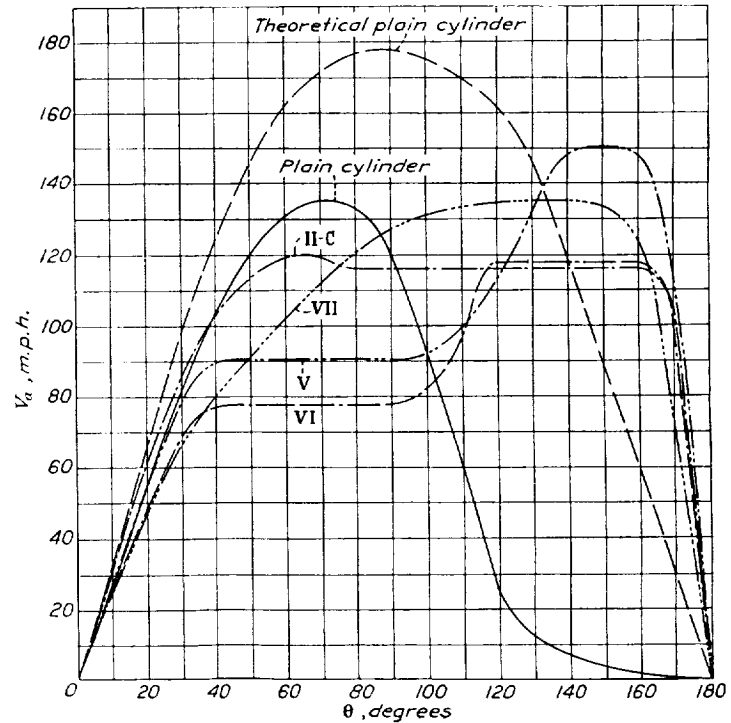
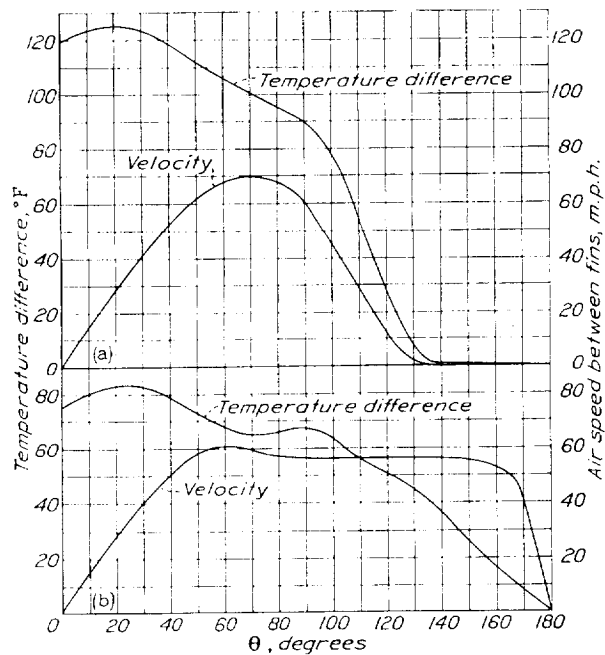


FIGURE 13.—Effect of design on the flow conditions of several baffles on a 4.66-inch diameter cylinder. V_a , 100 m. p. h.; fin width, three-fourths inch; fin space, one-fourth inch.



(a) Finned cylinder with no baffles. (b) Finned cylinder with baffle II-C.

FIGURE 14.—Comparison of temperature and velocity curves. V_a , 50 m. p. h.

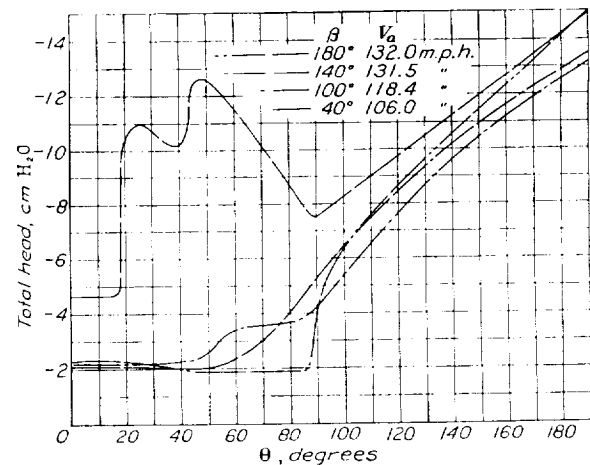


FIGURE 15.—Effect of entrance angle on the pressure drop around the cylinder with baffle II. V_a , 113 m. p. h.; fin width, three-fourths inch; fin space, one-fourth inch. The uniform loss in energy for the 140° opening results in good cooling.

sure drop through the baffle is very sensitive to changes in fin spacing. The rate of pressure drop $\frac{dP}{ds} = \alpha V^n$ where n is 1.8 and 1.6 for $\frac{1}{32}$ - and $\frac{1}{4}$ -inch spacing, respectively. Baffles giving a large loss in total head at the entrance or exit obviously cannot give a maximum interfin flow around the cylinders. Those having a uniform drop beginning just ahead of the baffle entrance gave the highest average air flow and over-all heat transfer.

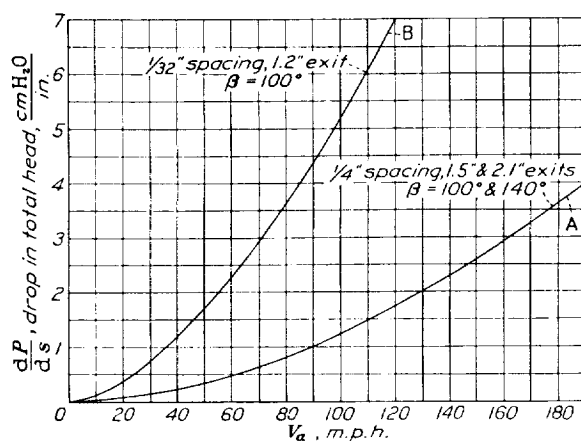


FIGURE 16.—Effect of fin spacing on differential pressure drop around the cylinder.

Some of the baffles in common use, termed "mixing" baffles, are placed in such a relation to the cylinder that they induce a mixing of the air at a point where more cooling is desired. As long as ample cooling is available, this practice is legitimate; but, when over-all cooling becomes a serious problem, such a wasteful practice cannot be continued.

CONCLUSIONS

1. The results presented here do not pretend to be directly applicable to solving the cooling problem on a cowled and baffled cylinder using *pressure cooling*. The results on pressure drop, the general behavior of the baffle in influencing the flow around the rear of the cylinder, and the study of fin spacing, however, are directly applicable. The study of entrance conditions

for a baffled cylinder obviously applies only to a cylinder in a free air stream. Special emphasis should be placed on the results of the tests of flow around the rear of the cylinder, which show the very great importance of close baffling for maximum heat transfer and minimum energy loss.

2. Flow characteristics around a cylinder are not as critical to changes in fin width as they are to fin spacing.

3. Velocity measurements check temperature measurements in the choice of the best baffle.

4. The position of the entrance of the baffle has a marked influence on its efficiency.

5. The maximum air flow and the maximum heat transfer are both obtained with the same exit opening.

LANGLEY MEMORIAL AERONAUTICAL LABORATORY,
NATIONAL ADVISORY COMMITTEE FOR AERONAUTICS,
LANGLEY FIELD, VA., November 7, 1935.

REFERENCES

1. Schey, Oscar W., and Rollin, Vern G.: The Effect of Baffles on the Temperature Distribution and Heat-Transfer Coefficients of Finned Cylinders. T. R. No. 511, N. A. C. A., 1934.
2. Schey, Oscar W., and Biermann, Arnold E.: Heat Dissipation from a Finned Cylinder at Different Fin-Plane/Air-Stream Angles. T. N. No. 429, N. A. C. A., 1932.
3. Doetsch, Hans: The Heat Transfer of Cooling Fins on Moving Air. T. M. No. 763, N. A. C. A., 1935.
4. Éliás, Franz: The Transference of Heat from a Hot Plate to an Air Stream. T. M. No. 614, N. A. C. A., 1931.
5. Thom, A.: The Flow Past Circular Cylinders at Low Speeds. (Abstract) R. & M. No. 1539, British A. R. C., 1933.
6. Thom, A.: The Boundary Layer of the Front Portion of a Cylinder. R. & M. No. 1176, British A. R. C., 1928.
7. Fage, A., and Falkner, V. M.: Further Experiments on the Flow around a Circular Cylinder. R. & M. No. 1369, British A. R. C., 1931.
8. Fage, A.: The Air Flow around a Circular Cylinder in the Region where the Boundary Layer Separates from the Surface. R. & M. No. 1179, British A. R. C., 1929.
9. Pye, D. R.: The Theory and Practice of Air Cooling. Aircraft Engineering, February 1933, pp. 31-33.
10. Pye, D. R.: The Principles of Air Cooling. Aircraft Engineering, March 1933, pp. 51-53; April 1933, pp. 79-86.

TABLE I.—DATA FOR THE 4.66-INCH CYLINDER WITH NO BAFFLES

Fin width, inches Fin space, inches		$\frac{V_2}{V_1} \times 100$, where $V_1 = \frac{50 \text{ m. p. h.}}{100}$				$\frac{V_2}{V_1} \times 100$, where $V_1 = \frac{50 \text{ m. p. h.}}{100}$			
		$\frac{3}{8}$	$\frac{1}{4}$	$1\frac{1}{2}$	3	$\frac{3}{8}$	$\frac{1}{4}$	$1\frac{1}{2}$	3
		$\theta = 15^\circ$				$\theta = 45^\circ$			
$\frac{1}{16}$		34.1	42.0	41.6	—	111.0	107.0	100.1	—
		36.2	42.5	40.2	—	111.5	108.3	100.4	—
		58.0	43.3	41.7	—	114.0	110.4	107.2	—
		37.2	43.6	40.7	38.0	117.0	111.7	114.2	93.0
$\frac{1}{8}$		33.7	38.5	38.5	41.3	113.7	108.4	104.2	98.3
		39.9	40.0	37.3	47.2	116.7	110.4	108.6	98.6
		37.2	42.9	42.1	34.7	118.7	114.2	106.6	99.2
$\frac{1}{4}$		38.0	38.7	40.0	36.6	120.6	111.9	109.0	102.4
		41.9	45.3	38.8	40.5	117.7	112.1	109.0	103.8
		28.7	46.7	42.2	34.5	117.2	116.0	109.2	102.0
$\frac{3}{8}$		40.6	42.2	40.4	35.1	120.0	114.8	110.8	103.2
		45.1	44.5	35.9	37.0	119.3	116.5	110.0	106.6
		$\theta = 90^\circ$				$\theta = 120^\circ$			
$\frac{1}{16}$		18.5	63.2	103.2	—	—	19.0	21.7	—
		34.0	81.2	101.0	—	—	10.2	21.1	—
		38.5	80.8	110.2	—	—	9.0	20.1	—
		70.2	110.1	112.4	114.8	—	20.1	42.0	52.4
$\frac{1}{8}$		101.2	116.2	114.8	115.6	—	—	56.5	59.4
		109.5	114.7	120.0	117.8	—	15.8	57.4	62.0
		140.0	120.8	126.0	114.5	28.0	24.1	68.0	79.3
$\frac{1}{4}$		133.5	118.8	123.5	121.3	46.2	22.2	96.6	84.7
		123.3	120.5	124.7	123.5	54.2	27.1	91.0	89.0
		157.7	123.8	122.0	123.5	31.8	60.1	85.0	76.1
$\frac{3}{8}$		150.8	134.5	134.8	125.6	47.7	41.2	110.8	92.0
		153.3	141.7	139.3	127.2	109.0	43.3	109.5	91.3

TABLE II.—DATA FOR THE 4.66-INCH CYLINDER HAVING $\frac{3}{4}$ -INCH FINNED AND $\frac{1}{4}$ -INCH SPACERS WITH BAFFLE I

		$\frac{V_2}{V_1} \times 100$, where $V_1 = \frac{50 \text{ m. p. h.}}{100}$	
Position		I_x Baffle contacting fins	I_L Baffle $\frac{1}{2}$ inch from fins
θ degrees			
15		42.2	49.6
		49.0	53.7
		49.7	52.7
		110.0	96.8
45		108.6	107.0
		108.4	106.0
		120.2	127.2
65		119.3	127.3
		120.5	127.0
		115.6	104.8
75		116.6	129.5
		119.4	127.3
		113.4	115.8
90		116.0	118.5
		117.8	120.2
		113.6	116.6
135		117.8	126.6
		121.3	125.0
		117.2	106.2
150		116.6	114.1
		120.6	117.8
		75.0	94.6
Exit		77.1	85.9
		77.5	87.7

TABLE III.—DATA FOR 4.66-INCH CYLINDER HAVING $\frac{1}{4}$ -INCH FINS AND $\frac{1}{4}$ -INCH SPACERS WITH BAFFLES II, III, AND IV

		$\frac{V_a}{V_t} \times 100$, where $V_t = 100$ 50 m. p. h. 150				$\frac{V_a}{V_t} \times 100$, where $V_t = 100$ 50 m. p. h. 150				
θ degrees	Exit width, inches									
		1.5	2.1	2.5	2.1	1.5	2.1	2.5		
$\beta = 40^\circ$										
15		57.6	71.0	60.8		15		45.2	45.2	45.4
		60.8	68.0	59.0				46.0	47.8	45.0
		58.9	68.3	59.5				49.0	48.6	47.0
		81.6	93.6	90.4				92.0	97.8	96.4
25		82.0	89.5	92.6		45		91.2	102.3	103.0
		85.3	95.8	94.6				90.2	101.8	103.0
		91.6	101.0	98.0				100.0	105.8	104.2
45		88.5	95.5	95.8		55		96.9	111.3	108.0
		87.8	100.0	99.3				101.9	111.7	110.7
		89.4	101.2	95.8	98.4			100.0	106.6	103.2
90		84.3	97.4	97.8	99.6	90		105.2	114.0	109.0
		90.6	98.7	99.3	98.0			102.9	117.9	112.1
		90.8	84.6	89.0				93.2	104.4	103.4
135		84.4	89.2	91.0		135		99.5	111.5	109.7
		83.0	89.5	91.7				104.8	116.0	111.5
		70.4	52.3	45.6	50.2			84.4	69.4	53.2
Exit		63.8	52.2	48.9	46.0	Exit		92.6	76.3	57.0
		66.7	52.7	50.8	47.6			94.2	77.5	60.3
$\beta = 100^\circ$										
15		45.6	42.2	46.4		15		43.4	45.0	42.4
		43.3	49.0	46.6				41.8	47.6	44.1
		45.2	49.7	46.5				43.0	48.8	43.6
		100.0	110.0	110.4				104.6	109.8	105.4
45		102.0	108.6	107.9		45		105.3	112.0	107.1
		103.6	108.4	109.9				105.3	113.4	110.0
		111.2	120.2	124.0				112.4	121.0	117.4
65		113.0	119.3	126.3		85		117.2	131.0	122.5
		113.2	120.5	127.4				118.6	131.3	123.4
		99.6	115.6	115.8				104.8	115.0	105.6
75		105.3	116.6	117.9		90		109.2	119.2	111.5
		105.7	119.4	120.5				110.2	121.3	113.3
		96.4	113.4	112.2				101.2	111.2	103.8
90		100.0	116.0	118.0		95		108.7	117.1	109.1
		101.1	117.8	117.8				109.5	120.4	111.2
		96.4	113.6	107.0				100.2	105.2	104.6
135		98.4	117.8	110.2		135		105.7	111.3	109.5
		101.1	121.3	111.7				107.0	115.2	113.2
			117.2					90.4	73.4	57.2
150			116.6			Exit		101.0	76.6	64.4
			120.6					101.0	79.7	63.1
Exit		91.0	76.0	71.0						
		94.2	77.1	68.8						
		95.7	77.5	67.3						
$\beta = 140^\circ$										
15		48.0	52.4	46.6		15		48.0	52.4	46.6
		47.0	51.2	47.1				47.0	51.2	47.1
		47.9	51.8	46.3				47.9	51.8	46.3
		112.4	113.6	108.0				112.4	113.6	108.0
45		113.8	113.7	109.8		45		113.8	113.7	109.8
		115.3	116.0	108.9				115.3	116.0	108.9
		132.6	131.0	126.0				132.6	131.0	126.0
90		136.4	133.0	131.4		90		136.4	133.0	131.4
		137.3	132.0	132.7				137.3	132.0	132.7
		102.4	104.0	101.0				102.4	104.0	101.0
105		114.0	107.6	107.2		105		114.0	107.6	107.2
		114.0	107.0	106.1				114.0	107.0	106.1
		82.6	90.0	81.6				82.6	90.0	81.6
115		88.4	90.5	88.5		115		88.4	90.5	88.5
		91.2	92.8	91.8				91.2	92.8	91.8
		72.4	75.0	78.6				72.4	75.0	78.6
135		90.7	89.4	92.6		135		90.7	89.4	92.6
		94.8	91.3	94.7				94.8	91.3	94.7
		73.4	63.0	51.6				73.4	63.0	51.6
Exit		82.4	61.7	52.2		Exit		82.4	61.7	52.2
		83.0	59.9	54.5				83.0	59.9	54.5

11, modified by rear fillet.

TABLE IV.—DATA FOR THE 4.66-INCH CYLINDER
HAVING 3/4-INCH FINS AND 1/4-INCH SPACERS WITH
BAFFLES V, VI, AND VII

		$\frac{V_a}{V_t} \times 100$, where $V_t = \frac{50 \text{ m. p. h.}}{150}$		
Battle α degrees	V	VI	VII	
15	41.2	36.8	39.4	
	41.2	36.4	38.2	
	89.4	77.0	38.0	
45	91.	78.8	83.2	
			85.3	
			118.0	
85			125.0	
			123.3	
			123.0	
90	86.4	74.6	132.0	
	94.2	79.7	132.0	
			132.0	
120	102.8	86.2	125.4	
	117.7	98.0	135.2	
	117.3		133.2	
135	133.8	108.6	133.8	
	140.1	128.2	136.5	
	141.5		138.4	
Exit	98.0	102.4	100.6	
	106.2	134.5	87.5	
	111.3		94.9	

TABLE V.- DATA FOR 7.0-INCH CYLINDER HAVING
3/4-INCH FINS AND 1/4-INCH SPACERS

		$\frac{V_r}{V_t} \times 100$, where $V_t = \frac{50 \text{ m. p. h.}}{150}$			
O degrees	No baffle	Baffle IX		Baffle X	
		A	B	A	B
15	50.0	43.8	40.6	45.6	47.2
	49.0	43.7	44.9	46.7	46.0
	48.7	44.0	44.9	46.7	46.5
45	111.4	103.2	102.8	104.6	106.4
	111.6	102.7	104.8	107.2	108.3
	113.3	103.0	104.2	106.6	108.0
65		112.0	112.6	112.6	118.6
		115.0	115.2	121.1	120.3
		115.7	115.0	123.3	120.3
75	130.2	104.4	104.0	96.4	95.4
	139.0	104.6	108.5	107.4	108.6
	139.3	107.0	111.7	111.3	111.0
90	103.8	93.8	99.0	91.4	87.8
	116.9	102.2	108.3	100.0	99.4
	116.6	106.5	109.0	103.3	102.7
135		90.2	100.4	99.6	98.0
		96.3	105.9	104.4	104.0
		99.6	109.0	108.0	104.6
Exit		69.2	67.2	41.4	46.4
		75.8	69.5	42.5	43.1
		77.6	75.5	45.4	45.6

TABLE VI.—DATA FOR 4.66-INCH CYLINDER HAVING
3/4-INCH FINS AND 1/2-INCH SPACERS WITH NO
BAFFLE AND WITH BAFFLE VIII

		$\frac{V_z}{V_1} \times 100$, where $V_1 = 100$ 50 m. p. h. 150				
θ degrees	β degrees	40	100	140	180	220
	No baffle	Baffle VIII				
15	43.6 49.8 52.7	36.2 38.0 38.1	33.6 37.9 38.6	37.2 37.1 38.6	38.2 43.0 45.2	39.2 45.2 45.7
25	50.4 53.4 50.0	50.0				
45	88.2 103.2 104.6	46.6 48.5 50.1	60.0 70.1 71.3	74.6 86.6 87.5	78.6 95.0 97.3	86.0 96.4 100.3
55			45.2 58.7 59.6			
65				55.6 74.3 82.0		
75	71.2 101.3 104.7			57.8 51.9 56.4		
85					45.0 60.4 61.3	
90	29.4 40.4 41.4	36.8 35.4 36.8	38.4 45.5 49.5	33.6 43.1 45.8	27.0 44.0 44.9	37.8 62.1 63.9
95					25.6 31.4 36.0	
105						13.0 12.3 12.9
115						
135		32.6 38.2 43.1	36.2 47.6 56.1	34.6 47.1 49.3	21.2 27.6 33.8	20.0 18.8 19.6
150						18.4 15.4 16.6
Exit		41.0 32.4 38.1				

REPORT No. 556

FURTHER STUDIES OF FLAME MOVEMENT AND PRESSURE DEVELOPMENT IN AN ENGINE CYLINDER

By CHARLES F. MARVIN, JR., ARMISTEAD WHARTON, and CARL H. ROEDER

SUMMARY

The investigation described in this report, was carried out at the National Bureau of Standards at the request and with the financial assistance of the National Advisory Committee for Aeronautics. Stroboscopic apparatus, previously described, for observing flame movement through a large number of small windows distributed over the head of a spark-ignition engine was used in following flame spread with combustion chambers of different shapes at two engine speeds and for a variety of spark-plug locations including single and twin ignition. The principal factors influencing flame movement in the engine are discussed, and the lack of reliable information regarding their separate effects upon the structure of the flame and its speed of propagation are emphasized.

INTRODUCTION

The explosion in a gasoline engine is not an instantaneous but a progressive process, a flame originating at the spark plug and spreading throughout the combustion chamber. The development of pressure and the resulting production of power is dependent upon the nature of this flame spread, as is also the "roughness" of the engine associated with explosion shock and and the "knock" that accompanies detonation. Knowledge of the fundamental facts regarding the actions in the gaseous contents of the engine cylinder during the combustion period is thus important in connection with the design of efficient and smoothly operating engines.

A previous report (reference 1) presented results showing flame movement to all parts of the combustion chamber and simultaneous pressure development in an engine operating on diverse gaseous fuels. The effects of varying the mixture ratio, degree of dilution, charge density, spark advance, and engine speed were measured using a flat cylinder head at compression ratios of 3.6 and 5. The experiments described in the present report give results of a similar nature, obtained by operating the engine on motor benzol with four differently shaped combustion chambers, each giving a compression ratio of 5, and with various arrangements of single and twin ignition. The results of both sets of measurements are reviewed in a general discussion of the major basic factors influencing flame velocities in the engine.

APPARATUS AND PROCEDURE

The 4-stroke-cycle, single-cylinder, L-head engine of 3 $\frac{3}{4}$ -inch bore and 4-inch stroke, the auxiliary apparatus, and the procedure described in reference 1 were used in the present measurements with only minor changes to facilitate observation and improve precision.

The four special cylinder heads of approximately 5:1 compression ratio with combustion chambers of different shape are shown in figure 1. Head B is the flat steel head used in the experiments of reference 1. Head C, domed over both cylinder and valves, was made from the original cast-iron head of the engine. Heads D and E, domed over the valves alone and with small clearance over the piston, were made of cast brass and differed only with respect to the inward protrusions shown clearly in the photograph of head E. All heads were water-cooled, head B having a separate system not connected with the block.

Each head was provided with a large number of small windows symmetrically distributed over the combustion chamber. These windows were observed through a stroboscope that provided a momentary view at the same point in successive cycles. By varying the timing of the view, it was possible to follow the progress of the flame as it spread from the spark plug to all parts of the charge. Possible positions of the spark gap are shown in the photograph of head B.

Pressure changes during combustion were measured with a balanced-diaphragm indicator of the type described in reference 2.

In order to check the visual observations and to secure a permanent record of the flame travel, photographs like those shown in figure 2 were taken through the stroboscope on many of the runs. The set-up used for this purpose is shown in figure 3. For convenience in analyzing the results, a cardboard mask, showing an outline of the combustion chamber and relative positions of piston and valves, was placed just over the head. Holes punched in the mask permitted a view of the flame through the windows. A small camera loaded with panchromatic motion-picture film was mounted at the stroboscope eyepiece and focused on the head as viewed in a mirror placed above the engine. The stroboscope thus acted as a high-speed shutter giving a very brief exposure once each

explosion at the same point in the cycle. When taking a picture, the camera shutter was usually left open for 30 seconds, thus exposing the film to a selected phase of about 250 explosions (at 1,000 r. p. m.). A run included a series of such composite pictures taken at successive 2° intervals during the period of inflamma-

tion. Motor benzol was used as fuel in all runs. Air and fuel flows were adjusted to maintain approximately optimum mixture ratio and a constant weight of charge per cycle equivalent to 75 percent volumetric efficiency for atmospheric conditions of 760 mm of mercury pressure and 20°C .

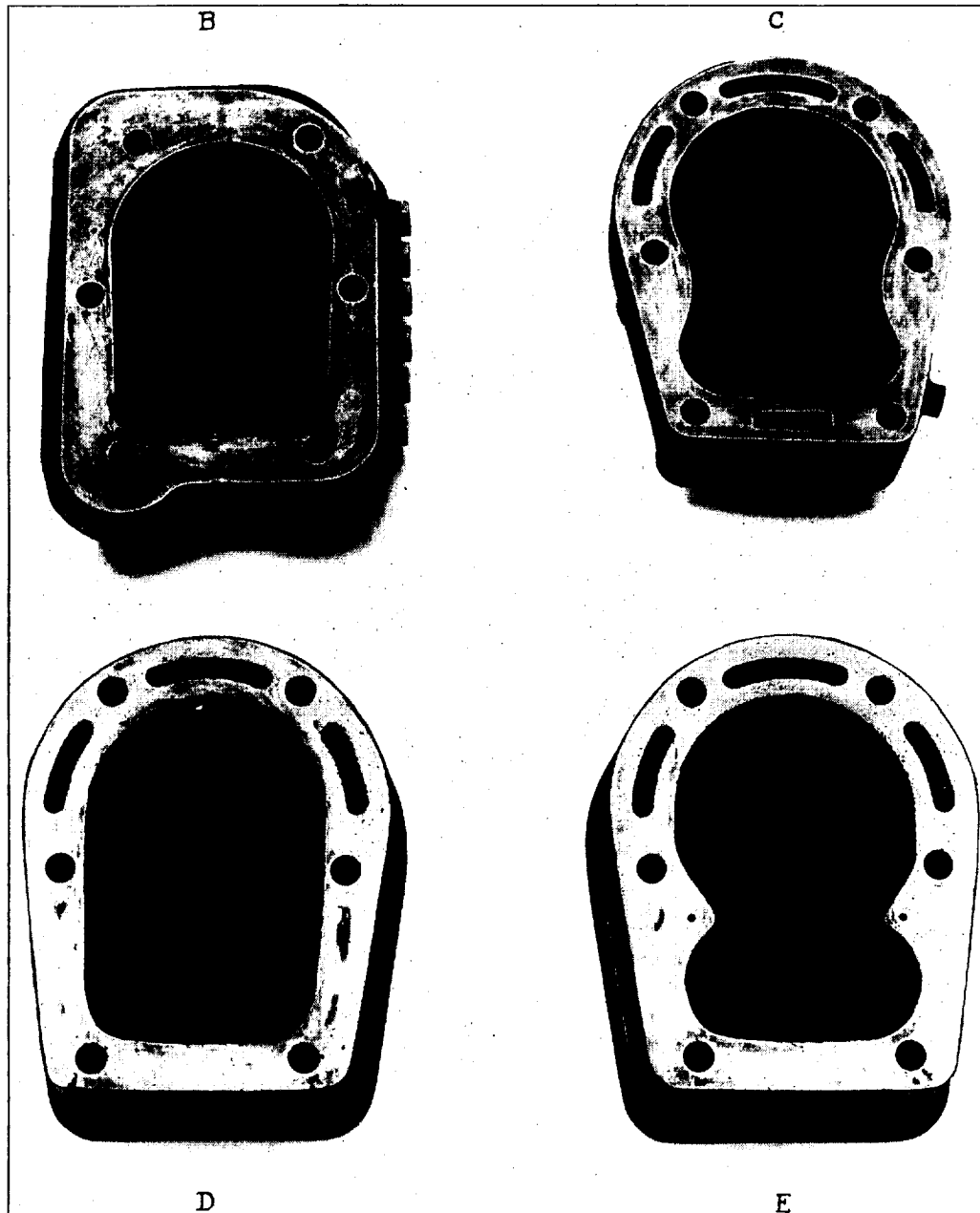


FIGURE 1.—Special engine heads used in flame-travel observations.

tion. Each negative was identified by including in the picture small cards showing run number and stroboscope setting, the latter being expressed in degrees of crank rotation before top dead center (BTDC) or after top dead center (ATDC).

RESULTS OF EXPERIMENTS

General characteristics.—During a normal explosion in the engine cylinder, the spark initiates a luminous region that spreads rapidly in all directions from the plug, gaining in brightness as it spreads until the whole

charge is inflated. Although the luminosity decreases as the piston recedes, it is usually visible far down on the expansion stroke.

just reached by the average flame front at a given stroboscope setting receive light from some explosions and not from others and therefore appear dimmer on

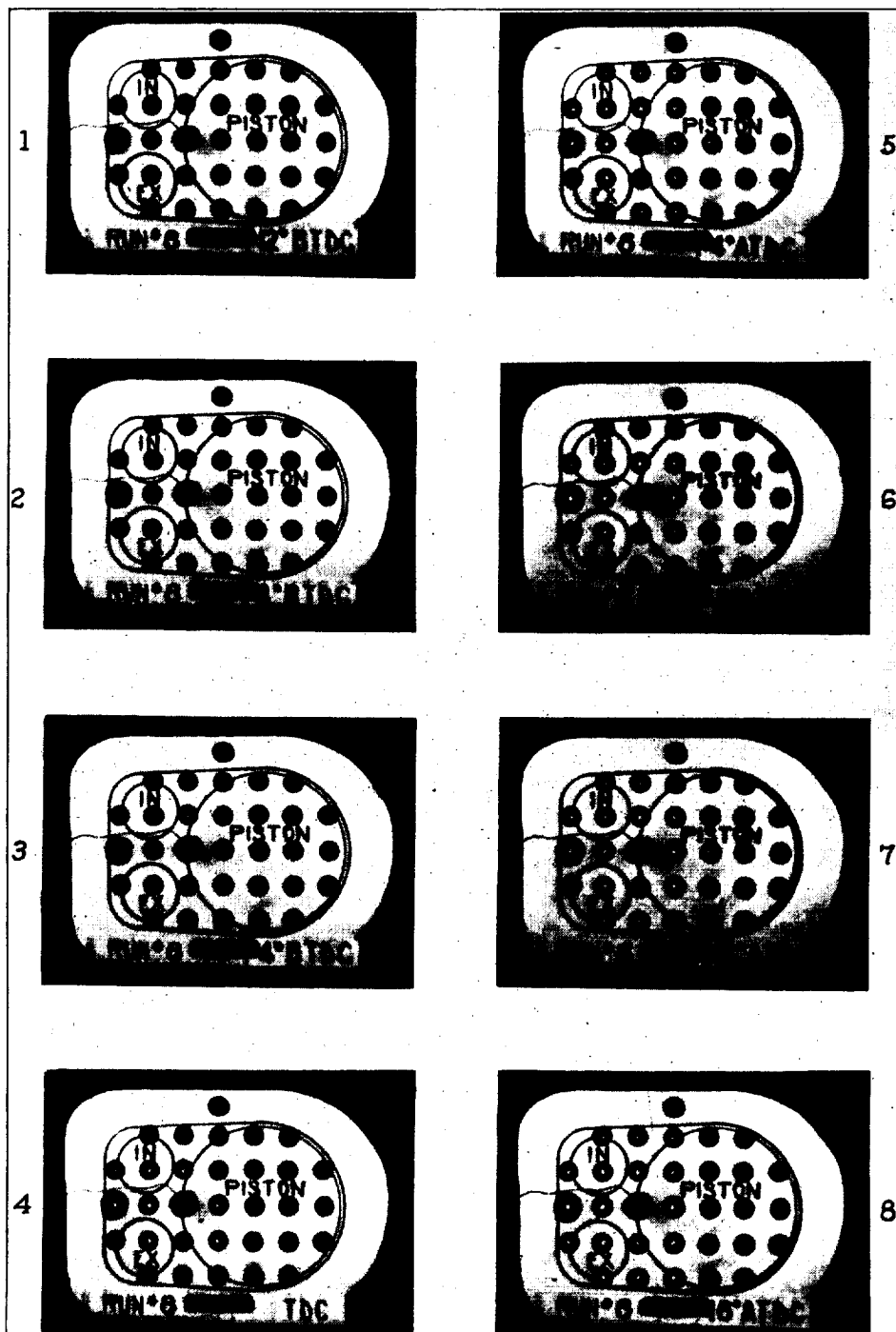


FIGURE 2.—Typical photographs showing spread of flame; 20° spark advance; head B; 1,000 r. p. m.

Successive explosions do not repeat exactly either in speed or general pattern of spread, and the diagrams presented here represent the average of many cycles. Owing to the irregularity from cycle to cycle, windows

the photographs than windows previously illuminated. The depth of the flame under these borderline windows is also likely to be small, especially in the region of the plug, owing to the probable curvature of the vertical

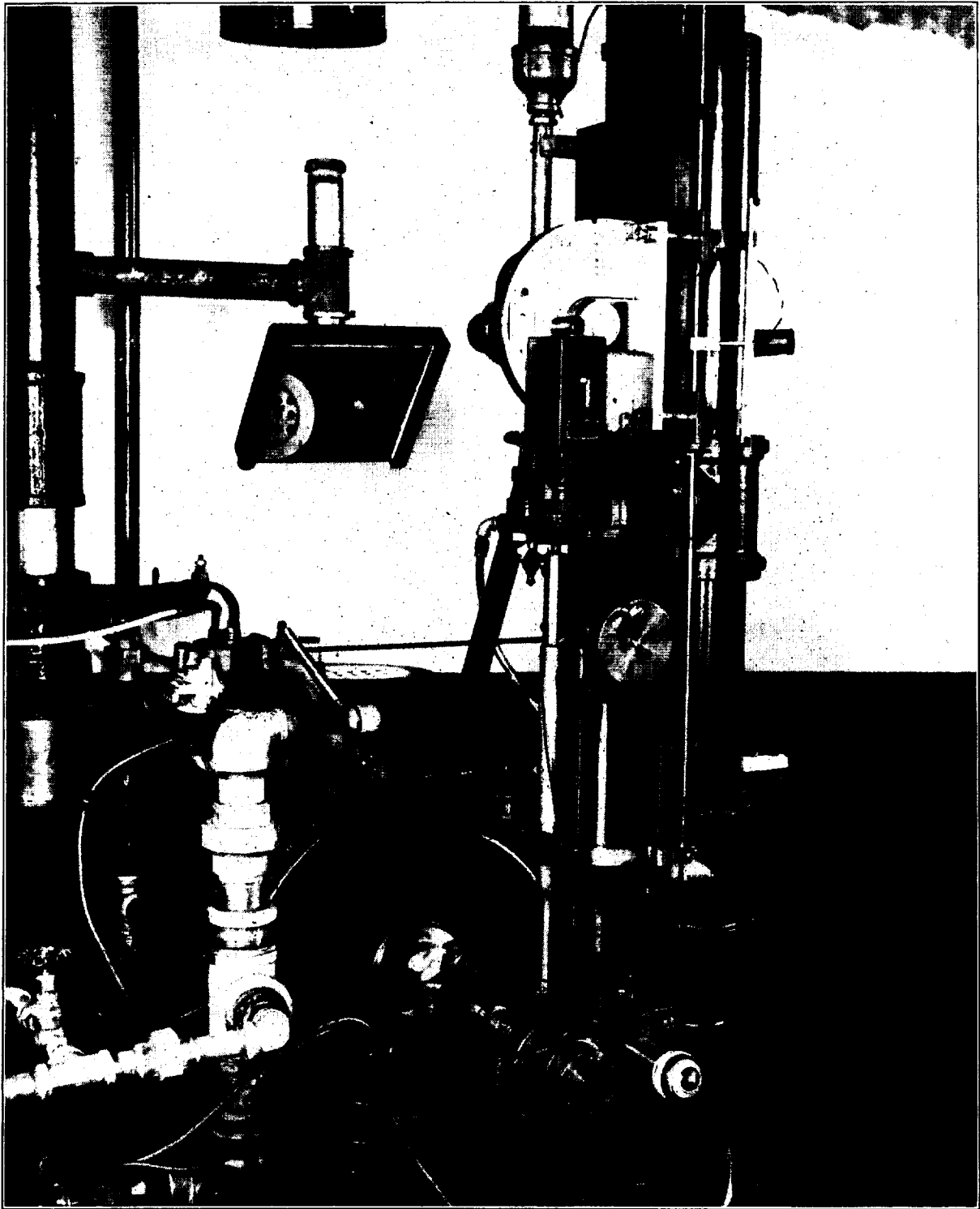


FIGURE 3.—Apparatus used in photographing flame spread.

section of the flame front. In the cases shown by the photographs of figure 2, the depth of the flame over the piston is somewhat less than that at other parts of the combustion chamber, owing to the fact that the piston face rises above the cylinder block. Moreover, this depth is variable to a slight extent due to piston movement. In the other three heads, variable depth results also from curvature of the ceiling of the combustion chamber. Although the windows were thoroughly cleaned before each run, some windows tend to accumulate a deposit of carbon sooner than others, which makes them appear relatively dimmer after a short period of operation. In addition, differences undoubtedly exist in the character and intensity of the illumination emitted at different points within the inflamed gases.

In spite of these time and space variations in the intensity of the illumination, there is usually a sharp distinction between the inflamed region and the adjacent dark gases, and it is generally possible for a number of operators to estimate, with an average uncertainty of about two crankshaft degrees, the time of arrival of the average flame front under a given window, either by visual observation through the stroboscope or by examination of the photographic records. Timing of the spark varied by less than one-quarter of a degree from cycle to cycle.

Effect of combustion-chamber shape.—In figures 4 and 5, flame-front positions at successive 5° intervals after ignition are shown on plan views and vertical center sections of each of the four combustion chambers for two different engine speeds. No observations of flame travel in the vertical plane were made, the flame positions in the vertical sections having been estimated from the plan views. Instantaneous positions of the piston face, where it intercepts the flame fronts, are shown by the dashes. Corresponding sets of indicator diagrams are given in figures 6 and 7. On these and succeeding indicator diagrams the points of complete inflammation, as judged from observations of the flames, are indicated by circles.

The striking feature of these results is their similarity, i. e., pronounced alterations in combustion-chamber shape and engine speed produce only minor changes in flame movement and pressure development as referred to crank or piston travel. Distortion of the flame diagrams from truly concentric spread is not very great in any case. Within a range of 6° (from 11° to 17° after top center) all the flame diagrams reach complete inflammation and all the indicator diagrams arrive at their peak pressures. The maximum rate of pressure rise (about 25 pounds per square inch per degree of crank angle) is approached rather closely in all the diagrams and maximum pressures range between 315 and 365 pounds per square-inch gage.

While differences between diagrams for the different heads are little greater than the experimental uncer-

tainty, some of them are sufficiently consistent to be of interest. Flame travel during the first 15° after the spark is most rapid for the flat head B, slower for the moderately domed head C, and still slower for the higher domes of D and E. The rates of pressure rise during the early stages of combustion show a similar order for the different heads, but the indicator diagram for head C crosses that for head B about 16° after the spark at both engine speeds. Throughout the major portion of the pressure rise, the indicator diagrams for the four heads are nearly parallel and are arranged in the same order at both engine speeds.

The higher maximum pressures attained with head B, together with the fact that compression and expansion lines at both speeds are steeper than for any of the other heads, indicate that the compression ratio for head B was a little higher than for the other heads, probably due to compression of the three gaskets used with this head.

Windows around the piston end of head C became sooted quickly and the very small depth of flame under these windows made readings very uncertain. No reliable readings were obtained in this region at 600 r. p. m.

Effect of engine speed.—As in previous experiments (reference 1), no significant variation in the general pattern of flame spread resulted from a change in engine speed, and the flame and pressure diagrams, plotted with respect to crank position, are nearly the same for 600 and 1,000 r. p. m. Although the differences are slight, they are consistent for all heads and indicate that flame velocity and the time rate of pressure development increase only a little more slowly than engine speed. The increase in the rate of combustion with increase in engine speed is well established and is generally attributed to greater turbulence (references 3 and 4).

Figure 8 is typical of the effect of change in engine speed on the indicator diagrams for all heads. A more gradual slope on the compression and a steeper slope on the expansion lines at 600 r. p. m. is evidence of the greater heat loss from the charge at the lower speed.

Effect of number and location of ignition points.—Special spark plugs that could be inserted at any window location were made to permit a study of the effect of the number and position of the points of ignition. The results with a normal spark advance of 20° are shown in figures 9 and 10. Severe preignition occurred when two of the "hot" special plugs were used simultaneously and, in order to eliminate this feature, a second series of runs (figs. 11 and 12) were made with the spark retarded to 10° . These runs compare single and double ignition under otherwise fixed conditions.

As would be expected, a more rapid pressure rise is accomplished by double ignition although the difference when compared with a single plug favorably placed near the center of the combustion chamber is negligible for the particular conditions of tests.

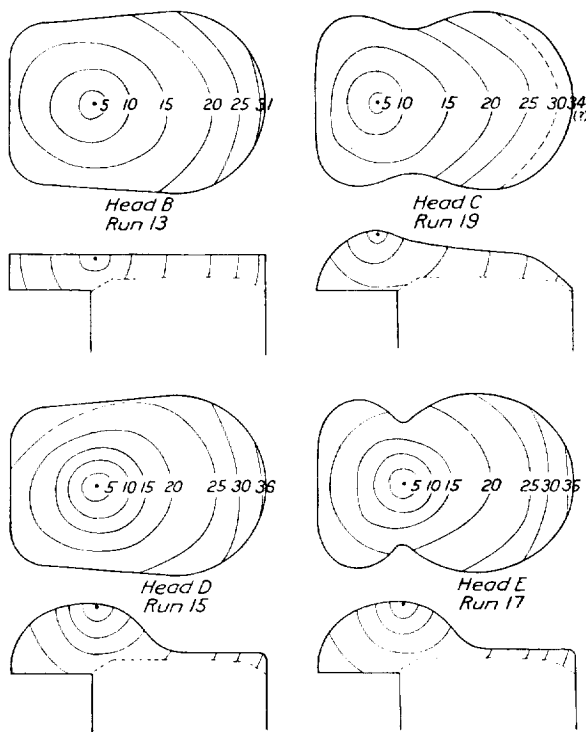


FIGURE 4.—Flame-travel diagrams for different combustion chambers—600 r. p. m.; 20° spark advance.

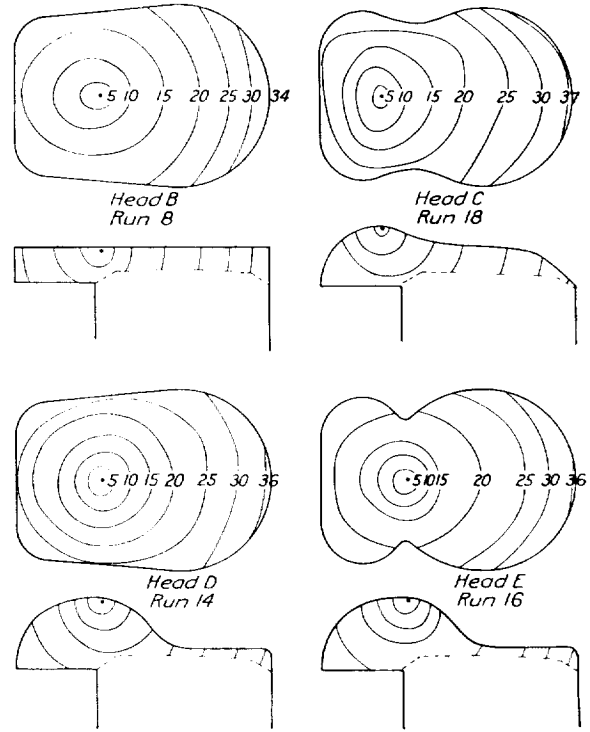


FIGURE 5.—Flame-travel diagrams for different combustion chambers—1,000 r. p. m.; 20° spark advance.

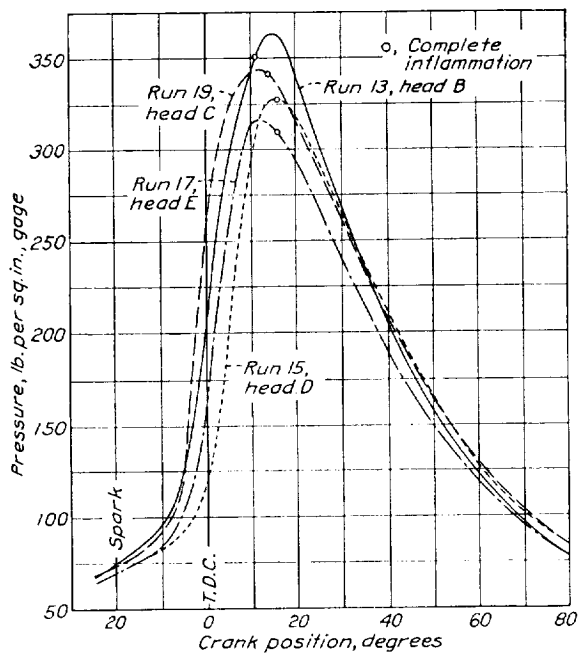


FIGURE 6.—Indicator diagrams for different combustion chambers—600 r. p. m.; 20° spark advance.

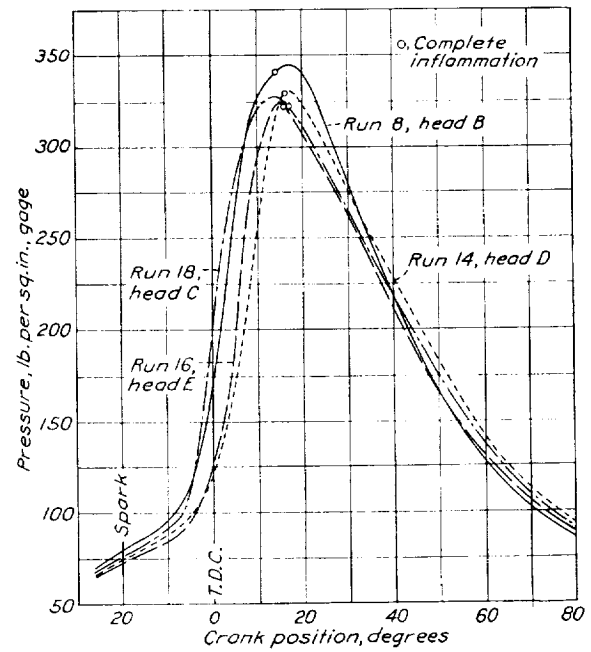


FIGURE 7.—Indicator diagrams for different combustion chambers—1,000 r. p. m.; 20° spark advance.

With single ignition, inflammation time was shortest and pressure rise most rapid when the spark plug was located near the center of the combustion chamber (runs 1 and 8). With side ignition (runs 4, 5, 11, and 12) the distance from the plug to the opposite wall is little greater than for the more central location and inflammation time was about the same except in run 4, which for some unknown reason is not consistent with the other runs of this group. The later pressure rise for the side ignition is probably due to the less rapid increase in area of flame in the early stages as compared with the more central ignition. Locating the single spark plug close to an end of the combustion chamber gave the longest inflammation time and the most gradual and prolonged pressure rise, which was to be expected since the distance the flame must travel is a maximum and the flame area is most restricted.

The marked differences in appearance of the indicator diagrams for the various plug locations and the accompanying differences in power developed would, of course, be greatly reduced if the optimum spark advance for each location had been substituted for the fixed advance used. A comparison of combustion characteristics when the charge is fired at various positions with optimum spark advance for each position is reported in reference 4.

Figure 13 shows the result of changing the spark-gap location from the ceiling of a domed head to a point midway between the ceiling and the block. The change made little difference in the flame spread as viewed from the top, but accomplished an earlier pressure rise because the flame could spread in all directions from the spark.

DISCUSSION IDEALIZED EXPLOSION

In the review of the many factors that operate more or less independently but simultaneously to influence flame movement in spark-ignition engines, it seems desirable first to recall very briefly the principal features of a highly idealized and simplified explosion. These features are illustrated in figure 14, which shows hypothetical conditions in a long column of gas ignited at one end.

If the tube containing the combustible mixture is open only at the ignition end so that the heated products can escape as they are formed, the flame front will advance into the unburned mixture, and hence along the tube, at a constant speed S_t , which may be called the "transformation velocity" because it is the linear rate at which the charge is transformed chemically.

If the tube is open only at the end opposite the source of ignition, the flame front will still advance into the unburned mixture at this same transformation velocity; but the heated products, now unable to escape to the rear, in expanding push the flame front and the unburned charge forward so that the velocity of the flame front along the tube, although still a constant, is now much greater than in the previous case.

If both ends of the tube are closed, the flame front will start to move at this higher velocity, the long column of unburned gas offering little resistance to the expansion of the first increment of charge to burn. As the flame front advances along the tube, however, the heated combustion products newly formed within it expand in both directions, this expansion being absorbed less and less by the diminishing column of unburned gas ahead and more and more by the increasing column of previously burned charge behind the flame front until, by the time the flame reaches the far end of the tube, all of the expansion is to the rear and the flame velocity in space has decreased to the transformation velocity as a limiting value. This

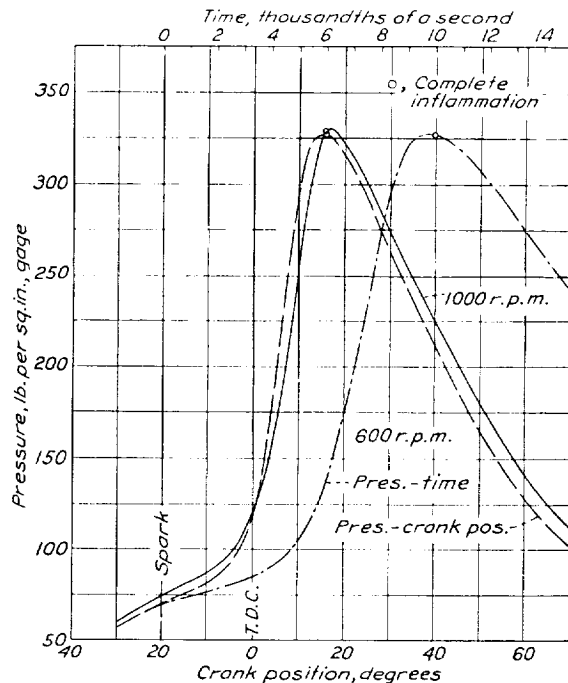


FIGURE 8.—Typical effect of engine speed on indicator diagram.

process has been described very clearly and in considerable detail by Ellis (reference 5).

Thus in normal spark-ignited explosions the velocity S_s of the flame front in space is the sum of the transformation velocity S_t or linear rate at which it advances with respect to the medium supporting it, plus what may be called the "gas velocity" S_u or rate at which the supporting gases are themselves moving through space, or

$$S_s = S_t + S_u \quad (1)$$

The light lines in the diagram show, for the hypothetical case, how elements of charge, originally equally spaced in the tube, move under the influence of the expanding reaction products. Since these lines divide the total mass of charge into equal fractions (tenths) the arrival of the flame front at each successive line completes the burning of another one-tenth of the mass.

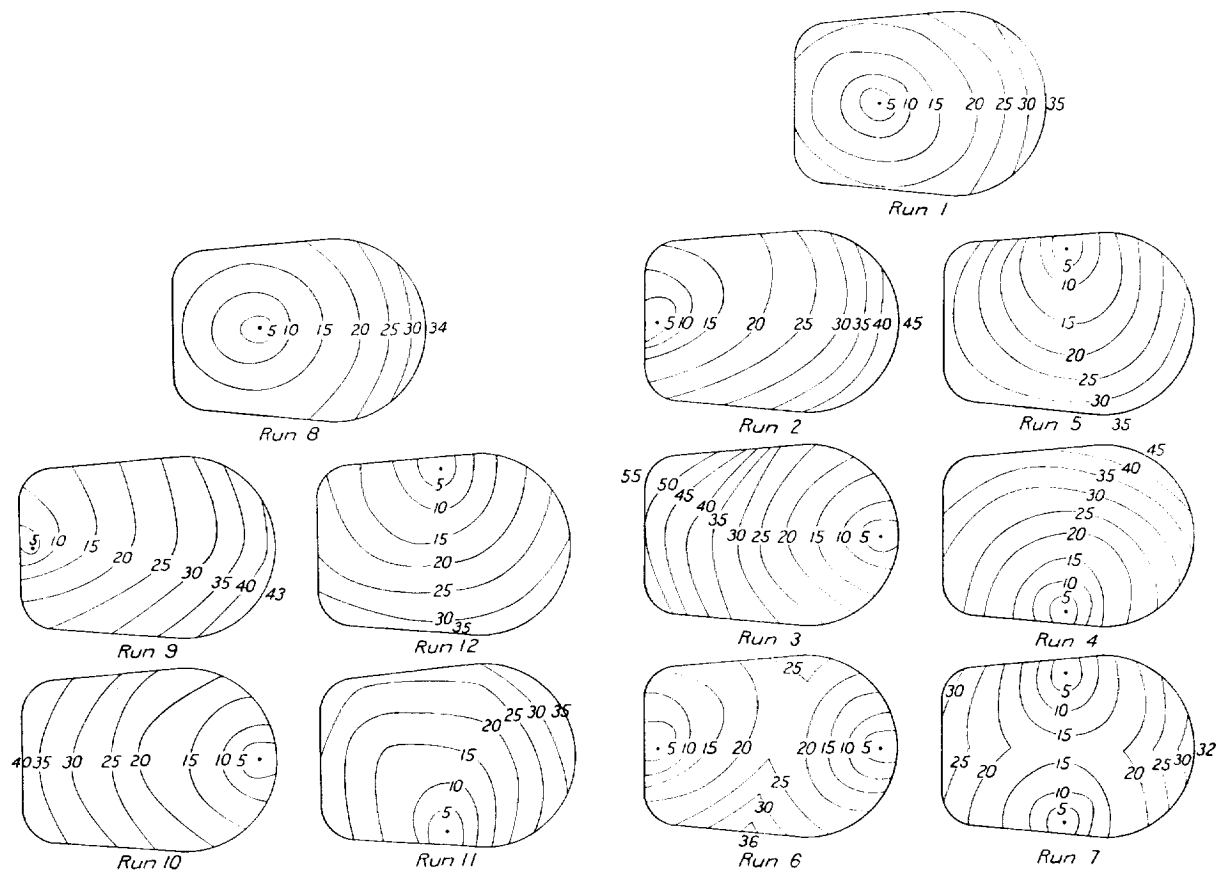


FIGURE 9.—Flame diagrams for different spark-plug locations—20° spark advance; head B; 1,000 r. p. m.

FIGURE 11.—Flame diagrams for different spark-plug locations—10° spark advance; head B; 1,000 r. p. m.

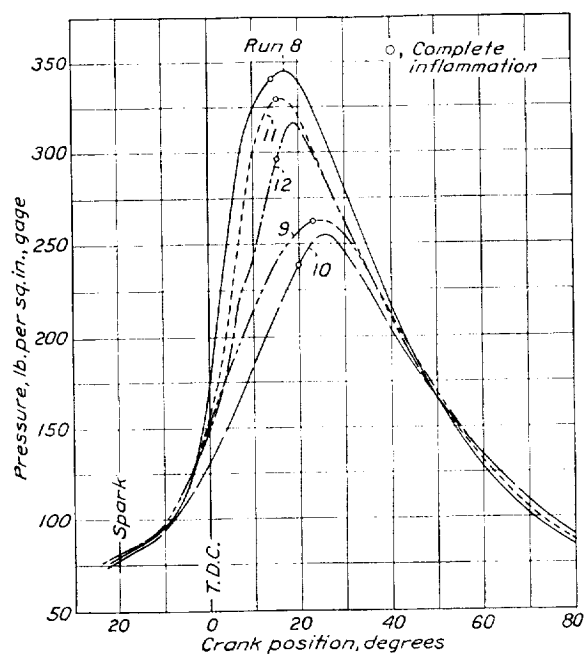


FIGURE 10.—Indicator diagrams for different spark-plug locations—20° spark advance; head B; 1,000 r. p. m.

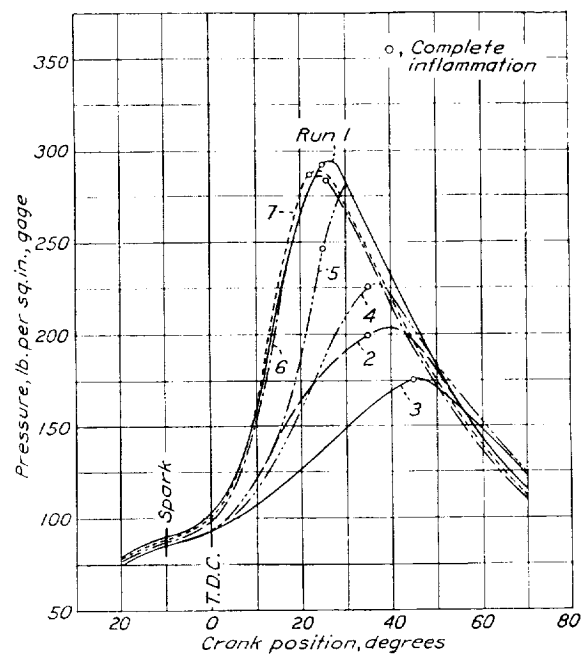


FIGURE 12.—Indicator diagrams for different spark-plug locations—10° spark advance; head B; 1,000 r. p. m.

If pressure rise is assumed proportional to mass burned, a pressure rise against time curve for the explosion may be plotted from the intersections of the flame-travel curve with the light lines.

The mass rate of burning, and hence the rate of pressure rise at any instant will obviously be:

$$M = AS_i D \quad (2)$$

where A is the area of the flame front and D is the density of the charge undergoing combustion. In the simple hypothetical case, A and S_i are constants so the increasing slope of the pressure curve reflects only the increasing density of the unburned charge. Since for a given explosion this density is determined by the in-

mixture. This conclusion is indicated by the fact that the cones of burners operating with constant gas flow are stationary and also by the uniform speed of flame spread in soap-bubble bombs (reference 6). This velocity might be expected to vary with (1) the composition of the unburned charge including both the character of the constituents and their proportions in the mixture, (2) the pressure of the system, (3) the temperature of the unburned charge, and (4) the degree of turbulence in the neighborhood of the flame front. Unfortunately, reliable quantitative information, either theoretical or experimental, as to the separate effects of these four variables upon S_i is either entirely lacking or extremely scarce.

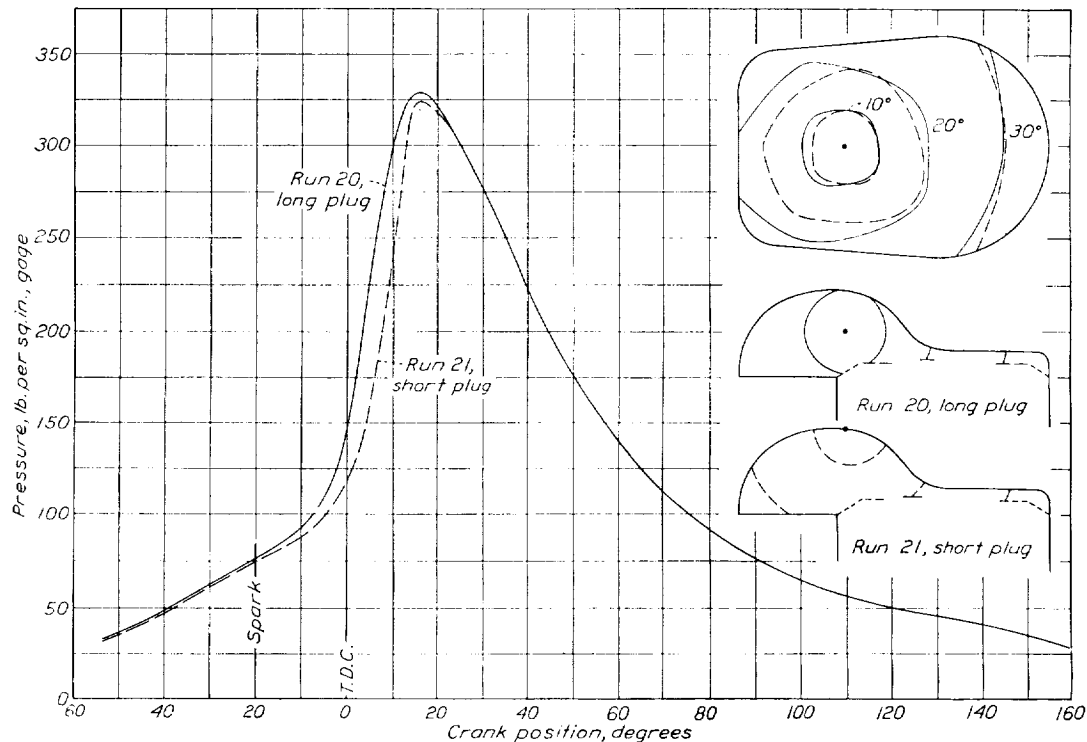


FIGURE 13. Flame and indicator diagrams for spark plugs with long and short electrodes.

stantaneous pressure, control of the rate of pressure rise must be accomplished through control of A or S_i .

This simple illustration gives a rough first approximation of the gross mechanism of a normal explosion in a spark-ignition engine, and equations (1) and (2) contain the principal factors upon which flame movement and pressure development in the engine depend. The two components of the flame's observed velocity may now be examined separately in greater detail.

FACTORS INFLUENCING TRANSFORMATION VELOCITY

The linear velocity S_i at which a flame front will advance into and transform a nonturbulent mixture of uniform composition and at given pressure and temperature would be expected to be a constant of the

In the engine, all of these factors may vary, generally to an indeterminate extent, from point to point in the combustion chamber and from instant to instant during a single explosion. Also, there is no reliable method of resolving the observed velocity S_i in the engine into its components S_i and S_u . The engine with its highly complicated combustion process is, obviously, not well adapted to the isolation and precise evaluation of the separate effects of fundamental factors, and experiments with the simplest types of gaseous explosions, begun by Professor Stevens, are being continued at the National Bureau of Standards as a means of obtaining this basic information.

Meanwhile, an effort has been made to detect in the engine diagrams any outstanding effects that might be

attributed to the four above-mentioned factors, with the realization that it is not possible to explain the observed variations in flame velocity with assurance and that all interpretations must be regarded as speculative to a considerable degree.

Charge composition.—Experiments (reference 1) with equivalent mixtures of different gaseous fuels show rather large differences in observed flame speed S_f . Since the heating values of these mixtures are about the same, little difference would be anticipated in the amount of expansion and, since the same engine-operating conditions were maintained in all runs, a variety of transformation velocities for the different fuels appears to be the only logical explanation for the considerable differences in observed flame speed.

A departure from optimum mixture ratio or an increase in the percentage of residual gases has been found (reference 1) to reduce the observed velocities in

stant-volume bomb made from the engine head (reference 1).

Temperature of the unburned charge.—A rise in temperature of the unburned charge may operate to change transformation velocity both directly through an increase in molecular velocities and indirectly, if the rise in temperature is great, by causing preflame reactions that alter composition.

The temperature of the charge at the time the spark occurs may be varied by changes in spark advance, compression ratio, or ratio of fresh to residual charge. Each of these factors was varied in this investigation but any effects of change in charge temperature upon reaction velocity were so confused with the effect of altered combustion-chamber proportions or charge composition as to be indistinguishable.

During the course of an explosion the unburned charge is constantly heated by compression and probably by preflame reactions, and the transformation velocity would be expected to show an accompanying increase. Such an increase would tend to offset the decrease in the gas-velocity component predicted by the idealized explosion and thus minimize variations in the velocity of the flame front in space. A few of the diagrams show a nearly constant velocity throughout the inflammation period. The great majority, however, exhibit low initial velocities, increasing velocities during the early stages and decreasing velocities near the end of the inflammation period. Relatively low velocities at the start and finish are also prominent features of many flame diagrams obtained by other investigators in the absence of detonation. (See references 8, 9, and 10.)

The diminishing velocity as the flame approaches the wall in a normal explosion shows that the increase in transformation velocity resulting from the rise in charge temperature is insufficient to offset entirely the decrease in gas velocity, even in the latter stages of the explosion where the greatest effects of rising temperature might be anticipated. It seems improbable, therefore, that relatively low-charge temperature is entirely responsible for the low-flame speeds during the early stages.

Turbulence.—It is well known that the rate of combustion increases with the degree of turbulence in explosive mixtures and it appears that this increase is brought about by a more rapid advance of the flame front with respect to the unburned mixture; that is, by a higher value of S_f rather than by a distortion of the pattern of flame spread by general swirling gas movements. The most satisfactory explanation for this phenomenon, as well as for the fact that flame speed increases with engine speed, seems to be that small-scale turbulence, in the form of small eddies of a highly random nature, exists throughout the charge in the cylinder and that the degree of this turbulence increases with engine speed.

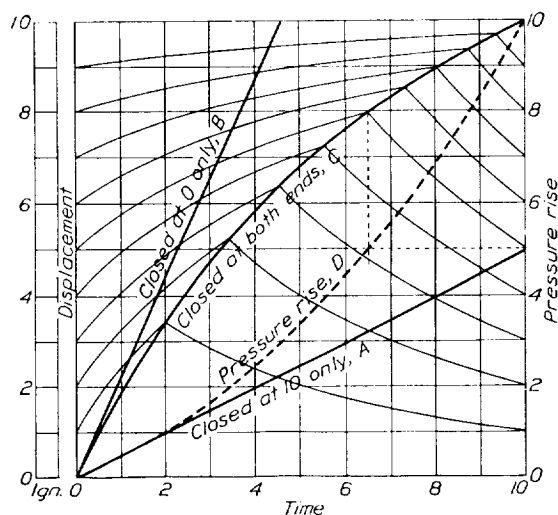


FIGURE 14.—Flame travel and pressure rise for simple idealized explosion in tube.
Curve A. Flame front displacement, tube closed at upper end only.
Curve B. Flame front displacement, tube closed at ignition end only.
Curve C. Flame front displacement, tube closed at both ends.
Curve D. Pressure rise, tube closed at both ends.
Light lines show displacement of planes 1-9, tube closed at both ends.

the engine, undoubtedly through a reduction in both transformation velocity and the amount of expansion in the reaction zone.

Pressure of the unburned charge.—Under conditions where variations in pressure so affect dissociation as to cause pronounced changes in the composition and specific volume of the burned gas, a considerable effect of pressure upon both S_f and S_u might be anticipated. An effect of pressure upon observed flame speed in space, which might be attributed to shifts in equilibrium conditions, has been reported by Flock and King (reference 7) for moist mixtures of CO and O₂ at initial pressures up to 1 atmosphere. For higher initial pressures in mixtures of hydrocarbons and air, however, these effects are apparently reduced to such an extent that no significant effect of pressure was detected in flame diagrams for the engine or for a con-

Kindling of the unburned charge must be accomplished largely, if not entirely, by direct collisions between newly formed materials from the flame and molecules of unburned charge, for the unburned gases can absorb little radiation and the time is not sufficient for conduction and convection to penetrate more than a very small distance ahead of the rapidly advancing flame.

In a perfectly quiescent mixture the process of diffusion alone controls the extent of intermingling of the burned, burning, and unburned phases in the neighborhood of the flame front. In such a mixture the number of collisions contributing to the combustion process per unit area of flame front in unit time is relatively small, and S_f has a minimum value characteristic of the mixture. It is this characteristic value of S_f that is approached or obtained in explosions of quiescent mixtures in bombs and in burner flames.

A vigorous random stirring of the gases in the neighborhood of the flame front, resulting in the mechanical mixture of burned, burning, and unburned materials in a zone of considerable depth would increase the probability of fruitful collisions and raise the value of S_f . Apparently it is through the action of some such local, perhaps even microscopic, turbulence that increased engine speed accomplishes a nearly proportional increase in flame speed.

Less of this type of turbulence in the high domes of combustion chambers D and E may be partly responsible for the slower flame spread and pressure rise in these cylinders as compared with those having the flatter heads. Very little is known about the character and mode of action of this turbulence but, if means can be devised for producing and modifying it locally in the engine cylinder, it should prove to be an effective medium for combustion control.

FACTORS INFLUENCING GAS VELOCITY

In addition to the small-scale random eddies that affect S_f , other more general movements of the charge will influence the observed flame speed S_f without altering S_f . The rate at which the flame front is transported bodily in a direction normal to its surface by such general movements of the gases supporting it has been briefly termed the "gas velocity", S_g . Large-scale gas movements capable of transporting the flame in this manner may be caused by (1) expansion of the burning gases, (2) piston motion during the burning period, or (3) the remnant of the swirl set up during the inlet or compression stroke.

Many published records of individual explosions, particularly in bombs and tubes, show that gas velocity may also be influenced by vibrations and wave effects. These effects are, however, not detected in the average diagrams for as many explosions as obtained by the stroboscopic method.

Expansion due to burning.—It has been seen that for the simple hypothetical explosion in the closed tube (fig. 14), gas velocity is a maximum just after ignition and decreases gradually to zero as the flame reaches the opposite end of the tube. In any so-called constant-volume explosion, each increment of charge overtaken by the advancing flame front is burned, not at constant volume, but more nearly at constant pressure and it therefore expands to an extent dependent largely upon the temperature rise for the reaction. When an increment of charge expands in the reaction zone, it compresses both the unburned charge ahead and the previously burned charge behind, the linear movement in each direction being approximately proportional to the relative volume of gas in that direction. In this process the flame front will be advanced only to the extent that the unburned charge is compressed. If it is assumed that reaction and heat liberation are confined to the flame front, the contribution of expansion to the flame's velocity will be a maximum just after ignition, for at this time the volume of unburned gas ahead of the flame is a maximum in all directions, and the whole expansion is effective in compressing the unburned gas and advancing the flame front. In a nonsymmetrical combustion chamber, the speed at which the flame front is carried away from the point of ignition will begin to slacken first in the direction of the nearest wall, for here the relatively shallow layer of unburned gas has the least freedom of movement normal to the flame with the net result that expansion takes place to the rear, where it contributes to the advance of the flame front in those regions still distant from a wall.

In general, the effect of gas movements set up by the burning of a charge in a nonsymmetrical container is to carry the flame front most rapidly toward the greatest volume of unburned gas; i. e., there is a tendency for the flame surface to shape itself to the container walls. This tendency is very strikingly demonstrated in many of the flame photographs published by Ellis (reference 11). It is detectable also in some of the diagrams reproduced in the present report.

Piston motion.—Both the position of the piston and its rate of motion influence flame velocities in a complicated manner dependent somewhat upon the combustion-chamber shape and spark-plug location.

When the spark occurs, the piston is normally moving upward near the top of the compression stroke. The resulting general compression opposes expansion in the reaction zone and thus tends to reduce gas velocity, the extent of this effect increasing with spark advance. The greater combustion-chamber volumes, however, at greater values of spark advance, favor higher gas velocities. Conflicting influences also control the transformation velocity. With greater spark advance, charge temperature will be lower but local

turbulence may be higher for some combustion chambers. That the net effect of these opposing factors upon flame speed in space may be very small, has been shown by the similarity of the flame diagrams (reference 1) obtained with spark advances of 65°, 47°, and 26° in head B.

As the piston moves upward the surge of gas ahead of it tends to blow the newly formed flame away from the piston. This action probably accounts for the first appearance of the flame in the windows on the side of the spark plug remote from the piston, prominent in the photographs of figure 2.

With excessively retarded spark or with slowly burning mixtures, the downward motion of the piston on expansion may noticeably affect flame movement. Figure 11 shows two diagrams (runs 2 and 3) made with the spark plug at opposite ends of the combustion chamber but otherwise under similar conditions. As the spark advance was 10°, the flame front had moved only a short distance from the spark plug when the piston started downward. The rush of gas to occupy the volume vacated by the piston carried the flame front forward when the spark plug was over the valves (run 2) but it blew against the flame when the spark plug was over the piston (run 3) decreasing gas velocity and prolonging the inflammation period about 10°. With a more normal spark advance (20°), inflammation was completed before piston velocity became great enough to produce these effects, as will be seen by a comparison of run 9 and run 10 in figure 9. This effect of piston motion on combustion time, and the influence of spark advance upon it, are also well illustrated in figure 11 of reference 4.

While recession of the piston may either increase or decrease gas velocity, depending upon whether the resultant flow of charge is with or against the advance of the flame front, the total inflammation time is likely to be increased in either case. Thus, if the flame is approaching the piston from above, the layer of gas next to the piston face will always recede faster than the following surge can carry the flame front toward it and transformation velocity will presumably suffer a decrease as the temperature of the expanding charge drops.

General swirl.—The distortion of the diagrams for run 9 of figure 9 and run 2 of figure 11, as though general swirl had carried the flame front forward on one side of the combustion chamber and retarded it on the other, is characteristic of all diagrams obtained with the spark plug in the position shown, although the direction of rotation is frequently reversed. With the spark plug at other locations, the distortion is sometimes noticeable but seldom pronounced. No rational explanation has been found for its erratic behavior, but it would seem that this lack of symmetry could be due only to a general rotary motion of the charge, set up by some unknown cause, or to local regions of

high temperature or unfavorable charge composition, which for obscure reasons shift from one side of the combustion chamber to the other.

PRESSURE DEVELOPMENT

The power of an internal-combustion engine is derived solely from pressure developed by combustion of the fuel. Theoretically, power and efficiency are a maximum for instantaneous and complete combustion at top dead center and both increase with increase in compression ratio. Too rapid combustion results, however, in rough operation, whereas increasing the compression ratio tends to cause detonation. The practical problems of combustion control are, therefore, (1) the attainment of the maximum rate of pressure rise consistent with satisfactory smoothness and (2) the suppression of detonation at high compression ratios.

Since flame spread is roughly concentric about a point of ignition, the shortest flame travel and the most rapid pressure rise with a single spark plug will be obtained by placing the gap near the geometrical center of the combustion chamber. A single plug should not be placed so that the flame is traveling away from the piston face as it recedes on the down stroke. With slow-burning mixtures or with retarded spark, such a location will cause great additional delay in combustion and pressure development.

Use of more than one plug will further reduce flame travel and increase rate of pressure rise. A detailed study of combustion control by appropriate placing of single and multiple spark plugs, covering a range of speed, spark advance and compression ratio, is reported in reference 4.

CONCLUSIONS

The following conclusions have been drawn from a consideration of the present and previous (reference 1) studies of flame travel and pressure development in a spark-ignition engine.

1. Under all conditions covered, the flame spreads in a roughly concentric pattern about the point or points of ignition.
2. It follows that with single ignition, the shortest combustion time will be obtained by placing the spark plug near the center of the combustion chamber.
3. Still shorter combustion times can be secured by using two or more plugs.
4. Flame velocities are dependent upon the character of the fuel and are reduced by the addition of residual gases to the charge or by departures from the mixture ratio giving maximum power.
5. For normal explosions in engines, flame speeds appear to be independent of pressure and, while they probably increase with temperature, evidence of pronounced effects is lacking.
6. Flame speeds and the rate of pressure development increase nearly as fast as engine speed, which

explains why engines can be operated at very high speeds with only a moderate increase in spark advance.

7. The increase in flame speed with engine speed is believed to be due to an increase in small-scale random turbulence, which affects the structure and depth of the reaction zone and influences the rate at which the flame advances into the unburned charge.

8. For a properly timed explosion of well-prepared charge, there will be very little piston movement during combustion.

9. For excessively retarded spark or slow-burning mixtures, combustion time may be greatly prolonged by downward movement of the piston, especially if the last of the charge to burn is remote from the piston.

10. In general, the spread of flame in the combustion chamber of a spark-ignition engine is controlled by at least six basic factors of major importance that operate more or less independently but simultaneously to determine instantaneous flame velocities in space. Three of these factors—(1) the composition of the unburned charge, (2) the temperature of the unburned charge, and (3) the degree of local turbulence—influence the linear rate at which the reaction advances into and transforms the unburned charge, and are thus of direct importance in determining the rate of pressure rise. The other three—(4) expansion of the gases in the reaction zone, (5) piston movement, and (6) general swirl—affect the rate at which the flame front is carried in a direction normal to its surface by mass movement of the gases comprising it. There is no adequate theory and little or no conclusive experimental evidence now available from which the separate effects of the first three factors upon flame speed can be formulated.

11. It is believed that experiments in bombs conducted under special conditions permitting the accurate evaluation of the speed of the flame front with respect to the active gases (not merely the speed in space) offer the most promising means of securing fundamental information regarding the structure of flame, the mechanism of spread, and the effect of fundamental factors such as charge composition and pressure and temperature in the low temperature range.

12. In the engine, preflame reactions alter the composition and temperature of the unburned charge to an unknown extent, which probably varies for different fuels. Since these reactions are associated with rela-

tively high temperatures and extremely short heating periods, it would appear that they can be produced and their effects studied with certainty only in an engine or a high-speed compression machine.

NATIONAL BUREAU OF STANDARDS,
WASHINGTON, D. C., September 1935.

REFERENCES

1. Marvin, Charles F., Jr., and Best, Robert D.: Flame Movement and Pressure Development in an Engine Cylinder. T. R. No. 399, N. A. C. A., 1931.
2. Dickinson, H. C., and Newell, F. B.: A High-Speed Engine Pressure Indicator of the Balanced Diaphragm Type. T. R. No. 107, N. A. C. A., 1921.
3. Schnauffer, K.: Combustion Velocity of Benzine-Benzol-Air Mixtures in High-Speed Internal-Combustion Engines. T. M. No. 668, N. A. C. A., 1932.
4. Rabezzana, Hector, and Kalmar, Stephen: Factors Controlling Engine Combustion. *Auto. Indus.*, March 2, 1935, pp. 324-329; March 9, 1935, pp. 354-357; March 16, 1935, pp. 394-397.
5. Ellis, Oliver Coligny de Champfleury: The Rationale of the Movement of Flame through Explosive Mixtures of Gases. *Jour. Soc. Chem. Indus.*, vol. 50, 1931, p. 403.
6. Stevens, F. W.: A Constant Pressure Bomb. T. R. No. 176, N. A. C. A., 1923.
Stevens, F. W.: The Gaseous Explosive Reaction—The Effect of Inert Gases. T. R. No. 280, N. A. C. A., 1927.
Stevens, F. W.: The Gaseous Explosive Reaction—A Study of the Kinetics of Composite Fuels. T. R. No. 305, N. A. C. A., 1929.
Stevens, F. W.: The Gaseous Explosive Reaction at Constant Pressure—The Reaction Order and Reaction Rate. T. R. No. 337, N. A. C. A., 1929.
Stevens, F. W.: The Gaseous Explosive Reaction—The Effect of Pressure on the Rate of Propagation of the Reaction Zone and upon the Rate of Molecular Transformation. T. R. No. 372, N. A. C. A., 1930.
7. Fiock, Ernest F., and King, H. Kendall: The Effect of Water Vapor on Flame Velocity in Equivalent CO-O₂ Mixtures. T. R. No. 531, N. A. C. A., 1935.
8. Glyde, H. S.: Experiments to Determine Velocities of Flame Propagation in a Side-Valve Petrol-Engine. *Jour. Inst. Petroleum Technologists*, November 1930, p. 756.
9. Schnauffer, Kurt: Engine-Cylinder Flame-Propagation Studied by New Methods. *S. A. E. Jour.*, January 1934, pp. 17-24.
10. Withrow, Lloyd, Lovell, W. G., and Boyd, T. A.: Following Combustion in the Gasoline Engine by Chemical Means. *Ind. Eng. Chem.*, September 1930, p. 945.
11. Ellis, O. C. de C.: Flame Movement in Gaseous Explosive Mixtures. (In 8 parts.) *Fuel in Science and Practice*, vol. 7, 1928.

REPORT No. 557

PRELIMINARY TESTS IN THE N. A. C. A. FREE-SPINNING WIND TUNNEL

By C. H. ZIMMERMAN

SUMMARY

Typical models and the testing technique used in the N. A. C. A. free-spinning wind tunnel are described in detail. The results of tests of two models afford a comparison between the spinning characteristics of scale models in the tunnel and of the airplanes that they represent.

The models are built of balsa wood and ballasted with lead to the proper mass distribution. A clockwork delayed-action mechanism is mounted in the model to move the control surfaces during the spin.

In steady-spin tests, observations are made of the rate of rotation and of the air speed necessary to hold the model at test height. Moving-picture records are taken from which the spinning attitudes are obtained. In recovery tests, moving-picture records are taken of the model from the instant the controls move until recovery is effected or failure to recover is definite.

The models of the XN2Y-1 and F4B-2 airplanes gave good approximations to the spinning characteristics of the airplanes, in both steady spins and recoveries. Since these models were scaled from somewhat similar biplanes, no conclusions are drawn as to the reliability of model results in general.

INTRODUCTION

Although the problem of the spin has been the object of a great deal of research, airplanes of recent design are occasionally found to have undesirable spinning characteristics. The prevalence of this condition is the result of a combination of factors that may be summarized as follows: A very great amount of experimental work is necessary before spinning characteristics can be accurately predicted by analysis; and designers are unwilling to go, possibly unnecessarily, to extreme measures to insure good spinning characteristics. Consequently, it has become very desirable to develop a method of determining the spinning characteristics of an airplane while it is in the design stage.

About 10 years ago members of the N. A. C. A. laboratory staff studied means of improving the spinning characteristics of two airplanes by noting the

behavior of dynamic scale models when launched in spins from the top of a balloon shed. (See reference 1.) Although the method showed promise, it was abandoned because of the difficulty of making satisfactory tests with the short free drop available (105 feet). There was also considerable doubt at the time concerning the fidelity with which scale models indicated full-scale behavior.

This method of studying spinning was adopted by research workers in England, who obtained a great deal of interesting and valuable information (reference 2). They likewise were hampered by the limited free drop available and, in an effort to avoid this restriction, built a small vertical wind tunnel in which it was possible to cause models to continue spinning for long periods of time without restraint other than that of the air. The model tunnel showed such promise that a 12-foot-diameter vertical tunnel was built for testing models of sufficient size for practical results (reference 3). This tunnel has been in operation since 1932.

The N. A. C. A., realizing the need of a satisfactory method of predicting spinning behavior and aware of the value of the results of the tests in the British free-spinning tunnel, constructed a tunnel, the operation of which is described in this report. The tunnel is expected to provide American designers with a ready means of determining whether changes are necessary in their airplane designs without the expense and danger of full-scale flight tests and the expense and delay incident to changes after construction.

The tunnel was completed in September 1934. Alterations to improve the air flow, velocity and turbulence surveys, and a calibration of the air-speed indicator were completed in March 1935. The first spin tests were made in April 1935. A large number of tests, both of steady spins and of recoveries, have been made to obtain data from which comparisons can be made between the spinning behavior of the XN2Y-1 and the F4B-2 airplanes (references 4 and 5) and scale models of them. These tests served as a calibration of the tunnel and the results are therefore included in this report.

DESCRIPTION OF MODELS

Dimensional characteristics.—The models used are generally $\frac{1}{10}$ to $\frac{1}{16}$ scale. (See fig. 1.) The size of the models is limited by the wing span and the wing loading. The maximum span allowable is about 36 inches; the maximum wing loading is about 1.3 pounds per square foot. Since the model wing loading must be equal to the airplane wing loading multiplied by the scale ratio (reference 6), 1.3 pounds per square foot corresponds to 13 pounds per square foot for the airplane when the model is $\frac{1}{10}$ scale or 21 pounds per square foot when the model is $\frac{1}{16}$ scale.

Balsa wood is the usual structural material because of its low density. It is necessary to hollow out the

must be built of balsa wood and be subjected to the rather rough treatment incidental to free-spinning tests. Consequently, tolerances somewhat larger than normal in model construction are permitted. Tolerances that appear to be satisfactory are ± 0.01 inch on wing- and tail-surface profiles, ± 0.02 inch on all other dimensions under 6 inches, and ± 0.03 inch on all other dimensions over 6 inches. Angular relationships are held to $\pm 0.5^\circ$. Details of fittings, air scoops, propellers, and other protuberances are omitted.

The fuselage, tail surfaces, and landing gear are finished with clear shellac, sanded smooth. The wings are finished with clear shellac or with wax, depending on whether difficulty is encountered in keeping the wings sufficiently light for the required mass distribution.

Mass characteristics.—Models to be used for free-spinning tests must be scaled from the airplane in mass distribution as well as in dimensional characteristics. In order to preserve dynamic similarity the weight of the model must be that of the airplane multiplied by the scale ratio to the third power, the center of gravity must be in the same relative location as in the airplane, and the moments of inertia must be those of the airplane multiplied by the scale ratio to the fifth power. Values of weight and moment of inertia are corrected for the difference between the air density in the tunnel and the density at the altitude at which the full-scale tests have been or are expected to be made.

The weight, the center-of-gravity location, and the moments of inertia are adjusted to the proper values by suitably disposed lead weights. The center-of-gravity location is determined by suspending the model by a thread in two or more attitudes and determining the point of intersection of vertical lines passing through the point of support.

The distribution of mass is determined by swinging the model as part of a compound pendulum and timing the oscillations. A knife-edge mounted in a vacuum chamber (see fig. 2) serves as support for the pendulum. The moments of inertia are determined in this manner about the X , Y , and Z axes of the model and also about an axis in the plane of symmetry at 45° to the X and Z axes. In the cases of airplanes of which the full-scale moments of inertia have been determined by swinging tests, the model is swung in air at sea-level density and its moments of inertia so determined are brought into proper scale relationship with the virtual moments of inertia of the airplane (reference 7). In the cases of other models the true moments of inertia are determined by swinging the model at several reduced air densities and extrapolating the plots of moment of inertia against density to zero density. The true moments of inertia so determined are brought into proper scale relationship with the calculated true moments of inertia of the airplane.

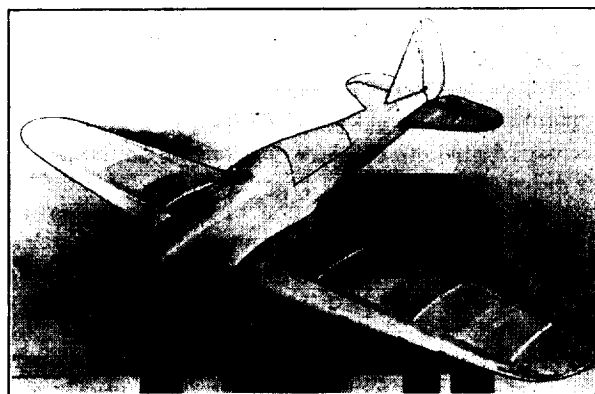
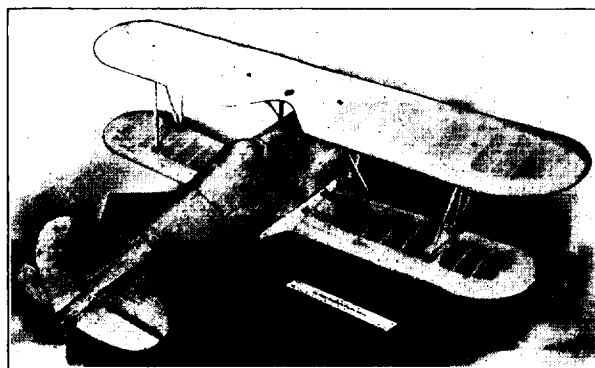


FIGURE 1.—Typical models used in the free-spinning tunnel.

after portion of the fuselage and to cut out a large portion of the wood in the wings to permit proper mass distribution. The wing cut-outs are covered with silk tissue paper. The leading and trailing edges and tips of the wings are fitted with strips of spruce, pattern pine, or bamboo inset into the edge of the balsa to prevent disfigurement from accidental blows or from striking the safety netting. Lead is used for ballast.

Exact scale models are very expensive. Furthermore, it is impracticable to attempt to maintain an extreme degree of dimensional accuracy in models that

The accuracy of the means of measurement is such that the quantities can be determined within the following limits:

Weight.....	± 0. 1 percent.
Center-of-gravity location.....	± 0. 01 inch.
Moment of inertia.....	± 3 percent.

Because of the effects of humidity upon the weight and mass distribution and the difficulty often encountered in placing ballast to give exactly the desired values, the mass quantities are not kept within the limits of accuracy of the measurements, but are held to the desired values within the following limits:

Weight.....	± 1 percent.
Center-of-gravity location.....	± 1 percent of chord.
Moments of inertia.....	± 5 percent.

Automatic-control mechanism.—In order that the behavior of models during recovery from the spin may be studied, a clockwork mechanism has been developed for moving the control surfaces while the model is spinning. This mechanism consists essentially of a watch spring, gears, and an escapement mechanism that drive a movable table. The table, in turn, carries small projecting plugs that actuate cam mechanisms and permit the control surfaces to be moved by springs. Three sets of cam mechanisms and related parts are provided so that each of three controls can be moved independently of the other two. The control surfaces can be caused to move either slowly or quickly and in any order desired with intervals between the movements of different controls as great as one-half minute by disposing the projecting plugs suitably in the movable table.

The mechanism is connected to the control surfaces by threads that transmit the movement. In order that observers may know the exact instant of movement of the control surface a small paper disk is clamped lightly to the side of the fuselage and connected to the control horn by a thread. Movement of the control horn pulls the paper disk free and it trails behind the spinning model.

TESTING TECHNIQUE

Launching the model.—At the beginning of a test the model is mounted upon a launching spindle about the axis of which it is free to rotate. This spindle is on the end of a wooden rod and is held in the center of the tunnel by one of the operators standing in the observation chamber. With the spindle vertical the attitude of the model is such that the fuselage axis is approximately 35° to the horizontal, nose down, and the wings are 10° to the horizontal with the left wing tip the lower (for a right spin). When the model is in this attitude, air flowing upward through the tunnel causes it to rotate fairly rapidly. The air speed is increased by a second operator until the air force on the model is equal to its weight. The model then

automatically disengages itself from the spindle and continues to float in the air stream entirely free of mechanical restraint. The launching spindle is immediately withdrawn from the tunnel. The air speed is adjusted until it just equals the rate of descent the model would have in still air and the model is at approximately eye level in the test section.

Steady spins.—With the model spinning steadily in the tunnel, observations are made of the air speed and rate of rotation; the air speed is taken from a calibrated tachometer and the rate of rotation is determined by noting with a stop watch the time required for 50 turns in the spin. Moving pictures are taken of the spinning

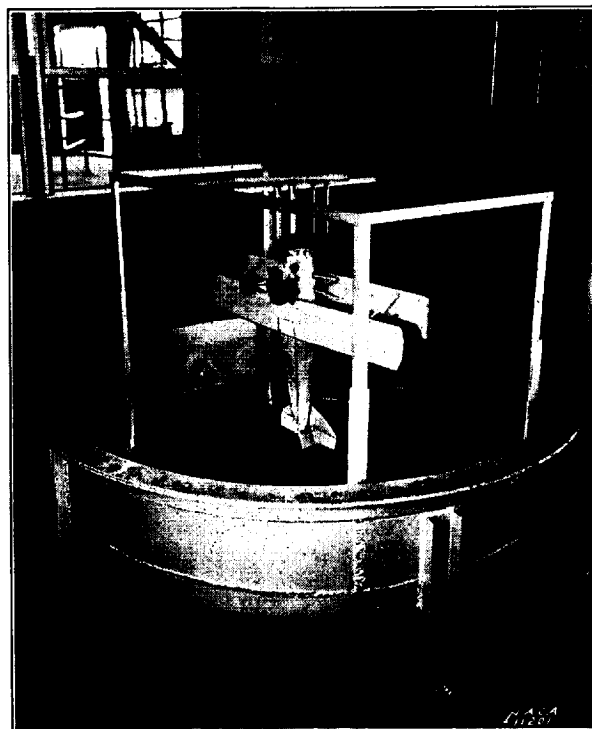


FIGURE 2.—Model-swinging gear.

model for a permanent record of its spinning attitude and any oscillatory tendencies or unsteadiness. The pictures are taken on 16 mm film at the rate of 64 per second. About 10 turns of the spin are photographed.

After the observations have been made, the model is lowered into a net held in the air stream by one of the operators or into a large bowl-shaped net at the bottom of the test section. When lowered into the large net, the model is retrieved with a long-handled clamp.

Recoveries.—When making recovery tests, the clockwork mechanism is wound, set to operate the controls after a time interval of approximately 1 minute, and started before the model is launched. The model is then launched as previously described. About 2 seconds before the controls are to move, the camera is

started and pictures are taken continuously at the rate of 16 per second until the model has dived into the netting or has definitely established a new spinning condition. For comparison with the camera records, one of the operators estimates the number of turns from the time the controls operate until the spin ceases. At least two, and frequently more, of these recovery tests are made for each test condition. The first recovery for each test condition is made with the model well down in the bowl-shaped net to determine whether the model tends to go immediately into a stalled glide, carrying it rapidly toward the side of the tunnel, or whether it goes into a nearly vertical dive. One or two recoveries cautiously made in this manner prevent unnecessary damage to the model. When the typical behavior of the model for the particular test condition has been determined, the model is allowed to start recovery as high in the test section as the trial tests have indicated to be safe.

Reduction of data.—The data from a steady-spin test consist of the film record (fig. 3), the air speed, and the rate of rotation. The angles of the fuselage (X) axis and the span (Y) axis to the horizontal are measured on the film using a film-viewing machine provided with a cross hair and a protractor. The intersections of the fuselage axis with the nose and tail are used as reference points in determining the fuselage-axis angle; corresponding points on the wing tips, which define a line parallel to the span axis, serve as reference points in determining the span-axis angle. Experience has shown that the angles can be readily obtained to within $\pm 1^\circ$ by this method. The angles so measured are designated as θ and ϕ , respectively, where θ is the angle of the fuselage axis to the horizontal, negative when the model is inclined nose downward; and ϕ is the angle of the span axis to the horizontal, positive when the left wing is higher than the right.

The radius of the spin is calculated from the rate of rotation and the value of θ on the assumption that the resultant aerodynamic force on the model is perpendicular to the X and Y axes. That this assumption is close to the true condition has been found to be the case with the N. A. C. A. spinning balance (reference 8). On this basis the radius is determined as in reference 9 by the relationship,

$$\text{Radius} = \frac{g \tan(-\theta)}{\Omega^2}$$

where g is the acceleration of gravity.

Ω , the rate of rotation in radians per second. In a number of cases of full-scale data this approximate equation has been found to give the true radius to within ± 10 percent, except for unusually large angles of sideslip. For most cases it is within ± 3 percent of the true value.

The angle of sideslip in the spin is determined from the relationship

$$\beta = \phi - \sigma$$

where β is the angle of sideslip equal to the $\sin^{-1} v/V$, σ , the helix angle equal to the $\sin^{-1} \Omega \text{ radius}/V$. This relationship is true to within $\frac{1}{2}^\circ$ or less for spinning attitudes.

The angle of attack is determined from the relationship

$$\alpha = 90^\circ - (-\theta)$$

This equation is an approximation, giving values of α from 1° to 2° higher than the true value for ordinary spinning attitudes. This discrepancy increases with the deviation of the wings from the horizontal, computed values being as much as 5° or 6° too high with large amounts (15° to 20°) of inward sideslip, and 3° to 4° too low with large amounts of outward sideslip.

The data from a recovery test consist of film records of one or more recoveries (fig. 4) and the observer's estimate of the number of turns required for recovery. The number of turns made by the model from the time the signal disk is pulled from its clamp until rotation ceases is obtained from the film and compared with the observer's estimate. In all recoveries for which film records are obtained the film-record value is used for the recorded data. In other cases the observer's estimate is used. The turns can be determined to within one-quarter of a turn from the film record. The observer's estimate is generally within one turn of the value obtained from the film record.

COMPARISON BETWEEN AIRPLANE SPINNING CHARACTERISTICS AND THE CHARACTERISTICS OF SCALE MODELS IN THE TUNNEL

One of the principal reasons for abandonment by the N. A. C. A. of the method of dropping models for spin study was doubt concerning the fidelity with which scale models indicated the spinning behavior of the airplanes from which they were scaled. When dynamic similarity is preserved, the Reynolds Number of the model is equal to that of the airplane multiplied by $N^{\frac{1}{2}}$ where N is the scale ratio ($\frac{1}{10}$, $\frac{1}{2}$, etc.). Furthermore, it is impracticable to reproduce the airplane in exact detail in a scale model. Comparisons between results from the N. A. C. A. spinning balance and full-scale flight tests have indicated considerable scale effect upon aerodynamic characteristics in spinning attitudes (references 8, 10, and 11). Tests in the British free-spinning tunnel have also given indications of scale effect that must be carefully taken into account in interpreting model free-spinning results (references 3 and 12).

In view of the uncertainty existing about the reliability of the results of model tests, it was thought highly desirable that tests be made in the N. A. C. A.

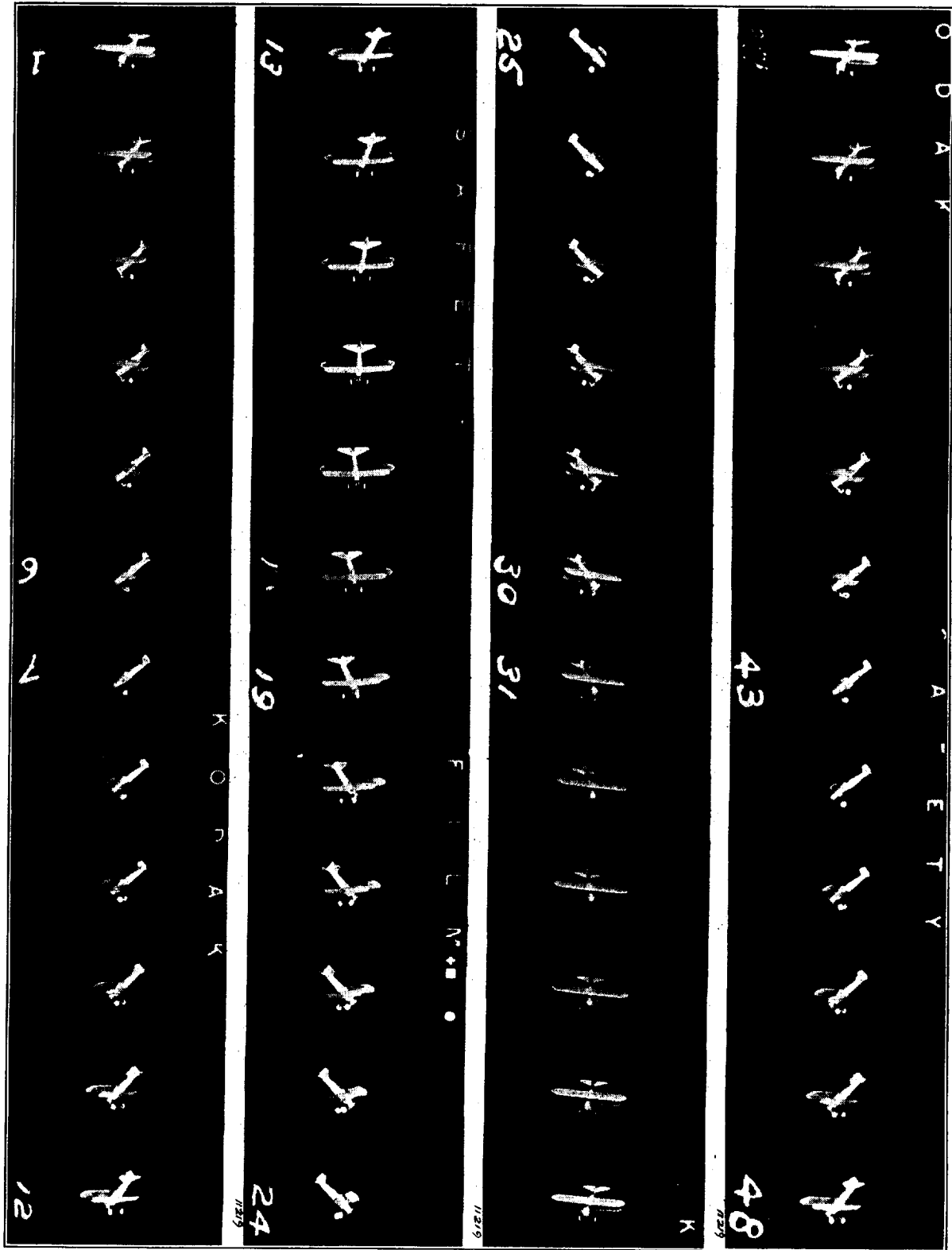


FIGURE 3. Portion of a film record of a steady spin.

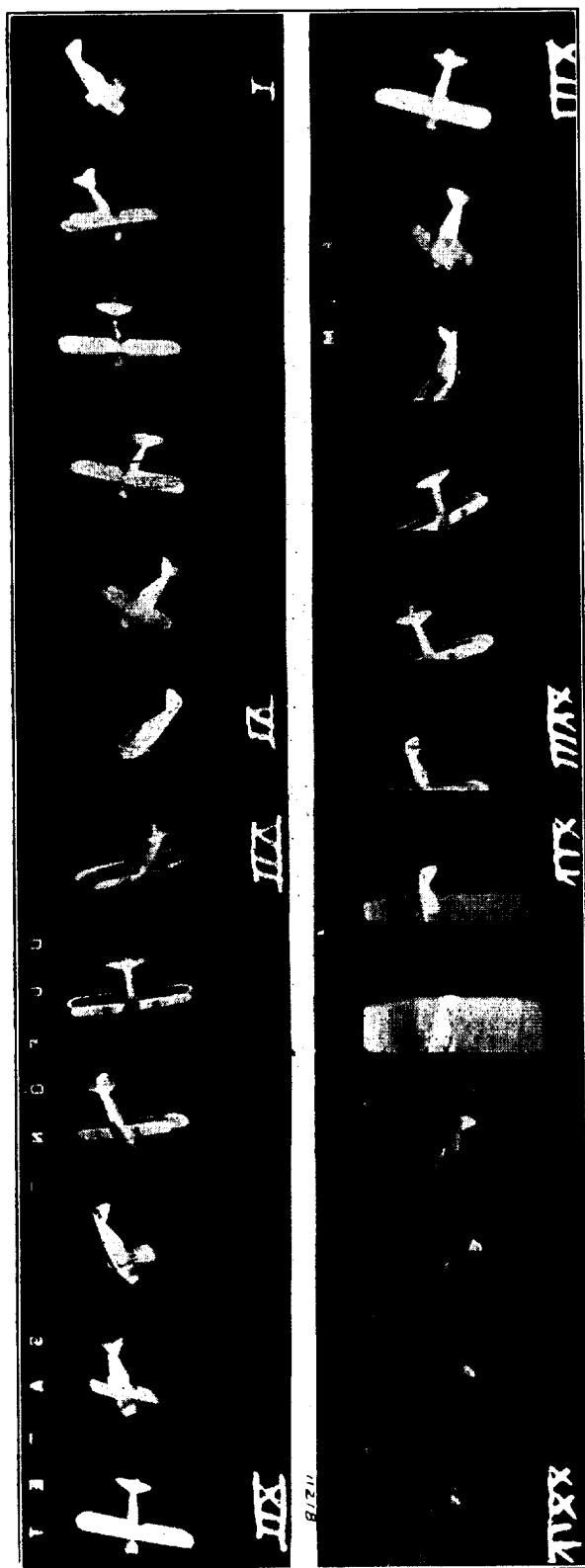


FIGURE 4.—Portion of a film record of a recovery.

free-spinning tunnel with models of airplanes for which the full-scale spinning characteristics are well known. Such tests should indicate the accuracy of the model results and the corrections that should be made to allow for the difference between model and full-scale behavior. Such a series of tests was also considered advisable as an opportunity to acquire experience in operation of the tunnel and to develop the testing technique.

The spinning characteristics of an XN2Y-1 and an F4B-2 airplane have been thoroughly studied by the N. A. C. A. (references 4 and 5). A $\frac{1}{10}$ -scale model of the XN2Y-1 and a $\frac{1}{12}$ -scale model of the F4B-2 were accordingly built and tested both for behavior in steady spins and for recovery characteristics.

MODELS

The XN2Y-1 model.—The $\frac{1}{10}$ -scale model of the XN2Y-1 is shown in figure 5. A drawing of the airplane is included in reference 4. The model was



FIGURE 5.—One-tenth-scale model of the XN2Y-1 airplane.

originally made entirely of balsa wood except for the bamboo struts and the silk tissue paper used to cover the wings where the wood was removed for lightness. Dimensions were held to ± 0.01 inch. The control mechanism was mounted just back of the wing cellule.

The original balsa tail surfaces, which were very thin and insecurely attached to the fuselage, were replaced by pattern-pine surfaces after the first trial of the model in the tunnel. The original wing cellule was used for the series of steady-spin tests but was demolished in a crash before recovery tests were started. A new wing cellule was built up with spruce spars and bamboo tips for added strength. It was found necessary to hollow out these wings until they were virtually shells to bring the moment of inertia about the fuselage axis to its proper value. As a result the tip of each wing warped outboard of the interplane strut attachments giving from $\frac{1}{2}^\circ$ to 1° washout at the extreme tip. One steady-spin test, as a check, and all the recovery tests were made with this latter wing cellule.

The F4B-2 model.—The $\frac{1}{12}$ -scale model of the F4B-2 is shown in figure 6. A three-view drawing and photographs of the airplane are given in reference 5. In the construction, dimensions were held to ± 0.01 inch. The wings were built up with spruce spars, ribs, and trailing-edge pieces and were covered with silk tissue paper. The leading portions and the tips were balsa. Bamboo strips were inset into the tips to prevent damage from contact with the safety netting. The leading edges were unprotected. The ribs, spars, leading portions, and tips were hollowed out for lightness. The after portion of the fuselage was hollowed out. The control mechanism was mounted at the center of gravity, access to it being provided by a door in the side of the fuselage.

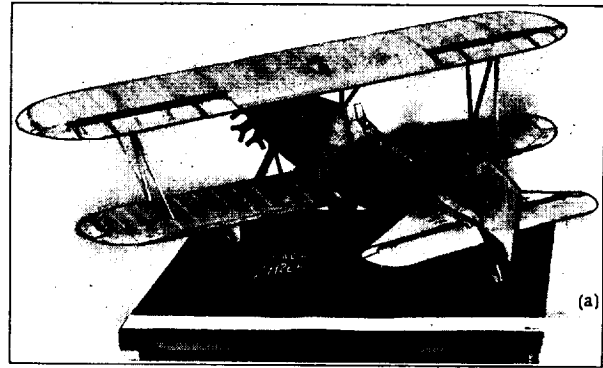
The tail surfaces were balsa, reinforced with spruce. Three interchangeable sets of surfaces were provided, which were held to the fuselage by close-fitting hardwood dowels. The various tail-surface combinations are shown in figure 6. They are designated as the F4B-2 surfaces; the F4B-2 stabilizer with F4B-4 fin and F4B-3 rudder (hereinafter referred to as the F4B-4 fin and rudder, as in reference 5); and the F4B-4 fin and rudder with the F4B-2 stabilizer set on the fin at a height corresponding to 1.54 feet (full-scale) above its normal location. In addition to these combinations, two auxiliary fins similar to those designated as fin 2 and fin 3 in reference 5 were provided.

This model was provided with movable ailerons made carefully to scale not only as regards general dimensions but also as regards the nose shape, the hinge-axis location, and the slot between the aileron and the wing. The ailerons were held in place by copper-wire hinges and the neutral settings were maintained by tack-gluing the aileron to the wing.

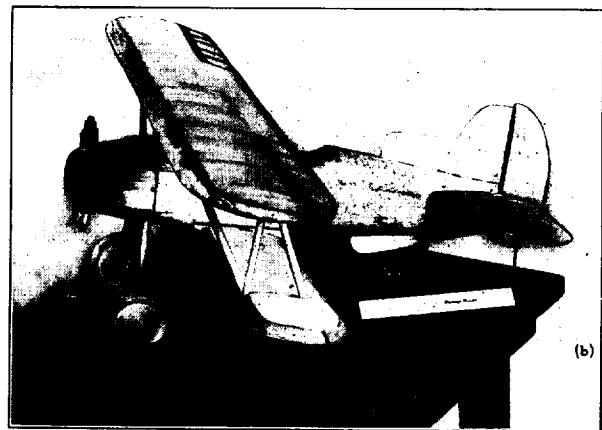
During the course of the tests, which involved approximately 250 spins, it was necessary to repair the wing tips a number of times and once to make extensive repairs to the entire wing cellule. The leading portions and the tips were disfigured somewhat through contact with the safety netting and in making repairs. It has been found impracticable to maintain close tolerances on repairs.

TEST CONDITIONS

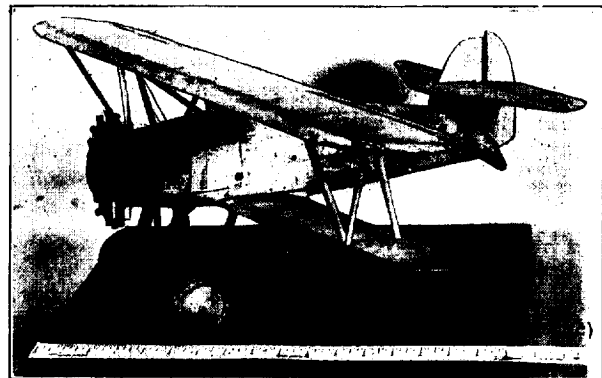
Steady spins.—In addition to the test conditions given in table 1 for the XN2Y-1 model, steady spins were made with rudder settings 41° , 18° , and 4° with the spin, elevator 24° up, with ballast at the wing tips; and rudder setting 41° with the spin, elevator 26.5° down, with ballast at the wing tips.



(a) Original surfaces.



(b) F4B-4 surfaces and auxiliary fins 2 and 3.



(c) F4B-4 surfaces and intermediate stabilizer.

FIGURE 6.—One-twelfth-scale model of the F4B-2 airplane.

Normal loading corresponded to the following true mass distribution values for the XN2Y-1 airplane when operated at 6,000 feet altitude:

Weight.....	1,762 pounds.
A.....	808 slug-ft. ²
B.....	1,114 slug-ft. ²
C.....	1,501 slug-ft. ²
C _g	0.34.
$\frac{z}{c}$	-0.02.

where A, the moment of inertia about the X axis, equal to mk_x^2 .

B, the moment of inertia about the Y axis, equal to mk_y^2 .

C, the moment of inertia about the Z axis, equal to mk_z^2 .

C_g, the center-of-gravity coefficient, the ratio of the distance of the center of gravity back of the leading edge of the mean aerodynamic chord to the length of the mean aerodynamic chord.

$\frac{z}{c}$, the ratio of the distance of the center of gravity below the thrust line to the length of the mean aerodynamic chord.

For the loading condition designated "ballast at tips" a weight corresponding to 18 pounds on the airplane was added to each lower wing tip bringing the true mass values to:

Weight.....	1,798 pounds.
A.....	1,012 slug-ft. ²
B.....	1,114 slug-ft. ²
C.....	1,705 slug-ft. ²
C _g	0.34.
$\frac{z}{c}$	-0.02.

In addition to the test conditions listed in table II for the F4B-2 model, tests were made with the rudder 30° and 15° with the spin, neutral, and 15° and 30° against the spin for elevator settings of 28.3° up, 15° up, neutral, 15° down, and 30.5° down with the normal+radio+raft loading and with the F4B-2 and F4B-4 fin and rudder combinations. In table II control settings are based on maximum deflection of the rudder of ±30°, maximum deflection of the elevator 28.3° up and 30.5° down, and maximum deflection of the ailerons 23° up and 16° down. The setting of the stabilizer relative to the thrust line was zero in all cases.

The mass distribution of the model for the specified loading conditions corresponded to the following true airplane mass distributions at a test altitude of 8,500 feet:

Stripped, F4B 4 fin and rudder:

Weight.....	2,728 pounds.
A.....	1,041 slug-ft. ²
B.....	1,876 slug-ft. ²
C.....	2,457 slug-ft. ²
C _g	0.34.
$\frac{z}{c}$	-0.03.

Normal+radio+raft, F4B-4 fin and rudder:

Weight.....	2,915 pounds.
A.....	1,078 slug-ft. ²
B.....	1,876 slug-ft. ²
C.....	2,455 slug-ft. ²
C _g	0.33.
$\frac{z}{c}$	-0.03.

Carrier overload, F4B-4 fin and rudder:

Weight.....	3,334 pounds.
A.....	1,131 slug-ft. ²
B.....	1,899 slug-ft. ²
C.....	2,426 slug-ft. ²
C _g	0.34.
$\frac{z}{c}$	-0.03.

Recoveries.—The recovery test conditions for the XN2Y-1 model are given in table III. In all recovery tests the controls were moved sharply and simultaneously from the original to the final setting listed. The settings specified are based on maximum rudder settings of ±41° and on maximum elevator settings of 24° up and 26.5° down.

The recovery test conditions for the F4B-2 are given in table IV. The original setting in each case during the steady spin was rudder full with the spin, elevator up, ailerons neutral. In all tests the surfaces were moved sharply and simultaneously to the setting listed in table IV.

RESULTS

Steady spins.—Results of the steady spins of the XN2Y-1 airplane and model are given in figures 7 to 11. For those cases in which direct comparisons were obtained, average values of airplane and model results are given in table I. The full-scale data were taken from a series of tests the results of which have not been published. The model data were obtained from observations and film records as described in the portion of this report dealing with the reduction of steady-spin data. All model data are listed as their full-scale equivalents, model values having been transformed to the full-scale equivalents by the relationships:

$$V_A = \frac{V_M}{\sqrt{N}}$$

$$\text{and} \quad \text{radius}_A = \frac{\text{radius}_M}{N}$$

where, subscript A refers to the airplane.
subscript M refers to the model.

Results of the steady spins of the F4B-2 airplane and model are given in figures 12 to 21. For those cases in which direct comparisons were obtained, average values of airplane and model results are given in table II. The full-scale data are taken from reference 5. All model data are listed as their full-scale equivalents.

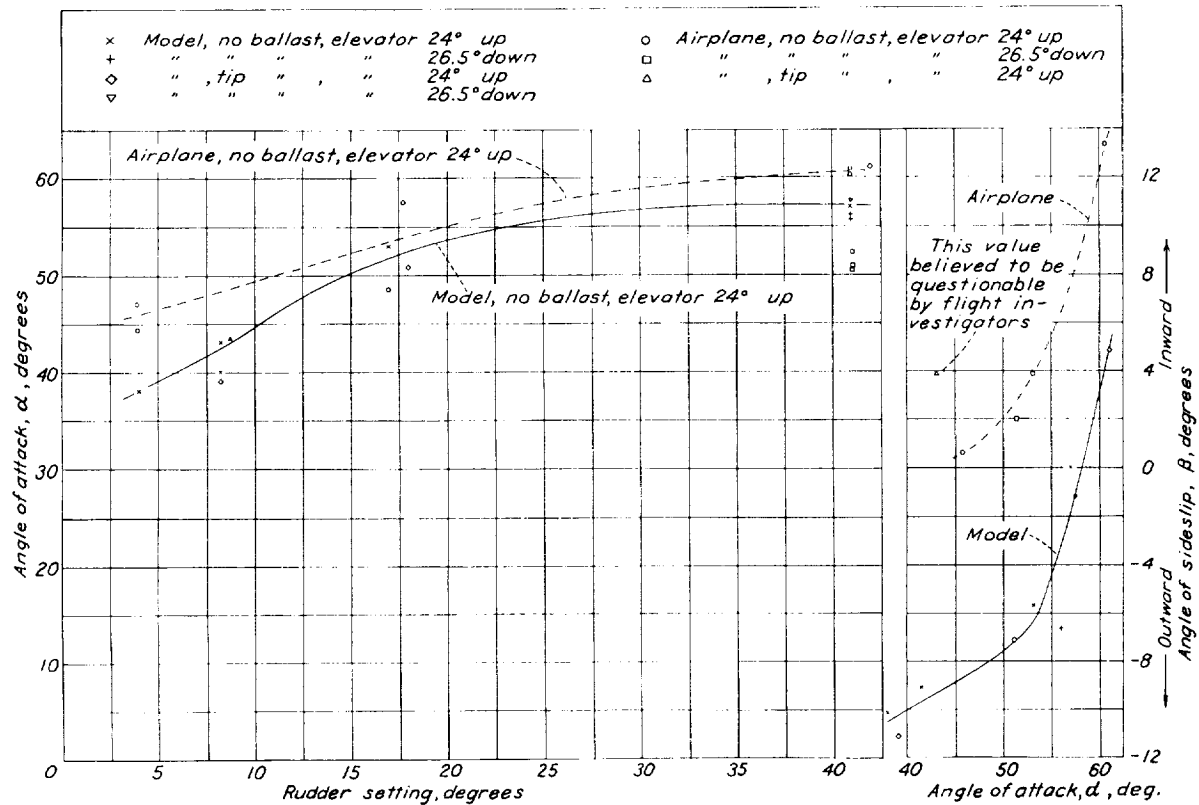


FIGURE 7.—Variation of angle of attack with rudder setting. XN2Y-1.

FIGURE 8.—Variation of angle of sideslip with angle of attack. XN2Y-1.

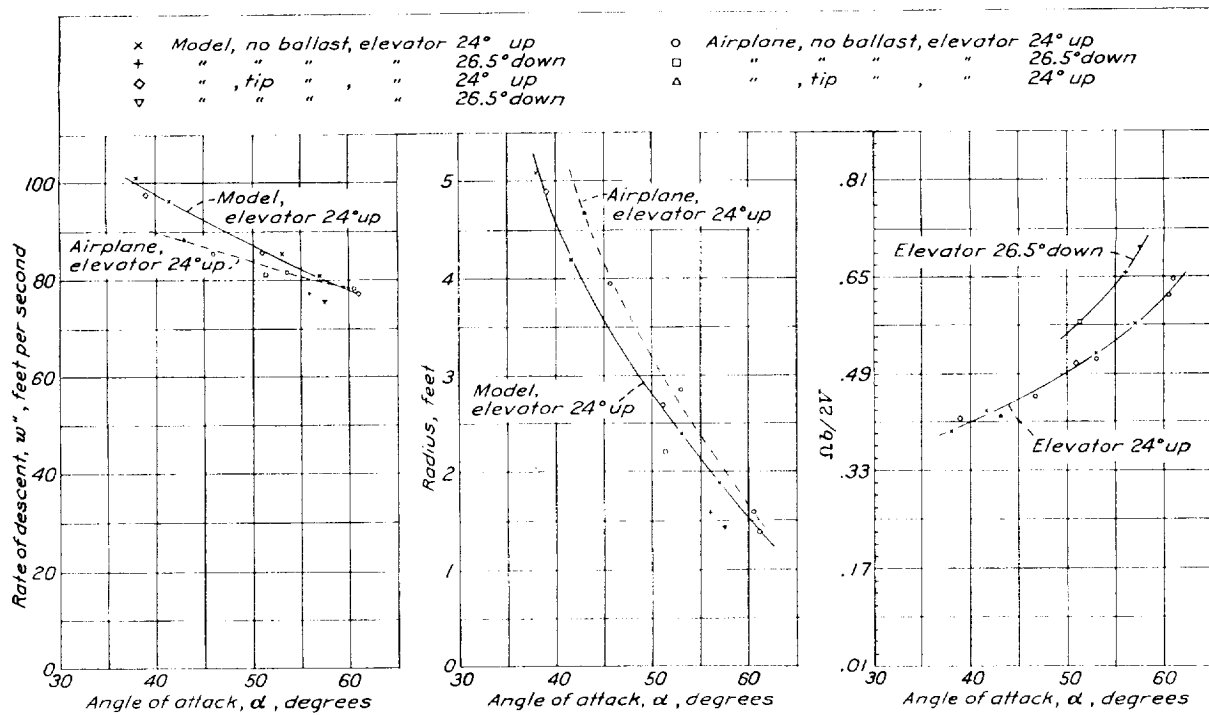


FIGURE 9.—Variation of rate of descent with angle of attack. XN2Y-1.

FIGURE 10.—Variation of radius with angle of attack. XN2Y-1.

FIGURE 11.—Variation of $\frac{Lb}{2V}$ with angle of attack. XN2Y-1.

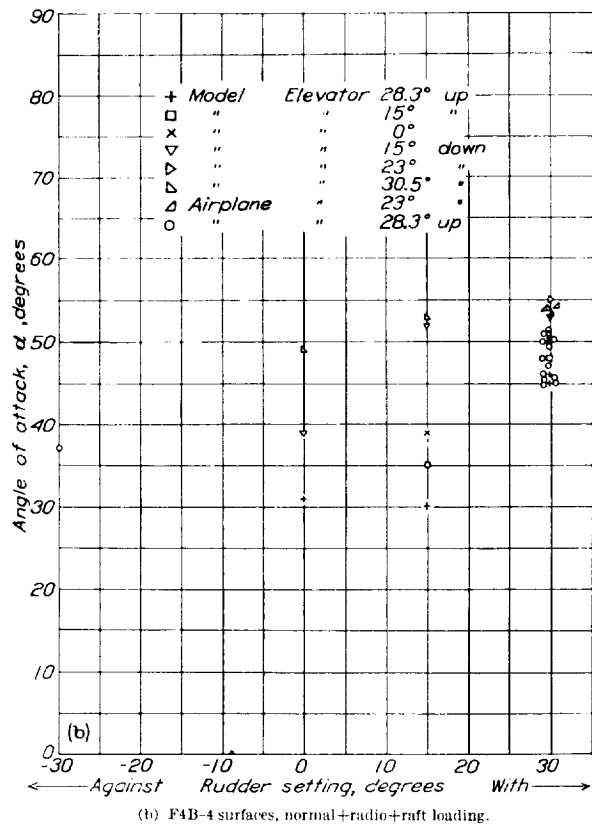
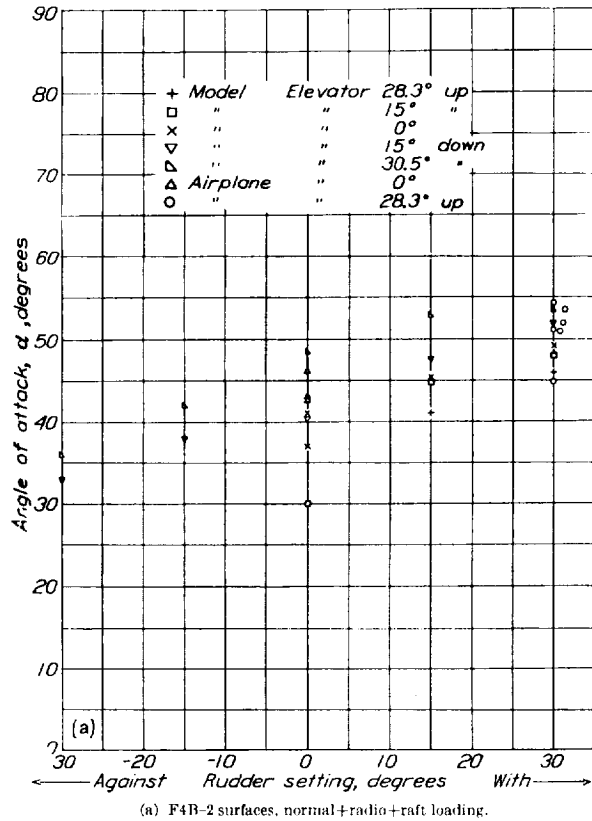


FIGURE 12. Variation of angle of attack with rudder setting. F4B-2.

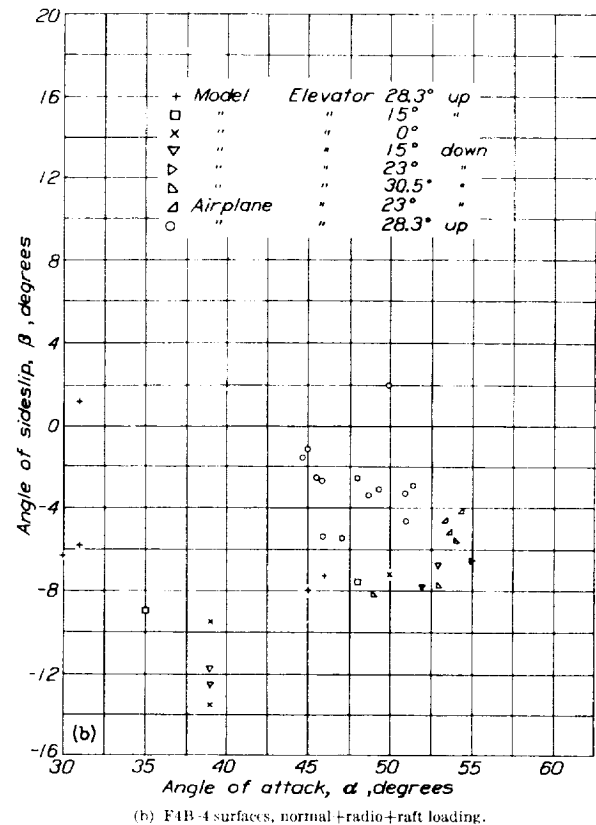
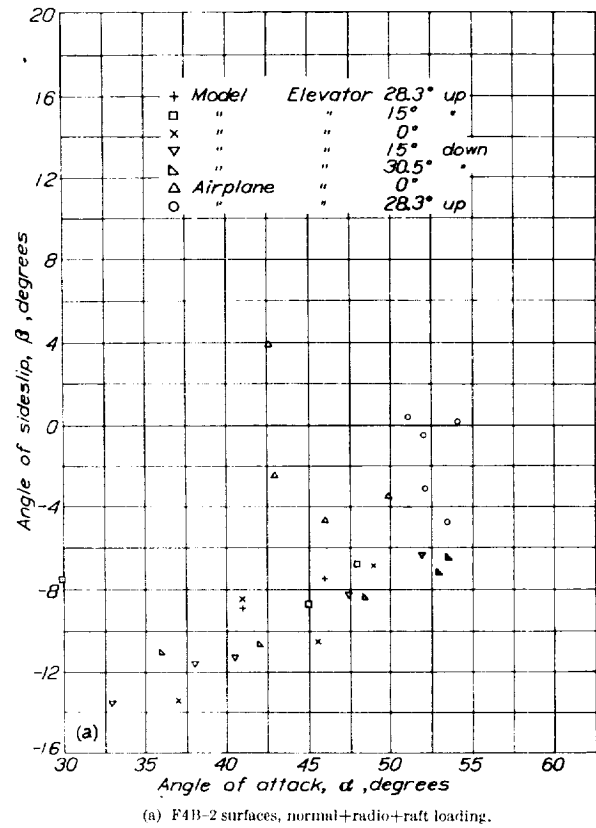
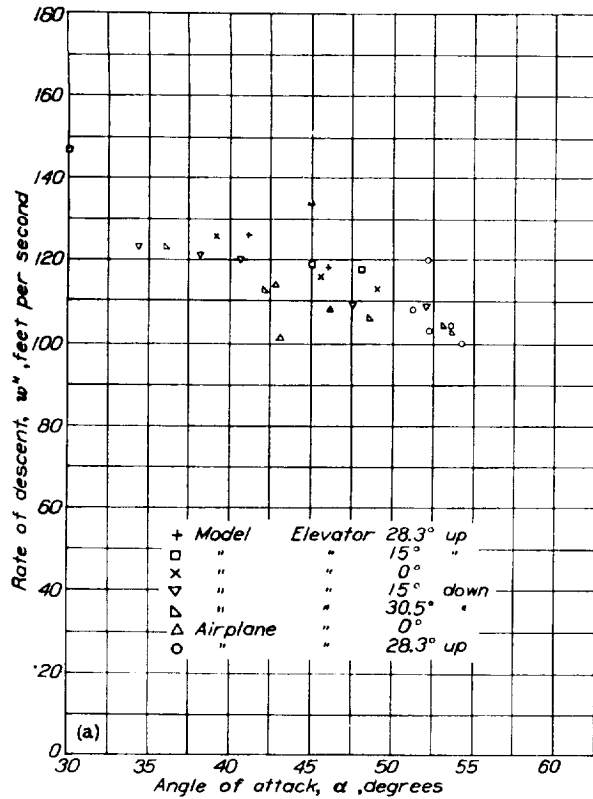
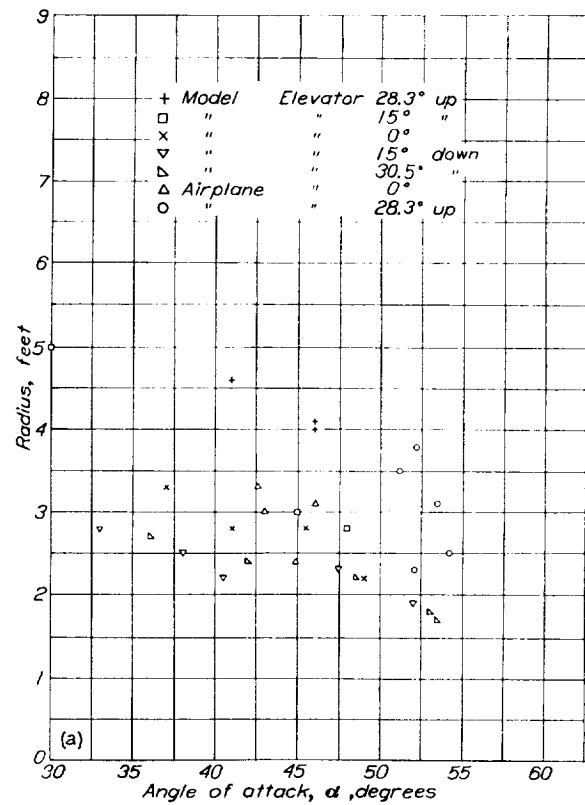


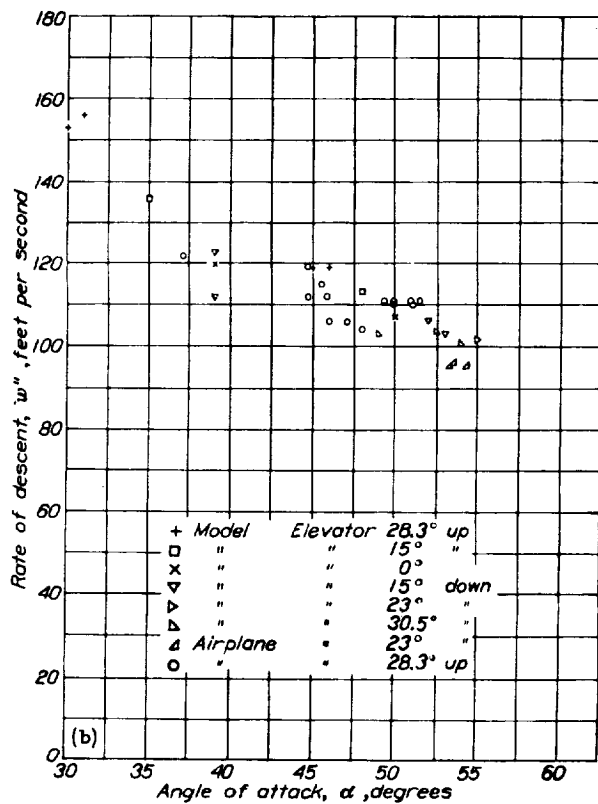
FIGURE 13. Variation of angle of sideslip with angle of attack. F4B-2.



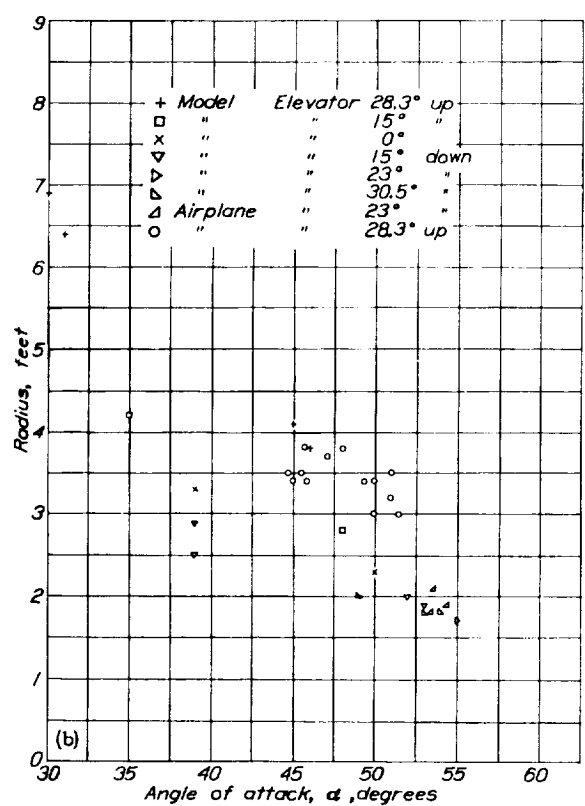
(a) F4B-2 surfaces, normal+radio+raft loading.



(a) F4B-2 surfaces, normal+radio+raft loading.



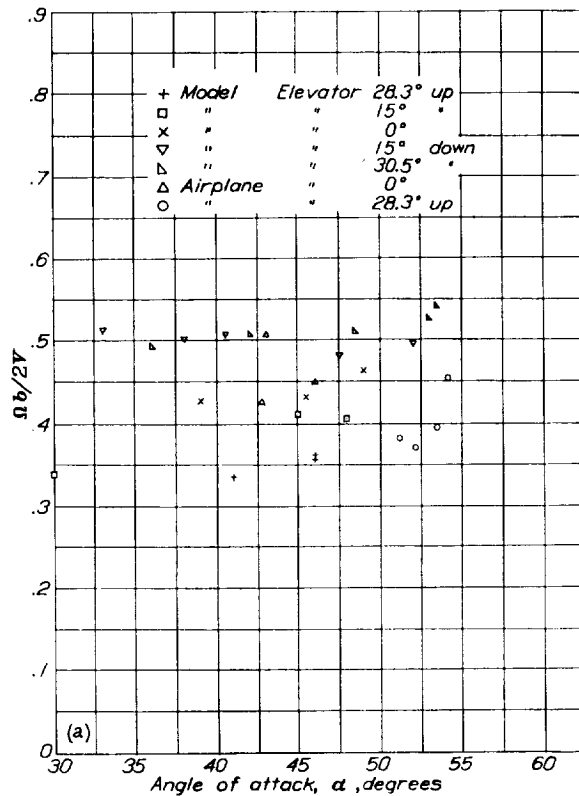
(b) F4B-4 surfaces, normal+radio+raft loading.



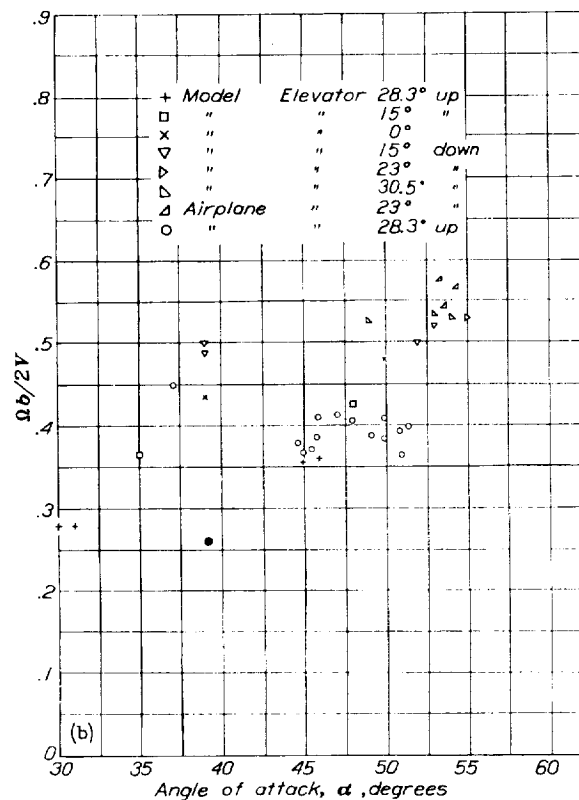
(b) F4B-4 surfaces, normal+radio+raft loading.

FIGURE 14. Variation of rate of descent with angle of attack. F4B-2.

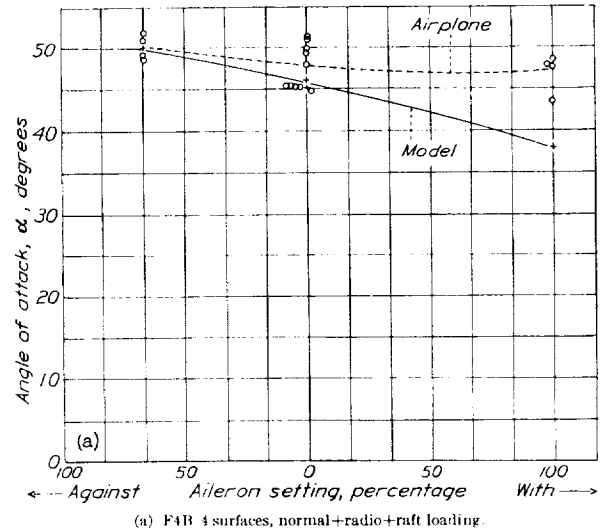
FIGURE 15. Variation of radius with angle of attack. F4B-2.



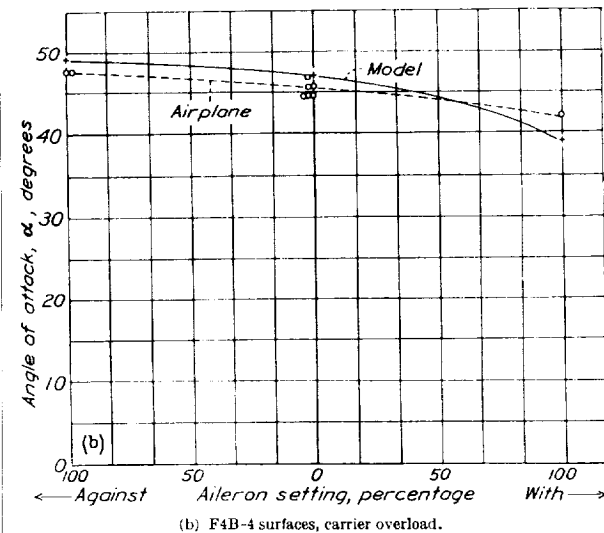
(a) F4B-2 surfaces, normal+radio+raft loading.



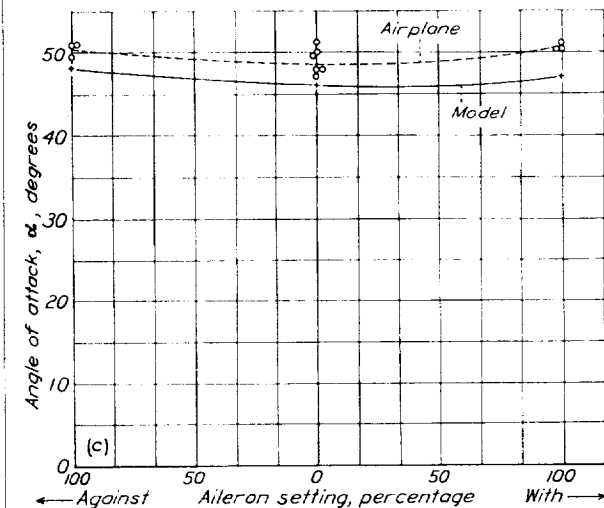
(b) F4B-4 surfaces, normal+radio+raft loading.

FIGURE 16. Variation of $\Omega b/2V$ with angle of attack F4B-2

(a) F4B-4 surfaces, normal+radio+raft loading.



(b) F4B-4 surfaces, carrier overload.



(c) F4B-4 fin, intermediate stabilizer, normal+radio+raft loading.

FIGURE 17. Variation of angle of attack with aileron setting. F4B-2

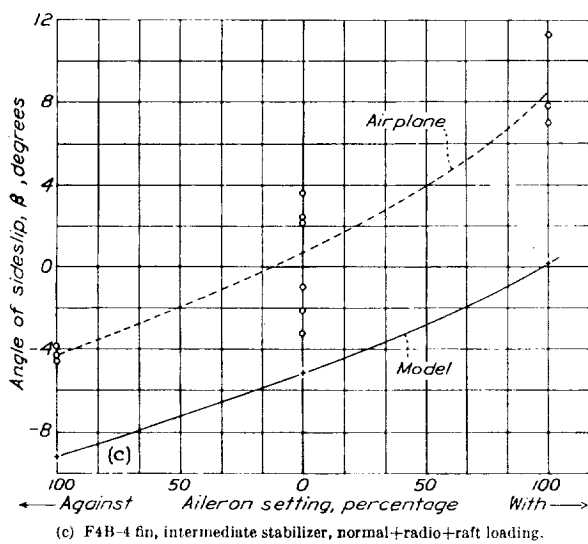
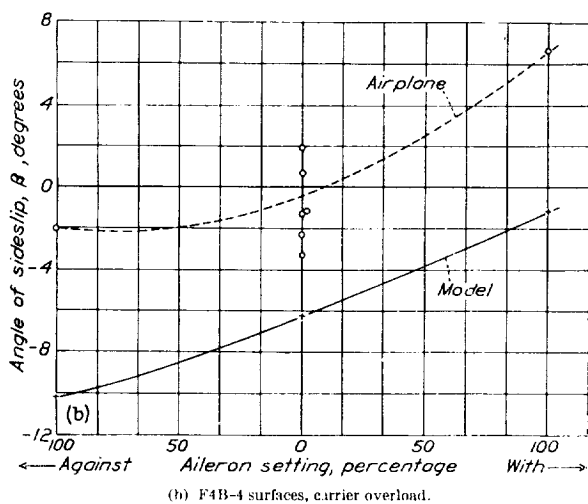
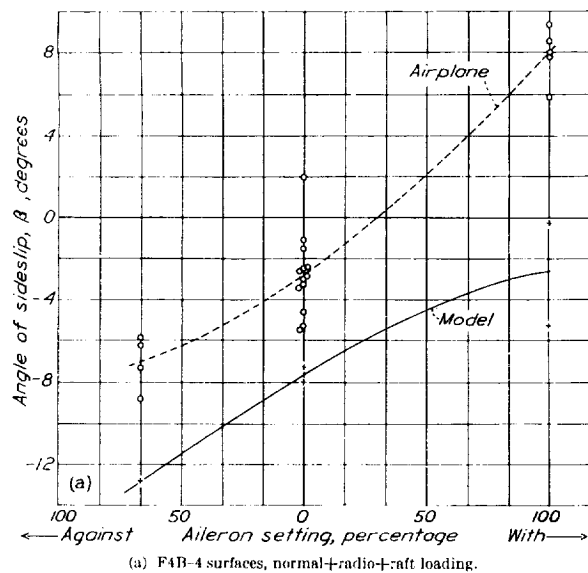


FIGURE 18.—Variation of angle of sideslip with aileron setting. F4B-2.

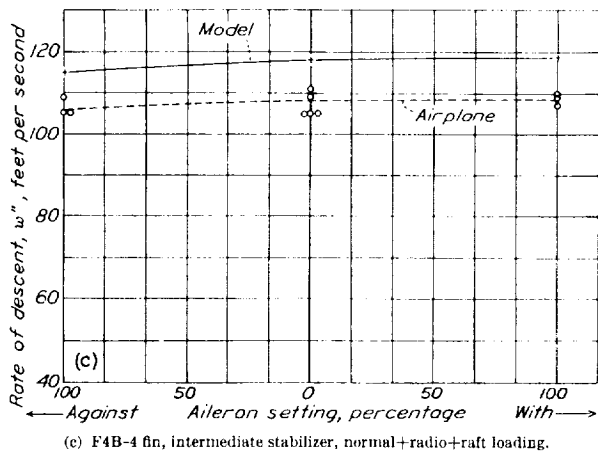
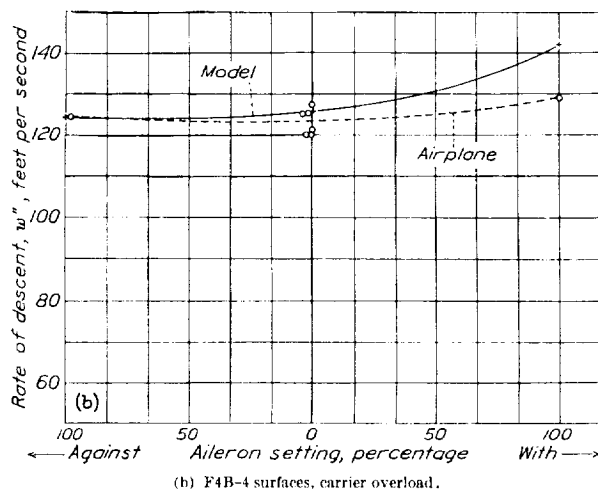
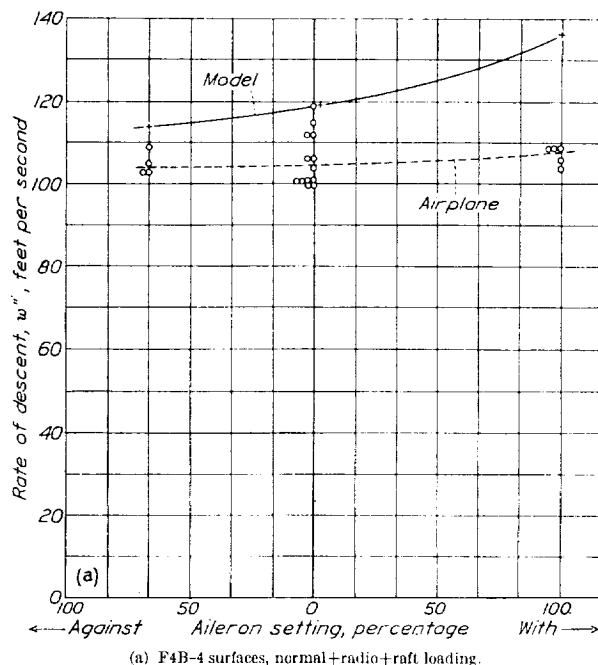


FIGURE 19.—Variation of rate of descent with aileron setting. F4B-2.

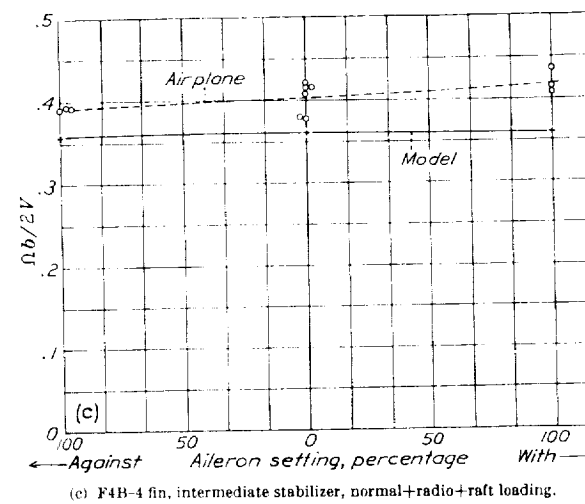
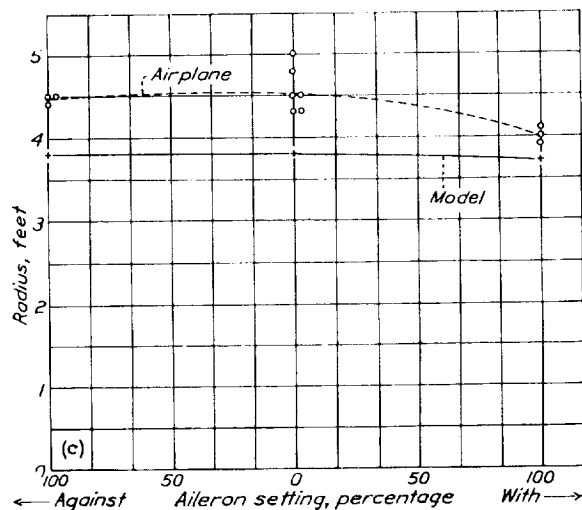
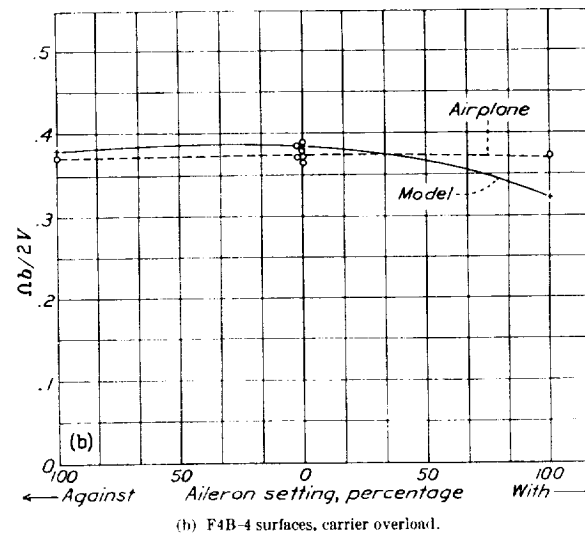
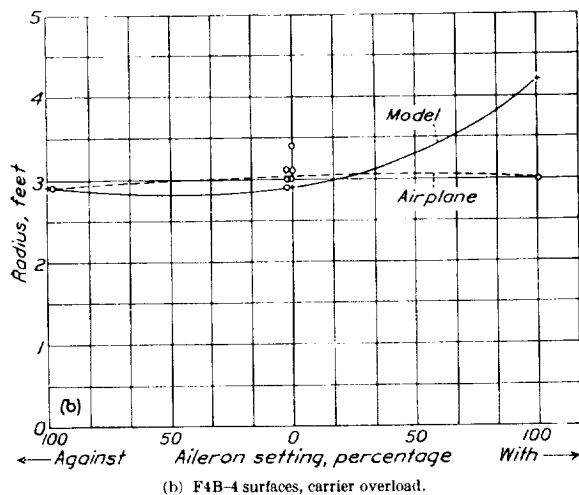
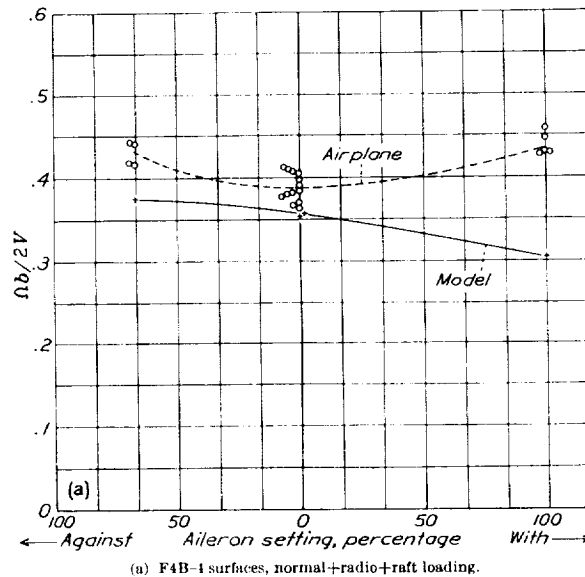
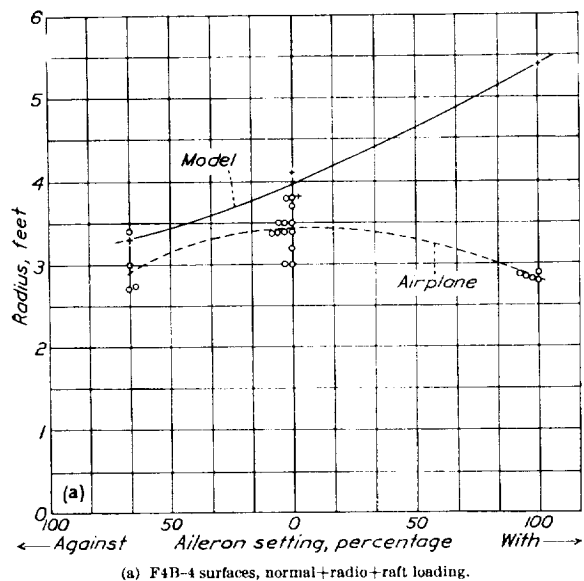


FIGURE 20.—Variation of radius with aileron setting. F4B-2.

FIGURE 21.—Variation of $\Omega b/2V$ with aileron setting. F4B-2.

Recoveries.—Results of comparable recovery tests with the XN2Y-1 airplane and model are given in table III, in which the full-scale data were obtained from a series of tests the results of which have not been published. The Model values are based in the camera records with the exceptions noted in the table. Similar results for the F4B-2 are given in table IV, the full-scale results of which were taken from reference 5.

Precision.—The test conditions were held within the following limits:

Control settings.....	$\pm 1\frac{1}{2}^\circ$.
Weight.....	± 1 percent.
Moments of inertia.....	± 5 percent.
C_θ and $\frac{z}{c}$	± 1 percent of chord.

These limits allow for errors in measuring values, changes due to temperature and humidity, and discrepancies permitted because of the time required to obtain more exact values.

The steady-spin data for the models are believed to be correct within the following limits:

Angle of attack.....	$\pm 3^\circ$.
Angle of sideslip.....	$\pm 1\frac{1}{2}^\circ$.
Air speed.....	± 2 percent.
Radius.....	± 10 percent.
$\Omega b/2V$	± 3 percent.

These limits allow for inaccuracies both in measurements and in method of reduction of the data. In cases where unsteady spins were obtained the data and limits apply to the mean values of the factors.

The recovery data for the models are believed to be correct within $\pm \frac{1}{4}$ turn.

The precision of the full-scale results is given in reference 5.

COMPARISON BETWEEN AIRPLANE AND MODEL RESULTS

Steady spins.—The XN2Y-1 model requires a somewhat greater rudder setting with the spin to attain a given angle of attack than did the airplane. The model spun with about 9° more outward sideslip than did the airplane at a given angle of attack throughout the angle-of-attack range. The model's rate of descent w'' (scaled to full-scale equivalent) was almost the same as that of the airplane at high angles of attack, but was about 10 percent greater at low angles. The model spin radius was somewhat shorter than that of the airplane at all angles of attack but the difference was more pronounced at the lower angles. The value of $\Omega b/2V$ for the model was in good agreement with that for the airplane throughout the angle-of-attack range.

For both model and airplane, deflecting the elevator down decreased the angle of attack but, for a given angle of attack, resulted in more outward sideslip, a lower rate of descent, a smaller radius, and a greater value of $\Omega b/2V$.

The comparison between airplane and model results for the F4B-2 is not clear-cut because both airplane and model were fairly unsteady in the spin. The scattering of the data from the flight tests indicates the nature of the results. The model results do not scatter so badly because they represent the mean condition in a prolonged spin. The following comparison is based on rough averages of the large number of full-scale points in figures 12 to 21.

The model required somewhat greater rudder setting with the spin to attain a given angle of attack than did the airplane. The model spun with about 5° more outward sideslip than did the airplane at a given angle of attack. The unsteadiness, which in some conditions was a definite oscillation, of the spins of both model and airplane was most apparent in the angle of sideslip. The rate of descent of the model was about the same as that of the airplane at the high end of the angle-of-attack range. No airplane data at the low angles of attack are available but, from the trend of the points at high and intermediate angles, the indications are that the model rate of descent was higher at the low angles of attack than that of the airplane would be. There was good agreement between the radii of spin at the same angle of attack within the limits of the data. The values of $\Omega b/2V$ were of the same order of magnitude for model and airplane.

For both model and airplane, moving the elevator down increased the angle of attack but, for a given angle of attack, made no definite change in sideslip, slightly decreased the rate of descent, decreased the radius, and increased $\Omega b/2V$.

Both model and airplane showed very little change in characteristics of the spin, except sideslip, with aileron movement when the stabilizer was at an intermediate height on the fin. Both model and airplane required from 9° to 15° more outward sideslip for spinning equilibrium with ailerons against the spin than with ailerons with the spin for the stabilizer both on the fin and in its normal location.

With the stabilizer in its normal location both model and airplane spun at lower angles of attack when the ailerons were with the spin than when they were neutral or against the spin. The change in angle of attack was much greater, however, for the model than for the airplane for both loadings tested. A similar, and related, discrepancy is apparent in the comparisons of effect of aileron setting on rate of descent; the rate of descent increased more rapidly with aileron setting against the spin for the model than for the airplane. The variation of radius and $\Omega b/2V$ with aileron setting for the carrier-overload condition was consistent with the variations of the other characteristics. With the normal+radio+raft loading the radius and $\Omega b/2V$ for the airplane varied in a manner opposite to what

would be expected from the angle-of-attack variation when the ailerons were changed from neutral to with the spin. The model values of these characteristics varied consistently with the variations of the other factors, giving a marked discrepancy with the airplane data.

Recoveries.—The turns required for recovery by the XN2Y-1 model were between the number required for the airplane in a right spin and those required in a left spin for cases in which the elevator was up during the steady spin. When the elevator was down in the steady spin, the recovery required about twice as many turns when the rudder was reversed for the model as for the airplane, and no recovery was obtained with the model when the controls were neutralized as compared with four or five turns for recovery in the case of the airplane. Placing ballast at the wing tips increased the number of turns necessary for recovery for both airplane and model.

The F4B-2 model recovery tests indicated that the F4B-2 fin and rudder combination was much less effective in bringing about recovery when the rudder was reversed than was the F4B-4 fin and rudder combination and that no recovery would be effected if the elevator were put down at the same time. In the airplane tests, recovery required about one turn more with the F4B-2 surfaces with the elevator down than with the F4B-4 surfaces, and recovery could be accomplished in less than three turns with either set of surfaces. When the F4B-2 surfaces were neutralized in the spin, the model in no case recovered. The airplane recovered from left spins but not from right spins with this control movement.

The airplane was in some cases slow in recovering from left spins but recovered satisfactorily from right spins with the F4B-4 surfaces and the normal +radio+raft and carrier-overload loadings. The model recovered satisfactorily under the same conditions in all cases tried. Recoveries were slow and uncertain for all cases of neutralization of the model controls, and also for the airplane in right spins; but recovery was generally definite in left spins. Both model and airplane were slightly improved in recovery characteristics by the addition of auxiliary fin 2. The airplane showed greater improvement in recovery characteristics when the stabilizer was raised to an intermediate position on the fin than did the model. Increasing the loading increased slightly, in general, the number of turns for recovery of both model and airplane.

Discussion.—In the consideration of the results from model tests certain fairly obvious facts must be borne in mind. A scale model cannot be expected to check full-scale spinning characteristics more closely than the agreement between right- and left-hand spins of a sym-

metrically rigged airplane with the propeller locked. Neither can they be expected to check full-scale characteristics more closely than the check between two airplanes built from the same set of drawings. The most that can be expected is a positive indication as to whether the airplane will be definitely slow to recover or uncontrollable in the spin, will be a borderline case with the possibility of uncontrollable spins with slight changes in loading or rigging, or will recover quickly under all probable conditions of loading and rigging.

From the tables and figures included herein it is evident that the XN2Y-1 and F4B-2 models gave good approximations to the spinning behavior of the respective airplanes. There are certain consistent differences between the model and the airplane steady-spinning characteristics that are in agreement with indications from other sources (references 3, 10, 11, and 12) and that had, in part at least, been specifically predicted in reference 11. There is one marked discrepancy between model and airplane results, i. e., in the effect of the ailerons on the spin of the F4B-2 with the F4B-4 surfaces. In this case, however, the full-scale characteristics seem inconsistent among themselves. Despite the differences in attitude between the model and airplane spins, the models would apparently spin with any control setting that would produce a spin on the airplane with the possible exception of one or two cases where full-scale spins were obtained only after repeated attempts with complicated control movements.

The agreement between model and airplane recovery characteristics is better than for the steady spins. The XN2Y-1 model recovered positively, but not quickly, with reversal of the rudder as did the airplane. The model, however, indicated recovery to be slowest from spins with the elevator down. For the airplane this behavior was true of left spins, but the opposite was true of right spins. The model could not be counted on to recover with controls neutral and recovery was slow in any event. The same was true in a general way of the airplane.

The recovery characteristics of the F4B 2 model with the F4B 2 fin and rudder were very poor, recovery not being possible with simultaneous reversal of both rudder and elevators although it could be effected by reversal of the rudder first and the elevator afterward. The indications from the model behavior are that relatively inexperienced pilots or pilots trained to make recoveries in a standard manner (i. e., by holding the elevator full up and the rudder full with the spin during the steady spin followed by simultaneous and quick reversal of both controls) would have difficulty with spins and such was apparently the case when the airplane was placed in service. The model indicated decidedly poorer re-

covery characteristics with these surfaces than did the F4B-2 airplane tested at Langley Field. The model recovered satisfactorily with all the other tail combinations when the rudder was reversed. Model recoveries were, in general, more positive with these latter tail combinations than recoveries with the airplane.

The model definitely would not recover when the controls were neutralized with the F4B-2 surfaces. Recoveries were slow and uncertain with the airplane. When the controls were neutralized with the F4B-4 fin and rudder, recoveries were slow and uncertain for both model and airplane.

Although the results of the tests with the two biplane models reported herein are very encouraging, the tests are not sufficiently general to warrant definite conclusions. Both models have quite similar general arrangements. An additional series of comparisons similar to those reported should be made with at least one dissimilar arrangement, preferably a monoplane. Only experience with a large number of models will give a true indication of the reliability of the results. It is too much to expect that the model results will be infallible. The present indications are, however, that the results are worthy of a certain amount of confidence and that carefully conducted tests should prove of great value in estimating spinning characteristics.

LANGLEY MEMORIAL AERONAUTICAL LABORATORY,
NATIONAL ADVISORY COMMITTEE FOR AERONAUTICS,
LANGLEY FIELD, VA., October 29, 1935.

REFERENCES

1. Soulé, Hartley A., and Scudder, N. F.: A Method of Flight Measurement of Spins. T. R. No. 377, N. A. C. A., 1931.
2. Stephens, A. V.: Free-Flight Spinning Experiments with Several Models. R. & M. No. 1404, British A. R. C., 1931.
3. Stephens, A. V.: Recent Research on Spinning. R. A. S. Jour., November 1933, pp. 944-955.
4. Scudder, N. F.: A Flight Investigation of the Effect of Mass Distribution and Control Setting on the Spinning of the XN2Y-1 Airplane. T. R. No. 484, N. A. C. A., 1934.
5. Scudder, N. F., and Seidman, Oscar: A Flight Investigation of the Spinning of the F4B-2 Biplane with Various Loads and Tail Surfaces. T. R. No. 529, N. A. C. A., 1935.
6. Scherberg, Max, and Rhode, R. V.: Mass Distribution and Performance of Free Flight Models. T. N. No. 268, N. A. C. A., 1927.
7. Soulé, Hartley A., and Miller, Marvel P.: The Experimental Determination of the Moments of Inertia of Airplanes. T. R. No. 467, N. A. C. A., 1933.
8. Bamber, M. J., and Zimmerman, C. H.: The Aerodynamic Forces and Moments Exerted on a Spinning Model of the NY-1 Airplane as Measured by the Spinning Balance. T. R. No. 456, N. A. C. A., 1933.
9. Stephens, A. V., and Francis, R. H.: Model Spinning Tests of an Interceptor Fighter. R. & M. No. 1578, British A. R. C., 1934.
10. Bamber, M. J., and Zimmerman, C. H.: The Aerodynamic Forces and Moments on a Spinning Model of the F4B-2 Airplane as Measured by the Spinning Balance. T. N. No. 517, N. A. C. A., 1935.
11. Bamber, M. J., and Zimmerman, C. H.: Spinning Characteristics of Wings. I—Rectangular Clark Y Monoplane Wing. T. R. No. 519, N. A. C. A., 1935.
12. Stephens, A. V.: Das Trudeln von Flugzeugen. Luftfahrtforschung, Bd. 11, Nr. 5, 25. Oktober 1934, S. 140-149.

TABLE I
COMPARISON OF AIRPLANE AND MODEL DATA
STEADY SPINS FOR THE XN2Y-1

[A, airplane; M, model]

Loading condition	Control setting			α		β		u''		Radius		$\Omega b/2V$	
	Aileron	Rudder	Elevator	°		°		ft./sec.		ft.		ft./sec.	
				A	M	A	M	A	M	A	M	A	M
Normal.....	Neutral.....	41° with	Up.....	60.5	53	13.4	0	78.2	81.8	1.6	1.9	0.620	0.562
Do.....	do.....	18° with	do.....	57.4	53	9.7	-5.7	79.0	85.6	2.2	2.4	.551	.523
Do.....	do.....	4° with	do.....	45.7	33	7	-10.1	85.8	101	4.0	5.1	.449	.392
Do.....	do.....	41° with	Down.....	51.3	53	2.0	-6.7	81.3	77.5	2.2	1.6	.575	.661
Ballast at tips	do.....	8° with	Up.....	43.0	33	*3.9	-11.1	88.5	98.0	4.7	4.9	.416	.419

* This value is believed by flight investigators to be questionable.

TABLE II
COMPARISON OF AIRPLANE AND MODEL DATA
STEADY SPINS FOR THE F4B-2

[A, airplane; M, model]

Loading condition	Tail combination	Control setting			α		β		v''		Radius		$\omega/2V$	
		Aileron	Rudder	Elevator	A	M	A	M	A	M	A	M	A	M
Stripped	B-4	Neutral	With	Up	44.5	47	-1.7	-6.2	111	118	3.9	3.8	0.376	0.356
Normal+radio+raft	B-2	do	do	do	52.6	46	-1.6	-7.5	107	118	3.1	4.1	404	360
Do	do	do	Neutral	Neutral	44.2	39	-1.7	-11.0	114	126	3.0	3.1	449	428
Do	B-4	do	With	Up	45.3	46	-2.0	-7.3	115	119	3.5	3.8	373	360
Do	do	do	do	$\frac{3}{4}$ down	53.7	55	-4.6	-6.5	95.5	102	1.9	1.7	563	530
Do	do	do	do	Up	47.1	38	7.9	-2.8	107	136	2.8	5.4	439	305
Do	do	$\frac{3}{4}$ against	do	do	50.1	50	-7.1	-12.8	105	114	3.0	3.3	436	376
Do	do	Neutral	do	do	49.3	46	-3.2	-7.3	109	119	3.4	3.8	395	360
Do	Intermediate stabilizer	do	do	do	48.9	46	-3	-5.2	107	119	4.6	3.8	401	360
Do	do	do	do	Down	47.3	49	-2.1	-7.9	103	110	3.7	2.1	520	495
Do	do	do	With	do	50.5	48	-4.3	-9.2	106	115	4.5	3.8	392	357
Do	do	do	do	Up	50.6	47	8.7	1	109	119	4.0	3.7	418	358
Carrier overload	B-4+fin 2	Neutral	do	do	48.9	43	-8	-8.5	110	124	3.7	4.1	393	353
Do	B-4 fin	do	do	do	45.3	47	0	-6.3	123	126	3.1	2.9	374	383
Do	do	Against	do	do	47.7	49	-2.1	-10.2	124	124	2.9	2.9	370	378
Do	do	With	do	do	42.2	39	6.6	-1.2	129	142	3.0	4.2	372	322
Do	B-4+fin 3	Neutral	do	do	46.4	47	2	-5.3	114	130	3.8	3.2	373	355

TABLE III
COMPARISON OF AIRPLANE AND MODEL DATA
RECOVERIES FOR THE XN2Y-1

Loading condition	Original setting		Final setting		Turns required for recovery		
	Rudder	Elevator	Rudder	Elevator	Airplane, right	Airplane, left	Model
Normal	With	Up	Neutral	Neutral	6, 6, 3 $\frac{1}{2}$	3, 2 $\frac{1}{2}$, 3	3 $\frac{1}{2}$, 4 $\frac{1}{2}$, 5
Do	do	do	Against	Down	3, 3, 3 $\frac{1}{2}$	2 $\frac{1}{2}$, 1 $\frac{1}{2}$, 1 $\frac{1}{2}$	2 $\frac{1}{2}$, 2 $\frac{1}{2}$
Do	do	Down	Neutral	Neutral	5, 5 $\frac{1}{2}$, 3 $\frac{1}{2}$	5, 4, 4 $\frac{1}{2}$	13, 13, 13
Do	do	do	Against	Down	2 $\frac{1}{2}$, 2 $\frac{1}{2}$, 2 $\frac{1}{2}$	1 $\frac{1}{2}$, 2 $\frac{1}{2}$, 2 $\frac{1}{2}$	4, 3, 4
Ballast at tips	do	Up	Neutral	Neutral	8, 9, 9 $\frac{1}{2}$	4 $\frac{1}{2}$, 3 $\frac{1}{2}$, 5 $\frac{1}{2}$	6, 6, 6
Do	do	do	Against	Down	4 $\frac{1}{2}$, 4 $\frac{1}{2}$, 4 $\frac{1}{2}$	2 $\frac{1}{2}$, 1 $\frac{1}{2}$, 2 $\frac{1}{2}$	3, 3

* No recovery in turns indicated. In the case of the model the spin was stopped by encounter with the safety net.
* Observer's estimate.

TABLE IV
COMPARISON OF AIRPLANE AND MODEL DATA
RECOVERIES FOR THE F4B-2

Loading condition	Tail combination	Control setting			Turns required for recovery		
		Aileron	Rudder	Elevator	Airplane, right	Airplane, left	Model
Stripped	B-2 fin	Neutral	Against	Down	2 $\frac{1}{2}$	2	∞ , 6, 5
Do	do	do	do	Neutral	2 $\frac{1}{2}$	1 $\frac{1}{2}$	3 $\frac{1}{2}$, 4, 5, 4, 5
Do	do	do	do	Up	2 $\frac{1}{2}$	2	2, 2, 1 $\frac{1}{2}$, 2
Do	do	do	Neutral	Neutral	6*	2 $\frac{1}{2}$	∞ , ∞ , 5
Do	B-4 fin	do	Against	Down	1 $\frac{1}{2}$, 1 $\frac{1}{2}$, 1 $\frac{1}{2}$	1 $\frac{1}{2}$, 1 $\frac{1}{2}$, 1 $\frac{1}{2}$	1 $\frac{1}{2}$, 1 $\frac{1}{2}$, 1 $\frac{1}{2}$
Do	do	do	do	Neutral	1 $\frac{1}{2}$	1 $\frac{1}{2}$	1, 1
Do	do	do	do	Up	2 $\frac{1}{2}$, 1 $\frac{1}{2}$, 1 $\frac{1}{2}$	2 $\frac{1}{2}$, 1 $\frac{1}{2}$, 2, 1 $\frac{1}{2}$	1, 1
Do	do	do	Neutral	Neutral	2 $\frac{1}{2}$, 1 $\frac{1}{2}$, 4, 6	1 $\frac{1}{2}$, 3, 3 $\frac{1}{2}$	3, 3, 3, 3
Do	B-4+fin 2	do	Against	Down	1 $\frac{1}{2}$, 1 $\frac{1}{2}$	1 $\frac{1}{2}$, 1 $\frac{1}{2}$	1, 1 $\frac{1}{2}$
Do	do	do	Neutral	Neutral	4 $\frac{1}{2}$, 3 $\frac{1}{2}$	5, 1 $\frac{1}{2}$	3, 2*
Do	B-4+fin 3	do	Against	Down	1 $\frac{1}{2}$	1 $\frac{1}{2}$	1 $\frac{1}{2}$, 1 $\frac{1}{2}$
Do	do	do	do	Up	1 $\frac{1}{2}$	1 $\frac{1}{2}$	1 $\frac{1}{2}$
Do	do	do	Neutral	Neutral	2 $\frac{1}{2}$	3 $\frac{1}{2}$	3 $\frac{1}{2}$, 3 $\frac{1}{2}$, 3 $\frac{1}{2}$
Do	do	do	do	Up	6, 6, 1 $\frac{1}{2}$	1 $\frac{1}{2}$, 1 $\frac{1}{2}$	4, 3, 3
Normal+radio+raft	B-4 fin	do	Against	Down	1 $\frac{1}{2}$, 1 $\frac{1}{2}$, 2	2, 1 $\frac{1}{2}$, 1 $\frac{1}{2}$	1 $\frac{1}{2}$, 1 $\frac{1}{2}$, 1
Do	do	do	do	Neutral	1 $\frac{1}{2}$, 2	1 $\frac{1}{2}$, 1 $\frac{1}{2}$	1, 1 $\frac{1}{2}$, 1 $\frac{1}{2}$
Do	do	do	do	Up	1 $\frac{1}{2}$	3 $\frac{1}{2}$, 4 $\frac{1}{2}$, 3 $\frac{1}{2}$, 2 $\frac{1}{2}$, 1 $\frac{1}{2}$	1, 1, 1
Do	do	do	do	Up	1 $\frac{1}{2}$	2 $\frac{1}{2}$, 1 $\frac{1}{2}$	
Do	do	do	Neutral	Neutral	5, 8 $\frac{1}{2}$, 6*	2, 3, 2	2 $\frac{1}{2}$, 3, 3, 3 $\frac{1}{2}$ *
Do	do	do	Against	Down	1, 1, 1		1 $\frac{1}{2}$, 1 $\frac{1}{2}$, 1 $\frac{1}{2}$
Do	Inter. stab	do	do	Neutral	1 $\frac{1}{2}$, 1 $\frac{1}{2}$	1 $\frac{1}{2}$, 1 $\frac{1}{2}$	1 $\frac{1}{2}$, 1 $\frac{1}{2}$, 1
Do	do	do	do	Up	1 $\frac{1}{2}$, 1 $\frac{1}{2}$	1, 1 $\frac{1}{2}$, 1 $\frac{1}{2}$, 1 $\frac{1}{2}$, 1 $\frac{1}{2}$	1, 1, 1 $\frac{1}{2}$
Do	do	do	Neutral	Neutral	4 $\frac{1}{2}$, 5*	2, 4 $\frac{1}{2}$	3*
Carrier overload	B-2 fin	do	Against	Down	2 $\frac{1}{2}$	2 $\frac{1}{2}$	5, 6, 5, ∞
Do	do	do	do	Neutral	4 $\frac{1}{2}$		6, 4, 3 $\frac{1}{2}$
Do	do	do	do	Up	6*	4	2, 2, 2, 2 $\frac{1}{2}$
Do	do	do	Neutral	Neutral	8*	3 $\frac{1}{2}$	∞
Do	B-4 fin	do	Against	Down	2, 1 $\frac{1}{2}$, 2, 1 $\frac{1}{2}$, 2 $\frac{1}{2}$	1 $\frac{1}{2}$, 1 $\frac{1}{2}$, 1 $\frac{1}{2}$, 2, 1 $\frac{1}{2}$	2, 1 $\frac{1}{2}$, 2 $\frac{1}{2}$
Do	do	do	do	Neutral	1 $\frac{1}{2}$, 2	1 $\frac{1}{2}$, 1 $\frac{1}{2}$	1 $\frac{1}{2}$, 1 $\frac{1}{2}$, 1 $\frac{1}{2}$
Do	do	do	do	Up	1 $\frac{1}{2}$, 1 $\frac{1}{2}$, 1 $\frac{1}{2}$	2 $\frac{1}{2}$, 6, 1 $\frac{1}{2}$, 4, 2, 5, 3	1 $\frac{1}{2}$, 1*
Do	do	do	do	Up	1 $\frac{1}{2}$, 1 $\frac{1}{2}$, 1 $\frac{1}{2}$	1 $\frac{1}{2}$, 2 $\frac{1}{2}$, 1 $\frac{1}{2}$	
Do	do	do	Neutral	Neutral	10, 12, 7*	2 $\frac{1}{2}$, 2 $\frac{1}{2}$, 2, 2 $\frac{1}{2}$	5*
Do	B-4+fin 2	do	Against	Down	1 $\frac{1}{2}$, 1 $\frac{1}{2}$	1 $\frac{1}{2}$, 1 $\frac{1}{2}$	1 $\frac{1}{2}$
Do	do	do	do	Neutral	1 $\frac{1}{2}$, 1 $\frac{1}{2}$	1, 1 $\frac{1}{2}$	1, 1
Do	do	do	do	Up	1 $\frac{1}{2}$, 1 $\frac{1}{2}$	1 $\frac{1}{2}$, 1 $\frac{1}{2}$	1, 1
Do	do	do	Neutral	Neutral	4 $\frac{1}{2}$, 6*	4, 4	2, 2 $\frac{1}{2}$ *
Do	B-4+fin 3	do	Against	Down	1 $\frac{1}{2}$	1 $\frac{1}{2}$	1 $\frac{1}{2}$, 1
Do	do	do	do	Neutral	2	1 $\frac{1}{2}$	1 $\frac{1}{2}$, 1, 1
Do	do	do	do	Up	1 $\frac{1}{2}$	5 $\frac{1}{2}$, 1 $\frac{1}{2}$	1 $\frac{1}{2}$
Do	do	do	Neutral	Neutral	6*	2 $\frac{1}{2}$	3, 7*

* No recovery in turns given. In the case of the model the spin was stopped by encounter with the safety net.

REPORT No. 558

TURBULENCE FACTORS OF N. A. C. A. WIND TUNNELS AS DETERMINED BY SPHERE TESTS

By ROBERT C. PLATT

SUMMARY

Results of drag and pressure tests of spheres having diameters of 2, 4, 6, 8, 10, and 12 inches in eight N. A. C. A. wind tunnels, in the air ahead of the carriage in the N. A. C. A. tank, and beneath an autogiro in flight are presented in this report. Two methods of testing were employed, one involving measurements of sphere drag and the other measurements of the pressure difference between the front stagnation point and the rear portion of the sphere. Satisfactory correlation between the two methods was obtained experimentally, as set forth in an appendix to the report.

The following table indicates the relative status of the wind tunnels tested as regards the amount of turbulence normally encountered in their air streams, the least turbulent being listed first:

Full-scale tunnel.
24-inch high-speed tunnel.
20-foot tunnel.
Model of the full-scale tunnel.
7- by 10-foot tunnel.
5-foot vertical tunnel.
Free-spinning tunnel.
Variable-density tunnel.

A "turbulence factor" for each wind tunnel, defined as the ratio of the critical Reynolds Number of a sphere in a nonturbulent air stream to the critical Reynolds Number in the tunnel, was obtained from sphere-test results. When the Reynolds Number of a model tested in a wind tunnel is multiplied by the turbulence factor for that tunnel, the resulting value is an "effective" Reynolds Number; that is, the Reynolds Number at which certain critical flow conditions obtained in the actual test would be approximately reproduced in a nonturbulent stream. When this method is used to obtain the scale-effect variation of maximum lift coefficient and drag coefficient at zero lift of certain well-known airfoils, data obtained in various wind tunnels under a wide variety of turbulent conditions are brought into satisfactory agreement.

INTRODUCTION

Air-stream turbulence has long been recognized as a source of discrepancy between forces measured on a model in a wind tunnel and forces that would occur on the model in free air under otherwise comparable conditions. Although the general effects of turbulence are now fairly well known, present knowledge is insufficient to permit either an exact determination of the nature and quantity of turbulence present in an air stream or the development of satisfactory corrections for its effect. It is possible, however, to determine by any one of several experimental methods a value indicative of the relative magnitude of the turbulence present in an air stream.

The effect of wind-tunnel turbulence in general on the aerodynamic characteristics of bodies has been estimated in some specific cases by the introduction of artificial turbulence into the tunnel air stream. In such cases an approximate determination of the amount of turbulence introduced relative to the initial turbulence has been of considerable assistance in extrapolating to the condition of zero turbulence. It is thus apparent that approximate measurements of air-stream turbulence, even though they fail to give completely satisfactory corrections, are of definite significance in wind-tunnel research.

A method commonly used to determine the turbulence of a wind tunnel involves measurement of the change in the drag coefficient of a sphere as the Reynolds Number of the sphere is varied. This method depends on a change in the nature of the flow about a sphere with changing Reynolds Number. At a low value of the Reynolds Number the flow separates approximately at the equator of the sphere and a large eddy wake with low pressure on the downstream side of the sphere results. In this condition the boundary layer of the sphere ahead of the point of separation is laminar. As the Reynolds Number is increased, transition from laminar to turbulent flow moves ahead of the point of separation with a resulting

backward, or downstream, movement of the point of separation and a consequent reduced wake area and drag. The Reynolds Number at which this sudden change of flow takes place has been called the "critical Reynolds Number." The change from laminar to turbulent flow in the boundary layer depends on the Reynolds Number and the initial turbulence of the air stream in such a way that the initial turbulence decreases the value of the Reynolds Number at which transition from laminar to turbulent flow in a boundary layer takes place. Thus the value of the critical Reynolds Number serves to indicate the amount of turbulence present in the air stream. In an extensive investigation by Dryden and Kuethe (reference 1) a relation was established between the critical Reynolds Number of a sphere in an air stream and the percentage turbulence of the air stream. The paper gives a clear account of the basic theory and proposes a quantitative method of determining the initial turbulence of an air stream from drag tests of spheres.

Sphere tests have come to be regarded as essential to the calibration of a wind tunnel, and some data of this nature have already been obtained in most of the existing wind tunnels. References 2 and 3 present the results of previous N. A. C. A. sphere tests in free air, in the old atmospheric wind tunnel, and in an early modification of the variable-density tunnel. The data obtained in the present investigation, however, are the first published material applicable to the various N. A. C. A. wind tunnels in their present forms.

The investigation was undertaken with the intention of determining the comparative turbulence of the present N. A. C. A. wind tunnels in such a way as to obtain an estimate of the effect of turbulence on test results. It was considered desirable to determine, if possible, the changes in aerodynamic characteristics resulting from the different turbulent conditions existing in free air and in wind tunnels. The determination of the comparative turbulence of free air was therefore considered an additional object of the investigation. The investigation was conducted during 1933-35 at such times as each of the eight tunnels at present in use became available.

APPARATUS AND METHODS

Wind tunnels.—The eight wind tunnels investigated, with references to descriptive material, are listed in the following table:

- The 7- by 10-foot tunnel, reference 4.
- The model of the full-scale tunnel, reference 5.
- The full-scale tunnel, reference 6.
- The 20-foot wind tunnel, reference 7.
- The 5-foot vertical tunnel, reference 8.
- The 24-inch high-speed tunnel, reference 9. (Reference 10 gives a description of a similar high-speed tunnel of smaller size.)

The variable-density tunnel, reference 11.

The free-spinning tunnel, reference 12.

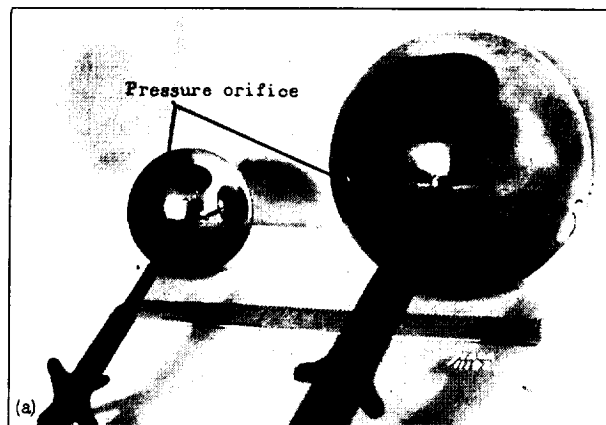
Data for free air were obtained by towing spheres beneath an autogiro in flight and ahead of the carriage in the canopy of the N. A. C. A. tank (reference 13).

Spheres.—Tests were made of five mahogany spheres (fig. 1(b)) having diameters of 4, 6, 8, 10, and 12 inches; the spheres were finished with lacquer and polished smooth. They were mounted on stings which could be attached to a balance for drag tests and which, in normal test position, extended directly downstream from the center of the sphere. Two holes, one at the front stagnation point and one 22° from the downstream axis of the sphere, were equipped with pressure leads to permit measurement of the front and rear pressures on each sphere. In addition to the wooden spheres, an 8-inch hard rubber bowling ball, a 2-inch steel ball bearing, and a 4-inch brass ball were used in some of the tests. The rubber sphere, which had a smooth, rubbed finish and which was not equipped with pressure holes, served as a check of the surface finish of the wooden spheres, which had to be repolished several times during the course of the tests. The steel and brass spheres (fig. 1(a)), which had only rear pressure holes, were polished to a mirror finish; they, in addition to serving as checks of the surface finish of the other spheres, were used for tests in which the other spheres were unsuitable. The nose pressures for these spheres were obtained from tunnel calibration data.

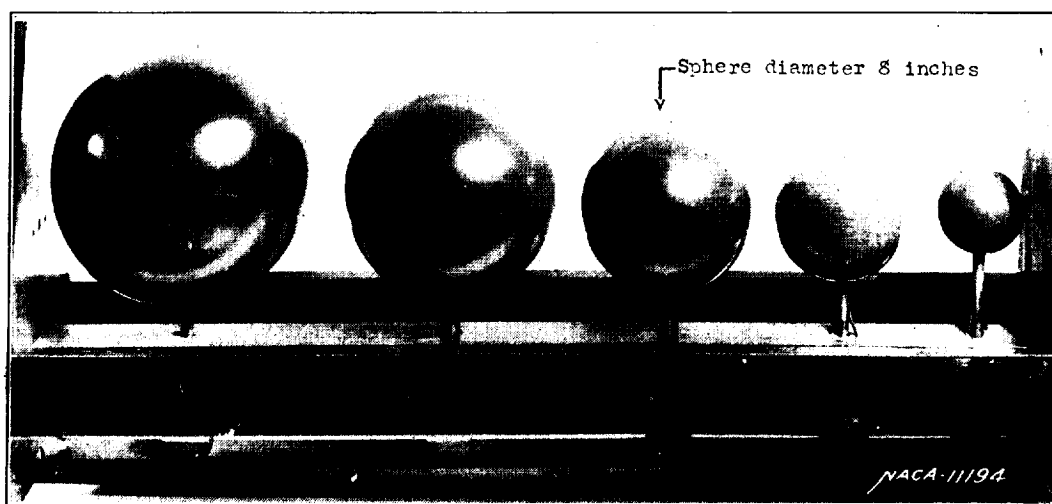
Balance and supports.—A portable drag balance (fig. 2a, b) especially designed to be easily mounted in various wind tunnels was constructed for use in this investigation. This balance consists of a round bar supported on Emery knife-edges inside a 2½-inch tube. The bar, which has a tapped hole in the forward end to take the sphere-support sting, is restrained longitudinally by a calibrated pressure capsule and can be balanced between contact points. The pressure required to produce balance is a measure of the drag force on the sphere.

A towing support (fig. 3) for use in making pressure measurements on the spheres was also constructed. This support consists of a bar with fins at the rear and with a tapped hole in the nose to take the sphere-support sting. With the sphere in place the unit was supported at its center of gravity by a cable and hung in any desired position with respect to an air-plane, to the carriage of the N. A. C. A. tank, or in the air stream of a wind tunnel.

Drag measurements.—For the drag measurements the special balance was supported rigidly in the tunnel under investigation and the drag forces on each of several spheres were measured at various air speeds. Drag measurements were made in the 7- by 10-foot tunnel, the model full-scale tunnel, and at two positions in the jet of the full-scale tunnel. In the 7- by 10-



(a) Metal spheres.



(b) Wooden spheres.

FIGURE 1.—Spheres used in the turbulence tests.

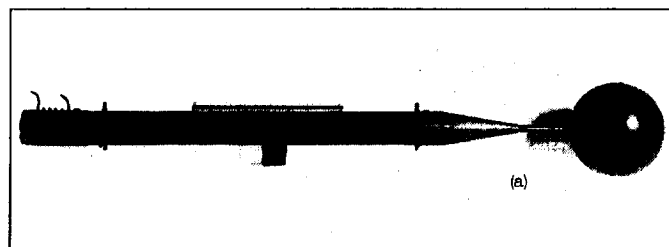


FIGURE 2a.—An 8-inch sphere mounted on the drag balance.

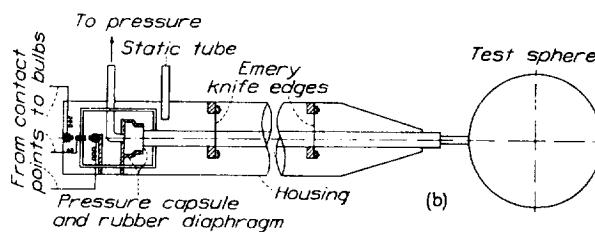


FIGURE 2b.—Sketch of the sphere drag balance.

foot-tunnel tests, two conditions of turbulence were obtained, one in the clear tunnel and one with a turbulence grid in the jet ahead of the sphere. This grid consisted of $\frac{1}{4}$ -inch square bars set edge on to the stream with their axes spaced $1\frac{1}{2}$ inches. The bars extended vertically and the entire unit was located 35 inches ahead of the center of the sphere.

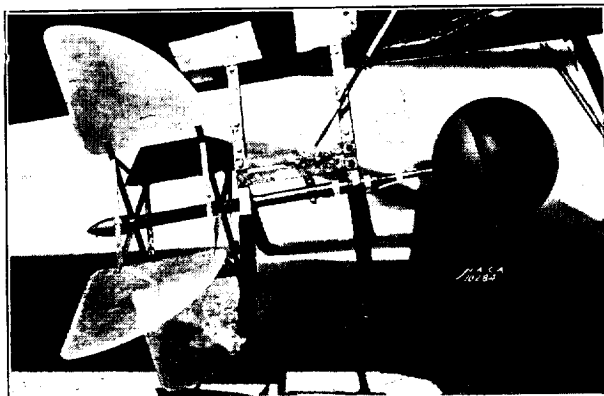


FIGURE 3.—Sphere towing unit with 10-inch sphere mounted on an autogiro.

Pressure measurements.—An alternative method of obtaining the critical Reynolds Number of a sphere was suggested for use in this investigation by Dr. H. L. Dryden, of the National Bureau of Standards. This

method consists of measuring the difference of pressure Δp between the front and rear portions of the sphere. If a pressure coefficient $\Delta p/q$ is plotted against appropriate values of Reynolds Number, a variation similar to the variation of the drag coefficient with Reynolds Number is found, thus permitting an approximate determination of the critical Reynolds Number. The method was independently developed by the D. V. L. in Germany; a complete description of the theory underlying it and the results of tests in which it is used have been published in reference 14. A résumé of the theory and a description of the tests correlating drag and pressure measurements are given in an appendix to the present report. The pressure method offers considerable advantage as compared with drag tests on account of the greater ease and rapidity with which results can be obtained both in flight and in wind tunnels. In addition, greater accuracy should result from the simplification of the technique of testing and the elimination of the need for damping the balance vibration.

Pressure tests were made at model location in the 7-by 10-foot tunnel with two conditions of turbulence and with normal turbulence in all of the other tunnels previously listed with the exception of the model of the full-scale tunnel, in which no pressure tests were made. In flight and in the tank, data were obtained solely by the pressure method.

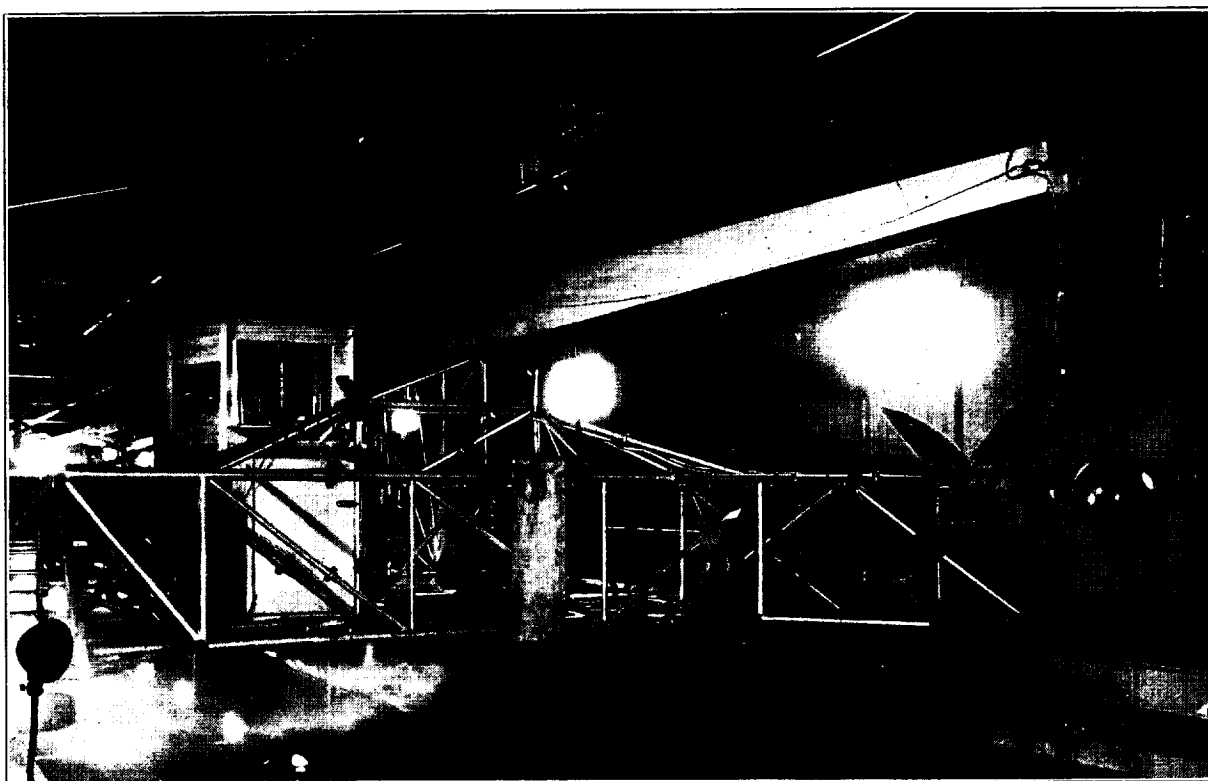


FIGURE 4.—Sphere towing unit in the N. A. C. A. tank

Mounting of spheres.—Several methods of mounting the spheres in the wind tunnels were employed. For the drag tests the drag balance was rigidly supported either by wires or by a clamp on a streamline tube braced with wires. In each case the center line of the sphere, sting, and balance unit was accurately aligned with the air stream. For some of the pressure tests the sphere was supported rigidly in the tunnel by wires attached to its sting. For the other pressure tests the towing support was hung by a V of wires permitting it to swing fore and aft but restraining the lateral motions. The fins in each case caused the sphere to maintain proper alignment in the air stream. In flight the sphere-towing support (fig. 3) was hung 70 feet below an autogiro by a cable. For the tests in the N. A. C. A. tank the towing support was hung on a special suspension of low frequency to reduce vibration of the sphere and was supported 15 feet ahead of the towing carriage near the center of the cross section of the tank canopy (fig. 4).

PRECISION

In general, errors in the sphere tests may be ascribed to faulty determination of the support interference and tare forces, to surface roughness, and to vibration of the sphere and the support. Support interference may be divided into two types: First, that resulting from a change in air flow caused by the junction of the support and sphere; and second, that resulting from a change in the air flow induced by the presence of bodies, such as the drag balance, behind the sphere.

The first type of support interference may be reduced to a negligible amount by having the point of attachment of the sphere to its support at the most downstream point of the sphere and by keeping the size of the support relatively small as compared with the size of the sphere (references 2 and 14). Satisfactory agreement between pressure measurements of duplicate set-ups with and without the sphere-drag balance in place indicates that the second type of interference is also negligible in these tests. Attempts to measure any tare force on the drag balance were unsuccessful. Since it is reasonable to suppose that errors in tare-force determination would be approximately proportional to the magnitude of the tare force itself, it seems probable that errors resulting from this source are very small. In cases where the nature of the support permitted visible vibration of the sphere, it was found that the critical Reynolds Number was appreciably reduced and care was taken to keep vibration at a minimum during the course of the testing.

From comparison of the results of check tests, it is believed that the variation of the observed critical

Reynolds Number caused by accidental errors lies within the following limits:

Drag tests in wind tunnels.....	± 5,000
Pressure tests in wind tunnels.....	± 5,000
Pressure tests in flight.....	± 8,000
Pressure tests in tank.....	± 5,000

The tests in flight and in the tank are thought to be free from error due to vibration because of the support employed. It seems very unlikely that vibrations from the autogiro could be transmitted down the 70-foot length of flexible cable used in the flight tests. The special spring suspension used in the tank showed a strong tendency to damp vibrations. Air turbulence as indicated by the motion of titanium tetrachloride smoke is considered to have been nonexistent in the air encountered by the sphere during the test runs in the tank canopy.

RESULTS AND DISCUSSION

Presentation of results.—Test data from the drag and the pressure tests have been reduced to the following nondimensional coefficient forms:

$$\text{Drag coefficient, } C_D = \frac{\text{drag force}}{qS}$$

$$\text{Pressure coefficient, } \frac{\Delta p}{q}$$

in which $q = \frac{1}{2}\rho V^2$, dynamic pressure.

$$S = \frac{\pi d^2}{4}, \text{ cross-sectional area of sphere.}$$

d , sphere diameter.

Δp , the pressure difference between the front and rear orifices in the sphere.

The values of the drag and the pressure coefficients are then plotted against Reynolds Number Vd/ν , in which V is the velocity of the air stream and ν is the kinematic viscosity of the air. The critical Reynolds Number R_c is chosen as that value of the Reynolds Number corresponding to a drag coefficient of 0.3 (reference 1) or to a pressure coefficient of 1.22 in accordance with the correlation of the results of the drag and pressure tests presented in the appendix.

The 7- by 10-foot wind tunnel.—Results of drag and pressure tests in the 7- by 10-foot wind tunnel are shown in figures 5 and 6. Figure 5 (a, b, c, d) shows curves of C_D and $\Delta p/q$ for spheres of different size in the clear tunnel, with normal turbulence. Figure 6 (a, b, c, d) shows curves of C_D and $\Delta p/q$ for different spheres in the tunnel with the turbulence grid in place. The discontinuity in the $\Delta p/q$ curve for the 8-inch sphere in figure 6 (c) should be noted as a phenomenon that has appeared in several other tests as well as in this one. (In such cases it has been possible to repeat these

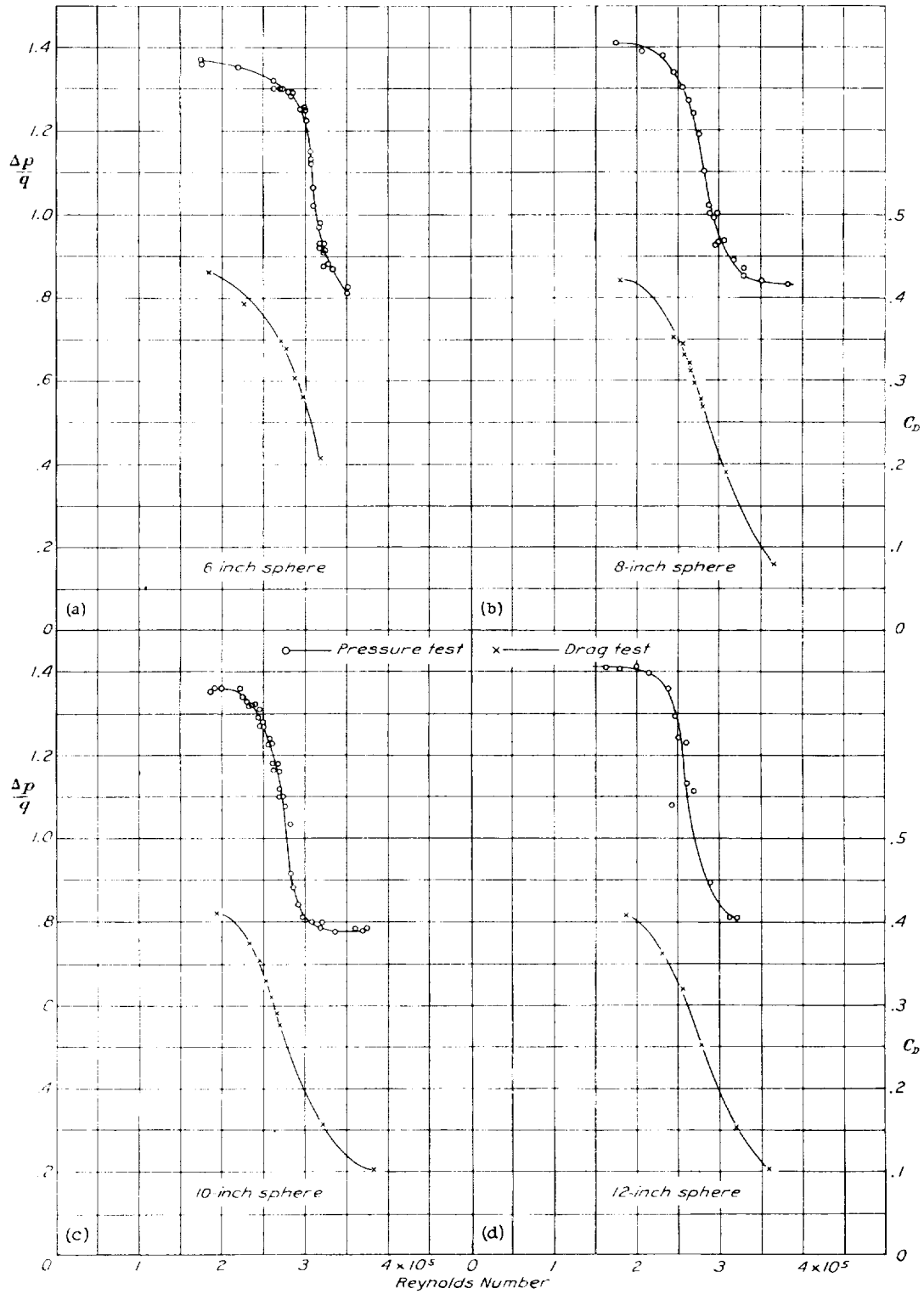


FIGURE 5 (a, b, c, d). Pressure and drag tests of spheres of different size in the 7- by 10-foot wind tunnel with normal turbulence.

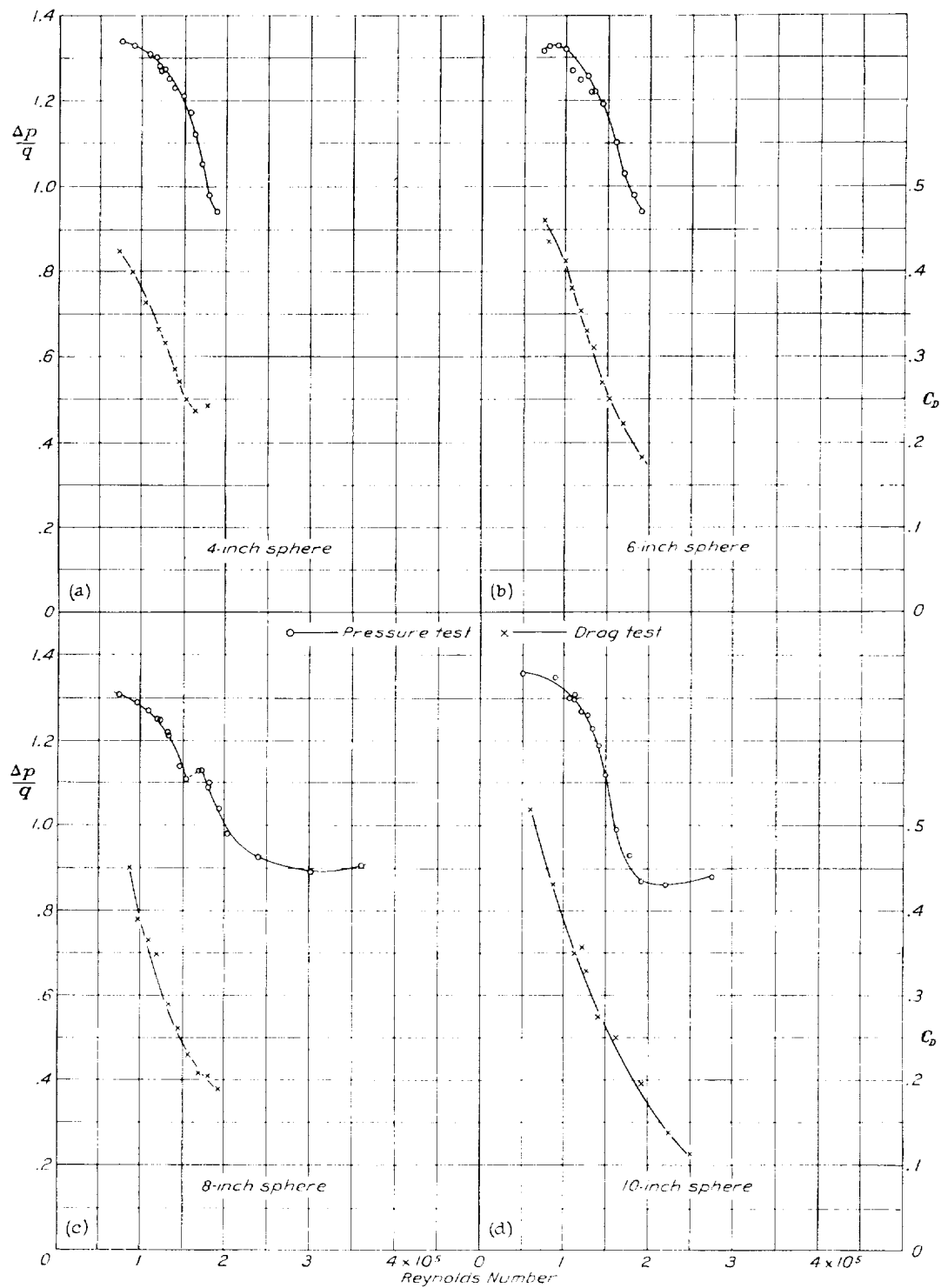


FIGURE 6 (a, b, c, d).— Pressure and drag tests of spheres of different size in the 7- by 10-foot wind tunnel with turbulence grid.

points in check tests.) Inasmuch as it does not, in general, extend to the critical value of $\Delta p/q$, no special consideration has been given to it in this investigation.

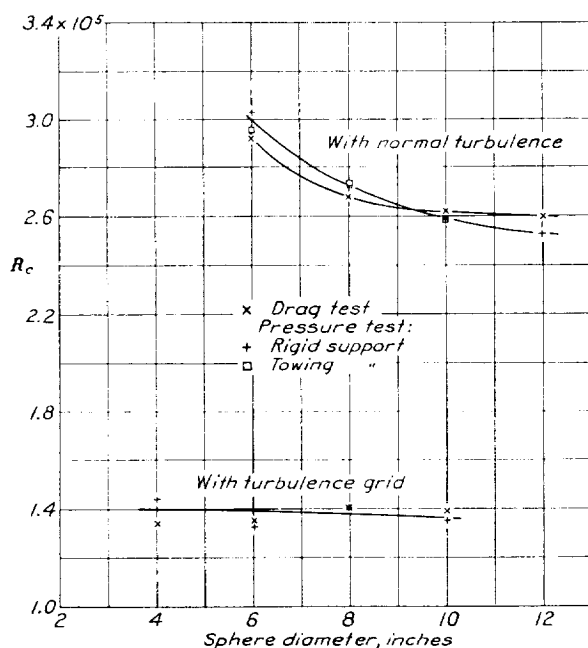


FIGURE 7. Variation of critical Reynolds Number with sphere diameter in the 7-by-10-foot wind tunnel.

Figure 7 shows the variation of critical Reynolds Number with sphere diameter. Since the air speed at which the critical Reynolds Number on a sphere occurs varies with the size of the sphere, it is possible that the

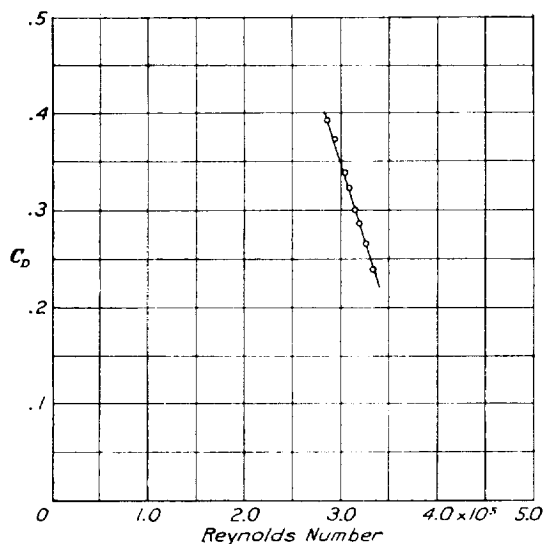


FIGURE 8. Sphere drag test in the model full-scale wind tunnel with the 8-inch sphere.

observed variation of the critical Reynolds Number with sphere size may result from a variation in tunnel turbulence with air speed. The fact that the energy

ratio of the wind tunnel changes with air speed tends to support this view, although data of references 1 and 15 indicate that the turbulence as measured by a hot-wire turbulence indicator is independent of the tunnel air speed. Although Harris and Graham (reference 16) suggest that the value of R_c varies with the ratio of sphere to tunnel diameter, subsequent data (discussed in Summary of Test Results) in the present report tend to invalidate this explanation of the observed effect. Figure 7 also shows the agreement of the pressure tests with the sphere supported on the drag balance and mounted at the same position in the air stream on the towing support. As stated previously, the agreement

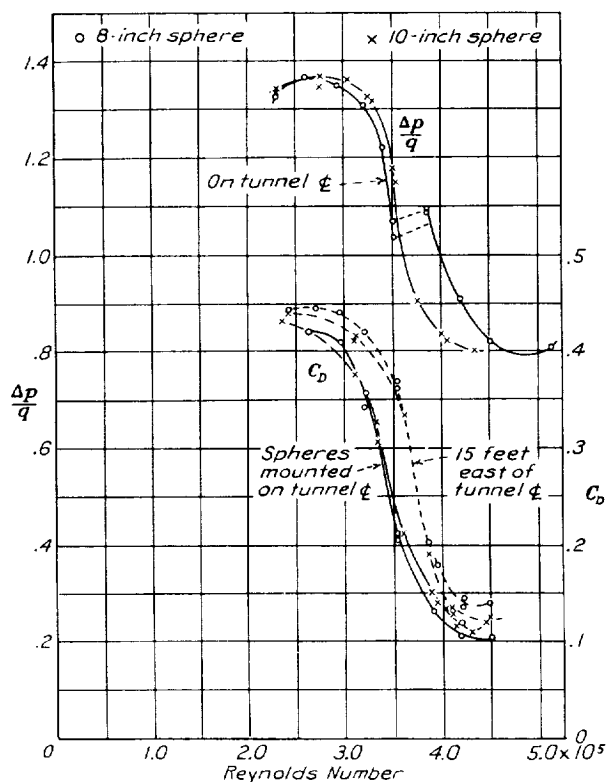
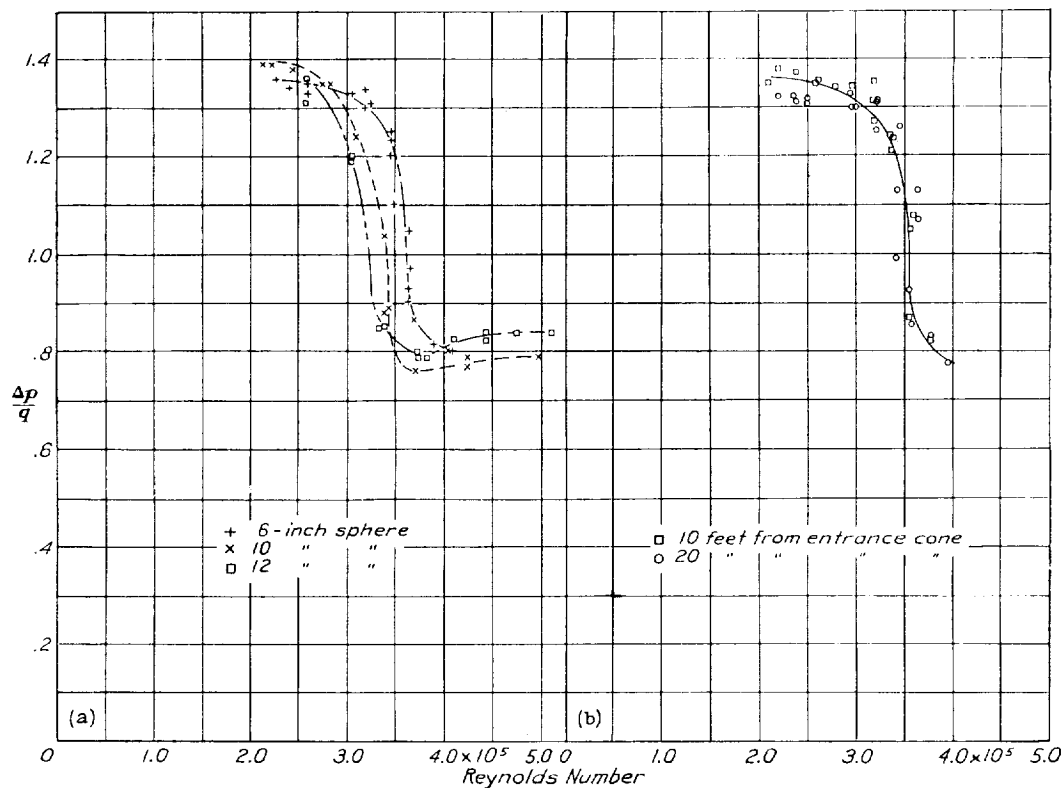


FIGURE 9. Pressure and drag tests of spheres of different size in the full-scale wind tunnel with normal turbulence.

between the tests indicates that the presence of the drag balance behind the sphere does not exert an appreciable effect on the air flow in the tunnel.

Model of the full-scale tunnel. Results of drag tests on an 8-inch rubber sphere, the one test made in the 1/15-scale model of the full-scale tunnel, are shown in figure 8.

Full-scale tunnel. Results of drag tests on two wooden spheres, each mounted 15 feet east of the vertical center line of the full-scale tunnel and on its horizontal center, and results of both drag and pressure tests with the spheres mounted at the intersection of the tunnel center lines are shown in figure 9. It is note-



(a) Three spheres mounted on tunnel center line.

(b) The 6-inch sphere mounted 2½ feet east of tunnel center line.

FIGURE 10.—Pressure tests of spheres of different size in the 20-foot wind tunnel with normal turbulence.

worthy that the turbulence appears to be definitely less 15 feet away from the center of the tunnel than on its vertical center line. A possible cause of the increased turbulence at the center may be the junction of the turbulent boundary layers from the outer walls of the return passages into a single disturbed region along the center of the jet.

Twenty-foot wind tunnel.—Results of pressure tests with three wooden spheres each mounted at various positions in the jet of the 20-foot wind tunnel are shown in figure 10 (a, b). As the full-scale and 20-foot tunnels have similar types of double return passage, it was intended to make tests at a position 5 feet off center, corresponding to the off-center position in the full-scale tunnel, but in this position it was found that an unsteadiness of flow in the jet caused the towing support to move unsteadily in the air stream, preventing satisfactory observation of the pressure differences. Tests were made 2½ feet off center where no unsteadiness was observed. No apparent difference was found in the amount of turbulence 10 feet and 20 feet from the entrance cone of this tunnel, which is in disagreement with the general belief that turbulence tends to be damped in an air stream. It is possible, however, that the turbulence had been so completely damped when the air reached the 10-foot station that there was very little further damping as it passed downstream.

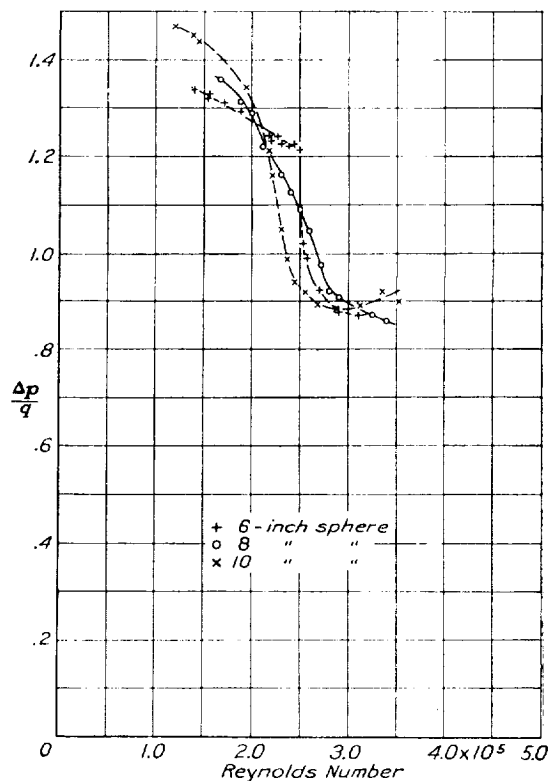
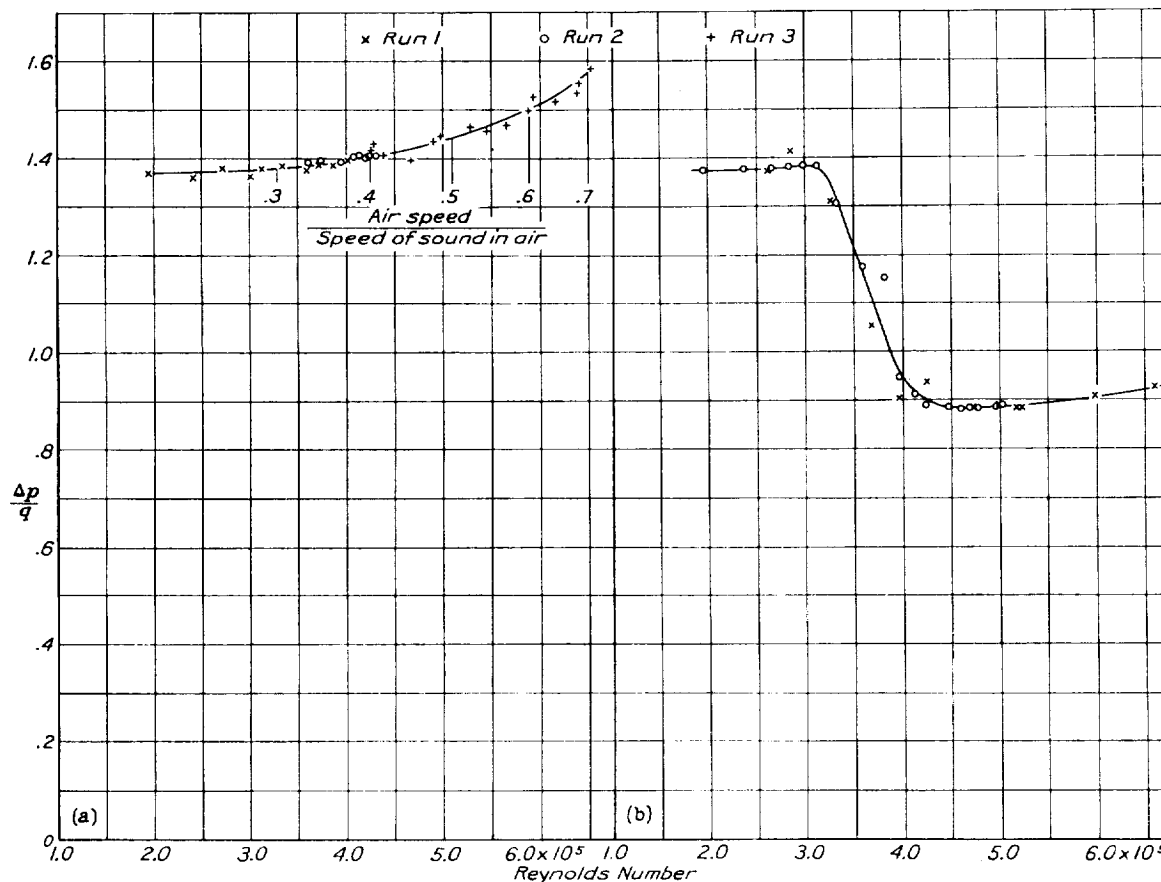


FIGURE 11.—Pressure tests of spheres of different size in the 5-foot vertical wind tunnel with normal turbulence. Spheres mounted on tunnel center line.

Five-foot vertical tunnel.—Results of pressure tests of three wooden spheres each located on the center line of the 5-foot vertical tunnel at the normal test position are shown in figure 11.

The 24-inch high-speed tunnel.—Results of pressure tests of the 2-inch steel and the 4-inch brass spheres in the 24-inch high-speed tunnel appear in figure 12 (a, b). Some tests of wooden spheres conducted before the final modifications and calibration of the tunnel indicated the $4\frac{1}{2}$ -inch off-center station to be representative of the average conditions across the jet

seems reasonable to conclude that the failure to obtain a critical Reynolds Number may be ascribed to an effect of compressibility in delaying the onset of boundary-layer turbulence, possibly through changing the pressure gradients on which compressibility is known to exert a powerful effect. It has been suggested that such an action might have occurred on the 4-inch sphere as well, resulting in a fictitious value of the critical Reynolds Number. The effect might be suggested as an explanation of the variation of the critical Reynolds Number with sphere diameter, al-



(a) The 2-inch sphere mounted $4\frac{1}{2}$ inches south of the tunnel center line. (b) The 4-inch sphere mounted $4\frac{1}{2}$ inches south of the tunnel center line.

FIGURE 12.—Pressure tests of two spheres in the 24-inch high-speed wind tunnel with normal turbulence.

at test level, and this position was accordingly chosen for the final tests.

The failure of the 2-inch sphere to reach a critical Reynolds Number is an interesting and apparently hitherto unobserved phenomenon. At a Reynolds Number of slightly over 300,000 where the pressure coefficient should begin to drop sharply, it begins to rise at a steadily increasing rate, giving a shape of curve suggestive of the variation of drag of an airfoil with air speed in the region in which compressibility begins to show an effect (references 9 and 10). It

though such an explanation seems very unlikely in the case of the observed variation in low-speed wind tunnels.

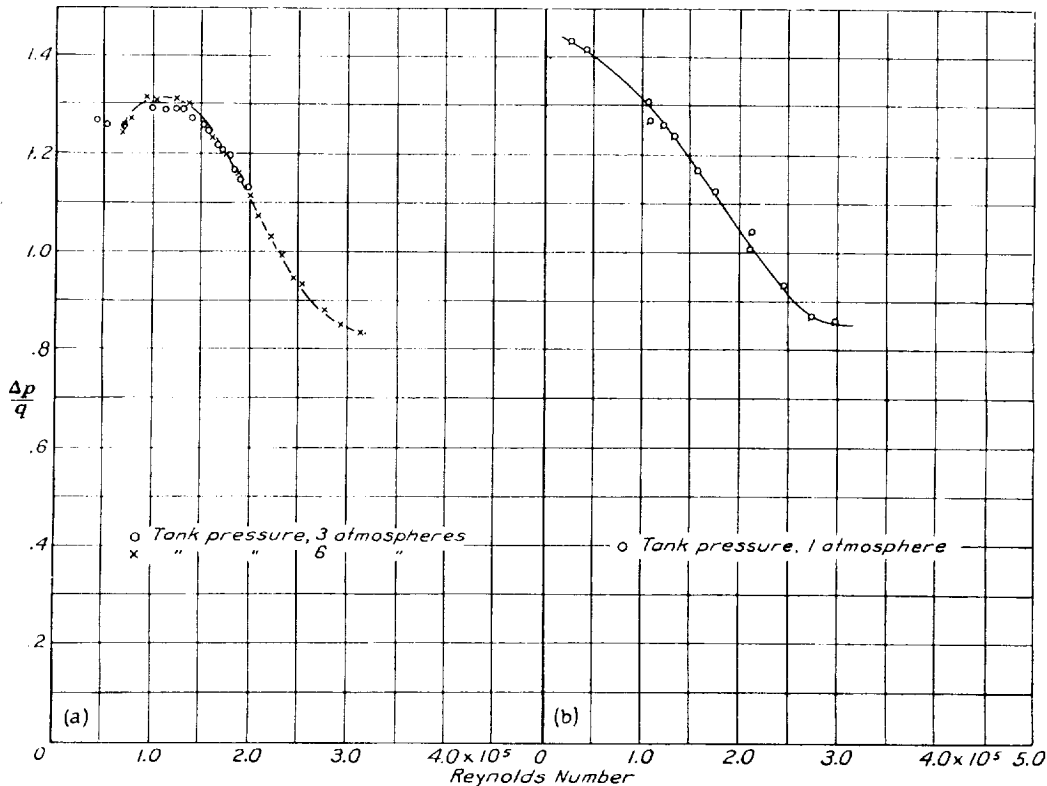
It is clear that at speeds greater than 0.4 the velocity of sound the effects of turbulence are seriously altered by compressibility, and full account of this effect must be taken before the significance of sphere tests in this range of speeds can be understood.

Variable-density tunnel.—Results of pressure tests of the 2-inch steel sphere and the 8-inch mahogany sphere in the variable-density tunnel are shown in

figure 13 (a, b). The results of tests at two different tank pressures, 3 and 6 atmospheres, indicate that variation of tank pressure does not exert an appreciable effect on the results of the sphere tests (see also reference 3); that is, variation of the pressure coefficient with Reynolds Number is the same regardless of the combination of speed and pressure used to produce a given Reynolds Number. Some tests at different positions indicate the variation of turbulence across the jet of the variable-density tunnel to be small. A comparison of the results for the 8-inch sphere with those for the 2-inch sphere indicate approximately the

with that found in the 20-foot tunnel, in which the turbulence was unaffected by downstream location, it is to be noted that there is definitely more turbulence in the free-spinning tunnel and that the test positions are much nearer to the source of turbulence than is the case in the 20-foot tunnel. The curve in figure 14 (d) appears to tend toward an asymptote and it might reasonably be supposed to check the indications of the 20-foot tunnel results satisfactorily if it were extended sufficiently far along the stream.

N. A. C. A. tank.—Pressure tests of two spheres each hung in the air 15 feet ahead of the towing carriage in



(a) The 2-inch sphere mounted on the tunnel center line.

(b) The 8-inch sphere mounted on the tunnel center line.

FIGURE 13.—Pressure tests of two spheres in the variable-density wind tunnel with normal turbulence.

same variation of the critical Reynolds Number with the sphere size as has been found in the tests in other tunnels.

Free-spinning tunnel.—Some results of tests of the 10-inch and 12-inch spheres and the variation of critical Reynolds Number with position in the jet of the free-spinning tunnel are shown in figure 14 (a, b, c, d). The low maximum speed available in the tunnel (50 feet per second) permitted testing only the large spheres; consequently only a small range of Reynolds Numbers was covered. In this tunnel the turbulence appears to be damped as the air passes downstream. Although this variation is apparently in disagreement

with the N. A. C. A. tank are shown in figure 15. Values of the pressure coefficient were obtained with the 10-inch sphere up to Reynolds Numbers of 350,000, the highest value obtainable with this sphere at the maximum speed of the carriage (approximately 80 feet per second). Corresponding pressure coefficients for the 12-inch sphere were obtained up to a Reynolds Number of 475,000. The curve for the 10-inch sphere appears to extrapolate satisfactorily through the value of the critical Reynolds Number indicated by the 12-inch sphere, that is, 385,000. Since the air is known to have been very still during the tests in which this value was obtained, it is considered representative of nonturbulent air. This

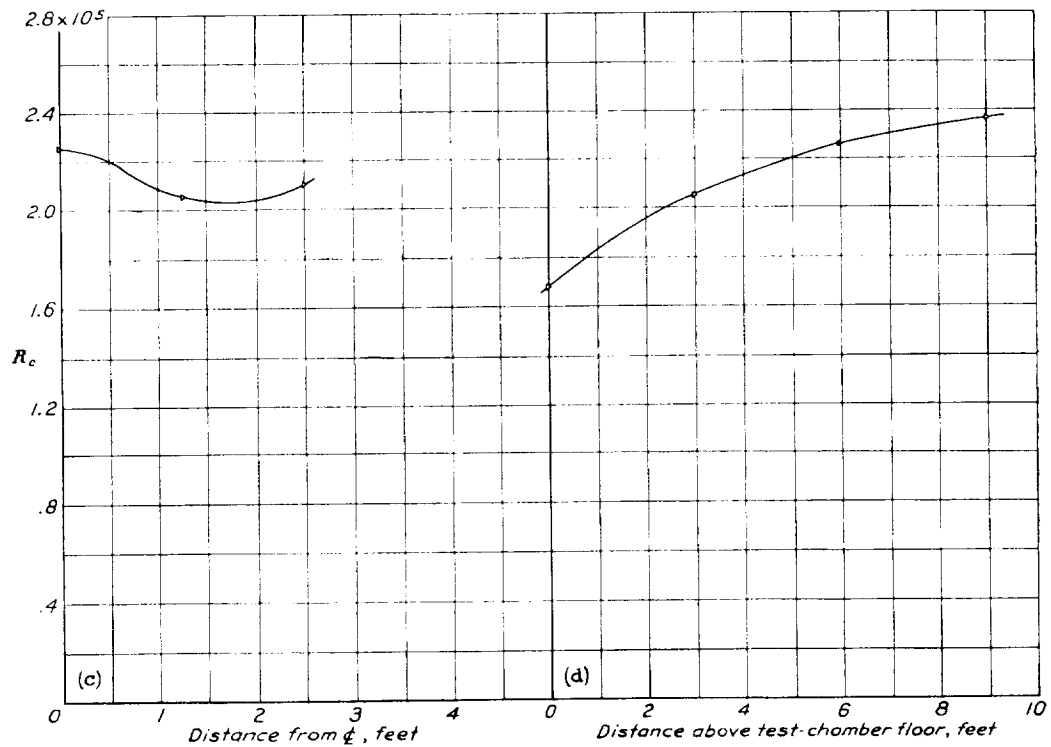
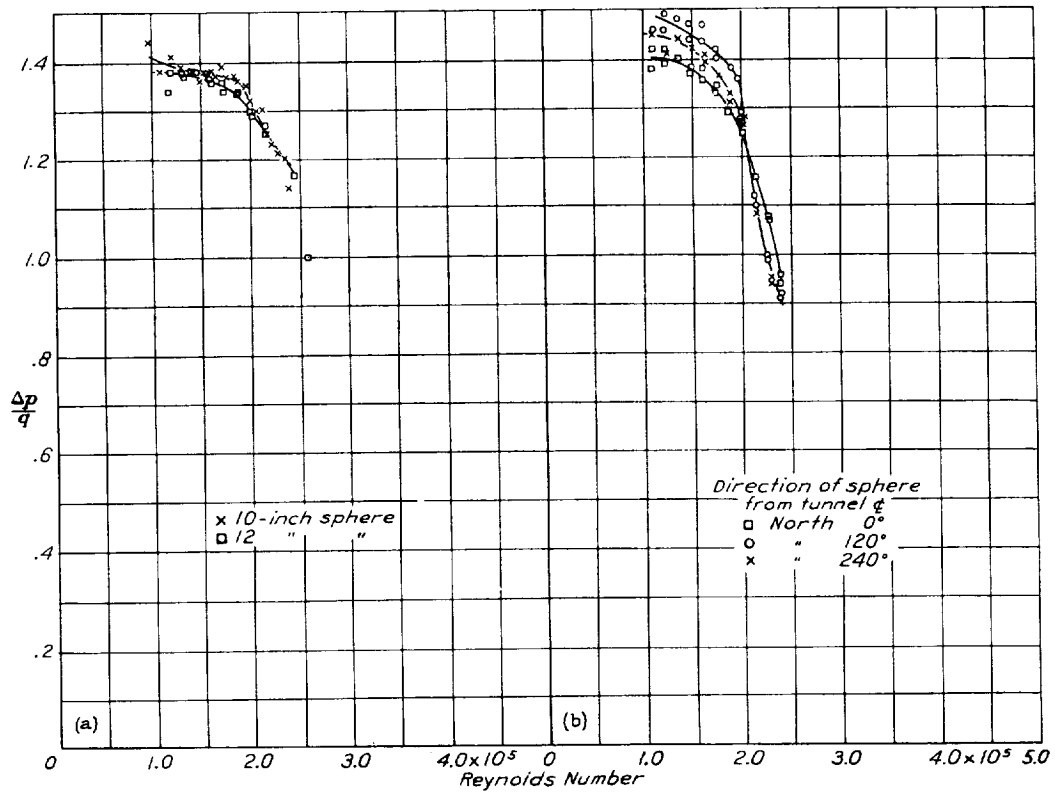


FIGURE 14. Pressure tests of two spheres in the 15-foot free-spinning wind tunnel with normal turbulence.

value agrees with the data presented in reference 14, in which the highest value of the critical Reynolds Number found with a sphere mounted above a motor car and tested in calm weather was 385,000. The value of 405,000 published in the reference resulted from the use of a slightly different value of the pressure coefficient $\Delta p/q$ as a criterion of the critical Reynolds Number.

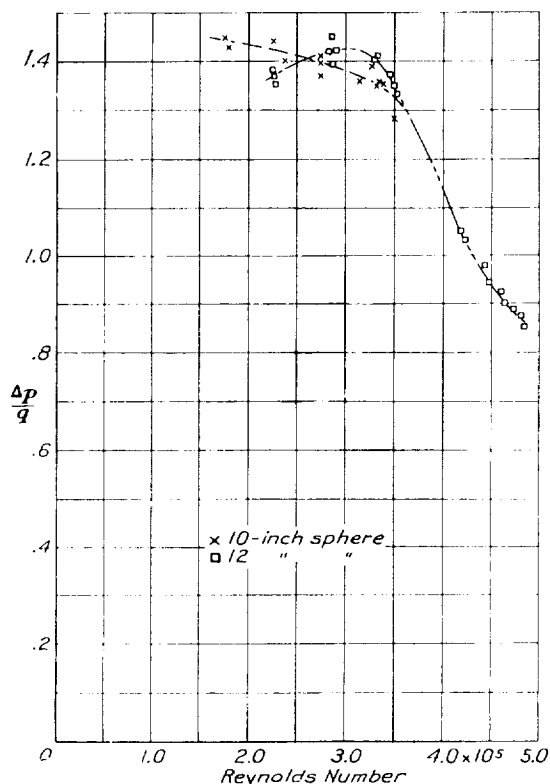


FIGURE 15.—Pressure tests of two spheres in the N. A. C. A. tank.

Flight tests.—Results of pressure tests of four spheres each hung 70 feet below an autogiro in flight are shown in figure 16 (a, b, c, d). No consistent variation of critical Reynolds Number with sphere size was found and the mean value, 385,000, agrees with the results obtained in the N. A. C. A. tank, as well as with the results in reference 14. The flight tests were conducted at altitudes of 2,000 to 5,000 feet in good weather but with varying amounts of wind. The results appear to indicate that under normal conditions the atmosphere may be regarded as nonturbulent insofar as its effect on flow about bodies having boundary layers of thickness comparable with those on the spheres used is concerned.

Summary of test results.—Average values of critical Reynolds Number for the wind tunnels investigated as well as for a number of other wind tunnels listed in references 14 and 16 appear in table I. Figure 17 shows the variation of critical Reynolds Number with sphere diameter for the cases in which these data were obtained.

All these wind tunnels show a fairly consistent variation with sphere size except the full-scale tunnel, which is the least turbulent of all those investigated and which appears to give conditions more directly comparable with those found in free air.

This consistent variation in the case of tunnels like the 20-foot tunnel and the 7- by 10-foot tunnel indicates that the explanation of the effect as depending directly on ratio of sphere to tunnel diameter is erroneous. It seems very unlikely that the sizes of sphere actually used could in any case have an effect on the 20-foot-tunnel jet comparable with their effect on the 7- by 10-foot jet. The most reasonable explanations suggested up to the present have involved the idea that flow similarity for spheres of different size in the same air stream does not exist because of the different ratio between turbulence grain and sphere diameter. Evidence at present available, however, seems insufficient to justify a definite conclusion regarding this matter.

CORRECTION OF AIRFOIL TESTS

It has been proposed (reference 17) that turbulence and Reynolds Number may be regarded as variations of the same fundamental phenomenon in that aerodynamic characteristics of bodies subject to scale effect are in general also subject to an effect of turbulence. Known effects of scale and turbulence on the air flow about bodies may be divided into two general types: First, an effective increase of viscosity in the fluid due to turbulent mixing; second, the effect of turbulence on characteristics associated with transition from laminar to turbulent flow in boundary layers and its relation to flow separation. It is worthy of note, at this point, that the turbulence normally present in a wind tunnel is of small magnitude as compared with that in the turbulent boundary layer of a model and that its effect on a laminar boundary layer ahead of the point of transition to turbulent flow appears to be negligible except in reducing the stability of the laminar boundary layer against the transition. (See reference 17.) The first type of scale and turbulence effect is characterized by a slow, continuous change of coefficient with Reynolds Number apparently related to the changing ratio of boundary-layer thickness to characteristic length of the body as, for example, in the case of the drag coefficient of a streamline body. (See reference 1, et al.) The second type is characterized by a more sudden change between two states of flow, one resulting from separation of the laminar boundary layer, the other from delayed separation of the turbulent boundary layer. In this category lie the effects of scale and turbulence that are observed in sphere-drag tests and on the maximum lift of airfoils. An intermediate state of flow, in which the transition of a free, or separated, boundary layer is the important factor

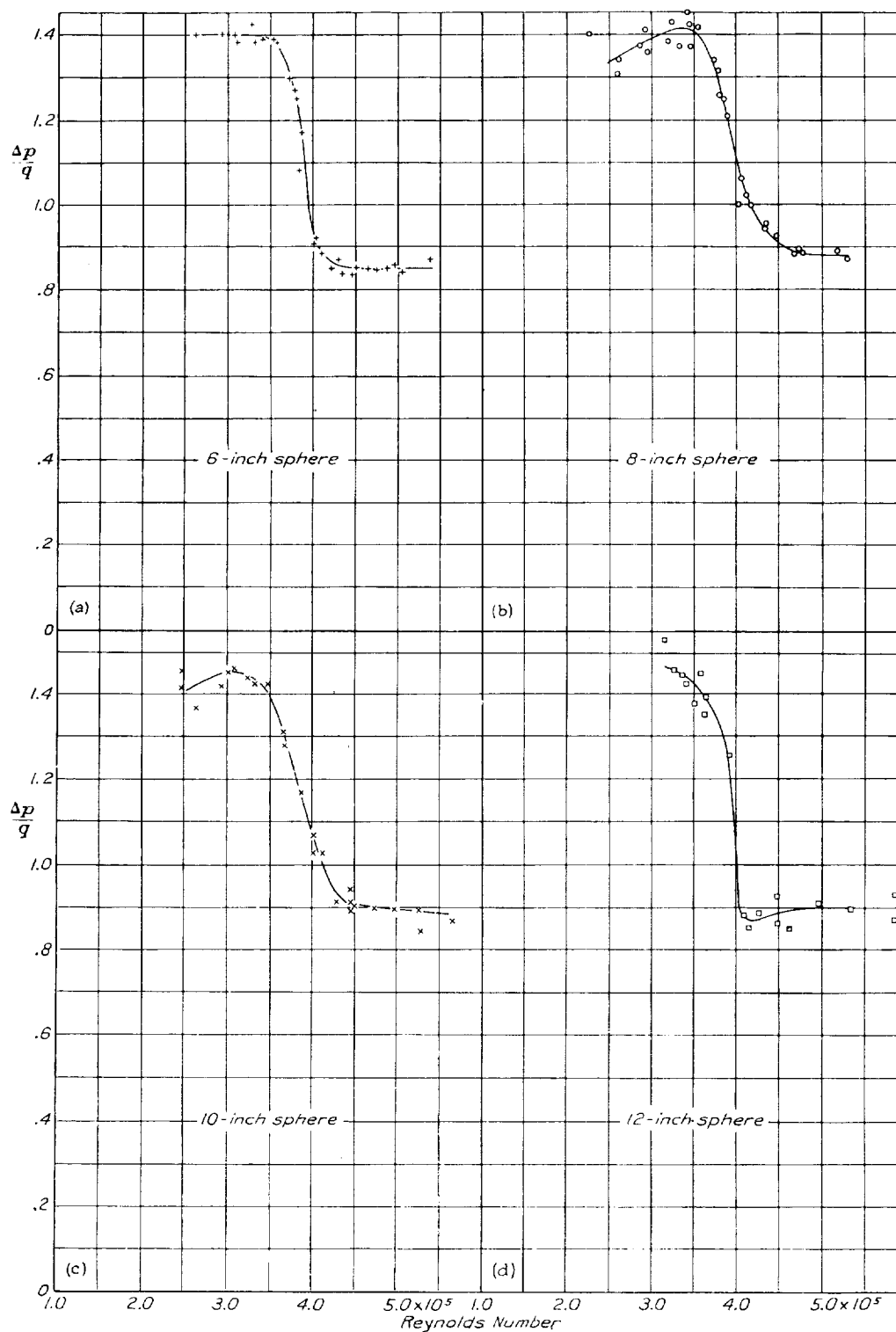


FIGURE 16 (a, b, c, d)—Pressure tests of spheres of different size towed beneath an autogiro in flight.

(reference 17), may exist and should not be excluded from considerations of the second type of scale and turbulence effect.

The variation of the maximum lift of an airfoil with Reynolds Number (see, for example, references 15 and 18) has been ascribed to the tendency of the turbulent boundary layer to delay separation of flow from a body. Thus, as the Reynolds Number of an airfoil is increased, the boundary layer in the region of separation becomes turbulent with resultant delay in the separation of flow from the airfoil and, consequently, a

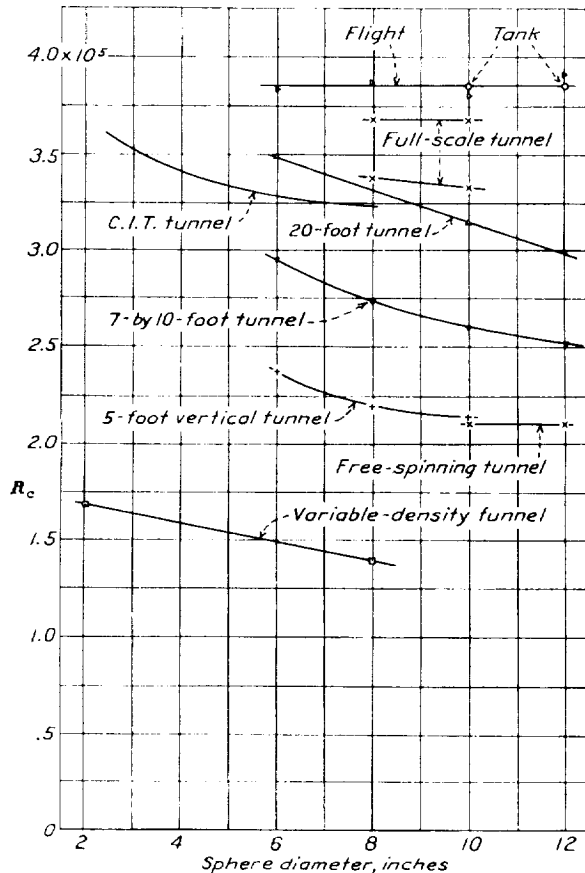


FIGURE 17.—Variation of critical Reynolds Number with sphere diameter for some of the wind tunnels listed in table I.

greater maximum lift coefficient. It has been found that the presence of initial turbulence in an air stream tends to cause this variation to take place at consistently lower values of Reynolds Number than would be the case in a nonturbulent stream and that, by multiplying values of test Reynolds Number in a turbulent stream by a factor depending in magnitude on the amount of turbulence present, it is possible to bring the variation of maximum lift of an airfoil with Reynolds Number as measured in a turbulent stream into reasonable agreement with the variation measured in a less turbulent stream (reference 18).

Comparison of the sphere tests in various wind tunnels indicates that the variation of the pressure coefficient with Reynolds Number in various turbulent streams may be brought into approximate agreement by a procedure similar to that adopted in the case of airfoils. Furthermore, the same value of the factor serves to correct sphere tests and airfoil tests from the same wind tunnel. If, then, the ratio of the value of the critical Reynolds Number for a sphere in free air to the value in a turbulent air stream be taken, the resulting constant is a factor by which the test Reynolds Number in the turbulent stream must be multiplied to obtain the Reynolds Number at which corresponding transition and separation phenomena occur in a nonturbulent stream. This ratio may be called the "turbulence factor" (T. F.) of the air stream in question.

In accordance with this definition, the turbulence factors for the N. A. C. A. wind tunnels have been

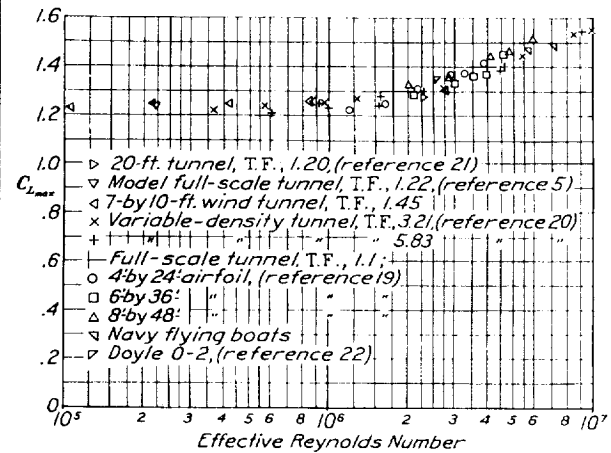


FIGURE 18. Variation of $C_{L,max}$ with effective Reynolds Number for a Clark Y airfoil.

calculated, using in each case a mean value of the critical Reynolds Number found by testing the spheres of various size in each tunnel, and are given in table I. Values for the other tunnels listed in the table are given for comparison, although the fact that these values were computed without reference to sphere size or test position tends to render them not exactly comparable.

The value of the turbulence factor for a nonturbulent stream is, by definition, 1 and, since the critical Reynolds Number of the sphere in flight is the same as that in nonturbulent air, correction of wind-tunnel test Reynolds Numbers according to the foregoing turbulence factors is equivalent to correcting to the free-flight condition.

Figure 18 shows measured values of maximum lift coefficient of a Clark Y airfoil obtained from a variety of sources (references 5 and 19 to 22) and corrected to

"effective Reynolds Number", i. e., test Reynolds Number times turbulence factor. It is interesting to note that when the results are corrected in this fashion they fall into a closely grouped band indicating a consistent variation of maximum lift of the Clark Y airfoil with Reynolds Number in free air. The data from the variable-density tunnel were obtained before the latest modifications were made to this tunnel and are therefore not representative of its present turbulence, as indicated by the different values of its turbulence factor in the figure and in table I. The dispersion of the experimental points obtained in the full-scale tunnel alone is almost as great as the dispersion of all the points plotted in this figure, which seems to indicate that apparent variations are a result of experimental inaccuracies throughout rather than of consistent differences caused by varying amounts of turbulence in the wind tunnels. Although flight determinations of maximum lift coefficient are subject to

Although the dispersion of the drag data is greater than that for maximum lift, consideration of the possible errors involved in the tests indicates that the data show no disagreement. The most widely divergent points in figure 19 should probably be disregarded for the following reasons. In the full-scale-tunnel data, the points for the two lowest Reynolds Numbers are subject to large percentage errors owing to the small magnitude of the measured forces relative to the tare forces and balance capacity. In the variable-density-tunnel tests with increased turbulence ($T. F. = 5.83$), the model was mounted in such close proximity to the turbulence screen that the individual wakes were not fully dissipated. In this condition some doubt must exist regarding both air-stream calibration and effective turbulence.

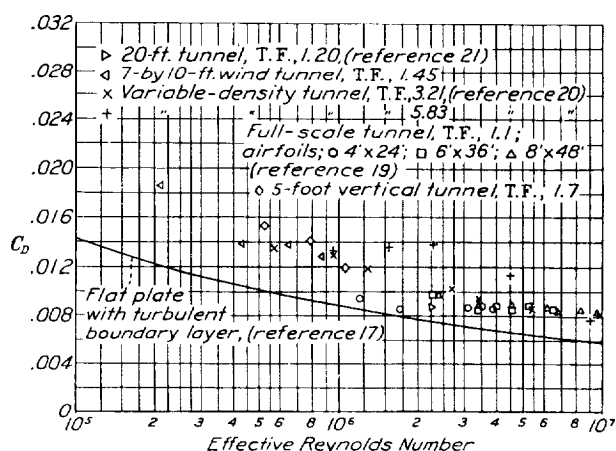


FIGURE 19.—Variation of C_D at zero lift with effective Reynolds Number for a Clark Y airfoil.

numerous sources of error, the results from tests in which special care has been taken to eliminate these errors appear to be in good agreement with the wind-tunnel results.

Figure 19 shows the variation of the drag coefficient at zero lift of the Clark Y airfoil with effective Reynolds Number, obtained from the same sources as the data of figure 18. An additional correction, however, is made to the drag data to make allowance for the difference in turbulent skin friction of the airfoil between the values of test Reynolds Number and effective Reynolds Number. This correction is made by deducting from the measured drag coefficient the change in skin friction involved in going from the test Reynolds Number to the effective Reynolds Number, as shown by the curve of turbulent skin friction of a flat plate against Reynolds Number in figure 19. An example of such correction with explanation is given in reference 18.

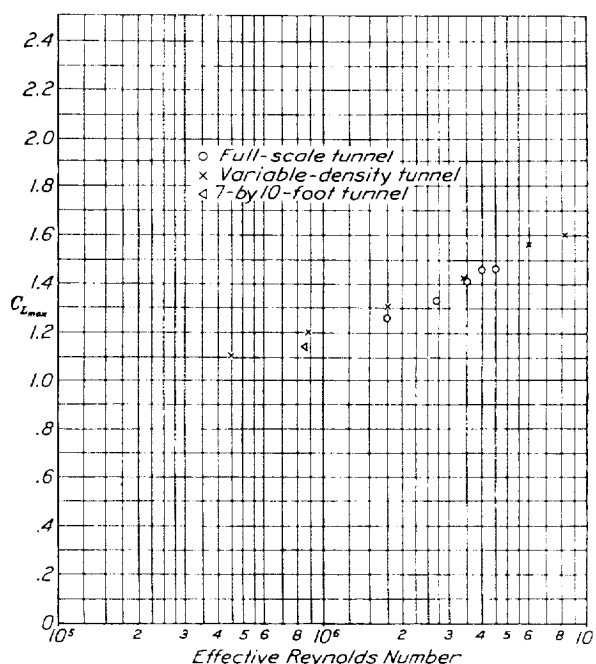


FIGURE 20.—Variation of $C_{L_{max}}$ with effective Reynolds Number for an N. A. C. A. 23012 airfoil.

Figures 20 and 21 show the variation of the maximum lift coefficient with Reynolds Number for the N. A. C. A. 23012 airfoil (reference 18) and the N. A. C. A. 2412 airfoil without and with a split flap. The data for the N. A. C. A. 2412 airfoil (fig. 21) are given in references 15 and 23, which present results of an extensive investigation of the effects of Reynolds Number and turbulence made at the California Institute of Technology. In figure 21(a) the results are plotted against test Reynolds Number for comparison with figure 21(b), in which they have been corrected to effective Reynolds Number. It is clear that when the results are corrected to effective Reynolds Number, a reasonably consistent variation of maximum lift of the N. A.

C. A. 2412 airfoil with Reynolds Number is established, although the results as plotted in figure 21(a) appear to show serious discrepancies between the maximum

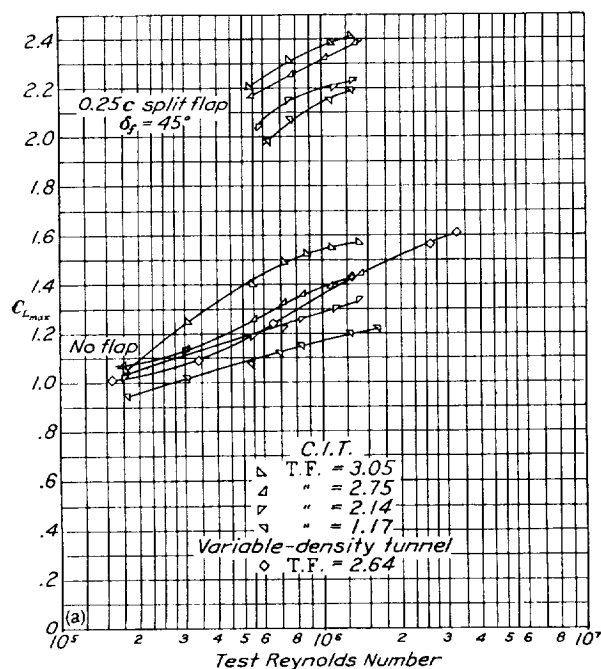
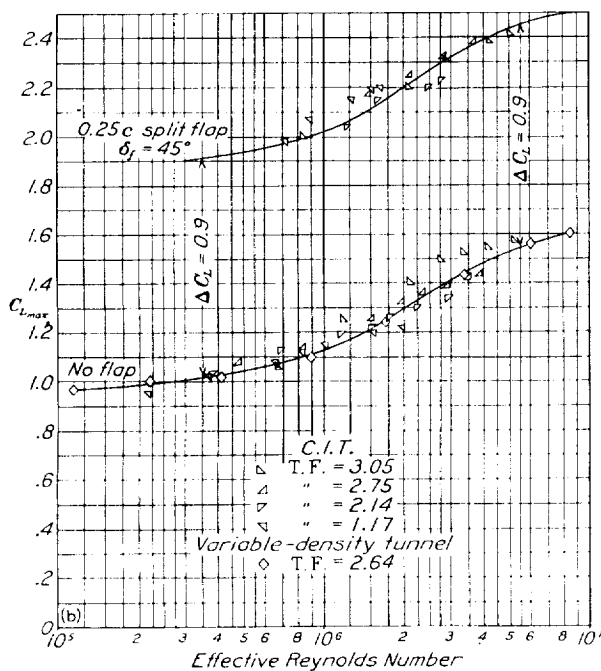


FIGURE 21 (a)

FIGURE 21 (a, b). Variation of $C_{L,max}$ with test and effective Reynolds Number for an N. A. C. A. 2412 airfoil.

lift coefficients obtained with various degrees of turbulence. The scattering of the test points about the mean curve does not appear to be seriously greater than

that found in the full-scale-tunnel tests with the Clark Y airfoil and is therefore believed to result from experimental inaccuracies rather than from consistent differences with the different amounts of turbulence employed. The apparently consistent differences may result from consistent errors caused by compressibility effect, model deflection under air load, difficulty of calibration of a highly turbulent air stream, and variation of critical Reynolds Number with sphere size.

In order to develop further the basis of the effective Reynolds Number concept, it is desirable to consider the conditions necessary for geometric similarity in aerodynamic tests. Four principal dimensions, relative to a linear dimension of the model, must be similar; namely, the thickness of the laminar boundary layer, the downstream distance of the point of transition from laminar to turbulent boundary layer, the thickness of the turbulent boundary layer, and the downstream distance of the point of separation. In streams having no turbulence the Reynolds Number serves as a criterion for similarity of all these factors but, when different amounts of turbulence are present in two different streams, dissimilarities of at least the last three items appear at the same test Reynolds Number, since the point of transition is moved forward by the presence of increased turbulence. If the test Reynolds Number of the model in the more turbulent stream is reduced to bring the point of transition into agreement, similarity is partly restored although the relative boundary-layer thicknesses are somewhat different. This procedure appears to be the most satisfactory method at present available for obtaining approximate similarity of tests in air streams with different amounts of turbulence and seems justifiable in cases where the direct effect of boundary-layer thickness is known, so that it can either be neglected or suitably corrected.

The use of sphere tests to indicate the relative values of Reynolds Number needed to give approximate similarity under different conditions of initial air-stream turbulence is based on the inference that when the sphere-drag coefficient C_D is equal to 0.3 (or $\frac{\Delta p}{q} = 1.22$) the point of transition has a given

downstream location, relative to the sphere diameter, although the value of the Reynolds Number at which this occurs may vary widely, depending on the initial air-stream turbulence. The validity of this inference depends on the assumption that the different boundary-layer thicknesses have only secondary effects on the pressure distribution around the body, an assumption sufficiently common in wind-tunnel testing to need no special verification for the purposes of the present discussion. If it is further assumed that the effect of turbulence on boundary-layer transition is approximately the same for spheres and airfoils in spite of the different pressure gradients that may be involved,

then the procedure required to obtain similarity in sphere tests should give approximate similarity for airfoil tests.

To summarize, it may be stated that the Reynolds Number serves as a criterion of geometric similarity of air flow about similar models in streams having zero turbulence; the effective Reynolds Number may possibly serve as a criterion of approximate geometric similarity in streams having different degrees of turbulence. Furthermore, a turbulence factor obtained from sphere tests may serve to indicate the approximate relation of effective Reynolds Number to test Reynolds Number for certain other aerodynamic bodies.

In the light of this discussion it is clear that for the data of figure 21 the test Reynolds Number has not served as a criterion of similarity. For all the maximum-lift data presented, however, the effective Reynolds Number does appear to have established the conditions of similarity, at least to a first approximation.

Perhaps there is less reason to regard the same effective Reynolds Number as a satisfactory criterion in the case of the drag coefficient, but it should at least be a more reliable criterion of similarity with respect to the point of transition than the test Reynolds Number. Here, however, the boundary-layer thickness exerts an appreciable influence, so after similarity with respect to transition has been obtained, a drag increment is required to allow for the dissimilar boundary-layer thicknesses. This procedure has been followed in several cases (references 18 and 24), partly because of the foregoing considerations and partly because it permits the presentation of all the data at the same value of the Reynolds Number. The data of figure 19 indicate that no disagreement results from this process as applied to the drag of the Clark Y airfoil at zero lift. Although certain doubts may be raised regarding the validity of the effective Reynolds Number concept as applied to the drag of airfoils, it is significant that the result obtained is in agreement with that predicted by a widely employed method of extrapolation (reference 25).

The limitations of the effective Reynolds Number concept are apparent from the foregoing discussion. Strictly speaking, its application is limited to effects resulting principally from the transition of the laminar boundary layer or from the interaction of this transition with flow separation. Where the effects associated with boundary-layer thickness are of primary importance the concept may still be applicable, but suitable correction for these effects must also be made and, if the effect is unknown but not negligible, the concept cannot be expected to give a clear interpretation of the phenomena involved.

A case of the failure of the concept may deserve mention. In certain unpublished tests of a slotted airfoil, a discontinuity observed in the curve of $C_{L_{max}}$ against Reynolds Number was attributed to the varying relation of boundary-layer thickness to slot size. Since both test Reynolds Number and point of transition affect this relation, it seems likely that neither test nor effective Reynolds Number will serve as a criterion of similarity in this case.

Consideration of these effects of turbulence, in combination with a method of correcting for them, suggests the possibility of extending the effective scale range of a wind tunnel for the measurement of certain aerodynamic coefficients by the introduction of artificial turbulence. The maximum effective Reynolds Number attainable is equal to the maximum test Reynolds Number times the turbulence factor. A certain arrangement of the variable-density tunnel having a turbulence factor of 5.8 gave the correct variation of $C_{L_{max}}$ with Reynolds Number for the Clark Y airfoil (see fig. 18), and it seems reasonable to expect that even higher values might be reached without affecting the interaction of scale and turbulence as applied to transition and separation phenomena.

CONCLUSIONS

1. The N. A. C. A. wind tunnels may be listed in order of increasing turbulence as follows:

- The full-scale tunnel.
- The 24-inch high-speed tunnel.
- The 20-foot tunnel.
- The model of the full-scale tunnel.
- The 7- by 10-foot tunnel.
- The 5-foot vertical tunnel.
- The free-spinning tunnel.
- The variable-density tunnel.

2. The effect of scale on the maximum lift coefficient of medium-camber, medium-thickness airfoils in a nonturbulent air stream may be obtained from tests in a turbulent stream by the application of a turbulence factor, obtained from sphere tests, to the test Reynolds Numbers of the models in the turbulent stream.

3. For determination of certain aerodynamic characteristics, the scale range of a wind tunnel may be extended to higher effective values of the Reynolds Number by the introduction of artificial turbulence into the air stream.

LANGLEY MEMORIAL AERONAUTICAL LABORATORY,
NATIONAL ADVISORY COMMITTEE FOR AERONAUTICS,
LANGLEY FIELD, VA., February 4, 1936.

APPENDIX

CORRELATION OF SPHERE DRAG AND PRESSURE TESTS

The air flow about a body that is not tapered to a point in the downstream direction is known to separate in the vicinity of the region where the pressure gradient on the surface of the body tends to oppose the normal direction of flow. (See also reference 14.) The low pressure on the surface of the body aft of the point of flow separation produces consequent large values of the drag coefficient. In the case of the sphere, this pressure drag is sufficiently large that, for purposes of approximate analysis, the skin-friction drag on the surface of the sphere may be neglected and the total drag of the sphere may be regarded as resulting from the pressure applied to the surface.

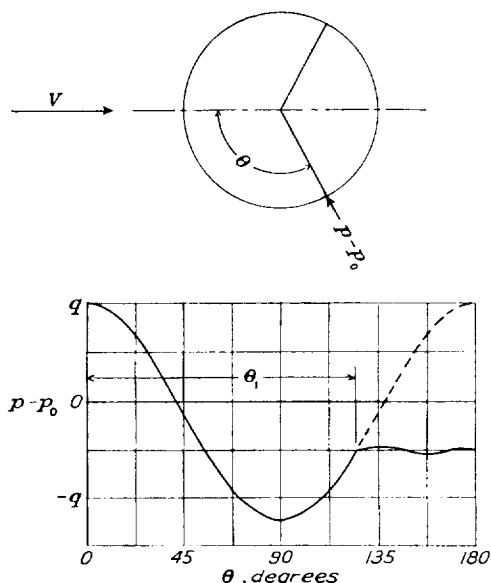


FIGURE 22.—Pressure distribution on a sphere.

Two phases of flow exist on a sphere in a stream of viscous fluid: that over the front portion, which approximates the theoretical flow in a nonviscous fluid; and an eddying wake region over the portion aft of the point of separation of the flow. If a sphere be considered cut by one branch of a circular cone with generating angle θ and with the apex at the center of the sphere (see fig. 22), then the pressure produced by the potential flow around the sphere at any circle of intersection of the sphere and cone is $\frac{p}{q} = 1 - 2\frac{1}{4}\sin^2\theta$ (reference 26) and the drag coefficient of the upstream part

of the sphere, by integration, is $C_D = \sin^2\theta (1 - \frac{9}{8}\sin^2\theta)$ where p is the increment of pressure on the surface above the normal static pressure of the stream, and $q = \frac{1}{2}\rho V^2$. The theoretical pressure distribution expressed by the foregoing equation is shown in figure 22. If the point at which the flow separates from the surface of the sphere be designated θ_1 , it has been found that the pressure aft of θ_1 on the surface of the sphere is approximately equal to the pressure at θ_1 . In other words, the surface of the sphere in the wake region is subjected to a uniform pressure approximately equal to the theoretical pressure at the point of separation of flow. It is possible then to express the pressure drag on the rear portion as

$$D = -\int p dA = -p\pi r^2 \sin^2\theta_1$$

or

$$C_D = -\frac{p}{q} \sin^2\theta_1$$

It is now possible to express the total drag coefficient of the sphere as equal to the sum of the drag due to the theoretical distribution ahead of the point of separation and the drag in the wake region behind the point of separation,

$$C_D = \sin^2\theta_1 \left(1 - \frac{9}{8}\sin^2\theta_1\right) - \frac{p}{q} \sin^2\theta_1$$

Collecting and substituting for p/q ,

$$C_D = \frac{9}{8} \sin^4\theta_1$$

It is also possible to calculate the pressure difference between the front and the rear portions of the sphere as a function of θ_1 . At the front $\frac{p}{q} = 1$, or front pressure equals q . Aft of the point of separation,

$$\frac{p_1}{q} = 1 - 2\frac{1}{4}\sin^2\theta_1$$

and the difference between the front and rear pressures,

$$\Delta p = q - p_1 = q - \left(q - 2\frac{1}{4}\sin^2\theta_1 q\right) = 2\frac{1}{4}\sin^2\theta_1 q$$

or

$$\frac{\Delta p}{q} = 2\frac{1}{4}\sin^2\theta_1$$

Substituting in the equation for C_D ,

$$C_D = \frac{9}{8} \left(\frac{4}{9} \frac{\Delta p}{q}\right)^2 = \frac{2}{9} \left(\frac{\Delta p}{q}\right)^2$$

Results from tests in the 7- by 10-foot tunnel and in the full-scale tunnel, in which corresponding drag and pressure tests were made, are plotted in figure 23 together with a curve plotted from the foregoing equation showing the relation between the drag and pressure coefficients. The tests cover a wide range of values of air-stream turbulence, the 7- by 10-foot wind tunnel being very turbulent with the grid in place and comparatively free from turbulence without the grid. The air stream in the full-scale tunnel is very nearly equivalent to nonturbulent air. The plotted results indicate no consistent difference in the relation between C_D and $\Delta p/q$ with the various amounts of turbulence. This

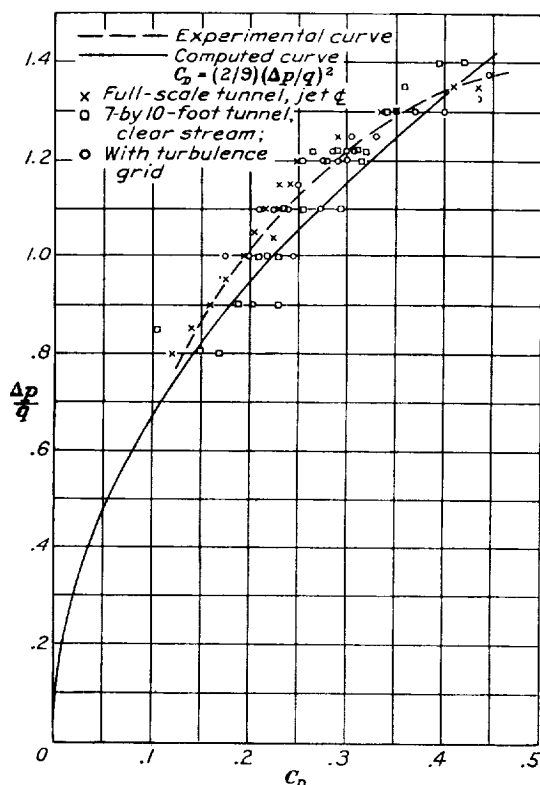


FIGURE 23.—Correlation of sphere drag and pressure measurements.

agreement is taken as evidence that the correlation between drag and pressure coefficients as found here is independent of the degree of air-stream turbulence and that a reliable indication of the critical Reynolds Number may be obtained from sphere pressure tests under any conditions in which it could be obtained from sphere drag tests. The mean value of $\Delta p/q$ at $C_D = 0.3$ is 1.22. Thus, in the sphere pressure tests the Reynolds Number corresponding to the value $\frac{\Delta p}{q} = 1.22$ is taken as the critical Reynolds Number. It is considered worthy of mention that the German tests correlating drag and pressure coefficients (reference 14)

made at only one degree of air-stream turbulence corroborate the relation between drag and pressure found in the present tests.

REFERENCES

1. Dryden, H. L., and Kuethe, A. M.: Effect of Turbulence in Wind Tunnel Measurements. T. R. No. 342, N. A. C. A., 1930.
2. Bacon, D. L., and Reid, E. G.: The Resistance of Spheres in Wind Tunnels and in Air. T. R. No. 185, N. A. C. A., 1924.
3. Jacobs, Eastman N.: Sphere Drag Tests in the Variable Density Wind Tunnel. T. N. No. 312, N. A. C. A., 1929.
4. Harris, Thomas A.: The 7 by 10 Foot Wind Tunnel of the National Advisory Committee for Aeronautics. T. R. No. 412, N. A. C. A., 1931.
5. Theodorsen, Theodore, and Silverstein, Abe: Experimental Verification of the Theory of Wind-Tunnel Boundary Interference. T. R. No. 478, N. A. C. A., 1934.
6. DeFrance, Smith J.: The N. A. C. A. Full-Scale Wind Tunnel. T. R. No. 459, N. A. C. A., 1933.
7. Weick, Fred E., and Wood, Donald H.: The Twenty-Foot Propeller Research Tunnel of the National Advisory Committee for Aeronautics. T. R. No. 300, N. A. C. A., 1928.
8. Wenzinger, Carl J., and Harris, Thomas A.: The Vertical Wind Tunnel of the National Advisory Committee for Aeronautics. T. R. No. 387, N. A. C. A., 1931.
9. Stack, John: The Compressibility Burble. T. N. No. 543, N. A. C. A., 1935.
10. Stack, John: The N. A. C. A. High-Speed Wind Tunnel and Tests of Six Propeller Sections. T. R. No. 463, N. A. C. A., 1933.
11. Jacobs, Eastman N., and Abbott, Ira H.: The N. A. C. A. Variable-Density Wind Tunnel. T. R. No. 416, N. A. C. A., 1932.
12. Zimmerman, C. H.: Preliminary Tests in the N. A. C. A. Free-Spinning Wind Tunnel. T. R. No. 557, N. A. C. A., 1936.
13. Truscott, Starr: The N. A. C. A. Tank—A High-Speed Towing Basin for Testing Models of Seaplane Floats. T. R. No. 470, N. A. C. A., 1933.
14. Hoerner, S.: Versuche mit Kugeln betreffend Kennzahl, Turbulenz und Oberflächenbeschaffenheit. Luftfahrtforschung, 28. März 1935, S. 42, 54.
15. Millikan, C. B., and Klein, A. L.: The Effect of Turbulence. Aircraft Engineering, August 1933, pp. 169-174.
16. Harris, R. G., and Graham, A.: Turbulence Tests of the R. A. E. Wind Tunnels. R. & M. No. 1662, British A. R. C., 1935.
17. Dryden, Hugh L.: Turbulence, Companion of Reynolds Number. Aero. Sci. Jour., April 1934, pp. 67-75.
18. Jacobs, Eastman N., and Clay, William C.: Characteristics of the N. A. C. A. 23012 Airfoil from Tests in the Full-Scale and Variable-Density Tunnels. T. R. No. 530, N. A. C. A., 1935.
19. Silverstein, Abe: Scale Effect on Clark Y Airfoil Characteristics from N. A. C. A. Full-Scale Wind-Tunnel Tests. T. R. No. 502, N. A. C. A., 1934.
20. Stack, John: Tests in the Variable Density Wind Tunnel to Investigate the Effects of Scale and Turbulence on Airfoil Characteristics. T. N. No. 364, N. A. C. A., 1931.
21. Wood, Donald H.: Tests of Large Airfoils in the Propeller Research Tunnel, Including Two with Corrugated Surfaces. T. R. No. 336, N. A. C. A., 1929.

22. Soulé, Hartley A., and Wheatley, John B.: A Comparison between the Theoretical and Measured Longitudinal Stability Characteristics of an Airplane. T. R. No. 442, N. A. C. A., 1932.
23. Millikan, Clark B.: Further Experiments on the Variation of the Maximum-Lift Coefficient with Turbulence and Reynolds' Number. A. S. M. E. Trans., November 1934, pp. 815-825.
24. Jacobs, Eastman N., and Pinkerton, Robert M.: Tests in the Variable-Density Wind Tunnel of Related Airfoils Having the Maximum Camber Unusually Far Forward. T. R. No. 537, N. A. C. A., 1935.
25. von Kármán, Th., and Millikan, Clark B.: The Use of the Wind Tunnel in Connection with Aircraft-Design Problems. A. S. M. E. Trans., Aero Eng., March 1934, pp. 151-166.
26. Zahn, A. F.: Flow and Drag Formulas for Simple Quadrics T. R. No. 253, N. A. C. A., 1927.

TABLE I

VALUES OF CRITICAL REYNOLDS NUMBER AND TURBULENCE FACTOR FOR VARIOUS WIND TUNNELS AND IN FREE AIR

Air stream	Remarks	Critical Reynolds Number R_c	Turbulence factor (T. F.)
Free air.....	N. A. C. A. flight.....	385,000	1.0
Still air.....	N. A. C. A. tank.....	385,000	1.0
N. A. C. A.:			
Full-scale tunnel.....	Average value.....	350,000	1.1
24-inch high-speed tunnel.....	4-inch sphere.....	350,000	1.1
20-foot tunnel.....	Average value.....	320,000	1.2
Model full-scale tunnel.....	8-inch sphere.....	315,000	1.2
7- by 10-foot tunnel.....	Average value.....	270,000	1.4
5-foot vertical tunnel.....	do.....	225,000	1.7
Free-spinning tunnel.....	Normal test level.....	211,000	1.8
Variable-density tunnel.....	Average value.....	150,000	2.6
R. A. E.:			
5-foot tunnel.....	do.....	250,000	1.5
7-foot tunnel.....	2 tunnels.....	185,000	2.1
N. P. L. compressed-air tunnel.....		190,000	2.0
Göttingen:			
Large tunnel.....		320,000	1.2
Small tunnel.....		280,000	1.4
Propeller tunnel.....		310,000	1.2
D. V. L. 1.2-meter tunnel.....	Average value.....	325,000	1.2
Braunschweig tunnel.....	do.....	300,000	1.3
Turin tunnel.....		200,000	1.9
Japanese navy 2.52-meter tunnel.....		310,000	1.2
Mitsubishi Co. tunnel.....		330,000	1.2
Kawanishi Co. tunnel.....		270,000	1.4
Aichi Tokai Co. tunnel.....		270,000	1.4
C. I. T. 10-foot tunnel.....	Average value.....	335,000	1.1
Akron vertical tunnel.....	do.....	250,000	1.5
Bureau of Standards:			
10-foot tunnel.....		230,000	1.7
4.5-foot tunnel.....		265,000	1.5
3.0-foot tunnel.....		270,000	1.4
M. I. T. 7.5-foot tunnel.....		185,000	2.1
Wright Field 5-foot tunnel.....	Average value.....	260,000	1.5
Free air.....	D. V. L. test..... (corrected to $\Delta p/q = 1.22$)	385,000	
Do.....	C. I. T. test.....	364,000	
Do.....	M. I. T. test.....	290,000	

¹ Reference 11.

REPORT No. 559

THE FORCES AND MOMENTS ACTING ON PARTS OF THE XN2Y-1 AIRPLANE DURING SPINS

By N. F. SCUDDER

SUMMARY

The magnitudes of the yawing moments produced by various parts of an airplane during spins have previously been found to be of major importance in determining the nature of the spin. Discrepancies in resultant yawing moments determined from model and full-scale tests, however, have indicated the probable importance of scale effect on the model. In order to obtain data for a more detailed comparison between full-scale and model results than has hitherto been possible, flight tests were made to determine the yawing moments contributed by various parts of an airplane in spins. The inertia moment was determined by the usual measurement of the spinning motion, and the aerodynamic yawing moments on the fuselage, fin, and rudder were determined by pressure-distribution measurements over these parts of the airplane. The wing yawing moment was determined by taking the difference between the gyroscopic moment and the fuselage, fin, and rudder moments.

The numerical values of the wing yawing moments were found to be of the same order of magnitude as those measured in wind tunnels. A direct comparison between wind-tunnel and flight results will be possible as soon as the tests of a model of this airplane have been completed on the N. A. C. A. spinning balance. The pressure-distribution tests incidentally demonstrated the favorable interference produced by the horizontal tail surfaces on the part of the vertical surfaces below them and the unfavorable interference produced on the part above them.

INTRODUCTION

Several earlier studies of spinning have shown that the nature of the spin may be controlled by relatively small changes in yawing moment. Knowledge of the resultant yawing moment and particularly of the components of this moment contributed by various parts of the airplane is therefore necessary for further progress toward a final solution of the problem of spinning. Although this subject has previously been studied by means of wind-tunnel tests, it has long been recognized that values obtained from tests of small-scale models are subject to scale-effect errors and that correction factors are necessary. Comparisons of the resultant

aerodynamic yawing moments have been made between the results of model tests in wind tunnels and flight tests of the corresponding airplanes at various laboratories, but these comparisons do not give information regarding correction factors that can be applied generally because the resultant moment is composed of several components, some of which, according to present knowledge, are affected by scale considerably more than others. At present it is to be expected from the nature of the flow over the wing that the wing yawing moment is the most sensitive to scale of all the components of yawing moment and, since the wing moment is the largest component assisting the spin, true information regarding the scale correction for wing yawing moments is particularly desirable.

In order to obtain full-scale data for comparison with results of measurements on models, an investigation of the yawing moments produced by various parts of an airplane in spins was made. The values of the separate components, including that produced by the wing, were obtained by simultaneously measuring the motion of the spin and the distribution of pressure over the vertical surfaces of the fuselage, fin, and rudder. The wing yawing moment was taken as the difference between the resultant determined from the spinning motion and that contributed by the fuselage and vertical tail surfaces. In the only previous case where similar pressure measurements were obtained (reference 1) the motion in the spin was not recorded so that the results, although of interest, cannot be properly analyzed for the present purpose.

APPARATUS AND METHOD

The airplane used for these tests was the XN2Y-1 training biplane. Since the completion of previous spin tests with this airplane (reference 2), the leading edges of the wings have been covered with sheet metal in order to obtain a smooth leading edge, free of fabric sag, that could be more easily reproduced in a model. The metal fairing extended back to the front spar on both upper and lower surfaces of each wing. The general dimensions and control ranges of the airplane are given in figure 1. The weight was 1,762

pounds at take-off for all tests except one, in which 36 pounds of lead was bolted to the tips of the front lower spars, making the total weight 1,798 pounds. The true moments of inertia were:

A = 802 slug-ft. ²	} without wing-tip ballast and
B = 1,080 slug-ft. ²	
C = 1,526 slug-ft. ²	
A = 1,006 slug-ft. ²	} with ballast at tips.
B = 1,080 slug-ft. ²	
C = 1,730 slug-ft. ²	

The center of gravity was at 35.4 percent of the mean chord for all tests. The propeller was stopped for all

The quantities measured to determine the spin motion were the same as for previous spin tests (reference 2). A pinhole camera instead of three angular-velocity recorders was used to determine angular velocities. This instrument was a simple pinhole camera with a solenoid shutter and an adjustable base permitting tilting to any angle necessary to orient its normal axis to an approximately vertical direction during the spin. The record trace was made on a photographic plate. The other instruments used were: an air-damped 3-component accelerometer, an electric timer, a control-position recorder, a statoscope,

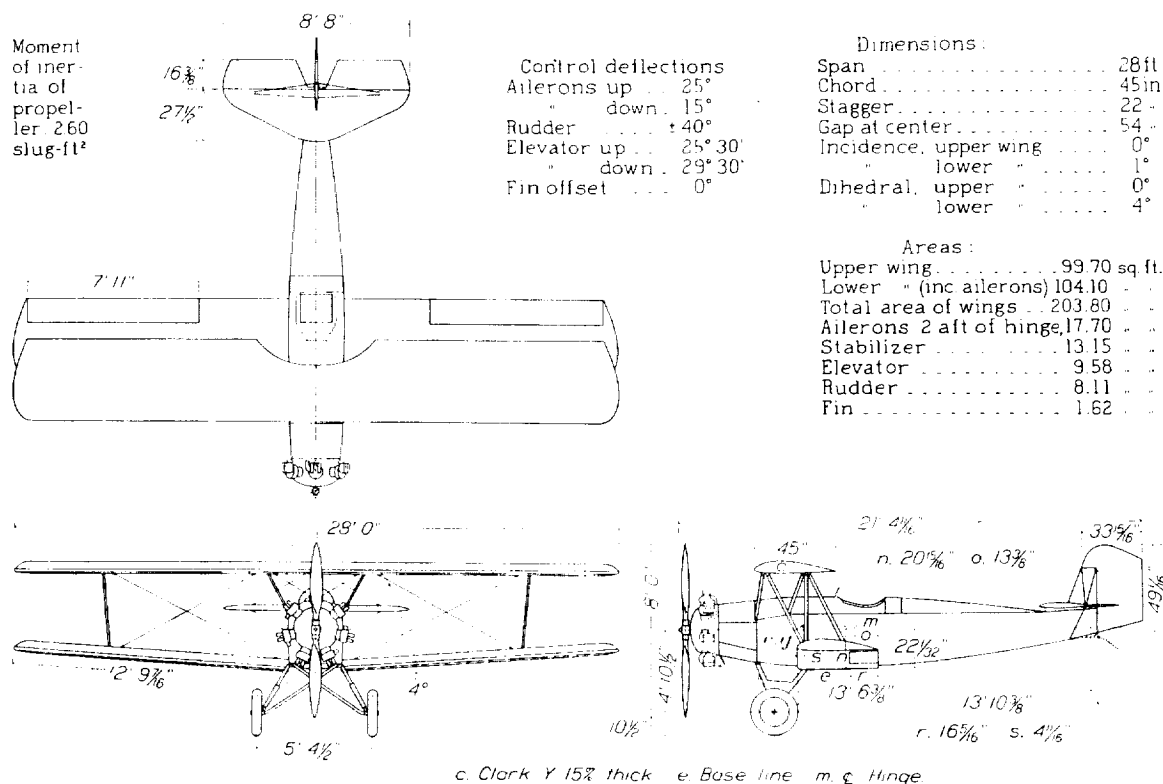


FIGURE 1.—Line drawing and general dimensions of the XN2Y-1 airplane.

tests, but no provision was made for stopping it in one fixed position.

Equipment for the measurement of pressures consisted of a 60-cell recording manometer connected to orifices located on the side of the fuselage and the vertical tail surfaces, as shown in figure 2. Each pressure cell was connected to an opposing pair of orifices to record resultant pressure on the fuselage and tail. The combined internal volumes of the tubing and pressure cells were adjusted for each pair of tubes so that no error would be introduced by the flow of air in the tubing and cells induced by the change of altitude during the spin. Since pressures were measured at 64 points, a switching valve was used to close off one set of tubes and open another.

a sensitive indicating altimeter, and a strut thermometer having a 9-second lag (reference 3).

For the determination of vertical velocity the altitude interval ΔZ was found from the relation (reference 4)

$$\Delta Z = RT_m \log_e \frac{p + \Delta p}{p}$$

where R is the gas constant for dry air.

T_m , the harmonic mean absolute temperature.

p , the pressure.

Temperatures corresponding to different pressure altitudes were observed at 500-foot intervals during the climb preceding the spin. The pressure p at the start of the spin was determined from the altimeter reading,

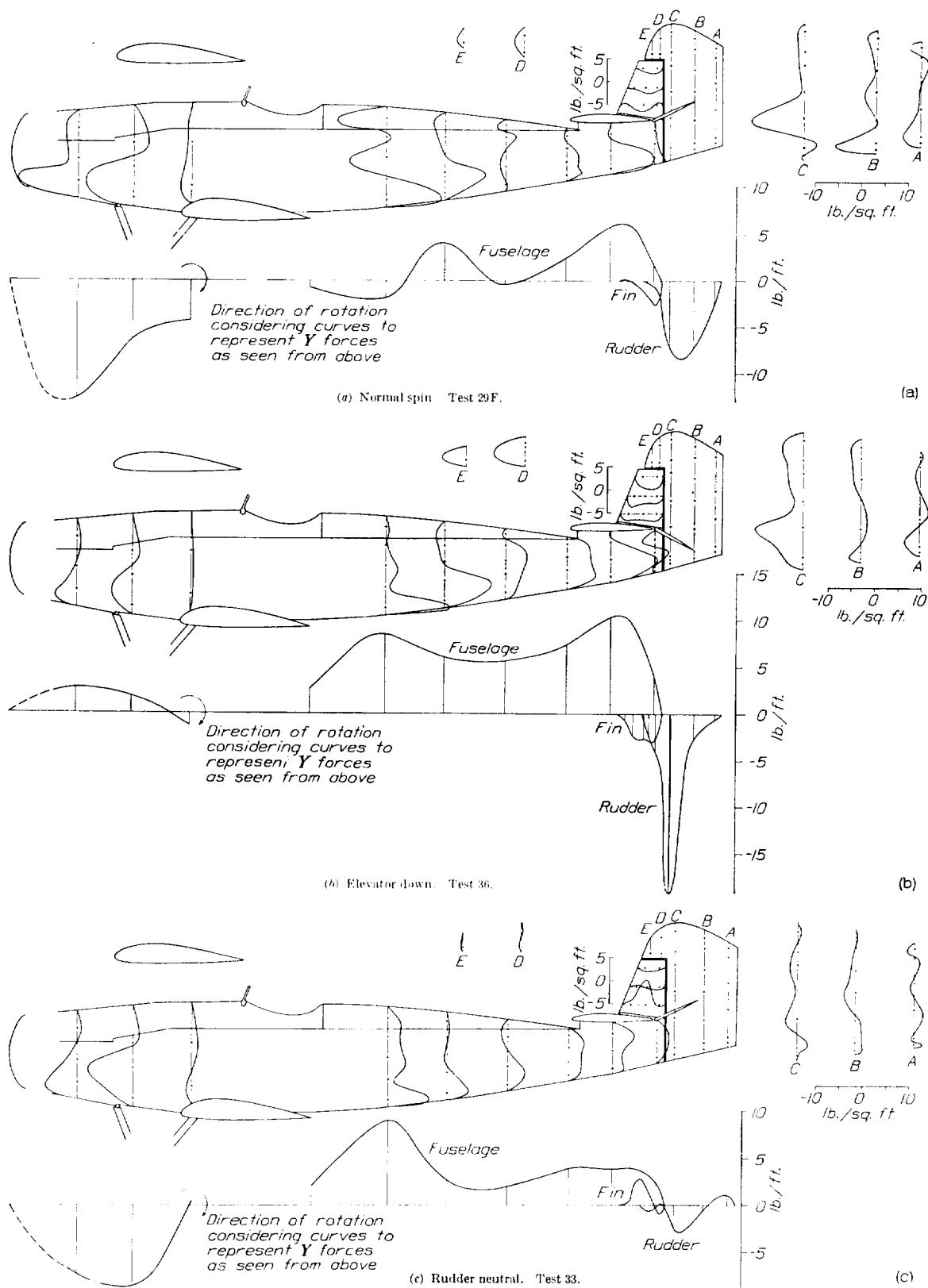


FIGURE 2.—Orifice positions and pressure and force curves for right-hand spins.
(Forces plotted to right or up are into the page on the side elevation of the airplane.)

and the change in pressure Δp from the reference was recorded on the time scale by means of a recording statoscope. The mean temperature was taken simply as the arithmetic mean of temperature for the altitude interval, as it differed only slightly from the harmonic mean temperature.

The spins were started at 6,000 feet altitude with motor stopped and allowed to continue for 1,000 to 1,500 feet descent to establish steady conditions. The instruments were then started at an altitude noted on the altimeter. The pinhole-camera shutter was opened for about $1\frac{1}{4}$ turns; the exact time was indicated by marks made photographically on the accelerometer film record. When about half of the 1,000 feet altitude loss to be recorded had passed, the manometer switching lever was operated. Four of the less important pressure points were connected to the manometer at this time in place of four other points at which pressures were recorded in the first part of the test

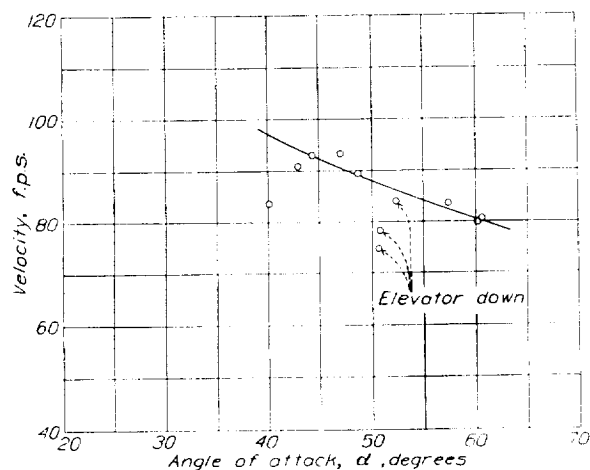


FIGURE 3.—Velocity against angle of attack for spins of the XN2Y-1 airplane.

record. The records were stopped at the end of exactly 1,000 feet of altitude loss, indicated by the altimeter.

The lateral forces and yawing moments arising from the air forces on the sides of the fuselage, fin, and rudder were obtained by plotting the pressure measurements to scale and integrating mechanically in the order made evident by the pressure and force curves shown in figure 2. Corrections were made to the plotted values for changes in rudder angle from the standard setting.

PRECISION

An exact statement regarding the precision of the determination of air forces and moment by the pressure-distribution method is difficult to make. An analysis of the errors and an estimate of the probable magnitude of such errors are given in reference 5. Because the pressures measured were small, the greatest care was taken concerning the physical factors affecting the

accuracy of these tests. Repeated calibrations at regular intervals during the course of the tests showed negligible changes in the slopes of the manometer-calibration curves; the installation was well made with regard to smoothness of the orifices; the pressure tubes were accurately balanced for capacity effect; the manometer was so oriented as to minimize acceleration effects; and the personal errors were kept at a minimum. The precision suffered to some extent because it was not possible to use a sufficient number of orifices; in fact, it was impracticable to include some parts of the airplane, such as the struts, landing gear, wheels, and engine in the measurements. Some difficulty was experienced because of large fluctuations of pressure caused by turbulent flow at many of the pressure points. These sources of error, however, were not serious because the yawing moments contributed by the parts not measured could not have been great and the orifices were distributed so that the large spacings were on areas near the yawing-moment axis. Likewise, the errors due to the fluctuating pressures could be kept small by carefully reading mean values on the pressure records. It is therefore considered safe to estimate that the errors in the air moment measurements are within limits of ± 8 percent. These limits are twice as broad as those estimated for the work reported in reference 5.

The measurement of spin motion was made particularly difficult by oscillations in the spin, which were much more troublesome in these tests than in previous tests with the same airplane. In fact, the records included in the present report represent only 15 percent of the records made; many had to be discarded because of oscillations and the remainder because of other faults made evident by the appearance of the records. All of the records except one taken when the wing tips were ballasted were discarded and it is possible that the one retained was incorrect because of oscillations in the spin. The usual method of detecting the oscillations was to note whether or not the pinhole-camera record was a regular figure; if, however, the period of an oscillation was the same as the period of rotation, this record might appear to be regular. If such an error did occur in these tests, it would affect the values of angular velocity in pitch, sideslip, and inertia yawing moment in the first order, and all the other variables of the spin motion in the second order. These particular effects would be expected because the oscillations of this airplane during the spin were mainly about the longitudinal axis.

The method employed for measuring the vertical velocity should have a good degree of precision for the determination of vertical interval, since the pressures could be determined to closer than 0.1 percent and the temperature to within a fraction of a degree. The lag of the thermometer was of the order of 0.2° F . It was

not practicable to determine the humidity; in the warmest weather or for two or three of the records reported herein, there may have been an error of 0.8 percent involved in assuming the air to be dry. It is

For this reason the values that fell some distance below the curve were arbitrarily moved up to it as a correction for vertical air currents.

The estimated limits of error for the fundamental measurements of motion are summarized as follows:

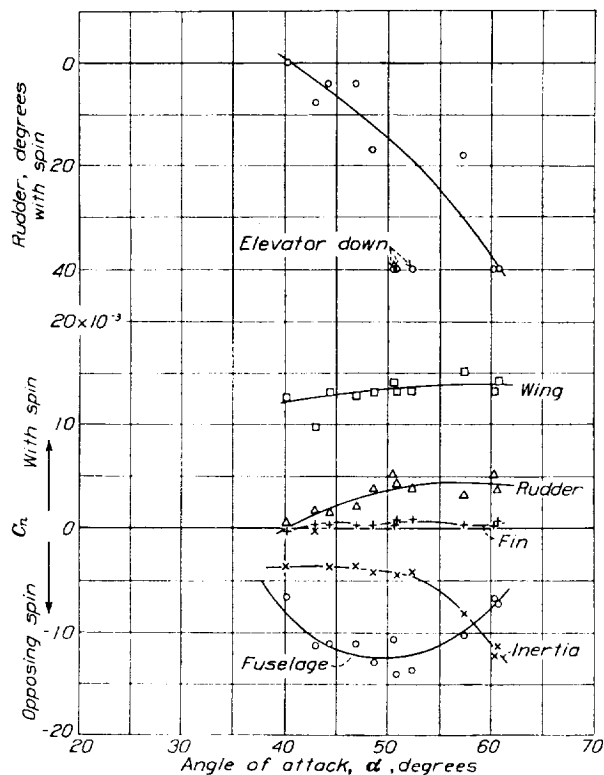


FIGURE 4.—Variation of yawing-moment coefficient and rudder angle with angle of attack for spins of the XN2Y-1 airplane.

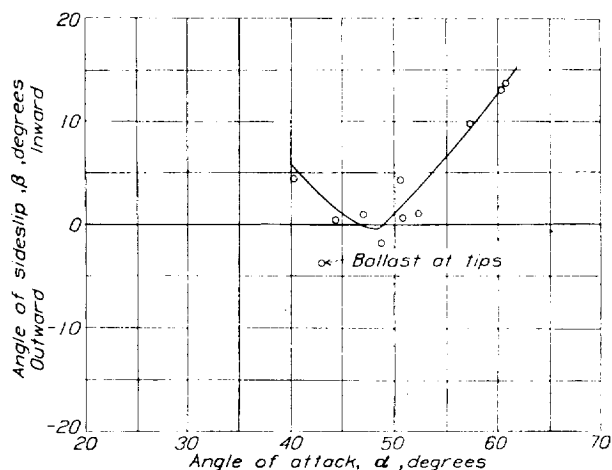


FIGURE 5.—Angle of sideslip against angle of attack for spins of the XN2Y-1 airplane.

to be noted, however, that velocity computed on the basis of change of density height, which refers to distance above the earth, does not take into account the possible existence of vertical currents in the atmosphere. Plotting the values of velocity obtained by this method (fig. 3) shows evidence of such a condition.

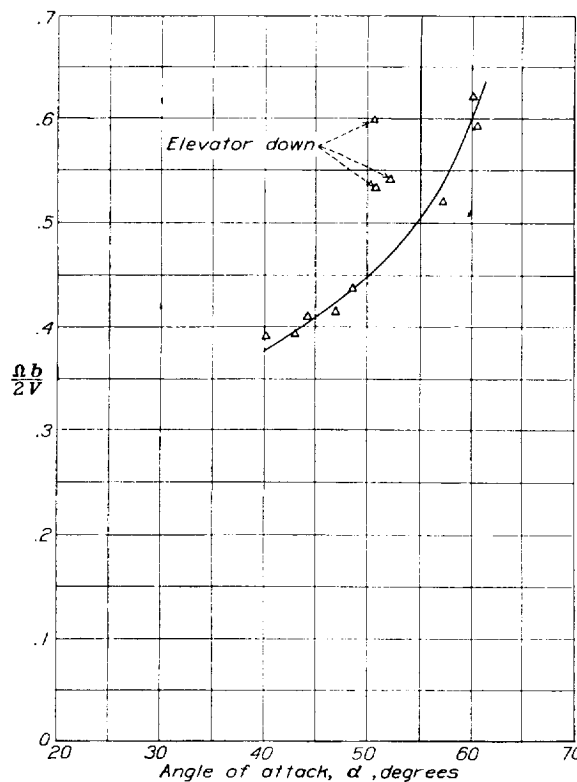


FIGURE 6.—Spin coefficient $\Omega b / 2V$ against angle of attack for spins of the XN2Y-1 airplane.

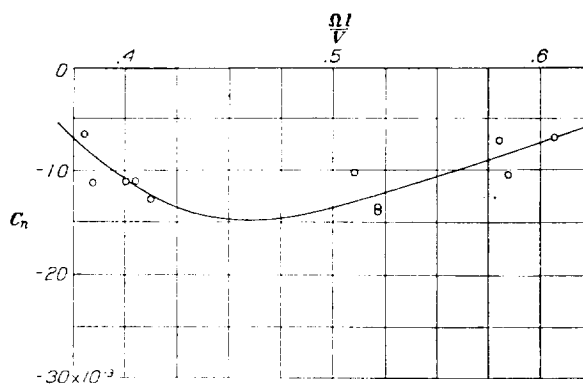


FIGURE 7.—Fuselage yawing-moment coefficient against Ω/V for spins of the XN2Y-1 airplane.

Components of angular velocity, ± 3 percent; acceleration, $\pm 0.05 g$; interval of altitude, ± 1 percent; time, ± 2 percent; weight, ± 1 percent; and moments of inertia, ± 2.5 percent, ± 1.3 percent, and ± 0.8 percent for A, B, and C, respectively, for airplane-swinging measurements. The increment of moment of inertia added as ballast is probably known very accurately.

A consideration of the probability of occurrence of large accidental errors shows that the possible limits of the errors previously stated would seldom be reached in individual measurements and, when they were, a wide scattering of points would be obtained. Since the scattering of points is not great, it seems apparent that the accidental errors were small, especially as the one divergent point is known to be subject to a highly probable error. In addition to the accidental errors there may be a residual error dependent upon the precision of the moment-of-inertia measurements. The limit of the inertia-yawing-moment error taken from the limits of the moment-of-inertia errors is 12 percent for the tests without ballast and 46 percent for the test with ballast. The 12-percent limit of residual error would introduce error limits of about 10 percent for high angles of attack and of about 2.8 percent at low angles of attack into the wing yawing-moment results. Whatever error in inertia yawing moments exists as a result of errors in moment-of-inertia measurements is of the same absolute value for the test with ballast as for tests without ballast, but the percentage error is 3.7 times as great. In conclusion, it may be stated that the values for wing yawing moments are believed to be well within ± 10 percent at all but the highest angles of attack tested and that this limit may be reached at the high angles.

RESULTS AND DISCUSSION

The important parameters of the spins reported are given in table I.

Coefficients of the components of yawing moment for the fuselage, fin, rudder, and wings are plotted against angle of attack in figure 4. The rudder deflections are plotted for reference on the same angle-of-attack scale.

For purposes of studying the results, curves showing the variation of three other parameters are given; the angle of sideslip β plotted against angle of attack in figure 5, the spin coefficient $\Omega b/2V$ plotted against angle of attack in figure 6, and the coefficient $\Omega l/V$ (l is the length from the center of gravity to the rudder hinge) plotted against fuselage yawing-moment coefficient in figure 7.

The absolute values of the wing yawing-moment coefficient, insofar as they are used consistently with the precision of these tests, are probably the most important results of the investigation. They provide a means of checking the results of wind-tunnel tests for this very important factor in spinning equilibrium. Full-scale measurements are very desirable since the yawing moment depends on the separation of flow over the wings and is therefore likely to be affected by scale and turbulence. The values obtained in these tests are within the range and toward the upper limit of values obtained in earlier wind-

tunnel tests. A comparison of these flight results with the most nearly applicable wind-tunnel tests made up to the present time with the N. A. C. A. six-component spinning balance should not be attempted because there is too much difference in stagger, airfoil section, gap/chord, and dihedral. Tests of a model of the XN2Y-1 airplane are now being undertaken.

Attention is called to the fact that, although the wing yawing-moment coefficients are plotted against angle of attack, changes in other variables may have had some effect on the values measured. The angle of sideslip and the spin coefficient both varied considerably, as shown by figures 5 and 6.

The wing yawing-moment curve (fig. 4) was not drawn through the point at $\alpha = 43.0^\circ$ because judgment would indicate that a sharp depression should not exist in the curve in this range. Since the algebraic sum of the ordinates of the five yawing-moment curves is zero, an error occurring in the measurement of one of the four independently measured quantities produces an error of equal magnitude in the wing yawing moment. An inspection of the curves indicates that the measured value of inertia yawing moment might be in error the amount necessary to move the point most of the way up to the curve. The possibility of this particular error is discussed in the section on Precision.

The yawing moment produced by the fin is, as expected from its size and position, very small.

The yawing moment produced by the fuselage reaches a maximum at 50° angle of attack and decreases rapidly as the angle of attack increases to 60° . In the absence of changes of other parameters, it would be expected that an increase in either angle of attack or $\Omega l/V$ would cause an increase in fuselage yawing-moment coefficient. It is to be noted, however, that the angle of sideslip becomes large inward in this angle-of-attack range. A rough estimate of the increment of lateral velocity at the tail, due to increases in angle of attack and in the parameter $\Omega l/V$, shows the effect to be of about equal magnitude and opposite sign to the corresponding increment due to the increased inward sideslip.

The yawing moment produced by the rudder in steady spins varied only slightly throughout the angle-of-attack range of the tests, even though the rudder angle was varied from 0° to 40° with the spin. It is interesting to note that the rudder set full with the spin produced about as much yawing moment with the spin when the elevator was down as it did at a setting of 15° with the spin and the elevators full up.

The distribution of lateral force over vertical areas of the fuselage, fin, and rudder shows points of interest. The curves in figure 2(a) are for test 29F, which was a normal right spin. Figures 2(b) and 2(c) give, respectively, the curves for the right spin with elevator

down (test 36) and for the right spin with rudder neutral (test 33). It will be noted that in test 29F the largest pressures occurred on the nose aft of the engine. This condition occurred frequently, particularly for spins at high angles of attack, which, in these tests, were associated with large inward sideslip. The forces were such as to produce moments resisting the spin but not ones of large magnitude because of the proximity of the area to the center of gravity. In the case of the PW-9 airplane, which spins with large inward sideslip as may be deduced from the pitch angular-velocity records of reference 1, the forces on the nose were large against the spin and, because of the great area, the spin-resisting moments were large enough to be very important. On the tail of the fuselage of the XN2Y-1 large forces were produced under the stabilizer. Very little lateral force was exerted on the section of the fuselage just forward of the stabilizer. This configuration of the force curve, involving a maximum under the stabilizer and a minimum just forward of the stabilizer, was observable in some form on every pressure record taken. Figures 2(b) and 2(c) show how changes in control position and the associated changes in spin conditions affected the pressure distribution.

The low-pressure area ahead of the stabilizer suggests the possibility of improving the fuselage yawing-moment characteristics by extending the stabilizer forward. This change, as a matter of fact, was made several years ago by the manufacturers of the airplane, although for a different purpose. They installed a stabilizer and elevator of aspect ratio 1, the area being the same as that for the standard stabilizer and elevator. The chord was therefore very great, extending forward over most of the region shown in these tests to give low pressures. The effect was a large improvement in an otherwise dangerous spin. In the light of present knowledge on the subject, it is evident that a considerable increase in fuselage yawing moment was obtained. It seems that this low-pressure region may also occur on other airplanes. The British have tested and found beneficial what they call an "antispin fillet" (reference 6). It is a forward extension of the stabilizer having a span of about 4 inches on each side of the fuselage. Such a horizontal surface might possibly induce beneficial interference similar to that induced by the stabilizer.

Examination of the pressure curves for the rudder shows the effects of the presence of the stabilizer and elevator. Large forces are developed on the lower portion of the rudder; in the wake of the stabilizer and elevator the forces are small.

It is interesting to consider the effect on the spin of adding an increment of pure yawing moment. The

change in rudder yawing moment obtained by changing the rudder setting is such a moment except for the associated changes in interference yawing moment on the fin and fuselage, and possibly a small amount of interference pitching moment. The rudder moment-coefficient curve indicates that a change of $C_n = -0.003$ was sufficient to change the equilibrium angle of attack from 60.5° to 40° . The interference yawing moment on the fin and fuselage could reasonably be expected to be appreciably less than another increment of -0.003 . These values indicate, then, that a very small increment of yawing-moment coefficient ($C_n < -0.006$) is all that is required to change the equilibrium of a flat spin to that of a definitely steep spin.

CONCLUSION

The components of yawing moment produced by various parts of an airplane have been measured in flight. The numerical results for the wing were of the same order of magnitude as similar quantities measured in wind tunnels; a direct comparison between model and flight results will be possible when the tests of a model of this airplane have been completed. An incidental feature of the tests was a clear demonstration of the strong favorable interference effects of the horizontal tail surfaces on the vertical areas under them and the corresponding unfavorable interference on the vertical areas above them.

LANGLEY MEMORIAL AERONAUTICAL LABORATORY,
NATIONAL ADVISORY COMMITTEE FOR AERONAUTICS,
LANGLEY FIELD, VA., February 20, 1936.

REFERENCES

1. Rhode, Richard V.: The Pressure Distribution over the Wings and Tail Surfaces of a PW-9 Pursuit Airplane in Flight. T. R. No. 364, N. A. C. A., 1930.
2. Scudder, N. F.: A Flight Investigation of the Effect of Mass Distribution and Control Setting on the Spinning of the XN2Y-1 Airplane. T. R. No. 484, N. A. C. A., 1934.
3. Henrickson, H. B.: Thermometric Lag of Aircraft Thermometers, Thermographs, and Barographs. Research Paper No. 222, Bur. Standards Jour. Res., Sept. 1930, pp. 695-709.
4. Diehl, Walter S.: Standard Atmosphere—Tables and Data. T. R. No. 218, N. A. C. A., 1925.
5. Rhode, R. V.: The Pressure Distribution over the Horizontal and Vertical Tail Surfaces of the F6C-4 Pursuit Airplane in Violent Maneuvers. T. R. No. 307, N. A. C. A., 1929.
6. Anon.: The New Type Park. The Acroplane, July 4, 1934, pp. 10-12 and 21-22.

TABLE I.—SPIN DATA

Test	p	q	r	$\frac{X^1}{mg}$	$\frac{Y^1}{mg}$	$\frac{Z^1}{mg}$	Ω	$\frac{Z''}{mg}$	α_x	β	γ	V	Radius	$\frac{\Omega b}{2V}$	C_l	C_m	C_n	Control settings
	rad./sec.	rad./sec.	rad./sec.				rad./sec.		°	°	°	ft./sec.	Feet					
29F ¹	1.51	1.01	2.88	-0.018	0.062	1.13	3.40	0.969	60.7	13.7	86.0	80.2	1.6	0.563	0.035	-0.084	0.011	Normal. ⁴
29G	1.60	1.02	2.99	-0.052	.059	1.12	3.55	.935	60.4	13.0	86.0	79.9	1.6	.622	.037	-.084	.012	Do.
20	2.22	.61	2.78	-.011	.043	1.25	3.61	.967	50.6	4.3	84.5	84.5	2.0	.598	.018	-.106	.009	Elevator down 26°35'.
30	1.91	.33	2.55	.008	-.010	1.20	3.20	.955	52.4	1.0	85.0	83.8	2.3	.535	.009	-.088	.004	Do.
36	1.99	.34	2.50	-.035	.019	1.23	3.21	.977	50.9	.6	84.5	84.2	2.3	.534	.009	-.087	.004	Do.
33	1.95	.65	1.75	-.027	.040	1.56	2.70	.988	40.2	4.4	80.2	97.0	2.7	.390	.009	-.043	.003	Rudder neutral.
31	1.80	.40	2.11	-.009	.023	1.30	2.80	.973	48.6	-1.9	83.7	89.7	3.5	.437	.008	-.059	.004	Rudder 17° with spin.
32C	1.83	.36	2.03	-.000	.005	1.35	2.76	.995	47.0	.9	83.4	93.2	3.9	.414	.007	-.055	.004	Rudder 4° with spin.
34B	1.87	.34	1.97	-.006	.006	1.35	2.73	.966	44.4	.4	83.2	93.0	4.0	.411	.006	-.053	.004	Do.
35	1.56	.76	2.58	-.035	.049	1.60	3.11	.957	57.4	9.7	85.3	83.2	2.2	.523	.022	-.074	.008	Rudder 18° with spin.
27B ²	1.91	.18	1.82	.014	-.026	1.41	2.64	.980	43.0	-3.9	82.1	94.0	4.7	.393	.004	-.047	.0005	Rudder 8° with spin.

¹ Accelerometer readings corrected to c, g ² Angle of attack for airplane X axis.³ Normal control setting: Ailerons neutral. Elevator up 23°50'. Rudder 40° right. Stabilizer 0°48.6' to X axis.⁴ All right-hand spins.⁵ 36 pounds of ballast added at wing tips.

REPORT No. 560

A SIMPLIFIED APPLICATION OF THE METHOD OF OPERATORS TO THE CALCULATION OF DISTURBED MOTIONS OF AN AIRPLANE

By ROBERT T. JONES

SUMMARY

A simplified treatment of the application of Heaviside's operational methods to problems of airplane dynamics is given. Certain graphical methods and logarithmic formulas that lessen the amount of computation involved are explained.

The problem of representing a gust disturbance or control manipulation is taken up and it is pointed out that in certain cases arbitrary control manipulations may be dealt with as though they imposed specific constraints on the airplane, thus avoiding the necessity of any integration whatever.

The application of the calculations described in the text is illustrated by several examples chosen to show the use of the methods and the practicability of the graphical and logarithmic computations described.

INTRODUCTION

The theory of airplane dynamics in its present form is due mainly to the original researches of Lanchester and Bryan on the stability of airplanes. Later investigators, notably Bairstow and Wilson (reference 1), applied and extended the original conceptions of the theory. Bryant and Williams (reference 2) have recently shown how the operational mathematics of Heaviside may be used in applying the theory to problems of the disturbed motions of airplanes.

Although the calculation of disturbed motions of aircraft is important in problems of flight safety, little experience has been gained in the practical application of the theory owing to its mathematical complexity. The present paper gives the results of researches in the mathematical application of the theory. It has been found, as suggested by Bryant and Williams, that the Heaviside method affords the simplest and most direct solution of these problems. In order to bring out the advantages of this method, a treatment of its application is given and certain formulas and graphical constructions are explained that make the calculations easier.

In their usual form, problems of airplane dynamics depend for solution on the integration of simultaneous linear differential equations. Methods for the integra-

tion of such equations are given by Wilson and Routh (references 1 and 3) and in mathematical textbooks. The problems met in airplane dynamics are often more complex than the examples treated in textbooks and, when an attempt is made to apply the given methods to their solution, difficulties of computation arise.

In view of the importance of investigating these problems and since their solutions involve lengthy calculations, it is desirable that as many mathematical simplifications as possible be employed. Heaviside's method gives such a simplification, the solution of the differential equations being accomplished symbolically by a single "expansion theorem."

THE DIFFERENTIAL EQUATIONS FOR THE DISTURBED MOTIONS

An airplane in uniform flight may be thought of as a free rigid body in equilibrium. Deviations of the airplane from this equilibrium condition may be caused by reactions due to control movement, gustiness in the air, or by some influence such as the stopping of an engine. The motions of the airplane following such a disturbance may be calculated if the momentary accelerations or forces are known. It is obvious that this computation may be performed by taking small intervals of the time and calculating the velocities and displacements generated by the known accelerations step by step, assuming the accelerations momentarily constant.

The component linear and angular motions of the airplane in its deviations from equilibrium are given exact definition by constructing a set of axes rigidly fixed in the machine and considering its motions as being those of the axes themselves. The motions spoken of are then velocities and displacements of the airplane axes relative to the earth or the air. When the airplane is in steady flight, it maintains a certain equilibrium attitude with respect to the air and to the earth. Thus for climbing flight at a given engine speed a definite angle of attack and a definite angle of pitch must be preserved. Deviations from equilibrium in either sense will introduce reactions; hence motions of the airplane axes relative to both air and earth must be considered.

The aerodynamic reactions to the motions arise from changed relative air velocities over the different parts of the airplane. The calculation or measurement of these component aerodynamic reactions leads to quantities known as "resistance derivatives" or "stability derivatives," which are taken as constant factors of proportionality between the reactions and the velocities or displacements of the motions. For a more detailed exposition of the concept of stability derivatives, the reader is referred to standard textbooks on aeronautics.

On account of the bilateral symmetry of the airplane it is customary to divide the motions into two independent groups, the lateral and the longitudinal, each consisting of three degrees of freedom:

- | | |
|--------------------------|--|
| (A) Lateral motions | Rolling.
Yawing.
Sideslipping. |
| (B) Longitudinal motions | Pitching.
Vertical translation.
Forward translation. |

Presumably the reactions to small increments of longitudinal speed or displacement do not sensibly influence the lateral motions and the two groups may be independently treated. In order to illustrate the calculation of the history of a motion due to a given disturbance, examples of lateral motions are chosen although the methods used are equally applicable to any set of degrees of freedom of the airplane. The quantities that arise in the consideration of the lateral motions are defined in the following table:

Velocities and displacements of airplane axes:

- U_0 , equilibrium flight velocity along X axis.
- v , component of flight velocity along Y axis (sideslipping).
- p , component of angular velocity about X axis (rolling).
- r , component of angular velocity about Z axis (yawing).
- ϕ , angle of bank (relative to gravity).

Forces and moments resolved along airplane axes:

- Y , component of force along Y axis.
- L , component of moment about X axis (rolling moment).
- N , component of moment about Z axis (yawing moment).

Accelerations of airplane:

- $Y_0 = Y/m$ (force per unit mass).
- $L_0 = L/mk_x^2$ (moment per unit moment of inertia).
- $N_0 = N/mk_z^2$ (moment per unit moment of inertia).

Gust velocities resolved along airplane axes:

- v_0 , component of gust velocity directed along Y axis.
- r_0 , component of angular velocity of gust about Z axis.
- p_0 , component of angular velocity of gust about X axis.

NOTE.—The signs of the gust velocities are so chosen that a positive gust produces the same aerodynamic reaction on the airplane as a positive velocity of the airplane in still air. The resolution of gust velocities along the moving axes is exact only to the first order of the small quantities involved.

Airplane characteristics used as parameters:

Y_e	Stability derivatives in terms of accelerations of airplane, thus:
Y_r	
L_p	$Y_r = \frac{\partial Y}{\partial v}/m$
L_e	
L_r	$L_r = \frac{\partial L}{\partial r}/mk_x^2$
N_p	
N_r	$N_p = \frac{\partial N}{\partial p}/mk_z^2$
N_e	

With the definition of the component motions that are to be considered, the stability derivatives will be of the form:

$$\frac{\partial L}{\partial p}, \frac{\partial N}{\partial v}, \frac{\partial Y}{\partial r}, \text{etc.}$$

where L , N , Y , respectively, are the rolling moment, the yawing moment, and the sidewise force, as they are customarily defined.

It has been found convenient to transform all stability derivatives and disturbing effects into terms of accelerations of the airplane rather than retaining them as moments and forces. This transformation is accomplished by dividing out the appropriate moments of inertia and the mass of the machine.

For example, $\frac{\partial L}{\partial p}/mk_x^2$ may be written simply as L_p ; similarly $\frac{\partial N}{\partial v}/mk_z^2 = N_r$ and $\frac{\partial Y}{\partial r}/m = Y_r$.

If the flight path is assumed to be horizontal (or nearly so) and the main forward velocity U_0 to be substantially constant, the equations of motion in a lateral disturbance may be written:

$$\left. \begin{aligned} \text{(In sideslipping)} \quad \frac{dv}{dt} &= g\phi - rU_0 + vY_e + rY_r + Y_0 \\ \text{(In rolling)} \quad \frac{dp}{dt} &= vL_e + pL_p + rL_r + L_0 \\ \text{(In yawing)} \quad \frac{dr}{dt} &= vN_e + pN_p + rN_r + N_0 \end{aligned} \right\} \quad (1)$$

In these equations the terms Y_0 , L_0 , and N_0 represent known disturbing or controlling accelerations, assumed to be given as functions of the time t . In the first equation the terms $g\phi$ and $-rU_0$ are, respectively, the accelerations due to gravity and to the rotation of the moving axes. Since the axes chosen will ordinarily lie

near the axes of the principal moments of inertia of the airplane, terms involving the products of inertia have been neglected.

INTEGRATION OF EQUATIONS FOR VELOCITIES AND DISPLACEMENTS

As previously mentioned, equations (1) may be integrated by taking small intervals of the time and calculating the velocities, and finally the displacements, by assuming the accelerations $\frac{dv}{dt}$, etc., to be momentarily constant. Although this method is sometimes useful, it naturally leads to extensive numerical work. The operational mathematics of Heaviside appear to offer the most promising means of performing these integrations.

The first step in integrating the equations of motion by the operational method is to replace the symbol $\frac{d}{dt}$ by the so-called "differential operator" D , which is to be treated as though it were an ordinary algebraic quantity; the equations are then rearranged with the known disturbance effects on the right-hand side:

$$\begin{aligned}(D - Y_r)v - g\varphi + (U_0 - Y_r)r &= Y_0 \\ -L_v v + (D - L_p)p - L_r r &= L_0 \\ -N_v v - N_p p + (D - N_r)r &= N_0\end{aligned}\quad (2)$$

Since $D\varphi = p$, the first equation may be operated on throughout by D , reducing all to the same variables (v, p, r):

$$\begin{aligned}D(D - Y_r)v - gp + D(U_0 - Y_r)r &= DY_0 \\ -L_v v + (D - L_p)p - L_r r &= L_0 \\ -N_v v - N_p p + (D - N_r)r &= N_0\end{aligned}\quad (2a)$$

With the equations in this form, they may be solved for v, p , or r by ordinary algebraic means; thus,

$$v = \begin{vmatrix} DY_0 & -g & D(U_0 - Y_r) \\ L_0 & (D - L_p) & -L_r \\ N_0 & -N_p & (D - N_r) \\ \hline D(D - Y_r) & -g & D(U_0 - Y_r) \\ -L_v & (D - L_p) & -L_r \\ -N_v & -N_p & (D - N_r) \end{vmatrix} \quad (3)$$

The expansion of the determinant of the numerator in terms of minors results in:

$$\begin{vmatrix} (D - L_p) & -L_r \\ -N_p & (D - N_r) \end{vmatrix} DY_0 + \begin{vmatrix} D(U_0 - Y_r) & -L_r \\ (D - N_r) & -L_r \end{vmatrix}$$

In the calculation of any of the velocity components the same denominator appears; if this determinant is denoted by $F(D)$, the forms of these components are:

$$\begin{aligned}v &= \frac{f_{11}(D)}{F(D)} Y_0 + \frac{f_{12}(D)}{F(D)} L_0 + \frac{f_{13}(D)}{F(D)} N_0 \\ p &= \frac{f_{21}(D)}{F(D)} Y_0 + \frac{f_{22}(D)}{F(D)} L_0 + \frac{f_{23}(D)}{F(D)} N_0\end{aligned}\quad (5)$$

etc.

Thus far the solution of the equations of motion has progressed simply on algebraic grounds, the required quantities (v, p , etc.) having been found explicitly in terms of the symbol D . The symbol D was defined as the operation of derivation with respect to the time t , expressed by writing

$$D = \frac{d}{dt}$$

The terms of the solution $f(D)/F(D)$ indicate that the formal operations are to be performed on whatever functions follow them as factors. Since they contain the symbol D in their denominators, it becomes necessary to define the operation indicated by $1/D$ or D^{-1} . As D is an operation and not a number, its reciprocal is defined as the inverse of the operation of differentiation, rather than as the derivative itself divided into 1. The inverse of differentiation is integration: thus,

$$D^{-1} = \int \dots dt$$

The operations indicated by the ratios of polynomials in D that occur in the terms of our solution then consist of a succession of differentiations $[f(D)]$ and a succession of integrations $[F(D)]^{-1}$. It is clear that the nature of the problems at hand requires that the resultant of these operations be an integration, which is shown by the fact that the polynomial $F(D)$ is invariably of higher degree in D than any of the polynomials $f(D)$.

THE EXPANSION EQUATION

By treating the disturbances (such as Y_0, N_0, L_0) as discontinuous functions of the time, Heaviside obtained solutions of equations similar to the foregoing by a simple theorem. The substitution of Y_0 into Heaviside's theorem results in

$$\frac{f(D)}{F(D)} Y_0 = Y_0 \left[\frac{f(0)}{F(0)} + \sum_{\lambda} \frac{f(\lambda)}{\lambda F'(\lambda)} e^{\lambda t} \right] \quad (6)$$

where the λ 's are the roots of the polynomial equation $F(D)=0$. This polynomial, $F(D)=0$, is used in the study of the stability of motion, being called the "stability equation." Its roots, $\lambda_1, \lambda_2, \dots, \lambda_n$, give an

$$\begin{vmatrix} -g & D(U_0 - Y_r) \\ -N_p & -L_r \end{vmatrix} L_0 + \begin{vmatrix} -g & D(U_0 - Y_r) \\ (D - L_p) & -L_r \end{vmatrix} N_0 \quad (4)$$

indication of the natural tendencies of an airplane's motion and are used in the definition of stability.

In order to apply the foregoing theorem to the integration of equations of airplane motion it is necessary to assume that the disturbance terms (Y_0 , N_0 , etc.) due to the control or gust in question are instantly applied at the assumed origin of the time scale ($t=0$) and remain constant thereafter. In the general case the disturbance terms in the equations of motion cannot be thus represented as remaining constant although in practical problems they may almost invariably be represented by means of functions of the form $Y_0 e^{nt}$. The interpretation of Heaviside's theorem (equation (6)) when this form of function is used is (see reference 2):

$$\frac{f(D)}{F(D)} Y_0 e^{nt} = Y_0 \left[\frac{f(n)}{F'(n)} e^{nt} + \sum_{\lambda} \frac{f(\lambda)}{(\lambda - n) F'(\lambda)} e^{\lambda t} \right] \quad (7)$$

When dealing with variable disturbance terms, it is important to note that a discontinuity of the function representing the disturbance at $t=0$ is implied as in equation (6).

By the substitution of (in) for n in equation (7), expressions that can be used when the disturbances

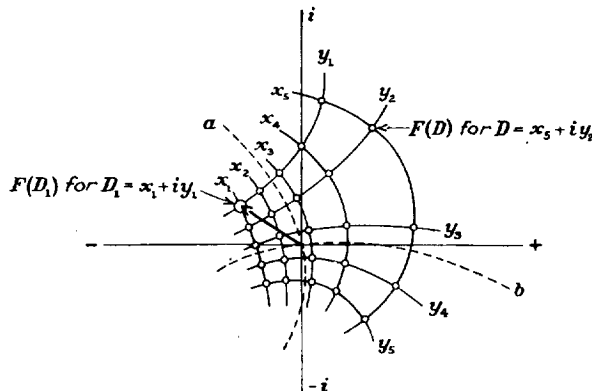


FIGURE 1.—Map of polynomial. $F(D) = D^4 + aD^3 + bD^2 + cD + d$ near zero. $F(D) \rightarrow F(\lambda) = 0$ when $D \rightarrow a \pm ib$.

are represented by forms involving $\sin nt$ or $\cos nt$ are obtained

$$\frac{f(D)}{F(D)} Y_0 e^{int} = Y_0 \left[\frac{f(in)}{F'(in)} (\cos nt + i \sin nt) + \sum_{\lambda} \left(\frac{\lambda + in}{\lambda^2 + n^2} \right) \frac{f(\lambda)}{F'(\lambda)} e^{\lambda t} \right] \quad (7a)$$

If $\frac{f(in)}{F'(in)} = A + iB$, then the expressions for the sine and cosine forms separately become

$$\frac{f(D)}{F(D)} Y_0 \sin nt = Y_0 \left[A \sin nt + B \cos nt + \sum_{\lambda} \left(\frac{n}{\lambda^2 + n^2} \right) \frac{f(\lambda)}{F'(\lambda)} e^{\lambda t} \right] \quad (8)$$

$$\frac{f(D)}{F(D)} Y_0 \cos nt = Y_0 \left[A \cos nt - B \sin nt + \sum_{\lambda} \left(\frac{\lambda}{\lambda^2 + n^2} \right) \frac{f(\lambda)}{F'(\lambda)} e^{\lambda t} \right] \quad (9)$$

These latter forms are particularly useful because almost any arbitrary variation of gust or control may be expressed as a sum of sine or cosine terms. Thus if

$$Y_0 = K_1 \sin n_1 t + K_2 \sin n_2 t + \dots + \text{etc.}$$

$$\frac{f(D)}{F(D)} Y_0 = \frac{f(D)}{F(D)} K_1 \sin n_1 t + \frac{f(D)}{F(D)} K_2 \sin n_2 t + \dots + \text{etc.} \quad (10)$$

Each of these terms may be evaluated by equation (8).

SOLUTION OF OPERATIONAL EQUATIONS

FINDING THE ROOTS OF THE EQUATION $F(D)=0$

The expansion equations given for the forms $f(D)/F(D)$ require the roots of the complementary equations $F(D)=0$ for their solution. In cases of airplane motions this equation is normally of the fourth degree in D ; hence it is not practicable to find the roots directly. Although a number of methods for approximating the roots of such equations have been devised, the most direct way is to draw a curve of the function $F(D)$ against D , locating the real roots as the points crossing the D axis. Usually in equations of this type near roots may be isolated by separating the equation into two parts. Thus, if

$$F(D) = D^4 + aD^3 + bD^2 + cD + d = 0 \quad (11)$$

there will usually be a large real root near $D^4 = -aD^3$, or $D = -a$, and a small one near $D = -\frac{d}{c}$. This division follows from the consideration that large roots are more dependent on the coefficients of the higher powers of D and small roots, on the lower powers.

If the natural motion of the airplane contains oscillatory components, as it usually does, there will be pairs of conjugate complex roots of the polynomial $F(D)=0$ in addition to the real roots. The determination of these roots is naturally more difficult, although if real roots have been previously found they may be used to reduce the degree of the equation by synthetic division and the determination of further roots will become progressively easier. Complex roots of such an equation may be directly found by plotting a map of the polynomial $F(D)$ for various values of D using the coordinates $D = x + iy$ and finding the zero point, or root, by interpolation, as is shown in figure 1. If a very accurate value of the root is required it may be convenient to plot the region of $F(D)$ near the origin to a magnified scale. Since the polynomial is what is known as an "analytic function" (reference 4),

$$\frac{\partial F(D)}{\partial x} = -i \frac{\partial F(D)}{\partial y} \quad (12)$$

and the map in its smallest parts will consist of squares. In this way a more accurate interpolation may be made or a process analogous to Newton's method may be applied.

It will be found most convenient to calculate the various values of $F(D)$ by means of a vector diagram

as shown in figure 2. If trial values of D are expressed in the form $R(\cos \theta + i \sin \theta)$ or $Re^{i\theta}$, vectors representing each of the terms of the polynomial may be simply calculated. The problem is to make all terms of the polynomial balance each other and it is readily seen how this may be accomplished by varying θ to change the relative inclinations of the vectors and by varying R to change their relative lengths. The advantage of this method is that it enables a close approximation of the value of a root with a minimum number of trials, the diagram making apparent how nearly all the vectors cancel each other.

SOLUTION OF EXPANSION EQUATIONS

The numerical operations indicated in the expansion equations (6) to (9) call for calculations with complex numbers (i. e., roots of $F(D)=0$). A great deal of the labor involved in these computations may be saved by the use of graphical and logarithmic methods.

Thus, if it is desired to calculate values of the complex terms occurring in equation (6), the logarithmic formula

$$\log \frac{f(\lambda_1)}{\lambda_1 F'(\lambda_1)} e^{\lambda_1 t} = \lambda_1 t + \log f(\lambda_1) - \log \lambda_1 - \log F'(\lambda_1) \quad (13)$$

is used. For the purpose of calculating these logarithms, it is convenient to express the complex numbers (λ_1 , $f(\lambda_1)$, etc.) as vectors of radius R and angle θ , writing, for example,

$$\lambda_1 = a + ib = R_1(\cos \theta_1 + i \sin \theta_1) = R_1 e^{i\theta_1} \quad (14)$$

by De Moivre's formula.

A complex term of equation (6) may then be written,

$$\begin{aligned} \frac{f(\lambda_1)}{\lambda_1 F'(\lambda_1)} e^{\lambda_1 t} &= \frac{R_2 e^{i\theta_2}}{R_1 e^{i\theta_1} R_3 e^{i\theta_3}} e^{\lambda_1 t} \\ &= \frac{R_2}{R_1 R_3} e^{\lambda_1 t + i(\theta_2 - \theta_1 - \theta_3)} \\ &= R_0 e^{\lambda_1 t + i\theta_0} \end{aligned} \quad (15)$$

Then

$$\log \frac{f(\lambda_1)}{\lambda_1 F'(\lambda_1)} e^{\lambda_1 t} = \lambda_1 t + \log R_0 + i\theta_0 \quad (16)$$

and the resultant logarithm may be plotted as a straight line $\lambda_1 t + \text{constant}$, which is then divided or extended to represent any division or extension of the time t over which the calculation is made. (See fig. 3.) The final vectors will represent the complex values of

$$\frac{f(\lambda_1)}{\lambda_1 F'(\lambda_1)} e^{\lambda_1 t}$$

and it is seen that the ordinates of the points of the line $\lambda_1 t + \text{constant}$ are the angles of these final vectors while the abscissas are the logarithms of their radii.

By a separation of the two components of the imaginary root $\lambda = a + ib$, the logarithmic formula may be reduced to

$$\begin{aligned} \log \frac{f(a+ib)}{(a+ib)F'(a+ib)} e^{(a+ib)t} &= (a+ib)t + \log R_0 + i\theta_0 \\ &= (\log R_0 + at) + i(\theta_0 + bt) \end{aligned} \quad (17)$$

The final formula, where $\lambda_1 = a + ib$, then becomes

$$\frac{f(\lambda_1)}{\lambda_1 F'(\lambda_1)} e^{\lambda_1 t} = R_0 e^{at} e^{i(b t + \theta_0)} \quad (18)$$

or, by De Moivre's theorem,

$$\frac{f(\lambda)}{\lambda F'(\lambda)} e^{\lambda t} = R_0 e^{at} [\cos (bt + \theta_0) + i \sin (bt + \theta_0)] \quad (19)$$

The points thus plotted will lie on a logarithmic spiral (fig. 3); the deviation of this spiral from a circle

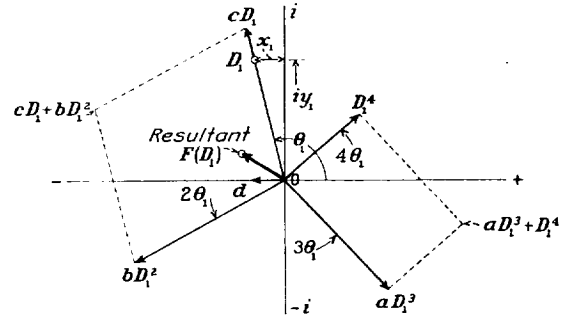


FIGURE 2.—Graphical method of locating values of $F(D)$ near zero, where $F(D) = D^4 + aD^3 + bD^2 + cD + d$. $D_1 = x_1 + iy_1 = R_1 e^{i\theta_1} = R_1(\cos \theta_1 + i \sin \theta_1)$

shows the influence of damping on the natural motion of the airplane.

The summation indicated in equation (6) calls for the plotting of such a logarithmic spiral for each of the complex roots. Since these roots always occur in conjugate pairs, the calculation may be carried out for one of such a pair and a spiral calculated for the second would be exactly conjugate to the first. Thus, it is only necessary to perform the foregoing calculations for one root of each pair, the summations indicated in the equations being carried out in effect by merely doubling the abscissas of the points of one of the conjugate spirals. If $\lambda_1 = a + ib$ and $\lambda_2 = a - ib$, this summation may be written:

$$\sum_{\lambda_1} \frac{f(\lambda)}{\lambda F'(\lambda)} e^{\lambda t} = 2R_0 e^{at} \cos (bt + \theta_0) \quad (20)$$

The formulas for the integration of terms containing $\sin nt$ and $\cos nt$ may be put into a more convenient form for the graphical or logarithmic calculations, i. e.,

$$\frac{f(D)}{F(D)} Y_0 \sin nt = Y_0 \left[\text{imaginary coordinate of } \frac{f(in)}{F(in)} e^{int} + \sum_{\lambda} \frac{n}{\lambda^2 + n^2} \frac{f(\lambda)}{F'(\lambda)} e^{\lambda t} \right] \quad (21)$$

$$\frac{f(D)}{F(D)} Y_0 \cos nt = Y_0 \left[\text{real coordinate of } \frac{f(in)}{F(in)} e^{int} + \sum_{\lambda} \frac{\lambda}{\lambda^2 + n^2} \frac{f(\lambda)}{F'(\lambda)} e^{\lambda t} \right] \quad (22)$$

kinematic constraint, or prescribed acceleration, imposed by the control as to assume that the pilot uses the control in an arbitrary way. This assumption leads to the inversion of the integration problems heretofore considered, because the motion of the airplane is itself predetermined and the forces and moments (or, more properly, accelerations) required to be supplied by the controls are calculated by differentiation. The ability of various control devices to produce a given maneuver of the airplane may thus be compared and the degree of coordination required of the other controls may be studied.

The foregoing procedure is a particularly useful way of studying the lateral-control effectiveness in turns. Turn maneuvers, which usually begin and end in level

naturally follows by differentiating this equation. If the turn is to be "perfect," that is, with no sideslipping, the rate of yawing throughout must bear a definite relation to the angle of bank, namely,

$$r = \frac{g}{U_0} \sin \varphi \quad (28)$$

or, simply,

$$r = \frac{g}{U_0} \varphi \text{ if } \varphi \text{ is under } 30^\circ$$

Differentiating the expressions for p and r gives the accelerations in rolling and yawing and hence the

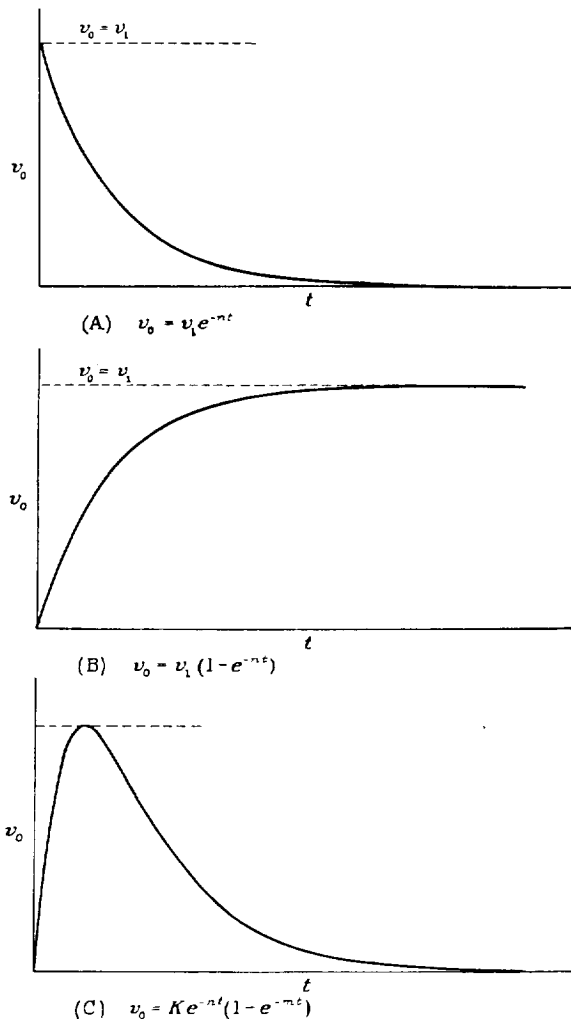


FIGURE 4.—Curves of different formulas for representing gusts.

flight, may be described by means of a few sine or cosine terms. For example, the angle of bank φ may be given by

$$\varphi = \text{constant} + A_1 \cos nt + A_2 \cos 2nt + \text{etc.} \quad (27)$$

(See fig. 5.) The rate of rolling at every instant

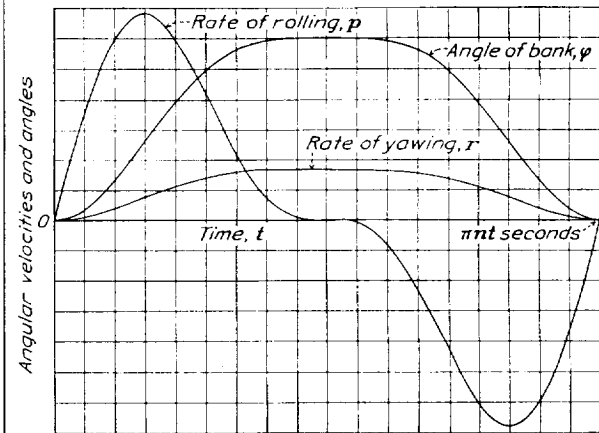


FIGURE 5.—Specifications for a turn maneuver in which the constraints are given by

$$\varphi = 1\frac{1}{4}A_1 + A_1 \cos nt + \frac{1}{4}A_1 \cos 2nt; \quad p = \frac{d\varphi}{dt}; \quad r = \frac{g}{U_0} \varphi.$$

moments, which will arise from two sources: the reactions due to natural stability and the reactions produced by the displaced controls. The reactions arising from the motions are found by combining the known stability derivatives with the angular velocities p and r , obtained from the specification equations (27) and (28). The parts of the moments necessarily supplied by the controls are then obtained by deducting these from the total moments. In the case of the aileron control, secondary moments in yaw result from the application of rolling moment, which modify the amount of rudder control displacement necessary.

CONTROL AGAINST GUSTS OR ENGINE FAILURE

In order to deal with attempted control of a given disturbance it is important to consider that there is invariably a lag in the pilot's reaction in countering the motion. In these cases it is possible to assume that the disturbance arises instantly, or nearly so (whether persistent or not), and that the pilot's displacement of the corrective control takes place according to the law

$$\delta = \delta_0 (1 - e^{-nt}) \quad (29)$$

(see fig. 4(B)) where δ_0 is the assumed maximum control deflection, which occurs more or less quickly as $-n$ is made large or small.

EXAMPLES SHOWING APPLICATION OF OPERATIONAL METHODS TO PROBLEMS OF AIRPLANE MOTION

The following examples illustrate the application of the various methods to specific problems of airplane motion. The airplane assumed in these calculations is a typical 2-passenger machine having the following characteristics:

CHARACTERISTICS OF TYPICAL AIRPLANE

Type: Monoplane; aspect ratio 6; rectangular, rounded tip, Clark Y wing; dihedral angle, 1° .

Dimensions:

Gross weight.....	1,600 lb.
Wing span.....	32 ft.
Wing area.....	171 sq. ft.
mk_x^2	1,216 slug-ft. ²
mk_z^2	1,700 slug-ft. ²

Stability derivatives:

U_0 (ft./sec.)	C_L	L_p	L_r	$U_0 L_r$	N_p	N_r	$U_0 N_r$
150	0.35	-5.44	1.11	-2.16	-0.207	-0.913	5.52
88.5	1.0	-3.23	1.88	-1.11	-0.301	-0.663	2.04
66	1.8	-2.46	2.51	-1.66	-0.310	-0.977	1.46

* Flaps down.

The calculated principal lateral-stability derivatives of this machine given with the other characteristics refer to motions of a set of axes fixed in the airplane but so inclined that the X axis points in the direction of the relative wind in straight flight at the lift coefficient specified. The axes, nevertheless, move with the machine during the small oscillations considered and hence depart slightly from instantaneous reference axes fixed in the wind direction.

ILLUSTRATION OF SOLUTION WITH CONSTANT DISTURBANCE TERM

Example I, Rolling motion produced by deflecting ailerons at low speed:

(a) Assume the machine to be in level steady flight at a speed of 88.5 feet per second ($C_L=1.0$) and that a rolling moment corresponding to $C_l=0.04$, with an adverse yawing moment $C_n=-0.01$, is applied suddenly at the time $t=0$. This condition corresponds approximately to a full deflection of ordinary ailerons at this speed.

(b) The equations of the motion in the three degrees of lateral freedom may be set up without including the expressions for the lateral air force, since this force is small and may be neglected in this case. The equations are:

$$\left. \begin{aligned} \frac{dv}{dt} &= g\phi - rU_0 \\ \frac{dp}{dt} &= vL_r + pL_p + rL_r + L_0 \\ \frac{dr}{dt} &= vN_r + pN_p + rN_r + N_0 \end{aligned} \right\} \quad (30)$$

The terms L_0 and N_0 represent the accelerations due to the constant control moments suddenly applied at $t=0$. They are

$$\begin{aligned} L_0 &= \frac{C_l q S b}{m k_x^2} \\ N_0 &= \frac{C_n q S b}{m k_z^2} \end{aligned} \quad (31)$$

The substitution of D for d/dt , and the rearrangement of the equations result in

$$\left. \begin{aligned} D^2 v - gp + DU_0 r &= 0 \\ -L_r v + (D - L_p)p - L_r r &= L_0 \\ -N_r v - N_p p + (D - N_r)r &= N_0 \end{aligned} \right\} \quad (32)$$

Since the rolling motion is desired, the equations will be solved for p . The algebraic solution is:

$$p = \frac{\begin{vmatrix} D^2 & 0 & DU_0 \\ -L_r & L_0 & -L_r \\ -N_r & N_0 & (D - N_r) \end{vmatrix}}{\begin{vmatrix} D^2 & -g & DU_0 \\ -L_r & (D - L_p) & -L_r \\ -N_r & -N_p & (D - N_r) \end{vmatrix}} \quad (33)$$

which is then reduced to the form required for expansion in equation (6),

$$p = \frac{f_1(D)}{F(D)} L_0 + \frac{f_2(D)}{F(D)} N_0 \quad (34)$$

The calculation of the various polynomials in D results in:

$$\left. \begin{aligned} f_1(D) &= D^3 - N_r D^2 + U_0 N_r D \\ f_2(D) &= L_r D^2 - U_0 L_r D \\ F(D) &= D^4 - (L_p + N_r) D^3 + (L_p N_r - L_r N_p + U_0 N_r) D^2 \\ &\quad + U_0 (L_r N_p - L_p N_r - \frac{g}{U_0} L_r) D + g(L_r N_r - L_r N_r) \end{aligned} \right\} \quad (35)$$

At the assumed speed of 88.5 feet per second ($C_L=1.0$), the constant rolling and yawing accelerations are

$$\begin{aligned} L_0 &= 1.68 \\ N_0 &= -0.301 \end{aligned} \quad (36)$$

Using these numerical values, combined with those given for the stability derivatives, the polynomials in D become.

$$\left. \begin{aligned} f_1(D) &= D^3 + 0.663 D^2 + 2.04 D \\ f_2(D) &= 1.88 D^2 + 1.11 D \\ F(D) &= D^4 + 3.89 D^3 + 4.75 D^2 + 10.33 D - 1.13 \end{aligned} \right\} \quad (35a)$$

In order to perform the expansion of $\frac{f(D)}{F(D)}$ by Heaviside's theorem it is necessary to determine the roots of the complementary equation $F(D)=0$. When the

polynomial $F(D)$ is plotted as a function of a real variable (D), two real roots of this equation are found:

$$\left. \begin{aligned} \lambda_1 &= -3.41 \\ \lambda_2 &= 0.104 \end{aligned} \right\} \quad (37)$$

By the use of vector diagrams (see fig. 2) and the plotting of a map of the polynomial considered as a function of a complex variable ($D=x+iy$), the following root was found by interpolation:

$$\lambda_3 = 1.78 (\cos 1.73 + i \sin 1.73) \quad (38)$$

An additional complex root that is the conjugate of λ_3 is known to exist and completes the four roots of the fourth-degree equation,

$$\lambda_4 = 1.78 (\cos 1.73 - i \sin 1.73) \quad (39)$$

The next step is to set up the integration equation and perform the indicated operations. Since the applied control moments L_0 and N_0 are constants, form (6) will be used

$$p = \frac{f_1(D)}{F(D)} L_0 + \frac{f_2(D)}{F(D)} N_0 = L_0 \left[\frac{f_1(0)}{F(0)} + \sum_{\lambda} \frac{f_1(\lambda)}{\lambda F'(\lambda)} e^{\lambda t} \right] + N_0 \left[\frac{f_2(0)}{F(0)} + \sum_{\lambda} \frac{f_2(\lambda)}{\lambda F'(\lambda)} e^{\lambda t} \right] \quad (40)$$

The various terms to be substituted in this formula are found to be:

$$\left. \begin{aligned} \frac{f_1(0)}{F(0)} L_0 + \frac{f_2(0)}{F(0)} N_0 &= 0 \\ f_1(\lambda) L_0 + f_2(\lambda) N_0 &= 1.68 \lambda^3 + 0.54 \lambda^2 + 3.09 \lambda \\ \lambda F'(\lambda) &= 4 \lambda^4 + 11.67 \lambda^3 + 9.49 \lambda^2 + 10.33 \lambda \end{aligned} \right\} \quad (41)$$

These terms are to be calculated for the four (real and complex) values of the roots. In the case of the real roots the calculation is made without resorting to graphical methods. For $\lambda_1 = -3.41$, the value

$$\frac{f_1(\lambda_1) L_0 + f_2(\lambda_1) N_0}{\lambda_1 F'(\lambda_1)} = -0.484 \text{ results,} \quad (42)$$

and for $\lambda_2 = 0.104$

$$\frac{f_1(\lambda_2) L_0 + f_2(\lambda_2) N_0}{\lambda_2 F'(\lambda_2)} = 0.277 \quad (43)$$

It will be convenient to perform graphical calculations to determine the other parts of the solution, corresponding to the complex terms. This result is accomplished by calculating the square, cube, and fourth power of the absolute length of λ_3 and by multiplying each of these values by the proper coefficients in the polynomials $f(D)$ and $F(D)$. By vector addition the value of the first polynomial was determined as

$$f_1(\lambda_3) L_0 + f_2(\lambda_3) N_0 = 3.99 (\cos 5.23 + i \sin 5.23) \quad (44)$$

and the second

$$\lambda_3 F'(\lambda_3) = 40.6 (\cos 5.60 + i \sin 5.60). \quad (45)$$

Since the quotient of these values is to be multiplied into $e^{\lambda_3 t}$ for a series of values of t it will be convenient to use the logarithm of this quotient, simply adding to it the various values of $\lambda_3 t$ for which the calculation is to be made. This logarithm is

$$\log \frac{f_1(\lambda_3) L_0 + f_2(\lambda_3) N_0}{\lambda_3 F'(\lambda_3)} = (\log 3.99 - \log 40.6) + i(5.23 - 5.60) = -2.32 - 0.38 i \quad (46)$$

The logarithm of the result naturally occurs in the form $x+iy$. Plotting this point on the paper and constructing from it a line parallel to λ_3 , we obtain the locus of

$$\log \frac{f_1(\lambda_3) L_0 + f_2(\lambda_3) N_0}{\lambda_3 F'(\lambda_3)} e^{\lambda_3 t}$$

for various values of t (see fig. 3). The angles of the final points are given by the ordinates of these logarithms and the absolute lengths by the antilogarithms of the abscissas. The final points are found to lie on a logarithmic spiral whose radius decreases with the time (time measured as angle) showing the damping of this component of the motion. The summation over the two conjugate roots λ_3 and λ_4 is accomplished without any further calculation by merely doubling the abscissas of the points plotted above, as has been pointed out. The values thus obtained are listed in the following table:

Table of values obtained from graphical construction

t (Seconds)	$\sum_{\lambda} \frac{f_1(\lambda) L_0 + f_2(\lambda) N_0}{\lambda F'(\lambda)} e^{\lambda t}$
	(For λ_3 and λ_4)
0	0.184
.2	.186
.4	.166
.6	.130
.8	.082
1.0	-.030
1.5	-.080
2.0	-.110

At the time $t=0$, $e^{\lambda t}$ will be unity so that the initial condition of zero rate of rolling should be given by the sum of its coefficients. The summation

$$-0.484 + 0.277 + 0.184 = -0.023$$

shows how nearly this condition is attained. Figure 6 shows the resultant rate of rolling and the components of the solution corresponding to each of the four roots, λ_n . In addition to the rolling curve obtained by the foregoing methods, other curves obtained by step-by-step integrations of the same equations of motion are given. In the calculation of these curves, steps of one-tenth and one-twentieth second were taken, which resulted in the differences shown.

ILLUSTRATION OF SOLUTION WITH VARIABLE DISTURBANCE TERMS

Example II, Sideslipping during 2-control turn maneuver:

(a) Assume the airplane to perform a specified banking maneuver by application of a variable rolling moment. If no yawing moments (from either rudder or

aileron) are applied, the natural stability of the airplane will cause it to turn in a direction appropriate to the direction banked. Such a turn is called a "2-control turn," inasmuch as only two (aileron and elevator) of the three available controls are used. Since there will not be a very perfect coordination between the banking and yawing, some sideslip will result. It is of interest to know the approximate amount of this

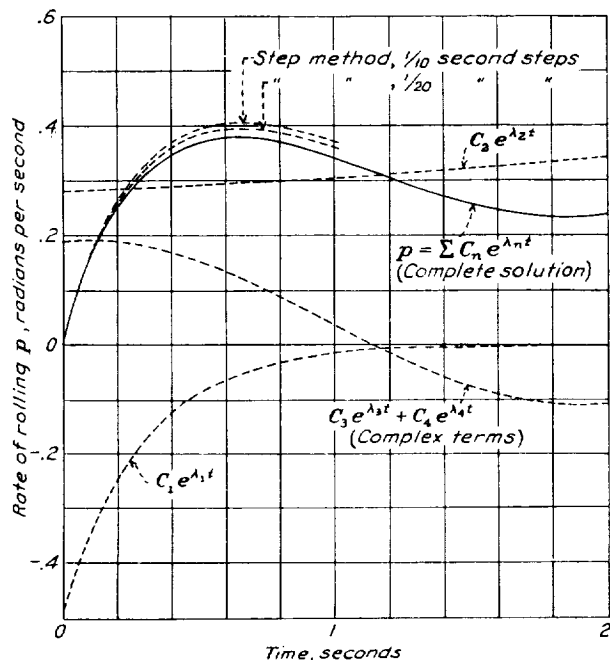


FIGURE 6.—Result of sample computation compared with step-by-step integrations; example I. Rolling motion following sudden deflection of ailerons. Typical 1,600-pound airplane. $C_L=1.0$; $C_T=0.04$; $C_A=-0.01$.

sideslip during such a turn in studying the practicality of 2-control operation.

(b) The first step in this problem is the determination of a suitable expression for the banking part of the maneuver. It was considered that the pilot would naturally conform his use of the control to the desired motion of the airplane rather than move the control in a predetermined way and accept whatever motion of the machine followed. Hence it seems more logical to specify the banking motion itself rather than to try to predetermine a law of application of rolling moment.

The airplane is thus assumed to be constrained in banking by the aileron control so as to follow a well-executed bank maneuver and recovery. The usual procedure in making a turn is to bank the machine up to a definite angle, holding this angle steadily for a short time while in the steady part of the turn, and then to recover to level flight on the completion of the desired angle of turn. A curve representing such a relation of bank angle against time may be represented by a series of only two cosine terms with a constant defining the

initial and terminal conditions of level flight, or zero bank angle. (See fig. 7.) For a fairly sharp turn with this small airplane the time required will be about 6 seconds if the maximum angle of bank is 30° . The specification decided on is:

$$\text{Bank angle, } \varphi = 0.327 - 0.262 [\cos t + \frac{1}{4} \cos 2t] \quad (47)$$

which reaches a steady value of 30° , and gives level flight at $t=0$ and $t=2\pi$ seconds. The rate of rolling is the rate of change of this angle of bank; or

$$p = \frac{d\varphi}{dt} = 0.262 \sin t + 0.131 \sin 2t \quad (48)$$

A constraint of the machine in one of its degrees of freedom having thus been specified, it is only necessary to consider the equations for free motion in the remaining two degrees. As before, the lateral motion will be assumed to be independent of the longitudinal. There remain only the sideslipping and yawing motions to be considered. Their equations are:

$$\left. \begin{aligned} \frac{dv}{dt} &= g\varphi - rU_0 \\ \frac{dr}{dt} &= vN_v + pN_p + rN_r \end{aligned} \right\} \quad (49)$$

Although the equations contain the rate of rolling and the angle of bank, these are to be considered as known

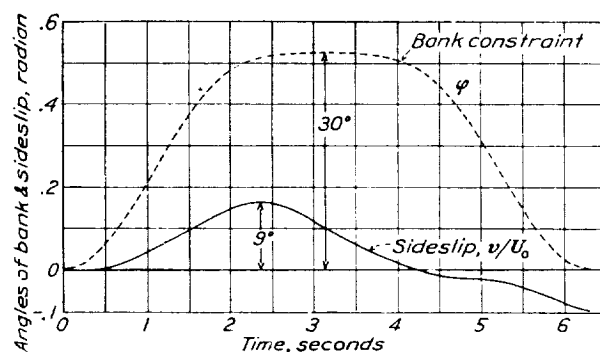


FIGURE 7.—Result of computation; example II. Sideslip during a 2-control turn maneuver.

from equations (29) and (30) and are, in fact, to be used as the disturbance terms. Calling

$$\left. \begin{aligned} Y_0 &= \frac{g}{U_0} \varphi \\ N_0 &= pN_p \end{aligned} \right\} \quad (50)$$

and rearranging the equations as in the other problems:

$$\left. \begin{aligned} D \frac{v}{U_0} + r &= Y_0 \\ -U_0 N_v \frac{v}{U_0} + (D - N_r) r &= N_0 \end{aligned} \right\} \quad (51)$$

Solving algebraically for v/U_0 :

$$\frac{v}{U_0} = \frac{\begin{vmatrix} Y_0 & 1 \\ N_0 & (D-N_r) \end{vmatrix}}{\begin{vmatrix} D & 1 \\ -U_0 N_r & (D-N_r) \end{vmatrix}} \quad (52)$$

or

$$\frac{v}{U_0} = \frac{f_1(D)}{F(D)} Y_0 + \frac{f_2(D)}{F(D)} N_0 \quad (52a)$$

where

$$\left. \begin{aligned} f_1(D) &= D - N_r \\ f_2(D) &= -1 \\ F(D) &= D^2 - N_r D + U_0 N_r \end{aligned} \right\} \quad (53)$$

If the airplane is to maintain its altitude while turning, the speed must be adjusted to give a higher lift than that at an equal lift coefficient in level flight. At an assumed lift coefficient of 1 the speed necessary to maintain altitude while turning at 30° bank is found to be 95 feet per second. Actually, if this speed is held throughout the specified maneuver, the longitudinal path will be accelerated somewhat; this condition will be neglected in the present problem. The necessary stability derivatives calculated for the new condition are:

$$\left. \begin{aligned} N_r &= -0.712 \\ U_0 N_r &= 2.40 \\ N_p &= -0.323 \end{aligned} \right\} \quad (54)$$

The "disturbance effects" Y_0 and N_0 are (see equations (46), (47), and (49))

$$\begin{aligned} Y_0 &= 0.111 - 0.0888 \cos t - 0.0222 \cos 2t \\ N_0 &= -0.0846 \sin t - 0.0423 \sin 2t \end{aligned} \quad (55)$$

and, finally,

$$\begin{aligned} \frac{v}{U_0} &= 0.111 \frac{f_1(D)}{F(D)} - 0.0888 \frac{f_1(D)}{F(D)} \cos t \\ &\quad - 0.0222 \frac{f_1(D)}{F(D)} \cos 2t - 0.0846 \frac{f_2(D)}{F(D)} \sin t \\ &\quad - 0.0423 \frac{f_2(D)}{F(D)} \sin 2t \end{aligned} \quad (56)$$

For the expansion of these terms in the integration equations (6), (8), and (9), it is necessary to know the roots of $F(D) = 0$. These are

$$\left. \begin{aligned} \lambda &= \frac{N_r \pm \sqrt{N_r^2 - 4 U_0 N_r}}{2} \\ \lambda &= -0.356 \pm 1.51i \end{aligned} \right\} \quad (57)$$

Since both these roots are complex, the operations indicated in the integration equations were performed graphically in the manner previously shown.

The results of these calculations are shown in figure 7. The fact that the error in meeting the zero sideslip condition at the start of the maneuver was very small (even though the graphical construction of several terms was required) gives an indication of the accuracy of the calculation.

LANGLEY MEMORIAL AERONAUTICAL LABORATORY,
NATIONAL ADVISORY COMMITTEE FOR AERONAUTICS,
LANGLEY FIELD, VA., February 19, 1936.

APPENDIX

EVALUATION OF ELEMENTARY OPERATORS

A simple differential equation may be used to illustrate briefly Heaviside's method of evaluating more elementary operational forms. Consider the case of an airplane executing pure rolling motion under the influence of a suddenly applied rolling moment of magnitude $mk_X^2 L_0$, which produces the impulsive acceleration L_0 in roll. The equation of motion may be written:

$$\frac{dp}{dt} = pL_p + L_0 \quad (58)$$

in which both p and L_0 are supposed to have the value zero at the time $t=0$.

The solution of this equation as ordinarily found will consist of two parts, one of which is a solution of

$$\frac{dp}{dt} - pL_p = 0 \quad (59)$$

the "complementary equation." In effect, Heaviside wrote both equations, (58) and (59), as one by introducing a discontinuous function of t into (58). Thus, (substituting the usual D)

$$Dp - L_p p = 1(t)L_0 \quad (60)$$

where the symbol $1(t)$ is termed the "unit function," and is supposed to have the value zero until the time $t=0$ and to take the value 1 thereafter. The algebraic solution of (60) is then written

$$p = \frac{1}{D - L_p} 1(t)L_0 \quad (60a)$$

and it is required to evaluate the form

$$\frac{1}{D - L_p} 1(t)$$

The procedure is to expand the fraction by the binomial theorem in ascending powers of L_p , thus,

$$(D - L_p)^{-1} = D^{-1} + D^{-2}L_p + D^{-3}L_p^2 + \dots + \text{etc.} \quad (61)$$

Since

$$\begin{aligned} D^{-1}1(t) &= \int 1(t)dt = 1(t)t \\ D^{-2}1(t) &= \int \int 1(t)dt dt = 1(t)\frac{t^2}{2!}; \text{ etc.,} \end{aligned} \quad (62)$$

performing the indicated integrations results in

$$(D - L_p)^{-1}1(t) = 1(t) \left(t + \frac{L_p t^2}{2!} + \frac{L_p^2 t^3}{3!} + \dots + \text{etc.} \right) \quad (63)$$

If this series is multiplied throughout by L_p it becomes identically the series for $e^{L_p t}$ except for the term 1, that is

$$[L_p(D - L_p)^{-1} + 1]1(t) = 1(t)e^{L_p t} \quad (64)$$

or

$$(D - L_p)^{-1}1(t) = \frac{1(t)}{L_p}(e^{L_p t} - 1) \quad (65)$$

The final solution of the original equation (1) follows as

$$p = 1(t) \frac{L_0}{L_p}(e^{L_p t} - 1) \quad (66)$$

Such forms as the left side of equation (60), involving the symbol D , are termed "operators." Equations (6) to (9) of the text are to be considered as evaluations of the more complex operators $f(D)/F(D)$ along the above-indicated lines. The evaluation of a number of such forms is given in reference 5.

Equation (6) of the text is a shorthand method of arriving at the foregoing solution. For the present problem this formula is:

$$p = \frac{f(D)}{F(D)} 1(t)L_0 = 1(t) \left[\frac{f(0)}{F(0)}L_0 + \sum_{\lambda} \frac{f(\lambda)L_0}{\lambda F'(\lambda)} e^{\lambda t} \right] \quad (67)$$

and the various terms are:

$$\left. \begin{aligned} f(D) &= 1 \\ F(D) &= D - L_p \\ f(0) &= 1 \\ F(0) &= -L_p \\ \lambda &= L_p \\ f(\lambda) &= 1 \\ F'(\lambda) &= 1 \end{aligned} \right\} \quad (68)$$

The substitution of these terms in (67) results in

$$p = 1(t) \frac{L_0}{L_p}(e^{L_p t} - 1) \quad (69)$$

as before.

REFERENCES

1. Wilson, Edwin Bidwell: Theory of an Aeroplane Encountering Gusts. T. R. No. 1, Part 2, 1915; II, T. R. No. 21, 1917; and III, T. R. No. 27, N. A. C. A., 1918.
2. Bryant, L. W., and Williams, D. H.: The Application of the Method of Operators to the Calculation of the Disturbed Motion of an Aeroplane. R. & M. No. 1346, British A. R. C., 1931.
3. Routh, E. J.: Advanced Rigid Dynamics, vol. II. The MacMillan Company, 1905.
4. Goursat, Edouard: Functions of a Complex Variable. Translated by E. R. Hedrick and Otto Dunkel, Ginn & Co., 1916.
5. Bush, V.: Operational Circuit Analysis. John Wiley and Sons, Inc., 1929.

REPORT No. 561

EFFECT OF NOZZLE DESIGN ON FUEL SPRAY AND FLAME FORMATION IN A HIGH-SPEED COMPRESSION-IGNITION ENGINE

By A. M. ROTHROCK and C. D. WALDRON

SUMMARY

Fuel was injected from different types of injection nozzles into the combustion chamber of the N. A. C. A. combustion apparatus, operated as a compression-ignition engine; high-speed motion pictures were taken at the rate of 2,200 frames per second of the fuel sprays and the combustion. Single-orifice nozzles of 0.008-, 0.020-, and 0.040-inch diameter, and multiorifice nozzles having 2, 6, and 16 orifices were tested. Nozzles having impinging jets and slit orifices were also included. The photographs indicate that the rate of vapor diffusion from the spray is comparatively slow and that this slow rate of diffusion for combustion chambers with little or no air flow prevents the compression-ignition engine, with the present methods of fuel injection, from giving the high performance inherent in the high compression ratios. The sprays from multiorifice nozzles destroyed the air movement to a greater extent than did those from single-orifice nozzles. It is concluded that high performance cannot be realized until the methods of distributing the fuel are improved by means of the injection-nozzle design, air flow, or both.

INTRODUCTION

In the high-speed compression-ignition engine the most difficult problem to solve is that of obtaining an intimate mixture of the fuel and the air so that the fuel may be burned both completely and efficiently. As yet no method has been devised to obtain a mixture that will completely utilize both the air and the fuel in the combustion chamber. Compression-ignition engines are therefore operated with an excess of air in order to obtain the low fuel consumption inherent in the high compression ratios.

Methods of mixing the fuel and air correctly are based on bringing the fuel to the air, on bringing the air to the fuel, or on both. During the past few years the N. A. C. A. has been conducting an extensive investigation of the effects of nozzle design on the general characteristics of fuel sprays for compression-ignition engines to learn to what extent the injection nozzle can be utilized in bringing the fuel to the air in the combustion chamber. Engine tests have been reported in

references 1 and 2, experiments on the distribution in the fuel sprays in references 3, 4, and 5, and experiments on fuel-spray disintegration in reference 6. In a more recent series of tests, the results of which will be later published, Lee has determined qualitatively the comparative distribution of the fuel from nozzles identical with or similar to those described in reference 5.

When the distribution of the fuel in the liquid stage has been determined, the next step is to determine the additional distribution caused by the diffusion of the fuel vapors. In order to make this determination it is necessary to conduct tests with the engine or with some special apparatus that reproduces very closely the engine conditions. Such tests, reported herein, have been conducted with the N. A. C. A. combustion apparatus (reference 7). By means of this apparatus high-speed motion pictures were taken of the fuel spray and flame formation in a single-cylinder test engine operating under load as a compression-ignition engine for a single cycle. These tests, in addition to forming a part of the general research on injection-nozzle design, also form a part of the general research on combustion being conducted by the Committee (references 8 and 9).

APPARATUS AND METHODS

The N. A. C. A. combustion apparatus (fig. 1) in its present form has been described in reference 9. The single-cylinder test engine is brought to speed by an electric motor. When the desired conditions are reached, a clutch is engaged and a camshaft makes a single revolution at one-half engine speed. This revolution of the camshaft causes a single charge of fuel to be injected into the combustion chamber of the engine. The compression-release valve is open for all engine revolutions except the one during which the injection of the fuel takes place. The following conditions were maintained constant during the tests:

Engine bore.....	inches..	5
Engine stroke.....	do.....	7
Height of inlet ports.....	do.....	0.5
Engine speed.....	revolutions per minute..	1,500

Compression ratio (based on 6.5-inch stroke)—

With windows in both sides.....	13.2
With indicator in one side.....	13.9
Engine-coolant temperature outgoing.....° F.....	150
Air-fuel ratio (see table I).....	17
Start of injection.....crankshaft degrees B. T. C.....	15

The different nozzles tested are shown in figure 2. Data on the atomization, penetration, and general appearance of the sprays from these or similar nozzles have been given in references 3, 4, and 5. The injection

indicator was again installed and two more indicator cards were taken as a check. Finally, the injection valve was removed and the fuel quantity again weighed. Because the injection valve was disassembled so frequently, it was impossible to hold the fuel quantity within the close limits maintained in the tests of air-fuel ratio reported in reference 9. Table I lists the various fuel quantities together with the actual deviation in weights and the estimated air-fuel ratios:

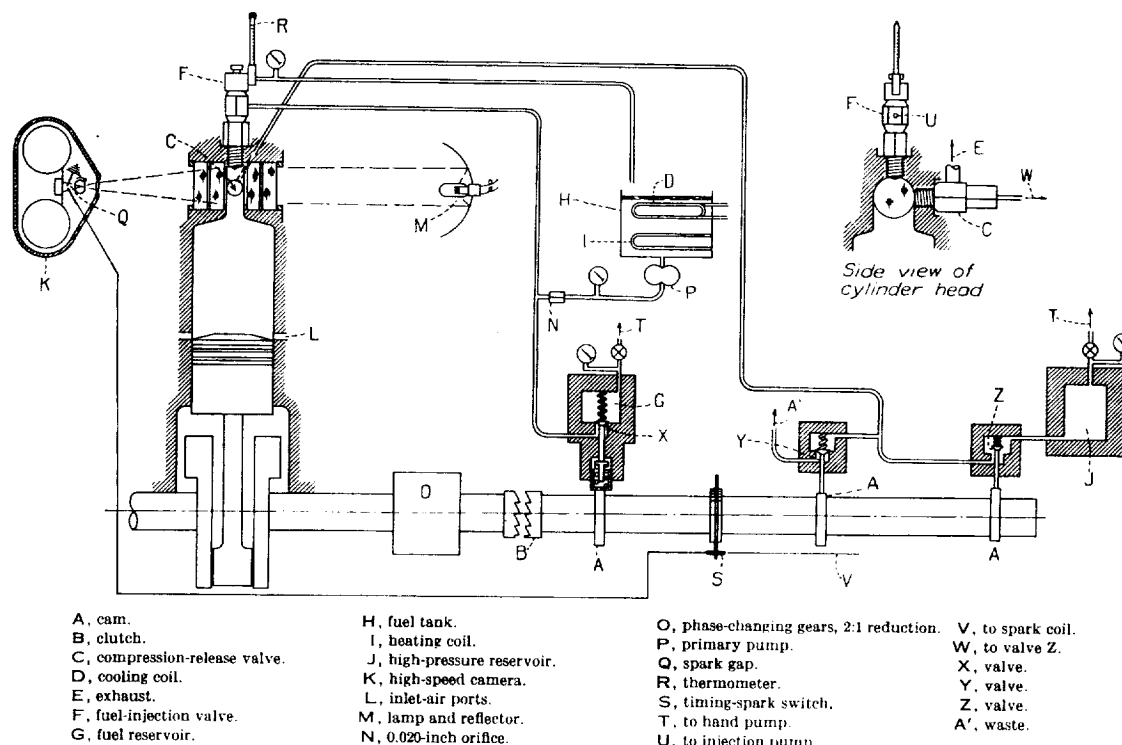


FIGURE 1.—Diagrammatic sketch of the N. A. C. A. combustion apparatus.

tion-valve opening pressure was adjusted to maintain as nearly as possible a constant injection pressure for all nozzles at the desired air-fuel ratio of approximately 17. In some cases the injection pressure varied appreciably from the mean. (See table I.) Although both the injection-valve opening pressure and the injection pressure varied, previous results obtained by the Committee (references 3 to 6) have shown that these variations do not affect the validity of the results.

The diesel fuel used in these tests was the same as that described in reference 9. For each of these tests the fuel-injection system was calibrated to determine the injection pressure necessary to obtain the desired fuel quantity. The injection valve was put into the engine and two indicator cards were taken. The indicator was removed, the glass windows were inserted in both sides of the cylinder head, and two series of motion pictures of the spray and combustion flame were taken. The

TABLE I
NOZZLE AND FUEL-INJECTION DATA

Nozzle	Fuel weight (Pounds)	Limits (Pound)	Injection pressure (lb./sq. in.)	Estimated air-fuel ratio ¹	Total discharge-orifice area (sq. in.)
Single 0.008-inch.....	2.99×10^{-4}	$\pm 0.15 \times 10^{-4}$	4,200	16.9	0.50×10^{-4}
Single 0.020-inch.....	2.87	$\pm .37$	5,950	17.6	3.14
Single 0.040-inch.....	2.97	$\pm .18$	3,900	17.0	12.56
2-orifice.....	2.93	$\pm .20$	6,000	17.2	9.83
6-orifice.....	2.95	$\pm .10$	6,000	17.1	9.73
16-orifice.....	2.95	$\pm .31$	5,000	17.1	20.57
Slit-orifice.....	2.95	$\pm .22$	5,750	17.1	4.40
Multiorifice-slit.....	2.97	$\pm .18$	5,500	17.0	
2-impinging-jets.....	3.02	$\pm .15$	5,500	16.7	19.25
4-impinging-jets.....	3.02	$\pm .26$	5,250	16.7	28.28

¹ See reference 9.

The indicator cards obtained in these tests were not sufficiently accurate to determine either the brake mean effective pressure developed during the power cycle or to obtain the specific fuel consumption. For this reason

the nozzles were also tested in the N. A. C. A. single-cylinder test engine using the combustion chamber described in reference 2. This combustion chamber is similar to that used in the N. A. C. A. combustion apparatus for the present tests. Nozzle K-4, described in reference 2, instead of the 6-orifice nozzle shown in figure 2, was used in the engine tests because of the differences in the combustion-chamber shapes.

RESULTS AND DISCUSSION

A composite of all the spray and flame photographs is shown as figure 3.¹ The rate at which the motion pictures were taken varied from 2,100 to 2,400 frames a second; hence, the timing sparks at 90 crankshaft degrees after top center are not in line. The time scale represents an average of all the runs.

Composites of the indicator cards obtained on the combustion apparatus with the different fuel-injection nozzles are shown as figure 4. The indicator cards show vibrations of the indicator diagram caused by the rate of pressure rise in the combustion chamber. These vibrations are not sufficiently intense to prohibit the use of the cards as an indication of the course of the combustion.

The analysis of the data presented in the report is chiefly based on the spray and flame photographs; consideration is also given to the data that were obtained with the test engine and are presented in table II. In table II the data are presented for the conditions of constant maximum cylinder pressure and of constant injection advance angle. Under either operating condition, the 6-orifice nozzle gave the best performance, and the 2-orifice nozzle the next best. The single 0.008-inch orifice was not tested on the engine because of its extremely long injection period. The other nozzles followed in fairly close order with some variation depending on whether the maximum cylinder pressure or the injection advance angle was kept constant.

TABLE II
ENGINE-PERFORMANCE TEST DATA

Nozzle	Constant maximum cylinder pressure, 800 pounds per square inch			Constant injection advance angle, 12 crankshaft degrees B. T. C.			
	B. m. e. p. (lb./sq. in.)	B. t. c. (lb./hp. hr.)	Air-fuel ratio	B. m. e. p. (lb./sq. in.)	B. t. c. (lb./hp. hr.)	Air-fuel ratio	Max. cyl. press. (lb./sq. in.)
Single 0.020-inch	84.8	0.654	17.0	66.0	0.823	17.3	545
Single 0.040-inch	79.0	.692	17.2	71.0	.790	16.8	690
2-orifice	91.3	.590	17.4	89.0	.628	16.8	745
6-orifice	115.0	.472	17.2	115.0	.472	17.2	800
16-orifice	90.0	.618	17.0	77.4	.720	16.9	650
Slit-orifice	85.8	.618	17.7	75.3	.716	17.4	645
Multiorifice-slit	87.7	.630	17.1	77.5	.716	16.9	675
2-impinging-jets	83.4	.690	16.2	62.0	.898	16.8	550
4-impinging-jets	83.4	.640	17.5	70.0	.784	17.1	585

¹ These results have also been prepared as a technical motion picture film (400 ft. 16 mm.) entitled "Effects of Nozzle Design on Combustion in a Compression-Ignition Engine," by A. M. Rothrock, E. C. Buckley, and C. D. Waldron, Technical Film No. 6, N. A. C. A., 1935. This film may be obtained on loan from the Committee.

A comparison of the indicator cards shown in figure 4 indicates that the 6-orifice nozzle and the multi-orifice-slit nozzle gave the best performance and that the 2-orifice nozzle was next. In a comparison of

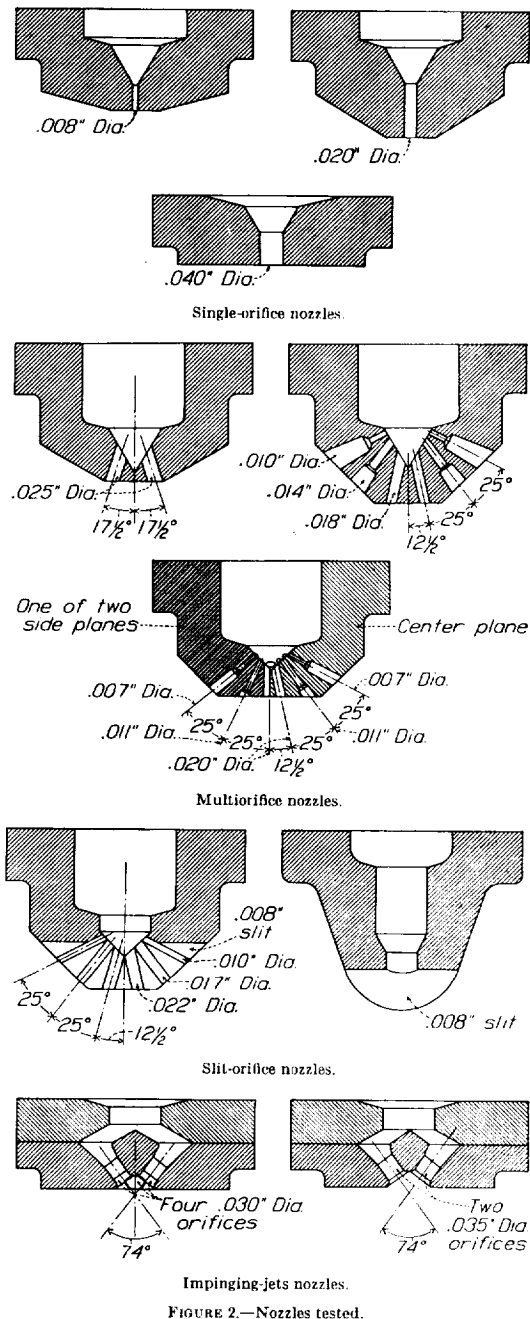


FIGURE 2.—Nozzles tested.

these results with those given in table II, allowance must be made for the differences in the combustion chambers and also in the air flow in the chambers.

In a previous report (reference 8) the form of combustion chamber used in these tests has been termed a

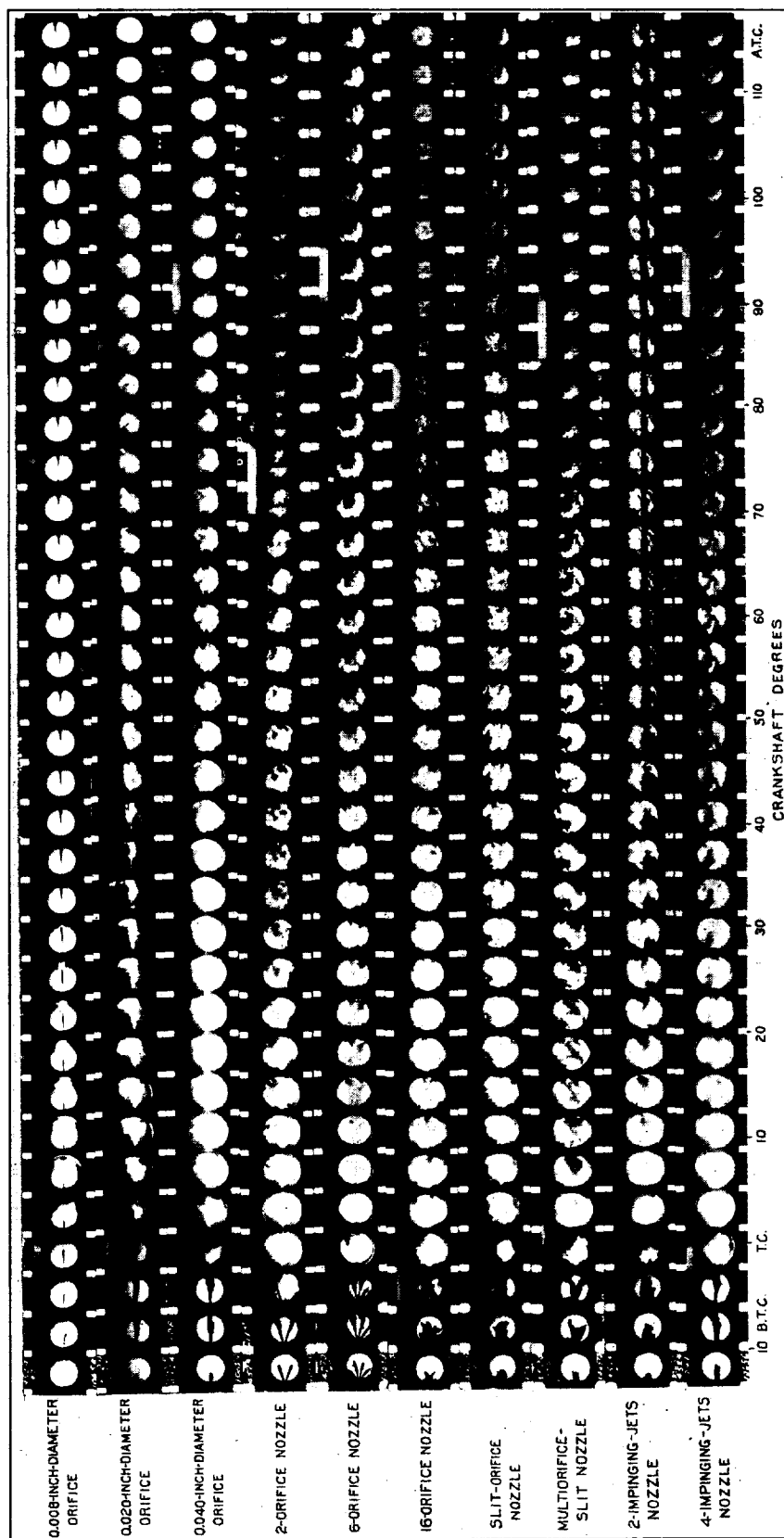


FIGURE 3. Effect of nozzle design on fuel spray and flame formation. Air-fuel ratio, 17; compression ratio, 13.2; speed, 1,500 r. p. m.; jacket temperature, 150° F.

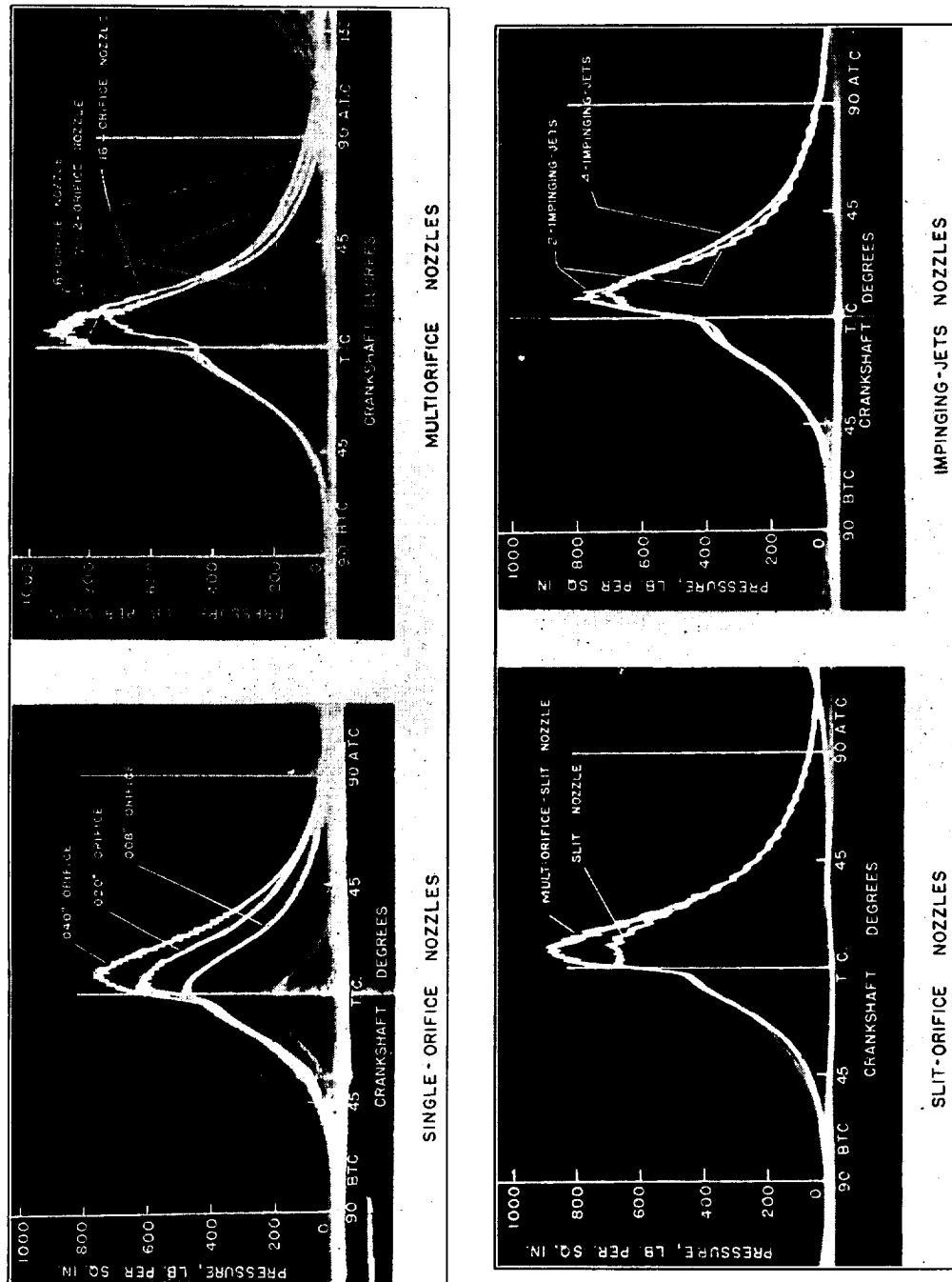


FIGURE 4.—Indicator cards obtained with different nozzles.

"quiescent" chamber. Subsequent tests (reference 9) have shown that air flow does exist in the combustion chamber, probably induced as the air enters the engine cylinder through the intake ports. Tests, the results of which are at present unpublished, show that this air movement consists of a vortex in the combustion chamber. A schlieren photograph of this vortex in the combustion chamber is shown in figure 5. The vortex appeared most intense in the left-hand side of the chamber and successive frames of the motion picture showed that it rotated in a counterclockwise direction and moved in the plane of the combustion chamber. As shown in figure 3 of reference 8, the inducted air entered the cylinder at a high pressure difference resulting in a high initial velocity. For this reason the air flow is comparable with that obtained in a highly supercharged engine.

Because the vortex itself, as well as the air within the vortex, is in motion, the fuel sprays may be bent first in one direction and then another. These spray

carried from the spray to the lower left-hand quarter of the combustion chamber, the flame being first photographed at about 4° after top center. The indicator card shows that the pressure rise caused by the combustion started at about 2° before top center. Figure 3 shows no flame at top center. The difference in the start of combustion is within the accuracy of the results. The flame then surrounds the spray in the portion of the chamber away from the nozzle and spreads more or less symmetrically to both sides. In the successive frames the visible portion of the flame grows smaller as the flame is apparently drawn down into the displacement volume of the engine. Beyond 30° after top center the flame is no longer visible although the fuel continues to be sprayed from the injection nozzle. In no case did the flame reach the top of the chamber at the injection nozzle. With the 0.008-inch orifice nozzle the actual discharge pressure at the orifice was probably considerably in excess of the 4,200 pounds per square inch in the injection reservoir (reference 10).

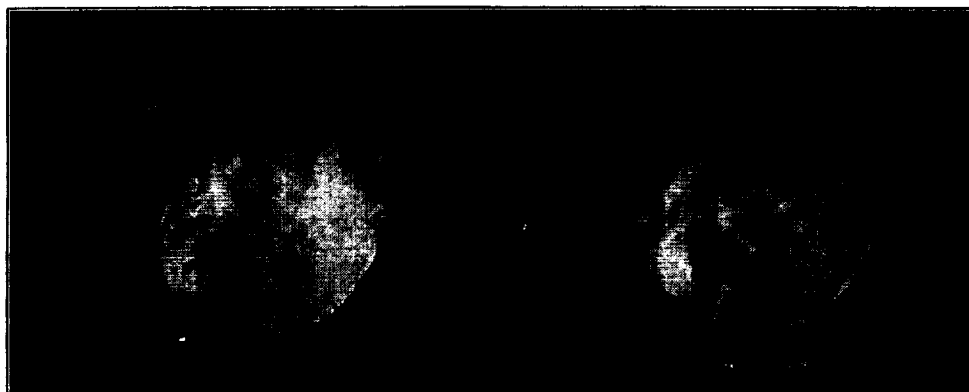


FIGURE 5.- Schlieren photograph of the air vortex in the combustion chamber. The air in the vortex is apparently rotating in a counterclockwise direction, and the vortex itself is rotating around the chamber in a counterclockwise direction.

movements are more visible in the enlargements of the fuel-spray development and of the first part of the burning, shown in figures 6 to 9. Since the purpose of this report is to discuss the effects of the nozzle design and not of the air movement, the effects of the air movement will be treated only incidentally.

Single-orifice nozzles (figs. 3, 4, and 6).—The most important fact to be learned from the photographs of the sprays and flame from the single-orifice nozzles is that the rate of vapor diffusion from the fuel spray is comparatively slow although it can be assisted to some extent by the nozzle design. With the single 0.008-inch orifice, the injection of the fuel lasted from 15° before top center to about 180° after top center. Such an injection period is, of course, entirely impracticable from considerations of engine operation, but it was used in the present series of tests to obtain additional information on spray diffusion. The spray traverses the combustion chamber comparatively slowly. The fuel that does vaporize and form a combustible mixture is

The high velocity and the small orifice both tended to lessen the mean drop diameter of the atomized fuel (reference 4). The fineness of the atomization in turn assisted the vaporization. Because of the slow mass rate of fuel discharge, however, the actual rate of vapor formation was probably low. This low rate of vaporization accompanied by the low rate of vapor diffusion (reference 9) resulted not only in a low rate of burning but also in limiting the flame to a small portion of the combustion chamber.

Holfelder (reference 11), using an apparatus somewhat similar to that described in the present report, has shown that when the combustion air is quiescent the burning starts close to the core of the fuel spray from a single-orifice nozzle and does not travel far from the volume included in the spray envelope.

When the orifice diameter was increased to 0.020 inch, the linear rate of fuel discharge was decreased (reference 10) but the mass rate and also the mean drop diameter (reference 4) were increased. The increased

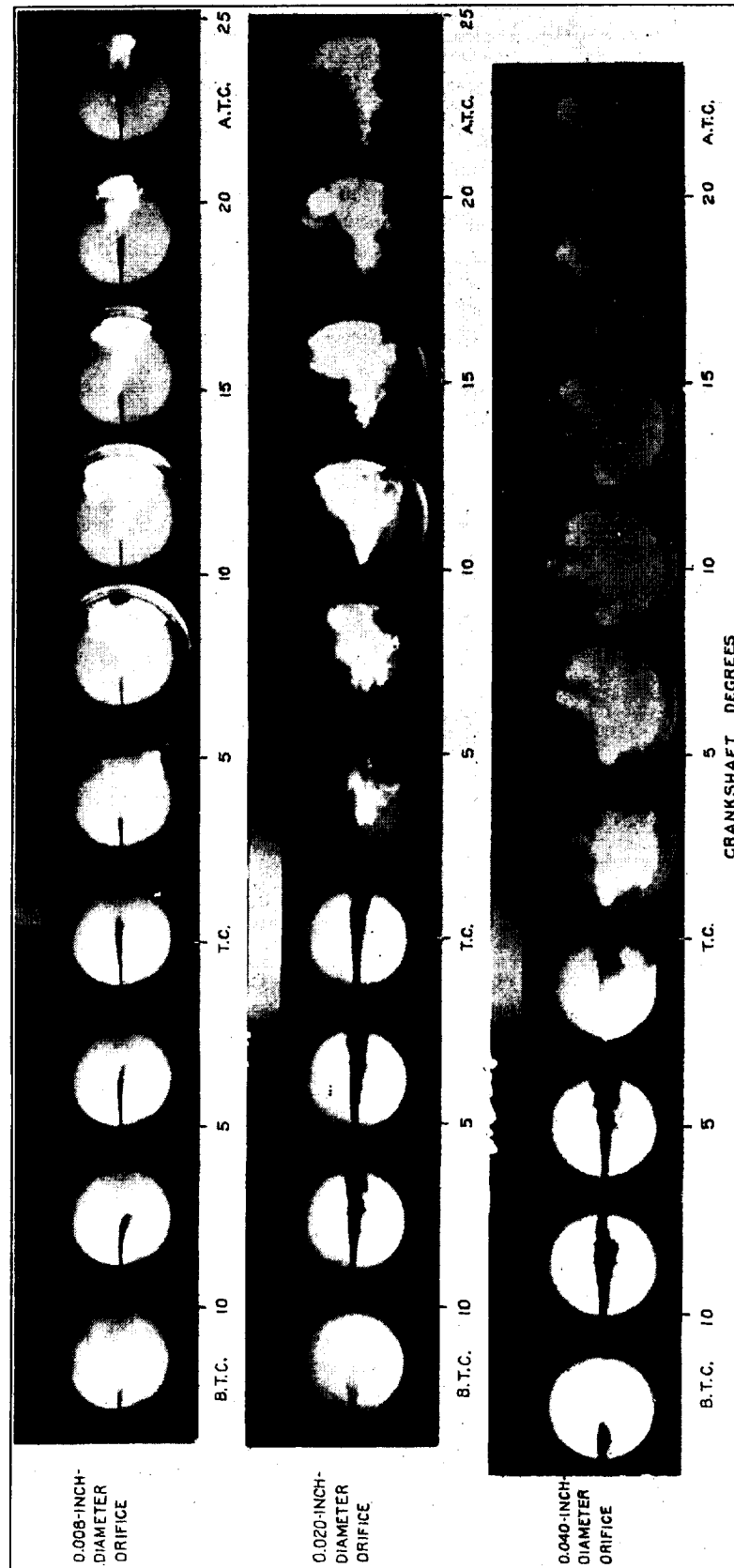


FIGURE 6.—Fuel spray and flame formation with single-orifice nozzles. Air-fuel ratio, 17; compression ratio, 13.2; speed, 1,500 r. p. m.; jacket temperature, 150° F.

mass rate of discharge more than compensated for the decreased atomization so that the rate of formation of a combustible mixture and its diffusion were increased. Consequently the flame spread to a greater area than it did with the smaller orifice. As the piston proceeded on its downward stroke, the flame did not disappear from view as it did when the 0.008-inch orifice nozzle was used but tended to remain in the visible portion of the combustion chamber. The photographs show clearly that the incandescent gases can remain in the combustion chamber without diffusing through the unburned portion of the gases. The results emphasize the slow rate of diffusion of the gases in the combustion chamber.

When the discharge-orifice diameter was increased to 0.040 inch, the area covered by the flame was still further increased although it did not fill the visible portion of the combustion chamber. The flame first appeared in the upper left-hand portion of the chamber. The comparison of the three series of photographs shows that, as the orifice diameter was increased, the first appearance of flame traveled from the bottom of the combustion chamber toward the top, always remaining on the leeward side of the spray. Examination of check runs made under the same or similar conditions showed that this tendency was definite. It is probable that, as the orifice diameter was increased, the velocity at the nozzle decreased and consequently the moving air was more able to deflect the spray envelope from its original path, thus forming a combustible mixture in the upper part of the chamber.

The indicator cards and the flame photographs both show that the ignition lag decreased as the orifice diameter was increased. This decrease is apparently caused by the earlier formation of a combustible mixture. The indicator cards show a large change in pressures as the orifice diameter is increased from 0.008 to 0.020 inch and a smaller change as the diameter is further increased to 0.040 inch. The cards also indicate that with the 0.040-inch orifice the amount of combustible mixture formed is the greatest, although the rate of pressure rise indicates that the rate of formation of the mixture is about the same as with the 0.020-inch orifice.

Multiorifice nozzles.—The results obtained with the multiorifice nozzles are shown in figures 3, 4, and 7. In each case the combustion reached a higher maximum pressure than with the single-orifice nozzles and was apparently more efficient. With the 2-orifice nozzle the flame covered a slightly greater area than with the single 0.040-inch orifice and the flame did not reach the upper portion of the chamber except close to the nozzle. When the number of orifices was increased to six, nearly all the combustion chamber was reached by flame; the air flow had no apparent effect on the spread of the flame other than at the start.

The fuel distribution was improved over that obtained with the single- or 2-orifice nozzles since it had to traverse only half the distance between each of the six sprays.

The results with the 16-orifice nozzle were disappointing as regards the resulting combustion. When so many orifices were provided, it was necessary to have a large over-all discharge area, 2.11 times that of the 6-orifice nozzle. The injection pressure was therefore still further decreased so that a point was reached at which the penetration was also decreased (reference 12) and the proportional distribution between the orifices was destroyed. Had the over-all area of the discharge nozzles been maintained constant, the penetration with the 16-orifice nozzle would still have been decreased because of the smallness of the orifices.

The first appearance of flame with the multiorifice nozzles was close to the fuel sprays, indicating that the multiorifice nozzles had an appreciable effect in destroying the air movement in the combustion chamber.

The indicator cards for the multiorifice nozzles show that the 6-orifice nozzle gave the highest maximum cylinder pressure. The expansion line for the 16-orifice nozzle crosses that for the 6-orifice nozzle. This pressure difference is, however, within the precision of the cards. The spread and duration of the flame with the 6-orifice nozzle indicate, as do the data of table II, that the maximum engine output was obtained with the 6-orifice nozzle. The results presented in figure 7 show why in many cases a nozzle that gives a spray which appears to be particularly good from design considerations may turn out to be inferior. When the over-all area of the nozzle becomes too great for the injection system as a whole, the spray penetration is decreased to such an extent that the decrease in the fuel dispersion results in a decrease in engine performance. The limitations of the injection pump may be such that the nozzle design most advantageous to the combustion chamber cannot be used.

High-distribution nozzles (figs. 3, 4, 8, and 9).—Nozzles giving uniformly distributed fuel sprays have been the subject of numerous tests. Most compression-ignition engines, however, employ either a multiorifice nozzle or a pintle nozzle. Although high-distribution nozzles present particularly interesting characteristics, they have not, in general, given satisfactory engine performance. The results shown in the photographs indicate that the trouble has been caused by an incorrect combination of combustion-chamber design, air flow, and nozzle design.

The slit nozzle shows distribution characteristics that are particularly interesting. The spray penetration is low so that probably this nozzle can be used beneficially only with air flow. When the slit is com-

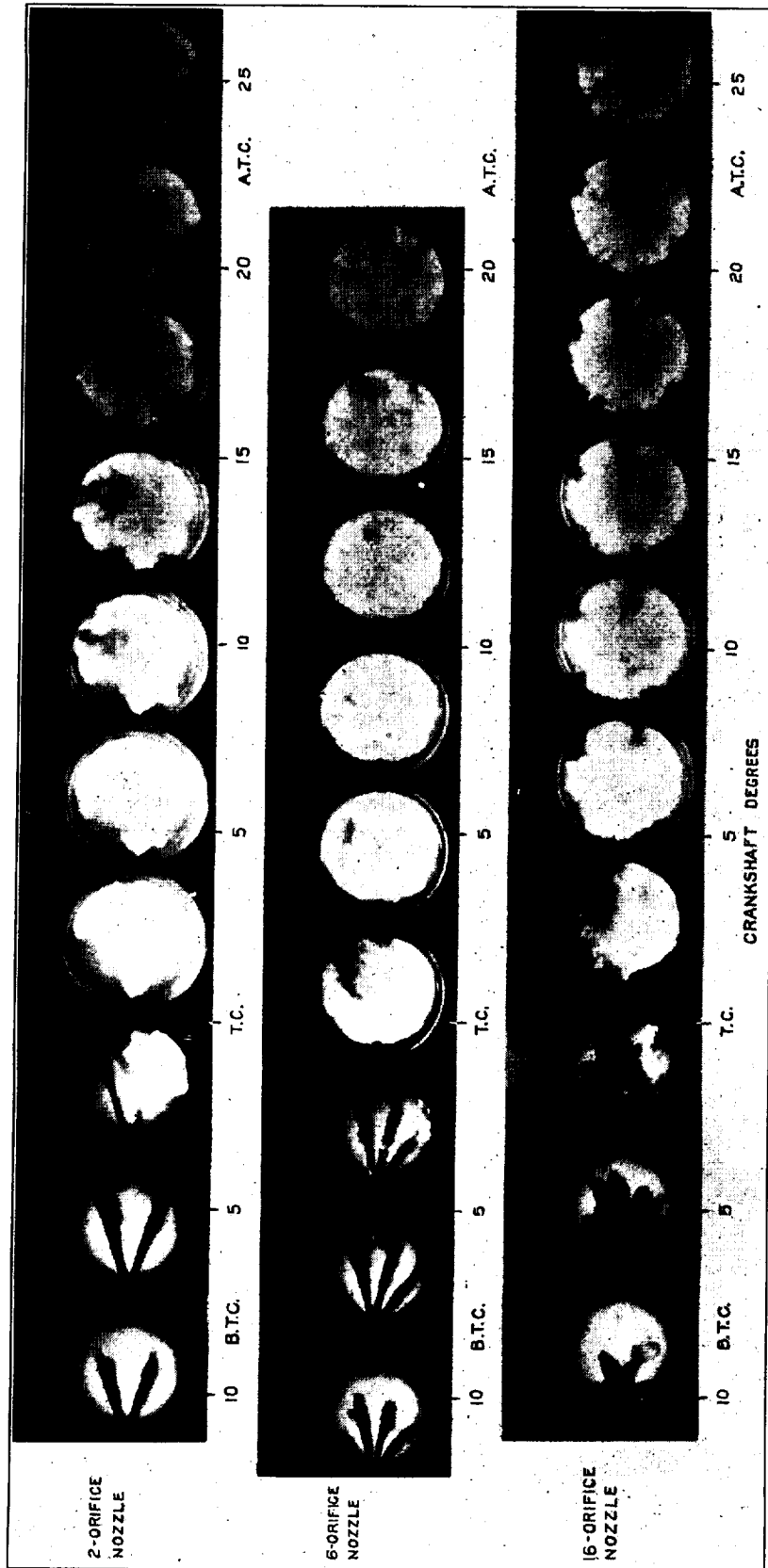


FIGURE 7. Fuel spray and flame formation with multiorifice nozzles. Air-fuel ratio, 17; compression ratio, 13.2; speed, 1,500 r. p. m.; jacket temperature, 150° F.

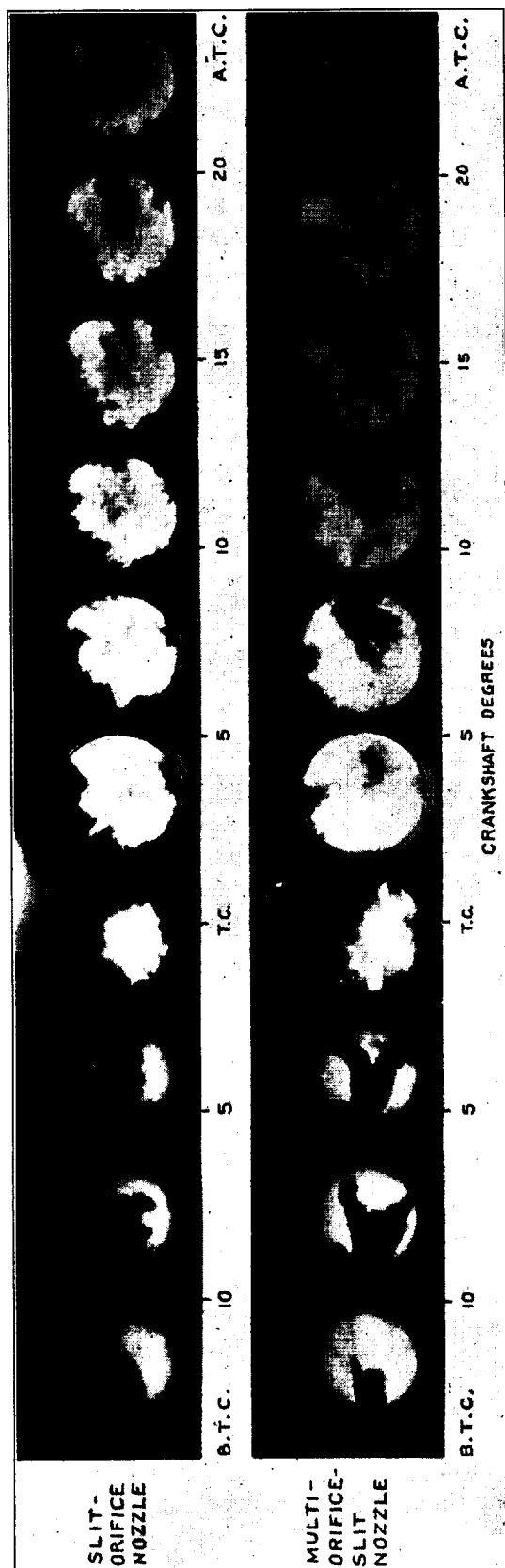


FIGURE 8.—Fuel spray and flame formation with slit-orifice and multiorifice-slit nozzles. Air-fuel ratio, 17; compression ratio, 13.2; speed, 1,500 r. p. m.; jacket temperature, 150° F.

combined with the multiorifice nozzle, the flow through the nozzle may be considerably different from that of either nozzle used separately. The photographs in figure 8 show that the slit gave an apparently symmetrical spray; the combination of the slit and multiorifice destroyed this symmetry. In neither case did the flame fill the combustion chamber, showing that, although the distribution within the spray may have been uniform, the fuel was too localized, resulting in an overrich mixture in the spray.

The 2-impinging-jets nozzle showed results somewhat similar to the slit nozzle. The 4-impinging-jets nozzle showed a spray of low penetrating ability, compared with a single-orifice nozzle, but one in which the core was of larger diameter and therefore of lower density. The indicator cards show that the rate of burning with this nozzle was comparatively slow, indicating a slow rate of diffusion of the fuel vapors into the unused air. For best results the low spray penetration must be assisted by air flow. The photographs show that the spray was more affected by the air movement in the chamber than was the case with the single-orifice nozzles.

In the construction of a high dispersion nozzle it is sometimes difficult to obtain a symmetrical spray. It can often be obtained only by trial and error, in which case considerable time can be saved by injecting the spray against some substance such as modeling clay (reference 3) in order to study the spray symmetry.

Comparison of all the nozzles.—By the comparison of all the nozzles, it is apparent that the distribution of the fuel relative to the combustion chamber can be regulated to a large extent by the design of the fuel-injection nozzle. This conclusion is not new in itself, but the extent to which the flame spread can be controlled by nozzle design, however, has not been known heretofore, and by the flame spread the diffusion of the fuel vapors is indicated. The results emphasize the fact that the rate of diffusion of the fuel vapor as well as of the fuel spray is a comparatively slow process and must be assisted by some other means if the combustion with little or no excess air is to be efficient. The indicator cards show that in some cases the difference in cylinder pressures is not so much as flame photographs might indicate, showing that the extent of flame spread is not the only criterion of the extent of combustion. From this fact it must be concluded that the extent of combustion within the flame area and also the rate must vary considerably. The tests emphasize again, as was brought out in reference 9, that in the high-speed compression-ignition engine the maximum performance of the engines is at present limited by the rate of diffusion of the fuel vapors and that, if the power and the economy are to be those inherent in the high compression ratio of the compression-ignition engine, the diffusion of the fuel by the injection nozzle and the air flow must be improved.

The results for all the nozzles show that in a nearly quiescent combustion chamber the best distribution of the fuel spray is obtained with a nozzle containing several plain round orifices. These results are in accordance with those already reported in references 1 and 2. In this type of chamber, good penetration of the fuel, which is very important, is best obtained by dense sprays from single round-hole orifices. It is possible that with extremely high injection pressures, e. g., in excess of 15,000 pounds a square inch, the high-dispersion nozzle might prove superior to the multiorifice nozzle.

CONCLUSIONS

The following conclusions are presented:

1. The rate of diffusion of the fuel vapors is too slow to provide satisfactory mixing of the fuel with the air in the combustion chamber.
2. The rate of fuel-spray distribution and the rate of fuel-vapor diffusion with respect to the combustion chamber and not the rate or fineness of fuel atomization, the rate of fuel vaporization, nor the rate of fuel injection are the chief obstacles to be overcome in the development of the high-speed compression-ignition engine.
3. The high performance inherent in the high compression ratio of the compression-ignition engine cannot be realized until a better method of distributing the fuel is obtained by improving the injection nozzle design, by the use of air flow, or by both.
4. Fuel sprays from a multiorifice nozzle destroy the air movement in a combustion chamber to a greater extent than do the sprays from single-orifice or high-dispersion nozzles.

LANGLEY MEMORIAL AERONAUTICAL LABORATORY,
NATIONAL ADVISORY COMMITTEE FOR AERONAUTICS,
LANGLEY FIELD, VA., March 19, 1936.

REFERENCES

1. Spanogle, J. A., and Whitney, E. G.: A Description and Test Results of a Spark-Ignition and a Compression-Ignition 2-Stroke-Cycle Engine. T. R. No. 495, N. A. C. A., 1934.
2. Foster, H. H.: The Quiescent-Chamber Type Compression-Ignition Engine. T. R. No. 568, N. A. C. A., 1936.
3. Lee, Dana W.: Experiments on the Distribution of Fuel in Fuel Sprays. T. R. No. 438, N. A. C. A., 1932.
4. Lee, Dana W.: The Effect of Nozzle Design and Operating Conditions on the Atomization and Distribution of Fuel Sprays. T. R. No. 425, N. A. C. A., 1932.
5. Lee, Dana W.: A Comparison of Fuel Sprays from Several Types of Injection Nozzles. T. R. No. 520, N. A. C. A., 1935.
6. Lee, Dana W., and Spencer, Robert C.: Photomicrographic Studies of Fuel Sprays. T. R. No. 454, N. A. C. A., 1933.

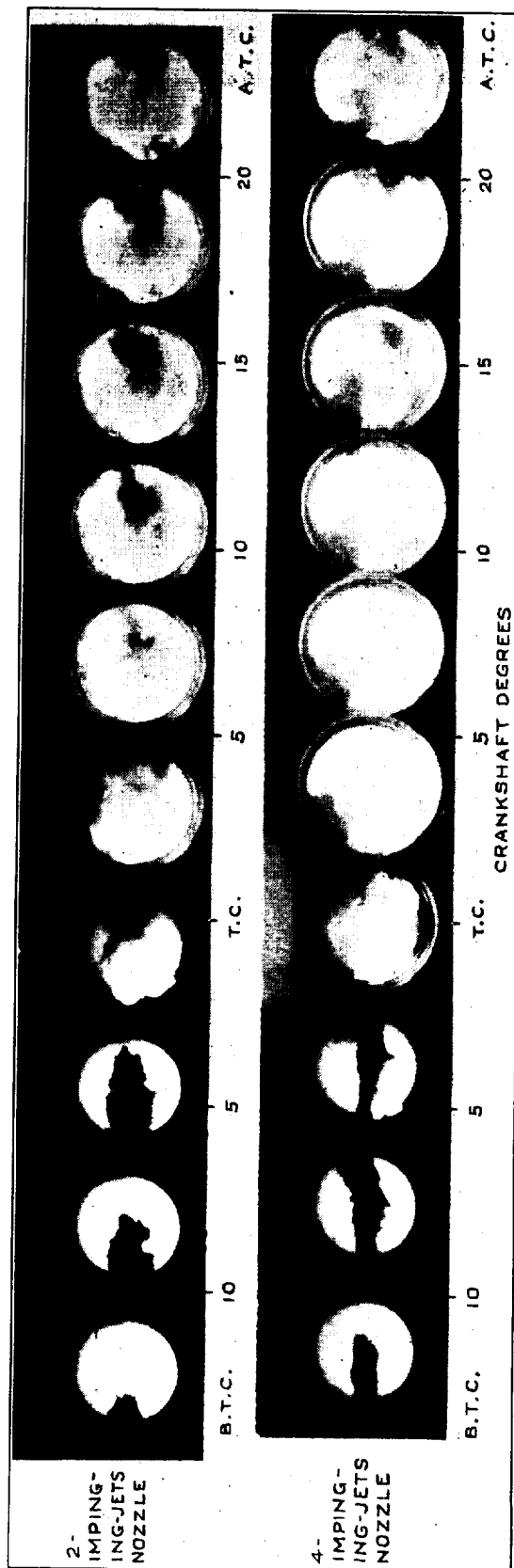


FIGURE 9.—Fuel spray and flame formation with impinging-jets nozzles. Air-fuel ratio, 17; compression ratio, 13.2; speed, 1,500 r. p. m.; jacket temperature, 16° F.

7. Rothrock, A. M.: The N. A. C. A. Apparatus for Studying the Formation and Combustion of Fuel Sprays and the Results from Preliminary Tests. T. R. No. 429, N. A. C. A., 1932.
8. Rothrock, A. M., and Waldron, C. D.: Some Effects of Injection Advance Angle, Engine-Jacket Temperature, and Speed on Combustion in a Compression-Ignition Engine. T. R. No. 525, N. A. C. A., 1935.
9. Rothrock, A. M., and Waldron, C. D.: Effects of Air-Fuel Ratio on Fuel Spray and Flame Formation in a Compression-Ignition Engine. T. R. No. 545, N. A. C. A., 1935.
10. Rothrock, A. M.: Hydraulics of Fuel Injection Pumps for Compression-Ignition Engines. T. R. No. 396, N. A. C. A., 1931.
11. Holfelder, Otto: Ignition and Flame Development in the Case of Diesel Fuel Injection. T. M. No. 790, N. A. C. A., 1936.
12. Gelalles, A. G.: Effect of Orifice Length-Diameter Ratio on Fuel Sprays for Compression-Ignition Engines. T. R. No. 402, N. A. C. A., 1931.

REPORT No. 562

AIR FLOW IN THE BOUNDARY LAYER NEAR A PLATE

By HUGH L. DRYDEN

SUMMARY

The published data on the distribution of speed near a thin flat plate with sharp leading edge placed parallel to the flow (skin friction plate) are reviewed and the results of some additional measurements are described. These experiments were carried out at the National Bureau of Standards with the cooperation and financial assistance of the National Advisory Committee for Aeronautics for the purpose of studying the basic phenomena of boundary-layer flow under simple conditions.

When the distribution of mean speed is measured in a stream without pressure gradient, it is found that the flow for some distance from the leading edge corresponds to that derived theoretically by Blasius from Prandtl's equations for laminar flow. At a definite value of the Reynolds Number formed from the distance to the leading edge and the speed of the stream at a considerable distance from the plate, the flow departs from the Blasius distribution and after a long transition region has the characteristics of fully developed turbulent flow, hereinafter designated "eddy flow." The Reynolds Number at which transition occurs is a function of the initial turbulence of the air stream, decreasing as the turbulence is increased.

Small pressure gradients in the air stream greatly change the critical Reynolds Number for a given turbulence.

From measurements of the amplitude of the u-fluctuation of speed it was found that the laminar region exhibits comparatively large fluctuations induced by the turbulence of the general flow. The laminar and eddy regions cannot be distinguished on the basis of the magnitude of the speed fluctuation, but the principal fluctuations in the eddy region are of higher frequency than those occurring in the laminar region.

INTRODUCTION

It is becoming increasingly evident that the solution of problems of great importance to aircraft designers, especially the influence of Reynolds Number or scale effect and the influence of initial turbulence, demands a more complete knowledge of the flow near surfaces, that is, in boundary layers. Even in the simple case of boundary-layer flow near a skin-friction plate, i. e., a thin flat plate of great length and width placed

parallel to the flow, our knowledge is far from complete. Studies of this simplified case are much needed to discover the basic laws of boundary-layer flow and thereby to prepare the way for a better understanding of the flow mechanism in the many cases of interest to the designer.

The concept of the boundary layer and the equations describing the laminar flow within it were announced by Prandtl in 1904 (reference 1). Four years later Blasius (reference 2) gave the solution of these equations for the skin-friction plate. A general acceptance of the boundary-layer concept was delayed for 20 years until experimental technique advanced to the point where the inner structure of the boundary layer could be explored in detail. The pioneer measurements were made by Burgers and his assistant, van der Hegge Zijnen, at Delft in 1924 (reference 3) with the aid of a hot-wire anemometer. Further measurements with pitot tubes were made a few years later by Hansen (reference 4) and by Eliás (reference 5) at Aachen. Later developments have shown that the comparatively good agreement between the results at Delft and Aachen was somewhat fortuitous. It seemed worth while to make some further measurements in an air stream of considerably smaller turbulence and, in view of the development of equipment for measuring the velocity fluctuations parallel to the mean direction of flow, to study the fluctuations as well as the mean speed.

The primary interest in this work is in the field of flow (distribution of speed in the vicinity of the plate), and not in the skin friction itself, which is more easily studied by force measurements. Th. von Kármán has recently (reference 6) given a review of the data on skin friction.

ACKNOWLEDGMENT

The author wishes to acknowledge the assistance of A. M. Kuethe, W. C. Mock, Jr., and S. S. West in connection with the experimental program and the reduction of observations; of W. H. Boyd in the design and construction of the traversing equipment; and of E. R. Frisby in the computation of the effect of the "simplified turbulence."

PREVIOUS EXPERIMENTAL WORK

The essential features of the flow in the boundary layer of a skin-friction plate may be described by a consideration of the measurements of Burgers and van der Hegge Zijnen (reference 3). The results are presented in the dissertation of van der Hegge Zijnen in the form of numerous tables and curves giving the observed speeds at several hundred points, whose x and y coordinates with respect to the leading edge of the plate are tabulated, for five speeds of the approaching air stream. The original dissertation should be consulted for detailed results. Only the general features can be discussed here.

Dimensional analysis enables one to devise a method of representation that gives a general view of the hundreds of measurements. The speed u at any point (x, y) at distance x from the leading edge and at distance y from the plate is a function of the speed U_0 of the approaching air stream, of the density ρ and the viscosity μ of the air, and of x and y . By the principles of dimensional analysis

$$\frac{u}{U_0} = f\left(\frac{U_0 x}{\nu}, \frac{U_0 y}{\nu}\right) \quad (1)$$

where ν is the kinematic viscosity μ/ρ . The independent variables may be considered as x -Reynolds Number and y -Reynolds Number, since a nondimensional product obtained by multiplying $\frac{U_0}{\nu}$ by a linear dimension

is ordinarily called a "Reynolds Number." If the foregoing factors are the only ones determining the flow, the flow can be pictured by a three-dimensional model or, more conveniently, by a contour diagram of the three-dimensional model. This representation is entirely independent of any theory of the flow and its validity rests only on the completeness of the list of controlling quantities.

A contour diagram of this type for the measurements of van der Hegge Zijnen is given in figure 1. The contours are for values of u/U_0 in steps of 0.1, the corresponding x and y being found by interpolation in the original tables. For convenience, the scale of y -Reynolds Number has been magnified 200 times. If one wishes to think in terms of x and y , the numbers along the abscissas represent for an air speed of 200 feet per second distances in inches, while each square along the ordinates represents one one-thousandth of an inch. Or for an air speed of 20 feet per second, the numbers along the abscissas are tens of inches and each square along the ordinates is one one-hundredth of an inch.

The diagram contains data for five speeds and, in general, the results are very consistent. The deviations correspond to about 0.02 in u/U_0 or 0.005 inch on the average in y . When examined on a large scale there are certain systematic differences between the results at different speeds, which are to be ascribed to the influence of a slight pressure gradient in the air stream in which the measurements were made.

Near the leading edge the contour lines are approximately parabolic in shape and correspond approximately to the theoretical result of Blasius for laminar flow (cf. theoretical treatment). For this reason, the flow in this part of the field is labeled "laminar."

At an x -Reynolds Number of about 300,000, the contours for small values of u/U_0 approach the axis of abscissas, indicating an increasing speed along the plate while the contours for large values bend away from the axis, indicating a rapid thickening of the layer. The process continues over the range from 300,000 to about 500,000, a region usually designated as the "transition" region.

There follows a different type of speed distribution which resembles very closely that found in eddying (fully developed turbulent) flow in pipes. In the part marked "eddying layer," there is at any x -Reynolds Number, a logarithmic relation between u and the y -Reynolds Number, often approximated by a power law. The relations are different near the wall, a region commonly termed the "laminar sublayer" because the distribution resembles that in the laminar layer. It should be noted that the laminar sublayer accounts for only a small part of the thickness of the layer but for two-thirds of the fall in speed.

The contour for $\frac{u}{U_0} = 1$ is not shown, for the reason that u approaches U_0 asymptotically. Various unambiguous procedures can be used to define the "thickness" of the layer of fluid affected by the presence of the plate. We may perhaps think of the distribution as approximated by some specific mathematical expression, and the thickness δ as the value of y which, substituted in that expression, gives $u = U_0$. Or δ may be taken as the value of y , for which $u = 0.99 U_0$ or $0.995 U_0$ or some other convenient value. The "displacement thickness" δ^* defined as $\int_0^\infty \left(1 - \frac{u}{U_0}\right) dy$ is often the most convenient measure of the thickness.

Burgers and van der Hegge Zijnen made another significant observation, namely, that the presence of strong fluctuations in the flow of air approaching the plate moved the transition to an x -Reynolds Number of about 85,000. The fluctuations were produced by a square-mesh wire screen immediately ahead of the plate, the wire diameter being 0.08 cm and the mesh being 0.4 cm.

In air streams, especially those produced by artificial means in wind tunnels, the motion is never absolutely steady, and there are always present small ripples or fluctuations that usually do not exceed a few percent of the average speed. It is difficult to believe that the presence of these fluctuations, usually of frequencies of the order of 20 to perhaps 1,000 per second, could play any part in determining the nature of the flow around an object placed in the stream. Yet it has been experimentally found that these fluctuations

exert a comparatively large influence in many cases. The basic effect in all these cases is believed to be the effect on the transition from laminar to eddying flow in the boundary layer.

No method by which the initial turbulence could be numerically evaluated was known in 1924 and the methods are still in process of development. No completely satisfactory method can be developed until a satisfactory theory of the effect of turbulence is available. It is now possible to measure directly (reference 7) the mean fluctuation of the speed at any point with time by means of a hot-wire anemometer, with a wire of small diameter, an amplifier, an electrical network to compensate for the lag of the wire, and an alternating current milliammeter. The speed fluctuation is converted into an alternating electric current whose intensity is measured. The turbulence may then be defined as the ratio of the average fluctuation to the mean speed and is usually expressed as a percentage. Such a method was used in the experiments described in this paper.

Because of certain small discrepancies between the experimental results of van der Hegge Zijnen in the region of laminar flow near the leading edge and the theory of Blasius, the measurements were repeated by M. Hansen at Aachen (reference 4), using small pitot tubes. In general appearance, a contour diagram of the results would resemble figure 1. The data of Hansen are not given in sufficient detail to permit the preparation of an accurate contour diagram. The transition occurred at nearly the same value of the x -Reynolds Number, a fact which the experiments in the present paper show to be a coincidence. The principal differences between the two sets of measurements at Delft and Aachen are: (1) the Aachen results agree very well with the Blasius theory, whereas the Delft results show small discrepancies; and (2) when the speed distribution in the eddying region is approximated by a power law, the exponent is about $1/5$ in the Aachen experiments as compared with $1/7$ in the Delft experiments.

Hansen showed that the Delft experiments were made in an air stream in which the static pressure decreased along the plate and that therefore the experiments could not be expected to check the theory of Blasius, which assumed a constant static pressure along the plate. An approximate allowance for the effect of the pressure gradient brought the Delft experimental results into agreement with the Blasius theory.

Hansen made some studies of the effect of the shape of the leading edge of the plate and of the roughness of the surface. A poorly shaped leading edge sets up turbulence which has an effect similar to that of increased turbulence in the air stream. For rough plates, the flow was eddying at all points investigated.

Elías (reference 5) also made measurements of the speed distribution near a plate in connection with

measurements of heat transfer. The results are similar to those of Hansen and were presumably made in the same wind tunnel. Transition occurred at an x -Reynolds Number of about 150,000 to 200,000.

THEORETICAL TREATMENT

Laminar flow.—The equations given by Prandtl for the steady flow of an incompressible fluid in a thin boundary layer along a two-dimensional plane surface are as follows:

$$u \frac{\partial u}{\partial x} + v \frac{\partial u}{\partial y} = \nu \frac{\partial^2 u}{\partial y^2} - \frac{1}{\rho} \frac{\partial p}{\partial x} \quad (2)$$

$$\frac{\partial p}{\partial y} = 0 \quad (3)$$

$$\frac{\partial u}{\partial x} + \frac{\partial v}{\partial y} = 0 \quad (4)$$

where u is the component of the velocity parallel to the surface, v the normal component, x the distance measured along the surface, y the distance measured normal to the surface, ν the kinematic viscosity, and p the pressure. The boundary conditions are: (1) at the surface, $u=v=0$; (2) at a great distance $u=U$, the speed in the potential flow. By (3) the pressure is independent of y and hence equal to that in the potential flow. By Bernoulli's theorem $p + \frac{1}{2}\rho U^2$ is constant and hence, $\frac{\partial p}{\partial x} = \rho U \frac{dU}{dx}$.

Blasius discussed the case where U , the speed at a considerable distance from the plate, is constant, i. e., $\frac{dU}{dx} = 0$ and therefore $\frac{\partial p}{\partial x} = 0$. This constant value of U will be designated U_0 .

By virtue of equation (4), a stream function ψ may be introduced, such that

$$u = -\frac{\partial \psi}{\partial y}, \quad v = \frac{\partial \psi}{\partial x} \quad (5)$$

Equation (2) becomes for $\frac{dp}{dx} = 0$

$$-\frac{\partial \psi}{\partial y} \frac{\partial^2 \psi}{\partial x \partial y} + \frac{\partial \psi}{\partial x} \frac{\partial^2 \psi}{\partial y^2} = \nu \frac{\partial^3 \psi}{\partial y^3} \quad (6)$$

Introducing new variables Z and X defined by

$$Z = \frac{1}{\sqrt[3]{\alpha}} \frac{\psi}{\sqrt{\nu U_0 x}}, \quad X = \frac{\sqrt[3]{\alpha}}{2} \sqrt{\frac{U_0}{\nu x}} y \quad (7)$$

in which α is a numerical constant whose significance and value will be determined later, equation (6) becomes

$$\frac{d^3 Z}{dX^3} + Z \frac{dZ}{dX} = 0 \quad (8)$$

Setting $u = \frac{u}{U_0}$ and $y = y \sqrt{\frac{U_0}{\nu x}}$, it may be shown from

$$(5) \text{ and } (7) \text{ that } \bar{u} = \frac{\alpha^{2/3}}{2} \frac{dZ}{dX} \text{ and } \bar{y} = \frac{2}{\alpha^{1/3}} X \quad (9)$$

¹ In view of the more complete derivations published elsewhere, for example, reference 2, only the principal steps in the method of solution will be outlined.

Likewise

$$\frac{d\bar{u}}{d\bar{y}} = \frac{\alpha}{4} \frac{d^2 Z}{dX^2} \text{ and } \frac{d^2 \bar{u}}{d\bar{y}^2} = \frac{\alpha^{2/3}}{8} \frac{d^3 Z}{dX^3} \quad (10)$$

The boundary conditions, $u=v=0$ at the surface and $u=U_0$ for large values of y become in the new variables

$$\frac{dZ}{dX}=0, Z=0 \text{ at } X=0 \text{ and } \frac{\alpha^{2/3}}{2} \frac{dZ}{dX}=1 \text{ at } X=\infty \quad (11)$$

In the solution of equation (8) it is convenient to begin the solution at the surface. By the introduction

and $\frac{d^2 u}{d\bar{y}^2}$ are readily computed. These quantities are also given in table I.

It is significant that the complete solution can be represented by a single curve of \bar{u} plotted against \bar{y} . Thus the speed distributions at various values of x are similar, the same speed occurring at values of y proportional to the square root of $\frac{\nu x}{U_0}$. This similarity of the speed distributions is the physical expression of the

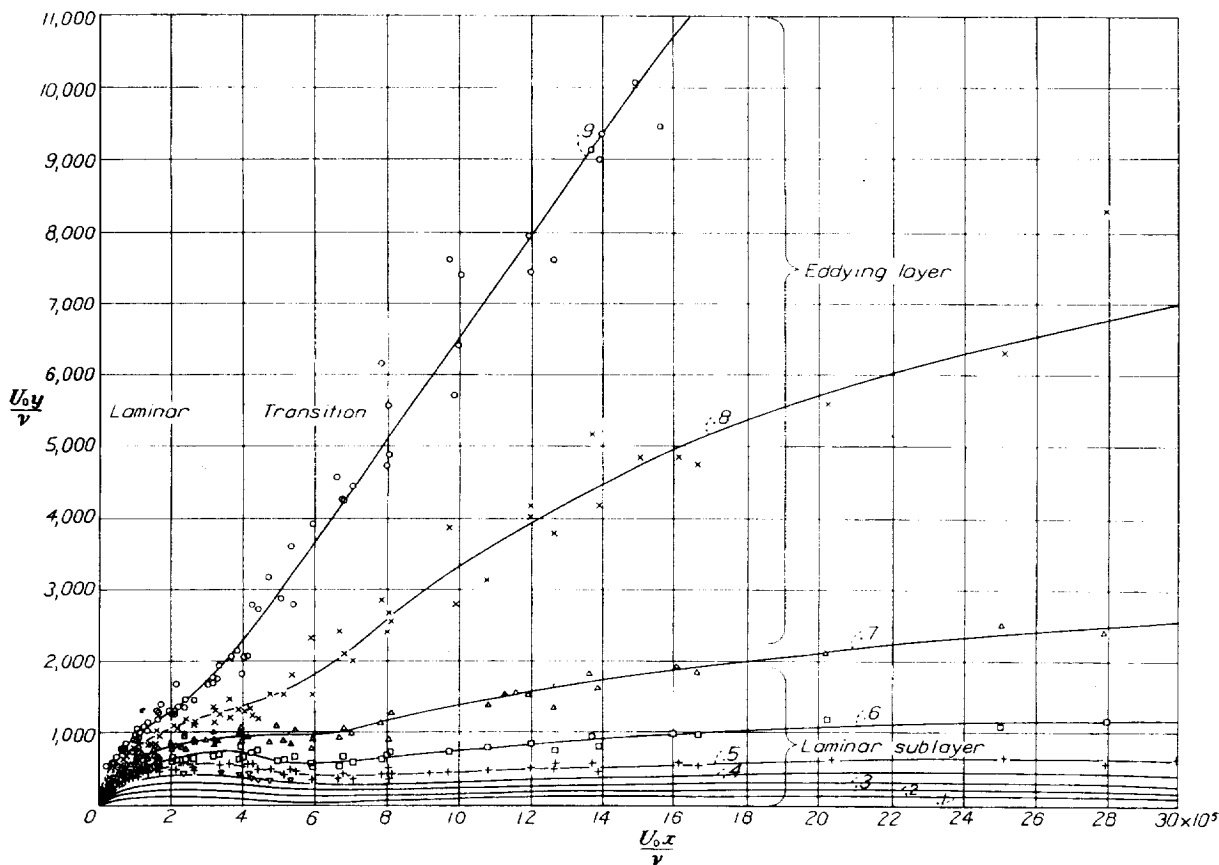


FIGURE 1.—Distribution of mean speed near skin-friction plate. Measurements made by van der Hegge Zijnen. x is the distance measured along the plate from the leading edge, y the distance from the plate, U_0 the speed of the free stream, ν the kinematic viscosity. The contours are contours of equal mean speed, the number on each contour being the corresponding value of u/U_0 , where u is the local speed.

of the numerical constant α , the value of $\frac{d^2 Z}{dX^2}$ at $X=0$

may be assumed equal to 1, this boundary condition temporarily replacing condition (11). When the solution has been obtained, α may then be chosen to satisfy (11). It may be noted that α does not appear in (8).

Equation (8) may be solved numerically by the Runge-Kutta method (reference 8). The results are given in table I. The value of α is found to be 1.328238.

From this value and equations (9) and (10), \bar{y} , \bar{u} , $\frac{d\bar{u}}{d\bar{y}}$,

reduction of the partial differential equation to a total differential equation. On the representation of the laminar speed distribution by a contour diagram similar to figure 1, it is readily seen that a constant value of \bar{y} corresponding to a given \bar{u} is indicated by a constant value of the ratio of the y -Reynolds Number to the square root of the x -Reynolds Number, which ratio numerically equals \bar{y} . Hence the contours are parabolas. The values of \bar{y} at even values of \bar{u} for the theoretical laminar distribution are given in the following table:

\bar{u}	\bar{v}	\bar{u}	\bar{v}
0.1	0.301	0.6	1.890
.2	.603	.7	2.276
.3	.908	.8	2.739
.4	1.220	.9	3.385
.5	1.544		

The equations of the contour lines are

$$\frac{U_0 y}{\nu} = \bar{y} \sqrt{\frac{U_0 x}{\nu}} \quad (12)$$

The "displacement thickness" δ^* is readily computed from table I to be $1.7207 \sqrt{\frac{\nu x}{U_0}}$, and hence the δ^* Reynolds Number is 1.7207 times the square root of the x -Reynolds Number.

When a pressure gradient is present so that $\frac{dp}{dx}$ is not zero, the similarity of the speed distributions disappears except in special cases, and the partial differential equation must be solved. Various approximate methods have been proposed, for example, those described in references 9, 10, 11, and 12. For small pressure gradients with the pressure decreasing downstream, the computed effect on the contour diagram representation is to move the contours closer to the axis of abscissa, i. e., to decrease the rate of thickening of the boundary layer. The \bar{u} or \bar{v} curve is not independent of x ; in general \bar{u} increases with \bar{y} more rapidly than for the Blasius case and approaches the asymptote to a given approximation at a smaller value of \bar{y} . The departure from the Blasius curve increases with increasing x . The effect of a small gradient is surprisingly large.² The references cited may be consulted for a detailed discussion.

Transition.—The physical factors that determine the transition from laminar to eddying flow are not clearly understood. The principal theoretical developments have proceeded from the assumption that the origin of eddying flow is to be sought in the instability of the laminar flow under certain circumstances. The difficult mathematical computations have been made by Tollmien (reference 13) and Schlichting (reference 14) of the Göttingen group for the following idealized case. A steady two-dimensional laminar flow is assumed in which the velocity depends only on the coordinate normal to the direction of flow. Small disturbances are superposed on this basic flow in the form of waves propagated in the direction of flow. These disturbances are assumed to satisfy the Navier-Stokes equations and the usual boundary conditions. It is then determined whether waves of any given frequency are damped or amplified.

In the computation it is found necessary, in order to obtain a *linear* differential equation, to assume the amplitude of the disturbances sufficiently small that

only first-order terms need be retained. The viscosity effects are assumed small, zero in fact, except near the boundary and in a critical layer where the wave velocity of the disturbance equals the speed of the basic flow. If the viscosity were neglected everywhere, the amplitude of the disturbance would become infinite in this critical layer, thus invalidating the neglect of terms of higher order than the first.

The results obtained for the Blasius distribution of the preceding section as the basic flow are given in figure 2. The region marked "unstable" represents those values of Reynolds Number and wave length for which small disturbances are amplified. Disturbances for wave lengths and Reynolds Numbers outside that region are damped. The displacement thickness δ^* is used as the characteristic length in the Reynolds Number and as the unit for measuring the wave length.

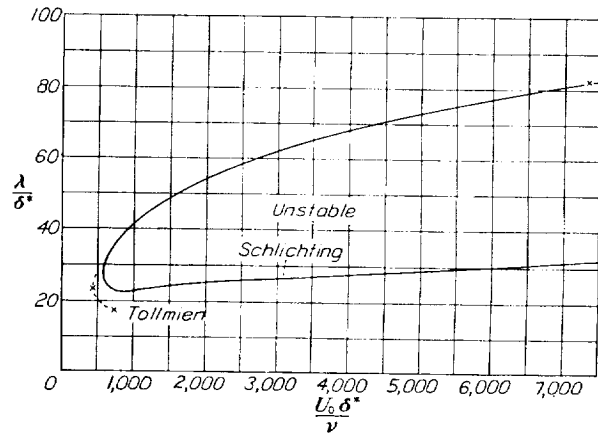


FIGURE 2.—Wave length of sinusoidal disturbances which produce instability of laminar flow near a plate according to Tollmien and Schlichting. λ is the wave length, δ^* is the displacement thickness of the boundary layer, U_0 the speed of the free stream, ν the kinematic viscosity.

Tollmien (reference 15) has shown that velocity distributions having an inflection point, which occur in boundary layers when the pressure increases downstream, are unstable and that the amplification of small disturbances is of a higher order of magnitude than the one found for the Blasius distribution. Thus the non-dimensional amplification factor is of the order of 0 to 0.05 for the distribution with inflection point as compared with 0 to 0.007 for the Blasius distribution.

These theoretical calculations are of the utmost importance in the study of the origin of eddying flow. The amplified disturbances do not, however, in themselves constitute eddying flow. The wave lengths of the amplified disturbances are of the order of 25 to 50 or more times the displacement thickness. Schlichting (reference 14) computed the maximum possible amplification of the disturbances and concluded that a fourfold to ninefold amplification appeared sufficient to produce eddying flow from the long-wave disturbances as judged by a comparison of experimentally observed transition points with the theoretically computed maximum amplification in passing along the plate to the

² See also page 341

observed transition point. It appears to be the opinion of Tollmien that the formation of velocity distributions with inflection points constitutes an intermediate step in the development of eddying flow, these distributions arising as the long-wave length disturbance increases in amplitude.

An attempt was made by Nikuradse (reference 16) to check the theory. A glass plate with a faired leading edge of metal was set up in a water channel provided with slightly diverging walls to give constant static pressure along the plate. The disturbances in the flow were reduced as much as possible, giving a transition at an x -Reynolds Number of 655,000 or a δ^* -Reynolds Number of 1,400. Artificial disturbances of approximately sinusoidal character and of varying frequency were produced by a varying suction applied to holes in the faired leading-edge strip. Except for three points at very low frequency, transition occurred at a δ^* -Reynolds Number between 790 and 1,050, the majority of the points scattering about a value of 850. There was no indication that the frequency of the disturbance had any marked effect as would be inferred from the computations of Tollmien and Schlichting. Nikuradse states, "Perhaps the explanation is that, since the disturbance impressed on the boundary layer is not of perfectly sinusoidal form, some harmonic of the disturbance acts to produce turbulence. A clear decision for or against the Tollmien theory is accordingly still lacking."

In the opinion of the author the numerous experiments on the critical Reynolds Number of spheres and airship models in relation to measurements of the fluctuations present in the air stream furnish additional evidence that it is the amplitude of the disturbances initially present rather than their frequency which is of primary importance and, as in Nikuradse's experiments, if the amplitude is fixed, the point of transition is but little affected by the frequency, provided the frequency is not too low.³

The theory of small vibrations in which only first-order terms are retained cannot give any information as to the influence of amplitude of the fluctuations originally present in the flow. In reference 17 the author outlined briefly the following conception of the mechanism of transition:

The observed fluctuations of speed at a fixed point may be taken as an indication that at any one time there are variations of speed along the outer edge of the boundary layer. With the speed variations there will be associated variations of pressure, and in the regions where the speed is decreasing, the pressure will be increasing. The magnitude of the pressure gradient depends on the amplitude and frequency of the speed fluctuations, increasing as either increases. At a sufficient distance from the leading edge, the thickness of the boundary layer will be such that there will be a reversal of the direction of flow near the surface in those places where the pressure is increasing downstream. Larger speed fluctuations bring larger

pressure gradients and an earlier reversal of flow. It seems very probable that such a reversal would give rise to the formation of eddies.

This conception differs from that of Tollmien in that (1) the disturbances are "forced" by the external turbulence rather than being "free vibrations" and (2) the eddying flow is assumed to originate in velocity distributions with reversed flow which occur as a result of separation rather than in distributions which have only inflection points.

Some computations have been made to show the sensitivity of a boundary layer to small pressure gradients and the facility with which separation occurs. The computations were made by a modification of Pohlhausen's method, which has been described in reference 11. The problem treated was that of the laminar boundary layer of a plate in a steady external flow

$$\frac{U}{U_0} = 1 + 0.02 \sin \left(2\pi \frac{x}{\lambda} - \alpha \right)$$

In other words, a sinusoidal variation (with distance x) of amplitude equal to 2 percent of the mean speed, wave length λ , and phase α relative to the leading edge of the plate was superposed on the uniform flow of speed U_0 . Computations were made for ten values of α corresponding to displacement of the sine wave by steps of 0.1λ . The speed distributions obtained for two values of α are shown in figure 3. Separation occurs at the points indicated.

Each of these computations refers to a steady flow, the distribution being independent of the time. As a rough approximation to a traveling wave we may, however, consider the sine wave slowly displaced along the plate and inquire as to the value of the mean speed at a given point and of the variation of the speed at that point. The mean speed is found to be practically identical with the Blasius distribution. The speed fluctuations expressed as root-mean-square values are plotted in figure 4.

The essential features of the results to which we shall have occasion to refer are as follows:

1. The mean speed is practically unaffected by this simplified turbulence of the external flow.
2. There are speed variations within the boundary layer which are much larger than those in the external flow. Their amplitude increases with distance from the leading edge of the plate.
3. The point of separation is not fixed but moves back and forth within certain limits.
4. The position of the separation point and the distribution of the speed variations depend on the wave length λ .
5. While computations for only one amplitude have been made in full, it may be shown that there is a marked dependence of the location of the separation point on the amplitude of the speed variation in the external flow.

³ It is known that there is some effect of "average size of eddies" on the critical Reynolds Number of a sphere, but the effect is of a lower order of magnitude than the effect of amplitude of the speed fluctuation.

The variation of speed in the external flow along the plate at any given instant is not sinusoidal in character, and it is not at all evident that the quasi-stationary method of computation is justified. All the results listed, however, are in agreement with experimental data except 4, the effect of wave length. The two theories of the transition are, in a sense, supplementary. If the fluctuations are extremely small, eddying flow may arise in the Tollmien manner from accidental disturbances. If the fluctuations are sufficiently large,

view of the large effect of frequency required by both, which was not found in Nikuradse's experiments.

Eddying flow.—In experimental work on eddying flow, the distribution of mean speed near a wall is found to be represented fairly well by a power law of the form $u=ay^n$, where u is the mean speed, y the distance from the wall, and a and n are empirical constants. For Reynolds Numbers that are not too large, n is approximately $1/7$ and this value has been much used as the starting point in computing the friction.

This purely empirical representation has been superseded by a formula having some theoretical backing, namely,

$$u = \left(\frac{\tau_0}{\rho}\right)^{1/2} \left[a + \frac{1}{k} \log \left(\frac{\tau_0}{\rho} \right)^{1/2} \frac{y}{\nu} \right] \quad (13)$$

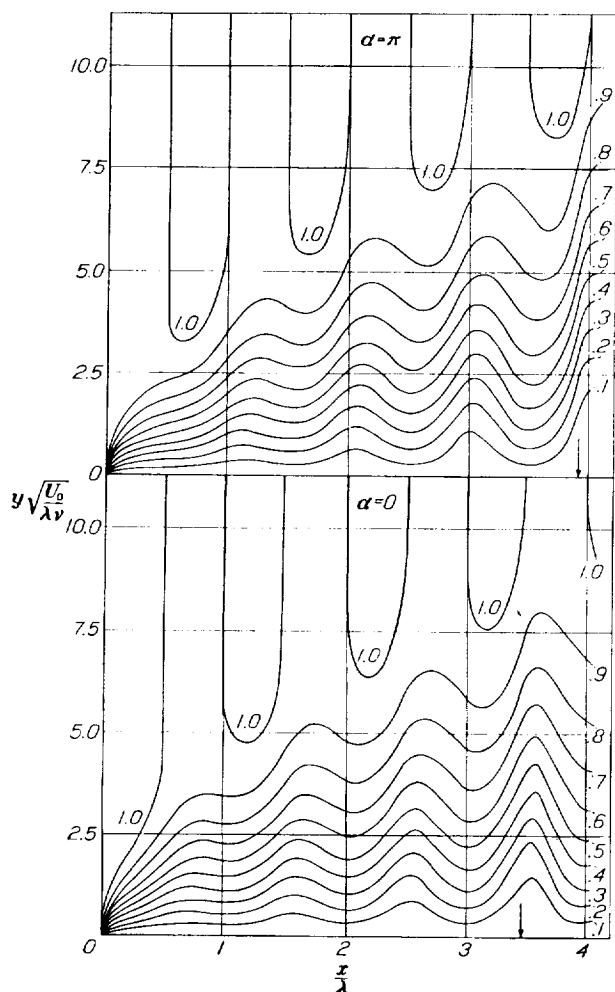


FIGURE 3.—Computed distribution of mean speed in the boundary layer of a plate for the external flow $U/U_0 = 1 + 0.02 \sin(2\pi x/\lambda - \alpha)$. The contours are contours of equal values of u/U_0 . Separation begins at the points indicated by arrows.

as probably happens in most practical cases, the eddying flow arises from the forced fluctuations of the boundary layer. The two pictures agree in exhibiting fluctuations of wave lengths that are long as compared with the thickness of the boundary layer. These fluctuations produce pressure gradients as a preliminary step. The long-wave disturbances do not themselves constitute eddying flow, although they involve comparatively large speed fluctuations. The correctness of either picture must be left an open question in

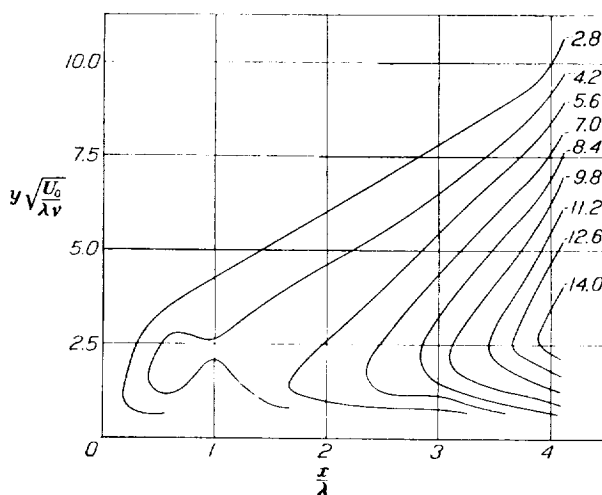


FIGURE 4.—Computed root-mean-square fluctuation of speed for the flow of figure 3 when α is varied from 0 to 2π . The contours are contours of equal values of the root-mean-square u -fluctuation expressed in percent of the speed of the free stream. In the free stream the fluctuation is 1.4 percent of the mean speed.

where τ_0 is the shearing stress at the wall, ρ is the density of the fluid, ν the kinematic viscosity, and a and k are constants. This equation is due to von Kármán. (See reference 6.)

The original paper should be consulted for a detailed discussion of the theory. The formula is derived for the idealized case of a constant shearing stress transferred in parallel flow along a wall. Both in a pipe and near a wall, the shearing stress is not constant but decreases with increasing distance from the wall. Nevertheless the formula is found experimentally to fit the velocity distribution as far as the center of the tube or the outer edge of the boundary layer, and the constant k is nearly the same whether computed from velocity distribution in smooth or rough pipes or near a wall, or from skin-friction measurements in smooth or rough pipes or on plates.

For the case of the skin-friction plate, it is convenient to set $\frac{2\tau_0}{\rho U_0^2} = c_f$ the local friction coefficient,

and to write equation (13) in the form

$$\frac{u}{U_0} = \left(\frac{c_f}{2}\right)^{1/2} \left[a + \left(\frac{1}{k}\right) \log \left(\frac{c_f}{2}\right)^{1/2} \left(\frac{U_0 y}{\nu}\right) \right] \quad (14)$$

Then setting $y = \delta$ for $\frac{u}{U_0} = 1$ and subtracting the resulting equation from (14), we find

$$\frac{u}{U_0} - 1 = \frac{(c_f/2)^{1/2}}{k} \log \frac{y}{\delta} \quad (15)$$

In order to show the similarity with the power-law formula, (15) may be written

$$e^{\frac{u}{U_0} - 1} = \left(\frac{y}{\delta}\right)^{\frac{(c_f/2)^{1/2}}{k}} \quad (16)$$

For small values of $\frac{u}{U_0} - 1$, the term on the left may be expanded in the series $1 + \left(\frac{u}{U_0} - 1\right) + \frac{1}{2} \left(\frac{u}{U_0} - 1\right)^2$ etc., whence, retaining only the first two terms

$$\frac{u}{U_0} = \left(\frac{y}{\delta}\right)^{\frac{(c_f/2)^{1/2}}{k}} \quad (17)$$

Thus the exponent in the empirical power law representation may be expected to be a function of the local friction coefficient, and the power law representation itself may be expected to be valid only for small values of $\frac{u}{U_0} - 1$.

The velocity distribution in the laminar sublayer near the wall may be approximated by solving the equation $\tau_0 = \mu \frac{du}{dy}$, assuming τ_0 constant. The result is

$$u = \frac{\tau_0}{\rho \nu} y \text{ or } \frac{u}{U_0} = \frac{c_f}{2} \frac{U_0 y}{\nu} \quad (18)$$

From von Kármán's universal velocity distribution near a smooth wall, which was based on the data of Nikuradse, the transition between (18) and (14) extends from $(c_f/2)^{1/2} \frac{U_0 y}{\nu} = 8$ to $(c_f/2)^{1/2} \frac{U_0 y}{\nu} = 100$. For $c_f = 0.01$, the range of $\frac{U_0 y}{\nu}$ is from 113 to 1,413; for $c_f = 0.001$, the range is from 358 to 4,473. Hence (14) cannot be expected to hold accurately for $\frac{U_0 y}{\nu} < \text{about } 4,000$.

MEASUREMENTS AT THE NATIONAL BUREAU OF STANDARDS

APPARATUS

Wind tunnel.—The measurements were made in the 3-foot wind tunnel of the National Bureau of Standards from December 1929 to November 1930. A sketch of the tunnel and a brief description are given in reference 18. The tunnel is of the room return type with closed cylindrical working section, 6 feet long and 3 feet in diameter. The area of the entrance cross section, at which the honeycomb is located, is 5.44 times the working cross section. The turbulence at the working section is 0.5 percent, the critical Reynolds Number for a 5-inch sphere being 270,000.

The plate.—Two plates were used in the course of the work. Each was a polished aluminum plate, $\frac{1}{8}$ inch thick and 2 feet wide. In the preliminary series of measurements, the plate was 49 inches long and the leading edge was beveled as indicated at E in figure 5. Since the preliminary measurements indicated a considerable disturbance at the leading edge, this plate

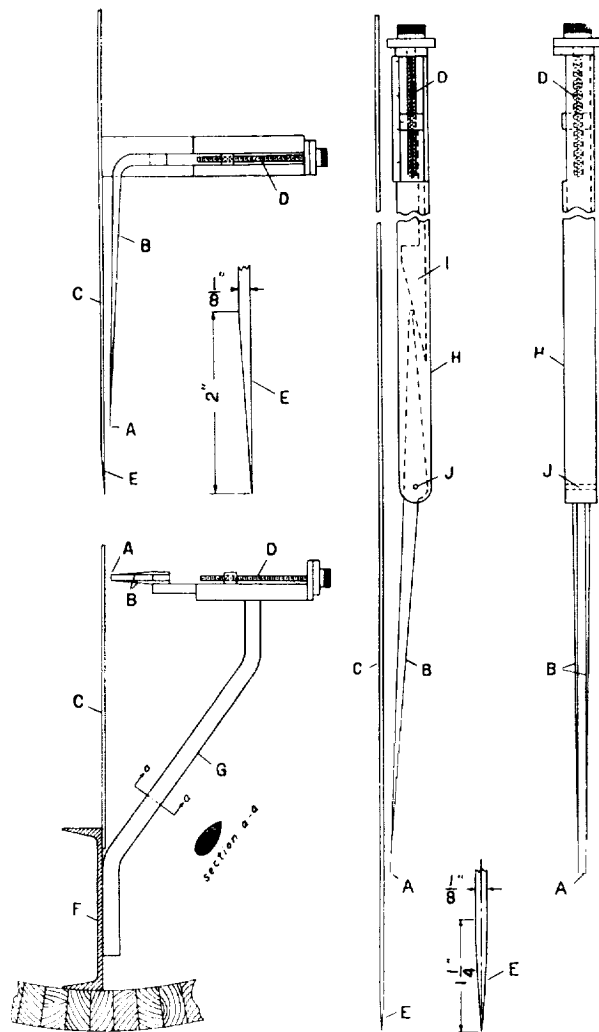


FIGURE 5.—Traverse mechanism and leading edge shape used in the preliminary measurements (series A).

FIGURE 6.—Traverse mechanism and leading edge shape used in the later measurements (series B, C, and D).

was discarded. A new plate, 60 inches long, with leading edge sharp and symmetrically shaped as shown at E in figure 6 was used for all other measurements.

The plate was mounted on two light 7-inch channels as shown at F in figure 5. The channels ran longitudinally parallel to the axis of the wind tunnel, one flange of each channel being fastened to the tunnel wall. The webs furnished supports for the edges of the plate and filled the gap between the edges of the plate and the tunnel wall.

The upstream edge of the plate was approximately 2 feet downstream from the upstream end of the working section and the downstream edge was within the expanding exit cone.

The hot-wire anemometer.—The speeds were measured by a hot-wire anemometer and associated equipment. The wire used was a platinum wire 0.017 mm in diameter and about 8 mm long. This very small wire was used to permit measurements of rapid fluctuations in speed as well as the mean speed.

In the preliminary series of measurements, the mounting shown in figure 5 was used. The wire A was mounted at the ends of the prongs B which ran downstream from the wire for about 12 inches. The prongs were bent at right angles and supported on a movable slide, which in turn was supported from the lower channel F by the bent streamline bracket G. The position of the wire relative to the plate C was varied by means of the micrometer screw D. The reading of the screw for zero distance was determined either by moving the wire in until the prongs touched the plate as determined by an auxiliary electric circuit or, better, by observing the reflection of the wire in the mirror surface of the plate. When observing the reflection, the mounting could be adjusted by shimmiing the bracket until the wire was accurately parallel to the plate.

Since the wire expands when heated and contracts when cooled, the prongs must be flexible. Otherwise a wire which is taut and straight when cool will become slack when heated or, if adjusted when heated, it will break when the heating current is shut off. Satisfactory results were obtained by using fine steel needles for the extreme tips. The fine platinum wire was electrically welded to the needles.

The long bracket G of this mounting tended to vibrate at high wind speeds, making the distances of the wire from the plate uncertain and a small but measurable effect on the static pressure at the position of the wire was detected. The slide and bracket block an undesirably large percentage of the area of the air stream. Hence when the preliminary measurements were completed, a new and improved mounting was constructed.

The improved mounting (fig. 6) was contained wholly within a tube H having a cross section about 1 inch square. The axis of the tube was parallel to the air flow and the tube was clamped directly to the plate with small spacing blocks between the tube and the plate. The wire prongs were rotated about the fulcrum J (fig. 6) by the cam I, which was moved by the micrometer screw D. The wire was 13.28 inches from the fulcrum, so that for small lateral displacements the wire moved practically at right angles to the plate. The micrometer screw was calibrated in terms of lateral movement of the wire in an auxiliary apparatus in which the lateral displacement was measured by means of a second micrometer screw.

The improved mounting showed no observable effect on the static pressure at the wire position and the blocking was inappreciable. The vibration of the wire relative to the plate was greatly reduced. There is perhaps some slight deflection of the prongs at high wind speeds because of wind pressure on the prongs.

The associated equipment is essentially as described in the appendix to reference 18. The fundamental theory of the hot-wire anemometer as used for measuring mean speed and fluctuations in the mean speed is given in reference 7. The performance of the particular equipment used in these measurements as regards accuracy of compensation for the lag of the wire is given in figure 1 of reference 17. The measurements were completed before the development of the improved equipment described in reference 19.

REDUCTION OF OBSERVATIONS

At a given distance from the front edge of the plate and for a given speed, the following observations were made:

1. Micrometer reading for $y = 0$.
2. Voltage of potentiometer battery (by comparison with standard cell).
3. Resistance of wire at air temperature.
4. Voltage drop across wire for various air speeds with wire about 1 inch from plate (i. e., in free air stream).
5. For 10 or 15 values of y , values of the average voltage drop and the root-mean-square voltage fluctuation. The average current through the wire was adjusted to be 0.2 ampere at each value of y . The resistance to be used in the compensation circuit of the amplifier was computed and the adjustment made at each value of y . The amplifier was calibrated before and after the series.
6. Items 1, 2, 3, 4 were repeated in reverse order.
7. Frequent observations were made of air temperature, and the barometric pressure was read at the beginning and end of the series.

Calibration of the wire.—The relationship between the heat loss H and the speed u is given by the formula

$$H = (A + B\sqrt{u})\theta \quad (19)$$

where θ is the difference in temperature between the wire and the air and A and B are constants for a given wire. If i is the heating current and R the resistance of the heated wire (exclusive of the leads) when exposed to the stream, $H = i^2 R$. Denoting the resistance of the wire at air temperature by R_0 and the temperature coefficient of resistance referred to that temperature by α

$$\theta = \frac{R - R_0}{R_0 \alpha} \quad (20)$$

Thus the calibration formula (19) may be written in the form

$$\frac{H}{\theta} = \frac{i^2 R R_0 \alpha}{R - R_0} = A + B\sqrt{u} \quad (21)$$

The product $R_0\alpha$ is equal to the slope of the curve of resistance plotted against air temperature and is approximately independent of the air temperature.

Two typical calibration runs are shown in table II and figure 7. In the table the details of the computation of the true speed u from the pressure developed by a reference static plate and the air density are omitted, since the procedure is well known. The two calibrations at the beginning and end of the series of observations show very satisfactory agreement. Such good agreement was not obtained in all cases, especially when the wire was subjected to speeds of 130 to 150 feet per second. In those instances where the calibration curves were different, an interpolation was made. In about one-third of the 62 series of observations made, the calibration curves at the beginning and end agreed as well as those shown in figure 7. In some 25 series the

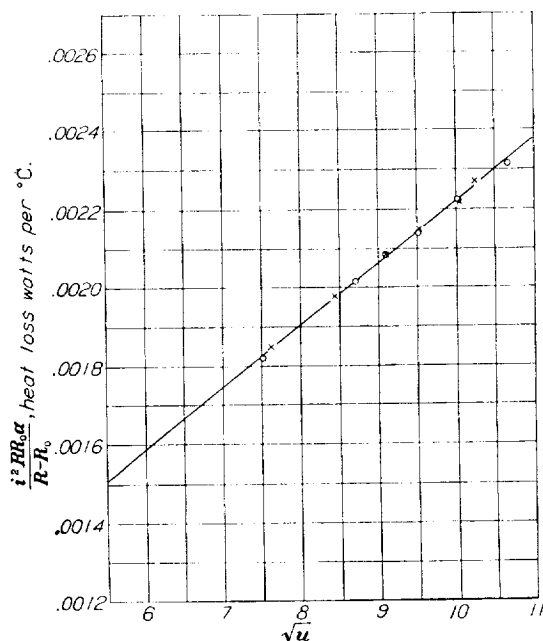


FIGURE 7.—Calibration curves for hot-wire anemometer. u is the air speed in feet per second. See text for explanation of other symbols. The dots and crosses distinguish the calibrations at the beginning and end of a series of observations of distribution of mean speed and speed fluctuation.

difference corresponded to a shift in the value of u/U_0 of 0.01 to 0.03, so that the interpolated values have a probable precision of about 0.01. In the remaining 16 series, the difference corresponded to a shift in u/U_0 greater than 0.03, rarely exceeding 0.06. In these cases the interpolated values have a probable precision of about 0.02. The use of the small diameter wire required to obtain fluctuation measurements impairs somewhat the precision of the measurements of mean speed.

Determination of the mean speed.—The determination of the mean speed in one series is illustrated in table III. The detailed micrometer readings and potentiometer readings are omitted, only the final values of y and of the voltage drop being given. The

procedure may seem somewhat cumbersome, since one might plot the observed voltage drop in the calibration runs against speed and from such curves read off the speeds corresponding to the observed voltage drop in table III. The advantage of the procedure followed is the linear form of the calibration curve and its independence of air temperature. The final values obtained are not significantly affected by comparatively large changes in R_0 and α so that these quantities do not need to be known with high precision.

Heat loss due to presence of the plate.—When a hot-wire anemometer is used near a solid wall, the heat loss at a given speed is probably affected by the presence of the wall. In still air, the effect is quite perceptible at distances of about 0.08 inch from the wall. The magnitude of the effect is known to be a function of the speed, decreasing as the speed increases (reference 20). No entirely satisfactory procedure has been devised for this effect.

Van der Hegge Zijnen determined the heat loss in still air as a function of the distance from the surface and the temperature difference between the wire and the surroundings. He then deducted from the observed heat loss in his experiments the excess heat loss found in still air at the same distance and temperature difference above the heat loss at a large distance from the plate.

A similar determination of the heat loss in still air was made in the present series of experiments and it was found that for temperature differences θ from 100° C. to 400° C., distances y 0.004 to 0.070 inch, the heat loss H_p due to the plate could be represented by the empirical formula

$$H_p = 0.0000000127 \frac{l}{y} \theta^2 \quad (22)$$

where l is the length of the wire in inches, and H_p is measured in watts.

The result of applying this correction to the results of table III is shown in table IV. The value of u/U_0 at $y=0.015$ inch is reduced by 0.05.

Van der Hegge Zijnen noted that in some instances application of the correction gave S-shaped curves. He also found that the speed-distribution curves did not pass through the zero of the diagram and he arbitrarily decreased the y values by amounts from 0 to 0.005 inch to make them pass through zero. It is significant that application of the heat-loss correction based on still air determinations will produce a change in the intercept on the y axis in the direction observed.

On the basis of the results obtained for the laminar part of the boundary layer, which will be discussed later and the results of Schubauer (reference 21), it seems best to make no correction for heat loss when the flow is laminar and the speed is greater than 3 feet per second. In the absence of further information on the behavior of the wire when the flow is eddying, no correction has been made in that case either.

Determination of fluctuations.—The root-mean-square fluctuation in speed may be determined by measuring the root-mean-square fluctuation in voltage drop across the wire by means of a calibrated amplifier suitably compensated for the lag of the wire. Since the cooling is approximately independent of the direction of the air flow, the fluctuations are fluctuations of the absolute value of the velocity but, since the u -component of the fluctuation adds algebraically to the mean speed u whereas the v -component is at right angles, the fluctuation is primarily the u -fluctuation and is so designated in this paper.

The relation between speed fluctuation and voltage fluctuation may be found by differentiating (21) permitting i and R to vary, as follows:

$$\frac{2iRR_0\alpha}{R-R_0}di - \frac{i^2R_0^2\alpha}{(R-R_0)^2}dR = \frac{B}{2} \frac{du}{\sqrt{u}} \quad (23)$$

To connect di and dR , we have the relation

$$12 = i(R+r) \quad (24)$$

where 12 is the battery voltage and r is the resistance of the heating circuit, excluding that of the wire. Hence

$$di = \frac{-i dR}{R+r} = -\frac{i^2 dR}{12} \quad (25)$$

and we find on substitution in (23), setting $i dR = dE$

$$\frac{du}{u} = -\frac{2}{B\sqrt{u}} \left[\frac{iR_0^2\alpha}{(R-R_0)^2} + \frac{1}{6} \frac{i^2RR_0\alpha}{R-R_0} \right] dE \quad (26)$$

If root-mean-square values are considered, the minus sign may be omitted.

A typical determination, omitting details of the computation of the compensation resistance and calibration of the amplifier, is shown in table V.

If a correction had been applied for heat loss according to (22), it is easily shown that a third term is added within the brackets on the right-hand side of (26) equal to $\frac{0.000\ 000\ 0127}{yiR_0\alpha}$. The effect of making this correction to the results of table V is shown in table VI.

The values of $\frac{du}{u}$ are modified but there is very little change

in the values of $\frac{du}{U_0}$.

Fairing of results for preparation of contour diagrams.—In order to prepare contour diagrams, the results of each series were plotted as shown in figure 8 and values read from faired curves at even intervals of u/U_0 and du/U_0 as illustrated in table VII. The x and y Reynolds Numbers were computed. It may be remarked in passing that figure 8 illustrates the distribution of mean speed and u -fluctuation near the beginning of the transition region.

It does not seem practicable to present the original observations of the 62 series of observations. The sample series gives some idea of the precision and accuracy of the observations. In general, it is believed that the errors in y do not exceed 0.003 inch (except in

the preliminary series A), the errors in u/U_0 do not exceed 0.02, and the errors in $100 \frac{du}{U_0}$ do not exceed 0.2 except for the very high values in the transition region. The contour diagrams used to present the results can be read easily to this precision.

No corrections have been applied for heat loss to the plate.

PRELIMINARY MEASUREMENTS WITH PRESSURE GRADIENT

The measurements now regarded as preliminary measurements (series A) were not so intended when the work was begun. They are here reported in spite of some inadequacies because some of the results are of interest and the experiments with pressure gradient were not repeated with the improved equipment.

The plate (fig. 5) and the traversing apparatus have already been described. The equipment was installed in the wind tunnel and the plate was alined to give a symmetrical wake as determined by a pitot tube. This installation required setting the plate at an angle of approximately 0.1° to the axis of the tunnel. Although

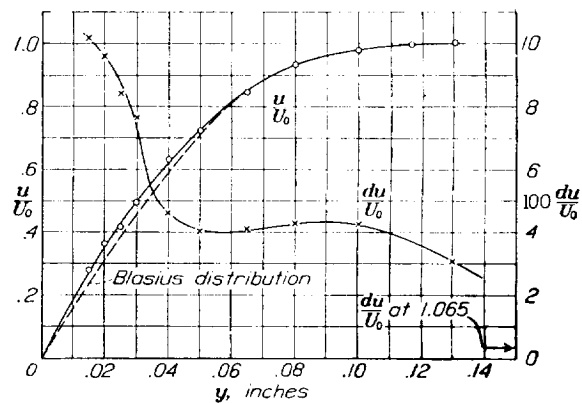


FIGURE 8.—Distribution of mean speed and u -fluctuation at $x=23$ inches for $U_0=105.2$ feet per second. Turbulence of free stream, 0.5 percent.

this necessity indicated at once that the leading-edge form was probably not the most desirable one, it was decided to proceed with some measurements.

The pressure gradient along a line parallel to and 9 inches from the plate is shown in figure 9. For the most part the pressure gradient is not constant. There is, however, a distance of about 2 feet, beginning about 8 inches downstream from the leading edge, over which the pressure falls at the rate of about 1.7 percent of the velocity pressure per foot.

The test speed chosen was approximately 100 feet per second. If transition had occurred at the same x -Reynolds Number (300,000) as in the measurements of van der Hegge Zijnen, it should have been found 6 inches behind the leading edge. Measurements at 6.32 inches and 17.5 inches gave distributions of mean speed of the laminar type although the u -fluctuations were considerably larger than in the general flow. After some study of a very pronounced disturbance

at the leading edge, measurements were made at 35.63 inches from the leading edge where the flow still was of the laminar type. The speed was then increased to 145 and finally to 175 feet per second, at which speeds the transition type of distribution was found at a distance of about 35 inches.

The results of the measurements of mean speed are shown in figure 10, omitting two runs which will be discussed separately. Transition begins at an x -Reynolds Number of approximately 1,800,000. From the plot the values of y appear to be subject to a systematic error, since the 0.3 speed contour is much closer to the wall than three times the distance between the 0.3 and 0.4 speed contour. A detailed study by means of cross plots and comparison with the Blasius distribution led to the conclusion that the values of y are probably too small by about 0.008 inch, corresponding at a speed of 102 feet per second to a displacement of the values of R_y by 400. It appeared

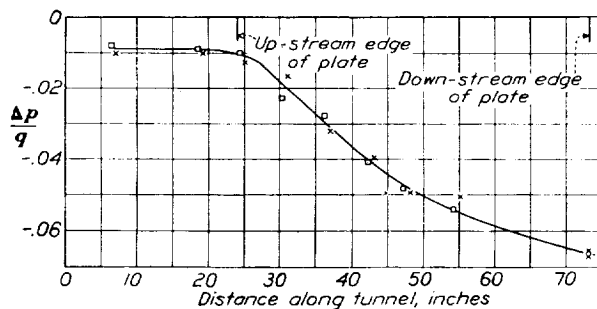


FIGURE 9.—Pressure gradient for measurements of series A (figs. 10 to 14, inclusive). q is the reference velocity pressure. The crosses denote measurements of static pressure; the circles, changes in the velocity pressure plotted with sign reversed. The velocity pressure increases as the static pressure decreases but at the same rate.

that the mounting of figure 5 was not sufficiently rigid. It was found that the mounting vibrated somewhat in the wind with a vibrating motion of perhaps 0.005 inch at the wire. For this reason no great reliance can be placed on the values of y , but the general character of the speed distribution and the value of the x -Reynolds Number for transition are not affected by this uncertainty.

Two runs which have been omitted from figure 10 are worthy of special consideration. After the observations at 102 feet per second were completed, observations were made at 145 feet per second, beginning at a distance of 35.3 inches from the leading edge, then 29.44 inches, each giving a transition type of curve. On the following day measurements were made at 23.31 inches and, surprisingly, the distribution was that characteristic of fully developed turbulent flow. This result seemed unreasonable and the next day a repeat run was made without disturbing the apparatus. The curve obtained was of the transition type, not checking the previous run. A week end intervened and 3 days later a second repeat run was begun. After one observation, which appeared to fall in with the immediately preceding run, it was noticed that the

plate was somewhat dusty and it was decided to clean the plate. This was done and the run continued. The distribution then observed was of the laminar type, the run being that plotted in figure 10 for an x -Reynolds Number of 1,615,000.

The three distributions, all obtained within a few days under presumably identical conditions except for the amount of dust on the plate, are shown in figure 11. This plot gives the essential difference in character of the distribution of mean speed in the laminar, transition, and eddying regimes.

The corresponding u -fluctuations are shown in figure 12. There are illustrated the characteristic distributions of u -fluctuations for the laminar, transition, and eddying regimes.

The observations of u -fluctuations are hardly complete enough to enable the plotting of an accurate contour diagram. The values from faired curves are indicated in figure 13, the two runs previously discussed being omitted. The solid contours are drawn on the assumption that the observations at x -Reynolds Numbers of 117,000 and 1,773,000 are not to be considered. Since the necessity of keeping dust removed from the plate was not appreciated, the various measurements may not be comparable. The location of the contours has been guided to some extent by the results of the later measurements.

One interesting feature is the disturbance near the leading edge. The u -fluctuation in the free stream was only 0.5 percent of the mean speed, whereas in this disturbance the u -fluctuation is 5.0 percent of the mean speed in the free air stream. Evidently the stagnation point is on the inclined leading edge and the flow around the sharp corner sets up an increased turbulence. This turbulence is damped out to some extent along the plate, then increases, slowly at first, but very rapidly in the transition region. The primary purpose of presenting these exploratory measurements is to show that with an accelerating pressure gradient present the strong leading-edge disturbance is not sufficient to produce an early transition.

At 35.5 inches, the flow was still of the transition type, so that completely eddying flow was not obtained in this series of measurements.

When it was realized that the traverse mechanism was not giving sufficiently accurate values of y , that the leading edge shape was very poor, that the plate must be kept free of dust, and that the influence of the pressure gradient was very large, it was decided to make a completely fresh start.

MEASUREMENTS WITH SMALLER PRESSURE GRADIENT

Normal air stream.—As already described a new plate was obtained with sharp symmetrical leading edge and a new traversing mechanism was constructed (fig. 6). In addition, an attempt was made to secure the condition of zero pressure gradient. It was first thought that the desired result might be obtained by a

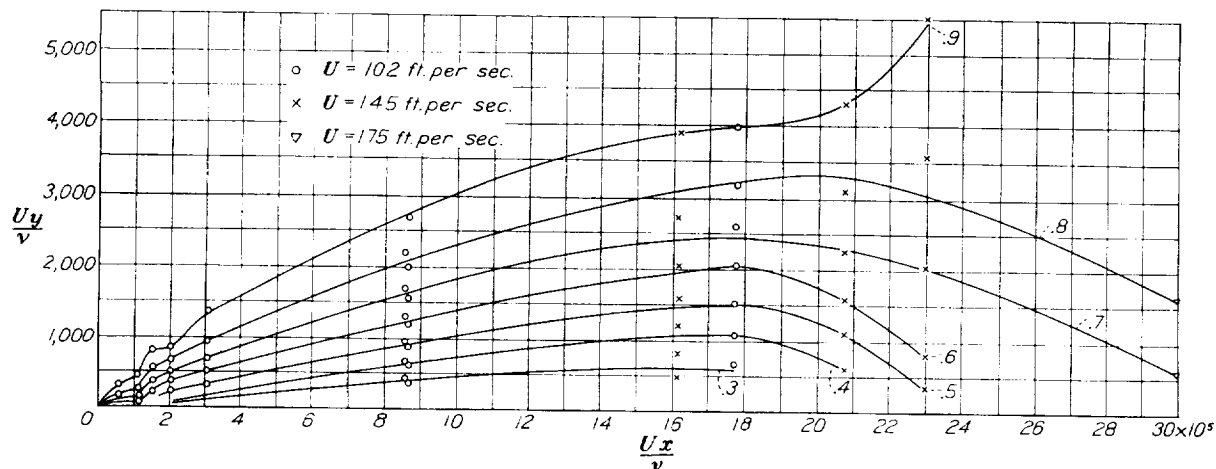


FIGURE 10.—Distribution of mean speed, preliminary series A, with pressure gradient of figure 9, turbulence of free stream, 0.5 percent. See legend of figure 1 for notation. U , the speed of the free stream, increases slightly along the plate. The contours are contours of equal u/U .

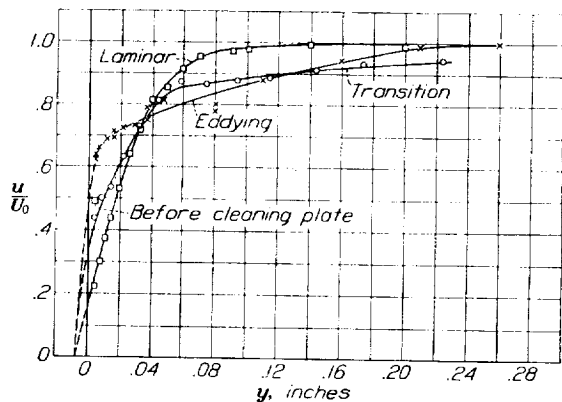


FIGURE 11.—Distribution of mean speed at $x = 23.3$ inches for $U = 145.2$ feet per second, showing effect of roughness produced by dust on the plate. The three curves illustrate distributions of the laminar, transition, and eddying types.

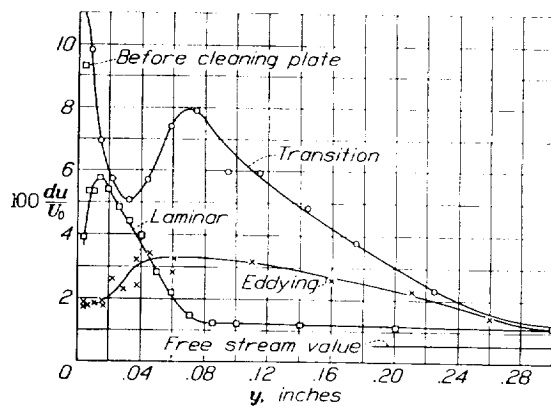


FIGURE 12.—Distribution of u -fluctuation at $x = 23.3$ inches for $U = 145.2$ feet per second, showing effect of roughness produced by dust on the plate. The three curves illustrate distributions of the laminar, transition, and eddying types.

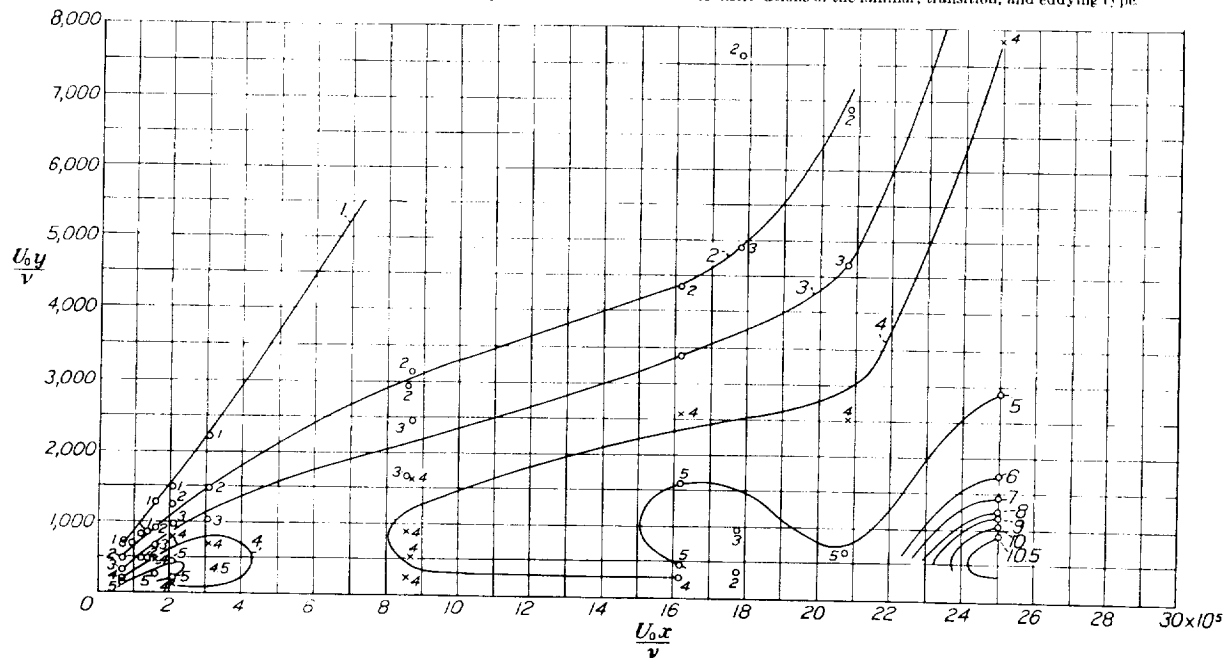


FIGURE 13. Distribution of u -fluctuation, preliminary series A, with pressure gradient of figure 9, turbulence of free stream, 0.5 percent. The contours are contour of equal values of the root-mean-square speed fluctuation expressed in percent of the speed of the free stream. See legend of figure 1 for notation. Note intense leading edge disturbance.

slight inclination of the plate to produce an expanding cross section between the working side of the plate and the wall. Pressure surveys showed considerable local variations near the plate of the nature found for small

Several weeks were spent in modifications of the contour of the blisters to secure approximately zero pressure gradient. The ideal was in no wise attained and the first series of measurements with the improved

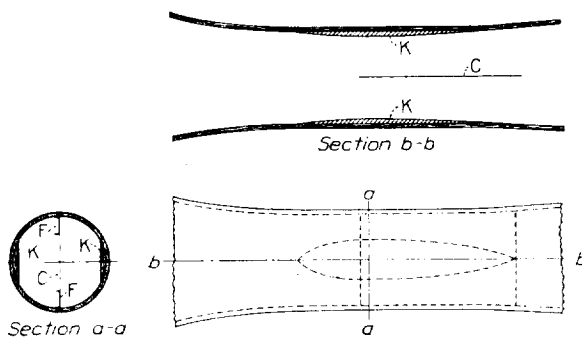


FIGURE 14.—“Blisters” installed in wind tunnel to reduce pressure gradient.

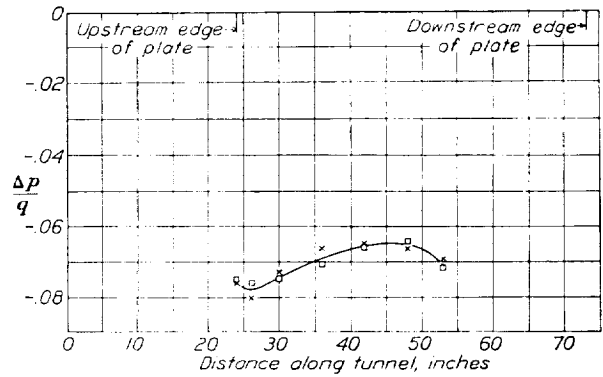


FIGURE 15.—Pressure gradient for measurements of series B and D (figs. 16 to 22, inclusive). See legend of figure 9. The speed of the free stream departs from the mean value by a maximum of 0.4 percent.

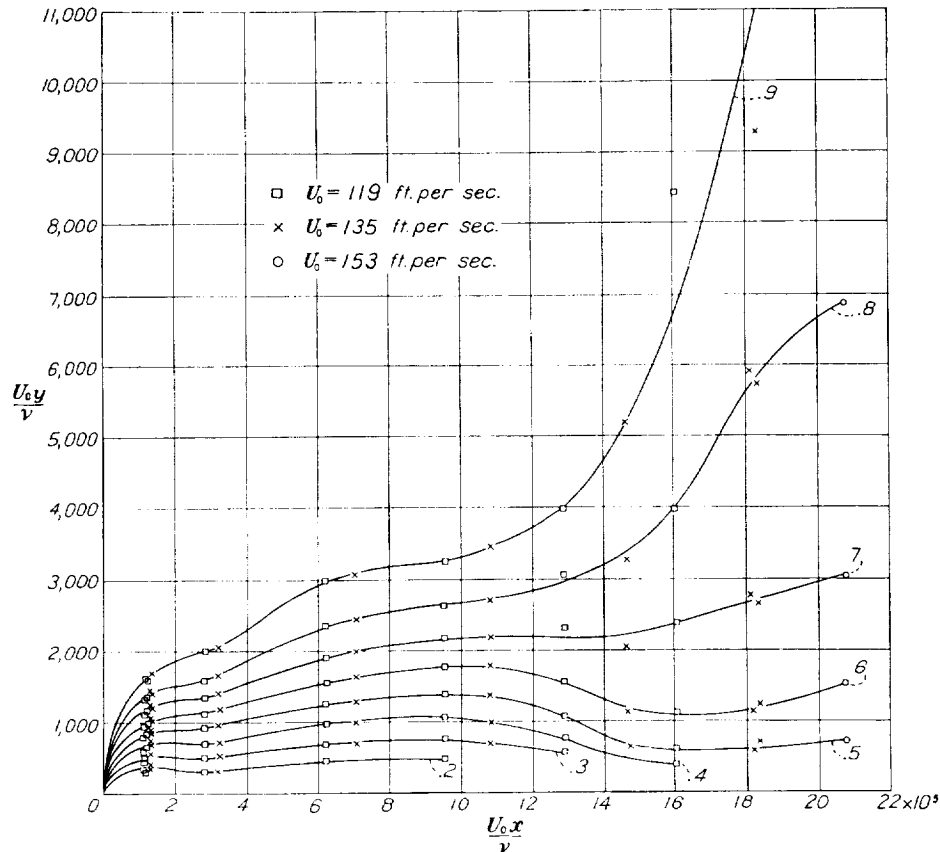


FIGURE 16.—Distribution of mean speed, series B, with pressure gradient of figure 15, turbulence of free stream, 0.5 percent. See legend of figure 1 for notation.

plates set at a small angle of attack. Attention was then turned toward producing the expanding cross section by suitable blocking at the tunnel walls. The general form and scale of the “blisters” applied to the tunnel wall is shown in figure 14 at K.

apparatus was made under the pressure gradient shown in figure 15. The pressure falls slightly for 2 inches, then rises at the rate of about 0.9 percent of the velocity pressure per foot for about 19 inches, then falls at a rate of about 1 percent of the velocity pressure per

foot. By comparison with figure 9, the total range in pressure has been reduced to one-fourth of that previously found and the maximum gradient has been reduced to about one-half that previously found, with gradients of both signs occurring.

In the first series of measurements (series B), only mean speeds were determined. Sixteen traverses were

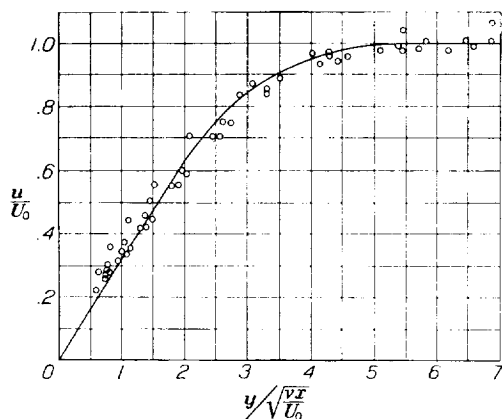


FIGURE 17.—Distribution of mean speed, for $x=5, 11$, and 17 inches, series B, plotted for comparison with the Blasius distribution.

made in all, at distances 2, 5, 11, 17, 22.8, and 28.8 inches from the leading edge, at speeds of 119 and 135 feet per second except for one run at 28.8 inches for which the speed was 153 feet per second. The contour

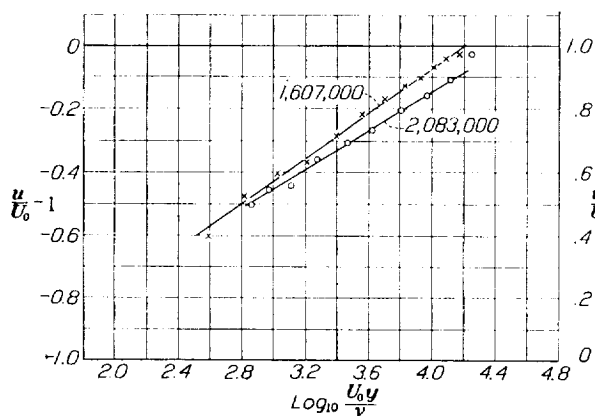


FIGURE 18.—Distribution of mean speed, for x -Reynolds Numbers 1,607,000 and 2,083,000, series B, plotted for comparison with the logarithmic distribution.

diagram prepared from faired curves similar to figure 8 is shown in figure 16.

Transition begins at an x -Reynolds Number of about 1,100,000. The observations for the several speeds are quite concordant and there is no indication of any systematic error in the values of y , except possibly at the 2-inch station (x -Reynolds Number about 120,000).

Figure 17 shows that the results for the 5-, 11-, and 17-inch stations are in very satisfactory agreement with the Blasius theoretical curve. In this figure, the original observations, not faired values, are plotted. The agreement would not have been so good had the

heat loss to the wall in still air been applied as a correction to the observed heat loss.

The data available in the eddying region are hardly sufficient to make possible any extensive analysis. In figure 18 observations for x -Reynolds Numbers of 1,607,000 and 2,083,000 are plotted in a form suggested by equation (15). This equation represents the data

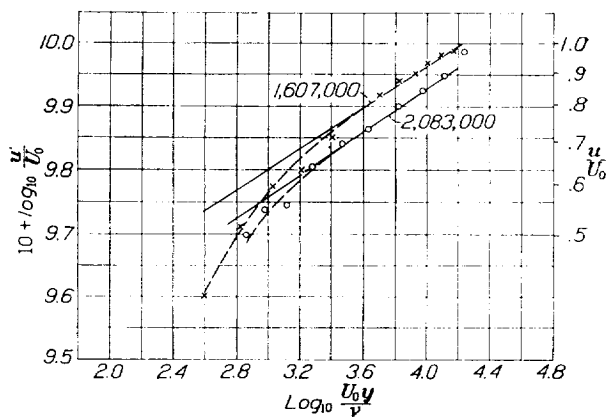


FIGURE 19.—Distribution of mean speed, for x -Reynolds Number 1,607,000 and 2,083,000, series B, plotted for comparison with the power-law distribution.

well within the precision of the observations over a wider range than the power law representation shown in figure 19. The lines drawn in figure 19 correspond to exponents of 0.16 and 0.17.

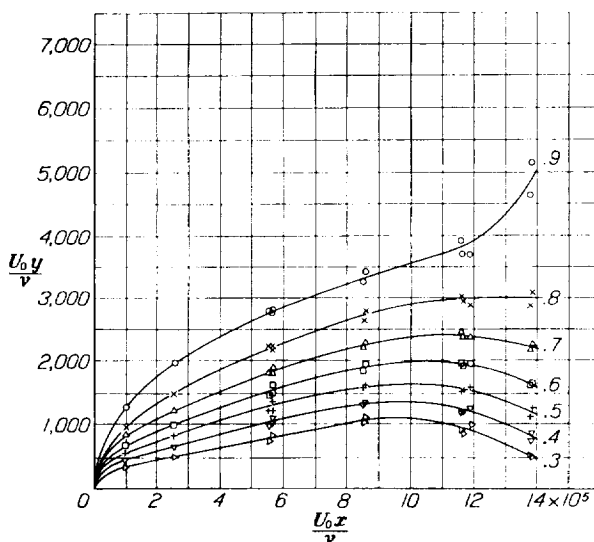


FIGURE 20.—Distribution of mean speed, series D, with pressure gradient of figure 15, turbulence of free stream, 0.5 percent. See legend of figure 1 for notation.

The first series of measurements of mean speed only (series B) was made during the month of June 1930. In October, after the completion of some measurements with increased turbulence of the wind stream, a second series of measurements (series D) was made in which both mean speed and u -fluctuations were determined. Twelve traverses were made, at distances of 2, 5, 11, 17, 23 and 28 inches, at a speed of 105

feet per second. The contour diagram of the distribution of mean speed is shown in figure 20.

Comparison of the original observations for the 2-, 5-, 11-, and 17-inch stations with the Blasius curve is made in figure 21. There is some evidence of a systematic error in y of the order of 0.001 inch, the observed values being too large. From the construction of the traverse mechanism, the effect of wind load on the prongs would be to deflect the mounting toward the plate. Such an effect is not indicated, however, in the earlier series (fig. 17). In view of the difficulty of the measurements, it seems quite clear that the Blasius curve is an accurate representation of the laminar portion of the velocity field near a plate with sharp

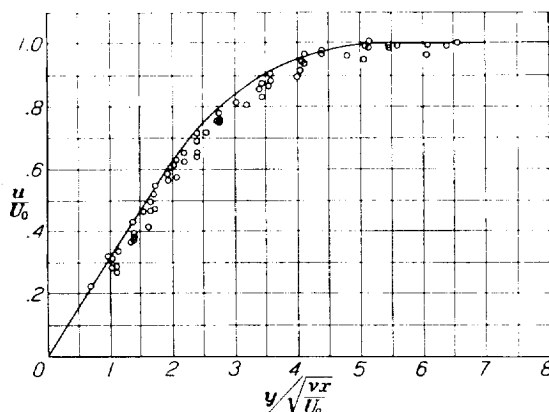


FIGURE 21.—Distribution of mean speed, for $x=2, 5, 11$, and 17 inches, series 1D, plotted for comparison with the Blasius distribution.

symmetrical leading edge in a stream without appreciable pressure gradient.

No observations of this series fall within the eddying region.

The contour diagram of the u -fluctuations is shown in figure 22. It is not possible without greatly confusing the diagram to show either original observations or faired values. In one traverse at 11 inches, the fluctuations were abnormally large and not concordant with two additional traverses at the same station. The cause is not known, and results for this one traverse have not been considered. Otherwise, the individual traverses were reasonably concordant, and it has only been necessary to smooth out minor inconsistencies. The faired values from which figure 22 was prepared are given in table VIII. The u -fluctuation in the free air stream was 0.5 percent of the mean speed.

The interesting features of figure 22 are the leading-edge disturbance, which has not been completely eliminated; the fluctuations in the laminar region of magnitude about three times the free-stream fluctuation; the increasing amplitude of fluctuation beginning at an x -Reynolds Number of 700,000, as compared, with transition at 1,100,000 as inferred from the distribution of mean speed; and the large amplitude of fluctuation in the transition region.

Artificially turbulent air stream.—The very high value of the x -Reynolds Number, 1,100,000, for transition, as compared to the value 300,000 observed by van der Hegge Zijnen and Hansen, is undoubtedly to be attributed to the small magnitude of the u -fluctuations in the normal air stream of the 3-foot wind tunnel. In order to definitely confirm this statement, the turbulence was artificially increased by the introduction of a wire screen of $\frac{1}{8}$ -inch mesh 39 inches ahead of the leading edge of the plate. Some 200 small aluminum tags about $1\frac{1}{4}$ inches by 1 inch by $\frac{1}{32}$ inch were fastened to the screen by paper clips. The tags, fluttering in the wind, produced a large distributed u -fluctuation whose root-mean-square value was about 3.0 percent of the mean speed of the air stream. The fluctuations normally present were accordingly increased by a factor of 6.

The u -fluctuation decreased slightly along the plate, from about 3.2 percent at the leading edge to about

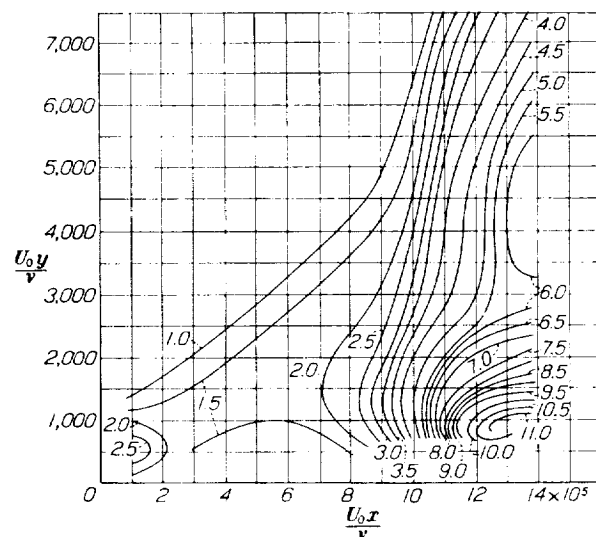


FIGURE 22.—Distribution of u -fluctuation, series D, with pressure gradient of figure 15, turbulence of free stream, 0.5 percent. See legend of figure 13.

2.8 percent at 28 inches from the leading edge. The maximum single value observed was 3.42 and the minimum, 2.56 percent.

The pressure gradient along the plate was that shown in figure 23. The variation is similar to that of figure 15, but the approximation to constant pressure was somewhat better.

Twelve traverses were made at a speed of about 65 feet per second at distances 2, 4, 5, 6, 7, 8, 10, 11.5, 13, 18, 23, and 28.5 inches from the leading edge, and ten traverses were made at a speed of about 32.5 feet per second at distances 4, 8, 10, 12, 14, 16, and 28 inches. In six cases, therefore, approximately the same x -Reynolds Number was obtained at two speeds differing by a factor of 2. The choice of speeds considerably lower than 100 feet per second permitted some increase in precision. The contour diagram prepared from faired curves is shown in figure 24.

Transition begins at an x -Reynolds Number of the order of 100,000; i. e., very close to the leading edge. The results for the two speeds are reasonably concordant and, in the six cases where the same Reynolds Number was obtained at the two speeds, there is no

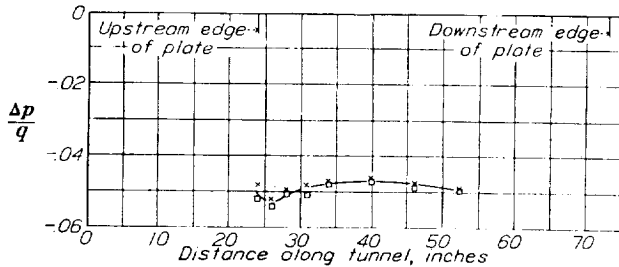


FIGURE 23.—Pressure gradient for measurements of series C (figs. 24 to 26, inclusive). See legend of figure 9. The speed of the free stream departs from the mean value by a maximum of 0.2 percent.

evidence of a systematic difference. Comparison of figure 24 with figures 16 and 20 will emphasize the very great influence of the initial turbulence of the wind tunnel on the velocity distribution and hence on the skin friction. Only the measurements at the

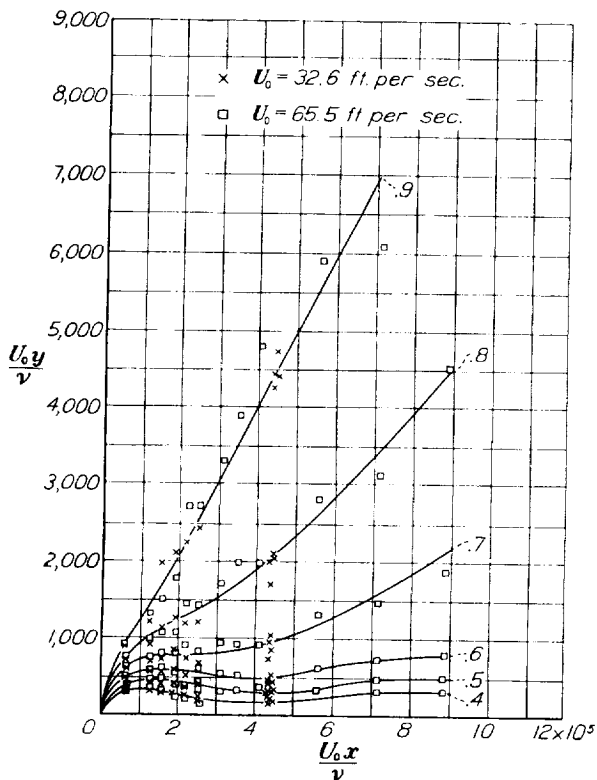


FIGURE 24.—Distribution of mean speed, series C, with pressure gradient of figure 23, turbulence of free stream, 3.0 percent. See legend of figure 1 for notation.

2-inch station are in the laminar region. These two traverses agree well with the Blasius distribution.

Figure 25 shows the results of four traverses in the eddying region at an x -Reynolds Number of approximately 435,000 and one traverse at 888,000 plotted in the form suggested by equation (15). The four repeat

runs show that the precision of the measurements is not sufficiently great to determine the slope with very great accuracy.

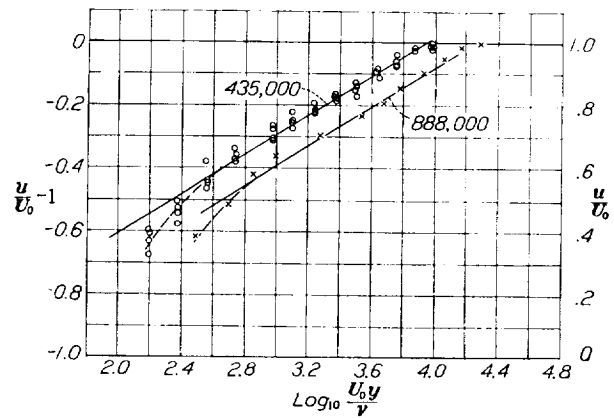


FIGURE 25.—Distribution of mean speed, for x -Reynolds Numbers 435,000 and 888,000, series C, plotted for comparison with the logarithmic distribution.

The contour diagram of the u -fluctuation is shown in figure 26. The faired values from which the dia-

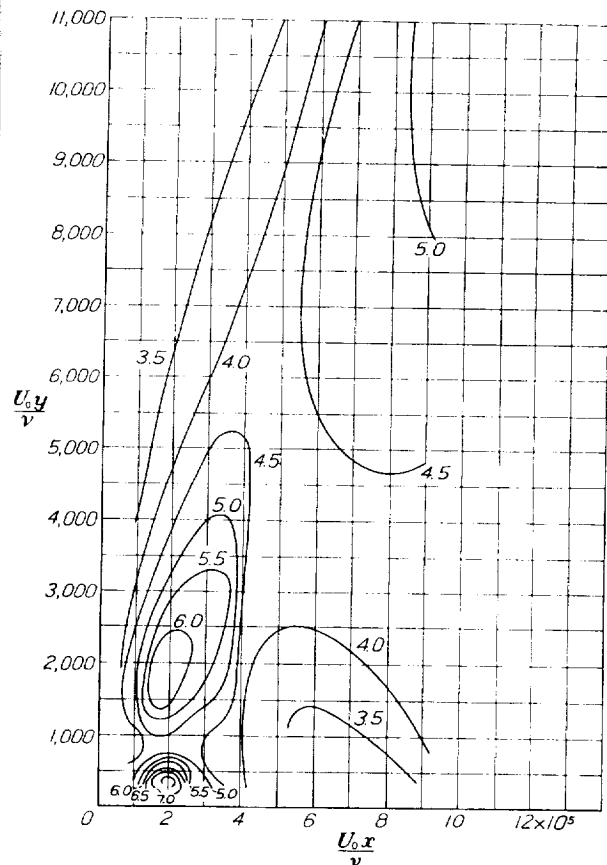


FIGURE 26.—Distribution of u -fluctuation, series C, with pressure gradient of figure 23, turbulence of free stream, 3.0 percent. See legend of figure 13.

gram was prepared are given in table IX. The region of maximum u -fluctuation occurs at an x -Reynolds Number of about 200,000, corresponding roughly to the middle of the transition region. In the eddying

region the magnitude of the fluctuation is of the order of 4 or 5 percent of the mean speed as compared with the free stream value of about 3 percent.

DISCUSSION

Meaning of fluctuations in laminar region.—The distinction between laminar and eddying flow is usually based on the nature of the variation of the skin friction with speed or on the nature of the speed distribution as has been more fully discussed in the section on Previous Experimental Work. The skin friction and speed distribution in laminar flow are generally computed on the assumption of steady flow, and the agreement between experimental results and theoretical calculations leads us to picture the laminar flow near a plate as a steady flow. The experiments described in this paper clearly show that the conclusion is incorrect; the experiments together with the computations illustrated in figures 3 and 4 indicate that it is possible to have large speed fluctuations with no measurable effect on the distribution of mean speed.

On the other hand, it has long been known that eddying flow is characterized by fluctuations of speed at a given point and hence there is a temptation to identify speed fluctuations with turbulence. Here again the experiments described in this paper show that large fluctuations are not confined to the region of eddying flow. It is not possible to determine by measurement of amplitude of fluctuation alone whether the flow is laminar or eddying.

This result and a brief account of the measurements described in this paper were reported to the Fourth International Congress of Applied Mechanics at Cambridge, England, in 1934. Tollmien discussed this account in reference 22 and emphasized by examples the importance of considering the correlation between the several components of the velocity fluctuations. He says "In order to produce a shearing stress a correlation is necessary between the components of the velocity fluctuations in two different directions. This is of course well known. But one has hitherto frequently regarded the mere existence of velocity fluctuations as sufficiently characteristic of turbulence in the tacit expectation that a correlation between the components of the fluctuations would be present. It is therefore necessary in general to give the greatest attention to the correlation between any, even theoretical, velocity fluctuations which have been determined, in order to be certain of the effect of the fluctuations on the form of the velocity distribution curve." One of the interesting examples in Tollmien's paper is the von Kármán vortex street, which shows no correlation between the longitudinal and lateral components of the velocity fluctuations.

It may be remarked that the fluctuations in the free stream of the wind tunnel are of this uncorrelated type having no influence on the distribution of mean speed. Since these fluctuations have generally been

called "turbulence", the author denotes a flow with the correlated type of fluctuations as "eddying" flow. Whether these particular names are generally adopted or not, there should be some clear distinction by means of different names between fluctuations whose components are uncorrelated and those which show correlation. Most experimenters would consider the flow in a von Kármán vortex street as highly turbulent.

In the discussion at the Congress of Applied Mechanics, it was pointed out that the fluctuations in the laminar layer were, generally speaking, of lower frequency than the fluctuations in the eddying layer. At the time the measurements described in this paper were made, a suitable oscillograph was not available. In 1934, after the Cambridge meeting, a plate was installed in the 4½-foot wind tunnel at the National Bureau of Standards and records of the fluctuations made with a cathode ray oscillograph. For convenience, the flow was made more turbulent by a wire screen of 1-inch mesh placed about 4.5 feet upstream from the plate. The u -fluctuation of the free stream was approximately 1.3 percent of the mean speed, giving transition at an x -Reynolds Number of about 500,000. The pressure gradient was not determined and the values of y were not accurately measured; hence these values are not comparable with the data reported in the preceding section. The records obtained are shown, in part, in figure 27. They were not made simultaneously. It is seen that the fluctuations in the laminar region (position 2) are much less rapid than those in the eddying region (position 5).

It should perhaps be pointed out that "slow" and "fast" are in this connection purely relative terms, the absolute magnitude of the rate of change of speed being a function of mean speed and of the thickness of the boundary layer. In any given flow, the distinction between laminar and eddying flow can be made on this basis, but in two different flows at widely different speeds and with boundary layers of widely different thickness, the use of this simple criterion would not be safe.

In the opinion of the author, the fluctuations in the laminar layer are to be regarded as forced oscillations produced by the turbulence of the wind-tunnel air stream. The qualitative distribution is very similar to that computed in the highly simplified manner described in the theoretical treatment of the transition and pictured in figure 4. Since, however, the distribution in the "free" oscillations as computed by Schlichting (reference 23) is also of much the same character, the general shape of the distribution curve cannot serve as a criterion of whether the fluctuations are forced or free.

Transition from laminar to eddying flow.—Figures 1, 10, 16, 20, and 24 show a gradual transition region extending over a range of x -Reynolds Numbers of 200,000 or more. It is very difficult to state definitely where the transition begins. The departures from the

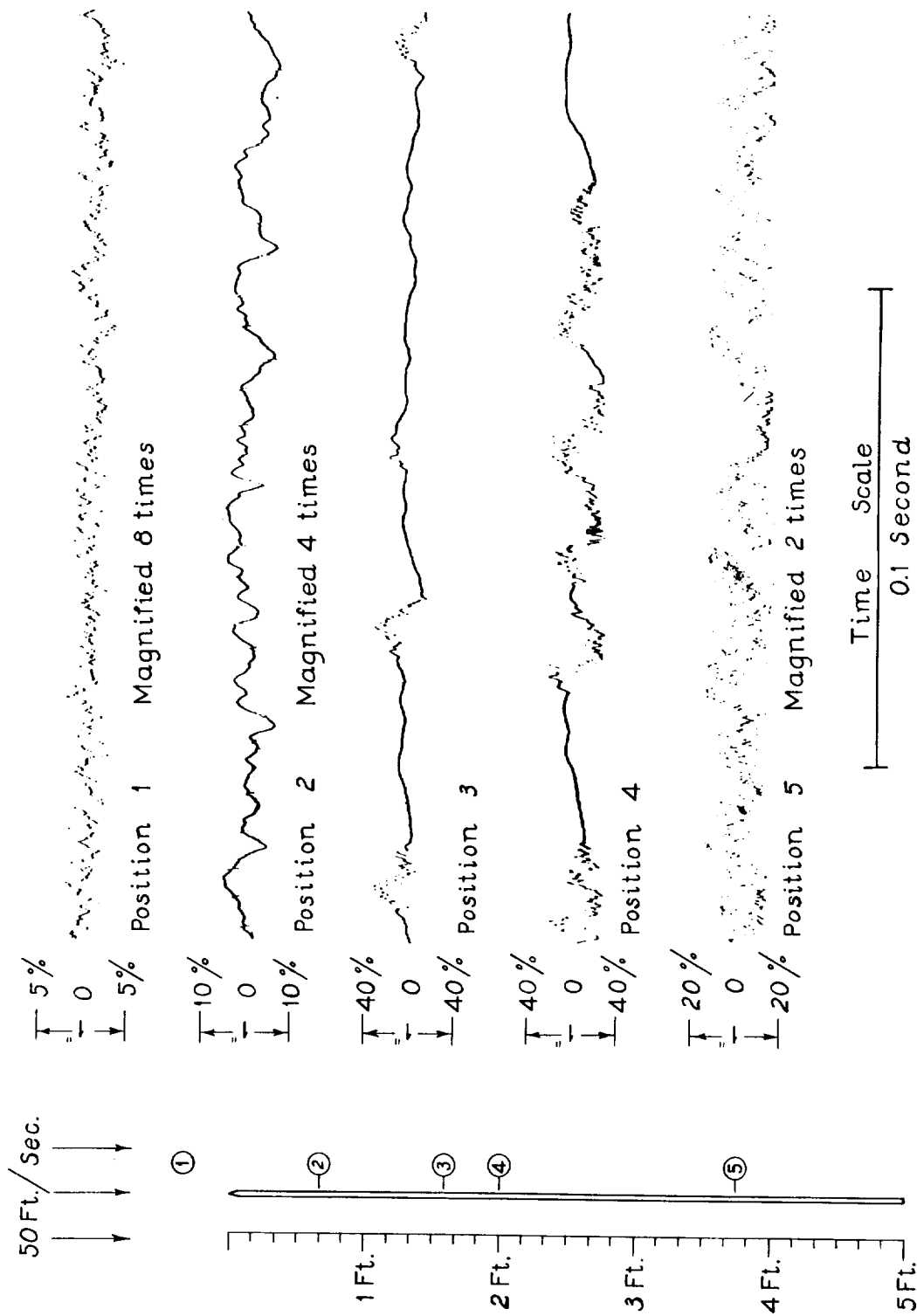


FIGURE 27.—Oscillograph records of u -fluctuation at several points near a plate.

Blasius distribution begin earlier for speed contours in the neighborhood of 0.4 or 0.5 than for the 0.9 contour. The layer begins to thicken rapidly at a somewhat greater x -Reynolds Number than that at which the speed near the surface begins to be accelerated. The character of the first noticeable change may perhaps best be seen in figure 8.

Figures 22 and 26 show that the rate of increase of the amplitude of the u -fluctuation is accelerated at an x -Reynolds Number considerably lower than that for which noticeable departures from the Blasius distribution of mean speed occur.

Finally, figure 27 shows that the transition is in fact a sudden phenomenon. Near the upstream limit of the transition region, eddying flow occurs intermittently at infrequent intervals, the flow being of the eddying type for only a small fraction of the time

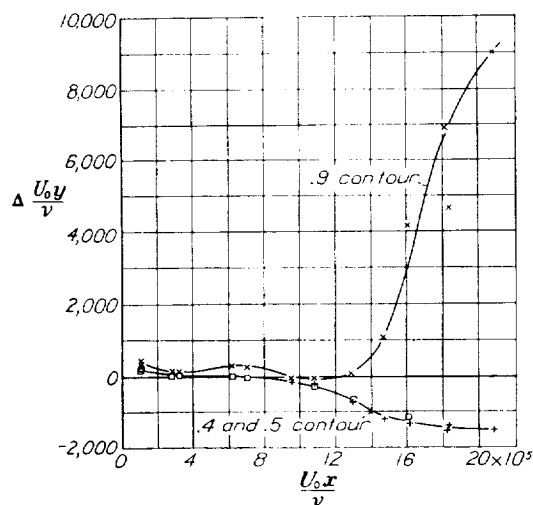


FIGURE 28.—Departure of the 0.4, 0.5, and 0.9 contours of mean speed in figure 16 from the Blasius positions. The ordinates represent the observed y -Reynolds Numbers for the speed contours minus the y -Reynolds Number computed from Blasius' solution for a laminar boundary layer.

covered by the record. Near the downstream limit, laminar flow occurs infrequently.

The process may be pictured somewhat as follows:

Transition is a sudden phenomenon controlled by the instantaneous pressure distribution arising from the turbulence of the free air stream. As the pressure distribution fluctuates, the point of transition fluctuates back and forth along the plate. At a given point in the transition region the flow is sometimes laminar and sometimes eddying—more frequently laminar as the point of observation is moved upstream and more frequently eddying as the point is moved downstream. Since the turbulence of the free stream is constant only in a statistical sense, there is a point of transition only in a statistical sense. The designation of the Reynolds Number at which transition occurs becomes then a matter of definition.

No entirely satisfactory definition has been found. The values quoted can be regarded only as approxi-

mate. In figure 28, the departures of the distribution of mean speed of figure 16 from the Blasius distribution are plotted for the 0.4, 0.5, and 0.9 contours. The value of the x -Reynolds Number for transition has been given as 1,100,000. It is obvious that significant departures occur at a somewhat lower x -Reynolds Number for the 0.4 and 0.5 contours, perhaps as low as 900,000 whereas the 0.9 contour does not show significant departures until 1,300,000.

The use of a Reynolds Number based on the "displacement thickness" δ^* , which equals $\int_0^\infty (1 - u/U_0) dy$, has often been suggested. A plot of δ^* -Reynolds Number against x -Reynolds Number, compared with a similar plot of the δ^* -Reynolds Number computed from the Blasius distribution, is not found to give clear indications of transition, because the departures

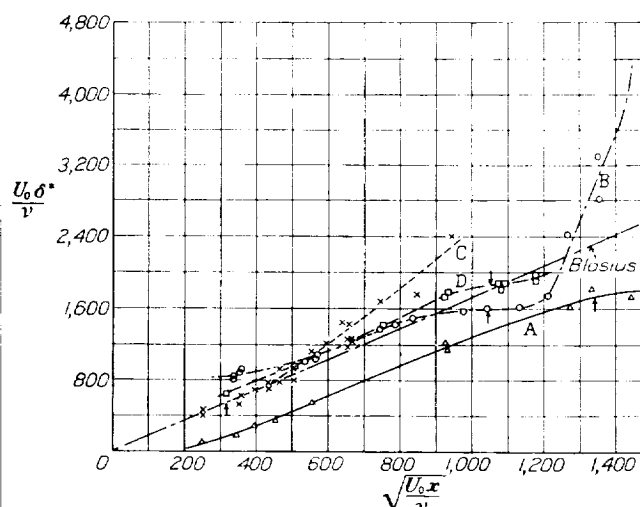


FIGURE 29.—The δ^* -Reynolds Number for the several series of observations as a function of the square root of the x -Reynolds Number. The transition begins at the values indicated by the arrows as determined from the distribution of mean speed.

from the Blasius distribution expressed as differences in y -Reynolds Number for a given speed are in one direction for the 0.4 and 0.5 contours and in the opposite direction for the 0.8 and 0.9 contours. The two effects partly compensate and lead to only moderate departures of the δ^* -Reynolds Number from the Blasius result, which are sometimes masked by experimental errors.

The comparison was made, however, and the results are given in figure 29. The values of the δ^* -Reynolds Number were computed by Simpson's rule from the faired values similar to those of table VII. Between the lowest value of u/U_0 (0.3 in table VII) and zero, a linear interpolation was used. The transition points are indicated in figure 29 by arrows. The points for the preliminary observations of series A show the apparent systematic error of about 400 in the value of $U_0 y/\nu$ to which reference has previously been made.

If correction is made for this shift, the δ^* -Reynolds Number at transition appears to be about 2,200.

Series B shows a somewhat earlier transition than series D as may also be seen from a careful examination of figure 16 and figure 20. In view of the difficulties of measurement, the results may be averaged to give a δ^* -Reynolds Number of about 1,700.

The curves for series A, B, and D show a bending away from the Blasius curve toward lower values with approach to slowly changing δ^* -Reynolds Number with increasing x -Reynolds Number. This deflection is followed for series B by a rapid increase. The same effects are not marked for the series C observations. From figure 24, it is clear that transition begins at an x -Reynolds Number of about 100,000 corresponding to a δ^* -Reynolds Number of about 560. No perceptible departure of the δ^* -Reynolds Number curve in figure 29 from the Blasius curve occurs until much higher values.

It is possible to suggest an unambiguous definition of the Reynolds Number of transition; for example, that for which the 0.4 contour deviates from the theoretical Blasius position by a y -Reynolds Number of 100. But so long as the effects of experimental errors combined with the effects of unavoidable departures from the uniform pressure assumed in the theory are of the order of 300 or 400, accurate determinations cannot be made in accordance with such a definition.

Effect of turbulence.—In the experiments of van der Hegge Zijnen and of Hansen, the turbulence of the air stream was not measured, no method then being known. From the dimensions of the honeycombs and their location and published data (for example, that in reference 17), we may estimate that the turbulence was between 1 and 2 percent. The corresponding x -Reynolds Number for transition was about 300,000, and the δ^* -Reynolds Number for transition about 940.

The experiments described in this paper give the following results:

Turbulence percent	x -Reynolds Number	δ^* -Reynolds Number
0.5	1,100,000	1,700
3.0	100,000	560

The available data do not suffice to construct a well-defined curve such as that established for the relation between the critical Reynolds Number of a sphere and the turbulence (reference 18). Nevertheless, there is little doubt that such a relation exists. The effect of turbulence is obviously very great. It is believed that the evidence presented supports the view that in an air stream of approximately uniform static pressure and for a smooth plate with sharp leading edge, the x -Reynolds Number for transition is a function of the turbulence varying from about 1,100,000 to 100,000.

Effect of pressure gradient.—The preliminary series of experiments showed that the effect of a pressure

gradient such as shown in figure 9 was to increase the x -Reynolds Number for transition in a stream of turbulence 0.5 percent from 1,100,000 to 1,800,000. The change in the δ^* -Reynolds Number is not so definitely established in view of the apparent systematic error in the preliminary series, but the author believes that with the pressure gradient the δ^* -Reynolds Number was increased from 1,700 to about 2,200; in other words, approximately in the same ratio as the square roots of the x -Reynolds Numbers.

The effect of an accelerating pressure gradient is then to delay the transition. This effect does not contradict the picture of the mechanism of transition described in the theoretical treatment, for the addition of a steady accelerating pressure gradient to the fluctuating pressure gradients of the turbulence of the air stream would reduce the magnitude of the instantaneous retarding gradients and hence delay separation. It is interesting to speculate on the effect of an accelerating gradient so large as to suppress entirely the retarding gradients in the fluctuations. A fundamental investigation of the effect of pressure gradient with constant turbulence is urgently needed. It is desirable that such experiments be made with both low and high degree of turbulence in the air stream.

Speed distribution in eddying region.—From the slopes of the lines in figure 18 and von Kármán's value, 0.4, of the universal constant k , the local friction coefficient may be computed according to equation (15). The values obtained are 0.0076 and 0.0057, respectively, which are unreasonably high.

Similarly the slopes of the lines in figure 25 give values of the local skin-friction coefficient computed from equation (15) for $k=0.4$ of 0.0057 and 0.0062 which again are unreasonably high. From von Kármán's table (reference 16) values of the order of 0.0045 and 0.0038 would be expected. Such a large difference is not accounted for by any reasonable assumption as to the errors in the velocity determinations. Application of the still-air heat-loss correction would increase the discrepancy.

The explanation of the discrepancy is that in the thin boundary layer nearly all stations are sufficiently near the wall that the effects of viscosity cannot be neglected, the y -Reynolds Numbers being less than 4,000.

Since no independent determination of local skin-friction coefficients was possible in the present experiments, no direct comparison can be made. It is of interest, however, to estimate the local skin-friction coefficients c_f from von Kármán's table and to plot the distributions of figures 18 and 25 with $\left(\frac{2}{c_f}\right)^{1/2} \frac{u}{U_0}$ as ordinate and $\log_{10} \left(\frac{c_f}{2}\right)^{1/2} \frac{u}{U_0}$ as abscissa. This has been done in figure 30. The solid curve is that determined by von Kármán from Nikuradse's measurements in pipes. In the estimation of c_f , the Reynolds Number used was

that obtained by assuming the eddying layer to begin at the beginning of the transition region.

The measurements with artificial turbulence lie about 4 percent above von Kármán's curve but sensibly parallel. On the other hand, the measurements with very small turbulence in the air stream show a different slope. The exact significance of this difference is not clear. The speed fluctuation at the center of a pipe in which the flow is eddying is of the order of that at the outer edge of the boundary layer in the experiments with artificial turbulence. The observations now

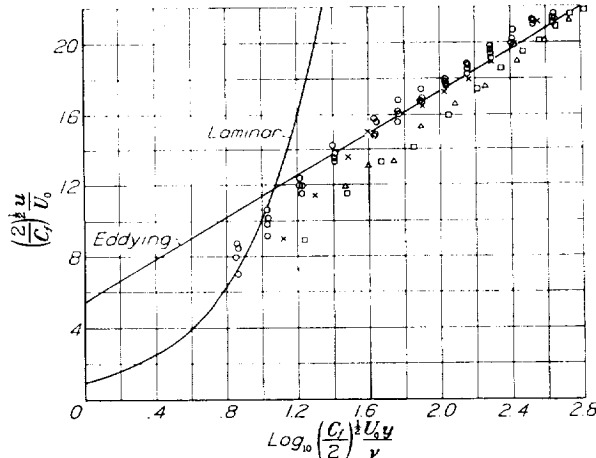


FIGURE 30.—Distribution of mean speed in eddying region for comparison with Kármán's formula. The data are those shown in figures 18 and 25. The local friction coefficient C_f , is estimated by assuming that the eddying begins at the beginning of the transition region.

available are too few to be certain that the shape of the speed-distribution curve near a plate is actually a function of the turbulence of the stream, as suggested by figure 30.

CONCLUSION

The intensive study of the boundary-layer flow near a thin flat plate promises to yield considerable information as to the origin of eddying flow and the effect of turbulence in wind-tunnel experiments. The information now available shows that the velocity field varies greatly with the turbulence of the air stream, and with the pressure gradient. The Reynolds Number at which transition occurs in a stream without pressure gradient decreases greatly as the turbulence is increased.

The presence of fluctuations is not an indication of the presence of eddy shearing stresses. The laminar layer shows speed fluctuations of amplitude considerably greater than that in the free stream. These fluctuations do not produce departures from the theoretical Blasius distribution for laminar flow. They are of lower frequency than the fluctuations in the eddying boundary layer.

Transition is a sudden phenomenon, but the point of transition moves back and forth within rather wide limits.

NATIONAL BUREAU OF STANDARDS,
WASHINGTON, D. C., March 1936.

REFERENCES

1. Prandtl, L.: *Motions of Fluids with Very Little Viscosity*. T. M. No. 452, N. A. C. A., 1928.
2. Blasius, H.: *Grenzschichten in Flüssigkeiten mit kleiner Reibung*. Z. f. Math. u. Phys., Band 56, Nr. 1, 1908, S. 1-37.
3. van der Hegge Zijnen, B. G.: *Measurements of the Velocity Distribution in the Boundary Layer along a Plane Surface*. Report 6, Aero. Lab. Tech. H. S., Delft, 1924.
4. Hansen, M.: *Velocity Distribution in the Boundary Layer of a Submerged Plate*. T. M. No. 585, N. A. C. A., 1930.
5. Éliás, Franz: *The Transference of Heat from a Hot Plate to an Air Stream*. T. M. No. 614, N. A. C. A., 1931.
6. von Kármán, Th.: *Turbulence and Skin Friction*. Jour. Aero. Sci., January 1934, pp. 1-20.
7. Dryden, H. L., and Kuethe, A. M.: *The Measurement of Fluctuations of Air Speed by the Hot-Wire Anemometer*. T. R. No. 320, N. A. C. A., 1929.
8. Runge, C., and König, H.: *Numerisches Rechnen*. Julius Springer (Berlin), 1924, p. 311.
9. Pohlhausen, K.: *Zur näherungsweise Integration der Differentialgleichung der laminaren Grenzschicht*. Z. f. a. M. M., Band I, Nr. 4, 1921, S. 252.
10. Falkner, V. M., and Skan, Sylvia W.: *Some Approximate Solutions of the Boundary Layer Equations*. R. & M. No. 1314, British A. R. C., 1930.
11. Dryden, Hugh L.: *Computation of the Two-Dimensional Flow in a Laminar Boundary Layer*. T. R. No. 497, N. A. C. A., 1934.
12. von Kármán, Th., and Millikan, C. B.: *On the Theory of Laminar Boundary Layers Involving Separation*. T. R. No. 504, N. A. C. A., 1934.
13. Tollmien, W.: *The Production of Turbulence*. T. M. No. 609, N. A. C. A., 1931.
14. Schlichting, H.: *Zur Entstehung der Turbulenz bei der Plattenströmung*. Nach. Gesell. d. Wiss. z. Gött. M. P. K., 1933, S. 181.
15. Tollmien, W.: *General Instability Criterion of Laminar Velocity Distribution*. T. M. No. 792, N. A. C. A., 1936.
16. Nikuradse, J.: *Experimentelle Untersuchungen zur Turbulenzentstehung*. Z. f. a. M. M., Band 13, 1933, S. 174.
17. Dryden, Hugh L.: *Reduction of Turbulence in Wind Tunnels*. T. R. No. 392, N. A. C. A., 1931.
18. Dryden, H. L., and Kuethe, A. M.: *Effect of Turbulence in Wind Tunnel Measurements*. T. R. No. 342, N. A. C. A., 1930.
19. Mock, W. C., Jr., and Dryden, H. L.: *Improved Apparatus for the Measurement of Fluctuations of Air Speed in Turbulent Flow*. T. R. No. 448, N. A. C. A., 1932.
20. Piercy, N. A. V., and Richardson, E. G.: *On the Flow of Air Adjacent to the Surface of an Aerofoil*. R. & M. No. 1224, British A. R. C., 1928.
21. Schubauer, G. B.: *Air Flow in a Separating Laminar Boundary Layer*. T. R. No. 527, N. A. C. A., 1935.
22. Tollmien, W.: *Über die Korrelation der Geschwindigkeitskomponenten in periodisch schwankenden Wirbelverteilungen*. Z. f. a. M. M., Band 15, 1935, S. 96.
23. Schlichting, H.: *Amplitudenverteilung und Energiebilanz der kleinen Störungen bei der Plattenströmung*. Nach. Gesell. d. Wiss. z. Gött., M. P. K., Band I, 1935, S. 47.

TABLE I
SOLUTION OF BLASIUS EQUATION FOR FLOW IN A LAMINAR BOUNDARY LAYER

X	Z	$\frac{dZ}{dX}$	$\frac{d^2Z}{dX^2}$	$\frac{d^3Z}{dX^3}$	$\bar{y} = y \sqrt{\frac{U_\infty}{\nu x}}$	$\frac{u}{U_\infty} = \bar{u}$	$\frac{d\bar{u}}{d\bar{y}}$	$\frac{d^2\bar{u}}{d\bar{y}^2}$
0	0	0	1	0	0	0	0.3320	0
0.1	0.00500	0.10000	0.99983	-0.00500	0.1819	0.0604	.3320	-0.0009
.2	.02000	.19993	.99967	-.01997	.3639	.1208	.3316	-.0036
.3	.04498	.29966	.99551	-.04478	.5458	.1812	.3306	-.0082
.4	.07992	.39894	.98939	-.07907	.7278	.2410	.3285	-.0144
.5	.12474	.49741	.97940	-.12217	.9097	.3005	.3252	-.0223
.6	.17936	.59466	.96470	-.17303	1.0917	.3593	.3203	-.0316
.7	.24362	.69017	.94459	-.23012	1.2736	.4170	.3137	-.0420
.8	.31732	.78338	.91853	-.29147	1.4556	.4733	.3050	-.0532
.9	.40020	.87367	.88623	-.35467	1.6375	.5278	.2943	-.0647
1.0	.49193	.96042	.84763	-.41698	1.8194	.5803	.2815	-.0761
1.1	.59214	1.04299	.80296	-.47547	2.0014	.6301	.2666	-.0868
1.2	.70037	1.12082	.75276	-.52721	2.1833	.6772	.2500	-.0962
1.3	.81613	1.19339	.69784	-.56952	2.3653	.7210	.2317	-.1039
1.4	.93886	1.26027	.63925	-.60016	2.5472	.7614	.2123	-.1095
1.5	1.06798	1.32116	.57825	-.61756	2.7292	.7982	.1920	-.1127
1.6	1.20289	1.37588	.51620	-.62093	2.9111	.8313	.1714	-.1133
1.7	1.34295	1.42441	.45452	-.61040	3.0931	.8606	.1509	-.1114
1.8	1.48757	1.46684	.39456	-.58693	3.2750	.8862	.1310	-.1071
1.9	1.63613	1.50342	.33751	-.55221	3.4569	.9083	.1121	-.1008
2.0	1.78807	1.53448	.28441	-.50855	3.6389	.9271	.0944	-.0928
2.1	1.94285	1.56046	.23502	-.45855	3.8208	.9428	.0784	-.0837
2.2	2.10001	1.58185	.19282	-.40492	4.0028	.9557	.0640	-.0739
2.3	2.25909	1.59920	.15506	-.35029	4.1847	.9662	.0515	-.0639
2.4	2.41973	1.61305	.12272	-.29694	4.3667	.9745	.0408	-.0542
2.5	2.58160	1.62392	.09557	-.24672	4.5486	.9811	.0317	-.0450
2.6	2.74443	1.63232	.07323	-.20096	4.7305	.9862	.0243	-.0367
2.7	2.90800	1.63871	.05520	-.16052	4.9125	.9900	.0183	-.0293
2.8	3.07212	1.64348	.04093	-.12575	5.0944	.9929	.0136	-.0230
2.9	3.23665	1.64700	.02986	-.09665	5.2764	.9951	.0099	-.0176
3.0	3.40149	1.64954	.02143	-.07289	5.4583	.9966	.0071	-.0133
3.1	3.56654	1.65135	.01513	-.05394	5.6403	.9977	.0050	-.0098
3.2	3.73174	1.65262	.01050	-.03919	5.8222	.9985	.0035	-.0072
3.3	3.89705	1.65350	.00717	-.02795	6.0042	.9990	.0024	-.0051
3.4	4.06243	1.65409	.00482	-.01957	6.1861	.9993	.0016	-.0036
3.5	4.22786	1.65448	.00318	-.01346	6.3680	.9996	.0011	-.0025
3.6	4.39332	1.65474	.00207	-.00909	6.5500	.9997	.0007	-.0017
3.7	4.55881	1.65491	.00132	-.00603	6.7319	.9998	.0004	-.0011
3.8	4.72430	1.65502	.00083	-.00393	6.9139	.9999	.0003	-.0007
3.9	4.88981	1.65508	.00051	-.00251	7.0958	.9999	.0002	-.0005
4.0	5.05522	1.65512	.00031	-.00158	7.2778	1.0000	.0001	-.0003
4.1	5.22063	1.65515	.00019	-.00097	7.4597	-----	.0001	-.0002
4.2	5.38635	1.65516	.00011	-.00059	7.6417	-----	0	-.0001
4.3	5.55187	1.65517	.00006	-.00035	-----	-----	-----	-----
4.4	5.71738	1.65518	.00004	-.00021	8.0055	-----	-----	-----
4.5	5.88290	1.65518	.00002	-.00012	8.1875	-----	-----	-----
5.2	7.04153	1.65518	0	0	9.4611	-----	-----	-----

TABLE II
CALIBRATIONS OF WIRE N18 ON OCT. 14, 1930

	Beginning	End
Resistance of wire and leads, $R+R_0$, ohms.....	5.388	5.405
Resistance of leads, R_0 , ohms.....	.445	.446
Resistance of wire, R , ohms.....	4.943	4.959
Temperature, °C.....	29.0	29.6
Barometric pressure, in Hg.....	29.68	29.68

Heating current 0.2 ampere. $R_{0a} = 0.01653$.

FIRST CALIBRATION							
Temperature °C	Speed, u ft./sec.	\sqrt{u}	Voltage drop $i(R+R_0)$	$R+R_0$ ohms	R ohms	R_0 ohms	$\frac{iRR_{0a}}{R-R_0}$
28.5	56.6	7.52	1.638	8.190	7.745	4.933	0.001820
	64.5	8.02	1.602	8.010	7.565	-----	.001898
29.0	75.7	8.70	1.561	7.805	7.360	4.943	.002013
	82.7	9.09	1.538	7.690	7.245	-----	.002080
29.0	90.6	9.51	1.520	7.600	7.155	-----	.002138
	100.6	10.03	1.496	7.480	7.035	-----	.002221
29.0	113.9	10.66	1.474	7.370	6.925	-----	.002310
SECOND CALIBRATION							
30.0	105.2	10.25	1.492	7.460	7.014	4.967	0.002267
	100.1	10.05	1.505	7.525	7.079	-----	.002213
30.0	90.8	9.52	1.526	7.630	7.184	-----	.002143
	82.8	9.10	1.546	7.730	7.284	-----	.002080
30.0	71.3	8.44	1.583	7.915	7.469	-----	.001972
	58.2	7.62	1.637	8.185	7.739	-----	.001845

TABLE III
DETERMINATION OF MEAN SPEED FOR $x=23$ INCHES, $U_0=105.2$ FT./SEC. ON OCT. 14, 1930

SEE TABLE II FOR DATA ON WIRE. SEE FIGURE 7 FOR CALIBRATION CURVE										
Temperature °C	y inches	Voltage drop $i(R+R_0)$	$R+R_0$ ohms	R ohms	R_0 ohms	$\frac{iRR_{0a}}{R-R_0}$	\sqrt{u}	u ft./sec.	$\frac{u}{U_0}$	
29	0.015	1.862	9.310	8.865	4.943	0.001494	5.42	29.4	0.280	
29.5	.020	1.765	8.825	8.379	4.954	.001616	6.19	38.3	.364	
29.5	.025	1.720	8.600	8.154	-----	.001684	6.62	43.8	.417	
29.5	.030	1.666	8.330	7.884	-----	.001778	7.21	52.0	.494	
30.0	.040	1.602	8.010	7.565	4.967	.001926	8.15	66.4	.632	
30.0	.050	1.566	7.830	7.384	-----	.002021	8.75	76.5	.728	
30.0	.065	1.529	7.645	7.199	-----	.002130	9.45	89.2	.848	
30.0	.080	1.508	7.540	7.096	-----	.002203	9.91	98.3	.935	
30.0	.100	1.499	7.495	7.049	-----	.002237	10.13	102.6	.976	
30.0	.130	1.493	7.465	7.019	-----	.002259	10.26	105.3	1.001	
30.0	.180	1.490	7.450	7.004	-----	.002274	10.36	107.6	1.024	
30.0	.230	1.490	7.450	7.004	-----	.002274	10.36	107.6	1.024	
30.0	1.065	1.493	7.465	7.019	-----	.002259	10.26	105.3	1.001	

TABLE IV

RESULTS OF TABLE III CORRECTED FOR HEAT LOSS TO PLATE ON BASIS OF STILL AIR CORRECTION

WIRE LENGTH-0.342 INCH. $K=0.000\ 000\ 00435$						
y inches	$\frac{R-R_0}{R_0} = \theta$ ° C.	$\frac{K\theta}{y}$	$\frac{i^2 RR_0 \alpha}{R-R_0} - \frac{K\theta}{y}$	$\sqrt{u_e}$	u_e ft./sec.	$\frac{u_e}{U_0}$
0.015	237.2	0.000069	0.001425	4.93	24.3	0.231
.020	207.2	.000045	.001571	5.90	34.8	.331
.025	193.6	.000034	.001650	6.40	41.0	.390
.030	177.2	.000026	.001752	7.06	49.8	.473
.040	157.1	.000017	.001909	8.05	64.8	.616
.050	146.2	.000013	.002008	8.68	75.3	.716
.065	135.1	.000009	.002121	9.38	88.0	.836
.080	128.7	.000007	.002196	9.85	97.0	.922
.100	126.0	.000005	.002232	10.09	101.8	.968
.130	124.1	.000004	.002255	10.25	105.0	.998
.180	123.2	.000003	.002271	10.35	107.5	1.022
.230	123.2	.000002	.002272	10.35	107.5	1.022
1.065	124.1	0	.002259	10.26	105.3	1.001

TABLE V

DETERMINATION OF SPEED FLUCTUATION FOR $x=23$ INCHES, $U_0=105.2$ FT./SEC. ON OCT. 14, 1930

SEE TABLE II FOR DATA ON WIRE, TABLE III FOR MEAN SPEED, FIG. 7 FOR CALIBRATION CURVE $B=0.0001580$ (from fig. 7)								
1	2	3	4	5	6	7	8	9
y inches	\sqrt{u}	$\frac{i^2 R_0^2 \alpha}{(R-R_0)^2}$	$\frac{i^2 RR_0 \alpha}{6(R-R_0)}$	(3)+(4)	$\frac{2(5)}{B\sqrt{u}}$	dE (volts)	$\frac{du}{u}$	$\frac{du}{U_0}$
0.015	5.42	0.001061	0.000249	0.001310	3.06	0.1190	0.364	0.1019
.020	6.19	.001396	.000269	.001665	3.40	.0776	.284	.0961
.025	6.62	.001597	.000281	.001878	3.59	.0563	.202	.0843
.030	7.21	.001905	.000296	.002201	3.86	.0403	.1555	.0768
.040	8.15	.002436	.000321	.002757	4.28	.0171	.0732	.0482
.050	8.75	.002812	.000337	.003149	4.56	.0122	.0556	.0405
.065	9.45	.003290	.000355	.003645	4.88	.0099	.0483	.0410
.080	9.91	.003623	.000367	.003990	5.10	.0090	.0459	.0429
.100	10.13	.003780	.000373	.004153	5.19	.00838	.0435	.0425
.130	10.26	.003896	.000376	.004272	5.27	.00582	.0307	.0307
.180	10.36	.003958	.000379	.004337	5.29	.00360	.0191	.0196
.230	10.36	.003958	.000379	.004337	5.29	.00266	.0141	.0144
1.065	10.26	.003896	.000376	.004272	5.27	.00115	.0061	.0061

TABLE VI

RESULTS OF TABLE V CORRECTED FOR HEAT LOSS TO PLATE ON BASIS OF STILL AIR CORRECTION

WIRE LENGTH 0.342 INCHES $K=0.000\ 000\ 00435$							
1	2	3	4	5	6	7	8
y inches	$\sqrt{u_e}$	$\frac{K}{y i R_0 \alpha}$	Column (5) of table V +(3)	$\frac{2(4)}{B\sqrt{u_e}}$	dE volts	$\frac{du_e}{u_e}$	$\frac{du_e}{U_0}$
0.015	4.93	0.000088	0.001398	3.59	0.1190	0.427	0.0986
.020	5.90	.000066	.001731	3.72	.0776	.289	.0957
.025	6.40	.000053	.001931	3.82	.0563	.215	.0838
.030	7.06	.000044	.002245	4.03	.0403	.1612	.0763
.040	8.05	.000033	.002790	4.39	.0171	.0751	.0463
.050	8.68	.000026	.003175	4.63	.0122	.0565	.0404
.065	9.38	.000020	.003665	4.95	.0099	.0490	.0410
.080	9.85	.000016	.004006	5.15	.0090	.0463	.0427
.100	10.09	.000013	.004166	5.23	.00838	.0438	.0424
.130	10.25	.000010	.004282	5.29	.00582	.0308	.0307
.180	10.35	.000007	.004344	5.31	.00390	.0191	.0195
.230	10.35	.000006	.004343	5.31	.00296	.0141	.0144
1.065	10.26	.000001	.004273	5.27	.00115	.0061	.0061

TABLE VII

FAIRED VALUES FOR $x=23$ INCHES, $U_0=105.2$ FT./SEC.

Average temperature 30° C. Pressure 29.68 inches Hg $\nu=0.0001732$ ft ² /sec. $\frac{U_0 \nu}{\nu} = 1,164,000$					
$\frac{u}{U_0}$	y inch	$\frac{U_0 y}{\nu}$	$100 \frac{du}{U_0}$	y	$\frac{U_0 y}{\nu}$
0.3	0.0166	841	10	0.0166	841
.4	.0230	1,165	9	.0237	1,200
.5	.0301	1,525	8	.0282	1,428
.6	.0378	1,915	7	.0310	1,570
.7	.0468	2,371	6	.0327	1,656
.8	.0560	2,938	5	.0367	1,859
.9	.0727	3,682	4	.057	2,888
			3	.110	5,575
			2	.132	6,690
				.179	9,070

TABLE VIII

y -REYNOLDS NUMBERS CORRESPONDING TO VARIOUS VALUES OF u -FLUCTUATION USED IN PLOTTING FIGURE 22

$100 \frac{du}{U_0}$	x -Reynolds Number											
	102000	256200	567000 ¹	567000	555000	863000	869000	1188000	1160000	1164000	1380000	1383000
11											400 1130	1270
10.5									960 1560		1230	1330
10.0									890 1590	760	1350	1410
9.5								1330	830 1530	1030	1470	1510
9.0								1480	790 1660	1160	1580	1610
8.5								1620	1700	1280	1700	1730
8.0								1770	1730	1420	1830	1880
7.5								1920	1800	1570	1970	2020
7.0								2080	1890	1660	2120	2220
6.5								2270	2000	1750	2290	2450
6.0								2500	2150	1820	2470	2770 2790 2840
5.5								2820	2300	1910	2680 3740 5900	5960
5.0			1080 1390					3250	2620	1980	6410	6420
4.5			770 1510					3670	2990 4390	2090	6950	6940
4.0			1870					4180	5400	5570	7640	7560
3.5			2000					4960	5860	6080	8480	8360
3.0			2140			1010 1530 1900	1190 1470		6360	6690	9320	9090
2.5	780 330		2320			1170 1330 2010	1860		7170	7770	10100	10050
2.0	1000		2570		1260	2990	3100			9070	11920	11160
1.5	1190	1380	2830	1060 2560	510 2440	4120	3800			11250	12760	12350
1.0	1380	1880	3270	3170	3200	4650	4590				13550	13630

¹ Not considered, because not concordant with repeat runs.

TABLE IX

y -REYNOLDS NUMBERS CORRESPONDING TO VARIOUS VALUES OF u -FLUCTUATION USED IN PLOTTING FIGURE 26

$U_0 = 32.6 \text{ ft./sec.}$								
$100 \frac{du}{U_0}$	x -Reynolds Number							
	62800	123400	156100	186400	215300	251200	439500	437300
8.0			255 435					
7.5			210 490	270 455				
7.0			190 500	240 500	240 385			
6.5		300 450	165 645	205 570	175 460			
6.0		255 535	155 770	190 670	170 495			
				1505 2105	1660 2355			
5.5		215 865 1740	1090 1560	160 810 1300	160 505 915	310 460 1040		
5.0		170 2070	2475	2525 155 1025 1125	2695 155 3220	2830 230 580 880		
4.5				2835		3450 190	1995	1780
4.0	630 1180	2700	2730	3265	3695	4100 150	6080 785	5810 335
3.5	475 1515	3135	2940	3835	4540	4770	7535	7060
3.0	375		3330	4700	5545	5540	11450	9210 185

$U_0 = 65.5 \text{ ft./sec.}$												
$100 \frac{du}{U_0}$	x -Reynolds Number:											
	63000	125200	156000	188500	217300	252200	307500	352000	406000	558000	716000	888000
7.5				380	250 355							
7.0			265 395	460	425							
6.5			435 500	530	500							
6.0			595 1390 2180	575 1400 2390	575 1555 2715	2095 2400						
						355 485						
5.5		470 1385 1720	560 1185 1810	660 1200 2710	645 1335 3075	1750 1545 2360	2875 3170	3245				
						335 585						
5.0		550 1165 2110	640 960 2775	715 975 3080	800 1135 3540	400 1355 3650	400 1005 5065	1620 4375				8250 12140
4.5	670 1560	650 960 2380	3230	3640	4160	320 4550	540 1005 5065	280 1185 5260	3305 4930	6195	4790 11470	4795 13700
4.0	2060	2850	4055	4555	5070	6000	6070	6710	1695 7490	2540 14980	2070 14980	995 15880
3.5		3960	5550	9430	6890		7940	8960	10730	1395 14340	20680	305 19620

REPORT No. 563

CALCULATED AND MEASURED PRESSURE DISTRIBUTIONS OVER THE MIDSPAN SECTION OF THE N. A. C. A. 4412 AIRFOIL

By ROBERT M. PINKERTON

SUMMARY

Pressures were simultaneously measured in the variable-density tunnel at 54 orifices distributed over the midspan section of a 5- by 30-inch rectangular model of the N. A. C. A. 4412 airfoil at 17 angles of attack ranging from -20° to 30° at a Reynolds Number of approximately 3,000,000. Accurate data were thus obtained for studying the deviations of the results of potential-flow theory from measured results. The results of the analysis and a discussion of the experimental technique are presented.

It is shown that theoretical calculations made either at the effective angle of attack or at a given actual lift do not accurately describe the observed pressure distribution over an airfoil section. There is therefore developed a modified theoretical calculation that agrees reasonably well with the measured results of the tests of the N. A. C. A. 4412 section and that consists of making the calculations and evaluating the circulation by means of the experimentally obtained lift at the effective angle of attack; i. e., the angle that the chord of the model makes with the direction of the flow in the region of the section under consideration. In the course of the computations the shape parameter ϵ is modified, thus leading to a modified or an effective profile shape that differs slightly from the specified shape.

INTRODUCTION

Pressure-distribution measurements over an airfoil section provide, directly, the knowledge of the air-force distribution along the chord that is required for some purposes. In addition, such data, when compared with the results of potential-flow (nonviscous fluid) theory, provide a means of studying the effects of viscous forces on the flow about the airfoil section.

The results of experimental pressure measurements for a few miscellaneous airfoils may be found in various publications. The general application of this method of obtaining design data, however, is limited because of the expense of making such measurements.

A method of calculating the pressure distribution is developed in references 1 and 2. This method, based on the "ideal fluid" or potential-flow theory, gives the

local velocities over the surface; the pressures are calculated by means of Bernoulli's equation. Although this method provides an inexpensive means of obtaining the distribution of pressure, the results may not be in satisfactory agreement with measured results. Such disagreement, however, is not surprising since the theory does not account for the effects of the viscous boundary layer.

A reasonably accurate method of calculating the pressure distribution over an airfoil section is desirable and might be obtained by two procedures. First, such a method might be found by the development of a complete theory. Such a theory, however, must take into account all the factors or phenomena involved and must give satisfactory agreement with actual measurement. A second procedure, the most feasible one at present, is the development of a rational method of correcting the application of the potential-flow theory to minimize the discrepancies between the theoretical and measured results.

It was realized, however, that unusually reliable experimental pressure-distribution data for comparison with calculations were not available. The experiments to obtain such data consisted of pressure measurements at a large number of points around one section of an airfoil. Because the investigation was primarily intended to study deviations of the actual from the ideal, or potential, flow, the tests were made in the variable-density tunnel over a range of values of the Reynolds Number, representing varying effects of viscosity. In addition, tests were made in the 24-inch high-speed tunnel at certain corresponding values of the Reynolds Number obtained by means of high speeds, thereby bringing out the effects of compressibility. Parts of this experimental investigation outside the scope of this report are still incomplete.

The present report, which presents the most important of the experimental results (those corresponding to the highest value of the Reynolds Number), is divided into two parts. The first part comprises the description and discussion of the experimental technique: Materials that are essential to establish the fact that the measured results are sufficiently accurate and reliable to meet the demands of the subsequent analysis. The

second part presents a comparison of theoretically calculated results with measured results and an analysis of the differences and probable causes. A method is developed to modify the application of potential-flow theory in order to minimize discrepancies from the measured pressure distributions.

EXPERIMENTAL PRESSURE DISTRIBUTION

APPARATUS AND TESTS

The experimental investigation described herein was made in the variable-density wind tunnel (reference 3). The model used was a standard duralumin airfoil having

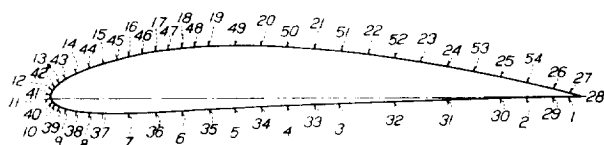


FIGURE 1.—Distribution of pressure orifices about the N. A. C. A. 4412 airfoil.

the N. A. C. A. 4412 section and a rectangular plan form with a span of 30 inches and a chord of 5 inches. It was modified by replacing a midspan section 1 inch in length with a brass section in which the pressure orifices were located. The 54 orifices, each 0.008 inch in diameter, were drilled perpendicularly into the airfoil surface and placed in 2 rows about the airfoil. The method and accuracy of construction of the model are described in reference 3. In order to evaluate the pressure force parallel to the chord, a relatively large number of orifices were located at the nose of the airfoil (fig. 1); well-defined distributions of pressure along a normal to the chord were thus assured. The locations of the pressure orifices are included in table 1. Brass tubes were connected to the orifices and carried in grooves in the lower surface of the airfoil to the planes of the supporting struts where they were brought out of the model. After the model was assembled, the grooves were covered with a plate carefully faired into the surface. The tubing extended through the tunnel wall into the dead-air space and the part exposed to the air stream together with the support struts was faired into a single unit (fig. 2). The tubes were connected by rubber tubing to a photorecording multiple-tube manometer mounted in the dead-air space.

Figure 3 shows the 60-tube manometer, composed of 30-inch glass tubes arranged in a semicircle and connected at the lower ends to a common reservoir. The total-head pressure of the air stream was chosen as the reference pressure and was measured by a pitot head, mounted as shown in figure 2, to which four equally spaced manometer tubes were connected. The dynamic pressure of the air stream was determined by two tubes connected to the calibrated static-pressure orifices used in the normal operation of the tunnel. One tube was connected to a set of four orifices spaced around the inner wall of the return passage and the other tube to a set of four orifices spaced around the entrance cone

near the test section. The remaining 54 tubes, used to measure the pressure at the orifices on the airfoil, were connected to the tubes leading to the airfoil model.

A lighttight box mounted on the flat side of the semicircle contained drums for holding photostat paper and the necessary operating mechanism. The manometer was arranged so that it could be operated from outside the tank that houses the tunnel.

The manometer characteristics determined by trial included the time required for the menisci to become steady and the proper exposure of the photostat paper.

A record of the heights of the manometer fluid in the glass tubes was taken at each of 17 angles of attack

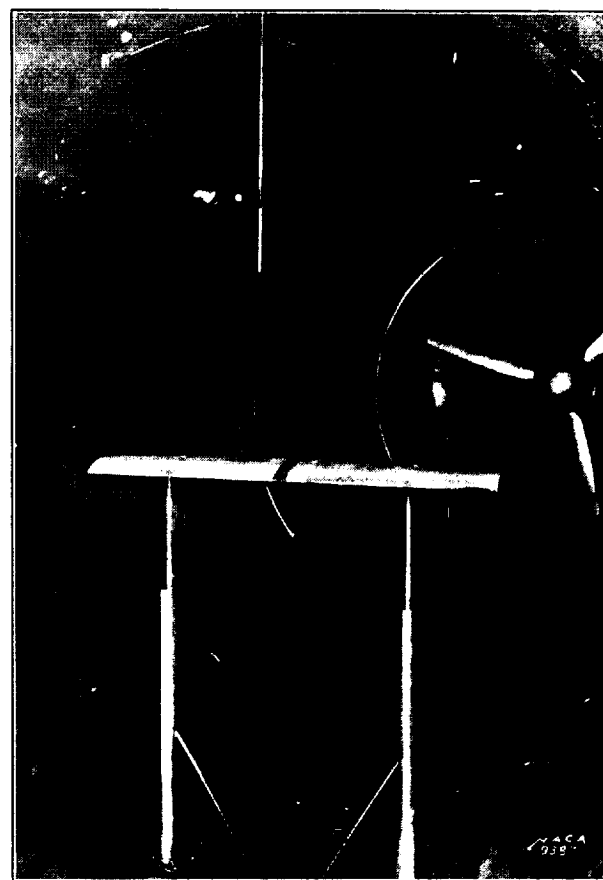


FIGURE 2.—Pressure-distribution model mounted in the tunnel.

from -20° to 30° at a Reynolds Number of approximately 3,000,000.

In order to keep the results as accurate as possible, it was necessary to obtain large deflections of the manometer liquids, which was accomplished by using two liquids of widely different specific gravities.

Liquid:	Specific gravity
Mercury.....	13.6
Tetrabromoethane.....	3.0

The proper choice of the angle-of-attack groups and of the liquid enabled the use of large and comparable

deflections throughout the angle-of-attack range. Repeat tests, using the same and different manometer liquids, provided data on the precision of the tests.

RESULTS

A copy of a sample photostat record is shown in figure 4. The pressures in inches of manometer fluid were measured to 0.01 inch. All measurements were made from a reference line obtained by drawing a line connecting the menisci of the four reference tubes. The quantities thus obtained from the photostat records were:

$$\Delta p = H - p$$

where H is the total-head pressure of the stream and p , the pressure at the airfoil orifice; and

$$q = \text{factor} \times \Delta p,$$

where q is the dynamic pressure and Δp is the difference in pressure between the static-pressure orifices in the entrance cone and those in the return passage. The factor was previously determined by comparing values of Δp_s with simultaneous values of the dynamic pressure obtained with a calibrated pitot-static tube mounted in the air stream in the absence of a model. Finally, the pressures on the airfoil were computed as ratios to the dynamic pressure, thereby making the results independent of manometer liquid.

Bernoulli's equation for the undisturbed stream becomes

$$p_\infty + \frac{1}{2}\rho V^2 = H$$

where p_∞ is the pressure and V the velocity. The pressure of the fluid at the wing orifice is given by

$$p = H - \Delta p$$

Substitute for H from the previous equation and remember that $\frac{1}{2}\rho V^2 = q$, the dynamic pressure, then

$$p = p_\infty + q - \Delta p$$

Consider p_∞ as the datum pressure. The pressure coefficient then becomes

$$P = \frac{p - p_\infty}{q} = 1 - \frac{\Delta p}{q}$$

where Δp and q are quantities obtained from the photostat records as previously described. Values of P at each orifice on the airfoil and for all angles of attack are tabulated in table I.

Figure 5 (a, b, c) presents plots of P against orifice position along the chord and against position perpendicular to the chord for each angle of attack. Large-scale plots similar to those presented here were mechanically integrated to obtain the normal-force, the chord-force,

and the pitching-moment coefficients, which are defined by the following expressions:

$$c_n = \frac{1}{c} \int P dx$$

$$c_c = \frac{1}{c} \int P dy$$

$$c_{m_{c/4}} = \frac{1}{c^2} \left[\int P \left(\frac{c}{4} - x \right) dx + \int P y dy \right]$$

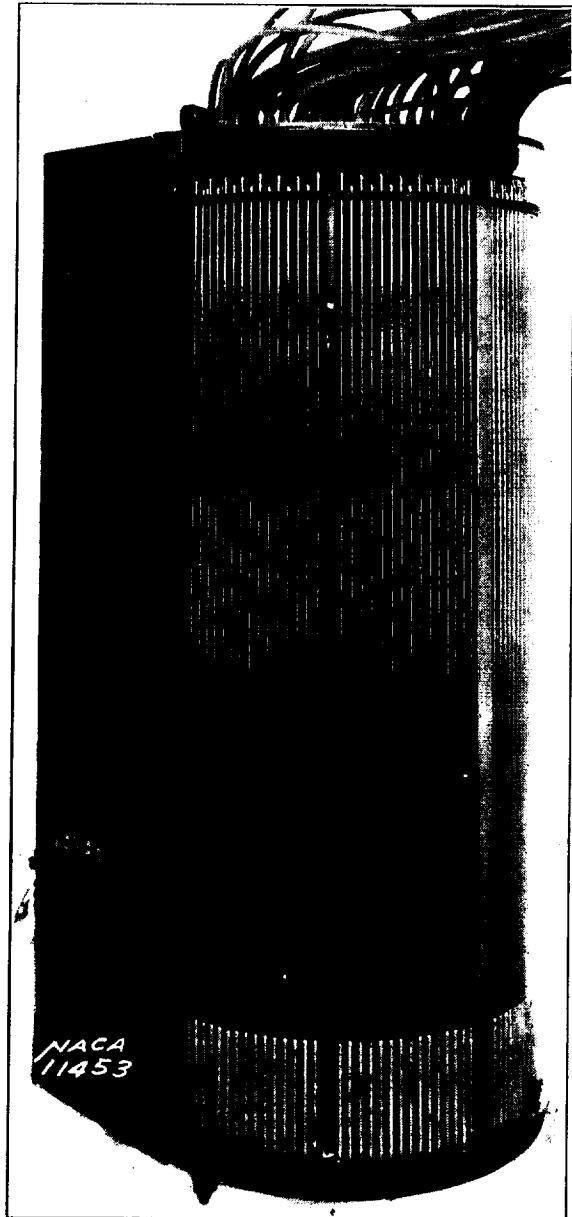


FIGURE 3. Photorecording multiple-tube manometer.

where c is the chord, x is the orifice station along the chord, and y is the orifice ordinate measured from the chord. The lower-case symbols c_n , c_c , $c_{m_{c/4}}$ designate

section characteristics and refer respectively to the normal-force, chord-force, and pitching-moment coefficients for the midspan section of the airfoil. Plots of these coefficients (see table II) against geometric angle of attack are given in figure 6. The geometric angle of attack α is measured from the mean direction of the flow in the tunnel. This direction is defined as the zero-lift direction of a symmetrical airfoil in the tunnel and was found to be equivalent to $20'$ of upflow. In order to have true section characteristics (2-dimensional) for comparison with theoretical calculations, a determination must be made of the effective angle of attack, i. e., the angle that the chord of

where w is the induced normal velocity produced by the vortex system of the airfoil, including the tunnel-wall interference, and V is the velocity of the undisturbed flow. In order to calculate the induced velocity w , the distribution of the lift (or circulation) along the span of the airfoil must be determined. A theoretical method of obtaining this distribution is given in reference 4 and, when applied to this problem, gives for the induced angle of attack of the midspan section

$$\alpha_i = 1.584 c_l$$

where c_l is the lift coefficient for the midspan section. This lift coefficient is obtained from the pressure

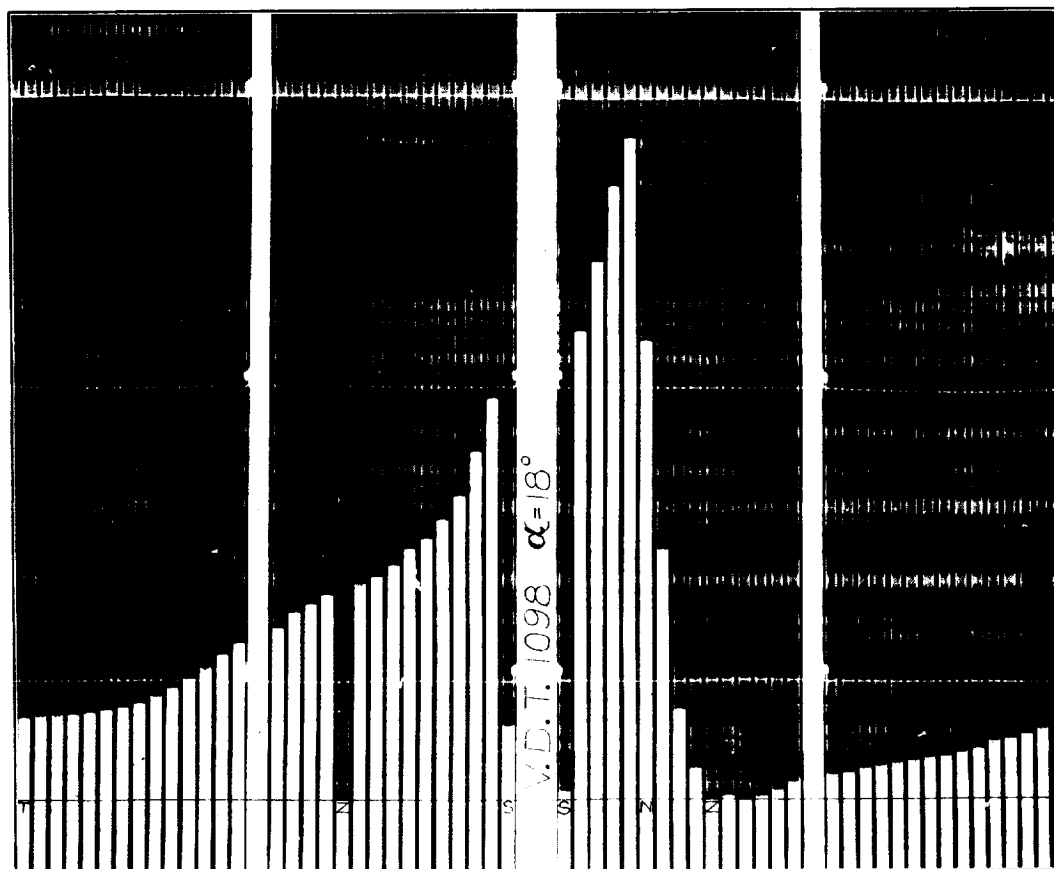


FIGURE 4.—Copy of sample record. N, leading-edge orifice tube; S, static-pressure tubes; T, trailing-edge orifice tube; and Z, reference-pressure tubes.

the model makes with the direction of flow in the region of the midspan section of the model.

The effective angle of attack, corresponding to the angle for 2-dimensional flow, is given by

$$\alpha_0 = \alpha - \alpha_i$$

where α_i is the angle that the flow in the region of the airfoil section makes with the direction of the undisturbed flow. The amount of this deviation is small and can be calculated from

$$\alpha_i = \frac{w}{V}$$

measurements by means of the equation

$$c_l = c_n \cos \alpha - c_e \sin \alpha$$

Values of c_l , α_i , and α_0 are given in table II.

PRECISION

The reliability of the results of the pressure measurements reported herein may be determined by consideration of the technique of obtaining and measuring the pressure records, of the deviations of the pressure diagrams obtained from several tests at the same angle of attack, and of the method of calculating the effective angle of attack.

The method of obtaining the pressure records is a direct, simultaneous, photographic recording of the height of the liquid in the manometer tubes. Since the pressure coefficients used in the analysis are ratios

to become steady and by delaying the taking of the record at each angle of attack until sufficient time had elapsed. As a further check, a zero record was taken at the end of each test run under the same conditions.

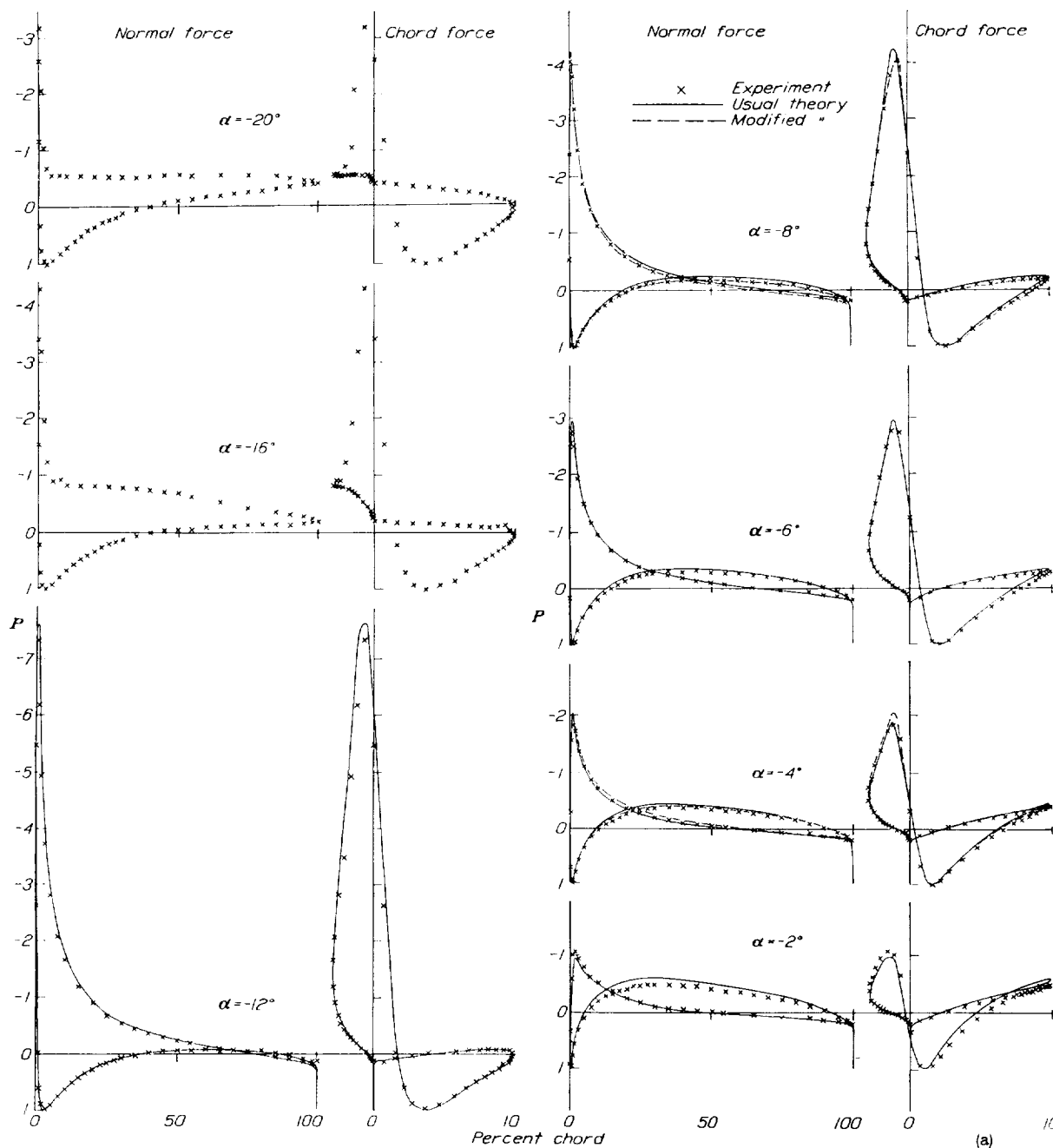


FIGURE 5a. -Experimental and theoretical pressure-distribution diagrams for the N. A. C. A. 4412 airfoil at several angles of attack.

of quantities taken from the same record, the primary source of error therefore lies in the unequal damping in the tubes connecting the airfoil orifices to the manometer. This source of error was minimized by determining the time required for the liquid in all the tubes

In addition, the tubes were checked for leaks before and after each run. In order to minimize any possible error in reading the photostatic records (fig. 4) measurements of the recorded pressures were made independently by two persons. The readings were then com-

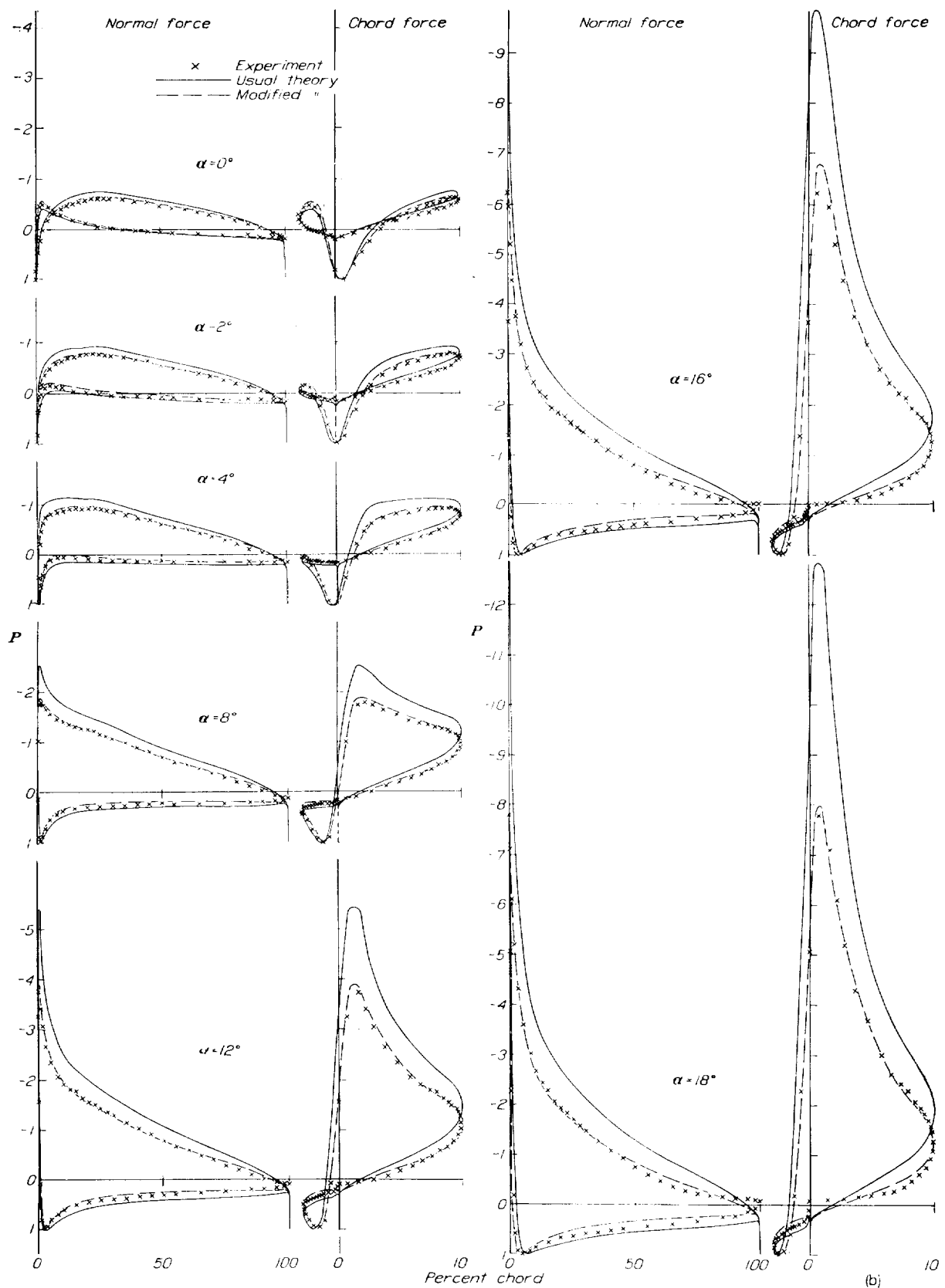


FIGURE 5b.—Experimental and theoretical pressure-distribution diagrams for the N. A. C. A. 4412 airfoil at several angles of attack.

pared and a compromise was made where differences occurred. The differences between any two such independent readings rarely exceeded 0.01 inch except in the case of obvious errors. Possible errors due to

from several tests at the same angle of attack. Figure 7 presents such diagrams at two angles of attack, -4° and 8° . Tetrabromoethane, because of the larger deflections, gave more accurate results, which agreed

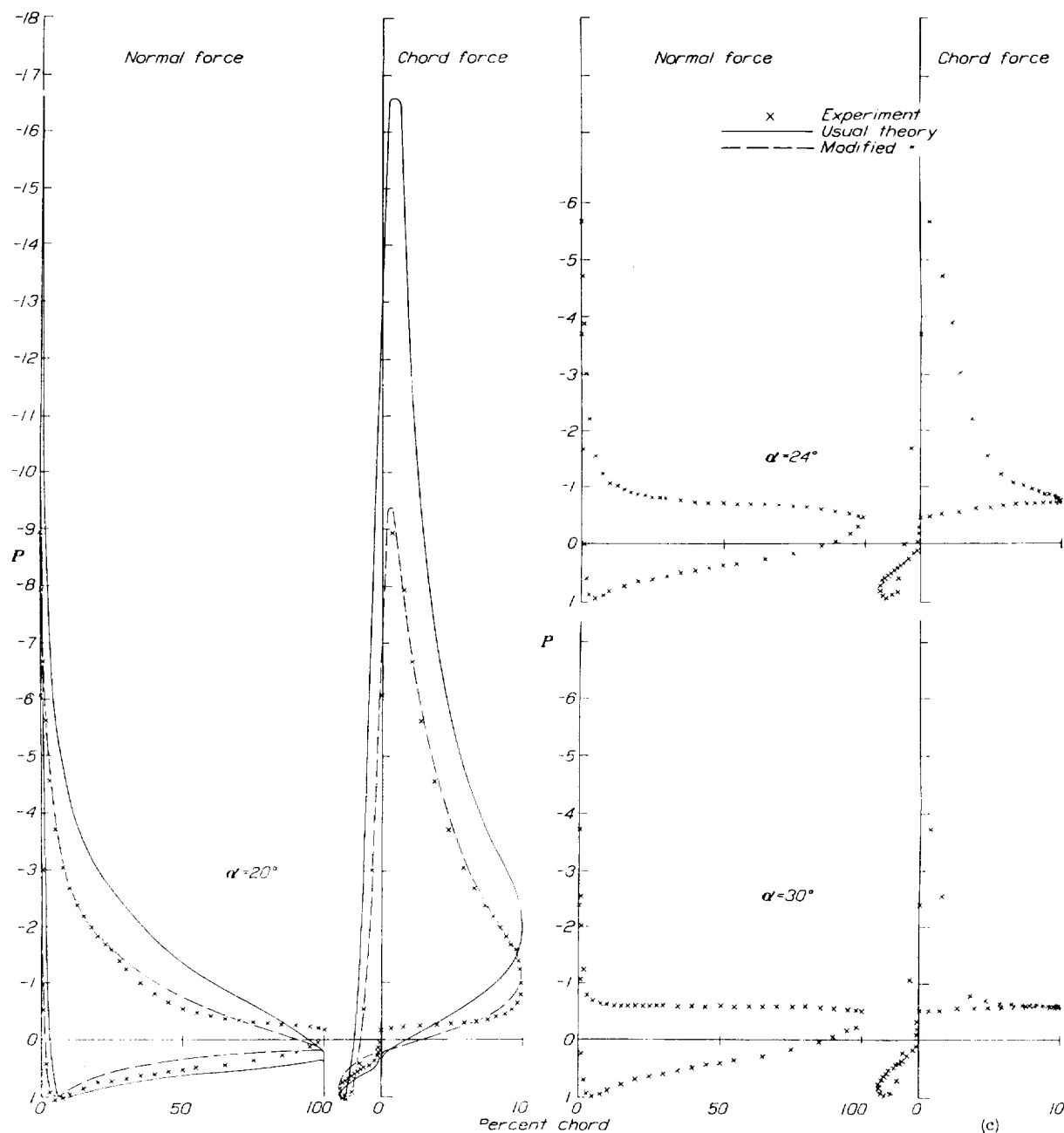


FIGURE 5c. Experimental and theoretical pressure-distribution diagrams for the N. A. C. A. 4412 airfoil at several angles of attack.

shrinkage of the records were avoided by the use of the ratio of two pressures obtained from the same record; namely, the ratio of the pressure at a wing orifice to the dynamic pressure.

The precision of the measured results is indicated by the variations of the pressure diagrams obtained

very closely with the mean values obtained from repeated mercury tests, of which the greatest deviation from the mean values was approximately ± 3 percent of the dynamic pressure. This deviation is not a random scattering of points from any given test but is a consistent difference between repeat tests and may

be partly accounted for by a possible small difference in angle of attack. Figure 7(b) also includes the results of tests made before and after carefully polishing the midspan section of the model. The change in surface smoothness and a slight change in fairness had no discernible effect on the distribution; the differences were

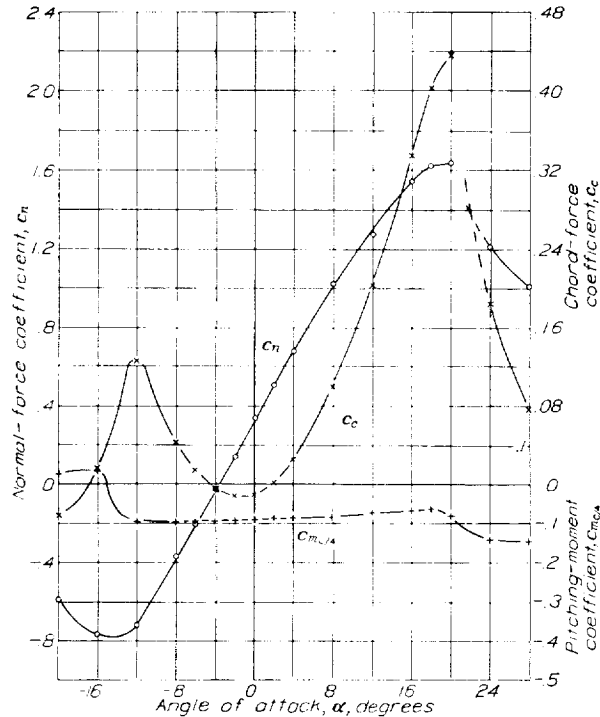


FIGURE 6.—Normal- and chord-force coefficients, and pitching-moment coefficients about the quarter-chord point. The numerical value of C_c should be prefixed by a minus sign.

less than those obtained by repeat tests of the same surface.

The determination of the effective angle of attack of the midspan section entails certain assumptions that are subject to considerable uncertainty. First, the angle of attack of this section may be in error because of the assumption that the deviation of the air-stream axis from the tunnel axis is uniform along the span of the model; i. e., that the geometric angle of attack α is the same for all sections along the span. Actually there is some variation of the air-stream direction across the tunnel. Because of the interference of the support struts, the deflection of the stream in this region might reasonably be expected to exceed the deflection at the midspan section; hence, the deflection at the midspan section is probably less than the effective mean value. Furthermore, a zero deflection of the stream at the midspan section would bring the angle of zero lift obtained from the pressure tests into agreement with force-test results.

A second and rather large source of error lies in the determination of the induced angle of attack. The method used probably produces erroneous results

because of the fact that the tips of a rectangular wing carry a larger proportion of the load than is indicated by the theoretical calculations on which the method is based. To make an accurate experimental determination of the lift distribution on which to base the induced-angle calculations would require pressure measurements at several sections along the span, especially near the tips. An estimate can be made, however, of the possible error in the induced angles of attack given herein by comparison of the deduced slopes of the lift curve for infinite aspect ratio obtained from these tests and from the best force-test data available. Such a comparison indicates that the induced angle of attack may be approximately two-thirds of the calculated values given herein, which would mean a possible error of approximately $\frac{1}{2}^\circ$ for a lift coefficient of 1.

It is evident, therefore, that the effective angles of attack are subject to a considerable error of uncertain magnitude. Approximate possible errors have been

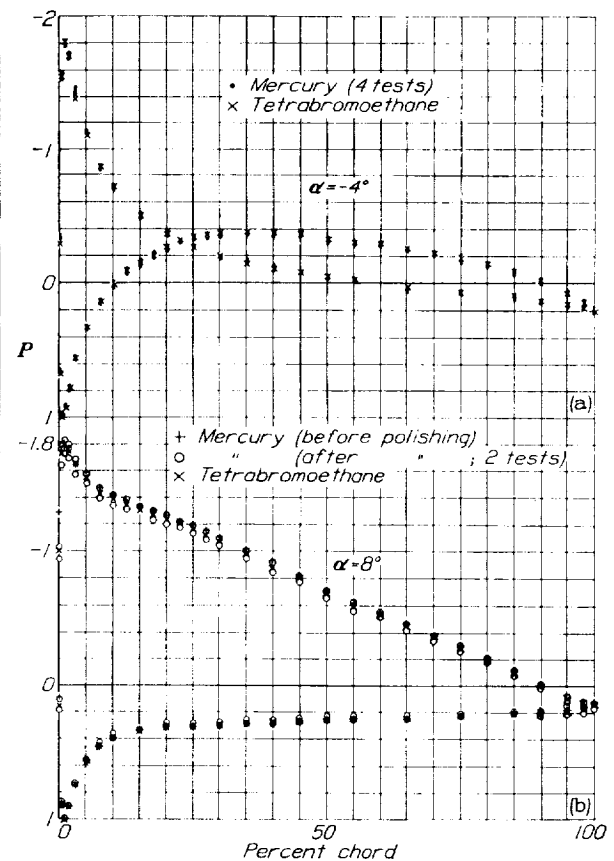


FIGURE 7.—Pressure-distribution diagrams from several tests at two angles of attack.

estimated and summarized as follows: The values of the angles as given may be too large by a constant error of approximately $\frac{1}{4}^\circ$ because of a possible error in the assumed direction of the stream. On the other hand, the angles may be too small by approximately $c_l/2^\circ$, owing to the error in the induced-angle calculations.

THEORETICAL PRESSURE DISTRIBUTION

POTENTIAL-FLOW THEORY

A theoretical determination of the distribution of pressure about an airfoil section has been developed for potential flow and assumes an ideal fluid that is

mined by means of the same transformations. References 1 and 2 present detailed discussions of the underlying theory and the derivation of the necessary equations for the calculation of the characteristics of the potential field about the airfoil.

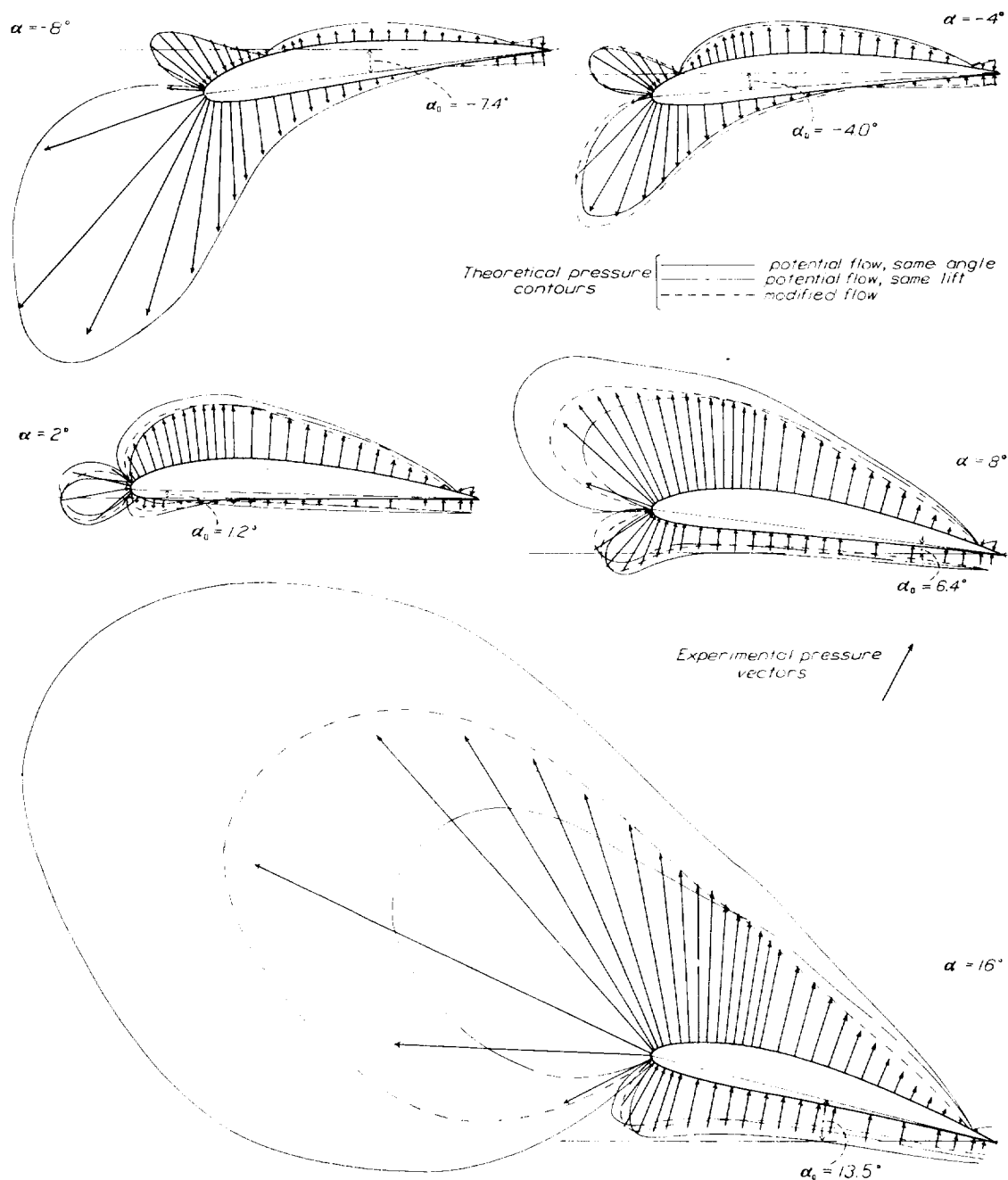


FIGURE 8.—Pressure-vector diagrams for the N. A. C. A. 4412 airfoil at several angles of attack.

nonviscous and incompressible. Briefly, the method consists of the conformal transformation of the airfoil section into a circle. Then, inasmuch as the flow about the circle can readily be calculated, the flow characteristics about the airfoil section can be deter-

The general equation for the local velocity about an airfoil section in a potential flow as given in reference 1

$$v = V \left[\sin(\theta + \epsilon + \alpha) + \frac{\Gamma}{4\pi R V} \right] \quad (1)$$

where

$$k = \frac{\left(1 + \frac{d\epsilon}{d\theta}\right)e^{\psi_0}}{\sqrt{(\sinh^2\psi + \sin^2\theta)\left[1 + \left(\frac{d\psi}{d\theta}\right)^2\right]}} \quad (2)$$

V is the velocity of the undisturbed stream.

α , the angle of attack (2-dimensional).

Γ , the circulation.

θ, ψ, ϵ , parameters that are functions of the airfoil coordinates.

ψ_0 , the mean value of ψ .

$R = ae^{\psi_0}$, the radius of the conformal circle about which the flow is calculable.

In order to calculate the velocity field from equation (1) the circulation must be evaluated. This evalua-

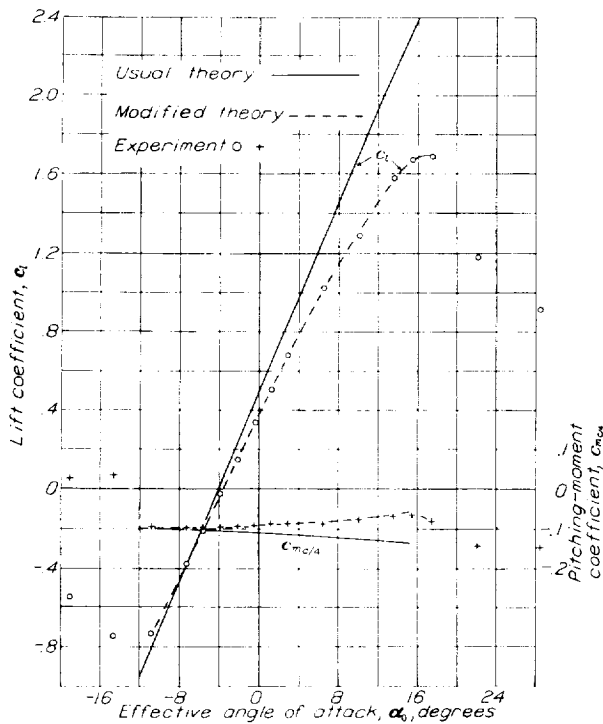


FIGURE 9. Lift and pitching-moment section characteristics for the N. A. C. A. 4412 airfoil.

tion is done by the use of the Kutta condition, which requires that the velocity at the trailing edge ($\theta = \pi$) be zero so that equation (1) becomes

$$v = Vk[\sin(\theta + \epsilon + \alpha) + \sin(\alpha + \epsilon_T)] \quad (1a)$$

where ϵ_T is the value of ϵ at $\theta = \pi$ (trailing edge).

The angle of zero lift is equal to $-\epsilon_T$.

The necessary equations and a step-by-step description of the calculation of the velocity field are given later. The pressure coefficients are computed by means of Bernoulli's equation,

$$P = \frac{p - p_\infty}{q} = 1 - \left(\frac{v}{V}\right)^2 \quad (3)$$

where p is the pressure at the airfoil surface and p_∞ the pressure of the free stream.

COMPARISON OF THEORY AND EXPERIMENT

The theoretical distributions of pressure have been calculated for the 2-dimensional angles of attack corresponding to the measured distributions on the N. A. C. A. 4412 airfoil. Comparisons of the calculated and measured distributions are presented in figure 5 (excluding the diagrams after the airfoil has stalled) and in figure 8. Figure 5 presents the usual normal- and chord-component pressure diagrams and provides a means for a general study of the differences between the theory and experiment as a function of angle of attack. Figure 8 provides a more detailed study at a few angles of attack and presents vector diagrams for the angles of -8° , -4° , 2° , 8° , and 16° . These diagrams were obtained by plotting the pressure coefficients normal to the airfoil profile; the perpendicular distance from the profile line represents the magnitude of the coefficient. The experimental pressures are represented by the drawn vectors and the theoretical pressures by the solid contour line. The other contour lines represent certain modified calculations to be discussed later.

It is immediately evident that the theoretical results do not satisfactorily agree with the actual measurements except for angles of attack near -8° , corresponding approximately to the angle at which the experimental and theoretical lifts are the same (fig. 9). The comparisons in figure 5 show, moreover, that with increasing angle of attack the differences between theory and experiment become larger as predicted by the higher slope of the theoretical lift curve. A detailed study of the vector diagrams (fig. 8) shows how these differences vary around the profile of the airfoil. The largest differences occur in the regions of low pressures, or the high-velocity areas, and as previously stated they increase with increasing angle of attack. Furthermore, the percentage difference in pressure is larger near the trailing edge than in the region of the nose, indicating a progressive influence on the flow as it moves over the airfoil surface.

The effect of these differences in the pressure distribution on the pitching-moment characteristics is shown in figure 9. The theoretical pitching moment about the quarter-chord point was obtained by integrating theoretical pressure diagrams. The results show an increasing diving moment with increasing angle of attack, whereas the diving moment actually decreases.

The comparisons have thus far been made at the same relative angle of attack, that is, for the angle of attack in 2-dimensional flow. Another condition of comparison that has been used more or less regularly in previous studies is suggested; it allows a comparison at the same lift and consists in comparing the theoretical distribution calculated at an angle of attack that gives a theoretical lift equal to the experimental

value. This method has been used for the diagrams in figure 8 and the distributions thus calculated are represented thereon by the long-and-short-dash contour lines. Again the differences are too large to be neglected, especially at angles of attack where a large lift is obtained. At -8° the curve coincides with the previously described contour, since the angle and the lift are the same, while at -4° the distribution calculated on the basis of the same lift is approximately the same as the dashed contour representing a third calculation presented herein. At the higher angles of attack the calculated distributions depart progressively in shape from the measured distributions. It may therefore be concluded that, on the basis of these comparisons, the usual calculations from the potential theory do not give an accurate determination of the distribution of pressure about an airfoil.

The inaccurate prediction of the forces on an airfoil by the usual potential-flow theory is not surprising since the theory neglects the frictional force of the viscous fluid acting on the airfoil. The direct effect of this force, which acts tangential to the direction of the local flow, is important only on the drag and contributes what is known as the "skin-friction" drag. Because of the small magnitude and the direction of this force, the component in the direction of the lift is probably negligible, the lift being determined entirely by the pressure forces. The indirect effect, however, of this friction force is the deceleration of the air in a thin layer near the surface of the airfoil and the production of the so-called "boundary-layer" phenomena, which are important in the development of lift by an airfoil. In the boundary layer the velocity changes rapidly from zero at the surface of the airfoil to the value of the local stream velocity at the outer limit of the layer. The loss of energy involved in overcoming the friction forces results in a cumulation of slowly moving air as the flow moves back along the airfoil; hence the boundary-layer thickness increases toward the trailing edge. This cumulative effect is indicated by the progressive increase in the differences between the theoretical and measured pressures.

From this discussion it is not to be presumed that agreement between the measured and calculated results should occur at zero lift, except approximately for a symmetrical airfoil section. The velocity distributions over the upper and lower surfaces of an asymmetrical section are not the same, even at zero lift. The viscous effects on the flow over the two surfaces at the calculated angle of zero lift are therefore different and a lift is measured, which is negative for most sections. Actually, then, the experimental and theoretical angles of zero lift are not the same and for normal sections the two lift curves intersect at a negative value of the lift coefficient.

Outside the boundary layer the viscous forces can probably be considered negligible and the flow a

potential one; probably the pressures may also be considered as being transmitted undiminished through the thin boundary layer. The actual flow might therefore be replaced by a potential flow about a shape slightly different from that defined by the airfoil coordinates, which would require the determination of the boundary-layer thickness to define the effective profile shape. The pressure about the new shape could then be computed by the potential theory. Boundary-layer calculations, however, are at present subject to uncertainties that would cast doubt on the validity of the results and, in addition, the computations are difficult and tedious.

MODIFIED THEORETICAL CALCULATIONS

A simpler and more practical method of calculating the pressure over an airfoil section has been developed

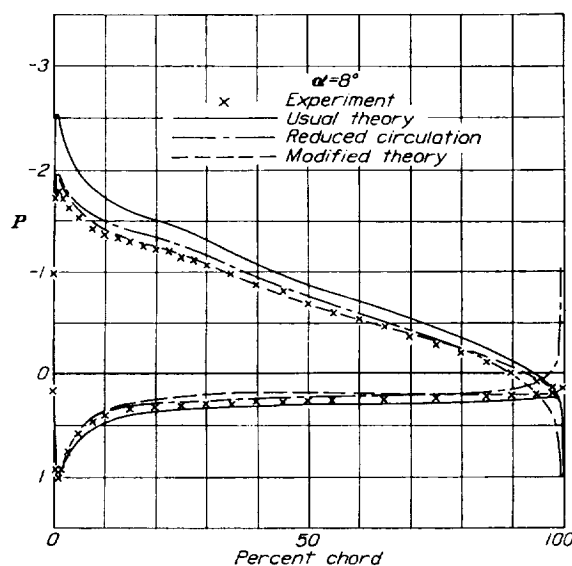


FIGURE 10.—Effect of an arbitrary reduction of the circulation on the calculated pressure distribution.

as a result of the foregoing analysis. The analysis shows that theoretical distributions calculated at the true angle of attack are similar in shape to the true distributions but give too high a lift. Conversely, when the theoretical distributions are calculated at an angle of attack that gives the same lift as the experimental distribution, the two distributions are dissimilar in shape.

The modified calculation is made at the effective angle of attack but the circulation is determined from the experimentally measured lift instead of by the Kutta-Joukowski method. The preliminary calculations made on this basis resulted in an excessive velocity and a consequent high suction pressure at the trailing edge, as shown in figure 10. This unsatisfactory result (shown by the dot-dash line in fig. 10) was finally avoided by means of a further modification subsequently described.

Since a change in the effective profile shape has been predicted by boundary-layer considerations, an arbitrary modification of the shape parameter ϵ is made so that the velocity becomes zero at $\theta = \pi$. (See equation (1).) The shape is thus altered to satisfy again the Kutta-Joukowski condition. In order to maintain the continuity of the ϵ curve, a study has been made of the manner in which ϵ should be modified. The indicated cumulative effects of the viscous forces toward the trailing edge show that most of the change in ϵ should

tions obtained by means of the modified calculations are given by the dashed lines. The relative merit of the unaltered potential theory and the modified method for the calculation of the pressure distribution about an airfoil section is shown in figures 5, 8, and 9.

The following step-by-step description of the computations required to obtain the calculated pressure distribution is given in sufficient detail to enable the calculations for any airfoil to be made. The local velocity about the airfoil is computed by means of equation (1)

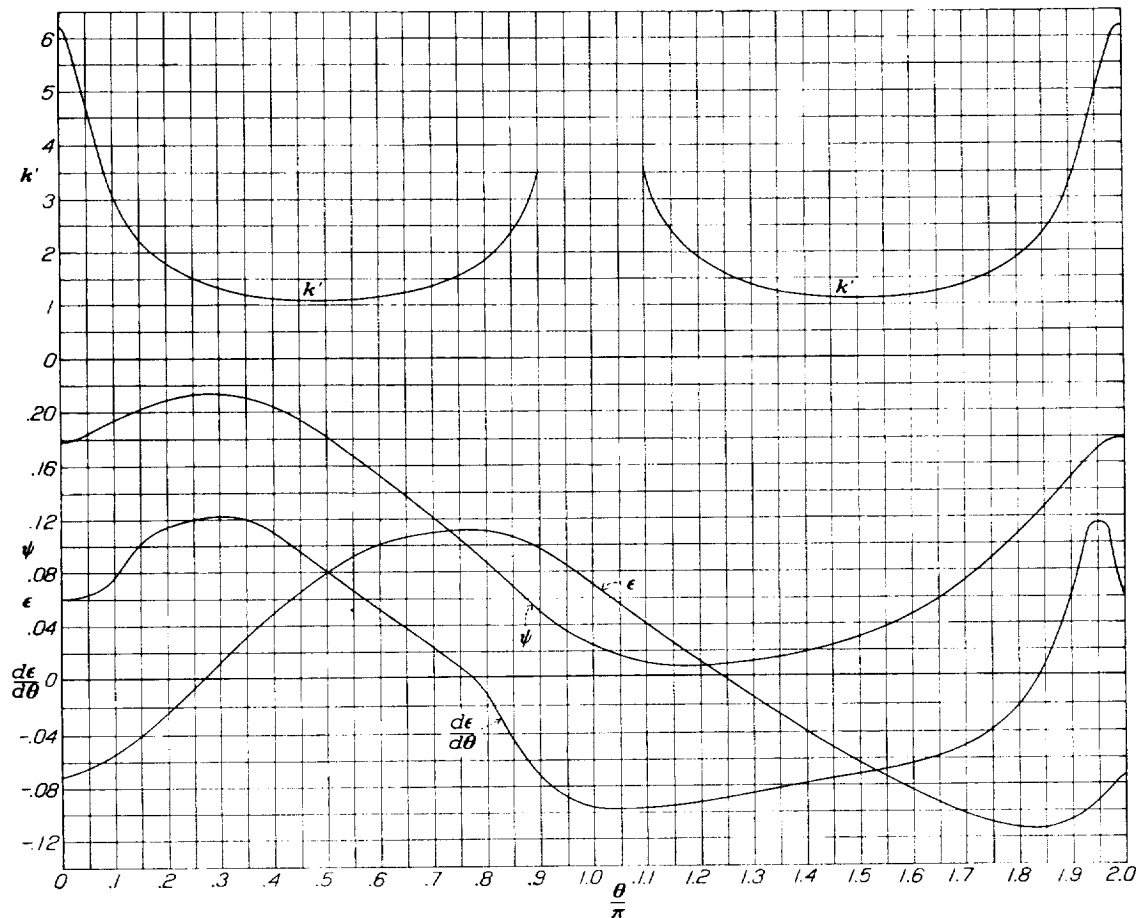


FIGURE 11.—Theoretical parameters required to compute the theoretical pressures on the N. A. C. A. 4412 airfoil.

probably be made in that region. Inasmuch as the effect of changing ϵ is not critical for different distributions of the change, provided that most of the change is made near the trailing edge of the airfoil, a purely arbitrary distribution is chosen that permits ready application, namely, a sinusoidal variation with θ .

The ϵ curve and subsequently the other parameters must be modified for each angle of attack. This modification has been made and the corresponding pressure distributions determined for several angles of attack. (See figs. 5 and 8.) At -8° the distribution is the same as that shown by the solid line representing the unaltered theory. In the other diagrams the distribu-

modified as indicated by the preceding discussion. The detailed forms of the modifications are introduced as they appear in the course of routine computations.

In order that the transformation from the airfoil to its conformal circle may be of a convenient form, the coordinate axes are selected so that the profile is as nearly as possible symmetrical about them. (See reference 1.) The x axis is chosen as the line joining the centers of the leading- and trailing-edge radii. The origin is located midway between a point bisecting the distance from the leading edge to the center for the leading-edge radius and the corresponding point at the trailing edge; the coordinates of these points are

respectively $(2a, 0)$ and $(-2a, 0)$. In the following discussion the coordinate scale has been chosen so that a is unity. (For practical purposes it is probably sufficient to choose the chord joining the extremities of the mean line as the x axis.)

The following equations express the relationship between the airfoil coordinates previously described and the parameters θ and ψ .

$$\begin{aligned} x &= 2 \cosh \psi \cos \theta \\ y &= 2 \sinh \psi \sin \theta \end{aligned} \quad (4)$$

In order to compute values of θ corresponding to any given point on the airfoil profile, equations (4) are solved for $\sin^2 \theta$.

$$\sin^2 \theta = \frac{1}{2} (h + \sqrt{h^2 + y^2}) \quad (5)$$

where

$$h = 1 - \left(\frac{x}{2}\right)^2 - \left(\frac{y}{2}\right)^2$$

A similar solution for $\sinh^2 \psi$ can be obtained but experience has shown that a more usable solution is given by the equation below

$$\sinh \psi = \frac{1}{2} \frac{y}{\sin \theta} \quad (6)$$

A plot of ψ as a function of θ for the N. A. C. A. 4412 airfoil is given in figure 11. The function ψ_0 is given by

$$\psi_0 = \frac{1}{2\pi} \int_0^{2\pi} \psi d\theta$$

and can be determined graphically from the ψ curve or by a numerical evaluation. The value of ψ_0 for the N. A. C. A. 4412 airfoil is

$$\psi_0 = 0.1044$$

The parameter ϵ as a function of θ is given by the definite integral,

$$\epsilon_n = -\frac{1}{2\pi} \int_0^{2\pi} \psi \cot \frac{\theta - \theta_n}{2} d\theta \quad (7)$$

where the subscript n refers to the particular value of θ for which the corresponding value of ϵ is to be determined. A 20-point numerical evaluation of this integral is derived in reference 1 and is included here for convenience. The integral is evaluated at 20 equal interval values of θ , namely,

$$\begin{aligned} \theta_0 &= 0 = \theta_{20} \\ \theta_1 &= \frac{\pi}{10} = \theta_{19} \\ \theta_2 &= \frac{2\pi}{10} = \theta_{18} \\ &\vdots \\ \theta_{20} &= 2\pi = \theta_0 \end{aligned}$$

The value of ϵ at $\theta_n = \frac{n\pi}{10}$ is given by the following equation.

$$\begin{aligned} \epsilon_n = -\frac{1}{\pi} \left[\frac{\pi}{10} \left(\frac{d\psi}{d\theta} \right)_n + 1.091 (\psi_{n+1} - \psi_{n-1}) \right. \\ \left. + 0.494 (\psi_{n+2} - \psi_{n-2}) \right. \\ \left. + 0.313 \right. \\ \left. + 0.217 \right. \\ \left. + 0.158 \right. \\ \left. + 0.115 \right. \\ \left. + 0.0804 \right. \\ \left. + 0.0511 \right. \\ \left. + 0.0251 (\psi_{n+9} - \psi_{n-9}) \right] \end{aligned} \quad (8)$$

where the subscripts designate the particular θ at which the named quantity is taken. A plot of ϵ as a function of θ for the N. A. C. A. 4412 airfoil is given in figure 11. Thus far the calculations are identical with those made for the potential theory.

As stated in the discussion of the modified theoretical calculations, the circulation is evaluated by the experimentally known lift of the airfoil section. The well-known equation relating the lift and the circulation is

$$L = \rho V \Gamma$$

Also by definition

$$L = \frac{1}{2} \rho V^2 c c_l$$

Expressing the circulation in terms of the lift coefficient,

$$\Gamma = \frac{cV}{2} c_l$$

and finally

$$\frac{\Gamma}{4\pi R V} = \frac{c}{8\pi R} c_l \quad (9)$$

Substituting the numerical values for the N. A. C. A. 4412,

$$\frac{\Gamma}{4\pi R V} = \frac{1}{6.915} c_l \quad (9a)$$

The prediction of unreasonable velocities around the trailing edge is avoided by altering the ϵ function so that the velocity is zero at $\theta = \pi$. The altered function is designated ϵ_a and is arbitrarily assumed to be given by

$$\epsilon_a = \epsilon + \frac{\Delta\epsilon_T}{2} (1 - \cos \theta) \quad (10)$$

where $\Delta\epsilon_T$ is the increment of ϵ required to give zero velocity at $\theta = \pi$ and is a function of the angle of attack. The quantity $\Delta\epsilon_T$ is given by

$$\Delta\epsilon_T = \epsilon_{aT} - \epsilon_T$$

where ϵ_{aT} is determined by equating equation (1) to zero and substituting from equation (9).

$$\sin (\pi + \alpha + \epsilon_{aT}) + \frac{c}{8\pi R} c_l = 0$$

Solving for ϵ_{aT} gives,

$$\epsilon_{aT} = \sin^{-1} \frac{c}{8\pi R} c_l - \alpha$$

The parameters ϵ and ψ are conjugate functions of θ , and ψ is given by

$$\psi_n = \frac{1}{2\pi} \int_0^{2\pi} \epsilon \cot \frac{\theta - \theta_n}{2} d\theta + \psi_0$$

where the definite integral can be evaluated in the same manner as equation (7). The coordinates of the profile corresponding to the modified ϵ function can be obtained from the new ψ function by equations (4). Figure 12 gives the modified shape obtained by this method for the N. A. C. A. 4412 airfoil at $\alpha = 8^\circ$ and 16° .

The profiles given in figure 12 are, of course, only effective profiles corresponding to the calculations. The actual profile about which a potential flow might be considered as being established would be blunt at the trailing edge and would have the thickness of the wake at that point. The thickness of the boundary layer on the upper surface, however, is greater than that on the lower surface; therefore, if the trailing edge were taken as the midpoint of the wake and the after portion of the profile were faired to that point, the



FIGURE 12.—Change in profile shape associated with the modified theoretical calculation of pressure.

resulting shape would be similar to the effective profiles in figure 12.

The influence of the changes in ψ on the value of k are found to be negligible so that k_α may be written

$$k_\alpha = \left(1 + \frac{d\epsilon_\alpha}{d\theta}\right) k'$$

where

$$k' = \frac{e^{\psi_0}}{\sqrt{(\sinh^2 \psi + \sin^2 \theta) \left[1 + \left(\frac{d\psi}{d\theta}\right)^2\right]}}$$

Differentiating equation (10)

$$\frac{d\epsilon_\alpha}{d\theta} = \frac{d\epsilon}{d\theta} + \frac{\Delta\epsilon_\tau}{2} \sin \theta$$

Plots of $\frac{d\epsilon}{d\theta}$ and k' as functions of θ for the N. A. C. A. 4412 airfoil are given in figure 11. Equation (1) for the velocity at any point on the airfoil profile is now written

$$v = V k_\alpha \left[\sin (\theta + \epsilon_\alpha + \alpha) + \frac{c}{8\pi R} c_l \right] \quad (1b)$$

The generality of the preceding method of calculating the pressure distribution about an airfoil section is supported by the following evidence. First, no restricting assumptions have been made in the development of the method. Second, the circulation is determined by a known quantity, the experimentally measured lift. Third, the change in the effective airfoil shape is in the direction indicated by boundary-layer considerations. Finally, the computed and measured pressures agree satisfactorily.

LANGLEY MEMORIAL AERONAUTICAL LABORATORY,
NATIONAL ADVISORY COMMITTEE FOR AERONAUTICS,
LANGLEY FIELD, VA., March 25, 1936.

REFERENCES

1. Theodorsen, T., and Garrick, I. E.: General Potential Theory of Arbitrary Wing Sections. T. R. No. 452, N. A. C. A. 1933.
2. Theodorsen, Theodore: Theory of Wing Sections of Arbitrary Shape. T. R. No. 411, N. A. C. A., 1931.
3. Jacobs, Eastman N., and Abbott, Ira H.: The N. A. C. A. Variable-Density Wind Tunnel. T. R. No. 416, N. A. C. A., 1932.
4. Millikan, Clark B.: On the Lift Distribution for a Wing of Arbitrary Plan Form in a Circular Wind Tunnel. Publication No. 22, C. I. T., 1932.

TABLE I.—EXPERIMENTAL DATA—N. A. C. A. 4412 AIRFOIL

[Average pressure (standard atmospheres): .21; average Reynolds Number: 3,100,000]

Orifices			Values of pressure coefficient, $P = \frac{p - p_\infty}{q}$, for different angles of attack																		
Designation	Station (percent c from L. E. of chord)	Ordinate (percent c above chord)	-20°	-16°	-12°	-8°	-6°	-4°	-2°	0°	2°	4°	6°	8°	10°	12°	16°	18°	20°	24°	30°
28	100.00	0	-0.421	-0.199	0.114	0.198	0.217	0.204	0.207	0.200	0.181	0.158	0.134	0.101	0.010	-0.062	-0.173	-0.466	-0.513		
1	97.92	-16	-0.454	-0.251	.159	.224	.181	.178	.180	.183	.164	.157	.167	.160	.140	.121	.094	.049	-.291	-.304	
29	94.86	-16	-0.406	-0.291	.107	.185	1.52	1.51	1.58	1.66	.154	.156	.180	.166	.179	.166	.127	.160	-.167		
2	89.90	-22	-0.505	-0.330	.074	.153	.122	.128	.140	.156	.152	.160	.203	.199	.231	.237	.224	-.030	-.036		
30	84.94	-28	-0.538	-0.382	.035	.107	.072	.082	.098	.118	.118	.158	.211	.212	.257	.270	.283	.049	-.042		
31	74.92	-52	-0.558	-0.454	-.043	.055	.049	.068	.095	.126	.136	.158	.231	.251	.322	.348	.374	.179	.179		
32	64.94	-84	-0.564	-0.539	-.101	.002	.000	.028	.062	.104	.120	.154	.244	.283	.374	.407	.453	.270	.289		
3	54.48	-1.24	-0.571	-0.643	-.199	-.082	-.063	-.024	.021	.072	.100	.157	.250	.309	.414	.452	.492	.348	.368		
33	49.98	-1.44	-0.571	-0.695	-.252	-.115	-.099	-.053	-.005	.050	.091	.134	.252	.316	.426	.472	.531	.381	.407		
4	44.90	-1.64	-0.571	-0.721	-.304	-.160	-.128	-.075	-.017	.048	.088	.140	.268	.342	.459	.505	.570	.413	.446		
34	39.98	-1.86	-0.558	-0.754	-.368	-.206	-.169	-.105	-.041	.031	.071	.136	.265	.362	.485	.544	.609	.466	.498		
5	34.90	-2.10	-0.551	-0.773	-.447	-.258	-.217	-.146	-.073	.010	.066	.133	.290	.387	.516	.576	.642	.504	.544		
35	29.96	-2.30	-0.545	-0.786	-.545	-.358	-.274	-.190	-.105	-0.011	.048	.116	.293	.414	.551	.609	.687	.557	.596		
6	24.90	-2.54	-0.545	-0.806	-.688	-.427	-.367	-.266	-.165	-0.054	.025	.115	.313	.433	.589	.661	.726	.609	.648		
36	19.98	-2.76	-0.551	-0.819	-.799	-.591	-.490	-.365	-.244	-0.111	-0.093	.321	.472	.627	.687	.752	.824	.700	.733		
7	14.94	-2.90	-0.558	-0.825	-1.178	-.799	-.663	-.502	-.348	-.180	-.053	.076	.345	.518	.713	.785	.857	.733	.778		
37	9.96	-2.86	-0.551	-0.832	-1.660	-1.143	-.946	-.716	-.501	-.279	-0.111	.059	.402	.616	.818	.883	.948	.824	.876		
8	7.38	-2.72	-0.577	-0.916	-2.070	-1.407	-1.153	-.867	-.596	-.333	-0.131	.071	.462	.713	.896	.961	1.019	.902	.941		
38	4.94	-2.46	-0.571	-0.897	-2.807	-1.861	-1.490	-1.106	-.777	-.428	-.150	.109	.508	.818	.980	1.013	1.046	.948	.980		
9	2.92	-2.06	-0.702	-1.242	-3.745	-2.408	-1.931	-1.380	-.932	-.467	-.098	.231	.748	.948	.993	.948	.909	.883	.941		
39	1.66	-1.60	-1.053	-1.947	-4.940	-3.198	-2.478	-1.709	-1.059	-.366	0.028	.409	.916	.974	.991	.966	.933	.902	.941		
10	.92	-1.20	-2.082	-3.212	-6.177	-3.770	-2.765	-1.812	-.995	-.266	.254	.643	1.013	.831	.294	-.279	-.173	-.518	.003	-.244	
40	.36	-0.70	-3.204	-4.300	-7.337	-4.052	-2.732	-1.559	-.631	.156	.639	.924	.905	.094	-1.379	-2.285	-3.012	-1.671	-1.059		
11	0	0	-2.623	-3.433	-5.480	-2.397	-1.232	-.296	-.356	.834	.989	.952	.157	-1.555	-3.648	-5.000	-6.073	-3.695	-2.382		
41	0	.68	-1.178	-1.549	-2.625	-.538	.184	.681	.945	1.010	.854	.473	-1.000	-3.250	-6.230	-7.775	-8.941	-5.660	-3.730		
12	.44	1.56	.322	.231	-.043	.765	.955	.994	.948	.720	.336	-.202	-1.740	-3.738	-5.961	-7.125	-7.954	-4.698	-2.552		
42	.94	2.16	.739	.720	-.586	.974	1.009	.939	.770	.468	.055	-.456	-1.793	-3.399	-5.210	-6.110	-6.681	-3.881	-2.006		
13	1.70	2.78	.928	.935	-.883	1.000	.939	.782	.569	.246	-.148	-0.611	-1.743	-3.053	-4.478	-5.160	-5.620	-3.010	-1.249		
43	2.94	3.64	.987	1.000	-.974	.896	.761	.559	.332	.118	-.336	-.728	-1.647	-2.637	-3.765	-4.285	-4.562	-2.200	-.786		
14	4.90	4.68	.922	.935	-.896	.713	.512	.333	.110	-.179	-.485	-.813	-1.547	-2.343	-3.190	-3.570	-3.731	-1.529	-.695		
44	7.50	5.74	.804	.798	-.752	.498	.344	.139	-.066	-.312	-.568	-.831	-1.432	-2.057	-2.709	-2.981	-3.060	-1.235	-.644		
15	9.96	6.56	.687	.687	-.622	.374	.208	.017	-.168	-.388	-.623	-.872	-1.391	-1.912	-2.440	-2.662	-2.681	-1.059	-.630		
45	12.58	7.34	.583	.576	-.498	.263	.089	-.091	-.271	-.468	-.676	-.899	-1.350	-1.802	-2.240	-2.440	-2.440	-0.611	-.599		
16	14.92	7.88	.498	.485	-.407	.178	.014	-.152	-.309	-.500	-.700	-0.912	-1.308	-1.769	-2.149	-2.285	-2.180	-.955	-.604		
46	17.44	8.40	.414	.407	-.329	.100	-.052	-.210	-.360	-.537	-.721	-0.910	-1.272	-1.620	-1.952	-2.062	-1.984	-.910	-.604		
17	19.96	8.80	.335	.335	-.257	.036	-.111	-.262	-0.402	-.568	-.740	-0.914	-1.239	-1.548	-1.841	-1.927	-1.815	-.870	-.598		
47	22.44	9.16	.263	.257	-.172	0.024	-.176	-.322	-.452	-.599	-.769	-0.930	-1.224	-1.502	-1.758	-1.822	-1.685	-.851	-.591		
18	24.92	9.52	.212	.211	-.140	-0.063	-.196	-.332	-.454	-.599	-.746	-.895	-1.163	-1.418	-1.640	-1.692	-1.592	-.825	-.591		
48	27.44	9.62	.166	.165	-.100	-0.096	-.228	-.355	-.471	-.566	-.742	-.881	-1.122	-1.347	-1.535	-1.573	-1.391	-.812	-.591		
19	29.88	9.76	.114	.133	-.068	-0.114	-0.241	-.364	-.469	-.594	-.722	-.851	-1.071	-1.280	-1.438	-1.463	-1.254	-.786	-.591		
49	34.98	9.90	.036	.055	-.009	-.154	-.275	-.381	-.473	-.596	-.693	-.804	-.982	-1.144	-1.269	-1.255	-1.005	-.760	-.591		
20	39.90	9.84	-.017	.009	-.030	-.173	-.272	-.370	-.447	-.542	-.635	-.732	-.880	-1.007	-1.099	-1.059	-.798	-.554	-.591		
50	44.80	9.64	-.095	-.044	-.069	-.194	-.291	-.371	-.439	-.519	-.619	-.691	-.809	-.902	-.961	-0.910	-.655	-.420	-.591		
21	49.92	9.22	-.121	-.056	-.075	-.173	-.256	-.329	-.389	-.455	-.525	-.595	-.690	-.759	-.786	-.734	-.538	-.315	-.591		
51	54.92	8.76	-.147	-.069	-.075	-.161	-.238	-.303	-.351	-.406	-.471	-.527	-.601	-.649	-.649	-.544	-.473	-.300	-.591		
22	59.94	8.16	-.199	-.101	-.095	-0.161	-.214	-.268	-.342	-.391	-.438	-.487	-.541	-.576	-.551	-.460	-.414	-.295	-.591		
52	64.90	7.54	-.225	-.108	-.082	-.128	-.174	-.214	-.266	-.324	-.378	-.421	-.456	-.460	-.414	-.343	-.369	-.288	-.591		
23	69.86	6.76	-.252	-.121	-.082	-.115	-.181	-.225	-.250	-.282	-.319	-.351	-.371	-.375	-.316	-.264	-.337	-.282	-.591		
53	74.90	5.88	-.277	-.128	-.056	-.082	-.148	-.183	-.200	-.222	-.252	-.279	-.285	-.264	-.212	-.212	-.310	-.255	-.591		
24	79.92	4.92	-.297	-.147	-.069	-.076	-.115	-.144	-.155	-.169	-.191	-.210	-.199	-.180	-.147	-.173	-.291	-.242	-.578		
54	84.88	3.88	-.330	-.154	-.024	-.024	-.068	-.091	-.094	-.101	-.116	-.113	-.106	-.082	-.082	-.140	-.271	-.246	-.565		
25	89.88	2.74	-.356	-.161	.022	.028	-.006	-.019	-.016	-.017	-.026	-.032	-.009	-.004	-.043	-0.114	-.246	-.265	-.552		
55	94.90	1.48	-.388	-.174	.075	.100	.073	.069	.078	.082	.076	.070	.079	.062	.016	-.095	-.226	-.519	-.519		
26	98.00	.68	-.434	-.200	.127	.165	.141	.139	.147	.150	.143	.127	.120	.088	-0.004	-0.075	-.200	-.479	-.506		
27	98.00	.68																			
28	100.00	0																			

* Test, variable-density tunnel 1008; manometer liquid, mercury.

† Test, variable-density tunnel 1009-4; manometer liquid, tetrabromoethane.

TABLE II.—INTEGRATED AND DERIVED CHARACTERISTICS—N. A. C. A. 4412 AIRFOIL

α

TABLE III.—THEORETICAL PARAMETERS—N. A. C. A. 4412 AIRFOIL

Station (percent c)	Ordinate (percent c)	x	y	$\frac{\theta}{\pi}$	ψ	$\theta + \epsilon$	Ordinate (percent c)	x	y	$\frac{\theta}{\pi}$	ψ	$\theta + \epsilon$
Upper surface							Lower surface					
		2.032	0	0	0.178	deg. min.		2.032	0	0	0.178	deg. min.
0	0.62	2.031	.0121	.007	0.178	-4 10	0	2.031	-.0129	-.012	0.178	-4 10
.25	1.25	2.021	.0375	.034	-----	-2 1	.60	2.021	-.0371	-.034	-----	-6 20
.5	1.64	2.011	.0532	.046	-----	4 35	.88	2.011	-.0484	-.043	-----	-10 49
1.25	2.44	1.981	.0855	.073	.186	9 48	-1.43	1.980	-.0706	-.069	.162	-18 1
2.5	3.39	1.931	.1239	.103	.194	15 29	-1.95	1.930	-.0916	-.098	.151	-23 48
5	4.73	1.830	.1784	.146	.201	23 48	-2.49	1.829	-.1130	-.140	.133	-31 47
7.5	5.76	1.730	.2203	.179	.205	30 19	-2.74	1.729	-.1227	-.172	.119	-37 39
10	6.59	1.629	.2542	.207	.208	35 58	-2.86	1.628	-.1271	-.200	.108	-42 36
15	7.89	1.427	.3075	.254	.213	45 25	-2.88	1.426	-.1271	-.249	.090	-51 11
20	8.80	1.225	.3446	.296	.213	53 56	-2.74	1.224	-.1210	-.292	.076	-58 32
25	9.41	1.024	.3696	.333	.211	61 26	-2.50	1.023	-.1110	-.330	.064	-65 2
30	9.76	.824	.3845	.369	.208	68 32	-2.26	.820	-.1005	-.366	.055	-71 6
40	9.80	.418	.3873	.435	.197	81 42	-1.80	.417	-.0807	-.435	.041	-82 47
50	9.19	-.0149	.3640	.500	.181	94 32	-1.40	-.0137	-.0633	-.500	.030	-93 45
60	8.14	-.389	.3229	.560	.163	106 11	-1.00	-.390	-.0460	-.560	.023	-103 50
70	6.69	-.792	.2655	.628	.143	119 0	-.65	-.793	-.0307	-.629	.017	-115 12
80	4.89	-1.196	.1940	.702	.121	132 48	-.39	-1.197	-.0190	-.704	.012	-127 32
85	3.83	-1.398	.1518	.745	.106	140 32	-.30	-1.398	-.0149	-.746	.010	-134 28
90	2.71	-1.600	.1074	.793	.089	149 23	-.22	-1.600	-.0109	-.795	.009	-142 25
95	1.47	-1.802	.0577	.855	.065	159 56	-.16	-1.802	-.0081	-.856	.009	-152 31
98	.68	-1.924	.0262	.910	.047	169 18	-.14	-1.924	-.0069	-.912	.012	-161 34
100	.13	-2.003	0	1.000	.025	184 3	-.13	-2.003	-.0013	-1.000	.025	-175 57

TABLE IV.—THEORETICAL PARAMETERS—N. A. C. A. 4412 AIRFOIL

$\frac{\theta}{\pi}$	ψ	$\frac{d\psi}{d\theta}$	k'	ϵ	$\frac{d\epsilon}{d\theta}$
0	0.1780	0	6.201	-0.0727	0.0600
.1	.1924	.0611	3.041	-.0548	.0755
.2	.2082	.0395	1.777	-.0258	.1135
.3	.2128	-.0116	1.326	.0120	.1220
.4	.2035	-.0527	1.139	.0492	.1095
.5	.1806	-.0866	1.088	.0797	.0800
.6	.1519	-.0942	1.147	.1002	.0515
.7	.1214	-.1028	1.350	.1087	.0230
.8	.0863	-.1166	1.856	.1109	-.0130
.9	.0501	-.1016	3.528	.0975	-.0720
1.0	.0250	-.0590	-----	.0706	-.0960
1.1	.0118	-.0249	3.589	.0403	-.0970
1.2	.0088	.0020	1.887	.0115	-.0925
1.3	.0120	.0169	1.372	-.0153	-.0860
1.4	.0192	.0284	1.167	-.0385	-.0785
1.5	.0302	.0434	1.109	-.0612	-.0720
1.6	.0470	.0661	1.163	-.0837	-.0640
1.7	.0736	.0976	1.351	-.1029	-.0505
1.8	.1080	.1211	1.845	-.1126	-.0210
1.9	.1488	.1351	3.205	-.1070	.0640
2.0	.1780	0	6.201	-.0727	.0600

REPORT No. 564

TESTS OF A WING-NACELLE-PROPELLER COMBINATION AT SEVERAL PITCH SETTINGS UP TO 42°

By RAY WINDLER

SUMMARY

A 4-foot model of Navy propeller No. 4412 was tested in conjunction with an N. A. C. A. cowled nacelle mounted ahead of a thick wing in the 20-foot propeller-research tunnel. A range of propeller pitches from 17° to 42° at $0.75R$ was covered, and for this propeller the efficiency reached a maximum at a pitch setting of 27° ; at higher pitches the efficiencies were slightly lower. The corrected propulsive efficiency is shown to be independent of the angle of attack for the high-speed and the climbing ranges of flight. A working chart is presented for the selection of similar propellers over a wide range of airplane speed, engine power, and propeller revolution speed.

INTRODUCTION

Of the numerous N. A. C. A. reports on the characteristics of metal propellers, probably the most widely used is reference 1, which provides working charts for the selection of propellers for use with engines located in the various shapes of fuselages commonly used at the time of publication. A sufficient range of airplane speed, engine power, propeller pitch, and propeller revolution speed was covered in these tests to meet and even to exceed the needs at that time. The recent increase in high speed and the use of more highly powered and of geared engines has, however, necessitated additional propeller tests.

Current research of the N. A. C. A. on wing-nacelle-propeller arrangements, confined mainly to a propeller pitch of 17° at $0.75R$, has shown that position B of reference 2, with the nacelle located in line with and about 30 percent of the chord ahead of the leading edge of the wing, is one of the desirable combinations for use with radial engines. Accordingly, this position was selected for an extension of the program to include tests of a propeller-pitch range from 17° to 42° at $0.75R$. The subject paper presents the results of these tests in a form suitable for the selection of a propeller for a wide range of conditions; the results cover the present needs as well as some future possibilities.

APPARATUS AND METHODS

The tests were conducted in the N. A. C. A. 20-foot propeller-research tunnel (reference 3). The wing of

5-foot chord and 15-foot span, the nacelle, and the propeller described in reference 2 were used. The single sting was replaced by a double one with offsets at the rear, partly for convenience and partly to secure a larger negative angle of attack. (See fig. 1.)

The method of testing was similar to that of reference 2 except that tare runs were omitted because previous tests had shown that the tare was independent of lift and therefore not required in the analysis. The wing was tested for airfoil characteristics from -10° to 10° angle of attack with and without the nacelle. Propeller tests were then made with propeller pitches



FIGURE 1.—Test set-up.

from 17° to 42° at $0.75R$ for wing angles of attack from -8° to 5° .

The V/nD range for each pitch was obtained in the following manner: A revolution speed was set that would require about the maximum torque of the motor at the ground point. This revolution speed was held constant and the air speed gradually increased up to about 102 miles per hour. In order to obtain the higher values of V/nD , the air speed was held at 102 miles per hour and the revolution speed decreased. The following values of propeller speed (within ± 15

r. p. m.) were used for the constant revolution-speed portion of the tests.

Pitch at 0.75R	Propeller speed
Degrees	r. p. m.
17	2,800
22	2,300
27	1,950
32	1,700
37	1,475
42	1,400

RESULTS

These results are presented in the same graphic and tabular form as in previous wing-nacelle reports. A detailed discussion of the accuracy and manner of presentation may be found in references 2 and 4. The

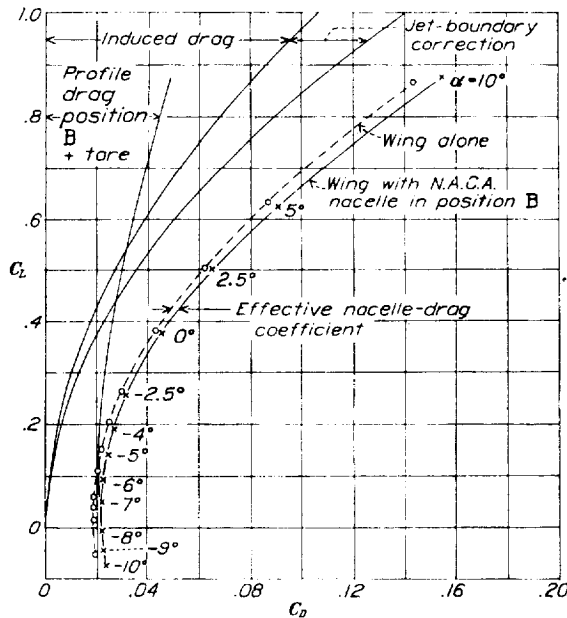


FIGURE 2.—Airfoil curves, propeller removed.

nondimensional coefficients and symbols employed are given and defined as follows:

$$\begin{aligned}
 C_L &= \frac{\text{lift}}{qS} \quad (\text{propeller removed}) \\
 C_D &= \frac{\text{drag}}{qS} \quad (\text{propeller removed}) \\
 C_{LP} &= \frac{\text{lift}}{qS} \quad (\text{propeller operating}) \\
 C_T &= \frac{(T - \Delta D)}{\rho n^2 D^4} = \frac{(R + D)}{\rho n^2 D^4} \\
 C_{T_{corr.}} &= \frac{R + D_L}{\rho n^2 D^4} \\
 C_P &= \frac{P}{\rho n^2 D^5} \\
 \eta &= \frac{(T - \Delta D)V}{P} = \frac{(R + D)V}{P} = \left(\frac{C_T}{C_P} \right) nD \\
 \eta_{corr.} &= \frac{(R + D_L)V}{P} = \left(\frac{C_{T_{corr.}}}{C_P} \right) nD
 \end{aligned}$$

$$C_s = \sqrt[5]{\frac{\rho V^5}{P n^2}} = \sqrt[5]{\frac{nD}{C_P}}$$

where

q , dynamic pressure ($\frac{1}{2} \rho V^2$).

ρ , mass density of the air.

V , velocity.

S , area of the wing.

T , thrust of propeller operating in front of a body (tension in crankshaft).

R , resultant forward force.

D , drag at given angle with propeller removed.

D_L , drag with propeller removed at the lift obtained with the propeller operating (same dynamic pressure).

ΔD , change in drag of body due to action of propeller.

n , revolutions per unit time.

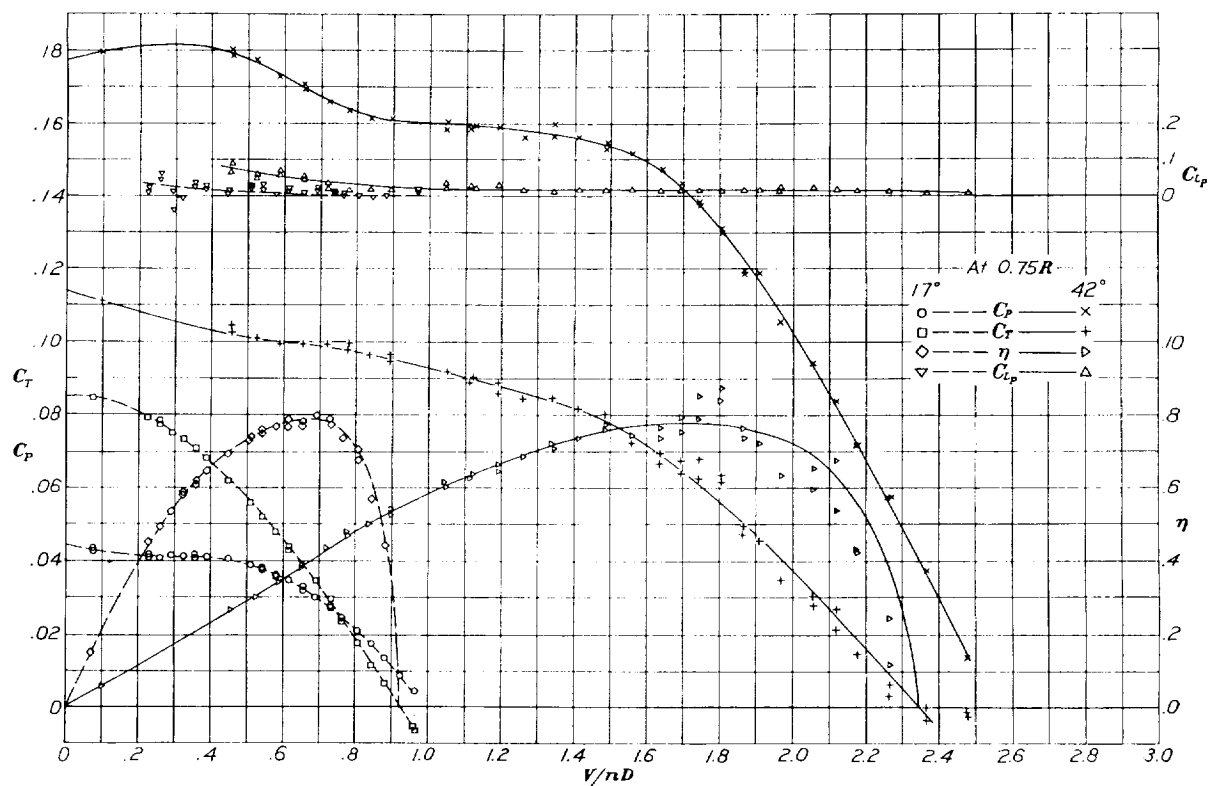
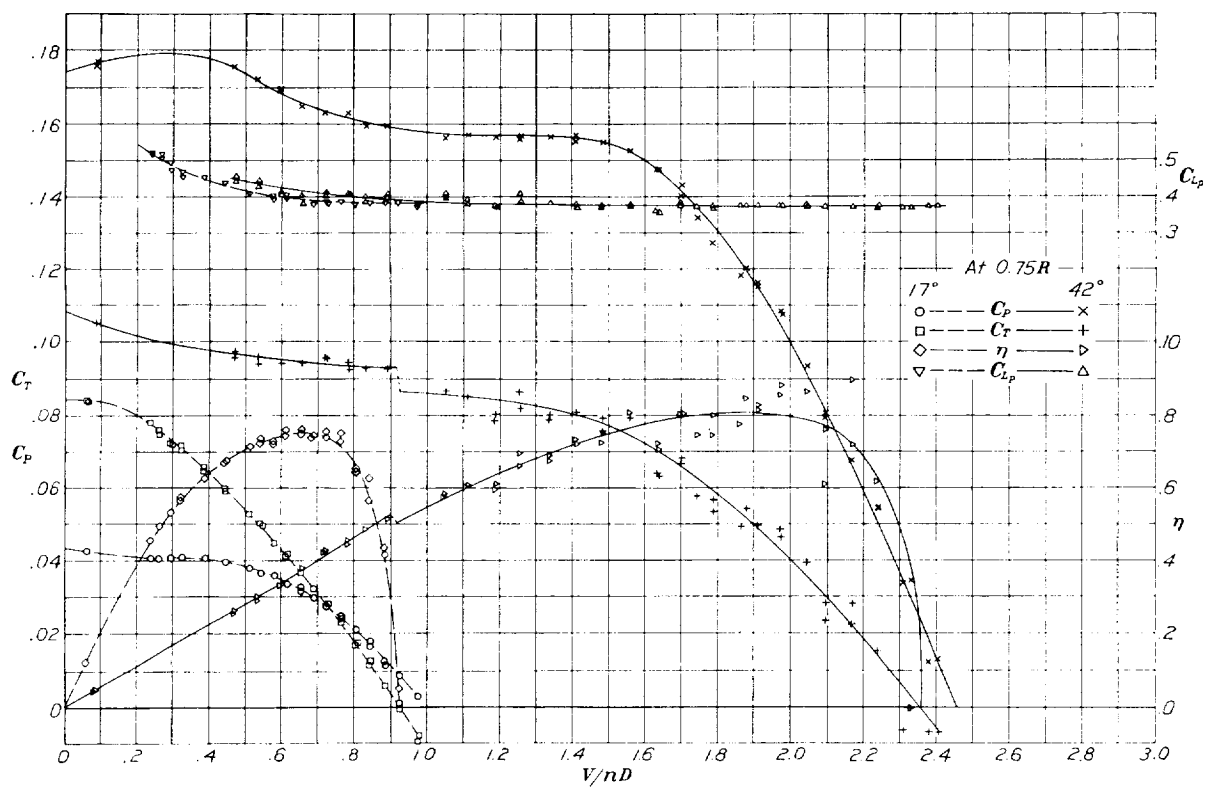
D , propeller diameter.

P , power.

The airfoil characteristics of the wing alone and for the wing with nacelle are given in figure 2. No tare corrections have been made. It should be noted that measurements have been made for close increments of angle of attack, especially in the region of minimum drag.

Although propeller tests were made at 17°, 22°, 27°, 32°, 37°, and 42° pitch at 0.75R at each of -8°, -5°, -2.5°, 0°, 2.5°, and 5° angle of attack, only a few sample test curves are shown. Figures 3 and 4, which are for the two extremes of pitch tested, show a considerable scattering of the test points, particularly of the thrust at the high pitch (42°). The power variations are largely a function of pitch, not angle of attack, and all power data are reliable, since the torque was measured directly and is not a computed value as is the thrust (thrust = resultant force + drag). The efficiency points, being computed from the thrust and power, show a dispersion similar to the thrust.

In tests of this type there is an inherent scattering of thrust-coefficient points at maximum efficiency and beyond, which increases as either the angle of attack or propeller pitch is increased. Three reasons exist for this dispersion. First, scattering occurs because the thrust, a computed value, is determined as the algebraic sum of the two measured quantities R and D . As zero thrust is approached these quantities are of the same order of magnitude but of opposite sign and consequently a small error in either may be a large percentage error in the effective thrust. Second, increasing the angle of attack, in addition to increasing the drag force, introduces correspondingly larger force fluctuations that are independent of propeller pitch. Third, and probably most important, in order to obtain the higher values of V/nD that correspond to higher pitches, the revolution speed of the propeller must be decreased because the tunnel air speed is

FIGURE 3. Sample curves, uncorrected. Right-hand propeller No. 4412, 4-foot diameter, $\alpha = -8^\circ$.FIGURE 4. Sample curves, uncorrected. Right-hand propeller No. 4412, 4-foot diameter, $\alpha = 0^\circ$.

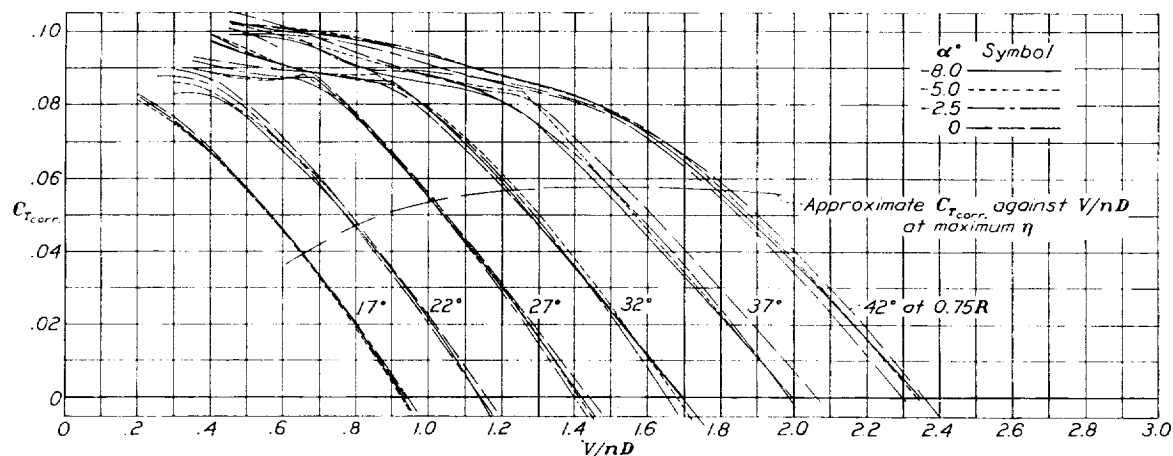


FIGURE 5.- Composite of corrected thrust. Right-hand propeller No. 4412, 4-foot diameter.

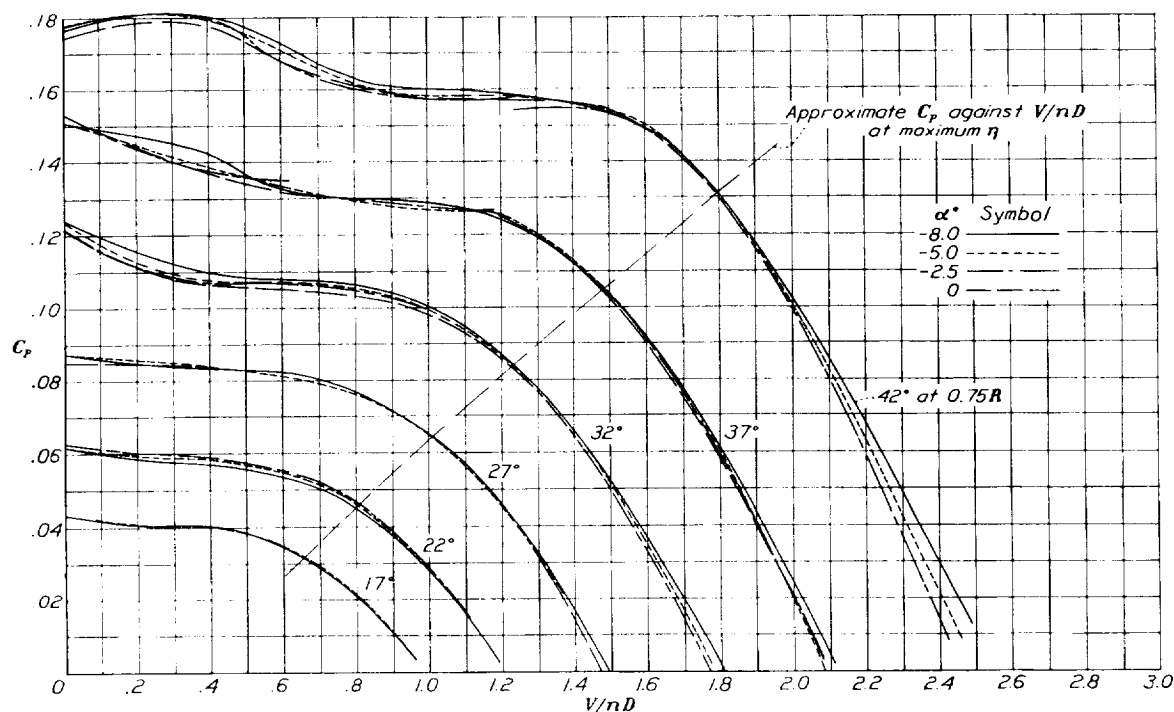


FIGURE 6.- Composite of power. Right-hand propeller No. 4412, 4-foot diameter.

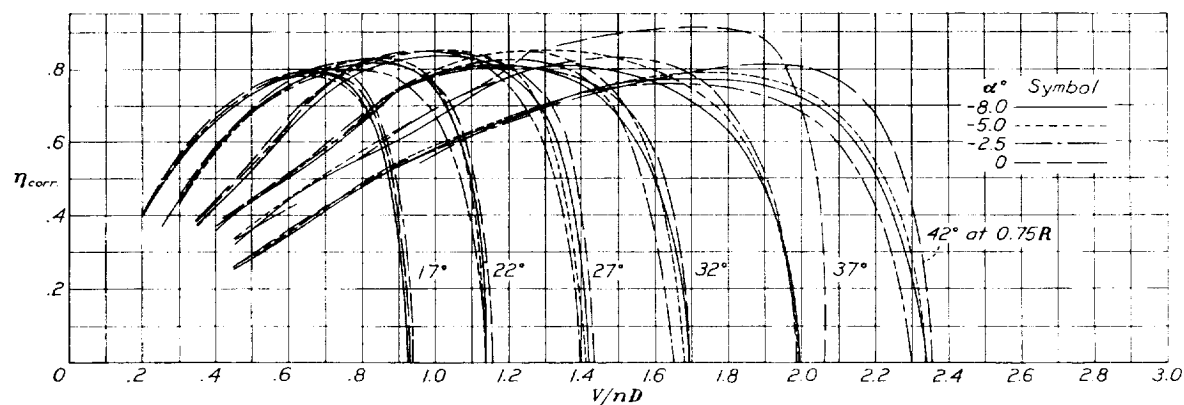


FIGURE 7.- Composite of corrected propulsive efficiency. Right-hand propeller No. 4412, 4-foot diameter.

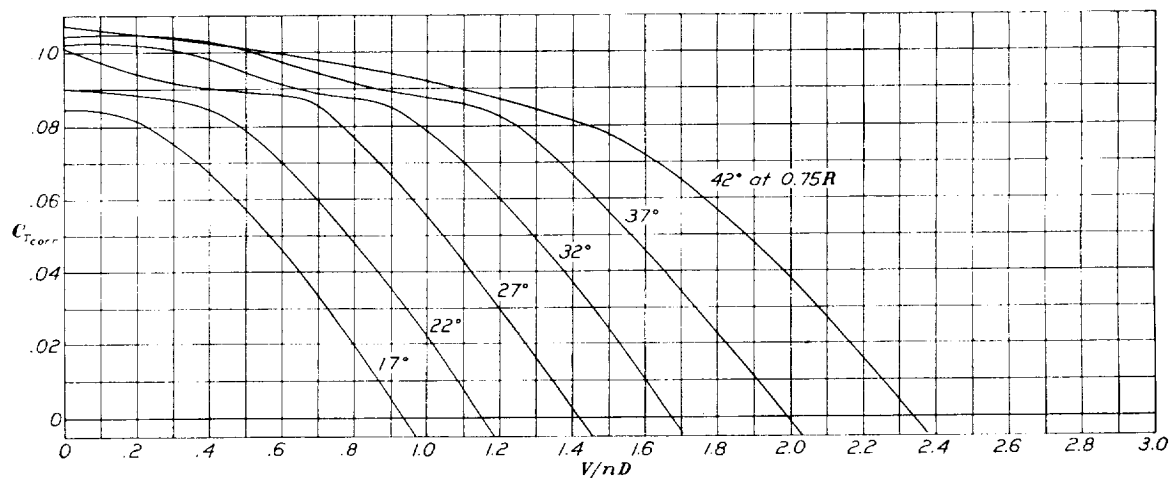


FIGURE 8. -- Average corrected thrust. Right-hand propeller No. 4412, 4-foot diameter.

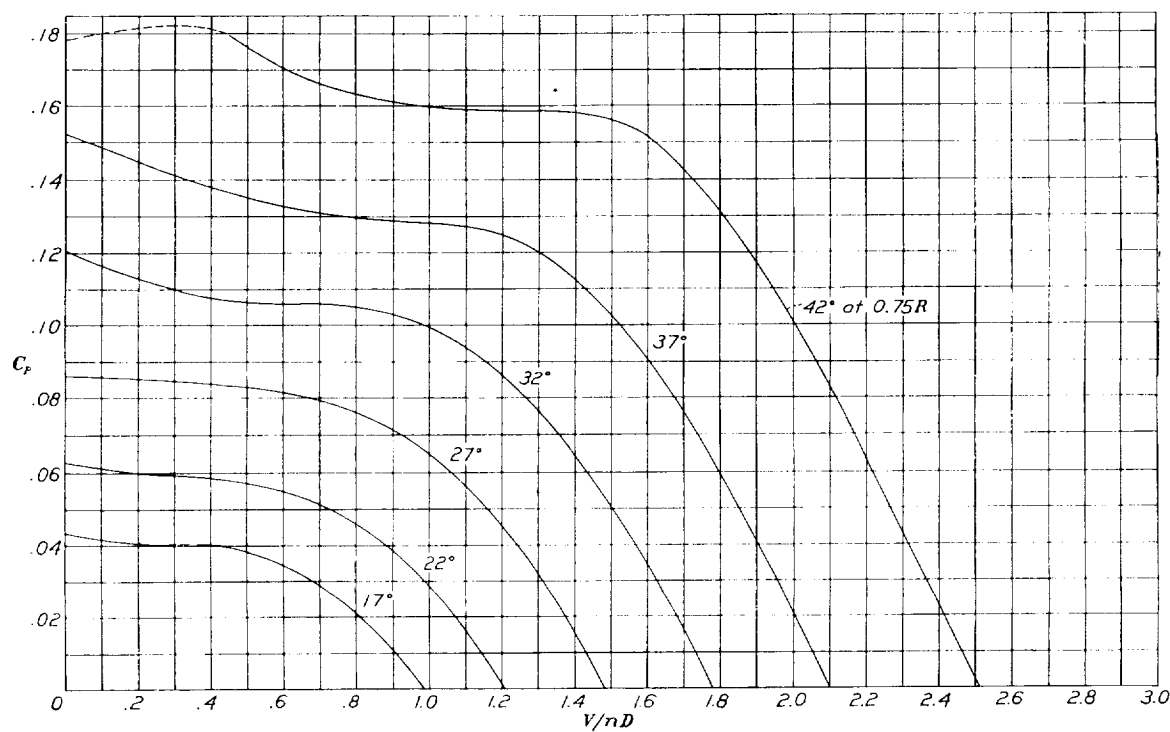


FIGURE 9. Average power. Right-hand propeller No. 4412, 4-foot diameter.

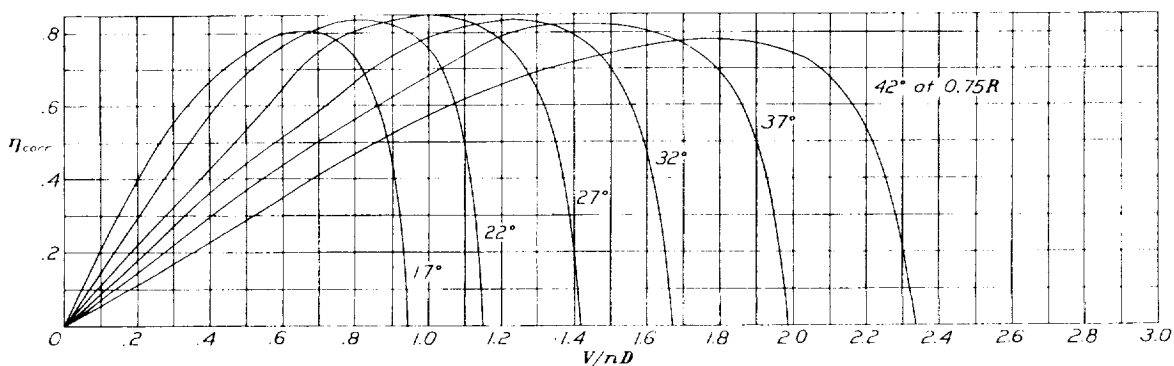


FIGURE 10. Average corrected propulsive efficiency. Right-hand propeller No. 4412, 4-foot diameter.

limited. As the thrust coefficient varies directly as the thrust and inversely as n^2 , the scattering with propeller pitch will vary roughly as $(V/nD)^2$ for the same value of thrust coefficient and the same value of

pitch as at the lowest. The curves for the 37° propeller pitch at 0° angle of attack of the wing are an example of what would result if most of the test points were obtained under adverse conditions resulting from

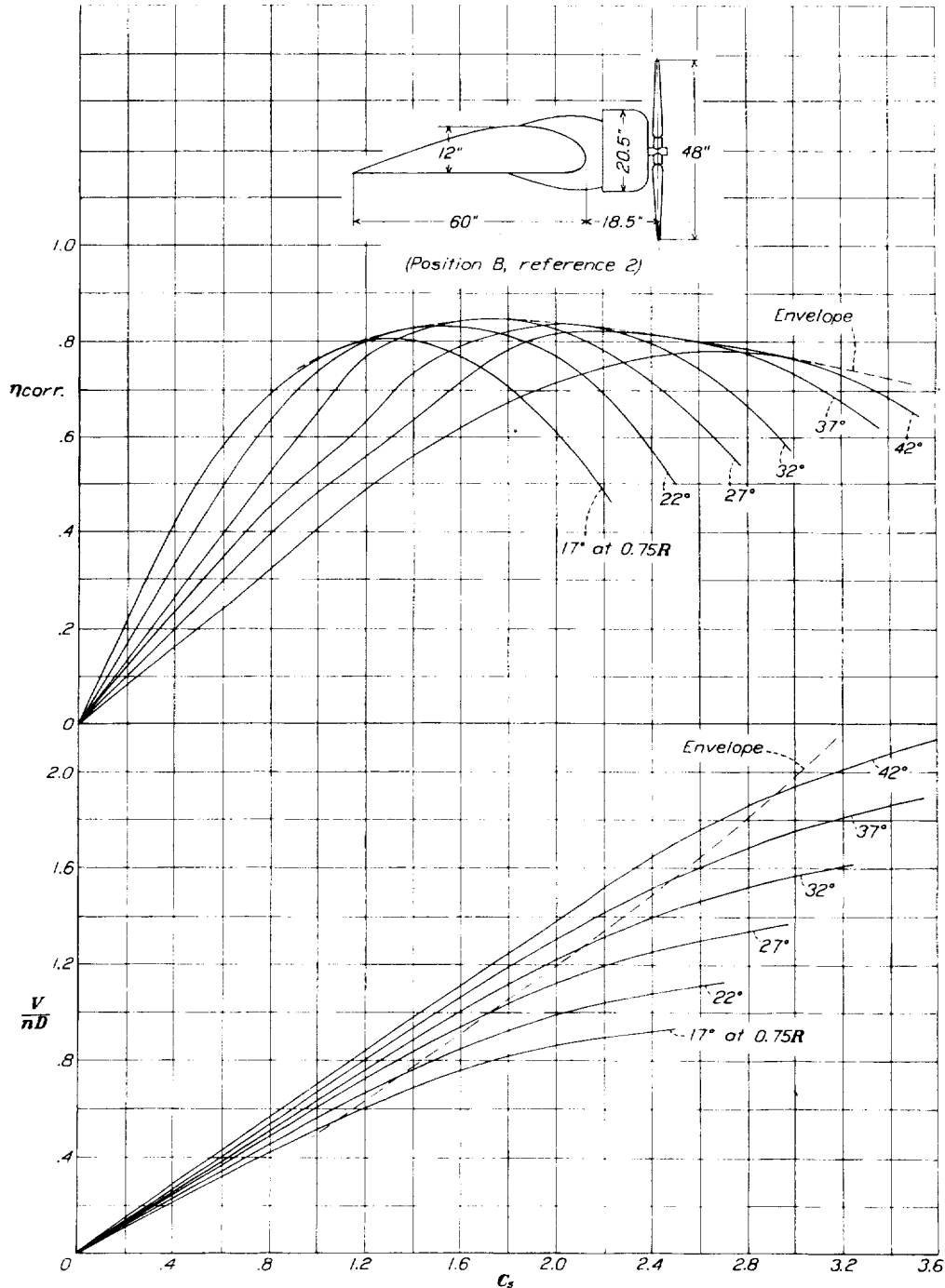


FIGURE 11. Working chart, N. A. C. A. nacelle in line with thick wing. Right-hand propeller No. 4412, 4-foot diameter.

force fluctuations. On this basis the fluctuations of the thrust coefficient would increase with pitch and would be from 4 to 10 times as great at the highest

the three reasons discussed. The thrust is high and the effect on the efficiency is more obvious; this thrust curve was omitted in obtaining average values.

METHOD OF ANALYSIS

A full discussion of the difficulties and methods of comparing wing-nacelle-propeller combinations is given in references 2 and 4 and need not be repeated here. The "corrected propulsive efficiency" was introduced in reference 4 and is the basis on which these data are analyzed.

Figures 5, 6, and 7 are composite curves of corrected thrust, power, and corrected propulsive efficiency for all the pitches tested from -8° to 0° angle of attack of the wing; the curves for 2.5° and 5° are not included on account of the scattering of points previously mentioned. These data have been corrected similarly to those of reference 4 except that, instead of computing the difference in induced drag and jet-boundary correction, it was read directly from figure 2 and therefore includes a slight change in profile drag. This method of correction, considered admissible since previous tests have shown the tare drag to be independent of the lift, gives slightly higher values of thrust and efficiency than the method of reference 4, which assumes no change in profile drag. The difference in thrust and efficiency obtained by these two methods is small, especially near maximum efficiency, and certainly does not exceed the limits of accuracy of the tests.

The composite curves in figures 5, 6, and 7 indicate that, up to 0° angle of attack, the limit to which the data are considered to be reliable, the corrected thrust, power, and corrected propulsive efficiency are independent of angle of attack. Average curves were accordingly drawn from figures 5 and 6, omitting the thrust for 37° pitch at 0° angle of attack. Figures 8 and 9 show these average values of thrust and power and figure 10 shows the recomputed corrected propulsive efficiency, based on the foregoing averages. Table I lists these values together with the computed value of the operating coefficient C_s .

Figure 11 presents the data of table I in working-chart form. Figure 12 is a plot of C_{Lp} against C_s giving average values for all pitches. Table II lists values read from figure 12.

DISCUSSION

The airfoil curves for the wing alone and the wing with nacelle as shown in figure 2 are conventional. In general, the effective nacelle-drag coefficient at a constant lift is in good agreement with that of reference 2. Although the effective nacelle-drag coefficient varies somewhat with lift, it may be taken as 0.0026 for this combination over the high-speed range of flight.

Figure 7 indicates a tendency of the corrected propulsive efficiency to increase with angle of attack. This same trend is also shown by the data in reference 2 when the corrected propulsive efficiency is computed. Over the high-speed and climbing range of lift coefficients the change in corrected propulsive efficiency

is small, being almost within the accuracy of the experiments. The corrected propulsive efficiency may therefore be considered to be independent of the angle of attack except in very special cases and may be taken as the average over the high-speed and the climbing range.

The working chart given in figure 11 is to be used in the same manner as those of reference 1. This chart is, of course, based on certain fixed test conditions and in its application due allowances should be made for the effects of changes in propeller diameter, power input, and other variables.

The effect of the propeller on the lift is shown in figure 12. The curves apply only to these particular test conditions and must not be considered to have general application. They have been inserted to give the change in lift caused by the propeller and also to show that for a given arrangement the effect of propeller pitch is slight with a fixed-diameter propeller at constant values of C_s . No test points (see figs. 3 and

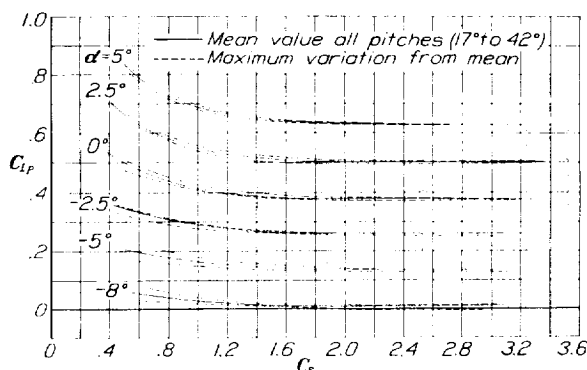


FIGURE 12.—Effect of propeller on lift.

4) are given, but the maximum variation of the faired curves for each pitch is shown. The small effect of propeller pitch may seem unusual but a few simple computations at the different pitches, assuming C_s , velocity, propeller diameter, and angle-of-attack constant, will show that the thrust is about the same for all pitches and, since the change in lift for any combination is mainly a function of propeller thrust, it is not unreasonable that the lift variation with propeller pitch should be small.

These are the first published results of tests made in the propeller-research tunnel of propellers at pitches greater than about 27° at $0.75R$. It is hoped that they may be useful in indicating trends for higher pitches from previous tests for lower pitches as well as be useful to the designer of modern high-speed airplanes. The reason for the falling off in efficiency as early as 27° is not fully explained. One possibility is that there may be increasing interference with the wing as the pitch of the propeller is increased. Available data (reference 5) covering the values of propeller pitches only up to 23° provide evidence that the tendency of

the wing interference is to increase as the propeller pitch is increased. The pitch distribution of the propeller used in this investigation is not considered particularly good for the higher pitches and a series of full-scale tests with more favorable pitch distribution is contemplated. It is expected that some improvement in the efficiency in the higher pitch range can be obtained.

LANGLEY MEMORIAL AERONAUTICAL LABORATORY,
NATIONAL ADVISORY COMMITTEE FOR AERONAUTICS,
LANGLEY FIELD, VA., November 12, 1935.

REFERENCES

1. Weick, Fred E.: Working Charts for the Selection of Aluminum Alloy Propellers of a Standard Form to Operate

with Various Aircraft Engines and Bodies. T. R. No. 350, N. A. C. A., 1930.

2. Wood, Donald H.: Tests of Nacelle-Propeller Combinations in Various Positions with Reference to Wings. Part I. Thick Wing—N. A. C. A. Cowled Nacelle—Tractor Propeller. T. R. No. 415, N. A. C. A., 1932.
3. Weick, Fred E., and Wood, Donald H.: The Twenty-Foot Propeller Research Tunnel of the National Advisory Committee for Aeronautics. T. R. No. 300, N. A. C. A., 1928.
4. Wood, Donald H., and Bioletti, Carlton: Tests of Nacelle-Propeller Combinations in Various Positions with Reference to Wings. VI—Wings and Nacelles with Pusher Propeller. T. R. No. 507, N. A. C. A., 1934.
5. Weick, Fred E., and Wood, Donald H.: The Effect of the Wings of Single Engine Airplanes on Propulsive Efficiency as Shown by Full Scale Wind Tunnel Tests. T. N. No. 322, N. A. C. A., 1929.

TABLE I.—AVERAGE VALUES

[Corrected for lift]

[Right-hand propeller No. 4412, 4-foot diameter]

V/nD	Set 17° at 0.75 R				Set 22° at 0.75 R				Set 27° at 0.75 R				Set 32° at 0.75 R				Set 37° at 0.75 R				Set 42° at 0.75 R						
	C _{T_{corr.}}	C _P	η _{corr.}	C _S	C _{T_{corr.}}	C _P	η _{corr.}	C _S	C _{T_{corr.}}	C _P	η _{corr.}	C _S	C _{T_{corr.}}	C _P	η _{corr.}	C _S	C _{T_{corr.}}	C _P	η _{corr.}	C _S	C _{T_{corr.}}	C _P	η _{corr.}	C _S			
0	0.0846	0.0433	0	0	0.0900	0.0628	0	0	0.1010	0.0862	0	0	0.1020	0.1208	0	0	0.1043	0.1523	0	0	0.1070	0.1780	0	0			
.05	.0846	.0423	.100	.09	.0893	.0620	.072	.09	.0990	.0860	.057	.08	.1022	.1187	.043	.08	.1046	.1505	.035	.07	.1067	.1789	.030	.07			
.10	.0842	.0417	.202	.19	.0890	.0612	.145	.17	.0970	.0858	.113	.16	.1023	.1167	.088	.15	.1047	.1486	.070	.15	.1060	.1797	.059	.14			
.15	.0831	.0410	.304	.28	.0887	.0607	.219	.26	.0954	.0853	.167	.25	.1021	.1148	.134	.23	.1048	.1467	.107	.22	.1054	.1805	.087	.21			
.20	.0817	.0408	.400	.38	.0881	.0600	.294	.35	.0940	.0850	.222	.33	.1019	.1130	.180	.31	.1047	.1449	.144	.29	.1049	.1819	.115	.28			
.25	.0786	.0403	.499	.47	.0877	.0593	.370	.44	.0927	.0849	.274	.41	.1012	.1113	.228	.39	.1043	.1430	.182	.37	.1042	.1822	.143	.35			
.30	.0750	.0404	.556	.57	.0870	.0591	.441	.53	.0918	.0844	.326	.49	.1005	.1100	.274	.47	.1040	.1413	.220	.44	.1035	.1825	.170	.42			
.35	.0711	.0403	.618	.67	.0860	.0589	.511	.62	.0909	.0841	.378	.57	.0993	.1088	.320	.55	.1033	.1397	.259	.52	.1030	.1823	.198	.49			
.40	.0670	.0400	.670	.76	.0844	.0584	.579	.71	.0900	.0839	.429	.66	.0980	.1078	.364	.63	.1028	.1381	.297	.60	.1022	.1812	.226	.56			
.45	.0621	.0393	.711	.86	.0821	.0579	.637	.80	.0894	.0834	.481	.74	.0961	.1070	.404	.70	.1018	.1367	.335	.67	.1017	.1795	.254	.63			
.50	.0571	.0381	.749	.96	.0788	.0570	.691	.89	.0890	.0830	.536	.82	.0942	.1064	.442	.78	.1006	.1352	.371	.75	.1009	.1762	.286	.71			
.55	.0518	.0365	.780	1.07	.0745	.0560	.731	.98	.0887	.0823	.592	.91	.0926	.1062	.479	.86	.0990	.1340	.406	.82	.1000	.1732	.317	.78			
.60	.0459	.0344	.800	1.18	.0699	.0549	.764	1.07	.0880	.0815	.648	.99	.0910	.1061	.515	.94	.0971	.1329	.439	.90	.0992	.1703	.349	.85			
.65	.0395	.0319	.804	1.30	.0649	.0531	.794	1.17	.0873	.0804	.706	1.08	.0898	.1061	.550	1.02	.0957	.1319	.471	.97	.0983	.1679	.381	.93			
.70	.0330	.0289	.800	1.42	.0594	.0512	.811	1.27	.0852	.0792	.751	1.16	.0888	.1060	.586	1.10	.0940	.1310	.502	1.05	.0975	.1660	.411	1.00			
.75	.0261	.0251	.780	1.57	.0540	.0489	.829	1.37	.0818	.0779	.788	1.25	.0880	.1058	.624	1.18	.0928	.1303	.534	1.13	.0968	.1644	.441	1.07			
.80	.0192	.0210	.731	1.73	.0479	.0459	.835	1.48	.0770	.0761	.810	1.34	.0873	.1050	.665	1.26	.0913	.1298	.563	1.21	.0959	.1631	.469	1.15			
.85	.0121	.0182	.635	1.94	.0416	.0425	.831	1.60	.0720	.0740	.827	1.43	.0866	.1041	.707	1.34	.0902	.1291	.593	1.26	.0950	.1621	.498	1.22			
.90	.0049	.0101	.436	2.26	.0351	.0344	.822	1.73	.0662	.0713	.836	1.53	.0850	.1030	.743	1.42	.0890	.1286	.623	1.30	.0939	.1612	.524	1.29			
.95	.0028	.0048	2.76	.0285	.0338	.800	1.87	.0608	.0682	.846	1.63	.0821	.1015	.769	1.50	.0881	.1283	.651	1.44	.0929	.1603	.550	1.36			
1.000218	.0287	.760	2.04	.0549	.0648	.848	1.73	.0783	.0993	.788	1.59	.0874	.1281	.681	1.51	.0919	.1598	.576	1.45			
1.050146	.0228	.672	2.24	.0488	.0609	.841	1.84	.0742	.0968	.805	1.68	.0868	.1279	.714	1.59	.0908	.1592	.598	1.52			
1.100072	.0162	.489	2.51	.0426	.0561	.836	1.96	.0698	.0937	.820	1.77	.0858	.1272	.740	1.67	.0896	.1590	.620	1.59			
1.150001	.0091	2.94	.0360	.0510	.811	2.08	.0650	.0901	.829	1.86	.0844	.1263	.767	1.74	.0883	.1588	.640	1.66			
1.200292	.0451	.778	2.23	.0600	.0860	.837	1.96	.0825	.1250	.792	1.82	.0871	.1586	.660	1.74			
1.250226	.0390	.725	2.39	.0545	.0815	.836	2.06	.0797	.1229	.811	1.89	.0858	.1586	.676	1.81			
1.300158	.0320	.640	2.59	.0488	.0763	.831	2.17	.0755	.1201	.816	1.98	.0841	.1585	.690	1.88			
1.350091	.0240	.487	2.85	.0428	.0707	.816	2.29	.0710	.1187	.822	2.08	.0829	.1583	.705	1.95			
1.400023	.0158	.206	3.22	.0368	.0646	.796	2.42	.0661	.1126	.823	2.16	.0813	.1580	.720	2.02			
1.450304	.0578	.762	2.56	.0612	.1080	.823	2.26	.0795	.1573	.733	2.10			
1.500239	.0465	.719	2.72	.0562	.1029	.820	2.36	.0777	.1562	.745	2.17			
1.550170	.0427	.616	2.92	.0510	.0971	.814	2.47	.0750	.1544	.753	2.24			
1.600102	.0343	.476	3.14	.0456	.0904	.808	2.59	.0720	.1513	.761	2.32			
1.650031	.0258	.198	3.43	.0400	.0834	.791	2.71	.0687	.1472	.770	2.42			
1.700039	.0161	3.88	.0342	.0759	.766	2.85	.0651	.1424	.777	2.50		
1.750285	.0677	.737	3.00	.0611	.1370	.781	2.61		
1.800228	.0591	.694	3.17	.0568	.1310	.780	2.70		
1.850168	.0500	.621	3.37	.0521	.1239	.780	2.80		
1.900108	.0407	.504	3.61	.0474	.1168	.772	2.92		
1.950047	.0308	.298	3.90	.0424	.1089	.760	3.04		
2.000012	.0206	4.35	.0373	.1006	.742	3.17	
2.050321	.0919	.716	3.31	
2.100268	.0828	.680	3.46	
2.150211	.0734	.619	3.63	
2.200156	.0632	.542	3.83	
2.250099	.0534	.418	4.05	
2.300041	.0431	.218	4.32	
2.350018	.0329	4.66

TABLE II.—AVERAGE VALUES OF C_{L_p} FOR ALL PITCHES (17° TO 42°)

[Right-hand propeller No. 4412, 4-foot diameter]

C_S	Angle of attack, α						C_S	Angle of attack, α					
	-8°	-5°	-2.5°	0°	2.5°	5°		-8°	-5°	-2.5°	0°	2.5°	5°
0.6	0.054	0.194	0.331	0.474	0.628	0.789	2.0	0.009	0.137	0.258	0.380	0.501	0.631
.8	.039	.177	.308	.438	.579	.726	2.2	.009	.136	.258	.379	.500	.630
1.0	.028	.163	.289	.413	.547	.688	2.4	.009	.135	.258	.379	.500	.630
1.2	.019	.153	.278	.397	.527	.663	2.6	.009	.134	.258	.378	.500	.629
1.4	.013	.147	.269	.388	.513	.649	2.8	.009	.133	.258	.378	.500	.629
1.6	.011	.140	.262	.381	.507	.640	3.0	.009	.133	.258	.378	.500	.629
1.8	.009	.138	.259	.380	.503	.634							

REPORT No. 565

MEASUREMENTS OF FUEL DISTRIBUTION WITHIN SPRAYS FOR FUEL-INJECTION ENGINES

BY DANA W. LEE

SUMMARY

Two methods were used to measure fuel distribution within sprays from several types of fuel-injection nozzles. A small tube inserted through the wall of an airtight chamber into which the sprays were injected could be moved about inside the chamber. When the pressure was raised to obtain air densities of 6 and 14 atmospheres, some air was forced through the tube and the fuel that was carried with it was separated by absorbent cotton and weighed. Cross sections of sprays from plain, pintle, multiple-orifice, impinging-jets, centrifugal, lip, slit, and annular-orifice nozzles were investigated, at distances of 1, 3, 5, and 7 inches from the nozzles.

Sprays that were symmetrical about their axes were also tested by a second method in which the injection valve was inserted through the top of a pressure chamber containing a nest of eight concentric cups, the axis of which coincided with the nozzle axis. The injected fuel was caught by the cups, drained into receptacles below, and weighed. Tests were made at 1, 6, and 14 atmospheres, at the same distances from the nozzles used in the first method.

It was found that the distribution of the fuel within the sprays always improved with increasing distance from the nozzle and usually with increasing air density, the effect of both factors being greatest with sprays of high penetrating power. Distribution within sprays from plain nozzles improved slightly with an increase in the injection pressure or with a decrease in the fuel viscosity. Changing the orifice length-diameter ratio of plain nozzles had little effect on fuel distribution.

INTRODUCTION

Laboratory research on compression-ignition engines has resulted in recent years in continued increases in speed and mean effective pressure, particularly when some form of controlled air swirl is used to improve the distribution of fuel throughout the combustion chamber. Another effective method of increasing the specific power output is to improve the fuel distribution through changes in the nozzle design and injection pressure, and it is believed that the work described in this report will be useful to those who are working along such lines. Spark-ignition engines employing

fuel injection having shown definite advantages over carburetor-equipped engines, distribution tests were also made at low air densities.

Outstanding among previous measurements of fuel distribution within sprays are those made at the Pennsylvania State College, where the weights of fuel reaching various stations on a "dispersion rack" were accurately determined (reference 1). The effects of injection pressure, air density, fuel viscosity, orifice diameter, and distance from the nozzle were determined using plain cylindrical nozzles. The results are complete only at 14 inches from the nozzle; at nearer stations the weights at the center of the spray could not be obtained. At a later date, the total amounts of fuel reaching various distances from the nozzle were caught and weighed by a "tipping cup" (reference 2).

Several previous experiments on the distribution of fuel in sprays have also been made at this laboratory. The relative amounts of fuel reaching different distances from the nozzle were obtained in connection with atomization measurements and the results are given in reference 3. The structure of fuel sprays and the process by which they are formed were studied by means of spark photographs taken under a wide variety of conditions (reference 4), and the study was continued by means of photomicrographs of the sprays (reference 5). The approximate dimensions of the high-velocity cores of sprays from several types of nozzles were obtained by injecting them against pieces of plasticine, and the outlines of the sprays were obtained from spark photographs. Cross-sectional sketches of the sprays made from these measurements are shown in reference 6.

The present tests, which were made to obtain quantitative data on the distribution of fuel within sprays from several types of nozzles, are divided into two parts, each using a different test method. The first method gave the relative amounts of fuel reaching any particular point in the spray; the second gave the actual weight reaching each of a series of annular areas concentric about the spray axis. The variables studied were: Air density, nozzle design, fuel viscosity, and injection pressure. Results were obtained at 1, 3, 5,

and 7 inches from the nozzles with the air at 1, 6, and 14 times atmospheric density and at room temperature. The tests were made at the Committee's laboratories at Langley Field, Va., during the first 6 months of 1935.

APPARATUS

SAMPLING TUBE

The apparatus used to determine the relative amounts of fuel reaching different points in the sprays will be referred to as the "sampling-tube apparatus" because it consisted essentially of a small copper tube that removed a small amount of fuel from each spray passing its open end. The tube was soldered to a traversing-screw mechanism by which it could be moved linearly at right angles to the spray axis. (See fig. 1.) The tube could enter the chamber through

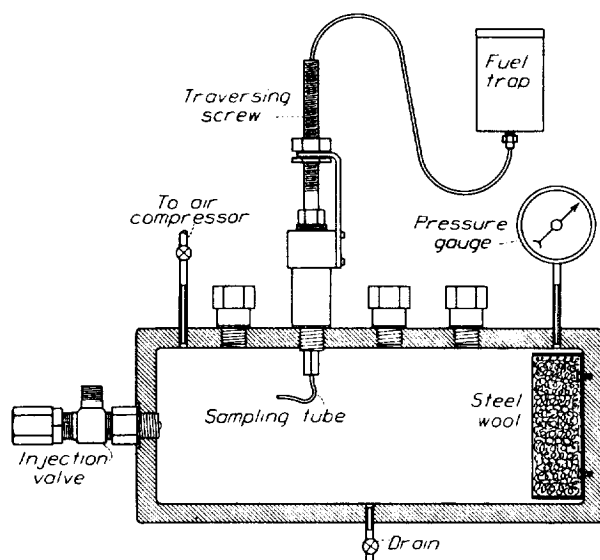


FIGURE 1.—Sampling-tube apparatus.

any one of the four holes shown, the others then being closed. The inside and outside diameters of the tube were 0.040 and 0.080 inch, respectively, and the open end was filed to a sharp edge to minimize splashing of the fuel. The tube extended through the hollow center of the traversing screw into the fuel trap. The inside of the spray chamber was 10¼ inches long, 3¾ inches high, and 4 inches wide. Some of the early tests were made with a glass window installed in one side of the chamber, and it was found that steel wool was very useful in reducing the amount of fuel that splashed from the end wall and was carried back into the spray by the circulating air currents.

In order to make a test, the valve in the compressed-air line was adjusted until the desired pressure was maintained in the chamber and then the fuel-injection pump was started. Because the air pressure inside the chamber was greater than that outside, air flowed through the tube to the fuel trap, carrying with it all

the fuel reaching the end of the tube. Absorbent cotton in the trap retained the fuel but allowed the air to escape. After about 400 sprays had been injected the pump was stopped, the pressure-release valve was opened, and the fuel trap was detached and weighed on an analytical balance. From its weight increment during the test and the number of sprays injected, the "grams of fuel collected per 1,000 sprays" was computed. This value was used as a measure of the fuel concentration in the spray at the end of the sampling tube. Although it is desirable to express the results as grams of fuel per square inch per injection, it is impossible because air flowed into the tube from an area greater than the tube area and the extent of that area is not known.

A series of exploratory tests was always made before starting the final traverse across the spray, the tube being bent sidewise by hand as well as being moved vertically by the screw. The purpose of these preliminary tests was to locate the regions of maximum fuel concentration, which were frequently quite small and might otherwise be missed.

The principal advantages of the sampling-tube method are: Sprays of any shape may be tested; as many readings may be made during a traverse as are necessary to determine the shape of the distribution curve; the traverse may be made at any distance from the nozzle; and the fuel distribution is only slightly altered by the presence of the small tube. The principal disadvantage is that the results cannot be expressed in terms of fuel weight per unit spray cross-sectional area.

CONCENTRIC CUPS

The apparatus used to obtain more accurate data on the distribution of fuel sprays will be referred to as the "concentric-cups apparatus." (See fig. 2.) The fuel sprays were caught by a nest of concentric cups mounted on a framework, which was lowered into a pressure chamber. Fuel caught by the cups drained through small tubes into receptacles on the shelf below. The distance between the nozzle and the upper edges of the cups was adjustable at 2-inch intervals from 1 to 7 inches. The inside diameters of the eight collecting cups were: 0.104, 0.25, 0.50, 0.75, 1, 1.50, 2, and 3 inches. The wall thickness of the cups was 0.010 inch and the rims were sharpened to minimize splashing. The inside diameter of the pressure chamber was 4 inches so that there was an annular space 0.5 inch wide outside the largest cup. This apparatus is suitable for testing only sprays that are symmetrical about their axes. Tests were made with the plain, the pintle, and the 4-impinging-jets nozzles; the nozzles, as well as the injection valves and the pump, were the ones used in the sampling-tube tests.

Before each test, several sprays were injected against a thin layer of plasticine mounted just above the cups. The framework was then adjusted so that the true

spray axis, as indicated by the deepest part of the impression in the plasticine, coincided with the axis of the concentric cups.

After the eight fuel receptacles were weighed and placed in position, the entire framework was lowered into the pressure chamber and the cover bolted down. The injection tube from the pump was attached to the injection valve, and compressed air was admitted until the desired air density was reached. It was necessary to operate the injection pump intermittently, injecting for five cycles and idling for about 20 seconds, in order to let the fuel drain from the cups to the receptacles through the small tubes. When the pump was continuously operated, the fuel splashed from one cup to

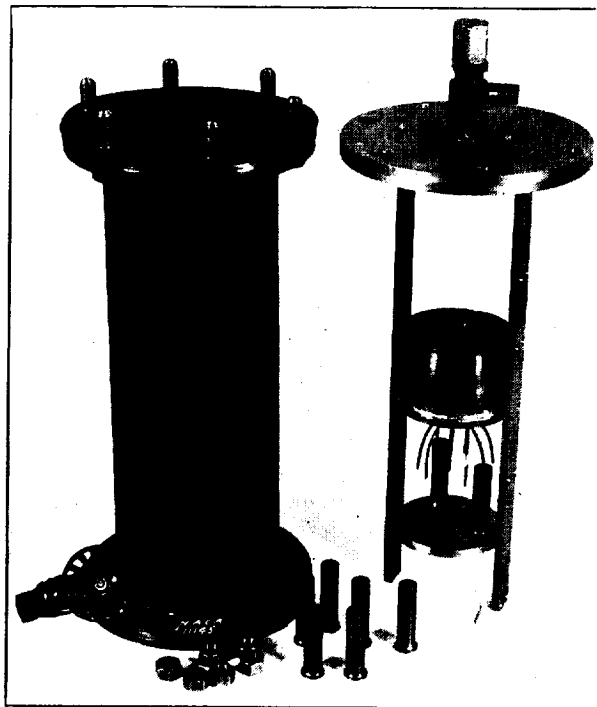


FIGURE 2.—Concentric-cups apparatus.

another. The cups were thoroughly drained after every 100 cycles, and the receptacles reweighed. From the weight increments, the areas of the corresponding compartments, and the number of cycles, the grams of fuel per square inch per cycle were computed for each annular area. The amount of fuel discharged from the nozzle during each test was determined by subsequent tests during which the pump was operated as before but in which the fuel was caught in a bottle and weighed.

The principal advantage of the concentric-cups method is that the results can be expressed in terms of fuel weight per unit spray cross-sectional area. The disadvantages are that only symmetrical sprays can be tested, the number of test readings is limited to the number of cups, and the presence of the cups some-

what alters the fuel distribution. The two test methods serve as a check on each other, the weak points of one being the strong points of the other.

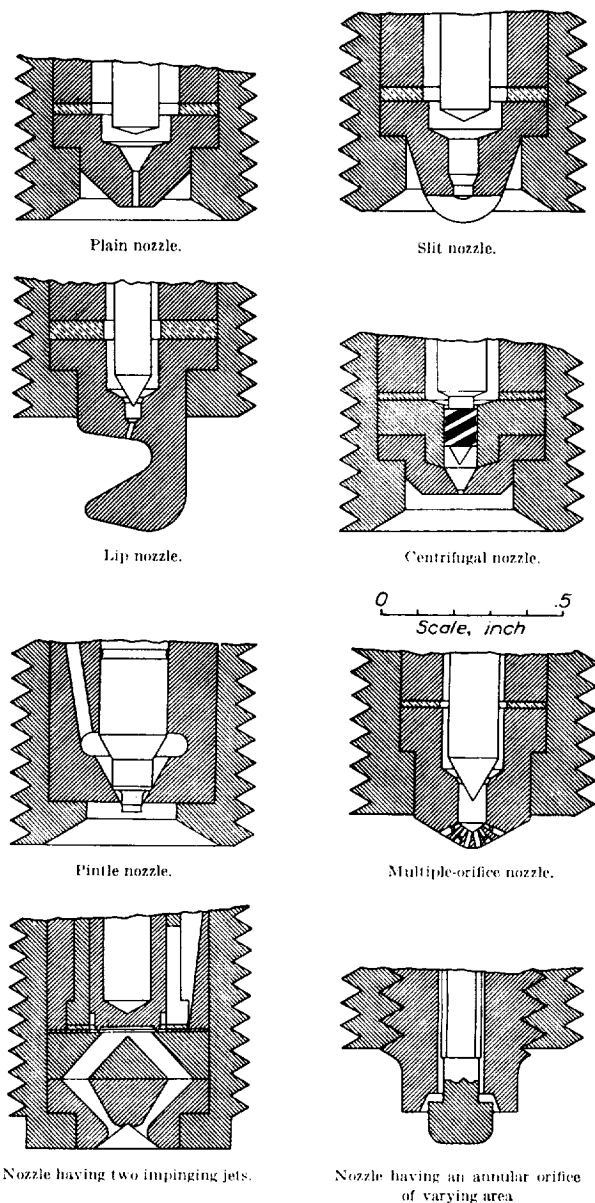


FIGURE 3.—Types of nozzles used.

INJECTION EQUIPMENT

Sketches of the types of nozzles used are shown in figure 3. Six *plain nozzles*, that is, nozzles having single cylindrical orifices, were tested. Nozzles with orifice diameters of 0.008, 0.014, 0.020, and 0.030 inch were used and, unless otherwise stated, the orifice length-diameter ratio was 2. Two *pintle nozzles* were tested, one having an orifice diameter of 0.063 inch and a nominal spray cone angle of 20° and the other having an orifice diameter of 0.059 inch and a nominal spray

cone angle of 30° . The *lip nozzle* used had an orifice diameter of 0.014 inch, an orifice length of 0.028 inch, and the angle between the axis of the fuel jet and the surface of the lip was 45° . Two *impinging-jets nozzles* were tested, one having two orifices each 0.020 inch in diameter and the other having four orifices each 0.030 inch in diameter. In the 4-orifice nozzle (not shown in fig. 3) the plane through two of the orifices was at right angles to that through the other two, all four jets meeting at a common point. The angle between opposite jets was 74° in each case. With the *annular-orifice nozzle* the space between the enlarged end of the valve stem and the valve body constituted the orifice. This space varied with the injection pressure, and the cone angle of the hollow spray produced was about 45° . The *multiple-orifice nozzle* had six orifices in one plane. The two center orifices had diameters of 0.019 inch, the next two 0.014 inch, and the outer two 0.008 inch. The length of each orifice was twice its diameter and the angle between adjacent jets was 20° . The *slit nozzle* had an orifice width of 0.008 inch, a length of 0.055 inch, and an average depth of about 0.050 inch. The bottom of the short cylindrical passage above the slit was spherical, with a radius of about 0.060 inch; the radius of the spherical end of the nozzle was about 0.110 inch. The *centrifugal nozzle* had an orifice diameter of 0.020 inch and a length of 0.010 inch. There were four grooves on the valve stem to produce the whirling of the fuel; their helix angle was 30° , and the total area of the grooves and clearance space was 0.00052 square inch (equivalent to a single 0.026-inch orifice).

The nozzles were used in automatic spring-loaded injection valves, all but one valve being of the lapped-stem differential-area type. The exception was the valve with the annular orifice, the stem of which was not lapped but was guided by lands. Sketches of these injection valves may be found in reference 6. The injection valves used with the pintle and annular-orifice nozzles were obtained from commercial concerns; the other valves and nozzles were made at this laboratory.

Extensive tests of the rates of discharge of the Bosch fuel-injection pump that was used for these tests are reported in reference 7; some of the characteristics of fuel sprays produced by it are given in reference 8. The injection tube was 55 inches long and its inside diameter was 0.125 inch. The fuel discharged was practically independent of pump speed but varied slightly with orifice area, the extreme values being 0.27 gram per cycle with the 0.008-inch orifice and 0.31 gram per cycle with the annular orifice. An electrical revolution counter attached to the pump automatically recorded the number of injections made.

Except for some tests to determine the effect of fuel viscosity on distribution, the fuel used was a high-grade Diesel fuel. The following test conditions were considered standard: pump speed, 750 r. p. m.; injection-valve opening pressure, 3,500 pounds per square inch.

TEST RESULTS

SAMPLING-TUBE TESTS

The results of the sampling-tube tests of fuel distribution within sprays from the different nozzles are presented graphically in figures 4 to 15, values of grams of fuel collected per 1,000 sprays being plotted against distances from the spray axis. Distances above the spray axis are plotted to the left, those below to the right. When a spray was known to be symmetrical about its axis, only one traverse of the sampling tube was necessary at each condition, and it was not usually carried entirely across the spray but extended from the upper part of the chamber to a little below the spray axis. With unsymmetrical sprays, two traverses at right angles to each other were made for each condition. The test points are shown on the curves, connected by solid lines. The uncompleted traverses are extended with broken lines that match the solid parts. As the air in the chamber was not changed during any one test, it always became fogged with fuel particles. The fuel concentration in this mist is indicated by the level at which the curves flatten out to the horizontal, and this level should be considered as the zero line when comparisons are made between curves. Some of the tests showed a slightly higher fuel concentration in the lower parts of the spray than in the upper parts. This difference was probably caused by the increasing interference of the traversing screw as it was lowered into the chamber, deflecting more and more of the fuel from the central to the outer portions of the spray.

Sampling-tube tests were made only at air densities of 6 and 14 atmospheres. In order to obtain them at 1 atmosphere, it would be necessary to put the fuel trap in an evacuated chamber. The air velocity through the sampling tube was the same for all tests, for with an air density of either 6 or 14 atmospheres, the ratio of the pressures at the inner and outer ends of the tube was greater than the critical value of 1.9.

CONCENTRIC-CUPS TESTS

The results of the concentric-cups tests are given in table I. The cups are numbered from 1 to 8, beginning at the center. The term "percentage of fuel caught" means the total weight of the fuel collected by the cups divided by the weight discharged from the nozzle during the test, multiplied by 100. Vaporization can account for only a small part of the fuel not collected because at room temperature the rate of vaporization of Diesel fuel is negligible. Most of the fuel not caught by the cups was carried off by air currents set up by the sprays and was deposited on the walls of the chamber; from there it drained to the bottom and was removed at the end of the test.

Although tables of data are concise, any systematic trends are much more evident when the test results are presented in a graphical form. Therefore the data

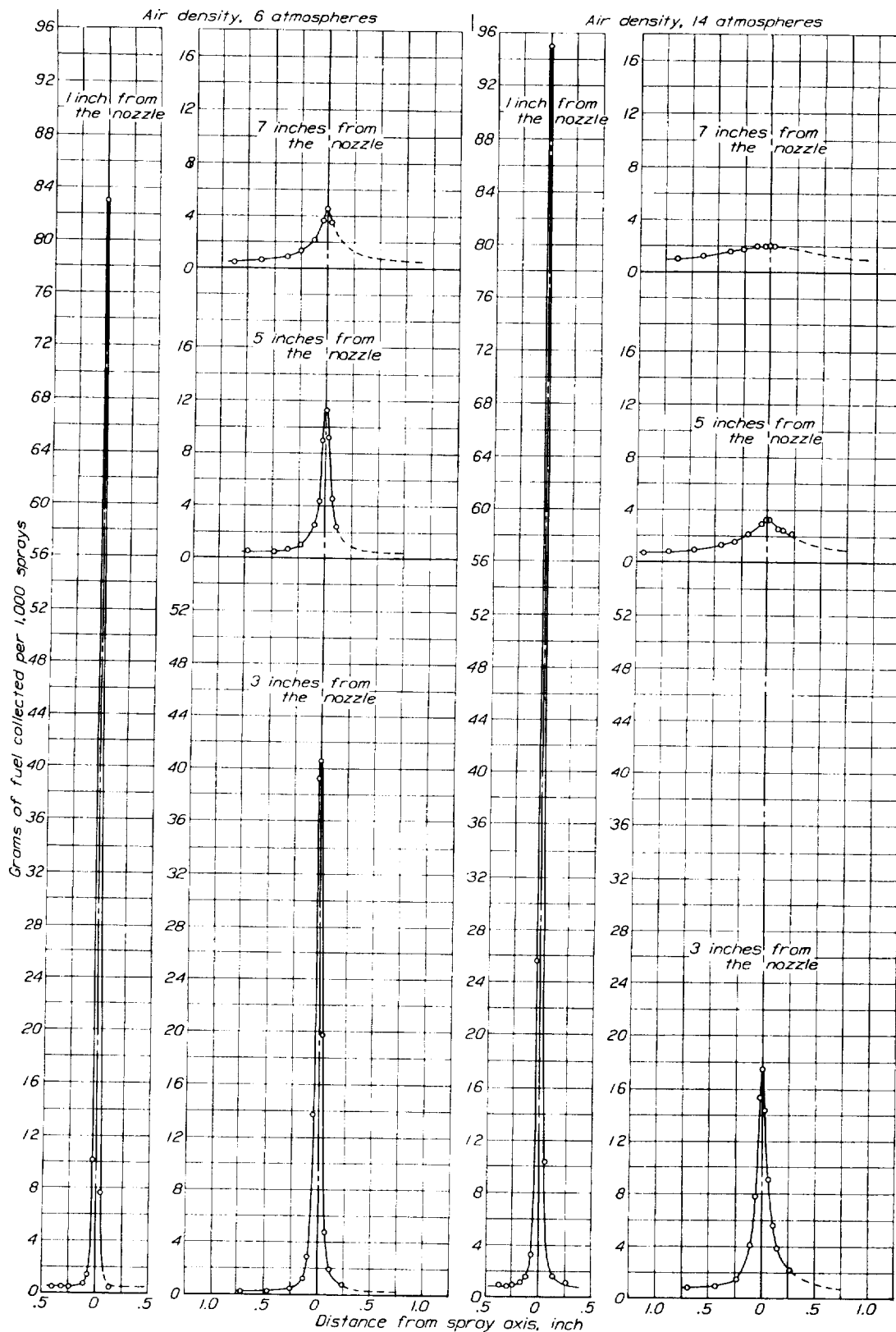


FIGURE 4.—Sampling-tube tests with a plain nozzle. Orifice diameter, 0.020 inch; orifice length-diameter ratio, 2.

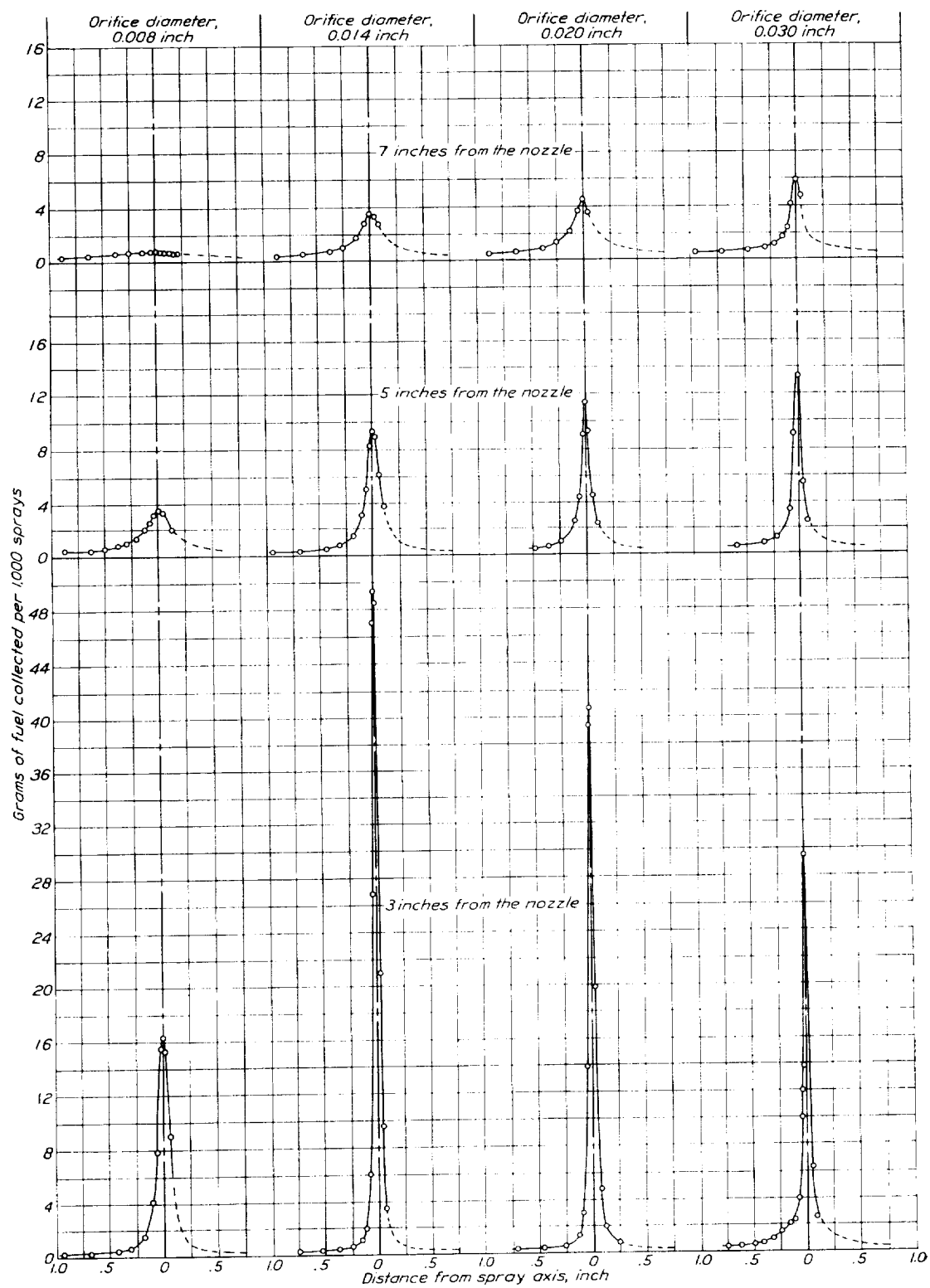


FIGURE 5.—Sampling-tube tests with plain nozzles having different orifice diameters. Orifice length-diameter ratio, 2; air density, 6 atmospheres.

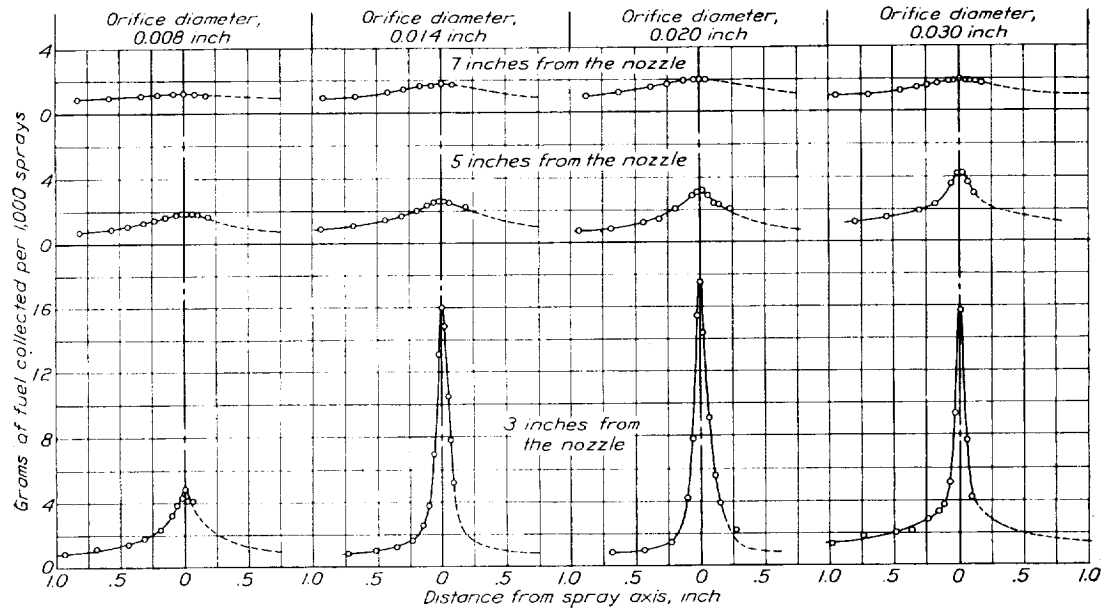


FIGURE 6.—Sampling-tube tests with plain nozzles having different orifice diameters. Orifice length-diameter ratio, 2; air density, 14 atmospheres.

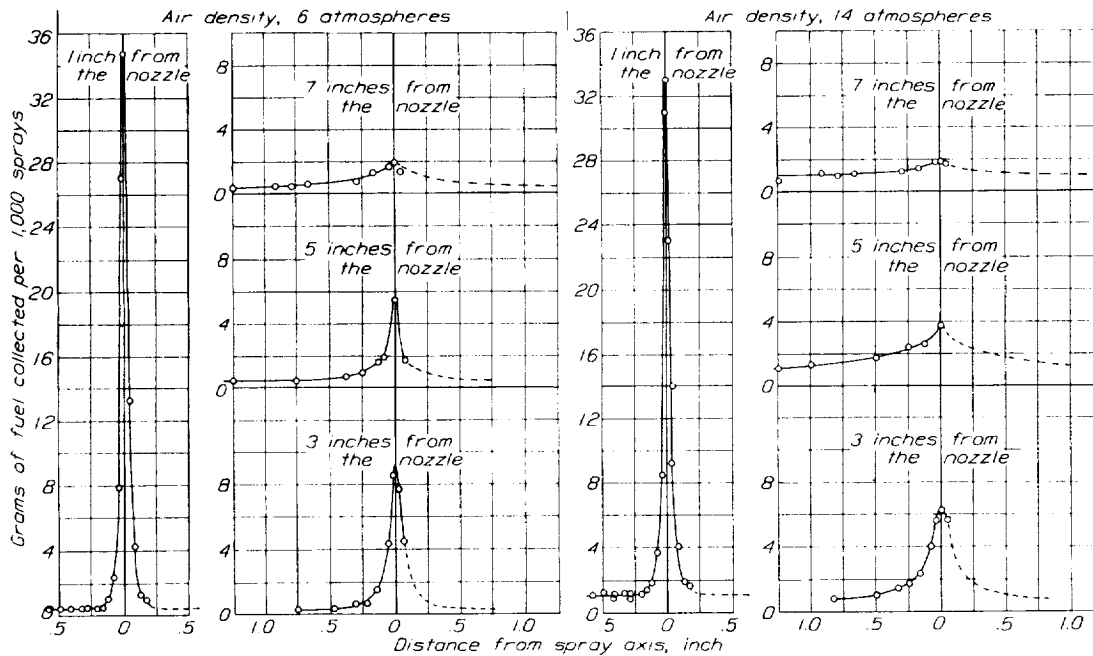


FIGURE 7.—Sampling tube tests with a pintle nozzle. Pintle dispersion angle, 20°.

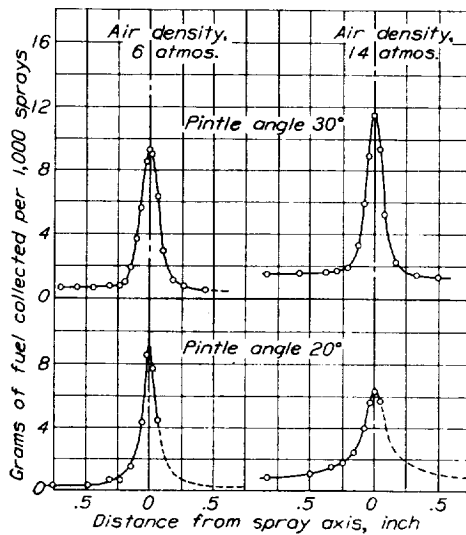


FIGURE 8.—Sampling-tube tests with pintle nozzles having different dispersion angles. All tests at 3 inches from the nozzle.

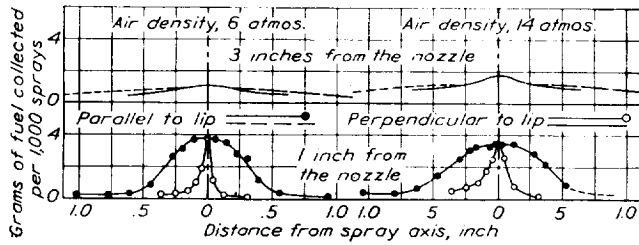


FIGURE 9.—Sampling-tube tests with a lip nozzle.

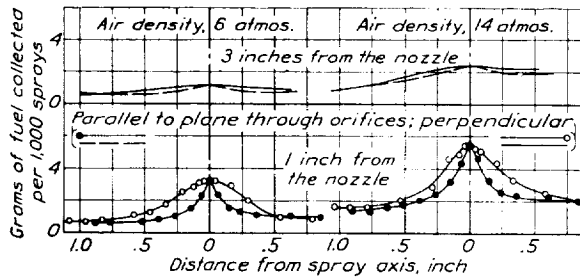


FIGURE 10.—Sampling-tube tests with a 2-impinging-jets nozzle.

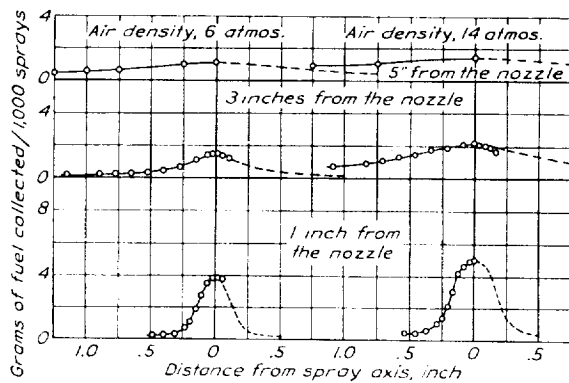


FIGURE 11.—Sampling-tube tests with a 4-impinging-jets nozzle.

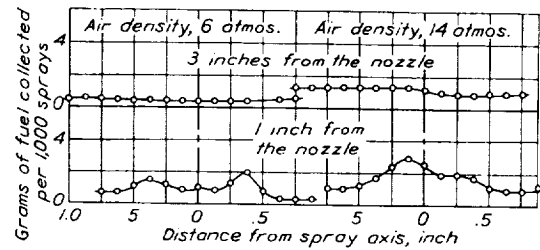


FIGURE 12.—Sampling-tube tests with an annular-orifice nozzle.

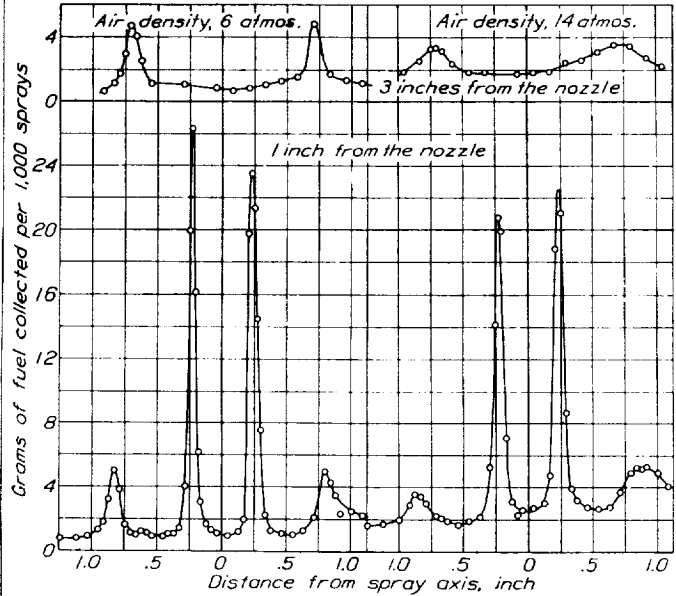


FIGURE 13.—Sampling-tube tests with a multiple-orifice nozzle.

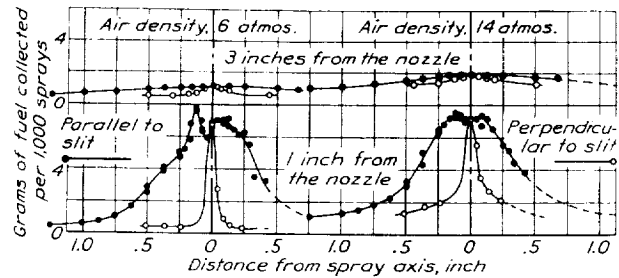


FIGURE 14.—Sampling-tube tests with a slit nozzle.

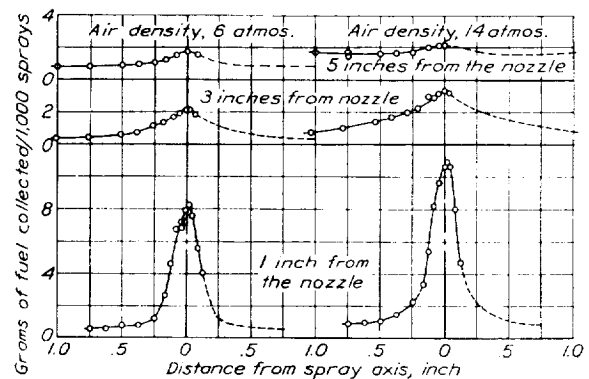


FIGURE 15.—Sampling-tube tests with a centrifugal nozzle.

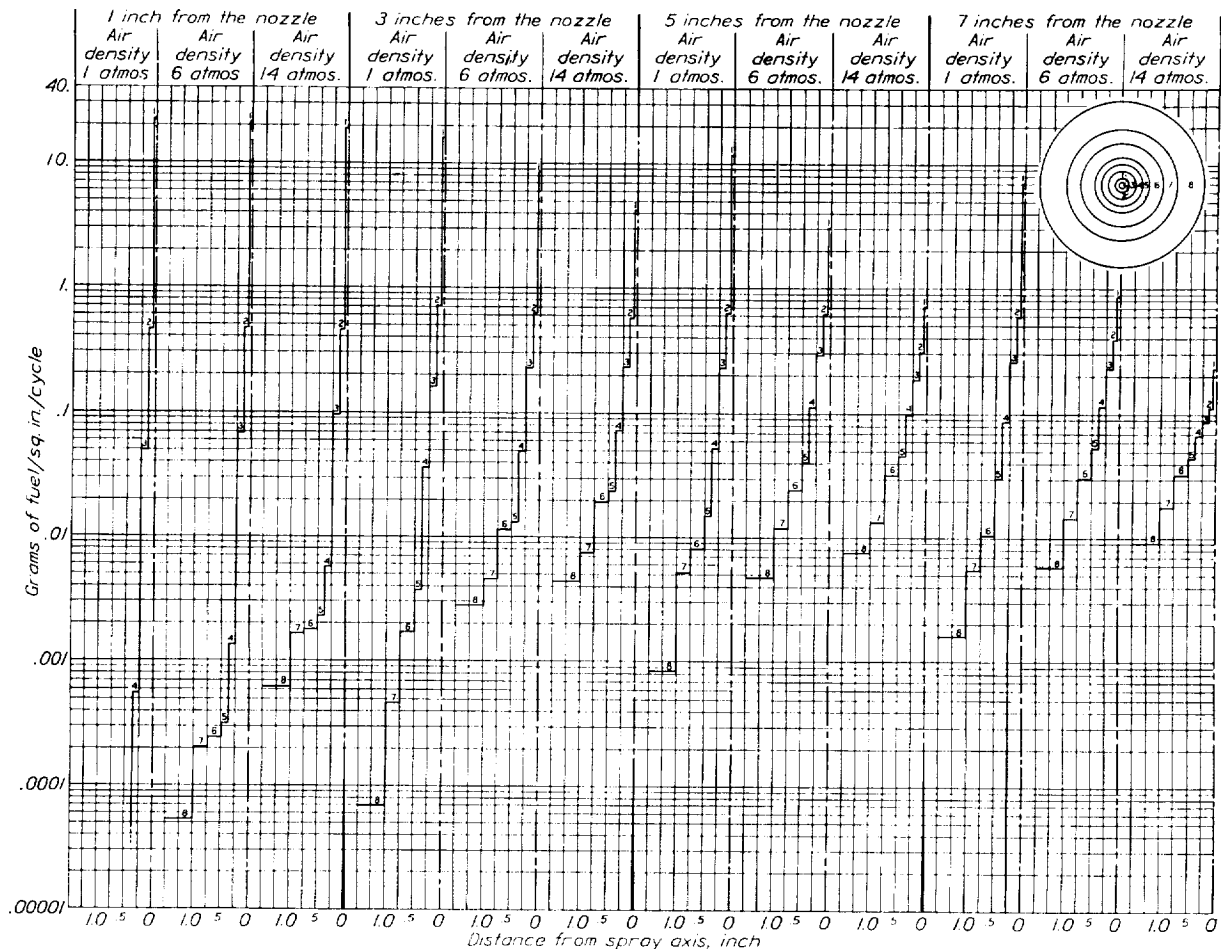


FIGURE 16.—Concentric-cups tests with a plain nozzle. Orifice diameter, 0.020 inch; orifice length-diameter ratio, 2.

given in table I for sprays from the plain nozzle with a 0.020-inch diameter orifice are also shown graphically in figure 16, grams of fuel per square inch per cycle being plotted vertically in steps, the widths of which are proportional to the distances between the walls of the cups. The great range of fuel concentrations (415,000:1) made it advisable to use a logarithmic vertical scale, thus making it much easier to read the smaller values. A sketch showing the relative diameters of the concentric cups is included, the scale being the same as the horizontal scale of the plots. The identifying numbers of the eight cups are shown, and the steps in the plots are labeled with the numbers of the cups they represent.

COMPARISON OF RESULTS OF THE TWO TEST METHODS

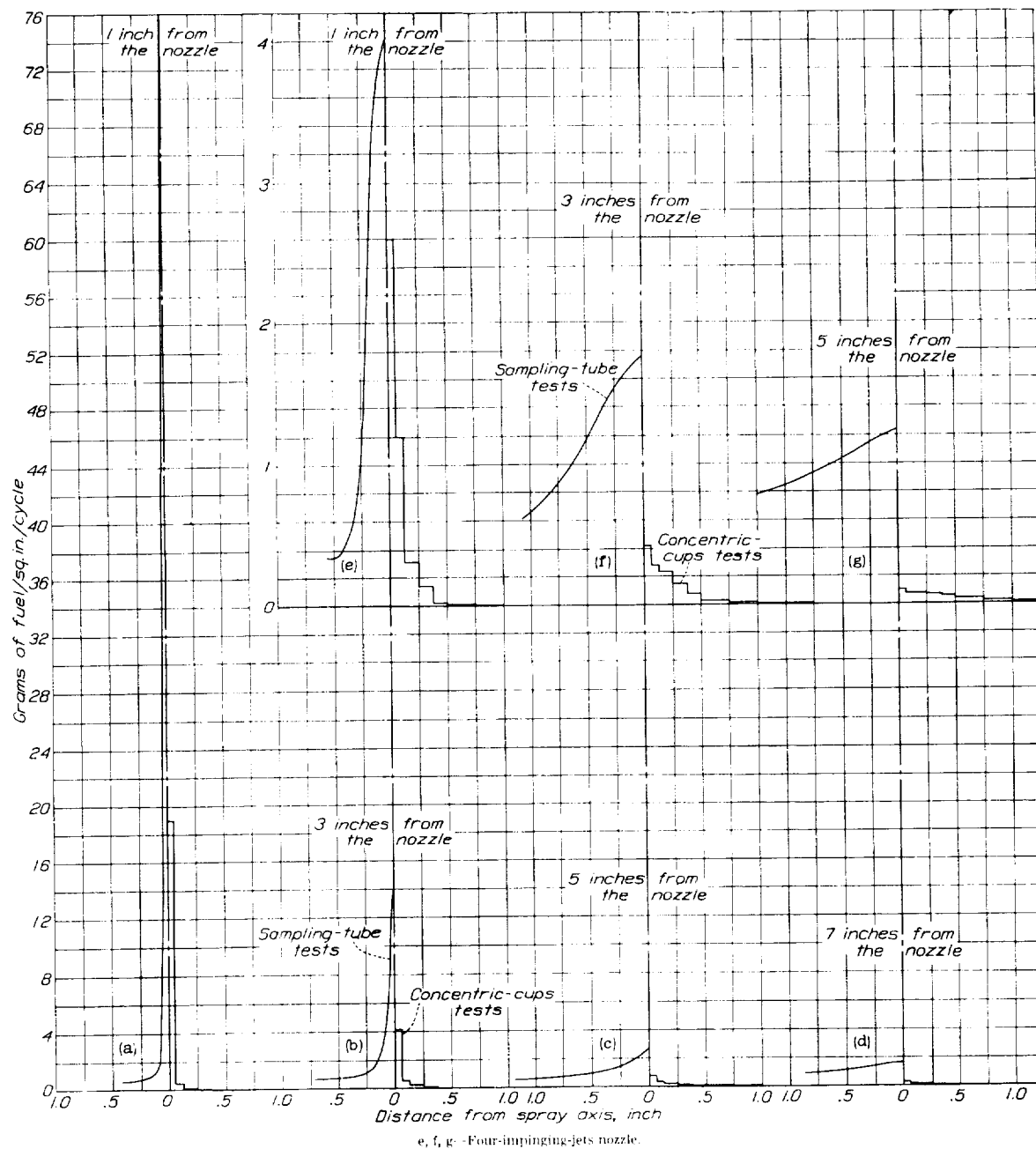
For each of the tests made with the concentric-cups apparatus at air densities of 6 and 14 atmospheres, a corresponding test was made with the sampling-tube apparatus. In order to make a direct comparison of the results of the two methods, the fuel weights obtained in some of the sampling-tube tests were divided

by the tube area and the number of injections made and were then plotted opposite the concentric-cups data for the same conditions. (See fig. 17.) The comparison shows that there is good general agreement as to the effect of different variables on fuel distribution but that the values are much greater for the sampling-tube tests. It is therefore believed that the area from which fuel was gathered by the sampling tube was much greater than the area of the tube itself.

DISCUSSION

FUEL DISTRIBUTION IN SPRAYS FROM DIFFERENT TYPES OF NOZZLES

In the study of the results of the tests described in this report, it is necessary to keep clearly in mind the distinction between *distribution of fuel within a spray* and *distribution of fuel throughout a combustion chamber*. Distribution of liquid fuel within the sprays was measured in this investigation; but other factors such as spray penetration, air-flow velocity, and engine temperature also influence the distribution of fuel throughout a combustion chamber. For instance, wide sprays



e, f, g.—Four-impinging-jets nozzle.
 a, b, c, d.—Plain nozzle; orifice diameter, 0.020 inch; orifice length-diameter ratio, 2.
 FIGURE 17.—Comparison of sampling-tube and concentric-cups tests with a 4-impinging-jets and a plain nozzle. Air density, 14 atmospheres

are desirable in cases for which high penetration is not required, such as the injection of fuel during the intake stroke of spark-ignition engines; but in compression-ignition engines such sprays usually fail to penetrate to all parts of the chamber and it becomes necessary to use plain, pintle, or multiple-orifice nozzles which, despite poorer distribution within the sprays, may produce better distribution in the combustion chamber. Data for the rates of penetration of the various types of sprays tested are presented in reference 6 and should be particularly useful in connection with the results

herein presented because, in most cases, the same nozzles were used.

The following discussion refers only to the fuel distribution within the sprays and the conclusions reached are largely based on the rate at which the fuel concentration decreased with increasing distance from the center line of the spray.

Plain nozzles.—Figures 4 to 6 and the data in table I show that the distribution of the fuel within sprays from the plain nozzles was very poor and that it improved rapidly as the air density or the distance from

the nozzle was increased. The results of the sampling-tube tests with plain nozzles having different orifice diameters indicate that at 5 and 7 inches from the nozzle the distribution became poorer as the orifice diameter was increased but at 3 inches from the nozzle the distribution was about the same for the 0.014-, 0.020-, and 0.030-inch nozzles and inferior to that for the 0.008-inch nozzle. Tests reported in reference 7 show that the injection pressure rapidly decreased as the orifice diameter was increased. As will be shown later, a decrease in the injection pressure results in poorer fuel distribution, and this factor is at least partly responsible for the change in distribution with orifice size shown by the present tests.

Some sampling-tube tests were made with plain nozzles having orifice diameters of 0.020 inch and orifice length-diameter ratios of 0.5, 2, and 5, but the effect of orifice length-diameter ratio on fuel distribution was very slight, and the results of the tests are not included in this report.

Pintle nozzles.—Figure 7 and table I show that the fuel distribution in the sprays from the 20° pintle nozzle was better than in those from all of the plain nozzles except the one with the 0.008-inch orifice. Increasing the air density from 1 to 6 atmospheres resulted in poorer fuel distribution, but a further increase to 14 atmospheres resulted in an improvement. The improvement with distance from the nozzle was not so rapid as with plain nozzles.

The results of sampling-tube tests with a 30° pintle nozzle at 3 inches from the nozzle are shown in figure 8 and corresponding curves for the 20° nozzle are included to facilitate comparison. The concentric-cups data in table I show that raising the air density from 1 to 6 atmospheres caused the fuel distribution to become much poorer, but a further increase to 14 atmospheres had little effect. The unusual change in fuel distribution between 1 and 6 atmospheres for both pintle nozzles was probably caused by narrowing of the spray core. (See reference 6.) At 1 atmosphere the fuel in sprays from the 30° nozzle was much better distributed than in those from the 20° nozzle, at 6 atmospheres there was little difference, and at 14 atmospheres the sprays from the 20° nozzle had the better distribution.

Lip nozzle.—Sprays from the lip nozzle are shaped like a narrow fan, extending outward from the lip surface. Two traverses by the sampling tube at each condition were therefore necessary to obtain a true picture of the fuel distribution. One traverse was made perpendicular to the plane of the lip surface, displacements above this plane (on side toward the orifice) being plotted to the left and those below it to the right. The results of the tests 1 inch from the nozzle (fig. 9) show that the plane of maximum fuel concentration coincided with that of the lip surface, but that more of the fuel was above that plane than

below it. The second traverse was made in the plane of the lip surface, the nozzle having been rotated 90° after making the first traverse. The results show that at 1 inch from the nozzle the distribution of the fuel in the plane of the lip surface was much better than in the plane at right angles to it but that at 3 inches from the nozzle there was little difference. The curves for the two traverses made at 3 inches from the nozzle are so close to each other that the test points have been omitted. When the air density was increased from 6 to 14 atmospheres, the fuel distribution at 1 inch from the nozzle improved slightly in both planes but at 3 inches from the nozzle it became poorer.

Impinging-jets nozzles.—Cross sections of sprays from a 2-impinging-jets nozzle are approximately elliptical, the minor axis of the ellipse lying in the plane containing the axes of the two jets. Sampling-tube traverses were made first through the narrow parts and then through the wide parts of the spray. Figure 10 shows that fuel distribution along the lines of both traverses improved with distance from the nozzle but that increasing the air density from 6 to 14 atmospheres had very little effect.

Sprays from 4-impinging-jets nozzles are symmetrical about the spray axis so that only one traverse was necessary for each condition. Figure 11 shows that the distribution of fuel near the nozzle was very good and improved slowly with increasing air density and distance from the nozzle.

Annular-orifice nozzle.—The injection valve used for the annular-orifice nozzle tests was designed for the injection of gasoline into air at atmospheric density, a condition requiring relatively low injection pressures. The valve was set at its maximum valve-opening pressure, about 1,000 pounds per square inch, with the result that the mean injection pressure was considerably less for these tests than for those with the other nozzles.

Only one traverse was made at each condition when testing the annular-orifice nozzle, although previous work (reference 6) had shown that this particular nozzle does not produce symmetrical sprays. Figure 12 shows that this nozzle dispersed the fuel very quickly and that as the air density was increased the fuel distribution became poorer. Experience with several annular-orifice nozzles at this laboratory indicates that the production of unsymmetrical sprays is a common fault of this type of nozzle and that its usefulness is thereby decidedly reduced.

Multiple-orifice nozzle.—Each of the jets from a multiple-orifice nozzle is symmetrical about its axis, so that a single traverse in the plane of the jet axes was sufficient. The size of the pressure chamber limited the traverse at 1 inch from the nozzle to four of the six jets, and at 3 inches from the nozzle only the two central jets could be included. Figure 13 shows that the various jets remained distinct, very little fuel being

deflected into the spaces between them. The traverse was carried in a straight line across the spray and intersected the two central jets at an angle of 80° and the other two jets at 60° . Before each jet was traversed, however, the end of the sampling tube was bent parallel to the axis of that jet. The test results show that the distribution of fuel in the two central jets from the multiple-orifice nozzle was better than in sprays from a plain nozzle having nearly the same orifice diameter. This difference may be attributed to the more turbulent flow through the orifices of the multiple-orifice nozzle, which have no conical approaches to help stabilize the flow. (See reference 5.)

Slit nozzle.—Results of sampling-tube tests with the slit nozzle are shown in figure 14. Sprays from this nozzle resemble those from the lip nozzle but are somewhat thinner and broader. Tests made at this laboratory have shown that the fuel distribution in sprays from slit nozzles is greatly influenced by the shape of the fuel passage between the stem seat and the slit. With nozzles having cylindrical passages, the shape of the bottom of that passage is important, a flat bottom resulting in a narrow spray and a conical bottom often breaking the spray into two parts. A spherical bottom has been found to be the best, but even with it the fuel distribution may be irregular, as shown by the results of sampling-tube traverses made parallel to the slit at 1 inch from the nozzle. The curves in figure 14 show that increasing the air density had little effect on fuel distribution along a line parallel to the slit but did improve the distribution at right angles to the slit. Fuel distribution in both directions improved with increasing distance from the nozzle.

Centrifugal nozzle.—As the whirling fuel leaves the centrifugal nozzle it spreads out to form a hollow cone. At the same time, however, the thin sheet of fuel begins to disintegrate into drops and, as the fuel gets farther from the nozzle, the sides of the cone thicken until the hollow center is entirely filled. The disintegration of the spray core continues to send fuel drops into the central part of the spray from all directions as well as to send them to the outer parts of the spray, with the result that the fuel concentration becomes greatest at the center of the spray. In air at atmospheric density the process may not be completed until the fuel has traveled an inch or more from the nozzle, but at 6 and 14 atmospheres it is completed in a shorter distance, as shown by the curves in figure 15. Distribution of the fuel improved with increasing distance from the nozzle but became slightly worse when the air density was increased from 6 to 14 atmospheres.

Comparison of the various types of sprays.—After a careful study of the data presented in this report, the following nozzles have been listed in the order of improving distribution of fuel within their sprays: Plain nozzle, pintle nozzle, centrifugal nozzle, lip

nozzle, slit nozzle, 4-impinging-jets nozzle, 2-impinging-jets nozzle, and annular-orifice nozzle. There was little difference between the lip and slit nozzles, and the listing of the annular-orifice nozzle as producing sprays with the best distribution is questionable because of the nonsymmetry of the sprays. The multiple-orifice nozzle was not included in this list because only the central portion of its spray could be investigated.

EFFECT OF INJECTION PRESSURE ON FUEL DISTRIBUTION

Tests were made both with the sampling tube and with the concentric cups to measure the effect of injection pressure on fuel distribution. The plain nozzle with the 0.020-inch orifice was used; the valve-opening pressure was reduced to 730 pounds per square inch and the pump speed, to 487 r. p. m. These values were chosen because the tests of the injection pump reported in reference 7 showed that making these two changes resulted in reducing the mean effective injection pressure from 2,500 to 1,250 pounds per square inch. The curves in figure 18 and the data in table I show that the fuel distribution was slightly better at the higher injection pressure.

EFFECT OF FUEL VISCOSITY ON DISTRIBUTION

Sampling-tube tests were made with a hydrogenated safety fuel, a Diesel fuel, and S. A. E. 30 lubricating oil in air at a density of 14 atmospheres. The high volatility of the safety fuel made it necessary to apply a correction to the results of tests using this fuel. The correction was obtained by running an evaporation test at the end of alternate fuel-collecting tests; air flowed through the fuel trap for the same length of time as for the fuel-collecting tests, but there were no sprays in the chamber. The decrease in the weight of the fuel trap during each evaporation test was added to the fuel weight collected during the preceding and following tests to give the correct amount of fuel collected. This correction varied from 12 percent of the fuel collected at the centers of the sprays to 84 percent at the edges. Concentric-cups tests were made with the safety fuel and the Diesel fuel but not with the lubricating oil, as it would not flow through the small drain tubes. The plain nozzle with the 0.020-inch orifice was used at the standard injection conditions, and all the tests were made at 3 inches from the nozzle. The viscosities of the safety fuel, Diesel fuel, and lubricating oil were measured at 22°C . and at atmospheric pressure and found to be 0.0058, 0.052, and 3.1 poises, respectively.

The results of the sampling-tube tests (fig. 19) indicate that the fuel distribution became poorer as the fuel viscosity was increased, but the concentric-cups tests showed little difference between the distribution in Diesel and safety-fuel sprays.

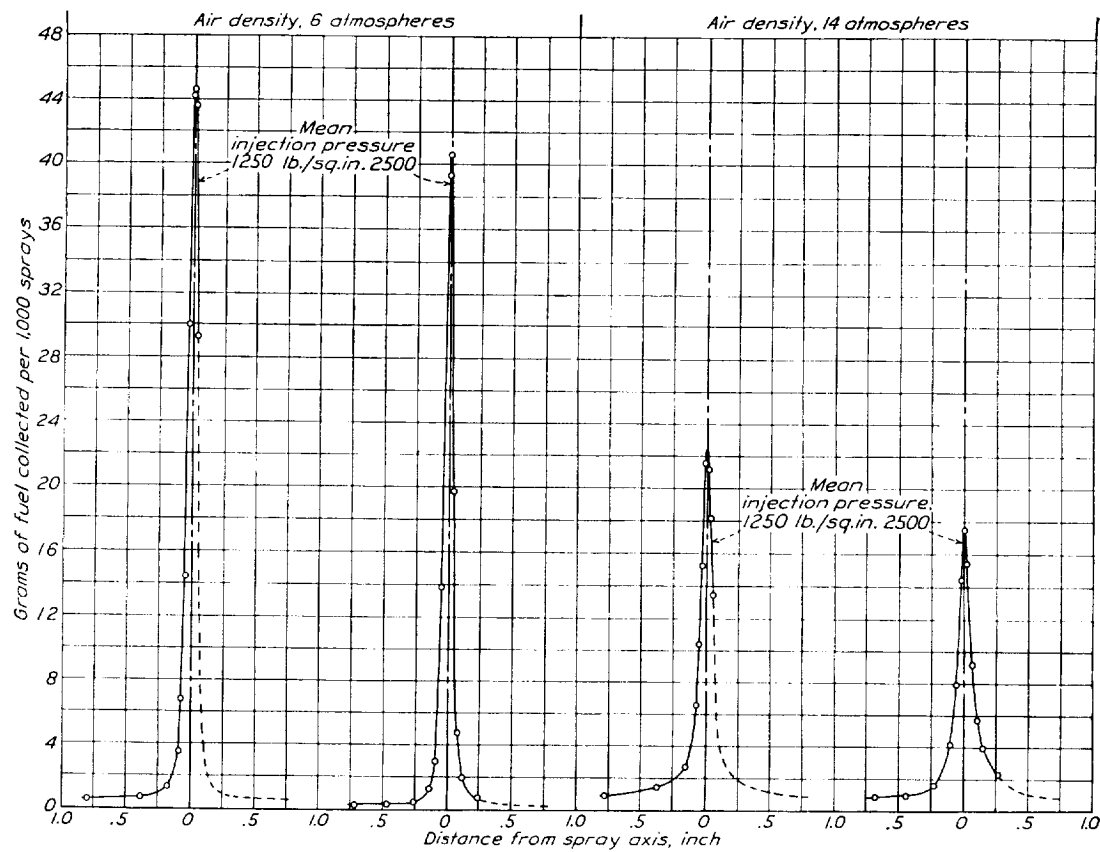


FIGURE 18. Sampling-tube tests using different mean injection pressures. Plain nozzle; orifice diameter, 0.020 inch; orifice length-diameter ratio, 2; distance from nozzle, 3 inches; pump speeds, 487 and 750 r. p. m.; injection-valve opening pressures, 730 and 3,500 pounds per square inch.

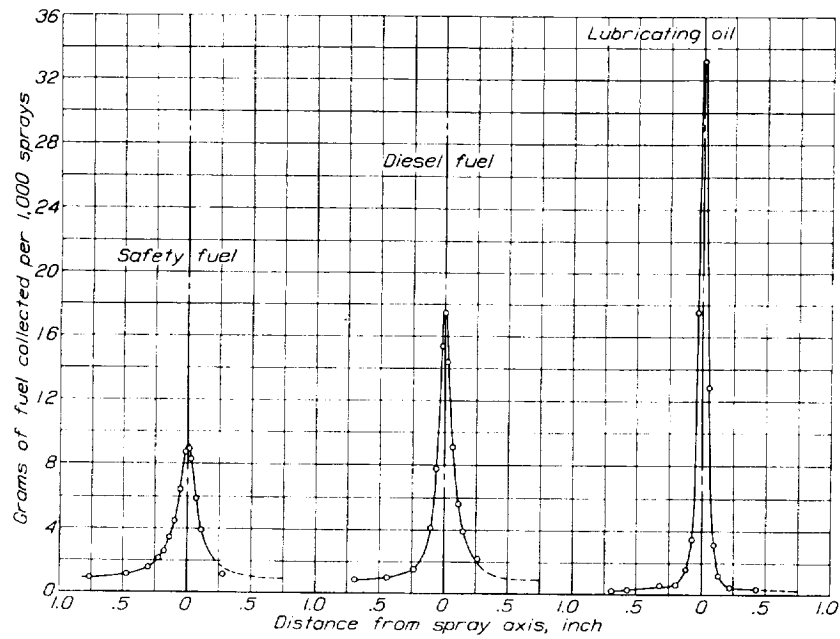


FIGURE 19.—Sampling-tube tests using different fuels. Plain nozzle; orifice diameter, 0.020 inch; orifice length-diameter ratio, 2; air density, 14 atmospheres; distance from nozzle, 3 inches.

EFFECTS OF VAPORIZATION AND AIR MOVEMENT ON FUEL DISTRIBUTION

The present results have shown the distribution of the fuel in the liquid phase. The additional effects of vaporization and diffusion and of air movement on the distribution of the fuel can be estimated by comparing these data with those presented in references 9 and 10. The photographs of the combustion in reference 9 show that the fuel was distributed over a larger area than indicated by the distribution in the liquid phase. With a plain nozzle, for example, the flame volume was more than five times the liquid spray volume and, although the present tests show that in the liquid phase without air flow there was very little fuel distributed between the jets of the multiple-orifice nozzle, the combustion photographs show that, when the same nozzle is used under conditions closely simulating engine conditions, a considerable amount of fuel reached the area between the visible sprays. Test results for an engine with very little or no air flow (reference 11) show that, although a combustible mixture is formed over a considerable area even with a single-orifice nozzle, the effectiveness of the combustion is low unless a sufficient number of orifices is used to give an angle between sprays of about 25° . When air flow is employed, the optimum angle between the sprays may be the same or greater. (See references 12 and 13.)

The photographs reproduced in reference 9 show that when high-dispersion nozzles, such as the slit or impinging-jets nozzles, are used, the distribution within the sprays is good but that apparently the air-fuel ratio is too low for good combustion efficiency.

CONCLUSIONS

Distribution of the liquid fuel within sprays is only one of the factors that determine whether the fuel will be well distributed to all parts of the combustion chamber; some of the other factors are rate of spray penetration, air-flow velocity, and engine temperature. Satisfactory combinations of these factors must be determined by engine tests, but the results herein presented and summarized as follows should reduce the required amount of such test work.

1. Fuel distribution in all types of sprays improved with increasing distance from the nozzle, the improvement being the most rapid in sprays of high penetrating power.

2. Fuel distribution within sprays having high penetrating power improved greatly when the air density was increased, but the improvement was much less in sprays having low penetrating power; in some widely dispersed sprays the distribution became poorer.

3. Increasing the injection pressure resulted in a small improvement in the fuel distribution in sprays from plain nozzles.

4. Sampling-tube tests showed that increasing the viscosity of the fuel resulted in poorer fuel distribution in sprays from plain nozzles.

5. The nozzles used for these tests are listed as follows in the order of improving distribution of fuel within their sprays: Plain nozzle, pintle nozzle, centrifugal nozzle, lip nozzle, slit nozzle, 4-impinging-jets nozzle, 2-impinging-jets nozzle, and annular-orifice nozzle.

6. Changing the orifice length-diameter ratio of one of the plain nozzles had very little effect on the fuel distribution in the sprays.

7. Fuel distribution in the two central jets of sprays from the multiple-orifice nozzle was better than in sprays from a plain nozzle having nearly the same orifice diameter.

LANGLEY MEMORIAL AERONAUTICAL LABORATORY,
NATIONAL ADVISORY COMMITTEE FOR AERONAUTICS,
LANGLEY FIELD, VA., April 8, 1936.

REFERENCES

- DeJuhasz, Kalman J., Zahn, O. F., Jr., and Schweitzer, P. H.: On the Formation and Dispersion of Oil Sprays. Eng. Exp. Sta. Bull. No. 40, Penn. State Coll. 1932, pp. 26-61.
- Schweitzer, P. H.: The Penetration of Oil Sprays in Dense Air. Tech. Bull. No. 20, Penn. State Coll. 1934, pp. 108-124.
- Lee, Dana W.: The Effect of Nozzle Design and Operating Conditions on the Atomization and Distribution of Fuel Sprays. T. R. No. 425, N. A. C. A., 1932.
- Lee, Dana W.: Experiments on the Distribution of Fuel in Fuel Sprays. T. R. No. 438, N. A. C. A., 1932.
- Lee, Dana W., and Spencer, Robert C.: Photomicrographic Studies of Fuel Sprays. T. R. No. 454, N. A. C. A., 1933.
- Lee, Dana W.: A Comparison of Fuel Sprays from Several Types of Injection Nozzles. T. R. No. 520, N. A. C. A., 1935.
- Gelalles, A. G., and Marsh, E. T.: Rates of Fuel Discharge as Affected by the Design of Fuel-Injection Systems for Internal-Combustion Engines. T. R. No. 433, N. A. C. A., 1932.
- Rothrock, A. M., and Marsh, E. T.: Penetration and Duration of Fuel Sprays from a Pump Injection System. T. R. No. 455, N. A. C. A., 1933.
- Rothrock, A. M., and Waldron, C. D.: Effect of Nozzle Design on Fuel Spray and Flame Formation in a High-Speed Compression-Ignition Engine. T. R. No. 561, N. A. C. A., 1936.
- Rothrock, A. M., and Waldron, C. D.: Effects of Air-Fuel Ratio on Fuel Spray and Flame Formation in a Compression-Ignition Engine. T. R. No. 545, N. A. C. A., 1935.
- Spanogle, J. A., and Foster, H. H.: Basic Requirements of Fuel-Injection Nozzles for Quiescent Combustion Chambers. T. N. No. 382, N. A. C. A., 1931.
- Moore, C. S., and Foster, H. H.: Performance Tests of a Single-Cylinder Compression-Ignition Engine with a Displacer Piston. T. N. No. 518, N. A. C. A., 1935.
- Spanogle, J. A., and Whitney, E. G.: A Description and Test Results of a Spark-Ignition and a Compression-Ignition 2-Stroke-Cycle Engine. T. R. No. 495, N. A. C. A., 1934.

TABLE I
RESULTS OF THE CONCENTRIC-CUPS TESTS

Nozzle	Valve-opening pressure	Fuel	Distance from the nozzle	Air density	Grams of fuel per square inch per cycle								Percentage of fuel caught
					Cup no.								
					1	2	3	4	5	6	7	8	
	lb./sq. in.		Inches	Atmospheres									
Plain, orifice diameter 0.008 inch	3,500	Diesel	1	9	24	0.18	0.0071	0.00073	0	0	0	0	96.2
				14	22	.21	.013	.0012	.00073	.00021	.00011	.00003	91.3
				1	19	.36	.072	.0036	.0016	.0015	.0020	.00058	87.5
				6	19	.46	.090	.0071	.00043	.00026	.00011	.00004	89.6
			3	6	5.8	.58	.28	.055	.010	.0058	.0032	.0022	67.4
				14	1.4	.33	.18	.083	.030	.015	.0067	.0046	55.6
			5	1	13	.57	.24	.032	.0089	.0025	.00061	.00020	84.4
				6	.79	.33	.19	.094	.049	.023	.0073	.0031	60.0
			7	14	.31	.11	.079	.065	.047	.029	.013	.0061	54.2
				1	7.2	.70	.33	.064	.025	.0087	.0023	.00061	79.7
				6	.30	.16	.11	.080	.052	.031	.014	.0046	58.3
				14	.14	.056	.045	.044	.040	.028	.019	.0094	56.0
Plain, orifice diameter 0.014 inch	3,500	Diesel	1	23	32	.064	.00097	0	0	0	0	97.6	
				6	23	.27	.032	.0056	.00041	.00035	.00030	.00014	95.8
				14	22	.27	.054	.0021	.00087	.00047	.00031	.00018	94.2
				1	19	.59	.14	.015	.0034	.0011	.00041	.00025	96.0
			3	6	14	.40	.16	.042	.012	.0067	.0029	.0019	85.0
				14	5.6	.41	.23	.058	.018	.014	.0063	.0045	71.0
			5	1	15	.61	.14	.047	.012	.0042	.0012	.00048	92.0
				6	4.7	.55	.27	.087	.035	.019	.0080	.0038	81.4
			7	14	.78	.26	.15	.084	.041	.032	.014	.0076	69.4
				1	11	.72	.21	.059	.022	.0090	.0030	.0010	87.5
				6	1.3	.41	.19	.094	.045	.030	.012	.0054	73.0
				14	.20	.091	.067	.055	.039	.029	.016	.0087	56.7
Plain, orifice diameter 0.020 inch	3,500	Diesel	1	22	46	.050	.00053	0	0	0	0	96.4	
				6	21	.47	.070	.0013	.00032	.00024	.00020	.000053	94.8
				14	19	.45	.097	.0057	.0023	.0018	.0017	.00063	89.3
				1	16	.71	.16	.037	.0037	.0017	.00047	.000069	91.7
			3	6	8.6	.61	.22	.049	.013	.012	.0046	.0028	79.2
				14	4.2	.57	.23	.072	.024	.020	.0075	.0044	73.5
			5	1	12	.62	.23	.052	.015	.0081	.0052	.00084	83.7
				6	3.1	.61	.28	.11	.041	.024	.012	.0047	81.6
			7	14	.72	.31	.19	.098	.040	.032	.013	.0075	70.7
				1	7.2	.59	.26	.088	.031	.011	.0055	.0016	79.6
				6	.87	.39	.23	.12	.054	.032	.014	.0058	89.0
				14	.23	.11	.087	.068	.044	.033	.018	.0091	65.3
Pintle, spray angle 20°	3,500	Diesel	1	1	8.3	.41	.50	.097	.016	.0046	.0021	.00016	83.0
				6	13.2	.54	.15	.017	.0047	.0038	.0022	.00013	70.9
				14	13.3	.51	.12	.021	.0095	.0079	.0042	.00018	75.5
			3	1	2.6	.52	.23	.19	.082	.021	.0043	.0020	77.8
				6	4.7	.52	.16	.066	.023	.014	.0065	.0042	62.0
			5	14	2.5	.49	.21	.078	.030	.019	.010	.0063	66.8
				1	1.1	.46	.26	.12	.061	.034	.015	.0038	78.0
			7	6	1.5	.43	.23	.11	.043	.020	.0095	.0045	63.7
				14	.60	.23	.17	.092	.047	.029	.014	.0072	64.2
				1	.19	.20	.16	.12	.078	.035	.015	.0063	70.3
				6	.29	.18	.15	.095	.062	.031	.014	.0059	62.5
				14	.17	.08	.078	.064	.046	.030	.018	.0082	57.6
Pintle, spray angle 30°	3,500	Diesel	1	1	.21	.17	.18	.21	.17	.054	.012	.0017	89.7
				6	4.1	.61	.21	.083	.025	.016	.0093	.0046	67.4
				14	5.4	.63	.23	.068	.026	.019	.011	.0062	77.3
			3	1	1.6	1.3	.52	.21	.055	.014	.0016	.00010	95.6
				6	2.3	1.6	.27	.21	.031	.0078	.0025	.0010	85.0
			5	14	2.6	1.2	.31	.14	.021	.0080	.0040	.0022	74.8
				1	.29	.25	.20	.15	.10	.056	.019	.0042	89.3
			7	6	.62	.42	.29	.16	.080	.028	.0071	.0035	76.9
				14	.42	.28	.23	.15	.078	.026	.0094	.0061	73.7
				1	.10	.087	.086	.076	.061	.045	.027	.010	74.6
				6	.13	.10	.10	.090	.080	.044	.019	.0067	69.3
				14	.10	.069	.069	.064	.055	.036	.019	.0092	61.2
Plain, orifice diameter 0.020 inch	730	Diesel	3	1	19	.89	.18	.020	.0036	.0016	.0012	.00067	89.2
				6	15	.87	.15	.033	.010	.0055	.0032	.0024	84.0
Plain, orifice diameter 0.020 inch	3,500	Diesel	3	14	8.0	.81	.21	.060	.023	.015	.0082	.0049	76.5
				1	16	.71	.16	.037	.0037	.0017	.00047	.000069	91.7
Plain, orifice diameter 0.020 inch	3,500	Safety	3	6	8.6	.61	.22	.049	.013	.012	.0046	.0028	79.2
				14	4.2	.57	.23	.072	.024	.020	.0075	.0044	73.5
Plain, orifice diameter 0.020 inch	3,500	Safety	3	1	16	.43	.085	.036	.0064	.0020	.0020	.00088	74.9
				6	9.6	.52	.12	.052	.017	.0098	.0059	.0032	68.5
				14	3.7	.45	.20	.074	.030	.022	.011	.0049	66.5

REPORT No. 566

GROUND-HANDLING FORCES ON A 1/40-SCALE MODEL OF THE U. S. AIRSHIP "AKRON"

By ABE SILVERSTEIN and B. G. GULICK

SUMMARY

An investigation was conducted in the N. A. C. A. full-scale wind tunnel to determine the ground-handling forces on a 1/40-scale model of the U. S. airship "Akron." Ground-handling conditions were simulated by establishing a velocity gradient above a special ground board in the tunnel comparable with that encountered over a landing field. The tests were conducted at Reynolds Numbers ranging from 5,000,000 to 19,000,000 at each of six angles of yaw between 0° and 180° and at four heights of the model above the ground board.

The ground-handling forces vary greatly with the angle of yaw and reach large values at appreciable angles of yaw. Small changes in height, pitch, or roll did not critically affect the forces on the model. In the range of Reynolds Numbers tested, no significant variation of the forces with the scale was disclosed.

INTRODUCTION

At the request of the Bureau of Aeronautics, Navy Department, an investigation was conducted in the N. A. C. A. full-scale wind tunnel to determine the ground-handling forces on a 1/40-scale model of the U. S. airship *Akron*.

Correlated data on the forces and moments encountered in handling airships near the ground have not been available. Previous work of a similar nature conducted at low Reynolds Numbers has shown conflicting results (references 1 and 2). Actual handling experiences with the large airships have shown under some conditions the existence of extremely large forces and moments that may endanger the airship unless properly anticipated. The prediction of the numerical values of the handling forces by wind-tunnel research is not satisfactory owing to the relatively small size of the models. It was believed, however, that the 1/40-scale *Akron* model was large enough to enable the direction and trend of the forces to be predicted.

Ground-handling conditions were closely simulated by establishing a velocity gradient above the ground board comparable with that encountered over a landing field. Tests were made at six angles of yaw between 0° and 180°, at four heights of the model above the

ground board, and at air speeds from 28 to 100 miles per hour. Several special conditions of pitch and roll were also investigated.

WIND TUNNEL AND EQUIPMENT

The wind tunnel used for these tests is described in reference 3. The tunnel was modified by the addition of a horizontal ground board, 30 feet wide, to simulate the landing field. The board was installed at the level of the lower surface of the entrance cone, making a continuous surface with the entrance cone and extend-

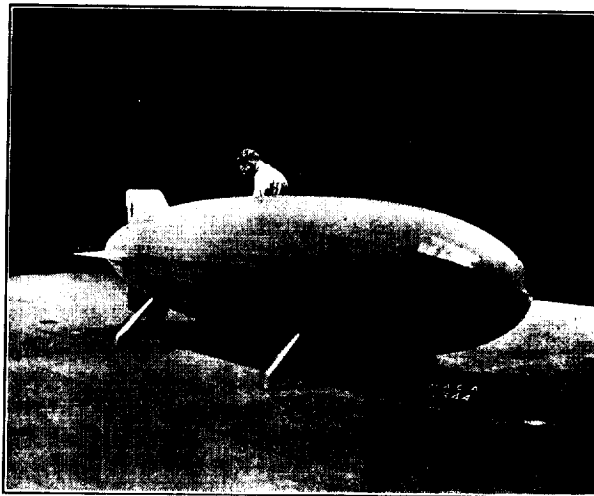


FIGURE 1.—The 1/40-scale model of the U. S. airship *Akron* on ground board at 0° yaw.

ing to within a few feet of the exit cone. Figure 1 shows the model in position above the ground board.

Forces, moments, and velocity distribution about the model were measured with the standard wind-tunnel equipment. The model was supported by four struts projecting through the ground board and rigidly attached at their lower ends to the floating frame of the balance (fig. 1). The portions of the struts extending above the ground board were shielded by streamline fairings to eliminate tare forces.

Smoke was used to show the flow of air over the model. The smoke was generated by passing kerosene

through heated coils and was ejected through small tubes into the air stream a short distance ahead of the model. Pictures were taken of the flow with a standard movie camera using 16 millimeter film and taking 16 frames a second.

MODEL

The *Akron* model previously tested in the propeller-research tunnel (reference 4) was fitted with the Mark II fins and control surfaces. The model is of hollow wood construction of polygonal cross section with 36 sides over the fore part of the hull faired into 24 sides near the stern. The surface was refinished so as to be comparable with well-doped fabric. The principal dimensions of the model are listed in the following table:

Ratio of distance from nose to total length	Radius (circumscribed circle)
a/L	Inches
0	0
.02	4.95
.05	9.96
.10	14.20
.15	16.65
.20	18.39
.25	19.12
.30	19.61
.35	19.85
.40	19.90
.45	19.90
.50	19.80
.55	19.59
.60	19.12
.65	18.46
.70	17.50
.75	16.15
.80	14.44
.85	12.29
.90	9.61
.95	6.52
1.00	0

Length, 19.62 ft.; volume, 115 cu. ft.; $(vol)^{1/3}$, 23.62 sq. ft.; $(vol)^{1/3}$, 4.86 ft.; center of buoyancy, $a/L=0.404$.

VELOCITY GRADIENT

One of the important variables affecting the airship handling forces is the gradient of the wind velocity with height above the landing field. This velocity gradient is not constant and depends largely on the terrain and the weather conditions. In the present investigation it

was not expedient to test with more than one velocity gradient so that a representative gradient obtained in tests at Langley Field (reference 5) was adopted. This reference velocity gradient indicates that the average increase in velocity with height above the ground is proportional to the $1/7$ power of the height ($V \propto h^{1/7}$) or, in terms of the dynamic pressure, $q \propto h^{2/7}$. This velocity gradient is similar to that in the boundary layer of a flat plate immersed in a turbulent stream at high Reynolds Numbers and may be considered as the most probable gradient over a flat landing field free of obstructions.

The velocity at 200 feet above the ground was arbitrarily chosen as a reference. It corresponds to a height of 5 feet above the ground board for the model tests; consequently all velocity computations are based on the velocity at this height. The gradients as represented by the foregoing relation and as determined from the results of dynamic-pressure surveys for the positions occupied by the model are compared in figure 2.

CORRECTIONS

The results were corrected for the blocking effect of the model on the air stream. (See reference 6.) Inasmuch as the model was small in proportion to the size of the jet, no tunnel-boundary corrections were applied to the data. Surveys showed the variation of the static pressure over the length of the model to be negligible, therefore no corrections for static-pressure gradient were made.

TESTS

Force tests. The lift, drag, and cross-wind forces and the pitching, rolling, and yawing moments were measured for four heights, $25\frac{1}{2}$, 27, $28\frac{1}{2}$, and $31\frac{1}{2}$ inches, of the model center line above the ground board (fig. 3). These heights gave clearances between the ground board and the model at the maximum diameter of 5.6, 7.1, 8.6, and 11.6 inches, respectively. Tests were made at each height for the following six angles of yaw relative to the wind: 0° , 30° , 60° , 90° , 180° , and

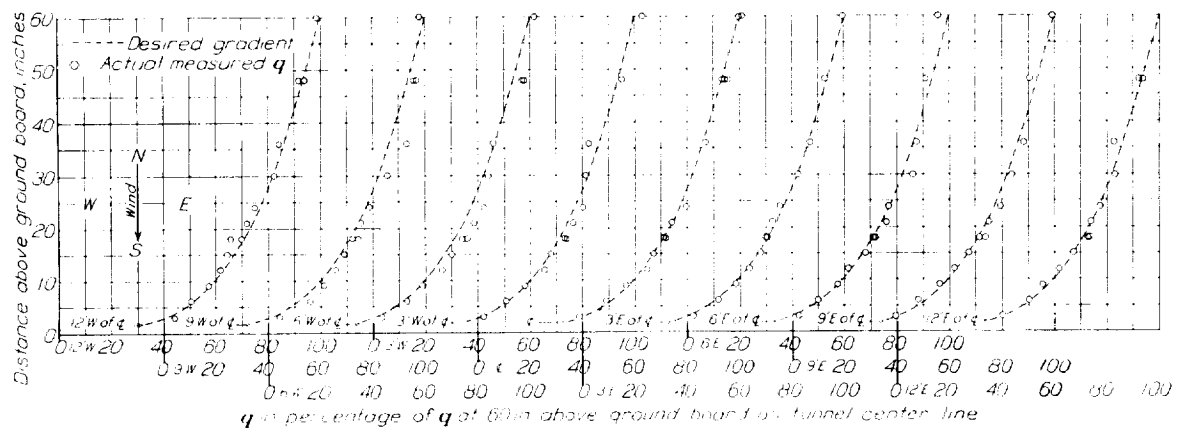


FIGURE 2.—Velocity gradient for ground-handling tests of the 1/40-scale model of the U. S. airship *Akron*.

210°. The angle of yaw of 210° instead of 150° was used for convenience in testing. The magnitudes of the forces and moments are obviously the same for the two angles but the direction is opposite for the cross-wind force and the rolling and yawing moments. For the comparison of the results, the coefficients for 210° yaw angle were converted to 150° yaw.

At the 28½-inch height, tests were made with the model rolled to the right through an angle of 10° while yawed at angles of 30° and 90°. The effects of small angles of pitch were obtained by pitching the model 2° and -2° (fig. 3); the forces and moments were measured for the 0°, 30°, and 180° yaw positions.

For the tests with the model in roll, the Reynolds Numbers ranged from 5,000,000 to 8,000,000. All other tests were made at Reynolds Numbers ranging from 5,000,000 to 19,000,000, which correspond to air speeds from 28 to 100 miles per hour. The Reynolds Number values are based on the length of the hull,

$$\text{Reynolds Number} = \frac{\rho V l}{\mu}$$

and are 4.04 times those based on (vol)^{1/3}, which have been used in a number of airship investigations.

Smoke flow.—Motion pictures were taken of smoke flow over several sections along the model for all angles of yaw with the model 28½ inches above the ground board. Enlarged prints (fig. 4) illustrate the nature of the flow.

Wake surveys.—Surveys were made of the dynamic pressure and total head in the field of the model when yawed 90° to the wind.

RESULTS

The results of the force tests are presented (figs. 5 to 24) in the form of nondimensional coefficients defined as follows:

Lift coefficient,

$$C_L = \frac{\text{lift}}{q(\text{vol})^{2/3}}$$

Drag coefficient,

$$C_D = \frac{\text{drag parallel to wind axes}}{q(\text{vol})^{2/3}}$$

Longitudinal-force coefficient,

$$C_X = \frac{\text{force parallel to longitudinal body axes}}{q(\text{vol})^{2/3}}$$

Cross-wind force coefficient,

$$C_{ss} = \frac{\text{cross-wind force}}{q(\text{vol})^{2/3}}$$

Cross-force coefficient,

$$C_Y = \frac{\text{force normal to longitudinal body axes}}{q(\text{vol})^{2/3}}$$

Resultant-force coefficient,

$$C_R = \frac{\text{resultant force}}{q(\text{vol})^{2/3}}$$

Rolling-moment coefficient,

$$C_l = \frac{\text{rolling moment about C. B.}}{q(\text{vol})}$$

Pitching-moment coefficient,

$$C_m = \frac{\text{pitching moment about C. B.}}{q(\text{vol})}$$

Yawing-moment coefficient,

$$C_n = \frac{\text{yawing moment about C. B.}}{q(\text{vol})}$$

in which (vol) is the volume of the hull in cubic feet and q is the dynamic pressure in pounds per square foot at a point 5 feet above the ground board, which corresponds to 200 feet above the ground for the full-size airship. When applying the wind-tunnel results to the actual airship, the wind velocity at a point 200 feet above the ground should be used as a base. All moment coefficients are presented with reference to the body axes of the model.

The important results are presented in their simplest form in figure 5, a three-view drawing of the measured

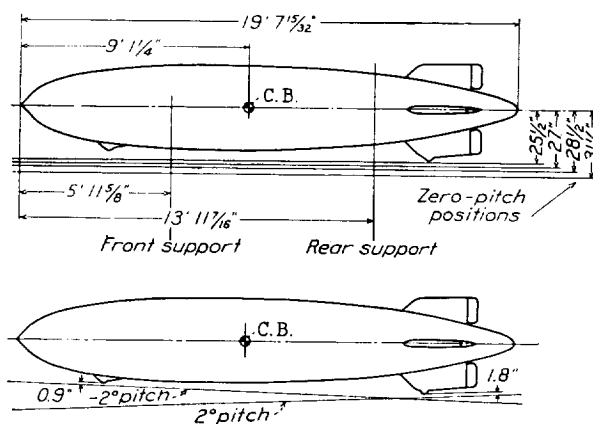
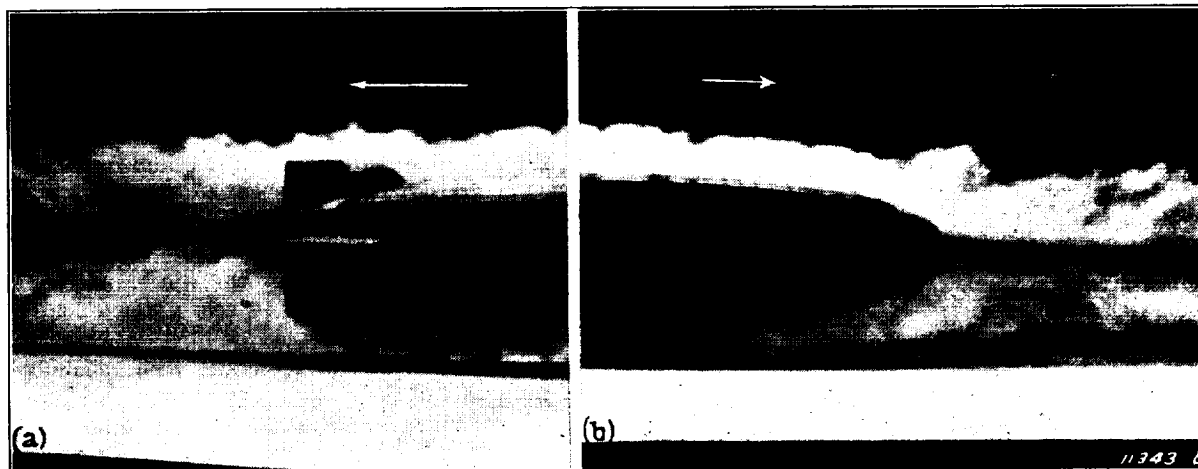


FIGURE 3.—Positions of the airship model relative to the ground board.

resultant-force vectors on the airship for the angles of yaw that were tested for a single height of the model above the ground. The vectors are to scale and show the magnitude and direction of the forces and the moments about the three coordinate axes.

Lift.—The measured vertical forces on the airship model were positive, or upward, for the entire range of angles of yaw tested and for all heights of the model above the ground plane (fig. 6). The lift coefficient is negligible at 0° angle of yaw but increases with angle of yaw and reaches a maximum at an angle of about 60° to the relative wind. With increasing angles of yaw from 60° the lift decreases rapidly until at 90° it has a small positive value. In the angle range between 90° and 180° the lift decreases slowly and almost uniformly and becomes negligible again at 180° yaw.

In the scale range investigated the lift showed only a small variation with Reynolds Number for the 0° angle position but, at the 90° yaw angle, decreased at a small but constant rate with increasing Reynolds Number (figs. 7 and 8). The lift varies appreciably with the height of the model above the ground plane;



(a) Flow over tail at 0° yaw.

(b) Flow over nose at 180° yaw.



(c) Flow over midsection at 30° yaw, side view.

(d) Flow over midsection at 30° yaw, top view.



(e) Flow over tail at 30° yaw.

(f) Flow over midsection at 60° yaw.

FIGURE 4.—Smoke flow over 1/40-scale model of the U. S. airship *Akron*. Center line of model 28½ inches above the ground board.



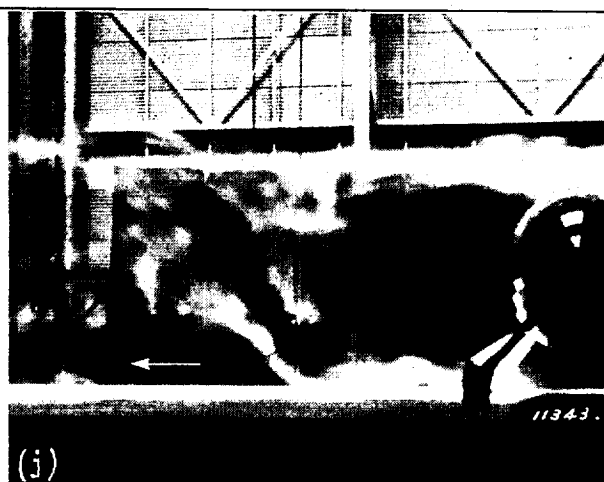
(g) Flow over midsection at 60° yaw.



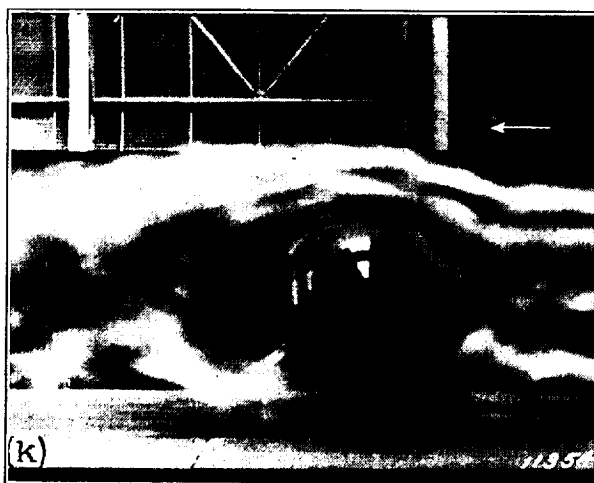
(h) Flow over tail at 60° yaw.



(i) Flow over tail at 90° yaw.



(j) Flow over midsection at 90° yaw.



(k) Flow over nose at 90° yaw.



(l) Flow over tail at 210° yaw.

FIGURE 4. -Continued. Smoke flow over 1/40-scale model of the U. S. airship *Akron*. Center line of model 28½ inches above the ground board.

however, the results showed that there were no critical heights in the range investigated. The lift on the model increases as the ground board is approached (fig. 6), showing the greatest absolute increase at about 60° yaw at which angle the lift is highest, but showing the greatest percentage increase in the angle range between 90° and 180°. Rolling the airship 10° made no appreciable change in the lift (fig. 9).

and is relatively unaffected by any of the changes in model height or roll (fig. 12).

The effect of scale on the longitudinal force is relatively unimportant in the Reynolds Number range tested as is shown in figures 7 and 8 for the 0° and 90° angles, respectively.

Cross-wind force.—Like the drag, the cross-wind force showed very little change with any of the varia-

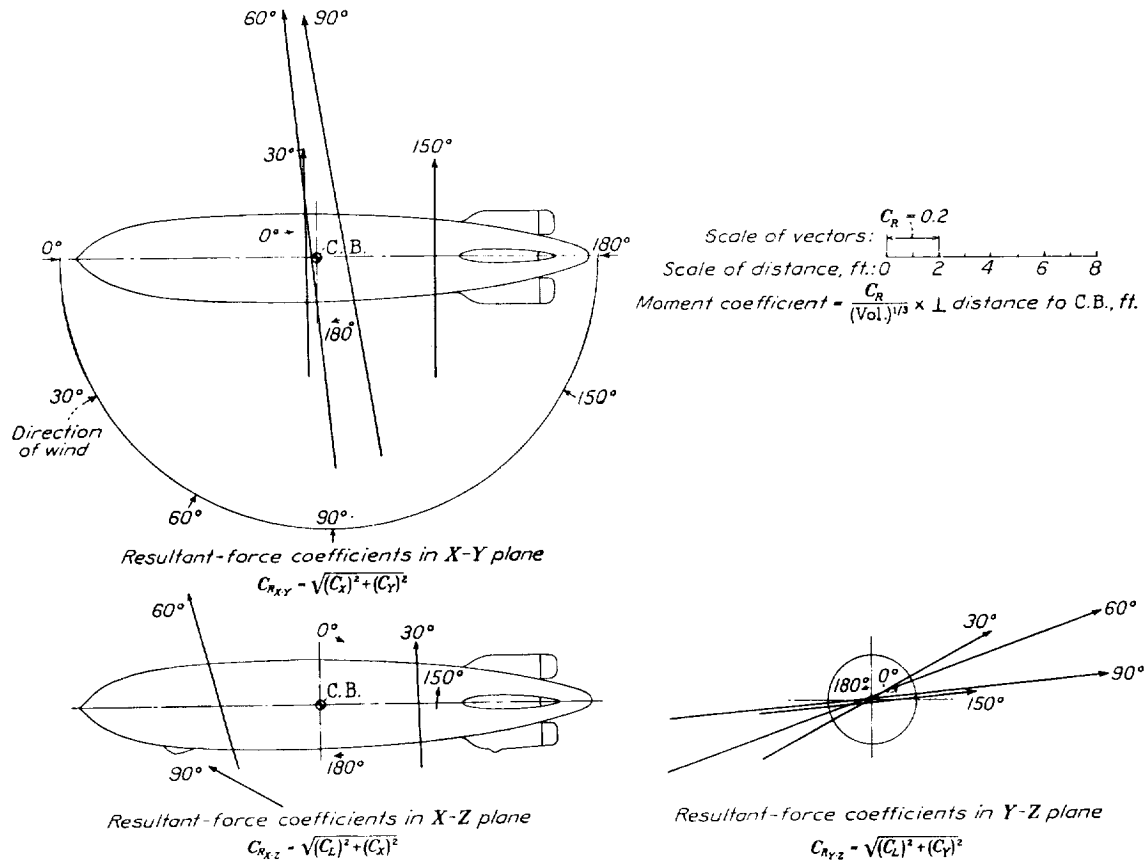


FIGURE 5.—Three-view drawing showing resultant forces on the 1/40-scale model of the U. S. airship *Akron*. Model 28½ inches above ground board. Reynolds Number, 16,000,000.

Drag.—The drag coefficients with reference to the wind axis increase as the angle of yaw increases and reach a maximum with the airship at 90° yaw. The drag curve is almost symmetrical about the 90° ordinate, and the drag coefficient drops to a value of about 0.030 for both the 0° and 180° angles (fig. 10). The height of the model above the ground plane proved to be an unimportant variable in the drag except in the range of angles near 90°. At the 90° angle the drag is lower for positions closer to the board.

The longitudinal-force coefficient (figs. 11 and 12) changes from a small positive value at 0° to a rather large negative or stern-to-bow force at 90°, the transition from positive to negative force occurring at about 30° yaw. The curve is essentially symmetrical

in model height, pitch, or roll (figs. 13, 14, and 15). In the range of angles near 90° yaw (fig. 14) the cross force (body axis) changes with model height, increasing with the greater distance from the board.

The cross force showed a greater variation with the Reynolds Number than did the longitudinal force, dropping off at the lower values to about 8 percent below the value for the high Reynolds Numbers (fig. 8).

Pitching moment.—The pitching moment was not critically affected by any of the variations in model height, pitch, or roll, and the results (figs. 16 and 17) again show that the effects of these variables were relatively unimportant compared with the changes in the pitching moment for small changes in the angle of yaw.

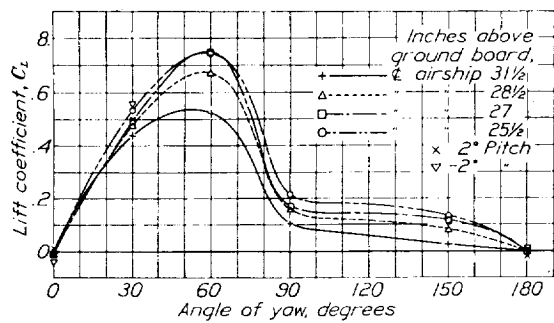


FIGURE 6.—The variation of the lift coefficient with angle of yaw, angle of pitch, and height above the ground board at a Reynolds Number of 16,000,000.

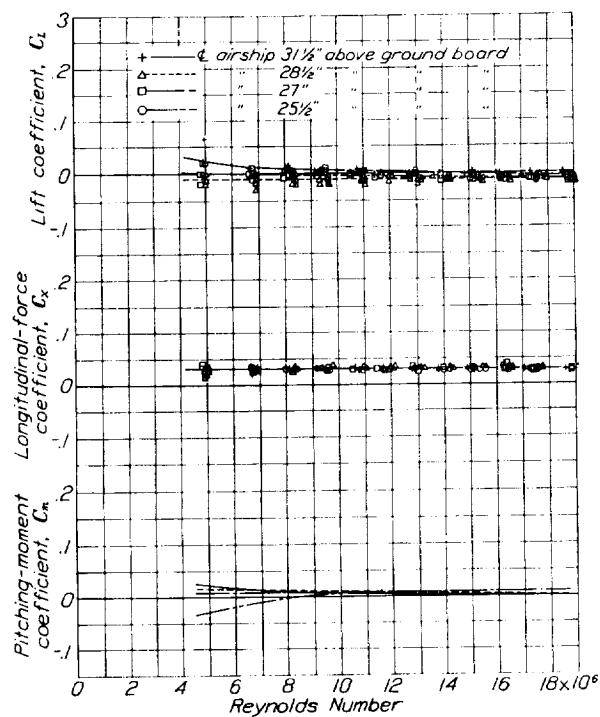


FIGURE 7.—The variation of the pitching-moment coefficient, the longitudinal-force coefficient, and the lift coefficient with Reynolds Number. Model at 0° yaw.

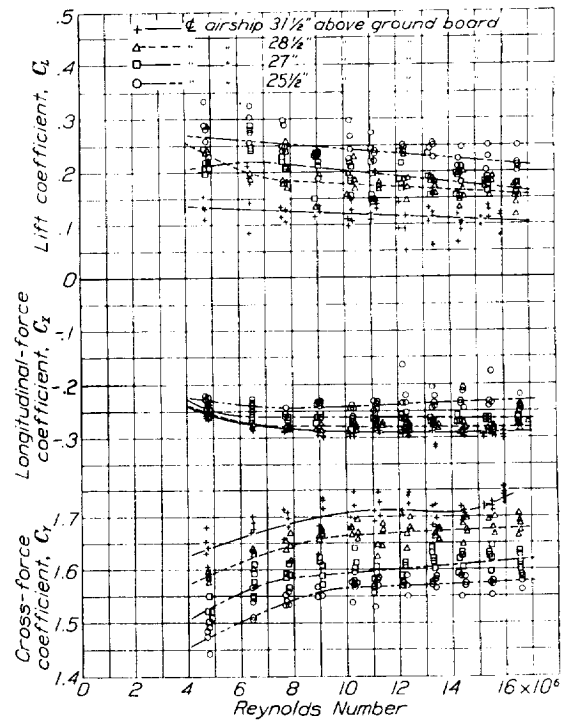


FIGURE 8.—The variation of the cross-force coefficient, the longitudinal-force coefficient, and the lift coefficient with Reynolds Number. Model at 90° yaw.

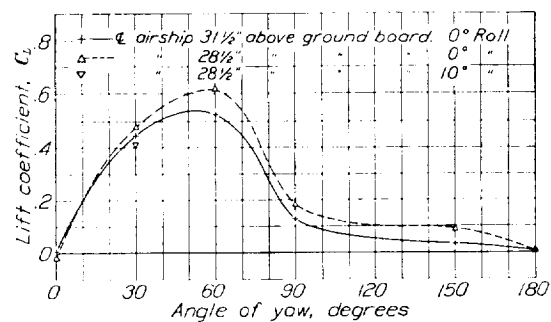


FIGURE 9.—The variation of the lift coefficient with angle of yaw, angle of roll, and height above the ground board at a Reynolds Number of 8,000,000.

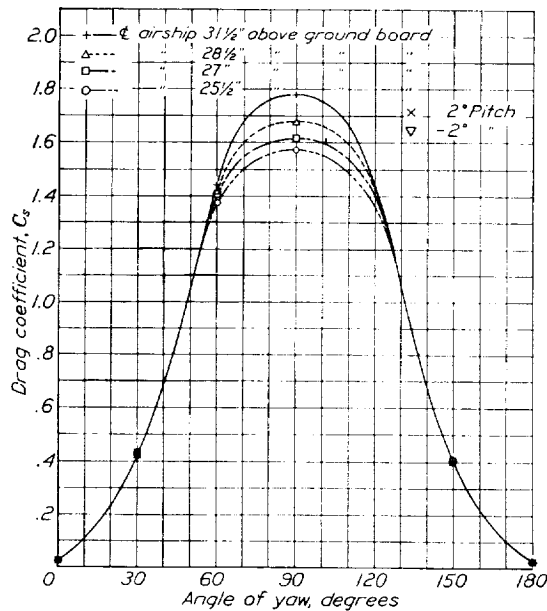


FIGURE 10.—The variation of the drag coefficient with angle of yaw, angle of pitch, and height above the ground board at a Reynolds Number of 16,000,000.

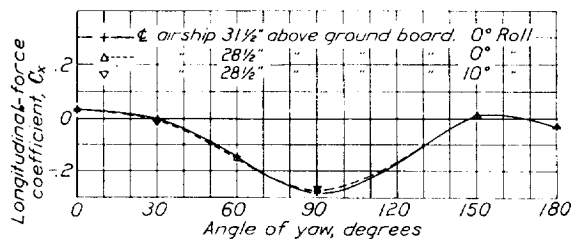


FIGURE 12.—The variation of longitudinal-force coefficient with angle of yaw, angle of roll, and height above the ground board at a Reynolds Number of 8,000,000.

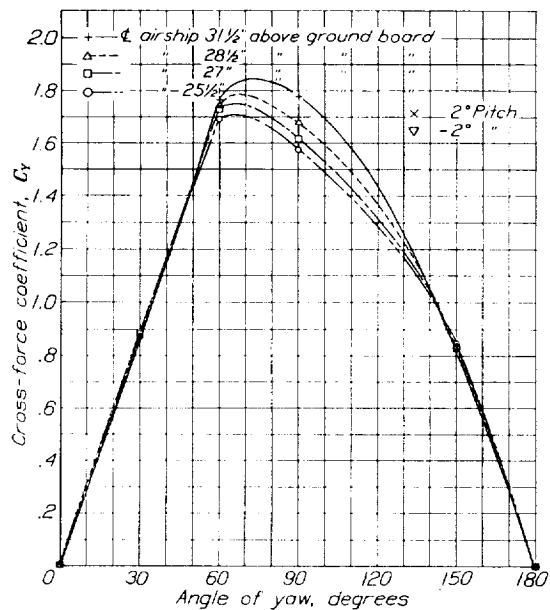


FIGURE 14.—The variation of cross-force coefficient with angle of yaw, angle of pitch, and height above the ground board at a Reynolds Number of 16,000,000.

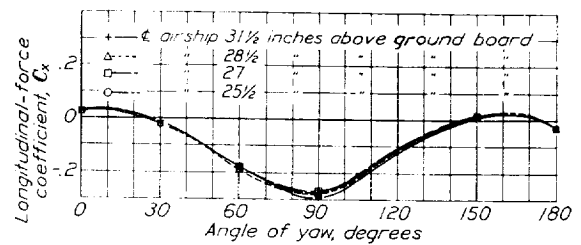


FIGURE 11.—The variation of the longitudinal-force coefficient with angle of yaw and height above the ground board at a Reynolds Number of 16,000,000.

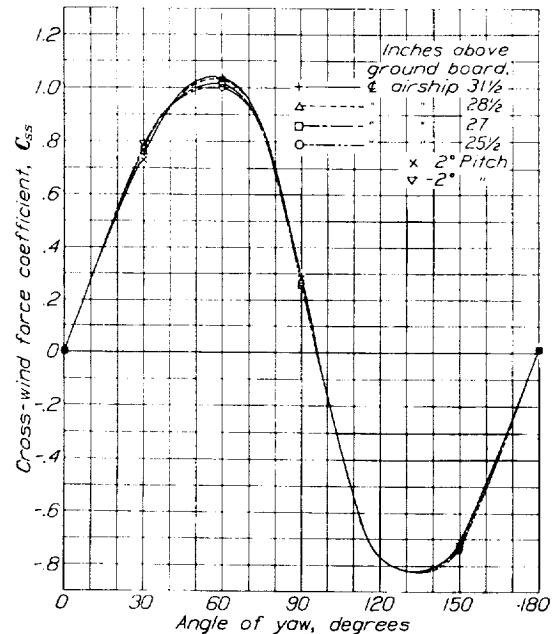


FIGURE 13.—The variation of cross-wind force with angle of yaw, angle of pitch, and height above the ground board at a Reynolds Number of 16,000,000.

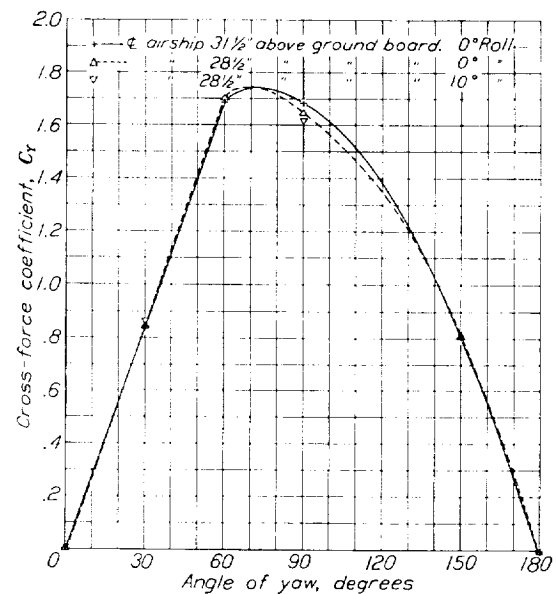


FIGURE 15.—The variation of cross-force coefficient with angle of yaw, angle of roll, and height above the ground board at a Reynolds Number of 8,000,000.

The variations of the pitching moment with the Reynolds Number were small and inconsistent as shown by figures 7 and 18 for the 0° and 90° yaw positions, respectively.

An interesting reversal of the sign of the pitching moment occurs in the yaw-angle range between 30° and 60°, the pitching-moment coefficient changing from about -0.35 at 30° to 0.55 at 60°.

Yawing moment.—The yawing-moment coefficients for angles of yaw in the range between 0° and 60° are small but reach large negative values at 150° (figs. 19 and 20). The effects of model height are unimportant except in the angle range between 0° and 60°, where the moments are small. The effects of roll and pitch are also relatively unimportant. The variation with Reynolds Number is small (fig. 18).

Rolling moment.—The rolling-moment coefficients are almost zero for the full range of the tests, and none of the variations in model height, pitch, roll, or Reynolds Number showed any marked or appreciable effects (figs. 18, 21, and 22).

Wake surveys.—The dynamic and total pressures in the wake of the airship at 90° yaw are presented in figures 23 and 24, respectively. The dead-wake size varies with position along the hull and is largest behind the tail surfaces.

DISCUSSION

The test results presented in figures 5 to 24 give directly the measured forces and moments on the 1/40-scale airship model for the conditions that were tested. It is desirable that some understanding be obtained of the origin of these forces and the nature of the flow about the airship to aid in the large extrapolation of the measured results to full-scale Reynolds Numbers. An attempt has therefore been made in the following paragraphs to analyze the test data and the general problem with a view to determining the nature of the flow about the airship when adjacent to the ground and to obtain some conception of the applicability of the results to the full-size airship. These fundamental conceptions are usually provided by the theory; however, the complex interaction of the effects of the ground gradient with those of the ground-plane interference makes any theoretical treatment without innumerable assumptions very difficult, if not impossible. The motion pictures taken of the smoke flow over the model, a few frames of which are presented in figure 4, greatly assisted in the flow analysis.

The following problems are considered to be of particular interest and importance and will be discussed in the succeeding paragraphs:

1. The source of the positive lifting force on the model.
2. Possibilities of extrapolating the lift results to Reynolds Numbers of the full-size airship.

3. Origin of negative or stern-to-bow longitudinal force on airship model at 90° yaw.

4. Comparison of the drag results on the *Akron* model above the ground board in the full-scale tunnel with those measured in the 20-foot tunnel in free-air conditions.

5. Reason for the reversal of the pitching-moment coefficients of the model in the yaw-angle range between 30° and 60°.

6. The large yawing moments encountered at 150° yaw in contrast to the relative ineffectiveness of the vertical tail surfaces at angles of yaw between 0° and 60°.

Origin of lift on airship.—In the analysis of the flow and the aerodynamic forces on the airship the model has been considered as divided into sections of unit length of simple geometric form about which the flow may be predicted. Thus at small angles of yaw, sections through the airship parallel to the relative wind have profiles similar to thick symmetrical airfoils; whereas at larger angles of yaw, these sections parallel to the wind are deformed into approximately elliptical shapes that become circles at 90°. The flows over both the symmetrical airfoil sections and the bluff elliptical and circular sections are well known and have been the subject of many previous investigations. It has been shown that to obtain a lift from these sections, i. e., the airfoil or circular sections, it is required that a circulation exist, the circulation manifesting itself by different velocities and pressures over the bottoms and tops of the profiles.

The existence of a lift on the airship model therefore indicates a circulation about the sections and, inasmuch as the angle of attack of the profiles is 0°, the entire circulation may be attributed to the interference of the ground board and ground gradient. This same conclusion is obvious from the symmetry of the model and, in the absence of a ground plane and velocity gradient, no lift would be expected on the model.

It is believed that the resultant circulation producing a vertical force may be contributed from the three following sources:

1. Contraction of flow between model and ground board.
2. Unsymmetrical flow in the wake of the model due to the ground-board restraint.
3. Unsymmetrical pressure distribution over top and bottom of model due to the velocity gradient.

The contraction of the flow between the airship and the ground board produces lower pressures on the bottom side of the model with a resultant downward or negative lift, which increases as the model approaches the ground. The magnitude of this effect may be theoretically computed (reference 7) assuming potential flow over the model and no ground gradient. For this calculation the ground plane is replaced by a

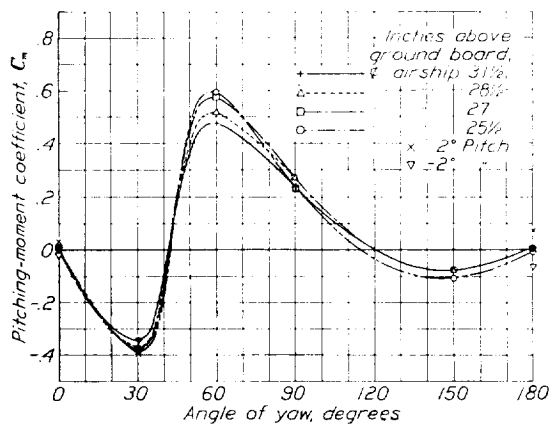


FIGURE 16.—The variation of pitching-moment coefficient with angle of yaw, angle of pitch, and height above the ground board at a Reynolds Number of 16,000,000.

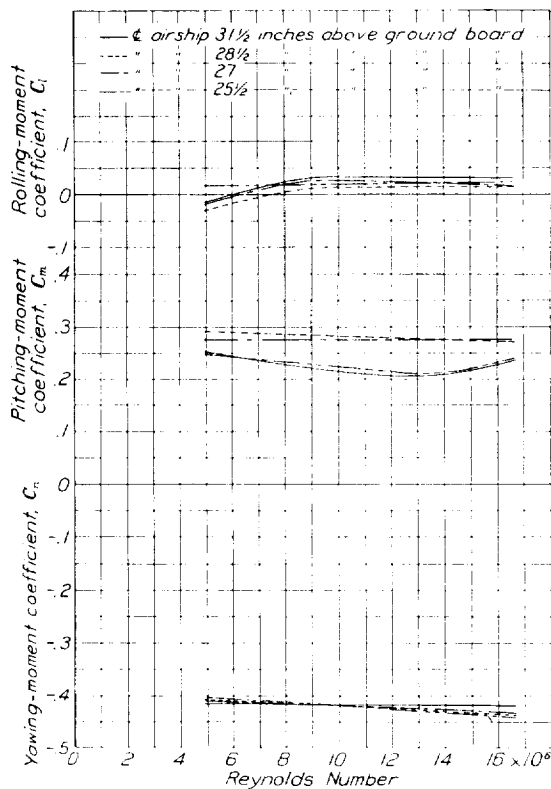


FIGURE 18.—The variation of yawing-moment coefficient, pitching-moment coefficient, and rolling-moment coefficient with Reynolds Number. Model at 90° yaw.

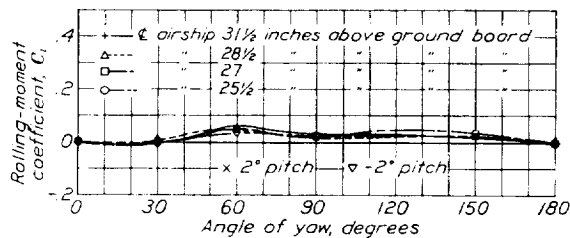


FIGURE 21.—The variation of rolling-moment coefficient with angle of yaw, angle of pitch, and height above the ground board at a Reynolds Number of 16,000,000.

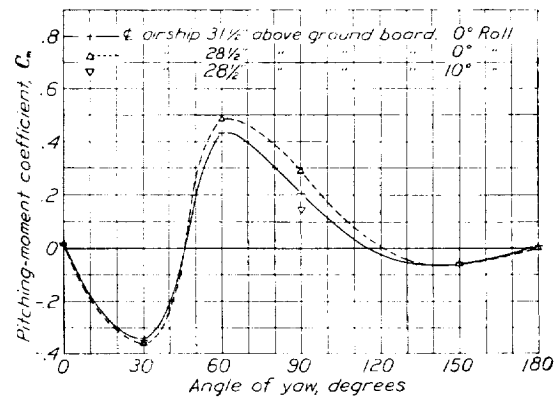


FIGURE 17.—The variation of pitching-moment coefficient with angle of yaw, angle of roll, and height above the ground board at a Reynolds Number of 8,000,000.

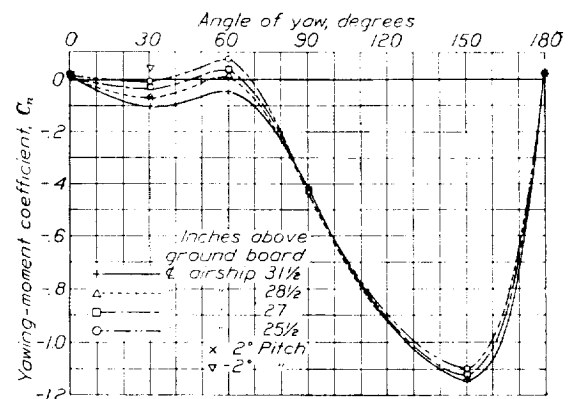


FIGURE 19.—The variation of yawing-moment coefficient with angle of yaw, angle of pitch, and height above the ground board at a Reynolds Number of 16,000,000.

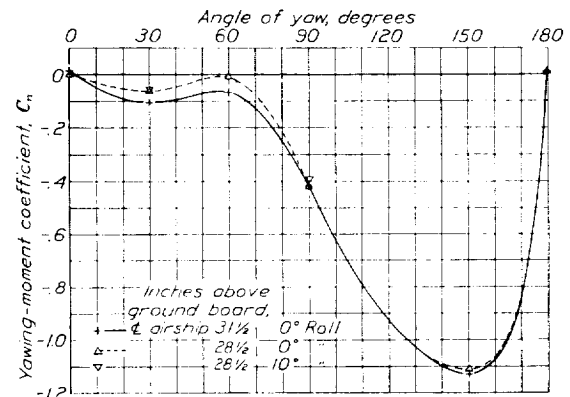


FIGURE 20.—The variation of yawing-moment coefficient with angle of yaw, angle of roll, and height above the ground board at a Reynolds Number of 8,000,000.

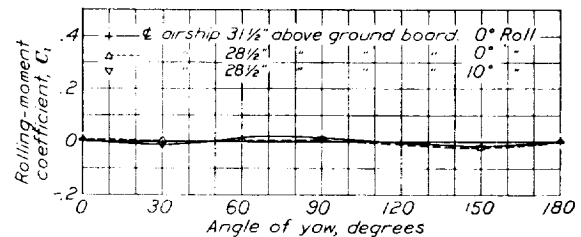


FIGURE 22.—The variation of rolling-moment coefficient with angle of yaw, angle of roll, and height above the ground board at a Reynolds Number of 8,000,000.

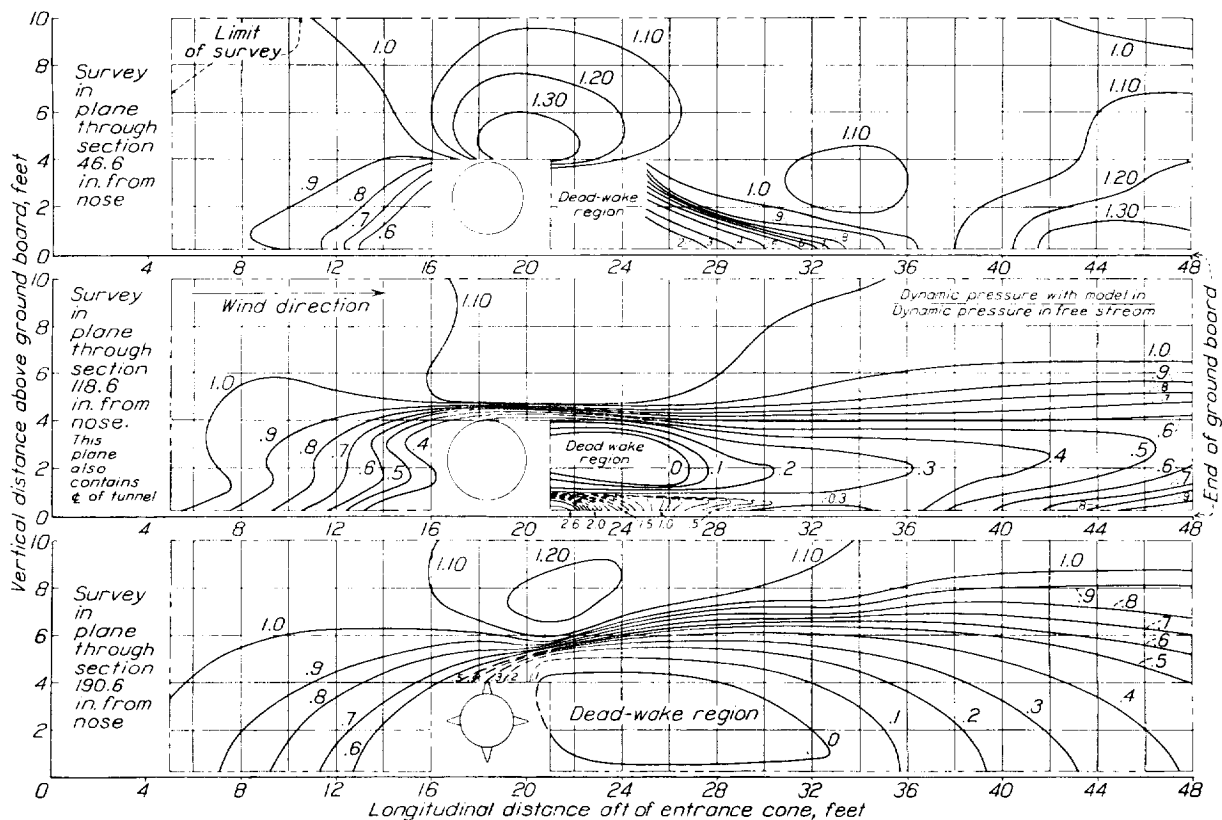


FIGURE 23.—Survey of dynamic pressure in the wake of the airship model at 90° yaw.

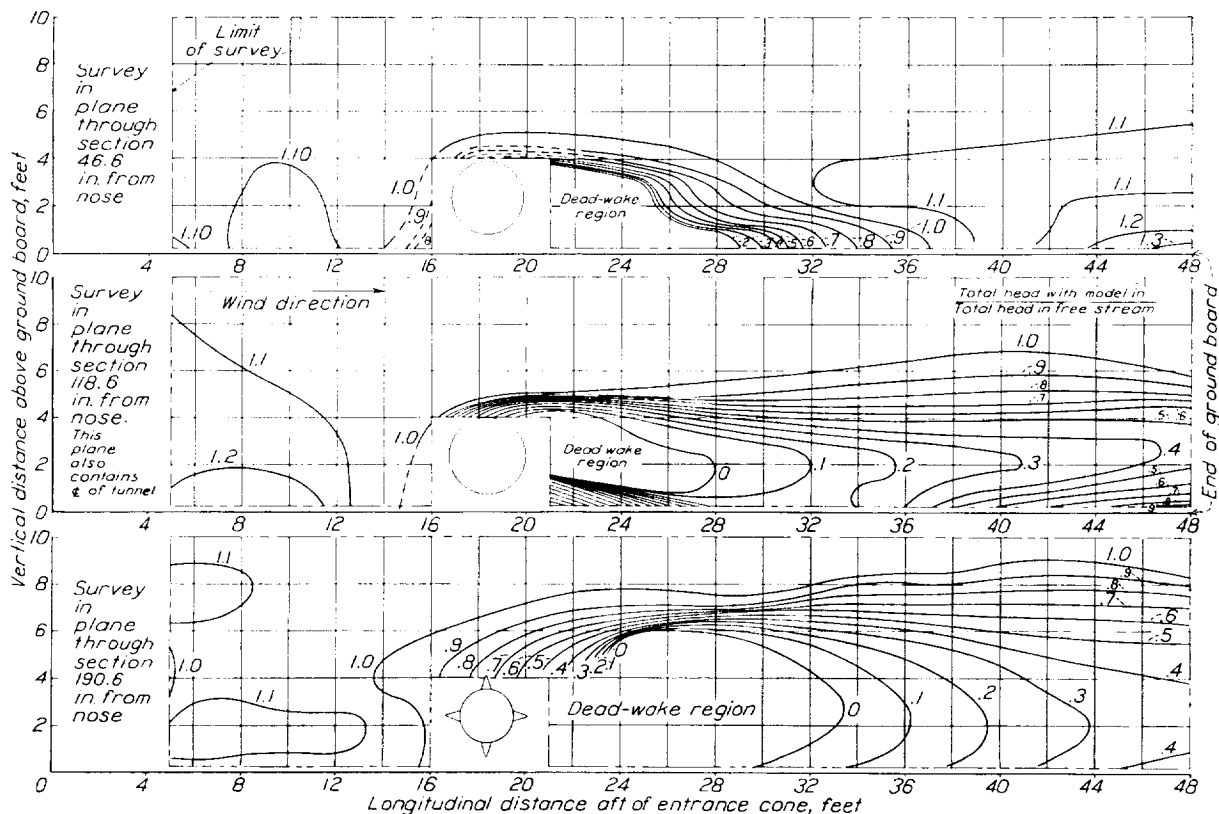


FIGURE 24.—Survey of the total pressure in the wake of the airship model at 90° yaw.

reflected image of the model in the ground plane. Computations of this type made for the condition of the airship at 90° yaw indicate that, if the flow over the model were truly potential, the attraction of the model to the ground plane would be large and the resultant lift force negative rather than positive.

The assumption of potential flow over the model is wholly erroneous, in fact, it is only at angles of yaw near 0° that any similarity exists between the theoretical and the actual flow over the hull. This disparity with the theoretical condition is caused by the breakaway of the flow from the surface of the model over the rear of the sections owing to the losses in the boundary layer. The air flow will not follow the hull but separates forming a dead-air region of negative pressure behind the model. The size of the dead-air region is dependent on the shape of the sections over which the air passes, being smallest for the 0° yaw condition (fig. 4(a)) and largest for the 90° yaw angle. (See smoke pictures fig. 4(j) and 4(k) and the wake surveys behind the model at 90° yaw in figs. 23 and 24.) Approximate computations based on flows over the airship model including separation over the rear of the model revealed much smaller negative-lift effects arising from the contraction than were previously computed from the potential flow and indicate that the contraction effect may be one of the less important of the effects contributing to the resultant vertical force.

The second source of lift is similar to the first in that it is related to the effect of the ground plane on the flow. It particularly depends on the effect of the ground board on the flow over the leeward portions of the airship profiles and on the point of separation of the flow from the surface. Previous tests have shown the point of separation to be very sensitive to any type of interference effect, and several stable types of flow are possible, depending upon the particular set of external interference conditions. The effect of the unsymmetrical restraint is to rotate the flow in front of the model upward and to induce a positive angle of attack in the flow over the model. The flow over the bottom of the airship therefore tends to follow farther along the circumference of the model before separation than the flow over the top side, and the dead-wake region of negative pressure on the leeward side of the model is rotated upward, resulting in a positive lifting force. Indications of these effects are shown by the smoke pictures. The flow over the model at 60° yaw (maximum-lift angle) is shown in figure 4(g) and it may be observed that the dead-air region is shifted upward and that the flow follows much farther around the lower half of the model than over the upper half. This unsymmetrical pattern in the wake is also shown in figures 4(e) and 4(i). The upflow in front of the model for the 30° yaw condition is shown in figure 4(c), and for the 90° yaw condition in figures 4(i) and 4(k). The effect of the ground board on the breakaway appears

to be smallest for the 90° angle (figs. 4(j) and 4(k)) probably because of the shorter effective chord in the direction of the flow. This observation is also a check on the smaller positive force measured at this angle.

The third factor contributing to the vertical force is the ground gradient. Inasmuch as the pressures on the surface of the body are a function of the dynamic pressures outside the field of the body, the pressures over the surface at positions where the outside velocity is highest will reach larger values. In this particular case, therefore, with a positive gradient, that is, a velocity increasing with height above the ground board, the pressures on the upper side of the airship model will reach higher negative values than those on the lower surface and produce a positive lift. Trial computations were made assuming average velocities over the top and bottom half of the airship when at 90° yaw; integration of the computed pressures over the surface of the model gave a positive lift of the same sense but of slightly greater magnitude than the measured one. The method was, of course, approximate, inasmuch as the velocity varies continuously with the height, and it was also necessary to make assumptions as to the pressure distribution over the cylindrical profile. The results indicate, however, that the ground gradient is an important factor contributing to the lifting force.

The large effect of the velocity gradient on the lift force suggests that further tests be made with other velocity gradients than the one employed in the present investigation. Generally the results should indicate greater positive lifts with higher velocity gradients than that of the present investigation, and conversely.

All three factors to which the vertical force has been attributed—streamline contraction, unsymmetrical wake restraint, and ground gradient—vary with the height, and the measured lift force did show a slight change with the model height; in the range of the tests, however, there were no critical points at which either sudden changes or reversals of forces existed.

Extrapolation of results.—The results showing a positive lift on the model airship are of particular interest in regard to the possibility of predicting the lift of the full-size airship. The extrapolation of results from the model to the full-size airship is lengthy inasmuch as the Reynolds Numbers for the full-scale airship at wind velocities of 20 miles per hour are about eight times the maximum value for the tests in the full-scale tunnel. A direct extrapolation by continuation of the curves of model results to the Reynolds Numbers of the full-size airship is not believed justified or satisfactory, inasmuch as the extension of a curve to eight times its original length will, no doubt, lead to erroneous conclusions.

A more satisfactory method is to consider the flows about the body for the two cases of model and full scale to see if any critical changes in the flow are to be expected in passing through the scale range to be

extrapolated. It has been previously mentioned that at large angles of yaw longitudinal sections of the airship become elliptical and, at 90° , become circular. Two stable types of flow over a cylinder at right angles to the flow may occur, depending upon the Reynolds Number. For Reynolds Numbers below the critical (400,000 to 500,000 based on cylinder diameter) the flow is characterized by an early separation on the rear of the cylinder, the breakaway occurring slightly before the point of maximum width (fig. 25(a)). For Reynolds Numbers above the critical the boundary layer becomes turbulent and the breakaway occurs farther back along the circumference (fig. 25(b)). Quite marked differences would therefore be expected in the flow over the airship and in the forces on the model in passing through this Reynolds Number range. In the present model tests the Reynolds Number was above the critical for all but a few of the smallest sections near the bow and stern of the model.

Tests have been made in other wind tunnels of cylinders adjacent to ground boards (references 1 and 2) but, owing to the fact that all of the results were obtained close to the critical Reynolds Numbers, they show different results from the full-scale-tunnel data. Once the critical range has been passed, the flow in cylinder tests has shown no marked changes with the Reynolds Number, and it is believed that the flow over the full-size airship will be generally similar to that over the model as tested in the full-scale tunnel. It may be further pointed out that the portion of the lift caused by the ground gradient should scale almost directly to the larger Reynolds Numbers. It is believed that the lift curve (fig. 8), which show a decreasing lift with increasing Reynolds Number, will tend to flatten out at the very high Reynolds Numbers and show a more nearly constant value.

If the measured lift coefficients on the model airship at the highest Reynolds Numbers tested in the tunnel are scaled directly to the case of the full-size airship, the resultant vertical forces are of large magnitude for appreciable angles of yaw and moderate wind velocities. For example, the lift on an airship of the size of the *Akron* at 30° yaw in a 20-mile-per-hour wind velocity when its center line is about 95 feet above the ground is 17,800 pounds; for a yaw angle of 60° and the same wind velocity, the lift would reach a maximum of about 25,600 pounds. The Reynolds Number of this typical case is about eight times the highest value reached in the tunnel tests. The 95-foot height in full scale corresponds to the $28\frac{1}{2}$ inch test height with the model.

Longitudinal force.—The large negative longitudinal force (with reference to body axis) at 90° yaw is of interest and may be accounted for by the unsymmetrical flow over the bow and stern of the airship. The flow over the bow produces a negative pressure region

over almost its entire area, whereas the flow over the stern is distributed by the tail surfaces and the static pressure is positive on the windward side and negative on the leeward (figs. 4(k) and 4(i)). The result is a longitudinal force in the direction of the nose. On the bare hull without tail surfaces the large negative value would not be expected.

Comparison with drags measured in 20-foot tunnel.—The model tested in the full-scale tunnel adjacent to the ground board had previously been tested in the N. A. C. A. 20-foot tunnel in the center of the free stream (reference 4). The minimum drag coefficient of 0.024 obtained from these tests may be compared with the 0° yaw value from the full-scale-tunnel tests. The

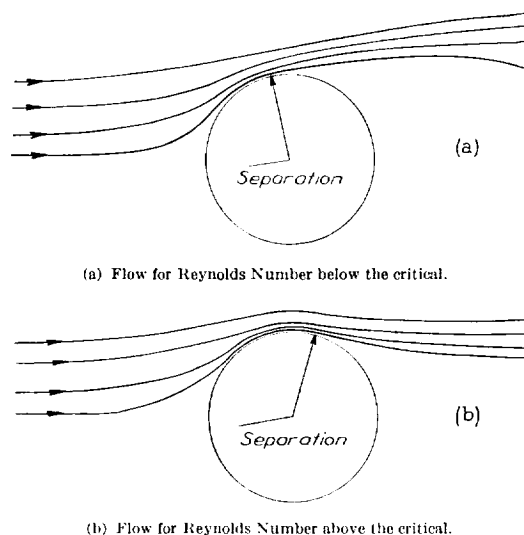


FIGURE 25.—Flow over circular cylinders showing separation.

comparison indicates the magnitude of interference effect on the drag owing to the ground board and the ground gradient. In the comparison, consideration must be given to the fact that coefficients for the full-scale-tunnel tests were not based on the average velocity over the model but on the velocity at 5 feet above the board. If the true average dynamic pressure over the model is used, the drag coefficient for the full-scale-tunnel tests at 0° yaw becomes 0.039, indicating that the interference increased the drag approximately 60 percent above the 20-foot-tunnel value. Approximate computations for the 90° angle of yaw, considering the airship to consist of a series of cylinders and the tail surfaces to be flat plates, gave a free-air drag coefficient of 1.27. This value was compared with the measured drag coefficient at 90° yaw corrected to the actual dynamic pressure over the model, and the interference of the ground plane and gradient on the drag was again shown to be in the order of 60 to 70 percent. The increase in drag may be attributed largely to the disturbed wake of the model.

Reversal of pitching moment.—The reversal of the sign of the pitching moments in the yaw-angle range between 30° and 60° is probably caused by the changing force on the horizontal tail surfaces. The large negative moment at 30° is caused by a large positive lift on the horizontal tail surfaces, inasmuch as the smoke pictures in figure 4(e) show the average flow in the tail vicinity to be inclined upward. At the 30° angle the flow over the windward horizontal surface is not yet shielded by the vertical surfaces, the blanketing action being counteracted by the tendency of the flow to follow along the hull and reduce the effective angle of yaw. Figures 4(c) and 4(e) show this effect clearly. At the 60° angle, however, the vertical surfaces effectively shield the flow over the entire horizontal surfaces and the areas become inactive (fig. 4(h)). The hull pressures are, moreover, in the correct direction to create a positive moment, as is observed in figure 4(f), which indicates that the flow between the airship and the ground plane is toward the stern. In all probability there is a low-pressure region under the stern and a down force at the tail. For the 30° angle it may be observed that the smoke streamers passing between the board and the airship are turned toward the bow.

Effect of yaw angle on yawing moment.—The measured yawing moments were small in the range of yaw angles between 0° and 60° but changed to large negative values at 150° (figs. 19 and 20).

The small yawing moments in the yaw-angle range between 0° and 60° are explained somewhat by the smoke picture 4(e), which shows that the air is turned by the hull and flows along the hull in the region of the tail. The effective angle of attack of the fin, and therefore the fin lift, is thus reduced. For the 150° yaw angle, however, the fin is ahead of the hull and operates in an air stream free of interference. The effectiveness of the fin when forward of the hull is shown in figure 4(l) where the large bending of the smoke streamers owing to the downwash from the fin is readily apparent. These results verify previous experimental information showing the effectiveness of bow elevators.

CONCLUSIONS

1. Changes in the angle of yaw of the airship greatly affect the ground-handling forces; whereas, in the range of Reynolds Numbers between 5,000,000 and 19,000,000 (Reynolds Numbers based on model length), small changes in height, pitch, or roll of the airship have a negligible effect.
2. In the scale range investigated the ground-handling forces are not importantly affected by changes in Reynolds Numbers.
3. The curves of the model results should not be extrapolated to the Reynolds Numbers of the full-size airship but may be used with some reliability directly from the measured values at the highest Reynolds Numbers.
4. The application of the measured results to the full-size airship shows very large handling forces for appreciable angles of yaw and moderate wind velocities.

LANGLEY MEMORIAL AERONAUTICAL LABORATORY,
NATIONAL ADVISORY COMMITTEE FOR AERONAUTICS,
LANGLEY FIELD, VA., April 8, 1936.

REFERENCES

1. Knoblock, F. D., and Troller, Th.: Tests on the Effect of Sidewind on the Ground Handling of Airships. Daniel Guggenheim Airship Inst., Publication No. 2, 1935, pp. 53-57.
2. Bradfield, F. B., and Cohen, J.: Wind Tunnel Test of Lift and Drag Measured in a Velocity Gradient. R. & M. No. 1489, British A. R. C., 1932.
3. DeFrance, Smith J.: The N. A. C. A. Full-Scale Wind Tunnel. T. R. No. 459, N. A. C. A., 1933.
4. Freeman, Hugh B.: Force Measurements on a 1/40-Scale Model of the U. S. Airship "Akron." T. R. No. 432, N. A. C. A., 1932.
5. Thompson, F. L., Peck, W. C., and Beard, A. P.: Air Conditions Close to the Ground and the Effect on Airplane Landings. T. R. No. 489, N. A. C. A., 1934.
6. Theodorsen, Theodore, and Silverstein, Abe: Experimental Verification of the Theory of Wind-Tunnel Boundary Interference. T. R. No. 478, N. A. C. A., 1934.
7. Garrick, I. E.: Potential Flow about Arbitrary Biplane Wing Sections. T. R. No. 542, N. A. C. A., 1936.

REPORT No. 567

PROPULSION OF A FLAPPING AND OSCILLATING AIRFOIL

By I. E. GARRICK

SUMMARY

Formulas are given for the propelling or drag force experienced in a uniform air stream by an airfoil or an airfoil-aileron combination, oscillating in any of three degrees of freedom: vertical flapping, torsional oscillations about a fixed axis parallel to the span, and angular oscillations of the aileron about a hinge.

INTRODUCTION

It is the object of this paper to investigate theoretically the horizontal forces experienced by an airfoil or an airfoil-aileron combination in a uniform air stream made to execute flapping motion or to perform angular oscillations about a fixed axis parallel to the span. The problem treated is that of an infinite wing, or wing and aileron, performing steady sinusoidal oscillations in any of three degrees of freedom: vertical flapping at right angles to the direction of motion, oscillations about an arbitrary fixed axis parallel to its span, and oscillations of the aileron about a hinge.

The work of Wagner (reference 1) for calculating the distribution of vorticity in the wake of an airfoil in nonuniform motion appears as a starting point. A vortex wake is generated by the oscillatory motion, which in turn affects the entire nature of the forces experienced by the wing. Beautiful experimental checks of Wagner's theory of the manner in which the circulation builds up have been obtained by Farren and Walker. (Cf. reference 2, ch. 9 for a more detailed bibliography.) Birnbaum and Küssner (reference 3) have also attacked the problem of obtaining the lift forces on an oscillating wing by certain series expansions that are rather cumbersome to handle. Glauert (reference 4) has treated the case of an oscillating airfoil and has obtained expressions for the forces and moments that check with Wagner. Theodorsen (reference 5) has developed compact expressions for the lift and moments in the case of an airfoil-aileron combination of three independent degrees of freedom and has applied the results to an analysis of the wing-flutter problem. The foregoing references are concerned only with the lift forces, not with the horizontal forces; however, von Kármán and Burgers, who present in reference 2 a résumé of the work (to 1934) on non-

uniform motion, calculate there the propulsion effect on a flapping wing. The present paper makes application of the compact formulas developed by Theodorsen and of the method outlined by von Kármán and Burgers to treat the propulsion on a wing oscillating in three independent degrees of freedom.

The assumptions underlying the theory are small amplitudes in the various degrees of freedom and a (infinitely) narrow width of the rectilinear vortex wake, as well as the usual assumption of a perfect fluid. Quantitative agreement with experimental values, which are not very abundant, can hardly be expected since the finite width of the wake is important with regard to considerations of the resistance; nevertheless the results can be useful for interpreting such experiments as exist on the so-called "Katzmayr effect" (reference 6) and for clearing up certain aerodynamic features of the nature of the flight of birds.¹ Experimental tests on an oscillating and flapping wing are being conducted at the present time by the N. A. C. A.

This paper is not concerned with the problem of flutter, which is an instability phenomenon that manifests itself in certain critical frequency ranges and is due to an interaction and feedback of energy because of coupling in the various degrees of freedom. (Cf. references 3 and 5.) Profile drag is to be considered as additive to the horizontal forces obtained.

FORCES AND MOMENTS ON AN OSCILLATING AIRFOIL

Consider an airfoil represented by the straight line of figure 1. The airfoil chord is of length $2b$ and (its mean position with b as reference unit length) is assumed to extend along the x axis from the leading edge $x = -1$ to the trailing edge $x = +1$. The coordinate $x = a$ represents the axis of rotation of the wing, $x = c$ the coordinate of the aileron hinge. The airfoil is assumed to undergo the following motions with small amplitudes: A vertical motion h of the entire wing, positive downward; a rotation about $x = a$ of angle of attack α , positive clockwise and measured by the direction of the velocity v at infinity and the instantaneous position of the wing; an aileron motion about the hinge $x = c$ of angle β ,

¹ It is interesting to observe that the Katzmayr effect occurs in nature also in the motion of fish. See "The Physical Principles of Fish Locomotion," by E. G. Richardson, Jour. Exp. Biol., vol. XIII, no. 1, Jan. 1936, pp. 63-74.

measured with respect to the undeflected position of the wing itself.

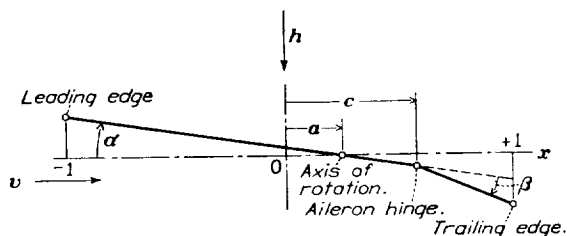


FIGURE 1.—Parameters of the airfoil-aileron combination.

Let us consider sinusoidal oscillations in the various degrees of freedom and use the complex-number notation

$$\left. \begin{aligned} \alpha &= \alpha_0 e^{i(pt + \varphi_0)} \\ \beta &= \beta_0 e^{i(pt + \varphi_1)} \\ h &= h_0 e^{i(pt + \varphi_2)} \end{aligned} \right\} \quad (1)$$

The constants α_0 , β_0 , and h_0 represent the maximum amplitudes in the various degrees of freedom, φ_0 , φ_1 , and φ_2 are phase angles, and the parameter p determines the frequency of the oscillations. By means of the relation

$$p = \frac{kv}{b} \quad (2)$$

an important parameter k is defined, i. e., $k = pb/v$. It will be seen that $2\pi/k$ is the wave length between successive waves in the vortex wake in terms of the half-chord b as reference length.

The following three formulas for the lift and moments on an oscillating airfoil of three degrees of freedom are due to Theodorsen and are taken from reference 5:²

$$P = -\rho b^2(v\pi\dot{\alpha} + \pi\ddot{h} - \pi ba\ddot{\alpha} - vT_4\dot{\beta} - T_1b\ddot{\beta}) - 2\pi\rho vbC(k)Q \quad (3)$$

$$M_a = -\rho b^2 \left[\pi \left(\frac{1}{2} - a \right) vb\dot{\alpha} + \pi b^2 \left(\frac{1}{8} + a^2 \right) \ddot{\alpha} + T_{13}v^2\dot{\beta} + T_{16}vb\ddot{\beta} + 2T_{13}b^2\ddot{\beta} - a\pi b\ddot{h} \right] + 2\rho vb^2\pi \left(a + \frac{1}{2} \right) C(k)Q \quad (4)$$

$$M_\beta = -\rho b^2 \left[T_{17}vb\dot{\alpha} + 2T_{13}b^2\ddot{\alpha} + \frac{1}{\pi}v^2T_{18}\dot{\beta} - \frac{1}{2\pi}vbT_{19}\ddot{\beta} - \frac{1}{\pi}T_3b^2\ddot{\beta} - T_1b\ddot{h} \right] - \rho vb^2T_{12}C(k)Q \quad (5)$$

where

$$Q = v\alpha + \dot{h} + b \left(\frac{1}{2} - a \right) \dot{\alpha} + \frac{1}{\pi}T_{10}v\beta + \frac{b}{2\pi}T_{11}\dot{\beta}$$

These equations are to be interpreted as follows: The real part of P denotes the lift force (positive downward)

² The writer wishes to record the fact that in order to establish a check on these general relations he has compared them with the widely varying expressions given by Wagner, Glauert, von Kármán and Burgers, and Küssner in their special cases (references 1 to 4). Identical agreement has resulted in all cases, except that in the case of Küssner's formulas a numerical check was made since an analytic check was not feasible. The numerical agreement was good except in the case of the wing-aileron combination where Küssner makes some rough approximations.

A recent paper by Cicala (reference 7) deserves mention. Cicala derives expressions for the lift and moment on an oscillating airfoil that seem to agree with the results of Theodorsen, although the method is somewhat more involved. The functions denoted by Cicala as λ' and λ'' correspond to $1-F$ and $-G$ defined in equation (6).

associated with the motion given by the real parts of (1); i. e., $\alpha = \alpha_0 \cos(pt + \varphi_0)$, $\beta = \beta_0 \cos(pt + \varphi_1)$, and $h = h_0 \cos(pt + \varphi_2)$. The imaginary part of P denotes the lift force associated with the motions $\alpha = \alpha_0 \sin(pt + \varphi_0)$, $\beta = \beta_0 \sin(pt + \varphi_1)$, and $h = h_0 \sin(pt + \varphi_2)$. Similarly M_a and M_β denote in complex form the moments (positive clockwise in fig. 1) about $x=a$ and $x=c$, respectively, due to the motions (1). (The mean value of α or β is considered zero. When the mean values are different from zero, the forces and moments arising from constant values α_m and β_m are to be added.) In equations (3), (4), and (5) there occur various symbols that have not yet been defined. The T 's, i. e., T_1 , T_3 , T_4 , etc., are constants defined completely by the parameters c and a (reference 5, p. 5). For reference they are listed in appendix 1, where there is also given a collection of the symbols employed in the notation of this paper. The function $C(k)$ is a useful complex function of the parameter k (see (2)) and is given by

$$C(k) = F(k) + iG(k) \quad (6)$$

where

$$F = \frac{J_1(J_1 + Y_0) + Y_1(Y_1 - J_0)}{(J_1 + Y_0)^2 + (Y_1 - J_0)^2}$$

$$G = -\frac{Y_1Y_0 + J_1J_0}{(J_1 + Y_0)^2 + (Y_1 - J_0)^2}$$

Functions J_0 , J_1 , Y_0 , and Y_1 are standard Bessel functions of the first and second kinds of argument k . Figure 2 and table I, which are taken from reference 5 (with certain minor changes), illustrate these functions.

In what follows we shall be interested only in one part of the preceding complex equations. It is an arbitrary matter whether to employ the real or imaginary parts. The choice made here is to treat the imaginary parts, and we write down for reference the imaginary parts of equations (1), (3), (4), and (5):

$$\left. \begin{aligned} \alpha &= \alpha_0 \sin(pt + \varphi_0) \\ \beta &= \beta_0 \sin(pt + \varphi_1) \\ h &= h_0 \sin(pt + \varphi_2) \end{aligned} \right\} \quad (7)$$

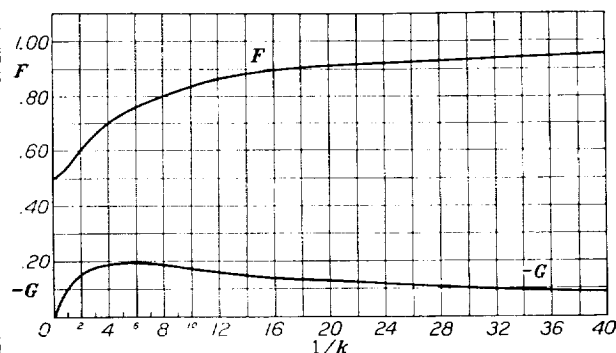


FIGURE 2.—The functions F and $-G$ against $1/k$.

$$\begin{aligned}
P = & -\rho b^2 [v\pi\alpha_0 p \cos (pt + \varphi_0) - \pi h_0 p^2 \sin (pt + \varphi_2) + \pi b a \alpha_0 p^2 \sin (pt + \varphi_0) \\
& - v T_4 \beta_0 p \cos (pt + \varphi_1) + T_1 b \beta_0 p^2 \sin (pt + \varphi_1)] \\
& - 2\pi \rho v b F \left[v\alpha_0 \sin (pt + \varphi_0) + h_0 p \cos (pt + \varphi_2) + b \left(\frac{1}{2} - a \right) \alpha_0 p \cos (pt + \varphi_0) \right. \\
& \left. + \frac{T_{10}}{\pi} v \beta_0 \sin (pt + \varphi_1) + \frac{T_{11}}{2\pi} b \beta_0 p \cos (pt + \varphi_1) \right] \\
& - 2\pi \rho v b G \left[v\alpha_0 \cos (pt + \varphi_0) - h_0 p \sin (pt + \varphi_2) - b \left(\frac{1}{2} - a \right) \alpha_0 p \sin (pt + \varphi_0) \right. \\
& \left. + \frac{T_{10}}{\pi} v \beta_0 \cos (pt + \varphi_1) - \frac{T_{11}}{2\pi} b \beta_0 p \sin (pt + \varphi_1) \right] \quad (8)
\end{aligned}$$

$$\begin{aligned}
M_\alpha = & -\rho b^2 \left[\pi \left(\frac{1}{2} - a \right) v b \alpha_0 p \cos (pt + \varphi_0) - \pi b^2 \left(\frac{1}{8} + a^2 \right) \alpha_0 p^2 \sin (pt + \varphi_0) \right. \\
& + T_{13} v^2 \beta_0 \sin (pt + \varphi_1) + T_{18} v b \beta_0 p \cos (pt + \varphi_1) \\
& \left. - 2 T_{13} b^2 \beta_0 p^2 \sin (pt + \varphi_1) + a \pi b h_0 p^2 \sin (pt + \varphi_2) \right] \\
& + 2 \rho v b^2 \pi \left(a + \frac{1}{2} \right) F \left[v\alpha_0 \sin (pt + \varphi_0) + h_0 p \cos (pt + \varphi_2) \right. \\
& + b \left(\frac{1}{2} - a \right) \alpha_0 p \cos (pt + \varphi_0) + \frac{T_{10}}{\pi} v \beta_0 \sin (pt + \varphi_1) \\
& + \frac{T_{11}}{2\pi} b \beta_0 p \cos (pt + \varphi_1) \left. \right] + 2 \rho v b^2 \pi \left(a + \frac{1}{2} \right) G \left[v\alpha_0 \cos (pt + \varphi_0) \right. \\
& - h_0 p \sin (pt + \varphi_2) - b \left(\frac{1}{2} - a \right) \alpha_0 p \sin (pt + \varphi_0) + \frac{T_{10}}{\pi} v \beta_0 \cos (pt + \varphi_1) \\
& \left. - \frac{T_{11}}{2\pi} b \beta_0 p \sin (pt + \varphi_1) \right] \quad (9)
\end{aligned}$$

$$\begin{aligned}
M_\beta = & -\rho b^2 \left[T_{17} v b \alpha_0 p \cos (pt + \varphi_0) - 2 T_{13} b^2 \alpha_0 p^2 \sin (pt + \varphi_0) + \frac{1}{\pi} v^2 T_{18} \beta_0 \sin (pt + \varphi_1) \right. \\
& \left. - \frac{1}{2\pi} v b T_{19} \beta_0 p \cos (pt + \varphi_1) + \frac{1}{\pi} T_3 b^2 \beta_0 p^2 \sin (pt + \varphi_1) + T_1 b h_0 p^2 \sin (pt + \varphi_2) \right] \\
& - \rho v b^2 T_{12} F \left[v\alpha_0 \sin (pt + \varphi_0) + h_0 p \cos (pt + \varphi_2) + b \left(\frac{1}{2} - a \right) \alpha_0 p \cos (pt + \varphi_0) \right. \\
& + \frac{T_{10}}{\pi} v \beta_0 \sin (pt + \varphi_1) + \frac{T_{11}}{2\pi} b \beta_0 p \cos (pt + \varphi_1) \left. \right] - \rho v b^2 T_{12} G \left[v\alpha_0 \cos (pt + \varphi_0) \right. \\
& - h_0 p \sin (pt + \varphi_2) - b \left(\frac{1}{2} - a \right) \alpha_0 p \sin (pt + \varphi_0) + \frac{T_{10}}{\pi} v \beta_0 \cos (pt + \varphi_1) \\
& \left. - \frac{T_{11}}{2\pi} b \beta_0 p \sin (pt + \varphi_1) \right] \quad (10)
\end{aligned}$$

In addition to these equations we will need the expression for the force on the aileron. This equation is obtained in complex form as (use formulas on pp. 5-8, reference 5)

$$\begin{aligned}
P_\beta = & -\rho b^2 \left(-v T_4 \dot{\alpha} - T_4 \ddot{h} + b T_9 \ddot{\alpha} - \frac{1}{2\pi} v T_5 \dot{\beta} - \frac{b}{2\pi} T_2 \ddot{\beta} \right) \\
& - 2 \rho b v \sqrt{1-c^2} \left[\frac{b}{2} (1-c) \dot{\alpha} + \frac{1}{\pi} v \sqrt{1-c^2} \beta + \frac{b}{2\pi} (1-c) T_{10} \dot{\beta} \right] \\
& - 2 \rho v b T_{20} C(k) Q
\end{aligned}$$

And the imaginary part is

$$\begin{aligned}
P_\beta = & -\rho b^2 \left[-v T_4 \alpha_0 p \cos (pt + \varphi_0) + T_4 h_0 p^2 \sin (pt + \varphi_2) - b T_9 \alpha_0 p^2 \sin (pt + \varphi_0) \right. \\
& \left. - \frac{1}{2\pi} v T_5 \beta_0 p \cos (pt + \varphi_1) + \frac{b}{2\pi} T_2 \beta_0 p^2 \sin (pt + \varphi_1) \right] - 2 \rho b v \sqrt{1-c^2} \left[\frac{b}{2} (1-c) \alpha_0 p \cos (pt + \varphi_0) \right. \\
& + \frac{1}{\pi} v \sqrt{1-c^2} \beta_0 \sin (pt + \varphi_1) + \frac{b}{2\pi} (1-c) T_{10} \beta_0 p \cos (pt + \varphi_1) \left. \right] - 2 \rho v b T_{20} F \left[v\alpha_0 \sin (pt + \varphi_0) \right. \\
& + h_0 p \cos (pt + \varphi_2) + b \left(\frac{1}{2} - a \right) \alpha_0 p \cos (pt + \varphi_0) + \frac{T_{10}}{\pi} v \beta_0 \sin (pt + \varphi_1) \\
& + \frac{T_{11}}{2\pi} b \beta_0 p \cos (pt + \varphi_1) \left. \right] - 2 \rho v b T_{20} G \left[v\alpha_0 \cos (pt + \varphi_0) - h_0 p \sin (pt + \varphi_2) \right. \\
& \left. - b \left(\frac{1}{2} - a \right) \alpha_0 p \sin (pt + \varphi_0) + \frac{T_{10}}{\pi} v \beta_0 \cos (pt + \varphi_1) - \frac{T_{11}}{2\pi} b \beta_0 p \sin (pt + \varphi_1) \right] \quad (11)
\end{aligned}$$

Following the method of von Kármán and Burgers (reference 2), the average horizontal force will be determined in two ways: (1) by the energy formula given in equation (12), and (2) by the force formula given in equation (13). The agreement of the results of the two methods will thus furnish a check on the work.

ENERGY FORMULA

$$\bar{W} = \bar{E} + \bar{P}_x v \quad (12)$$

where \bar{W} represents the average work done in unit time in maintaining the oscillations (7) against the forces and moments (8), (9), and (10); \bar{E} represents the average increase in kinetic energy in unit time in the vortex wake and; $\bar{P}_x v$ denotes average work done in unit time by the propulsive force P_x .³

FORCE FORMULA

$$P_x = \pi \rho S^2 + \alpha P + \beta P_\beta \quad (13)$$

where P_x is the propelling force; α and β are given in (7); P in (8), and P_β in (11); S is obtained from the relation $S = \lim_{x \rightarrow -1} \frac{1}{2} \gamma \sqrt{x+1}$ where γ is the vorticity distribution. The value of S is finite, since γ is infinite in the order of $\frac{1}{\sqrt{x+1}}$ at the leading edge $x = -1$, and is given in equation (25) and derived in appendix II.⁴

We proceed first to evaluate \bar{W} in equation (12). The instantaneous rate at which work is done in maintaining the oscillations is

$$\dot{W} = -(P\dot{h} + M_\alpha \dot{\alpha} + M_\beta \dot{\beta})$$

For the average work done in unit time we have

$$\bar{W} = -\frac{p}{2\pi} \int_0^{2\pi} (P\dot{h} + M_\alpha \dot{\alpha} + M_\beta \dot{\beta}) dt \quad (14)$$

On employing equations (7) to (10) and performing the indicated integrations, we obtain after some lengthy but elementary reductions

$$\bar{W} = \pi \rho b^2 \frac{2\gamma^3}{k} (B_1 h_0^2 + B_2 \alpha_0^2 + B_3 \beta_0^2 + 2B_4 \alpha_0 h_0 + 2B_5 \beta_0 h_0 + 2B_6 \alpha_0 \beta_0) \quad (15)$$

where

$$B_1 = F$$

$$B_2 = b^2 \left\{ \frac{1}{2} \left(\frac{1}{2} - a \right) - \left(a + \frac{1}{2} \right) \left[F \left(\frac{1}{2} - a \right) + \frac{G}{k} \right] \right\}$$

$$B_3 = b^2 \left[-\frac{T_{19}}{4\pi^2} + \frac{T_{12}}{2\pi} \left(\frac{T_{11}}{2\pi} F + \frac{T_{10}}{\pi} \frac{G}{k} \right) \right]$$

³ When the energy released in the wake in unit time is less than the work required in unit time to maintain the oscillations, i. e., $\bar{E} < \bar{W}$, then P_x is positive and is a true propelling force. When $\bar{E} > \bar{W}$, then P_x is negative and denotes not *propulsion* but *resistance or drag*.

⁴ Formula (13) is obtained by a slight extension of the method of reference 2, pp. 305-306. The "suction" force $\pi \rho S^2$ arising from the infinite vorticity at the leading edge is explained in reference 2 (pp. 52 and 306) along lines laid down by Grammel and Cisotti. (See also reference 8, pp. 135 and 203.) The fact that this infinity occurs implies that the ideal flow for an infinitely thin wing is unrealizable. We are regarding this case, however, as a limiting one of a wing that is rounded and smooth at the leading edge and sharp at the trailing edge.

$$B_4 = \frac{b}{2} \left[\left(\frac{1}{2} - 2aF + \frac{G}{k} \right) \cos (\varphi_2 - \varphi_0) - \left(\frac{F}{k} - G \right) \sin (\varphi_2 - \varphi_0) \right]$$

$$B_5 = \frac{b}{2} \left[\left(-\frac{T_4}{2\pi} + \frac{T_{11} + T_{12}}{2\pi} F + \frac{T_{10}}{\pi} \frac{G}{k} \right) \cos (\varphi_2 - \varphi_1) - \left(\frac{T_{10}}{\pi} \frac{F}{k} + \frac{T_4}{\pi} G \right) \sin (\varphi_2 - \varphi_1) \right]$$

$$B_6 = \frac{b^2}{2} \left\{ \left[\frac{T_{11}}{4\pi} - \left(\frac{1}{2} - a \right) \frac{T_4}{2\pi} + \left(\frac{T_4}{2\pi} - \frac{T_{11} + T_{12}}{2\pi} a \right) F - \left(\left(a + \frac{1}{2} \right) \frac{T_{10}}{\pi} - \frac{T_{12}}{2\pi} \right) \frac{G}{k} \right] \cos (\varphi_1 - \varphi_0) + \left[\frac{T_{15}}{2\pi} \frac{1}{k} - \left(\left(a + \frac{1}{2} \right) \frac{T_{10}}{\pi} + \frac{T_{12}}{2\pi} \right) \frac{F}{k} + \left(\frac{T_{11} + T_{12}}{4\pi} - \frac{T_4}{\pi} a \right) G \right] \sin (\varphi_1 - \varphi_0) \right\}$$

In order to calculate \bar{E} in equation (12), we need the expression for the vorticity in the wake. The magnitude of the vorticity in the wake is given in complex form by

$$U = U_0 e^{i\varphi} e^{ip \left(t - \frac{(x-1)b}{v} \right)} \quad (16)$$

where $U_0 e^{i\varphi}$ is a complex quantity determined in (19). (Cf. reference 5, p. 8, in which x instead of $x-1$ is used in the exponent.) From the definition of the circulation about the airfoil as the integral of the vorticity in the wake we have in complex form,

$$\Gamma = \int_1^\infty U dx = -\frac{i}{k} U_0 e^{i\varphi} e^{ip t} \quad (17)$$

Also from reference 5, equation (8), the condition for smooth flow at the trailing edge leads to the relation

$$\frac{1}{2\pi} \int_1^\infty \sqrt{\frac{x+1}{x-1}} U dx = v\alpha + h + b \left(\frac{1}{2} - a \right) \dot{\alpha} + \frac{T_{10}}{\pi} v\beta + b \frac{T_{11}}{2\pi} \dot{\beta} = Q \quad (18)$$

Combining (17) and (18) we may write

$$\Gamma = 2\pi Q - \int_1^\infty \left(\sqrt{\frac{x+1}{x-1}} - 1 \right) U dx$$

On equating coefficients of $e^{ip t}$ on both sides of this relation and solving for the quantity $U_0 e^{i\varphi}$ (for the evaluation of the definite integral in terms of Bessel functions see reference 5, p. 8), we obtain

$$U_0 e^{i\varphi} = -4(A + iB)(J + iK)e^{-ik} \quad (19)$$

where,

$$J = \frac{J_1 + Y_0}{D}, K = \frac{Y_1 - J_0}{D},$$

$$D = (J_1 + Y_0)^2 + (Y_1 - J_0)^2, J^2 + K^2 = \frac{1}{D}$$

and

$$\left. \begin{aligned} A &= v\alpha_0 \cos \varphi_0 - h_0 p \sin \varphi_2 - b \left(\frac{1}{2} - a \right) \alpha_0 p \sin \varphi_0 \\ &\quad + \frac{T_{10}}{\pi} v\beta_0 \cos \varphi_1 - \frac{T_{11}}{2\pi} b\beta_0 p \sin \varphi_1 \\ B &= v\alpha_0 \sin \varphi_0 + h_0 p \cos \varphi_2 + b \left(\frac{1}{2} - a \right) \alpha_0 p \cos \varphi_0 \\ &\quad + \frac{T_{10}}{\pi} v\beta_0 \sin \varphi_1 + \frac{T_{11}}{2\pi} b\beta_0 p \cos \varphi_1 \end{aligned} \right\} \quad (20)$$

When the imaginary part of U is denoted by γ , which is the only part of interest, the vorticity in the wake is given by

$$\gamma = A_0 \cos kx + B_0 \sin kx \quad (21)$$

where

$$\begin{aligned} \frac{1}{4}A_0 &= (BK - AJ) \sin pt - (AK + BJ) \cos pt \\ \frac{1}{4}B_0 &= (BK - AJ) \cos pt + (AK + BJ) \sin pt \end{aligned}$$

The induced vertical velocity at a great distance x downstream is

$$w_z = \frac{1}{2\pi} \int_{-\infty}^{\infty} \frac{\gamma(x')}{x-x'} dx' = \frac{1}{2} (A_0 \sin kx - B_0 \cos kx)$$

The difference in potential at points of the x axis in the wake is

$$\phi_2 - \phi_1 = b \int \gamma dx = \frac{b}{k} (A_0 \sin kx - B_0 \cos kx)$$

and the kinetic energy in the wake (per unit length) at a point x along the surface of discontinuity far from the airfoil is⁵

$$\begin{aligned} E_1 &= \frac{1}{2} \rho w_z (\phi_2 - \phi_1) \\ &= \frac{1}{2} \rho \frac{b}{2k} (A_0 \sin kx - B_0 \cos kx)^2 \\ &= 4\rho \frac{b}{k} [(BK - AJ) \cos (pt + kx) \\ &\quad + (AK + BJ) \sin (pt + kx)]^2 \end{aligned} \quad (22)$$

The mean value of E_1 with respect to time is independent of x and is given by

$$\bar{E}_1 = \frac{p}{2\pi} \int_0^{2\pi/p} E_1 dt = \frac{2\rho b}{kD} (A^2 + B^2)$$

And, finally, the average value of the increase in energy in the field in unit time is

$$\bar{E} = v \bar{E}_1 = \frac{2\rho b v}{kD} (A^2 + B^2)$$

or also

$$\begin{aligned} \bar{E} &= \pi \rho b^2 \frac{p^3}{k} [C_1 h_0^2 + C_2 \alpha_0^2 + C_3 \beta_0^2 + 2C_4 \alpha_0 h_0 \\ &\quad + 2C_5 \beta_0 h_0 + 2C_6 \alpha_0 \beta_0] \end{aligned} \quad (23)$$

where

$$\begin{aligned} C_1 &= \frac{2}{\pi k D} \\ C_2 &= \frac{2b^2}{\pi k D} \left[\frac{1}{k^2} + \left(\frac{1}{2} - a \right)^2 \right] \\ C_3 &= \frac{2b^2}{\pi k D} \left[\left(\frac{T_{10}}{\pi k} \right)^2 + \left(\frac{T_{11}}{2\pi} \right)^2 \right] \\ C_4 &= \frac{2b}{\pi k D} \left[-\frac{1}{k} \sin (\varphi_2 - \varphi_0) + \left(\frac{1}{2} - a \right) \cos (\varphi_2 - \varphi_0) \right] \\ C_5 &= \frac{2b}{\pi k D} \left[-\frac{T_{10}}{\pi} \frac{1}{k} \sin (\varphi_2 - \varphi_1) + \frac{T_{11}}{2\pi} \cos (\varphi_2 - \varphi_1) \right] \\ C_6 &= \frac{2b^2}{\pi k D} \left[\left(\frac{T_{10}}{\pi} \frac{1}{k^2} + \left(\frac{1}{2} - a \right) \frac{T_{11}}{2\pi} \right) \cos (\varphi_1 - \varphi_0) \right. \\ &\quad \left. + \frac{1}{k} \left(\frac{T_{10}}{\pi} \left(\frac{1}{2} - a \right) - \frac{T_{11}}{2\pi} \right) \sin (\varphi_1 - \varphi_0) \right] \end{aligned}$$

Equation (12) now defines $\bar{P}_z v$ and hence \bar{P}_z . We have

$$\bar{P}_z v = \bar{W} - \bar{E}$$

or

$$\begin{aligned} \bar{P}_z &= \pi \rho b p^2 [A_1 h_0^2 + A_2 \alpha_0^2 + A_3 \beta_0^2 + 2A_4 \alpha_0 h_0 \\ &\quad + 2A_5 \beta_0 h_0 + 2A_6 \alpha_0 \beta_0] \end{aligned} \quad (24)$$

where from equations (15) and (23)

$$A_1 = B_1 - C_1, \quad A_2 = B_2 - C_2, \text{ etc.}$$

We shall now proceed to the direct calculation of P_z from (13). The value of S is derived in appendix II and in complex form is given by

$$S = \frac{\sqrt{2}}{2} \left[2C(k)Q - b\alpha - \frac{2}{\pi} \sqrt{1-c^2} v\beta + \frac{T_1}{\pi} b\beta \right]$$

Again we shall use only the imaginary part of this expression which is

$$S = \frac{\sqrt{2}}{2} (M \sin pt + N \cos pt) \quad (25)$$

where

$$\begin{aligned} M &= 2F \left[v\alpha_0 \cos \varphi_0 - h_0 p \sin \varphi_2 - b \left(\frac{1}{2} - a \right) \alpha_0 p \sin \varphi_0 + \frac{T_{10}}{\pi} v\beta_0 \cos \varphi_1 - \frac{T_{11}}{2\pi} b\beta_0 p \sin \varphi_1 \right] \\ &\quad - 2G \left[v\alpha_0 \sin \varphi_0 + h_0 p \cos \varphi_2 + b \left(\frac{1}{2} - a \right) \alpha_0 p \cos \varphi_0 + \frac{T_{10}}{\pi} v\beta_0 \sin \varphi_1 + \frac{T_{11}}{2\pi} b\beta_0 p \cos \varphi_1 \right] \\ &\quad + b\alpha_0 p \sin \varphi_0 - \frac{2}{\pi} \sqrt{1-c^2} v\beta_0 \cos \varphi_1 - \frac{T_1}{\pi} b\beta_0 p \sin \varphi_1 \end{aligned}$$

⁵ The expression $\frac{1}{2} \rho w_z (\phi_2 - \phi_1)$ is actually equal to $\frac{1}{2} \rho \phi \frac{\partial \phi}{\partial n}$ taken along the surface of discontinuity (the x axis) where $\phi = \phi_2 - \phi_1$ and $\frac{\partial \phi}{\partial n} = w_z$. The latter expression is equal to $\frac{1}{2} \rho \left[\left(\frac{\partial \phi}{\partial t} \right)^2 + \left(\frac{\partial \phi}{\partial z} \right)^2 \right]$ taken over a proper space interval, i. e., represents the kinetic energy in a certain volume.

and

$$\begin{aligned} N = & 2F \left[v\alpha_0 \sin \varphi_0 + h_0 p \cos \varphi_2 + b \left(\frac{1}{2} - a \right) \alpha_0 p \cos \varphi_0 + \frac{T_{10}}{\pi} v \beta_0 \sin \varphi_1 + \frac{T_{11}}{2\pi} b \beta_0 p \cos \varphi_1 \right] \\ & + 2G \left[v\alpha_0 \cos \varphi_0 - h_0 p \sin \varphi_2 - b \left(\frac{1}{2} - a \right) \alpha_0 p \sin \varphi_0 + \frac{T_{10}}{\pi} v \beta_0 \cos \varphi_1 - \frac{T_{11}}{2\pi} b \beta_0 p \sin \varphi_1 \right] \\ & - b \alpha_0 p \cos \varphi_0 - \frac{2}{\pi} \sqrt{1-c^2} v \beta_0 \sin \varphi_1 + \frac{T_4}{\pi} b \beta_0 p_0 \cos \varphi_1 \end{aligned}$$

The mean value of $\pi \rho S^2$ with respect to time is

$$\frac{p}{2\pi} \int_0^{2\pi/p} \pi \rho S^2 dt = \frac{\pi \rho}{4} (M^2 + N^2)$$

This expression becomes, after a considerable number of terms cancel,

$$\pi \rho \bar{S}_1^2 = \pi \rho b p^2 (a_1 h_0^2 + a_2 \alpha_0^2 + a_3 \beta_0^2 + 2a_4 \alpha_0 h_0 + 2a_5 \beta_0 h_0 + 2a_6 \alpha_0 \beta_0) \quad (26)$$

where

$$\begin{aligned} a_1 = & F^2 + G^2 \\ a_2 = & b^2 \left\{ (F^2 + G^2) \left[\frac{1}{k^2} + \left(\frac{1}{2} - a \right)^2 \right] + \frac{1}{4} - \left(\frac{1}{2} - a \right) F - \frac{1}{k} G \right\} \\ a_3 = & b^2 \left\{ (F^2 + G^2) \left[\left(\frac{T_{10}}{\pi k} \right)^2 + \left(\frac{T_{11}}{2\pi} \right)^2 \right] + \frac{1-c^2}{\pi^2 k^2} + \frac{T_4^2}{4\pi^2} \right. \\ & \left. + F \left(-\frac{2T_{10}\sqrt{1-c^2}}{\pi^2 k^2} + \frac{T_4 T_{11}}{2\pi^2} \right) + \frac{G}{k} \left(\frac{T_4 T_{10}}{\pi^2} + \frac{T_{11}\sqrt{1-c^2}}{\pi^2} \right) \right\} \\ a_4 = & b \left\{ (F^2 + G^2) \left[-\frac{1}{k} \sin (\varphi_2 - \varphi_0) + \left(\frac{1}{2} - a \right) \cos (\varphi_2 - \varphi_0) \right] - \frac{F}{2} \cos (\varphi_2 - \varphi_0) + \frac{G}{2} \sin (\varphi_2 - \varphi_0) \right\} \\ a_5 = & b \left\{ (F^2 + G^2) \left[-\frac{T_{10}}{\pi k} \sin (\varphi_2 - \varphi_1) + \frac{T_{11}}{2\pi} \cos (\varphi_2 - \varphi_1) \right] + \frac{F}{2} \left[\frac{2\sqrt{1-c^2}}{\pi k} \sin (\varphi_2 - \varphi_1) + \frac{T_4}{\pi} \cos (\varphi_2 - \varphi_1) \right] \right. \\ & \left. + \frac{G}{2} \left[\frac{2\sqrt{1-c^2}}{\pi k} \cos (\varphi_2 - \varphi_1) - \frac{T_4}{\pi} \sin (\varphi_2 - \varphi_1) \right] \right\} \\ a_6 = & b^2 \left\{ (F^2 + G^2) \left[\left(\frac{T_{10}}{\pi k^2} + \frac{T_{11}}{2\pi} \left(\frac{1}{2} - a \right) \right) \cos (\varphi_1 - \varphi_0) + \left[\frac{T_{10}}{\pi} \left(\frac{1}{2} - a \right) - \frac{T_{11}}{2\pi} \right] \frac{1}{k} \sin (\varphi_1 - \varphi_0) \right] \right. \\ & + \frac{F}{2} \left[-\frac{2\sqrt{1-c^2}}{\pi k^2} + \frac{T_4}{\pi} \left(\frac{1}{2} - a \right) - \frac{T_{11}}{2\pi} \right] \cos (\varphi_1 - \varphi_0) - \left[\frac{2\sqrt{1-c^2}}{\pi} \left(\frac{1}{2} - a \right) + \frac{T_4 + T_{10}}{\pi} \right] \frac{1}{k} \sin (\varphi_1 - \varphi_0) \\ & + \frac{G}{2} \left[-\frac{2\sqrt{1-c^2}}{\pi k^2} + \frac{T_4}{\pi} \left(\frac{1}{2} - a \right) + \frac{T_{11}}{2\pi} \right] \sin (\varphi_1 - \varphi_0) + \left[\frac{2\sqrt{1-c^2}}{\pi} \left(\frac{1}{2} - a \right) + \frac{T_4 - T_{10}}{\pi} \right] \frac{1}{k} \cos (\varphi_1 - \varphi_0) \\ & \left. + \frac{\sqrt{1-c^2}}{2\pi} \frac{1}{k} \sin (\varphi_1 - \varphi_0) - \frac{T_4}{4\pi} \cos (\varphi_1 - \varphi_0) \right\} \end{aligned}$$

We proceed to calculate the average values of the terms αP and βP_β in (13) by employing equations (7), (8), and (11). Their results

$$\overline{\alpha P} = \pi \rho b p^2 (b_2 \alpha_0^2 + 2b_4 \alpha_0 h_0 + 2b_6 \alpha_0 \beta_0) \quad (27)$$

where

$$\begin{aligned} b_2 = & b^2 \left[-\frac{a}{2} - \frac{F}{k^2} + \left(\frac{1}{2} - a \right) \frac{G}{k} \right] \\ b_4 = & \frac{b}{2} \left[\left(\frac{1}{2} + \frac{G}{k} \right) \cos (\varphi_2 - \varphi_0) + \frac{F}{k} \sin (\varphi_2 - \varphi_0) \right] \\ b_6 = & \frac{b^2}{2} \left[\left(-\frac{T_1}{2\pi} - \frac{F}{k^2} \frac{T_{10}}{\pi} + \frac{G}{k} \frac{T_{11}}{2\pi} \right) \cos (\varphi_1 - \varphi_0) \right. \\ & \left. + \left(-\frac{T_4}{2\pi} + F \frac{T_{11}}{2\pi} + \frac{G}{k} \frac{T_{10}}{\pi} \right) \frac{1}{k} \sin (\varphi_1 - \varphi_0) \right] \end{aligned}$$

Also

$$\overline{\beta P_\beta} = \pi \rho b p^2 (c_3 \beta_0^2 + 2c_5 \beta_0 h_0 + 2c_6 \alpha_0 \beta_0) \quad (28)$$

where

$$\begin{aligned} c_3 = & b^2 \left[-\frac{T_2}{2\pi^2} - \frac{1-c^2}{\pi^2 k^2} - \frac{F}{k^2} \frac{T_{10} T_{20}}{\pi^2} + \frac{G}{k} \frac{T_{11} T_{20}}{2\pi^2} \right] \\ c_5 = & \frac{b}{2} \left[\left(-\frac{T_4}{2\pi} + \frac{T_{20} G}{\pi k} \right) \cos (\varphi_2 - \varphi_1) + \frac{T_{20} F}{\pi k} \sin (\varphi_2 - \varphi_1) \right] \\ c_6 = & \frac{b^2}{2} \left[\left[\frac{T_9}{\pi} - \frac{T_{20}}{\pi} \frac{F}{k^2} + \frac{T_{20}}{\pi} \left(\frac{1}{2} - a \right) \frac{G}{k} \right] \cos (\varphi_1 - \varphi_0) \right. \\ & + \left[\frac{T_4 - (1-c)}{2\pi} \frac{\sqrt{1-c^2}}{\pi} - \frac{T_{20}}{\pi} \left(\frac{1}{2} - a \right) F \right. \\ & \left. \left. - \frac{T_{20} G}{\pi k} \right] \frac{1}{k} \sin (\varphi_1 - \varphi_0) \right] \end{aligned}$$

Finally from (13) the average propulsive force is

$$\bar{P}_z = \pi \rho b p^2 [a_1 h_0^2 + (a_2 + b_2) \alpha_0^2 + (a_3 + c_3) \beta_0^2 + 2(a_4 + b_4) \alpha_0 h_0 + 2(a_5 + c_5) \beta_0 h_0 + 2(a_6 + b_6 + c_6) \alpha_0 \beta_0] \quad (29)$$

In order that equations (24) and (29) agree we must have that

$$\begin{aligned} A_1 &= a_1 \\ A_2 &= a_2 + b_2 \\ A_3 &= a_3 + c_3 \\ A_4 &= a_4 + b_4 \\ A_5 &= a_5 + c_5 \\ A_6 &= a_6 + b_6 + c_6 \end{aligned} \quad (30)$$

Each of these relations may be reduced to an identity, e. g., consider A_1 and a_1 . From (15), (23), and (26)

$$\begin{aligned} A_1 &= B_1 - C_1 = F - \frac{2}{\pi k D} \\ a_1 &= F^2 + G^2 \end{aligned}$$

In order that $A_1 = a_1$ the following relation must hold

$$F = F^2 + G^2 + \frac{2}{\pi k D} \quad (31)$$

To show that this is true note that

$$F = \frac{J_1(J_1 + Y_0) + Y_1(Y_1 - J_0)}{(J_1 + Y_0)^2 + (Y_1 - J_0)^2} = \frac{J_1^2 + Y_1^2 + J_1 Y_0 - J_0 Y_1}{D}$$

$$F^2 + G^2 = (F + iG)(F - iG) = \frac{J_1^2 + Y_1^2}{D}$$

(cf. reference 5, p. 8) and from a well-known property of the Bessel functions,

$$J_1 Y_0 - J_0 Y_1 = \frac{2}{\pi k}$$

Hence equation (31) follows.

By the use of the relation (31) and the definitions of the various T 's given in the appendix, it can be verified that the remaining relations in (30) are also identities.

It may be of interest to consider the special cases of one degree of freedom. Let the motion of the wing consist only of the vertical motion h at right angles to the direction of flight, i. e., flapping motion. The propelling force is then ⁶

$$\bar{P}_z = \pi \rho b p^2 h_0^2 (F^2 + G^2) \quad (32)$$

Consider in this case the ratio

$$\begin{aligned} \frac{\bar{P}_z v}{W} &= \frac{\text{energy of propulsion}}{\text{total energy}} \\ &= \frac{F^2 + G^2}{F} \end{aligned} \quad (33)$$

This function, shown in figure 3, represents the theoretical efficiency of the flapping motion (unity = 100 per-

cent). It is observed that a propelling force exists in the entire range of $1/k$, the efficiency being 50 percent for infinitely rapid oscillations and 100 percent for infinitely slow flapping.

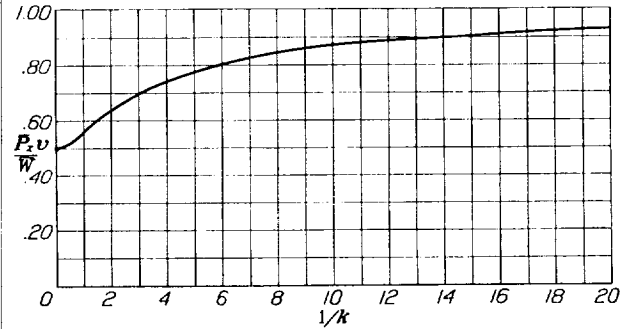


FIGURE 3.—The ratio of energy of propulsion to the energy required to maintain the oscillations ($\frac{P_z v}{W}$) as a function of $1/k$ for the case of pure flapping.

For the special case of angular oscillations about α alone ($h=0$, $\beta=0$) the horizontal force is

$$\begin{aligned} \bar{P}_z &= \pi \rho b p^2 h_0^2 \alpha_0^2 \left[(F^2 + G^2) \left[\frac{1}{k^2} + \left(\frac{1}{2} - a \right)^2 \right] \right. \\ &\quad \left. + \frac{1}{2} \left(\frac{1}{2} - a \right) - \frac{F}{k^2} - \left(\frac{1}{2} - a \right) \frac{G}{k} \right] \end{aligned} \quad (34)$$

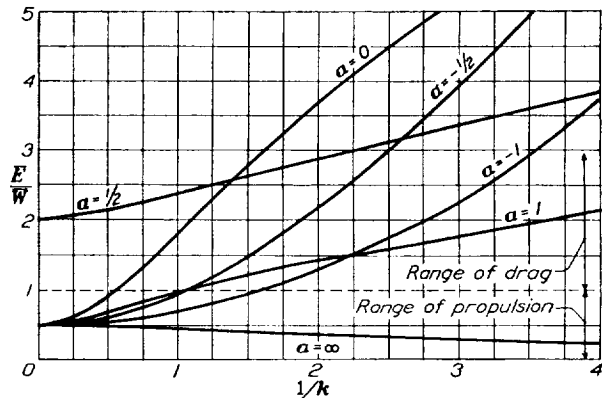


FIGURE 4.—The ratio of the energy dissipated in the wake to the energy required to maintain the oscillations (E/W) as a function of $1/k$ for the case of pure angular oscillations about α .

In figure 4 there is shown the ratio \bar{E}/\bar{W} , in this case for several positions of the axis of rotation. These curves give the ratio of the energy per unit time released in the wake to the work per unit time required to maintain the oscillations. In the range of values $0 < \bar{E}/\bar{W} < 1$, \bar{P}_z is positive and denotes a thrust or propelling force; for other values it is negative and denotes a drag force.

⁶ This result agrees with the formula of von Kármán and Burgers (reference 2, p. 306). The expressions of reference 2 denoted by

$$\begin{aligned} b_1 &= 1 + A_1 - \lambda A_1 (Q - S) + \lambda A_2 (P - C) \\ b_2 &= A_2 - \lambda A_1 (Q - S) - \lambda A_1 (P - C) \end{aligned}$$

reduce in our notation simply to $2F$ and $2G$, respectively.

APPENDIX I

NOTATION

α , angle of attack (fig. 1).
 β , aileron angle (fig. 1).
 h , vertical distance (fig. 1).
 $\dot{\alpha} = \frac{d\alpha}{dt}$, $\ddot{\alpha} = \frac{d^2\alpha}{dt^2}$, etc.
 $\alpha_0, \beta_0, h_0, \varphi_0, \varphi_1, \varphi_2$, amplitudes and phase angles of the oscillations (equation (7)).
 b , half chord, used as reference length.
 x , coordinate in direction of airfoil chord.
 t , time.
 v , velocity of the general motion in direction of x axis.
 p , 2π times the frequency of the oscillations.
 k , reduced frequency (equation (2)). The wave length between successive waves in the vortex wake is $2\pi b/k$.
 a , coordinate of axis of rotation (fig. 1).
 c , coordinate of aileron hinge (fig. 1).
 i , imaginary unit $\sqrt{-1}$.
 e , base of natural logarithms.
 ρ , mass density of air.
 P , lift force on airfoil (+downward in fig. 1).
 M_a , moment on airfoil about a (+clockwise in fig. 1).
 M_b , moment on aileron about c (+clockwise in fig. 1).
 P_b , lift force on aileron (+downward in fig. 1).
 $C(k), F, G, J_0, J_1, Y_0, Y_1, J, K, D$, Bessel functions of the argument k . (Cf. equations (6) and (19), fig. 2, and table I.)
 \bar{W} , average work done in unit time in maintaining the oscillations.
 \bar{E} , average increase of kinetic energy in the wake in unit time.
 \bar{P}_x , average force in the direction of the x axis (+propulsion, -drag).
 $A_1 \dots A_6, B_1 \dots B_6, C_1 \dots C_6, a_1, \dots, a_6, b_1, b_2, b_3, b_4, b_5, c_3, c_5, c_6$, coefficients.
 Q , defined by equation (18).
 A, B , defined by equation (20).
 A_0, B_0 , defined by equation (21).
 M, N , defined by equation (25).
 U , distribution of vorticity in the wake in complex form (equation (16)).

$U_0 e^{i\varphi}$, coefficient of U , given in equation (19).
 γ , imaginary part of U .
 S , defined by equation (13); see also appendix II.
 Γ , circulation about the airfoil, defined by equation (17).

DEFINITIONS OF THE T 's

$$\begin{aligned}
 T_1 &= -\frac{1}{3}(2+c^2)\sqrt{1-c^2} + c \cos^{-1} c \\
 T_2 &= c(1-c^2) - (1+c^2)\sqrt{1-c^2} \cos^{-1} c + c(\cos^{-1} c)^2 \\
 &\quad [T_2 = T_4(T_{11} + T_{12})] \\
 T_3 &= -\frac{1}{8}(1-c^2)(5c^2+4) + \frac{1}{4}c(7+2c^2)\sqrt{1-c^2} \cos^{-1} c \\
 &\quad - \left(\frac{1}{8} + c^2\right)(\cos^{-1} c)^2 \\
 T_4 &= c\sqrt{1-c^2} - \cos^{-1} c \\
 T_5 &= -(1-c^2) + 2c\sqrt{1-c^2} \cos^{-1} c - (\cos^{-1} c)^2 \\
 T_6 &= T_2 \\
 T_7 &= \frac{1}{8}c(7+2c^2)\sqrt{1-c^2} - \left(\frac{1}{8} + c^2\right) \cos^{-1} c \\
 T_8 &= -\frac{1}{3}(1+2c^2)\sqrt{1-c^2} + c \cos^{-1} c = -\frac{1}{3}(1-c^2) - cT_4 \\
 T_9 &= \frac{1}{2} \left[\frac{1}{3}(1-c^2)^2 + aT_4 \right] \\
 T_{10} &= \sqrt{1-c^2} + \cos^{-1} c \\
 T_{11} &= (2-c)\sqrt{1-c^2} + (1-2c) \cos^{-1} c \\
 T_{12} &= (2+c)\sqrt{1-c^2} - (1+2c) \cos^{-1} c \\
 &\quad [T_{12} - T_{11} = 2T_4] \\
 T_{13} &= -\frac{1}{2}(T_7 + (c-a)T_1) \\
 T_{14} &= \frac{1}{16} + \frac{1}{2}ac \\
 T_{15} &= T_4 + T_{10} = (1+c)\sqrt{1-c^2} \\
 T_{16} &= T_1 - T_8 - (c-a)T_4 + \frac{1}{2}T_{11} \\
 &\quad \left[T_{16} + T_{17} = -\left(\frac{1}{2}-a\right)T_4 + \frac{1}{2}T_{11} \right] \\
 T_{17} &= -2T_9 - T_1 + \left(a - \frac{1}{2}\right)T_4 \\
 T_{18} &= T_5 - T_4T_{10} \\
 T_{19} &= T_4T_{11} \\
 T_{20} &= -\sqrt{1-c^2} + \cos^{-1} c \\
 &\quad [T_{20} = T_{10} - 2\sqrt{1-c^2}]
 \end{aligned}$$

APPENDIX II

EVALUATION OF S (EQUATION (25))

From reference 5 (p. 7) we have that the condition for smooth flow at the *trailing edge* is obtained from the equation

$$\frac{\partial}{\partial x}(\varphi_r + \varphi_a + \varphi_h + \varphi_a + \varphi_\beta + \varphi_\beta)_{x=1} = 0 \quad (1)$$

where the φ 's are as follows (a \pm sign is to be prefixed to each φ , + for the upper surface, - for the lower surface):

$$\begin{aligned} \frac{\partial \varphi_r}{\partial x} &= \frac{1}{2\pi} \int_1^\infty \sqrt{\frac{x_0^2-1}{1-x^2}} \frac{1}{x_0-x} U dx_0 \\ \varphi_a &= v\alpha b \sqrt{1-x^2} \\ \varphi_h &= \dot{h} b \sqrt{1-x^2} \\ \varphi_a &= \dot{\alpha} b^2 \left(\frac{1}{2} x - a \right) \sqrt{1-x^2} \\ \varphi_\beta &= \frac{1}{\pi} v\beta b [\sqrt{1-x^2} \cos^{-1} c - (x-c) \log N] \\ \varphi_\beta &= \frac{1}{2\pi} \beta b^2 [\sqrt{1-c^2} \sqrt{1-x^2} + (x-2c) \sqrt{1-x^2} \cos^{-1} c \\ &\quad - (x-c)^2 \log N] \end{aligned}$$

where

$$N = \frac{1-cx - \sqrt{1-c^2} \sqrt{1-x^2}}{x-c}$$

Condition (1) leads to the relation (cf. (18))

$$\begin{aligned} \frac{1}{2\pi} \int_1^\infty \sqrt{\frac{x_0+1}{x_0-1}} U dx_0 &= v\alpha + \dot{h} + b \left(\frac{1}{2} - a \right) \dot{\alpha} + \frac{T_{10}}{\pi} v\beta \\ &\quad + b \frac{T_{11}}{2\pi} \beta = Q \end{aligned} \quad (2)$$

The *leading-edge* vorticity may be written as

$$2 \frac{\partial}{\partial x} (\varphi_r + \varphi_a + \varphi_h + \varphi_a + \varphi_\beta + \varphi_\beta)_{x=1} = \frac{2S}{\sqrt{1+x}}$$

On substituting for the φ 's, making use of relation (2) and of equation XI, reference 5, which is

$$C(k) = \frac{\int_1^\infty \frac{x_0}{\sqrt{x_0^2-1}} e^{-ikx_0} dx_0}{\int_1^\infty \frac{x_0+1}{\sqrt{x_0^2-1}} e^{-ikx_0} dx_0}$$

there results

$$S = \frac{\sqrt{2}}{2} [2C(k)Q - b\dot{\alpha} - \frac{2}{\pi} \sqrt{1-c^2} v\beta + \frac{T_4}{\pi} b\beta]$$

REFERENCES

1. Wagner, Herbert: Über die Entstehung des dynamischen Auftriebes von Tragflügeln. Z. f. a. M. M., Band 5, Heft 1, Feb. 1925, S. 17-35.
2. von Kármán, Th., and Burgers, J. M.: General Aerodynamic Theory—Perfect Fluids. Aerodynamic Theory, W. F. Durand, ed., vol. II, Julius Springer (Berlin), 1935.
3. Küssner, Hans Georg: Schwingungen von Flugzeugflügeln. DVL-Jahrbuch 1929, S. 313-334.
4. Glauert, H.: The Force and Moment on an Oscillating Aerofoil. R. & M. No. 1242, British A. R. C., 1929.
5. Theodorsen, Theodore: General Theory of Aerodynamic Instability and the Mechanism of Flutter. T. R. No. 496, N. A. C. A., 1935.
6. Katzmayr, R.: Effect of Periodic Changes of Angle of Attack on Behavior of Airfoils. T. M. No. 147, N. A. C. A., 1922.
7. Cicala, Placida: Le Azioni Aerodinamiche sui Profili di Ala Oscillanti in Presenza di Corrente Uniforme. Roy. Acad. Sci. Torino, 1935.
8. Pistolesi, Enrico: Aerodinamica. Unione Tipografica—Editrice Torinese, 1932.

TABLE I.—VALUES OF THE BESSEL FUNCTIONS

k	$1/k$	J_0	J_1	Y_0	Y_1	D	F	$-G$
∞	0	—	—	—	—	0	0.5000	0
10	$\frac{1}{10}$	—0.2459	0.0435	0.0557	0.2490	.2548	.5006	.0124
6	$\frac{1}{6}$	—0.1506	—0.2767	—0.2882	—0.1750	.4251	.5017	.0206
4	$\frac{1}{4}$	—0.3971	—0.0660	—0.0169	.3979	.6389	.5037	.0305
2	$\frac{1}{2}$.2239	.5767	.5104	—0.1070	1.2913	.5129	.0577
1	1	.7652	.4401	.0883	.7812	2.6706	.5394	.1003
.8	$\frac{1}{1.25}$.8463	.3688	—0.0868	.9780	3.4076	.5541	.1165
.6	$\frac{1}{1.67}$.9120	.2867	—0.3085	—1.2604	4.7198	.5788	.1378
.5	$\frac{1}{2}$.9385	.2423	—0.4446	—1.4714	5.8486	.5979	.1507
.4	$\frac{1}{2.5}$.9604	.1960	—0.6060	—1.7808	7.6823	.6250	.1650
.3	$\frac{1}{3.33}$.9776	.1483	—0.8072	—2.2929	11.130	.6650	.1793
.2	$\frac{1}{5}$.9900	.0995	—1.0510	—3.2235	19.570	.7276	.1886
.1	$\frac{1}{10}$.9975	.0499	—1.5342	—6.460	57.810	.8320	.1723
.05	$\frac{1}{20}$.9994	.0250	—1.979	—12.8	194.26	.9090	.1305
.025	$\frac{1}{40}$.9999	.0125	—2.430	—25.6	713.4	.9545	.0872
.01	$\frac{1}{100}$	1.000	.0050	—3.006	—63.7	4195	.9824	.0482
0	∞	1.000	0	∞	∞	∞	1.000	0

REPORT No. 568

THE QUIESCENT-CHAMBER TYPE COMPRESSION-IGNITION ENGINE

By H. H. FOSTER

SUMMARY

The performance of a single-cylinder 4-stroke-cycle compression-ignition engine having a vertical disk form of combustion chamber without air flow has been determined. The number, size, and direction of the orifices of the fuel-injection nozzles used were independently varied. A table and graphs are presented showing the performance of the engine with different nozzles; results of tests at different compression ratios, boost pressures, and coolant temperatures are also included.

The best unboosted performance was obtained at a compression ratio of 15.3 at an engine speed of 1,500 revolutions per minute, using water as a coolant. The increase in indicated mean effective pressure with boost pressure was proportional to the increase in weight of inducted air for equal air-fuel ratios and comparable maximum cylinder pressures. The engine operation was smoother with boosting.

The engine power and fuel economy obtained with a 6-orifice nozzle was equal to or better than that obtained with nozzles having any other form, number, or combination of orifices. The optimum value for the number, direction, or size of the orifices is not sharply defined. Results indicate that impingement of the fuel spray on the piston and chamber walls, although it may be detrimental to efficient combustion, may aid distribution and consequently increase the power output. Although the results do not afford a rational basis for nozzle design that can be reduced to an analytical or empirical formula, they do show that engine performance can be improved by careful design of the injection nozzle.

The large percentage of the total fuel in the relatively solid spray core injected from round-hole orifices and the short time available preclude the probability of obtaining a homogeneous mixture of the fuel and air in a quiescent combustion chamber using a multiple-orifice nozzle. The resultant inferior performance compared with that obtained from the same combustion chamber with forced air flow, despite the easy starting, easy scavenging, low mechanical losses, and freedom from knock, renders the quiescent-chamber engine unattractive for aircraft-engine use.

INTRODUCTION

In the course of the general investigation of the possibilities and limitations of the compression-ignition engine for aircraft use, the N. A. C. A. has been investigating the performance of a single-cylinder 4-stroke-cycle test engine with a vertical disk-shaped combustion chamber. This combustion chamber has been designated "quiescent" because there is evidence that any air movement which may occur in the chamber has no marked effect on the distribution of the fuel (reference 1). In order to obtain as nearly a homogeneous mixture of the fuel and air as possible, it is therefore necessary to meter and distribute the fuel to the air in the combustion chamber by means of the injection system.

Determination of the optimum distribution of the fuel to the air in this combustion chamber was undertaken in two ways. The first was the commonly used method of conducting a series of engine-performance tests and systematically varying the number, size, and direction of the orifices until the test results indicated an optimum value in any series of changes. The second method consisted in mathematically proportioning the area of each orifice to the volume of air into which the spray from this orifice would be injected. As a matter of convenience and in order to have a basis of comparison, results from the first method were used as a starting point for the second. Some of the results of nozzle investigations, started in 1927 and continued into 1933, have been published as technical notes (references 2 and 3). The purpose of this report is to summarize the nozzle investigations and to present further results obtained at different compression ratios, boost pressures, and coolant temperatures. All the data presented were obtained at the N. A. C. A. engine-research laboratories at Langley Field, Va.

APPARATUS AND METHODS

The test unit used in this work is shown in figure 1. The engine has a 5-inch bore and a 7-inch stroke and is connected to an electric dynamometer. Necessary

auxiliaries and apparatus for obtaining the performance data are shown grouped about the engine. Parts of the engine are, as far as practicable, the same as those of the N. A. C. A. universal test engine (reference 4), the main exception being the cylinder head, which has a vertical disk-shaped combustion chamber between the heads of horizontally opposed intake and exhaust valves, as shown in figure 2. Changes in compression ratio were obtained by varying the length of the removable throat-orifice ring between the combustion chamber and the cylinder while keeping the mechani-

period was 27 crank degrees; and a high rate, in which the injection period was 20 crank degrees at an engine speed of 1,500 r. p. m. for full-load fuel quantity. The pump was driven from the crankshaft through a reduction gear in which there was an adjustment for changing the angular relation between the crankshaft and the pump cam. A spring-loaded automatic injection valve, set to open at 3,000 pounds per square inch, was installed in the top hole of the combustion chamber. The valve and pump were connected by a steel tube 36 inches long and of one-eighth inch inside diameter.



FIGURE 1.—Test engine and auxiliary equipment.

cal clearance between the piston crown and cylinder head at about 0.032 inch.

A detail drawing of the injection pump is shown in figure 3. It differs from the pump as actually used only in having micrometer screws instead of levers for controlling the position of the start-and-stop cam blocks, which control the closing and opening of the bypass valve, thus changing the time and period of injection. Shifting of the position of the control blocks, combined with the variable-velocity cam, varies the quantity and the rate of fuel discharge.

Figure 4 shows a comparison of two representative rates of injection: a low rate, in which the injection

Figure 5 shows enlarged sections of the nozzles. The length-diameter ratio of the orifices is 2. The fuels used were conventional Diesel engine fuels described in reference 5 as fuels 1 and 2. The rate of fuel consumption was obtained by timing the consumption of 0.50 pound of fuel. Full-load fuel quantity (zero excess air), 0.000325 pound per cycle, is the fuel quantity required for a chemically correct mixture with the quantity of air inducted per cycle by this engine at a volumetric efficiency of 82 percent.

Information regarding spray penetration and spray interference in the combustion chamber was desired as an aid in nozzle design; accordingly, a full-scale

model following the outline of the disk-shaped combustion chamber was placed in the N. A. C. A. spray-photography pressure chamber and photographs of the spray formation in this chamber were obtained. The edges of the combustion-chamber shape were slightly obscured in the photographs by the pressure-chamber cover plate. Injection pressures were of the

engine. Motoring tests showed the optimum length of air-intake pipe for maximum charging efficiency at an engine speed of 1,500 r. p. m. to be approximately 6 feet, which determined the height of the surge tank above the engine. Air consumption was determined by timing the displacement of 80 cubic feet of air from a 100-cubic-foot gasometer by means of an electrically

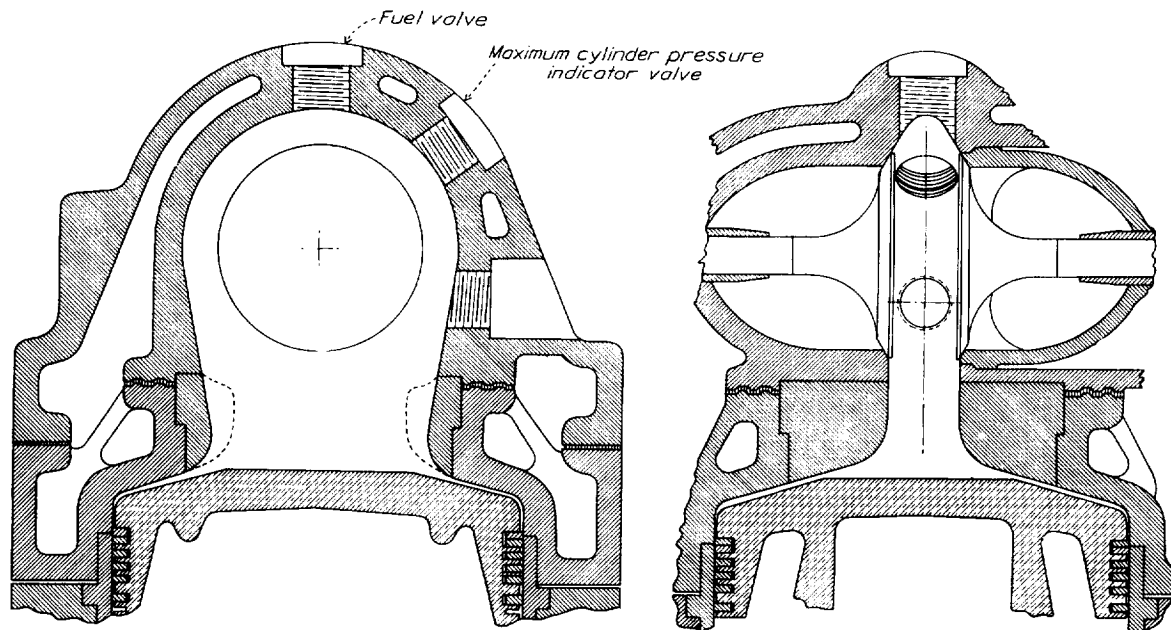


FIGURE 2. Combustion chamber.

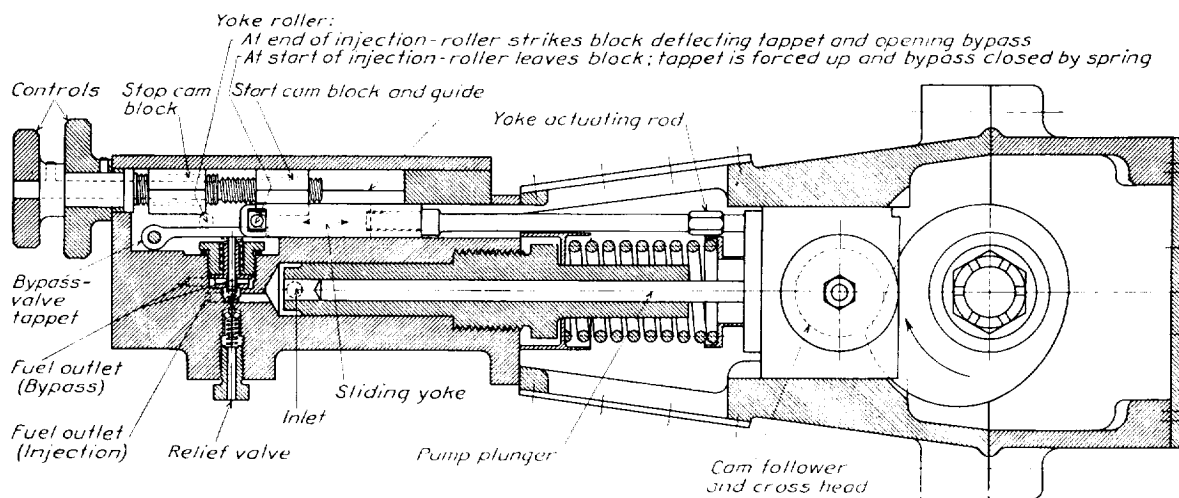


FIGURE 3. Fuel-injection pump.

same order as those used in the full-load engine tests. The spray-chamber air density was made to approximate that of the combustion chamber at the time of injection.

Figure 6 is a schematic diagram of the air system used in this investigation. Rubber diaphragms were placed over the ends of the overhead drums to damp pulsations and to give a smooth flow of air to the

operated stop watch. The inlet-air temperature was maintained at 95° F. Water and oil temperatures (out) were maintained at 170° and 140° F., respectively. For the special variable-coolant temperature tests Prestone and glycerin were used.

Maximum cylinder pressures were indicated by a calibrated Bourdon spring gage connected to an N. A. C. A. disk-type check valve operated by the pressure

of the gases in the cylinder. This instrument, designated a "trapped-pressure" indicator, was used because it afforded an easy and reliable means of directly

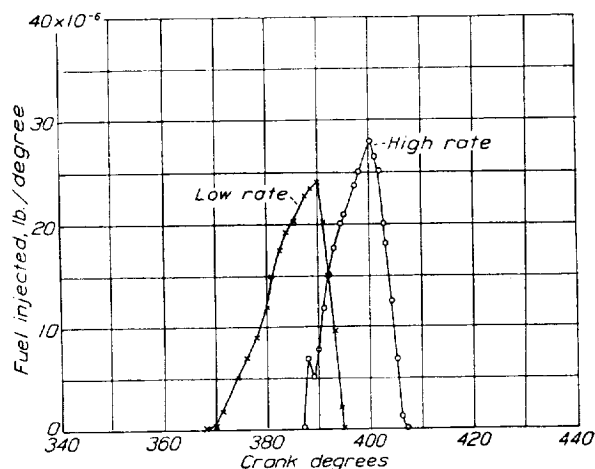


FIGURE 4.—Comparison of the injection rates used in the engine-performance tests; full load; 1,500 r. p. m.

observing the pressure readings as the engine controls were changed. Trapped-pressure readings are usually 5 to 25 pounds per square inch lower than those of the

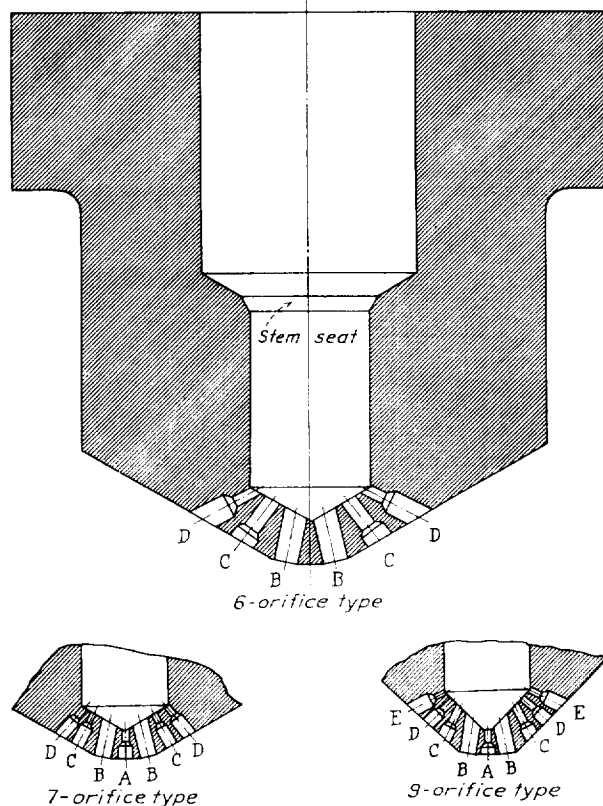


FIGURE 5.—Fuel-injection nozzles.

balanced-diaphragm type of indicator in the range of permissible rates of pressure rise. The difference in readings increases with an increase in the rate of

pressure rise. Indicator cards were taken with the Farnboro electric indicator (reference 6) during the course of its remodeling.

No attempt was made to operate the engine at a particular value of maximum cylinder pressure in the early test work, inasmuch as undesirable knock was encountered before objectionable cylinder pressures were reached; instead, the fuel pump was adjusted to give the desired fuel quantity and then the timing was advanced until a faint knock was heard. Immediately after a power test the engine was motored and friction readings were obtained to which were added the brake readings in order to calculate values of indicated mean effective pressure and fuel consumption.

Engine speed was determined by a revolution counter and a stop watch, both of which were electrically

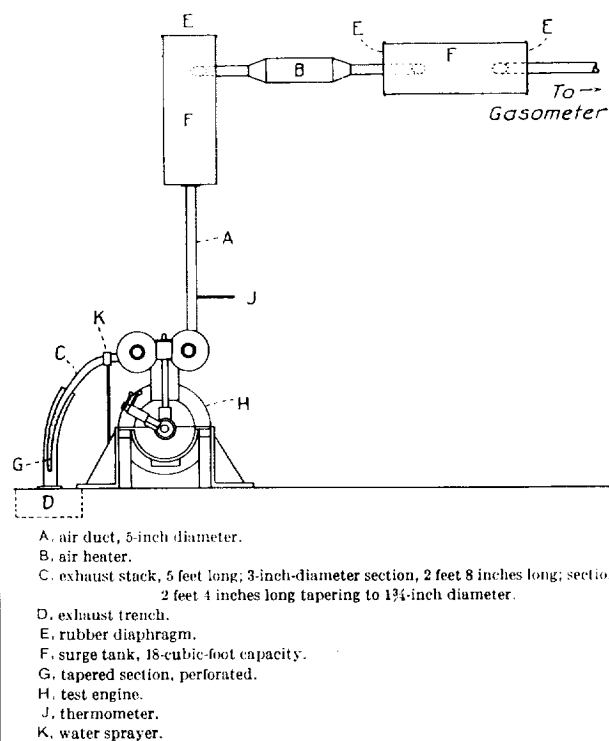


FIGURE 6. Diagrammatic representation of air system.

operated. The standard test speed of 1,500 r. p. m., unless otherwise noted, was used in all the tests.

TESTS AND RESULTS

PRELIMINARY INVESTIGATION

The test results obtained on the engine with different arrangements of fuel-valve nozzles are presented in chronological order in table I, which lists the nozzles used, the number, size, and direction of their discharge orifices, and their corresponding engine performance. The nozzles are classified into different series, each of which is discussed in detail and for which variable fuel-quantity performance curves are shown.

Miscellaneous series.—The first experimental nozzles were built with the idea of injecting fuel into the

available air without impingement on either the piston crown or the combustion-chamber walls. Figure 7 shows the engine performance obtained with nozzles 3, 4, and 7 and the limited fuel-quantity range imposed by the use of the relatively small orifice areas to prevent impingement; it also shows the engine performance with both the high and low rates of injection.

sprays from the small orifices with their shorter penetration would distribute fuel to that part of the combustion chamber nearer the injection nozzle and thus give a more uniform mixture of the fuel and the air. A comparison of the performance curves for the high and low rates of injection of nozzle 9 (fig. 7) shows that they are quite similar except for the maximum cylinder

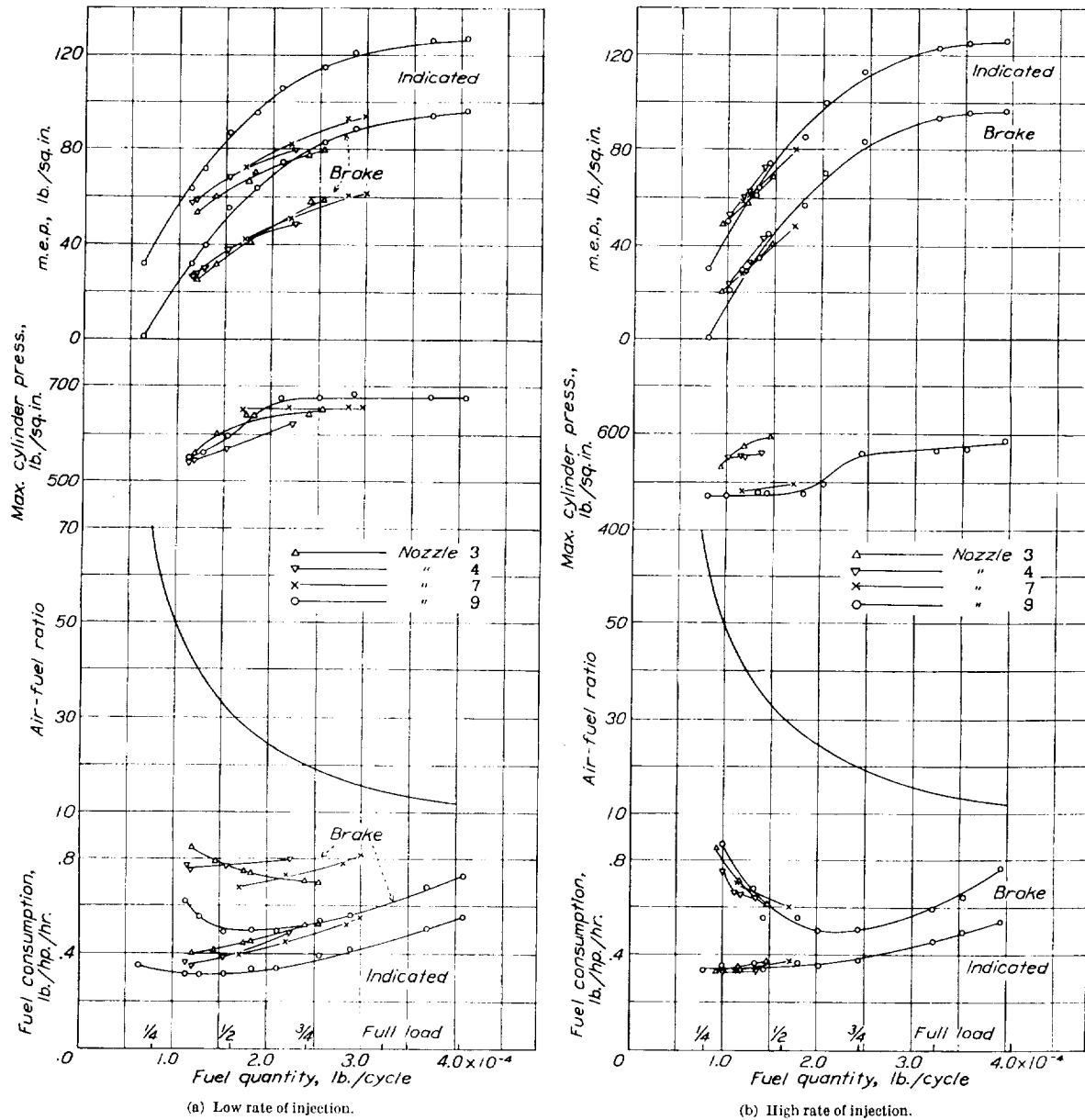


FIGURE 7.—Comparison of engine performance using preliminary nozzles.

(See fig. 4.) The fuel-quantity range of the small-area nozzles is slightly extended by the use of a lower rate of injection and the accompanying longer injection period.

Seven-orifice series.—The design of nozzle 9, the first of the 7-orifice type having alternate large and small orifices, was based on the assumption that the

pressure, which is higher for the low rate of injection. Engine operation was considerably smoother with the low rate of injection but the exhaust was smokier for the same air-fuel ratios. The high rate of injection with its shorter injection period resulted in earlier completion of combustion, a cleaner exhaust, and somewhat higher rates of pressure rise with conse-

quently rougher engine operation. The high rate of injection was adopted for all subsequent tests and fuel nozzles were developed for its use.

The engine performance obtained with nozzle 9 warranted the continuation of tests to determine the effect on engine performance of varying, first, the two main orifices that deliver fuel to the air charge in the rectangular throat and directly above the piston crown and, second, the other orifices that deliver fuel to the air in the upper part of the combustion chamber. Figure 8 shows comparative engine performance for a range of

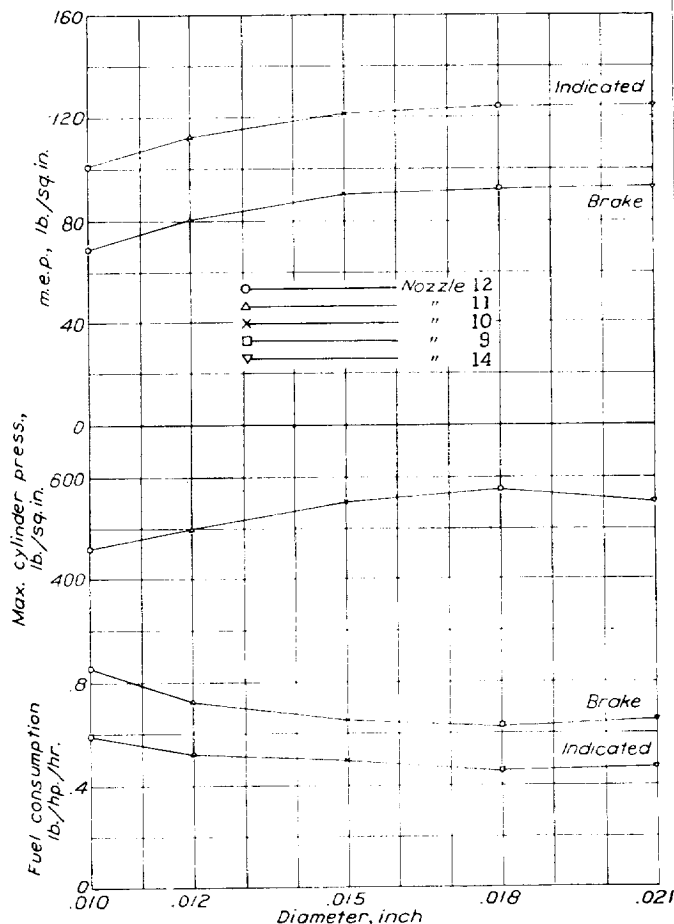


FIGURE 8.—Effect of changing the diameter of the two main orifices B on engine performance at full load.

sizes of the two main orifices B (fig. 5) from 0.010 to 0.021 inch diameter. The results show that 0.018 inch is the optimum diameter for the two main orifices of this combination.

An inspection of the carbon formation on the piston crown showed that the sprays from orifices of 0.012-inch diameter or larger impinged upon the piston crown. Inasmuch as the specific fuel consumption decreased as the B orifices were enlarged to 0.018 inch, it is concluded that impingement of a spray does not necessarily affect the combustion adversely. The larger quantity

of fuel injected from the 0.018-inch orifices, compared with that injected from the 0.012-inch orifices, was apparently necessary for the utilization of the available air.

Variation in volumetric efficiency with fuel quantity is shown in figure 9. The decrease in volumetric efficiency is attributed to an increase in the quantity of residual gases in the combustion chamber and also to an increase in temperature of the combustion chamber and cylinder walls, as the fuel quantity or load is increased.

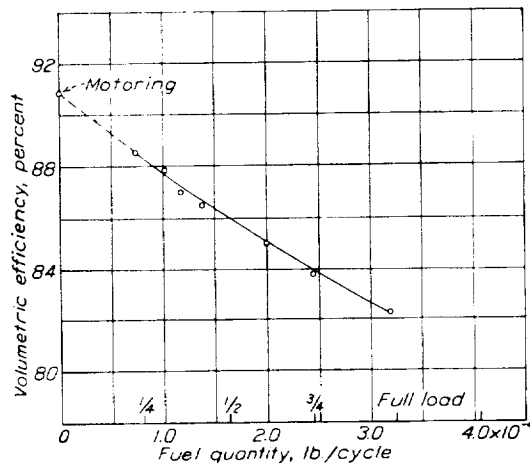


FIGURE 9.—Effect of load on volumetric efficiency.

Figure 10 shows the effect on engine performance of changing the diameters of only the outside orifices D (fig. 5), which deliver fuel to the air in the uppermost part of the combustion chamber, from 0.006 inch to 0.012 inch in nozzles having two 0.018-inch-diameter main orifices. From the results, 0.010 inch appears to be the optimum diameter for the outside orifices. An increase in diameter of these two orifices from 0.010 to 0.012 inch caused a slightly smokier exhaust with no measurable change in power output. Table I shows the effect on engine performance of changing the C orifices from 0.005 inch to 0.012 inch. The difference in performance between nozzles 17 and 18 indicates that the C orifices should be considered as fillers when used in combination with the larger D orifices. This change from 0.005 to 0.012 inch decreased the power output and increased the fuel consumption. Spray photographs (see fig. 19 (b)), taken afterward, showed that the spray tips from orifices C and D were projected into the same space, which probably resulted in localized overrich mixtures of fuel and air and a consequent decrease in engine performance.

PROPORTIONAL-AREA INVESTIGATION

Nine-orifice series.—The 9-orifice series was so designed that the orifice areas were proportional to the volume of air served by each orifice. The two main 0.018-inch-diameter orifices, which were apparently a

better established optimum than the other sizes of orifice and which could be compared with previous data, were used as a beginning for the investigation. When the air volume for each orifice was computed, the air in the clearance between the piston crown and cylinder head was included in that served by the main sprays. The angular spacing of the orifices in this series was slightly closer than that used in the 7-orifice series and an additional orifice was added on each end of the line, making a total of nine in one plane. Nothing

air that had not been reached by the two main sprays.

Effect of number of orifices, E series.—Figure 12 gives a comparison of engine performance with one of the best 7-orifice and one of the best 9-orifice nozzles. It was decided to continue the use of the proportional-area principle but to substitute for the original angular spacing (fig. 5) one based upon the spray-photography data. The spray photographs showed that the spray cone angle for sprays under comparable conditions,

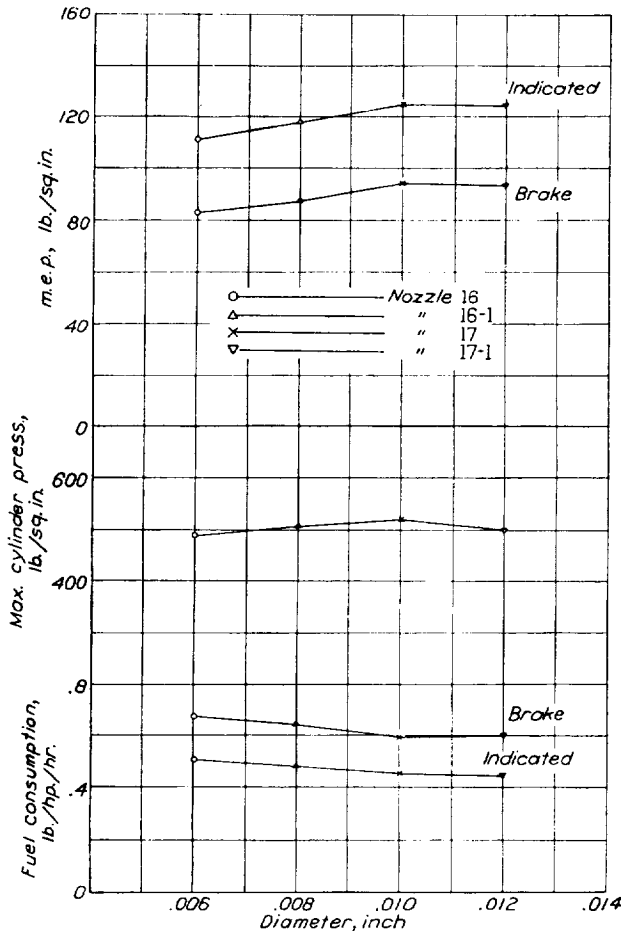


FIGURE 10.—Effect of changing the diameter of the two outside orifices D on engine performance at full load.

either in the performance data or in the spray photographs (see fig. 19(f)) indicates that these additional orifices discharged enough fuel to make any difference in performance; therefore their addition is considered an unwarranted complication.

The first nozzle of this series was built without the small center orifice A (fig. 5) (which has no place in the proportional-area arrangement) in an attempt to determine its value. The increase in engine performance (see fig. 11) showed the effect of this center orifice. The center spray of this particular orifice combination and angular spacing apparently reached

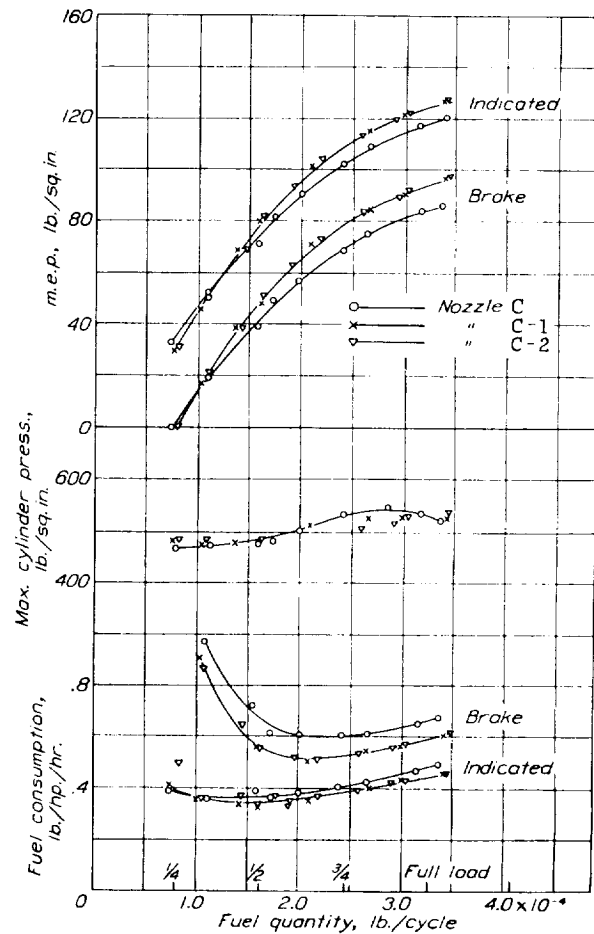


FIGURE 11.—Effect of the center orifice A on engine performance.

except for temperature, varied from 18° to 22°. Accordingly, 20° was adopted as the angular spacing of all the orifices.

In order to determine just how far it was advisable to follow the proportional-area principle, comparative performance tests were made with nozzles designed to extend the idea beyond practicable limits in the construction of nozzles for commercial engines. Before these tests were started the throat orifice connecting the cylinder and combustion chamber (fig. 2) was enlarged by increasing its width. This alteration increased the clearance volume and thereby decreased

the compression ratio from 13.6 to 12.6. It was desired to continue to use a nozzle design that would be comparable with the designs used in former tests; therefore the diameters of the two main orifices were maintained at 0.018 inch and the volume of air in the mechanical clearance space between the piston crown and the cylinder head was added to that served by the main orifices. These nozzles are designated by the letter E; the subscript denotes the number of orifices in the nozzle at the time of test. Thus this series was started with nozzle E₂, which contained only the two main orifices. The number of orifices was increased

involved is smaller than the experimental error. The performance tests shown in figures 14 and 15 indicate that no justifiable gain would be obtained by using more than six orifices for this combustion chamber. The test points of figure 14 have been omitted to save confusion. These results simplified subsequent nozzle design.

Effect of angular spacing, F series.—There were a number of indications during these tests that the 20° angle between sprays was not the optimum. About this time the results of the work on dispersion at Pennsylvania State College were published (reference 7) and, according to the method outlined by deJuhasz the boundaries of combustion were laid out for the F₆ nozzle as shown in figure 16. If the volumes within these boundaries are assumed to be the minimum space requirements for combustion, it is evident that the sprays overlap and probably interfere with each other during combustion. An investigation was accordingly made of the effect on engine performance of varying the angle between the spray axes of the individual sprays; the corresponding orifice sizes were maintained constant.

When the series of nozzles using different angular spacing of the orifices was designed, it was again necessary to deviate from the proportional-area principle because the volume of air served by each orifice changed with the angle. The fact that the corresponding orifice sizes were maintained the same for all angles caused a departure from the proportional-area principle of about 1 percent, which was neglected as it was less than the error in the determination of performance values.

The nozzles of this series are designated by the letter F with a subscript denoting the angle between the axes of the orifices. Thus, the F₆ and the F₂₀ are identical nozzles, with six orifices spaced at 20°. The performance tests of these nozzles showed very little variation, as evidenced by the curves in figure 17, but observation of the exhaust gases and the sensitiveness to controls led to a decision to standardize on an angle of 25° for further work with this combustion chamber. As a check on this decision, two 0.005-inch orifices were added to the center of the F₂₅ nozzle to see if any unused air remained between the two main sprays. The resulting increase in performance, as shown in the curves of figure 18, indicated that the small filler sprays are effective when the angle between the sprays on either side is too great.

From the test results it was concluded that a nozzle having an angular spacing of 25° would give the best performance and that any increase which could be obtained by further refinements in nozzle design would not be commensurate with the complication involved in its construction. The results, however, did not show angular spacing to be very critical within the range covered in these tests, possibly because of the

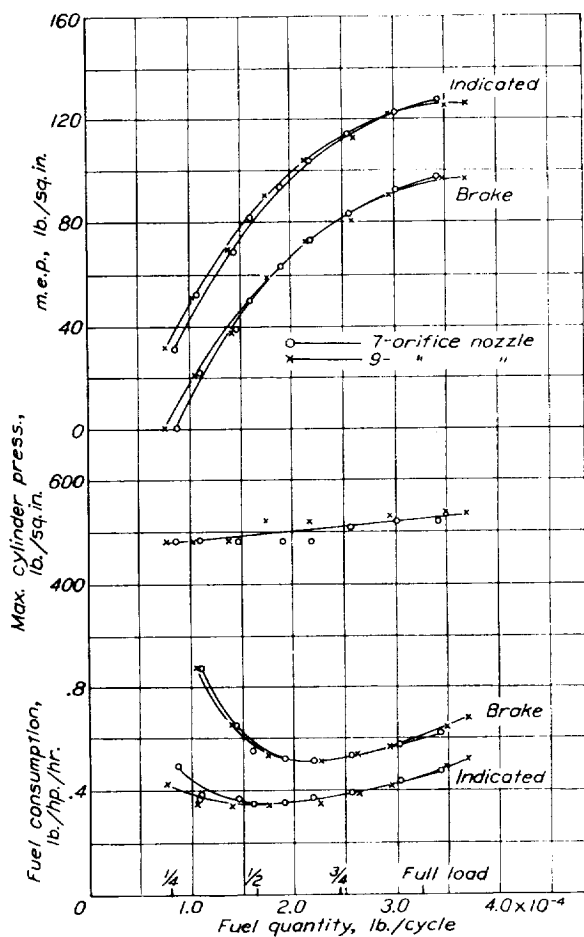


FIGURE 12.—Comparison of engine performance using one of the best 7-orifice and one of the best 9-orifice nozzles.

by increments of two and the nozzle performance tested for each increment. At the end of the series there were 6 orifices in one plane and 5 orifices in a plane on each side of the first, with angular spacing of 20° between orifices and 10° between planes. (See fig. 13.)

There is a slight deviation from the proportional-area principle in the E series after E₁₂ because it was considered impracticable to use orifices smaller than 0.005-inch diameter. This deviation is not serious because the percentage of the total orifice area in-

small percentage of fuel in the outer part of the spray as shown by the dispersion data in reference 7.

Effect of total orifice area, H series.—In anticipation of boosting tests to be started with this cylinder head, it was considered that an increase in total orifice area should be investigated because, with more air available for combustion, it would naturally follow that more fuel should be supplied.

The nozzles of this series were designated by the letter H. The increase in the total orifice area over that of the best of the E and F series, E₆, was 24 percent, 39 percent, 15 percent, and 65 percent, for nozzles H-1, H-2, H-3, and H-4, respectively. The

The nozzle-area requirements, then, depend not upon air density but rather upon the combustion chamber size and shape, the injection period desired, the rate of injection, the engine speed, and the capacity of the injection pump.

Correction to proportional-area design.—One of the assumptions in the application of the proportional-area principle in nozzle design is that the same discharge pressure will be acting on each orifice in a multiple-orifice nozzle. Observation of the fuel spray in the atmosphere indicated that, as the areas of the orifices were increased for greater discharge area, the flow of fuel from the large main orifices reduced the effective

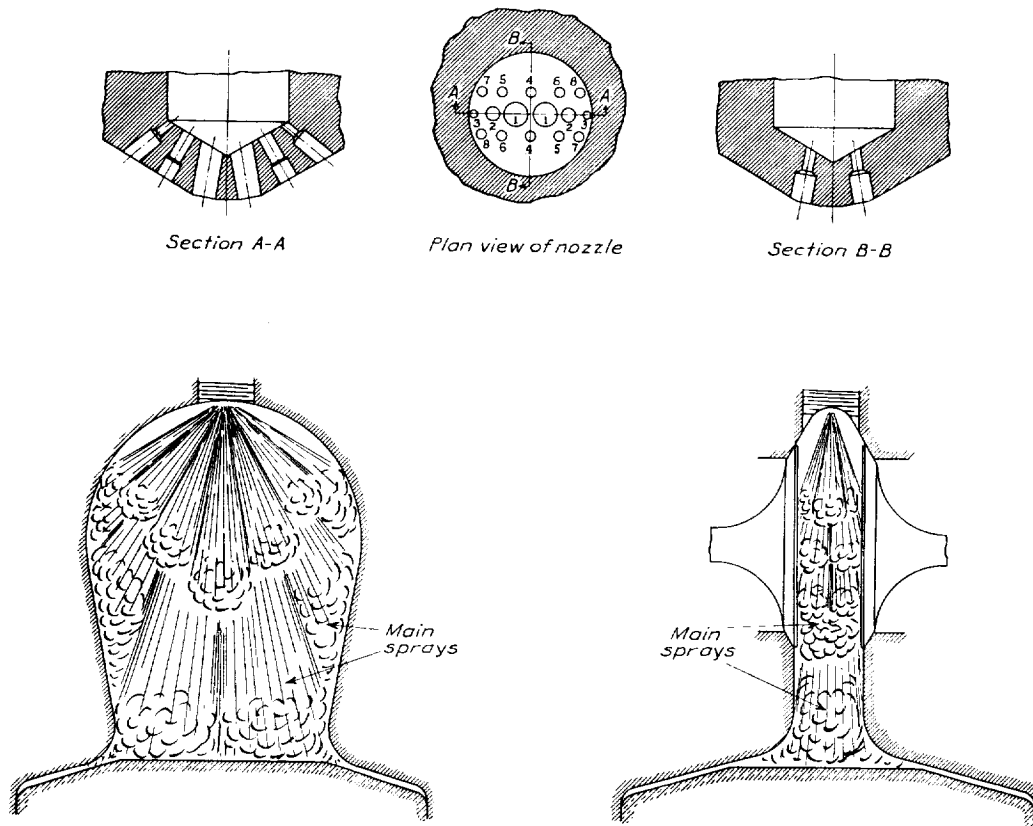


FIGURE 13.—Projected spray distribution using nozzle E₁₄.

increase in air density for 9 inches of mercury boost pressure is about 24 percent. The corresponding orifices in nozzle H-1 were therefore increased 24 percent in area. In nozzles H-2, H-3, and H-4 the two large orifices were chosen to give successive increases in discharge area and the smaller orifices were proportionally increased.

The nozzles of this series produced but little difference in the unboosted performance (table I) or in subsequent tests with boosting. They did, however, give smoother engine operation than the nozzles of smaller area owing to localized overrich mixtures in the combustion chamber, resulting in lower rates of burning and consequently lower rates of pressure rise.

pressure on the other orifices and, therefore, the fuel distribution did not fulfill the requirements expected of the particular nozzle. This lack of proportion was verified by catching sprays from individual orifices in a container with a long neck (reference 8). The sum of the weights of the sprays from the individual orifices caught in this way checked within ± 1 percent the weight of the sprays from all the orifices caught simultaneously under the same conditions. The areas of the orifices discharging insufficient fuel were increased until all spray discharges were in the proper ratio. A nozzle designed for a shortened combustion chamber (compression ratio 15.3) and designated K-4 was developed by this procedure and is considered the

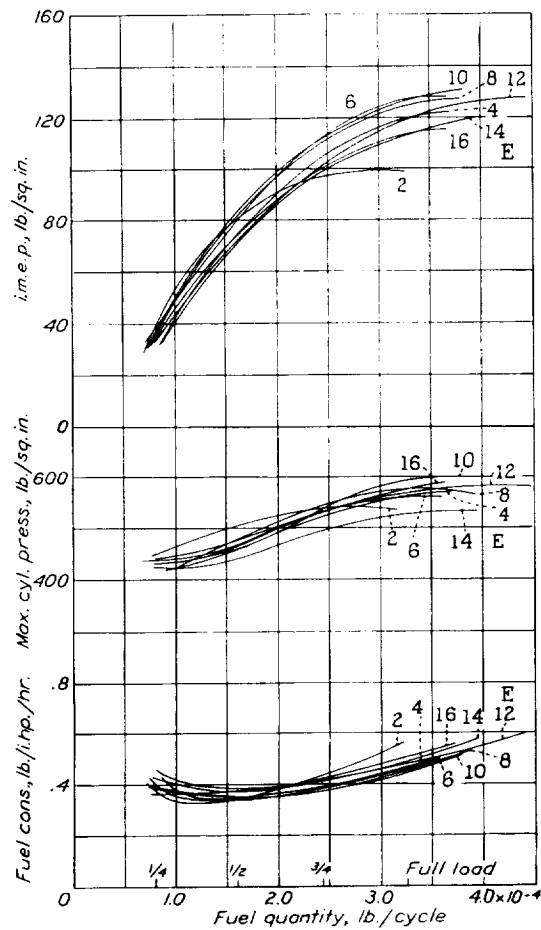


FIGURE 14. -- Comparison of engine performance using injection nozzles E_2 to E_{16} , variable fuel quantity.

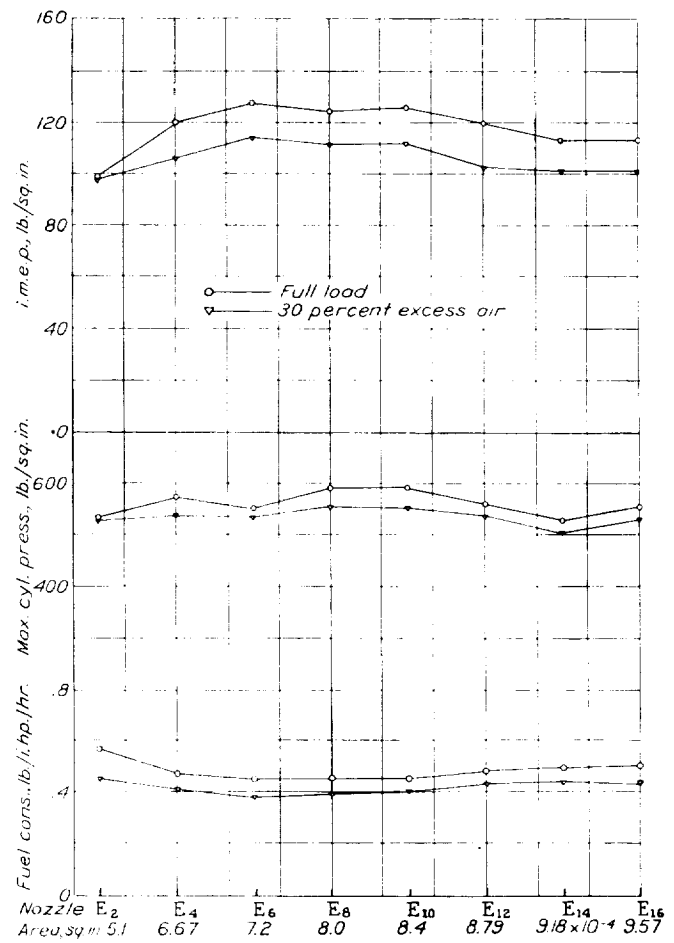


FIGURE 15. -- Comparison of engine performance using injection nozzles E_2 to E_{16} .

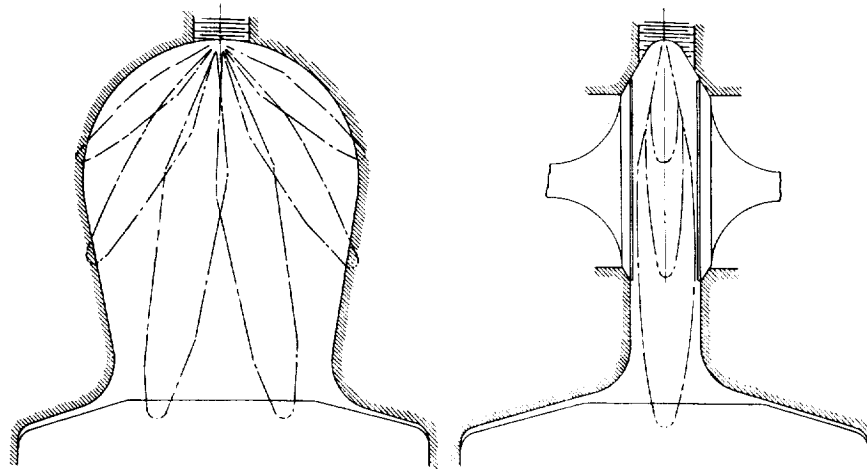


FIGURE 16. -- Boundaries of combustion for nozzle E_4 .

best of the development series. Knowledge gained from the tests of the preceding H-series nozzles and of the original K nozzle with its subsequent alterations aided in determining the final orifice sizes of nozzle K-4.

SPRAY PHOTOGRAPHS

The spray photographs shown in figure 19 were taken during development work with the 7- and 9-orifice series. Figures 19(a) and 19(b) show photographs of the sprays from nozzle 9 with injection pressures of 4,750 and 3,200 pounds per square inch, corresponding

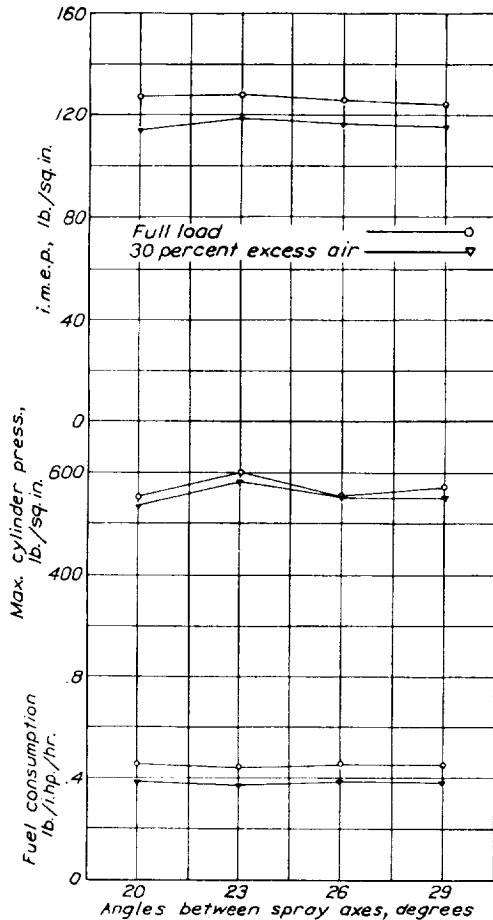


FIGURE 17.—Effect of spray spacing on engine performance, F nozzles.

to the maximum injection pressure at full load for the high and low rates of injection, respectively.

Figure 19(c) shows a photograph of the sprays from nozzle 17-1, which is similar to nozzle 9 except that the outer orifices are of 0.012-inch diameter instead of 0.008-inch. The outer sprays in this nozzle struck the sides of the chamber and were deflected downward into otherwise unreachable air, thereby aiding the fuel distribution. Figure 19(d) shows spray photographs for nozzle 16-2 with 0.008-inch-diameter outer orifices.

136892—37—29

Figure 19(e) shows photographs of sprays from nozzle 12, which had two main orifices of 0.010-inch diameter as compared with an 0.018-inch diameter for all other nozzles. Owing to the reduced orifice area, the pressure at the high injection rate was 6,800 pounds per square inch as compared with 4,750 pounds per square inch for other nozzles.

Figure 19(f) comprises photographs of sprays from the 9-orifice nozzle C-2. Lack of a more pronounced outline of the sprays may be caused by crowding these comparatively large sprays.

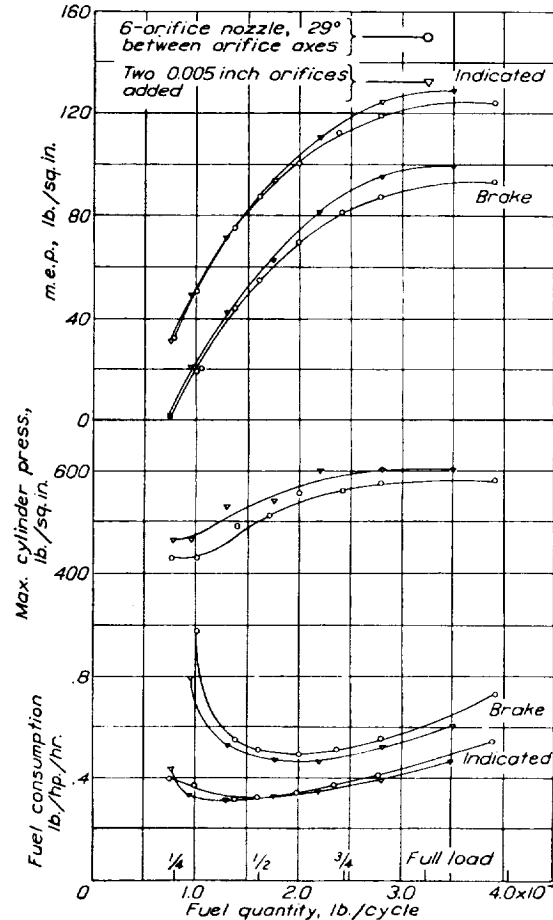
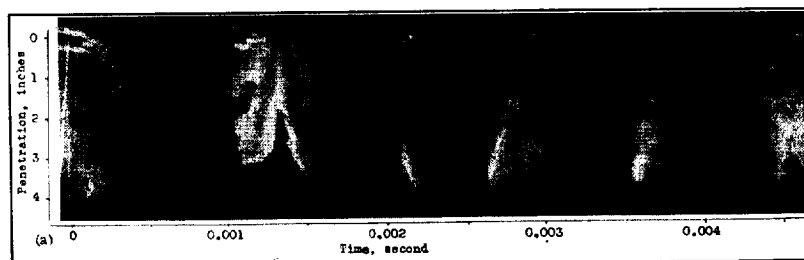
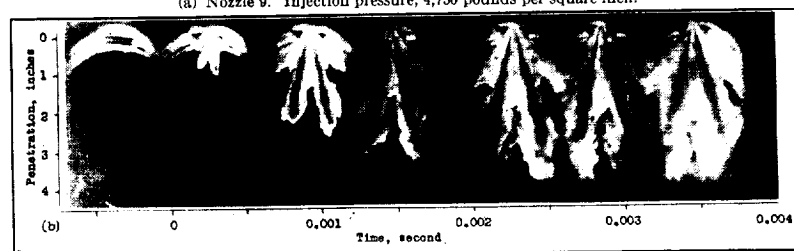


FIGURE 18.—Effect on engine performance of adding auxiliary orifices to nozzle F₁₂.

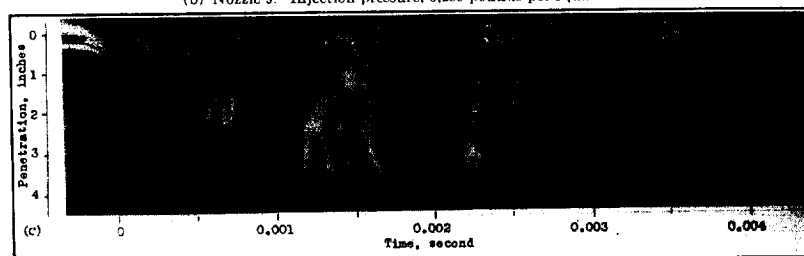
Owing to the very uneven distribution of the fuel in the sprays, visual observation of fuel injected into the air or photographs of sprays from multiple-orifice nozzles are not to be relied upon as bases for judging the fuel distribution in a combustion chamber or for estimating the relative engine performance of a particular nozzle design. This conclusion is based on the general results obtained with this quiescent combustion chamber and is borne out particularly by the E-series nozzles.



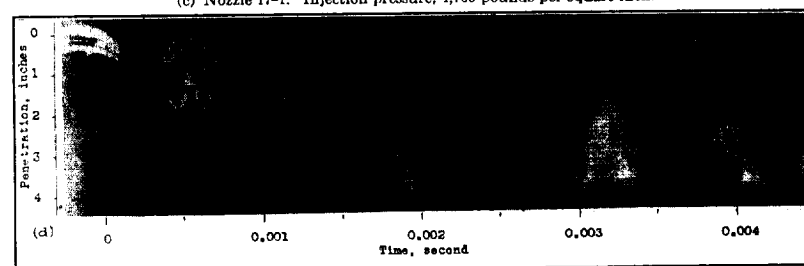
(a) Nozzle 9. Injection pressure, 4,750 pounds per square inch.



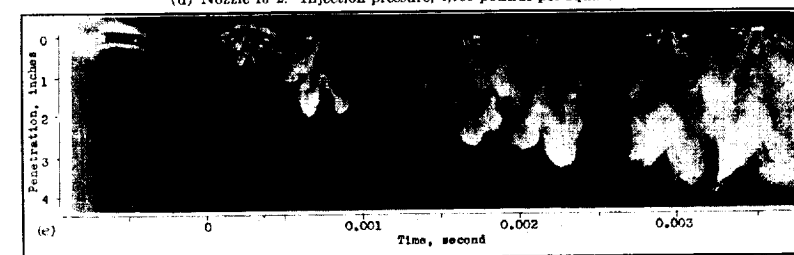
(b) Nozzle 9. Injection pressure, 3,200 pounds per square inch.



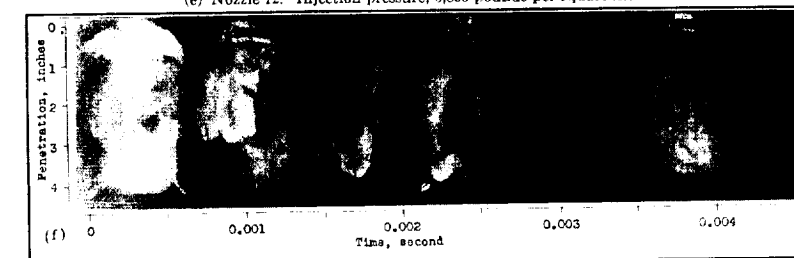
(c) Nozzle 17-1. Injection pressure, 4,700 pounds per square inch.



(d) Nozzle 16-2. Injection pressure, 4,700 pounds per square inch.



(e) Nozzle 12. Injection pressure, 6,800 pounds per square inch.



(f) Nozzle C-2. Injection pressure, 4,700 pounds per square inch.

FIGURE 19.—Photographs of fuel sprays.

MISCELLANEOUS ENGINE TEST RESULTS

Variable engine speed.—Figure 20 shows engine performance for a speed range of from 700 to about 1,700 r. p. m. for a compression ratio of 15.3 and full-load fuel quantity, using the K-4 nozzle. Operation at full load below 700 r. p. m. was not satisfactory, although the engine could be idled at 175 r. p. m. The downward trend in the indicated mean effective pressure at

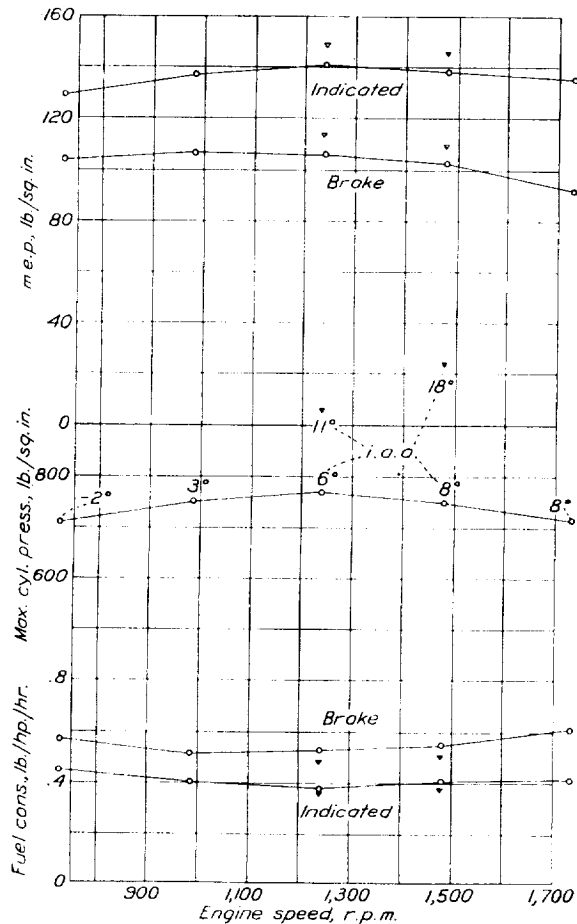


FIGURE 20.—Effect of engine speed on engine performance at full load; nozzle K-4; i. a. a., indicated.

the higher speed is caused by decreased volumetric efficiency because the valve timing was better suited to the 1,200–1,500 r. p. m. range than to the higher speed range.

The effect upon performance of increasing the injection advance angle and therefore the maximum cylinder pressure is shown for the 1,200–1,500 r. p. m. speed range. Although mechanical limitations made it inadvisable to operate the single-cylinder test engine at higher speeds, there was nothing in the fuel-system or engine-combustion characteristics to indicate that higher speeds could not be advantageously used.

Boosting.—The effect of boosting when the quiescent combustion chamber is used will be only briefly mentioned since a complete report of the boosting results with and without valve overlap has already been published (reference 8). The indicated power generally increases proportionately with the increase in weight of the inducted air charge available for combustion. This proportionality is, of course, affected by air-fuel ratio, injection-advance angle, and scavenging. Boosting, then, merely extends the performance curves and does not essentially change their characteristics.

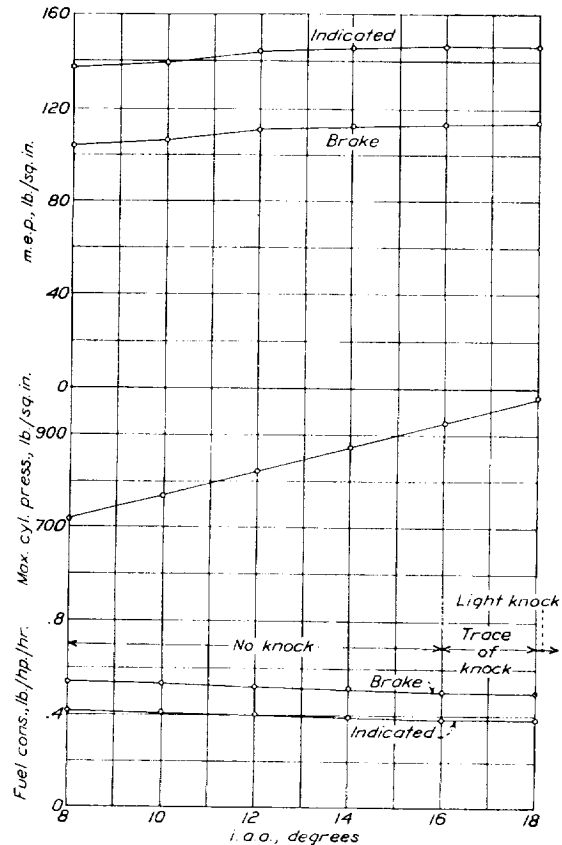


FIGURE 21.—Effect of injection advance angle on engine performance at full load; nozzle K-4.

It was found that the engine operated considerably smoother when boosted. The balanced-diaphragm maximum-cylinder-pressure indicator showed that the difference in maximum cylinder pressure between individual cycles becomes considerably less than when the engine is unboosted. This condition is again indicated by the smooth, even line and by the absence of scattered points on the indicator card.

Compression ratio.—In addition to performance tests at the adopted standard compression ratios of 13.6 and 12.6, performance tests were conducted at compression ratios of 10.6 and 15.3, which are about

the practicable limits obtainable with this cylinder head. The preliminary test results showed little difference in specific power output and fuel consumption for compression ratios of 10.6, 12.6, 13.6, and 15.3 for the same ratio of maximum cylinder pressure to compression pressure. The engine-operating characteristics, however, were found to be quite different. At a compression ratio of 10.6, starting was difficult and the ignition lag under standard test conditions was more

The more homogeneous mixture of fuel and air and the shorter ignition lag permitted the use of higher cylinder pressures, which resulted in better engine performance.

Figure 21 shows the effect of injection advance angle on engine performance. This performance, with the K-4 nozzle, is the best obtained with the quiescent chamber with normal aspiration. The valve timing was changed to give a very small overlap, which prob-

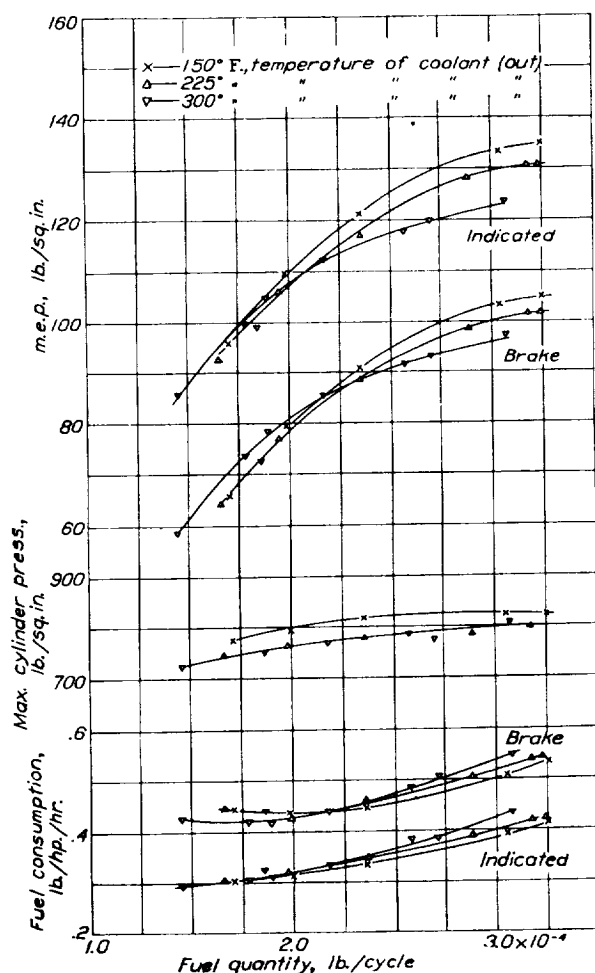


FIGURE 22.—Effect of coolant temperature on engine performance; i. a. a., 21°; nozzle H-1.

than one-third longer than that obtained at a compression ratio of 15.3. The rate of pressure rise at the lower compression ratio as determined from indicator cards was nearly double the corresponding values obtained at a compression ratio of 15.3. Starting was easy at the higher compression ratio, the explosion pressures were more uniform, and the engine operation was considerably smoother than at the lower compression ratios.

The shortened, compact combustion chamber at the compression ratio of 15.3 simplified fuel distribution.

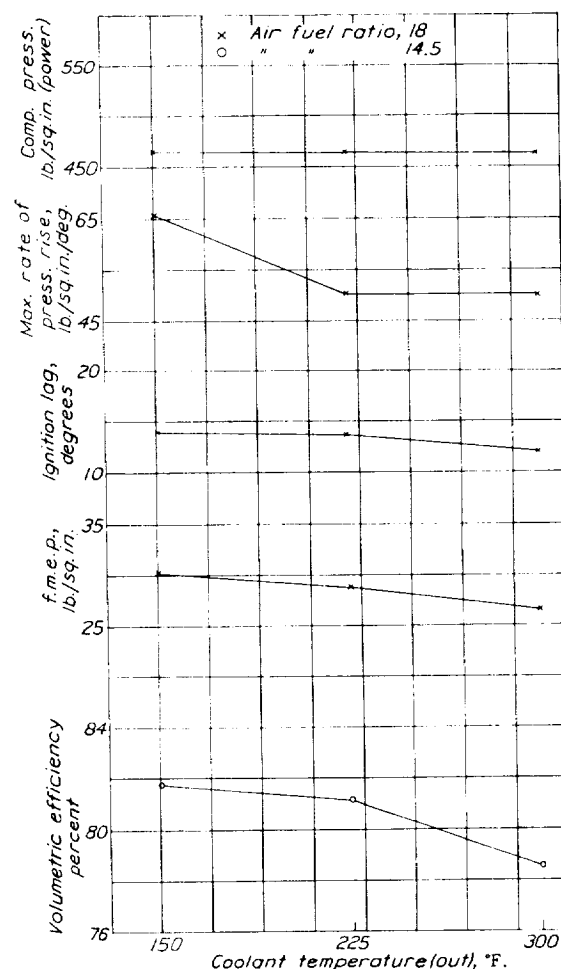


FIGURE 23.—Effect of coolant temperature on engine operating characteristics; i. a. a., 21°; nozzle H-1.

ably aided in scavenging the combustion chamber and improving combustion. (See reference 8.)

High-temperature cooling.—Figures 22 and 23 show some of the effects on engine performance and operating characteristics of increasing the coolant temperature from 150° to 300° F. in an attempt to reduce the ignition lag. The test results and observations showed: a 4-percent decrease in volumetric efficiency, objectionable breather smoke from the hot piston at full load, difficulty in maintaining the high boiling point of the coolant due to absorption of moisture, an 8-percent

decrease in power and a corresponding increase in fuel consumption at full load, a 12-percent decrease in friction mean effective pressure, a decrease in ignition lag, a decrease in the rate of pressure rise in the cylinder, and smoother engine operation. Obviously the gain obtained from the decreased friction losses and probably lower losses to the coolant when using high-temperature cooling cannot compensate for the loss in performance occasioned by the lowered volumetric

and Waldron (reference 9) regarding the effect of engine-jacket temperature on combustion in a compression-ignition engine.

Because of the high temperatures and the small volume of the coolant used, it was not practicable to investigate the heat losses to the coolant. With water as the coolant and at standard operating temperatures, however, the heat loss to the coolant was about 24 percent of the total heat of the fuel and changed little

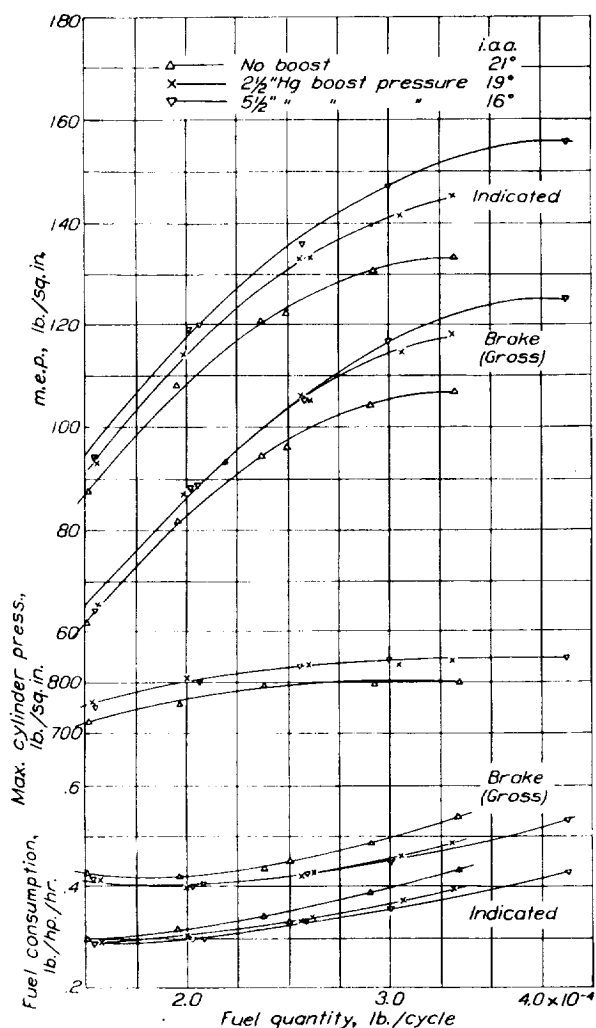


FIGURE 24.—Effect of boost pressure on engine performance at a coolant temperature of 265° F.; nozzle H-1.

efficiency and the adverse effect on combustion. The reduction in the ignition lag resulted in a correspondingly earlier occurrence of high temperatures in the combustion chamber, which probably caused fuel from the latter part of the injection to pass through regions of high temperatures which, in turn, reduced the penetration and prevented some of the fuel from reaching sufficient air for combustion. These results and conclusions are in agreement with those of Rothrock

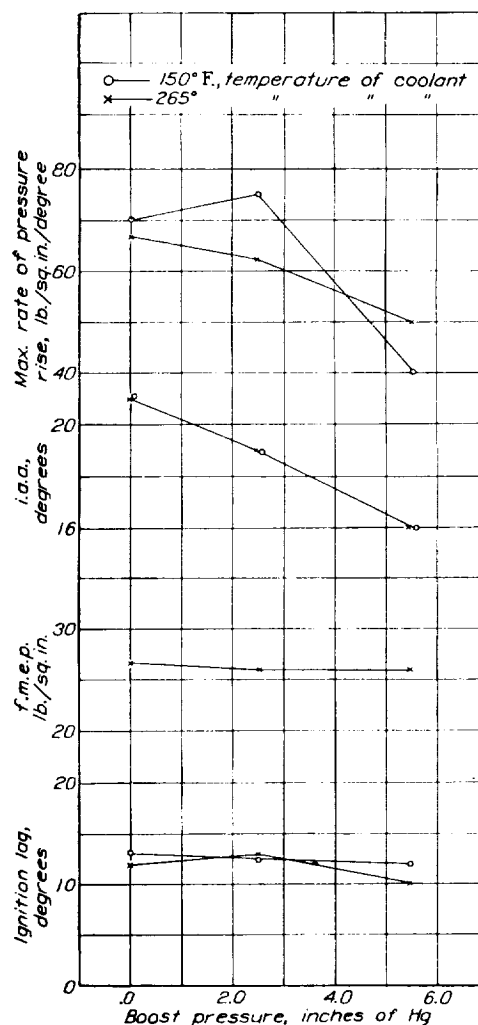


FIGURE 25.—Effect of boost pressure and coolant temperature on engine-operating characteristics; nozzle H-1.

with change in load. Figures 24 and 25 show that boosting did not change the trend of the curves for the general operating characteristics or for the performance at high coolant temperatures.

Indicator cards.—Figure 26 shows a typical pressure-time card of the quiescent combustion-chamber engine for a compression ratio of 15.3, full-load fuel quantity, and 1,500 r. p. m., with both an optimum and a retarded injection advance angle. The line cut was

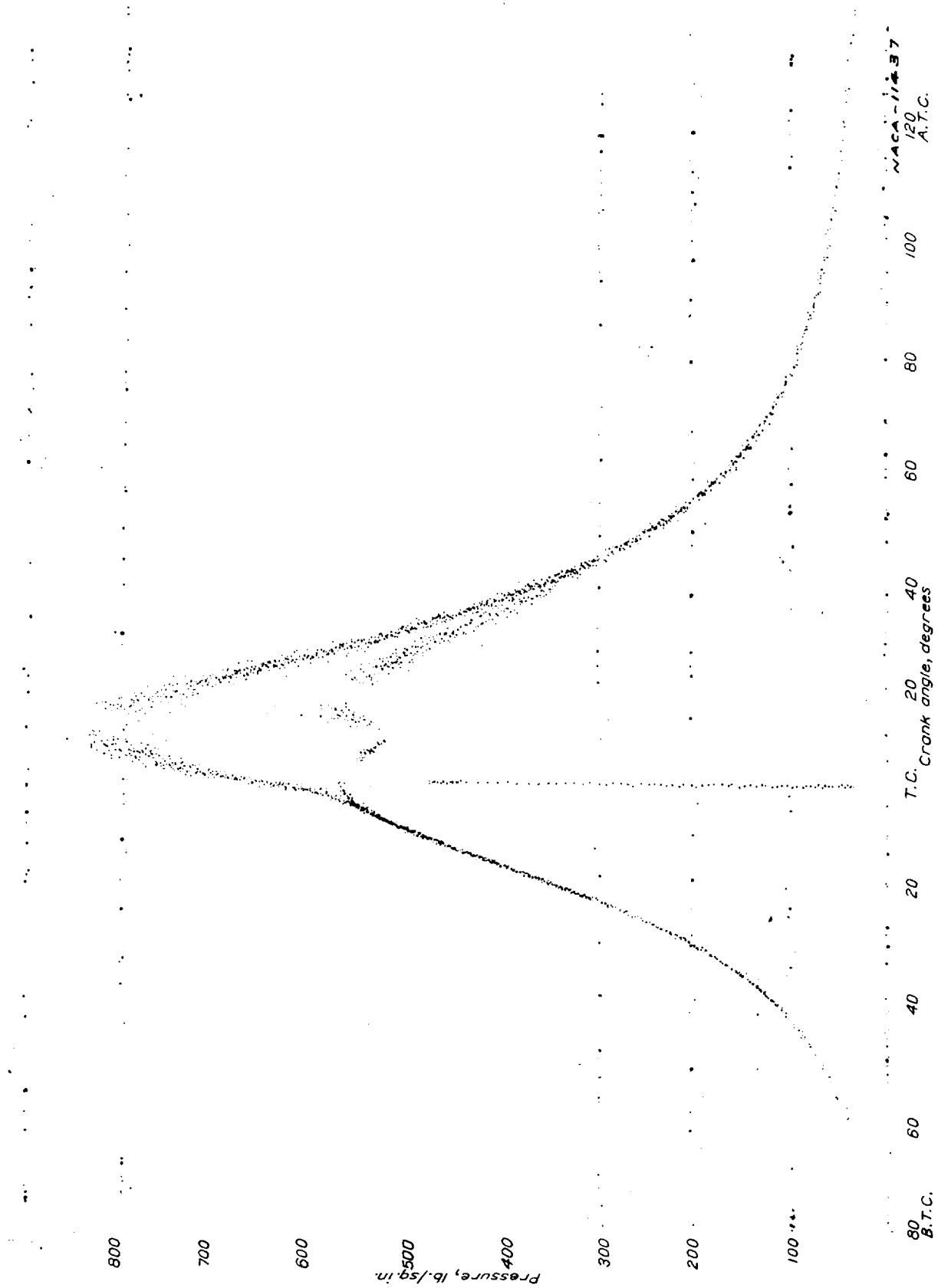


FIGURE 26 - Typical indicator cord, optimum and retarded i. a. a.

made from a copy of the original card recorded directly on a special thin white paper. With the optimum injection advance angle, two general rates of pressure rise may be noted—in this case 40 and 20 pounds per square inch per degree; the breakaway occurs about 4° before top center. The earlier occurrence of the higher rate is believed to be caused by comparatively rapid and uncontrolled combustion when burning starts, owing to the ignition lag and the more favorable

that orifices smaller than 0.008 inch or larger than 0.020 inch need not be used.

A study of fuel-dispersion data (reference 11) shows the very uneven fuel distribution in the fuel spray and the large percentage of the total fuel contained in the relatively solid core of the spray; these factors are reflected in the values of specific fuel consumption, power output, and cloudy exhaust. These results show the futility of trying to obtain a truly homogeneous mixture of fuel and air in a quiescent combustion chamber with a nozzle having round-hole orifices. Random tests with two injection valves, the other two valve locations, and nozzles having other types of orifices, such as the impinging jets, the pintle, and the slit (reference 11), resulted in engine performance considerably inferior to the performance obtained with nozzles having round-hole orifices in one valve in the top location. It thus appears that the quiescent combustion chamber has inherent limitations that prevent it from attaining the high performance ultimately expected of the compression-ignition aircraft engine.

At the beginning of 1934 this quiescent chamber was converted into an air-flow chamber by the use of a displacer piston. The preliminary performance results (reference 12) were so satisfactory and so far superior to those obtained with the quiescent chamber (fig. 27) that work with the quiescent chamber has been discontinued. The air-flow type of combustion chamber apparently offers considerably greater possibilities of development than the quiescent chamber.

CONCLUSIONS

The results of these investigations indicate that:

1. The engine performance obtained by proportioning the areas of the orifices to the volumes of air to be served by each orifice was approximately the same as that obtained by varying all the orifice sizes and determining from the engine power the optimum combination. Neither method, however, is complete in itself; the use of both should yield the best results.

2. In a multiorifice fuel-injection valve nozzle for a vertical disk-type quiescent combustion chamber, there is no sharply defined optimum value for the number, direction, or size of the orifices. A 6-orifice nozzle gave power and economy equal to or better than that obtained with any other number and arrangement of orifices.

3. The rate of injection influences the rate of pressure rise in the cylinder and apparently the severity of combustion shock.

4. Although the results do not afford a rational basis of nozzle design that can be reduced to an analytical or empirical formula, they do show that engine performance can be improved by careful design of the injection nozzle.

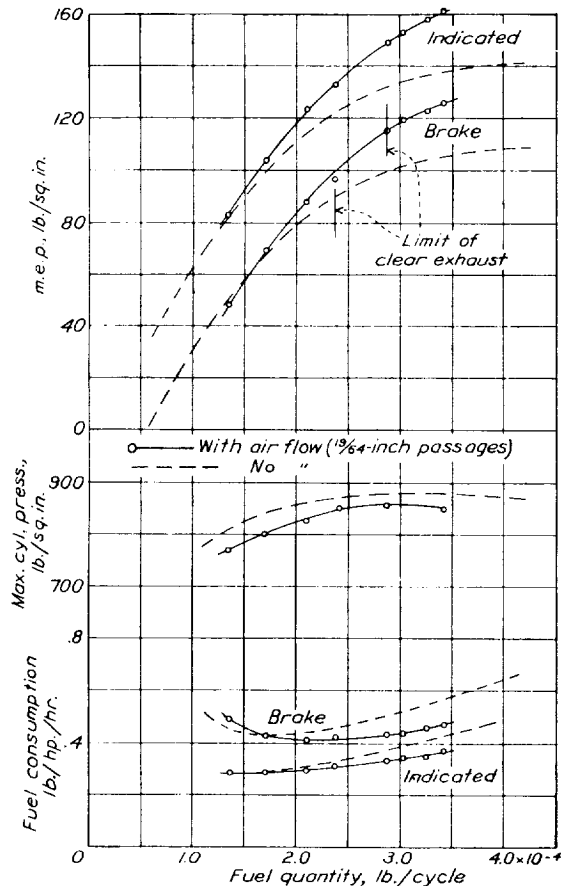


FIGURE 27.—Comparison of engine performance with and without air flow. Double-passage displacer; 1,500 r. p. m.

conditions in the combustion chamber for air and fuel mixing. Fuel injected after the burning starts reaches the remaining available air with increasing difficulty; hence there are slower burning and lower rates of pressure rise for the last part of the fuel injected. These conclusions are in agreement, generally, with those of Ricardo (reference 10) and with those regarding the behavior of this engine observed over a wide range of test conditions.

Remarks.—No trouble was experienced on account of the clogging of the small orifices in the fuel-valve nozzle. The fuel was usually centrifuged and the test runs were intermittent rather than of long duration, rarely exceeding 4 hours. The engine tests indicate

TABLE I.—NOZZLE CHARACTERISTICS AND CORRESPONDING ENGINE PERFORMANCE; ENGINE SPEED, 1,500 R. P. M.—Continued


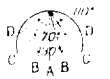




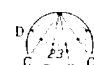
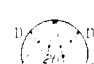
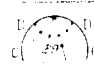

Orifice arrangement	Nozzle	Total orifice area (sq. in.)	Orifice diameter (inch)	Total orifice area (percent)	I. m. e. p.		Indicated fuel consumption		Maximum cylinder pressure (lb./sq. in.)	Full-load fuel with clear exhaust (percent)	Compression ratio
					¾ full load (lb./sq. in.)	Full load (lb./sq. in.)	¾ full load (lb./i. hp.-hr.)	Full load (lb./i. hp.-hr.)			
7-ORIFICE SERIES—HIGH RATE OF INJECTION FOR THIS AND SUBSEQUENT SERIES											
	9	0.00069	A = .007 B = .018 C = .005 D = .008	A = 5.58 B = 36.8 C = 2.84 D = 7.25	112	124	0.380	0.420	573	66	13.6
	10	.00053	A = .007 B = .015 C = .005 D = .008	A = 7.26 B = 33.2 C = 3.7 D = 9.42	100	121	.430	.490	550	64	13.6
	11	.00041	A = .007 B = .012 C = .005 D = .008	A = 9.52 B = 28.0 C = 4.85 D = 12.3	97	112	.435	.520	500	62	13.6
	12	.00034	A = .007 B = .010 C = .005 D = .008	A = 11.5 B = 23.5 C = 5.08 D = 14.9	92	101	.460	.580	460	58	13.6
	14	.00087	A = .007 B = .021 C = .005 D = .008	A = 4.43 B = 30.75 C = 2.25 D = 5.75	106	123	.405	.465	550	66	13.6
	16	.00064	A = .007 B = .018 C = .005 D = .006	A = 6.0 B = 39.7 C = 3.06 D = 4.42	97	111	.460	.500	490		13.6
	16-1	.00069	A = .007 B = .018 C = .005 D = .008	A = 5.58 B = 36.8 C = 2.84 D = 7.25	112	124	.380	.450	575	66	13.6
	16-2	.00072	A = .007 B = .018 C = .007 D = .008	A = 5.18 B = 35.1 C = 5.32 D = 6.9	110	123	.370	.455	535	68	13.6
	17	.00074	A = .007 B = .018 C = .005 D = .010	A = 5.19 B = 34.25 C = 2.64 D = 10.6	112	125	.370	.450	520	81	13.6
	17-1	.00081	A = .007 B = .018 C = .005 D = .012	A = 4.75 B = 31.25 C = 2.42 D = 23.95	112	124	.360	.445	500	71	13.6
	18	.00093	A = .007 B = .018 C = .012 D = .010	A = 4.14 B = 27.30 C = 12.15 D = 8.45	95	111	.440	.500	510	72	13.6
	18-1	.00097	A = .010 B = .018 C = .012 D = .010	A = 8.10 B = 26.2 C = 12.65 D = 8.10	95	111	.440	.500	510	72	13.6
	18-2	.00107	A = .012 B = .018 C = .012 D = .012	A = 10.5 B = 23.7 C = 10.5 D = 10.5	104	112	.400	.500	475	67	13.6
9-ORIFICE SERIES											
	C	0.00084	A = .007 B = .018 C = .010 D = .008 E = .007	A = 30.2 B = 9.35 C = 5.98 D = 4.58	104	118	0.410	0.480	540	74	13.6
	C-1	.00088	A = .007 B = .018 C = .010 D = .008 E = .007	A = 4.37 B = 28.8 C = 8.91 D = 5.69 E = 4.37	112	125	.360	.460	540	74	13.6
	C-2	.00092	A = .010 B = .018 C = .010 D = .008 E = .007	A = 8.53 B = 27.60 C = 8.52 D = 5.44 E = 4.18	111	125	.380	.450	535	73	13.6
	C-3	.00078	A = .007 B = .018 C = .008 D = .007 E = .006	A = 4.93 B = 32.50 C = 6.40 D = 4.94 E = 3.63	102	122	.415	.460	500	71	13.6

TABLE I.—NOZZLE CHARACTERISTICS AND CORRESPONDING ENGINE PERFORMANCE; ENGINE SPEED, 1,500 R. P. M.—Continued

Orifice arrangement	Nozzle	Total orifice area (sq. in.)	Orifice diameter (inch)	Total orifice area (percent)	I. m. e. p.		Indicated fuel consumption		Maximum cylinder pressure (lb./sq. in.)	Full-load fuel with clear exhaust (percent)	Compression ratio
					$\frac{3}{4}$ full load (lb./sq. in.)	Full load (lb./sq. in.)	$\frac{3}{4}$ full load (lb./l. hp.-hr.)	Full load (lb./l. hp.-hr.)			
E SERIES											
	E ₂	0.00051	B = 0.018	B = 50	98	99	0.440	0.570	530	55	12.6
See figure 13	E ₄	.00067	$\left\{ \begin{array}{l} B = .018 \\ C = .010 \end{array} \right.$	$\left\{ \begin{array}{l} B = 37.9 \\ C = 11.7 \end{array} \right.$	104	120	.390	.470	570	73	12.6
	E ₅	.00072	$\left\{ \begin{array}{l} B = .018 \\ C = .010 \\ D = .006 \end{array} \right.$	$\left\{ \begin{array}{l} B = 35.25 \\ C = 10.90 \\ D = 3.92 \end{array} \right.$	112	127	.380	.450	550	73	12.6
	E ₈	.00080	$\left\{ \begin{array}{l} E_5 + \text{two} \\ 0.007 \end{array} \right.$		110	124	.380	.450	590	62	12.6
	E ₁₀	.00084	$\left\{ \begin{array}{l} E_8 + \text{two} \\ 0.005 \end{array} \right.$		112	126	.390	.450	590	68	12.6
	E ₁₂	.00088	$\left\{ \begin{array}{l} E_{10} + \text{two} \\ 0.005 \end{array} \right.$		104	120	.420	.480	560	65	12.6
	E ₁₄	.00092	$\left\{ \begin{array}{l} E_{12} + \text{two} \\ 0.005 \end{array} \right.$		100	113	.420	.490	530	66	12.6
	E ₁₅	.00096	$\left\{ \begin{array}{l} E_{14} + \text{two} \\ 0.005 \end{array} \right.$		100	113	.430	.500	570	71	12.6
	E ₅	.00066	$\left\{ \begin{array}{l} A = .018 \\ B = .014 \\ C = .008 \end{array} \right.$	$\left\{ \begin{array}{l} A = 38.4 \\ B = 23.6 \\ C = 7.5 \end{array} \right.$	114	123	.370	.460	550	75	12.6
F SERIES											
	F ₂₀	0.00072	$\left\{ \begin{array}{l} B = 0.018 \\ C = .010 \\ D = .006 \end{array} \right.$	$\left\{ \begin{array}{l} B = 35.25 \\ C = 10.90 \\ D = 3.92 \end{array} \right.$	112	127	0.380	0.450	550	73	12.6
	F ₂₁	.00072	$\left\{ \begin{array}{l} B = .018 \\ C = .010 \\ D = .006 \end{array} \right.$	$\left\{ \begin{array}{l} B = 35.25 \\ C = 10.90 \\ D = 3.92 \end{array} \right.$	114	128	.365	.440	600	75.5	12.6
	F ₂₆	.00072	$\left\{ \begin{array}{l} B = .018 \\ C = .010 \\ D = .006 \end{array} \right.$	$\left\{ \begin{array}{l} B = 35.25 \\ C = 10.90 \\ D = 3.92 \end{array} \right.$	114	126	.380	.450	550	80	12.6
	F ₂₉	.00072	$\left\{ \begin{array}{l} B = .018 \\ C = .010 \\ D = .006 \end{array} \right.$	$\left\{ \begin{array}{l} B = 35.25 \\ C = 10.90 \\ D = 3.92 \end{array} \right.$	114	124	.375	.460	570	74.5	12.6
H SERIES											
	H 1	0.00089	$\left\{ \begin{array}{l} B = 0.020 \\ C = .011 \\ D = .007 \end{array} \right.$	$\left\{ \begin{array}{l} B = 35.10 \\ C = 10.60 \\ D = 4.30 \end{array} \right.$	119	128	0.360	0.440	600	73	12.6
	H-2	.00100	$\left\{ \begin{array}{l} B = .022 \\ C = .011 \\ D = .006 \end{array} \right.$	$\left\{ \begin{array}{l} B = 38.00 \\ C = 9.50 \\ D = 2.83 \end{array} \right.$	115	128	.360	.450	600	70	12.6
	H-3	.00083	$\left\{ \begin{array}{l} B = .020 \\ C = .010 \\ D = .0055 \end{array} \right.$	$\left\{ \begin{array}{l} B = 37.80 \\ C = 9.42 \\ D = 2.85 \end{array} \right.$	117	124	.360	.450	600	72	12.6
	H 4	.00119	$\left\{ \begin{array}{l} B = .024 \\ C = .012 \\ D = .0065 \end{array} \right.$	$\left\{ \begin{array}{l} B = 37.80 \\ C = 9.45 \\ D = 2.77 \end{array} \right.$	114	128	.365	.445	590	64	12.6
	K 4	.00097	$\left\{ \begin{array}{l} B = .019 \\ C = .014 \\ D = .008 \end{array} \right.$	$\left\{ \begin{array}{l} B = 29.1 \\ C = 15.8 \\ D = 5.2 \end{array} \right.$	123.5	136	.340	.410	880	73.7	15.3

REPORT No. 569

WING-NACELLE-PROPELLER INTERFERENCE FOR WINGS OF VARIOUS SPANS FORCE AND PRESSURE-DISTRIBUTION TESTS

By RUSSELL G. ROBINSON and WILLIAM H. HERRNSTEIN, JR.

SUMMARY

An experimental investigation was made in the N. A. C. A. full-scale wind tunnel to determine the effect of wing span on nacelle-propeller characteristics and, reciprocally, the lateral extent of nacelle and propeller influence on a monoplane wing. The results provide a check on the validity of the previous research on nacelles and propellers with 15-foot-span wings tested in the 20-foot wind tunnel and reported in Technical Reports 415, 436, 462, 505, 506, and 507.

The 4/9-scale propeller and the N. A. C. A. cowling used in the former researches were tested in three typical tractor locations with respect to a thick wing of 5-foot chord and 30-foot span. The span was progressively reduced to 25, 20, and 15 feet and the same characteristics were measured in each case.

The efficiency factors—propulsive efficiency, nacelle drag efficiency, and net efficiency—were obtained for each wing length by means of force tests and the values are compared to determine the effect of span. Pressure-distribution measurements show the lateral extent of the nacelle interference and the propeller-slipstream effect on the span loading for the various conditions. Complete polar curves and curves showing the variation of nacelle drag with lift coefficient are also included.

Force and pressure-distribution tests concur in indicating that, for engineering purposes, the influence of a nacelle and of a propeller, in a usual combination, may be considered to extend laterally on a wing the same maximum distance, or about five nacelle diameters or two propeller diameters outboard of their common axes. All important effects of 4/9-scale nacelle-propeller combinations may be measured within practical limits of accuracy by tests of a 15-foot-span wing.

INTRODUCTION

Several years of research in the N. A. C. A. 20-foot tunnel have provided data comparing the merits of most practicable wing-nacelle-propeller combinations for air-cooled radial engines. There have been tested a tractor propeller with an N. A. C. A. cowled nacelle and a thick wing (reference 1), with various radial-engine cowlings and a thick wing (reference 2), with

various radial-engine cowlings and a Clark Y wing (reference 3); tandem propellers with a thick wing and various radial-engine cowlings (reference 4); a tractor propeller with a Clark Y biplane cellule and N. A. C. A. cowled nacelle (reference 5); and a pusher propeller with various wings and radial-engine cowlings (reference 6). For all these investigations a 4/9-scale reproduction of a Wright J-5 Whirlwind engine was used in conjunction with engine nacelles and cowlings of various forms. The propeller was 4 feet in diameter in every case. The thick wing was of 5-foot chord and 15-foot span; the Clark Y wing, of 38-inch chord and 15-foot 10-inch span. The magnitude of these dimensions relative to each other and to the 20-foot-diameter air stream in which the tests were made are among the factors that determine the degree to which the tunnel tests reproduce flight conditions.

The validity of all the data reported in references 1 to 6 depends on the effects of certain departures from flight-operating conditions. The most obvious difference is the limited span of the test wing compared with the greater spans of actual wings used in flight. If the field of flow were appreciably altered beyond the tips of the test wing by the nacelle or the propeller, then the total effect that would be produced on a large airplane wing would be different from that measured on the test wing and the test data could not be applied directly to an airplane design. The "blocking" of such a large test wing in a 20-foot-diameter jet is another possible source of error in that a possible higher velocity near the edges of the stream, compared with the velocity in the center, is a condition not reproduced in flight. The jet boundary may also introduce undesirable effects.

British tests (reference 7), the only known experimental work on the subject, suggested that the influence of a nacelle without propeller extends about 6 or 7 diameters outboard of the nacelle center. Thus a wing of at least 20-foot span, or aspect ratio 4, would be required to measure the complete nacelle effect, and it might be supposed (in the absence of test results) that the propeller effect extends farther than the nacelle effect.

The influence of any such disturbing bodies as nacelles or propellers moving in free air obviously extends laterally an infinite distance. The disturbance is relatively great in the immediate vicinity of the disturbing element, but the magnitude of the flow change diminishes rather rapidly with increasing distance from its source and becomes asymptotic to a zero value. When a nacelle or a propeller or both are tested on a wing, they influence the flow over the whole of the wing, from tip to tip, regardless of the span. It is therefore improper to speak of a limit to, or a lateral extent of, the influence of nacelle or propeller and useless to

effects have been measured on the 15-foot-span wing. The blocking effect mentioned previously is considered to be a known quantity in the full-scale tunnel as a result of airplane tests and its numerical value is probably smaller than that for the same wing tested in the 20-foot tunnel. The jet-boundary corrections are also smaller, being, for a 15-foot-span wing, less than 30 percent of the values in the 20-foot tunnel because of the proportionately larger jet area. In order to define more closely the limits of the nacelle and propeller influences, pressure-distribution tests were made to give the required span-load curves.

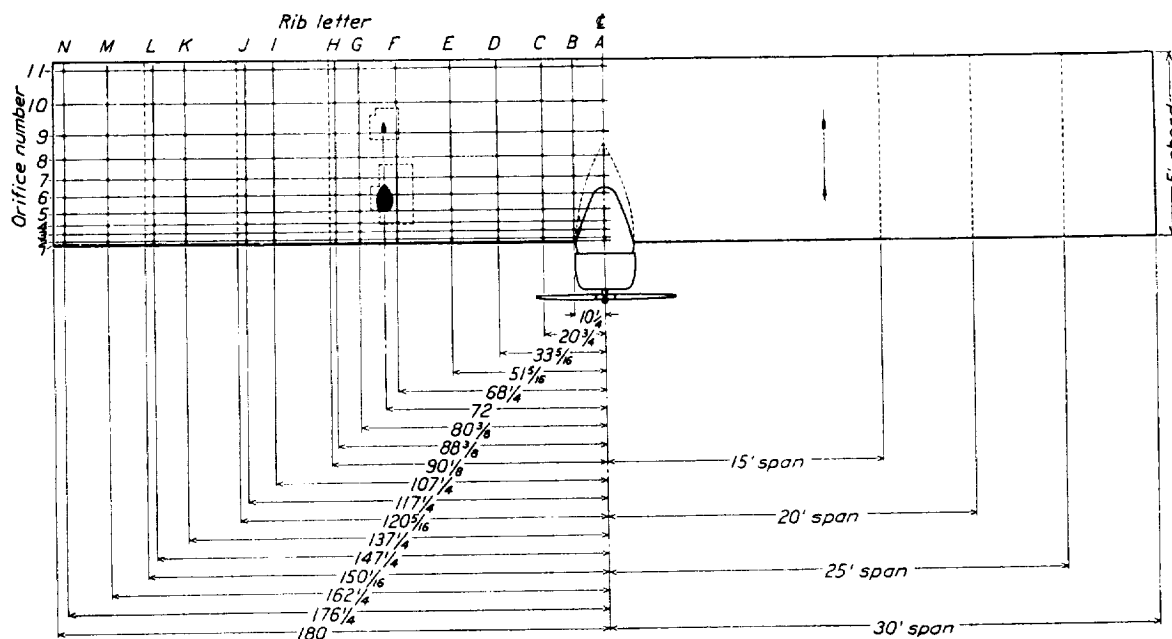


FIGURE 1.—Plan of test wing; lower surface showing pressure-orifice locations.

attempt to determine a wing span that includes within its tips the whole flow change. However, since the effect of nacelles and propellers becomes inappreciable for engineering usage at some distance laterally and becomes less than the limits of measurement at approximately the same point, it is convenient to consider the lateral extent of such effect to be the distance at which the local effect (for pressure-distribution tests) or the total effect (for force tests) becomes less than the limits of accuracy of the test for any increase of the span over which the effects are measured. Throughout the present paper the lateral extent is considered to have the limits just enumerated.

The present investigation was planned to evaluate the aforementioned effects in the full-scale wind tunnel. Force tests, repeated on wings of 5-foot chord and 15-, 20-, 25-, and 30-foot spans, were made to determine propulsive efficiencies, nacelle drag efficiency factors, and net efficiencies. Comparison of the values for the different spans shows to what extent the complete

APPARATUS AND METHODS

The full-scale wind tunnel, its balance, and the wing supports used in these tests are described in reference 8.

The apparatus will not be described in detail because a great deal of it is the same equipment that was used in the prior tests in the 20-foot tunnel. (See reference 1.) The wooden wing specially built for the tests to the ordinates specified in table I was of 30-foot span, 5-foot chord, and had a thickness equal to 20 percent of the chord. It was built to allow its being shortened symmetrically about its center to spans of 25, 20, and 15 feet. At each of 14 rib stations on the left half of the wing (fig. 1) 22 copper tubes terminated flush with the wing surfaces. These tubes passed inside the wing to flexible connections at the wing-support points. At the support points, the wing was provided either with large cut-outs through which the tubing passed during pressure-distribution tests or with small closely fitting cut-outs during force tests, the tubing being concealed inside the wing in the latter case. A number of flush

cover plates on the upper and lower surfaces of the center section were provided to allow attachment of the nacelle in various positions.

TABLE I.—WING ORDINATES

Station		Upper		Lower	
Percent chord	Inches	Percent chord	Inches	Percent chord	Inches
0	0	6.7	4.00	6.7	4.00
2.5	1.50	12.0	7.20	3.0	1.82
5	3.00	14.2	8.50	1.8	1.10
10	6.00	17.1	10.26	.6	.34
15	9.00	18.7	11.24	.2	.10
20	12.00	19.6	11.75	0	.02
30	18.00	20.0	12.00	0	0
40	24.00	18.9	11.34	0	0
50	30.00	16.9	10.14	0	0
60	36.00	14.1	8.48	0	0
70	42.00	11.0	6.58	0	0
80	48.00	7.5	4.52	0	0
90	54.00	3.8	2.30	0	0
100	60.00	0	0	0	0

The 4/9-scale model of a Wright J-5 radial air-cooled engine and N. A. C. A. cowled nacelle, the same as used in previous tests, is illustrated in figure 2. The

For pressure-distribution tests the orifices were connected to two multiple-tube manometers in the balance house by tubing attached to the support fairings. The recording manometers pictured in figure 4 are fully described in reference 9.

Force tests and pressure-distribution tests were made of the wing alone and of the wing with the nacelle in three positions. A 30-foot span wing was first used; by cutting and refinishing both tips, the span was reduced progressively to 25, 20, and 15 feet. Similar measurements were made in each case.

Figures 5 to 9 show the different spans, nacelle locations, and support conditions that make up the 32 combinations tested. Pressure-distribution tests were run, separately from the force tests, with the tubing that is attached to the strut fairings joined to the flexible ends of the tubing in the wing, and the bundle of connections faired, as nearly as could be, into a streamline shape as shown in figures 6 and 9.

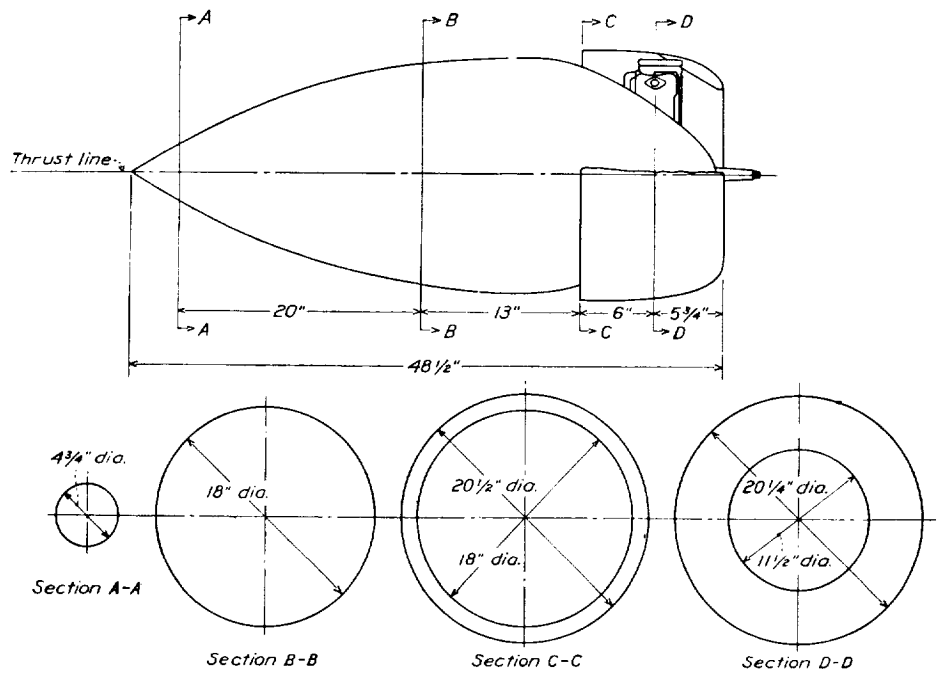


FIGURE 2.—The N. A. C. A. cowled nacelle and engine assembly.

nacelle contains a 25-horsepower 220-volt direct-current motor and an electric tachometer. A 4-foot aluminum-alloy model of the right-hand Navy No. 4412, 9-foot adjustable propeller, set 17° at $0.75 R$, was normally used, but for a part of the pressure-distribution tests, to simulate flow over the half of the wing without pressure orifices, a geometrically similar left-hand propeller was fitted and pressure readings were taken on the same wing orifices as before. The three typical nacelle locations used in the present tests are shown in figure 3 and are designated by the numbering system of reference 1.

Force tests were made of the wing alone for each span at an air speed of approximately 60 miles per hour over an angle-of-attack range from -12° to 25° by 2° intervals, except that the intervals were closer near minimum drag and maximum lift. In addition, force tests and pressure-distribution measurements were made for the wing alone at angles of attack of -5° , 0° , 5° , 10° , and 15° at air speeds of approximately 30, 50, 80, and 100 miles per hour.

For each span and for each nacelle location, with propeller removed, force measurements at the same 5° intervals were made at various air speeds between 2

and 100 miles per hour. Pressure-distribution measurements were made at the same angles at air speeds of 30, 50, 80, and 100 miles per hour.

For each span and for each nacelle location, with right-hand propeller, propeller operating force tests were made at angles of attack of -5° , 0° , 5° , and 10° at 12 values of V/nD obtained by varying the air speed between 27 and 100 miles per hour and by throttling the motor at the highest air speed. Pressure-distribution tests were made at the same angles at four values of V/nD , between 0.23 and 0.76, obtained at approximately 30, 50, 80, and 100 miles per hour. Both types of test were repeated for the 15- and 30-foot spans with the left-hand propeller.

Tare force tests were made on the 30-foot-span wing by suspending it independently and measuring the air forces on the supports. The tare values obtained on the 30-foot-span wing were used for all spans.

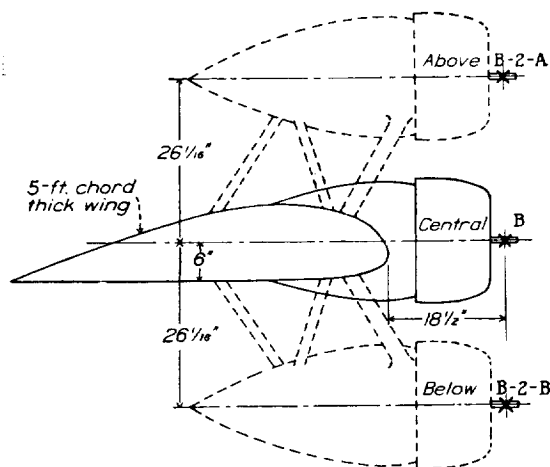


FIGURE 3.—Nacelle test locations.

In all force tests the lift, drag, angle of attack, and air speed were measured and, in the propeller-operating tests, the torque and propeller revolution speed in addition. Double or triple readings were taken for each test condition. In the pressure-distribution tests, single readings of angle of attack, air speed, and pressure at individual orifices were taken and, in tests with propeller operating, the propeller speed as well.

RESULTS

The conditions during these tests represent approximately one-fifth the full-scale Reynolds Number of a large, modern, high-speed transport airplane. The results for "high-speed flight," defined subsequently, were taken at about 88 miles per hour (Reynolds Number approximately 4,000,000) and those for "climbing flight" at about 57 miles per hour (Reynolds Number approximately 2,500,000). The degree of turbulence in the full-scale tunnel is discussed in references 10 and 11, which indicate that the effects of

turbulence are of secondary importance. The same references show that agreement may be expected between tests in the 20-foot tunnel and in the full-scale tunnel. For the purposes of this report the present results may be considered directly comparable, as regards scale and turbulence, with results from the 20-foot tunnel and may also be considered representative of flight conditions.

FORCE TESTS

The force-test data were corrected by the method described in reference 6 that allows comparison of different wing-nacelle combinations at the same angle of attack. This method involves computation of propulsive efficiencies, nacelle drag efficiency factors, and net efficiencies, all at the same angle of attack (for the same span), and correction for the jet-boundary drag and induced drag resulting from the differences in lift caused by the nacelle and propeller combinations. This procedure eliminates certain discrepancies that develop when the data are reduced in accordance with the method used in references 1 to 5. The corrections are explained in detail in reference 6, but the method and factors involved will be briefly enumerated in the following section.

Propulsive efficiency η is the ratio of the effective thrust power (total thrust power less loss caused by increased drag of parts in the slipstream) to the motor power.

$$\begin{aligned}\eta &= \frac{\text{effective thrust} \times \text{velocity of advance}}{\text{motor power}} \\ &= \frac{(T - \Delta D)V}{P} \\ &= \frac{C_T}{C_P} \frac{V}{nD} + \frac{\Delta C_{D_i} + \Delta C_{D_j}}{C_P} \frac{S}{2D^2} \left(\frac{V}{nD} \right)^3\end{aligned}$$

where all symbols have their usual meanings except as noted.

$$C_T = \frac{T - \Delta D}{\rho n^2 D^4}$$

where

T is thrust of propeller (shaft tension).

ΔD , change in drag of body (nacelle plus wing) due to action of propeller.

$T - \Delta D$, effective thrust, the quantity actually inferred from the measurements because of the difficulty in measuring T and ΔD separately; equal to the gross propeller-operating thrust of a wing-nacelle-propeller combination plus the drag of the same wing-nacelle combination, propeller off, at the same attitude and air speed.

ΔC_{D_i} , change in induced drag due to a change in lift. In the present case the lift change caused by the propeller is put in the form of the equivalent drag change by assuming the latter equal

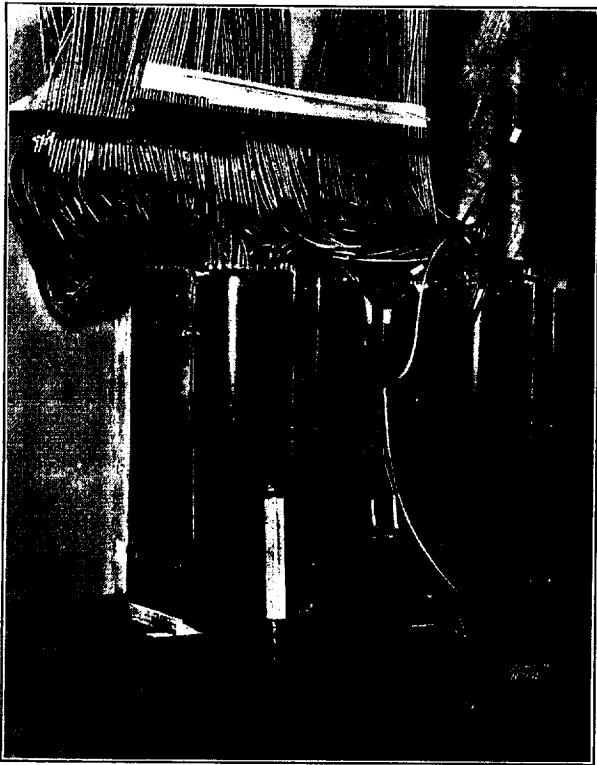


FIGURE 4.—Multiple-tube recording manometers, model 4, connected for pressure-distribution tests.

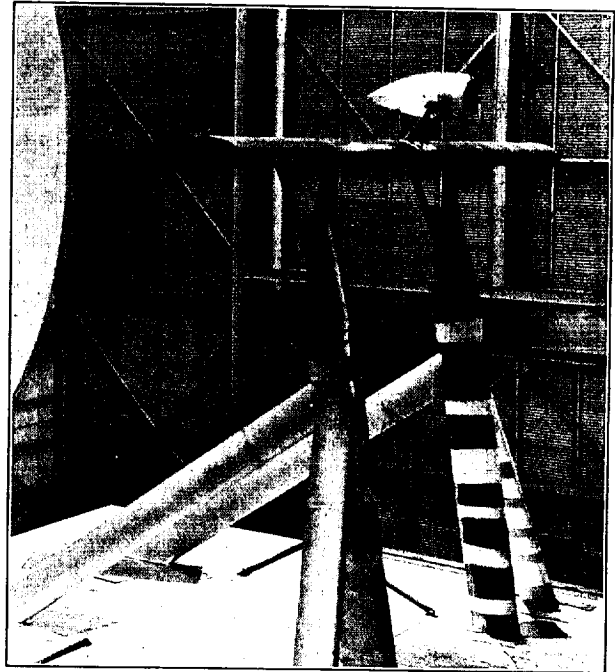


FIGURE 5.—Force test; 5- by 30-foot wing, nacelle above.

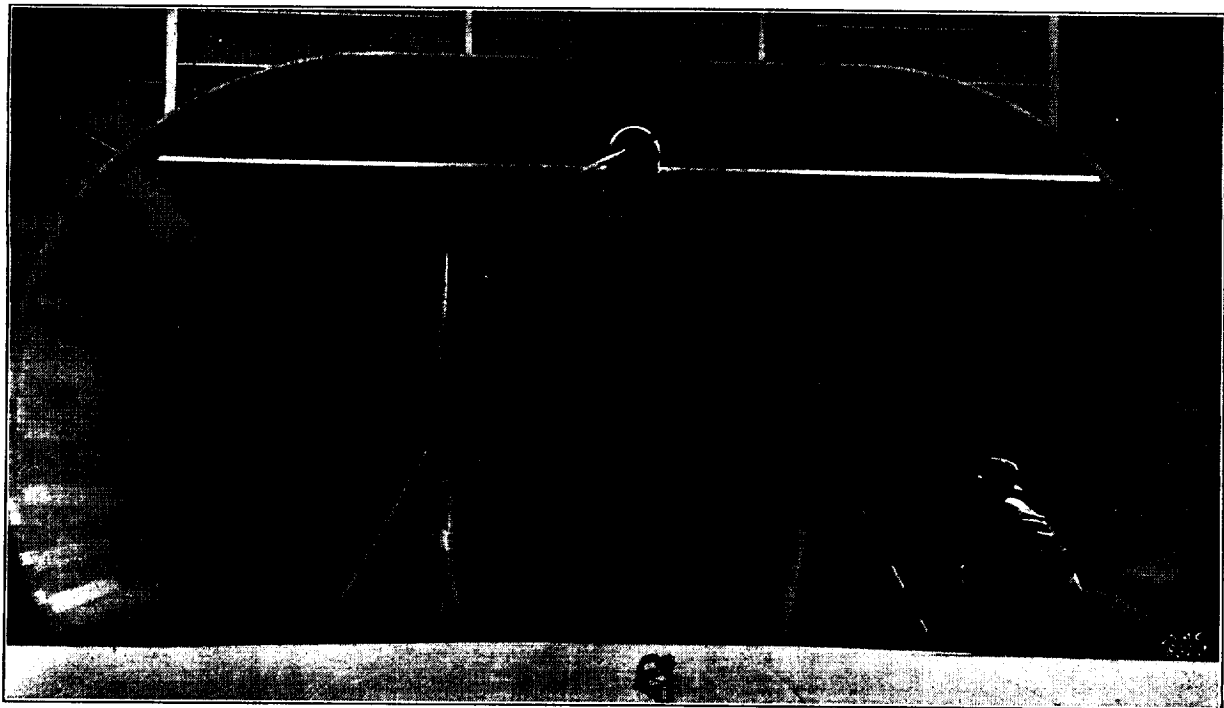


FIGURE 6.—Pressure-distribution test; 5- by 30-foot wing, nacelle central.

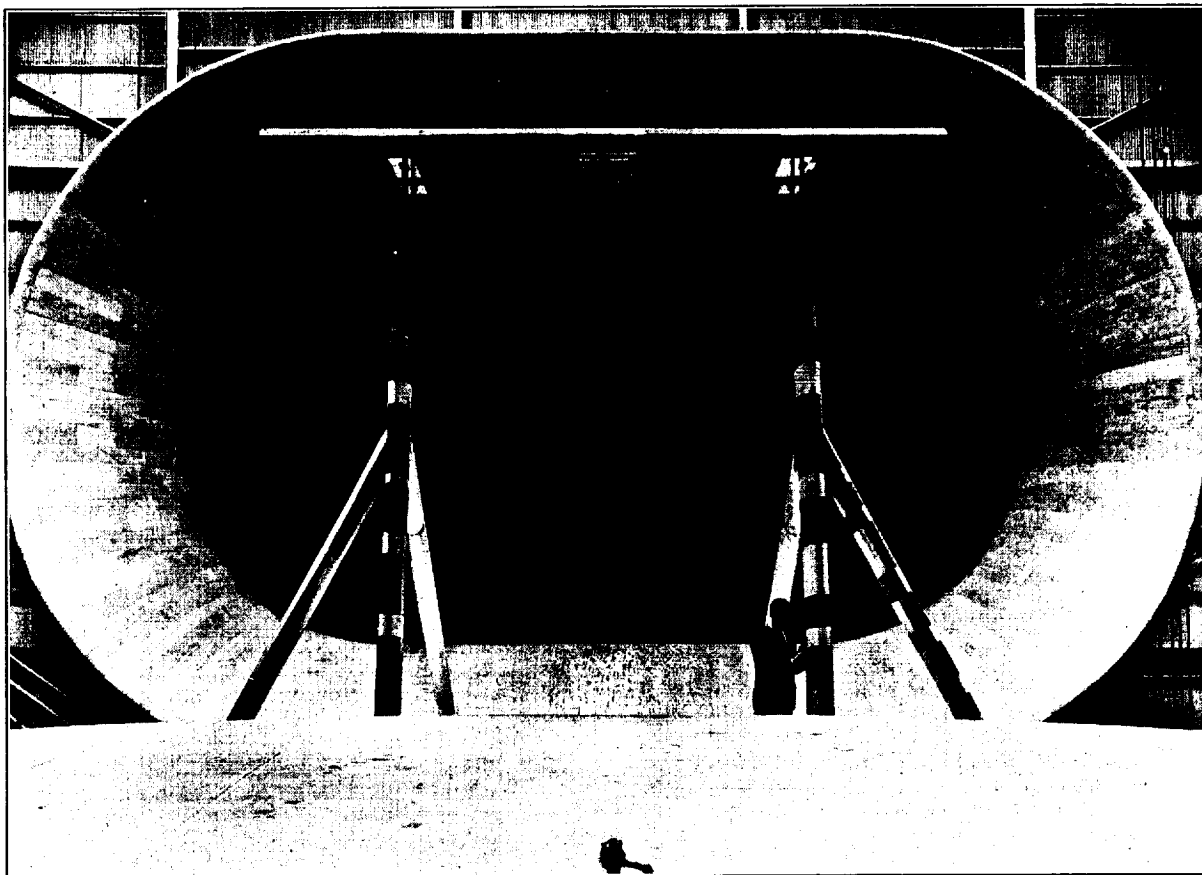


FIGURE 7.—Force test; 5- by 20-foot wing alone.

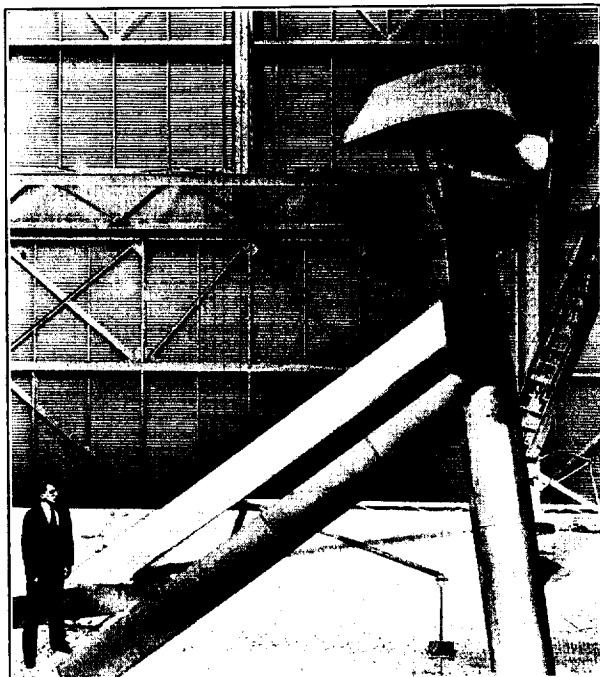


FIGURE 8.—Force test; 5- by 25-foot wing, nacelle below.



FIGURE 9.—Pressure-distribution test; 5- by 15-foot wing, nacelle central.

to the change in induced drag experienced by an elliptically loaded wing of the same aspect ratio when its lift is changed from the actual measured lift, propeller removed, to the measured lift, propeller operating.

$$\Delta C_{D_i} = \frac{(C_{L_p}^2 - C_{L_c}^2)}{\pi \times A}$$

where

C_{L_p} is lift coefficient, propeller operating, of a wing-nacelle-propeller combination at a given angle of attack.

C_{L_c} , lift coefficient, propeller removed, of the same wing-nacelle combination at the same angle of attack.

A , aspect ratio.

ΔC_{D_j} , change in jet-boundary drag correction due to a change in lift; for the same reasons and based on the same lift change as ΔC_{D_i} .

$$\Delta C_{D_j} = \left(\delta \frac{S}{C} \right) (C_{L_p}^2 - C_{L_c}^2)$$

where

δ is the nondimensional jet-boundary correction factor.

C , cross-sectional area of the jet, 1,608 square feet.

Nacelle drag efficiency factor N. D. F. is the ratio of power absorbed by nacelle drag and interference to the motor power.

$$\text{N. D. F.} = \frac{(C_{D_w} - C_{D_{wc}} + \Delta C_{D_i} + \Delta C_{D_j})}{C_p} \times \frac{S}{2D^2} \times \left(\frac{V}{nD} \right)^3$$

where

C_{D_w} is drag coefficient, wing alone, at a chosen angle of attack.

$C_{D_{wc}}$, drag coefficient of wing-nacelle combination at the same angle of attack.

ΔC_{D_i} , change in induced drag due to a change in lift; in this case, the lift change caused by the nacelle.

$$\Delta C_{D_i} = \frac{(C_{L_w}^2 - C_{L_c}^2)}{\pi \times A}$$

C_{L_w} , lift coefficient of wing alone at the same angle of attack as C_{L_c} is taken.

ΔC_{D_j} , change in jet-boundary drag due to a change in lift; for the same reasons and based on the same lift change as ΔC_{D_i} .

$$\Delta C_{D_j} = \left(\delta \frac{S}{C} \right) (C_{L_w}^2 - C_{L_c}^2)$$

Net efficiency η_0 is the percentage of the motor power available for uses other than for overcoming the losses,

direct and indirect; of the nacelle-propeller combination; that is, the fraction of the engine brake horsepower available for overcoming the drag of the complete airplane without nacelles, nacelle supports, if any, and propellers.

$$\eta_0 = \eta - \text{N. D. F.}$$

The results are compared for two flight conditions: $C_L=0.2$, $V/nD=0.65$; and $C_L=0.6$, $V/nD=0.42$, values which represent high-speed (not necessarily full-speed) and climbing conditions, respectively, for airplanes utilizing the pitch setting used in these tests (17°). The three types of tests—wing alone, wing and nacelle with propeller removed, and wing-nacelle combination with propeller operating—were all compared, for any one span, at the same two angles of attack at which the wing alone showed the chosen lift coefficients; differences in lift were taken into account as detailed in reference 6 and as described briefly in the preceding paragraphs. All results were corrected for blocking and for the air-stream angle known to exist in the tunnel. Both these corrections were determined by airplane tests and by Clark Y airfoil tests reported in reference 10 and by air-stream surveys made in the jet. All results are finally corrected for jet-boundary effects. The values of the factor δ used for these corrections are: -0.203 for 15-foot span, -0.206 for 20-foot span, -0.208 for 25-foot span, and -0.210 for 30-foot span.

Results of the force tests are summarized in figure 10, which shows the variation of propulsive efficiency, nacelle drag efficiency factor, and net efficiency with span. The plotted points are not observed values but are computed from values taken from faired curves. They are included only to show the degree of dispersion from the faired curve. Since the present comparisons are made at different values of C_L than those chosen in reference 1, the results are also compared for the conditions ($C_L=0.409$, $V/nD=0.65$; $C_L=0.652$, $V/nD=0.42$) used in that reference and the numerical values are given in table II.

TABLE II.—COMPARISON OF 15-FOOT-SPAN RESULTS

Tunnel	Nacelle above			Nacelle central			Nacelle below		
	N. D. F.	η	η_0	N. D. F.	η	η_0	N. D. F.	η	η_0
High speed; $\alpha=0^\circ$; $C_L=0.409$; $V/nD=0.65$									
20-foot ¹	0.155	0.802	0.647	0.042	0.776	0.734	0.086	0.763	0.677
Full-scale ²	.137	.784	.647	.051	.813	.762	.097	.794	.697
Climbing; $\alpha=5^\circ$; $C_L=0.652$; $V/nD=0.42$									
20-foot ¹	0.035	0.663	0.628	0.017	0.683	0.666	0.028	0.644	0.616
Full-scale ²	.034	.677	.643	.020	.734	.714	.065	.659	.654

¹ Data from reference 1, corrected by method of reference 6.

² Data from present tests, corrected by method of reference 6.

Complete polars of the wing and wing-nacelle combinations (fig. 11) for the four spans show the variation of nacelle drag with lift coefficient. It is apparent, however, that if the nacelle drags are identical when nacelles are mounted on two wings of unequal span and area, other conditions being the same, the nacelle drag coefficients will not be the same in both cases because of the different wing areas on which the coefficients are

nacelle drag coefficient." This coefficient is then a constant independent of span or area if the actual nacelle drag is constant for different spans. The factors and the resulting effective nacelle drag coefficients are shown in figure 12. In figure 13 the variation of effective nacelle drag coefficient with span is shown for the three nacelle positions at the high-speed condition.

In figure 14 are plotted some results obtained incidentally during the main research. They show the variation with span of effective profile drag coefficient at $C_L=0.2$, maximum lift coefficient, and angle of attack for maximum lift, all corrected to free-air conditions.

PRESSURE-DISTRIBUTION TESTS

The basis for comparison of the pressure-distribution tests is the same as for the force tests, i. e., high-speed and climbing conditions, with the same criteria as in the force tests. The normal-force coefficient C_N for each rib was first plotted against angle of attack α and, for propeller-operating tests, at a constant V/nD . At the angle of attack at which the force tests showed that the chosen C_L would be realized, the value of C_N for each rib was read. For propeller-operating tests these points were cross-plotted against V/nD and values at the chosen V/nD were used. These values of rib C_N were then plotted at appropriate rib positions to give the span loading for the two flight conditions considered.

Results of the pressure-distribution tests are collected in figures 15, 16, and 17. These figures show the span-load curves for high-speed and climbing flight for the wing alone and for the nacelle above, central, and below. The charts show the loading as seen from upstream, looking at the leading edge, with the propeller turning in the direction indicated. The plotted points are not observed values but are obtained by cross-fairing and are included as the best guide in judging the limits to which the curves should be read. For the following reasons the curves do not show directly the resultant free-air load distribution of the complete span. Measurements were taken on only one half of the wing and a left-hand propeller was used to simulate the slipstream effect on the other half of the wing. A blocking effect in the tunnel (reference 12) results in slightly different local velocities at each rib; but, for simplicity, the rib coefficients are computed on the basis of average velocity. No correction for the jet boundary was made to the span loading, but this effect is known to be small. The previously mentioned conditions, however, do not make the results any less valid for the present comparison; in fact, the use of right- and left-hand propellers eliminates the effect of any asymmetry of air flow and wing profile and permits an easier and more accurate determination of the slipstream effect.

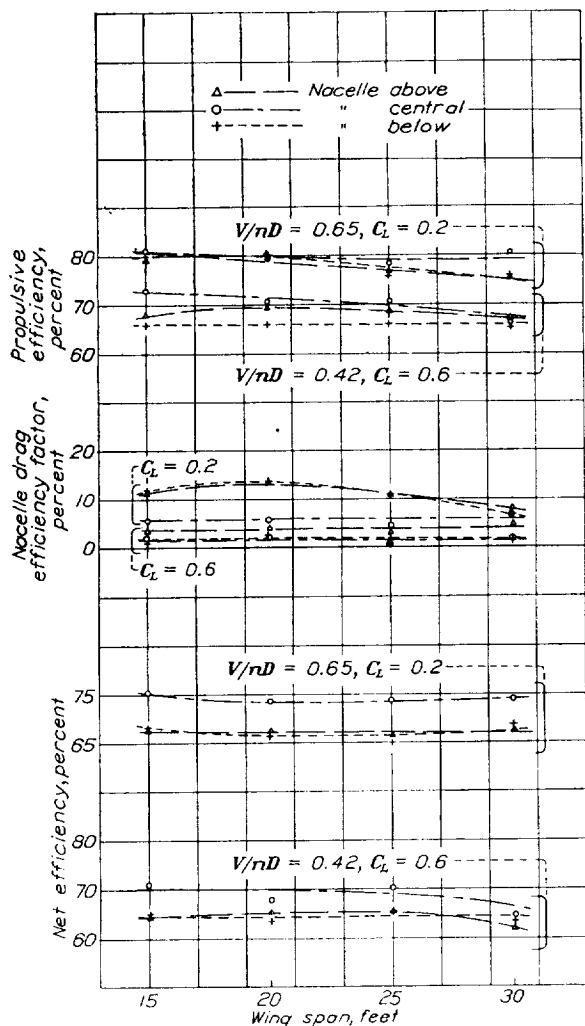


FIGURE 10.—Variation with span of nacelle-propeller efficiency factors.

based; that is, on the 30-foot-span wing a nacelle drag of 4.6 pounds at 100 miles per hour gives a nacelle drag coefficient ΔC_D of 0.0012; whereas, if the nacelle has the same drag when mounted on the 15-foot-span wing, the nacelle drag coefficient ΔC_D is equal to 0.0024 based on the reduced wing area. In order that any variation with span, as well as variation with lift coefficient, may be shown on a plot of nacelle drag coefficients, each coefficient is multiplied by a factor K equal to the ratio of the wing areas and the result is termed the "effective

PRECISION

The precision of the force tests was about the same as for the earlier tests in the 20-foot tunnel. The angle of attack of the wing was set within 0.1° . Tachometer readings were accurate to within one-half of 1 percent. Lift readings were taken to the nearest pound and drag

results should be accurate to within ± 2 percent for the efficiencies and ± 20 percent at low lift coefficients for the nacelle drag coefficients.

The pressure-distribution results are less precise than the force results. Only single observations were taken for a given set of conditions but cross-fairing tended to

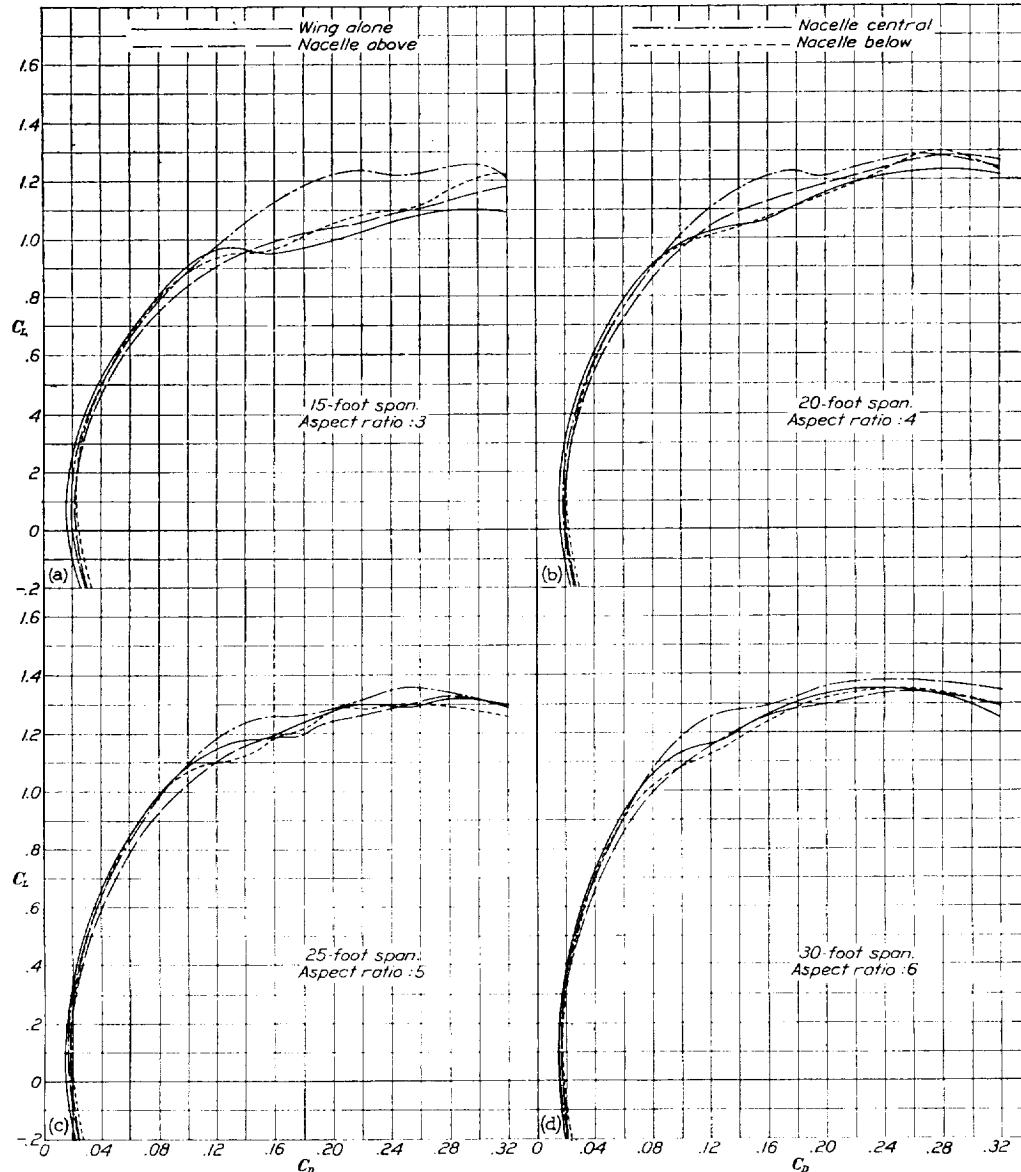


FIGURE 11. (a, b, c, d).—Comparison of lift and drag characteristics of wing alone and N. A. C. A. cowled nacelle combination, propeller removed, in three positions, corrected for tunnel effects; Reynolds Number, 2,800,000; full-scale tunnel.

readings to the nearest 0.1 pound. The magnitude of the tare forces aided in securing high accuracy; tare drag was approximately 7 percent of $C_{D_{min}}$ for the 15-foot span and approximately 4 percent for the 30-foot span. The over-all precision is, of course, less on the larger spans on account of obtaining small differences by deducting forces of correspondingly larger magnitudes. On the 15-foot span, at least, the final

diminish the effect of individual erratic readings. The scatter of points on plots of rib C_N against α shows the dispersion to be more nearly a given absolute value than a given percentage so that the accuracy will be less at the lower lift coefficients. Below the stall, however, the dispersion of observed points might be placed at ± 5 percent and the accuracy of the final span-load curves at ± 3 percent.

DISCUSSION

FORCE TESTS

An examination of figure 10 indicates the extent to which the nacelle-propeller efficiency factors may vary with the span of the test wing. Propulsive efficiencies,

factors show the same tendency except that the indicated variation is greater in some cases. The nacelle drag efficiency factor is useful mainly for comparison with results previously reported; a more useful and more accurately determined quantity and its variation

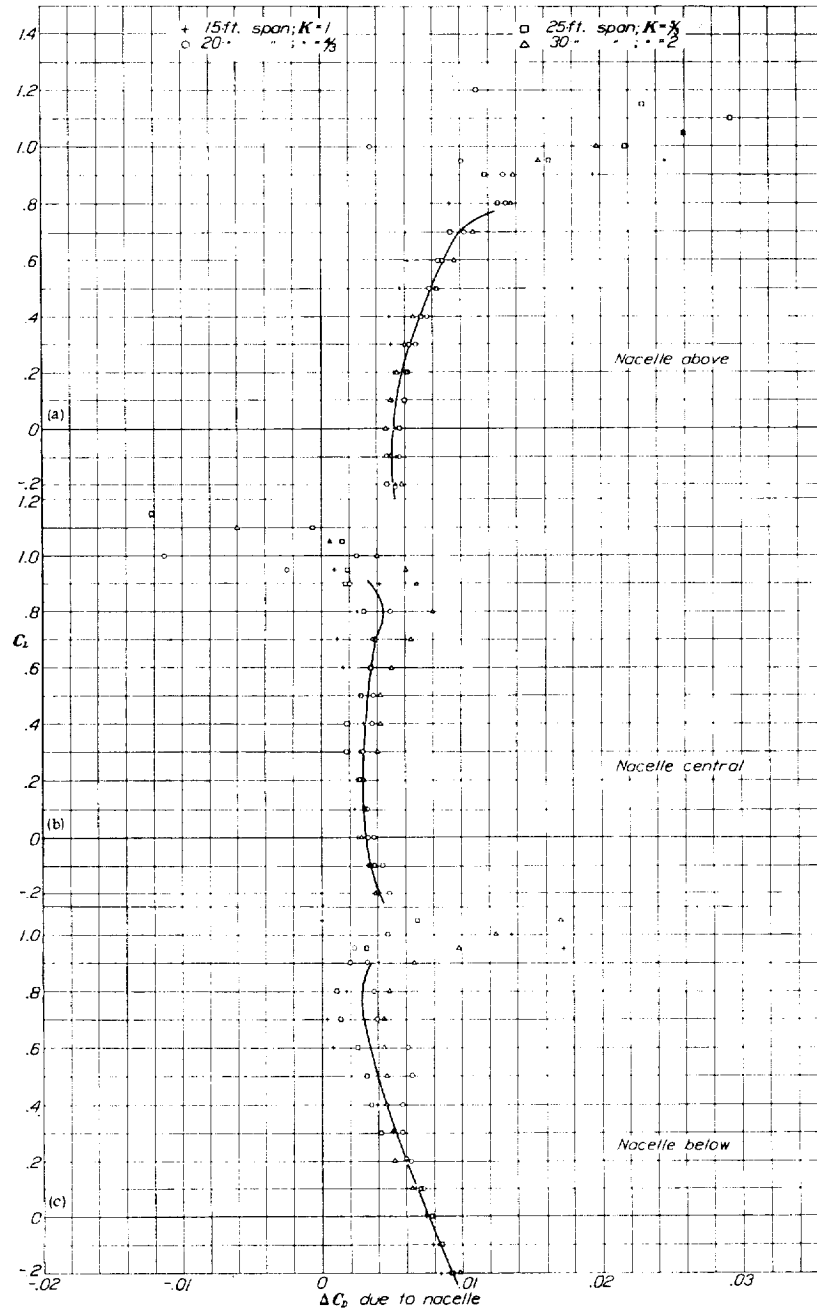


FIGURE 12 (a, b, c). Effective nacelle drag coefficients for four spans. Based on wing area of 75 square feet; engine diameter, 20 inches. $\Delta C_D = K(C_{D_e} - C_{D_s})$.

both in high-speed and climbing conditions, generally tend to increase slightly as the wing is shortened from 30 to 15 feet. The best combination, nacelle central, shows small variation in propulsive efficiency, especially at the high-speed condition. The nacelle drag efficiency

with span will presently be discussed. A comparison of the propulsive-efficiency curves and the curves of the nacelle drag efficiency factor demonstrates that the propeller, in spite of its larger diameter, is no more affected by span than is the nacelle. Because the

propulsive-efficiency curves and N. D. F. curves have similar tendencies, the net-efficiency curves show even less variation with span than the curves from which they are derived. The maximum over-all variation of any of the net-efficiency curves is little over 3 percent. These curves generally show their greatest departure from constant values for the 30-foot span for which the experimental errors are known to be largest.

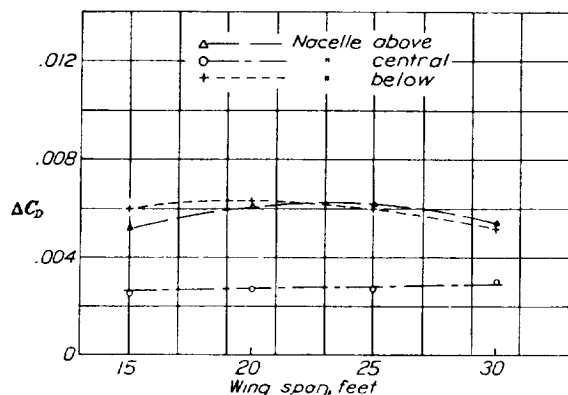


FIGURE 13.—Variation with span of effective nacelle drag coefficients for $C_L=0.2$.

It has been determined (reference 13) that the most accurate way to apply nacelle-propeller data to airplanes, the design speed of which is considerably in excess of the wind-tunnel speeds at which the data were taken, as is now usually the case, is to use an experimentally determined propulsive efficiency and the effective nacelle drag coefficient (which includes interference) scaled to the proper engine size and wing area, instead of using a net efficiency value. At the higher flying speeds the nacelle drag assumes a greater importance than formerly and accurate data on this portion of the airplane loss are accordingly more valuable. For this reason the nacelle drag, in the form of an effective nacelle drag coefficient, is obtained from the original data with as little loss in accuracy as possible by taking the difference in effective profile drag coefficients, nacelle off and nacelle on, at the same lift coefficients. These results (fig. 12) are readily usable for design purposes; it is recommended that the faired-curve values be used in each case. Because of their simple and more accurate derivation and because the results are represented for the whole useful-lift range instead of for the two conditions ($C_L=0.2$ and $C_L=0.6$) previously used, these results provide a good basis for judging the effect of span.

All the results cited thus far, especially the curves of effective nacelle drag coefficient, indicate no systematic variation of nacelle and interference drag with span and imply that all effects, within the precision of the measurements, are therefore included by the 15-foot-span wing. Figure 13, derived from figure 12, is typical and illustrates the condition for a high-speed lift-coefficient value. Similar figures, constructed for

larger values of lift coefficient, show a greater dispersion of points but cannot definitely be interpreted to show consistent variations of nacelle and interference drag with span.

The comparison in table II of 20-foot-tunnel data with the corresponding data from the full-scale tunnel demonstrates that both series of tests are substantially in agreement. As explained in reference 6, the pro-

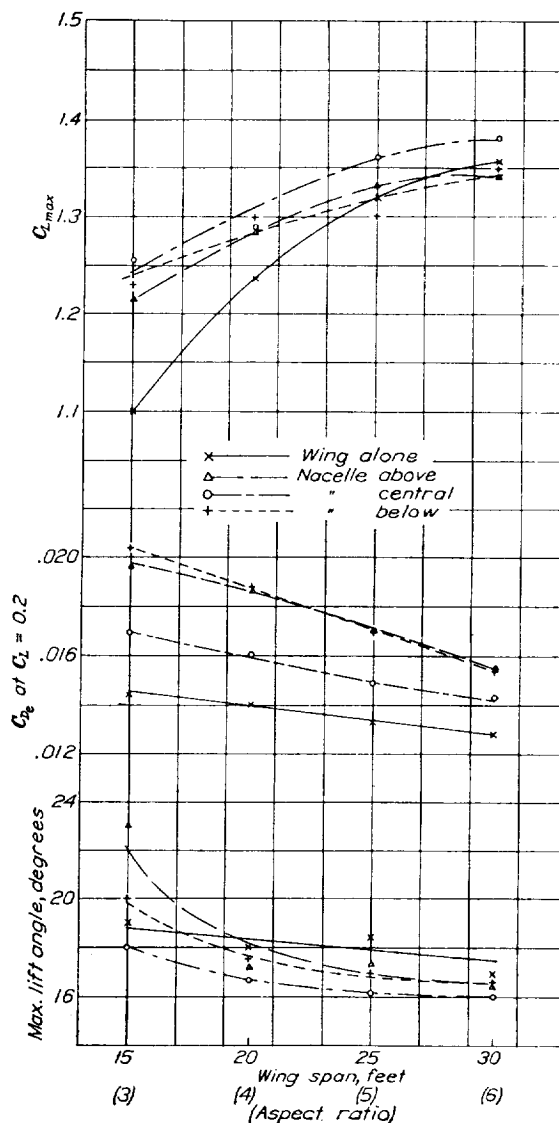


FIGURE 14.—Variation with span of wing-nacelle characteristics. Corrected for tunnel effects; Reynolds Number 2,800,000; full-scale tunnel.

pulsive efficiencies and nacelle drag efficiency factors given in reference 1 will change when corrected for the induced-drag effects but, because the power coefficients and lift-curve slopes remain nearly constant, the net efficiencies will not change perceptibly.

The values of all quantities measured in the full-scale wind tunnel are generally higher than those from the 20-foot tunnel but, compared with the precision of the

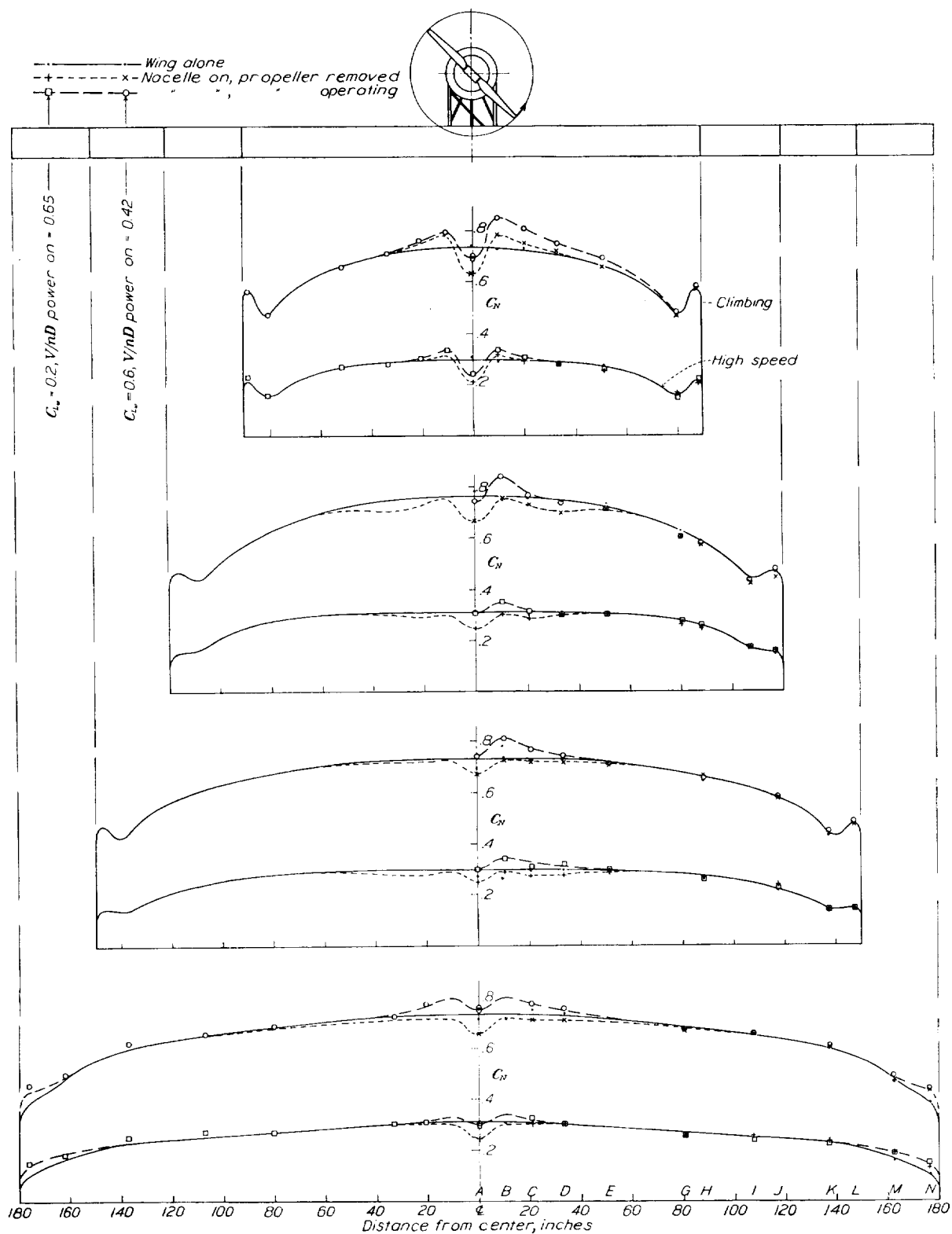


FIGURE 15.—Span-load curves. Wing alone and nacelle above; propeller removed and propeller operating; various spans.

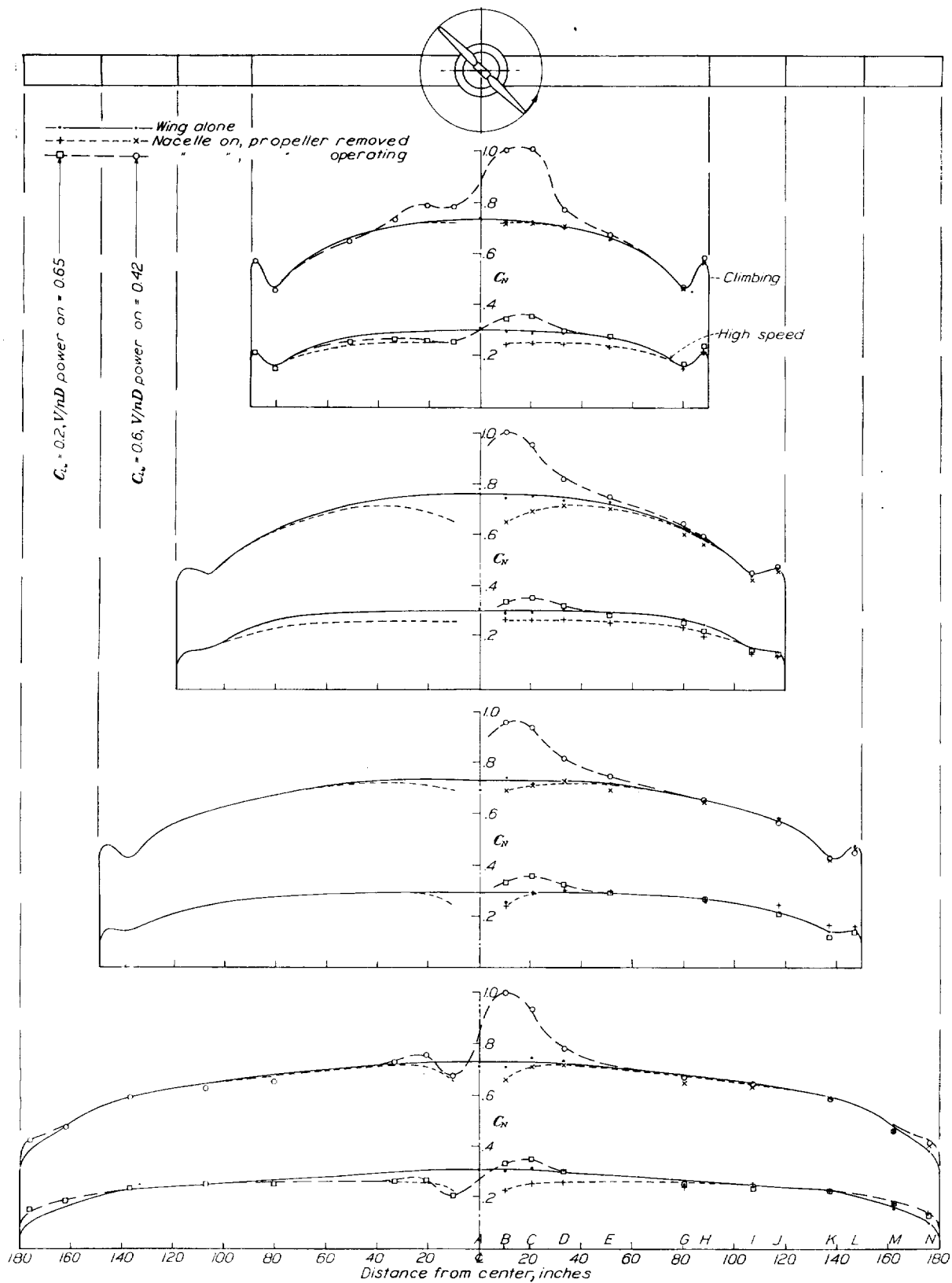


FIGURE 16.—Span-load curves. Wing alone and nacelle central; propeller removed and propeller operating; various spans.

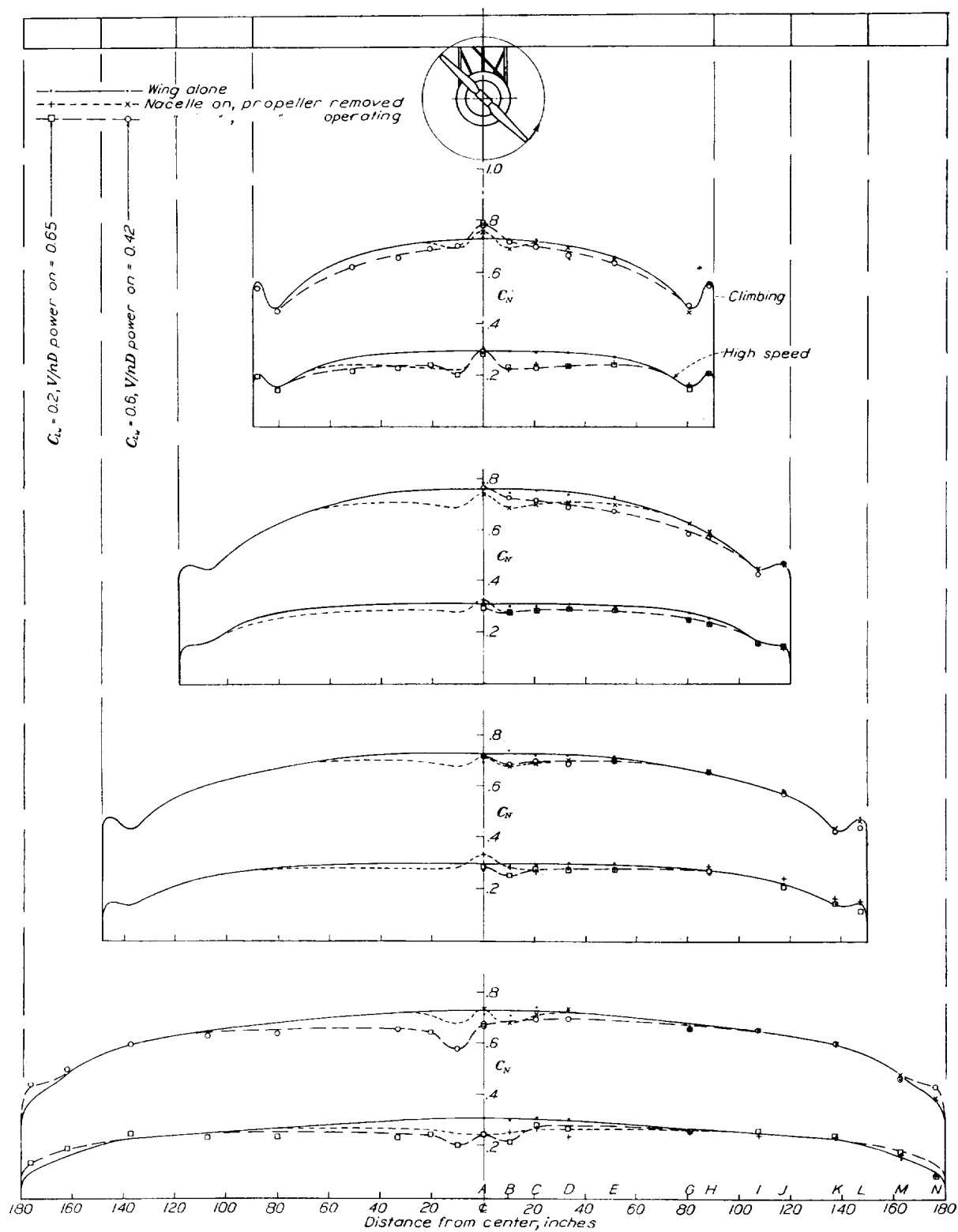


FIGURE 17.—Span-load curves. Wing alone and nacelle below; propeller removed and propeller operating; various spans.

tests, the difference is not great. Propulsive efficiencies for the three nacelle locations average 0.017 higher for high-speed and 0.026 higher for climbing; nacelle drag efficiency factors average 0.001 higher for high-speed and 0.008 higher for climbing; and net efficiencies average 0.016 and 0.034 higher, respectively.

The incidental results plotted in figure 14 show the usual trend for wings of medium aspect ratio. The wings with nacelles show decreasing maximum lift coefficients as the aspect ratio is decreased from 6 to 3, but the decrease is only about half that for the wing alone. The minimum drag coefficient of the wing alone increases with decreasing aspect ratio because a tip loss, which must be nearly constant in absolute value for the spans tested, accounts for a larger portion of the coefficient as the area is reduced. In the same way the nacelle, with its drag a constant independent of span, raises the coefficient most for the shortest span because of the smaller area on which the coefficient is based. If allowance is made for this fact, the variation of minimum drag coefficient is about the same for the wing-nacelle combinations as for the wing alone. The various combinations show an increase of angle for maximum lift, with decrease of aspect ratio, similar to the wing alone except that the increase is more rapid for the lower aspect ratios.

PRESSURE-DISTRIBUTION TESTS

If only the more marked effects that would be important in engineering practice are considered, the pressure-distribution curves of span load (figs. 15, 16, and 17) also show that the nacelle and propeller effects do not extend appreciably beyond the limits of a 15-foot-span wing, approximately four and one-half nacelle diameters or two propeller diameters outboard of the center. Figure 15, nacelle above the wing, shows that the effects of the nacelle extend in no case beyond 80 or 100 inches (four or five nacelle diameters) from the center. Figure 16, nacelle central, shows that although the loading at the center is changed more radically than for nacelle above or below, the effects do not extend beyond 100 inches. Figure 17, nacelle below the wing, shows that the effects of the nacelle extend about 100 inches as a maximum. Contrary to the previously expressed supposition, most of the curves show that the lateral extent of the propeller effect is no greater than that of the nacelle without propeller.

Consideration of the degree to which all the nacelle locations tested in the present research indicate like values of the lateral extent of their influence and consideration of the results of reference 7, which indicate that the magnitude, but not the lateral extent,

of the interference increases for high-drag nacelles (comparable to uncowl engines) and very poor locations (touching the upper or lower surface of the wing), lead one to believe that the present conclusions are applicable to usual wing-nacelle-propeller combinations. One of the variables not tested was wing thickness, but this variable is shown by other results (reference 3) to be of secondary importance. The case of the pusher propeller probably represents the greatest departure, but this case probably affects wing-nacelle characteristics less because the inflow, in which a part of the wing lies, is more regular and of smaller intensity than the slipstream of a tractor propeller.

The present tests indicate that the optimum span on which to test the 4/9-scale nacelle and propeller in a large wind tunnel is about 20 feet (semispan equal to six nacelle diameters or two and one-half propeller diameters, approximately). For smaller spans the pressure-distribution results show appreciable effects, in some cases to the point at which the tip effects begin, a condition which it seems desirable to eliminate. For larger spans the precision of the force tests decreases. The 15-foot span wing, however, is sufficiently large to measure all effects within practical limits of accuracy.

CONCLUSIONS

1. Force and pressure-distribution tests concur in indicating that for engineering purposes the influence of a nacelle may be considered to extend laterally along a wing no farther than about five nacelle diameters from its center.
2. Similar tests indicate that a propeller operating with a usual wing-nacelle combination may be considered to influence the wing no farther laterally than does the nacelle alone, that is, about two propeller diameters from its center.
3. All important effects of a 4/9-scale nacelle-propeller combination may be measured within practical limits of accuracy on a 15-foot-span wing in the jet of the 20-foot tunnel.
4. The present test results show substantial agreement, for the same operating conditions, with results previously obtained in the 20-foot tunnel.
5. The foregoing conclusions probably apply approximately to all usual wing-nacelle-propeller combinations.

LANGLEY MEMORIAL AERONAUTICAL LABORATORY,
NATIONAL ADVISORY COMMITTEE FOR AERONAUTICS,
LANGLEY FIELD, VA., April 21, 1936.

REFERENCES

1. Wood, Donald H.: Tests of Nacelle-Propeller Combinations in Various Positions with Reference to Wings. Part I—Thick Wing—N. A. C. A. Cowled Nacelle—Tractor Propeller. T. R. No. 415, N. A. C. A., 1932.
2. Wood, Donald H.: Tests of Nacelle-Propeller Combinations in Various Positions with Reference to Wings. II—Thick Wing—Various Radial-Engine Cowlings—Tractor Propeller. T. R. No. 436, N. A. C. A., 1932.
3. Wood, Donald H.: Tests of Nacelle-Propeller Combinations in Various Positions with Reference to Wings. III—Clark Y Wing—Various Radial-Engine Cowlings—Tractor Propeller. T. R. No. 462, N. A. C. A., 1933.
4. McHugh, James G.: Tests of Nacelle-Propeller Combinations in Various Positions with Reference to Wings. IV—Thick Wing—Various Radial-Engine Cowlings—Tandem Propellers. T. R. No. 505, N. A. C. A., 1934.
5. Valentine, E. Floyd: Tests of Nacelle-Propeller Combinations in Various Positions with Reference to Wings. V—Clark Y Biplane Cellule—N. A. C. A. Cowled Nacelle—Tractor Propeller. T. R. No. 506, N. A. C. A., 1934.
6. Wood, Donald H., and Bioletti, Carlton: Tests of Nacelle-Propeller Combinations in Various Positions with Reference to Wings. VI—Wings and Nacelles with Pusher Propeller. T. R. No. 507, N. A. C. A., 1934.
7. Ower, E., and Hutton, C. T.: On the Interference of a Streamline Nacelle on a Monoplane Wing. R. & M. No. 1395, British A. R. C., 1931.
8. DeFrance, Smith J.: The N. A. C. A. Full-Scale Wind Tunnel. T. R. No. 459, N. A. C. A., 1933.
9. Parsons, John F.: Full-Scale Force and Pressure-Distribution Tests on a Tapered U. S. A. 45 Airfoil. T. N. No. 521, N. A. C. A., 1935.
10. Silverstein, Abe: Scale Effect on Clark Y Airfoil Characteristics from N. A. C. A. Full-Scale Wind-Tunnel Tests. T. R. No. 502, N. A. C. A., 1934.
11. Platt, Robert C.: Turbulence Factors of N. A. C. A. Wind Tunnels as Determined by Sphere Tests. T. R. No. 558, N. A. C. A., 1936.
12. Theodorsen, Theodore, and Silverstein, Abe: Experimental Verification of the Theory of Wind-Tunnel Boundary Interference. T. R. No. 478, N. A. C. A., 1934.
13. Wood, Donald H.: Engine Nacelles and Propellers and Airplane Performance. S. A. E. Jour., April 1936, pp. 148-160.

REPORT No. 570

THE EFFECT OF LATERAL CONTROLS IN PRODUCING MOTION OF AN AIRPLANE AS COMPUTED FROM WIND-TUNNEL DATA

By FRED E. WEICK and ROBERT T. JONES

SUMMARY

An analytical study of the lateral controllability of an airplane has been made in which both the static rolling and yawing moments supplied by the controls and the reactions due to the inherent stability of the airplane have been taken into account. The investigation was undertaken partly for the purpose of coordinating the results of a long series of wind-tunnel investigations with phenomena observed in flight tests; for this reason a hypothetical average airplane, embodying the essential characteristics of both the wind-tunnel models and the full-size test airplanes, was assumed for the study.

Stability derivatives for the average airplane and for several of the actual flight-test airplanes were computed, and computations were made in an attempt to reproduce by the theory the conditions of several actual flight tests. Computations made of forced rolling and yawing motions of an F-22 airplane caused by a sudden deflection of the ailerons were found to agree well with actual measurements of these motions.

The conditions following instantaneous full deflections of the lateral control have been studied, and some attention has been devoted to the controlling of complete turn maneuvers. A portion of the work was devoted to a study of controllability at stalling angles, and the results of this application of theory were found to agree qualitatively with flight-testing experience.

The angle of bank produced in 1 second, ϕ_1 , by a deflection of the rolling control may be taken as a relative measure of the control effectiveness. In the analysis of controllability below the stall, it was found that a simple measure of the rolling effectiveness of a control is given by the sum of a constant times the rolling moment and a con-

stant times the yawing moment. Thus a relative weight or importance is given to the secondary yawing moment produced by the rolling control. It was concluded that the importance of such secondary moments can be minimized by alteration of the moments of inertia of the airplane. Increasing the yawing moment of inertia reduces the effectiveness of a given yawing control in producing either yawing or rolling motion. Changes of rolling moment of inertia have little direct effect on either the rolling or yawing motion produced by a given rolling-control moment.

The study of conditions above the stall indicated that satisfactory control could not be expected without some provision to maintain the damping in rolling and that a dangerous type of instability would arise if the damping were insufficient. The quantity $L_p N_r - L_r N_p < 0$ was found to give a good measure of this type of instability.

INTRODUCTION

For some time the N. A. C. A. has been conducting a program of research on lateral control for the specific purpose of obtaining information that would lead to improvement of control at the low speeds and high angles of attack above the stall, a region in which present conventional ailerons are known to be unsatisfactory. Several series of wind-tunnel investigations have been completed and an attempt has been made to compare a number of widely different lateral-control devices on the basis of what has been considered their primary function—the provision of rolling moment. Some of the secondary characteristics, such as the yawing moments given by the controls and their effect on the damping in rolling, were considered but only by comparing the various values separately. Flight

tests were then made with the devices that seemed to promise the best lateral control at the stall. Some of them did not perform as had been expected from the wind-tunnel tests (see reference 1), indicating that the first approximation, based largely on the rolling moments given by the devices, was an insufficient basis for comparison and that the complete interaction of the secondary factors must very likely be considered.

References 2 to 5 describe important work that has been done on the lateral control of airplanes in both normal and stalled flight. Reference 2 gives a general account of the problem of control of the stalled airplane; references 3 and 4 describe investigations of the lateral control and stability of different biplane types.

The present report contains the results of a study of control effectiveness made by means of computations that take into account the secondary factors including the yawing moments given by the controls, their effect on the damping in rolling, the other lateral-stability derivatives, and the moments of inertia of the airplane.

Two methods of computation are used. In the first, the rolling and yawing motions are computed step by step for the conditions following a sudden deflection of the lateral control; in the second method a complete turn is arbitrarily specified and the control moments and deflections necessary to perform the maneuver are found. The first method is used to compare the effectiveness below the stall of various lateral-control devices and to investigate primarily the effects of changed stability characteristics above the stall.

The results of calculations made for normal unstalled conditions are compared with measurements made in flight using different types of lateral-control devices. The effects of certain changes in the lateral-stability characteristics below the stall are also studied. The method used in the study of complete turn maneuvers has proved to be a very practical way of dealing with specific control problems. Here all the stability characteristics of the airplane are taken into account but the lengthy and tedious integration of the equations of motion is avoided by predetermining the actual movements of the airplane in the form of some desired maneuver and then finding the manipulation of the controls that would be necessary to execute the specified maneuver. The coordination of the rudder with different types of ailerons has been studied in this way.

MOTION FOLLOWING SUDDEN CONTROL APPLICATION

The method used for calculating the motion following a sudden application of the controls consists of a step-by-step integration. In most cases the control moments were assumed to be applied constantly throughout the motion.

Assumptions and symbols.—The assumptions usually made in the study of airplane stability were used here, including:

1. That the air forces and moments arising from displacements of the airplane, relative to its steady condition of flight, are proportional to the displacements or to their rates.
2. That the components of moment due to the different components of motion are additive (i. e., the rolling moment due to the combined rolling and sideslipping may be computed as though the rolling and sideslipping had occurred separately).

The axes used in specifying the moments, angular velocities, etc., are fixed in the airplane and therefore move relatively to the air and to the earth. The X axis passes through the center of gravity of the airplane in the plane of symmetry and is chosen to point directly into the line of the relative wind when the airplane is flying steadily. In other respects the axes form a conventional trihedral system, intersecting at the center of gravity of the airplane, the Z axis pointing downward in the plane of symmetry and the Y axis pointing along the direction of the right wing. The motions discussed are those of the moving axes relative to the undisturbed air with the exception of the angle of bank, which is measured relative to the horizontal.

The symbols used in the various formulas are defined as follows:

U_0 , velocity along X axis in steady flight.

v , velocity of sideslip.

p , angular velocity in rolling.

r , angular velocity in yawing.

φ , angle of bank.

$\beta = \frac{v}{U_0}$, angle of sideslip.

δ , angle of control setting.

Y , component of force along Y axis.

L , rolling moment (about X axis).

N , yawing moment (about Z axis).

$L_p = \frac{\partial L}{\partial p} / mk_x^2$, rolling acceleration due to rolling.

$N_p = \frac{\partial N}{\partial p} / mk_z^2$, yawing acceleration due to rolling.
etc.

$\delta L_i = \frac{C_i q S b}{mk_x^2}$, where C_i is the control rolling-moment coefficient.

$\delta N_i = \frac{C_n q S b}{mk_z^2}$, where C_n is the control yawing-moment coefficient.

b , wing span.

c , wing chord.

S , wing area.

l , tail length (distance from c. g. to tail post).

mk_x^2 , moment of inertia of airplane about X axis.

mk_z^2 , moment of inertia of airplane about Z axis.

Γ , dihedral angle.

Λ , sweepback angle.

Equations of motion.—The moments acting on the airplane during its maneuvers are considered to be divided into two main groups: (1) Those due to the deflected controls, and (2) those arising from the motions of the airplane. The motions are usually supposed to be started by the action of the controls alone but, at each succeeding instant, to be conditioned by factors that vary directly in magnitude with the motions or displacements relative to the air. The effects of the motions are described by quantities known as "resistance," or "stability," derivatives. The part of a rolling moment due to rolling motion is calculated by the expression $p \frac{\partial L}{\partial p}$; the partial rolling moment due to combined yawing and rolling is given by:

$$p \frac{\partial L}{\partial p} + r \frac{\partial L}{\partial r}$$

It will be found convenient to replace the actual moments by their corresponding angular accelerations, which are proportional to them. Since

$$\frac{\frac{\partial L}{\partial p}}{mk_x^2} = L_p$$

the component of rolling acceleration due to rolling motion is simply

$$pL_p$$

If the airplane is moving in all its degrees of lateral freedom with deflected controls, the total acceleration in rolling is expressed by

$$\frac{dp}{dt} = \delta L_\delta + pL_p + rL_r + \beta L_\beta \quad (1)$$

where δL_δ is the part of the acceleration due to the control. Likewise the sum of the components of yawing acceleration is

$$\frac{dr}{dt} = \delta N_\delta + pN_p + rN_r + \beta N_\beta \quad (2)$$

The equation for the angle of sideslip contains both the centrifugal effect due to turning and the effect of gravity,

$$\frac{d\beta}{dt} = \frac{g}{U_0} \sin \varphi - rU_0 \quad (3)$$

It is to be noted that, when the angle of sideslip β was computed, the component accelerations due to the

sidewise air forces (i. e., terms containing Y) were neglected. The most important term here is Y_β ; a rough estimate shows that its greatest probable effect would be negligible for the type of maneuver investigated.

Since the axes change their orientation in the airplane with different lift coefficients, they will not be directly in line with the axes of the principal moments of inertia. The corrections are small, however, and have been neglected.

Integration of equations.—The equations show that in order to calculate the acceleration of the motion at any time, the velocities p , r , and the angle of sideslip β must be known. This knowledge is, of course, available only when all accelerations before the time in question are known; an integration is therefore necessary. This integration may be conveniently performed by dividing the time during which the motion occurs into very small steps and by assuming that the velocities remain constant over these small intervals. If a particular instant is denoted by the subscript n , the accelerations at this instant may be calculated by the formulas

$$\left. \begin{aligned} \left(\frac{dp}{dt} \right)_n &= (\delta L_\delta)_n + p_n L_p + r_n L_r + \beta_n L_\beta \\ \left(\frac{dr}{dt} \right)_n &= (\delta N_\delta)_n + p_n N_p + r_n N_r + \beta_n N_\beta \end{aligned} \right\} \quad (4)$$

If the preceding time instant is denoted by $n-1$, the accelerations at each succeeding instant may be calculated step by step, using the velocities computed from the previous instant. Thus:

$$\left. \begin{aligned} p_n &= \left(\frac{dp}{dt} \right)_{n-1} \times \Delta t + p_{n-1} \\ \varphi_n &= p_{n-1} \times \Delta t + \varphi_{n-1} \\ r_n &= \left(\frac{dr}{dt} \right)_{n-1} \times \Delta t + r_{n-1} \\ \beta_n &= \left(\frac{d\beta}{dt} \right)_{n-1} \times \Delta t + \beta_{n-1} \end{aligned} \right\} \quad (5)$$

The right-hand sides of these equations contain only quantities known from the preceding instant. At the start, $n=0$, all the velocities and angles are taken as zero, and the accelerations are caused by the control moments alone,

$$\left. \begin{aligned} \left(\frac{dp}{dt} \right)_0 &= \delta L_\delta = \frac{C_{lq} S b}{mk_x^2} \\ \left(\frac{dr}{dt} \right)_0 &= \delta N_\delta = \frac{C_{nq} S b}{mk_z^2} \\ \left(\frac{d\beta}{dt} \right)_0 &= 0 \end{aligned} \right\} \quad (6)$$

A typical example illustrating the step-by-step computation is given in table I.

Comparison of computed and measured motions.—The results of a number of flight tests of the F-22 airplane equipped with several widely different lateral-

control devices have been used as checks of the computations. These tests were conducted by gliding the airplane at various steady speeds and suddenly deflecting the aileron control to its full extent. Instrument records of the resulting rolling and yawing angular

of a series of lateral-control devices (reference 7). The wind-tunnel program included experiments to determine several important lateral-stability characteristics as well as the static rolling and yawing moments produced by the control devices; the results of these

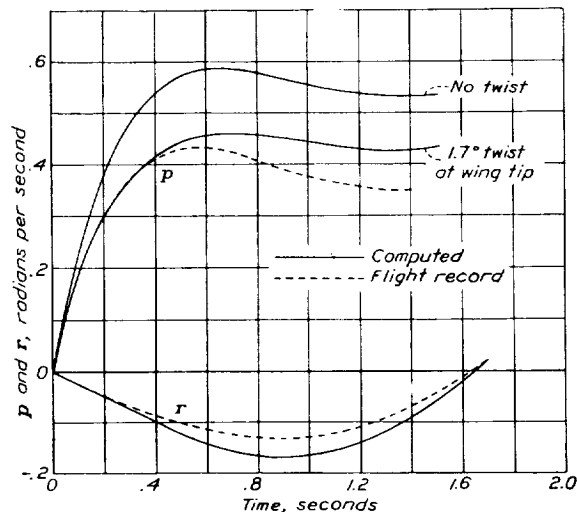


FIGURE 1.—Rolling and yawing motion of F-22 airplane with long narrow ailerons. Flaps up; $C_L=1.0$.

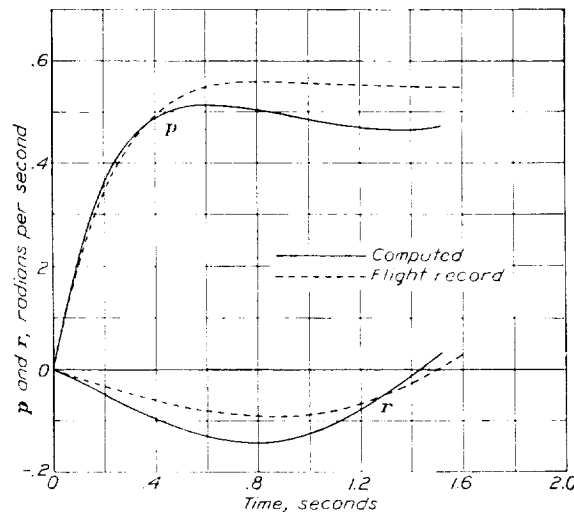


FIGURE 3.—Rolling and yawing motion of F-22 airplane with balanced short wide ailerons. Flaps up; $C_L=1.10$.

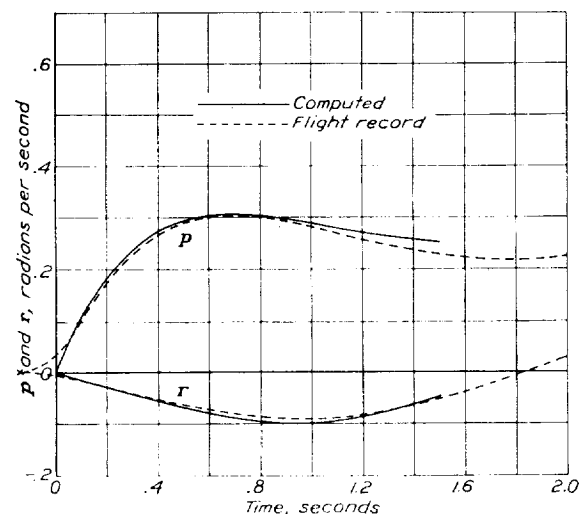


FIGURE 2.—Rolling and yawing motion of F-22 airplane with long narrow ailerons. Flaps down; $C_L=1.75$.

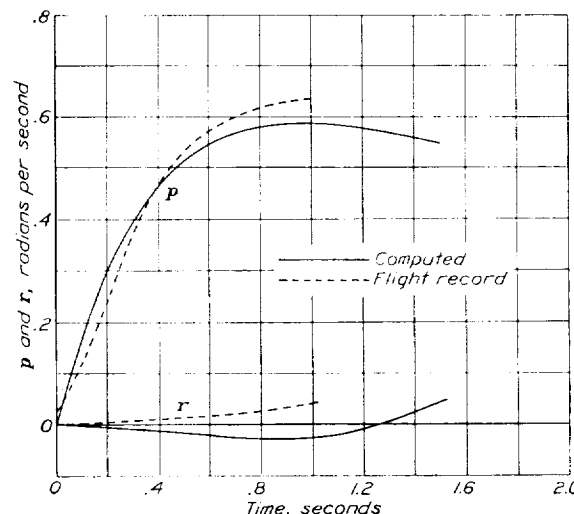


FIGURE 4.—Rolling and yawing motion of F-22 airplane with retractable ailerons. Flaps up; $C_L=1.0$.

velocities were made as a measure of the effectiveness of the various controls. (See references 1 and 6.)

The procedure in these experiments simulated very closely the conditions assumed in the computations, although the flight records showed that about 0.15 second was actually required to accomplish the full deflection of the control, which was assumed to be instantaneous in the computations. In the comparisons included, this discrepancy was eliminated by appropriate shifts of the time scales.

The flight tests were intended to supplement a program of tests made in the 7- by 10-foot wind tunnel

experiments furnished the necessary basis for reproducing the conditions of the flights in the computations. The quantities needed in the computations, including the resistance derivatives, were determined from the known dimensions of the F-22 airplane by the methods given in appendix I.

When computed motions and flight records were first compared, it was found that in many cases the initial accelerations in roll predicted from the rolling moments obtained in the wind tunnel were larger than those shown by the motions recorded in flight. Thus, the full value of the rolling moment measured on the

models was apparently not realized in flight. Examination showed this lack of agreement to be especially apparent in the cases of devices that would be expected to exert the greatest twisting effect on the wings and, since appreciable twisting of the actual wings had been observed in full-scale wind-tunnel experiments, the discrepancy was attributed to this effect. Calculation showed that in the most extreme case (that of ordinary narrow-chord ailerons) a linearly distributed angle of twist reaching 1.7° at the wing tip would account for the observed difference and that the rolling-moment coefficient would be reduced from 0.056 to 0.043. In this case the flight test was made at a dynamic pressure of 9 pounds per square foot. With this first correction as a basis, a general correction formula was used in which the reduction in rolling moment was given as a proportion of the dynamic pressure and the change in section pitching-moment coefficient produced by deflecting the controls.

Figures 1 and 2 show the rolling and yawing motions of the F-22 equipped with long, narrow ailerons. This particular airplane was also equipped with flaps that retracted into the wing ahead of the ailerons. (See reference 6.) Figure 1 illustrates the effect attributed to twisting of the wings. The higher curve was obtained when a value of the rolling-moment coefficient based on a wind-tunnel test of a solid wooden model was used. The yawing angular velocity curves showed remarkably good agreement in these two cases, especially as regards the period of the oscillation of this motion.

The comparison of the yawing curves in figures 3 and 4 is not so favorable as in the former cases. In figure 3 it appears that the yawing-moment coefficient as computed from the wind-tunnel data was slightly greater than that recorded. In this case the control moment coefficients used in the computations were obtained from full-scale wind-tunnel tests of the actual airplane; hence no correction for wing twist was applied. The curves of figure 4 apply to a modified F-22 airplane equipped with retractable ailerons. It is possible that this control device, which is similar to a spoiler, has some effect on the yawing moment due to rolling. The disagreement in the yawing curves would seem to indicate that too large a negative value was assumed in the computations.

The curves of computed rolling motion show no consistent disagreements with the curves plotted from the flight measurements, the differences being of opposite sign in several cases. It seems probable that these comparisons represent the general accuracy obtainable either in the experiments or in the calculations.

COMPUTATIONS FOR AVERAGE AIRPLANE IN UNSTALLED FLIGHT

The results of the flight experiments with the F-22 airplane were not suitable for direct comparisons of the effectiveness of the various controls used because the airplane was modified considerably during the progress of the experiments (see references 1 and 6) so that

different sets of stability derivatives and moments of inertia had to be used in the computations to represent the different individual tests. In order to secure data of more general significance and to make a more systematic investigation of control effectiveness than was possible in the flight experiments, it was thought desirable to make a series of computations based on a standard set of airplane characteristics, including standard resistance derivatives and moments of inertia. At the same time it was desired to retain the basic dimensions of the F-22 machine so that there would be at least a partial check with the flight-test work at all times.

Specifications of average airplane.—With these considerations in mind the specifications of an arbitrary standard airplane were devised. The weight and the wing area and span of the F-22 airplane were retained but, since other dimensions were obtained from statistical averages, the machine was called an "average airplane." These statistical averages were obtained by studying the specifications of a number of conventional airplanes of different sizes, weights, and types. Data from 20 to 40 airplanes were used for the determination of average values of the following characteristics:

1. The ratio of the total fin and rudder area to the wing area.
2. The ratio of the tail length (i. e., distance from *c. g.* of airplane to the tail post) to the wing span.
3. The ratios of the radii of gyration in rolling and yawing to the wing span.

The moments of inertia were obtained from data listed in reference 8. That the characteristics thus obtained did not differ appreciably from those of the F-22 is shown by the following table:

	Range of characteristics of F-22 airplane used in flight tests	Characteristics of average airplane
Weight.....pounds..	1,500-1,650	1,600
Wing span.....feet..	30- 32.8	32
Wing area.....square feet..	161- 172	171
Area of fin and rudder.....do..	10.1	10.8
Tail length.....feet..	14.5	14.6
mk_z	696-1,554	1,216
mk_z^2	1,520-2,118	1,700

Computations based on a purely dimensionless average airplane were considered, but it was thought that the results would have a more concrete meaning if they were presented in terms of an airplane of particular size, especially since they could then be directly compared with the flight results.

Unstalled-flight computations.—Most of the lateral-control devices tested in the wind tunnel did not cause any change in the stability derivatives of the wings (spoiler devices are a notable exception). In such cases the sole effect of the control in producing motions can

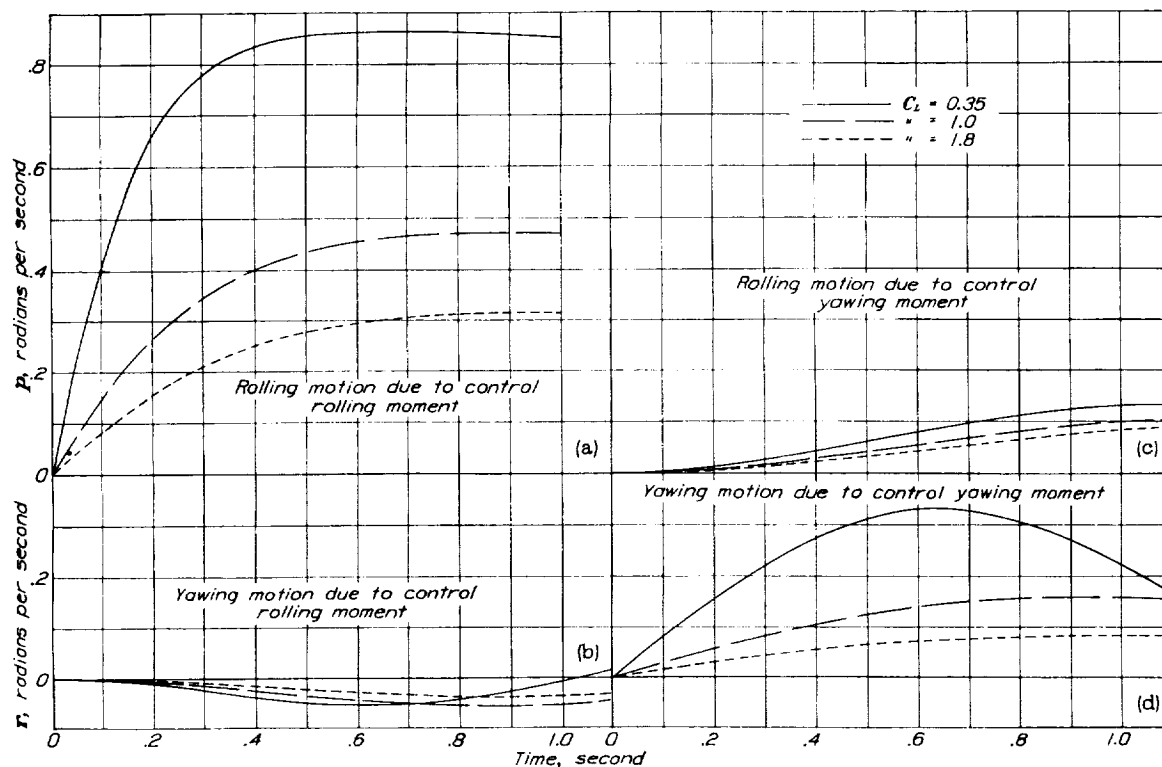
(a) (b) $C_L = 0.04$ $C_N = 0$ (c) (d) $C_L = 0$ $C_N = 0.01$

FIGURE 5 (a, b, c, d).—Computed rolling and yawing motions of average airplane.

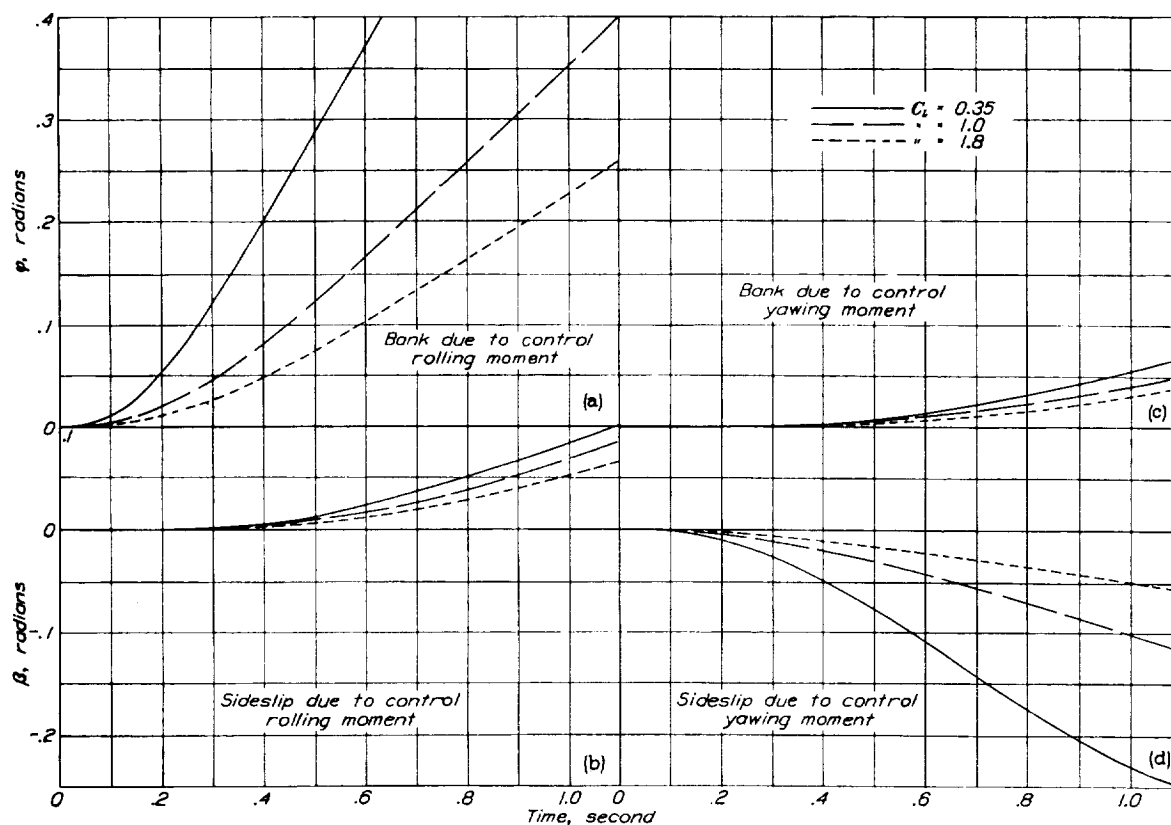
(a) (b) $C_L = 0.04$ $C_N = 0$ (c) (d) $C_L = 0$ $C_N = 0.01$

FIGURE 6 (a, b, c, d).—Computed angles of bank and sideslip of average airplane.

be attributed to the static rolling and yawing moments produced; consequently, a large class of devices could be investigated, in effect, by extending computations over a suitable range of combinations of static rolling and yawing moments.

On account of the linearity of the equations of motion it was possible to calculate the effects of yawing moments and rolling moments separately and later to add them in any desired proportion. Thus, at each of the three lift coefficients two computations were made, one to determine the motion due to a yawing moment and the other to determine the motion due to a rolling moment. The following table lists the values of the coefficients that were used:

C_L : 0.35; 1.0; and 1.8 (20 percent c split flaps, full span).

C_n : 0.01 and 0.

C_l : 0 and 0.04.

In these cases the dihedral angle assumed for the average airplane was 1° . Several additional computations were made to investigate the effect of variation of this factor, assuming angles of 5° and 9° .

Stability derivatives of average airplane.—The stability derivatives used in these computations were obtained by methods described in appendix I and are given in the following table; in the calculation the average airplane was assumed to have rounded-tip wings with 1° dihedral.

	L_p	L_r	L_β	N_p	N_r	N_β
$C_L=0.35$	-5.44	1.11	-2.16	-0.207	-0.913	5.52
Cruising speed $U_0=150$ feet per second						
$C_L=1.0$	-3.23	1.88	-1.11	-.301	-.663	2.04
Gliding speed $U_0=88.5$ feet per second						
$C_L=1.8$	-2.46	2.51	-1.66	-.310	-.977	1.46
Low speed (flaps) $U_0=66$ feet per second						

Results of below-stall computations.—The results of the series of computations for the condition below the stall are shown in figures 5 to 9. Calculated examples of the complete motion are given in figures 5 and 6, which show the rates of rolling and yawing and the angles of bank and sideslip plotted against time for the different flight speeds.

It was thought that the amount of motion produced in 1 second would be a reasonable measure of the control effectiveness. As previously mentioned, the motion produced by a given yawing moment can be added to that produced by a given rolling moment to get the simultaneous effect of both. Thus the formulas for the motion produced in 1 second by any combination of rolling and yawing moments are

$$\left. \begin{aligned} p_1 &= C_l \frac{\partial p_1}{\partial C_l} + C_n \frac{\partial p_1}{\partial C_n} \\ \varphi_1 &= C_l \frac{\partial \varphi_1}{\partial C_l} + C_n \frac{\partial \varphi_1}{\partial C_n} \\ r_1 &= C_l \frac{\partial r_1}{\partial C_l} + C_n \frac{\partial r_1}{\partial C_n} \\ \beta_1 &= C_l \frac{\partial \beta_1}{\partial C_l} + C_n \frac{\partial \beta_1}{\partial C_n} \end{aligned} \right\} \quad (7)$$

where $\frac{\partial p_1}{\partial C_n}$, $\frac{\partial \varphi_1}{\partial C_l}$, etc., are parameters that depend on the speed of flight and the stability characteristics of the airplane. These parameters are shown plotted against lift coefficient (as a measure of the flight speed) in figures 7 and 8 and represent the principal results of the series of computations for unstalled flight.

Discussion of below-stall computations.—The factors shown in figures 7 and 8 may be used to compare the effectiveness of various lateral-control devices on the basis of the motions and displacements they would produce on a 1,600-pound airplane of average stability characteristics. By showing the effect of secondary control moments in producing motion of the airplane, they give a measure of the relative weight to be assigned such secondary moments in comparing different devices. These factors will, of course, be somewhat different for airplanes of different stability characteristics and the relative effects of secondary control moments will be expected to be somewhat different also. The average airplane is simply a convenient yardstick in this respect.

If the factors given in figures 7 and 8 are used as absolute measures of the amount of motion produced in 1 second (aside from their use simply in comparing various control devices), a greater error will be committed in applying them to airplanes of different size than in applying them to airplanes of somewhat different stability characteristics. Reference 9 gives the necessary rules for correctly applying the present data to airplanes of any size or weight in which certain definite aspects of similarity are preserved. The theory requires that the airplanes be geometrically similar although they may have different densities. Practically, this requirement necessitates that the outward forms of the airplanes be similar and that the ratios of the radii of gyration about each axis to the wing span be the same. The motions of the different sized airplanes are compared at equal values of the lift coefficient. With equal values of the wing loading the angular velocities are inversely proportional to the spans: Thus,

and

$$\left. \begin{aligned} \frac{p'_1 b'}{2U_0} &= \frac{p_1 b}{2U_0} \\ \frac{\varphi'_1 b'}{2U_0} &= \frac{\varphi_1 b}{2U_0} \end{aligned} \right\} \quad (8)$$

With similar airplanes of different wing loadings the state of motion existing at a given time for one will generally pertain to a different instant for another, which is also true of an airplane of the same size and loading but flying in air of different density. Given the motion of the average airplane at 1 second, the instant to which this state of motion (as indicated by

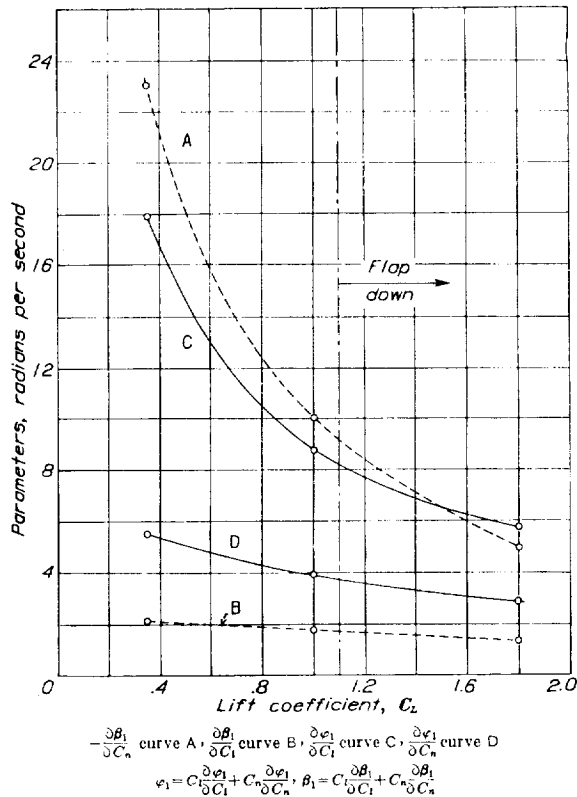


FIGURE 7.—Parameters for computing displacement of average airplane at end of 1 second with various combinations of rolling and yawing moments.

the value of $pb/2U_0$) pertains on a similar airplane may be found from:

$$t' = 1 \times \frac{S_2^p U_0}{S_2' p' U_0'} \quad (9)$$

Plots representing the motion of an airplane in non-dimensional terms have as abscissa

$$\frac{S_2^p U_0}{m} \times t$$

and as ordinate

$$\frac{pb}{2U_0}$$

or

$$\frac{S_2^p b}{\varphi \frac{p}{2m}}$$

etc.

In the case of the average airplane the influence of moderate dihedral on the lateral controllability below

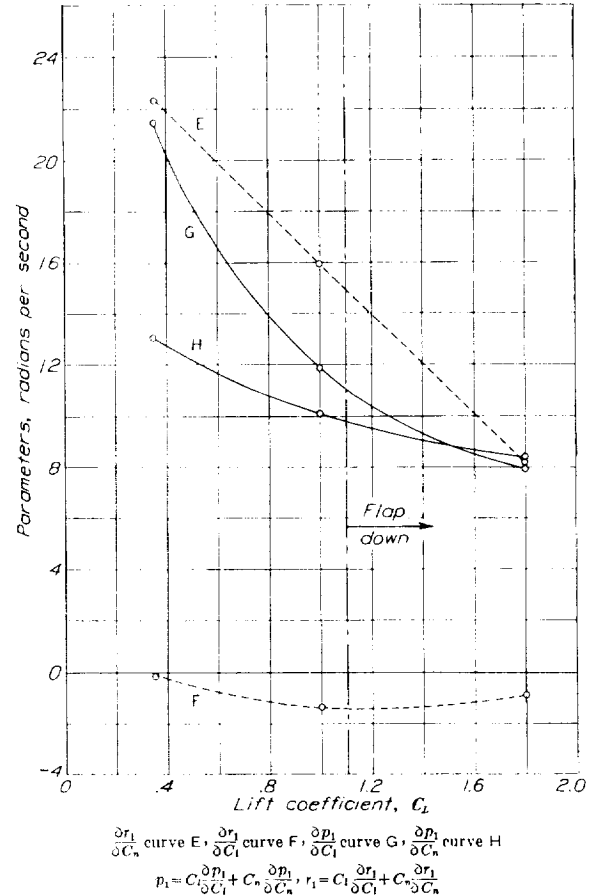


FIGURE 8.—Parameters for computing motion of average airplane at end of 1 second with various combinations of rolling and yawing moments.

the stall was small, as is shown in figure 9. If, however, a large dihedral effect is combined with considerable adverse yawing tendency from the ailerons, the lateral control may become ineffective. This condition is most likely to occur at low speeds with flaps deflected because under these conditions the wings show their greatest tendency to roll when yawed (dihedral effect) and because the aileron yawing moment is usually greatest at high lift coefficient. Figure 9 shows that with a dihedral angle of 9° and an adverse yawing moment of one-fourth of the rolling moment, the aver-

age airplane actually reversed its normal roll, rolling against the ailerons less than 2 seconds after they were applied. The magnitude of the tendency for a given adverse yawing moment to render the lateral control ineffective depends to some extent on all the stability characteristics of the airplane but principally on the ratio of rolling to yawing moments in sideslip, i. e., on $\frac{dC_l/d\beta}{dC_n/d\beta}$. For the various cases depicted in figure 9 these ratios were:

Dihedral angle, degrees	$\frac{dC_l/d\beta}{dC_n/d\beta}$
1	0.8
5	1.2
9	2.4

Large values of this ratio decrease the aileron control effectiveness if the secondary yawing moments are ad-

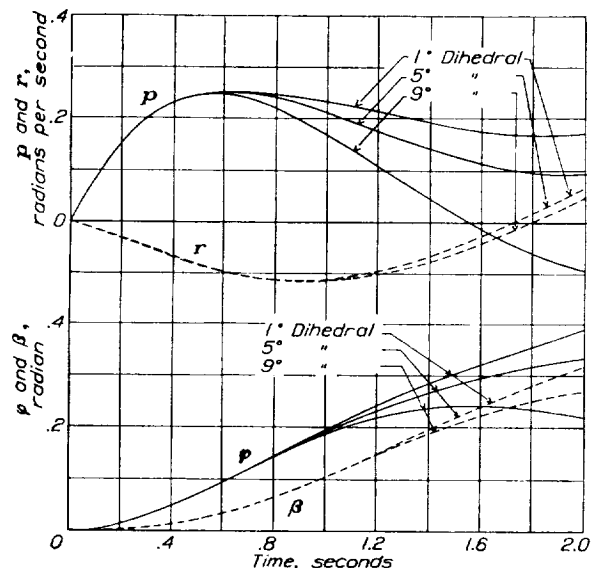


FIGURE 9.—Effect of dihedral combined with adverse yawing moment on rolling control. Flaps down; $C_L=1.8$; $C_L=0.04$; $C_N=-0.01$.

verse but will tend to increase it if they are favorable.

The curves of rolling motion given in figures 1 to 5 show that the rate of rolling rises quickly at the start on account of the relatively great rolling moment but soon becomes almost steady. This steady rate is attained in about 0.3 second at high speed and occurs when the air damping of the rolling motion is large enough to overcome the control moment. Obviously the lateral moment of inertia (mk_x^2) cannot have much influence on this portion of the curve since the airplane is not accelerating appreciably, and its effect will be shown mainly on the starting slope of the curve. (See fig. 10.) It may be seen that the area under the curve at, say, 1 second would not be appreciably affected by changes in this slope; hence the angle of bank reached in 1 second would not be much affected by the moment of inertia in rolling. This fact has been borne out by flight ex-

periments made by the N. A. C. A. in which the test pilots were unable to detect with certainty the effects of changes in rolling moment of inertia of as high as 50 percent. (See also reference 10.)

The yawing-motion curves indicate a different phenomenon. Here the damping is relatively small and the effects of moment of inertia in yaw are fairly large. Thus it appears that the magnitude of the rudder moments should be accommodated to the airplane moment of inertia, while the principal consideration determining the rolling-control moments should be the air-damping factor.

Since the amount of yawing motion produced by a given yawing moment is primarily governed by the moment of inertia in this motion, it appears that the unfavorable influence of secondary aileron yawing moments could be effectively reduced by increasing this moment of inertia. Furthermore, since the direct effect of roll moment of inertia on the rolling motion is apparently slight, it is possible that increasing mk_z^2 by

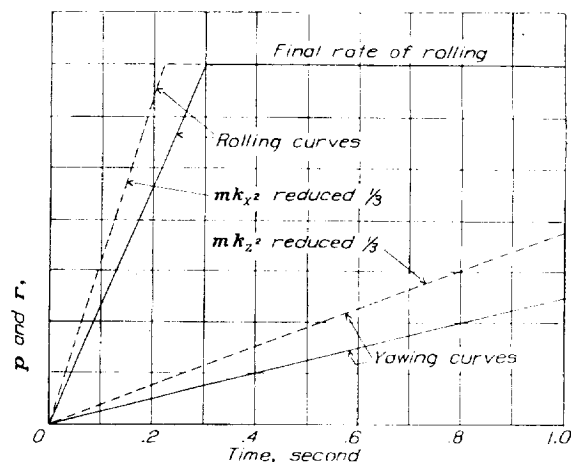


FIGURE 10.—Diagram illustrating effect of change of moments of inertia on rolling and yawing control.

distributing weight along the wing span would actually increase the aileron effectiveness if considerable adverse yawing moment were present.

COMPUTATIONS FOR STALLED FLIGHT

Experiments with lateral control at angles of attack above the stall having been made both in the flight and the wind-tunnel research projects, it was desired to extend the present investigation to cover this condition also. Accordingly, a study of the results of both series of tests was made with the object of determining whether the conditions encountered in practice could be reproduced in theory.

Unfortunately, the wind-tunnel experiments showed that no certain determination of the factors (resistance derivatives) involved in the motion of a stalled airplane was possible. On the other hand, the flight experiments indicated that these factors apparently had no definite values (according to their usual definition), inasmuch

as the action of the airplane could not be foretold from one experiment to the next. For example, the outcome of a simple aileron movement might in one instance be a roll in the direction urged by the control; whereas at another time, under practically the same conditions, the roll would be the reverse of that intended.

Stability derivatives above stalling angles.—The reasons for the apparently contradictory results of the flight tests may be found in the wind-tunnel measure-

ment in rolling changes sign and becomes an "aiding" (autorotational) moment.

Obviously many of the assumptions of the method as used in investigating unstalled-flight phenomena are not true in the case of stalled flight. In particular, the assumed independence of small longitudinal and lateral motions, which is supported by both experience and reason for the ordinary-flight range, cannot be said to hold under these new conditions because the values of the derivatives change very rapidly with small changes of longitudinal attitude (angle of attack). The assumption that the components of a moment arising from different sources may be added together as though their causes occurred separately is apparently borne out only in the abstract sense of representing the average condition.

In spite of these limitations of the method, it was considered feasible to extend the computations to the condition of stalled flight in the study of the general conditions encountered in controlling such flight, although the results of the computations made for these conditions do not have the same significance as those made for conditions below the stall. The former results gave quantitative estimates of the amount of motion produced by given control moments; the extension of the computations to stalled flight will only illustrate the various phenomena that may result from the conditions predicted by the wind-tunnel experiments.

Experience in attempting controlled flight above the stall has shown that the possibility of controlling such flight depends as much on the natural stability characteristics of the airplane as on the possibility of securing adequate controlling moments. Because of this fact the present computations were made primarily to investigate the effects of changed stability characteristics (derivatives). Another important reason for choosing various combinations of stability derivatives is the fact that no very definite values can be assigned to them for a particular lift coefficient, as was possible in the unstalled-flight range.

For these reasons the investigation of controllability above the stall is necessarily presented in a manner different from that used in the cases of ordinary flight. The wind-tunnel measurements were studied to find the approximate variation of the resistance derivatives over a range of angles of attack definitely above the stall, chosen to include the region of most violent instability. The particular lift coefficient assumed was necessarily somewhat loosely defined ($C_L=1.2$); it was so taken to represent extreme stalling as well as intermediate conditions. The calculation of the stability derivatives at these angles is given in appendix I.

In the variation of the stability characteristics to take account of the range of possible conditions, the effects of the parts of the airplane other than the wings were not considered. The wing characteristics which

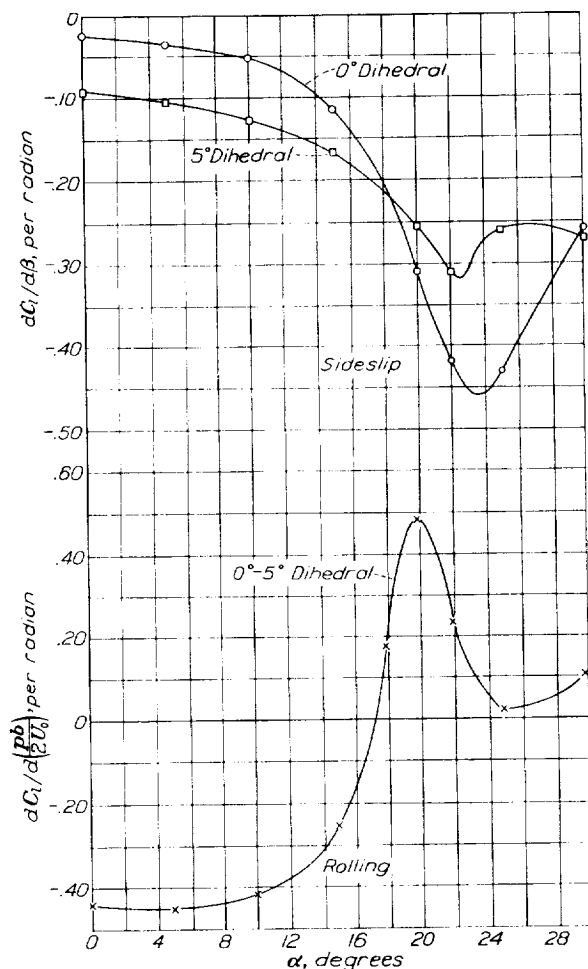


FIGURE 11.—Coefficients of rolling moment due to rolling and sideslip at various angles of attack. Rectangular Clark Y monoplane; data from tests in the 7- by 10-foot wind tunnel.

ments of the stability characteristics made at these high angles; these measurements show that motions of the wings may develop unstable moments, which could quickly overpower static rolling or yawing moments given by the controls. Figure 11 shows typical measurements of coefficients by which these quantities are determined. These curves show that the rolling moment due to sideslip of a straight wing increases enormously as the stall is approached, reaching values 7 or 8 times as great as those at medium angles below stalling. Under the same conditions the damping

show the greatest variation in this region and which apparently have the greatest effect on the stability are:

1. The damping in rolling, L_p .
2. The rolling reaction due to sideslip, L_β .
3. The yawing reaction due to rolling, N_p .

Accordingly, three values for each of these were chosen, covering the range shown by the wind-tunnel data and representing two extremes and one mean condition. These values were designated a, b, and c and are listed in table II.

TABLE II.—VALUES OF STABILITY DERIVATIVES USED ABOVE STALL

Designation	L_p	L_β	N_p
a	-1.75	-7.4	-0.20
b	0	-11.4	.53
c	3.50	-14.4	1.06

In each case it will be noted that letter c denotes the most extreme condition likely to be encountered. Condition a may be fairly assumed to apply only to cases where some provision is made to prevent the wing tips from stalling, which may be accomplished by washout or twist or by means of some such device as tip slots. (See appendix I for determination of these derivatives.)

The computations were made to cover more than a dozen different combinations of these values of the derivatives in conjunction with a given fixed pair of control rolling and yawing moments. These arbitrary controlling moments were chosen to represent rolling- and yawing-moment coefficients somewhat greater than those obtained with ordinary ailerons but which might be attained in practice with rather large ailerons, especially those of the short, wide type described in reference 7, I. As in the previous computations (below stall), the sign of the standard yawing-moment coefficient was alternated, giving the effect of favorable and adverse, as well as zero, secondary yawing moment.

Range of investigation of stalled flight.—Since in these computations the plan was to study the *possibility of control* rather than to obtain any numerical measure of control effectiveness, the procedure of the computations was sometimes varied in such a way as to represent attempts of the control to check motions of the airplane as well as to start them. In some cases the motion was assumed to be due to some external cause and to exist at the start of the computations, while in other cases the initial setting of the control was reversed after a short interval in an attempt to check the motion it had already produced. The effects of both favorable and adverse yaw were tried in these cases.

Results of computations.—Figure 12 shows rolling motions resulting from suddenly applied and continuously maintained aileron deflections giving a rolling-moment coefficient of 0.04 and an adverse yawing-

moment coefficient of -0.02 . The different angular-velocity curves are the results of assuming different combinations of the stability derivatives listed in table II. In accordance with the plan of table II, the first letter in each symbol designation attached to the curves indicates the value of the damping factor L_p used; the second, the value of L_β ; and the last, N_p .

These curves appear to represent the same erratic phenomena as were observed in the flight experiments. It will be noted that in some instances the direction of motion of the airplane after a short interval was the reverse of that urged by the rolling control, while in other instances it rolled with increasing acceleration in the direction urged. Either of these phenomena

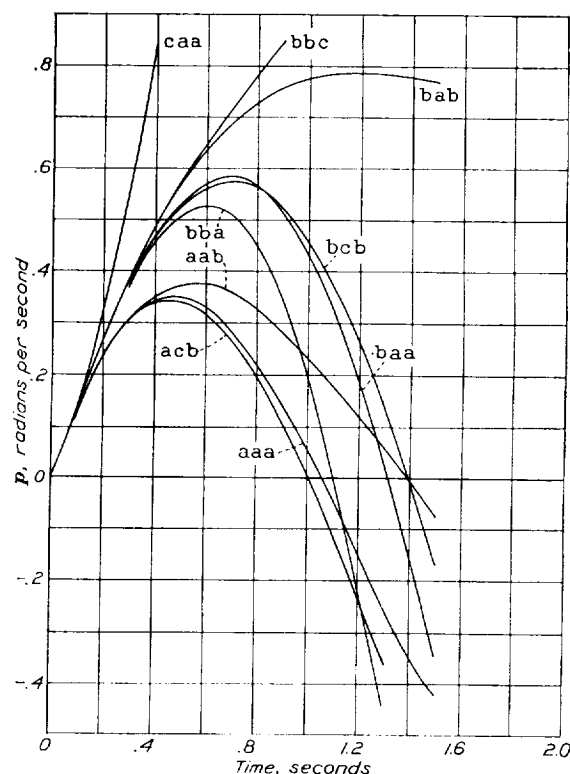


FIGURE 12. Rolling motions resulting from application of adverse-yaw aileron control in stalled flight with different combinations of stability derivatives; $C_l=0.04$; $C_n=-0.02$.

occurred within the predictable range of the stability derivatives.

The effects of smaller control rolling and yawing moments may be visualized simply by reducing the scales of the motions. Thus in figure 12 the motions calculated for $C_l=0.02$ and $C_n=-0.01$ would be just half those plotted.

Figure 13 shows the results of attempts to check an initial disturbance in rolling with both favorable- and adverse-yaw ailerons. The failure of the adverse-yaw ailerons is due mainly to the yawed attitude they produce, although the actual yawing motion accounts for an appreciable effect. Figure 14 differs from figure 13 in that it includes also conditions in which the initial

motion countered by the ailerons was assumed to be due to the action of the control rather than to an external disturbance in rolling. Here the ailerons were called upon to check whatever yawing motion they had previously produced. In this case it will be noted that the favorable-yaw ailerons encountered difficulty because it was hard to recover from the initial motion they had produced.

Figure 15 shows the effect of a delay in attempting to recover from rolling and yawing motion. Because of the instability of the airplane, the motion could not be checked even though the yawing moment of the ailerons was favorable. Thus, for the particular case illustrated, a delay of 0.1 second in reversing the control changed the action from one in which the airplane followed the

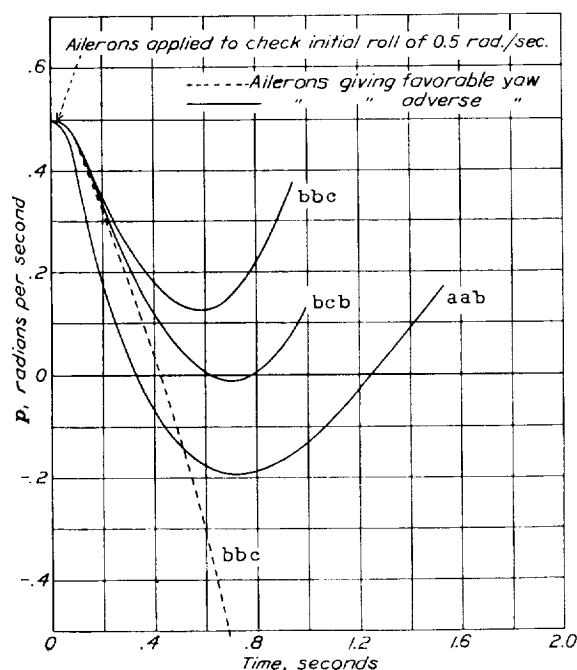


FIGURE 13.—Rate-of-rolling curves illustrating attempts to control initial motion in pure rolling. Stalled flight; $C_l = -0.04$; $C_a = \pm 0.02$.

control to one in which it continued to roll against it.

Discussion in terms of stability derivatives.—The motion of the average airplane in stalled flight is apparently governed more by its natural tendencies than by the applied control moments, a condition illustrated by the curves previously described which showed that the airplane developed tendencies that were uncontrollable in some instances. When using the step-by-step method, it was found convenient to tabulate each separate component of the rolling and yawing accelerations due to the stability factors as well as the components of motion. (See table I.) In this way a complete history of the contribution of each factor was obtained, thus enabling a study of the controllability in terms of the stability derivatives.

Undoubtedly the most important single factor contributing to the uncontrollable instability above the

stall is the loss of the damping in rolling. Below the stall this damping is the most powerful constraint of the airplane, and the effects produced by its sudden drop to zero or to a negative value exert a great influence on the behavior of the machine. Apparently no airplane can be considered safely controllable above the stall if the autorotational tendencies observed in wind-tunnel tests of plain wings are retained.

During a roll maneuver in stalled flight there may be, in addition to the control moment, certain other factors that tend to accelerate the rolling. These factors arise because the rolling motion by itself usually tends to

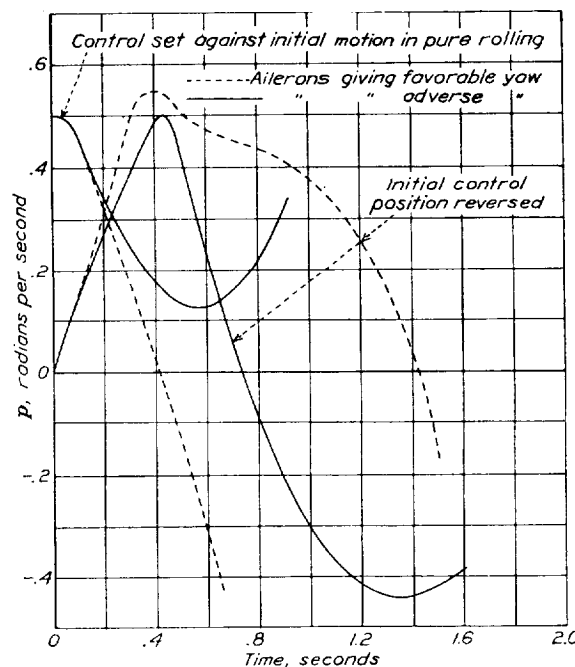


FIGURE 14.—Rate-of-rolling curves showing effect of favorable and adverse aileron yawing moments in attempting to control initial motion in pure rolling and in reversing initial control position. Case bbc; $C_l = 0.04$; $C_a = \pm 0.02$.

induce a favorable yawing action above the stall. Thus when the right wing is dropping, its added drag causes a yaw to the right, retarding the wing tip and causing a loss of lift due to decreased speed and tending to aggravate the dropping of the wing. The factors that directly oppose these rolling and yawing motions by damping tend to check this sequence if they are present. The first two effects, which aid the angular motion indirectly, relate to L_r and N_p , proportional, respectively, to the rolling moment due to yawing and the yawing moment due to rolling. Evidently if these moments overcome the direct damping tendencies, the angular motion will tend to accelerate of its own accord or will diverge. Suppose for the moment that these opposing tendencies just balance each other, that is,

$$\begin{cases} pL_p + rL_r = 0 \\ pN_p + rN_r = 0 \end{cases} \quad (10)$$

Inasmuch as p and r are simultaneous, there will exist a relation between the derivatives that is independent of p and r ; i. e.,

$$L_p N_r - L_r N_p = 0 \quad (11)$$

If this sum is zero, L_r and N_p are sufficiently large to equilibrate the stabilizing damping terms; and, if it is negative, any combined rolling and yawing motion will tend to diverge with increasing acceleration even though the direct dampings are present. The relation between this criterion and the behavior of the airplane in lateral motions above the stall is shown in table III, which gives values for the cases shown in figures 12 to 16.

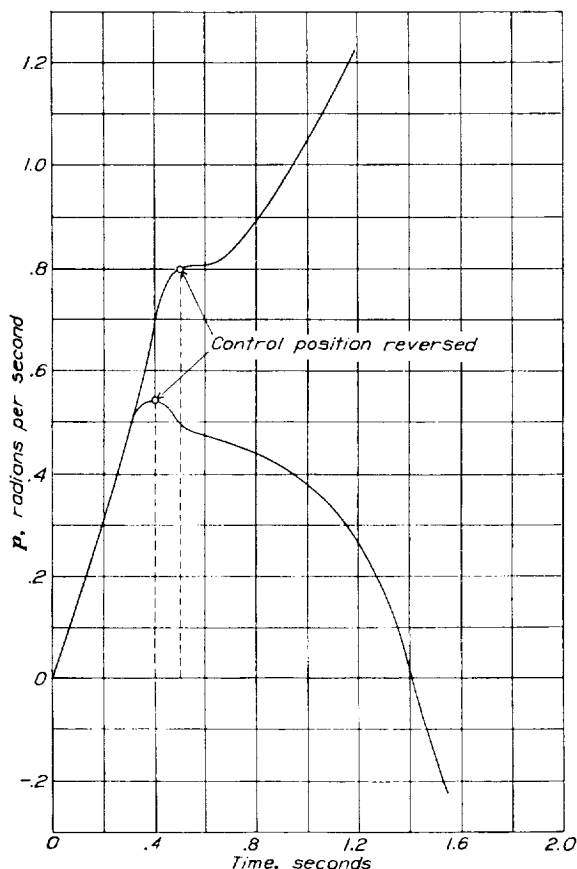


FIGURE 15.—Effect of delay in attempting to recover from motion started by ailerons with favorable yaw. Stalled flight. Case bbc; $C_l=0.04$; $C_h=0.02$.

It will be noted that the curves of figure 12 which indicate the greatest tendency toward continued rolling in the direction started correspond to the greatest negative values of $L_p N_r - L_r N_p$. In the curves shown, the rolling control was assumed to give an adverse yawing moment that served to oppose the tendency toward divergence indicated by negative values of this criterion. If a rolling moment with no secondary yawing moment had been assumed in these cases, each curve would have shown an increasing acceleration in rolling greater than that given by the control and ac-

cording to the magnitude of the tendency exhibited by the value of the criterion, as shown in figure 16. After a definite interval this tendency would have exceeded the power of the controls, and recovery would have been impossible.

Below the stall this criterion appears to be in every case positive, indicating stability. Relatively large positive values indicate relatively great damping of combined rolling and yawing motion.

The foregoing considerations do not take account of any sideslipping effects. These considerations, when combined with the factors determining the sideslipping tendency, give a more complete idea of the controllability characteristics of the airplane at high angles of attack and in stalled flight.

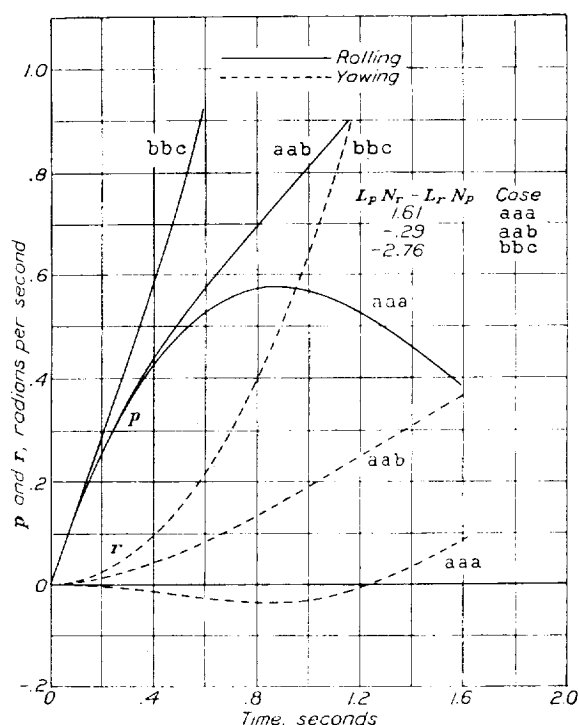


FIGURE 16.—Rolling and yawing motions resulting from application of rolling moment without secondary yawing moment showing effect of different degrees of damping; $L_p N_r - L_r N_p$; $C_l=0.04$, $C_h=0$.

It may be shown that the question of whether the airplane tends to sideslip inward or outward at the beginning of a rolling motion depends on the magnitude of N_p compared with g/U_0 . As rolling commences from level flight the yawing tendency due to the rolling (which is usually positive above the stall) causes the downgoing wing to be dragged back, creating an outward sideslipping tendency. This tendency is opposed by the action of gravity when the plane is banked, tending to produce inward sideslip. The condition that the outward and inward accelerations cancel is that

$$r U_0 = g \phi \quad (12)$$

assuming $\sin \varphi$ equal to φ . The angular acceleration in yawing requisite to this condition is

$$\frac{dr}{dt} = \frac{g}{U_0} p \quad (13)$$

In a rolling disturbance the yawing angular acceleration will be due only to N_p , or:

$$\frac{dr}{dt} = p N_p \quad (14)$$

Hence the condition that a rolling disturbance from level flight result in neither outward nor inward sideslipping is that

$$N_p = \frac{g}{U_0} \quad (15)$$

and the relative magnitudes of these quantities may be taken as an indication of the resultant tendency.

The airplane may diverge in the combined rolling and yawing motion previously discussed without sideslipping although such will not generally be the case. Near stalling angles the magnitude of the dihedral effect of the wings increases enormously (especially if the actual dihedral angle is small) and, if the tendency of the airplane is to sideslip outward while rolling and turning, any divergence in the rolling and yawing motion (indicated by negative $L_p N_r - L_r N_p$) will be greatly aggravated. The question of whether the dihedral effect will increase the instability is determined by the sign of the quantity $(N_p - g/U_0)$. The magnitude of the effect of the sideslipping tendency thus determined obviously depends on the stability derivatives in sideslip L_β and N_β or, more conveniently, on L_β/N_β . The values of N_p computed for the stalled-flight conditions b and c were considerably larger than g/U_0 , indicating that the natural tendency would be toward outward sideslip during a lateral maneuver. In such cases N_β would exert a stabilizing influence, tending to straighten out the skid. The values of these sideslipping criterions for the cases shown in figures 12 to 16 are given in table III.

TABLE III.—CONTROLLABILITY CRITERIONS FOR CASES SHOWN IN FIGURES 12 TO 16

Designation (see fig. 12)	Damping of rolling L_p	Combined damping $L_p N_r - L_r N_p$	Sideslip indication $N_p - g/U_0$	Sideslip stability factor $-L_\beta/N_\beta$
	(1)	(2)	(3)	
aaa	-1.75	1.61	-0.60	2.73
aab	-1.75	-.29	.13	2.73
acb	-1.75	-.29	.13	3.76
baa	0	.52	-.60	2.73
bab	0	-1.38	.13	2.73
bba	0	.52	-.60	3.40
bcb	0	-1.38	.13	3.76
caa	3.50	-1.65	.60	2.73
bbe	0	-2.76	.66	3.40

¹ Positive values indicate instability.

² Negative values indicate instability.

³ Positive values indicate outward sideslipping tendency.

Possible modifications of characteristics to improve stability above the stall.—Of the factors influencing

the lateral controllability, the stability characteristics that depend on the moments developed by the wings appear to be most important, since it is to be expected that they will be changed most by stalling. In addition to the damping in rolling, the wing moment characteristics that show marked change at the stalling point and contribute to the instability are L_r , L_β , and N_p . The factor L_r , proportional to the rolling moment due to yawing, depends on the lift coefficient and on the spanwise distribution of lift. Obviously, the greater the lever arm of the supporting lift, the greater L_r will be and, since it is desired to make L_r smaller, tapering the wings or shortening their span should help. The factor L_β at normal angles of attack depends also on this spanwise lever arm of the lift and on the dihedral angle. At stalling angles different tip shapes have considerable effect and the relation between the dihedral angle and the rolling moment reverses, the greatest moment being shown by the straight wing with square or upturned tips. (See fig. 11.) Here also, shortening the span and tapering the wing should improve conditions. The use of a moderate dihedral angle appears desirable in the stalled condition. The other wing characteristic, N_p , would be favorably affected by shortening the span of the wings. Here its magnitude depends mainly on the rate of increase of the profile drag of the wings and on the effective arm of the increase. If no damping in rolling (L_p) is present, there will be no induced N_p but in this case the slope of the wing profile-drag curve is almost certain to be very great, more than accounting for the induced effect. (See appendix I.) Taper or washout of the wings should help this situation. The provision of damping in rolling calls for keeping the wing tips from stalling; this requirement is compatible with all the others mentioned except that for small L_r . The desirability of maintaining the damping, however, far outweighs this consideration.

In the consideration of modifications of wing design to improve the controllability at high angles, it is important to take account of the premature tip-stalling phenomena exhibited by tapered wings. As was pointed out in the previous discussion, reducing the lift and the slope of the drag curve near the tips would lead to improved conditions. If this improvement is effected simply by tapering the wings, however, the net result may be detrimental to controllability on account of the premature loss of roll damping due to the stalling of the tips. In the case of any wing with an extreme reduction of chord, the downwash distributes itself in such a manner as to tend to maintain a more uniform distribution of the actual lift, so that the lift coefficient, and hence the effective angle of attack, of the reduced-chord sections is greater than at other sections. Pressure-distribution tests show that the tip portions of a 5:1 tapered wing reach their maximum lift coefficients at angles as much as 5° below the stalling angle of the center portions of the wing. Thus,

tapering the wings cannot be expected to improve the controllability at low speeds unless the taper is accompanied by some washout, or unless other provision is made to prevent the tips from stalling.

It may be inferred from the foregoing discussions that the effects of high aspect ratio will be detrimental to controllability and stability above the stall. It is easily seen how the unstable tendencies of the wings would be more unfavorable to controllability if the wings were of large span. If the span is large in proportion to the lever arm of the rudder control, the wings may easily develop yawing tendencies that will completely overpower the rudder moments. Furthermore, since rapid yawing motion induces a rolling moment through L_r , it is important to provide a large damping in yawing as an indirect check on the rolling as well as on the yawing motions. Thus it appears that considerable tail length and fin area are desirable to increase both N_r and N_β . Inasmuch as there ordinarily exists a great disproportion between the dampings in rolling and yawing below the stall, it is probable that fairly large increases in N_r would be permissible without causing undesirable stiffness of the rudder control at high speeds. Increasing N_β by using larger vertical tail surfaces is especially desirable because in that way the available rudder control is increased. Data on conventional airplanes show that the rudders used produce the weakest of the three controlling moments; their maximum moment is often smaller than the secondary yawing moment of the ailerons, yet the rudder deals with the largest moment of inertia of the airplane and should be the most effective control in checking the unstable yawing tendencies of the wings (as, for instance, in spinning). It appears that considerable improvement in these characteristics could be effected by enlarging the fin surface of conventional machines. If the increased rudder control is found to be undesirable at high speed because of too great sensitiveness, a corresponding increase in N_r , the damping in yawing, should remedy this trouble and still further improve the controllability at high angles. Thus if the tail is made longer as the vertical surface is increased, the control characteristics at high speed should not be unfavorably affected. It appears unlikely, however, that such improvements could result in the retention of satisfactory control above the stall if the autorotational tendencies shown by ordinary wings in wind-tunnel experiments are developed.

TURN MANEUVERS

The foregoing computations were designed to represent the procedure employed in a particular type of flight test to compare the efficiency of various control devices purely on the basis of their independent action in producing roll. Another type of flight test, qualitative in nature, consisted of performing normal turn

maneuvers with the airplane, using the device in conjunction with the other controls and observing the amount of coordination that was required.

The first type of computation together with the flight tests showed that the roll-producing effectiveness of some devices would be influenced by the occurrence of considerable incidental sideslipping, much of the apparent improvement due to favorable secondary yaw being obtained by the production of outward sideslipping.

Since it was not known in any quantitative way how the presence of this sideslipping tendency due to the secondary aileron moments would affect the controllability in making actual turn maneuvers, it was decided to make an analysis of these conditions, representing analytically as nearly as possible the second stage of the flight tests.

EXPLANATION OF METHOD OF COMPUTATIONS

In certain instances in the former computations a simple sort of controlled maneuver was used in which an initial deflection of the ailerons was reversed, representing an attempt to check a motion previously produced by them. (See fig. 13.) It was realized that an extension of this procedure could be applied to the present problem by means of step-by-step integrations of the motion due to any arbitrarily specified way of applying the controls. This adaptation of the former method would have required a knowledge of the control manipulations necessary to perform a normal turn, as well as lengthy step-by-step calculations. For these reasons it was considered more feasible to predetermine the actual motion of the airplane than to fix on an arbitrary way of applying the controls. Furthermore it seemed reasonable to presume that the pilot of an airplane would conform his use of the controls to suit a desired maneuver, rather than to prescribe beforehand his use of the control and accept whatever motion of the airplane followed. He would then judge the effectiveness of the control by the way it had to be used to obtain a desired result.

As the outcome of these considerations, the problem of investigating turn maneuvers presented itself in a way inverse to the previous problems. Here the motion of the airplane was given and the requisite use of the controls was sought. Previously the airplane motions had been determined from the controlling accelerations by integration, whereas here the accelerations incident to a given motion were to be determined; thus the process would simply be a differentiation.

Periodic or trigonometric functions of the time naturally suggested themselves for the representation of the angular velocities and displacements during a turn maneuver. By the use of trigonometric functions of the time, any conceivable maneuver of the airplane that begins and ends in level flight may be specified; that is, any given manner of varying the attitude or

angular velocity of the airplane during a given interval may be described by a formula such as

$$p, \text{ or } \varphi, \text{ or } \dots \text{ etc.} \\ = A_1 \sin nt + A_2 \sin 2nt + A_3 \sin 3nt + \text{etc.} \quad (16)$$

By a suitable choice of n the maneuver may be made to extend over as long or as short a time as desired.

In the present case it was intended that the airplane roll up to a moderate angle of bank, starting with the wings level, and check its rate of rolling so as to maintain this bank angle steadily, then roll back to the level condition after a definite time interval. Throughout this interval the airplane was to be yawing appropriately while banking and in the correct amount to prevent sideslipping during every part of the maneuver. Thus the turn was to be "perfect" in that no sideslip was permitted and the coordination of the lateral controls (ailerons and rudder) necessary to accomplish such a maneuver was to be studied.

A few trials in plotting cosine curves against time showed that the expression

$$\varphi = -A_1 \cos nt - \frac{1}{4} A_1 \cos 2nt + \text{constant} \quad (17)$$

would represent a bank that assumed a steady angle at the midpoint of the maneuver, starting with zero at the time $t=0$ and becoming zero again at $t=\pi/n$. Arranging for the bank to become steady at the midpoint of the maneuver and choosing nt so as not to coincide with the natural period of the free motions of the airplane obviated the possibility of any reinforced oscillation phenomena during the maneuver. The form of the curve of bank angle against time plotted to this formula is shown in figure 17.

In order to attain the specified bank at every instant, a definite rate of rolling is required at all times, which is obviously found by differentiating the bank equation; thus

$$p = \frac{d\varphi}{dt} = nA_1 \sin nt + \frac{2n}{4} A_1 \sin 2nt \quad (18)$$

In order for the airplane to turn without sideslipping, there must be a coordination between the banking and yawing at all times. The outward and inward accelerations must cancel, that is:

$$rU_0 = g \sin \varphi \quad (19)$$

(See equation (12).)

This equation enables the calculation of r from φ , assuming the condition that

$$r = \frac{g}{U_0} \sin \varphi \quad (20)$$

is satisfied. The curve of yawing angular velocity plotted against time is thus very similar in shape to the bank-angle curve, reaching a steady value at its midpoint.

The specification of the angular velocities and angles of the airplane in the foregoing manner is analogous to the specification of constraints of the motion. The total accelerations necessary to constrain the airplane to the specified motions are calculated by differentiating the expressions for the angular velocities, p and r . (See equations (17) and (18).)

$$\frac{dp}{dt} = \frac{d^2\varphi}{dt^2} = n^2 A_1 \cos nt + \frac{4n^2}{4} A_1 \cos 2nt \quad (21)$$

and

$$\frac{dr}{dt} = \frac{g}{U_0} p \cos \varphi \quad (22)$$

These accelerations are not furnished altogether by the controls but have components due to the air reactions on the moving airplane. The air reactions are calculated from the resistance derivatives and, when deducted from the total accelerations, give the components necessarily supplied by the deflected controls. Thus the acceleration supplied by the rolling control will be

$$\delta L_s = \frac{dp}{dt} - pL_p - rL_r \quad (23)$$

If the application of rolling control is accompanied by a secondary (adverse or favorable) yawing moment, the rudder control will have to accommodate this moment as well as the residual acceleration of the yawing motion. This secondary yawing moment may be considered to be a function of the rolling moment and its acceleration written as $f(\delta L_s)$; then

$$\delta N_s = \frac{dr}{dt} - pN_p - rN_r - f(\delta L_s) \quad (24)$$

Equation (24) gives the amount of rudder coordination necessary with a given aileron-control device. The rolling- and yawing-moment coefficients corresponding to these accelerations may be calculated by known means from the speed of flight and the airplane dimensions.

In the derivation of the equations for the turn maneuvers no account was taken of the pitching motion involved. Obviously if a banked airplane is turning without loss of altitude there will be a component of pitching involved in the motion. As was explained in the description of the step-by-step method of computation the pitching motion may be considered separately and independently of the lateral motions since the airplane is symmetrical about the plane in which pitching occurs. Presumably, the only ways in which pitching motions can influence the lateral motions are by a change of speed or attitude introducing changes in the lateral-stability derivatives or by gyroscopic couples. In the case of a prescribed turn maneuver the maximum gyroscopic couple may be estimated in advance and the relative importance of its effect may be foreseen. The other secondary influence may be partly accounted for

by assuming a certain increased speed throughout the turn. Either the air speed or the attitude will, in general, vary continuously throughout the turn if no altitude is lost or gained. For turns up to 30° angle of bank the change in stability derivatives thus produced will be slight and may be satisfactorily compen-

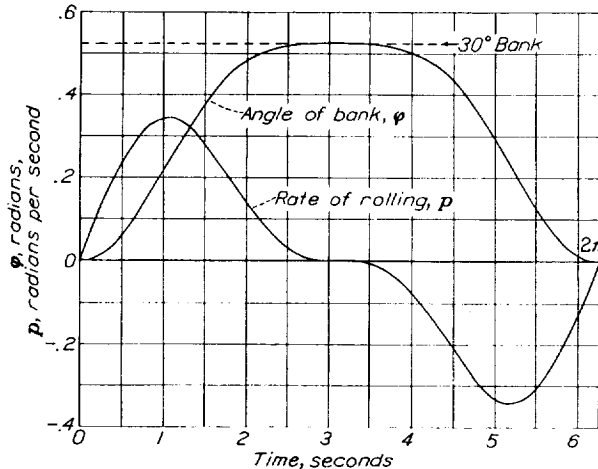


FIGURE 17.—Angle of bank and rate of rolling during specified turn maneuver. $\phi = -0.262[\cos t + \frac{1}{4} \cos 2t] + 0.327$; $p = d\phi/dt$.

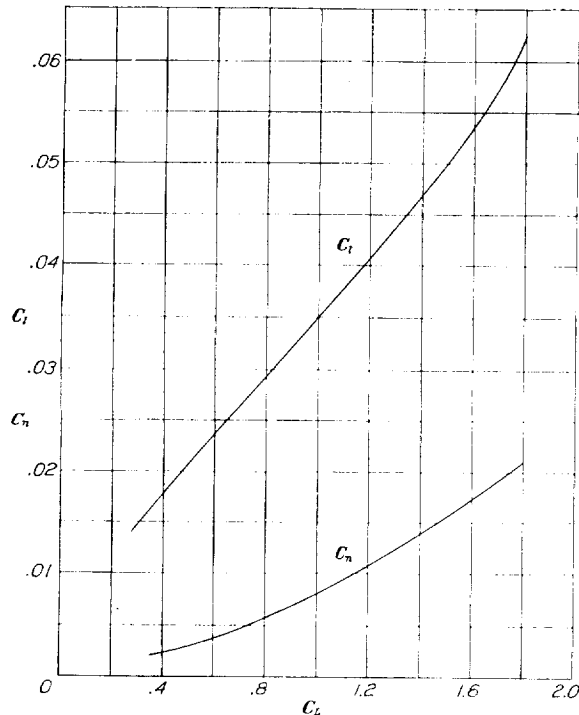


FIGURE 19.—Maximum control-moment coefficients required in performing a turn maneuver at various lift coefficients; average airplane (for 30° bank turn completed in 6.28 seconds).

sated by assuming an average value of the speed U somewhat greater than that for level flight. This speed may be calculated from the relation:

$$q = \frac{q_0}{\cos \phi} \quad (25)$$

where q_0 is the dynamic pressure at steady-flight speed and ϕ is the angle of bank at which the airplane is assumed to lose or gain no altitude.

RESULTS AND DISCUSSION

The foregoing procedure was applied to the case of the average airplane performing 30° banked turns at various speeds. The time taken to complete the specified maneuver was chosen as approximately 6.28 (2π) seconds, since at the lowest speeds under consideration comparatively large rolling and yawing moments were required to execute the maneuver with this rapidity. Inasmuch as the angle-of-bank relation was held the

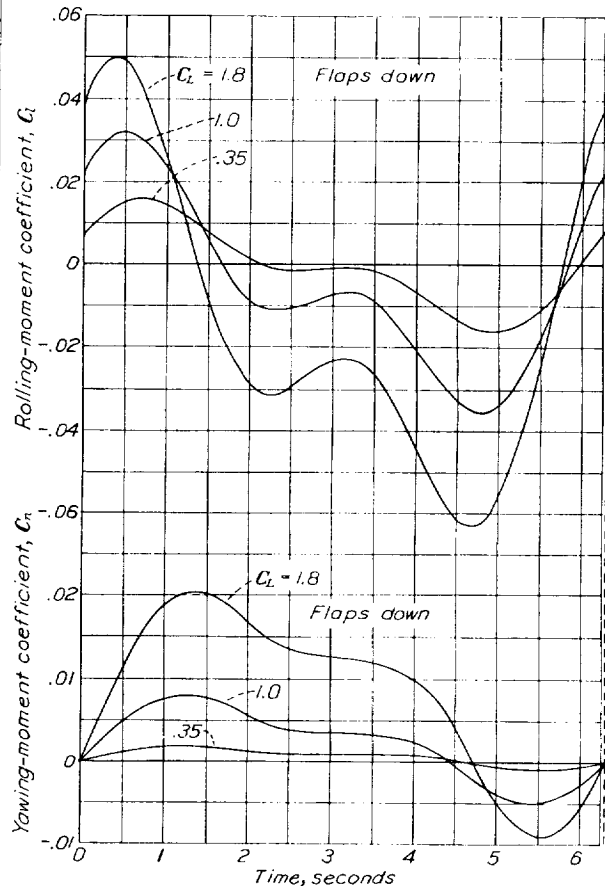


FIGURE 18.—Control rolling- and yawing-moment coefficients necessary to perform 30° bank turn without sideslipping at various lift coefficients.

same for all speeds, the rate of yawing was necessarily different and hence the actual angle of turn, or the changed heading of the airplane, was different for the different speeds. As in the previous computations, lift coefficients of 0.35, 1.0, and 1.8 were assumed, although the corresponding speeds were increased somewhat over those in the previous computations to account for the additional lift while turning, as previously explained. With the assumption of no loss of altitude at 30° bank, the speeds were increased by the factor

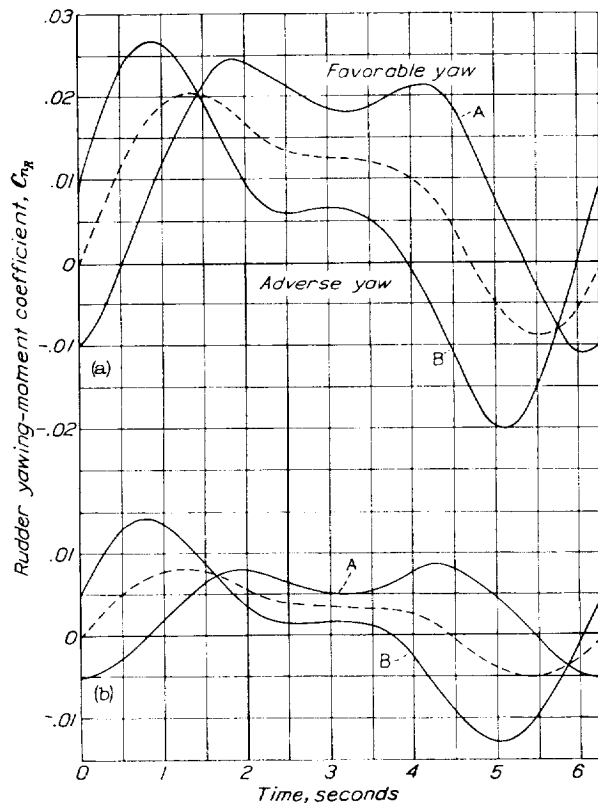
$$\sqrt{\frac{1}{0.866}} = 1.074$$

The values of L_p , L_r , N_p , N_r , corresponding to the given lift coefficients, were also multiplied by this factor. (See appendix I.)

The curves of rolling motion and angle of bank calculated for these maneuvers are those shown in figure 17. The formula for the bank angle was

$$\varphi = -0.262 (\cos t + 1/4 \cos 2t) + 0.327 \quad (26)$$

reaching a maximum of 30° at π seconds. This formula determined the angular velocities and accelerations by the principles already demonstrated. Inasmuch as the turn reaches a steady rate at its midpoint, the whole



(a) Low speed, flaps down, $C_L = 1.8$.
(b) Gliding speed, $C_L = 1.0$.

FIGURE 20. Rudder control-moment coefficients during 30° bank turn, showing effect of secondary aileron yawing moments on rudder control necessary to perform a turn maneuver without sideslipping. Assumed aileron yawing moment, $\pm 1/4$ aileron yawing moment. $C_{n\delta}$ is secondary aileron yawing-moment coefficient.
 $C_{n\delta} = 1/4 C_{l\delta}$ curve A $C_{n\delta} = -1/4 C_{l\delta}$ curve B

maneuver may be presumed to be of any time extent by assuming a continuation of this steady point, which occurs at π seconds.

The results of a series of these computations showed principally the effect of flight speed on the degree of control deflection necessary to perform a given maneuver and the effect of favorable-yaw and of adverse-yaw ailerons on the amount of rudder control required. Figure 18 shows the rolling- and yawing-moment coefficients necessary to accomplish the maneuver at speeds corresponding to the three different lift coefficients. For the average airplane these were:

C_L	U
0.35	161 feet per second.
1.0	95 feet per second
1.8	71 feet per second (flaps deflected).

In this case no secondary aileron yawing moments were included and such moment coefficients would have to be added to or deducted from the yawing-moment curves. These computations showed that the maximum yawing moment necessary at the lowest speed was 10 times as great as that at high speed, while the maximum rolling-moment coefficient increased only 4 times under the same circumstances. Figure 19 illustrates this increase of coefficient necessary to perform the specified maneuver in the same time at the lower speeds.

Figure 20 shows the effects of favorable and adverse secondary aileron yawing moments on the rudder control necessary throughout the turn. Positive yawing moments indicate a setting of the rudder in a direction to aid the turning. It will be noted that the existence of any secondary aileron moment calls for a counteracting movement of the rudder applied simultaneously with the ailerons at the beginning of the turn. With no secondary aileron moments the curves show that the simultaneous initial deflection of both ailerons and rudder is not required, the turn being initiated by the ailerons alone with the rudder being applied after the start. In the case of favorable secondary yawing moments an initial setting of the rudder opposite to the direction of the turn is required, while on beginning the recovery the rudder has to be moved slightly in a direction that would normally tend to continue the turning. It appears that ailerons giving no secondary yawing moments of either sign would require the least rudder coordination in making turns without sideslipping.

CONCLUSIONS

1. The agreement of the computations with the results of flight tests verifies the usefulness of the method utilizing stability derivatives for the study of controllability both above and below the stall.

2. The angle of bank produced in 1 second, φ_1 , by a full deflection of the lateral control may be taken as a relative measure of the control effectiveness. In the case of a conventional airplane this measure is given by a simple formula involving the static rolling and yawing moments produced by the control, namely:

$$\varphi_1 = \text{constant} \times C_l + \text{constant} \times C_n$$

3. The effect of secondary adverse yawing moments on the aileron control may be moderated by increasing the moment of inertia about the yaw axis, although it is to be expected that the power of the rudder will be correspondingly reduced. Increasing the moment of inertia about the roll axis should have little direct

influence on the lateral-control effectiveness with a given rolling-control moment.

4. The tendency for a given adverse yawing moment to render the lateral control ineffective becomes greater with increasing dihedral. In no case should the ratio of the control adverse yawing moment to the rolling moment be allowed to exceed (in absolute magnitude) either:

(a) The ratio of yawing to rolling moment acting on the airplane in sideslip; or

(b) The ratio of yawing to rolling moment acting on the airplane in yawing.

5. It appears that ailerons giving nearly zero yawing moment would require the least coordination of the rudder control in executing turn maneuvers without sideslip.

6. The study of conditions above the stall indicates that satisfactory control cannot be expected unless

some provision is made to maintain the damping in rolling at these angles.

7. For control at high angles of attack it is important that the damping in both rolling and yawing be maintained above a definite minimum to avoid an uncontrollable form of instability arising from the interaction of these motions. The minimum damping is given by the condition that

$$L_p N_r > L_r N_p$$

This condition appears to be next in importance to direct damping in rolling.

LANGLEY MEMORIAL AERONAUTICAL LABORATORY,
NATIONAL ADVISORY COMMITTEE FOR AERONAUTICS,
LANGLEY FIELD, VA., April 20, 1936.

TABLE I.—STEP-BY-STEP COMPUTATION OF MOTION OF AVERAGE AIRPLANE

[$C_L=1.0$; $C_D=0.04$; $C_n=0$]

Time	$\left(\frac{dp}{dt}\right)_n$	p_n	φ_n	$\left(\frac{v'}{U_0}\right)_n$	$\left(\frac{dr}{dt}\right)_n$	r_n	β_n	β_n	ΣL_i			ΣN_i		
	$\delta L_1 + \Sigma L_i$ ($\delta L_1 = 1.68$)	$\left(\frac{dp}{dt}\right)_{n-1} \times \Delta t + p_{n-1}$	$p_{n-1} \times \Delta t + \varphi_{n-1}$	$\frac{32.2}{88.5} \times \Delta t \times \sin \varphi_{n-1} + \left(\frac{v'}{U_0}\right)_{n-1}$	$\left(\frac{dr}{dt}\right)_{n-1} \times \Delta t + r_{n-1}$	$\delta N_1 + \Sigma N_i$ $\delta N_1 = 0$	$\beta_{n-1} \times \Delta t + \beta_{n-1}$	$\beta_{n-1} + \left(\frac{v'}{U_0}\right)_n$	$p_n L_p + r_n L_r + \beta_n L_\beta$			$p_n N_p + r_n N_r + \beta_n N_\beta$		
									$p_n \times -3.23$	$r_n \times 1.88$	$\beta_n \times -1.11$	$p_n \times -0.301$	$r_n \times -0.663$	$\beta_n \times 2.04$
sec.														
0	1.680	0	0	0	0	0	0	0	0	0	0	0	0	0
.05	1.409	.084	0	0	-.025	0	0	0	-.271	0	0	-.025	0	0
.10	1.181	.154	.004	0	-.045	-.001	0	0	-.497	-.002	0	-.046	.001	0
.20	-.790	.272	.019	0	-.078	-.006	0	0	-.879	-.011	0	-.082	.004	0
.30	.518	.351	.046	.001	-.093	-.014	.001	.002	-1.134	-.026	-.002	-.106	.009	.004
.40	.329	.403	.081	.003	-.096	-.023	.002	.005	-1.302	-.043	-.006	-.121	.015	.010
.50	.109	.436	.121	.006	-.089	-.033	.004	.010	-1.408	-.062	-.011	-.131	.022	.020
.60	.109	.456	.165	.010	-.074	-.042	.007	.017	-1.473	-.079	-.019	-.137	.028	.035
.70	.050	.467	.211	.016	-.054	-.049	.011	.027	-1.508	-.092	-.030	-.141	.032	.055
.80	.009	.472	.257	.024	-.024	-.054	.016	.040	-1.525	-.102	-.044	-.142	.036	.082
.90	-.013	.473	.304	.033	.005	-.056	.021	.054	-1.528	-.105	-.060	-.142	.037	.110
1.00	-.027	.472	.351	.044	.039	-.055	.027	.071	-1.525	-.103	-.079	-.142	.036	.145

APPENDIX I

CALCULATION OF STABILITY DERIVATIVES¹

In the report all moments and angular velocities are measured from axes fixed in the airplane along the directions perpendicular and parallel to the relative wind in the steady flight just previous to the maneuver computed.

In the computations of the stability derivatives as well as in the consideration of their modification by alteration of the design of an airplane, it is convenient to separate those governed by the wing characteristics from those depending mainly on the body and the tail.

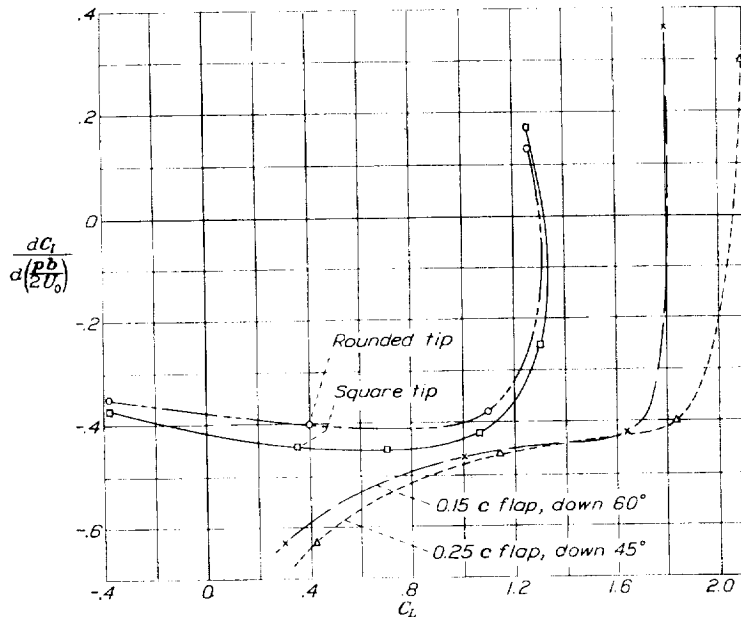


FIGURE 21.—Damping in rolling of rectangular wing. Aspect ratio, 6; 7- by 10-foot wind-tunnel measurements.

In the case of conventional airplanes, the derivatives that depend almost wholly on the wings are

$$L_p, L_r, L_\beta, \text{ and } N_p$$

The other two factors considered in the report, N_r and N_β , depend primarily on the disposition and area of the vertical tail and on the fuselage.

ROLLING ACCELERATION DUE TO ROLLING, L_p

The factor L_p may be determined from the results of tests of the damping in rolling of wings, such as the tests that have been made in the 7- by 10-foot wind tunnel. The test results are given in the form of the

¹ The authors desire to acknowledge valuable aid received from Mr. C. H. Zimmerman of the laboratory staff in the preparation of this section.

coefficient $\frac{dC_l}{d\left(\frac{pb}{2U_0}\right)}$ and are summarized in figure 21,

which shows values of the coefficient measured on rectangular Clark Y wings of aspect ratio 6. The effects of deflected split flaps and tip rounding are also shown. Correction factors to convert these values to those for tapered wings and wings of different aspect ratio are given in figure 22. These correction factors are based on theoretical calculations of the load distribution on wings having a uniform twist which, in effect, reproduced the conditions encountered by a rolling wing as far as the rolling moment is concerned. The data for these corrections were deduced from calculations given in reference 11.

The actual damping moment of a full-size wing calculated from the coefficient is

$$L = p \times \frac{dC_l}{d\left(\frac{pb}{2U_0}\right)} S^p_2 U_0 \frac{b^2}{2} \quad (27)$$

The derivative, as used in the report, is obtained by dividing the coefficient of p by the moment of inertia of the airplane in rolling: i. e.,

$$L_p = \frac{dC_l}{d\left(\frac{pb}{2U_0}\right)} S^p_2 U_0 \frac{b^2}{2mk_x^2} \quad (28)$$

It will be readily appreciated that parts of the airplane other than the wings contribute only a negligible amount of this damping; for example, if the tail plane has an area 15 percent of that of the wing and a span of 25 percent b , its contribution will be less than

$$0.15 \times (0.25)^2 = 0.019, \text{ or 2 percent}$$

of that due to the wing.

The rolling moment due to rolling of a biplane may be estimated by using its equivalent monoplane aspect ratio in figure 22.

For the damping of rolling above stalling angles, wind-tunnel tests show that there is no consistent linear relation between the damping moment and the rate of rolling even at very slow rates; hence there actually exists no definite L_p in the sense previously defined. Arbitrary values may be assumed to repre-

sent roughly certain conditions, as was done in the described stalled-flight computations. In the case of wings with devices to prevent stalling at the tips, recourse must be had to wind-tunnel tests.

ROLLING ACCELERATION DUE TO YAWING, L_r

The rolling moment developed by a wing in circling flight may be easily calculated from the consideration that this motion brings about a difference in velocity along the span. If the yawing velocity is r and the spanwise distance from the reference origin (center of gravity) is y , this additional velocity will be ry . The lift on an element of the wing is proportional to the square of the whole velocity, or:

$$(U_0 \pm ry)^2 = U_0^2 \pm 2ryU_0 + (ry)^2 \quad (29)$$

The rolling moment produced by the change in lift on either side of the wing is directly proportional to r . A

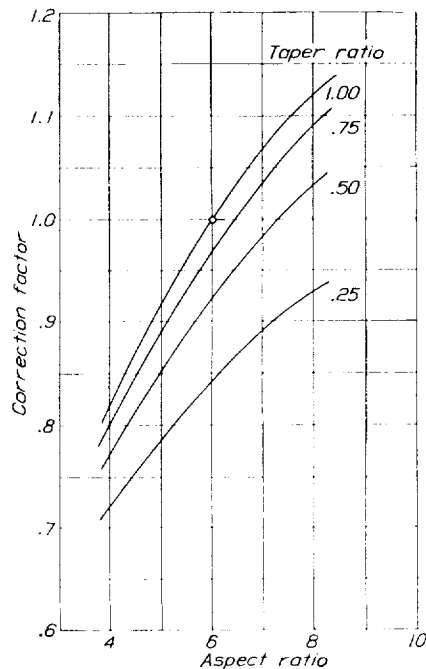


FIGURE 22.—Factors for correcting wind-tunnel values of $dC_L/d\left(\frac{pb}{2U_0}\right)$ for aspect ratio and taper.

simple integration shows the moment for a straight wing to be:

$$L = r \frac{b^2}{6} S \frac{\rho}{2} U_0 C_L \quad (30)$$

if the lift is distributed uniformly along the span. Such a distribution is approximated in the case of a rectangular wing at stalling angles, hence the foregoing formula was used in the stalled-flight computations. Below the stall the actual distribution of lift on the wings in circling flight should be taken into account. This distribution is modified somewhat by the fact that the induction of the circular trail of vortices differs from the induction in straight flight. These phenomena

have been treated by Glauert and Wieselsberger for the cases of rectangular and elliptical wings in circling flight and curves derived from their calculations are shown in figure 23. (See reference 12.) The derivative L_r is obtained from the coefficient by the formula

$$L_r = F_1 C_L S \frac{\rho}{2} U_0 \frac{b^2}{2mk_x^2} \quad (31)$$

It appears that the value of $\frac{1}{2}F_1$ previously calculated from simple integration as one-sixth should be more nearly one-eighth for aspect ratio 6, as indicated by the chart. Although no calculations have been made for tapered wings, it may be presumed that the interpolated curves given in figure 23 will apply with good approximation. The part of L_r due to the body and tail will be treated in a later paragraph.

ROLLING ACCELERATION DUE TO SIDESLIP, L_s

Measurements of the rolling moment due to sideslip have been made on a large number of wing models in the 7- by 10-foot wind tunnel. The results of these

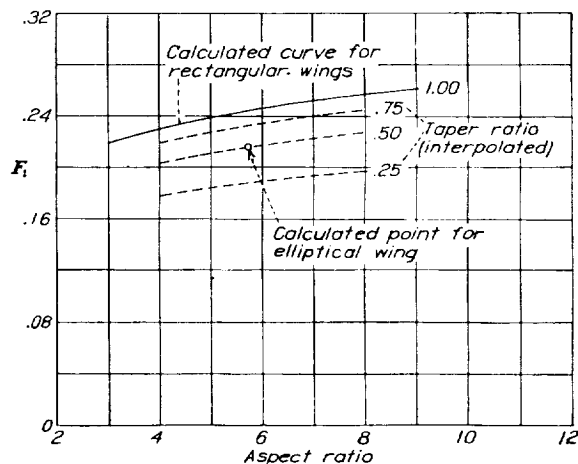


FIGURE 23.—Factors for calculating rolling moment in circling flight.

$$dC_L/d\left(\frac{rb}{2U_0}\right) = F_1 C_L$$

tests are summarized in figure 24, which shows the influence of tip rounding and deflected split flaps on the dihedral effect of Clark Y wings without actual dihedral angle. Further tests made on wings with varying degrees of dihedral showed that the additional effect due to this angle was the same regardless of the tip shape or the lift coefficient of the wing (below the stall). Sweepback of the wings is known to have an effect similar to dihedral, although comparatively few tests have been made. Unlike the rolling moment due to dihedral angle, however, the rolling effect of sweepback appears to be approximately proportional to the lift coefficient, disappearing at zero lift as would be expected. Presumably, its effect may be added to the others as in the case of the dihedral. These considerations result in the following formula for the total rolling moment in sideslip

$$\frac{dC_l}{d\beta} = \left(\frac{dC_l}{d\beta} \right)_{\Gamma, \Lambda=0} + \Gamma \frac{\partial}{\partial \Gamma} \left(\frac{dC_l}{d\beta} \right) + \Lambda \frac{\partial}{\partial \Lambda} \left(\frac{dC_l}{d\beta} \right) \quad (32)$$

where Γ is dihedral angle and Λ is angle of sweepback.

An analysis of the available data indicates the following values for the parameters:

$$\left. \begin{aligned} \frac{\partial}{\partial \Gamma} \left(\frac{dC_l}{d\beta} \right) &= -0.012 \\ \frac{\partial}{\partial \Lambda} \left(\frac{dC_l}{d\beta} \right) &= -0.0045 C_L \end{aligned} \right\} \quad (33)$$

(see reference 13),
and

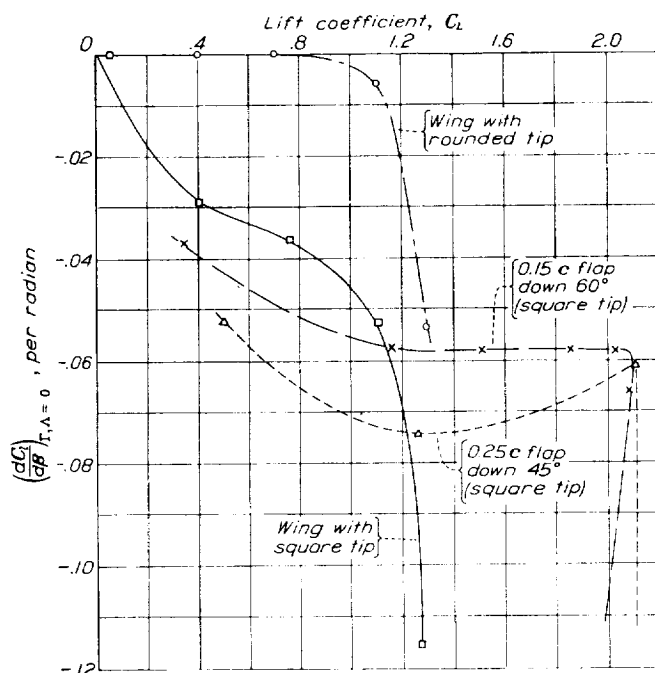


FIGURE 24.—Rolling moment due to sideslip. Untapered wings without dihedral; aspect ratio, 6; 7- by 10-foot wind-tunnel measurements.

where $dC_l/d\beta$ is in terms of radians and Γ and Λ are measured in degrees. The derivative L_β follows from the formula:

$$L_\beta = \frac{dC_l}{d\beta} S q \frac{b}{mk_x^2} \quad (34)$$

Inasmuch as the wind-tunnel tests were of rectangular wings of aspect ratio 6, the formula (33) applies directly to them. Correction factors for calculating the rolling moment due to the dihedral of yawed wings of different aspect ratios and taper ratios are given in figure 25. These corrections were deduced from theoretical calculations made at the Laboratory (reference 11) on the span load distribution of wings having their right and left semispan portions set at different angles of attack and are somewhat different from those deduced previously for the damping in rolling.

Above stalling angles none of the given formulas or correction factors apply. In this region a straight

wing shows a far greater rolling tendency when yawed than wings with either sweepback or dihedral. Adding either sweepback or dihedral tends to reduce this tendency and may on this account be desirable to a certain degree. Tests of wings with very large sweepback, such as are used on tailless airplanes, have been made in which the rolling moment due to yaw actually reversed its sign when the stall was reached.

YAWING ACCELERATION DUE TO ROLLING, N_y

It is assumed that the effect of a rolling motion of the wing can be replaced by a relative rolling motion

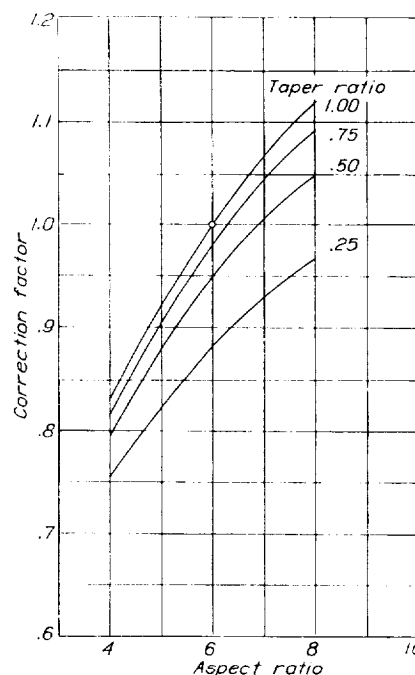


FIGURE 25.—Factors for correcting wind-tunnel value of $\partial \left(\frac{dC_l}{d\beta} \right) / \partial \Gamma$ for aspect ratio and taper.

of the air about the X axis of the airplane. Thus in positive rolling the relative air stream is rising toward the right wing tip and descending on the left. The lift vectors, being perpendicular to the relative wind at each point of the span, are inclined forward with respect to the Z axis on the right and backward on the left, resulting in a negative yawing moment for positive rolling of the wing. (This varying resolution of the lift vectors along the span is unimportant in computing the rolling moment due to rolling since the angle $pb/2U_0$ is small.)

In addition to the changed resolution of the lift vectors along the span, there is an increased drag on the downgoing wing that tends to reduce the negative yawing tendency. It should be noted that an asymmetrical change in the lift distribution, such as that caused by rolling, results in greater changes in the induced drag at various sections of the wing than would be produced by symmetrical lift changes. (See

reference 14.) Hence the uncorrected results of measurements made on the wing in direct lifting cannot be used in computing the rolling or yawing moments of a rolling wing.

Figure 26 shows the resolution of the lift at a point of the span y on the downgoing side of the wing. The air stream initially rising toward the section at the inclination py/U_0 is deflected somewhat by the resulting increased lift at that point so that the air meets the wing at the additional effective angle of attack, $\Delta\alpha_0 = \frac{py}{U_0} - \Delta\frac{w}{U_0}$. This additional angle of attack may be found at each point of the span if the corresponding lift increment is known, since

$$\Delta\alpha_0 = \frac{\Delta C_L}{\left(\frac{dC_L}{d\alpha}\right)_0} \quad (35)$$

where $\left(\frac{dC_L}{d\alpha}\right)_0$ is the slope of the lift curve for infinite aspect ratio. The lift vector on the wing in straight flight C_L is increased by the amount ΔC_L and inclined forward through the angle $\Delta\alpha_0$. If the usual assumptions regarding small angles are made, the total effect may be integrated along the span as

$$N = -2\frac{\rho}{2}U_0^2 \int_0^{b/2} C_L \times \Delta\alpha_0 \times c \times y \times dy \quad (36)$$

It will be noted that it is unnecessary to consider the resolution of the lift increments ΔC_L by the angles $\Delta\alpha_0$ since they are sensibly equal and opposite on either side of the wing and their yawing effects cancel, resulting simply in a bending moment about the mid-

point. Replacing $\Delta\alpha_0$ by $\frac{\Delta C_L}{\left(\frac{dC_L}{d\alpha}\right)_0}$ and calculating the coefficient

$$C_n = -\frac{2}{Sb\left(\frac{dC_L}{d\alpha}\right)_0} \int_0^{b/2} C_L \times \Delta C_L \times c \times y \times dy \quad (37)$$

Since $-\frac{2}{Sb} \times \Delta C_L \times c \times y \times dy = dC_u$, an approximate expression of this formula is

$$\left. \begin{aligned} C_n &= -\frac{C_L}{\left(\frac{dC_L}{d\alpha}\right)_0} C_L \\ \text{whence} \quad \frac{dC_n}{d\left(\frac{pb}{2U_0}\right)} &= \frac{C_L}{\left(\frac{dC_L}{d\alpha}\right)_0} \frac{dC_L}{d\left(\frac{pb}{2U_0}\right)} \end{aligned} \right\} \quad (38)$$

This approximation is based on the assumption of constant lift coefficient across the span and hence corresponds to an elliptical wing. The resolution of this yawing moment along the general wind direction results in:

$$\frac{aC_n}{d\left(\frac{pb}{2U_0}\right)} = \frac{dC_L}{d\left(\frac{pb}{2U_0}\right)} \left[\frac{C_L}{\left(\frac{dC_L}{d\alpha}\right)_0} - \frac{C_L}{\pi R} \right] \quad (39)$$

Reference 11 gives the lift and lift-increment distributions for both rectangular and tapered wings and these may be used in conjunction with the foregoing formulas if a more accurate theoretical value of N_p is desired.

A component of N_p due to the profile-drag effect may be estimated by a simple integration, assuming the slope of profile-drag coefficient with effective angle of attack to be constant across the span. Thus, if $\left(\frac{dC_D}{d\alpha}\right)_0$ is the slope of the drag curve for infinite aspect ratio at the lift coefficient in question

$$\Delta N = 2\frac{\rho}{2}U_0^2 \int_0^{b/2} \Delta\alpha_0 \left(\frac{dC_D}{d\alpha}\right)_0 cy dy \quad (40)$$

or, making the same substitutions as before, the coefficient giving the effect of profile drag is

$$\frac{dC_n}{d\left(\frac{pb}{2U_0}\right)} = -\frac{dC_{D_0}}{dC_L} \frac{dC_L}{d\left(\frac{pb}{2U_0}\right)} \quad (41)$$

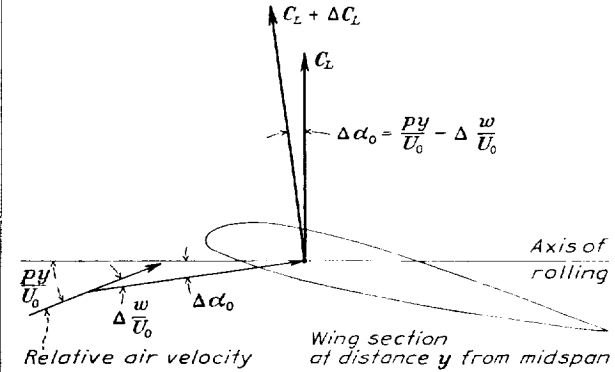


FIGURE 26.—Resolution of air velocity and lift at section of rolling wing

where C_{D_0} is the profile-drag coefficient of the airfoil section. The final formula for N_p is

$$N_p = \frac{dC_n}{d\left(\frac{pb}{2U_0}\right)} S \frac{\rho}{2} U_0^2 \frac{b^2}{2mk_z^2} \quad (42)$$

where $\frac{dC_n}{d\left(\frac{pb}{2U_0}\right)}$ is the sum of the portions given by equations (39) and (41).

Above stalling angles the slope of the profile-drag coefficient with angle of attack reaches large values, and it is to be expected that N_p will change its sign. The foregoing theoretical formulas cannot be used at these angles, because the lift is no longer proportional to the angle of attack. A tentative formula for $\frac{dC_n}{d\left(\frac{pb}{2U_0}\right)}$ in the stalled condition is

$$\frac{dC_n}{d\left(\frac{pb}{2U_0}\right)} = \left[\left(\frac{dC_D}{d\alpha}\right)_0 - C_L \right] \frac{4}{Sb^2} \int_0^{b/2} cy^2 dy \quad (43)$$

or simply

$$\frac{dC_n}{d\left(\frac{pb}{2U_0}\right)} = \frac{1}{6} \left[\left(\frac{dC_D}{d\alpha} \right)_0 - C_L \right] \quad (44)$$

for rectangular wings.

In the case of an airplane with a long fuselage, a certain increment of N_p at high angles of attack due to the effect of the body and fin must be considered, as will be explained later.

YAWING ACCELERATION DUE TO YAWING, N_r

Unlike the damping in rolling, the damping in yawing N_r , cannot be attributed to any single predominant factor. It is convenient, however, to consider it as primarily effected by the disposition and area of the vertical tail surface. Since only a few isolated experiments have been made for the determination of this derivative and since it is not known

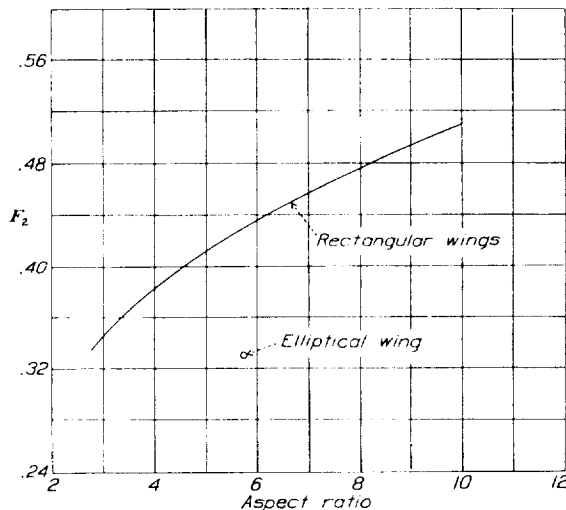


FIGURE 27.—Factors for calculating the yawing moment due to the induced-drag distribution in circling flight.

$$dC_n/d\left(\frac{rb}{2U_0}\right) = -F_2 C_{D_i}$$

to what extent certain incalculable factors influence it, only a rough estimate of its value in any given case is possible.

The part of the damping of yawing due to the wings may be calculated from considerations similar to those employed in the determination of L_r . Here the changed drag distribution along the span in circling flight is to be considered and the resulting yawing moment found. The theoretical calculations of Glauert and Wieselsberger that were employed in the determination of L_r may be applied in this case as well. Here, however, it will be necessary to include the effect of profile drag of the wings and their attachments, since it is the actual magnitude of the drag that counts in determining N_r and not its rate of increase with angle of attack. On the assumption that the profile-drag coefficient is nor-

mally the same at all sections of the span, a simple integration (see L_r) gives the formula

$$\frac{dC_{n_0}}{d\left(\frac{rb}{2U_0}\right)} = -\frac{1}{3} C_{D_i} \quad (45)$$

for the part due to the profile drag of a rectangular wing. Figure 27 shows the results of the previously mentioned calculations, which were extended to the determination of the distribution of induced drag while circling. With the factor shown in the figure included, the formula for the total wing effect becomes

$$\frac{dC_n}{d\left(\frac{rb}{2U_0}\right)} = -F_2 C_{D_i} - \frac{1}{3} C_{D_i} \quad (46)$$

where C_{D_i} is the induced-drag coefficient, i. e.,

$$C_{D_i} = \frac{C_L^2}{\pi R} \quad (47)$$

The part of N_r due to the vertical tail surfaces may be very simply calculated. The yawing angular velocity r about an axis through the center of gravity produces an effective sidewise velocity of the vertical tail equal to rl . Its change in angle of attack relative to the air stream is then rl/U_0 . The yawing moment due to this effect is

$$N = \frac{rl}{U_0} \left(\frac{dC_y}{d\beta} \right)_f \frac{S_f S_f^p}{S} \frac{U_0^2 l}{2} \quad (48)$$

where $(dC_y/d\beta)_f$ is the slope of the normal-force coefficient of the fin against the sidewise angle of attack β and S_f is the area of the fin. An average value for $dC_y/d\beta$ is -2.2 . Combining these factors and writing the expression in a form involving the span as the fundamental length results in

$$\frac{dC_n}{d\left(\frac{rb}{2U_0}\right)} = \frac{dC_y}{d\beta} \left(\frac{l}{b} \right)^2 \frac{S_f}{S} \times 2 \quad (49)$$

Expressing the various factors thus calculated in the form of a single dimensionless coefficient, the formula for the total damping derivative in yawing becomes

$$N_r = \frac{dC_n}{d\left(\frac{rb}{2U_0}\right)} S \frac{U_0^2 b^2}{2mk_z^2} \quad (50)$$

in which $\frac{dC_n}{d\left(\frac{rb}{2U_0}\right)}$ may be determined from an aerodynamic test of a complete model or may be estimated from the sum of several contributing factors.

It is not known how the body of the airplane influences its damping in yawing, although it is unlikely that its effect is as powerful as that of the vertical fin. In the case of the average airplane treated in this

report, an allowance equal to 60 percent of the fin effect was made for the fuselage and parts of the airplane other than the wings.

YAWING ACCELERATION DUE TO SIDESLIP, N_s

Measurements of the yawing moments in sideslip have been made on a large number of complete models in the course of routine wind-tunnel testing of military airplanes. A study of the results of these tests indicated that at low angles of attack the yawing moment may be estimated from the area and disposition of the vertical fin with a suitable allowance for the fuselage effect. Although airplane bodies when tested alone almost invariably show an unstable yawing tendency about the center of gravity, when tests of a complete model are made the results may show an additional stabilizing influence of the fuselage, possibly due to interference effects. At high lift coefficients the wings may exert considerable influence. The effect of the fuselage depends, of course, on its disposition with respect to the center of gravity and also on the nose shape. Models, especially those with uncowed radial engines, often show only 40 or 50 percent of the righting moment calculated for the fin and rudder alone.

The part of the yawing moment in yaw due to the vertical fin surface may be estimated by means of the data previously used for the calculation of N_r ,

$$N_{s_r} = -\left(\frac{dC_p}{d\beta}\right) \frac{l}{b} \frac{S_f}{S} S q \frac{b}{mk_z^2} \quad (51)$$

In cases of airplanes having wings set at a dihedral angle some provision must be made for an additional yawing moment in yaw that arises as a consequence of the setting of the wings. In straight flight, lift vectors drawn on each wing half, being inclined inward by the angle of dihedral, would intersect on the Z axis vertically above the center of gravity. These lift vectors remaining at the same time perpendicular to the leading-edge lines and to the relative wind direction do not intersect when the wing is yawed, giving rise to a couple. A simple approximation results in

$$C_n = -\frac{1}{5} \Gamma \beta C_L \quad (52)$$

Since this component of yawing moment is attributed to dihedral setting, it may be represented by

$$\frac{\partial}{\partial \Gamma} \frac{dC_n}{d\beta} = -\frac{1}{5} C_L \quad (53)$$

for calculation.

In addition to the simple dihedral effect, an induced yawing moment on the yawed wing must be considered as a secondary effect of the rolling moment. An approximate formula for this yawing moment derived from data given in reference 13 is

$$\left. \begin{aligned} C_n &= -\frac{1}{4} C_L C_l \\ \text{or} \quad \frac{dC_n/d\beta}{dC_l/d\beta} &= -\frac{1}{4} C_L \end{aligned} \right\} \quad (54)$$

These formulas agree with the results of tests made in the 7- by 10-foot wind tunnel except near the region of zero lift. A formula for the total yawing-moment coefficient of the wings is

$$\left(\frac{dC_n}{d\beta}\right)_w = -C_L \left(0.0035 \Gamma + \frac{1}{4} \frac{dC_l}{d\beta}\right) \quad (55)$$

where Γ is given in degrees.

CERTAIN CORRECTING TERMS AT HIGH ANGLES OF ATTACK

At high angles of attack the body of the airplane will be inclined appreciably to the reference axis about which the rolling moments are measured. The formulas given for the effects of the fin (and body) on the damping in yawing and yawing moment in yaw should for exactness have included the factor $\cos \alpha$, since the lever arm of the moment-producing effects will actually be shortened somewhat by the inclination. This correction is of no importance, however, and need not be considered. The same is true of the logical correction that should be applied to the wind-tunnel measurements of rolling moment in yaw, which were actually made about an axis pointing directly upstream and hence not quite in line with the axes considered in the report. The only correcting terms that are of sufficient magnitude to be considered here are those affecting L_r , L_β , and N_p and arising from the fact that the fin and body surfaces are disposed below the rolling axes. These terms are

$$\left. \begin{aligned} \Delta L_r &= N_r \sin \alpha \times \frac{k_z^2}{k_x^2} \\ \Delta L_\beta &= N_\beta \sin \alpha \times \frac{k_z^2}{k_x^2} \\ \Delta N_p &= N_r \sin \alpha \end{aligned} \right\} \quad (56)$$

Only the components of N_r and N_β attributed to the fuselage and vertical fin of the airplane should be used here.

REFERENCES

1. Weick, Fred E., Soulé, Hartley A., and Gough, Melvin N.: A Flight Investigation of the Lateral Control Characteristics of Short Wide Ailerons and Various Spoilers with Different Amounts of Wing Dihedral. T. R. No. 494, N. A. C. A., 1934.
2. Jones, B. Melvill: Research on the Control of Airplanes. T. M. No. 485, N. A. C. A., 1928.
3. Halliday, A. S., and Burge, C. H.: Lateral Stability Calculations for the Bristol Fighter Aeroplane. R. & M. No. 1306, British A. R. C., 1930.
4. Jones, B. Melvill, and Trevelyan, A.: Step-by-Step Calculations upon the Asymmetric Movements of Stalled Aeroplanes. R. & M. No. 999, British A. R. C., 1925.
5. Stability and Control Panel: The Lateral Control of Stalled Aeroplanes. R. & M. No. 1000, British A. R. C., 1926.
6. Soulé, H. A., and McAvoy, W. H.: Flight Investigation of Lateral Control Devices for Use with Full-Span Flaps. T. R. No. 517, N. A. C. A., 1935.
7. Wind-Tunnel Research Comparing Lateral Control Devices, Particularly at High Angles of Attack.
 - I. Ordinary Ailerons on Rectangular Wings, by Fred E. Weick and Carl J. Wenzinger. T. R. No. 419, N. A. C. A., 1932.

- II. Slotted Ailerons and Frise Ailerons, by Fred E. Weick and Richard W. Noyes. T. R. No. 422, N. A. C. A., 1932.
- III. Ordinary Ailerons Rigged up 10° When Neutral, by Fred E. Weick and Carl J. Wenzinger. T. R. No. 423, N. A. C. A., 1932.
- IV. Floating Tip Ailerons on Rectangular Wings, by Fred E. Weick and Thomas A. Harris. T. R. No. 424, N. A. C. A., 1932.
- V. Spoilers and Ailerons on Rectangular Wings, by Fred E. Weick and Joseph A. Shortal. T. R. No. 439, N. A. C. A., 1932.
- VI. Skewed Ailerons on Rectangular Wings, by Fred E. Weick and Thomas A. Harris, T. R. No. 444, N. A. C. A., 1932.
- VII. Handley Page Tip and Full-Span Slots with Ailerons and Spoilers, by Fred E. Weick and Carl J. Wenzinger. T. N. No. 443, N. A. C. A., 1933.
- VIII. Straight and Skewed Ailerons on Wings with Rounded Tips, by Fred E. Weick and Joseph A. Shortal. T. N. No. 445, N. A. C. A., 1933.
- IX. Tapered Wings with Ordinary Ailerons, by Fred E. Weick and Carl J. Wenzinger. T. N. No. 449, N. A. C. A., 1933.
- X. Various Control Devices on a Wing with a Fixed Auxiliary Airfoil, by Fred E. Weick and Richard W. Noyes. T. N. No. 451, N. A. C. A., 1933.
- XI. Various Floating Tip Ailerons on Both Rectangular and Tapered Wings, by Fred E. Weick and Thomas A. Harris. T. N. No. 458, N. A. C. A., 1933.
- XII. Upper-Surface Ailerons on Wings with Split Flaps, by Fred E. Weick and Carl J. Wenzinger. T. R. No. 499, N. A. C. A., 1934.
- XIII. Auxiliary Airfoils Used as External Ailerons, by Fred E. Weick and Richard W. Noyes. T. R. No. 510, N. A. C. A., 1935.
8. Miller, Marvel P., and Soulé, Hartley A.: Moments of Inertia of Several Airplanes. T. N. No. 375, N. A. C. A., 1931.
9. Glauert, H.: A Non-Dimensional Form of the Stability Equations of an Aeroplane. R. & M. No. 1093, British A. R. C., 1927.
10. Aerodynamics Staff of the R. A. E.: The Effect upon the Control of an Aeroplane of Carrying Load Distributed along the Planes. R. & M. No. 849, British A. R. C., 1922.
11. Pearson, H. A.: Theoretical Span Loading and Moments of Tapered Wings Produced by Aileron Deflection. T. N. No. 589, N. A. C. A., 1937.
12. Glauert, H.: Calculation of the Rotary Derivatives Due to Yawing for a Monoplane Wing. R. & M. No. 866, British A. R. C., 1923.
13. Shortal, Joseph A.: Effect of Tip Shape and Dihedral on Lateral-Stability Characteristics. T. R. No. 548, N. A. C. A., 1935.
14. Munk, Max M.: A New Relation between the Induced Yawing Moment and the Rolling Moment of an Airfoil in Straight Motion. T. R. No. 197, N. A. C. A., 1924.

REPORT No. 571

PRESSURE DISTRIBUTION OVER A RECTANGULAR AIRFOIL WITH A PARTIAL-SPAN SPLIT FLAP

By CARL J. WENZINGER and THOMAS A. HARRIS

SUMMARY

Pressure-distribution tests of a Clark Y wing model with a partial-span split flap were made to determine the distribution of air loads over both the wing and the flap. The model was used in conjunction with a reflection plane in the N. A. C. A. 7- by 10-foot wind tunnel. The 20-percent-chord split flap extended over the inboard 60 percent of the semispan. The tests were made at various flap deflections up to 45° and covered a range of angles of attack from zero lift to approximately maximum lift for each flap deflection.

The results are given as airfoil section, or rib, pressure diagrams for the wing with flap neutral. Increments of airfoil section pressures are given for various amounts of flap deflection so that combined wing and flap section pressure diagrams may be obtained by a simple addition. Calculated coefficients of section loads and moments and of wing loads and moments are also given for the wing and flap combination and for the flap alone.

It was found that deflecting a partial-span split flap affected the pressures and the section normal-force and pitching-moment coefficients over the entire wing span. The flap loads and moments were almost constant over the span of the partial-span flap for a given angle of attack and flap deflection. The maximum normal-force

and hinge-moment coefficients were about the same for the partial-span split flap of the present tests as for a full-span split flap previously tested.

INTRODUCTION

A considerable amount of aerodynamic and air-load data is available for simple split flaps extending along the entire span of the wing. (See references 1 to 3.) However, because of the general use on present-day airplanes of the outer portion of the wing span for ailerons, most of the installations of split flaps have been limited to the inner 40 to 60 percent portion of the wing span. Some aerodynamic information on partial-span split flaps is available from wind-tunnel force tests of both rectangular and tapered wings equipped with such flaps (references 4 and 5). There are available, however, very few air-load and moment data suitable for the design of wings with partial-span split flaps.

The present investigation was made to obtain information, particularly of span load distribution, that would be suitable for application to design problems involving partial-span split flaps. The data were obtained from pressure-distribution tests of a wing model with a 20-percent-chord split flap in the N. A. C. A. 7- by 10-foot wind tunnel. The results are given as

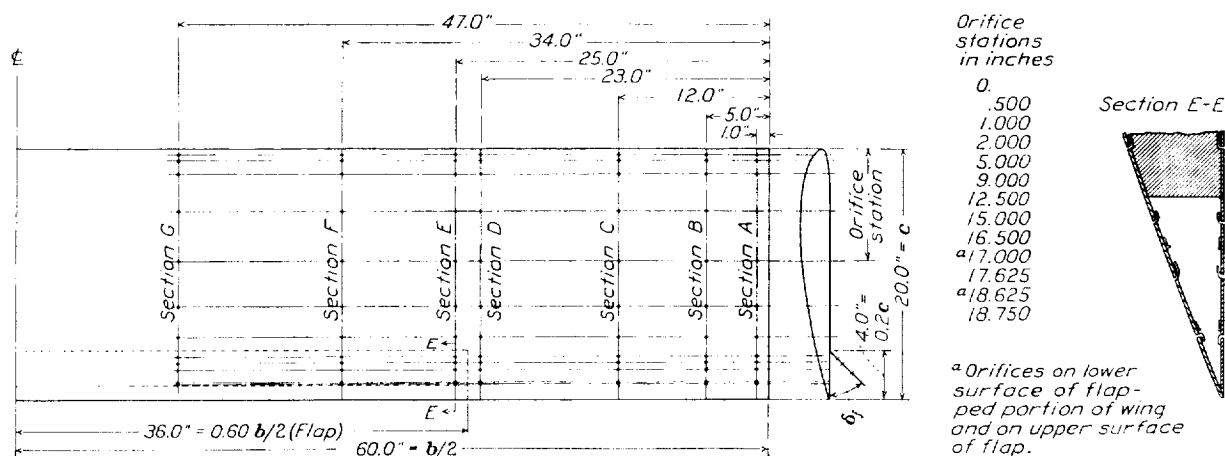


FIGURE 1. Diagrammatic drawing of semispan Clark Y airfoil with split flap showing pressure orifices.

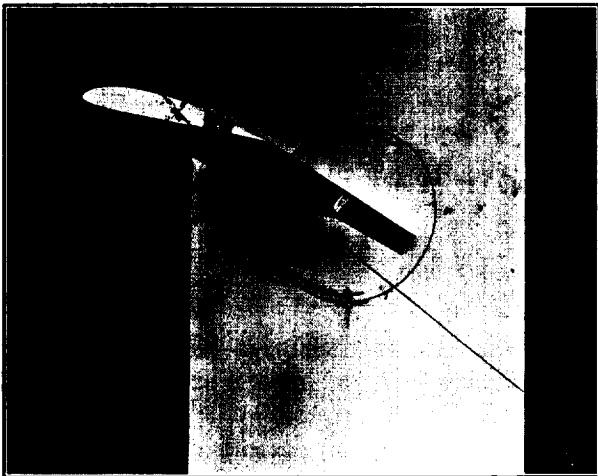


FIGURE 2.—Side view of model in tunnel.



FIGURE 3.—Front view of model in tunnel.

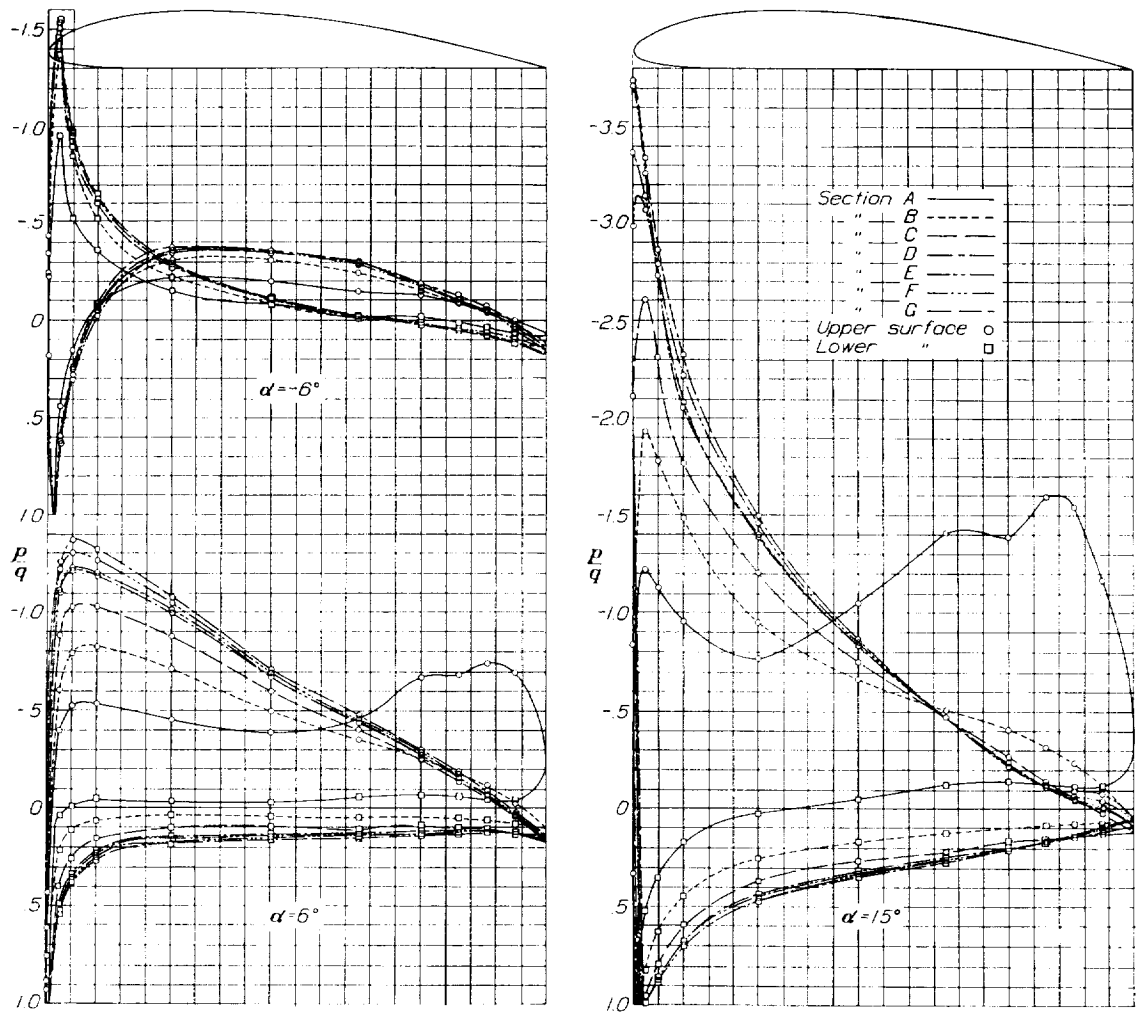


FIGURE 4.—Pressure distribution over airfoil sections at three angles of attack; $\delta_f = 0^\circ$.

pressure diagrams for the basic wing and as increments in pressure or load for the flap-deflected conditions. The characteristics are given for the wing-and-flap combination and for the flap alone.

MODEL AND APPARATUS

WING MODEL

The Clark Y wing used for these tests had a 20-inch chord and a 60-inch semispan (fig. 1); the portion extending back to 80 percent of the wing chord was con-

and was set at the various deflections by suitable spacer blocks as shown in figure 2. The gap between the leading edge of the flap and the wing was sealed with plasticine for all tests.

Pressure orifices were built into the upper and lower surface of both the wing and flap at several sections along the semispan, 166 individual pressure orifices being installed. The tubes from the orifices were brought through the model and out at the inboard end. Two orifices on both the upper surface of the flap and

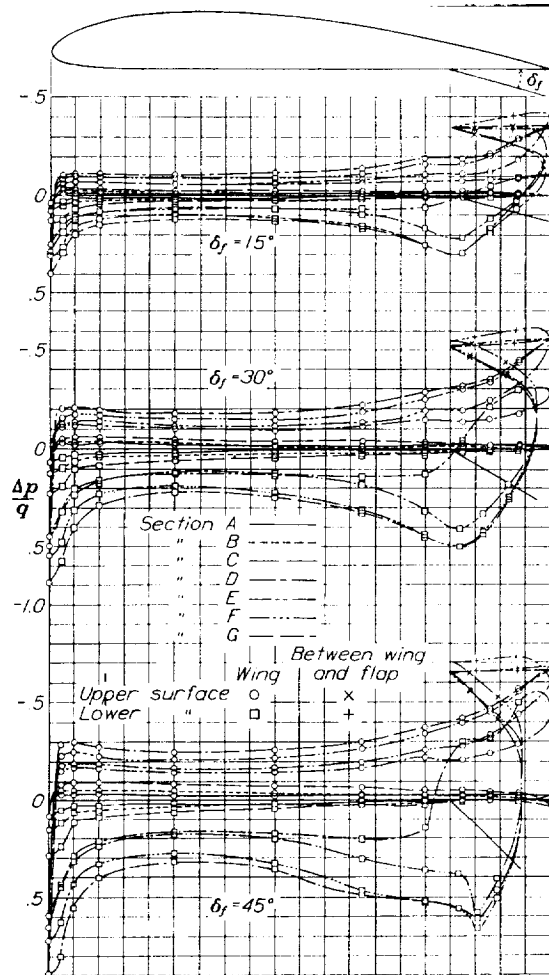


FIGURE 5.—Increments of pressure over airfoil sections at -6° angle of attack with the flap deflected various amounts.

structed of laminated mahogany. The trailing-edge, upper portion was constructed of $\frac{1}{16}$ -inch-thick steel plate rolled to the contour and attached to the wooden part of the wing with screws. The flap, which had a 4-inch chord and a 36-inch semispan (20 percent c by 60 percent $b/2$), was formed by hinging the inboard 60 percent of the metal lower surface of the rear part of the wing about its leading edge. The flap was supported at its leading edge by small piano-type hinges

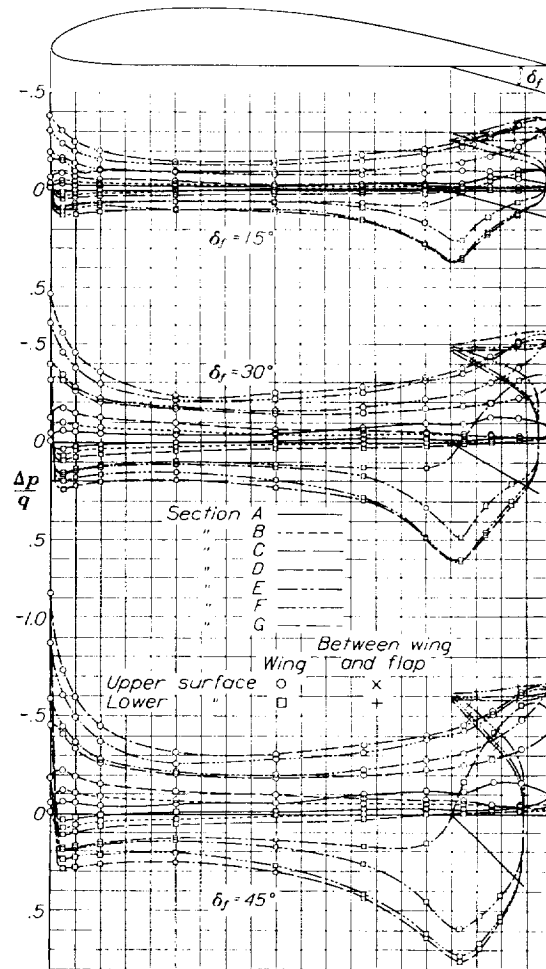


FIGURE 6.—Increments of pressure over airfoil sections at 6° angle of attack with the flap deflected various amounts.

on the lower surface of the wing at sections E, F, and G (fig. 1) were used to obtain the pressures between the flap and the wing.

MANOMETERS

Two N. A. C. A. multiple-tube photographic-recording manometers (described in reference 6) were used to record the point pressures on the model. The manometer was connected to the orifices by means of rubber tubing, so arranged as not to affect the air flow over the wing.

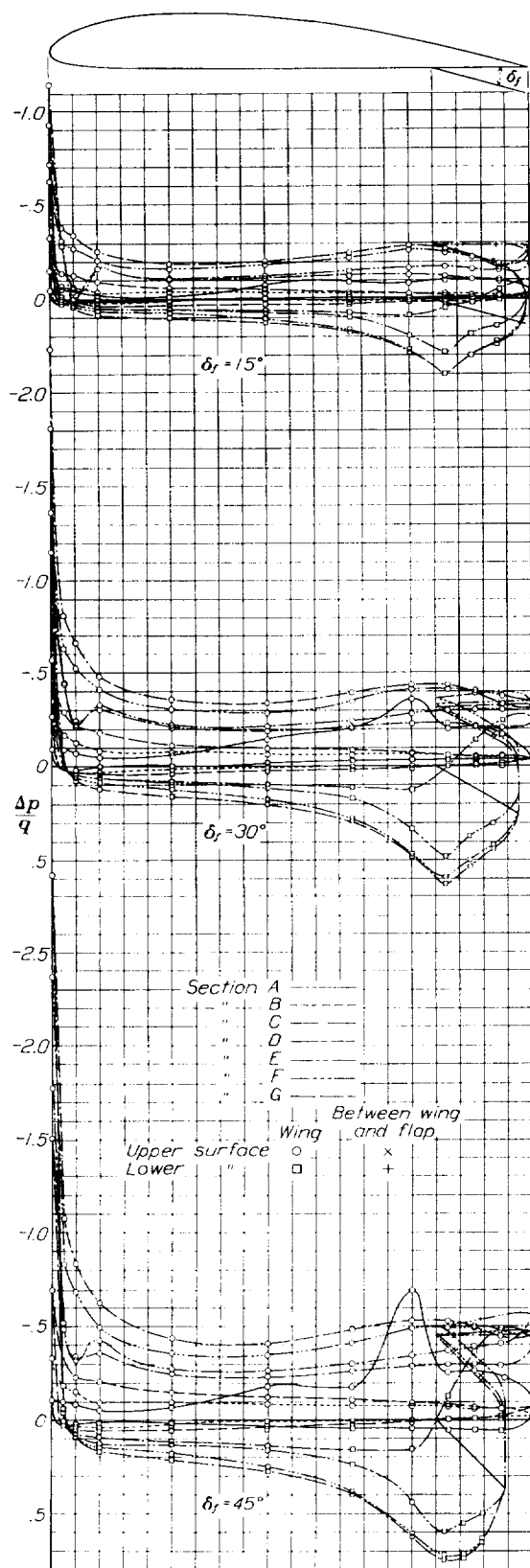


FIGURE 7.- Increments of pressure over airfoil sections at 15° angle of attack with the flap deflected various amounts.

TEST ARRANGEMENT

The model was mounted in the N. A. C. A. 7- by 10-foot wind tunnel (reference 7) in conjunction with a reflection plane at the inboard end. (See figs. 2 and 3). This plane extended from the top to the bottom of the air stream and some distance ahead of and behind the model and was so located that the model was placed symmetrically with respect to the tunnel center line. The tubes from the pressure orifices were brought horizontally through a rotatable section of this plane to the edge of the jet and were grouped together to form a streamline shape so that the air flow on the opposite side of the plane, on which the model was located, was not appreciably disturbed.

TESTS

The static reference pressure used to maintain the dynamic pressure constant during the tests was calibrated against dynamic-pressure surveys at the model location with the model removed from the tunnel. The longitudinal static pressure at the model location was also measured and used to correct the point pressures to the correct reference pressure.

All the tests were made at a dynamic pressure of 16.37 pounds per square foot, corresponding to an air speed of 80 miles per hour under standard sea-level atmospheric conditions. The average Reynolds Number of the tests, based on the wing chord, was approximately 1,220,000.

The model was tested with flap angles of 0°, 15°, 30°, and 45°. The angles of attack covered a range from approximately zero lift to 15° (approximately $C_{L_{max}}$) with each flap setting, test points being taken at 3° intervals. When the model had been fixed at a given angle of attack with a given flap setting, a few minutes were allowed for conditions to become constant; a record was then taken of the pressures at the orifices by means of the photographic manometer.

PRESENTATION OF DATA

Section or rib pressure diagrams with the flap neutral (fig. 4) are given as ratios of point pressure p to dynamic pressure q for a low angle of attack (-6°), an intermediate angle of attack (6°), and a high angle of attack (15°). In addition to the section pressure diagrams with the flap neutral, the increments of point pressure with the flap deflected over the point pressure with the flap neutral (both in terms of the dynamic pressure) are given (figs. 5 to 7) for all flap deflections and for the three previously mentioned angles of attack. On these diagrams the flap pressures are plotted from the deflected flap chord but normal to the wing chord. The principal advantage of the increment diagrams is that they may, by the principle of superposition, be applied to pressure diagrams of any other basic wing section that does not depart too greatly from the Clark Y section of which the tests were made.

The data computed from the integrated pressure diagrams are given as nondimensional coefficients. The coefficients for the wing-and-flap combination include the loads of the flap projected onto the wing chord. The coefficients are defined as follows:

$$c_{n_w} = \frac{n_w}{qc_w}, \text{ airfoil section normal-force coefficient.}$$

$$C_{m_{c/4}} = \frac{M_{w_{c/4}}}{qc_w^2 b_w}, \text{ wing pitching-moment coefficient about quarter-chord point.}$$

$$c_{h_f} = \frac{h_f}{qc_f^2}, \text{ flap section hinge-moment coefficient about flap hinge.}$$

$$C_{h_f} = \frac{H_f}{qc_f^2 b_f}, \text{ flap hinge-moment coefficient about flap hinge.}$$

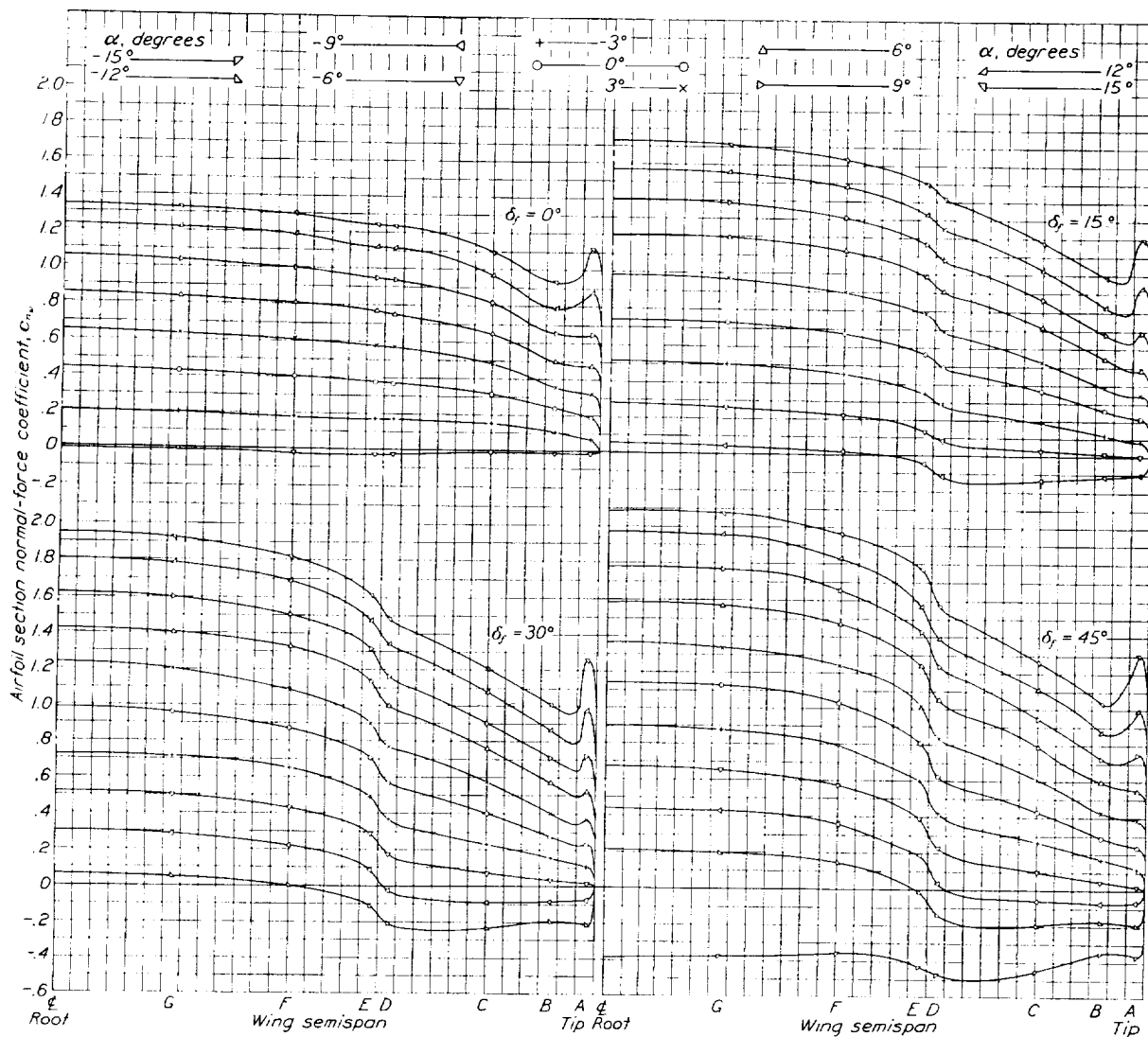


FIGURE 8.—Span load distribution on the airfoil with the flap deflected various amounts.

$$C_{N_w} = \frac{N_w}{qc_w b_w}, \text{ wing normal-force coefficient.}$$

$$c_{n_f} = \frac{n_f}{qc_f}, \text{ flap section normal-force coefficient.}$$

$$C_{N_f} = \frac{N_f}{qc_f b_f}, \text{ flap normal-force coefficient.}$$

$$c_{m_{c/4}} = \frac{m_{w_{c/4}}}{qc_w^2}, \text{ airfoil section pitching-moment coefficient about quarter-chord point.}$$

$$(c.p.)_w = \left(0.25 - \frac{C_{m_{c/4}}}{C_{N_w}} \right) \times 100, \text{ airfoil section longitudinal center of pressure in percentage of wing chord from wing leading edge.}$$

$$(C.P.)_w = \left(0.25 - \frac{C_{m_{c/4}}}{C_{N_w}} \right) \times 100, \text{ wing center of pressure in percentage of wing chord from wing leading edge.}$$

$(c.p.)_f = \left(-\frac{c_{h_f}}{c_{n_f}} \right) \times 100$, flap section center of pressure in percentage of flap chord from hinge.

$(C.P.)_f = \left(-\frac{C_{h_f}}{C_{n_f}} \right) \times 100$, flap center of pressure in percentage of flap chord from hinge.

$(C.P.)_{w_{lat}} = \left(\frac{M_{w_{lat}}}{N_w b_w} \right) \times 100$, wing lateral center of pressure in percentage of wing semispan from wing root.

$M_{w_{c/4}}$, wing pitching moment about the quarter-chord point.

h_f , flap section hinge moment per unit span about the flap hinge.

H_f , flap hinge moment about the flap hinge.

$M_{w_{lat}}$, moment of wing semispan load about wing root.

$M_{f_{lat}}$, moment of flap semispan load about inboard end of flap.

q , dynamic pressure.

c_w , wing chord.

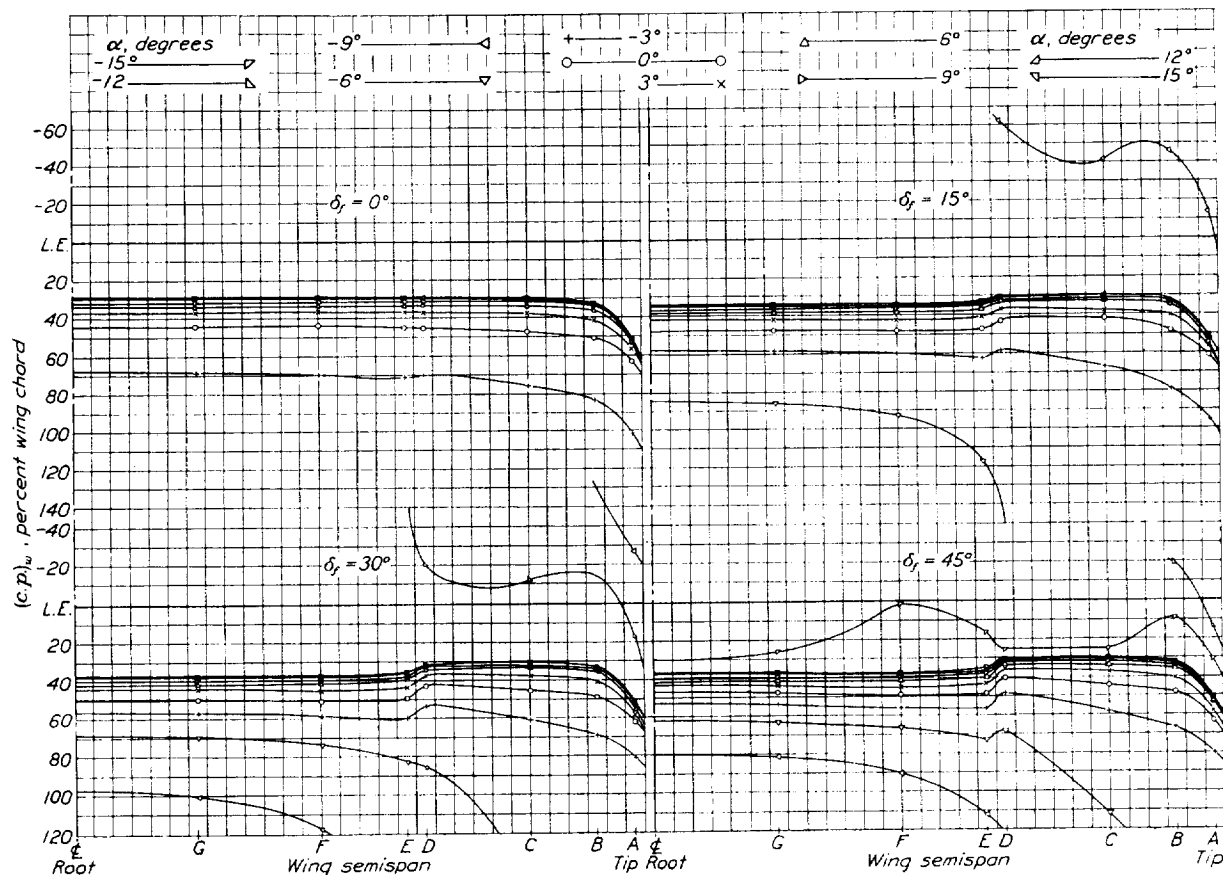


FIGURE 9.—Airfoil section longitudinal centers of pressure against span of wing with the flap deflected various amounts.

$(C.P.)_{f_{lat}} = \left(\frac{M_{f_{lat}}}{N_f b_f} \right) \times 100$, flap lateral center of pressure in percentage of flap semispan from inboard end of flap.

where

n_w is the airfoil section normal force per unit span.

N_w , wing normal force.

n_f , flap section normal force per unit span.

N_f , flap normal force.

$m_{w_{c/4}}$, airfoil section pitching moment per unit span about the quarter-chord point.

c_f , flap chord.

b_w , wing span.

b_f , flap span.

In these coefficients it is to be noted that the chord forces on the airfoil have been neglected; i. e., the longitudinal center-of-pressure positions and the pitching-moment coefficients were derived solely from considerations of the normal forces.

The airfoil section normal-force coefficients are plotted against the wing semispan in figure 8 for all flap deflections and all angles of attack tested. The

airfoil section centers of pressure are plotted similarly in figure 9. In addition to these data, the increments of airfoil section normal-force and pitching-moment coefficients, Δc_n and Δc_m , for the three angles of attack previously mentioned are given in figure 10. The airfoil section coefficients c_n and c_m are also plotted against angle of attack for all the flap deflections in figure 11. The wing normal-force and pitching-moment coefficients and longitudinal centers of pressure are plotted against angle of attack for all flap deflections in figure 12, and the wing lateral centers of pressure are given for all flap deflections in figure 13.

The flap section normal-force coefficients are plotted against flap semispan in figure 14 for all flap deflections and angles of attack. It should be noted that for $\delta_f = 0^\circ$ the coefficients were computed for the load on only the lower surface of the flap, whereas for the other flap deflections the coefficients include the loads on both the upper and lower surfaces of the flap. This condition also applies to the flap centers of pressure and hinge-moment coefficients. The flap section centers of pressure for all flap deflections and angles of attack are plotted against flap semispan in figure 15. The flap normal-force and hinge-moment coefficients and longitudinal centers of pressure are plotted against wing normal-force coefficients in figure 16 for all flap deflections. The flap lateral centers of pressure are plotted against angle of attack in figure 17.

PRECISION

Inasmuch as no air-flow alinement tests were made in the wind tunnel with the test arrangement used for this investigation, the absolute setting of the angle of attack may be slightly in error; the relative angles are, however, accurate to within $\pm 0.1^\circ$. The flap deflections were set to the specified angles to within $\pm 0.1^\circ$. The point pressures based on check tests in which both the angle of attack and the flap settings were changed independently showed that they agreed to within ± 2 percent, with the exception of the upper-surface pressures near the wing leading edge which, at high angles of attack, checked to within ± 5 percent. The dynamic pressure recorded on each diagram was accurate to within ± 0.25 percent for all tests. Since the dynamic pressure was recorded on each diagram, there is no relative error between it and the point pressure; therefore variations of the dynamic pressure do not introduce any error in computing the coefficients. None of the data has been corrected for the effects of the jet boundaries.

RESULTS AND DISCUSSION

SECTION PRESSURE DISTRIBUTION

The distribution of pressure over the airfoil sections with the flap neutral (fig. 4) is typical of that for wings of rectangular plan form. The expected high tip

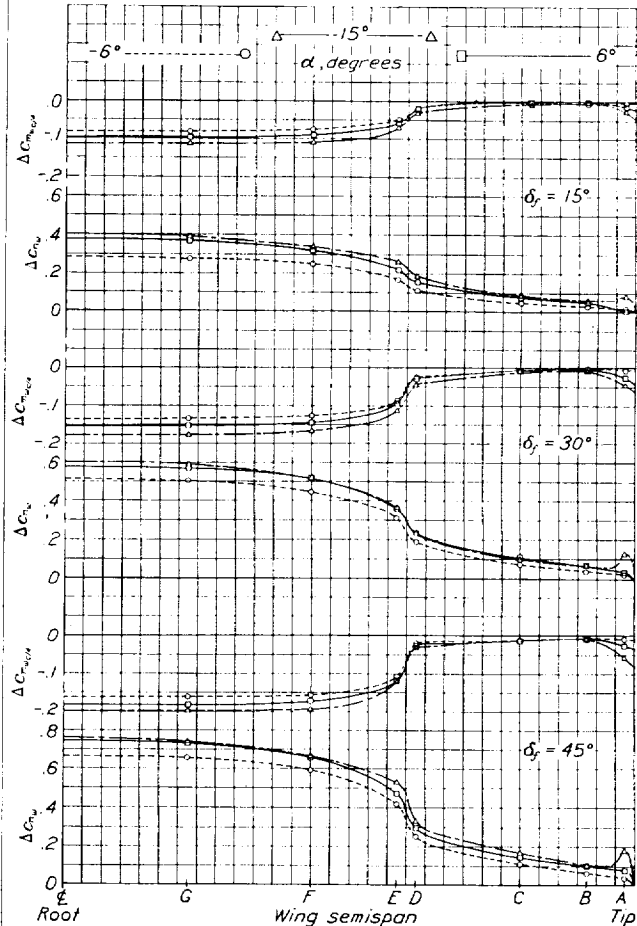


FIGURE 10.—Increments in airfoil section normal-force and pitching-moment coefficients with the flap deflected various amounts.

loads at the high angle of attack verify previous conclusions that structurally the rectangular tip shape is poor. The data for angles of attack other than those shown were not believed to be of sufficient general interest to include in this report.

The increments of pressure due to the deflected flap at the low angle of attack, -6° , (fig. 5) show that the partial-span flap affects the load distribution on all sections along the span of the wing. The first section outboard of the tip of the flap, section D, shows a

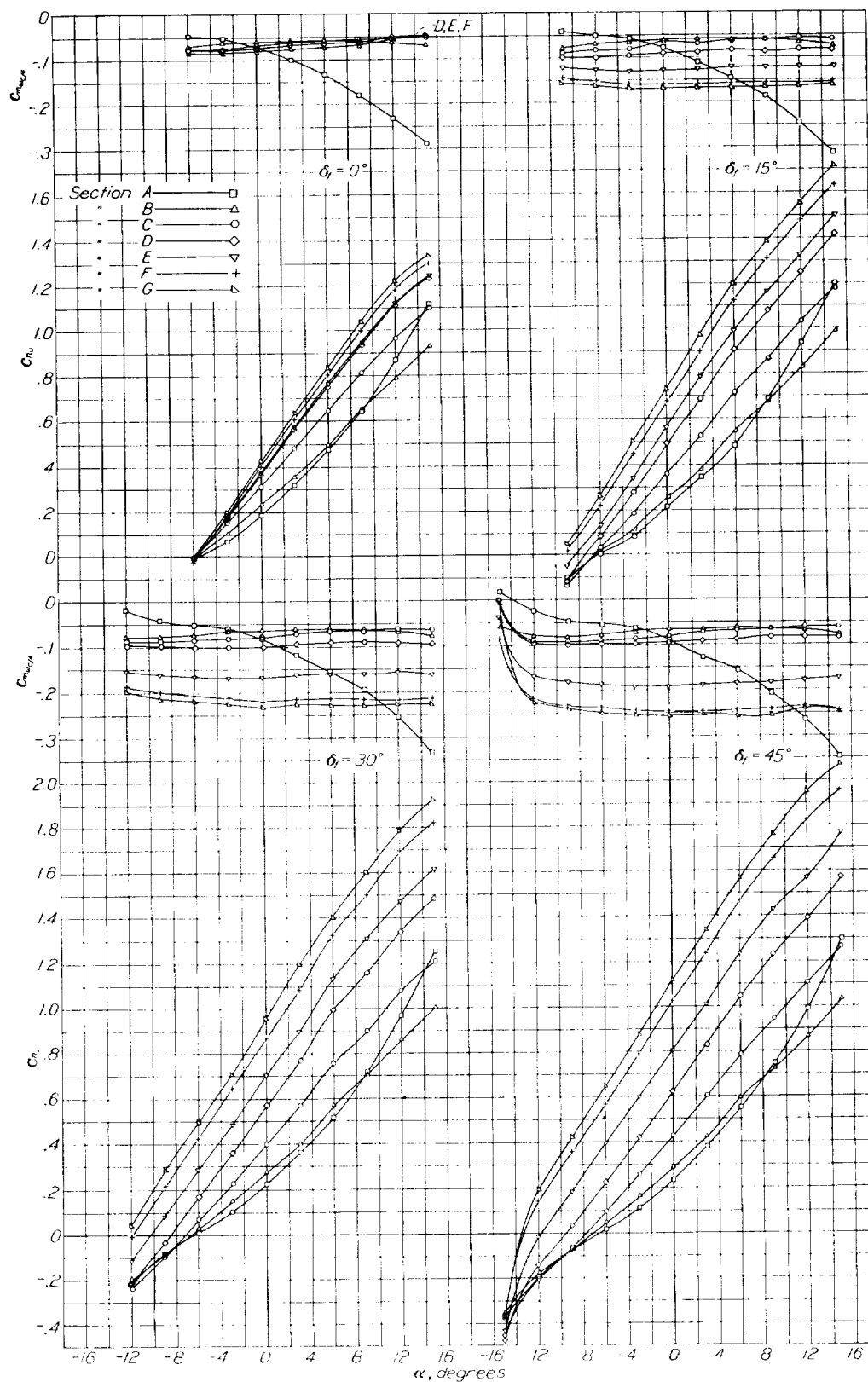


FIGURE 11. Airfoil section normal-force and pitching-moment coefficients with the flap deflected various amounts.

peculiar resultant down-load increment at the trailing edge of the wing, which increases as the flap is deflected downward. There is also a considerable resultant down-load increment on the trailing-edge portion of the wing covered by the flap when the flap is deflected, which increases with flap deflection. In addition, the positive pressures on the lower surface of the wing are

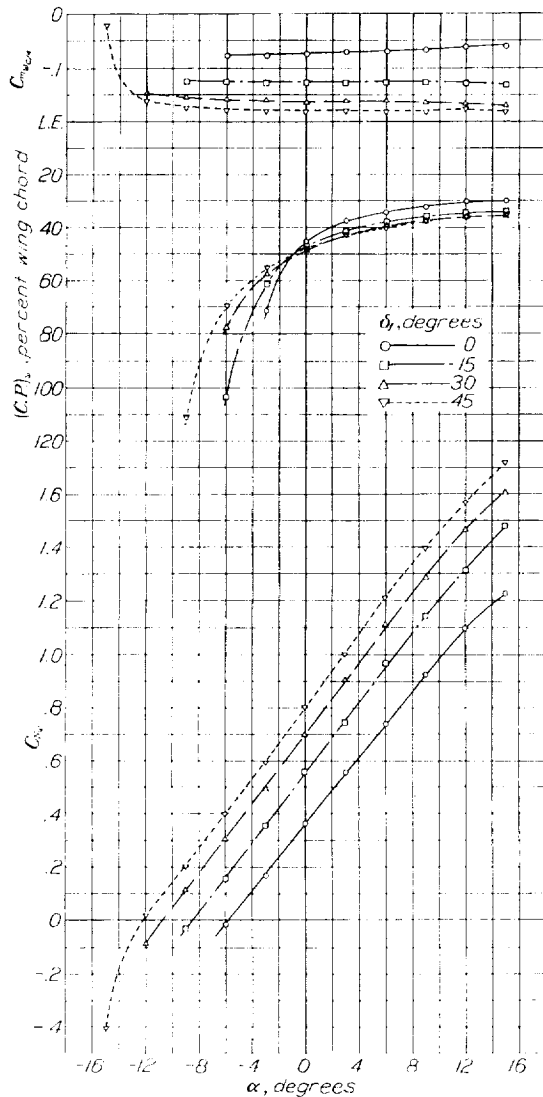


FIGURE 12—Normal-force coefficients, pitching-moment coefficients, and centers of pressure of the wing with the flap deflected various amounts.

increased more than the negative pressures on the upper surface at a given flap deflection. The pressures are increased the greatest amount near the flap hinge and near the leading edge of the wing.

At the intermediate angle of attack, 6° (fig. 6), there is a peculiar increase in load at the tip of the wing, which is probably a function of the wing plan as well as of the flap deflection. The increments of pressure at the trailing edge of the wing are quite similar to

those noted for the low angle of attack. In addition, the increase in positive pressure near the flap hinge on the lower surface of the wing is larger. This increase in load near the hinge may be critical in rib design because normally this portion of the rib does not have large loads. The negative pressure on the upper surface near the leading edge increases at this angle of attack by about 75 percent of the dynamic pressure with the maximum flap deflection.

At an angle of attack of 15° (fig. 7) the increase in load on the tip section is again evident. At this angle of attack the resultant down-load increment near the trailing edge at section D with the flap down is less than for the lower angles of attack. The load increment on the portion of the wing above the flap is very small but the increment on the wing outboard of the flap is large, increasing with flap deflection. The

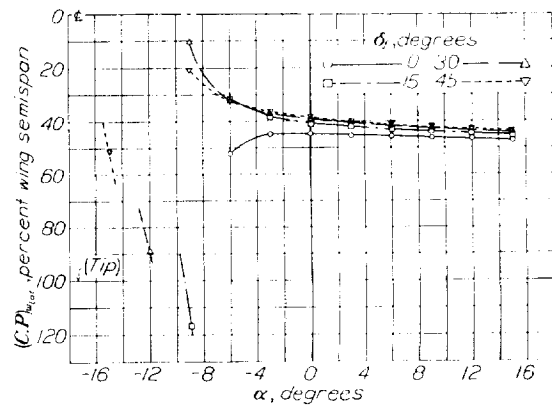


FIGURE 13—Lateral centers of pressure of wing with the flap deflected various amounts.

large increase in positive pressure near the flap hinge is also evident and is in agreement with the results of the tests reported in reference 3. The increased negative pressure at the wing leading edge is about three times the dynamic pressure when the flap is fully deflected.

WING LOADS AND MOMENTS

The airfoil section normal-force coefficients plotted in figure 8 show the actual distribution of the air load along the span for all the angles of attack and the flap deflections tested. With the flap neutral, the span load distribution is typical of that for rectangular airfoils. With the flap deflected, the section normal-force coefficient increases along the entire span of the wing. The rapid change in section normal-force coefficients at the tip of the flap is very noticeable. The curves show that the larger the flap deflection, the greater is the concentration of the load over the flapped portion of the wing for a given total load. The high tip loads may be attributed to the particular plan form of the wing.

The section centers of pressure plotted against the span of the wing with the flap neutral (fig. 9) are

typical of those for a wing of rectangular plan form. The center of pressure moves forward as the angle of attack is increased and is nearly uniform over the span except at the tips of the wing, which may be seen from the pressure-distribution diagrams (fig. 4). With the flap deflected (fig. 9), the center of pressure shifts rearward not only over the flapped portion of the wing but also over the rest of the wing to the outboard end for the high angles of attack. For the low angles of attack, the center of pressure shifts forward over the unflapped portion of the wing when the flap is deflected.

The increments of airfoil section normal-force and pitching-moment coefficients caused by deflecting the

and moment diagrams of plain wings having similar profiles and plan forms.

In order to complete the air-load information on wings with this type of flap, more tests are desirable with other wing profiles and plan forms and flaps of different spans and chords. Such additional data would establish the effect of profile and plan form on section-characteristic increments and on span-load and moment increments.

The curves of the section normal-force coefficient (fig. 11) show that for all sections except A and B the normal-force coefficient is linearly proportional to the angle of attack from zero lift to 15° angle of attack. The pitching-moment coefficient curves, except for section A, are regular, the moment increasing toward the center of the wing.

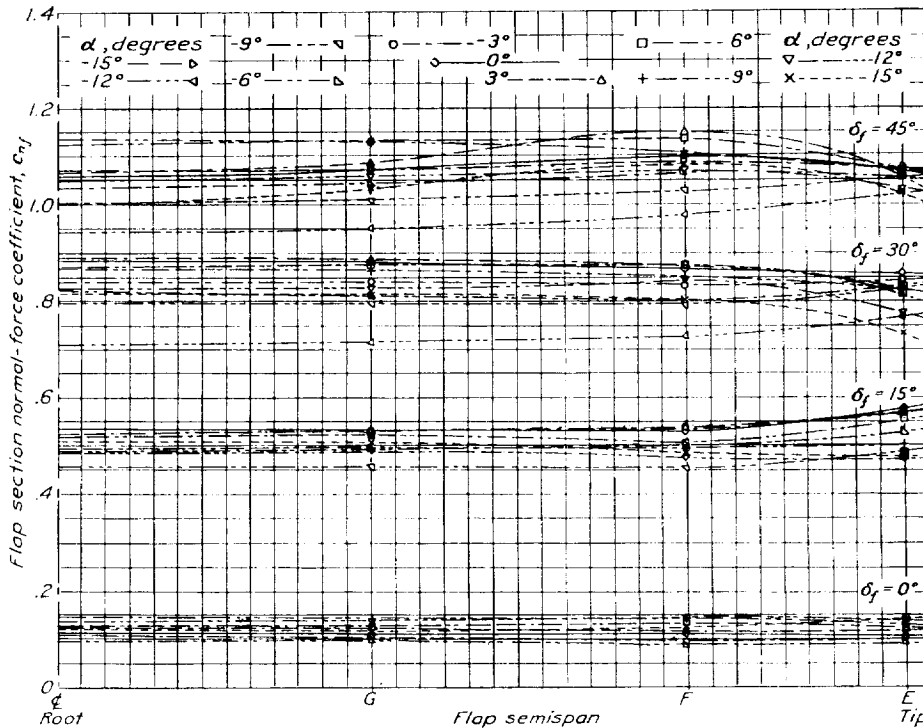


FIGURE 14.—Span load distribution on flap for various flap deflections.

flap (fig. 10) are probably of greater interest than the wing coefficients for a particular model. The largest changes in section normal-force coefficient, $\Delta c_n = 0.75$, and in section pitching-moment coefficient, $\Delta c_{m_{cl,4}} = -0.20$, occur at the maximum flap deflection used and at 15° angle of attack. The rapid change in both the wing normal-force and pitching-moment coefficients at the outboard end of the flap and the increase in the force and moment on the unflapped portion of the wing are clearly shown by these increment diagrams. The peak load and moment increments at the tip of the wing are probably a function of the rectangular tip shape and might not be encountered with rounded wing tips. It is probable that these increments of loads and moments may safely be superposed on known span load

As previously pointed out, the peculiar loads and moments at the tip section are a function of the tip shape.

The variation in the wing characteristics with angle of attack (fig. 12), caused by deflecting the partial-span flap a given amount, checks reasonably well with the results of force tests (data unpublished). The sudden change in normal force at high negative angles of attack with the flap down 45° is worthy of note. The same phenomenon was encountered in force tests with split flaps (references 2 and 4) and may result in critical loads when considering a down gust if flying at maximum allowable speed with the flap deflected. More data on conditions in this vicinity are desirable.

The lateral center of pressure on the wing (fig. 13) moves toward the plane of symmetry as the flap is deflected downward.

FLAP LOADS AND MOMENTS

The flap section normal-force coefficients are shown in figure 14 for all flap deflections and angles of attack plotted against flap span. For the zero flap deflection the load on only the lower surface of the flap was considered, but for the other flap deflections the load on both surfaces was included. The section normal-force coefficient of the flap increases with flap deflection but shows no consistent variation with angle of attack. For practical purposes the air-load distribution may be considered uniform over the span of the flap.

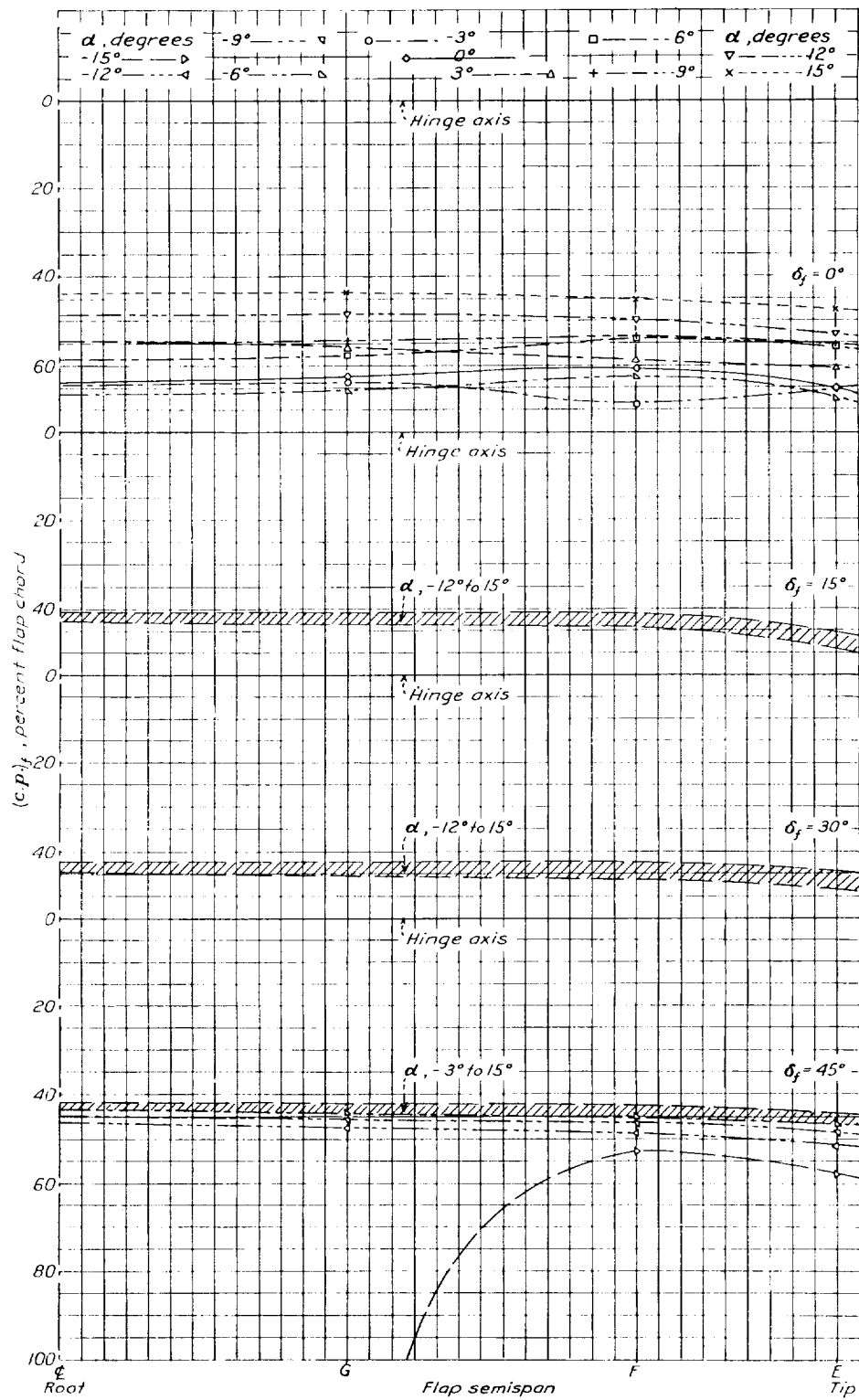


FIGURE 15.—Flap section longitudinal centers of pressure against span of flap for various flap deflections.

The flap section centers of pressure (fig. 15) with the flap neutral are rather erratic and vary over a large range; for other flap deflections the flap center of pressure is essentially constant between 40 and 50 percent of the flap chord from the hinge axis.

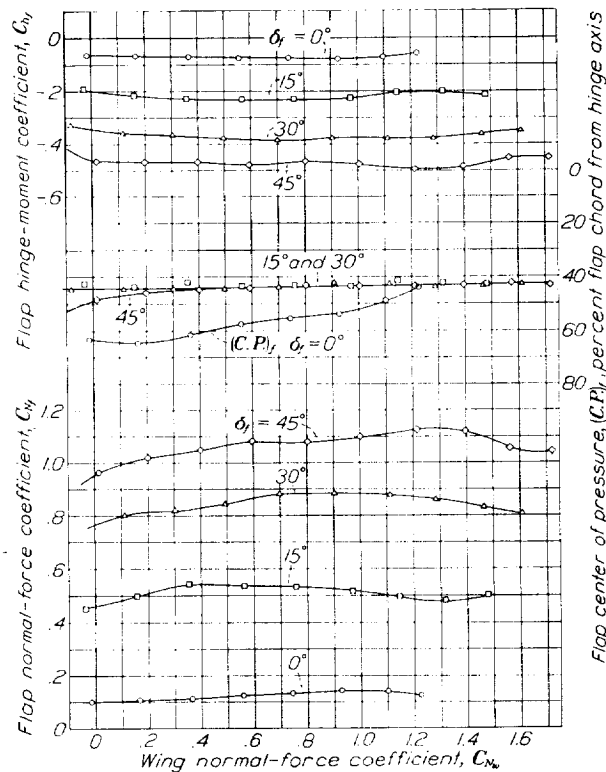


FIGURE 16.—Normal-force coefficients, hinge-moment coefficients, and centers of pressure of flap for various flap deflections.

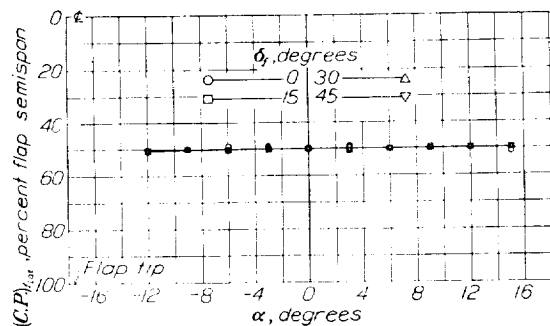


FIGURE 17.—Lateral centers of pressure of flap for various flap deflections.

The flap hinge-moment and normal-force coefficients (fig. 16) increase with flap deflection but show no consistent variation with wing normal-force coefficient. The maximum flap normal-force coefficient was 1.15, which checks the results of references 2 and 3 for the same flap deflection. The maximum hinge-moment coefficient of the flap was 0.5, which is about 10 percent less than that reported for the full-span flap of reference 2.

The longitudinal center of pressure on the flap (fig. 16) is about constant at 43 percent of the flap chord from the hinge axis except when the flap is neutral and

for small values of the wing normal-force coefficient with the flap down 45°. With the flap neutral the center of pressure moves to about 65 percent of the flap chord at small values of wing normal-force coefficient. The lateral center of pressure on the flap (fig. 17) is at 50 percent of the flap span from the plane of symmetry, within ± 0.5 percent, for all flap deflections and angles of attack tested.

The amount of leakage between the wing and a closed split flap largely determines the hinge-moment and normal-force coefficient for the neutral setting. If there is any negative pressure on the upper surface of the flap in the closed position, the hinge-moment and normal-force coefficients will be increased. It is possible that the force required to overcome the hinge moment when the flap is neutral may be critical for manual operation of the flap. Further tests of various flap-neutral conditions seem desirable.

CONCLUSIONS

The following conclusions may be drawn from the results of the tests reported herein:

1. Deflection of the partial-span split flap affected the pressures and section normal-force and pitching-moment coefficients over the entire span of the wing.
2. For the wing-flap combination tested, the flap loads and moments were practically constant over the span of the partial-span split flap for a given flap deflection and angle of attack of the wing.
3. The maximum normal-force and hinge-moment coefficients were about the same for the partial-span split flap of the present tests as for a previously tested full-span split flap.

LANGLEY MEMORIAL AERONAUTICAL LABORATORY,
NATIONAL ADVISORY COMMITTEE FOR AERONAUTICS,
LANGLEY FIELD, VA., April 28, 1936.

REFERENCES

1. Weick, Fred E., and Harris, Thomas A.: The Aerodynamic Characteristics of a Model Wing Having a Split Flap Deflected Downward and Moved to the Rear. T. N. No. 422, N. A. C. A., 1932.
2. Wenzinger, Carl J.: Wind-Tunnel Measurements of Air Loads on Split Flaps. T. N. No. 498, N. A. C. A., 1934.
3. Wallace, Rudolf: Investigation of Full-Scale Split Trailing-Edge Wing Flaps with Various Chords and Hinge Locations. T. R. No. 539, N. A. C. A., 1935.
4. Wenzinger, Carl J.: The Effect of Partial-Span Split Flaps on the Aerodynamic Characteristics of a Clark Y Wing. T. N. No. 472, N. A. C. A., 1933.
5. Wenzinger, Carl J.: The Effects of Full-Span and Partial-Span Split Flaps on the Aerodynamic Characteristics of a Tapered Wing. T. N. No. 505, N. A. C. A., 1934.
6. Parsons, John F.: Full-Scale Force and Pressure-Distribution Tests on a Tapered U. S. A. 45 Airfoil. T. N. No. 521, N. A. C. A., 1935.
7. Harris, Thomas A.: The 7 by 10 Foot Wind Tunnel of the National Advisory Committee for Aeronautics. T. R. No. 412, N. A. C. A., 1931.

REPORT No. 572

DETERMINATION OF THE CHARACTERISTICS OF TAPERED WINGS

By RAYMOND F. ANDERSON

SUMMARY

Tables and charts for use in determining the characteristics of tapered wings are presented. Theoretical factors are given from which the following characteristics of tapered wings may be found: The span lift distribution, the induced-angle-of-attack distribution, the lift-curve slope, the angle of zero lift, the induced drag, the aerodynamic-center position, and the pitching moment about the aerodynamic center.

The wings considered cover the complete range of taper ratios and a range of aspect ratios from 2 to 20. The factors given include the effects of sweepback and twist and apply to wings having a straight taper plan form with rounded tips and an elliptical plan form. The general formulas of the usual wing theory are also given from which the characteristics of a wing of any form may be calculated when the section characteristics are known from experiment.

In addition to the tables and charts, test results are given for nine tapered wings, including wings with sweepback and twist. The test results verify the values computed by the methods presented in the first part of the report. A final section is given outlining a method for estimating the lift coefficient at which a tapered wing begins to stall. This method, which should be useful for estimating the maximum lift coefficient of tapered wings, is applied to one of the wings tested.

INTRODUCTION

A large amount of work has been done on the determination of tapered-wing characteristics from airfoil theory. Glauert has given some of the characteristics of wings with straight taper for a limited range of aspect ratios (references 1 and 2). Hueber has given other characteristics of wings with straight taper for a large range of aspect ratios (reference 3). Several other papers have given various characteristics of tapered wings. The data of all the papers, however, have been limited by one or more of the following factors: Range of aspect ratio and taper ratio, number of characteristics given, and omission of data on wings with sweepback and twist. In order to provide more complete information, data are given in this report for a large range of aspect ratios, for the complete range

of taper ratios, and for wings with sweepback and twist. As airplane wings are usually rounded at the tips, the data are given for wings with rounded tips.

In addition to the theoretical characteristics, the results of tests of nine tapered wings, including wings with sweepback and twist, and a comparison of some of the test results with theoretical values are presented.

The characteristics are given for wings having a straight taper and rounded tips and for wings having an elliptical plan form, with an aspect-ratio range from 2 to 20. For these wings, formulas are given using factors that are presented in tables and charts. From the formulas and factors the following characteristics of tapered wings may be determined: Span lift distribution, induced-angle-of-attack distribution, lift-curve slope, angle of zero lift, induced drag, aerodynamic-center position, and pitching moment about the aerodynamic center.

METHOD OF OBTAINING DATA

BASIC CONCEPTS

When obtaining the data used to determine the characteristics of wings, a tapered wing is considered to consist of a series of airfoil sections that may vary in shape, chord length, and in angle of attack from root to tip. Each airfoil section is assumed to have an aerodynamic center through which the lift and drag act and about which the pitching moment is constant.

With the section characteristics as a basis, characteristics of the entire wing are obtained by integration across the span. Formulas for the integrations will first be given for a wing of any shape and zero dihedral; that is, the aerodynamic centers of all the sections along the span lie in a plane which passes through the root chord and which is perpendicular to the plane of symmetry. Wings of particular shape will be considered later and a method for including the effect of dihedral will be given.

For any tapered wing the span lift distribution may be considered to consist of two parts. One part, which will be called the "basic distribution," is the distribution that depends principally on the twist of the wing and occurs when the total lift of the wing is zero; it does not change with the angle of attack of the wing.

The second part of the span lift distribution, which will be called the "additional distribution," is the lift due to change of the wing angle of attack; it is independent of the wing twist and maintains the same form throughout the reasonably straight part of the lift curve.

In the designation of the characteristics of a wing, lower-case letters will be used for section characteristics and upper-case letters for the characteristics of the entire wing. The basic and additional section lift coefficients are then c_{l_b} and c_{l_a} . A complete list of symbols follows. It is convenient to find the additional lift coefficient for a wing C_L of 1 and it is then designated $c_{l_{a1}}$. The two coefficients are related by $c_{l_a} = C_L c_{l_{a1}}$. The total lift coefficient at any section is found from the basic and additional coefficients from

$$c_{l_0} = c_{l_b} + C_L c_{l_{a1}}$$

where c_{l_0} is the lift coefficient perpendicular to the local relative wind at any section as distinguished from c_l , which is perpendicular to the relative wind at a distance. For convenience, however, c_l will be used and may be considered equal to c_{l_0} .

SYMBOLS

- A , aspect ratio, b^2/S .
 b , span.
 c , chord at any section along the span.
 c_t , tip chord (for rounded tips, c_t is the fictitious chord obtained by extending the leading and trailing edges to the extreme tip).
 c_s , chord at root of wing or plane of symmetry.
 S , wing area.
 β , angle of sweepback, measured between the lateral axis and a line through the aerodynamic centers of the wing sections. (See fig. 1.)
 ϵ , aerodynamic twist in degrees from root to tip, measured between the zero-lift directions of the center and tip sections, positive for washin.
 x , longitudinal coordinate, parallel to the root chord.
 y , lateral coordinate, perpendicular to plane of symmetry.
 z , vertical coordinate in the plane of symmetry, perpendicular to the root chord.
 $x_{a.c.}$, x coordinate of wing aerodynamic center.
 a , wing lift-curve slope, per degree.
 a_0 , wing section lift-curve slope, per degree.
 m , wing lift-curve slope, per radian.
 m_0 , wing section lift-curve slope, per radian.
 α , angle of attack at any section along the span.
 α_s , wing angle of attack measured from the chord of the root section.
 α_{a_s} , absolute wing angle of attack measured from the zero-lift direction of the root section.
 α_{l_0} , angle of zero lift of the root section.
 α_{l_0t} , angle of zero lift of the tip section.

$\alpha_{s(L=0)}$, wing angle of attack for zero lift.

α_i , section induced angle of attack.

c_l , section lift coefficient perpendicular to the distant relative wind.

Subscripts for c_l :

0, refers to section lift coefficient perpendicular to the local relative wind.

b , refers to basic lift ($C_L=0$).

a , refers to additional lift (any C_L).

$a1$, refers to additional lift ($C_L=1$).

c_{d_i} , section induced-drag coefficient.

c_{d_0} , section profile-drag coefficient.

$c_{m_{a.c.}}$, section pitching-moment coefficient about section aerodynamic center.

l , section lift.

m_{l_a} , section pitching moment due to additional lift forces.

M_{l_a} , wing pitching moment due to additional lift forces.

$C_{m_{l_a}}$, wing pitching-moment coefficient due to additional lift forces.

C_{m_b} , wing pitching-moment coefficient due to basic lift forces.

C_{m_s} , wing pitching-moment coefficient due to the pitching moments of the wing sections.

$C_{m_{a.c.}}$, wing pitching-moment coefficient about its aerodynamic center.

C_L , wing lift coefficient.

C_{D_i} , wing induced-drag coefficient.

GENERAL FORMULAS

Formulas in terms of the section characteristics.—

The induced angle of attack at any section is obtained from c_l by

$$\alpha_i = \alpha - \frac{c_l}{m_0}$$

The section induced-drag coefficient is obtained from α_i and c_l from

$$c_{d_i} = \alpha_i c_l$$

and the induced-drag coefficient for the entire wing may be obtained by integration across the semispan from the section values:

$$C_{D_i} = \frac{2}{S} \int_0^{b/2} \alpha_i c_l c dy \quad (1)$$

In order to obtain the aerodynamic center and the pitching moment of the wings, a system of reference axes was used; the origin was at the aerodynamic center of the root section and the axes were as shown in figure 1. The x axis (fig. 1 (a)) is parallel to the root chord, and the y axis (fig. 1 (b)) is perpendicular to the plane of symmetry with positive directions following the vectors. The wing axis is the locus of the aerodynamic centers of the sections and lies in the x - y plane. The lift l and the coefficient c_l of any section along the span are represented in figure 1.

A typical section with the aerodynamic center located at a distance x from the y axis has a moment arm of

$$x \cos \alpha_s$$

and a pitching moment about the lateral axis (fig. 1) due to the additional lift force of

$$m_l = -x \cos \alpha_s l_a$$

but the lift increment of any section is

$$l_a = c_l q c$$

and the pitching moment for the entire wing is obtained from

$$M_l = -2q \cos \alpha_s \int_0^{b/2} c_l c x dy$$

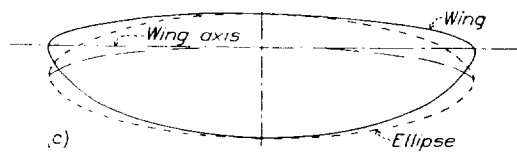
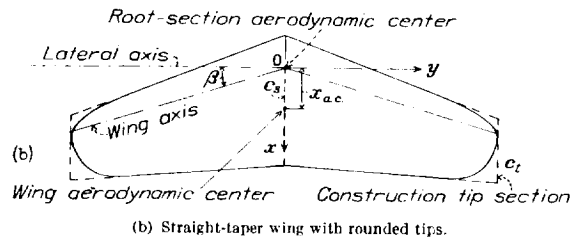
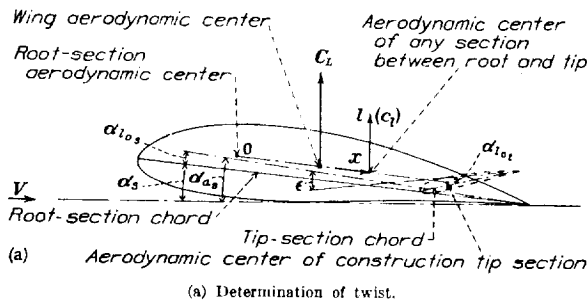


FIGURE 1.—Form of wings.

Pitching-moment coefficients for the entire wing will be based on a chord length of S/b so that

$$C_m = \frac{M}{qS^2}$$

The pitching-moment coefficient due to the additional lift forces then becomes

$$C_{m_l} = -\frac{2b}{S^2} \cos \alpha_s \int_0^{b/2} c_l c x dy$$

The additional lift forces have a centroid through which the lift may be considered to act. This point is the aerodynamic center of the wing and its x coordi-

nate will be designated $x_{a.c.}$ (See fig. 1.) This distance corresponds to d in reference 4. The term C_{m_l} then may also be expressed

$$C_{m_l} = -(x_{a.c.} \cos \alpha_s) \frac{b}{S} C_L$$

If the previous expression for C_{m_l} is used, $x_{a.c.}$ is obtained as a fraction of S/b by

$$\frac{x_{a.c.}}{S/b} = \frac{\frac{2b}{S^2} \int_0^{b/2} c_l c x dy}{C_L} \quad (2)$$

The moment due to the drag forces has been omitted because it is relatively small, except for wings with large amounts of sweepback or dihedral.

The pitching moment of the basic lift forces is a couple and is therefore independent of the axis about which it is determined. The lateral axis was used to facilitate computation but, when the pitching moment is used, it is convenient to consider it constant about an axis through the aerodynamic center. According to the method previously used, the pitching-moment coefficient due to the basic lift forces is

$$C_{m_b} = \pm \frac{2}{S^2} b \int_0^{b/2} c_l c x dy \quad (3)$$

The $\cos \alpha_{s(L=0)}$ (the cosine of the angle of zero lift of the wing measured from the root chord) has been omitted because it is practically equal to unity.

In addition to the basic lift forces, the pitching moment of each section also contributes to the pitching moment of the wing, which is obtained by

$$C_{m_s} = \frac{2b}{S^2} \int_0^{b/2} c_{m.a.c.} c^2 dy \quad (4)$$

The total moment about the aerodynamic center is then the sum of the two foregoing parts

$$C_{m_{a.c.}} = C_{m_b} + C_{m_s}$$

Formulas in terms of the coefficients of the Fourier series.—In order to obtain data from the foregoing formulas, the spanwise distribution of the lift coefficient (following Glauert) was expressed as the Fourier series:

$$c_l = \frac{4b}{c} \sum A_n \sin n\theta$$

where θ is related to the distance along the span (fig. 1) by $y = (-b/2) \cos \theta$ and only odd values of n are used. When c_l is expressed in the foregoing manner, it is possible to obtain the induced angle of attack in the form

$$\alpha_i = \sum n A_n \frac{\sin n\theta}{\sin \theta}$$

Also the coefficients A_n may be expressed in the form

$$A_n = B_n \alpha_a + C_n \epsilon$$

where α_a is the absolute angle of attack of the root section; that is, the angle of attack of the root section, measured from its direction of zero lift, and ϵ is the wing twist measured between the zero-lift directions of the root and tip sections.

When the preceding expressions for c_l and α_i are substituted in the foregoing formulas, the characteristics are obtained in terms of the coefficients B_n and C_n , which in turn are grouped into factors.

From (1) the induced-drag coefficient may be obtained in the form:

$$C_{Di} = \frac{C_L^2}{\pi A u} + C_L \epsilon a_0 v + (\epsilon a_0)^2 w$$

where A is the aspect ratio, and

$$\begin{aligned} \frac{1}{u} &= \frac{1}{B_1^2} \left[\sum_{n=3,5,7}^{\infty} n B_n^2 \right] + 1 \\ v &= \frac{2}{m_0 B_1} \left[\sum_{n=3,5,7}^{\infty} n B_n \left(C_n - \frac{C_1}{B_1} B_n \right) \right] \\ w &= \frac{\pi A}{m_0^2} \left[\sum_{n=3,5,7}^{\infty} n \left(C_n - \frac{C_1}{B_1} B_n \right)^2 \right] \end{aligned}$$

In the determination of the aerodynamic-center position, the wing axis is considered to be a straight line and the angle of sweepback is β (fig. 1), then

$$x = |y| \tan \beta$$

and from (2) the x coordinate of the aerodynamic center is obtained as

$$\frac{x_{a.c.}}{S/b} = H A \tan \beta$$

where

$$\begin{aligned} H &= \frac{2}{\pi B_1} \left(\frac{B_1}{3} + \frac{B_3}{5} - \frac{B_5}{21} + \frac{B_7}{45} + \dots \right) \\ &\quad \frac{B_n}{4} \left\{ \frac{\sin [(n-2)\pi/2]}{(n-2)} - \frac{\sin [(n+2)\pi/2]}{(n+2)} \right\} \end{aligned}$$

From (3) the moment due to the basic lift forces becomes

$$C_{m_{i_b}} = -G \epsilon a_0 A \tan \beta$$

where a_0 is the section lift-curve slope for the wing and

$$G = \frac{2A}{m_0} \left[\left(\frac{C_3}{5} - \frac{C_5}{21} + \frac{C_7}{45} - \dots \right) - \frac{C_1}{B_1} \left(\frac{B_3}{5} - \frac{B_5}{21} + \frac{B_7}{45} - \dots \right) \right]$$

(The term $C_{m_{i_b}}$ is equal to C_{m_T} in reference 4.)

Also from equation (4) the pitching moment of the wing due to the pitching moments of the sections is expressed as

$$C_{m_s} = E c_{m_{a.c.}}$$

where $c_{m_{a.c.}}$ is constant across the span and

$$E = \frac{2b}{S^2} \int_0^{b/2} c^2 dy$$

In addition to the foregoing formulas, the following formulas were obtained in terms of B_n and C_n for other

characteristics. The basic and additional lifts at any point along the span were expressed by the dimensionless quantities

$$L_b = \frac{4A}{m_0} \left[\sum_{n=3,5,7}^{\infty} \left(C_n - \frac{C_1}{B_1} B_n \right) \sin n\theta \right]$$

and

$$L_a = \frac{4}{\pi} \left[\sum_{n=1,3,5,7}^{\infty} \frac{B_n}{B_1} \sin n\theta \right]$$

so that

$$c_{i_b} = \frac{\epsilon a_0 S}{cb} L_b$$

and

$$c_{i_a} = \frac{S}{cb} L_a$$

The lift-curve slope was obtained in the form

$$a = \frac{\pi A B_1}{57.3}$$

By the introduction of the slope for an elliptical wing, a may be expressed

$$a = f \frac{a_0}{1 + \frac{57.3 a_0}{\pi A}}$$

where

$$f = \frac{a}{a_0} \left(1 + \frac{57.3 a_0}{\pi A} \right)$$

The angle of zero lift was obtained in the form

$$\frac{\alpha_{a_s}}{\epsilon} = -\frac{C_1}{B_1} = J$$

The angle of attack of a wing may then be given by

$$\alpha_s = \frac{C_L}{a} + \alpha_{i_0_s} + J \epsilon$$

where α_s is the angle of attack measured from the chord of the root section, and $\alpha_{i_0_s}$ is the angle of zero lift of the root section.

The general formulas and the factors used with them have now been outlined. The manner of obtaining the data will be completed by explaining the method of finding the coefficients B_n and C_n used in computing the factors.

Determination of the coefficients of the Fourier series.—The coefficients B_n and C_n depend on the shape of the wing. The two wing shapes used are shown on figure 1. Wing (b) has a straight taper plan form with rounded tips and (c) an elliptical plan form. The tapered wing is shown with sweepback and the elliptical wing without, but either wing may or may not have sweepback. The rounded tip of the tapered wing is formed within a trapezoidal tip of length c_t , and the taper of the wing is determined by the tip to root chord ratio c_t/c_s . The aerodynamic centers of the airfoil sections lie on a straight line across the semispan and form the wing axis. The elliptical wing is formed by distorting an ellipse until the wing axis becomes straight. In order to determine the wing axis, the

aerodynamic centers of the airfoil sections were taken at the quarter-chord point. The straight wing axis may then be given sweepback with each chord moving parallel to its original position. The same process would be used to change the sweepback of the tapered wing.

For the wings considered, the twist varies linearly from root to tip and the total angle of twist is ϵ . As shown in figure 1, ϵ is the twist measured between the zero-lift directions of the root and tip sections.

Tapered wing.—For the tapered wing the coefficients B_n and C_n were determined from the equation

$$\alpha_a = \Sigma A_n \sin n \theta \left(\frac{4b}{m_0 c} + \frac{n}{\sin \theta} \right) \quad (5)$$

where α_a is the absolute angle of attack at any section; that is, the angle of attack measured from the zero-lift direction for the section. The coefficients B_n and C_n are related to A_n by

$$A_n = B_n \alpha_{a_s} + C_n \epsilon$$

where α_{a_s} is the absolute angle of attack of the root section. The value of m_0 used in the preceding equation was 5.79 per radian, which approximates the lift-curve slope of good airfoil sections. For the linear taper α_a becomes

$$\alpha_a = \alpha_{a_s} + \epsilon \cos \theta$$

For a wing of any particular aspect ratio and taper ratio, equation (5) was satisfied at four points along the semispan by the usual method (except for $c_t/c_s = 0$ for which six points were necessary to obtain sufficient accuracy), and values of B_n and C_n for $n = 1, 3, 5$, and 7 were found.

The elliptical wing.—For the elliptical wing the foregoing fundamental equation may be simplified and a new series of coefficients, independent of aspect ratio, may be obtained. The coefficient A_n for $n = 3, 5, 7 \dots \infty$ may be obtained in the form

$$A_n = \frac{k_n \epsilon}{\pi A + n m_0}$$

where k_n is determined from

$$\cos \theta = k_3 \left(1 + \frac{\sin 3\theta}{\sin \theta} \right) - k_5 \left(1 - \frac{\sin 5\theta}{\sin \theta} \right) + k_7 \left(1 + \frac{\sin 7\theta}{\sin \theta} \right) \dots$$

The factors for the elliptical wing then take the form

$$L_b = 4A \left[\sum_{n=3,5,7,\dots,\infty} \frac{k_n}{\pi A + n m_0} \sin n \theta \right]$$

$$L_a = \frac{4}{\pi} \sqrt{1 - \left(\frac{y}{b/2} \right)^2}$$

$$a = \frac{a_0}{1 + \frac{57.3 a_0}{\pi A}}$$

$$f = 1$$

$$J = -k_3 + k_5 - k_7 \dots$$

$$u = 1$$

$$v = 0$$

$$w = \frac{\pi A}{m_0^2} \left[\sum_{n=3,5,7,\dots,\infty} \frac{n k_n^2}{\left(\frac{\pi A}{m_0} + n \right)^2} \right]$$

$$H = \frac{2}{3\pi}$$

$$G = \frac{2k_3}{5\pi \left(1 + \frac{3m_0}{\pi A} \right)} - \frac{2k_5}{21\pi \left(1 + \frac{5m_0}{\pi A} \right)} + \frac{2k_7}{45\pi \left(1 + \frac{7m_0}{\pi A} \right)} \dots$$

$$E = \frac{32}{3\pi^2} \quad (c_{m_{a.c.}} \text{ constant along the span})$$

The foregoing factors were obtained for the elliptical wing and for a straight-taper wing with trapezoidal tips for a range of aspect ratios from 3 to 20 and of taper ratios from 0 to 1. The factors were also obtained for the tapered wing with rounded tips for a sufficient number of aspect ratios and taper ratios so that the complete range could be covered using the factors for the wing with trapezoidal tips as a guide. Cross plots were then made to obtain figures 2 to 9 and the values for wings with rounded tips presented in tables I and II. Although the factors become less reliable as the aspect ratio is decreased, it was considered desirable to extrapolate the curves to an aspect ratio of 2 as the factors in the low-aspect-ratio range may be of use in the absence of other data. Additional spanwise lift-distribution data computed for the elliptical wing are given in table III.

USE OF TABLES AND CHARTS

In order to find the characteristics of a wing having a straight taper and rounded tips or having an elliptical plan form, the tables and charts may be used directly.

The properties of the wing should first be determined; that is, the taper ratio c_t/c_s , aspect ratio A , span b , the area S , the aerodynamic twist ϵ in degrees, the angle of sweepback β , and the average value of section lift-curve slope, as well as the section lift-curve slope a_0 , the section pitching-moment coefficient $c_{m_{a.c.}}$, and the chord c at convenient stations along the semispan.

The chord and a_0 should be found at the spanwise stations given in tables I and II to facilitate finding the spanwise lift distribution. Then, for the values of c_t/c_s and A , values of L_b and L_a may be found from tables I and II by interpolation if necessary. The section lift coefficients c_{l_b} and $c_{l_{a1}}$ are then found for each station along the semispan from

$$c_{l_b} = \frac{\epsilon a_0 S}{cb} L_b$$

$$c_{l_{a1}} = \frac{S}{cb} L_a$$

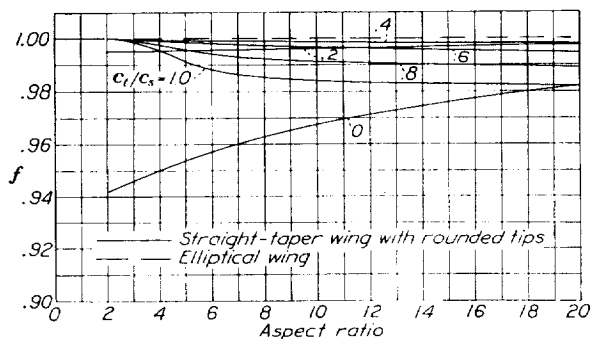
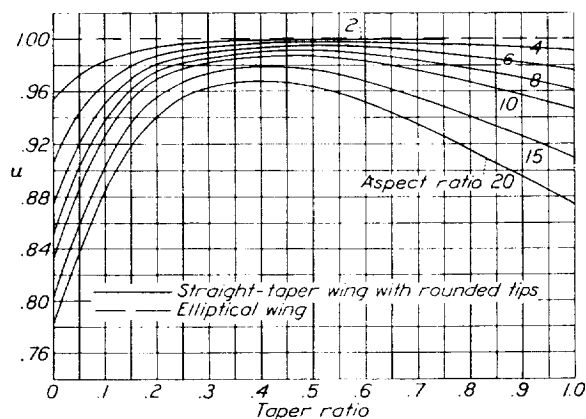


FIGURE 2.—Chart for determining lift-curve slope.

$$a = f \frac{a_0}{1 + \frac{57.3}{\pi A} a_0} \quad m = 57.3a$$

FIGURE 4.—Chart for determining induced-drag factor u .

$$C_{Di} = \frac{C_L^2}{\pi A u} + C_{L^2} e a_0^2 + (e a_0)^2 u$$

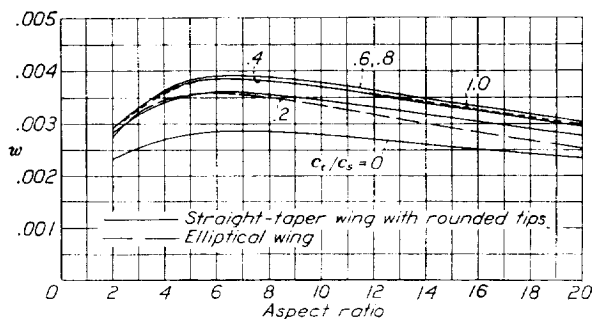
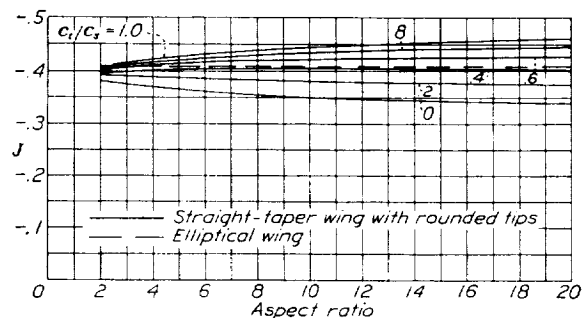
FIGURE 6.—Chart for determining induced-drag factor w .

FIGURE 3.—Chart for determining angle of attack.

$$\alpha_s = \frac{C_L}{a} + \alpha_{ts} + J\epsilon \quad \alpha_{s(L=0)} = \alpha_{ts} + J\epsilon$$

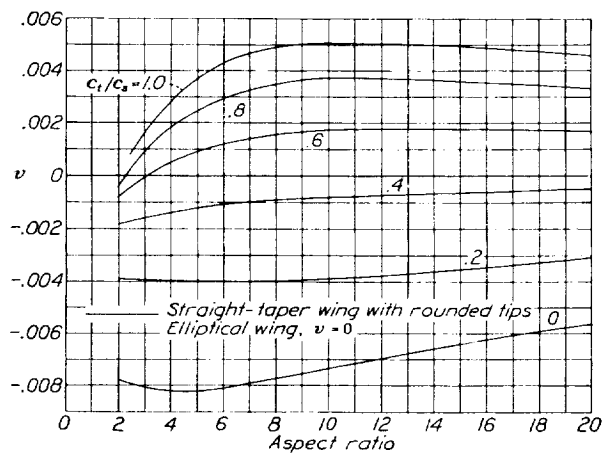
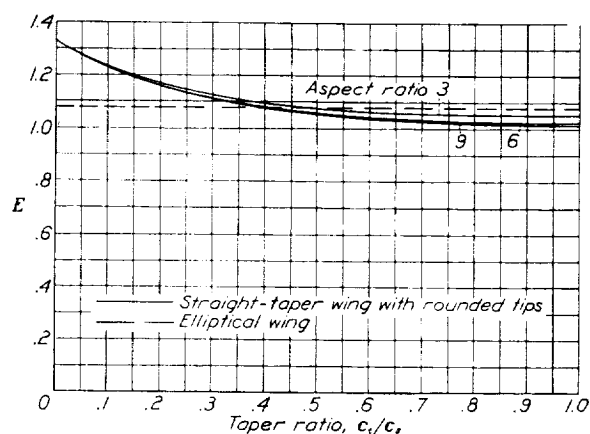
FIGURE 5.—Chart for determining induced-drag factor v .

FIGURE 7.—Chart for determining pitching moment due to section moment.

$$C_m = E c_{m_{a,s}}$$

For $c_{m_{a,s}}$, constant across the span.

and c_i for any value of C_L for the wing is obtained from

$$c_i = c_{i_b} + C_L c_{i_{a1}}$$

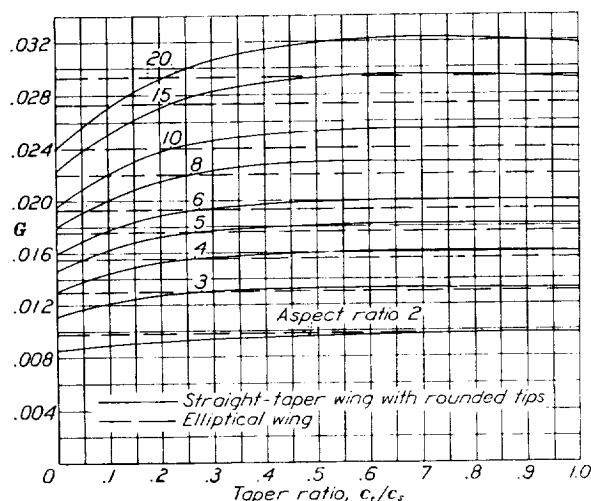


FIGURE 8.—Chart for determining pitching moment due to basic lift forces.
 $C_{m_{i_b}} = -G\epsilon a_0 A \tan \beta$

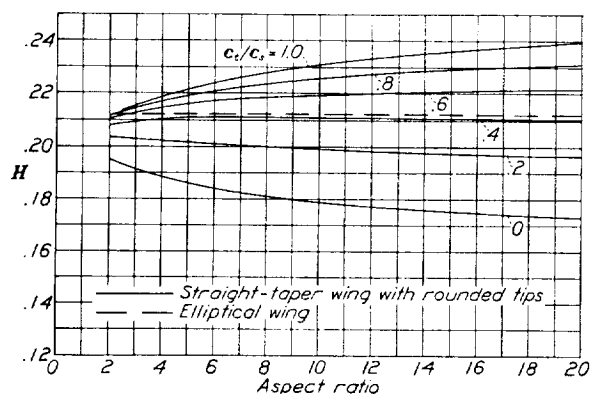


FIGURE 9.—Chart for determining aerodynamic-center position.

$$\frac{x_{a.c.}}{S/b} = HA \tan \beta$$

The actual basic, additional, and total lifts for any section of the wing may then be obtained from

$$\begin{aligned} l_b &= c_{i_b} q c \\ l_a &= C_L c_{i_{a1}} q c \\ l &= c_i q c \end{aligned}$$

Values of l may be computed for the various spanwise stations and the curve of the span lift-distribution may be plotted. Typical semispan lift-distribution curves are shown in figure 10.

The semispan induced angle-of-attack distribution may be obtained from

$$\alpha_{i_a} = \alpha_i - \frac{c_i}{a_0}$$

where

$$\alpha_a = \alpha_{a_s} + \frac{\eta}{b/2} \epsilon$$

$$\alpha_{a_s} = \frac{C_L}{a} + J\epsilon$$

The remaining characteristics are obtained simply by finding the required factor for the desired values of c_i/c_s and A from the charts and by computing the characteristics from the formulas previously given, using the average value of a_0 where a_0 is required. The formulas are summarized here for convenience.

Lift-curve slope:

$$a = f \frac{a_0}{1 + \frac{57.3 a_0}{\pi A}}$$

Angle of attack corresponding to any C_L :

$$\alpha_s = \frac{C_L}{a} + \alpha_{i_{0_s}} + J\epsilon$$

Angle of zero lift:

$$\alpha_{s(l=0)} = \alpha_{i_{0_s}} + J\epsilon$$

Induced-drag coefficient:

$$C_{D_i} = \frac{C_L^2}{\pi A u} + C_L \epsilon a_0 v + (\epsilon a_0)^2 w$$

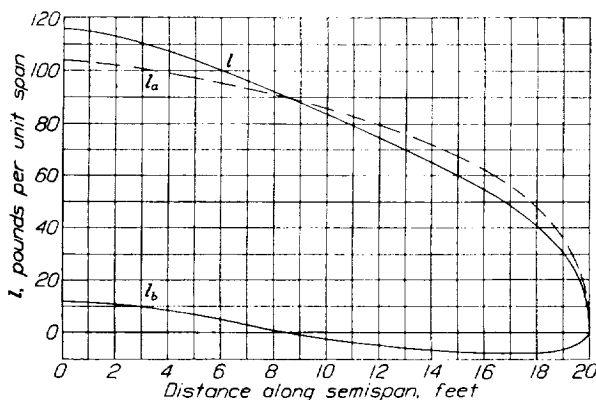


FIGURE 10.—Typical semispan lift distribution. $C_L = 1.2$.

Pitching-moment coefficient about an axis through the aerodynamic center:

$$\begin{aligned} C_{m_{a.c.}} &= C_{m_s} + C_{m_{i_b}} \\ C_{m_s} &= EC_{m_{a.c.}} \\ C_{m_{i_b}} &= -G\epsilon a_0 A \tan \beta \end{aligned}$$

Aerodynamic-center position (x coordinate):

$$\frac{x_{a.c.}}{S/b} = HA \tan \beta$$

Although C_{m_s} may usually be determined from the foregoing formula, equation (4) should be used if $C_{m_{a.c.}}$ varies considerably across the span.

Illustrative example.—In order to illustrate the method of using the charts, an example will be worked

out for a wing with straight taper and rounded tips having the following characteristics:

$$\begin{aligned} A &= 6 \\ c_t/c_s &= 0.5 \\ b &= 40 \text{ feet} \\ S &= 266.7 \text{ sq. ft.} \\ \beta &= 10^\circ \\ C_L &= 1.2 \\ q &= 10 \text{ lb./sq. ft.} \end{aligned}$$

Root section: Construction tip section:

N. A. C. A. 4415	N. A. C. A. 2409
$a_{0s} = 0.097$	$a_{0t} = 0.099$
$\alpha_{t0s} = -3.8^\circ$	$\alpha_{t0t} = -1.7^\circ$
$c_{ma,c_s} = -0.083$	$c_{ma,c_t} = -0.044$

The angle of twist measured between the chords of the root and construction tip sections is -5° (washout). Then, by the use of the angles of zero lift of the root and tip sections and by reference to figure 1, the angle of aerodynamic twist is determined to be -7.1° .

The chord at several stations along the semispan and the calculation of the lift distribution are given in table IV. In the table, a_0 and $c_{ma,c}$ are assumed to have a linear variation along the semispan. Values of L_b and L_a were obtained from tables I and II for an aspect ratio of 6 and a taper ratio of 0.5 and the basic, additional, and total lift distributions were computed and plotted in figure 10. The pitching-moment coefficient $c_{ma,c}$ varies so much along the semispan that C_{m_s} cannot be found by use of the factor E but must be found from (4). Accordingly, $c_{ma,c}c^2$ is plotted against y in figure 11 and C_{m_s} is found from the area under the curve to be -0.072 .

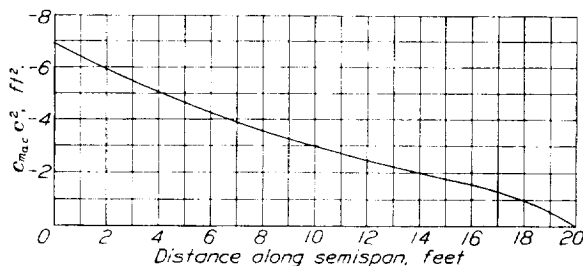


FIGURE 11.—Graphical determination of section pitching moment.

$$C_{m_s} = \frac{2b}{S} \int_0^{b/2} c_{ma,c} c^2 dy = -0.072$$

From figures 2 to 9 and the equations on page 7 the remaining factors and characteristics are determined to be

$f = 0.998$	$a = 0.0755$
$J = -0.408$	$\alpha_s = 15.0$
$u = 0.995$	$\alpha_{s(L=0)} = -0.9$
$v = 0.0001$	$C'_{Di} = 0.0786$
$w = 0.0039$	
$G = 0.0199$	$C_{m_{t0}} = 0.015$
$H = 0.214$	$x_{a,c} = 1.51 \text{ ft.}$
$C_{ma,c} = -0.072 + 0.015 = -0.057$	

Method for wing of special form.—If it is desired to find the characteristics of a wing having a chord distribution that lies between the chord distributions of the tapered and elliptical wings, such as a wing with a constant-chord center section, an interpolation may be made between the values for the tapered and elliptical wings to find most of the characteristics.

The lift distribution for such wings may be found by an approximate method that has been tried for a few wings having parallel center sections and has given satisfactory results. The method has been taken from reference 5 with the symbols converted to the notation of this report. Approximate values of L_a , which will be designated L_a' , may be calculated from

$$L_a' = \frac{\sqrt{1 - \left(\frac{y}{b/2}\right)^2}}{\sqrt{1 - \left(\frac{y}{b/2}\right)^2} + \frac{3}{8} \frac{m_0 c}{b/2}} \left(\frac{A}{2} \alpha_a + \frac{1}{\pi} \right)$$

where

$$\alpha_a = \frac{8}{\pi A} \left[\left(\frac{\sqrt{1 - \left(\frac{y}{b/2}\right)^2}}{\frac{m_0 c}{b/2}} \right)_{\text{mean}} + \frac{1}{8} \right]$$

The procedure is to choose a number of points at convenient intervals along the semispan (12 points should be sufficient for the usual plan forms); then from the

values of c at those points the mean value of $\frac{\sqrt{1 - \left(\frac{y}{b/2}\right)^2}}{\frac{m_0 c}{b/2}}$

is calculated. The value of α_a may then be found and from the values of y and c , L_a' at each point along the semispan may be computed. The values of L_a' should correspond to a C_L approximately equal to 1. The actual C_L may be found from

$$C_L = \int_0^1 L_a' d\left(\frac{y}{b/2}\right)$$

and C_L may be conveniently found from the area under a curve of L_a' plotted against $\frac{y}{b/2}$. Finally, L_a may be

found from $L_a = L_a' / C_L$. Values of c_{t0} may then be calculated by the previously indicated method and, if desired, C_{Di} and $\frac{x_{a,c}}{S/b}$ may be found from equations (1) and (2).

If a wing has considerable dihedral or a curved wing axis, an integration may be made directly from the section characteristics. For this purpose, the best procedure would be to resolve the section values c_{t0} and c_{d0} into components along and parallel to the x and z axes, where the z axis is perpendicular to the x axis and lies in the plane of symmetry. Owing to dihedral, there will be a vertical coordinate of the aero-

dynamic center and a pitching moment about the aerodynamic center of the force components in the x direction. The coordinates of the aerodynamic center and of the pitching moment about it may be found from integrations like (2) and (3) by substituting the appropriate values of the x and z force components. For example, $x_{a.c.}$ would be found from

$$x_{a.c.} = \frac{\frac{2}{S} \int_0^{b/2} c_{z_a} c x dy}{C_{z_a}}$$

where

$$C_{z_a} = \frac{2}{S} \int_0^{b/2} c_{z_a} c dy$$

The values of $x_{a.c.}$ and C_{z_a} may be found by plotting

to the desired angle of twist and the sections between the root and tip were then formed by using straight lines between corresponding stations of the root and tip sections. Formation of the wings in this manner results in a nonlinear distribution of twist along the semispan. In plan view the quarter-chord points of the sections lie on a straight line across the semispan; the sweepback was measured between this line and the lateral axis.

Three different amounts of sweepback, 0° , 15° , and 30° , and three types of airfoil sections, symmetrical, cambered, and reflexed, were used.

As the wings differ primarily in airfoil section, sweepback, and twist, a convenient designating number

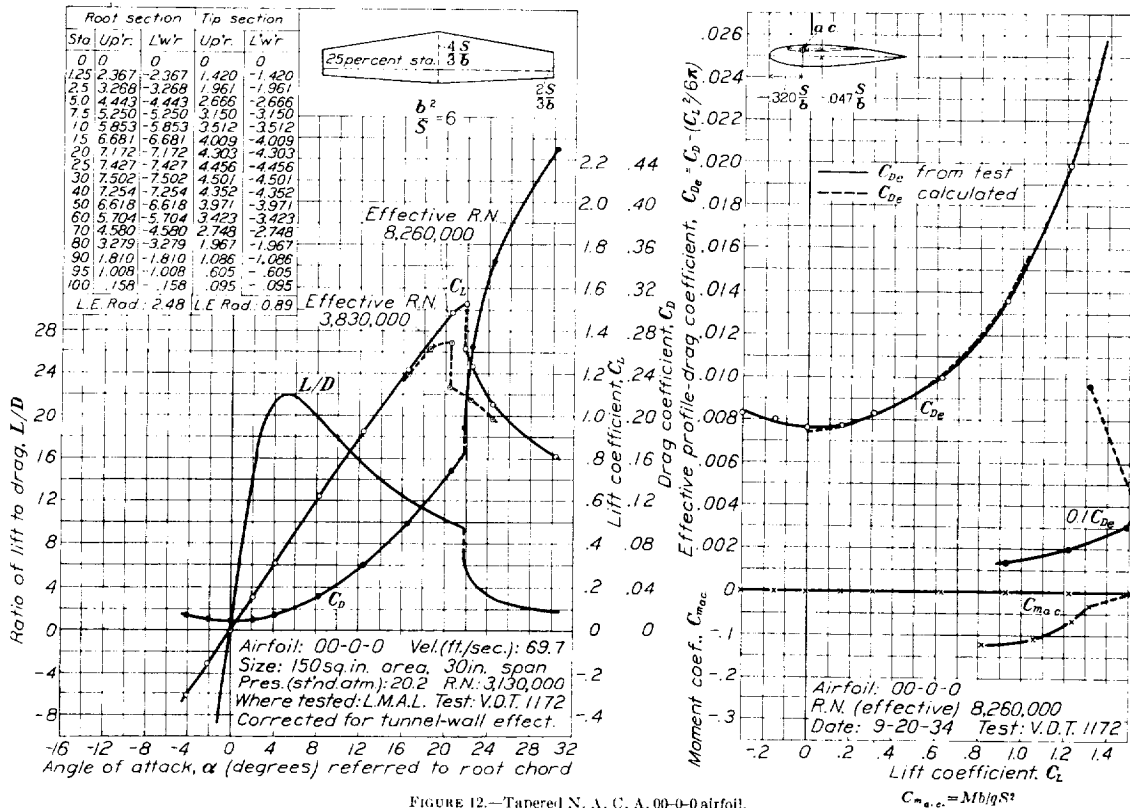


FIGURE 12.—Tapered N. A. C. A. 00-0-0 airfoil.

$c_{z_a} c x$ and $c_{z_a} c$ against the distance along the semispan and finding the area under the curves.

TESTS OF TAPERED WINGS

In order to provide test data on tapered wings, including wings with sweepback and twist, and to provide a check on the previously outlined method of computing characteristics, nine tapered wings were tested. The plan forms and sections of the wings are shown in figures 12 to 20. The aspect ratio of all the wings was 6; the taper ratio of eight of the wings was 0.5 and of one wing was 0.25. For all the wings the thickness ratio of the root section was 15 percent and of the tip sections 9 percent. The tip section was set

was used to distinguish the wings, such as 24-30-8.50. In this number 24 designates the N. A. C. A. airfoil mean line, i. e., 2 means 0.2 chord maximum camber and 4 that the maximum camber is at 0.4 chord; 30 gives the sweepback in degrees; and 8.50 gives the washout in degrees.

The wings are listed in table V. The first two wings have no sweepback and no twist and differ only in airfoil section. The next two have increased sweepback. The five remaining wings are examples of various methods of combining wings sweepback, twist, and airfoil section to obtain wings having a small positive pitching moment; such wings would be suitable for tailless airplanes. The amounts of twist and of

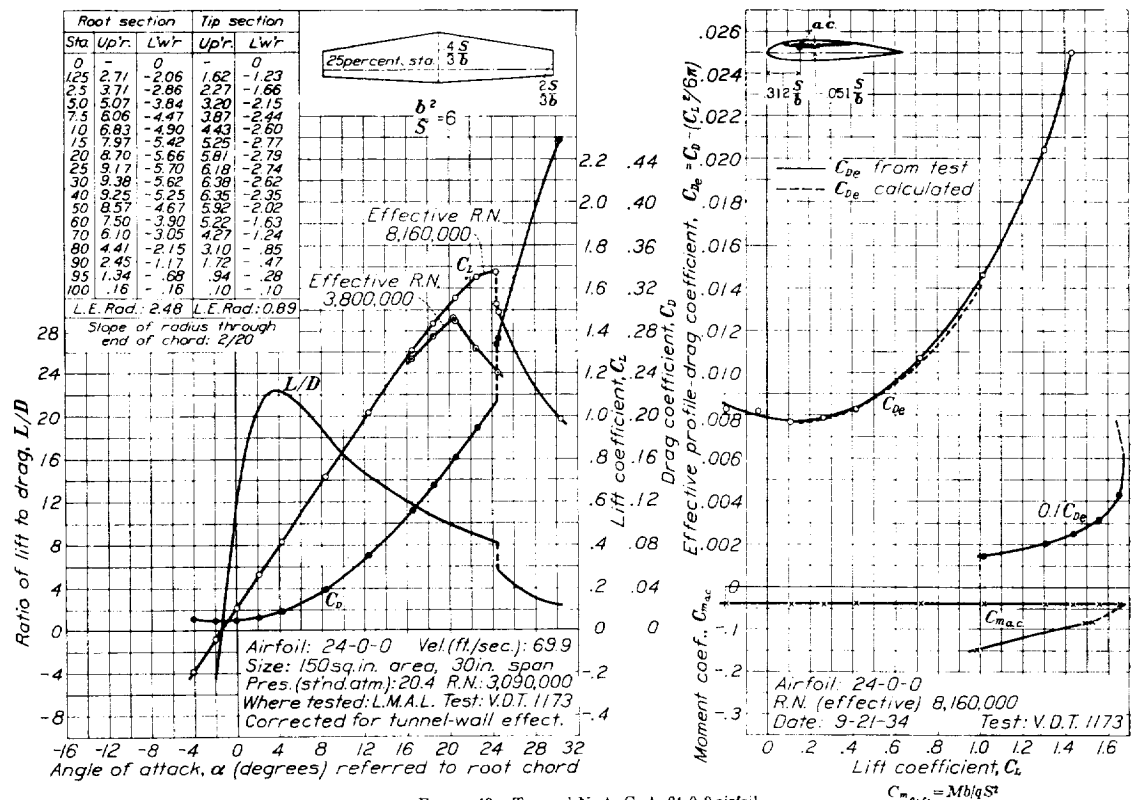


FIGURE 13.—Tapered N. A. C. A. 24-0-0 airfoil.

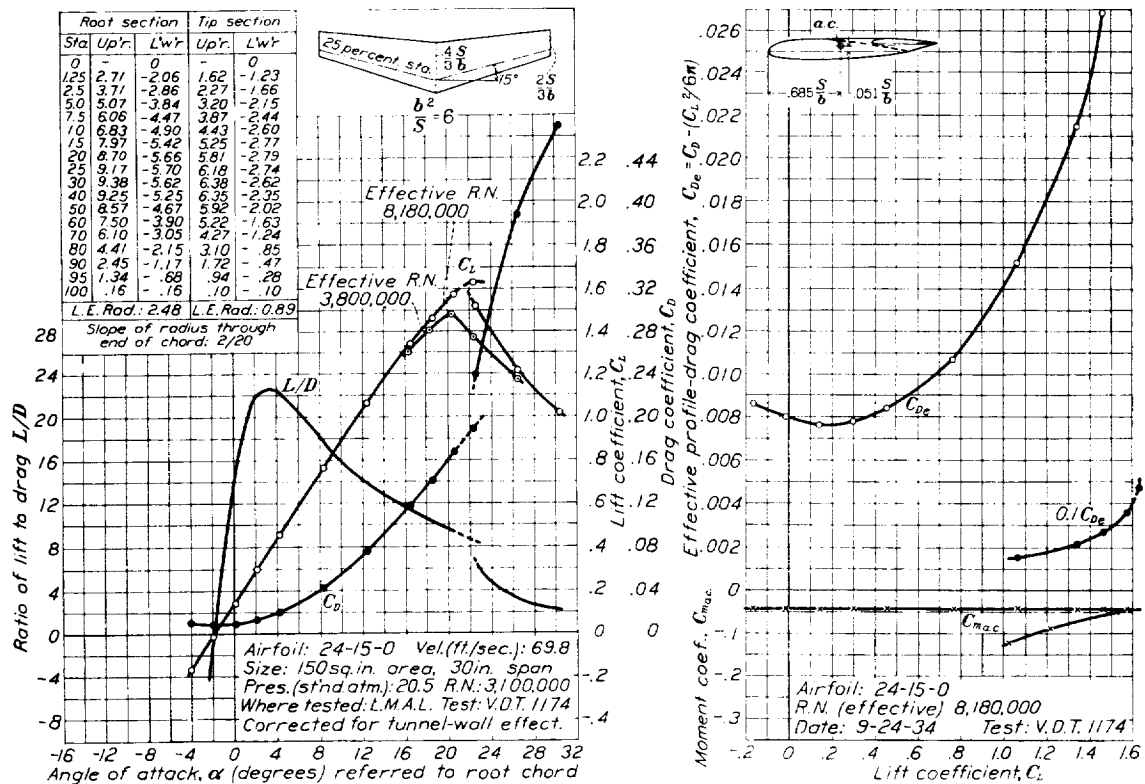


FIGURE 14.—Tapered N. A. C. A. 24-15-0 airfoil.

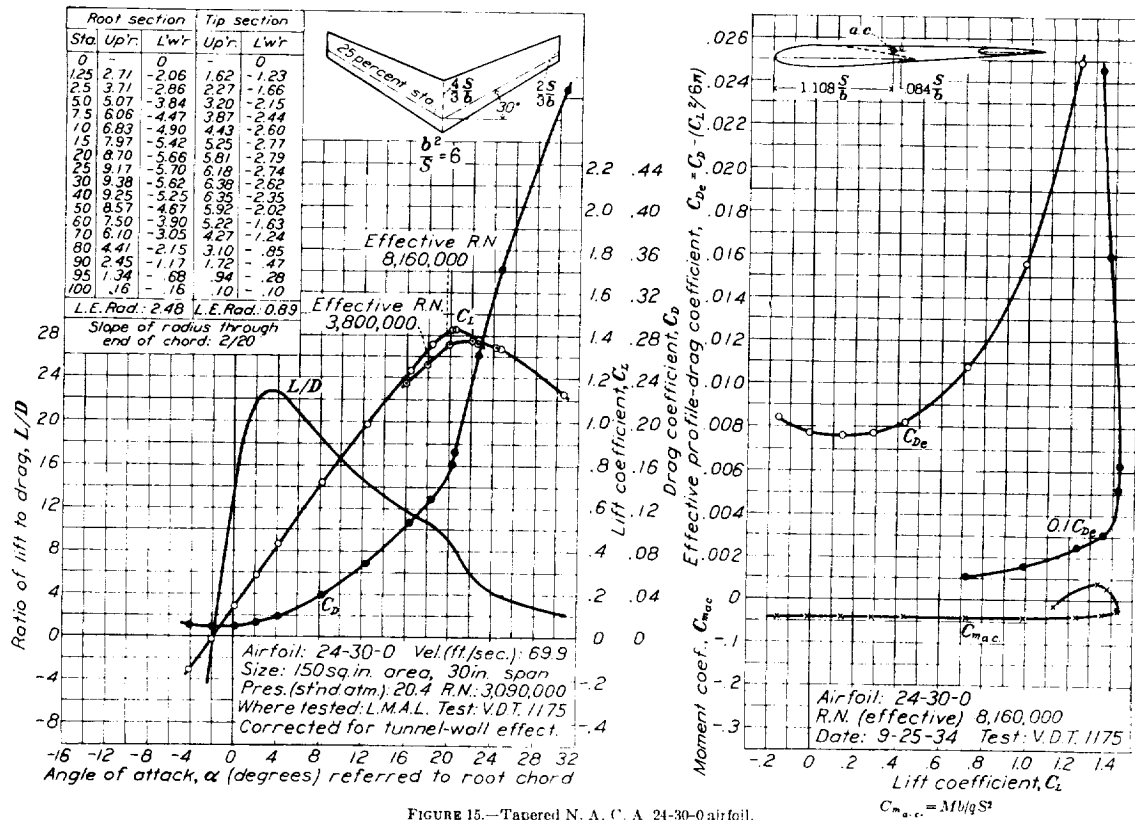


FIGURE 15.—Tapered N. A. C. A. 24-30-0 airfoil.

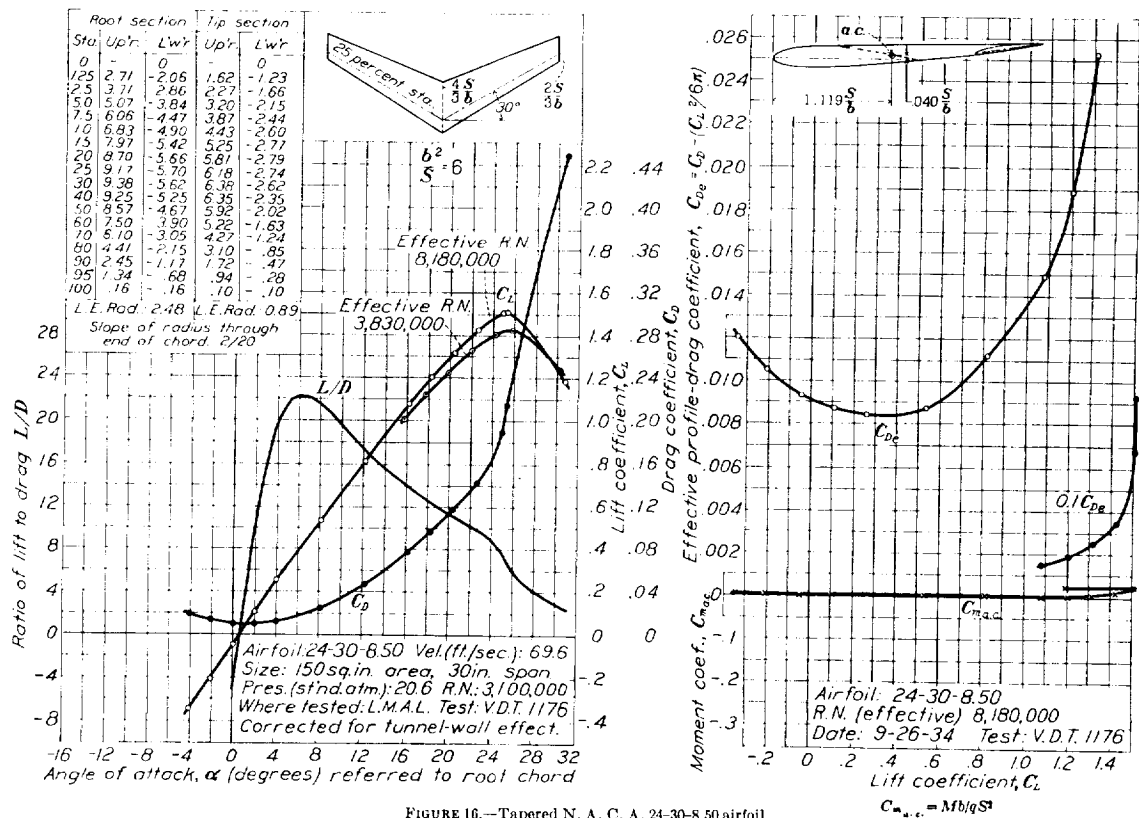
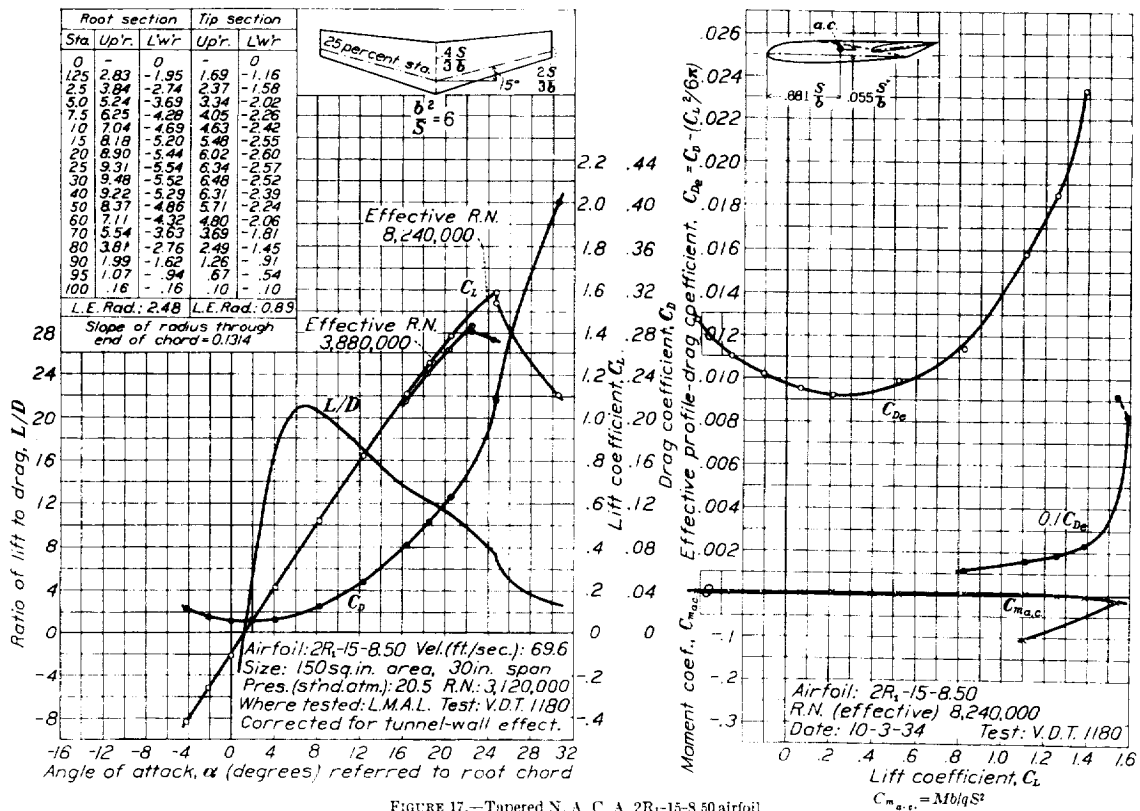
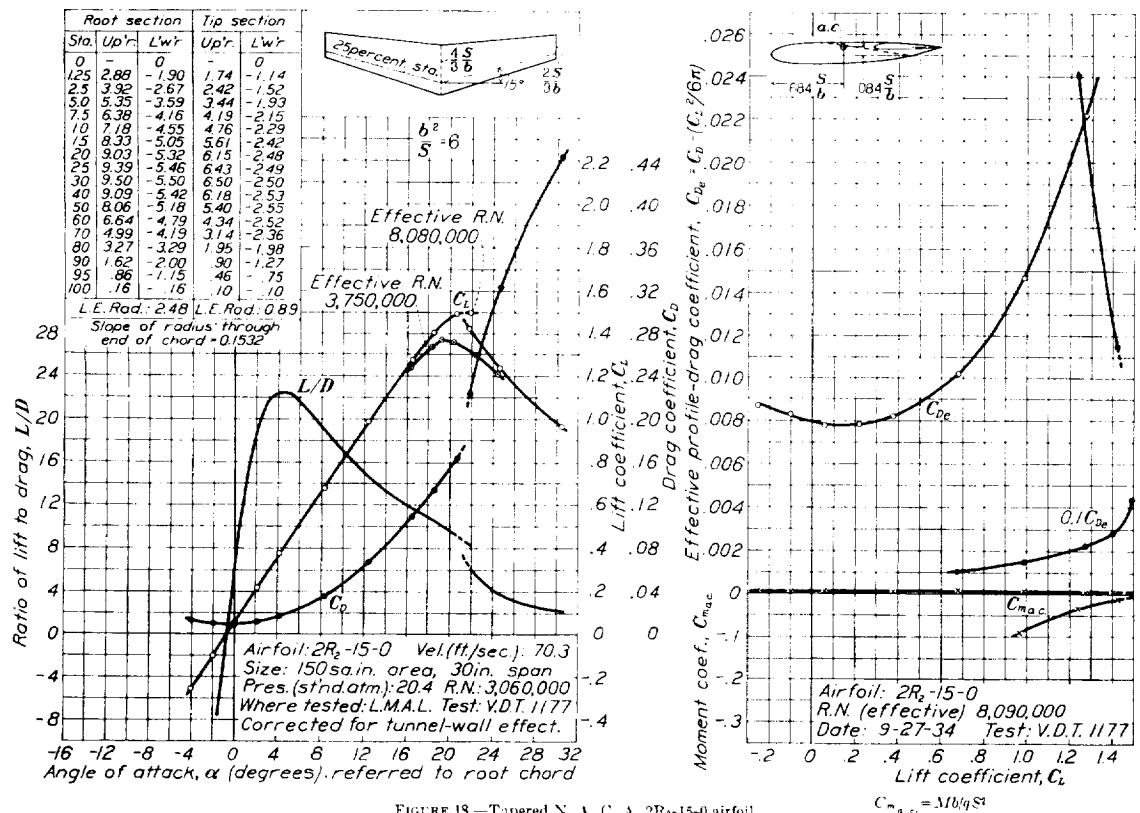


FIGURE 16.—Tapered N. A. C. A. 24-30-8.50 airfoil.

FIGURE 17.—Tapered N. A. C. A. 2R₁-15-8.50 airfoil.FIGURE 18.—Tapered N. A. C. A. 2R₂-15-0 airfoil.

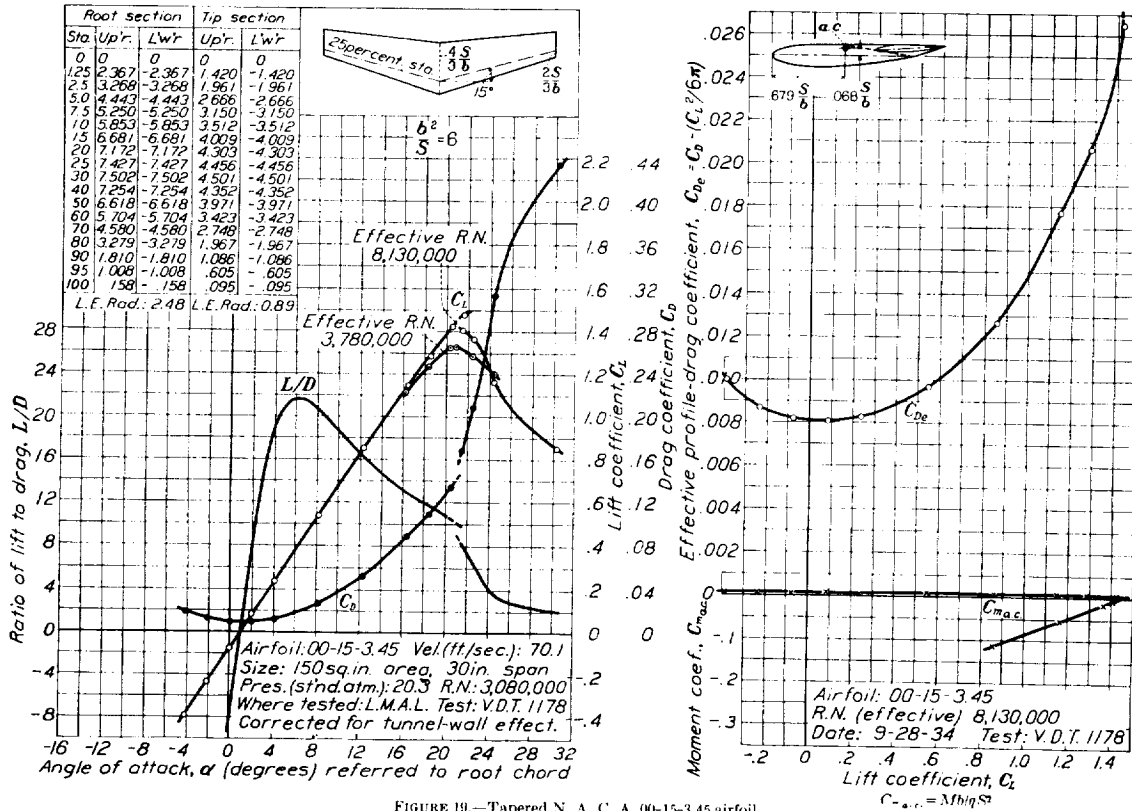


FIGURE 19.—Tapered N. A. C. A. 00-15-3.45 airfoil.

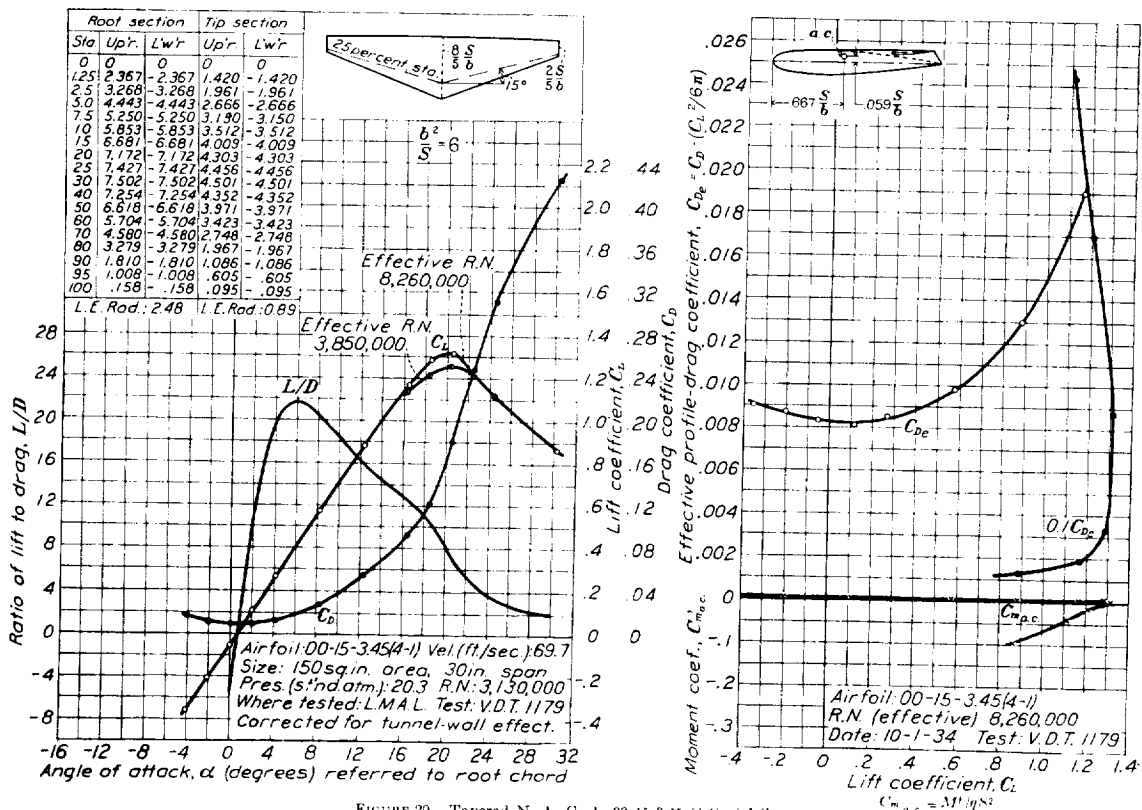


FIGURE 20.—Tapered N. A. C. A. 00-15-3.45 (4-1) airfoil.

sweepback necessary to obtain the desired pitching moment were determined by the method previously given for computing pitching moments, except that data for wings with trapezoidal tips were used. The 24-30-8.50 wing has sufficient twist to obtain the desired pitching moment using a cambered section and 30° sweepback. The 2R₁-15-8.50 wing has the same twist but half the sweepback and a reflexed airfoil section to obtain a positive pitching moment. The 2R₂-15-0 airfoil has no twist and increased reflex. A symmetrical section together with twist is used for the 00-15-3.45 wing, while the last wing has the same twist and sweepback as the previous wing but a taper ratio of 0.25.

The variable-density wind tunnel in which the tests were made is described in reference 6 together with the method of making tests. The lift, drag, and pitching moment of the wings were measured at a tank pressure of 20 atmospheres.

The results of the tests, corrected for tunnel-wall effect, are given in the form of dimensionless coefficients and are plotted in figures 12 to 20. The lift-curve peak is given for two values of effective Reynolds Number to indicate the scale effect. The effective Reynolds Number, at which the maximum lift coefficients apply in flight, is the test Reynolds Number multiplied by a turbulence factor, 2.64.

In order to make possible a more accurate reading of drag coefficients than can be made from the plots against angle of attack, a drag coefficient has been plotted against lift coefficient with the induced drag for elliptical span loading deducted; that is

$$C_{D_e} = C_D - \frac{C_L^2}{\pi A}$$

The coefficient C_{D_e} is called the "effective profile-drag coefficient" and is useful for comparing the drag of tapered wings, as it includes with the true profile drag any additional induced drag caused by a departure from the ideal elliptical lift distribution. Notice should be taken that C_{D_e} cannot be used like a profile-drag coefficient to compute the effect of change of aspect ratio but applies only to the particular wings tested. The values of C_{D_e} have been corrected to the effective Reynolds Number (references 7 and 8) by allowing for the reduction in skin-friction drag due to the change from the test to the effective Reynolds Number. The reduction amounted to $C_D = 0.0011$.

The pitching-moment coefficients plotted against the lift coefficient are given about an axis through the aerodynamic center of the wings in order to obtain a practically constant value of pitching-moment coefficient. The aerodynamic center was determined from the slope of the test pitching-moment curve. The location of the aerodynamic center is given on the plots by its distance from the leading edge and above the chord of the root section. These distances are given as fractions of the ratio of area to span, S/b .

The shapes of the lift and pitching-moment curves near maximum lift provide information on the nature of the stalling of the wings. The 24-0-0 wing has a sharp drop in lift after the maximum, indicating that stalling occurs almost simultaneously over a considerable portion of the wing. Also the $C_{m_{a.c.}}$ after the stall is like that of normal wings. In contrast to this wing, the 24-30-0 wing, which has the same airfoil sections but 30° sweepback, has a rounded lift-curve peak, indicating that stalling occurs progressively along the span. The pitching-moment coefficient is positive after the stall, which shows that stalling begins at sections behind the aerodynamic center. Washout, as in the case of the 24-30-8.50 wing, reduces the tendency to stall of sections behind the aerodynamic center, which may be verified by reference to the $C_{m_{a.c.}}$ curve. Stalling, however, still begins behind the aerodynamic center, as the $C_{m_{a.c.}}$ is positive after the stall. All the wings, except the 24-30-0 and 24-30-8.50, are stable after the stall.

The important test results for all the wings are summarized in table V. The coordinates of the aerodynamic center are expressed as fractions of S/b . The 24-0-0, 24-15-0, and 24-30-0 wings show a decrease of $C_{L_{max}}$ as the sweepback is increased. For the 24-30-8.50 wing, the effect of sweepback is partly compensated by twist, which reduces the tendency to stall of the low Reynolds Number sections near the tips and therefore increases $C_{L_{max}}$. The drag, however, is also increased. Of the wings designed to have a small positive C_{m_0} , the 2R₂-15-0 wing has the highest ratio of $C_{L_{max}}/C_{D_{min}}$.

COMPARISON OF TEST AND CALCULATED RESULTS

Pitching-moment characteristics, lift-curve slope, and drag.—The lift distribution and other theoretical data used to determine the desired pitching-moment coefficient of the wings are now used to predict other characteristics. In addition to C_{m_0} , the aerodynamic-center position, the angle of zero lift, and the lift-curve slope have been calculated. The values of a were calculated from the formula in figure 2. In this formula a value of a_0 corresponding to the a_0 for the N. A. C. A. 0012 and 2412 sections at a Reynolds Number of 3,000,000 was used, inasmuch as the effect of variations of a_0 with section and Reynolds Number is small. As the value of a_0 used in the formula was derived from tests of rectangular wings, a correction for square tips has been applied in order to obtain a better value of the section lift-curve slope. The correction, derived from tests of wings with rounded tips, is given in reference 9.

The calculated values of the pitching-moment coefficient at zero lift, the aerodynamic-center position, the angle of zero lift, and the lift-curve slope are generally in good agreement with the test values (table VI). The agreement of the pitching-moment coefficient at zero lift and the aerodynamic-center position, which are

calculated from the basic and additional lift distributions, respectively, indicate that the theoretical lift distributions must also agree reasonably well with the actual distributions.

In addition to the foregoing characteristics, the drag has been calculated for the 00-0-0 and 24-0-0 airfoils. The comparison between calculation and experiment is based on values of the effective profile-drag coefficient. The calculated values were obtained from

$$C_{De} = \frac{2}{S} \int_0^{b/2} c_{d0} c dy + C_{Di} - \frac{C_L^2}{\pi A}$$

In order to find the value of the integral, values of c_{d0} were determined as follows at several points along the semispan for convenient values of total wing C_L . For each value of C_L the distribution across the semispan of c_l , Reynolds Number, and thickness ratio were calculated. Then, for each point on the semispan, c_{d0} was found for the appropriate c_l , Reynolds Number,

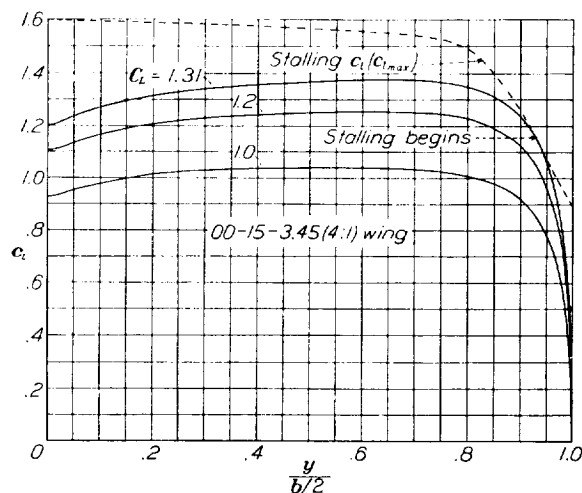


FIGURE 21.—Determination of the C_L at which a tapered wing begins to stall.

and thickness ratio, using data that are expected to be published soon in a report concerning scale effect on airfoils. From the values of c_{d0} , a curve of $c_{d0}c$ was plotted against y and the value of the integral was determined from the area under the curve. The value of C_{Di} was obtained for the formula previously given. The calculated and test values of C_{De} are compared in figures 12 and 13. The agreement is considered good.

Estimation of maximum lift coefficient.—A final characteristic to be estimated is the maximum lift coefficient, which should be nearly equal to the C_L at which stalling begins. The method of determining the C_L at which stalling begins is demonstrated for the 00-15-3.45 (4:1 taper) wing in figure 21. The lift coefficient at which each section along the semispan stalls (shown by the dashed curve) was obtained by

using the maximum lift coefficients of the symmetrical sections given in reference 10 but with the values of C_{Lmax} increased 3 percent. This correction was made for the same reason that a_0 was corrected; that is, to allow for the effect of square tips and thereby to obtain a closer approach to true section characteristics. Better section characteristics will be obtained as a result of an investigation in progress but the correction used is sufficiently accurate for the present purpose. As the values of C_{Lmax} given in reference 10 were for a Reynolds Number of 3,000,000, correction increments were applied to correct the values of C_{Lmax} to the actual Reynolds Number of each section along the span. Correction increments applying to various airfoil sections are expected to be published in the previously mentioned report concerning scale effect on airfoils.

The curves of c_l distribution for several values of wing C_L given in figure 21 were determined by the method previously given for finding c_l distribution. As soon as the c_l curve becomes tangent to the stalling c_{lmax} curve, the section at that point reaches its maximum lift coefficient and stalling should soon spread over a considerable part of the wing. Thus, for the 00-15-3.45 (4:1 taper) wing, stalling is indicated as beginning near the tips, at a C_L of 1.31. Stalling, however, is so close to the tip that it may be modified by the tip vortex. The measured C_{Lmax} is 1.32, but this value is probably low owing to the sweepback of the wing. This method, when applied to several other tapered wings without sweepback but having various taper ratios and aspect ratios, gave a stalling C_L that was within a few percent of the measured C_{Lmax} for all the wings; therefore, the method should prove useful for estimating the C_{Lmax} of tapered wings.

The 00-15-3.45 (4:1 taper) wing is an example of the harmful effect of excessive taper on C_{Lmax} . Large taper not only tends to cause a low C_{Lmax} but also tends to cause stalling near the tips, which results in poor lateral control at low speeds. Improvement could be obtained by using less taper and thicker sections near the tips.

Although all of the characteristics of tapered wings have not yet been satisfactorily calculated, it may be concluded that the following important aerodynamic characteristics—angle of zero lift, the lift-curve slope, the pitching-moment coefficient, the aerodynamic-center position, and the span lift distribution—can be calculated with sufficient accuracy for engineering purposes.

LANGLEY MEMORIAL AERONAUTICAL LABORATORY,
NATIONAL ADVISORY COMMITTEE FOR AERONAUTICS,
LANGLEY FIELD, VA., May 1, 1936.

REFERENCES

1. Glauert, H.: The Elements of Aerofoil and Airscrew Theory. Cambridge University Press, 1926.
2. Glauert, H., and Gates, S. B.: The Characteristics of a Tapered and Twisted Wing with Sweep-Back. R. & M. No. 1226, British A. R. C., 1929.
3. Hueber, J.: Die aerodynamischen Eigenschaften von doppeltrapezförmigen Tragflügeln. Z. F. M., 13. Mai 1933, S. 249-251; 29. Mai 1933, S. 269-272.
4. Anderson, Raymond F.: Charts for Determining the Pitching Moment of Tapered Wings with Sweepback and Twist. T. N. No. 483, N. A. C. A., 1933.
5. Lippisch, A.: Method for the Determination of the Spanwise Lift Distribution, T. M. No. 778, N. A. C. A., 1935.
6. Jacobs, Eastman N., and Abbott, Ira H.: The N. A. C. A. Variable-Density Wind Tunnel. T. R. No. 416, N. A. C. A., 1932.
7. Jacobs, Eastman N., and Clay, William C.: Characteristics of the N. A. C. A. 23012 Airfoil from Tests in the Full-Scale and Variable-Density Tunnels. T. R. No. 530, N. A. C. A., 1935.
8. Platt, Robert C.: Turbulence Factors of N. A. C. A. Wind Tunnels as Determined by Sphere Tests. T. R. No. 558, N. A. C. A., 1936.
9. Jacobs, Eastman N., and Pinkerton, Robert M.: Tests of N. A. C. A. Airfoils in the Variable-Density Wind Tunnel. Series 230. T. N. No. 567, N. A. C. A., 1936.
10. Jacobs, Eastman N., Ward, Kenneth E., and Pinkerton, Robert M.: The Characteristics of 78 Related Airfoil Sections from Tests in the Variable-Density Wind Tunnel. T. R. No. 460, N. A. C. A., 1933.

TABLE I.—BASIC SPAN LIFT-DISTRIBUTION DATA
VALUES OF L_b FOR TAPERED WINGS WITH ROUNDED TIPS $c_{l_b} = \frac{ea_0 S}{cb} L_b$

$A \backslash c_t/c_s$	0	0.1	0.2	0.3	0.4	0.5	0.6	0.7	0.8	0.9	1.0
SPANWISE STATION $\frac{y}{b/2} = 0$											
2.....	-0.118	-0.121	-0.122	-0.122	-0.122	-0.121	-0.121	-0.121	-0.120	-0.120	-0.120
3.....	-0.153	-0.160	-0.162	-0.163	-0.165	-0.164	-0.164	-0.163	-0.162	-0.161	-0.160
4.....	-0.183	-0.192	-0.197	-0.199	-0.199	-0.199	-0.198	-0.197	-0.196	-0.194	-0.192
5.....	-0.211	-0.221	-0.224	-0.226	-0.225	-0.225	-0.224	-0.224	-0.221	-0.219	-0.218
6.....	-0.235	-0.248	-0.253	-0.253	-0.252	-0.252	-0.250	-0.247	-0.244	-0.243	-0.242
7.....	-0.256	-0.269	-0.275	-0.276	-0.274	-0.272	-0.270	-0.268	-0.264	-0.261	-0.258
8.....	-0.274	-0.288	-0.293	-0.293	-0.291	-0.290	-0.288	-0.285	-0.282	-0.279	-0.276
10.....	-0.304	-0.318	-0.322	-0.323	-0.321	-0.320	-0.318	-0.315	-0.311	-0.305	-0.299
12.....	-0.329	-0.342	-0.350	-0.349	-0.348	-0.345	-0.341	-0.337	-0.331	-0.323	-0.317
14.....	-0.350	-0.364	-0.370	-0.370	-0.368	-0.365	-0.360	-0.355	-0.350	-0.342	-0.334
16.....	-0.367	-0.380	-0.386	-0.385	-0.382	-0.379	-0.375	-0.370	-0.362	-0.358	-0.348
18.....	-0.384	-0.399	-0.405	-0.403	-0.400	-0.393	-0.387	-0.380	-0.376	-0.368	-0.360
20.....	-0.398	-0.411	-0.417	-0.415	-0.410	-0.404	-0.399	-0.392	-0.386	-0.378	-0.369
SPANWISE STATION $\frac{y}{b/2} = 0.2$											
2.....	-0.076	-0.080	-0.082	-0.085	-0.086	-0.086	-0.086	-0.085	-0.085	-0.084	-0.083
3.....	-0.098	-0.108	-0.111	-0.112	-0.113	-0.113	-0.113	-0.112	-0.112	-0.110	-0.108
4.....	-0.117	-0.130	-0.135	-0.138	-0.137	-0.137	-0.137	-0.137	-0.137	-0.135	-0.132
5.....	-0.131	-0.148	-0.156	-0.159	-0.159	-0.158	-0.158	-0.158	-0.157	-0.156	-0.152
6.....	-0.145	-0.162	-0.173	-0.176	-0.176	-0.176	-0.176	-0.176	-0.175	-0.172	-0.170
7.....	-0.156	-0.178	-0.189	-0.192	-0.192	-0.192	-0.191	-0.191	-0.190	-0.190	-0.189
8.....	-0.168	-0.189	-0.200	-0.204	-0.204	-0.205	-0.205	-0.206	-0.205	-0.204	-0.204
10.....	-0.182	-0.207	-0.220	-0.224	-0.225	-0.225	-0.226	-0.226	-0.225	-0.225	-0.225
12.....	-0.197	-0.226	-0.239	-0.240	-0.239	-0.238	-0.238	-0.238	-0.237	-0.237	-0.237
14.....	-0.206	-0.234	-0.248	-0.249	-0.248	-0.248	-0.248	-0.248	-0.248	-0.248	-0.248
16.....	-0.212	-0.242	-0.256	-0.258	-0.257	-0.256	-0.256	-0.256	-0.256	-0.256	-0.255
18.....	-0.219	-0.247	-0.260	-0.264	-0.265	-0.265	-0.265	-0.265	-0.265	-0.264	-0.262
20.....	-0.222	-0.255	-0.269	-0.271	-0.271	-0.271	-0.272	-0.272	-0.272	-0.272	-0.270
SPANWISE STATION $\frac{y}{b/2} = 0.4$											
2.....	-0.006	-0.011	-0.013	-0.015	-0.016	-0.016	-0.016	-0.016	-0.016	-0.016	-0.015
3.....	-0.002	-0.010	-0.012	-0.015	-0.016	-0.016	-0.016	-0.016	-0.017	-0.018	-0.018
4.....	0	-0.006	-0.011	-0.012	-0.016	-0.016	-0.018	-0.019	-0.020	-0.020	-0.021
5.....	0.004	-0.004	-0.010	-0.012	-0.016	-0.018	-0.020	-0.021	-0.021	-0.022	-0.023
6.....	0.009	-0.002	-0.008	-0.012	-0.016	-0.018	-0.020	-0.021	-0.022	-0.024	-0.026
7.....	0.012	-0.001	-0.010	-0.013	-0.017	-0.018	-0.020	-0.022	-0.025	-0.027	-0.029
8.....	0.014	0	-0.008	-0.012	-0.017	-0.019	-0.021	-0.025	-0.029	-0.030	-0.030
10.....	0.021	0.007	-0.002	-0.010	-0.017	-0.020	-0.022	-0.027	-0.030	-0.032	-0.032
12.....	0.028	0.009	-0.001	-0.010	-0.017	-0.021	-0.025	-0.029	-0.032	-0.036	-0.038
14.....	0.036	0.013	0	-0.010	-0.017	-0.021	-0.028	-0.031	-0.035	-0.040	-0.042
16.....	0.043	0.019	0.002	-0.008	-0.016	-0.022	-0.029	-0.034	-0.038	-0.041	-0.045
18.....	0.049	0.022	0.004	-0.008	-0.015	-0.022	-0.031	-0.038	-0.041	-0.043	-0.046
20.....	0.050	0.023	0.006	-0.006	-0.014	-0.022	-0.031	-0.039	-0.041	-0.046	-0.049

TABLE I.—BASIC SPAN LIFT-DISTRIBUTION DATA—Continued
 VALUES OF L_b FOR TAPERED WINGS WITH ROUNDED TIPS $c_{lb} = \frac{\epsilon a_0 S}{cb} L_b$

c_l/c_s	0	0.1	0.2	0.3	0.4	0.5	0.6	0.7	0.8	0.9	1.0
A	SPANWISE STATION $\frac{y}{b/2} = 0.6$										
2	0.052	0.052	0.051	0.050	0.050	0.050	0.050	0.050	0.049	0.049	0.048
3	.070	.069	.068	.068	.068	.068	.068	.068	.068	.068	.068
4	.085	.082	.081	.080	.080	.080	.080	.080	.080	.080	.080
5	.099	.095	.092	.091	.091	.091	.091	.091	.090	.090	.090
6	.109	.107	.104	.102	.101	.101	.100	.100	.100	.100	.100
7	.119	.117	.114	.112	.111	.110	.110	.110	.110	.109	.108
8	.128	.122	.121	.120	.120	.119	.119	.118	.118	.117	.116
10	.139	.138	.135	.132	.131	.130	.130	.129	.128	.126	.124
12	.148	.145	.141	.140	.140	.139	.137	.135	.134	.132	.130
14	.155	.152	.150	.148	.145	.142	.141	.140	.139	.138	.135
16	.160	.158	.154	.151	.149	.146	.143	.141	.140	.139	.136
18	.165	.162	.160	.158	.152	.148	.145	.142	.140	.139	.138
20	.170	.169	.165	.159	.152	.148	.147	.143	.141	.140	.140
	SPANWISE STATION $\frac{y}{b/2} = 0.8$										
2	0.072	0.079	0.080	0.082	0.083	0.085	0.085	0.086	0.086	0.084	0.081
3	.088	.098	.101	.102	.104	.108	.109	.110	.110	.108	.106
4	.100	.113	.120	.123	.125	.128	.128	.130	.130	.130	.129
5	.109	.125	.135	.138	.140	.143	.147	.148	.148	.148	.149
6	.115	.135	.148	.152	.156	.160	.160	.162	.163	.164	.165
7	.121	.142	.158	.163	.169	.172	.173	.173	.174	.174	.175
8	.126	.149	.164	.174	.180	.182	.182	.183	.183	.184	.184
10	.136	.160	.178	.188	.195	.200	.201	.202	.203	.201	.198
12	.145	.170	.188	.200	.208	.212	.214	.216	.216	.214	.210
14	.152	.182	.200	.210	.216	.221	.223	.227	.228	.225	.220
16	.159	.186	.205	.216	.222	.229	.232	.233	.236	.232	.229
18	.161	.197	.215	.224	.230	.235	.239	.242	.243	.242	.238
20	.166	.201	.220	.232	.237	.241	.245	.248	.248	.248	.247
	SPANWISE STATION $\frac{y}{b/2} = 0.9$										
2	0.059	0.068	0.072	0.073	0.075	0.076	0.075	0.075	0.075	0.075	0.075
3	.068	.083	.092	.098	.099	.100	.100	.100	.100	.100	.100
4	.074	.098	.111	.118	.121	.122	.123	.123	.123	.123	.123
5	.081	.107	.122	.131	.138	.140	.141	.141	.142	.142	.142
6	.087	.117	.136	.148	.154	.159	.160	.160	.160	.160	.160
7	.090	.123	.146	.160	.167	.171	.171	.172	.172	.172	.172
8	.092	.131	.153	.170	.179	.182	.183	.184	.185	.186	.187
10	.098	.139	.166	.184	.197	.201	.203	.205	.207	.209	.210
12	.100	.147	.178	.198	.210	.218	.221	.225	.228	.229	.230
14	.102	.156	.188	.208	.220	.231	.238	.241	.243	.245	.246
16	.103	.161	.197	.219	.231	.241	.249	.253	.258	.259	.260
18	.105	.166	.202	.228	.243	.252	.260	.263	.269	.271	.275
20	.107	.172	.211	.233	.248	.260	.268	.273	.279	.282	.285
	SPANWISE STATION $\frac{y}{b/2} = 0.95$										
2	0.038	0.051	0.058	0.059	0.060	0.060	0.060	0.060	0.059	0.059	0.058
3	.044	.063	.073	.078	.079	.080	.080	.080	.080	.079	.078
4	.050	.072	.076	.092	.095	.097	.099	.100	.100	.100	.099
5	.052	.083	.100	.107	.110	.112	.113	.114	.116	.117	.116
6	.054	.088	.109	.119	.122	.125	.130	.132	.132	.131	.130
7	.056	.093	.116	.130	.135	.140	.144	.148	.150	.149	.145
8	.057	.100	.125	.140	.146	.152	.158	.160	.161	.160	.159
10	.058	.107	.138	.152	.162	.171	.178	.182	.186	.187	.183
12	.059	.112	.143	.165	.179	.189	.198	.200	.202	.205	.204
14	.060	.116	.151	.174	.190	.202	.211	.215	.218	.221	.222
16	.061	.121	.159	.184	.203	.218	.222	.229	.233	.236	.238
18	.061	.126	.166	.194	.213	.229	.236	.241	.248	.251	.255
20	.061	.128	.173	.203	.225	.239	.245	.251	.259	.265	.271
	SPANWISE STATION $\frac{y}{b/2} = 0.975$										
2	0.019	0.030	0.035	0.037	0.037	0.037	0.037	0.036	0.036	0.035	0.034
3	.022	.039	.045	.049	.050	.051	.052	.054	.053	.052	.051
4	.026	.043	.054	.060	.062	.064	.068	.069	.069	.068	.067
5	.029	.051	.065	.070	.071	.075	.078	.081	.082	.083	.083
6	.030	.055	.071	.079	.082	.088	.091	.094	.097	.097	.097
7	.030	.060	.078	.087	.091	.098	.101	.107	.110	.110	.110
8	.030	.062	.081	.091	.100	.107	.112	.120	.121	.121	.121
10	.031	.067	.090	.105	.115	.124	.132	.138	.141	.142	.143
12	.031	.069	.095	.115	.131	.141	.149	.153	.160	.161	.162
14	.031	.071	.102	.122	.143	.155	.163	.171	.175	.177	.178
16	.031	.077	.111	.138	.156	.169	.178	.182	.188	.190	.191
18	.032	.083	.121	.150	.169	.182	.191	.197	.200	.201	.202
20	.032	.086	.128	.158	.178	.193	.202	.208	.210	.212	.213

TABLE II.—ADDITIONAL SPAN LIFT-DISTRIBUTION DATA
VALUES OF L_a FOR TAPERED WINGS WITH ROUNDED TIPS, $c_{l_{at}} = \frac{S}{cb} L_a$

c_l/c_a A	0	0.1	0.2	0.3	0.4	0.5	0.6	0.7	0.8	0.9	1.0
SPANWISE STATION $\frac{y}{b/2} = 0$											
2	1.439	1.400	1.367	1.339	1.316	1.301	1.298	1.292	1.290	1.287	1.282
3	1.489	1.430	1.385	1.350	1.322	1.302	1.288	1.275	1.263	1.253	1.246
4	1.527	1.452	1.400	1.360	1.329	1.302	1.279	1.260	1.242	1.226	1.211
5	1.559	1.473	1.414	1.369	1.333	1.301	1.272	1.248	1.225	1.204	1.186
6	1.585	1.492	1.428	1.378	1.338	1.300	1.267	1.237	1.211	1.187	1.163
7	1.609	1.510	1.440	1.386	1.340	1.300	1.264	1.232	1.203	1.176	1.149
8	1.629	1.534	1.456	1.392	1.344	1.300	1.264	1.229	1.198	1.165	1.135
10	1.661	1.558	1.473	1.409	1.355	1.306	1.264	1.222	1.187	1.152	1.120
12	1.686	1.578	1.490	1.420	1.361	1.308	1.261	1.219	1.180	1.143	1.109
14	1.708	1.592	1.502	1.429	1.366	1.309	1.260	1.214	1.172	1.135	1.100
16	1.726	1.610	1.513	1.433	1.368	1.309	1.255	1.208	1.165	1.127	1.090
18	1.741	1.623	1.525	1.441	1.370	1.308	1.252	1.203	1.160	1.118	1.080
20	1.755	1.632	1.531	1.446	1.372	1.307	1.250	1.199	1.152	1.109	1.070
SPANWISE STATION $\frac{y}{b/2} = 0.2$											
2	1.369	1.329	1.300	1.279	1.267	1.260	1.258	1.253	1.253	1.250	1.248
3	1.405	1.346	1.308	1.279	1.260	1.248	1.241	1.234	1.228	1.221	1.214
4	1.434	1.363	1.318	1.284	1.260	1.243	1.232	1.220	1.209	1.198	1.186
5	1.459	1.377	1.324	1.288	1.260	1.240	1.223	1.208	1.194	1.181	1.168
6	1.477	1.388	1.329	1.290	1.259	1.236	1.218	1.200	1.184	1.169	1.151
7	1.491	1.393	1.332	1.291	1.259	1.236	1.211	1.193	1.174	1.157	1.138
8	1.502	1.401	1.338	1.294	1.261	1.236	1.212	1.189	1.168	1.148	1.129
10	1.513	1.411	1.347	1.299	1.265	1.236	1.209	1.182	1.158	1.137	1.114
12	1.520	1.417	1.349	1.302	1.265	1.233	1.202	1.172	1.148	1.126	1.102
14	1.527	1.423	1.354	1.307	1.268	1.232	1.201	1.170	1.144	1.119	1.094
16	1.532	1.428	1.358	1.308	1.269	1.232	1.199	1.164	1.135	1.110	1.087
18	1.539	1.429	1.359	1.309	1.270	1.231	1.195	1.160	1.130	1.103	1.078
20	1.547	1.431	1.360	1.311	1.271	1.230	1.190	1.155	1.123	1.098	1.069
SPANWISE STATION $\frac{y}{b/2} = 0.4$											
2	1.217	1.190	1.178	1.172	1.172	1.171	1.170	1.169	1.169	1.168	1.168
3	1.220	1.191	1.176	1.166	1.161	1.160	1.159	1.158	1.157	1.156	1.155
4	1.223	1.192	1.173	1.162	1.156	1.151	1.149	1.148	1.147	1.146	1.145
5	1.226	1.193	1.172	1.159	1.149	1.142	1.140	1.138	1.136	1.134	1.133
6	1.229	1.193	1.171	1.155	1.145	1.138	1.132	1.128	1.127	1.126	1.125
7	1.229	1.193	1.170	1.152	1.140	1.131	1.124	1.121	1.120	1.119	1.118
8	1.229	1.192	1.168	1.150	1.138	1.128	1.120	1.116	1.113	1.111	1.110
10	1.228	1.192	1.167	1.148	1.132	1.121	1.113	1.108	1.104	1.102	1.100
12	1.228	1.192	1.166	1.145	1.125	1.111	1.107	1.102	1.099	1.094	1.090
14	1.228	1.191	1.161	1.136	1.116	1.104	1.100	1.096	1.090	1.087	1.082
16	1.228	1.189	1.158	1.131	1.112	1.101	1.097	1.091	1.086	1.081	1.075
18	1.228	1.186	1.152	1.129	1.111	1.100	1.092	1.087	1.080	1.076	1.070
20	1.228	1.182	1.149	1.127	1.110	1.098	1.089	1.083	1.078	1.071	1.065
SPANWISE STATION $\frac{y}{b/2} = 0.6$											
2	0.970	0.976	0.984	0.992	1.003	1.010	1.012	1.014	1.016	1.018	1.019
3	.950	.962	.975	.985	.996	1.004	1.011	1.018	1.023	1.030	1.038
4	.932	.948	.962	.978	.992	1.002	1.008	1.014	1.023	1.035	1.050
5	.920	.938	.953	.971	.988	1.000	1.008	1.015	1.024	1.038	1.053
6	.909	.930	.948	.966	.981	.993	1.002	1.013	1.024	1.039	1.055
7	.900	.920	.940	.959	.975	.989	1.000	1.012	1.024	1.039	1.054
8	.891	.916	.938	.956	.972	.988	.999	1.011	1.024	1.039	1.053
10	.881	.907	.929	.947	.961	.976	.992	1.008	1.023	1.039	1.052
12	.872	.901	.923	.941	.958	.972	.989	1.006	1.022	1.038	1.051
14	.868	.895	.918	.937	.953	.969	.986	1.003	1.019	1.035	1.049
16	.861	.888	.912	.931	.948	.966	.983	1.000	1.017	1.033	1.048
18	.858	.883	.906	.925	.944	.963	.981	.998	1.015	1.032	1.047
20	.851	.876	.898	.920	.940	.959	.978	.995	1.012	1.028	1.046
SPANWISE STATION $\frac{y}{b/2} = 0.8$											
2	0.615	0.678	0.712	0.731	0.740	0.745	0.746	0.746	0.747	0.747	0.748
3	.589	.659	.700	.726	.743	.754	.761	.772	.782	.790	.799
4	.568	.644	.691	.723	.746	.764	.781	.795	.806	.816	.824
5	.548	.632	.685	.720	.748	.769	.790	.808	.822	.834	.845
6	.531	.619	.675	.717	.748	.775	.800	.820	.838	.851	.862
7	.517	.609	.670	.713	.748	.778	.802	.827	.845	.861	.875
8	.504	.600	.663	.710	.748	.779	.808	.834	.854	.872	.886
10	.486	.585	.653	.704	.748	.783	.815	.842	.868	.887	.905
12	.472	.576	.648	.702	.748	.788	.821	.850	.877	.899	.919
14	.462	.569	.641	.699	.748	.789	.825	.858	.887	.911	.933
16	.456	.564	.638	.698	.748	.791	.830	.862	.894	.921	.944
18	.450	.559	.636	.698	.750	.796	.835	.870	.901	.930	.953
20	.444	.545	.629	.698	.753	.801	.842	.878	.909	.937	.962

TABLE II.—ADDITIONAL SPAN LIFT-DISTRIBUTION DATA—Continued
VALUES OF L_a FOR TAPERED WINGS WITH ROUNDED TIPS, $c_{l_{a1}} = \frac{S}{cb} L_a$

c/c_s	0	0.1	0.2	0.3	0.4	0.5	0.6	0.7	0.8	0.9	1.0
A	SPANWISE STATION $\frac{y}{b/2} = 0.9$										
2	0.378	0.405	0.508	0.525	0.531	0.534	0.535	0.536	0.537	0.538	0.539
3	.352	.447	.500	.528	.543	.552	.559	.564	.568	.571	.575
4	.331	.435	.495	.532	.554	.569	.581	.590	.598	.603	.609
5	.314	.424	.490	.531	.560	.583	.600	.613	.622	.630	.636
6	.300	.416	.487	.531	.565	.595	.615	.631	.643	.652	.659
7	.290	.410	.484	.535	.572	.603	.628	.646	.660	.671	.678
8	.282	.403	.481	.536	.579	.612	.638	.658	.673	.686	.696
10	.265	.383	.472	.541	.590	.628	.656	.679	.698	.712	.723
12	.253	.378	.469	.542	.597	.639	.669	.698	.718	.736	.751
14	.245	.370	.468	.545	.602	.648	.684	.715	.739	.759	.776
16	.239	.366	.468	.547	.609	.659	.698	.729	.756	.780	.801
18	.234	.367	.470	.552	.618	.669	.710	.743	.773	.800	.822
20	.231	.368	.473	.560	.625	.679	.722	.759	.791	.819	.846
A	SPANWISE STATION $\frac{y}{b/2} = 0.95$										
2	0.231	0.296	0.334	0.358	0.370	0.379	0.381	0.383	0.386	0.388	0.390
3	.209	.290	.339	.369	.389	.401	.407	.412	.416	.418	.420
4	.191	.286	.342	.378	.402	.420	.428	.434	.440	.444	.446
5	.176	.281	.344	.384	.415	.436	.449	.458	.463	.469	.471
6	.166	.278	.346	.392	.428	.451	.466	.475	.482	.490	.496
7	.155	.272	.346	.398	.438	.464	.481	.494	.502	.510	.515
8	.148	.261	.346	.403	.446	.475	.495	.510	.521	.529	.534
10	.138	.255	.346	.410	.460	.495	.520	.538	.553	.566	.575
12	.132	.254	.348	.419	.473	.511	.542	.566	.583	.598	.608
14	.129	.252	.349	.423	.482	.529	.562	.588	.609	.628	.640
16	.126	.252	.351	.432	.495	.546	.581	.610	.635	.655	.671
18	.122	.254	.357	.439	.503	.558	.598	.629	.658	.682	.702
20	.121	.258	.364	.449	.516	.569	.613	.648	.680	.707	.730
A	SPANWISE STATION $\frac{y}{b/2} = 0.975$										
2	0.132	0.172	0.207	0.239	0.263	0.272	0.274	0.277	0.279	0.281	0.282
3	.119	.166	.210	.250	.278	.289	.291	.294	.298	.300	.301
4	.107	.163	.214	.258	.288	.304	.308	.311	.315	.319	.322
5	.098	.158	.217	.269	.304	.320	.322	.328	.333	.338	.342
6	.089	.158	.219	.272	.314	.332	.340	.344	.350	.357	.361
7	.081	.158	.222	.278	.320	.342	.351	.359	.366	.373	.381
8	.077	.158	.228	.283	.328	.352	.363	.374	.383	.391	.400
10	.069	.158	.233	.295	.343	.373	.390	.403	.415	.428	.438
12	.068	.161	.242	.308	.360	.395	.413	.430	.448	.461	.473
14	.066	.163	.248	.320	.376	.413	.438	.458	.478	.495	.510
16	.064	.166	.255	.331	.394	.435	.463	.488	.510	.529	.546
18	.063	.169	.263	.346	.412	.461	.492	.518	.539	.560	.580
20	.062	.171	.271	.363	.435	.483	.515	.544	.570	.593	.615

TABLE III.—ADDITIONAL SPAN LIFT-DISTRIBUTION
DATA FOR THE ELLIPTICAL WING, $c_{l_{a1}} = \frac{S}{cb} L_a$

$\frac{y}{b/2}$	L_a
0	1.273
.2	1.248
.4	1.167
.6	1.019
.8	.764
.9	.555
.95	.398
.975	.283

TABLE IV.—CALCULATION OF LIFT DISTRIBUTION FOR ILLUSTRATIVE EXAMPLE

$\frac{y}{b/2}$	c	a_0	L_b	L_a	$l_{c_{l_b}}$	$l_{c_{l_{a1}}}$	$C_L \times c_{l_{a1}}$	c_l	l_b	l_a	l	$c_{m_{a.e.}}$	$c_{m_{a.e.}} \times c^2$
0	9.13	0.097	-0.252	1.300	0.127	0.950	1.140	1.267	11.59	104.0	115.6	-0.083	-6.92
.2	8.22	.097	-.176	1.236	.098	1.003	1.205	1.303	8.05	99.0	107.2	-.075	-5.06
.4	7.30	.098	-.018	1.138	.012	1.039	1.248	1.260	.88	91.0	92.0	-.067	-3.57
.6	6.39	.098	.101	.993	-.073	1.036	1.242	1.169	-4.66	79.6	74.7	-.060	-2.45
.8	5.42	.099	.190	.775	-.138	.954	1.145	1.007	-7.48	62.0	54.6	-.052	-1.53
.9	4.49	.099	.159	.595	-.165	.884	1.061	.896	-7.41	47.7	40.3	-.048	-.97
.95	3.43	.099	.128	.451	-.175	.877	1.053	.878	-6.01	36.2	30.1	-.046	-.54
.975	2.47	.099	.088	.332	-.167	.896	1.076	.899	-4.13	26.6	22.4	-.045	-.27
1.0	0	(.099)	0	0	0	0	0	0	0	0	0	(-.044)	0

$$l_{c_{l_b}} = \frac{ea_0 S}{cb} L_b = -47.3 \frac{a_0}{c} L_b$$

$$l_{c_{l_{a1}}} = \frac{S}{cb} L_a = \frac{6.67}{c} L_a$$

TABLE V.—SUMMARY OF TEST RESULTS

[Effective Reynolds number, approximately 8,000,000]

Wing ¹	$C_{L_{max}}$	$C_{D_{min}}$	$C_{L_{max}}/C_{D_{min}}$	$\frac{x_p}{S/b}$	$\frac{x_h}{S/b}$	C_{m_0}
00-0-0.....	1.53	0.0076	201	0.320	0.047	0
24-0-0.....	1.68	.0077	218	.312	.051	-.040
24-15-0.....	1.63	.0076	215	.685	.051	-.043
24-30-0.....	1.43	.0076	188	1.108	.084	-.042
24-30-8.50.....	1.51	.0084	180	1.119	.040	.002
2R ₁ -15-8.50.....	1.59	.0092	173	.681	.055	.003
2R ₂ -15-0.....	1.50	.0078	192	.684	.084	.004
00-15-3.45.....	1.48	.0081	183	.679	.068	.007
00-15-3.45(4-1).....	1.32	.0082	161	.667	.059	.005

¹ The first group of numbers designates the mean line of the airfoil sections; the next group gives the angle of sweepback in degrees; the last group gives the angle of washout in degrees.

² Coordinates of the aerodynamic center: p is the distance from the leading edge of the root chord; and h is the distance above the root chord.

TABLE VI.—COMPARISON OF CALCULATED AND EXPERIMENTAL VALUES

Wing	C_{m_0}		$\frac{x_{ac}}{S/b}$		$\alpha_{\frac{1}{2}(L=0)}$		α	
	Calculated	Experimental	Calculated	Experimental	Calculated	Experimental	Calculated	Experimental
00-00.....	0	0	0	-0.014	0	0	0.074	0.075
24-0-0.....	-.043	-.040	0	-.022	-1.7	-1.7	.074	.074
24-15-0.....	-.043	-.043	.345	.352	-1.7	-1.9	.074	.075
24-30-0.....	-.043	-.042	.744	.775	-1.7	-1.9	.074	.072
24-30-8.50.....	.010	.002	.744	.786	.9	.7	.074	.076
2R ₁ -15-8.50.....	.006	.003	.345	.348	1.1	1.2	.074	.076
2R ₂ -15-0.....	.004	.004	.345	.351	-.6	-.7	.074	.078
00-15-3.45.....	.010	.007	.345	.346	1.1	1.0	.074	.076
00-15-3.45(4-1).....005	.345	.3347	.075	.076

REPORT No. 573

AERODYNAMIC CHARACTERISTICS OF N. A. C. A. 23012 AND 23021 AIRFOILS WITH 20-PERCENT-CHORD EXTERNAL-AIRFOIL FLAPS OF N. A. C. A. 23012 SECTION

By ROBERT C. PLATT and IRA H. ABBOTT

SUMMARY

The results of an investigation of the general aerodynamic characteristics of the N. A. C. A. 23012 and 23021 airfoils, each equipped with a 0.20c external-airfoil flap of N. A. C. A. 23012 section, are presented. The tests were made in the N. A. C. A. 7- by 10-foot and variable-density wind tunnels and covered a range of Reynolds Numbers that included values corresponding to those for landing conditions of a wide range of airplanes. Besides a determination of the variation of lift and drag characteristics with position of the flap relative to the main airfoil, complete aerodynamic characteristics of the airfoil-flap combination with a flap hinge axis selected to give small hinge moments were measured in the two tunnels. Some measurements of air loads on the flap itself in the presence of the wing were made in the 7- by 10-foot wind tunnel.

From the data obtained, the external-airfoil flap in combination with an airfoil appears to be one of the most generally satisfactory high-lift devices investigated to date. The combination tested offers a relatively high value of maximum lift coefficient with low profile drag in the high-lift range. At low lift coefficients it gives very nearly as low values of profile drag as a good plain airfoil of comparable thickness. Structural and stability problems associated with the large negative pitching moments occurring at high lift coefficients may be slightly greater than in the case of ordinary and split flaps.

INTRODUCTION

Consideration of the external-airfoil flap as a high-lift device indicates that it may be generally applied to improve airplane performance. Previous investigations of this device (see reference 1) have shown that it is capable of developing high lift coefficients and that it gives lower drag at these high lift coefficients than ordinary or split flaps. Thus it may be more favorable to such items of performance as take-off and ceiling. In addition, it can be balanced to have very low operating moments throughout its range of deflection and, if large adverse yawing moments are acceptable, it may be used to obtain lateral control while

still extending over the full wing span as a high-lift device.

Good aerodynamic characteristics have been obtained with an external-airfoil flap of Clark Y section (reference 1), especially when used in connection with a main airfoil of N. A. C. A. 23012 section. Consideration of known scale effect and drag characteristics of the Clark Y and N. A. C. A. 23012 airfoils indicated that substituting the N. A. C. A. 23012 section for the Clark Y section of the flap might improve the speed-range index of the combination. In addition, the small

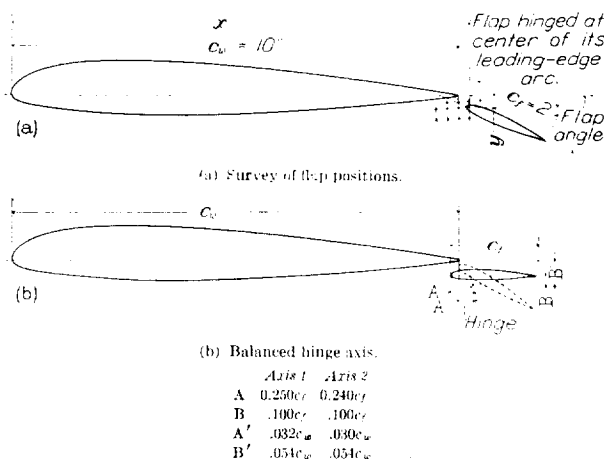


FIGURE 1.—Flap-setting details. The N. A. C. A. 23012 airfoil with 0.20c N. A. C. A. 23012 external-airfoil flap.

center-of-pressure travel of the N. A. C. A. 23012 airfoil indicated the possibility of hinging it as a flap in such a manner that operating moments lower than those of the Clark Y flap might be obtained.

A preliminary investigation of the N. A. C. A. 23012 section used for both the main airfoil and the flap was made in the 7- by 10-foot wind tunnel to determine the variation of lift and drag characteristics with position of the flap relative to the main airfoil. A hinge-axis location intended to give low operating moments and good aerodynamic characteristics was then selected and final force tests were made with the flap hinged at this position and set at various angles.

The tests in the 7- by 10-foot wind tunnel were concluded with a determination of the air loads and the hinge moments on the flap.

A series of tests with the flap set at a few selected angles was made in the variable-density tunnel to determine the full-scale characteristics of the airfoil-flap combination developed in the 7- by 10-foot wind tunnel. Tests were then made of the N. A. C. A. 23021 airfoil with the N. A. C. A. 23012 flap, using the same hinge-axis location as with the N. A. C. A. 23012 airfoil. Although no tests of the combination with the N. A. C. A. 23021 airfoil were made in the 7- by 10-foot tunnel, analysis of the data of reference 1 indicated that the same flap hinge axis was optimum for either airfoil. The variable-density-tunnel tests covered a range of Reynolds Numbers representative of the landing conditions of most modern airplanes.

number of flap angles were investigated to determine the values of $C_{L_{max}}$ and $C_{D_{min}}$ obtainable at each flap position. In these tests the flap was hinged at the center of its leading-edge arc.

On the basis of results obtained from the foregoing tests, a new hinge axis giving reduced flap hinge moments and optimum aerodynamic characteristics at the various flap-angle settings was selected. The model with the flap hinged about this point, designated axis 1 in figure 1 (b), was used in a series of final force tests to determine the lift, drag, and pitching-moment characteristics of the airfoil-flap combination at the various flap-angle settings. The tests were conducted in accordance with standard force-test procedure in the 7- by 10-foot wind tunnel at a dynamic pressure of 16.37 pounds per square foot, corresponding to a speed of 80 miles per hour in standard air. The average

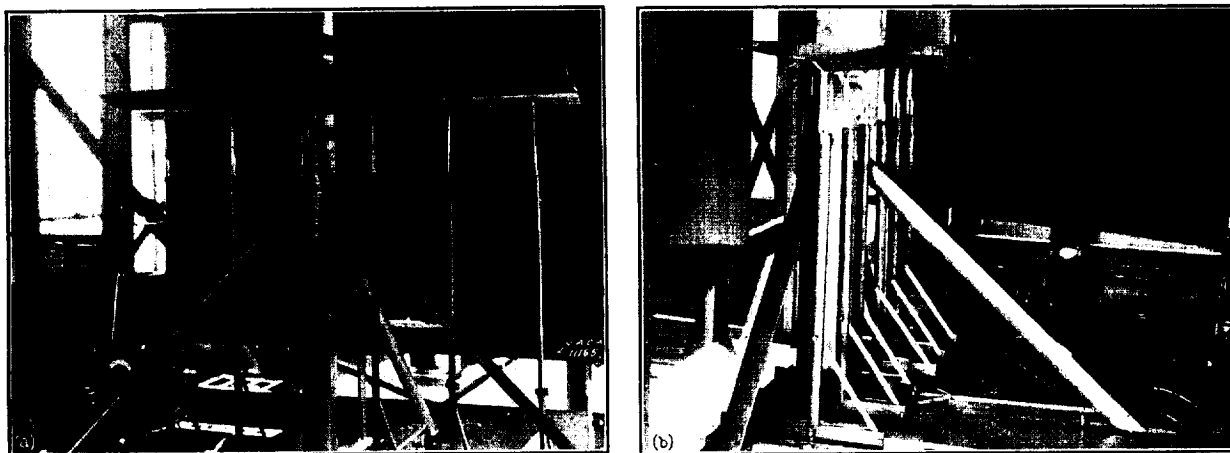


FIGURE 2.—Model arranged for flap-load tests in the 7- by 10-foot wind tunnel. The airfoil mounted on the balance; the flap separately supported.

APPARATUS, MODELS, AND TESTS

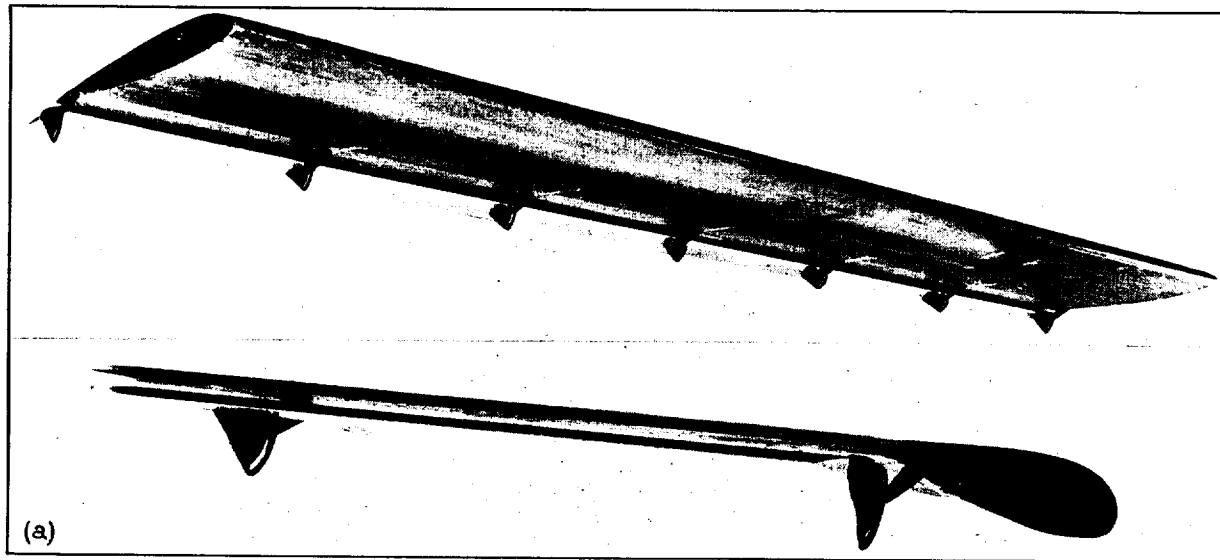
The tests were made during the summer of 1935 in the N. A. C. A. 7- by 10-foot and variable-density wind tunnels. Descriptions of the tunnels and the standard test procedures appear in references 2 and 3.

The model tested in the 7- by 10-foot wind tunnel was a rectangular airfoil of laminated mahogany having a span of 60 inches and a chord of 10 inches. The flap was a duralumin airfoil with a span of 60 inches and a chord of 2 inches. Fittings attached near the trailing edge of the airfoil supported the flap in any desired position relative to the airfoil. The N. A. C. A. 23012 airfoil model was the one used for the tests described in reference 1; likewise, the method of supporting the flaps, the program of testing, and the method of analyzing and presenting results were similar to those of reference 1. Figures 1, 2 and 3 are sketches and photographs of the models.

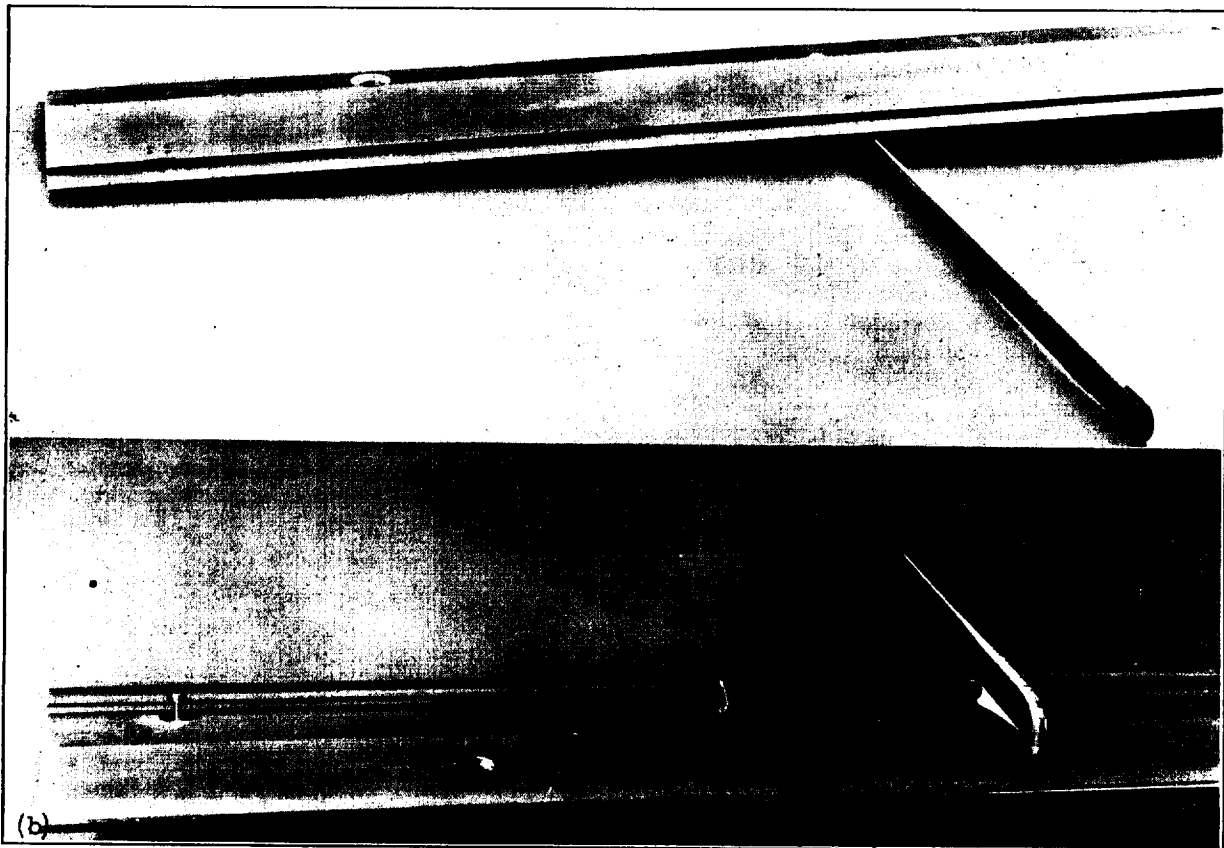
Tests in the 7- by 10-foot wind tunnel were first made to determine the variation of $C_{L_{max}}$ and $C_{D_{min}}$ of the airfoil-flap combination with the flap hinge located at each of the positions shown in figure 1 (a); a sufficient

test Reynolds Number based on the 12-inch chord (wing chord + flap chord) of the model was approximately 730,000.

The variation with flap angle of flap hinge moment about axis 1 at a series of angles of attack was determined by measuring the twist of a calibrated rod attached to one end of the flap, which for this test was hinged freely on its supports. For reasons that will appear later, additional hinge-moment measurements about an axis slightly ahead of axis 1, designated axis 2 in figure 1 (b), were also made. Air loads on the flap itself were determined by supporting the flap separately in the correct position with respect to the main airfoil and measuring forces on the main airfoil alone. The flap loads were then readily computed by deducting the loads measured on the airfoil alone with the flap in the correct position from the forces measured on the combination in the previous force tests. Figure 2 shows the model arranged for flap-load measurements in the 7- by 10-foot wind tunnel. Similar measurements of flap loads and hinge moments on split flaps and Fowler flaps are described in references 4 and 5.



(a) Model used in the 7- by 10-foot wind tunnel.



(b) Model used in the variable-density wind tunnel.

FIGURE 3.—The N. A. C. A. 23012 airfoil with 0.20c_u N. A. C. A. 23012 external-airfoil flap.

The models tested in the variable-density tunnel consisted of two duralumin airfoils of N. A. C. A. 23012 and N. A. C. A. 23021 sections using N. A. C. A. 23012 flaps made of stainless steel. The span of the models was 30 inches and the sum of the wing and flap chords, 5 inches. Small hinge brackets (fig. 3) were used to attach the flap to the main airfoils. Standard force tests were made at a Reynolds Number of about 3,000,000 (effective Reynolds Number about 8,000,000) of the combination using the N. A. C. A. 23012 section for the main airfoil with flap angles of -3° , 20° , 30° , and 40° . Similar tests with flap angles of -3° and 30° were made of the combination using the N. A. C. A. 23021 section for the main airfoil. Both combinations were tested inverted with the flap set at -3° (angle for minimum drag) to extend the characteristics through the negative-lift range. Maximum lift coefficients were also obtained for both combinations at lower values of the Reynolds Number.

PRECISION

The precision of force and load tests in the 7- by 10-foot wind tunnel is completely discussed in references 1, 4, and 5. A discussion of precision of force tests in the variable-density tunnel appears in references 3, 6, and 7. It is believed that the present test results may be considered free from any serious consistent errors and that they may be applied with normal engineering accuracy to free-flight conditions at the stated values of effective Reynolds Number.

RESULTS AND DISCUSSION

Form of presentation of results.—All test results have been reduced to standard nondimensional coefficient form based on total wing areas (sum of areas of airfoil and flap) and on total chord c (sum of chords of airfoil and flap), except the flap-load coefficients, which are based on the dimensions of the flap itself. The special coefficients used are defined as follows:

Subscript w refers to the main airfoil.

Subscript f refers to the flap.

$$C_{H_f} = \frac{\text{flap hinge moment}}{q(S_w + S_f)(c_w + c_f)}$$

$$C_{N_f} = \frac{\text{force on flap normal to flap chord}}{qS_f}$$

$$C_{D_f} = \frac{\text{force on flap parallel to flap chord}}{qS_f}$$

δ_f , angle between wing and flap chord lines, degrees.

$C_{m(a.c.)_0}$, pitching-moment coefficient computed about the aerodynamic center determined for the airfoil-flap combination with the flap set at the minimum-drag angle.

Standard corrections for the effects of jet-boundary and static-pressure gradient in the 7- by 10-foot wind tunnel were applied to the test results. Although the

nominal aspect ratio of the model having a span of 60 inches and a total chord of 12 inches was 5, the results have been corrected and are presented for aspect ratios of 6 and infinity. Infinite aspect ratio data are further corrected to an effective Reynolds Number to allow for the effects of air-stream turbulence, as explained in references 7 and 8.

The data obtained in the variable-density tunnel have been corrected in the usual manner (references 3, 9, and 10). The results are presented for an aspect ratio of 6 and as section data. The section characteristics, which have been corrected to the effective Reynolds Number and for the effect of rectangular tips (references 9 and 10), are distinguished from the wing characteristics by the use of lower-case letters, thus:

$$c_l, c_d, c_m, c.$$

Drag data obtained in both tunnels have been corrected by deducting the drag of the flap supports, estimated from tests with dummy supports. This correction was very small, varying in magnitude from 0 to 0.0005 at small and moderate values of the lift coefficient.

Determination of optimum flap hinge axis.—Results of the first series of tests in the 7- by 10-foot wind tunnel are given in figure 4. Contours showing the variation of $C_{L_{max}}$ with flap position at various flap angles appear in the figure, as well as contours of $C_{D_{min}}$ with the flap angle varying from -2° to -4° .

A balanced hinge axis for the flap was selected by investigating the characteristics of the wing-flap combination with the hinge axis near the $0.25 c_f$ point on the flap, where the flap hinge moments should be reduced to very small values. A profile of the flap drawn on transparent paper was laid on the various contour sheets and rotated about each of a series of hinge axes near the $0.25 c_f$ point on the flap and in various positions relative to the main airfoil; this procedure permitted the approximate determination of the values of $C_{L_{max}}$ and $C_{D_{min}}$ obtainable with the various axis locations. Hinge axis 1 (fig. 1 (b)) was finally selected as giving the best compromise between the requirements of low hinge moment, high $C_{L_{max}}$, and low $C_{D_{min}}$. The flap angles for $C_{L_{max}}$ and $C_{D_{min}}$ were 30° and -3° , respectively, and the loss of lift and drag characteristics incurred by hinging the flap at this axis was within the limits of accuracy of the tests in both cases.

Aerodynamic characteristics of selected airfoil combination.—Standard aerodynamic characteristics of the selected arrangement, as determined in the 7- by 10-foot wind tunnel, with the flap set at angles of -10° , -3° , 0° , 5° , 10° , 20° , 30° , and 40° are shown in figures 5 to 12, respectively. Similar data for the plain N. A. C. A. 23012 airfoil used in the tests are shown in figure 13.

It should be noted that the optimum flap angle for cruising and high-speed flight is not necessarily -3° but may vary somewhat with the lift coefficients corresponding to these speeds. The optimum angle for each design should probably be determined by flight test on account of possible variations resulting from such factors as the effect of attitude on fuselage and interference drag, the effect of pitching moment on tail drag, scale effect, and the variation with lift coefficient previously mentioned.

The results presented for the erect and inverted tests (figs. 14, 15, 19, and 20, and table I) overlap to some extent near zero lift and are not in strict agreement; the pitching-moment coefficients about the aerodynamic center, the positions of the aerodynamic center, and the values given in table I for the lift-curve slope, and for the angle of zero lift (indicated by the lift-curve slope) as obtained from the erect and inverted tests differ somewhat. These apparent discrepancies in table I arise from the fact that the

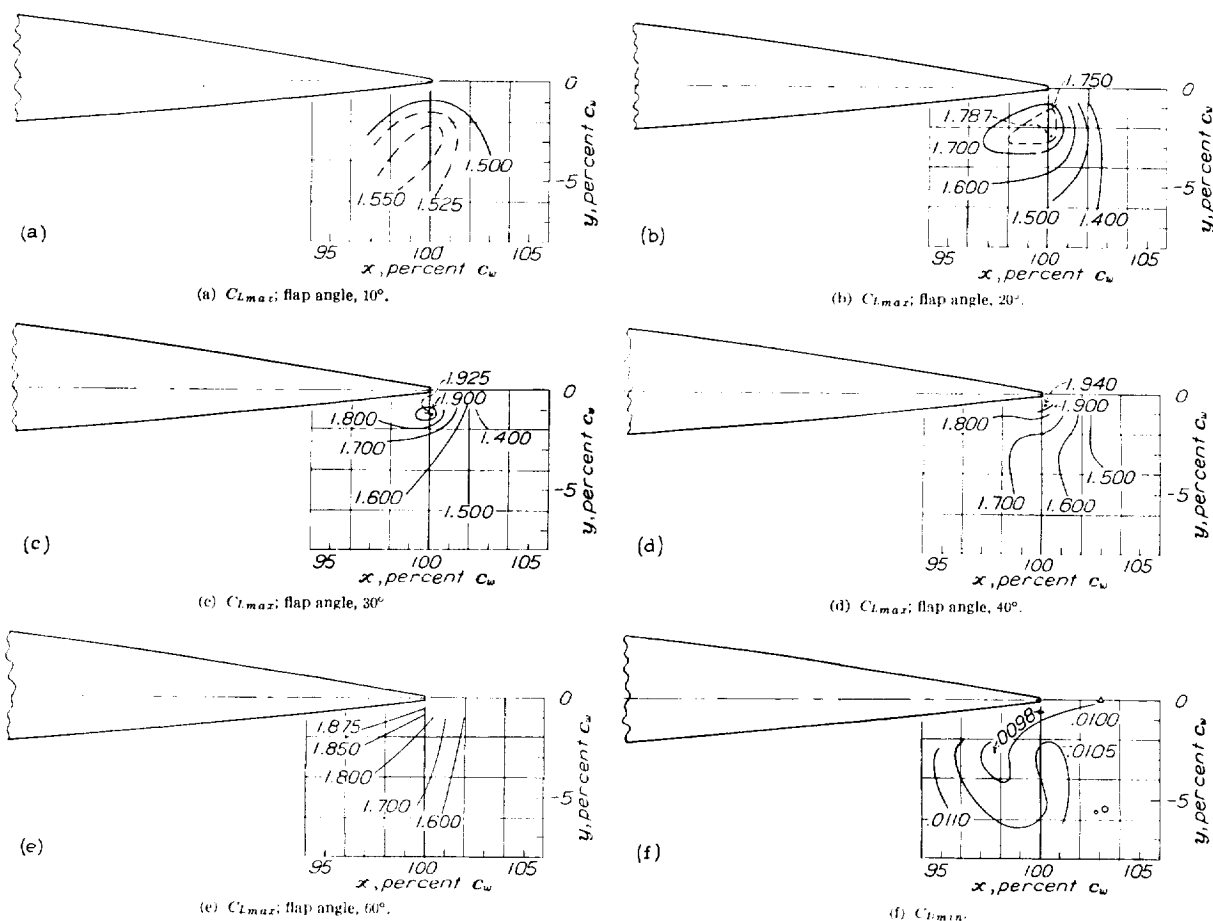


FIGURE 4.—Contours showing variation of $C_{L_{max}}$ and $C_{D_{min}}$ with flap position and angle. The N. A. C. A. 23012 airfoil with 0.20c_w N. A. C. A. 23012 external-airfoil flap. Plain wing: $C_{L_{max}}$, 1.150; $C_{D_{min}}$, 0.0103.

Standard large-scale aerodynamic characteristics of the N. A. C. A. 23012 airfoil with the N. A. C. A. 23012 external-airfoil flap hinged at axis 2 (fig. 1(b)) at angles of -3° (upright and inverted), 20° , 30° , and 40° as obtained in the variable-density tunnel are shown in figures 14 to 18. Similar data for the N. A. C. A. 23021 airfoil in combination with the N. A. C. A. 23012 external-airfoil flap set at angles of -3° (upright and inverted) and 30° appear in figures 19 to 21. Important characteristics of the two airfoil-flap combinations tested in the variable-density tunnel are summarized in table I.

Previously mentioned constants have been selected to give reasonably good agreement with the test results at moderate positive and negative angles of attack. The characteristic curves may be faired together at zero lift, giving preference to the positive-angle data; or the positive-angle data may be employed in the immediate neighborhood of zero lift.

Discussion of airfoil characteristics.—The high values of the maximum lift coefficient obtained, 2.37 for the N. A. C. A. 23012 airfoil with flap and 2.41 for the N. A. C. A. 23021 airfoil with flap at an effective Reynolds Number of about 8,000,000, compare favorably with those obtained for most other high-lift devices.

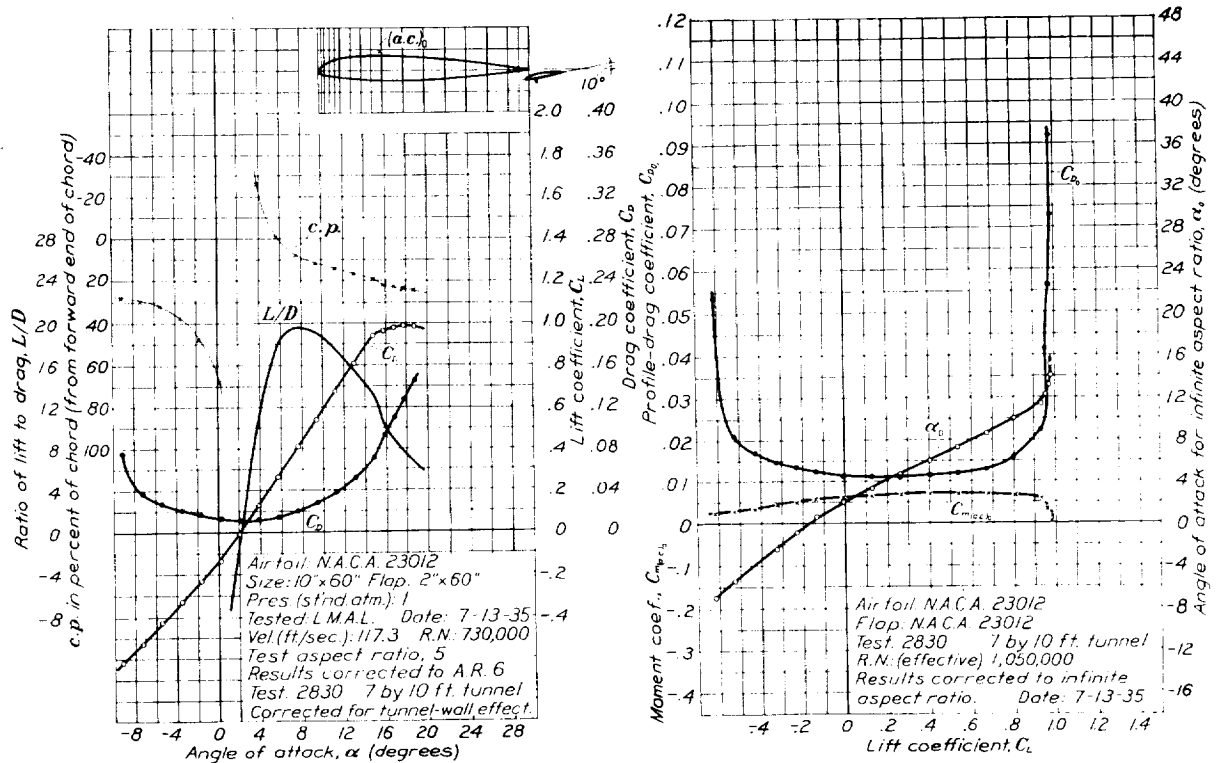


FIGURE 5.—The N. A. C. A. 23012 airfoil with 0.20 c_w N. A. C. A. 23012 external-airfoil flap. Flap angle, -10° . The airfoil is the same as used for test 2831-a (fig. 6), except the flap setting. The value of C_{m,c_0} is computed about the aerodynamic center used for test 2831-a.

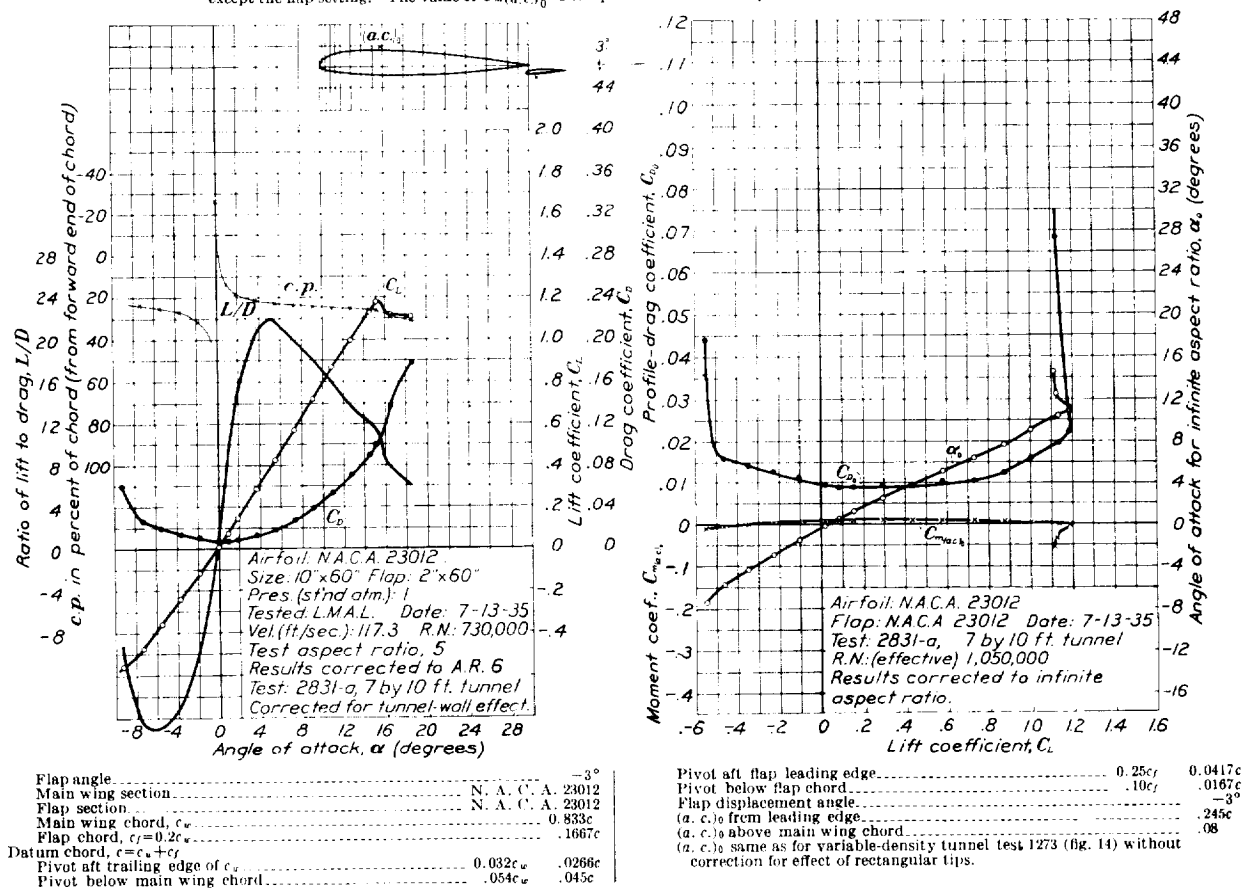


FIGURE 6.—The N. A. C. A. 23012 airfoil with 0.20 c_w N. A. C. A. 23012 external-airfoil flap.

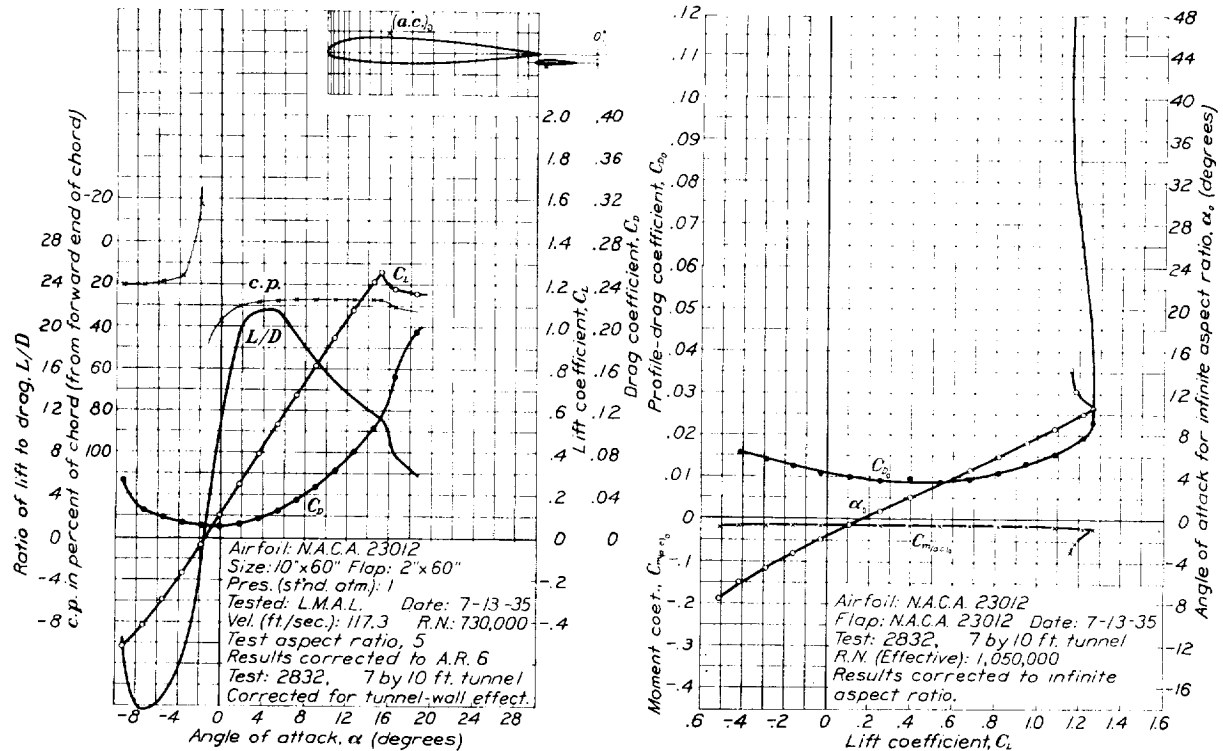


FIGURE 7.—The N. A. C. A. 23012 airfoil with 0.20c N. A. C. A. 23012 external-airfoil flap. Flap angle, 0°. The airfoil is the same as used for test 2831-a (fig. 6) except the flap setting. The value of $C_{m(a.c.)_0}$ is computed about the aerodynamic center used for test 2831-a.

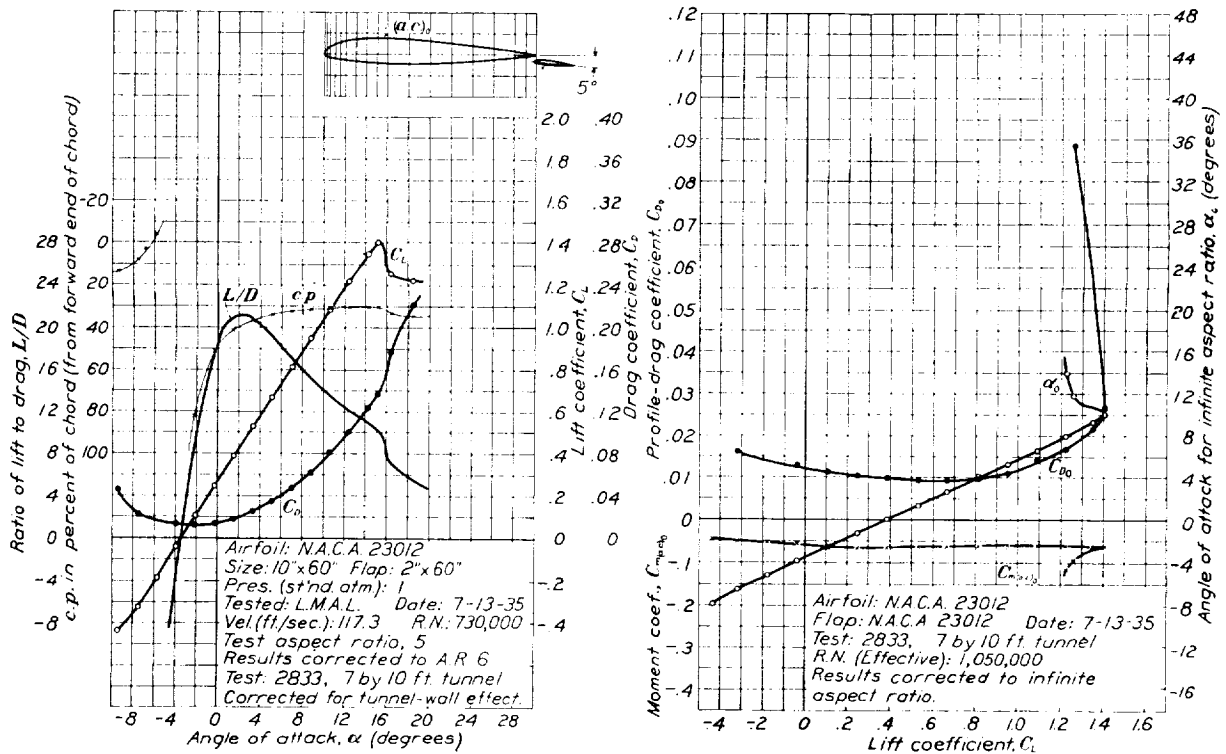


FIGURE 8.—The N. A. C. A. 23012 airfoil with 0.20c N. A. C. A. 23012 external-airfoil flap. Flap angle, 5°. The airfoil is the same as used for test 2831-a (fig. 6), except the flap setting. The value of $C_{m(a.c.)_0}$ is computed about the aerodynamic center used for test 2831-a.

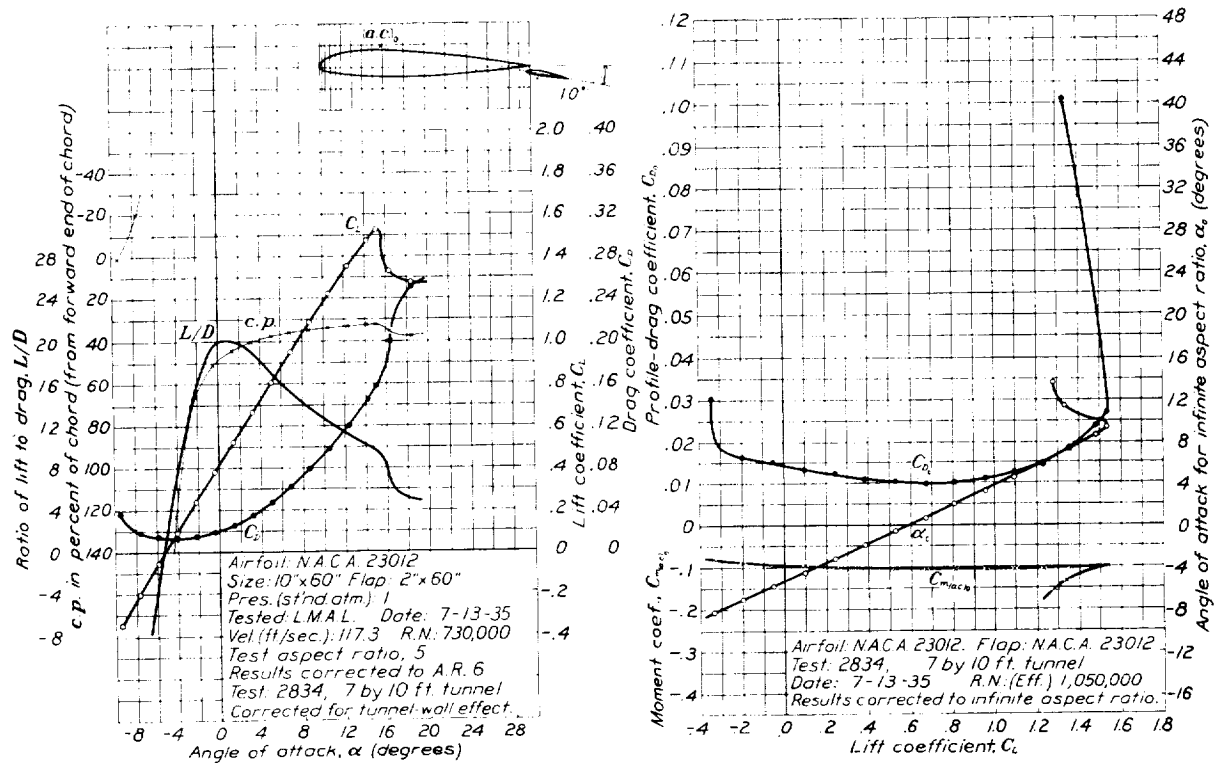


FIGURE 9.—The N. A. C. A. 23012 airfoil with 0.20 c_u N. A. C. A. 23012 external-airfoil flap. Flap angle, 10°. The airfoil is the same as used for test 2831-a (fig. 6), except the flap setting. The value of $C_{m(a.c.)_0}$ is computed about the aerodynamic center used for test 2831-a.

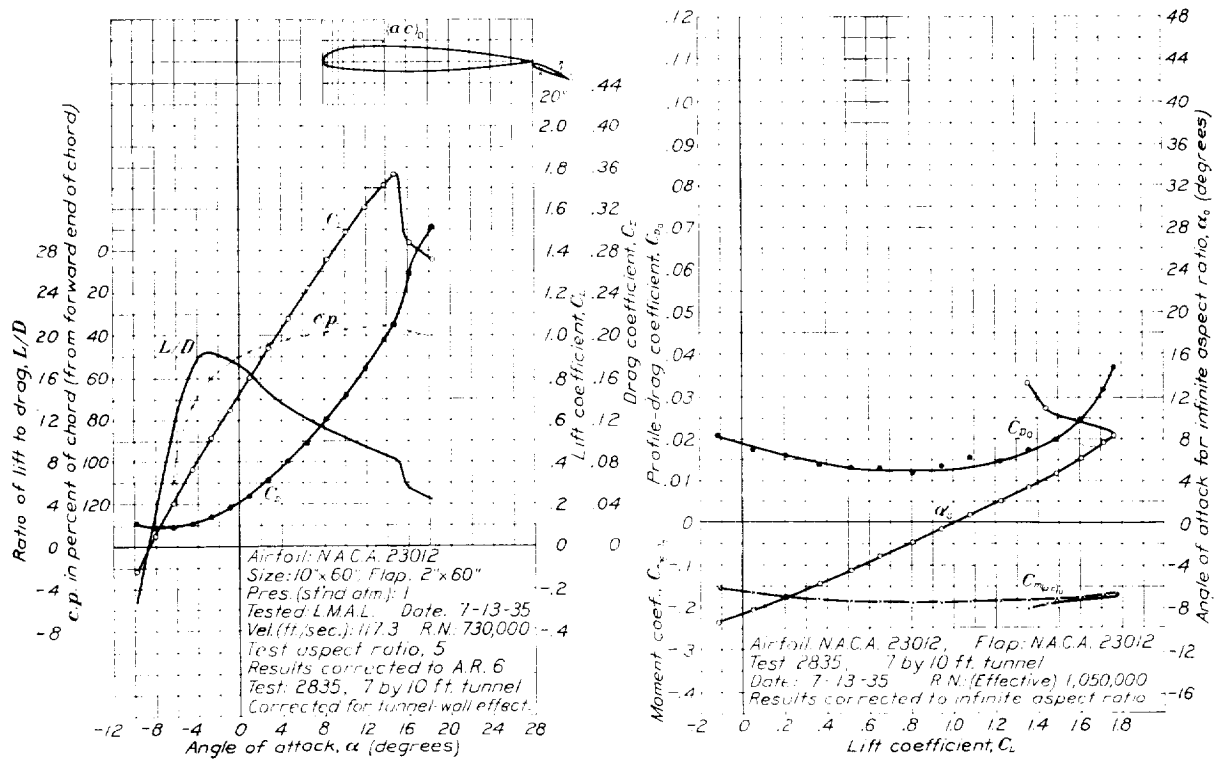


FIGURE 10.—The N. A. C. A. 23012 airfoil with 0.20 c_u N. A. C. A. 23012 external-airfoil flap. Flap angle, 20°. The airfoil is the same as used for test 2831-a (fig. 6), except the flap setting. The value of $C_{m(a.c.)_0}$ is computed about the aerodynamic center used for test 2831-a.

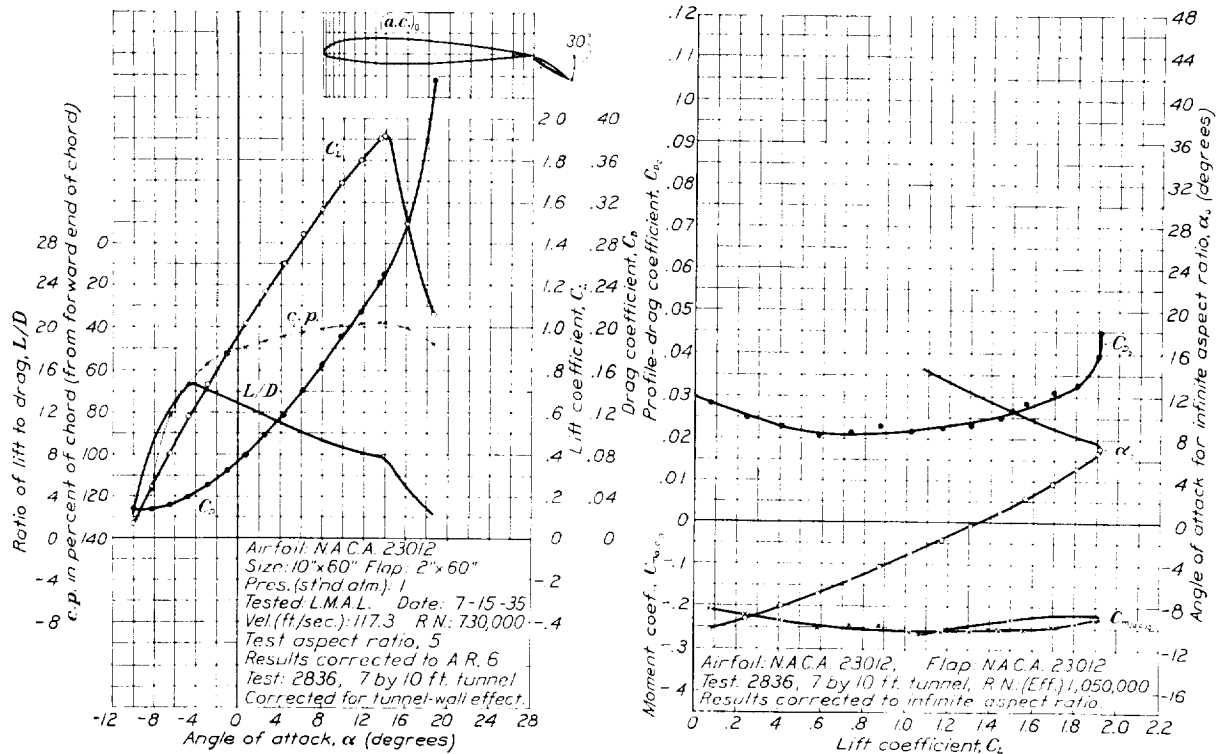


FIGURE 11.—The N. A. C. A. 23012 airfoil with 0.20c_a N. A. C. A. 23012 external-airfoil flap. Flap angle, 30°. The airfoil is the same as used for test 2831-a (fig. 6) except the flap setting. The value of $C_{m(a,c)_{j_0}}$ is computed about the aerodynamic center used for test 2831-a.

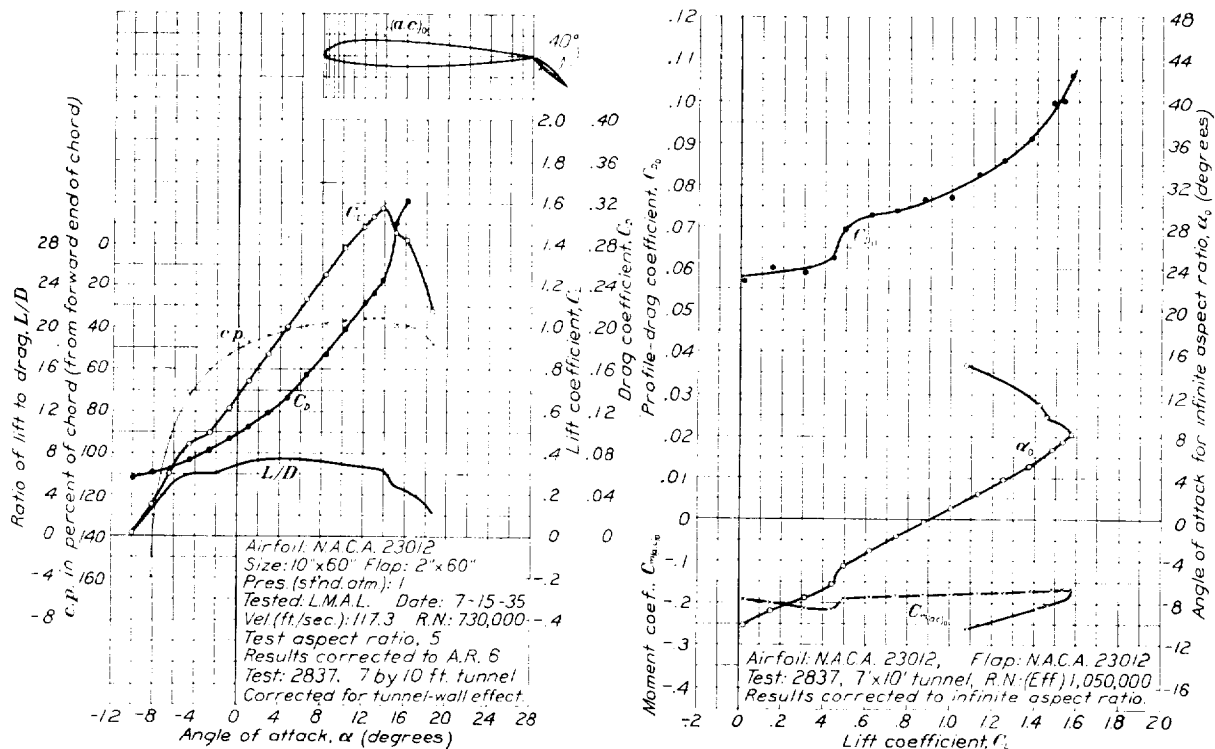


FIGURE 12.—The N. A. C. A. 23012 airfoil with 0.20c_a N. A. C. A. 23012 external-airfoil flap. Flap angle, 40°. The airfoil is the same as used for test 2831-a (fig. 6) except the flap setting. The value of $C_{m(a,c)_{j_0}}$ is computed about the aerodynamic center used for test 2831-a.

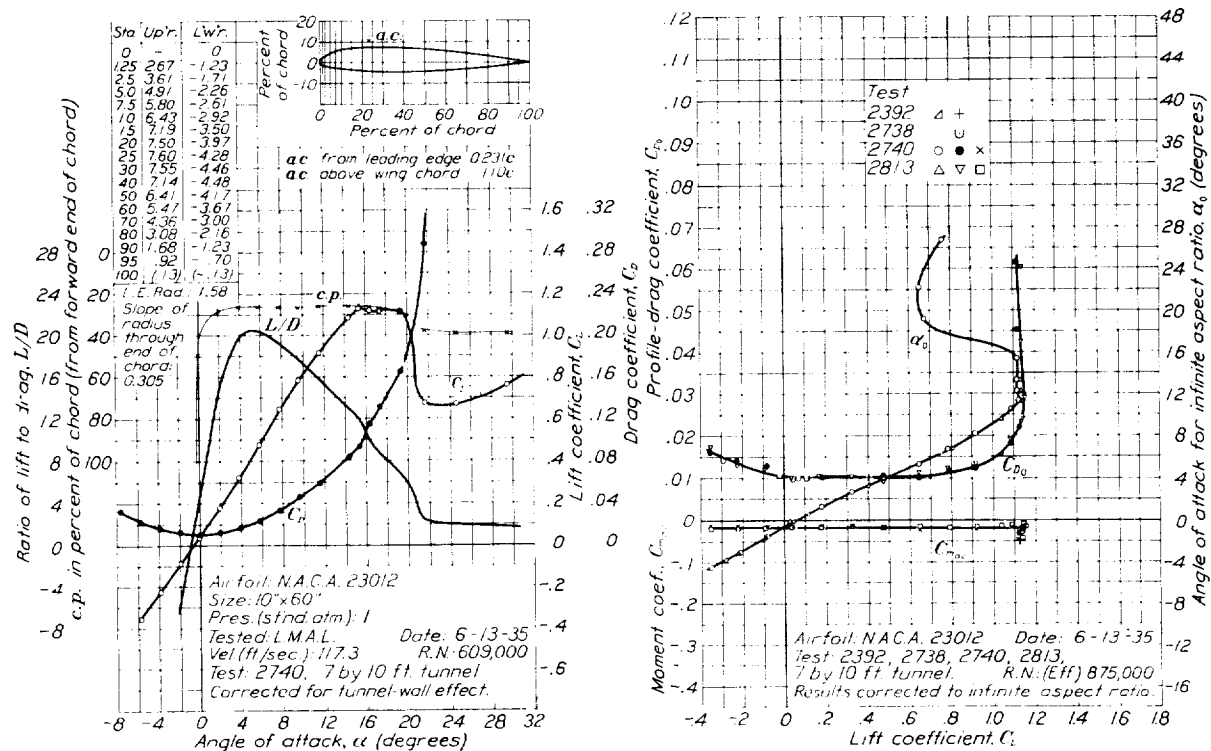


FIGURE 13.—The N. A. C. A. 23012 airfoil.

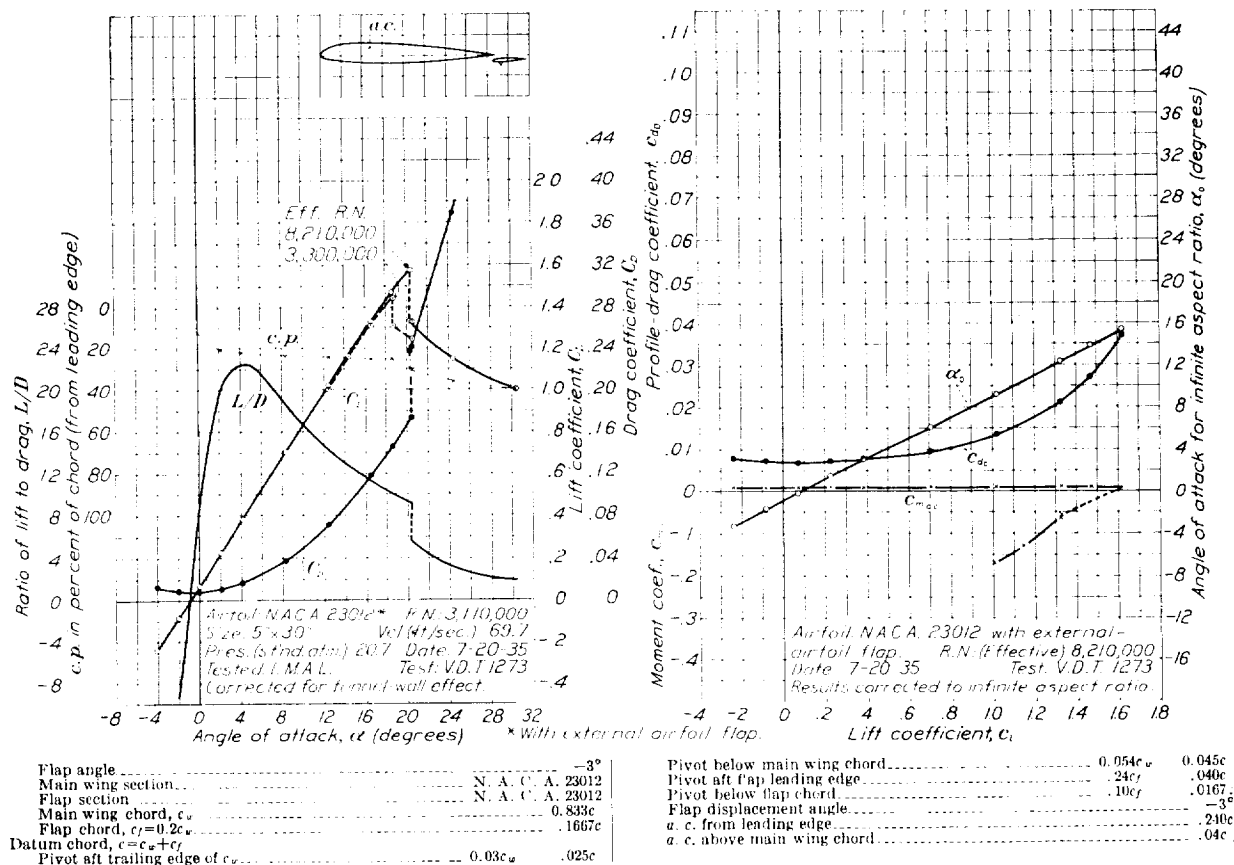


FIGURE 14.—The N. A. C. A. 23012 airfoil with 0.20c N. A. C. A. 23012 external-airfoil flap.

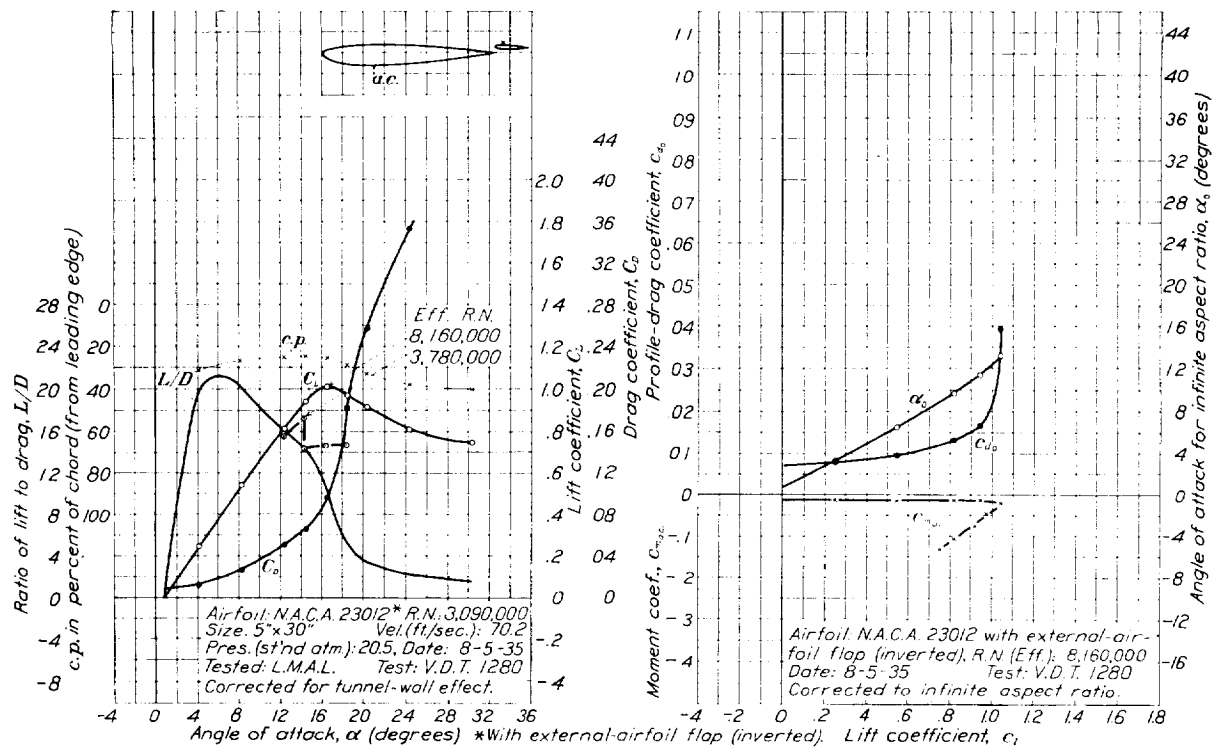


FIGURE 15.—The N. A. C. A. 23012 airfoil with 0.20c_m N. A. C. A. 23012 external-airfoil flap. Flap angle, -3°. The airfoil is the same as used for variable-density tunnel test 1273 (fig. 14) except inverted; a. c. from leading edge, 0.252; a. c. above main wing chord, -0.07c.

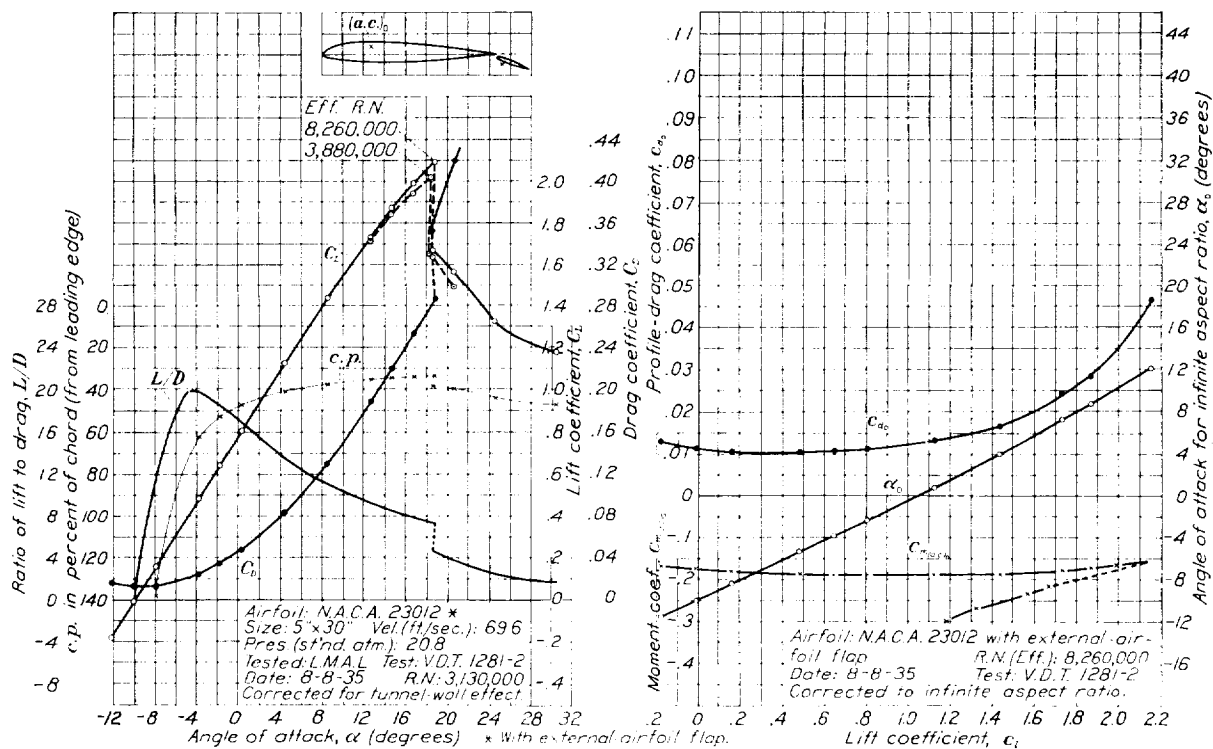


FIGURE 16.—The N. A. C. A. 23012 airfoil with 0.20c_m N. A. C. A. 23012 external-airfoil flap. Flap angle, 20°. The airfoil is the same as used for variable-density tunnel test 1273 (fig. 14) except the flap setting. The value of $c_{m(a.c.)_0}$ is computed about the aerodynamic center as determined for test 1273.

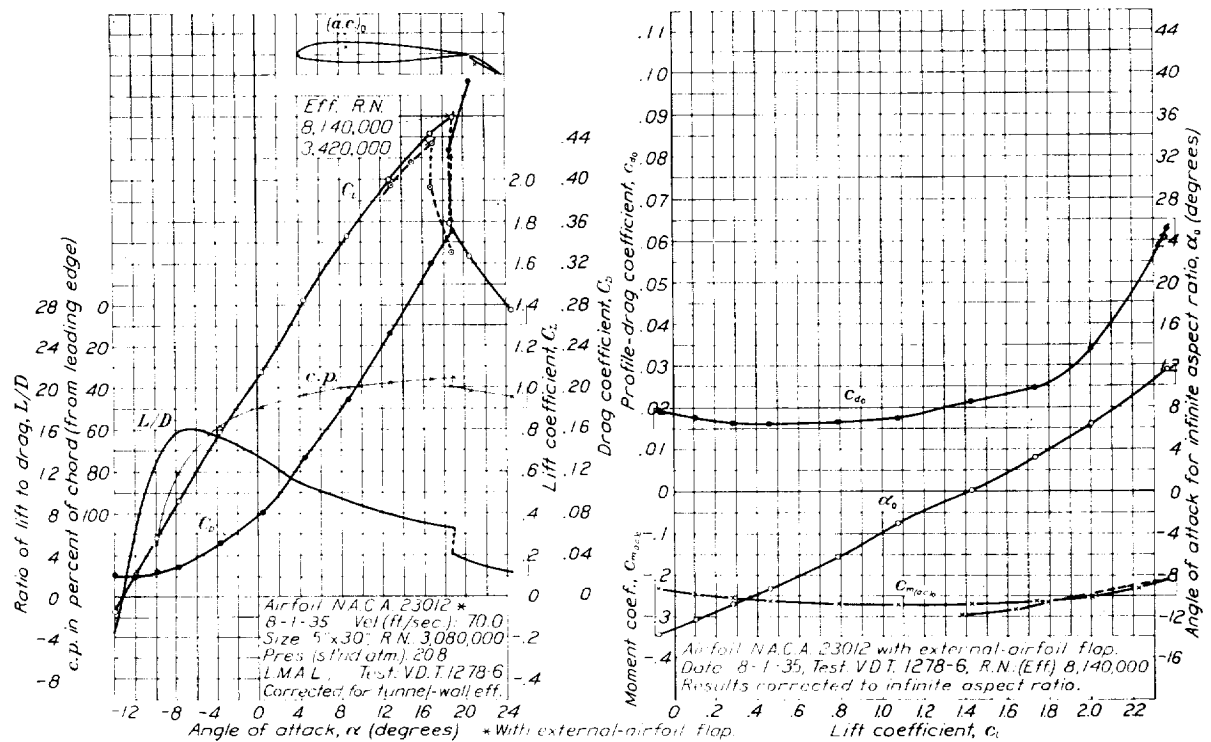


FIGURE 17.—The N. A. C. A. 23012 airfoil with 0.20c_w N. A. C. A. 23012 external-airfoil flap. Flap angle, 30°. The airfoil is the same as used for variable-density tunnel test 1273 (fig. 11) except the flap setting. The value of $c_{m(a,c)_0}$ is computed about the aerodynamic center as determined for test 1273.

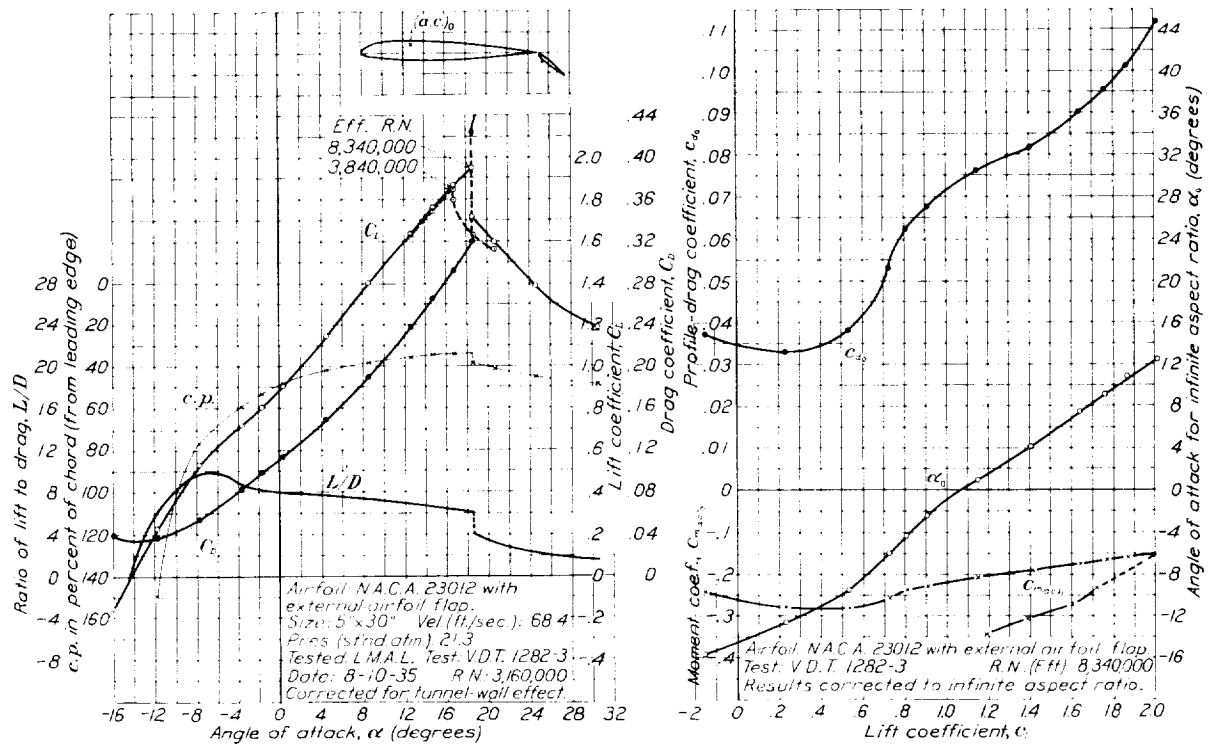
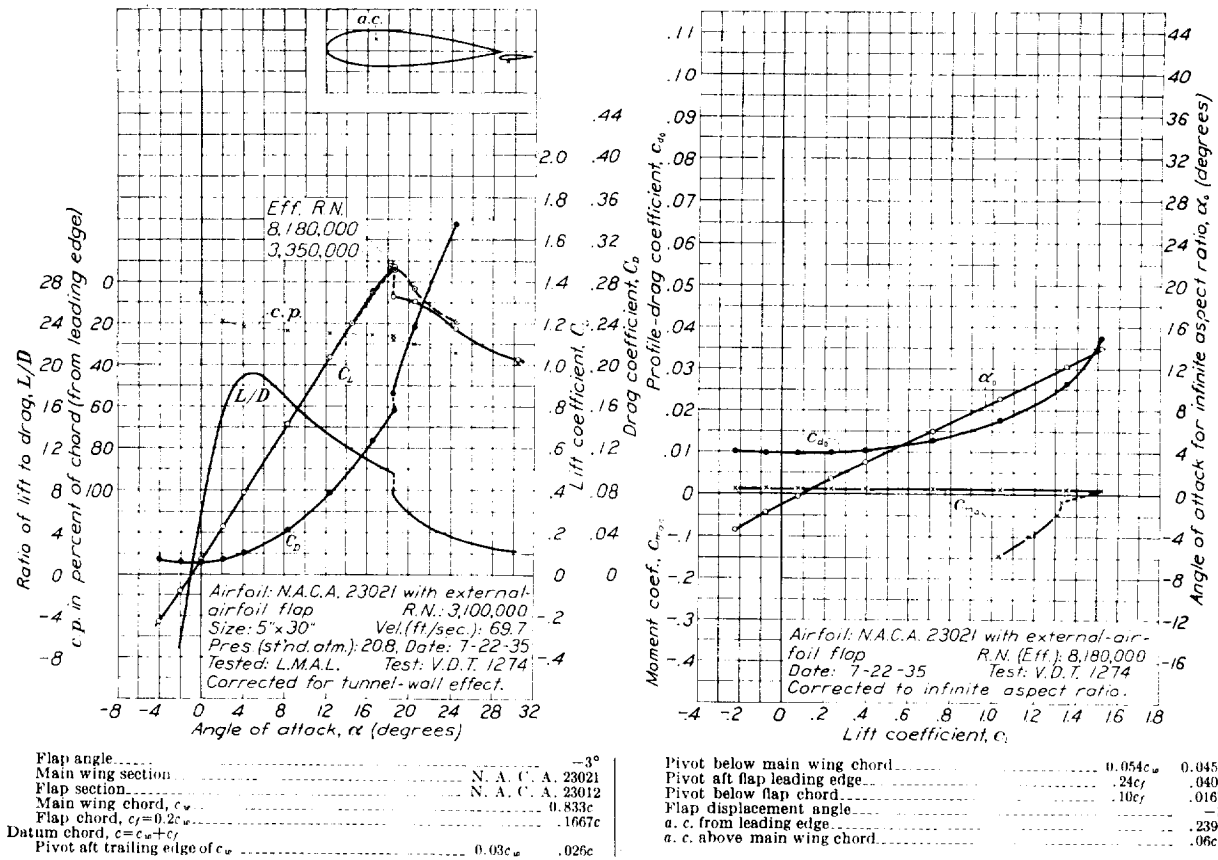
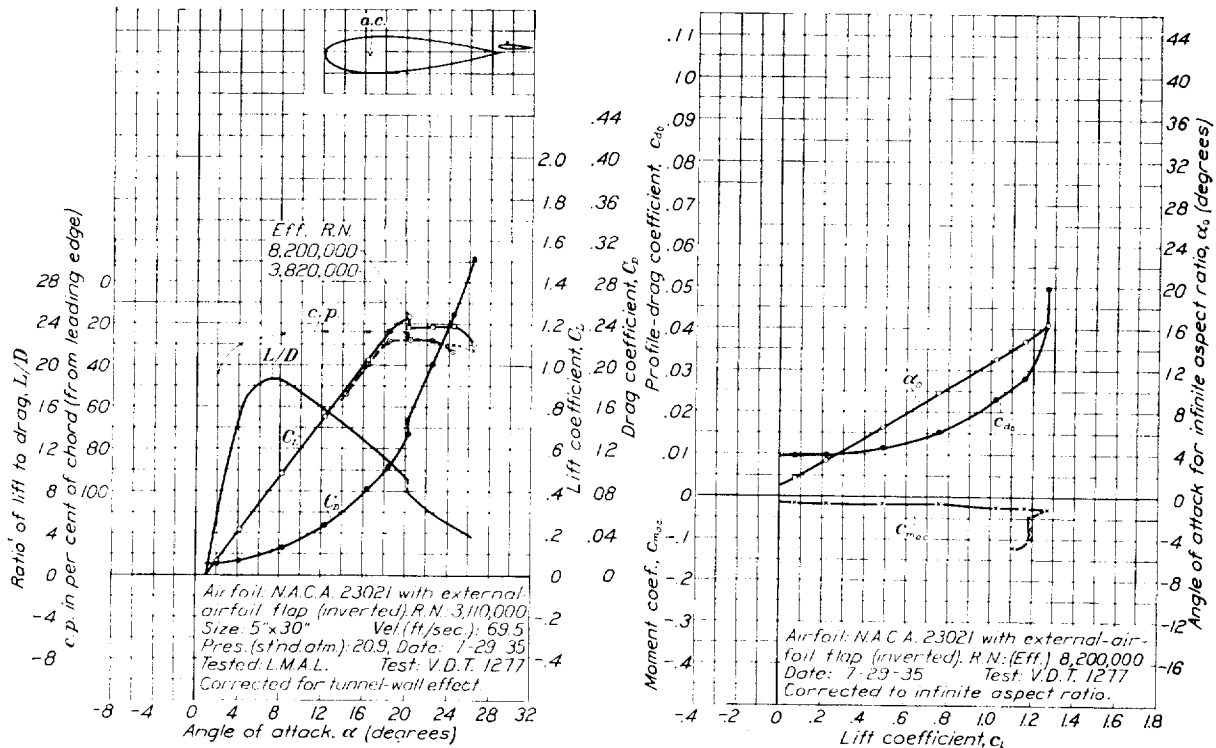


FIGURE 18.—The N. A. C. A. 23012 airfoil with 0.20c_w N. A. C. A. 23012 external-airfoil flap. Flap angle, 40°. The airfoil is the same as used for variable-density tunnel test 1273 (fig. 14) except the flap setting. The value of $c_{m(a,c)_0}$ is computed about the aerodynamic center as determined for test 1273.

FIGURE 19.—The N. A. C. A. 23021 airfoil with $0.20c$ N. A. C. A. 23012 external-airfoil flap.FIGURE 20.—The N. A. C. A. 23021 airfoil with $0.20c$ N. A. C. A. 23012 external-airfoil flap. Flap angle, -3° . The airfoil is the same as used for variable-density tunnel test 1274 (fig. 19) except inverted; a. c. from leading edge, $0.217c$; a. c. above main wing chord, $-0.01c$.

The minimum drag coefficients obtained for both airfoil-flap combinations indicate a slight favorable interference between the airfoil and the flap. The values obtained at an effective Reynolds Number of about 8,000,000 were 0.0069 and 0.0097, respectively, for the combinations using the N. A. C. A. 23012 and the N. A. C. A. 23021 airfoils for the main airfoil sections. These values are lower than those obtained for the N. A. C. A. 23012 and the N. A. C. A. 23021 sections alone, which have minimum drag coefficients of 0.0071 and 0.0101, respectively (reference 10). Airfoils of the N. A. C. A. 230 series of lower thickness ratios having the same maximum thickness for the same chord as the combination tested afford, however,

curves show the effects of scale on the characteristics plotted. It will be noted that the scale-effect curve for the maximum lift coefficient of the N. A. C. A. 23012 airfoil-flap combination as determined in the variable-density wind tunnel has a discontinuity at an effective Reynolds Number of about 1,700,000. The point obtained in the 7- by 10-foot wind tunnel at an effective Reynolds Number of only 1,000,000, however, lies on the extension of the curve obtained in the variable-density wind tunnel at higher Reynolds Numbers. Only two points were obtained for the combination using the N. A. C. A. 23021 section for the main airfoil in the variable-density tunnel, but for this case also it appears that a similar discontinuity may

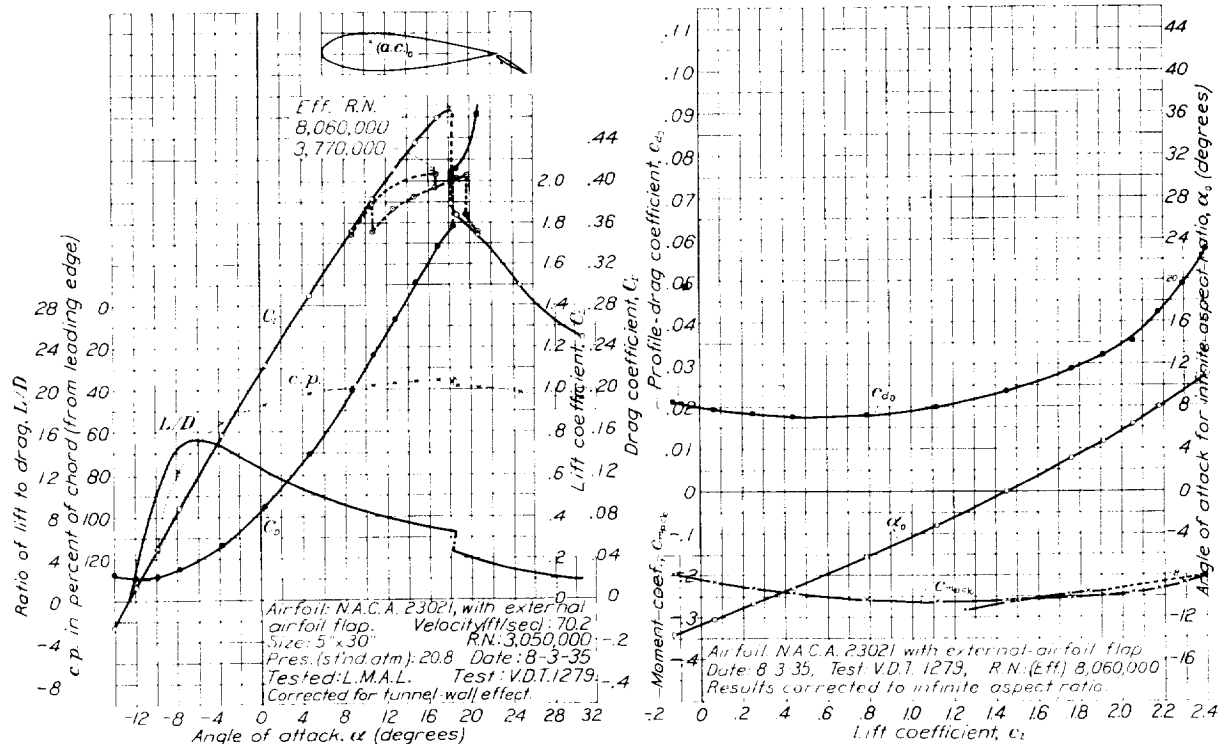


FIGURE 21.—The N. A. C. A. 23021 airfoil with 0.20c N. A. C. A. 23012 external-airfoil flap. Flap angle, 50° . The airfoil is the same as used for variable-density tunnel test 1274 (fig. 19) except the flap setting. The value of $c_{m(a.c.)_0}$ is computed about the aerodynamic center as determined for test 1274.

a better comparison. One such section is the N. A. C. A. 23010 predicted to have a minimum drag coefficient of 0.0067 and another is the N. A. C. A. 23018, which has a minimum drag coefficient of 0.0091 (reference 10). These values are slightly lower than those obtained with the comparable wing-flap combinations.

The variations of maximum lift and minimum drag coefficient with effective Reynolds Number are shown in figure 22. The data plotted in this figure are not corrected for hinge tares or for the effects of rectangular tips because these corrections were not known with certainty at all values of the effective Reynolds Number. The values plotted differ, therefore, from the fully corrected values given elsewhere, but the

exist, as evidenced by the low maximum lift coefficient obtained at an effective Reynolds Number of 3,800,000.

An explanation of this phenomenon and the apparent difference between the results from the two tunnels is indicated by the fact that the observed discontinuity tends to appear at a constant value of the test Reynolds Number rather than of the effective Reynolds Number. As pointed out in reference 8, the concept of effective Reynolds Number is applicable only when the scale effect is determined mainly by the influence of the transition from a laminar to a turbulent boundary layer. In the present case the flow through the slot probably is the important factor and depends upon the boundary-layer thickness relative to the slot size, which in turn is more nearly dependent on the

test Reynolds Number than on the effective Reynolds Number. Interpreted on this basis, the apparent conflict between the results obtained in the variable-density and the 7- by 10-foot wind tunnels disappears, and it is probable that wings in flight will show the discontinuity, if at all, at values of the Reynolds Number lower than the effective values at which the discontinuities occur in the variable-density tunnel.

The scale effect on minimum profile drag, as shown in figure 22, is about the same for both combinations.

Flap loads.—The variation of flap normal force, flap chord force, and flap center of pressure, with lift coefficient of the airfoil-flap combination is shown in figure 23. These data are in no case extended to the maximum lift coefficient of the combination at the flap angle in question on account of erratic points obtained in the tests. The data indicated that, with the flap supported separately, either the main airfoil or the flap had a tendency to stall prematurely, rendering the values in the region of $C_{L_{max}}$ inconsistent and unreliable.

The variation of flap hinge-moment coefficient C_{H_f} with flap angle about the two hinge-axis locations used is shown in figures 24 and 25. It will be noted that the flap is slightly overbalanced between angles of -5° and -10° when hinged at axis 1. Although the overbalance does not occur in the normal flap-operating range (-3° to 30°), it seems likely that overbalance might occur in operation of the flaps as ailerons with a neutral setting of -3° . For this reason the second location, axis 2 (fig. 1), was selected and used for further hinge-moment tests. This hinge axis is exactly 1 percent of the flap chord ahead of axis 1. Even with this axis, some slight degree of overbalance remains although it is considerably less than that encountered with axis 1 and is not considered likely to cause aileron overbalance in the high-speed condition.

Since the tests in the variable-density tunnel were based on the results of the 7- by 10-foot wind-tunnel tests, it was considered desirable to use flap hinge axis 2, which seems slightly more satisfactory than 1, in the variable-density-tunnel tests. Inasmuch as the flap was hinged at axis 1 for the 7- by 10-foot wind-tunnel tests, there is a slight discrepancy of flap position between the final force tests in the two tunnels. The rate of variation of lift and drag characteristics with flap position, as shown in figure 4, indicates, however, that the effect of this difference on the final force-test data may be regarded as negligible.

General features of combinations of airfoil and external-airfoil flap.—The present external-airfoil flap combinations appear to have as many desirable aerodynamic characteristics as other good high-lift devices tested up to the present. They give a high maximum lift coefficient and a low minimum drag coefficient; in these respects, however, their merit is approximately equal to that of such a device as the split flap. At the same time they give a much lower value of drag coefficient

throughout the high-lift range, provided that the flap is set at the proper angle, than do split flaps. If a large drag at a high lift coefficient is desired to obtain steep gliding ability, characteristics approaching those of the split flap can be obtained by deflecting the external-airfoil flap to larger angles than the optimum, thus causing the flap to stall and to give large increases of profile drag. A different hinge axis, selected with this characteristic in mind, should give large available values of profile drag at high lift coefficients without entailing much increase in the minimum values of profile drag obtainable throughout the lift range.

Another feature of external-airfoil flaps is the possibility of deflecting them as ailerons, while they cover the full span of the wing as a high-lift device. As explained in reference 1, disadvantages in connection with overbalance when the ailerons are deflected differentially and with large values of adverse yawing

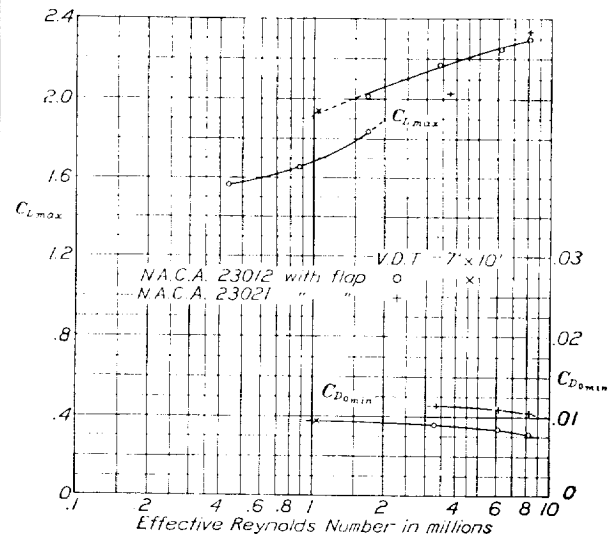


FIGURE 22. Scale effect on N. A. C. A. 23012 and N. A. C. A. 23021 airfoils with 0.20c N. A. C. A. 23012 external-airfoil flap. All values uncorrected for hinge fares and for effects of rectangular tips.

moment render their value as a lateral-control arrangement doubtful. Unfortunately the use of the full-span flap for glide control, as suggested previously, is incompatible with its use as a lateral-control device. An arrangement using the tip portions as combined ailerons and flaps, with the center portion capable of being deflected to much larger angles for glide control, appears to offer a possibility of combining these various features, provided that the large values of adverse yawing moment are acceptable.

With the data available at present, it is possible to determine the relative merit of the Clark Y and the N. A. C. A. 23012 airfoil sections for use as external-airfoil flaps on the N. A. C. A. 23012 main airfoil. Comparison of the results in this report with those of reference 1 indicates that the combination with the N. A. C. A. 23012 flap has appreciably lower drag

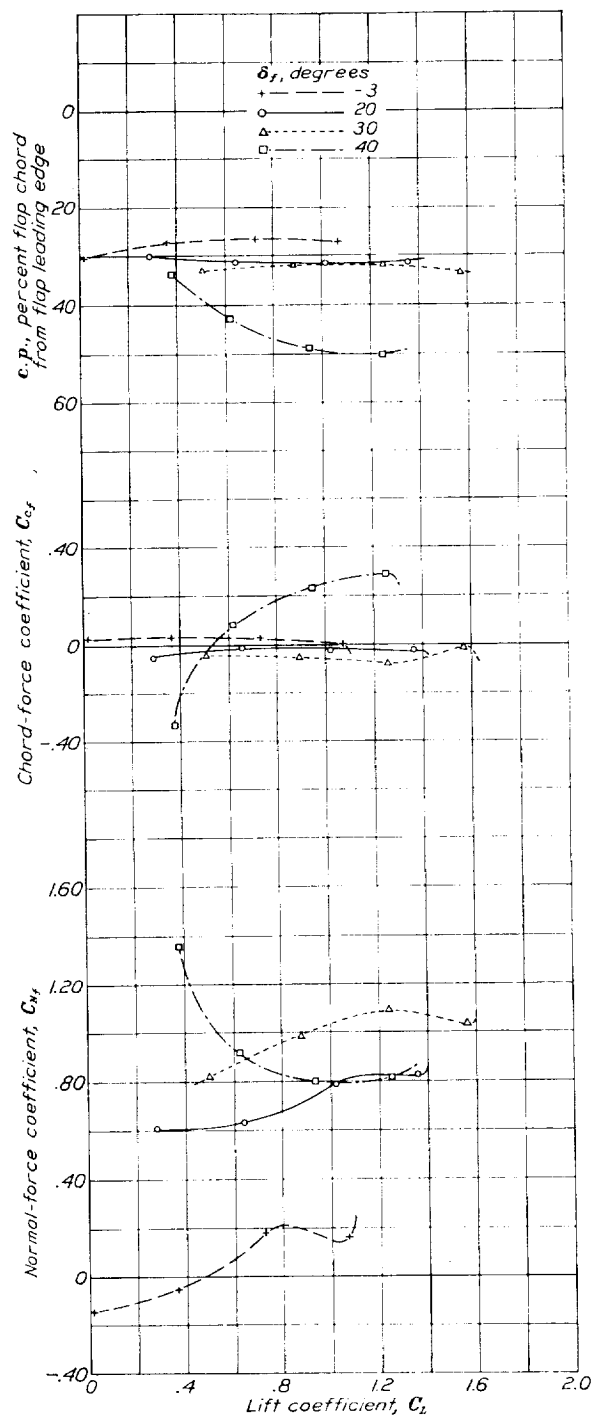


FIGURE 23.—Variation of air loads on flap with wing lift coefficient. N. A. C. A. 23012 airfoil with 0.20c_w N. A. C. A. 23012 external-airfoil flap.

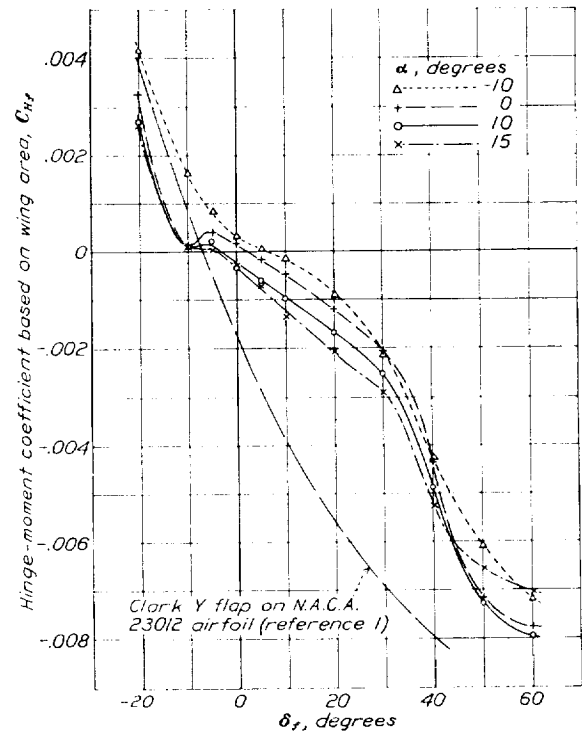


FIGURE 24.—Hinge-moment coefficients of flap. Hinge axis 1. N. A. C. A. 23012 airfoil with 0.20c_w N. A. C. A. 23012 external-airfoil flap.

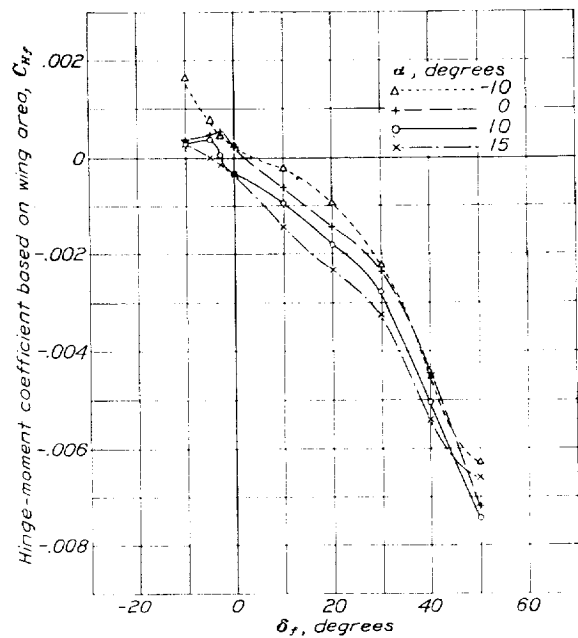


FIGURE 25.—Hinge-moment coefficients of flap. Hinge axis 2. N. A. C. A. 23012 airfoil with 0.20c_w N. A. C. A. 23012 external-airfoil flap.

throughout the whole lift range. The values obtained in the 7- by 10-foot wind tunnel of the speed-range index $C_{L_{max}}/C_{D_{min}}$, which may be considered representative of the relative merit of the two arrangements, are 192 for the N. A. C. A. 23012 flap on the N. A. C. A. 23012 airfoil and 174 for the Clark Y flap on the N. A. C. A. 23012 airfoil. Although the combination with the Clark Y flap gives a slightly higher maximum lift coefficient, it is apparent from the values of the speed-range index that the general maximum lift and minimum drag characteristics of the combination with the

in figures 26 and 27. The polar curves for the flap combinations are envelope curves of the series of polars obtained at the various flap-angle settings, thus giving at each lift coefficient the minimum profile-drag coefficient obtainable from the airfoil-flap combination. The envelope curves for the split-flap combinations were constructed from data obtained from reference 11 and from unpublished tests in the variable-density tunnel. In the case of the plain airfoil equipped with a split flap, no reduction of profile-drag coefficient is obtained by deflecting the flap except at lift coeffi-

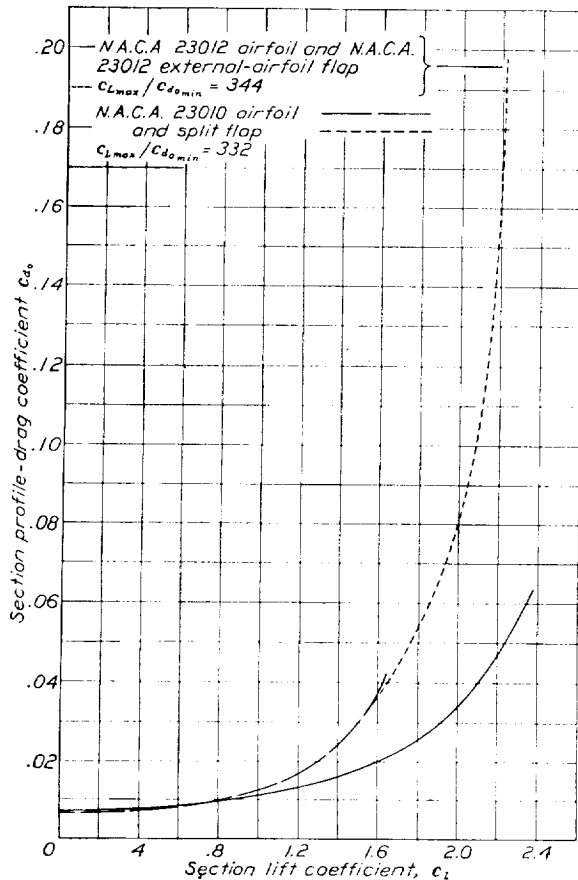


FIGURE 25.—Comparison of N. A. C. A. 23012 airfoil and $0.20c_u$ N. A. C. A. 23012 external-airfoil flap with N. A. C. A. 23010 airfoil and $0.20c_u$ split flap. Effective Reynolds Number, 8,200,000.

N. A. C. A. 23012 flap are more favorable. A study of the contour curves for maximum lift and minimum drag in this report and in reference 1 shows that the variation of optimum position of the flap with flap angle is more favorable for obtaining a hinge position giving low operating moments without sacrificing performance characteristics in the case of the N. A. C. A. 23012 flap than in the case of the Clark Y flap.

A comparison of the N. A. C. A. 23012 external-airfoil flap in combination with N. A. C. A. 23012 and N. A. C. A. 23021 airfoils, with the plain airfoils of comparable thickness equipped with split flaps is shown

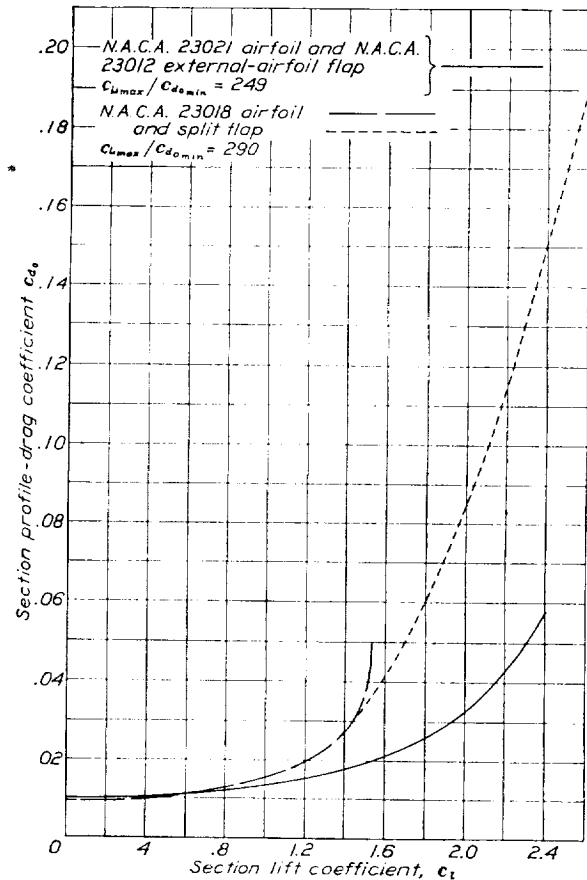


FIGURE 27.—Comparison of N. A. C. A. 23021 airfoil and $0.20c_u$ N. A. C. A. 23012 external-airfoil flap with N. A. C. A. 23018 airfoil and $0.20c_u$ split flap. Effective Reynolds Number, 8,200,000.

cients very near the maximum for the plain airfoil. The curves, therefore, show also the comparison of the external-flap device with a plain wing. Since the N. A. C. A. 23012 airfoil with a $0.20c_u$ N. A. C. A. 23012 external-airfoil flap has a maximum thickness equal to 10 percent of the over-all chord, it is considered directly comparable with the N. A. C. A. 23010 airfoil in that wings of these two types, having the same plan form and area, would have the same maximum thickness. The same is true of the N. A. C. A. 23021 airfoil with the N. A. C. A. 23012 external-airfoil flap in comparison with the N. A. C. A. 23018 plain airfoil.

From the data appearing in figures 26 and 27, the advantages of the external-airfoil flap over other types of high-lift flaps in general use at present are immediately apparent. The results show that, for flight at any lift coefficient above approximately 0.7, a wing with an external-airfoil flap is superior either to the comparable plain wing or to one equipped with a split flap. Since the maximum rate of climb of most airplanes occurs at an air speed corresponding to a lift coefficient near 0.7, it is apparent that the external-airfoil flap has no adverse effect on the maximum rate of climb, provided that other factors affecting the issue, such as wing loading and span, are the same for the types of wing arrangement being compared. It is further apparent that for an airplane of a given power, weight, wing area, span, and general "cleanness" the external-airfoil flap may give appreciable improvement over the plain wing in such performance features as take-off, angle of climb, ceiling, range, endurance, and minimum rate of descent, all of which may involve flight at lift coefficients in excess of 0.7. This feature may be particularly useful in increasing the single-engine ceiling of multiengine aircraft and in permitting such airplanes to maintain flight at lower speeds, in taking off for example, than would otherwise be possible with one engine stopped.

As far as manual operation of the flap in flight is concerned, the external-airfoil flap should be considerably superior to such devices as ordinary flaps and unbalanced split flaps on account of the low values of hinge moment that can be obtained throughout the operating range. If some degree of overbalance may be tolerated in cases where the flaps are not also used as ailerons, considerably more reduction in hinge moment should be obtainable by moving the flap hinge axis farther back on the flap chord without any loss of performance characteristics. Comparison of the hinge moments obtained for either of the present flap hinge axes with the data of reference 11 indicates that this arrangement of the external-airfoil flap requires about one-third the operating moment of comparable sizes of ordinary flap throughout the normal range. This ease of operation should facilitate adjustment of the glide path in approaches to a landing and permit the use of a direct flap-operating lever on airplanes of such

size that a more complicated mechanical drive would be necessary for conventional flaps. Certain other types of flap, as, for example, the Fowler or Zap, may be expected to give characteristics more nearly comparable with those of external-airfoil flaps than do the ordinary or split type. These other types, however, have extra mechanical complications in that they require some other type of motion than pure rotation, which contributes to the ease of installation and operation of external-airfoil flaps.

An undesirable feature of any trailing-edge high-lift device is the large negative pitching moment that it develops when operative. In this respect the external-airfoil flaps are slightly inferior at equal values of the maximum lift coefficient to ordinary or split flaps. In addition to the structural disadvantages involved, the problem of obtaining satisfactory balance and stability becomes more acute because of this characteristic. These features are somewhat compensated by the relatively small wake, indicated by the low drag, that occurs when the deflection of the external-airfoil flaps is less than the deflection giving the maximum lift coefficient. The reduction of tail effectiveness due to the low-speed wake, and incidentally the tendency to tail buffeting, should therefore be considerably less than with flaps that are deflected to large angles at maximum lift.

CONCLUDING REMARKS

From the data obtained in the present investigation, the external-airfoil flap in combination with an airfoil appears to be one of the most generally satisfactory high-lift devices investigated to date. The combination tested offers a relatively high value of maximum lift coefficient with low profile drag in the high-lift range. At low lift coefficients it gives very nearly as low values of profile drag as a good plain airfoil of comparable thickness. Structural and stability problems associated with the large negative pitching moments occurring at high lift coefficients may be slightly greater than in the case of ordinary and split flaps. A flight investigation of this type of device installed on a Fairchild 22 airplane, with full-span flaps arranged to operate also as ailerons, is now being conducted by the N. A. C. A.

LANGLEY MEMORIAL AERONAUTICAL LABORATORY,
NATIONAL ADVISORY COMMITTEE FOR AERONAUTICS,
LANGLEY FIELD, VA., *March 25, 1936.*

REFERENCES

1. Platt, Robert C.: Aerodynamic Characteristics of Wings with Cambered External-Airfoil Flaps, Including Lateral Control with a Full-Span Flap. T. R. No. 541, N. A. C. A., 1935.
2. Harris, Thomas A.: The 7 by 10 Foot Wind Tunnel of the National Advisory Committee for Aeronautics. T. R. No. 412, N. A. C. A., 1931.
3. Jacobs, Eastman N., and Abbott, Ira H.: The N. A. C. A. Variable-Density Wind Tunnel. T. R. No. 416, N. A. C. A., 1932.
4. Wenzinger, Carl J.: Wind-Tunnel Measurements of Air Loads on Split Flaps. T. N. No. 498, N. A. C. A., 1934.
5. Platt, Robert C.: Aerodynamic Characteristics of a Wing with Fowler Flaps Including Flap Loads, Downwash, and Calculated Effect on Take-Off. T. R. No. 534, N. A. C. A., 1935.
6. Jacobs, Eastman N., Ward, Kenneth E., and Pinkerton, Robert M.: The Characteristics of 78 Related Airfoil Sections from Tests in the Variable-Density Wind Tunnel. T. R. No. 460, N. A. C. A., 1933.
7. Jacobs, Eastman N., and Clay, William C.: Characteristics of the N. A. C. A. 23012 Airfoil from Tests in the Full-Scale and Variable-Density Tunnels. T. R. No. 530, N. A. C. A., 1935.
8. Platt, Robert C.: Turbulence Factors of N. A. C. A. Wind Tunnels as Determined by Sphere Tests. T. R. No. 558, N. A. C. A., 1936.
9. Jacobs, Eastman N., and Pinkerton, Robert M.: Tests in the Variable-Density Wind Tunnel of Related Airfoils Having the Maximum Camber Unusually Far Forward. T. R. No. 537, N. A. C. A., 1935.
10. Jacobs, Eastman N., and Pinkerton, Robert M.: Tests of N. A. C. A. Airfoils in the Variable-Density Wind Tunnel. Series 230. T. N. No. 567, N. A. C. A., 1936.
11. Wenzinger, Carl J.: Wind-Tunnel Investigation of Ordinary and Split Flaps on Airfoils of Different Profile. T. R. No. 554, N. A. C. A., 1936.

TABLE I.—AIRFOIL DATA

[See reference 9 for explanation of tabulated characteristics]

Airfoil	External airfoil flap setting, deg.	Classification		Effective R. N. mil- lions	$C_{L_{max}}$	α_0 at $C_{L_{max}}$, deg.	Fundamental section characteristics						Derived and additional characteristics that may be used for structural design									
		Chord	P. D.				S. E.	$C_{L_{max}}$	α_0 per degree	$C_{l_{opt}}$	$C_{d_{0min}}$	$\alpha C_{m_{0,c}}$	η c.		$\frac{C_{L_{max}}}{C_{d_{0min}}}$	c, p at $C_{L_{max}}$		Wing charac- teristics; $A=6$, round tips	Thickness		Cam- ber, per- cent c	
													Be- hind L. E., c, per- cent c	Above L. E., c, per- cent c		Com- puted, percent c	Actual, percent c		ma per rad.	$C_{D_{min}}$		0.15c, percent c
N. A. C. A. 23012.....	-3	A	8.21	1.62	15	-0.9	0.101	0.07	0.009	24.0	4	235	26	4.39	0.0070	8.90	6.88	10.00
	inverted	A	8.16	1.04	13	.3	.086	-.013	25.2	-7	25	3.58	8.90	6.88	10.00
	20	A	8.26	2.16	12	-9.9	.105	.35	208	33	4.52	.0112	8.90	6.88	10.00
	30	A	8.14	2.37	12	-13.6	.102	.45	147	35	4.43	.0181	8.90	6.88	10.00
N. A. C. A. 24021.....	40	A	8.34	2.51	12	-13.5	.102	.26	61	33	3.36	.0342	8.90	6.88	10.00
	-3	A	8.20	1.52	14	-9.9	.104	0	.012	23.9	6	157	26	4.49	.0097	15.58	12.03	17.50
	inverted	A	8.20	1.27	16	-7	.083	0	-.016	21.7	-1	131	24	3.77	.0097	15.58	12.03	17.50
	30	A	8.06	2.41	11	-13.4	.108	.58	137	35	4.62	.0197	15.58	12.03	17.50

• In these computations the chord length is the sum of the wing and the flap chords.

REPORT No. 574

PRESSURE DISTRIBUTION OVER AN AIRFOIL SECTION WITH A FLAP AND TAB

By CARL J. WENZINGER

SUMMARY

Pressure-distribution tests of a Clark Y airfoil with a flap and an inset tab were made in the N. A. C. A. 7-by 10-foot wind tunnel. The pressures were measured on both the upper and lower surfaces at one chord section. Calculations were made of the normal-force and pitching-moment coefficients of the airfoil section with flap and tab, the normal-force and hinge-moment coefficients of the flap section with tab, and the normal-force and hinge-moment coefficients of the tab section alone. In addition, comparisons were made of the theoretical and experimental values for an airfoil with a multiply hinged flap system.

It was found that peak values of the increments of resultant pressures due to flap or to tab deflection occurred at the flap and tab hinges, respectively. Also, the variations of increments of airfoil section normal-force and pitching-moment coefficients and of flap normal-force and hinge-moment coefficients, due to flap deflection with a given tab setting, were practically independent of the tab deflection. In addition, the variation of increments of tab normal-force and hinge-moment coefficients with tab deflection for a given flap setting was practically independent of flap deflection. Comparisons of the theoretical with the experimental forces and moments for the airfoil section with flap and tab show that the theory agrees fairly well with experiment for small flap deflections with the tab neutral, but that the theory indicates much greater effects than are actually obtained when the flap and tab are simultaneously deflected.

INTRODUCTION

A considerable number of airplanes are fitted with a small flap on one or more of the movable control surfaces. Such an auxiliary flap is ordinarily referred to as a "tab" and is usually set into the trailing edge of the control surface. When the tab is used to reduce the hinge moments of a control surface, it is known as a "balancing tab"; when used to trim the airplane in place of an adjustable stabilizer or fin, it is referred to as a "trimming tab."

The chief aerodynamic characteristics of tabs are covered in reference 1, which describes an investigation of a wing with several arrangements of ailerons and tabs, alone and in conjunction with other types of balancing arrangements. In reference 1 data are also

included from tests of a tail surface of average proportions with several different tabs.

Because of the rapidly increasing use of tabs, particularly on tail surfaces where they replace the adjustable fin and stabilizer, there is a demand for information that can be used for stress-analysis purposes. In this connection, the designer desires to know the magnitude and distribution of the air forces acting on the various surfaces and the moments about the hinge axes so that the structure, supports, and control mechanism can be designed for maximum efficiency. The present investigation was therefore undertaken to make available information that would be of immediate use in the foregoing design problems.

The tests consisted of pressure-distribution measurements over one chord section of an airfoil with a flap and a tab. From the data obtained, calculations were made of normal-force and pitching-moment coefficients for the airfoil section with flap and tab; both normal-force and hinge-moment coefficients were computed for the flap section with tab and for the tab section alone.

APPARATUS AND TESTS

The N. A. C. A. 7-by 10-foot wind tunnel, in which the tests were made, is described in reference 2. A half-span Clark Y airfoil (fig. 1) that had originally been built for pressure-distribution tests of high-lift devices was used. The model was altered by installing at the tip a flap having a chord 30 percent of the airfoil chord and a span 40 percent of the half-span model. An inset tab was mounted at the trailing edge of the flap, the tab size and location being selected as representative of the average. The tab chord was 20 percent of the flap chord and its span was 50 percent of the flap span. The gaps between the flap and the airfoil and those between the tab and the flap were sealed with plasticine for all tests.

The airfoil, flap, and tab were all constructed of laminated mahogany to within ± 0.010 inch of the specified ordinates. A row of small orifices was installed in the upper and lower surfaces at one chord section located at the center of the span of the flap and tab. (See fig. 1.) This location was 20 percent of the semispan of the model inboard of the rectangular tip so that satisfactory section characteristics could be obtained which

would be outside the influence of the usually high local tip pressures. The half-span model was set up in conjunction with a reflection plane at its inboard end, the plane extending from top to bottom of the air stream and some distance ahead of and behind the model. A multiple-tube alcohol manometer photographically recorded the pressures on the airfoil section.

Pressures were measured for flap settings of 0° , $\pm 15^\circ$, and $\pm 30^\circ$ with the tab neutral. With the flap neutral, pressures were measured for tab settings of $\pm 10^\circ$, $\pm 20^\circ$, and $\pm 30^\circ$. The pressures were then measured for various combinations of flap up with tab down and of flap down with tab up. The angles of attack used in the tests (-5° , 0° , 10° , and 15°) covered

RESULTS

The results of the investigation, in their original form, consisted of pressure diagrams for the section as tested at different angles of attack and for different tab and flap deflections. In order to facilitate the interpretation and application of these results, the pressure diagrams are presented in the form of "increment" diagrams, which represent the changes in pressure distribution due to changes in the significant variables. The pressure diagrams for the basic section (i. e., neutral tab and flap) are also given so that the resultant diagram for any case may be obtained by addition of the increment and the basic-section diagrams. The principal advantage of the increment

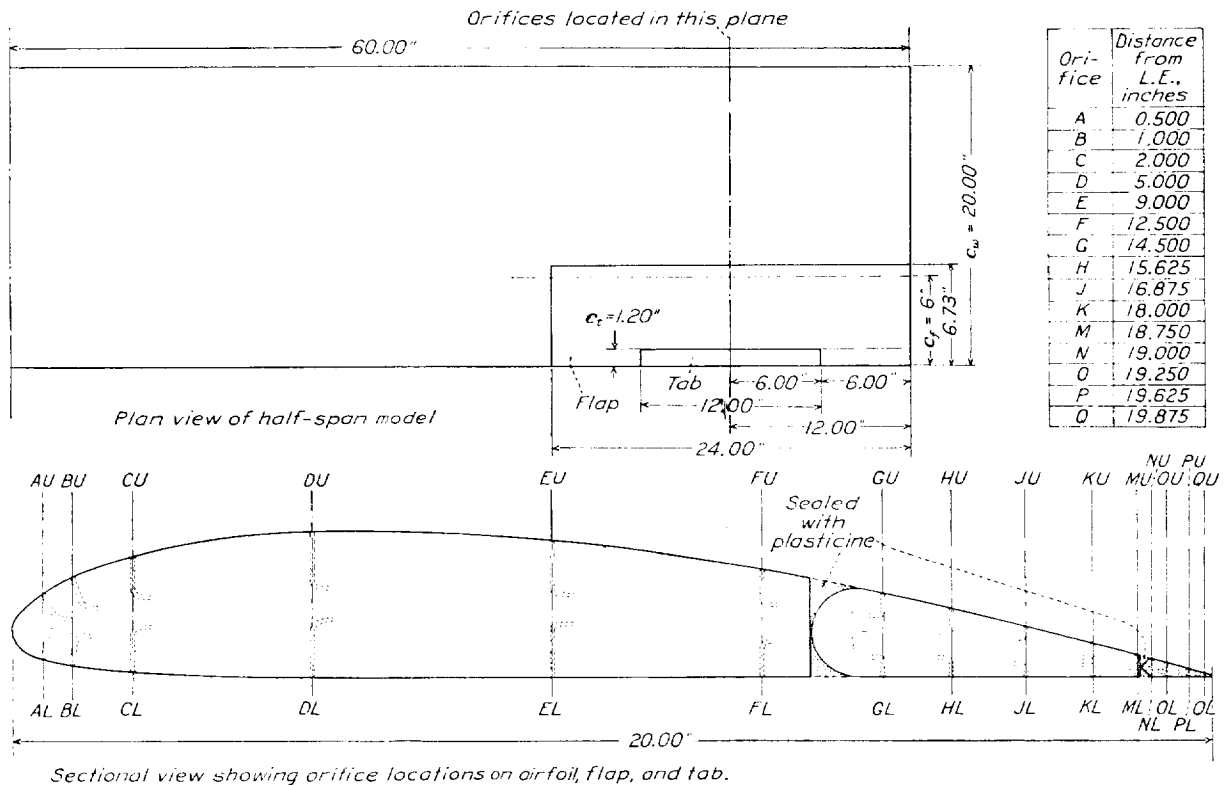


FIGURE 1.—Clark Y airfoil with tab and flap arranged for pressure-distribution tests.

approximately the range from zero lift to maximum lift.

Angles of attack and flap deflections were measured with respect to the airfoil chord; tab deflections were measured with respect to the flap chord. Positive flap or tab angles indicate a downward deflection with respect to the airfoil or flap chord. The tests were made at a dynamic pressure of 16.37 pounds per square foot, corresponding to an air speed of 80 miles per hour under standard sea-level conditions. The average Reynolds Number was 1,220,000, based on the airfoil chord of 20 inches as the characteristic length.

diagrams is that they may, by the principle of superposition, be applied to pressure diagrams for any other basic airfoil section, including the symmetrical section, that does not depart too greatly from the Clark Y section on which the tests were made. The diagrams of resultant-pressure distribution for the basic airfoil section are given in figure 2. The increments of resultant pressure for various tab and flap deflections are presented in figures 3 to 6. The figures give the results for a low-angle-of-attack condition, $\alpha = 0^\circ$, and for a high-angle-of-attack condition, $\alpha = 15^\circ$.

The important characteristics of the section as a whole and of the tab and flap, as functions of tab and

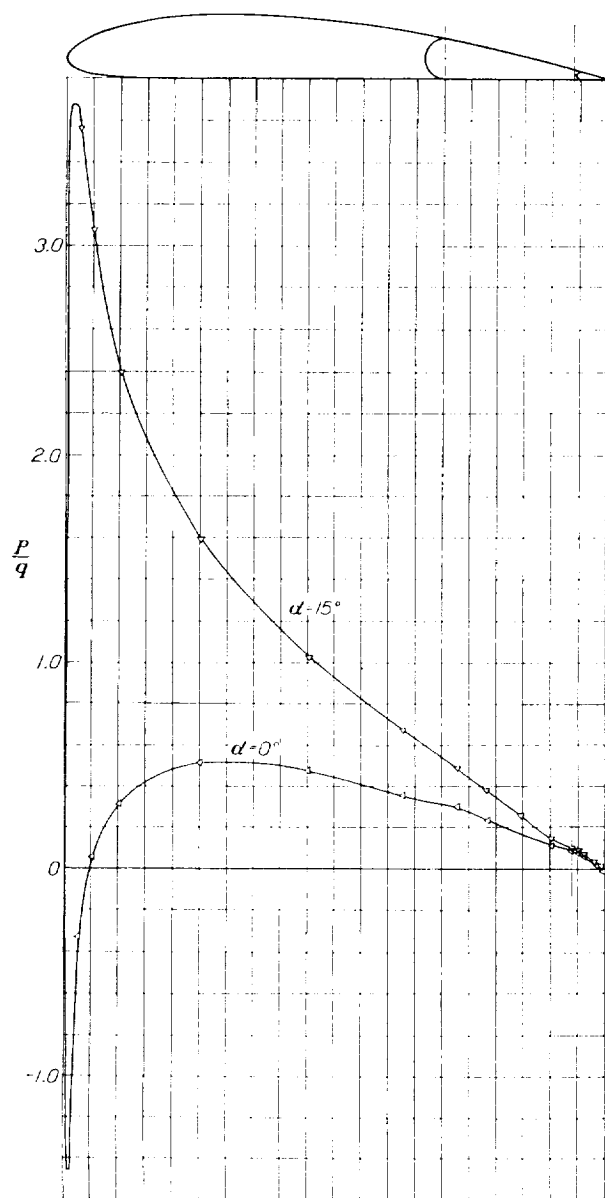


FIGURE 2.—Distribution of resultant pressure on airfoil section with flap and tab neutral. $\alpha = 0^\circ$ and 15° .

flap deflection, are also plotted as increments. These increments were obtained by deducting the basic section characteristics from those for the section with deflected flaps, the characteristics being determined in each case by integration of the original pressure diagrams. Calculations were made of the following quantities in which lower-case letters are used to indicate section coefficients:

Airfoil section normal-force coefficient, $c_{n_w} = \frac{n_w}{qc_w}$

Airfoil section pitching-moment coefficient, $c_{m_{c/4}} = \frac{m_w}{qc_w^2}$

Flap section normal-force coefficient, $c_{n_f} = \frac{n_f}{qc_f}$

Flap section hinge-moment coefficient, $c_{h_f} = \frac{h_f}{qc_f^2}$

Tab section normal-force coefficient, $c_{n_t} = \frac{n_t}{qc_t}$

Tab section hinge-moment coefficient, $c_{h_t} = \frac{h_t}{qc_t^2}$

in which

n_w is the resultant pressure force normal to the airfoil chord.

m_w , the corresponding pitching moment about the quarter-chord point.

n_f , the resultant pressure force normal to the flap chord.

h_f , the corresponding moment about the flap hinge.

n_t , the resultant pressure force normal to the tab chord.

h_t , the corresponding moment about the tab hinge.

The subscript w refers to the airfoil section with flap and tab; the subscript f to the flap section with tab; the subscript t to the tab section alone.

The integrated coefficients for the basic airfoil section are plotted in figure 7 against angle of attack. Curves giving the increments for various tab and flap deflections are presented in figures 8, 9, and 10.

Figures 11 and 12 are plots of theoretical parameters taken from reference 3 and modified so as to apply directly to N. A. C. A. absolute coefficients. Comparisons of theoretical with experimental values of the forces and moments for the Clark Y airfoil tested with several different deflections of the tab and flap are shown in figures 13, 14, and 15.

DISCUSSION

Pressure distribution.—The effects on the distribution of resultant-pressure increments due to tab or flap deflection are shown by figures 3 and 4. Deflections of the tab or of the flap produce peak values of the pressure increments at the tab hinge or at the flap hinge, respectively. If the tab and flap are deflected simultaneously (tab deflection opposite to that of flap), then peak values of the pressure increments occur at both hinge axes but the resultant pressures act in opposite directions. (See figs. 5 and 6.)

Section characteristics.—The characteristics of the basic airfoil section given in figure 7 (tab and flap neutral) exhibit no unusual tendencies. For a given setting of the tab, the flap and tab may be considered as a flap unit. Then the effect of deflection of such a unit will be similar to that for an ordinary flap (e. g., aileron, elevator, or rudder). Increments to the basic values of airfoil section normal-force and pitching-moment coefficients are given in figure 8 for various flap

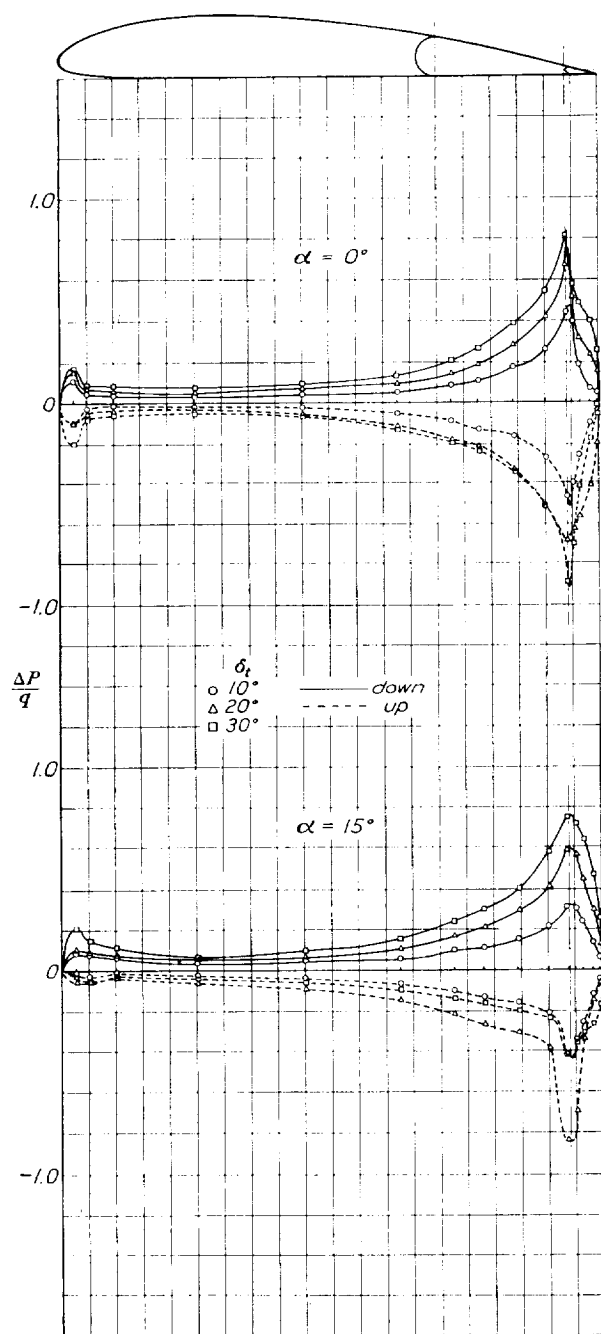


FIGURE 3.—Increments of resultant pressure due to tab deflection. Flap neutral.

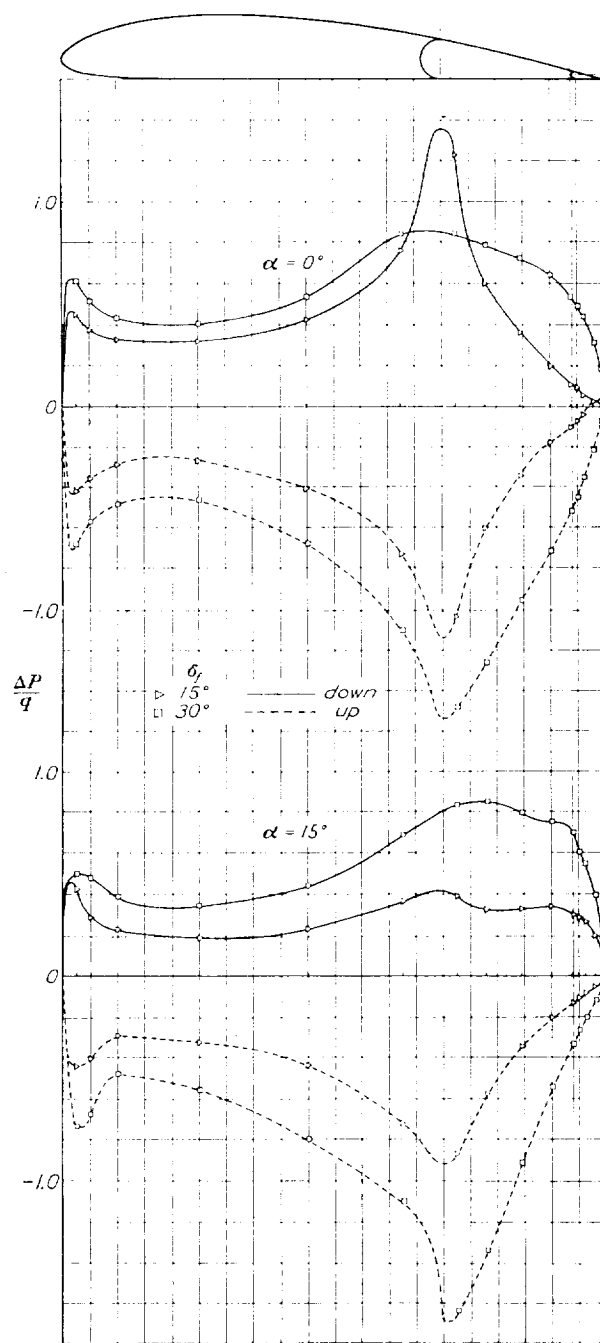


FIGURE 4.—Increments of resultant pressure due to flap deflection. Tab neutral.

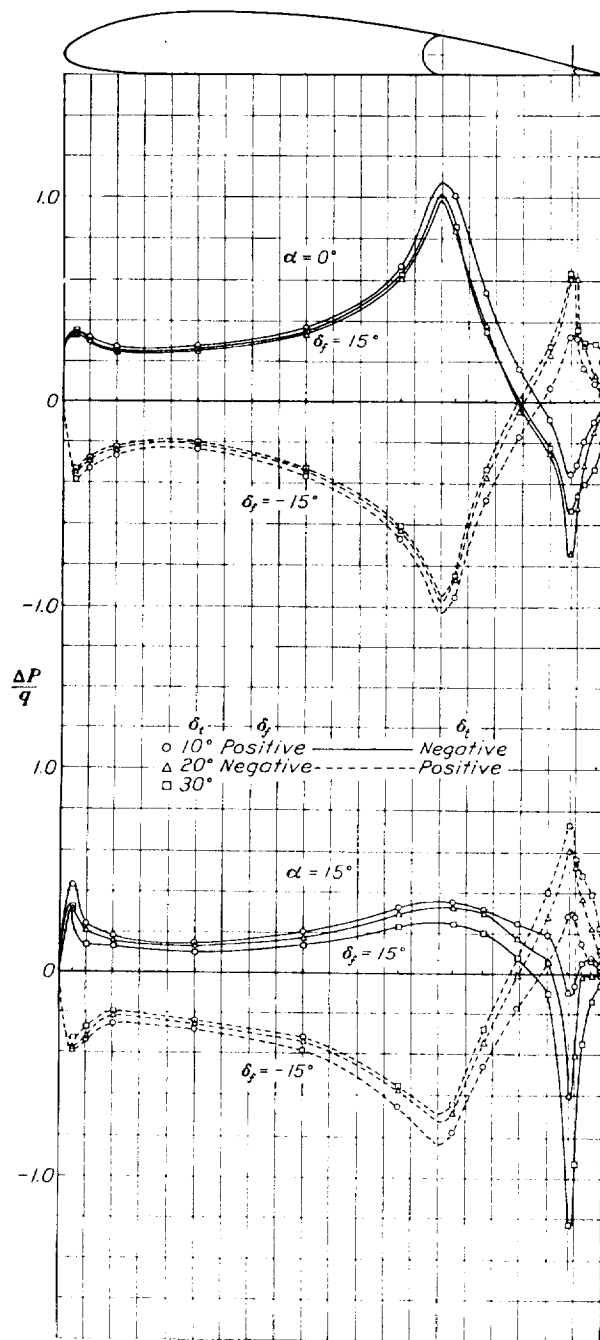


FIGURE 5.—Increments of resultant pressure due to combined tab and flap deflection. $\delta_t = \pm 15^\circ$.

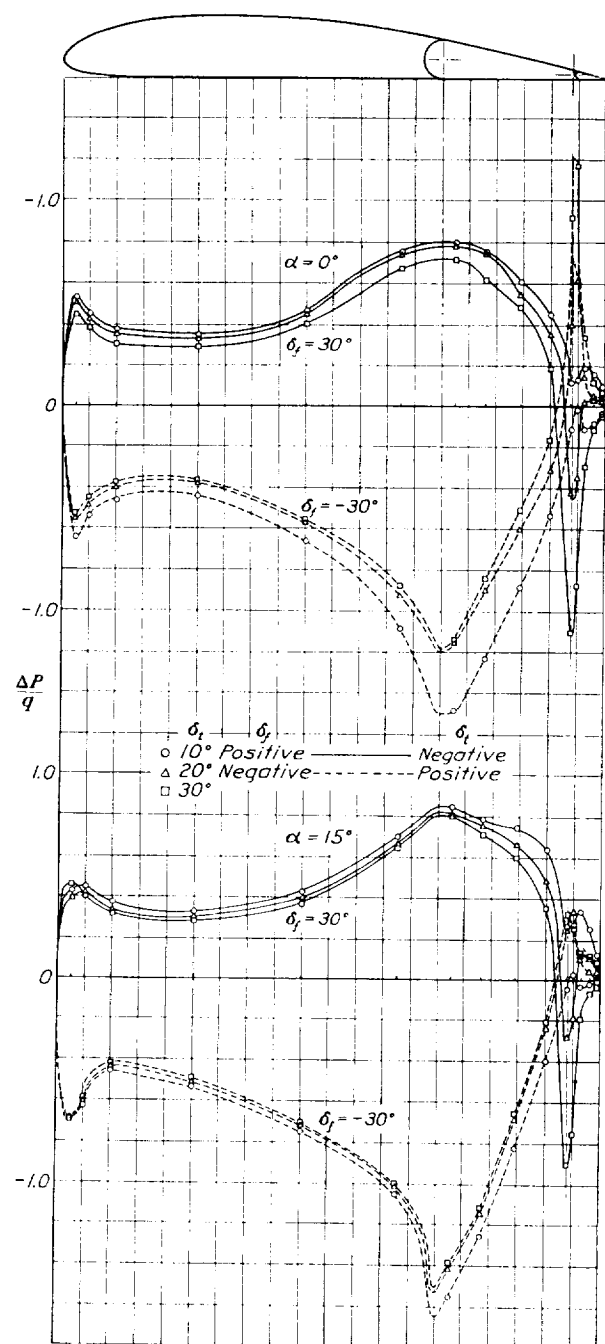


FIGURE 6.—Increments of resultant pressure due to combined tab and flap deflection. $\delta_t = \pm 30^\circ$.

deflections with given tab settings. With the tab deflected it will be noted that the curves are displaced parallel to the curve for the undeflected tab. This parallel nature of the curves shows that the variation of increments with flap deflection, considered with respect to any given initial tab deflection, is independent of tab deflection. At 30° deflection of the tab, however, the effectiveness of the tab appears to have been considerably reduced so that tab deflections of 20° should not be exceeded with the arrangements tested.

Increments to the basic values of flap section normal-force and hinge-moment coefficients are plotted in figure 9 for various flap deflections with given tab settings. The curves for the tab-deflected condition are displaced parallel to the curve for the undeflected tab, as was the case for the airfoil section increments. The variation of the flap increments with flap deflec-

Lift coefficient of airfoil:

$$C_L = \frac{dC_L}{d\alpha} \left(\alpha' + \frac{\partial \alpha}{\partial \delta_f} \delta_f + \frac{\partial \alpha}{\partial \delta_t} \delta_t \right) \quad (1)$$

Pitching-moment coefficient:

$$C_{m_{c/4}} = C_{m_0} + \frac{\partial C_m}{\partial \delta_f} \delta_f + \frac{\partial C_m}{\partial \delta_t} \delta_t \quad (2)$$

Hinge-moment coefficient of flap:

$$C_{h_f} = C_{h_{f_0}} + \frac{\partial C_{h_f}}{\partial C_L} C_L + \frac{\partial C_{h_f}}{\partial \delta_f} \delta_f + \frac{\partial C_{h_f}}{\partial \delta_t} \delta_t \quad (3)$$

Hinge-moment coefficient of tab:

$$C_{h_t} = C_{h_{t_0}} + \frac{\partial C_{h_t}}{\partial C_L} C_L + \frac{\partial C_{h_t}}{\partial \delta_f} \delta_f + \frac{\partial C_{h_t}}{\partial \delta_t} \delta_t \quad (4)$$

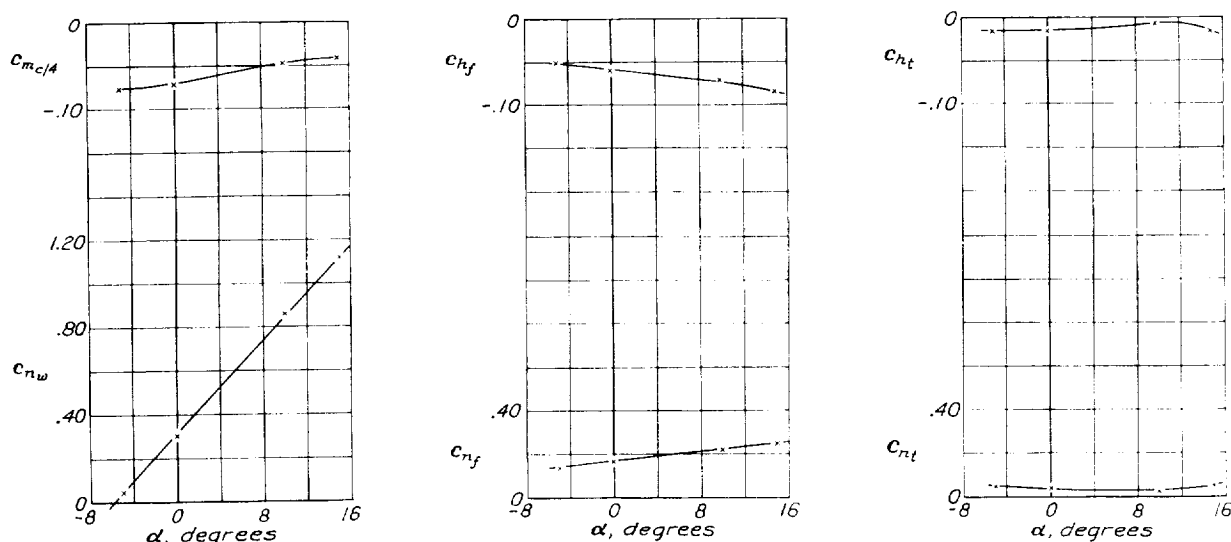


FIGURE 7.—Characteristics of the basic airfoil section. Tab and flap neutral.

tion for a given tab deflection are likewise independent of tab deflection.

Increments to the basic values of tab section normal-force and hinge-moment coefficients are given in figure 10 for various tab deflections with given flap settings. The curves for the flap-deflected condition are also displaced approximately parallel to the curve for the undeflected flap over the range of tab deflections from -20° to 20°. The curves show that the variation of increments with tab deflection for a given flap deflection is practically independent of flap deflection.

Comparison with theory.—Theoretical expressions for the lift, pitching moment, and hinge moment for a thin airfoil with any multiply hinged flap system have been derived by Perring (reference 3). The following relationships apply to a thin airfoil with a flap and a tab, N. A. C. A. absolute coefficients being used:

α' is the angle of attack of the main portion of the airfoil measured from zero lift of the undeformed section. (All angles are measured in radians.)

C_{m_0} , $C_{h_{f_0}}$, and $C_{h_{t_0}}$ are moment coefficients at zero lift of the undeformed airfoil.

Parameters $\frac{\partial \alpha}{\partial \delta_f}$, $\frac{\partial \alpha}{\partial \delta_t}$, $\frac{\partial C_m}{\partial \delta_f}$, $\frac{\partial C_m}{\partial \delta_t}$, $\frac{\partial C_{h_f}}{\partial C_L}$, $\frac{\partial C_{h_t}}{\partial C_L}$, $\frac{\partial C_{h_f}}{\partial \delta_f}$, $\frac{\partial C_{h_t}}{\partial \delta_t}$, are given in figure 11.

Parameters $\frac{\partial C_{h_f}}{\partial \delta_t}$ and $\frac{\partial C_{h_t}}{\partial \delta_f}$ are given in figure 12.

The curves given in figures 11 and 12 correspond to those given in reference 3 except that the values have been calculated and the curves redrawn on the basis of N. A. C. A. absolute coefficients.

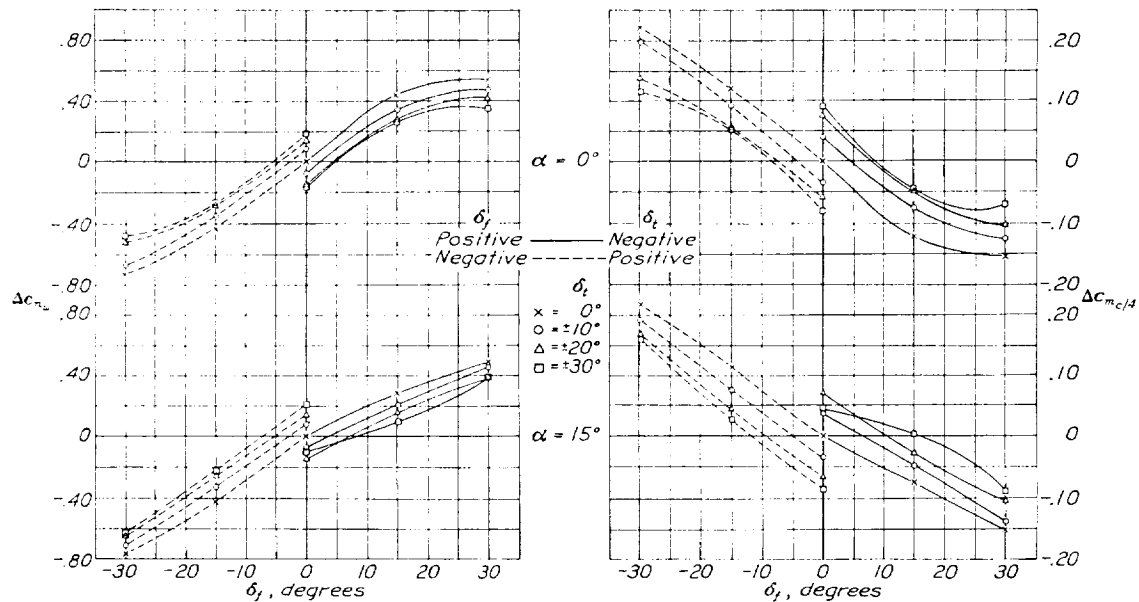


FIGURE 8.—Increments of airfoil section normal-force and pitching moment coefficients for various tab and flap deflections.

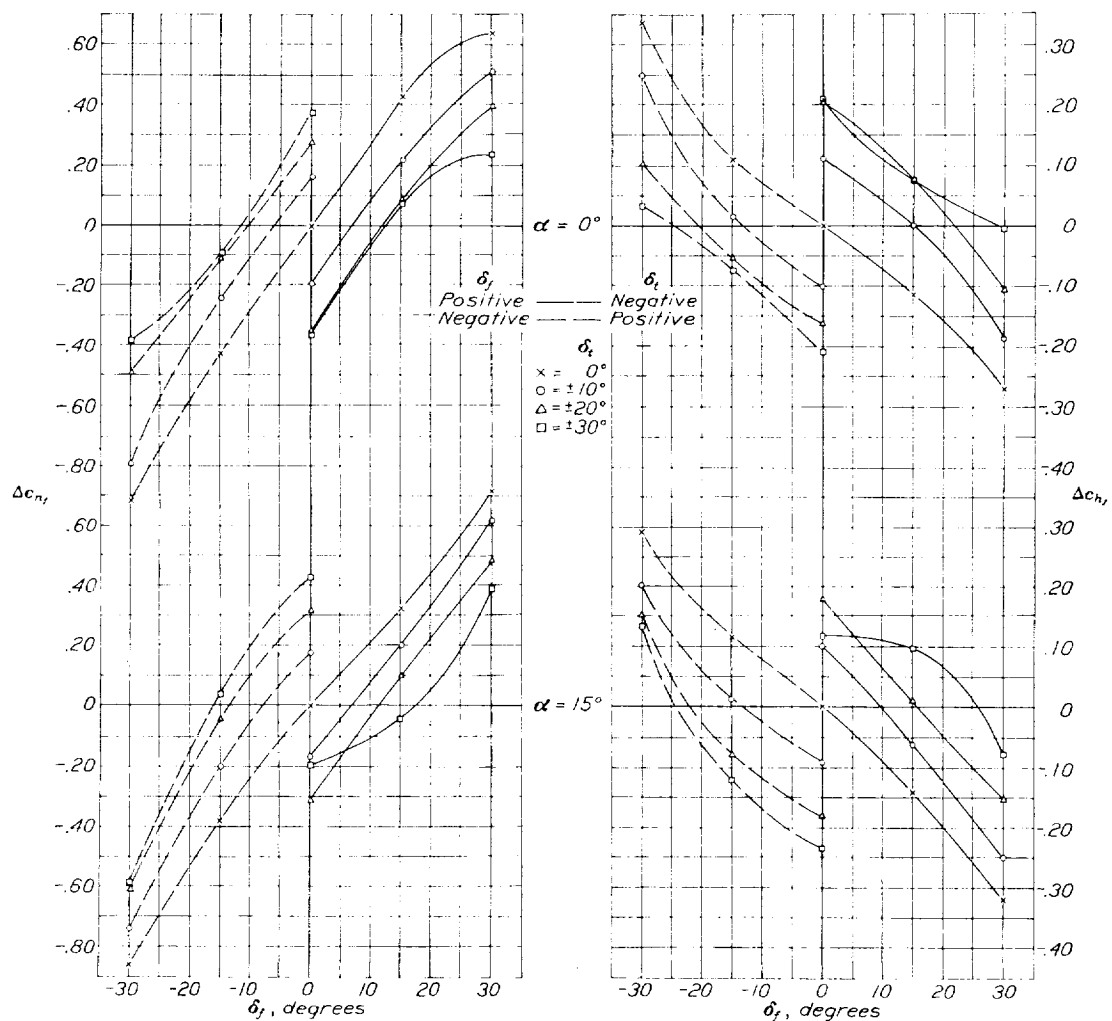


FIGURE 9.—Increments of flap normal-force and hinge-moment coefficients for various tab and flap deflections.

The theoretical and experimental values of airfoil section normal-force and pitching-moment coefficients are compared in figure 13. The data show that the theory agrees fairly well with experiment for flap deflections from 0° to $\pm 15^\circ$ with the tab neutral. Similar agreement was found in comparing data from reference 4 which deals with tests of a 30-percent-chord flap. Reference 5 also shows good agreement of theory with experiment for small angular deflections with flaps 20 percent of the airfoil chord. With the tab and flap both deflected, however, the present investigation shows that the theory indicates considerably greater

air near the trailing edge of the airfoil and is therefore unable to produce its full effect.

CONCLUSIONS

Based on the arrangement of airfoil section, flap, and tab tested, the following conclusions may be drawn:

1. Peak values of the increments of resultant pressures due to flap or to tab deflection occurred at the flap and tab hinges, respectively.
2. The variation of increments of airfoil section normal-force and pitching-moment coefficients and of flap normal-force and hinge-moment coefficients, due to

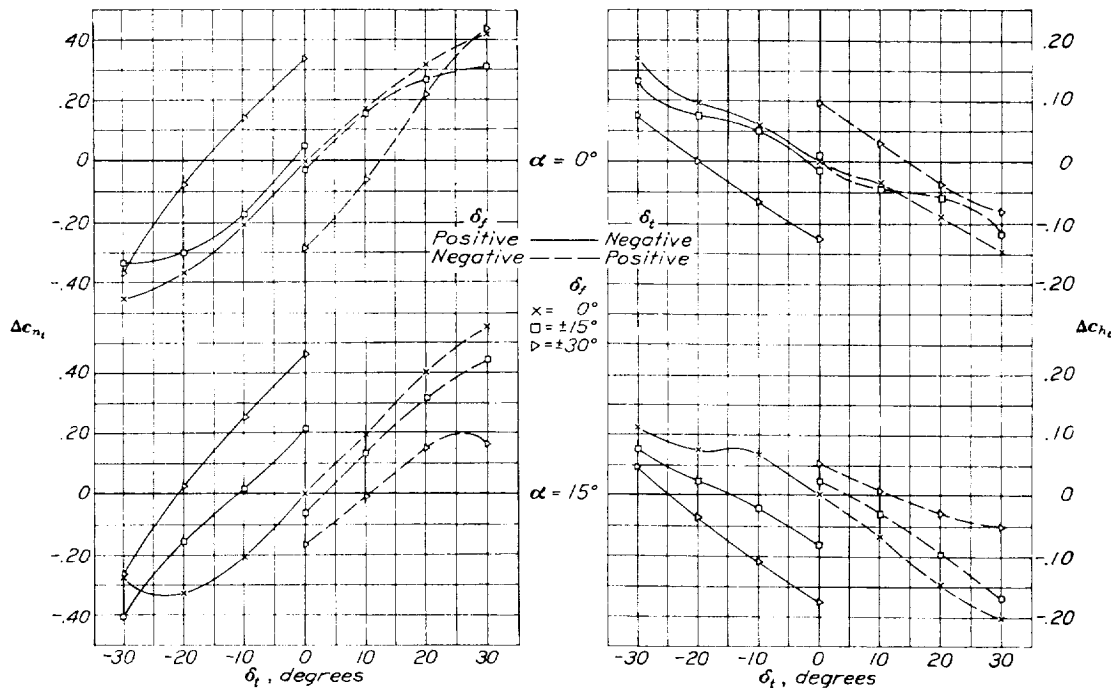


FIGURE 10.—Increments of tab normal-force and hinge-moment coefficients for various tab and flap deflections.

effects on the airfoil section normal-force and pitching-moment coefficients than are actually obtained by experiment.

Theoretical and experimental values of the flap hinge-moment coefficients are compared in figure 14. As in the case of the airfoil section coefficients, good agreement is shown between theory and experiment when the tab is neutral. With the tab deflected in a direction opposite to that of the flap, however, only one-half to two-thirds of the theoretical effect is obtained. Similar effects were shown by comparisons made in reference 6.

Values of the theoretical and experimental hinge-moment coefficients of the tab are compared in figure 15. This comparison shows a very poor agreement between theory and experiment, probably because of the small-chord tab (6 percent of the airfoil chord), which is operating in a somewhat turbulent region of

flap deflection with a given tab setting, was practically independent of the tab deflection.

3. The variation of increments of tab normal-force and hinge-moment coefficients with tab deflection for a given flap setting was practically independent of flap deflection.

4. Comparisons of the theoretical with the experimental forces and moments for the airfoil section with flap and tab shows that the theory agrees fairly well with experiment for small flap deflections with the tab neutral but that the theory indicates much greater effects than are actually obtained when the flap and tab are simultaneously deflected.

LANGLEY MEMORIAL AERONAUTICAL LABORATORY,
NATIONAL ADVISORY COMMITTEE FOR AERONAUTICS,
LANGLEY FIELD, VA., December 10, 1935.

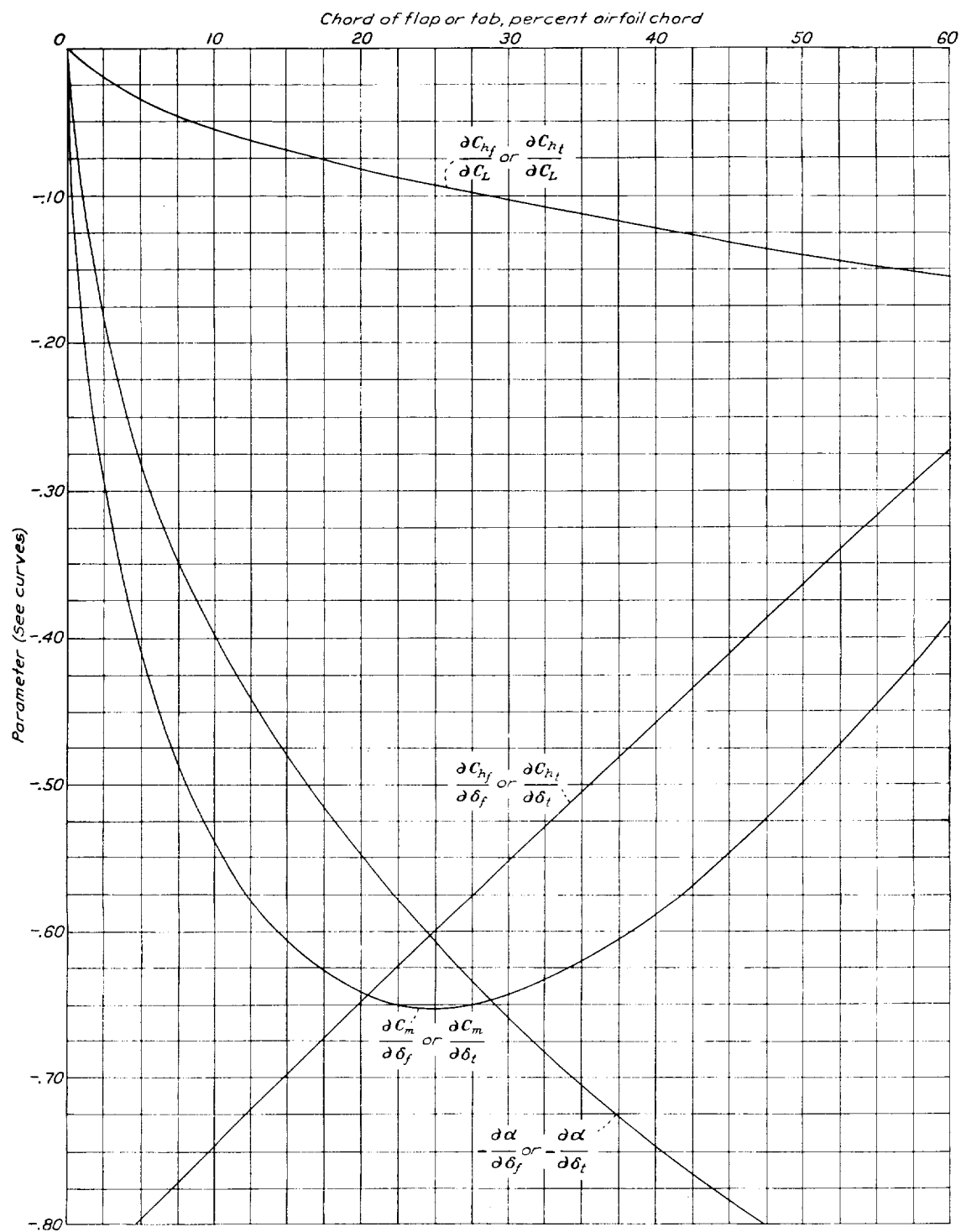


FIGURE 11.—Parameters for computing lift, pitching moment, and hinge moment.

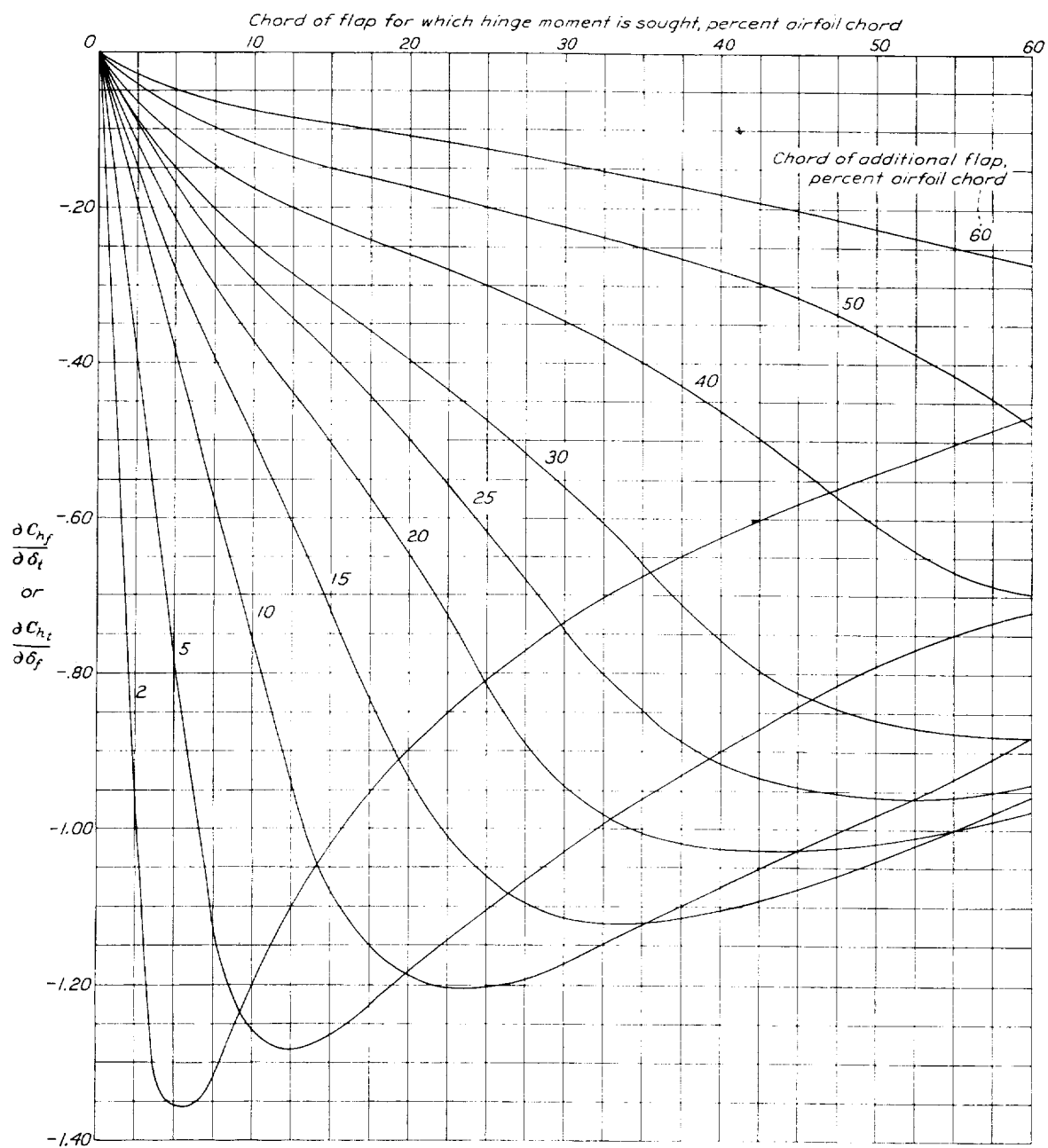


FIGURE 12.—Hinge-moment parameters. Increments in ratio of flap hinge moment to tab angle or tab hinge moment to flap angle.

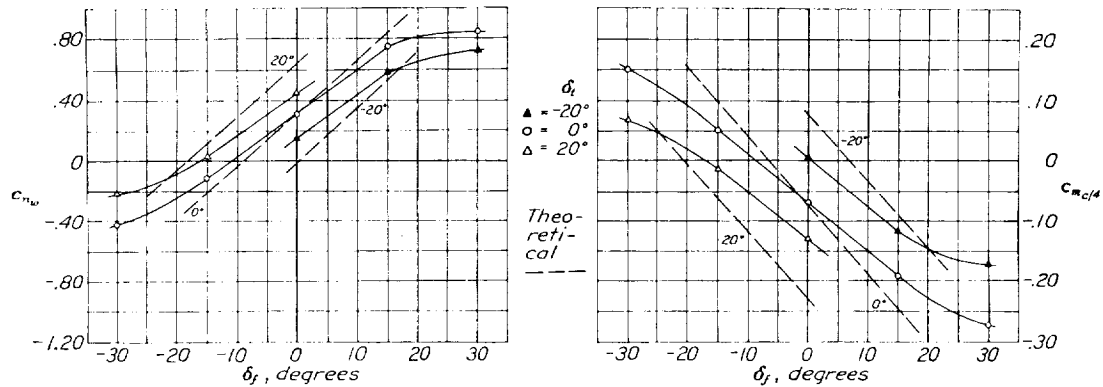


FIGURE 13.—Comparison of theoretical and experimental values of airfoil section normal-force and pitching moment coefficients. Clark Y section with flap and tab. $\alpha = 0^\circ$

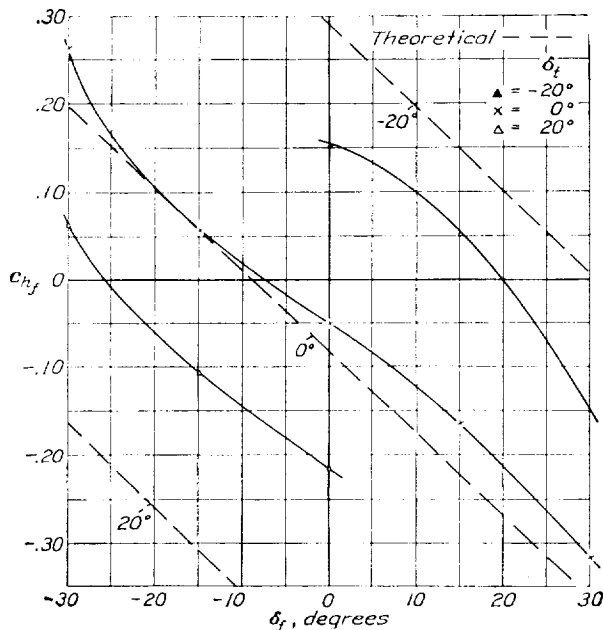


FIGURE 14.—Comparison of theoretical and experimental hinge-moment coefficients of flap with tab. Clark Y airfoil section. $C_L = 0.3$.

REFERENCES

1. Harris, Thomas A.: Reduction of Hinge Moments of Airplane Control Surfaces by Tabs. T. R. No. 528, N. A. C. A., 1935.
2. Harris, Thomas A.: The 7 by 10 Foot Wind Tunnel of the National Advisory Committee for Aeronautics. T. R. No. 412, N. A. C. A., 1931.
3. Perring, W. G. A.: The Theoretical Relationships for an Aerofoil with a Multiply Hinged Flap System. R. & M. No. 1171, British A. R. C., 1928.

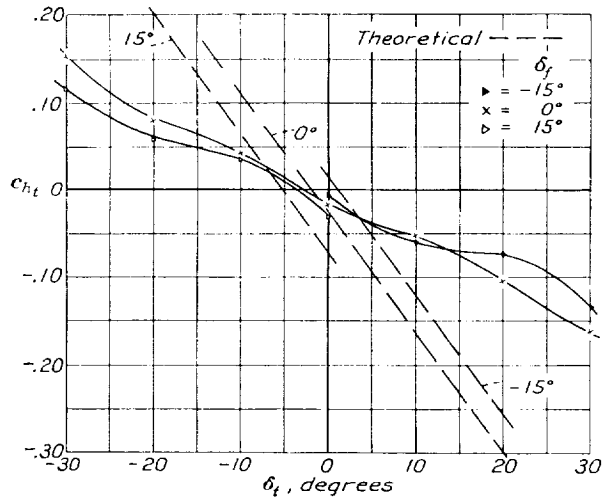


FIGURE 15.—Comparison of theoretical and experimental hinge-moment coefficients of tab. Clark Y airfoil section with flap and tab. $C_L = 0.3$.

4. Smith, R. H.: Lift, Drag, and Elevator Hinge Moments of Handley-Page Control Surfaces. T. R. No. 278, N. A. C. A., 1927.
5. Jacobs, Eastman N., and Pinkerton, Robert M.: Pressure Distribution over a Symmetrical Airfoil Section with Trailing Edge Flap. T. R. No. 360, N. A. C. A., 1930.
6. Lombard, A. E.: Control Surface Flaps for Trim and Balance. Jour. Aero. Sci., vol. 2, no. 1, January 1935 pp. 10-15.

REPORT No. 575

INTERFERENCE OF WING AND FUSELAGE FROM TESTS OF 28 COMBINATIONS IN THE N. A. C. A. VARIABLE-DENSITY TUNNEL

By ALBERT SHERMAN

SUMMARY

Tests of 28 wing-fuselage combinations were made in the variable-density wind tunnel as a part of the wing-fuselage interference program being conducted therein and in addition to the 209 combinations previously reported in N. A. C. A. Report No. 540. These tests practically complete the study of combinations with a rectangular fuselage and continue the study of combinations with a round fuselage and a tapered wing.

INTRODUCTION

An extensive wing-fuselage interference investigation has been undertaken in the N. A. C. A. variable-density wind tunnel as the second phase of a general program designed to cover the problem of interference. A discussion of this program is included in reference 1, which presents the basic part of the wing-fuselage interference investigation and contains test results for 209 combinations.

The present paper is a continuation of reference 1 and presents the results for some 28 additional wing-fuselage combinations that were indicated by the program outlined therein. The present tests practically conclude the study of combinations with a rectangular fuselage and continue the study of combinations with a round fuselage and a tapered wing. Future reports will cover further phases of the wing-fuselage interference investigation.

MODELS AND TESTS

The models employed for the combinations tested herein were those used in reference 1; they are the N. A. C. A. 0012 and the N. A. C. A. 4412 rectangular wings, the tapered N. A. C. A. 0018-09 wing, the round- and rectangular-section fuselages, the 9-cylinder radial engine, and the engine cowling. Fillets were carefully made up of plaster of paris as required.

The tests were of connected combinations only, 28 in all (see table V and figs. 8 to 11), and covered the effect of vertical displacement of the airfoil from the fuselage axis, k/c (see reference 1), the effect of fillets on various wings in combinations with the rectangular fuselage, and the effect of fillets and of a cowed engine on round-fuselage, tapered-wing combinations for various vertical wing positions. The wings were set in

combination at only one longitudinal location, $d/c=0$, and at zero incidence, $i_w=0$. (See figs. 1 to 7.) It should perhaps be mentioned here that the N. A. C. A. 4412 airfoil, because of its negative angle of zero lift, might be considered as having been at a positive angle of incidence, relative to the symmetrical airfoils.

The tests were run in the variable-density wind tunnel (reference 2) at a test Reynolds Number of approximately 3,100,000. In addition, values of maximum lift were obtained at a test Reynolds Number of approximately 1,400,000. The testing procedure and test precision, which are very much the same as for an airfoil, are fully described in reference 1. Since the tests of reference 1 were made, however, a small additional correction of less than -1 percent has been applied to the measurement of the dynamic pressure q as standard procedure to improve the precision of the results.

RESULTS

The test data are presented in the same manner as those of reference 1, in which the methods of analysis and presentation of the results are fully discussed.

Tables I and II present the characteristics of the wing and fuselage models separately (reference 1). Table III (continued from reference 1) presents the interference of the 28 wing-fuselage combinations. Table IV of reference 1 is not continued herein as no additional tests of disconnected combinations were made. Table V (continued from reference 1) presents the aerodynamic characteristics, combination descriptions, and profile diagrams of the combinations. In the present report, however, new values of the effective Reynolds Numbers at $C_{L_{max}}$ are given as a result of a new determination of the turbulence factor for the tunnel. The present turbulence factor for the variable-density tunnel is taken as 2.64, whereas a value of 2.4 was used in reference 1. The combinations in this report can be compared, however, with those in reference 1 on the basis of the test Reynolds Numbers, which remain the same.

Figures 1 to 7 show the polar characteristics of the interesting combinations investigated together with those of some combinations taken from reference 1 for comparison.

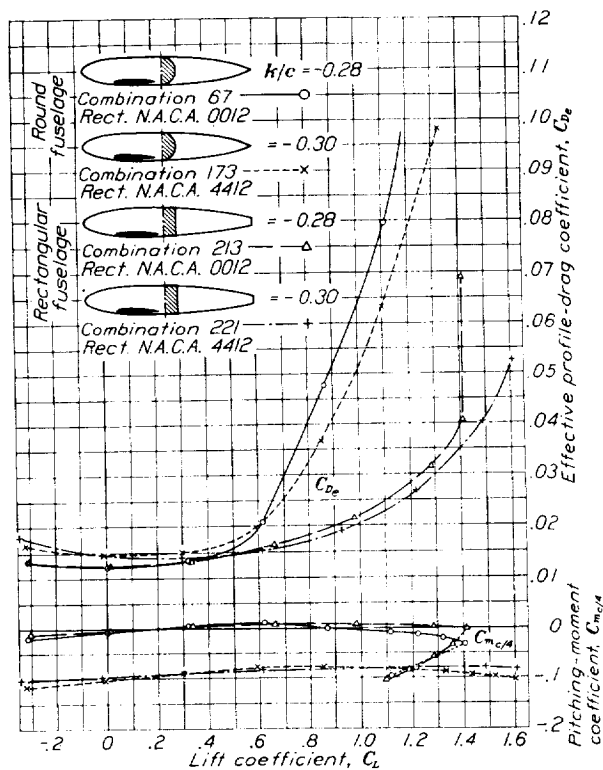


FIGURE 1.—Effect of fuselage section on wing-fuselage interference.

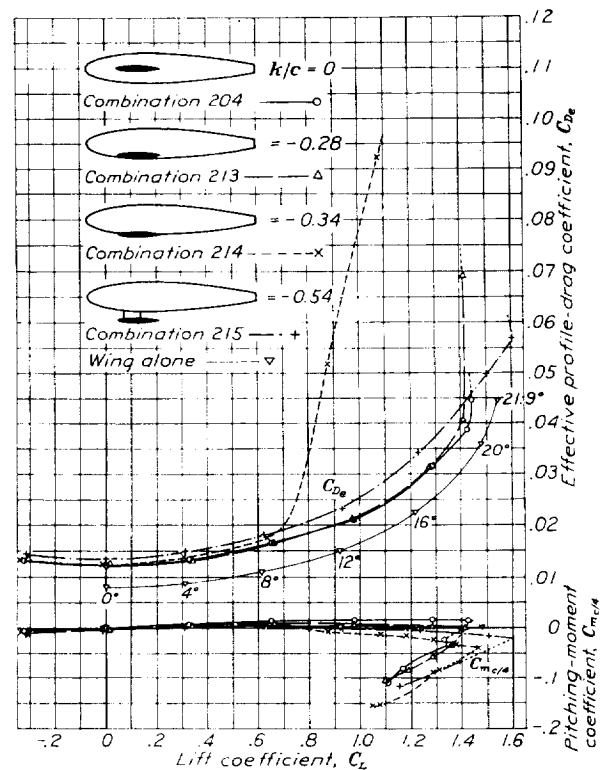
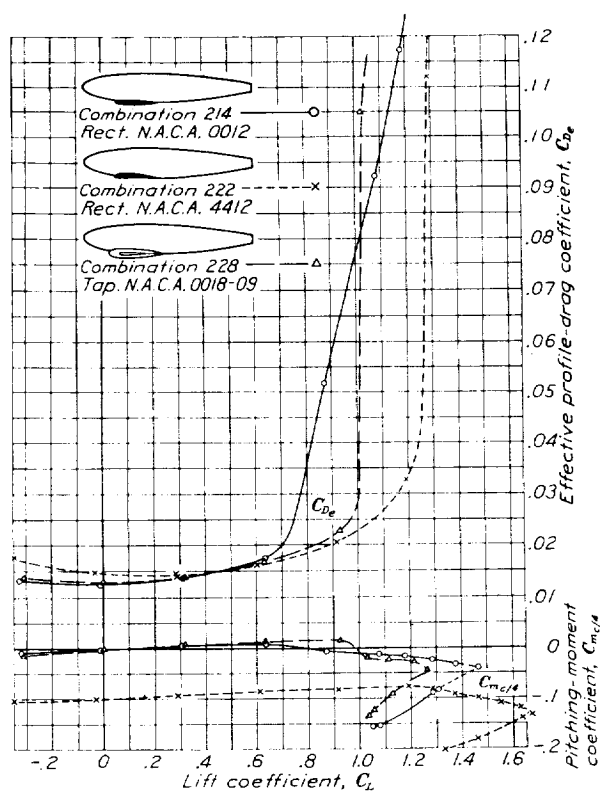
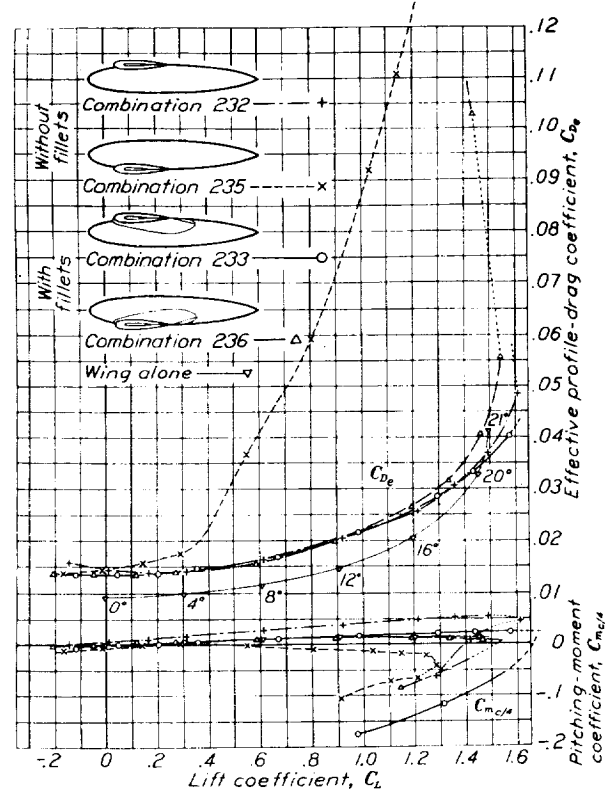


FIGURE 2.—Characteristics for various vertical wing positions. N. A. C. A. 0012 rectangular wing with rectangular fuselage.

FIGURE 3.—Characteristics for various wing shapes with rectangular fuselage; $k/c = -0.34$.FIGURE 4.—Effect of fillets on tapered-wing, round-fuselage combinations; $k/c = \pm 0.34$.

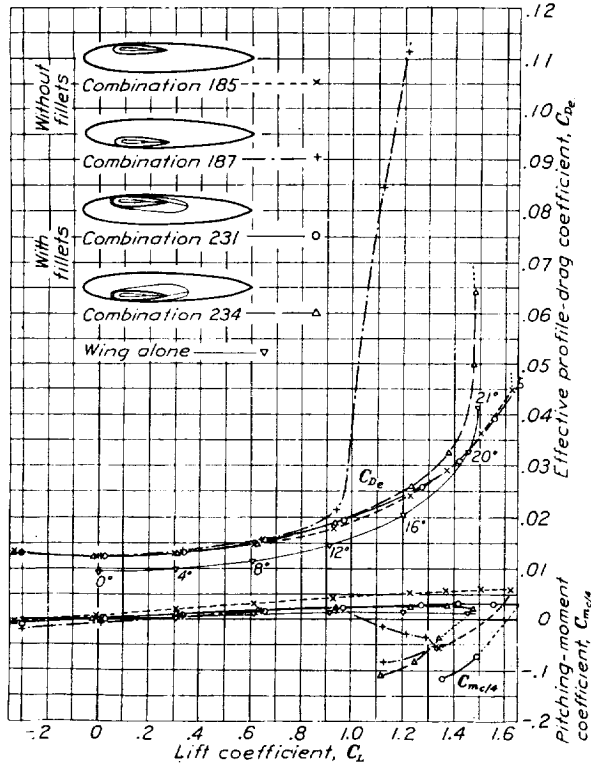


FIGURE 5.—Effect of fillets on tapered-wing, round-fuselage combinations; $k/c = \pm 0.22$.

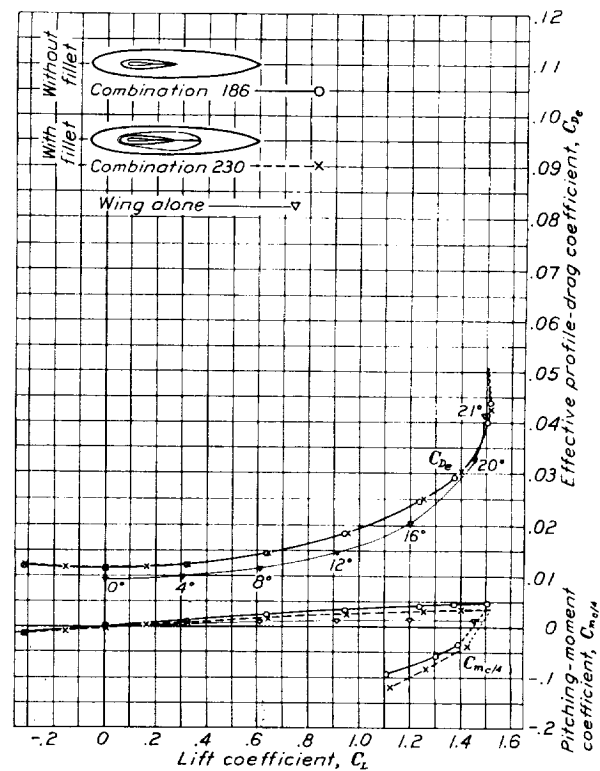


FIGURE 6.—Effect of fillets on tapered-wing, round-fuselage combinations; $k/c = 0$.

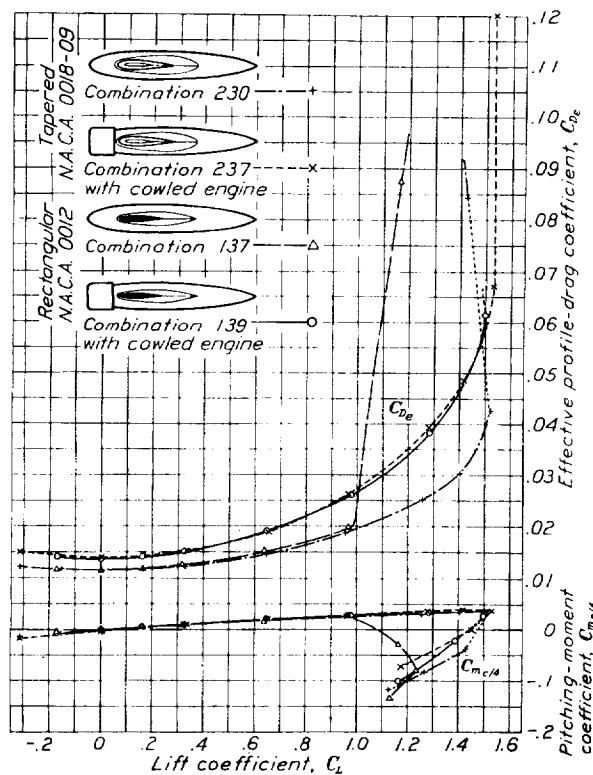


FIGURE 7.—Characteristics of cowled-engine, filleted combinations; $k/c = 0$.

DISCUSSION

Combinations with rectangular-section fuselage.—It was shown in reference 1 that the rectangular-section fuselage had a higher minimum drag than the round-section fuselage and that its drag, moreover, increased much more rapidly with angle of attack (table II). It was also shown, however, that when in combination with a wing the rectangular fuselage produced only a slightly greater drag increase with angle of attack than did the round fuselage, so that in its case the drag *interference* was generally more favorable. (See tables II and III.)

Low-wing combinations with the rectangular fuselage had generally better wing-root junctures than corresponding unfileted combinations with the round fuselage; there was less tendency to an early breakdown of the flow (see fig. 1), which is known as an "interference burble" (reference 1). Where an interference burble does occur for a combination with the round fuselage, substitution of the rectangular fuselage might result in a later-burbling combination having a drag almost as low as with the round fuselage and sometimes even lower (fig. 1).

Similar low-wing combinations with either fuselage showed approximately the same maximum lifts, but for midwing combinations with a rectangular wing the rectangular fuselage gave higher values.

Figure 2 shows the effect of the wing vertical position for the rectangular N. A. C. A. 0012 airfoil with the rectangular fuselage. As might be expected, there was little difference for combinations having the wing section wholly within the fuselage (tables III and V). The connected low-wing combination that exposed the leading edge of the wing exhibited an early flow breakdown but, surprisingly, no higher minimum drag than the others. The disconnected combination, in which no portion of the wing was shielded by the fuselage, had both a higher drag and higher maximum lift.

The rectangular fuselage had somewhat different interference when combined with differently shaped wings (table III). As previously shown in reference 1, the rectangular symmetrical N. A. C. A. 0012, the tapered symmetrical N. A. C. A. 0018-09, and the rectangular cambered N. A. C. A. 4412 wings were sensitive to the interference burble in the order named. This effect is very well demonstrated in figure 3, in which the three wings, combined in the only vertical position investigated that showed large interference, are compared. (See fig. 2.)

Fillets on rectangular-fuselage combinations had only a very small effect for the combinations investigated (tables III and V). Such a result was to be expected from the discussion in reference 1, which stated that fillets had only a small effect on combinations that were already fairly satisfactory.

Combinations with the round fuselage and tapered wing.—Figures 4, 5, and 6 present the polar characteristics of the tapered N. A. C. A. 0018-09 wing combined

with the round fuselage in various vertical positions both with and without fillets. The low-wing, unfileted combinations exhibited characteristic interference burlbles occurring progressively earlier as the wing was moved downward. Fillets eliminated this condition but the increase in minimum drag, as the wing departs from the midwing position, that operated for the unfileted combinations, held for the fileted combinations (table V). In the midwing and high-wing positions, fillets had very little effect except where an early interference burble at negative lifts produced an increase in the minimum drag. For such a combination, fillets served to reduce the minimum drag by eliminating the causative burble (fig. 4). Maximum lifts, as in most other combinations, were higher for the high-wing than for the low-wing positions whether or not the wing junctions were fileted.

The effect of a cowled engine at the nose of a tapered-wing combination is compared in figure 7 with a similar combination with a rectangular symmetrical wing. In the low-lift range, before the interference burble for the rectangular wing occurred, the effect for both wing shapes was practically identical. The tendency of a cowl toward suppressing the interference burble was evidently effective, and the polar curves for both cowled-engine combinations are virtually the same.

If the "speed-range index," the ratio of the maximum lift to a high-speed drag (see reference 1), be used as a criterion for comparing the combinations investigated in this report, the rectangular fuselage combined with the rectangular N. A. C. A. 4412 airfoil in a connected high-wing position would appear surprisingly good, inasmuch as it has one of the highest indexes of the combinations without high-lift devices investigated thus far. This combination does not have an exceptionally low drag coefficient, but the maximum lift coefficient is unusually high. If consideration be given, however, to the employment of various high-lift devices, the relative merit of the combinations may be changed and the minimum drag coefficient be shown to have much greater weight. Other favorable combinations in this report are the high-wing, rectangular-fuselage, tapered-wing combination and the midwing and semihigh-wing, round-fuselage, tapered-wing combinations with fillets.

LANGLEY MEMORIAL AERONAUTICAL LABORATORY,
NATIONAL ADVISORY COMMITTEE FOR AERONAUTICS,
LANGLEY FIELD, VA., March 12, 1936.

REFERENCES

1. Jacobs, Eastman N., and Ward, Kenneth E.: Interference of Wing and Fuselage from Tests of 209 Combinations in the N. A. C. A. Variable-Density Tunnel. T. R. No. 540, N. A. C. A., 1935.
2. Jacobs, Eastman N., and Abbott, Ira H.: The N. A. C. A. Variable-Density Wind Tunnel. T. R. No. 416, N. A. C. A., 1932.

TABLE I.—AIRFOIL CHARACTERISTICS

Airfoil	C_L	C_{D_s}	$C_{m_{c/4}}$	C_L	C_{D_s}	$C_{m_{c/4}}$	C_L	C_{D_s}	$C_{m_{c/4}}$
	$\alpha = 0^\circ$			$\alpha = 4^\circ$			$\alpha = 12^\circ$		
Rectangular N. A. C. A. 0012.....	0.000	0.0080	0.000	0.307	0.0087	0.003	0.920	0.0150	0.004
Tapered N. A. C. A. 0018-09.....	.000	.0093	.000	.305	.0099	.006	.910	.0146	.013
	$\alpha = -4^\circ$			$\alpha = 0^\circ$			$\alpha = 8^\circ$		
Rectangular N. A. C. A. 4412.....	-0.006	0.0097	-0.089	0.298	0.0095	-0.087	0.899	0.0136	-0.084

TABLE II.—FUSELAGE CHARACTERISTICS



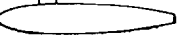

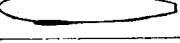
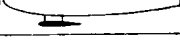
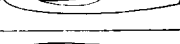
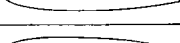
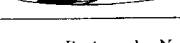

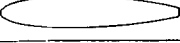
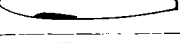
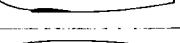
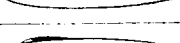
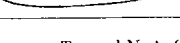


Fuselage	Engine	C_L	C_D	C_{m_p}	C_L	C_D	C_{m_p}	C_L	C_D	C_{m_p}	C_L	C_D	C_{m_p}	C_L	C_D	C_{m_p}
		$\alpha = 0^\circ$			$\alpha = 4^\circ$			$\alpha = 8^\circ$			$\alpha = 12^\circ$			$\alpha = 16^\circ$		
Round.....	None.....	0.000	0.0041	0.000	0.001	0.0042	0.016	0.005	0.0049	0.028	0.011	0.0062	0.035	0.019	0.0085	0.038
Do.....	Uncowled.....	.000	.0189	.000	.001	.0191	.015	.004	.0200	.027	.008	.0216	.037	.015	.0244	.041
Do.....	Cowled.....	.000	.0069	.000	.008	.0073	.013	.017	.0088	.025	.028	.0115	.035	.040	.0165	.044
Rectangular.....	None.....	.000	.0049	.000	.005	.0054	.009	.014	.0068	.015	.026	.0097	.018	.040	.0151	.015

¹ Pitching-moment coefficient about the quarter-chord point of the fuselage.

TABLE III.—LIFT AND INTERFERENCE, DRAG AND INTERFERENCE, AND PITCHING MOMENT AND INTERFERENCE OF FUSELAGE IN WING-FUSELAGE COMBINATIONS

Combination	ΔC_L	ΔC_{D_s}	$\Delta C_{m_{c/4}}$	ΔC_L	ΔC_{D_s}	$\Delta C_{m_{c/4}}$	ΔC_L	ΔC_{D_s}	$\Delta C_{m_{c/4}}$
	$\alpha = 0^\circ$			$\alpha = 4^\circ$			$\alpha = 12^\circ$		
210.....	-0.009	0.0043	0.003	0.001	0.0046	0.007	0.033	0.0079	0.015
211.....	.014	.0045	.002	.026	.0045	.005	.058	.0087	.014
212.....	.002	.0055	.005	.009	.0057	.007	.033	.0073	.011
213.....	.013	.0044	-.003	.027	.0045	.002	.057	.0064	.004
214.....	-.014	.0045	-.002	.001	.0051	.002	-.047	.0398	-.012
215.....	-.002	.0055	-.005	.003	.0062	-.002	.009	.0083	-.004
216.....	-.009	.0042	-.002	.015	.0043	.005	.049	.0058	.009
217.....	-.015	.0045	.005	-.002	.0045	.009	.036	.0073	.015
218.....	.015	.0045	-.005	.035	.0042	-.001	.068	.0061	-.001
	$\alpha = -4^\circ$			$\alpha = 0^\circ$			$\alpha = 8^\circ$		
219.....	-0.023	0.0037	-0.004	0.003	0.0034	0	0.038	0.0057	0.010
220.....	-.004	.0044	-.004	.018	.0036	0	.056	.0045	.009
221.....	-.019	.0048	-.010	-.002	.0044	-.005	.027	.0053	.002
222.....	-.025	.0050	-.012	-.010	.0045	-.006	.020	.0070	.002
223.....	-.027	.0049	-.006	-.006	.0043	-.002	.035	.0054	.011
224.....	-.006	.0039	-.005	.018	.0041	0	.053	.0050	.009
	$\alpha = 0^\circ$			$\alpha = 4^\circ$			$\alpha = 12^\circ$		
225.....	-0.006	0.0032	0.005	-0.001	0.0035	0.008	0.021	0.0064	0.019
226.....	.002	.0036	.004	.008	.0038	.008	.033	.0062	.015
227.....	.006	.0032	-.005	.024	.0034	-.003	.044	.0055	.002
228.....	-.002	.0036	-.004	.009	.0039	-.002	.017	.0081	.002
229.....	.003	.0033	-.002	.022	.0036	.004	.048	.0059	.011
230.....	.003	.0024	-.003	.023	.0024	.003	.042	.0040	.012
231.....	.022	.0031	0	.029	.0033	.002	.056	.0048	.010
232.....	.013	.0051	.007	.009	.0043	.011	.013	.0058	.025
233.....	.046	.0043	0	.054	.0048	0	.077	.0070	.004
234.....	.022	.0031	0	.001	.0032	.005	.024	.0044	.010
235.....	-.013	.0051	-.007	-.012	.0077	-.004	-.102	.0448	-.022
236.....	-.046	.0043	0	-.031	.0041	.001	-.017	.0053	-.001
237.....	.002	.0048	-.003	.025	.0055	.004	.055	.0117	.017

TABLE V.—PRINCIPAL AERODYNAMIC CHARACTERISTICS OF WING-FUSELAGE COMBINATIONS

Diagrams representing combinations	Combination	Remarks	Longitudinal position d/c	Vertical position k/c	Wing setting i_w	Lift-curve slope (per degree) at A. R. = 6.86	Span efficiency factor e	$C_{D_{max}}$	$C_{L_{opt}}$	Aerodynamic center position x_0	C_{m_0}	Lift coefficient at interference burble $^{1/2}C_{L_{b}}$	$^{1/2}C_{L_{max}}$ effective R. N. = 8.2×10^4	$^{1/2}C_{L_{max}}$ effective R. N. = 3.7×10^5
Rectangular N. A. C. A. 0012 airfoil with rectangular fuselage														
		Wing alone.....			Degrees	0.077	0.85	0.0080	0.00	0.010	0.000	A 1.5	c 1.54	e 1.39
210 	210		0.00	0.28	0	.080	.80	.0123	.00	.019	.003	A 1.3	b 1.33	b 1.31
211 	211		0	.34	0	.080	.85	.0126	.07	.021	.001	A 1.4	c 1.40	c 1.32
212 	212	Thin connecting plate (same as combination 149).....	0	.54	0	.079	.85	.0135	.04	.016	.005	A 1.6	c 1.64	c 1.46
213 	213		0	-.28	0	.080	.85	.0123	.00	.021	-.003	A 1.4	b 1.41	b 1.39
214 	214		0	-.34	0	.080	.80	.0126	-.07	.018	-.001	B 1.6	c 1.46	c 1.33
215 	215	Same as combination 212.....	0	-.54	0	.078	.80	.0135	-.04	.018	-.005	A 1.6	c 1.60	c 1.46
216 	216	Tapered fillets.....	0	.00	0	.081	.85	.0121	.00	.024	.000	A 1.5	c 1.52	c 1.41
217 	217	do.....	0	.28	0	.081	.80	.0122	-.03	.022	.005	A 1.3	b 1.30	c 1.33
218 	218	do.....	0	-.28	0	.082	.85	.0122	.03	.023	-.005	A 1.4	c 1.46	c 1.43
Rectangular N. A. C. A. 4412 airfoil with rectangular fuselage														
		Wing alone.....				.076	.90	.0094	.22	.006	-.089	A 1.6	A 1.64	A 1.51
219 	219		0	0.26	0	.080	.85	.0128	.30	.018	-.093	A 1.7	A 1.72	A 1.62
220 	220		0	.34	0	.080	.90	.0131	.31	.018	-.093	A 1.6	A 1.68	A 1.57
221 	221		0	-.30	0	.080	.85	.0139	.22	.021	-.098	A 1.6	A 1.67	A 1.57
222 	222		0	-.34	0	.080	.85	.0142	.24	.022	-.101	B 1.2	b 1.67	A 1.57
223 	223	Tapered fillets.....	0	.00	0	.081	.85	.0137	.29	.024	-.095	A 1.6	b 1.69	b 1.57
224 	224	Leading-edge fillets.....	0	.34	0	.080	.90	.0133	.15	.018	-.093	A 1.6	A 1.67	A 1.60
Tapered N. A. C. A. 0018-0009 airfoil with rectangular fuselage														
		Wing alone.....				.077	.90	.0093	.00	.020	.000	A 1.4	c 1.48	c 1.23
225 	225		0	0.22	0	.078	.85	.0124	.00	.030	.005	A 1.6	c 1.62	A 1.31
226 	226		0	.34	0	.078	.85	.0128	-.01	.027	.004	A 1.4	A 1.49	A 1.34

¹ Letters refer to types of drag curves associated with the interference burble. See footnote 1, p. 7.
² Letters refer to condition at maximum lift as follows: a, reasonably steady at CL_{max} ; b, small loss of lift beyond CL_{max} ; c, large loss of lift beyond CL_{max} ; and uncertain value of CL_{max} .

³ Poor agreement in high-speed range.

⁴ Poor agreement over whole range.

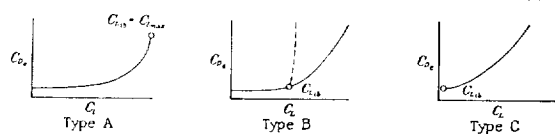
⁵ Poor agreement in high-lift range.

⁶ Rapid increase in drag preceding definite breakdown.

TABLE V.—PRINCIPAL AERODYNAMIC CHARACTERISTICS OF WING-FUSELAGE COMBINATIONS—Continued

Diagrams representing combinations	Combination	Remarks	Longitudinal position d/c	Vertical position k/c	Wing setting i_w	Lift-curve slope (per degree) a A. R. = 6.86	Span efficiency factor e	$C_{D_{min}}$	$C_{L_{opt}}$	Aerodynamic-center position x_0	C_{m_0}	Lift coefficient at interference burble $^1 C_{L_{ib}}$	$^2 C_{L_{max}}$ effective R. N. = 8.2×10^5	$^3 C_{L_{max}}$ effective R. N. = 3.7×10^6
Tapered N. A. C. A. 0018-0009 airfoil with rectangular fuselage Continued														
227	227		0	-.22	Degrees 0	.080	4.90	.0124	.00	.027	-.005	Δ 1.5	ϵ 1.51	Δ 1.27
228	228		0	-.34	0	.079	4.80	.0128	.01	.023	-.004	Δ 1.9	ϵ 1.26	Δ 1.10
229	229	Tapered fillets.....	0	.00	0	.079	.85	.0127	.00	.030	.000	Δ 1.5	ϵ 1.53	Δ 1.26
Tapered N. A. C. A. 0018-0009 airfoil with round fuselage														
230	230	Tapered fillets.....	0	0.00	0	.080	4.85	.0117	.00	.026	.000	Δ 1.5	ϵ 1.52	Δ 1.27
231	231	do.....	0	.22	0	.079	4.85	.0124	.00	.023	-.001	Δ 1.6	ϵ 1.65	Δ 1.37
232	232		0	.34	0	.076	.85	.0139	.17	.034	.006	Δ 1.6	ϵ 1.61	Δ 1.31
233	233	Tapered fillets.....	0	.34	0	.078	.85	.0135	-.07	.027	-.003	Δ 1.6	ϵ 1.69	Δ 1.38
234	234	do.....	0	-.22	0	.080	4.90	.0124	.00	.028	.001	Δ 1.4	ϵ 1.48	Δ 1.22
235	235		0	-.34	0	.076	4.60	.0139	-.17	.028	-.006	Δ 1.3	ϵ 1.28	Δ 1.09
236	236	Tapered fillets.....	0	-.34	0	.080	4.90	.0135	.07	.024	.003	Δ 1.5	ϵ 1.54	Δ 1.22
237	237	Tapered fillets and cowled engine.....	0	.00	0	.080	.80	.0142	.00	.040	-.003	Δ 1.5	ϵ 1.53	Δ 1.28

¹ Letters refer to types of drag curves associated with the interference burble as follows:



² Letters refer to condition at maximum lift as follows: a, reasonably steady at $C_{L_{max}}$; b, small loss of lift beyond $C_{L_{max}}$; c, large loss of lift beyond $C_{L_{max}}$ and uncertain value of $C_{L_{max}}$.

³ Poor agreement in high-speed range.

⁴ Poor agreement over whole range.

⁵ Poor agreement in high-lift range.

⁶ Rapid increase in drag preceding definite breakdown.

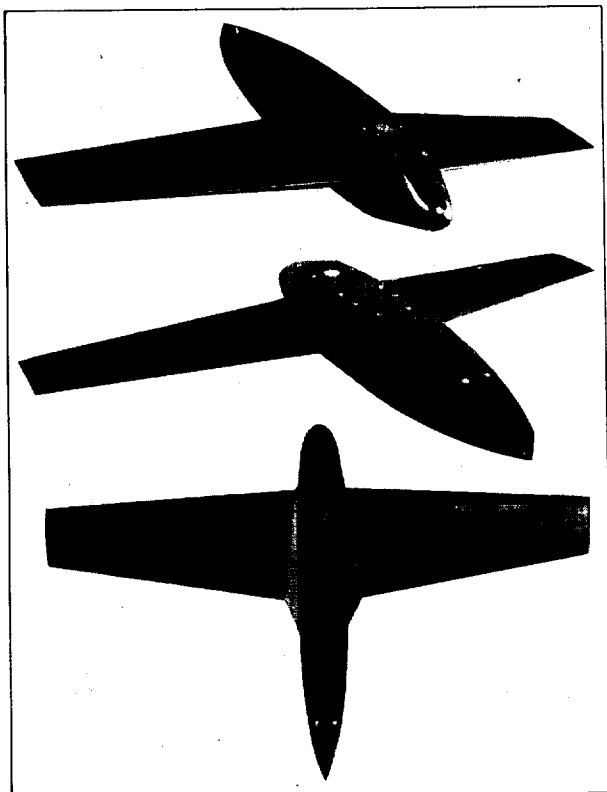


FIGURE 8.—Combination 229, showing tapered fillets.

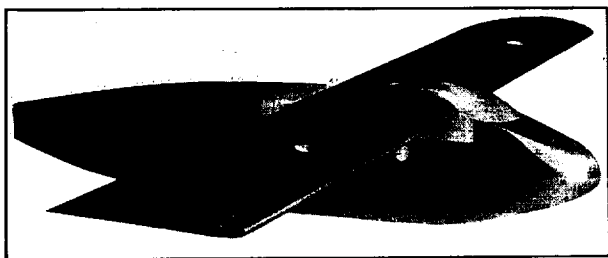


FIGURE 9.—Combination 224, showing a leading-edge fillet in the shape of a windshield

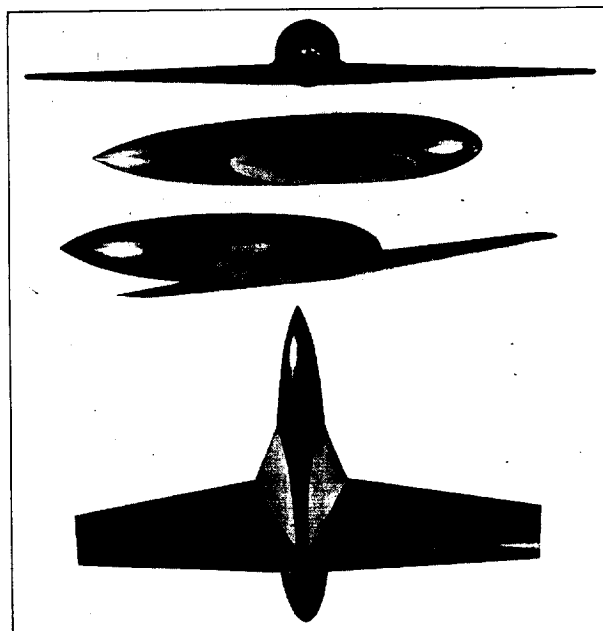


FIGURE 10.—Combination 234 (combination 231 inverted) showing tapered fillets.

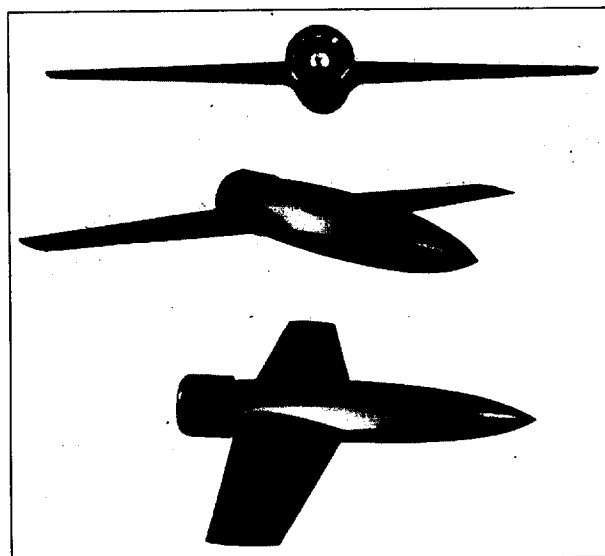


FIGURE 11.—Combination 237 showing a cowled engine and tapered fillets.

REPORT No. 576

AIRCRAFT ACCIDENTS

NATIONAL ADVISORY COMMITTEE FOR AERONAUTICS,
Washington, D. C., June 22, 1936.

GENTLEMEN:

As a result of the recent rapid advances in aeronautics, the need has arisen for the revision of Technical Report No. 357 "Aircraft Accidents—Method of Analysis" in which is presented an analysis method that has been for a number of years the standard method used by the War, Navy, and Commerce Departments. Since the publication of this report questions of interpretation of some of the definitions have arisen and incidents have occurred for which the specified classifications seemed inadequate. A revision of the report has therefore been prepared by the Committee on Aircraft Accidents in order to meet these conditions.

The revision of the report was conducted at a series of thirteen meetings, the first of which was held on October 30, 1935. At these meetings the form of the analysis chart and the classifications shown on the chart were carefully considered, as well as the definitions.

In accordance with resolution adopted at a meeting of the Committee on Aircraft Accidents held this date, I have the honor to recommend that the attached report be published as a technical report of the National Advisory Committee for Aeronautics, to supersede Technical Report No. 357.

Respectfully,

COMMITTEE ON AIRCRAFT ACCIDENTS,
EDWARD P. WARNER, *Chairman.*

THE EXECUTIVE COMMITTEE
National Advisory Committee for Aeronautics
Washington, D. C.

REPORT No. 576

AIRCRAFT ACCIDENTS

METHOD OF ANALYSIS

Report prepared by Committee on Aircraft Accidents

INTRODUCTION

PURPOSE AND HISTORY

This report is a revision of Technical Report No. 357, prepared by the Committee on Aircraft Accidents and published in 1930. The original report of the National Advisory Committee for Aeronautics on the analysis of aircraft accidents, of which Report No. 357 was the first revision, was prepared by a Special Committee on the Nomenclature, Subdivision, and Classification of Aircraft Accidents, and issued as Technical Report No. 308 of the National Advisory Committee for Aeronautics. The special committee was organized by the National Advisory Committee for Aeronautics in response to a request dated February 18, 1928, from the Air Coordination Committee, which consisted of the Assistant Secretaries for Aeronautics in the Departments of War, Navy, and Commerce. The request of the Air Coordination Committee was made "in order that practices used may henceforth conform to a standard and be universally comparable." The task of the special committee was, therefore, to prepare a basis for the classification and comparison of aircraft accidents, both civil and military.

The report of the special committee was approved by the Executive Committee of the National Advisory Committee for Aeronautics on October 3, 1928, and on recommendation of the National Advisory Committee the method of analysis outlined in the report was adopted for official use by the War, Navy, and Commerce Departments. As a result of recommendation of the special committee, a standing Committee on Aircraft Accidents was established for the consideration of questions regarding interpretation of the report and suggestions as to changes, and of such other questions relating to aircraft accidents as might arise from time to time.

Since the publication of the original report, the practical value of the method of accident analysis has been definitely proved by its use in the War, Navy, and Commerce Departments. However, during the first 2 years questions of interpretation of some of the definitions arose and incidents occurred for which the

specified classifications seemed inadequate. In order to meet these conditions Report No. 357 was prepared by the Committee on Aircraft Accidents. The recent rapid advances in aeronautics have resulted in the need for further revision, and this report has accordingly been prepared to supersede Report No. 357.

The membership of the Committee on Aircraft Accidents is as follows:

Representatives of the National Advisory Committee for Aeronautics:

Hon. Edward P. Warner, Chairman.
Dr. George W. Lewis.

Representatives of the Army Air Corps:

Capt. Lowell H. Smith, United States Army.
Captain E. V. Harbeck, United States Army.

Representatives of the Bureau of Aeronautics of the Navy:

Lt. Comdr. A. O. Rule, United States Navy.
Lt. S. B. Dunlap, United States Navy.

Representatives of the Bureau of Air Commerce:

Mr. Jesse W. Lankford.
Mr. J. T. Shumate.

GENERAL CONSIDERATIONS

DEFINITION OF AN AIRCRAFT ACCIDENT

An aircraft accident is an occurrence which takes place while an aircraft is being operated as such, as a result of which a person or persons are injured or killed or the aircraft receives appreciable or marked damage as a result of a failure of the aircraft structure or engine or through the forces of external contact, or through fire. For the purpose of analysis an aircraft is considered as "being operated as such" from the time the pilot or passengers board the aircraft with the intention of flight until such time as the pilot and passengers disembark from the aircraft upon completion of flight.

A collision of two or more aircraft should be analyzed and reported statistically as one accident. It is appreciated that in some cases, as where a collision involves two aircraft of different services, it will necessarily appear in two separate accident reports and that a certain amount of duplication in tabulation will inevitably be involved. In such a case each service involved will credit to its own account only those personnel injuries or fatalities occurring in the aircraft for which it is individually responsible.

AIRCRAFT ACCIDENT ANALYSIS FORM

In drawing up the aircraft accident analysis form and the accompanying definitions the committee had in mind the frequency rate of accidents from the various causes, the logical lines along which studies should be conducted, and the ease with which these studies can be made from this chart. It is recognized that to make a detailed study of accidents due to any one cause a further subdivision may be necessary. However, if all accidents are classified according to this chart the major causes can be easily determined and further investigation can be readily carried out for the purpose of eliminating these causes.

It was also recognized, in working out this chart, that the division of immediate causes between personnel and material as set forth in the chart and definitions was more or less arbitrary, since all defects of aircraft can in the last analysis be attributed to errors of personnel, whether in operation, inspection, maintenance, manufacture, or design. Since the purposes of the accident study seemed to be best served by drawing attention to defects of material, even though traceable ultimately to personnel errors, the line between personnel and material in the immediate causes was drawn at the operating or maintenance personnel of the aircraft. In other words, under the main heading "Personnel" there are included only those accidents for which personnel engaged in the operation or maintenance of the aircraft are responsible. Accidents due to material failure are classified under "Material" even though personnel charged with design, construction, or overhaul may be held responsible for the failure. Errors due to personnel other than those immediately accessory to the operation of the aircraft are shown in the "Underlying causes" or "Cross analysis", as set forth hereinafter, rather than in the main headings of immediate causes.

The plan as drawn up by the committee is not in any sense final or complete, but is presented to provide a working basis for the study of aircraft accidents from all sources.

WEIGHTING OF ACCIDENTS

Where two or more factors cause an accident, part will be charged to each; for example, in the case of an avoidable accident following an engine failure the responsibility for the accident might be considered to be equally divided between the pilot and the power plant, in which case 50 percent would be charged to "Personnel" and 50 percent to "Material." If the responsibility for the accident rested largely upon the pilot, "Personnel" would be charged with 60, 70, or 80 percent of the accident, or even more, depending upon the degree of responsibility decided upon. Conversely, in the above cases "Material" and "Miscellaneous" would be charged with a total of 40, 30, or 20 percent of the accident. This same division of responsibility might be carried out under "Personnel"

or other subheads. However, in the particular case cited "Errors of pilot" would be the only division of "Personnel" which could be charged with this accident. If 80 percent of the accident were charged to "Personnel" in the above instance, then 80 percent of the accident would be charged to "Errors of pilot." Then, assuming that the responsibility for such piloting error rested jointly upon error of judgment and poor technique, a still further subdivision would be made and 40 percent of the accident would be charged to "Error of judgment" and 40 percent to "Poor technique." Thus the factors of each crash could be traced down to the last subdivision under any heading and weighted in accordance with their importance.

CLASSIFICATION OF ACCIDENTS

For the purpose of comparative study aircraft accidents may be divided into groups of accidents of the same general characteristics. Accident prevention must be regarded as the primary purpose of aircraft accident study. Studies of accident causes point out needed remedies more clearly when they are supplemented by certain studies based upon the nature and results of the accident.

For example, in both bad landings and tail spins the principal cause is usually errors of the pilot. Statistics based upon the study of causes merely show that pilots' errors are responsible for more than half of all accidents, and the formulation of remedies for the situation appears difficult. If, however, the same accidents are classified according to their nature and results, it is found that the tail spin is the kind of accident that is by far the most prevalent among those which produce fatal consequences. It is apparent that new designs which decrease the tendency of airplanes to spin, or new training methods which increase the ability of pilots to avoid falling into spins and to recover from them quickly, will have a marked influence toward the prevention of fatal accidents.

Likewise, the study based upon nature and results indicates, in the case of collisions, that this kind of accident is third in importance among those which produce fatal results, and that these accidents are much more prevalent during winter months than in summer; and while remedies are not so obvious as in the case of tail spins some lines of attack immediately suggest themselves.

The following classifications for study of accidents according to their nature are recommended:

I. NATURE OF THE ACCIDENT

Under this head accidents are classified according to the type of accident which occurs.

1. *Class A—Collisions in full flight with other aircraft.*—This includes collisions with airplanes, balloons, or other aircraft while the colliding aircraft is at flying speed or at an altitude which permits free maneuvering.

It excludes collisions on the ground while taxiing, taking off, or landing. (See classes F and G.)

2. *Class B—Collisions in full flight with objects other than aircraft.*—This includes collisions while at flying speed and with engine functioning normally, with birds, towing lines, towed sleeves, trees, poles, wires, houses, mountain sides, or other objects. It includes collisions with the earth or water by diving. It excludes collisions on the ground while taxiing, taking off, or landing. It excludes accidents to an aircraft caused by parts of the same aircraft becoming detached in flight and flying back or striking other parts of the aircraft. (See classes F and G.)

3. *Class C—Spins or stalls following engine failure.*—This includes spins, stalls, and all collisions with the earth while the airplane is out of control due to loss of flying speed following engine failure.

4. *Class D—Spins or stalls without engine failure.*—This includes spins, stalls, and all collisions with the earth while the airplane is out of control following loss of flying speed, with the engine functioning normally. It includes spins due to defective handling qualities of the airplane.

5. *Class E—Forced landings.*—This covers accidents while making landings necessitated by conditions which could not be overcome while in flight.

Class E (1)—Emergency forced landings.—This covers accidents while making landings immediately necessitated by conditions which could not be overcome while in flight.

Class E (2)—Deferred forced landings.—This covers accidents while making landings necessitated by conditions which could not be overcome while in flight and which make continued flight inadvisable but do permit a reasonable time for the selection of a landing area.

6. *Class F—Landing accidents.*—This includes accidents occurring while the pilot is in the act of making a voluntary landing. It excludes forced landings, accidents while examining a field from the air or approaching it for a landing, and carrier, platform, and arresting-gear accidents.

7. *Class G—Take-off accidents.*—This includes accidents occurring between the time of starting the take-off and the time when flying speed permitting normal control has been attained with sufficient altitude to permit free maneuvering.

8. *Class H—Taxiing accidents.*—This includes accidents which occur while the aircraft is being operated as such and is maneuvering under its own power on land or water.

9. *Class I—Fires.*—This includes all accidents in which fires occur while the aircraft is being operated as such. It excludes fires which are the result of collision.

Class I (1)—Fires in the air.—This includes all accidents in which fires occur while the aircraft is being operated as such in the air.

Class I (2)—Fires on the ground.—This includes all accidents in which fires occur while the aircraft is being operated as such on the ground.

NOTE: FIRES AFTER ACCIDENT.—This is a secondary grouping for statistical purposes only, and should not be included under Class I.

10. *Class J—Carrier, platform, and arresting-gear accidents.*—This includes accidents occurring while the aircraft is landing upon or taking off from (1) the deck of a floating aircraft carrier, or (2) a platform intended for the landing and taking off of aircraft, but excludes launching-gear accidents.

11. *Class K—Launching-gear accidents.*—This includes accidents during take-off in which the aircraft is assisted in gaining flying speed by the application of an external force.

12. *Class N—Structural failure.*—This includes all accidents resulting in loss of control of the aircraft, as a result of a failure while in flight of any part of the aircraft structure or engine which is not due to contact with any external object.

13. *Class X—Miscellaneous.*—This includes accidents the nature of which is known but which do not fall into one of the above classifications.

14. *Class Y—Undetermined.*—This includes all accidents concerning the nature of which so little is known that any other classification cannot be intelligently made.

II. INJURY TO PERSONS

Under this head accidents are classified according to the injury suffered by persons.

1. *Class A.*—A "Class A" injury is one resulting in the death of the individual within a period of 90 days.

2. *Class B.*—A "Class B" injury is one resulting in serious injury to the individual. Because of the difficulties of classification, the opinion of a physician should be obtained whenever possible as to whether an injury is severe or minor. When a physician is not available, the following general rules should be followed: Any injury that results in unconsciousness; any fracture of any bone except simple fractures of the fingers and toes; lacerations that involve muscles or cause severe hemorrhage; any injury to any internal organ; or any other injury that it seems probable will incapacitate the individual for more than 5 days should be classed as a severe injury. All other injuries should be classed as minor.

3. *Class C.*—A "Class C" injury is one resulting in only minor injury to the individual.

4. *Class D.*—Any person who experiences an aviation accident with no personal injury shall be classified as "Class D."

NOTE.—The classification of an accident according to injury to persons shall contain a letter for each individual in the aircraft at the time of the accident, the first of these letters representing the pilot of the aircraft. For example, in an accident where the pilot is

killed, one passenger seriously injured, and the remaining passenger escapes with only minor injury the accident would be classified as a Class ABC accident. Had the pilot escaped with minor injury and both passengers been killed, it would have been a Class CAA accident.

III. DAMAGE TO MATERIAL

Under this head accidents are classified according to the amount of damage which occurs to material.

1. *Class A.*—This includes all accidents as a result of which the aircraft is of no further value except for possible salvage of usable parts.

2. *Class B.*—This includes all accidents as a result of which it is necessary to completely overhaul the aircraft before it would be again airworthy.

3. *Class C.*—This includes all accidents as a result of which it is necessary to replace some major assembly of the aircraft before it would be again airworthy, such as a wing, fuselage, undercarriage, tail, or engine.

4. *Class D.*—This includes all accidents resulting in minor and easily repairable damage to the aircraft, such as a broken wheel, bent rudder, bent propeller, broken cylinder, broken oil cooler, etc.

5. *Class E.*—This includes all accidents in which there is no damage to material.

CAUSES OF ACCIDENTS

The following classifications for the study of aircraft accidents according to their causes are recommended:

A. IMMEDIATE CAUSES OF AIRCRAFT ACCIDENTS

The following is a proposed list of immediate standard causes of aircraft accidents, with definitions where considered necessary for clarity.

I. *Personnel.*—This includes all accidents which can be traced to persons accessory to the operation or maintenance of the aircraft, either on the ground or in the air. This does not include accidents due to errors or omissions of personnel charged with the design, manufacture, or overhaul of aircraft.

1. *Errors of Pilot.*—This includes all accidents the responsibility for which rests upon the pilot. The pilot is the actual manipulator of the controls or the individual responsible for their correct manipulation.

(a) *Error of Judgment.*—This includes all accidents resulting from a decision made by the pilot which was not the correct one under existing circumstances.

(b) *Poor Technique.*—This includes all accidents resulting from lack of skill, dexterity, or coordination of the senses in handling aircraft controls, whether traceable to inherent inability to attain such or to infrequent flying, lack of experience in flying, lack of experience in flying under particular conditions or in the particular type of aircraft.

NOTE.—Judgment involves mental activity only for the purpose of arriving at decisions as to the ends to be attained and the general course to be followed.

Technique is the physical expression of the mental decisions which have been made.

See example on page 8.

(c) *Disobedience of Orders.*—This includes all accidents resulting from the violation or disobedience of local or general orders or regulations or provisions of law governing the operation of aircraft, such as low acrobatics, acrobatics in aircraft not to be used for such purposes, or any other type or manner of operation specifically forbidden by orders or regulations issued by competent authority.

(d) *Carelessness or Negligence.*—This includes all accidents resulting from the absence of care on the part of the pilot according to circumstances or the failure to use that degree of care which the circumstances justly demand, either on the ground or in the air, such as failure to make the proper mechanical adjustments necessary for take-off or landing.

(e) *Miscellaneous.*—This includes all accidents resulting from errors of the pilot not accounted for above.

2. *Errors of Other Personnel.*—This includes all accidents the responsibility for which rests upon personnel other than the pilot, such as section leaders, navigators, maintenance crew, operations officers, dispatchers, tower control men, or meteorological and communication personnel.

II. *Material.*—This includes all accidents resulting from failure of the airplane structure, power plant, accessories, and launching and arresting devices, whether traceable to material, faulty design, construction, modification, overhaul, or inspection incident to same.

1. *Power Plant.*—This includes all accidents resulting from failure or malfunctioning of the power plant and all auxiliaries essential to its proper functioning, exclusive of instruments. It includes the following:

- (a) FUEL SYSTEM.
- (b) COOLING SYSTEM.
- (c) IGNITION SYSTEM.
- (d) LUBRICATION SYSTEM.
- (e) ENGINE STRUCTURE.
- (f) PROPELLER AND PROPELLER ACCESSORIES.
- (g) ENGINE CONTROL SYSTEM (THROTTLE ROD, ETC.).
- (h) MISCELLANEOUS.
- (i) UNDETERMINED.

2. *Structural.*—This includes all accidents resulting from failure of the airplane exclusive of the power plant and instruments. It includes the following:

- (a) FLIGHT-CONTROL SYSTEM.
- (b) MOVABLE SURFACES.
- (c) STABILIZING SURFACES; STRUTS, WIRES, AND FITTINGS.
- (d) WINGS; STRUTS, WIRES, AND FITTINGS.
- (e) LANDING GEAR; STRUTS, WIRES, FITTINGS, AND RETRACTING MECHANISM.

N.A.C.A. AIRCRAFT ACCIDENT ANALYSIS FORM																					
CLASSIFICATION OF ACCIDENT NATURE : RESULTS : PERSONNEL (CLASS) MATERIAL (CLASS)				UNDERLYING CAUSES OF ACCIDENT																	
				ERRORS OF PILOT						MATERIAL					DESIGN ORIGINAL MODIFICATION UNDETERMINED						
				LACK OF EXPERIENCE		PHYSICAL AND PSYCHOLOGICAL		FAULTY IN-STRUCTIONS	INSPECTION	MATE-RIALS	STRENGTH (STRUCTURAL) ARRANGEMENT AERODYNAMIC UNDETERMINED										
				GENERAL	SPECIAL	DISEASE OR DEFECT	POOR RE-ACTION														
IMMEDIATE CAUSES OF ACCIDENT				TOTAL	RECENT	TOTAL	RECENT	INHERENT	TEMPORARY	INHERENT	TEMPORARY	OPERATING	MAINTENANCE	MANUFACTURING	OVERHAUL	MAINTENANCE	UNDETERMINED	ORIGINALLY DEFECTIVE	DETERIORATED	UNDETERMINED	
PER-SON-NE-L	ER-RORS OF PILOT	ERROR OF JUDGMENT																			
		POOR TECHNIQUE																			
		DISOBEDIENCE OF ORDERS																			
		CARELESSNESS OR NEGLIGENCE																			
		MISCELLANEOUS																			
MA-TER-IAL	POWER PLANT	FUEL SYSTEM																			
		COOLING SYSTEM																			
		IGNITION SYSTEM																			
		LUBRICATION SYSTEM																			
		ENGINE STRUCTURE																			
		PROPELLER AND PRO-PELLER ACCESSORIES																			
		ENGINE CONTROL SYSTEM																			
		MISCELLANEOUS																			
	STRUC-TURAL	UNDETERMINED																			
		FLIGHT CONTROL SYSTEM																			
		MOVABLE SURFACES																			
		STABILIZING SURFACES; STRUTS, WIRES & FITTINGS																			
		WINGS; STRUTS, WIRES, AND FITTINGS																			
		LANDING GEAR; STRUTS, WIRES, FITTINGS, AND RETRACTING MECHANISM																			
		WHEELS, TIRES & BRAKES																			
		SEAPLANE FLOAT OR HULL; STRUTS, WIRES & FITTINGS																			
		FUSELAGE, ENGINE MOUNT, AND FITTINGS																			
		COWLING, FAIRING & FITTINGS																			
		TAIL WHEEL ASSEMBLY AND SKID																			
		ARRESTING APPLIANCES ON AIRCRAFT																			
	MISCELLANEOUS																				
	UNDETERMINED																				
	HANDLING QUALITIES																				
		INSTRUMENTS																			
		LAUNCHING DEVICES																			
ARRESTING DEVICES																					
MIS-CEL-LAN-EOUS	WEATHER																				
	DARKNESS																				
	AIRPORT OR TERRAIN																				
	OTHER																				
UNDETERMINED																					

RECOMMENDED BY
 COMMITTEE ON AIRCRAFT ACCIDENTS
 JUNE 22, 1936
 APPROVED BY
 EXECUTIVE COMMITTEE
 NATIONAL ADVISORY COMMITTEE FOR AERONAUTICS
 JUNE 23, 1936

- (f) WHEELS, TIRES, AND BRAKES.
- (g) SEAPLANE FLOAT OR HULL; STRUTS, WIRES, AND FITTINGS.
- (h) FUSELAGE, ENGINE MOUNT, AND FITTINGS.
- (i) COWLING, FAIRING, AND FITTINGS.
- (j) TAIL-WHEEL ASSEMBLY AND SKID.
- (k) ARRESTING APPLIANCES ON AIRCRAFT.
- (l) MISCELLANEOUS.
- (m) UNDETERMINED.

3. HANDLING QUALITIES.—This includes all accidents resulting from those peculiar characteristics of certain types of aircraft affecting their controllability while on the ground or in the air, such as marked tendency to ground loop, inability to recover from a spin, etc.

4. INSTRUMENTS.—This includes all accidents resulting from failures of instruments which were essential to operation under the conditions of the flight.

5. LAUNCHING DEVICES.—This includes all accidents resulting from failure or malfunctioning of catapults or other launching devices.

6. ARRESTING DEVICES.—This includes all accidents resulting from failure or malfunctioning of arresting gear not a part of the aircraft.

III. *Miscellaneous*.—This includes all accidents not otherwise accounted for.

1. WEATHER.—This includes all accidents resulting from conditions of the weather which could not reasonably have been foreseen and avoided. (Mention may be made on the chart of contributing weather causes, as fog, gale, ice, hail, snow, rain, lightning, or low visibility.)

2. DARKNESS.—This includes all accidents resulting from conditions due to nightfall which could not reasonably have been foreseen and avoided.

3. AIRPORT OR TERRAIN.—This includes all accidents resulting from conditions of the airport or terrain which could not reasonably have been detected or avoided. (Forced landings should not be charged to airport or terrain unless the accident occurs on an area used for landing and take-off purposes.)

4. OTHER.—This includes all accidents resulting from causes not otherwise accounted for above.

IV. *Undetermined*.

B. UNDERLYING CAUSES OF AIRCRAFT ACCIDENTS

The following is a list of standard underlying causes of aircraft accidents, with definitions where considered necessary for clarity.

I. *Errors of pilot*.—Returning to "Errors of Pilot", paragraph I, subparagraph 1, the subdivisions of this paragraph were made according to the immediate causes of the errors attributed to the pilot, such as an "Error of judgment", "Poor technique", etc. The underlying causes of such errors may frequently be of more interest than the immediate causes themselves. These causes may be defined as those elements which contributed to the pilot's mental and physical equip-

ment at the time of the accident or to the deficiencies which existed in such equipment.

1. LACK OF EXPERIENCE.—This includes all accidents resulting from insufficient personal acquaintance with the actual conditions which had to be met under the circumstances.

(a) LACK OF GENERAL EXPERIENCE.—This includes all accidents resulting from a lack of experience in the general problems of aviation, such as landing, taking off, air work, etc.

(1) Lack of total general experience.—This includes all accidents resulting from a lack of general experience due to the fact that the individual concerned has never engaged in such work for a sufficient period of time to acquire the necessary experience to have avoided such accidents.

(2) Lack of recent general experience.—This includes all accidents resulting from a lack of general ability due to the fact that the individual concerned has too infrequently engaged in general flying activities prior to the accident, and consequently lost the ability he had originally acquired.

(b) LACK OF SPECIAL EXPERIENCE.—This includes all accidents resulting from a lack of experience in special problems of aviation, such as certain features of cross-country flying (which might, for example, require an intimate knowledge of the terrain of a certain section), carrier operations, night flying, instrument flying, etc.

(1) Lack of total special experience.—This includes all accidents resulting from a lack of special experience due to the fact that the individual had never engaged in such special problems for a sufficient period of time to acquire the necessary experience to have avoided such accidents.

(2) Lack of recent special experience.—This includes all accidents resulting from a lack of ability in the special problems due to the fact that the individual concerned has too infrequently engaged in special flying activities prior to the accident, and consequently lost the ability he had originally acquired.

2. PHYSICAL AND PSYCHOLOGICAL CAUSES.—This includes all accidents resulting from a demonstrable disease or defect or poor reaction.

(a) DISEASE OR DEFECT.—This includes all accidents resulting from a disease or defect, demonstrable by physical examination.

(1) Inherent disease or defect.—This includes all accidents resulting from a disease or defect which is not susceptible to remedy within a reasonable period of time, such as defective vision or judgment of distance; unconsciousness; hysterical or epileptic tendency; chronic air sickness; inability to withstand altitude, etc., any of which may lead to overshooting a field, faulty landings, or collision. The history of an individual may often be necessary to determine whether a disease or defect is inherent.

(2) **Temporary disease or defect.**—This includes all accidents resulting from a disease or defect which is remediable and one which may not be expected to repeat itself with undue frequency in the individual concerned, such as temporary illness, incomplete convalescence, etc.

(b) **POOR REACTION.**—This includes all accidents which result from no demonstrable disease or defect but from other causes which make the individual react either erroneously or slowly to a situation, such as selecting what is manifestly the poorer of two fields for an emergency landing, persisting on a course when better judgment would indicate that he should land or turn back, etc.

(1) **Poor reaction, inherent.**—This includes all accidents resulting from causes within this classification which apparently are not susceptible to correction within a reasonable period of time. The history of the individual would be a very important adjunct in determining whether such poor reaction were inherent and its repetition to be frequently expected.

(2) **Poor reaction, temporary.**—This includes all accidents resulting from causes within this classification which apparently are subject to correction within a reasonable period of time.

II. **Material.**—The underlying causes of material failures should also prove of considerable interest in analyzing accidents.

1. **FAULTY INSTRUCTIONS.**—This includes all accidents resulting from material failures which are traceable to errors or omissions in the standard instructions covering the use of the material.

(a) **FAULTY OPERATING INSTRUCTIONS.**—This includes all accidents resulting from material failures which are traceable to the operation of the material in accordance with standard instructions which prove to be incorrect or incomplete, such as instructions governing the use of the mixture control which when carried out are found to damage the engine, instructions governing the proper engine operating temperature which when carried out are found to damage the engine, etc.

(b) **FAULTY MAINTENANCE INSTRUCTIONS.**—This includes all accidents resulting from material failures which are traceable to the maintenance of the material in accordance with standard instructions which prove to be incorrect or incomplete, such as instructions specifying an improper grade of oil for use in an engine.

2. **FAULTY INSPECTION.**—This includes all accidents resulting from material failures which are traceable to errors or omissions in the inspection of the material.

(a) **FAULTY MANUFACTURING INSPECTION.**—This includes all accidents traceable to faulty inspection of material where errors or omissions occurred prior to the receipt of this material by the consumer.

(b) **FAULTY OVERHAUL INSPECTION.**—This includes all accidents traceable to faulty inspection of material where errors or omissions occurred during overhaul or storage of the material.

(c) **FAULTY MAINTENANCE INSPECTION.**—This includes all accidents traceable to faulty inspection of material where errors or omissions in such inspection occurred after the final delivery of this material to the operating unit.

(d) **FAULTY INSPECTION, UNDETERMINED.**—This includes all accidents traceable to faulty inspection of material where actual responsibility for the errors or omissions in inspection cannot be definitely placed.

3. **FAULTY MATERIALS.**—This includes all accidents resulting from material failures which are traceable to defective materials when the defects in materials could not reasonably have been detected and eliminated by a proper system of inspection.

(a) **ORIGINALLY DEFECTIVE MATERIALS.**—This includes all accidents traceable to faulty materials where the materials contained the defects when originally delivered.

(b) **DETERIORATED MATERIALS.**—This includes all accidents traceable to faulty materials where the defects of such materials occurred through deterioration after delivery.

(c) **FAULTY MATERIALS, UNDETERMINED.**—This includes all accidents traceable to faulty materials where it is not possible to determine the actual time or place when the defects first appeared.

4. **FAULTY DESIGN.**—This includes all accidents resulting from material failures which are traceable to errors or omissions in the design of the material.

(a) **FAULTY DESIGN, ORIGINAL.**—This includes all accidents traceable to faulty design where errors or omissions in such design occurred in the original design of the material, or in the course of changes in such design made prior to the final acceptance of the material by the operator.

(1) Faulty original design, structural strength.

(2) Faulty original design, arrangement.

(3) Faulty original design, aerodynamic.

(4) Faulty original design, undetermined.

(b) **FAULTY DESIGN, MODIFICATION.**—This includes all accidents traceable to faulty design where errors or omissions in such design occurred in modifications to the original design of the material made subsequent to the final acceptance of the material by the operator.

5. **UNDETERMINED MATERIAL FAILURE.**—This includes all accidents from material failures the exact cause of which cannot be determined.

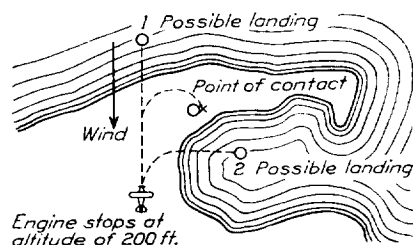
ALLOCATION OF ACCIDENTS

In compiling statistics an accident should be allocated to the service or organization having jurisdiction over or control of the operation of the aircraft at the time of the accident. In the case of collisions the accident itself should be analyzed as a single accident, but should be carried statistically by each of the organizations involved.

Injuries and fatalities should be allocated according to the aircraft in which they occur.

DESCRIPTION AND TYPICAL ANALYSIS OF AN ACCIDENT

Pilot John Doe was flying in a seaplane at an altitude of 200 feet over a point of land between a bay and the open sea when the engine stopped. Pilot Doe had an opportunity to land either directly into the wind in the open sea or cross wind in the bay. He started to land in the ocean but at 100 feet altitude he changed his mind and attempted to turn so as to land in the bay. In turning, Doe held the nose of the seaplane up, stalled it, and spun into the land. The seaplane was demolished, the pilot was seriously injured, and the passenger was killed.



Doe, according to his record, was an experienced aviator with 30 hours' flying during the preceding month and with recent experience in stunting airplanes.

Examination of the engine showed that one of the teeth in the magneto timing gear had stripped, the broken tooth having been drawn into the other teeth, causing the eventual stripping of all teeth. The original break was determined to be a visible hardening crack.

The NATURE of this accident is class C—tail spin following engine failure, as defined on page 3. The classification according to RESULTS is Personnel, class BA (pp. 3 and 4); Material, class A. (p. 4).

In analyzing this accident the IMMEDIATE CAUSE is charged, as indicated on the analysis chart, as 75 percent "Personnel" and 25 percent "Material", for the reason that the account of the accident shows that the pilot had two chances to make a safe landing and took advantage of neither of them. Considering the 75 percent which is charged to "Personnel", it is obvious that this is not chargeable to "Errors of other personnel", so that the whole weight, 75 percent, must be placed under "Errors of pilot." It appears that the errors of the pilot involved both errors of judgment and poor technique. He first decided to land straight ahead in the ocean, which was a proper decision. Then, after reaching an altitude at which turning without power is generally considered dangerous, he decided to turn and land in the bay. This was an error and showed poor judgment. Poor technique was displayed in the execution of this decision in that the pilot continued to pull the nose up, still further stalling the seaplane, when he should have sensed the approaching stall. It is considered that a charge of 35 percent to "Error of

judgment" and 40 percent to "Poor technique" represents as near an approximation as can be reached in this case.

UNDERLYING CAUSES

On analysis of UNDERLYING CAUSES it would appear that the "Error of judgment" and "Poor technique" were both due to a "Temporary poor reaction" with a strong possibility of such "Poor reaction" being "Inherent" rather than "Temporary." However, in the absence of a history of the individual this would have to be classified as "Temporary."

Considering the 25 percent charged to "II. Material", the entire 25 percent obviously should be assigned to "1. Power-plant failure", in the second order of subdivision, and again in the third order of subdivision the entire 25 percent should be charged to "(c) Ignition system."

The underlying cause of this material failure is unquestionably faulty manufacturing and accordingly on the cross analysis it would be placed under the head of "Manufacturing inspection."

INTERPRETATION OF DEFINITIONS AND METHODS

As was anticipated, questions have arisen regarding the proper interpretation of the definitions and the methods to be followed in using the proposed method of analysis. These questions have generally been referred to the committee for opinions or the interpretations followed have been communicated for approval. In this manner there has been established a sort of approved procedure.

An early criticism was the effect of the personal factor on the weights to be assigned to the various causes of an accident. That the average obtained from a considerable number of cases can not be far off is shown by the results from a test conducted by the original special committee, but not mentioned in its report. Six accidents were reported in identical form to each member of the committee and were analyzed independently by him. The percentages assigned the various causes were then averaged and the averages were compared with the individual ratings. Every member was willing to accept the average values as a fair analysis of the various accidents, and the differences between the values assigned by the individuals and averages were remarkably small.

CONCLUSION

The Committee on Aircraft Accidents believes that the practical value of the accident analysis chart prepared by the Committee on Aircraft Accidents, and the importance of the information which may be obtained from the use of this chart, have been clearly demonstrated in its use in service in the War, Navy, and Commerce Departments.

N.A.C.A. AIRCRAFT ACCIDENT ANALYSIS FORM																												
CLASSIFICATION OF ACCIDENT					UNDERLYING CAUSES OF ACCIDENT																							
					ERRORS OF PILOT					MATERIAL																		
					LACK OF EXPERIENCE		PHYSICAL AND PSYCHOLOGICAL		FAULTY IN-STRUC-TIONS	INSPECTION	MATE-RIALS	DESIGN																
					GENERAL	SPECIAL	DISEASE OR DEFECT	POOR RE-ACTION				ORIGINAL	MODIFICATION															
IMMEDIATE CAUSES OF ACCIDENT					TOTAL	RECENT	TOTAL	RECENT	INHERENT	TEMPORARY	INHERENT	TEMPORARY	OPERATING	MAINTENANCE	MANUFACTURING	OVERHAUL	MAINTENANCE	UNDETERMINED	ORIGINALLY DEFECTIVE	DETERIORATED	UNDETERMINED	STRENGTH(STRUCTURAL)	ARRANGEMENT	AERODYNAMIC	UNDETERMINED	UNDETERMINED		
75	PER-SON-NEL	75	ERRORS OF PILOT	35	ERROR OF JUDGMENT								35															
				40	POOR TECHNIQUE											40												
					DISOBEDIENCE OF ORDERS																							
					CARELESSNESS OR NEGLIGENCE																							
					MISCELLANEOUS																							
ERRORS OF OTHER PERSONNEL																												
15	MA-TER-IAL	15	POWER PLANT		FUEL SYSTEM																							
					COOLING SYSTEM																							
				25	IGNITION SYSTEM											25												
					LUBRICATION SYSTEM																							
					ENGINE STRUCTURE																							
					PROPELLER AND PRO-PELLER ACCESSORIES																							
					ENGINE CONTROL SYSTEM																							
					MISCELLANEOUS																							
			UNDETERMINED																									
		STRUCTURAL		FLIGHT CONTROL SYSTEM																								
				MOVABLE SURFACES																								
				STABILIZING SURFACES; STRUTS, WIRES & FITTINGS																								
				WINGS; STRUTS, WIRES, AND FITTINGS																								
				LANDING GEAR; STRUTS, WIRES, FITTINGS, AND RETRACTING MECHANISM																								
				WHEELS, TIRES & BRAKES																								
				SEAPLANE FLOAT OR HULL; STRUTS, WIRES & FITTINGS																								
				FUSELAGE, ENGINE MOUNT, AND FITTINGS																								
				COWLING, FAIRING & FITTINGS																								
				TAIL WHEEL ASSEMBLY AND SKID																								
				ARRESTING APPLIANCES ON AIRCRAFT																								
				MISCELLANEOUS																								
				UNDETERMINED																								
				HANDLING QUALITIES																								
				INSTRUMENTS																								
				LAUNCHING DEVICES																								
	ARRESTING DEVICES																											
MIS-CEL-LAN-EOUS		WEATHER																										
		DARKNESS																										
		AIRPORT OR TERRAIN																										
		OTHER																										
UNDETERMINED																												

RECOMMENDED BY
 COMMITTEE ON AIRCRAFT ACCIDENTS
 JUNE 22, 1936
 APPROVED BY
 EXECUTIVE COMMITTEE
 NATIONAL ADVISORY COMMITTEE FOR AERONAUTICS
 JUNE 23, 1936

As a result of experience, there have been introduced into the present report some minor changes in definitions and nomenclature, which changes, however, are in conformity with the classifications already set up.

The committee has given careful consideration to the physiological and psychological problems involved in the piloting of aircraft as having an important bearing on the number and types of accidents which occur.

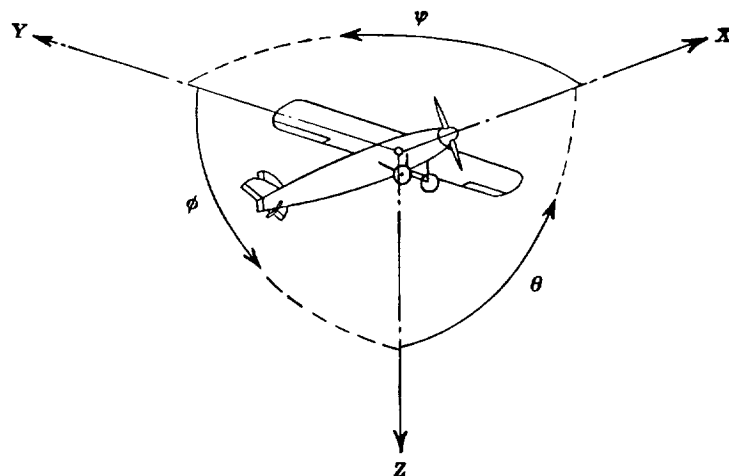
The report represents the experience of the committee and of the three departments concerned in the

study of aircraft accidents up to the present time. The study of aircraft accidents for the purpose of analyzing them in such a manner as to assist in reducing their frequency and severity is a task which can never be completed, but must be continued in step with the progress of the art.

Respectfully submitted.

COMMITTEE ON AIRCRAFT ACCIDENTS,
EDWARD P. WARNER, *Chairman*.

WASHINGTON, D. C., *June 22, 1936*.



Positive directions of axes and angles (forces and moments) are shown by arrows

Axis			Moment about axis			Angle		Velocities	
Designation	Sym- bol	Force (parallel to axis) symbol	Designation	Sym- bol	Positive direction	Designa- tion	Sym- bol	Linear (compo- nent along axis)	Angular
Longitudinal.....	X	X	Rolling.....	L	Y→Z	Roll.....	φ	u	p
Lateral.....	Y	Y	Pitching.....	M	Z→X	Pitch.....	θ	v	q
Normal.....	Z	Z	Yawing.....	N	X→Y	Yaw.....	ψ	w	r

Absolute coefficients of moment

$$C_l = \frac{L}{q b S}$$

(rolling)

$$C_m = \frac{M}{q c S}$$

(pitching)

$$C_n = \frac{N}{q b S}$$

(yawing)

Angle of set of control surface (relative to neutral position), δ . (Indicate surface by proper subscript.)

4. PROPELLER SYMBOLS

D , Diameter

p , Geometric pitch

p/D , Pitch ratio

V' , Inflow velocity

V_{∞} , Slipstream velocity

T , Thrust, absolute coefficient $C_T = \frac{T}{\rho n^2 D^4}$

Q , Torque, absolute coefficient $C_Q = \frac{Q}{\rho n^2 D^5}$

P , Power, absolute coefficient $C_P = \frac{P}{\rho n^3 D^5}$

C_{sp} , Speed-power coefficient $= \sqrt[5]{\frac{\rho V^5}{P n^3}}$

η , Efficiency

n , Revolutions per second, r.p.s.

Φ , Effective helix angle $= \tan^{-1} \left(\frac{V}{2\pi r n} \right)$

5. NUMERICAL RELATIONS

1 hp. = 76.04 kg-m/s = 550 ft-lb./sec.

1 metric horsepower = 1.0132 hp.

1 m.p.h. = 0.4470 m.p.s.

1 m.p.s. = 2.2369 m.p.h

1 lb. = 0.4536 kg

1 kg = 2.2046 lb.

1 mi. = 1,609.35 m = 5,280 ft.

1 m = 3.2808 ft.

